Natural Rubber Materials

Volume 2: Composites and Nanocomposites

RSC Polymer Chemistry Series

Titles in the Series:

1: Renewable Resources for Functional Polymers and Biomaterials
2: Molecular Design and Applications of Photofunctional Polymers and Materials
3: Functional Polymers for Nanomedicine
4: Fundamentals of Controlled/Living Radical Polymerization
5: Healable Polymer Systems
6: Thiol-X Chemistries in Polymer and Materials Science
7: Natural Rubber Materials Volume 1: Blends and IPNs
8: Natural Rubber Materials: Volume 2: Composites and Nanocomposites

Natural Rubber Materials
Volume 2: Composites and Nanocomposites

Edited by

Sabu Thomas, Hanna J. Maria, Jithin Joy
Mahatma Gandhi University, Kottayam, India
Email: sabuchathukulam@yahoo.co.uk, hannavidhu@gmail.com, jithinjoyjrf@gmail.com

Chin Han Chan
MARA University of Technology, Selangor, Malaysia
Email: cchan@salam.uitm.edu.my

and

Laly A. Pothen
Bishop Moore College, Mavelikkara, India
Email: lapothan@gmail.com

RSC Publishing

RSC Polymer Chemistry Series No. 8

ISBN: 978-1-84973-631-2
ISSN: 2044-0790

A catalogue record for this book is available from the British Library

Published by The Royal Society of Chemistry,
Thomas Graham House, Science Park, Milton Road,
Cambridge CB4 0WF, UK

Registered Charity Number 207890

For further information see our web site at www.rsc.org

Preface

The technology of natural rubber composites and nanocomposites is a versatile branch of materials science with several new prospects arising day to day. This family of composites is a structural material of high importance in the 21st century. The fast growing rubber industry is supported by research and development activities in a number of university research laboratories.

This book focuses on the synthesis and characterization of natural rubber composites and nanocomposites, the interaction between reinforcing agents and the rubber matrix and their effect on different properties. The reinforcing effect of traditional fillers in micro range and the effectiveness of these nanofillers are discussed. This book on natural rubber and nano composites comprises of the most recent research activities that will, unquestionably, be a vital reference book for scientists in both the academic and industrial sectors, as well as for individuals who are interested in natural rubber materials.

This is Volume 2 of *Natural Rubber Materials* and it covers natural rubber-based composites and nanocomposites in 27 chapters. It focuses on the different types of fillers, the filler–matrix reinforcement mechanisms, manufacturing techniques, and applications of natural rubber-based composites and nanocomposites. The first 4 chapters deal with the present state of art and manufacturing methods of natural rubber materials. Two of these chapters explain the theory of reinforcement and the various reinforcing nanofillers in natural rubber. Chapters 5 to 19 detail the natural rubber composites and nanocomposites with various fillers such as; silica, glass fibre, metal oxides, carbon black, clay, POSS and natural fibres etc. Chapters 20–26 discuss the major characterisation techniques and the final chapter covers the applications of natural rubber composites and nanocomposites. By covering recent developments as well as the future uses of rubber, this volume will be a standard reference for scientists and researchers in the field of polymer chemistry for many years to come.

RSC Polymer Chemistry Series No. 8
Natural Rubber Materials, Volume 2: Composites and Nanocomposites
Edited by Sabu Thomas, Hanna J. Maria, Jithin Joy, Chin Han Chan and Laly A. Pothen

Published by the Royal Society of Chemistry, www.rsc.org

We take this opportunity to thank all the people who have devoted their time and energy in making this book a success. We are also thankful to the reviewers for their support and time. We are also grateful to the editorial team of Royal Society of Chemistry for their guidance and continuous support in this venture. We are also thankful to one and all especially our co-workers, Vishak P. M., Poornima Vijayan, Sneha Mohan, Josmine P. Jose, Sangeetha Nair and Merin Sara Thomas for their support and help in preparing this book.

Contents

RSC Polymer Chemistry Series No. 8
Natural Rubber Materials, Volume 2: Composites and Nanocomposites
Edited by Sabu Thomas, Hanna J. Maria, Jithin Joy, Chin Han Chan and Laly A. Pothen

Published by the Royal Society of Chemistry, www.rsc.org

CHAPTER 1

Natural Rubber-Based Composites and Nanocomposites: State of the Art, New Challenges and Opportunities

C. H. CHAN,*[a] JITHIN JOY,[b] HANNA J. MARIA[b] AND S. THOMAS[a,b]

[a] Faculty of Applied Sciences, Universiti Teknologi MARA, Shah Alam, Malaysia; [b] Mahatma Gandhi University, Priyadarshini Hills P. O., Kottayam, Kerala 686 560, India
*Email: cchan@salam.uitm.edu.my; cchan_25@yahoo.com.sg

1.1 Introduction

Natural rubber (NR) is also known as *cis*-1,4-poly(isoprene) and has the chemical structure illustrated in Figure 1.1(a). NR is an elastomer originally derived from a milky colloidal suspension from the sap of some plants, called NR latex. Only the sap cultivated from the *Hevea brasiliensis* tree is of commercial importance (see Figure 1.1(b)).[1] *Hevea* is native to Brazil and produces a high molecular weight of $\sim$ 97% *cis*-1,4-poly(isoprene) (roughly 20,000 units of isoprene).[2] This signifies that the NR polymer chain continues on the same side of the double bond. *Hevea* yields high-quality latex over a sustainable period and is amenable to tapping for approximately 30 years. The typical

RSC Polymer Chemistry Series No. 8
Natural Rubber Materials, Volume 2: Composites and Nanocomposites
Edited by Sabu Thomas, Hanna J. Maria, Jithin Joy, Chin Han Chan and Laly A. Pothen

Published by the Royal Society of Chemistry, www.rsc.org

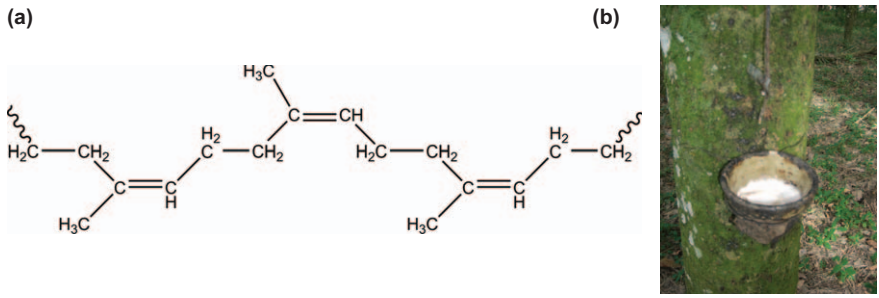

Figure 1.1 (a) Chemical structure of NR [*cis*-1,4-poly(isoprene)], where the chemical structure of isoprene is 2-methyl-1,3-butadiene and (b) NR latex from a *Hevea* tree on a rubber estate in Sungai Durian, Perak, Malaysia.

Table 1.1 Compositions of fresh NR latex in the form of an emulsion[3–5] and dry NR.[6]

	Component	*Composition (%)*
NR latex	Total solid content	36
	Dry rubber content	33
	Resinous substances	1–2.5
	Proteinaceous substances	1–1.5
	Inorganic salts (mainly K, P and Mg)	0.5
	Ash	< 1
	Sugars	1
	Water	60
Dry NR	Rubber content	93–95
	Resinous substances	2
	Proteinaceous substances	2–3
	Inorganic salts	< 0.2
	Sugars	< 0.2
	Cu and Mg	2–3 ppm
	Water	~ 0.5
Deproteinized dry NR	Rubber content	96
	Proteinaceous substances	0.12
	Ash	0.15
	Volatile matter content	0.3
	Dirt content	0.01

compositions of NR latex, dry NR and deproteinized dry NR (DPNR) are tabulated in Table 1.1. DPNR latex is a premier NR latex, treated with special enzymes or complexed with other chemicals to break down the naturally-occurring proteins. DPNR has improved resistance to fatigue failure for engineering applications.

The double bonds along the backbone of NR allow the attachment of pendant groups and/or provide chemically reactive sites for crosslinking or grafting. Naturally, NR is a soft and sticky solid with low tensile strength and low elasticity due to the weak van der Waals forces of its intermolecular attraction and occasional crosslinking. It softens at room temperature in tropical

Table 1.2 Properties of pure NR and vulcanized NR.

Properties	*Pure NR [reference]*	*Vulcanized NR [reference]*
Density at 20 °C (g cm^{-3})	0.9162 [23]	0.9093[23]
Thermal expansion coefficient at 20 °C (K^{-1})	6.6×10^{-4} [23]	6.4×10^{-4} [23]
Isothermal compressibility at atmospheric pressure (bar^{-1})	5.0×10^{-5} [23]	5.0×10^{-5} [23]
Thermal conductivity (W m^{-1} K^{-1})	0.13 [24]	0.153 [25, 26]
Specific heat capacity (J kg^{-1} K^{-1})	1.905×10^{3} [27]	1.828×10^{3} [28]
Glass transition temperature (°C)	−67 [29]	−63 [30]
Dielectric constant at 1 kHz	2.37–2.45 [24, 31]	2.68 [31]
Dissipation factor at 1 kHz	0.001–0.003 [31]	0.002–0.04 [31]
Conductivity (S m^{-1})	2.57×10^{-15} [24]	$2–100 \times 10^{-15}$ [24, 31]
Isothermal bulk modulus (Pa)	1.94×10^{6} [23]	1.95×10^{6} [23]
Storage modulus (Pa)	4.07×10^{5} [32]	4.07×10^{5} [33]
Loss modulus (Pa)	2.88×10^{4} [32]	6.31×10^{4} [33]
Ultimate elongation (%)	625 [34]	750–850 [35]
Tensile strength (MPa)	0.56 [34]	17–25 [35]

countries but hardens in cold weather[7,8] and it is highly crystallizable upon stretching.[9–15] It is soluble in some organic solvents, *e.g.* tetrahydrofuran, toluene, chloroform, methyl ethyl ketone, acetone, 2-butanone, *n*-hexane, benzene, *etc*. The properties of NR deteriorate drastically by sunlight, ozone and oxygen due to its high level of unsaturation, and such a material is of minimal interest in industry.[16] The properties of pure NR are tabulated in Table 1.2. Addition of carbon black (CB), and antiozonants and waxes, to NR enhances its resistance to UV and ozone, respectively.

In 1496, Christopher Columbus returned from his second voyage and brought back the first NR balls from the West Indies to the Iberian Peninsula. In 1736, Charles Marie de La Condamine introduced NR samples and reported the properties of NR to the Académie Royale des Sciences of France. He proposed that NR could be used as flexible tubes. Later, in 1770, Joseph Priestley, an English chemist, suggested the possibility of using NR as an eraser because of its ability to rub pencil marks off paper. This is the first recorded use of NR. Samuel Peal patented a method of waterproofing cloth by coating the cloth with a solution of NR in turpentine in 1791. In 1820, Nadier, a British industrialist, produced NR threads for clothing accessories. In London, Thomas Hancock invented a mastication machine to mix and soften NR, enabling it to be shaped. In 1823, Charles Macintosh produced waterproof garments by coating cloth with a solution of NR in benzene in a plant in Glasgow.

However, NR did not attain any commercial value until nearly a century later. The first important chemical modification of NR was vulcanization in 1839, which is generally credited independently to Charles Goodyear (USA) and Thomas Hancock (England). Crosslinks are introduced into NR chains in the process of vulcanization by heating up the NR with addition of sulfur, accelerator, fillers and antioxidants (see Figure 1.2). Vulcanization turns NR into a hard and non-sticky polymeric material with improved tensile strength

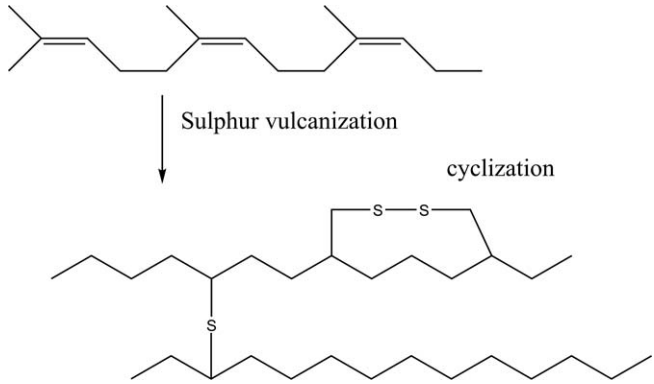

Figure 1.2 Schematic of sulfur vulcanization of NR. Adapted from ref. 17.

and higher resistance to organic solvents. This landmark in the history of NR has led to multibillion global NR industries.

In modern vulcanization processes,[18–22] NR is generally compounded (either under high or low temperature) with 0.5 to 1 wt% of accelerators, different concentrations of CBs (which act as a filler) (up to 45 wt% for tyre manufacturing), low concentrations of aromatic amines and phenols for antioxidation purposes and 5–8 wt% of sulfur. These types of vulcanized NR are commonly known as NR composites (when the filler dimension is on the microscale) or NR nanocomposites (when the filler dimension is on the nanoscale). NR-based composites or nanocomposites will be discussed in more detail in the following sections.

The vulcanized NR is elastic and flexible, but the process of vulcanization is irreversible. The properties of vulcanized NR are shown in Table 1.2. Since the 1980s there has been much attention paid to the disposal of used NR goods in an eco-friendly way. To address this environmental problem, recent years have seen scientific research into reversible chemical changes of NR, as well as the replanting of NR trees to enable a sustainable and renewable source of supply for NR production, whereas synthetic rubber (SR) is produced from depleting oil reserves.[36] The discovery of vulcanization of NR, led to a blossoming of NR industries, fuelled by additional supplies of NR from South-East Asia.

In 1876, Sir Henry Wickham transported 70,000 NR seedlings from the Amazon Basin to the Royal Botanic Gardens at Kew, of which only 2397 germinated. Some 1900 of these 2397 germinated seedlings were shipped on to Ceylon and Singapore (22 seedlings). Nine of the 22 seedlings from the Singapore Botanic Gardens were brought to Kuala Kangsar, Perak, Malaysia. These seedlings formed the nucleus of the NR industries in South-East Asia, which accounts for around 75% of all cultivated NR trees. Also at about this time, Sir Henry Nicholas Ridley (Director of the Singapore Botanic Gardens from 1888 to 1911) developed tapping techniques for the harvesting of NR latex from *Hevea*.[37] Early industrial applications of vulcanized NR are shown in Table 1.3. NR trees were first grown in 1873 at the Royal Botanic Gardens,

Table 1.3 Early industrial applications of vulcanized NR.[37,38]

Year		*Industrial applications*
1877	Patented by William Currie (USA)	Rubber golf balls
1884	Invented by C. McIntosh (UK)	Cushion tyres for bicycles
1888	Reinvented by John Boyd Dunlop	Pneumatic tyres for bicycles
1889	Manufactured by Pneumatic Tire Company (later known as Dunlop Rubber Company)	Pneumatic tyres
1889	Used by William Stewart Halsted (USA)	NR gloves (made by Goodyear Rubber Company) in the operating theatre
1892	Developed by Thomas Robins (USA)	Heavy-duty rubber belting for moving iron ore
1895	Introduced by Michelin (France) and designed by Daimler	First pneumatic automobile tyre
~1917		Pneumatic truck tyre in USA

Calcutta, India, and the first commercial NR plantations were established at Thattekadu in Kerala in 1902.

1.2 Supply and Demand of NR as Compared to SR

After a number of important scientific discoveries related to NR from the 1870s onwards, there was a quantum leap in terms of progress in the industrial applications of NR. The commercial production of automobiles by Karl Benz began in 1888 and later, from 1908 onwards, the mass production of cars by Henry Ford, increased the demand for pneumatic tyres, which were made exclusively from NR. The use of vehicles during World War I, coupled with the peace-time demand for motorized vehicles, was a golden age in terms of demand for NR. Before World War II, rubber products used 100% NR. Even today, around 60% of NR is used in the production of tyres.

During World War II, Japan's occupation of most of the countries of South-East Asia blockaded the supply of NR to industries in the West. This was a cause for concern and these countries responded vigorously, by investigating synthetic substitutes for NR and searching for large-scale supply of NR from other continents. The efforts to cultivate rubber trees in other countries did not actually pose a serious threat to the NR industries in South-East Asia. However, the development of SR, which was initiated politically and was strategically motivated, has emerged as the most serious threat to NR. SR production technology is intensive and is less dependent on a large and low-cost supply of labour compared to the production of NR latex on estates. Examples of SR are polybutadiene, ethylene/propylene copolymers, styrene butadiene rubber, *etc*. The production of SR was prompted by cheap and relatively constant supplies of petrochemical feedstock. In addition, the development of emulsion and stereoregular polymerization, new polymerization techniques, the availability of a wide range of suitable monomers, introduction of new monomers, and so on, has unveiled unprecedented opportunities and increased the

Table 1.4 Competitive strengths of SR as compared to NR and the strategized new dimensions of NR in the world market position.

Competitive strengths of SR as compared to NR	*Strategized new dimensions of NR in the world market position.*
1. Cheap and capacity of uninterrupted supply of petrochemical feedstock.	1. Changing from agricultural commodity to specialized industrial raw material.
2. Large corporation resources from established corporations.	2. Understanding the specific demands of consumers by tailoring the properties of NR.
3. Large captive markets.	3. Enhance the consistency in quality and chemical composition of NR as compared to SR.
4. Massive amount of R&D effort for tailoring the specific properties of SR to meet the specific requirements of consumers.	4. Improvement of performance of NR.
5. Perception of contributing to national security and independence, especially from the West.	5. NR shall be engineered as the biobased-feedstock for SR.
6. Consistency and specificity of chemical composition and quality.	
7. Huge variety of applications.	
8. SR manufacturing plants can be located close to major consumers, which will reduce the cost of transportation.	

Table 1.5 World consumption of rubbers and the maximum yield of NR latex in 1920 and 1970.[37,39]

Year	*Consumption of NR ('000 tons)*	*Consumption of SR ('000 tons)*	*Maximum yield of NR latex (kg/ha/year)*
1825	0.03 (100%)	–	
1840	0.38 (100%)	–	
1850	1.5 (100%)	–	
1860	2.7 (100%)	–	
1870	8 (100%)	–	
1880	13 (100%)	–	
1890	23 (100%)	–	
1900	50 (100%)	–	
1920	302 (100%)	–	500
1970	301 (35%)	5,590 (65%)	3000[a]

[a]Under ideal conditions for small- and pilot-scale plantings.

competitive strengths of SR as compared to NR, as summarized in Table 1.4. The early priority for Asian countries in terms of research was to increase the productivity of NR trees and to reduce the cost of production. However, new dimensions to position NR in the world rubber market have to be strategized, from agricultural commodity to specialized industrial raw material, as highlighted in Table 1.4. Trade statistics for the world consumption of NR and SR from 1825 to 1970 (see Table 1.5) illustrate the threat of SR to NR.

The increase in demand for NR over SR, which has dominated the world scene since World War II, is related to widespread concerns about global

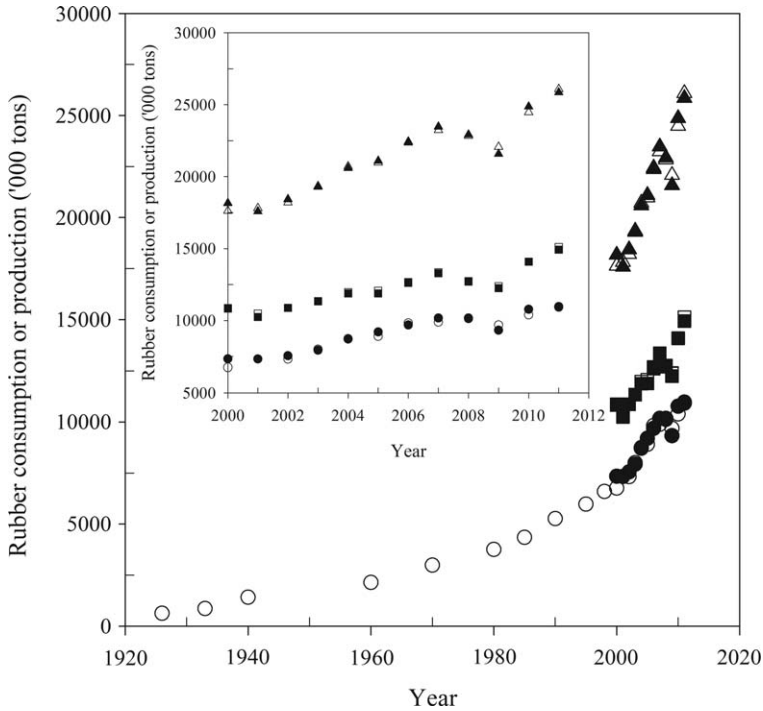

Figure 1.3 World consumption and production of NR, SR and total rubber from 1926 to 2011.[5,42] Consumption: ●, NR, ■, SR and ▲, total rubbers. Open symbols represent production.

warming, deteriorating ecosystems and depleting sources of fossil fuels. *Hevea* is one of the most effective trees for generating oxygen from carbon dioxide *via* photosynthesis. In general, planting one tree eliminates 1 ton of CO_2/year. An ecosystem of 33-year-old NR trees produces 450 tons/ha/year of biomass as compared to 475–664 tons/ha/year in Malaysian rainforests and 295–475 tons/ha/year in Brazilian and Thai rainforests.[40] However, it should also be noted that as industries urge towards sustainable farming practices for NR as demand rises, this may on the other hand drive deforestation.

Total world NR latex consumption gradually increased from 170,000 tons to 300,000 tons between 1960 and 1980. In the mid-1980s, total demand for NR latex took off, subsequently growing exponentially (see Figure 1.3). This marks the critical juncture of the transition of NR latex industries from the West to the East. The take-off was precipitated by prevention of transmission of human immunodeficiency virus (HIV) and hepatitis B with the increase in the use of NR latex gloves.[2] At first, gloves were mainly used during surgery, but nowadays examination gloves are used in virtually all contacts with patients, the driving force being the fear of transmittable diseases through physical contact. In addition the large-scale production of electronic parts and higher hygienic

Table 1.6 World consumption of NR and SR from 2000 to 2020.[42]

Year	*NR (%)*	*SR (%)*
2000	40.4	59.6
2001	41.7	58.3
2002	41.0	59.0
2003	41.2	58.8
2004	42.3	57.7
2005	43.6	56.4
2006	43.3	56.7
2007	43.4	56.6
2008	44.4	55.6
2009	43.2	56.8
2010	43.3	56.7
2011	42.3	57.7
2020	46.0[a]	54.0[a]

[a]Projection by IRSG.

standards in food production accelerated the usage of gloves during this period as well. There has been a marked increase in the demand for condoms, with their usage of condoms gradually diversifying from the prevention of pregnancy to the prevention of sexually transmitted diseases.[41]

World consumption and production of NR and SR from 1926 to 2011 are summarized in Table 1.6 and Figure 1.3.[42] In 2011, the world consumption of NR accounts for 42.3%, compared to SR at 57.7%. In 2011, 30% of NR was consumed by China. According to the former Secretary General of the International Rubber Study Group (IRSG) (Dr S. Evans), the projections for NR consumption and production in 2020 are 16.5 and 15.2 million tons, respectively. In other words, a deficit of 1.3 million tons of NR demand is expected. The major consumers of global NR production will be China ($\sim$7 million tons), followed by India (2.7 million tons), Europe, the USA and Japan. SR consumption in 2020 is expected to be 19.3 million tons.

1.3 Challenges and Opportunities for NR Industries

1.3.1 Challenges to Increase the Yield of NR Latex

Early research and development efforts on NR primarily focused on the increase in the yield of NR latex. As shown in Table 1.5, the maximum yield of NR latex increased from 500 to 3000 kg/ha/year from the 1920s to the 1970s.[5,37] Conventional horticultural techniques of plant breeding, selection of parents, selection of progenies from nurseries and selection of materials are the early attempts. However, this route demands long investigation period of 20 years by 1960s. New techniques, for examples gene manipulation and mutation breeding used in combination proven workhorse of tissue culture may push the yield of NR to the theoretical limit, up to 9000 kg/ha/year. By 1984, RRIM 900 series' clones of NR trees could produce around 5000 kg/ha/year under ideal soil and

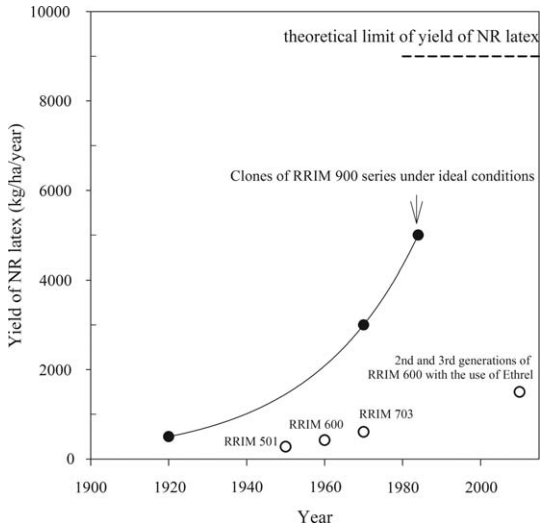

Figure 1.4 The yield of NR latex from the 1920s to 2010 in Malaysia.[37,39,43] ●, Maximum yield of NR latex under ideal conditions for small and pilot-scale plantings; ○, yield of NR from small stakeholders.

terrain conditions for small- and pilot-scale plantings[37] (Figure 1.4). However, a yield of NR latex of around 3000 kg/ha/year under ideal conditions is still common. This figure is still far below the theoretical yielding potential of NR trees (9000 kg/ha/year). Sustainable improvements in the yield of NR through plant breeding can only be achieved with the accessibility of a large genetic base, especially for countries outside Amazon basin.

In Malaysia, the yield of NR from small stakeholders (two-thirds of the total planting area for NR trees) is still around 1500 kg/ha/year. The common challenges of the small stakeholders include their increasing age and the lack of interest of the younger generation in NR plantations, old NR trees, and worker shortages. These lead to mature NR trees not being not tapped properly, and only around 4% of the NR trees from the small stakeholders use stimulants (*e.g.* ethereal) to increase the yield of NR latex. On the other hand, the yield of NR in plantations is around 2000 kg/ha/year. One of the targets is to increase the yield of NR from small stakeholders to 1960 kg/ha/year by 2020.[43]

Bridgestone Americas Center for Research and Technology successfully decoded the main genome sequence for *Hevea*, the data of which is expected to facilitate the development of improved breeding technologies and growing method of NR. Bridgestone expects to develop and improve *Hevea* clones with higher yield and quality.[44]

NR latex flows out from the latex vessels of NR trees after tapping. Best NR yield can be obtained for tapping at around 2 am. The latex vessels become plugged with particles after clotting is initiated by the flow of NR latex after several hours. When the cut is reopened on the following day, NR latex flows out again. The NR latex is collected daily for further processes. The production

of NR latex is labour intensive in most countries and the common practice to solve this predicament is by importing/recruiting indentured cheap labour. Generally, one tapper is needed for every 4 ha of NR plantation. However, this strategy serves as the short-term solution for the economic NR production. Regrettably, this common approach has delayed innovative discoveries for higher production of NR latex with minimal of manpower. By using gaseous stimulant (*e.g.* G-flex stimulant), 20–25 g NR/tap/day can be collected. The use of etherel (as stimulant) to prolong the flow of NR latex from a tapping cut and the use of chemical-contained polybag (to prevent premature coagulation of NR latex) may lead to the 10-day interval for the collection of NR latex from the polybag under ideal situation.[37] However, issues of collection of NR latex from polybags (in some cases up to $\sim$1 kg) by unauthorized people remain unsolved in unfenced NR plantations. Roughly 10% slurry of Ethrel® in palm oil is applied by hand with a paint brush on the NR bark near the tapping panel. Within days, hydrolysis of Ethrel® occurs and liberates ethylene and the absorption of ethylene within the NR tree tissues causes a dramatic increase in NR yield. Ethrel® can be reapplied at 2-month intervals.

An innovative tapping machine prototype was introduced by the Malaysian Rubber Board in October 2012,[43] with features of programmable tapping time, short tapping length (1 inch) with improved blade and solar energy with back-up DC battery. The solar energy panel also shields the NR tree from rain. This approach seems to be technically feasible, economically viable and with the hope of social acceptance. Issues such as the high installation costs of such tapping machines and the possibility of them being stolen from unfenced NR plantations are yet to be addressed.

1.3.2 Challenges and Opportunities to Promote NR Industries

NR suffers from inconsistent properties. Multiple stages of handling and transportation, and processes, are subject to contamination of NR latex (Figure 1.5). The grading of NR was correlated with a visual inspection of its dirt content in early years. Uniformity and purity of NR latex and dry NR as the commodity materials are overcome by introduction and enforcement of conformity of NR to strict technical specifications, *e.g.* Standard Malaysian Rubber (SMR, introduced in 1965 and revised in 1973 and 1991), Standard Thailand Rubber (STR), Standard Indonesian Rubber (SIR) and Standard Vietnam Rubber (SVR). Under SMR, tolerable amounts of nitrogen, dirt, volatile matter, copper and manganese are specified. STR, SIR and SVR are prepared based on SMR.

Until the early 1980s, NR woods were mainly used as fuel, where the main users were from the iron and steel industries. It has limited commercial applications due to its tendency to discolour and its appeal to insects. Chemical treatments were developed to prevent insect attack and fungal discolouration of NR wood. From the mid-1980s, it has been illegal to use NR wood as fuel in Malaysia and the wood is reserved mainly for the furniture industry. However,

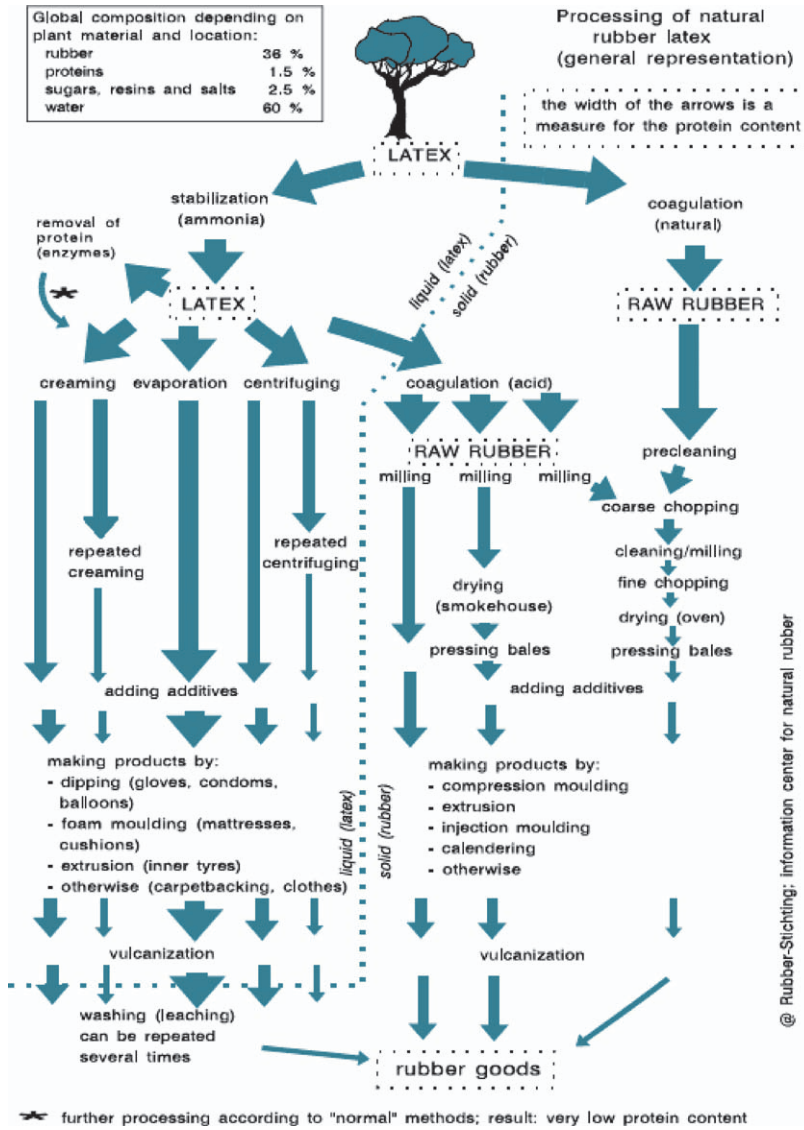

Figure 1.5 General representation of handling and the processes involved in turning NR latex into NR goods.[36] The thickness of the green arrows correlates with the protein content.

up to 70% of NR wood is wasted during the manufacture of furniture, in the form of low-quality logs, unusable cuts in the saw milling process and branches.[37]

Since the 1980s, Thailand, Indonesia and Malaysia (the top three NR-producing countries) have gradually diversified into manufacturing at the expense of the agricultural sector. It is predicted that the demand for NR will

overwhelm its supply. This may lead to an increase in the price of NR as a commodity material. Under these circumstances, the competitiveness of NR in relation to SR may be impaired, even though there have been technological developments in NR. The Asia/Pacific region will continue to account for more than 90% of world NR production in 2013. In 2008, Thailand and Indonesia produced almost 60% of NR, followed by Malaysia, India, Vietnam, China, the Philippines and Sri Lanka.

NR industries have been one of the leading industries for large-scale nanotechnology application, *i.e.* the use of CB for tyres. It is well known that smaller particle sizes of CBs (lead to higher reactivity) correlate with enhanced reinforcement of NR. Hence the quantities of additives used can be reduced, having a beneficial effect on the environment. However, the reduced amount of nanosized additives needed may not necessarily lead to a reduction in the cost of producing NR goods, because the nanosized additives are expensive.[45]

Competition between NR and bio-based SR (SR made from biosourced feedstock) should not be underestimated. For example in 2012, LANXESS is planning to produce the world's first SR, *i.e.* ethylene propylene diene monomer (EPDM) rubber (under the brand name of Keltan Eco) from ethylene derived from sugar cane at its Triunfo plant in Brazil. The ethanol is dehydrated into ethylene and polymerized to produce EPDM rubber.[46] Besides, bio-based SR is suggested to be the bio-based feedstock of poly(butadiene) rubber for tyre industries.

New challenges and opportunities to promote NR industries:[37]

1. Broadening the genetic base of NR tree for improving the productivity of NR latex.
2. Reduction of manpower in NR plantation by tapping the NR trees and collection of NR latex, let say, in every 10 days as compared to daily tapping and collection.
3. More economic use of fertilizers for NR plantation by:
   a. Judicious selection and tailoring the amount of fertilizers used to soil types.
   b. Controlled- and slow-release fertilizers shall be developed, *e.g.* encapsulation of fertilizers with thin coating of NR latex.
4. New and scientifically specified NR shall be designed with conformity to technical specifications in meeting the needs of buyers.
5. Waste NR woods shall be converted to chipboard/fibreboard composites and/or extraction of cellulose and lignin content from the waste. Cellulose may be converted into ethylene and butadiene or hydrolysed to sugars and then to alcohols. All these compounds may serve as the starting materials for polymer industry. Lignin may be used as filler, binder and extender or it may serve as a potential substitute for CB.
6. Modify and 'develop' NR as the feedstock for specific polymer architectures.
7. Advocate blends of NR and SR for manufacturing of goods to meet a specific customer's requirements.

8. There may increasingly be marketing challenges with derivation from both supply and demand of NR. The price of petroleum will continue to increase and therefore, the price of SR will correspondingly rise and inevitably, the price of NR will soar. Expansionary policy for the planting and replanting of NR trees shall be emphasized. Thailand and Indonesia have eventually taken up this policy.
9. Production cost of NR-based nanocomposites has to be optimized to the performance of the NR goods in order to capture market share. NR industries, in general, are comparatively conservative in nature compared to SR industries. Positive effects of nanotechnology on NR goods may become visible to the industries after extended studies.
10. Refocus the interest in NR latex or recycled NR in road construction as the ecological and environmentally choice as the modifier for asphalt. This will improve the durability of asphalt road surfaces. Extensive studies and market promotion shall be made.

All these challenges and opportunities call for innovative research and development. The proposals of the solutions shall be technically feasible and shall position the raw materials for futuristic applications with blue ocean strategy.

1.4 NR-Based Composites and Nanocomposites

Due to the reinforcement of filler in the matrix of NR; reduction in material costs, enhancement of desired properties and improvement in processing NR and so on are generally achieved.[47] Commercially used fillers in NR include CB, SiO_2 and calcium carbonate, *etc*. NR-based tyre industry is known to be the leading industry in using nanosized CBs. CB is the first reinforced filler for NR-based composites. Addition of CB to NR-based tyres reduces fuel consumption of vehicles by lowering the rolling resistance. Generally, a large amount of conventional fillers (*e.g*. 40%) are required to attain optimal mechanical properties for automobile parts.[48,49] The huge amount of added filler may reduce the processability of the materials, increase product weight as well as leading to brittleness and affecting the transparency of the finished goods. This leads to a continuous demand for new, low cost and low weight NR composites with improved properties. Under these circumstances, NR-based nanocomposites have regained special attention from industries and academia.[50,51] Mixing of micro- or nanosized fillers into NR is generally carried out by well-established mixing procedures and existing mixing equipment, such as two-roll mill mixing,[52–56] solution mixing,[57–60] melt mixing,[61] NR latex mixing followed by coagulation method,[62] *etc*.

1.5 An Overview of Common Fillers used in NR Composites

The essential criteria for improving abrasion tear, cutting and rupture resistance, stiffness and hardness of NR-based materials are strong interfacial

adhesion and uniform dispersion of the filler in the NR matrix. Commonly added fillers for NR are discussed in the following sections.

1.5.1 Carbon Black

Carbon black (CB) is indisputably the most widely used reinforcing filler in NR formulations. It improves tensile and tear strengths, modulus and hardness, abrasion and thermo-oxidative resistance, *etc*. of NR-based materials. CB is manufactured by a variety of processes, including the channel process, to produce furnace black, thermal black, lamp black and acetylene black.[63,64] NR-based composites and nanocomposites with the addition of CB exhibit the monotonous black colour to the finished goods.

Bhattacharya *et al*.[65] observed that NR nanocomposites with CB (N330) having a mean particle size of 30 nm shows an improvement in mechanical properties compared with pristine polymer. The tensile strength of the vulcanized nanocomposites increases from 20.6 to 22.1 MPa by 50 wt% CB filler loading. However, the elongation at break shows an opposite trend, where it decreases from 973 to 573%. Lin *et al*.[66] also reported the effect of CB (N234) on the NR matrix. In their study, tensile strength at 21.2 MPa with 50 wt% filler loading is recorded. Similarly, a decrease in the elongation at break is reported.

CB is often used together with other fillers to get obtain hybrid fillers to further enhance NR properties. Liu *et al*.[67] added nanosized CB and poly(ethylene glycol) (PEG) modified clay to prepare NR nanocomposites. They suggest that NR with hybrid fillers exhibits superior mechanical properties compared to NR with CB as the sole filler. Rattanasom *et al*.[22] also reported that the tensile strength and elongation at break increase from 15.3 to 25.4 MPa and 460 to 605%, respectively, for the CB-filled NR as compared to NR with hybrid fillers (CB and modified clay).

1.5.2 Clay

Clay (unmodified) has been an important NR filler for many years, but due to its large size and low surface activity, the reinforcing ability of clay is poor.[68] Layered silicates (LS) are the main active minerals in soils and clays. They are the most widely used 2D nanofillers (after exfoliation and/or intercalation), having two fused silicate tetrahedral sheets with an edge-shared octahedral sheet of metal atoms, such as Al or Mg in various fields. The layers are stacked by a weak dipole–dipole force and exhibit a net negative charge on the lamellar surface. The interlayers between the galleries are normally occupied by cations such as Na^+ and Ca^+. As the forces that hold the stacks together are relatively weak, the intercalation of small molecules between the layers can be done relatively easily.[69] However, the exfoliated nanolayers of LS may not be easily dispersed in most polymers due to their preferred face-to-face stacking in agglomerated tactoids. Dispersion of the tactoids into discrete monolayers is further hindered by the intrinsic incompatibility of hydrophilic LS and

Table 1.7 Mechanical properties of vulcanized NR with different fillers.[71]

Mechanical properties	*NR*	*NR/Na^+-MMT (10 phr)*	*NR/organo-MMT (10 phr)*	*NR/CB (10 phr)*	*NR/CB (40 phr)*
Elongation at break (%)	700	555	700	464	434
Hardness (Shore A)	28.8	20.7	43.5	30.5	38.3
Abrasion loss (mm^3)	286.2	–	217.5	282.0	199.3
Strain modulus 100% (MPa)	0.59	0.53	1.72	0.83	1.60

hydrophobic NR matrix. Therefore, LS have to be organically modified in order to become polymer-compatible clay, or organoclays. This has been well demonstrated by replacing the inorganic exchange cations in the cavities or 'galleries' of LS by alkylammonium surfactants.[70,71] The insertion of small amounts of organoclay into vulcanized NR may impart a radical improvement in mechanical properties such as tensile strength, modulus, hardness, abrasion resistance, tear strength, *etc*., solvent resistance, flammability resistance, gas barrier properties, and biodegradability of NR matrix.[56,72] The amounts of filler are expressed in phr (parts in wt per 100 parts in wt of dry rubber) in the following sections.

Arroyo *et al*.[73] prepared NR composites by using octadecylamine-modified montmorillonite (organo-MMT) as a substitute for CB (SPHERON 6400). Table 1.7 shows the mechanical properties of vulcanized NR with different fillers. They compared the organo-MMT with pristine clay (Na^+-MMT) and CB as fillers for NR, and observed that at similar filler contents, the reinforcing effect of the organo-MMT (which shows improved polymer–filler physical interactions) is better than that of Na^+-MMT and CB. The results reveal that the NR with 10 phr of organo-MMT shows maximum hardness (Shore A) at 43.5, when compared with 10 phr of Na^+-MMT and 10 and 40 phr of CB. The strain modulus at 100% elongation shows a similar tendency to the hardness. NR with 10 phr of organo-MMT shows a maximum value at 1.72 MPa. As deduced from Table 1.7, it is necessary to add 40 phr CB to obtain comparable mechanical properties to the nanocomposites with 10 phr organo-MMT.

1.5.3 Silica

Silica (SiO_2) is an excellent non-black spherical reinforcing filler that is widely used to produce coloured NR products. It is especially used in green tyre tread due to its low heat build-up and rolling resistance. SiO_2 can be produced by various methods, such as precipitation of an aqueous sodium silicate solution, fumed silica by pyrogenic process, silica from natural resources (*e.g*. rice husk ash[74] and fly ash[75]), and/or silica sol by the sol–gel process.[76] Ikeda *et al*.[77] prepared both a nano-SiO_2 filled NR composite (NR-71Si) and a commercial silica (Nipsil VN-3) filled NR composite (NR-71VN). They prepared NR-71Si using nano-SiO_2 (diameter 100–400 nm) by an *in situ* method *via* a sol–gel reaction of tetraethoxysilane up to approximately 80 phr. NR-71VN was prepared

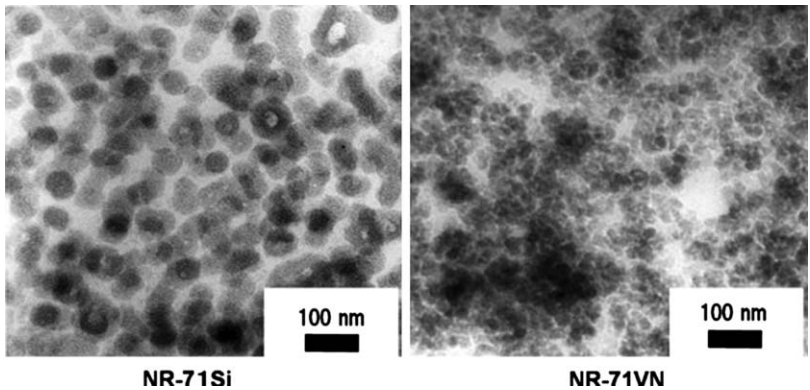

Figure 1.6 TEM image of *in situ* generated nano-SiO_2 and commercial SiO_2-filled NR vulcanizates.
Reproduced with kind permission from Springer.[75]

by a conventional method, with 71 phr SiO_2 content. Due to the high interaction between the *in situ* generated nano-SiO_2 and the NR matrix, the tensile strength of NR-71Si increases compared to NR-71VN. The NR-71Si shows lower stress at elongation up to 200% and higher stress at elongation beyond 200%. The high modulus at low elongation for conventional SiO_2-filled NR is due to the formation of larger aggregates of SiO_2. The *in situ* generated nano-SiO_2 exhibits an excellent reinforcing effect on NR vulcanizates. Transmission electron micrograph (TEM) images of *in situ* nano-SiO_2 and commercial SiO_2-filled NR vulcanizates is shown in Figure 1.6. Better dispersion of *in situ* generated nano-SiO_2 than that of the commercial SiO_2 in the NR matrix can be seen.

Arun *et al.*[78] prepared nano-SiO_2 and SiO_2-filled NR nanocomposites and composites by a co-vulcanization method. They compared the mechanical properties of NR composites with the corresponding nano-SiO_2 filled NR. The study suggests that nano-SiO_2 nanocomposites dispersed well at low filler loading (0.8 phr) in NR, possibly be due to the improved NR and nano-SiO_2 interaction. In the case of SiO_2-filled NR vulcanizates, the tensile strength slightly increases initially, and then decreases continuously with ascending amount of SiO_2 from 5 phr upwards. This is may be due to the poor NR and SiO_2 interaction and also less uniformity of the filler distribution. But in the case of nano-SiO_2 filled NR vulcanizates, the tensile strength increases gradually and reaches a maximum value of 35 MPa by the addition of 0.8 phr of nano-SiO_2 and then slightly decreases. It is noted that maximum tensile strength of the filled NR is observed at lower filler loading for nano-SiO_2 (0.8 phr) as compared to SiO_2 (10 phr). The elongation at break decreases with ascending amount of SiO_2 for SiO_2 filled NR. But in the case of nano-SiO_2 filled NR, the elongation at break steadily increases and reaches a maximum value 1550% and then decreases. The maximum value of elongation at break is noticed at a low level of nano-SiO_2 filler loading (0.8 phr) compared to the SiO_2 filler loading (2.5 to 10 phr). This may be due to the homogeneous distribution

Table 1.8 Effect of different shapes of ultrafine SiO_2 on the mechanical properties of vulcanized NR.[77]

		NR/cubical SiO_2 (phr)			*NR/elongated SiO_2 (phr)*			*NR/irregular SiO_2 (phr)*		
Properties	*NR gum*	*10*	*20*	*30*	*10*	*20*	*30*	*10*	*20*	*30*
Tensile strength (MPa)	17.5	21.1	23.8	23.2	21.4	24.4	24.1	21.8	25.2	24.9
Elongation at break (%)	930	970	972	985	955	965	982	980	985	1000
Hardness (Shore A)	41.2	43.8	45.0	46.2	44.0	46.2	49.0	44.4	47.0	49.8
Strain modulus at 100% elongation (MPa)	0.64	0.70	0.86	0.95	0.74	0.87	0.97	0.76	0.89	0.99

of nano-SiO_2 in the NR matrix and also due to the improved NR–nano-SiO_2 interfacial adhesion.

Idrus *et al.*[79] investigated the effects of different particle shapes of ultrafine SiO_2 used as a filler on the properties of vulcanized NR. Three shapes of filler (cubical, elongated and irregular with mean particle sizes of 1.25 μm, 1.18 μm, and 1.18 μm, respectively) were produced using the Hosokawa Alpine classifier mode with a 50 ATP-forced vortex classifier. The data in Table 1.8 depicts the mechanical properties of different shapes of SiO_2 in vulcanized NR. All the three shapes of SiO_2 show increasing tensile strength, elongation at break, hardness (shore A) and strain modulus at 100% elongation when the filler loading increases from 10 to 20 phr. Better dispersion of SiO_2 in NR matrix may be accountable for the enhancement of the mechanical properties within the range of the filler loading. However, at the higher SiO_2 loading (30 phr), the replacement of the SiO_2–NR interactions by SiO_2–SiO_2 interactions may lead to poorer tensile strengths. In general, the irregular SiO_2 filled NR shows higher tensile strength, elongation at break, tensile modulus and hardness, followed by the elongated and cubical SiO_2 filled NR. This may be because of the larger surface area of the irregular SiO_2, which may provide higher contact area between the SiO_2 and NR matrix; hence a positive reinforcing effect can be noticed.

1.5.4 Calcium Carbonate

Calcium carbonate ($CaCO_3$) (whiting) is widely used as non-reinforcing and reinforcing filler to impart desired colour and reduce product cost in NR-based composites. The two important types of $CaCO_3$ are ground limestone and precipitated $CaCO_3$. The ground limestone is prepared by grinding mineral limestone and the precipitated $CaCO_3$ is obtained by chemical precipitation from a salt solution. NR with the addition of ground $CaCO_3$ gives low tear resistance, however precipitated $CaCO_3$, in some cases with smaller particle size, enhances the tear strength of the NR product. Sobhy *et al.*[80] studied the cure characteristics and physicomechanical properties of $CaCO_3$ reinforced NR composite. They used $CaCO_3$ with mean particle size of 3.25 μm. Composites with 20 phr of $CaCO_3$ in NR show the highest tensile strength at 13.4 MPa and

elongation at break of 825%. At higher $CaCO_3$ content in NR matrix, tensile strength and elongation at break decrease. The use of $CaCO_3$ as a filler improves the physicomechanical properties of the aging resistance to γ-irradiation. Cai *et al.*[81] prepared NR composites reinforced with $CaCO_3$, with average particle diameter at 1.55 μm. The tensile strength and tear strength increase to 24.8 MPa and 70 kN/m, respectively, when the 15 phr of $CaCO_3$ was added. However, when the amount of $CaCO_3$ exceeds 15 phr, the mechanical properties decrease gradually. The elongation at break reduces with increasing loading of $CaCO_3$ in NR matrix.

1.5.5 Metal Particles

It is well known that the dielectric properties of an insulating medium, *e.g.* NR, can be modified by dispersing electrically conducting particles in the medium.[82] The insulating host material can be turned into conducting or semiconducting, depending on the amount of metal particles dispersed in the medium. Ferromagnetic iron, nickel and cobalt particles *etc.* are the choices as metallic magnetic fillers. Nickel particles are chemically more stable as compared to iron and cobalt and therefore they are the better candidates. Jamal *et al.*[83] tailored the magnetic properties of the NR/nickel composite by incorporating different amounts of nickel particles. The composites show a ferromagnetic behaviour and the saturation magnetization is found to increase with the nickel content. Dielectric permittivity increases with the increase in nickel content and decreases with the rise in temperature. Table 1.9 illustrates the magnetization and mechanical properties of different masses of nickel in vulcanized NR.

The increase in magnetic properties of vulcanized NR clearly shows that the ferromagnetic characteristics of nickel particles are retained in the composites. The elastic modulus of the samples shows improvement as the nickel content in the composites increases. The increase in the strains modulus as the amount of nickel increases reflects the reinforcing effect of nickel nanoparticles in NR matrix. However, there is a monotonous decrease in elongation at break with the increase in filler loading. This may be due the formation of agglomerates of filler particles in the NR matrix.

Table 1.9 Effect of different masses of nickel on the mechanical properties of vulcanized NR.[81]

Concentration of nickel (phr)	*Magnetization (emu/g)*	*Tensile strength (MPa)*	*Elongation at break (%)*	*Strain modulus at 100% (MPa)*
0	–	28.9	1210	0.75
20	7	26.7	1102	0.80
40	11	22.8	930	0.91
60	14	21.6	858	1.1
80	18	20.5	858	1.1
100	20	19.2	764	1.4

1.5.6 Bio-Based Fillers

Sustainability of the materials becomes one of the prime concerns in the research development in industries and academic institutions. The search for non-petroleum-based fillers has accelerated the research into bio-nanofillers from biomass. In some cases, bio-based nanocomposites show unique advantages over traditional inorganic nanoparticles. Commonly used bio-nanofillers in NR are whiskers of cellulose, chitosan, nanocrystals of starch *etc*. The studies on these fillers are aimed at competitive production cost and equivalent properties as compared to other petroleum-based fillers. In addition, biocompatibility and biodegradability of the bio-based fillers are hoped to be retained after dispersion in the NR matrix.

1.5.6.1 Chitin Whiskers

Chitin is the second most abundant semicrystalline polysaccharide. The natural sources of chitin include the external skeleton of shellfish (shrimp or crab shells contain 8 and 33% of chitin, respectively), insects and fibrous material of cellular walls in mushrooms and algae. Chitin macromolecules are made up of *N*-acetyl-D-glucosamine units. Chitin is non-toxic, odourless, biocompatible with living tissues and biodegradable. Removing the amorphous part of chitin leads to the production of crystalline chitin nanocrystals or chitin whiskers.[84] Figure 1.7 shows a TEM image of a dilute suspension of hydrolysed crab shell chitin (chitin whiskers).[85]

Gopalan Nair *et al*.[86,87] prepared chitin whiskers with slender parallel piped rods, by acid hydrolysis of chitin from crab shell. The mechanical properties, thermal stability and modulus of nanocomposites were improved by the

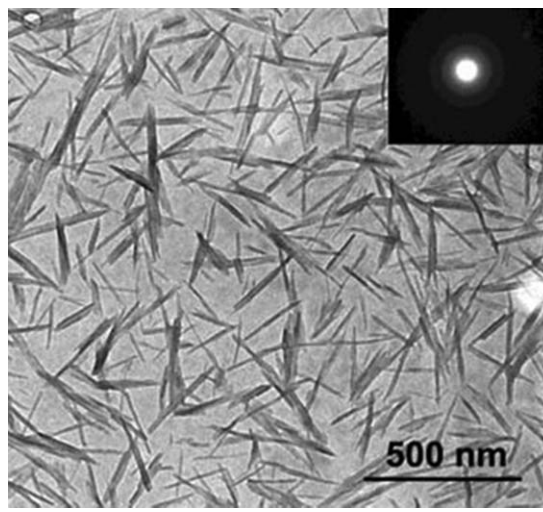

Figure 1.7 TEM image of chitin whiskers from crab shell. Reproduced with kind permission from Springer.[83]

incorporation of chitin whiskers in NR. The average length and width of chitin whiskers were estimated to be around 240 and 15 nm, respectively, with an aspect ratio close to 16. Tensile tests show a lower reinforcing effect for a chitin whisker filled vulcanized NR matrix compared to unvulcanized systems. Crosslinking of the NR matrix is suggested to interfere with the formation of a three-dimensional network of the whiskers. The presence of chitin whiskers in the NR matrix may result in a significant increase in the modulus, without much reduction in the elongation at break. The reinforcing effect of chitin whiskers strongly depends on their ability to form a rigid three-dimensional network, resulting from strong interactions such as hydrogen bonds between the whiskers.

Gopalan Nair *et al.*[88] chemically modified the chitin whiskers by using different coupling agents, namely phenyl isocyanate (PI), alkenyl succinic anhydride (ASA) and 3-isopropenyl-R, R′-dimethylbenzyl isocyanate (TMI). These various chemical treatments on chitin whiskers improve the adhesion between the chemically modified chitin whiskers and the NR matrix. However, the mechanical performances of these NR composites markedly decrease after chemical modification. This is due to the partial or total destruction of the three-dimensional network of chitin whiskers, which is assumed for the unmodified composites.

Ismail *et al.*[89] prepared chitosan-filled NR compounds by using chitosan powder with an average particle size of 90 μm. The results show that the tensile strength of the NR composite is reduced by the addition of chitosan. The irregular shape of the chitosan tends to decrease the mechanical strength of the composites due to the inability of the chitosan to support the stress transferred from the NR matrix. In general, the scorch time, cure time and elongation at break decrease with an increase in chitosan loading in NR. However, maximum torque and the tensile modulus of chitosan-filled NR can be observed.

1.5.6.2 Nano-cellulose

Cellulose is a homopolysaccharide comprised of 1,4-anhydro-D-glucopyranose units. Natural sources of cellulose include natural fibres (hemp, flax, rutabaga, wheat, banana, coir, *etc.*), wood fibres, and so on. The monomer units of cellulose have three hydroxyl groups. These hydroxyl groups may initiate hydrogen bonding with other molecules and/or macromolecules for oriented crystalline packing of cellulose and this governs the main physical properties of the materials developed. Nano-cellulose fibres with diameters from 5 to 60 nm can be extracted from various naturally-occurring plant fibres, such as bast, hemp, kraft pulp, corncob, oil palm wood flour, rutabaga, *etc.*[90–93] by different chemical treatments. Figure 1.8 shows TEM images obtained from dilute suspensions of cotton, sugar beet pulp and tunicin (the cellulose extracted from tunicate) whiskers.[85]

Ismail *et al.*[94] prepared NR/bamboo fibre composites with fibres having mean length 180–270 μm. Tensile strength and tear strength of the composites decreased with increasing fibre loading. The irregular shape of bamboo fibre, coupled with poor adhesion of the NR matrix, are the main factors in the deterioration of tensile strength and tear strength with increasing fibre loading. Ismail *et al.*[95] also prepared paper sludge-filled NR composites by

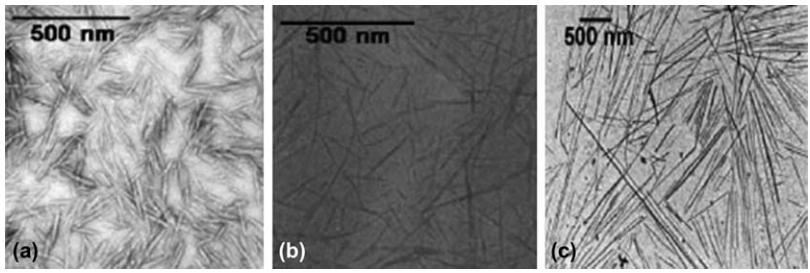

Figure 1.8 TEM images for nanowhiskers of (a) cotton, (b) sugar beet pulp and (c) tunicin starch.
Reproduced with kind permission from Springer.[83]

Table 1.10 Effect of different bio-based fillers on the mechanical properties of unvulcanized NR.

10 wt% cellulose whiskers (aspect ratio)	*Elongation at break (%)*	*Tensile strength (MPa)*	*Young's modulus (MPa)*	*Reference*
NR	625	0.56	0.50	34, 94
NR/bagasse whiskers (~ 13)	0.65	4.7	63	94
NR/Capim Dourado whiskers (~ 67)	0.11	12.0	258	95
NR/date palm whiskers (~ 43, ~ 30)	0.03	16.0	236	96
NR/maize starch whiskers (platelet-like particles)	0.90	2.9	7.5	97

incorporation of different loadings (10–40 phr) of paper sludge fillers with average filler size of 300 μm. They reported that the tensile strength of the composites decreases with filler content, and again this may be due to the irregular shape of the paper sludge filler.

Bras *et al.*[96] prepared nano-cellulose whiskers from sugar cane bagasse pulp with length from 84 to 102 nm and width from 4 to 10 nm. These nano-cellulose whisker reinforced NRs (unvulcanized) show an increase in tensile strength from 4 to 17 MPa by increasing the filler content from 7.5 to 10 wt%. This marked increase in tensile strength at 10 wt% may be due to the development of a mechanical percolation network that forms a rigid and continuous network by hydrogen bonding. The percolation threshold of rod-like whiskers with an aspect ratio of 13 is equivalent to ~ 7.7 wt% with the assumption of density of dry NR at 1 g cm^{-3} and crystalline cellulose at 1.5 g cm^{-3}. Table 1.10 depicts the mechanical properties of unvulcanized NR filled with different cellulose whiskers. Bagasse nano-cellulose has the lowest aspect ratio compared to Capim Dourado whiskers and date palm whiskers, which may lead to a lower tensile strength for these NR/bagasse whisker nanocomposites.

Angellier *et al.* (2005)[97] synthesized nanocrystal platelets from waxy maize starch of 6–8 nm thickness, 40–60 nm length and 15–30 nm width. They analyzed the properties of unvulcanized NR reinforced with these nanocrystals. The elongation at break of this nanocrystal filled NR decreases with increasing

nanocrystal content from 1960 (unfilled) to 920% (filled with 30 wt%). The storage relaxed modulus at 25 °C of the nanocomposite films containing 10, 20, and 30 wt% of filler is about 10, 75, and 200 times higher, than the one of the unfilled NR matrix.[98]

1.5.6.3 Starch Nanocrystals

Starch is the second most abundant biomass material in nature after cellulose. The major sources of starch are plant roots, stalks, crop seeds, and staple crops such as rice, corn, wheat, tapioca, potato, *etc*. The main components of starch are amylose, ranging from 72 to 82%, and amylopectins, ranging from 18 to 28%. Amylose is defined as a linear molecule of glucose units linked by (1-4)-α-D-glycosidic bonds, slightly branched by (1-6)-*R*-linkages. Amylopectin is a highly branched polymer consisting of relatively short branches of (1-4)-α-D-glucopyranose, which is interlinked by (1-6)-α-D-glycosidic linkages for approximately every 22 glucose units.[100]

Starch occurs as a flour-like white powder, which is insoluble in cold water after its extraction from plants. Native starches contain between 15 and 45% of crystalline material. Starch crystallite, starch nanocrystal, microcrystalline starch and hydrolysed starch all refer to the crystalline part of starch, which are obtained by different extents of acidic hydrolysis. We will focus on starch nanocrystals. Cellulose nanocrystals are 100% crystalline materials, but starch nanocrystals consist of 45% crystalline portion.

For waxy maize starch, a given weight of starch granules is mixed with H_2SO_4 solution at a known concentration. The suspension is stirred at a selected speed with an orbital shaking action. After various durations of hydrolysis, the suspension is washed by successive centrifugation in distilled water until neutrality.[101] Angellier *et al*.[99] synthesized nanocrystal platelets from waxy maize starch of 6–8 nm thickness, 40–60 nm length and 15–30 nm width. This starch nanocrystal, which is in the form of aggregates, has an average size of 4.4 μm. They analysed the properties of unvulcanized NR reinforced with this nanocrystal. Films were conditioned at 0% relative humidity (RH). The elongation at break of this nanocrystal-filled NR decreases with increasing nanocrystal content from 1960 (unfilled) to 920% (filled with 30 wt%). The tensile modulus increases almost exponentially with starch content, from 0.64 MPa for the unfilled NR matrix up to 77.8 MPa for composite films filled with 30 wt% of starch nanocrystal. The storage relaxed modulus at 25 °C of the nanocomposite films containing 10, 20 and 30 wt% of filler is about 10 (12.3 MPa), 75 (96 MPa) and 200 times (257 MPa) higher than that of the unfilled NR matrix (1.28 MPa).[99] Reduction in tensile modulus at higher filler content (*e.g*. 20 wt%) when the materials were exposed to 43% RH as compared the same filling loading at 0% RH. Elongation at break decreases to 1500% for 5–20 wt% filler loadings at 43% RH (see Table 1.11).[99,102] The hydrophilic nature of starch nanocrystals is responsible for the above deterioration in properties of starch nanocrystal-filled NR at high moisture content or RH. The possible formation of water-rich filler/NR matrix

Table 1.11 Tensil strength and elongation at break for waxy maize starch nanocrystal of unvulcanized NR nanocomposites.

Waxy starch nanocrystal (wt%)	*Tensile strength (MPa)*	*Elongation at break (%)*	*Ref.*
Relative humidity: 0%			
0	0.65	1960	99
5	1.60	1800	
10	4.90	1770	
15	12.5	1600	
20	26.5	1550	
30	77.8	920	
Relative humidity: 43%			
5	1.93	1500	102
10	5.77	1500	
20	14.8	1490	

interphase when storing the materials at high RH may hinder the stress transfer at the interface when the materials are subjected to mechanical tests.

1.5.7 Polyhedral Oligomeric Silsesquioxane

Polyhedral oligomeric silsesquioxane (POSS) is a relatively new class of nanofillers, and are the smallest particles of SiO_2. Conversely, each POSS molecule possesses covalently bonded reactive functionalities which may be able to initiate the polymerization of polymer or to trigger the grafting of POSS to the polymer chain. Besides, POSS molecule has non-reactive organic active sites which may account for solubility and compatibility of the POSS with various polymers.[103] The incorporation of POSS derivatives into polymeric materials can lead to striking improvements in properties, such as service temperatures, decomposition temperatures, oxidation resistance, surface hardening, mechanical properties, flammability resistance, heat evolution, and so on.[104] Up to now and to our knowledge, the incorporation of POSS into NR has not been reported. Hence, NR/POSS may be a new class of NR composites, well worth investigating by researchers. Baumann *et al.*[105] synthesized and characterized an elastomeric nanocomposite containing POSS molecules as both the crosslinker and filler within a poly(dimethylsiloxane) (PDMS) polymer matrix. Chen *et al.*[106] prepared room temperature vulcanized (RTV) silicone rubbers with POSS crosslinker, which exhibited enhanced mechanical properties compared to those of the PDMS filled with traditional crosslinkers. The observed improvement in mechanical properties could be attributed to the synergistic action of the structure of three-dimensional multi-arm crosslinker (vinyl-POSS derivative). Sahoo *et al.*[107] synthesized POSS with hydroxyl functional groups with an average diameter of 50 nm. They used POSS nanoparticles as curing agents in certain functionalized rubbers such as fluorocarbon rubber (FKM) and carboxylated nitrile rubber (XNBR).

1.5.8 Carbon Nanotubes

Carbon nanotubes (CNTs) are an allotrope of carbon with sp^2 hybridization and are cylindrical in shape. CNTs have a diameter in the order of a few nanometres, but they may be millimetres or even centimetres long. CNTs can be synthesized by arc discharge, laser ablation, high-pressure carbon monoxide (HiPCO) and various catalytic chemical vapour deposition (CVD) techniques.[108,109] CNTs can be classified into (i) single-walled carbon nanotubes (SWCNTs) and (ii) multi-walled carbon nanotubes (MWCNTs). Due to the high aspect ratio of CNTs and the high viscosity of NR, achieving a homogeneous dispersion of CNTs in an NR matrix is challenging. Pre-treatment and functionalization of CNTs, interfacial modification, and so on, are used to enhance the dispersion of NR-based CNT nanocomposites.[110] On the other hand, different sample preparatory techniques are used in order to attain optimum dispersion of CNTs in an NR matrix by reducing aggregation of the CNTs mainly by solution mixing,[111,112] sonication,[113,114] and by the use of surfactant.[115] Figure 1.9 shows a TEM image of raw MWCNTs.[116]

Ismail *et al.*[117] prepared NR/MWCNT nanocomposites by mechanical and solution mixing methods. They reported the effect of different preparatory methods (mechanical and solution mixing) on the properties of NR/MWCNT nanocomposites. The tensile strength of NR/MWCNT nanocomposites prepared by solution mixing is higher than those prepared by mechanical mixing. It was noted that with solution mixing of 5 phr CNTs, the tensile modulus increased, but the tensile strength decreased from 18 MPa to 12 MPa, and the fatigue life and elongation at break also decreased. The decrease in strength is attributed to the aggregation of CNTs in the NR matrix. NR/MWCNT nanocomposites produced by solution mixing with 0.5 phr CNTs showed a maximum

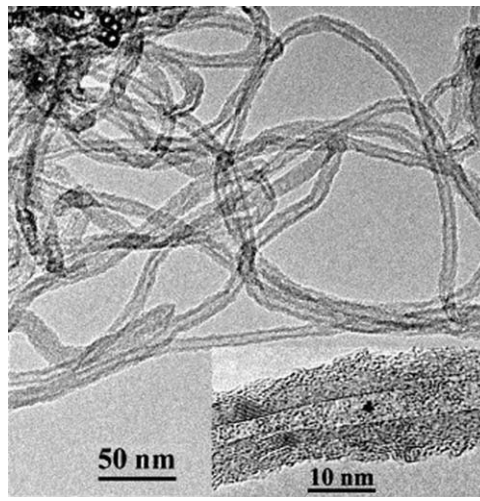

Figure 1.9 TEM image of raw MWCNTs.
Reproduced with kind permission from Elsevier.[112]

tensile strength at 18 MPa, due to better dispersion of MWCNTs in the NR matrix. Fakhru'l-Razi *et al.*[111] reported that addition of 1 phr of MWCNTs increases the stress level of NR nanocomposites from 0.28 to 0.56 MPa. At 10 phr MWCNTs, the stress value is 2.6 MPa, nine times higher than the pure NR.

Zhao *et al.*[114] prepared NR/SWNT nanocomposites and found that with the addition of 0.25 phr of SWCNTs, stain modulus increases about 20% higher than the pure NR samples on average at the same degree of vulcanization without sacrificing its elastic properties, and on the other hand retaining the tensile strength and elongation at break. Shanmugharaj *et al.*[115] prepared NR/silane-functionalized CNT nanocomposites, which exhibit higher modulus, tensile strength and elongation at break, due to the improved polymer–filler interaction between the silanized CNTs and NR vulcanizates. The tensile strength of these nanocomposites increases from 21.7 (unfilled) to 26.2 MPa (1 phr of silanized CNTs). However, elongation at break shows an opposite trend. It decreases from 593 to 559% by the incorporation 1 phr of silane-functionalized CNTs. Bhattacharyya *et al.*[116] found that there is a strong enhancement in the Young's modulus ($\sim$10-fold), tensile strength ($\sim$2-fold) and storage modulus ($\sim$60-fold) with up to 8.3 wt% of carboxylated MWCNTs, with a small reduction in elongation at break for unvulcanized NR. The tensile strength increases from 4.5 to 7.2 MPa. Cataldo *et al.*[118] prepared NR nanocomposites with hybrid fillers of CNTs and CB. The addition of MWCNTs (9.5 nm with an average length of 1500 nm) along with CB (N375 having a surface area of 90 m^2g^{-1}) to the NR composites causes a dramatic increase in the International Rubber Hardness Degrees (IRHD) of the cured NR nanocomposites. The hardness increases from 13 to 22%. It is also noted that the MWCNTs cause a strong stiffening effect, which leads to a reduction in the elongation at break of the nanocomposites. At 15 phr of MWCNTs, elongation at break reduces to 27% as compared with pristine NR. Sui *et al.*[113] prepared NR/CNT nanocomposites by solvent mixing. The CNTs used in this study were prepared by a CVD method. The diameters of raw CNTs vary from 20 to 50 nm, and lengths vary from 1 to 100 μm.

A comparison of the mechanical properties of NR/CNT and NR/CB composites with 25 phr of filler is shown in Table 1.12. NR/CNT nanocomposites exhibit marked enhancement of Shore A hardness, tensile modulus and tensile strength by 16, 32 and 10%, respectively, as compared to NR composites reinforced with the same filler loading of CB. This may be due to the strong

Table 1.12 Comparison of the mechanical properties of vulcanized NR composites with CNT and CB.[113]

Properties	*NR*	*NR/CNT (25 phr)*	*NR/CB (25 phr)*
Hardness (Shore A)	41 ± 2	63 ± 2	34 ± 2
Storage modulus at 300% elongation (MPa)	1.8 ± 0.2	12.5 ± 0.3	9.5 ± 0.3
Tensile strength (MPa)	7.2 ± 0.6	24.8 ± 2.0	22.5 ± 1.8
Elongation at break (%)	680 ± 20	495 ± 15	480 ± 20

interaction between the CNTs and the NR macromolecules in the NR matrix. The storage modulus of the NR/CNT nanocomposites is higher than that of the neat NR and CB/NR composites from low temperature to high temperature regions. The high modulus and specific surface area of CNTs enhance the stiffness of NR, which results in an increment in the storage modulus of the NR/CNT nanocomposites. Compared to CB, CNTs offer better anti-skid properties and lower rolling resistance than NR composites.

1.6 Applications of NR

Most NRs used are in the vulcanized form. The various types of NR and their major uses are demonstrated in Table 1.13. NR is largely used in tyres, with other uses accounting for less than 10% of total rubber production (Table 1.14).[119]

In order to reduce dependence on Asian NR (NR alternatives) and break out of the 'NR circle', Apollo Vredestein (a Dutch company) [a partner in the EU-based Production and Exploitation of Alternative Rubber and Latex Sources (EU-PEARLS) project, funded by the European Commission's 7th Framework Program] has been working with the Neiker-Tecnalia Research Centre at the Basque Institute for Agricultural Research and Development on genotyping of the guayule shrub (promising to Mediterranean areas) and the Russian dandelion plant (more suited to northern and eastern Europe). Apollo Vredestein and Wageningen UR Food & Biobased Research, the Netherlands, presented the first prototype of a tyre made from guayule and Russian dandelion at the recent 2012 Congress: BioRubber for Europe in Global Perspective, organized by the EU-PEARLS consortium to mark the end of the FP7 EU-PEARLS research project in Wageningen, the Netherlands.[120] Latex from both guayule and Russian dandelion also serve as potential commercial sources of NR latex for dipping. The US government is looking into the enhanced manufacturing processes, testing and utilizing guayule for the use in tyres and evaluating the remaining guayule plant biomass as a source of biofuel for the transportation industry.[44]

Table 1.13 Types and the major uses of NR.[2]

Type of NR	*Isoprene structure*	*Major commercial applications*
Hevea	*cis*-1,4	Tyres, latex gloves, footwear, weather stripping, shock absorbers, sports accessories, shoe soles, *etc.*[a]
Guayule[b]	*cis*-1,4	Latex gloves, tyres
Gutta percha[c,d]	*trans*-1,4	Wire coatings, textile belting, varnishes, orthopaedic devices, golf ball covers
Balata[d]	*trans*-1,4	Wire coatings, textile belting, varnishes
Chicle[d]	*cis*- and *trans*-1,4	Chewing gum

[a]Unvulcanized NR.
[b]Guayule rubber contains hypoallergenic proteins that do not trigger an allergic reaction.
[c]Harder, less soluble in organic solvents and more crystalline compared to *Hevea* rubber.
[d]Commands a very small commercial market in relation to *Hevea* rubber.

Table 1.14 General and engineering applications of NR.[6,37,121]

General and engineering goods	*Eco-friendly goods*
Tyres, especially for heavy-duty automobiles and aircraft. • Generally comprises 8% field coagulum NR, 18% smoked NR sheets, 18% NR latex, 6% plasticizer and 40% carbon black.	Rubberized coir forms for: seating in vehicles and has potential for replacement of polyurethane foam in inner sprung mattresses, cushions, geotextile pads, *etc*. (NR latex added with plant fibres). Stabilizing seashore lines, canal and river banks.
Medical devices, *e.g*. gloves, condoms, *etc*.	Prototype of non-fossil fuel resource tyres for passenger cars introduced by Sumitomo Rubber Industries, Ltd. • Generally comprises NR (matrix), epoxidized NR (dispersed phase), vegetable oil, silica and natural fibre (rayon).
Seismic bearings for protection of buildings, bridges and other civil engineering structures. • In Great Britain, bearings are almost always based on NR but in the USA, France and West Germany, mainly polychloroprene-based bearings are used. • For low temperatures, NR is preferred. For hot climates, polychloroprene is advantageous due to its better ozone and weathering resistance.	
Road rubberization • Bitumen is added with NR latex for binder and wearing courses of roads.	
Engineering products, *e.g*. engine mounts and shock absorbers.	

1.7 Conclusions

Based on technological properties, both NR and SR, which have their own merits, will be used continuously by the rubber industries. Inevitably, oil and gas resources are depleting. Biofeedstocks for synthesis of SRs or substitution of SRs by NR or chemically modified NR with equivalent properties may be the future direction of the research and development.

The focus on the research and development of NR industries shall be strategized as follows:

1. Improved productivity of NR latex
2. Shorter cycle times

3. Increased automation
4. Improved product performance
5. NR as the feedstock for specific polymer architectures
6. Blending of NR and SR for additive properties.

The research and development of NR-based composites shall be strategized on optimization of production cost of the composites coupled with enhancement of the mechanical properties of NR filled with nanofiller at lesser filler content as compared to that of the convention microfiller. The development of eco-friendly micro- and nanostructured functional materials based on NR is of commercial importance.

Replacement of inorganic fillers with bio-based fillers of NR-based composites is initiated by the academicians. However, inconsistencies of the properties due to the variation of sources, fluctuation of the supply of bio-based fillers, unsatisfactory mechanical performance of bio-based fillers and so on are challenges in convincing the industries for the replacement of inorganic fillers for NR-based composites. Environmental regulations and ethical concerns have triggered the search for materials that are environment friendly. Hence, great opportunity lies in near future for developing new bio-based products provided that the above mentioned challenges are addressed fully or partially. Botanists, biologists, chemists, technologists, *etc*. shall venture into different aspects of research and development for the substitution of inorganic fillers by sustainable bio-based fillers. Green materials will be the most sought after products in the days to come.

Acknowledgment

Some of the work of this chapter is partly supported by Research Intensive Faculty Grant from Universiti Teknologi MARA [600-RMI/DANA 5/3/RIF (858/2012)].

References

1. H. Brown, *Rubber: Its Source, Cultivation, and Preparation*, John Murray, London, 1918.
2. M. P. Stevens, *Polymer Chemistry: An Introduction*, 3rd edn, Oxford University Press, Oxford, 1999, pp. 476–479.
3. D. R. St. Cyr, in *Encyclopedia of Polymer Science and Engineering*, ed. H. F. Mark, N. Bikales, C. G. Overberger, G. Menges and J. I. Kroschwitz, Wiley-Interscience, New York, 2nd edn, 1990.
4. D. J. Hourston and J. O. Tabe, in *Polymeric Materials Encyclopedia*, ed. J. C. Salamone, CRC Press, New York, 2nd edn, 1996.
5. W. Resing, in *Natuurrubber (Natural Rubber)*, ed. J. v. d. Heijden and S. d. Meij, Rubber-Stichting Information Center for Natural Rubber, JA Delft, the Netherlands, 2000, p. 2.

6. N. M. Levin, in *Natuurrubber (Natural Rubber)*, ed. J. v. d. Heijden and S. d. Meij, Rubber-Stichting Information Center for Natural Rubber, JA Delft, the Netherlands, 1996, p. 9.
7. D. R. Burfield and Y. Tanaka, *Polymer*, 1987, **28**, 907.
8. D. R. Burfield, *Polymer*, 1984, **25**, 1823.
9. S. Toki, B. S. Hsiao, S. Amnuaypornsri and J. Sakdapipanich, *Polymer*, 2009, **50**, 2142.
10. E. H. Andrews, *Polymer*, 1964, **5**, 379.
11. A. M. Healey, P. J. Hendra and Y. D. West, *Polymer*, 1996, **37**, 4009.
12. C. H. Jones, *Spectrochim. Acta, Part A*, 1991, **47**, 1313.
13. W. Lin, M. Bian, G. Yang and Q. Chen, *Polymer*, 2004, **45**, 4939.
14. A. Suzuki, H. Oikawa and K. Murakami, *Polymer*, 1985, **26**, 97.
15. S. Toki, T. Fujimaki and M. Okuyama, *Polymer*, 2000, **41**, 5423.
16. M. L. Senyek, in *Encyclopedia of Polymer Science and Engineering*, ed. H. F. Mark, N. Bikales, C. G. Overberger, G. Menges, and J. I. Kroschwitz, Wiley-Interscience, New York, 2nd ed, 1990.
17. P. Saendee and P. Tangboriboonrat, *Colloid Polym. Sci.*, 2006, **284**, 634.
18. S. S. Choi, *Polym. Test.*, 2002, **21**, 741.
19. A. D. Drozdov and A. Dorfmann, *Int. J. Solids Struct.*, 2002, **39**, 5699.
20. M. Eskandari and H. Arastoopour, *Powder Technol.*, 2009, **189**, 454.
21. J. H. Kim and H. Y. Jeong, *Int. J. Fatigue*, 2005, **27**, 263.
22. N. Rattanasom, S. Prasertsri and T. Ruangritnumchai, *Polymer Test.*, 2009, **28**, 8.
23. L. A. Wood and G. M. Martin, *Rubber Chem. Technol.*, 1964, **37**, 850.
24. L. A. Wood, *Rubber Chem. and Technol.*, 1939, **12**, 130.
25. L. C. K. Carwile and H. J. Hoge, *Rubber Chem. Technol.*, 1966, **39**, 126.
26. M. N. Pilsworth Jr., H. J. Hoge and H. E. Robinson, *J. Mater.*, 1972, **7**, 580.
27. L. A. Wood and N. Bekkedahl, *J. Polym. Sci., Part B: Polym. Lett.*, 1967, **5**, 169.
28. W. H. Hamill, B. A. Mrowca and R. L. Anthony, *Rubber Chem. Technol.*, 1946, **19**, 622.
29. D. R. Burfield and K. L. Lim, *Macromolecules*, 1983, **16**, 1170.
30. L. A. Wood and F. L. Roth, *Rubber Chem. Technol.*, 1963, **36**, 611.
31. A. T. McPherson, *Rubber Chem. Technol.*, 1963, **36**, 1230.
32. L. J. Zapas, S. L. Shufler and T. W. DeWitt, *J. Polym. Sci.*, 1955, **18**, 245.
33. J. D. Ferry, R. G. Mancke, E. Maekawa, Y. Õyanagi and R. A. Dickie, *J. Phys. Chem.*, 1964, **68**, 3414.
34. G. Siqueira, S. Tapin-Lingua, J. Bras, D. da Silva Perez and A. Dufresne, *Cellulose*, 2011, **18**, 57.
35. B. B. S. T. Boonstra, in *Elastomers and Plastomers: Their Chemistry, Physics and Technology*, ed. R. Houwink, Elsevier, New York, 1948.
36. J. v. d. Heijden and J. Havinga, in *Natuurrubber (Natural Rubber)*, ed. J. v. d. Heijden and S. d. Meij, Rubber-Stichting Information Center for Natural Rubber, JA Delft, the Netherlands, 1997, p. 4.

37. U. Kallo, *B C Sekhar: Malaysia's Man for All Seasons*, Academy of Sciences, Kuala Lumpur, Malaysia, 2010.
38. B. C. Sekhar, *Mater. World*, 1997, **5**, 14.
39. S. T. Semegen, in *Encyclopedia of Physical Science and Technology*, ed. A. M. Robert, Academic Press, New York, 3rd edn, 2003, p. 381.
40. H. L. M. Kox, in *Natuurrubber (Natural Rubber)*, ed. J. v. d. Heijden and S. d. Meij, Rubber-Stichting Information Center for Natural Rubber, JA Delft, the Netherlands, 2000, p. 4.
41. J. S. Havinga, in *Natuurrubber (Natural Rubber)*, ed. J. v. d. Heijden and S. d. Meij, Rubber-Stichting Information Center for Natural Rubber, JA Delft, the Netherlands, 1997, p. 1.
42. International Rubber Study Group, Rubber Statistical Bulletin, International Rubber Study Group, Singapore, 2011.
43. S. Ahmad, in *International Rubber Technology and Economic Congress (IRTEC 12)*, Malaysian Rubber Board, One World Hotel, Petaling Jaya, Selangor, Malaysia, 2012.
44. *Polymers & Tyre Asia*, Dhanam House 29/609, August/September 2012, p. 48.
45. J. Havinga, in *Natuurrubber (Natural Rubber)*, ed. B. v. Baarle, Rubber-Stichting Information Center for Natural Rubber, Eindhoven, the Netherlands, 2004, p. 3.
46. *Rubber Asia*, Dhanuam Publications (Pvt) Ltd, Cochin, India, 2012, p. 55.
47. W. H. Waddell and L. R. Evans, *Rubber Chem. Technol.*, 1996, **69**, 377.
48. P. Deepalekshmi, P. M. Visakh, A. P. Mathew, A. K. Chandra and S. Thomas, in *Advances in Elastomers II*, ed. P. M. Visakh, S. Thomas, A. K. Chandra and A. P. Mathew, Springer, Berlin Heidelberg, 2013, p. 1.
49. D. Ponnamma, H. Maria, A. Chandra and S. Thomas, in *Advances in Elastomers II*, ed. P. M. Visakh, S. Thomas, A. K. Chandra and A. P. Mathew, Springer, Berlin Heidelberg, 2013, p. 69.
50. K. Ahmed, S. Nizami, N. Raza and K. Mahmood, *Int. J. Ind. Chem.*, 2012, **3**, 1.
51. S. Anandhan and S. Bandyopadhyay, in *Nanocomposites and Polymers with Analytical Methods*, ed. J. Cuppoletti, InTech, Rijeka, Croatia, 2011, p. 3.
52. J. B. Donnet, *Compos. Sci. Technol.*, 2003, **63**, 1085.
53. M. A. López-Manchado, J. Biagiotti, L. Valentini and J. M. Kenny, *J. Appl. Polym. Sci.*, 2004, **92**, 3394.
54. Q. Liu, Y. Zhang and H. Xu, *Appl. Clay Sci.*, 2008, **42**, 232.
55. H. Ismail and R. Ramli, *J. Reinf. Plast. Compos.*, 2008, **27**, 1909.
56. J. Carretero-González, H. Retsos, R. Verdejo, S. Toki, B. S. Hsiao, E. P. Giannelis and M. A. López-Manchado, *Macromolecules*, 2008, **41**, 6763.
57. M. Ganter, W. Gronski, P. Reichert and R. Mülhaupt, *Rubb. Chem. Technol.*, 2001, **74**, 221.
58. M. Pramanik, S. K. Srivastava, B. K. Samantaray and A. K. Bhowmick, *J. Appl. Polym. Sci.*, 2003, **87**, 2216.

59. R. Stephen, S. Thomas, K. V. S. N. Raju, S. Varghese, K. Joseph and Z. Oommen, *Rubber Chem. Technol.*, 2007, **80**, 672.
60. R. Stephen, S. Varghese, K. Joseph, Z. Oommen and S. Thomas, *J. Membr. Sci.*, 2006, **282**, 162.
61. Y. T. Vu, J. E. Mark, L. H. Pham and M. Engelhardt, *J. Appl. Polym. Sci.*, 2001, **82**, 1391.
62. P. Danwanichakul, R. Werathirachot, C. Kongkaew and S. Loykulnant, *Eur. J. Sci. Res.*, 2011, **62**, 537.
63. M.-J. Wang, C. A. Gray, S. A. Reznek, K. Mahmud and Y. Kutsovsky, in *Kirk-Othmer Encyclopedia of Chemical Technology*, John Wiley & Sons, Inc., New York, 2000, p. 761.
64. M. Voll and P. Kleinschmit, in *Ullmann's Encyclopedia of Industrial Chemistry*, Wiley-VCH Verlag GmbH & Co. KGaA, New York, 2000.
65. M. Bhattacharya and A. Bhowmick, *J. Mater. Sci.*, 2010, **45**, 6126.
66. Y. Lin, A. Zhang, L. Wang, C. Pei and Q. Gu, *J. Macromol. Sci., Part B: Phys.*, 2011, **51**, 1267.
67. Y. Liu, L. Li and Q. Wang, *J. Appl. Polym. Sci.*, 2010, **118**, 1111.
68. G. Gorrasi, M. Tortora, V. Vittoria, G. Galli and E. Chiellini, *J. Polym. Sci., Part B: Polym. Phys.*, 2002, **40**, 1118.
69. J. W. Kim, S. G. Kim, H. J. Choi, M. S. Suh, M. J. Shin and M. J. Jhon, *Int. J. Mod. Phys. B*, 2001, **15**, 657.
70. A. Ranade, N. A. D'Souza and B. Gnade, *Polymer*, 2002, **43**, 3759.
71. P. C. LeBaron, Z. Wang and T. J. Pinnavaia, *Appl. Clay Sci.*, 1999, **15**, 11.
72. K. N. Madhusoodanan and S. Varghese, *J. Appl. Polym. Sci.*, 2006, **102**, 2537.
73. M. Arroyo, M. A. López-Manchado and B. Herrero, *Polymer*, 2003, **44**, 2447.
74. S. Thongsang and N. Sombatsompop, *Polym. Compos.*, 2006, **27**, 30.
75. N. K. On, A. A. Rashid, M. M. M. Nazlan and H. Hamdan, *J. Appl. Polym. Sci.*, 2012, **124**, 3108.
76. D. Fragiadakis, L. Bokobza and P. Pissis, *Polymer*, 2011, **52**, 3175.
77. Y. Ikeda, S. Poompradub, Y. Morita and S. Kohjiya, *J. Sol–Gel Sci. Technol.*, 2008, **45**, 299.
78. K. J. Arun, P. J. Joseph Francis and R. Joseph, *Optoelectron. Adv. Mater., Rapid Commun.*, 2010, **4**, 1520.
79. S. S. Idrus, H. Ismail and S. Palaniandy, *Polym. Test.*, 2011, **30**, 251.
80. M. S. Sobhy, D. E. El-Nashar and N. A. Maziad, *Egypt. J. Solids*, 2003, **26**, 241.
81. H.-H. Cai, S.-D. Li, G.-R. Tian, H.-B. Wang and J.-H. Wang, *J. Appl. Polym. Sci.*, 2003, **87**, 982.
82. G. C. Psarras, *Composites, Part A*, 2006, **37**, 1545.
83. E. M. Jamal, P. A. Joy, P. Kurian and M. R. Anantharaman, *Polym. Bull.*, 2010, **64**, 907.
84. P. K. Dutta, J. Dutta and V. S. Tripathi, *J. Sci. Ind. Res.*, 2004, **63**, 20.
85. P. M. Visakh and S. Thomas, *Waste Biomass Valorization*, 2010, **1**, 121.
86. K. Gopalan Nair and A. Dufresne, *Biomacromolecules*, 2003, **4**, 657.

87. K. Gopalan Nair and A. Dufresne, *Biomacromolecules*, 2003, **4**, 666.
88. K. Gopalan Nair, A. Dufresne, A. Gandini and M. N. Belgacem, *Biomacromolecules*, 2003, **4**, 1835.
89. H. Ismail, S. M. Shaari and N. Othman, *Polym. Test*., 2011, **30**, 784.
90. H. Ismail, S. Shuhelmy and M. R. Edyham, *Eur. Polym. J*., 2002, **38**, 39.
91. V. G. Geethamma, K. Thomas Mathew, R. Lakshminarayanan and S. Thomas, *Polymer*, 1998, **39**, 1483.
92. H. Ismail, R. M. Jaffri and H. D. Rozman, *Polym. Int*., 2000, **49**, 618.
93. H. Ismail and R. M. Jaffri, *Polym. Test*., 1999, **18**, 381.
94. H. Ismail, M. R. Edyham and B. Wirjosentono, *Polym. Test*, 2002, **21**, 139.
95. H. Ismail, A. Rusli and A. A. Rashid, *Polym. Test*., 2005, **24**, 856.
96. J. Bras, M. L. Hassan, C. Bruzesse, E. A. Hassan, N. A. El-Wakil and A. Dufresne, *Ind. Crops Prod*., 2010, **32**, 627.
97. G. Siqueira, H. Abdillahi, J. Bras and A. Dufresne, *Cellulose*, 2010, **17**, 289.
98. A. Bendahou, Y. Habibi, H. Kaddami and A. Dufresne, *J. Biobased Mater. Bioenergy*, 2009, **3**, 81.
99. H. Angellier, S. Molina-Boisseau and A. Dufresne, *Macromolecules*, 2005, **38**, 9161.
100. D. b. Le Corre, J. Bras and A. Dufresne, *Biomacromolecules*, 2010, **11**, 1139.
101. H. Angellier, L. Choisnard, S. Molina-Boisseau, P. Ozil and A. Dufresne, *Biomacromolecules*, 2004, **5**, 1545.
102. H. Angellier, S. Molina-Boisseau, P. Dole and A. Dufresne, *Biomacromolecules*, 2006, **7**, 531.
103. L. Liu, M. Tian, W. Zhang, L. Zhang and J. E. Mark, *Polymer*, 2007, **48**, 3201.
104. G. Li, L. Wang, H. Ni and C. Pittman Jr, *J. Inorg. Organomet. Polym*., 2001, **11**, 123.
105. T. F. Baumann, T. V. Jones, T. Wilson, A. P. Saab and R. S. Maxwell, *J. Polym. Sci., Part A: Polym. Chem*., 2009, **47**, 2589.
106. D. Chen, J. Nie, S. Yi, W. Wu, Y. Zhong, J. Liao and C. Huang, *Polym. Degrad. Stab*., 2010, **95**, 618.
107. S. Sahoo and A. K. Bhowmick, *Rubber Chem. Technol*., 2007, **80**, 826.
108. M. Jose-Yacaman, M. Miki-Yoshida, L. Rendon and J. G. Santiesteban, *Appl. Phys. Lett*., 1993, **62**, 202.
109. P. L. Walker, J. F. Rakszawski and G. R. Imperial, *J. Phys. Chem*., 1959, **63**, 133.
110. P. C. Ma, J.-K. Kim and B. Z. Tang, *Carbon*, 2006, **44**, 3232.
111. A. Fakhru'l-Razi, M. A. Atieh, N. Girun, T. G. Chuah, M. El-Sadig and D. R. A. Biak, *Compos. Struct*., 2006, **75**, 496.
112. H. X. Jiang, Q. Q. Ni and T. Natsuki, *Key Eng. Mater*., 2011, **464**, 660.
113. G. Sui, W. H. Zhong, X. P. Yang, Y. H. Yu and S. H. Zhao, *Polym. Adv. Technol*., 2008, **19**, 1543.

114. Q. Zhao, R. Tannenbaum and K. I. Jacob, *Carbon*, 2006, **44**, 1740.
115. A. M. Shanmugharaj, J. H. Bae, K. Y. Lee, W. H. Noh, S. H. Lee and S. H. Ryu, *Compos. Sci. Technol.*, 2007, **67**, 1813.
116. S. Bhattacharyya, C. Sinturel, O. Bahloul, M.-L. Saboungi, S. Thomas and J.-P. Salvetat, *Carbon*, 2008, **46**, 1037.
117. H. Ismail, F. Ramly and N. Othman, *Polym.-Plast. Technol. Eng.*, 2010, **49**, 260.
118. F. Cataldo, O. Ursini and G. Angelini, *Fullerenes, Nanotubes, Carbon Nanostruct.*, 2008, **17**, 38.
119. International Rubber Study Group, Annual Report on Rubber Statistics, International Rubber Study Group, Wembley, United Kingdom, 2000.
120. N. Gevers and F. Kappen, in *BioRubber for Europe in Global Perspective*, EU-PEARLS Consortium Wageningen, the Netherlands, 2012, p. 34.
121. *Rubber Asia*, Dhanuam Publications (Pvt) Ltd, Cochin, India, 2012, p. 1.

CHAPTER 2

Nanofillers in Natural Rubber

MAURIZIO GALIMBERTI,*[a,b] VALERIA CIPOLLETTI[a] AND VINEET KUMAR[c]

[a] Politecnico di Milano, Department of Chemistry, Materials and Chemical Engineering, G. Natta, Via Mancinelli 7, 20131 Milano, Italy; [b] Consiglio Nazionale delle Ricerche, Istituto per lo Studio delle Macromolecole, Via E. Bassini 15, 20133, Milano (I); [c] Università degli Studi di Milano-Bicocca, Via R. Cozzi 53, 20125 Milano, Italy
*Email: maurizio.galimberti@polimi.it

2.1 Introduction

Nanofillers are playing an increasingly important role in the field of rubbers. They can be dispersed as individual particles in the polymer matrix, with at least one dimension at the nanoscale, defined "of the order of 100 nm or less".[1] The nanometric size implies features such as a large specific surface area and, as a consequence, a large interfacial area with the polymer matrix.

Most investigated nanofillers are clays (C),[2–6] organically modified clays (OC)[2–6] and carbon nanotubes (CNTs).[4,7] Nowadays, the focus of innovative research is on carbon nanofillers. Besides CNTs, there is great interest in graphene (GE), a single layer of graphite (G)[8] and in graphitic nanofillers made up of a few layers of graphene, called graphite nanoplatelets (GNPs),[9] graphite nanosheets, graphite nanoflakes and nano-graphite (nano-G).[10] Other nanofillers have been investigated, including nano-silica (SiO_2), nano calcium carbonate ($CaCO_3$) and nano metal oxides. Data are also available for the so-called nano carbon black (CB). This chapter focuses on C and OC, CNTs and nano-G: structural features of the nanofillers, processing methods for preparing them, organization of nanofillers in the polymer matrix, interaction

RSC Polymer Chemistry Series No. 8
Natural Rubber Materials, Volume 2: Composites and Nanocomposites
Edited by Sabu Thomas, Hanna J. Maria, Jithin Joy, Chin Han Chan and Laly A. Pothen

Published by the Royal Society of Chemistry, www.rsc.org

between the polymer and the nanofiller and properties of the nanocomposites are discussed. Nanocomposites based on nano-SiO_2,[4,11] nano-$CaCO_3$,[4] nano metal oxides[4] and nano-CB[4] are then briefly reviewed.

Much data has been reported, both in the scientific and in the patent literature, for C, OC and CNTs and, in particular, OC have already found application on the commercial scale.[12] Only preliminary investigations are available on GE and on the graphitic nanofillers based on a few layers of GE. However, they show great potential and thus deserve to be included in this chapter.

It will be demonstrated that nanofillers have a great impact on the properties of the rubber matrix. This chapter deals with natural rubber (NR) as the rubber matrix, but also considers synthetic poly(1,4-*cis*)-isoprene (IR) and epoxidized NR (ENR).

2.2 Nanofillers for NR: Structural Features

Nanofillers have a multiscale organization. The upper level of said organization refers to their distribution and dispersion in the rubber matrix. The lowest level of nanofiller organization refers to the structure of individual particles and of aggregates. In this section, the lowest level of nanofiller organization is discussed, presenting structural features of C, OC, CNT, GE and GNP, in their pristine state.

2.2.1 Clays and Organoclays

Clay minerals are layered.[13] As shown in Figure 2.1, montmorillonite (Mt), the most used clay mineral for the preparation of rubber composites, is made of layers 1 nm thick, with lateral dimensions between 100 and 1000 nm, with two tetrahedrally coordinated silicon atoms fused to an edge-shared octahedral sheet of either aluminium or magnesium hydroxide.

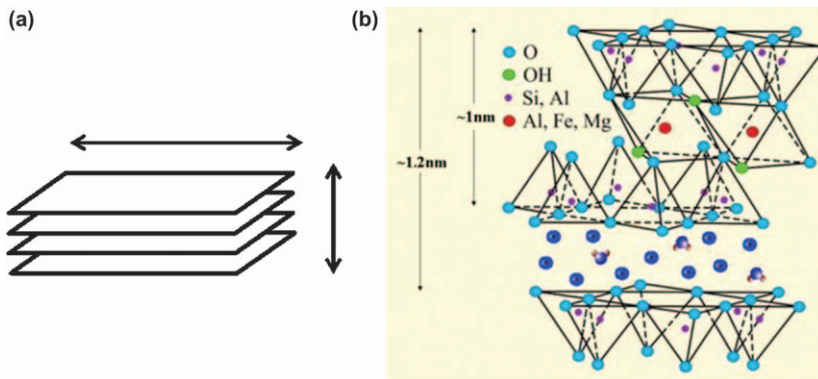

Figure 2.1 Montmorillonite: layered structure with significant difference in layer length with respect to thickness (a) and structure of a layer (b).

Layers are regularly stacked and are held together by van der Waals forces. Negative charges are generated inside the layers by isomorphic substitution (for example Al^{3+} with Mg^{2+}) and are counterbalanced by alkali and alkaline earth cations situated in the interlayer space. These cations can be easily involved in exchange reactions with other cations. Each silicate layer has oxygen atoms on the faces and oxygen atoms and hydroxide groups on the edges. Mt thus has a hydrophilic nature and needs a compatibilizer to be evenly dispersed in the rubber matrix.[3,14] Alkali and alkaline earth cations are exchanged with long chain quaternary alkyl cations (mostly ammonium cations), modifying the clay surface polarity and increasing the interlayer distance. Figure 2.2 shows XRD patterns of a pristine Na-Mt (a) and of a Na-Mt modified with an ammonium cation bearing two methyl and two tallow groups (b). In the pattern for pristine Mt, the (001) reflection at 7.2° as the 2θ value reveals an interlayer of 1.2 nm. In the case of the OC XRD pattern, the presence of (00ℓ) reflections, with $1 \leq \ell \leq 3$ for a periodicity of nearly 3.5 nm, clearly indicates the formation of an intercalate crystalline structure between clay and the ammonium compensating cation, whereas the presence of higher order (00ℓ) reflections indicates an ordered distribution of the alkylammonium cations in the interlayers.

From the peak width analysis it is possible to calculate the correlation length for the crystalline domain in the direction orthogonal to the structural layers ($D_{\perp}$) and the correlation length for the crystalline domain in the direction

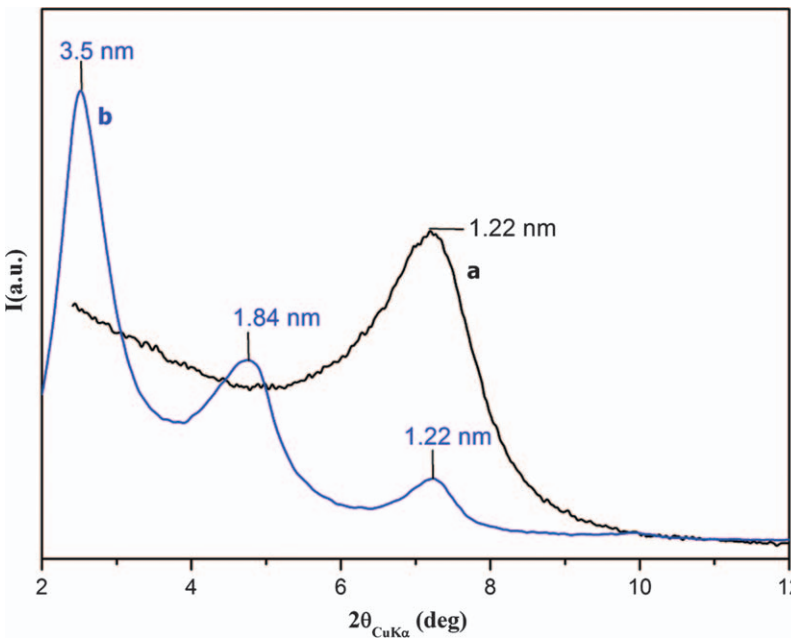

Figure 2.2 XRD patterns of (a) Na-Mt (Cloisite® from Southern Clay), (b) Na-Mt modified with an ammonium cation bearing two methyls and two hydrogenated tallow groups (Dellite® 67G from Laviosa Chimica Mineraria).

parallel to the structural layer ($D_{\parallel}$). The number of stacked layers can be estimated, taking into account the interlayer distance. Averages of about 4 and about 5 were calculated for C and OC, respectively.

The ratio between the longest and shortest dimensions of a filler is the filler aspect ratio. In the case of a clay, the aspect ratio is given by the ratio between the longest side and the thickness of the layer. As the clay has a thickness of about 1 nm, the aspect ratio can be as high as 1000. The aspect ratio is assessed through the analysis of transmission electron microscopy (TEM) images. As discussed in Chapter 24 of this book, TEM analysis gives 2D pictures: as a consequence, determining the dimensions of nanofiller particles could be affected by some uncertainty.

Infrared (IR) spectroscopy has been used to characterize OC, studying the interaction between the inorganic layer and the hydrocarbon chain of the compensating cations.[15–19] This technique gives precious information on interlayer structure and the molecular environment of alkylammonium substituents of the layered silicates. However, it appears difficult to distinguish between the clay interaction with the organophilic chains of the ammonium cation and with the polymer chains.

2.2.2 Nano-Graphite

A single layer of graphite is called graphene, a two-dimensional sheet made of sp^2-hybridized carbon atoms in an extended honeycomb network. Remarkable efforts are made to obtain GE or at least GNP, mainly through: (i) oxidation to graphite oxide with subsequent thermal or chemical reduction,[20] (ii) sonication of G suspension in appropriate solvents,[21] (iii) reactions on graphite derivatives.[22] However, types of G are already available with a low number of stacked layers and nano-dimensions. Figure 2.3 shows the structure of graphite (a) and the XRD pattern (b) of a particular type of commercially available graphite, characterized by nano-dimensions and a very high surface area (330 m^2/g).

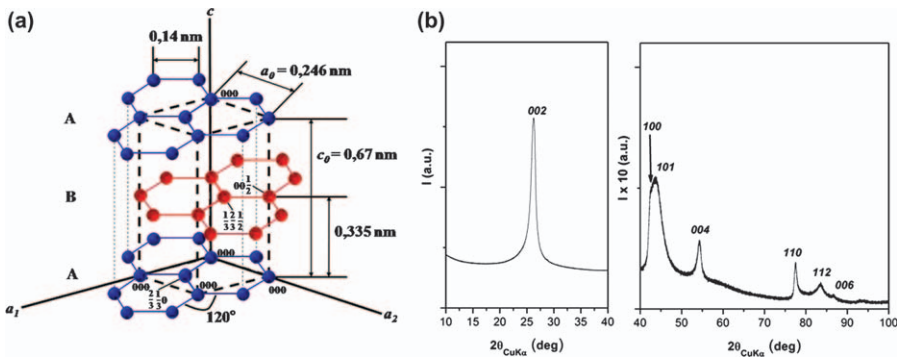

Figure 2.3 Graphite: (a) crystalline structure and (b) X-ray diffraction (CuKα) pattern in the 2θ range 5–80° of Synthetic Graphite 8427® from Asbury Graphite Mills Inc.

The following (00ℓ) reflections are detectable: (002) at 26.24° as 2θ value, corresponding to a d_{002} distance of 0.339 nm and (004) at 54.3° as 2θ value. The d_{002} distance corresponds to the distance between A and B planes. The crystalline order in the structural layer is indicated by 100 and 110 reflections at 42.7° and at 77.4°, as 2θ values, respectively.

Analogously to what reported above, from the peak width analysis a number of about 30 stacked layers was estimated and it was thus commented that this G grade, called nano-G, has nano-dimensions. Said nano-G was indicated as the ideal one for the preparation of nanocomposites and, in particular, of rubber nanocomposites, as it is endowed with the highest shape anisotropy, given by the $D_{\parallel}/D_{\perp}$ ratio, which means the ratio between the correlation length for the crystalline domain in the direction parallel and orthogonal to structural layers.[23]

Dimensions of graphite nanoplatelets are determined in the literature from the analysis of TEM micrographs: the minimum lateral size was shown to be about 500 nm.

2.2.3 Carbon Nanotubes

Carbon nanotubes (CNTs) are made by wrapped graphene layers. They are single-walled (SWCNTs) or multi-walled (MWCNTs). In the following, the acronym CNT will refer to the multi-walled type, unless otherwise indicated. Figure 2.4 shows the structures of both types of CNT (Figure 2.4(a)), the XRD pattern of a commercially available sample of CNT (Figure 2.4(b)), and the TEM micrograph showing bundles of CNTs (Figure 2.4(c)). The (002) reflection at 25.7° as 2θ value, corresponding to a d_{002} distance of 0.348 nm, is due to the regular overlapping of tube layers. XRD analysis can thus be used to calculate the number of walls in CNTs. The value obtained from the pattern in Figure 2.4(b) (about 10) lies in the middle of the range given in the technical data sheet (between 3 and 15). The number of CNT layers is usually estimated from the inspection of TEM micrographs, which also reveal the length of the tubes, which can be of micron size. As CNTs have a diameter of a few nanometres, they are endowed with a very large aspect ratio.

Raman spectroscopy measures the vibrational energies of molecules and there must be a change in the molecule polarizability to have a Raman active

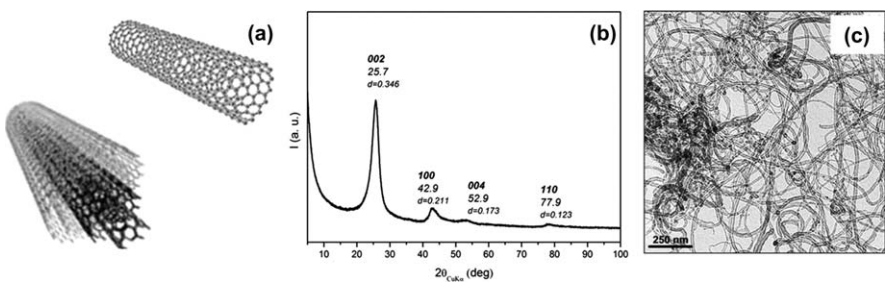

Figure 2.4 Carbon nanotubes: (a) structure of SWCNT and MWCNT, (b) XRD pattern of Baytube C150P, (c) TEM micrograph showing bundles of CNTs.

transition. It is widely acknowledged that Raman spectroscopy is a powerful and non-destructive technique able to characterize carbon-based materials, among them CNTs, leading to understanding many fundamental aspects of sp^2 carbon atoms.[24,25] Raman spectroscopy has been used to assess the effect on vibrational modes of the diameter of nanotubes,[26] of disorder in sp^2-hybridized carbon atoms[27] and of nanotube–nanotube interactions.[28] Some Raman bands have a strong frequency dependence on the excitation laser energy.[29–31] Two main typical graphite bands are present in the CNT Raman spectrum. The G band, at 1580 cm^{-1}, is assigned to the in-plane vibration of the C–C bond, with a shoulder around 1604 cm^{-1}, typical of defective graphite-like materials. The D band, at 1342 cm^{-1}, is due to the presence of disorder in carbon systems. Moreover, the G′ band at 2683 cm^{-1} is attributed to the overtone of the D band. As will be discussed in the following, Raman spectroscopy has been used to evaluate the state of dispersion of CNTs in polymer-based composites and the polymer–CNT interactions.

It should be emphasized that CNTs are available as bundles, with a large number of entanglements, as shown in Figure 2.4(c). Research efforts are spent in de-bundling CNTs, without damaging their structure, in particular without reducing their length. Over recent years, results have become available on the functionalization of CNTs.[32–36] The purpose of functionalizing CNTs is mainly to favour their dispersion in different matrices, either polar or apolar, improving mechanical strength and/or electrical conductivity. In most cases, functional groups contain oxygen atoms. Quantitative information on the concentration of said functional groups is obtained through X-ray photoelectron spectroscopy.[37–39]

Examination of the structure of nanofillers allows us to conclude that all of them have a layered structure. In the case of OC and G, the separation of layers from aggregates means an ultimate dispersion and a very high aspect ratio with a profound impact on the nanocomposite properties, as discussed below.

2.3 Processing Methods for the Preparation of Nanocomposites

OC, G and CNTs were blended with rubbers and, in particular, with isoprene rubbers through emulsion, melt and solution blending. As mentioned above, the upper level of nanofiller organization refers to their distribution and dispersion in the rubber matrix. This section summarizes the effect of blending technology on nanofiller dispersion.

2.3.1 Dispersion of Clays and Organoclays

Table 2.1 presents a summary of the information available in the scientific literature for C and OC dispersion in isoprene rubbers. The state of dispersion depends on the clay type, pristine or organically modified, and on the blending technology adopted. Table 2.2 shows that nanocomposites are formed with a pristine clay only through emulsion blending. In fact, the inorganic nature of clay layers hinders their compatibility with the rubber matrix.

Table 2.1 Blending technologies for C and OC in poly(*cis*-1,4)isoprene rubbers[23,40]

Nanofiller	*Rubber*	*Blending technology*
C[23,40]	NR	Emulsion, melt, solution
	IR	Melt, solution
	ENR	Melt
OC	NR	Emulsion, melt, solution
	IR	Melt, solution
	ENR	Melt, solution

Table 2.2 Dispersion of a pristine C in a poly(isoprene) matrix as a function of the blending method.[40]

Nanofiller	*Rubber*	*Blending method*	*Best silicate dispersion*
C = Mt, Bt, Fht	NR, IR, ENR	Melt	Simple incorporation of agglomerated clays, poor dispersion, poor interfacial adhesion.
C = Mt, Bt	NR	Solution	Conventional microcomposite, clay tactoids and agglomerates, big lumps of not exfoliated particles.
C = Mt, Bt, Fht	NR	Emulsion	Excellent clay dispersion: nanocomposites. Individual and stacked layers.

Instead, OC were shown to be able of forming nanocomposites with isoprene rubbers with any of the blending technologies. Compensating cations were: chlorhydrate of primary alkenyl amine and ammonium cations having: (i) three methyls and one long chain alkenyl substituent, (ii) two methyls and two larger alkenyl substituents, equal or different to each other: ethylhexyl, benzyl, talloyl, hydrogenated talloyl. In particular, many data are available with di(hydrogenated tallow)-dimethylammonium chloride (2HTCl). Aggregates with few layers and individual lamellae were clearly identified. Chapter 24 of this book reports TEM images that demonstrate said even dispersion. Results available in the scientific literature are reported and discussed in detail elsewhere.[2,40,41] More recent papers strengthen what was reported in said papers and give new suggestions for achieving a satisfactory dispersion of clay in NR. A suspension of Mt modified with octadecyl amine was added to NR latex.[42] Oligomeric and polymeric clay substituents were used in order to improve OC compatibility with the polymer matrix. A Mt modified with a compensating cation containing a $-CH_2CH_2OH$ group was reacted with a maleinized polybutadiene oligomer: a homogeneous dispersion was found both in NR and SBR matrices and an improved interaction was demonstrated with the SBR rubber.[43] Organic amines of varying chain lengths, from dodecyl- to octadecylamine as well as an amine-terminated butadiene-acrylonitrile copolymer were used to modify Mt and then prepare NR-based nanocomposites.[44] OC was reacted with fatty acids, as will be discussed in Section 2.4.1, and clay exfoliation was found to be dependent on the length of the fatty acid chain.[45]

A particularly interesting approach, in view of the larger-scale development of RCN, was proposed: OC based on a bentonite were prepared *in situ* in the polymer, used as the reaction medium. IR and NR were employed in most cases, achieving a homogeneous OC dispersion.[46,47] More recently, this approach was applied to both Mt and sepiolite.[48]

2.3.2 Dispersion of Nano-Graphite

Very few data are available for GNP and nano-G. To obtain GE, GNP has been sonicated in many different solvents and, in most cases, coating layers have been prepared,[21] but not with isoprene rubbers as the matrix. Melt blending has been reported in IR as the matrix:[10,49] even nano-G dispersion was obtained, although it was not possible to identify single GE layers in the final composite.

2.3.3 Dispersion of Carbon Nanotubes

CNTs were blended with isoprene rubbers through emulsion, solution and melt blending. The emulsion and solution approaches were adopted to achieve a satisfactory de-bundling of CNTs and to preserve as far as possible the original CNT length, *i.e.* the original aspect ratio. It was reported in Section 2.2.3 that functionalized CNTs are becoming more widely available and this will also make easier their dispersion in polyisoprene matrices. In this section, results reported in the scientific literature are reviewed as a function of the processing method.

Table 2.3 summarizes what arises from the scientific literature for the emulsion blending of CNTs in NR latex.

Polar groups were introduced onto the CNT surface, to prepare water dispersions which were then mixed with NR latex. Sonication of the polymer dispersion with CNTs was often adopted. Carboxylated groups were reported to lead to a strong CNT adhesion with the polymer, with CNTs embedded in the matrix and a layer of polymer on the CNT surface. Latex spheres were found to act as volume exclusion for CNTs and percolation was achieved at a low content. However, larger CNTs were dragged from the matrix, with unsatisfactory adhesion. A very good dispersion was also obtained by covering CNTs with a positively charged polymer. Table 2.4 shows results from solution blending.

A good dispersion was achieved, with the help of vigorous agitation (sonication), in particular by adding lipophilic groups such as octadecane onto the CNT surface. To promote a chemical linkage with the unsaturated rubber, a sulfur-containing silane such as bis[3-triethoxysilyl)propyl]tetrasulfane (TESPT) or resorcinol with a methylene donor such as hexamethylene tetramine (HMT) (with hydrated silica) were used. In fact, unmodified CNTs were observed as completely pulled out from the matrix from the scanning electron microscopy (SEM) analysis of fracture images.

Table 2.5 shows results from melt blending, which also produced a good and homogeneous CNT dispersion. However, protrusion of CNTs from the fracture plane was observed in SEM micrographs when CNTs were not modified. A remarkable reduction in CNT length was shown, when a step at the two-roll

Table 2.3 Dispersion of CNT in NR matrix through emulsion blending.

CNT treatment	*Blending procedure*	*Characterization techniques*	*Results: CNT dispersion*	*Ref.*
With acids: 1. HCl 2. HNO_3	1. Dispersion in water with SDS, 1/1 wt ratio. Sonication (bath sonicator) for 15 min. 2. Dispersion added to ammonia solution of pre-vulcanized NR. 3. Magnetic stirring for 24 h, sonication for 15 min (bath sonicator). 4. Poured into a Petri dish, dried at 60 °C for 24 h.	TEM	CNT strongly adhered to latex particle surface. Latex spheres act as exclusion volume for CNT. The available space for MWCNTs is drastically reduced: lower percolation threshold and formation of networks at the 'grain boundaries'.	111
		AFM	No aggregates. CNTs are properly embedded in the films and do not impede latex sphere coagulation.	
1. Pristine 2. With H_2SO_4/HNO_3: prior to treatment with SDS (Both 1 and 2 blended with NR as reported in the next column)	1. Dispersion in water with SDS, SDS/CNT = 1/1.5 wt ratio. Sonication (bath sonicator) for 2 h. 2. + NR latex, magnetic stirring. 3. Sonication (ultrasonic bath), 1 h (to remove bubbles): tick slurries. 4. Cast onto a flat plastic mould, dried in an oven under air, 50 °C, 24 h.	SEM	Heterogeneous cross-section. Fragments of CNT were cut by the microtome and larger CNTs were dragged: larger CNTs did not adhere to the matrix.	112
		TEM	High concentrations of oxygen and sulfur around CNT: surfactant molecules remain adhered to CNT surface and act as a bridge between the CNTs and the polymer.	
		AFM	CNTs covered by a layer of polymer: good adhesion between the two components. The polymer is 'softer' around the boundaries of CNT than in other regions: dissipative interfacial layer.	

1. SDS (CNT/SDS = 2/1) 2. pH adjusted to 10 with KOH: negatively-charged CNT 3. Positively-charged PDDA. CNT/PDDA = 10/1, magnetic stirring.	1. Pre-vulcanized NR latex (addition of curing system for 2 h at 60 °C). Total solids 50%. 2. CNT-PDDA (CNT) water suspension dropped into negatively-charged NR latex. Gentle magnetic stirring, RT, 24 h. 3. Cast onto glass plates, dried at 50 °C for 24 h.	TEM SEM	Untreated CNT aggregated and twisted form in the NR matrix. CNT-PDDA: more intimate with the matrix, individually attached to the NR particles like a little worm. Untreated CNTs severely aggregated in the matrix (twisting): incompatible CNT-PDDA: much improved dispersion. Interface with NR very smooth. PDDA: used as a bridge, to enhance the interfacial adhesion with the polymer. With CNT content < 3 wt%, almost all CNTs homogeneously distributed throughout the matrix as individual tubes. A further increase in CNT content had an unfavourable effect on dispersion in the latex.	65

Table 2.4 Dispersion of CNTs in NR matrix through emulsion blending.

CNT treatment	*Solvent and blending procedure*	*Characterization techniques*	*Results: dispersion of CNTs*	*Ref.*
=	Toluene, sonication (probe ultrasound)	TEM	Homogeneous distribution. More random orientation by increasing CNT content.	107
=	Toluene, sonication	SEM	Good dispersion (CNT = 1, 5, 10, 20 wt%).	60
=	Toluene, 3 wt% CNT, ultrasonication RT 30 min	SEM	Completely pulled out.	64
=	Toluene, sonication (mechanical probe sonicator)	FESEM	Short and long CNTs are seen. Homogeneous distribution without agglomeration. CNTs are observed to form percolating networks at 5 and 10 wt%. Lesser orientation of CNTs at higher concentration (5, 7 and 10 wt%).	113
1. Purification (with acids?) 2. Ball milling with H_2S: SH groups grafted onto the surface.	Toluene a. Ultra-Turrax (11000 rpm) b. Sonication, three steps of 3 min	TEM, AFM	Individual tubes and agglomerates, presence of agglomerates, independent of the type of CNT.	108
1. HF 2. Purification. HNO_3 : H_2SO_4 = 1 : 3 3. Functionalized hydrated silica : resorcinol : HMT = 15 : 10 : 6 (ball milling).	Toluene sonication (ultrasonic cleaner)	SEM	No aggregates were noted.	104

1. $KMnO_4$ with phase transfer catalyst: OH groups onto the surface. 2. Silanized with TESPT.	Toluene, 3 wt% CNT, ultrasonication RT 30 min	SEM images of fracture surfaces	Well dispersed in NR with no apparent aggregation. Embedded deeply in the matrix.	64
A. HF B. 1. HF 2. HNO_3/H_2SO_4 3. Resorcinol/HMT/silica	Toluene Sonication, ultrasonic cleaner	SEM	A. Not well dispersed. Outcrops from fracture surface. B. Good dispersion.	68
1. Acid treatment: OH and –COOH groups 2. Reaction with 1-octadecanol	Toluene, sonication for 30 min	TEM	The unmodified CNT-filled composites show individual CNT particles in the matrix along with a few loose agglomerates.	114
1. Acid treatment: OH and –COOH groups 2. Reaction with phenol	Toluene, sonication for 30 min	TEM	C18 modification of the nanotubes leads to their better dispersion in the NR matrix. Phenol-modified CNTs are better dispersed than unmodified CNTs.	114

Table 2.5 Dispersion of CNTs in NR and IR-based matrices through melt blending.

CNT treatment	*Blending procedure*	*Characterization techniques*	*Results*	*Ref.*
=	Haake® internal mixer S, MBTS added at two-roll mill 2 min, 100 °C	SEM	Protrusion of CNTs: lateral contraction of rubber on stretching, due to mismatch in Poisson's ratio between rubber and network of rigid fibres.	106
=	Two-roll mill, nip 0.2 mm, five times + 2 phr peroxide	TEM	Homogeneous dispersion. Tortuous configurations. 3D network structure. Longer CNTs (20 μm instead of 15 μm) relatively straighter.	119
=	Haake® internal mixer S, MBTS added at two-roll mill, 2 min, 100 °C	SEM	Good dispersion in unstretched state. By 15% stretching, long coil-like CNTs with smooth surfaces are seen to protrude out of fracture plane. By removing strain, CNTs slowly re-enter and only a few smooth outcrops of CNTs are observed. This indicates a weak interfacial interaction and easy slippage between CNTs and rubber matrix.	52

=	1. Brabender® internal mixer 2. Two-roll mill, nip 1 cm, 5 times, 50 °C	TEM	CNTs evenly dispersed and remarkably broken.	110
1. $H_2SO_4/K_2Cr_2O_7$ 2. AMEO	Two-roll mill, RT, 19 min Friction ratio 1 : 1.1, nip 1 mm	SEM	Pure CNTs: thin fibrous structures on the surface, more aggregation in the bulk. Acid-treated CNTs: individual fibrous structures, with less aggregation. Silane-treated CNTs: aggregated structure, due to hydrogen bonding between functionalized CNTs.	105
1. HF 2. Purification $HNO3 : H_2SO_4$ = 1 : 3 3. Functionalized hydrated silica : resorcinol : HMT = 15 : 10 : 6 (ball milling)	Banbury® internal mixer	SEM	Purified CNTs: entangled with each other. Functionalized CNTs: good dispersion in rubber matrix with improved interfacial bonding.	62

mill was adopted. As in the case of solution blending, CNT treatment with resorcinol and a methylene donor such as HMT led to improved dispersion in rubber and interfacial bonding.

As mentioned above, Raman spectroscopy has been used to evaluate the state of dispersion of CNTs in polymer-based composites. The shift to higher wavenumbers of the Raman bands has been taken as an indication of fewer inter-tube interactions. A further upshifting of Raman bands occurs when the tubes are disentangled and embedded in the polymer medium, as was reported for the SBR matrix.[50] Said upward shifts are also considered as the indication of intimate nanotube/polymer interaction, as will be discussed in Section 2.5.2.

It can thus be concluded that OC, CNTs and nano-G can be evenly distributed in a poly(isoprene) matrix using emulsion, melt and solution blending. It should be emphasized that the two first approaches have already been used on an industrial scale, at least for C, OC and CNTs as the nanofillers. Research is nowadays aimed at achieving an intimate nanofiller/rubber interaction, trying to avoid the slippage of nanofiller on polymer chains. A substantial reduction in tube length was reported for CNTs mixed through melt blending with a synthetic poly(isoprene).

2.4 Organization of Nanofillers in NR

Most properties of nanocomposites depend on the nanofillers structure in the NR matrix. The analysis proposed in Section 2.2 has thus to be performed on nanocomposites as well.

2.4.1 Clays and Organoclays

The structure of polymer nanocomposites based on C and, in particular, OC has been the subject of a huge number of investigations. Figure 2.5 summarizes the structures that are believed, by most authors, to be formed.

In particular, the intercalation of polymer chains is reported to play a very important role,[4–6] as it is considered not only to favour the improvement of the polymer properties but also to promote the clay exfoliation, leading to the ultimate clay dispersion. The enlargement of the interlayer distance, measured from XRD patterns, is assumed as the proof of the occurred polymer intercalation. However, an alternative mechanism is proposed to explain nanocomposites formation and clay exfoliation.[51–54] According to this alternative mechanism, only low molecular mass substances (compensating cations and polar molecules) are intercalated between two clay layers. The variation of the interlayer distance is due to the different arrangement of these substances and the exfoliation of clay aggregates, homogeneously dispersed in the polymer matrix, is due to the progressive peeling off of layers. Experiments in NR were at the basis of this alternative mechanism.[53] In fact, OC was prepared by performing the reaction between pristine Mt and the ammonium salt (di(hydrogenated tallow)-dimethylammonium chloride) in NR as the reaction medium: 6 nm was determined as the interlayer distance, in place of the usual

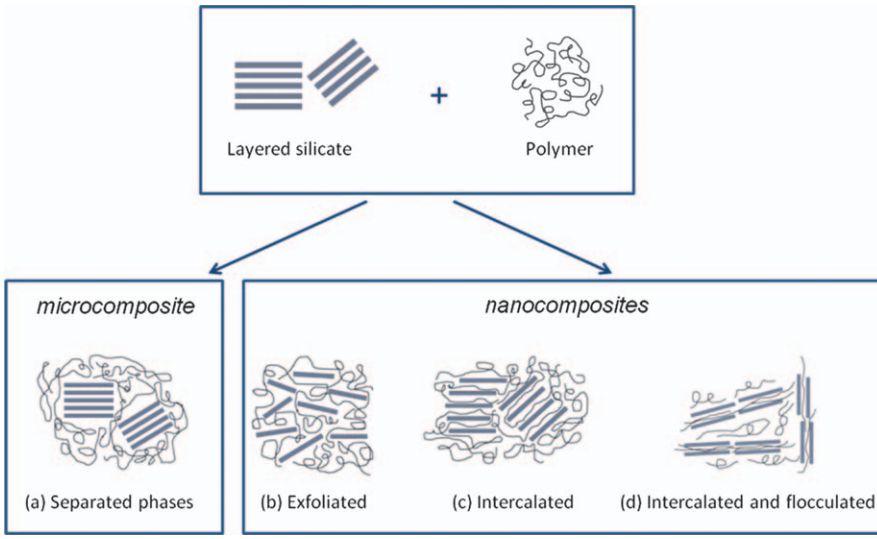

Figure 2.5 Structures of polymer (rubber) clay nanocomposites.

3.6–4 nm. The intercalation of the fatty acids, in particular of stearic acid, present in NR was commented to justify the increased d_{001} value and tailor made OC structures were then prepared, in successive works.

Figure 2.6 shows the mechanism to explain the formation of OC from pristine clay and a compensating ammonium cation, in the presence and in the absence of a fatty acid.

The expansion of the interlayer distance that occurs when OC are mixed with a polymer matrix is thus regarded as a crucial aspect in the field of PCN. In a nutshell, said expansion is considered to promote a better dispersion of OC and it is seen as preliminary for the final OC exfoliation. However, what reported in Figure 2.6 suggests that expansion might not necessarily mean exfoliation, as it might be due to crystalline structures with a higher degree of order. In another paper of 2007,[55] stearic acid was reported to promote the expansion of the interlayer distance of an analogous OC (with dimethyl dialkyl (C14-C18) ammonium cation), and the esterification of hydroxyl groups on Mt layers was commented to be the driving force for the intercalation of fatty acid. Stearic acid was reacted with a pre-formed OC and a maximum interlayer distance of 4 nm was achieved. More recently,[56–58] it has been confirmed that the reaction of OC with fatty acids leads to the expansion of the OC (with dimethyl distearyl ammonium cation) interlayer distance, which remains below 4 nm, however. In these papers, better OC dispersion, better mechanical properties and lower percolation thresholds are presented for the so-called 'expanded OC', which means for the OC reacted with a fatty acid. Summarizing, considering results reported previously,[51–58] it could be hypothesized that only the reaction of Mt with the ammonium cation in the presence of fatty acids leads to the formation of crystalline structures with a high degree of order, thanks to the presence of a

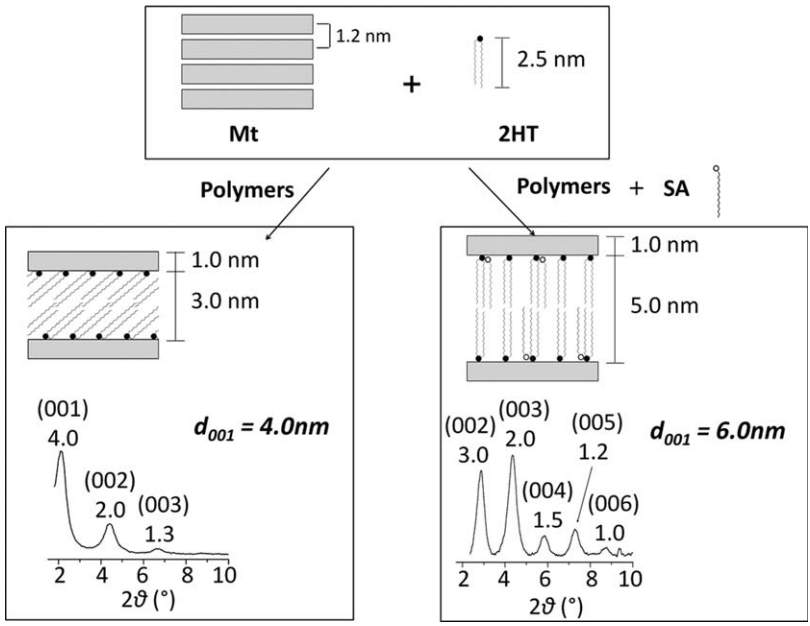

Figure 2.6 Mechanism for the formation of organoclay from Na-Mt and di(hydrogenated tallow)-dimethylammonium chloride (2HT), in the absence or in the presence of stearic acid (SA).

fatty acid. In these OC, the interlayer distance is dictated by the perpendicular bilayer arrangement of hydrocarbon substituents of the ammonium cation (see Figure 2.6). Conversely, the reaction of stearic acid with a pre-formed OC seems to lead to less ordered expanded structures. Both the approaches reported previously[51–54,55–58] led to a very homogeneous dispersion of OC.

2.4.2 Nano-Graphite

XRD analysis was performed on crosslinked nanocomposites based on synthetic polyisoprene and containing nano-G.[10,49] The (002) reflection was observed, as in Figure 2.3(b). Surprisingly, the peak width analysis led to calculate a higher number of overlapped layers. It was commented that the high pressure adopted for crosslinking the nanocomposites brings the nano-G structure to a minimum of energy, *i.e.* to a higher degree of organization.

2.4.3 Carbon Nanotubes

XRD analysis was as well performed on crosslinked nanocomposites based on synthetic poly(isoprene) and containing CNT.[49] The (002) reflection, reported in Figure 2.4b, was also observed in the pattern of the nanocomposite. Analogously to what reported above for nanocomposites with nano-G, the peak width analysis led to calculate a higher number of overlapped layers and

this finding was justified with the high pressure used for crosslinking the rubber sample.

2.5 Interaction between Isoprene Rubber and Nanofiller

One of the main subjects of research activity on polymer nanocomposites and, in particular, of nanocomposites based on isoprene rubber is the polymer/nanofiller interaction. To underline the importance of this subject, it could be simply said that the reinforcement by nanofillers depends essentially on the efficiency of load transfer to the nanofiller particles.

The investigation is performed at different *ranges*: (i) short range: the nanofiller–polymer interface, (ii) medium range: performing a strain of the composite up to about 25% (iii) long range, performing a strain of the composite higher than 25%, typically higher than 100%.

Table 2.6 summarizes the characterization techniques adopted, as a function of the investigation range, and the subjects of the investigation.

In Paragraph 2.3 and, in particular, in Tables 2.3, 2.4 and 2.5 data and comments were given on the nanofiller–polymer interface, arising from TEM and SEM microscopy as the characterization techniques. In this paragraph, what available in the literature is reviewed.

2.5.1 Clays and Organoclays

In the case of C, it was commented that the hydrophilic nature of clay layers allows their dispersion in the NR matrix only through the use of NR latexes. However, a poor interaction is achieved between the rubber and the pristine clay. OC can be easily dispersed in the NR matrix both through solution and melt blending. However, only non-bonding interactions are established with the polymer matrix. From TEM analysis, it has not been possible, so far, to tell apart rubber molecules from the organic part of the clay compensating cation and this hinders an intimate analysis of the interface. However, it has to be considered that chemical bonds are not established between OC and the rubber matrix and slippage of organically modified layers has to be expected. In fact, interesting findings were shown for nanocomposites based on IR and Mt/2HT as the OC. When said nanocomposites were crosslinked with peroxides, in stress–strain curves a remarkable decrease of the modulus was observed by

Table 2.6 Investigation of nanofiller–rubber interaction.

Range of the investigation	*Characterization techniques*	*Subject of the investigation*
Short range	TEM, SEM, solid-state NMR, Raman, bound rubber	Interface
Medium range	Dynamic-mechanical tests	Break-up of nanofiller network
Long range	Tensile, quasi-static tests, Raman	Strength of nanofiller–rubber interaction

increasing the strain, clearly indicating the slippage of OC on the polymer chains.[49]

2.5.2 Carbon Nanotubes

Data are not yet available for nano-graphite, whereas many investigations are dedicated to CNT, as a great impact on the composite properties is envisaged, provided that a strong interfacial bonding is achieved between CNT and the polymer molecules. It is clear that the chemical nature of CNT surface deeply affects their interaction with the polymer matrix. In general, CNT are treated with acids to remove catalytic residues, though in some papers this step is not indicated and, thus, it cannot be *tout court* supposed. In an early review, poor dispersion and poor interfacial bonding were commented, attributing the strong restriction in equilibrium swelling in toluene not to the filler matrix interfacial interaction but to the occlusion of rubber into the aggregates.[7] The poor interfacial interaction was reported to be in particular responsible for the poor composite ultimate properties.[59]

CNT apparently untreated were evenly dispersed in NR through solution blending in toluene[60] and FT-IR spectra revealed a shift to lower wavenumbers of typical NR bands when the content of CNT was increased. The introduction of polar groups on CNT led to their easy dispersion in aqueous medium but also to a weak interaction with non-polar NR and thus to self-aggregation.[60] Self aggregated CNT and outcrops from fracture surface were observed with purified CNT (containing polar groups) blended with NR in toluene solution,[61] whereas improved CNT dispersion and good interfacial bonding were achieved when CNT were treated with hydrated silica, resorcinol and a methylene donor. This treatment led to a strong interfacial bonding also by melt blending CNT and NR.[62] Thanks to the treatment of CNT with poly(diallyldimethylammonium chloride (PDDA), self-aggregation and twisting of CNT were greatly depressed and the interfacial adhesion with NR was remarkably enhanced.[63]

When CNT were grafted with TESPT, they could react with NR polymer chains and a strong interface was formed as it was shown by the remarkable increase (more than 30%) of the storage modulus in the glassy region.[64]

Raman spectroscopy. Raman spectroscopy has been used to study the polymer–CNT interface.[65,66] As mentioned in Section 2.3.3, the upfield shift of G, D and G' bands are taken as the indication that an intimate nanotube–polymer interaction is in place. In Figure 2.7[64] are reported the spectra of (a) pristine CNT, (b) NR/CNT and (c) NR/silanized-CNT. In the (c) case, TESPT was grafted onto the CNT surface and intimate interaction with the polymer was obtained.

Raman spectroscopy is as well applied to investigate the strength of the interface between the polymer and the nanotube surface when a strain is applied. A weak interface has been demonstrated so far for a rubber such as SBR.[67] However, when SWCNT were in NR as the polymer matrix,[68] they were found to provide effective load transfer, predominantly along the axis of

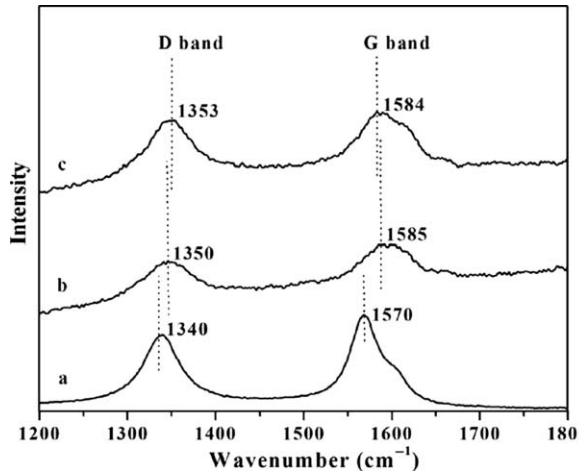

Figure 2.7 Raman spectra of pristine (a) CNT, (b) NR/CNT and (c) NR/silanized CNT composites.

the CNT bundles. It was commented that SWCNT carry most of the load in the nanocomposite, on the circumference of a nanorope. CNT/NR nanocomposites were formed *via* solution blending,[69] slight upfield shifts of the Raman bands were noted and were commented as due transfer from the matrix to the nanotubes.

Bound rubber. From bound rubber measurements, it was suggested[70] a weaker rubber–filler interaction for NR/CNT composite compared to the NR/CB composites, due to the weak adhesion between inner and outer CNT layers (that allows them to slip) and to the weak adhesion between outer layers and the rubber. The increase in mechanical properties of the nanocomposites was explained with the high aspect ratio of CNT.

2.6 Properties of NR/Clay Nanocomposites

Clay minerals, in NR, have a remarkable effect on (i) rheological properties, (ii) vulcanization efficiency, (iii) barrier properties, (iv) mechanical reinforcement, (iv) thermal properties, (v) degradation properties, (vi) flame resistance.

2.6.1 Rheological Properties

Clays compatibilized and evenly dispersed in the rubber matrix tend to build networks at low concentration. Rheological measurements allow us to observe the occurrence of the filler networking phenomenon at low filler content (even 4 phr) in rubber matrices such as IR, ENR, SBR, EPR.[71–75] At zero shear, the viscosity of RCN is thus higher than the one of the neat elastomer. However, OC reduces the steady shear viscosity of RCN, with pronounced shear-thinning behaviour, increasing with the clay content, a higher extent of extrudate, a

lower swelling and a better surface smoothness, by increasing the shear rate. Results are available in BR SBR, NBR.[76] This OC behaviour is opposite to that of traditional fillers and is attributed to the orientation of clay platelets along flow direction and to the slippage of platelets on the polymer chains. Processability of a polar rubber such as NBR[77] is particularly improved.

When NR was the rubber, a NR latex was mixed with Na-bentonite and Na-fluorohectorite, varying the concentration of clays from 1 to 2.5 phr and determining rheological properties with a coaxial cylinder viscometer. Viscosity increased with clay loading. Pseudo solid-like behaviour was observed in bentonite-filled composites at the loading of 2.5 phr, whereas a behaviour close to that of the Newtonian fluid was shown by unfilled NR. Stronger rubber–bentonite interaction was revealed by the higher viscosity, the lower power-law indexes and the slope of the Kraus plot.[78]

2.6.2 Vulcanization Efficiency

It is known that OC promote a faster sulfur-based cure of unsaturated polymer chains. The activation energy of the crosslinking reaction is decreased and the crosslinking density in enhanced.[79] To explain these effects by OC, the formation of tertiary amines from the thermal degradation of ammonium cations and the enhanced mobility of sulfur-accelerating anionic species were proposed.[80]

In NR, hexadecyltrimethyl ammonium, octadecyltrimethyl ammonium, tetraoctyl phosphonium, triphenyl vinylbenzyl phosphonium, octadecylamine chlorhydrate were used as the clay compensating cations.[79,81]

2.6.3 Barrier Properties

Barrier properties of a rubber matrix are remarkably improved thanks to clay addition. The tortuous path model is proposed to explain this phenomenon.[82,83] In a NR/Mt nanocomposite prepared from emulsion blending, 1, 2 and 3 phr of clay led to more than 35% and to about 45% and 50% reduction of oxygen permeability, respectively.[84] 3 phr of OC (Mt/ didodecyl methyl amine) gave a 50% reduction of the oxygen permeability and a 40% reduction of toluene absorption at 20 °C.[85] About 10% and 15% reduction of oxygen permeability were obtained with 5 and 10 phr of OC, respectively, and 30% reduction of toluene absorption was achieved with 15% OC, at 30 °C.[86]

2.6.4 Mechanical Reinforcement

According to the theories on reinforcement of polymer melts and elastomers by particulate fillers,[84] the initial modulus of a filled rubber composite is given by different contributions. Figure 2.8 reports the dependence of the shear complex modulus on the strain amplitude.

It is evident that three contributions to the modulus do not depend on the strain amplitude. They are due to: (i) the polymer network (entanglements,

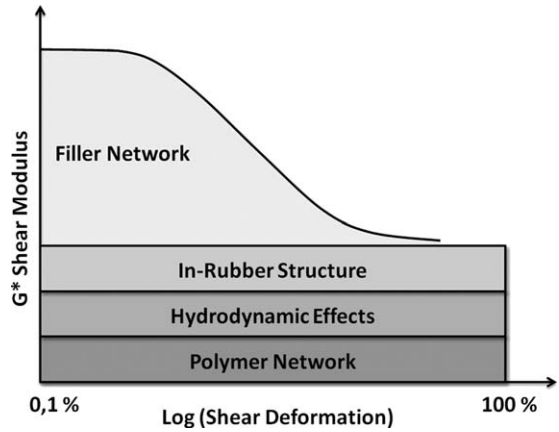

Figure 2.8 Shear modulus of a rubber compound filled with a particulate filler.

physical and chemical crosslinks), (ii) hydrodynamic effects (related to the filler volume fraction), (iii) the so-called 'in-rubber structure', that means the immobilization of rubber on filler particles (that transform a highly viscous liquid in a solid). It is also evident that the contribution to the modulus due to the filler network strongly depends on the strain amplitude. The filler network is formed when filler particles are joined together either directly or through polymer layers.

The initial modulus of the composite is correlated with the filler volume fraction through the Guth equation:

$$E = E_{\mathrm{m}}\left(1 + 0.67f\Phi + 1.62f^2\Phi^2\right) \tag{2.1}$$

The Guth equation was developed for composites filled with a nanostructured filler such as CB. In the equation, the quadratic term accounts for the mutual disturbance of filler particles and the factor f is the shape factor, which takes into account the irregular shape of aggregates of individual particles. In Section 2.2 the shape factor f was defined as the ratio between the longest and the shortest side of the nanofiller particle. It is evident the impact of the shape factor f on the value of the modulus, in particular when the filler content is high, that means when the quadratic term becomes important. Equation (2.1) holds up to the so-called filler percolation threshold, which means the filler content at which a continuous network is established in the rubber matrix and it accounts for the sum of the three contributions that do not depend on the strain amplitude. What reported so far has a general validity for nanocomposites based on either OC, or nano-G or CNT. In the case of a clay, the shape factor f is given by the ratio between the longest lateral side of the layer and the height of clay stacks, the highest f value being obtained in the case of a single clay layer. Therefore, the exfoliation of a clay not only favours a better clay dispersion but also improves the modulus of the compound. A modulus reduction factor of

about 0.7 was experimentally determined,[85] to take into account the lower contribution to the modulus of a platelet-like filler.

Discussing the rheological properties of OC-based nanocomposites, it was commented that a low clay concentration is needed to achieve the percolation threshold. Said percolation threshold was determined from the dependence of Young's modulus (obtained from stress–strain curves), on the OC concentration (OC was Mt/2HT) in an isoprene rubber matrix, either synthetic[86] or naturally occurring.[87] The excess of the Young's modulus was plotted, in a double logarithmic plot, versus the filler fraction, applying the Huber Vilgis model,[88] determining the percolation threshold, that was: 2.9 vol% in IR[86] and 4 vol % in NR.[87] The excess modulus scales with a power law with an exponent between 1.8 and 2.5 above the percolation threshold, lower with respect to the one typical of CB (about 4), probably as a consequence of the structural difference of the filler. As reported above, the filler network is responsible for the non-linearity of the dynamic-mechanical behaviour of rubber nanocomposites, a phenomenon known as the Payne effect.[87] Thanks to the easy formation of a filler network, clays promote a remarkable Payne effect, which was found to increase with the clay content, both in NR[90] and IR[86] based matrices. The dynamic modulus was observed to decrease by increasing the temperature,[91] probably as consequence of the 2-D melting[92] of the paraffinic chains substituents of the compensating ion.[87,93] Data available in the literature quantitatively demonstrate the improvement of mechanical properties of the rubber matrix (either NR or IR) by pristine clays and OC. The modulus of NR was observed to increase by adding up to 30 phr of clay, though in the presence of worse ultimate properties, when pristine Mt was dispersed in NR latex.[94] At 20 phr as clay content, higher 300% stress, shore A hardness, tensile strength and tear strength were obtained.[95] Lower concentrations of OC were required. 5 phr of Mt modified by tetraoctyl phosphonium bromide, in NR as the matrix, resulted in a three-fold increase of tensile strength[81] and best ultimate properties were obtained with 10 phr of OC (Mt/octadecyltrimethyl ammonium).[96] 2 phr of OC (Mt/octadecyltrimethylamine) in an NR/ENR blend (10 phr ENR50) led to increase both strain and stress at break values.[97]

An objective of the research activity was to achieve the same mechanical reinforcement of CB-based compounds with much less C or OC, thus preparing lighter compounds. A comparable mechanical reinforcement was obtained with 40 phr CB and 10 phr OC (Mt/octadecylamine), with almost twice the elongation at break, a lower compression set and similar abrasion loss.[98] With respect to 50 phr of CB, a much lower heat build-up was obtained with the same OC.[99]

Dynamic and loss moduli were investigated as a function of strain amplitude, preferentially in the shear mode. OC in NR matrix were found to promote a remarkable non-linear dynamic behaviour, demonstrated by a strong decrease of the storage modulus and by a maximum in the loss modulus.[90] These effects were shown to be absent in neat NR and to increase consistently with the OC content, becoming particularly evident above the OC percolation threshold. The non-linearity of the modulus with the strain amplitude is known as the

Payne effect and it is nowadays widely acknowledged that OC promotes noticeable Payne effect and hysteresis.

2.6.4.1 Hybrid OC/CB Filler System

Nowadays, it seems more reasonable to add a minor amount of C or OC to a compound filled with a much larger amount of CB. Hybrid OC/CB filler systems were used in IR,[86,100] NR,[91,101] NR/SBR blend,[102] ENR.[103] CB was used at a level typical of commercial applications (higher than 50 phr).[86,91,102] When the hybrid OC/CB filler system was used in IR, a change of the filler networking mode was observed at about 3.1 phr as OC content, whereas OC achieved its percolation threshold at about 5.9 phr when it was added to the neat IR matrix. In the case of the nanocomposite with the hybrid filler system, a transition was thus observed from a regime dominated by CB to another one in which the key role was played by the hybrid filler network. The presence of a continuous hybrid filler network was confirmed by TEM analysis.[86] The remarkable enhancement of material dynamic-mechanical properties led to comment a synergistic effect between the two fillers.[86] In fact, it was reported that the initial modulus values obtained with the hybrid CB-OMt filler system were much higher than those calculated by simply adding of the initial modulus values of composites with only CB or only OC.[10]

Dynamic-mechanical behaviour was investigated in the shear mode for nanocomposites based on IR and containing 60 phr of a furnace CB (N326) and various amounts of OC.[90] A pronounced Payne effect was detected, particularly at OC concentrations above the threshold required to have a change in the filler networking mode.

2.7 Properties of Isoprene Rubber/Nano-Graphite Nanocomposites

Nowadays, very few data are available for nanocomposites based on isoprene rubber and nano-G.[10,49] They essentially give information on the reinforcing ability of nano-G. Tensile measurements were taken on nanocomposites based on IR and containing an increasing amount of nano-G, from 1 to 60 phr. The percolation threshold of nano-G was calculated by applying the Huber–Vilgis model, as in the case of OC commented above. In the double logarithmic plot of the excess of initial modulus $(E - E_0)/E_0$ on nano-G content, two straight lines were identified, with slope 0.9 and 3.5, below and above the percolation threshold, found to be at 21.2 phr. The slope values are not far from the ones determined for CB (1 and 4) and the network formation occurs at a level not much lower than the one typical of CB (about 30 phr). In fact, it was shown that nano-G promotes higher reinforcement with respect to CB, but lower with respect to OC and CNT. However, nano-G does not require a sulfur-based vulcanization to express its reinforcing capability, as in the case of OC. Moreover, an interesting feature of nano-G is the ability to allow high

elongations at break for the nanocomposites, appreciably higher than for CB-based composites.

Hybrid nano-G/CB filler systems were prepared in IR as the matrix. In samples containing 60 phr of CB, a discontinuity was observed for the dependence of the excess of modulus on nano-G content, at about 6 phr as nano-G content, as if nano-G was able to establish a continuous network in the polymer matrix.

2.8 Properties of NR/CNT Nanocomposites

CNT, in NR, have effect on (i) vulcanization efficiency, (ii) mechanical properties, (iii) electrical properties and (iv) thermal properties.

2.8.1 Vulcanization Efficiency

The curing reaction rate of NR/CNT nanocomposites was found to be lower than that of pure NR, at the same temperature. The absorption of curatives on CNT was hypothesized to cause higher curing activation energy and lower reactivity.[61,104] As a consequence, the optimum cure time of NR increased. The absorption of curatives onto was also attributed to the presence on CNT surface of carboxylic acid groups and quinone oxygen atoms.

The scorch time, which is the measure of premature vulcanization, and the optimum cure of vulcanizates increased.[105]

The functionalization of CNT with TESPT led to the strong compatibilization with the rubber molecules, through the sulfur-based vulcanization.[64] This was confirmed by Raman spectra that showed shift of the D band to a higher wavenumber.

2.8.2 Mechanical Properties

Tensile measurements were taken in most cases to determine the mechanical properties of NR/CNT nanocomposites. Initial modulus, determined from stress–strain curves, was observed to remarkably increase with the filler content. At 1 wt%, the increase was 25.9%, compared to pure NR,[106] at 3, 5, 7 and 10 wt% the increase % was 142, 306, 680 and 850, respectively.[107] It was commented that the modulus increase is due to the hydrodynamic effect, further increased by the filler anisotropy, and by the presence of occluded rubber.[108] For composites with 37 wt% of CNT, the storage modulus was about three orders of magnitude higher than that of the pure rubber. CNT modification with resorcinol caused an increase in modulus at all CNT loadings, indicating improved filler–matrix adhesion.[109]

Initial modulus from stress–strain curves was as well used for determining the percolation threshold of CNT in IR.[110] Initial modulus values were elaborated through the Huber and Vilgis model,[88] reporting in a double logarithmic plot the excess of initial modulus $(E - E_0)/E_0$, versus the CNT content. Experimental data were interpolated with two different straight lines with slope 0.9 and 2.1, respectively, whose intersection gave the percolation threshold at

7.2 CNT phr. The discrepancy of the slope value with the one predicted by the model was interpreted with the peculiar shape of CNT.

Rapid decrease of E was observed with strain increase.[111] Pure NR and composites with a low CNT content (1 wt%) showed a moderate increase of stress up to about 75% strain, a sort of plateau up to 300% strain and a final more evident increase above 300%. Said increase could be due to rubber crystallization and to CNT alignment.[112] The stress-softening effect, known as Mullins effect, was observed at large strain and attributed to detachment of rubber molecules from the surface of filler particles.[106] The presence of CNT bundles (at 5, 7, 10 wt%) was commented to bring about a decrease of the stress.[113]

The tensile strength of the composites was found to linearly increase with CNT content,[111,106] up to 8.3 wt% as the maximum CNT content.[111] Composites with 5 wt% of CNT had a tensile strength approximately 300% higher compared to that of NR.[112] Tensile strength was increased four-fold with respect to neat NR and by 9% with respect to NR composites reinforced with the same level of CB.[62] Analogously, tensile strength was observed to achieve, at a CNT content of about 2 wt%, a maximum value that was about 50% more than that of pure NR.[63] CNT agglomeration occurred at higher CNT content, and led to a reduction in tensile strength. Tensile strength increased up to a maximum at about 5 phr of CNT content and then decreased.[107] At 1 and 3 wt% of CNT, the increment in tensile strength was higher than the one of the modulus whereas at 7 and 10 wt% the increment of the modulus was higher.[107] When CNTs were modified with octadecanoyl groups, tensile strength increased with the CNT loading, up to 10 phr.[114]

The elongation at break was found to increase with tensile strength, when CNTs were evenly dispersed thanks to modification with a paraffinic substituent.[114] A reduction in elongation at break was attributed to the restriction of molecular chain slipping on the CNT surface. NR/CNT nanocomposites with 5 wt% as CNT content showed a relatively low elongation at break (854%) compared to that of pure NR (945%)[65] when CNT was treated with PDDA (see Table 2.3) achieving an intimate interaction with the polymer. With CNT apparently untreated the increase in tensile strength brought about a reduction in elongation at break.[106] However, the contemporary decrease in tensile strength and elongation at break were attributed to poor interfacial interactions between CNT and the polymer matrix.[115]

The storage modulus determined from DMTA increased remarkably when CNT was added to the NR matrix: 33% increase was determined in the glassy region of the nanocomposite.[64] This result was obtained by grafting TESPT onto the CNT surface: TESPT functioned as a bridge with NR and brought to enhanced interface properties. It was assumed that the storage modulus increase was caused by the thicker interface. In the rubbery region, the modulus was about 1.8 times that of pure NR, similarly for CNT and silanized CNT. The increment of the elastic modulus in the rubbery state was observed to be quasi-linear and the increment slope was calculated of about 0.42 MPa/wt% at 300 K.[60] A strong interfacial bonding, achieved by treating CNT with hydrated silica, resorcinol and HMT, was found to promote a high storage modulus.[61]

The temperature corresponding to the maximum of tan delta was found to decrease when CNT concentration increased[111] and the height of tan delta peak, corresponding to the T_g of the elastomer, was reduced.[116] Glass transition temperature slightly increased from −61.3 °C for pristine NR to −59.8 °C for CNT filled sample[105] and marginally increased as well in the case of phenol functionalized CNT, remaining at about –62 °C.

A remarkable non-linear viscoelastic behaviour, known as the Payne effect was observed for NR/CNT nanocomposites. A sample with 10 phr of CNT displayed a great Payne effect.[7] It was reported that, below 3.8 wt% of CNT, the Payne effect was not observable.[108] It was reported as well a reduction of Payne effect for a composite with 9.1 wt% CNT, by increasing the temperature, from 298 K to 353 K. For this composite, the Payne effect was however much higher than for a composite with the same content of CB. It was commented that at this concentration CNT was above the percolation threshold. Remarkable Payne effect was observed also in IR based nanocomposites,[110] from strain sweep tests performed in the shear mode: it was noticed also below the percolation threshold of CNT (7.2 phr, see above) and it became much more evident above said threshold.

However, it was as well reported that the rebound resilience and the dynamic compression properties of the CNT/NR nanocomposites are better than that of CB-filled NR composites.[104]

Reinforcing effect by CNT was studied also in rubber blends. Blended latex of NR and SBR at dry wt ratio of 80/20 was reinforced with CNT in the range 0.1–0.4 phr and it was observed the increase of tensile strength, modulus at 300% strain and dynamic-mechanical properties, although in the presence of a reduction of elongation at break.[117]

2.8.2.1 *Hybrid CNT/CB Filler System*

Nanocomposites were prepared in IR with the hybrid filler system CB/CNT, with 60 phr of furnace CB N326 and various amounts of CNT (from 0 to 11 phr), determining a remarkable enhancement of the initial modulus values.[110] A change of the filler networking mode, at about 3 phr as CNT content, was observed, indicating a transition from a regime dominated by CB to another one in which the key role is played by the hybrid filler network. The presence of a continuous hybrid filler network was confirmed by TEM analysis. A synergistic effect between CB and CNT was commented, as the initial modulus values were much higher than those calculated through the simple addition of the initial modulus values of composites containing either only CB or only CNT.

CNT and CB dispersed in NR latex through ultrasonic assisted mixing process exhibited a synergistic reinforcing effect when co-coagulated, with a maximum of mechanical properties at 20 : 5 as CB/CNT weight ratio.[118]

Dynamic-mechanical properties were studied on the composites mentioned above, containing 60 phr of N326 CB and various amounts of CNT. Remarkable Payne effect was detected, particularly above the threshold of CNT concentration (3 phr as reported above) required to have a change in the filler networking mode.

2.8.3 Electrical Properties

The effect of CNT on electrical properties of the NR matrix becomes dramatic above the critical concentration required to establish a continuous CNT network, which means above the percolation threshold. An even CNT dispersion favours the achievement of the percolation threshold at low CNT content. However, conductivity occurs when CNT are not wrapped by insulating surfactants. In the case of composites from emulsion blending, in the presence of a homogeneous dispersion[112] the percolation threshold was achieved at 1–2 wt% and 2–3.5 wt% for CNT treated with sodium dodecyl sulfate (SDS) or only with the acid mixture, respectively. A decrease in electrical resistivity of seven orders of magnitude, with respect to neat NR, was observed for the sample that contains 10 wt% of CNT. In the case of composites from solution (toluene) blending, the resistivity was found to decrease abruptly by several orders of magnitude between 2.9 and 3.8 as CNT wt%, indicating the formation of a percolating network. Samples with 3.8 and 9.1 wt% of CB were not conductive.[108] The introduction of an octadecane group onto the CNT surface[114] led to an improved CNT dispersion. The drop of dielectric constant and the increase of dielectric loss were commented with the reduction of dipole–dipole interaction between nanotubes. When CNT/NR nanocomposites were prepared by solvent (toluene) mixing followed by two-roll compounding,[109] electrical resistivity was observed to remain unchanged even at 10 wt% as CNT content, when CNT were modified with resorcinol, in spite of the improved dispersion.

Composites prepared by melt blending revealed a transition change for the DC conductivity in a range from about 5 to about 8 phr as CNT content in IR[110] and in the range from 9 to 16 as CNT wt% in NR for the electrical volume resistance.[119] The electrical volume resistance of the composites was observed to dramatically drop (over 13 orders of magnitude) at a CNT concentration of 30 wt%.[119]

The DC conductivity of samples with the hybrid CB–CNT filler system[110] (with 60 phr as furnace CB, N326) was observed to be much higher than the one with CNT alone, monotonously increasing with the CNT content, without any discontinuity, as instead observed for the excess of initial modulus. NR based nanocomposites with 50 phr of furnace CB and CNT content from 1 to 5 phr[120] revealed specific absorbing properties of the nanocomposites, mainly coefficients of absorption and reflection of the electromagnetic waves and electromagnetic interference shielding effectiveness.

2.8.4 Thermal Properties

2.8.4.1 Degradation of NR/CNT Nanocomposites

The thermal stability of NR/CNT nanocomposites was evaluated through thermogravimetric analysis (TGA). The degradation curve of the NR/CNT nanocomposites showed a slight shift to higher temperature[63] and it was reported that the NR degradation occurs more slowly in the presence of CNT,[112] as indicated by the greater full-width at half-height of the calorimetric curves.

To explain the shift of rapid degradation region towards higher temperature, it was commented[104] that CNTs promote homogeneous heat conductivity, avoiding heat concentration.

The improved aging resistance of the NR/CNT nanocomposites was interpreted with the migration of the inorganic particles to the surface, at elevated temperatures, because of their relatively low surface potential energy.[63]

2.8.4.2 Thermal Conductivity

It was commented that the addition of CNT could improve thermal conductivity of the NR material because the thermal conductivity of CNTs is more than 10^4 times greater than that of polymer materials.[62]

2.9 Nano-silica

2.9.1 Sol–Gel Process for the *in situ* Generation of Silica

The generation of silica *in situ*, in the polymer matrix, has been performed by using the sol–gel process.[11] The typical aqueous sol–gel process[121] consists of the hydrolysis of metal alkoxides M(OR)x followed by condensation reaction. Reactions involved to prepare silica through the sol–gel process are reported as follows:

hydrolysis

$$Si(OR)_4 + nH_2O \rightarrow Si(OR)_{4-x} + 4ROH$$

water condensation

$$\equiv Si{-}OH + HO{-}Si\equiv \rightarrow + H_2O$$

alcohol condensation

$$\equiv Si{-}OR + HO{-}Si\equiv \rightarrow \equiv Si{-}O{-}Si\equiv + ROH$$

To prepare silica from sol–gel process, tetraethoxysilane (TEOS) is preferentially used.

When a polymer is present in the reaction environment, organic–inorganic hybrids are formed: spherical or quasi-spherical silica particles are obtained, with dimensions from few nanometres to submicron dimension, carrying out the so-called bottom-up preparation of nanofillers. Nanocomposites are thus formed with an intimate mixture of organic and inorganic phases.

Synthetic procedures adopted to prepare hybrid nanocomposites with nano-silica particles can be summarized as follows.

Solution procedure: (i) metal alkoxide and the rubber are dissolved in a common solvent (ii) water, sol–gel catalyst and vulcanization ingredients are added (iii) sol–gel process is performed, at given temperature and time (iv)

solvents and by-products are removed, by evaporation or precipitation (v) vulcanization is finally carried out.

Swelling procedure: *swelling of unvulcanized rubber:* (i) rubber is swollen in metal alkoxide (ii) swollen rubber is soaked in the sol gel catalyst solution (iii) sol–gel process is performed, at given temperature and time (iv) vulcanization ingredients are added through melt blending (v).

Swelling procedure: *swelling of vulcanized rubber:* this procedure is analogous to the previous one, obviously without step (iv).

The solution process is the preferred one to have a highly homogeneous dispersion of silica nanoparticles in the rubber matrix.

Drawbacks of the sol–gel *in situ* preparation of silica nanoparticles clearly appear from the reactions, reported above, involved in the process. They are the following: (i) the use of a large amount of chemicals (ii) the release of large amount of alcohols, such as for example ethanol.

2.9.2 Nanocomposites with *in situ* Silica

Nanocomposites with silica nanoparticles have been prepared in poly-dimethylsiloxanes, butadiene, styrene-butadiene, acrylonitrile-butadiene, acrylic and ethylene-propylene diene rubber. Nanocomposites in isoprene rubbers are here examined. In a nutshell, these nanocomposites were prepared adopting the three methods summarized above and nano-silica was reported to promote the mechanical reinforcement of poly (isoprene) matrices, less that CB but more than conventional silica, with lower viscosity.

NR based nanocomposites. Nanocomposites were prepared in NR with a content of silica formed *in situ* up to 21 phr.[122,123] Both the solution procedure and the swelling in vulcanized rubber were adopted. A significant reinforcing effect, due to the *in situ* generated silica, was shown by stress–strain curves, and stress values were found to be higher than those predicted by the Guth and Gold equation, allowing us to hypothesize the presence of filler–rubber interactions. Aggregation of silica particles *via* silanol groups was observed when this synthetic procedure was used and was, conversely, avoided when the procedure implying the swelling of vulcanized rubber was adopted.

The viscosity of composites with silica content from 10 to 70 phr, prepared with the solution procedure with an amine as catalyst, was found to increase with the silica content, being however lower than the viscosity of composites containing nanostructured silica.[124,125] This difference, attributed to the lower amount of silanols on the surface of *in situ* generated silica, could be also attributed to the lower structure of *in situ* silica, that means to the absence of occluded rubber. The *f* shape factor of the Guth equation (Equation (2.1)) was calculated to be 2.53.

By performing the formation of silica in swollen uncrosslinked NR,[126,127] modulus at low and high strains were found to be higher and lower, respectively, than those of composites containing conventional silica. These findings were attributed to the presence of larger agglomerates of conventional silica at low strain and to the better dispersion on *in situ* silica in the NR matrix, with a stronger interaction with polymer chains.

The reinforcement due to *in situ* silica was found to be in between that achieved with conventional silica (lower) and CB (higher).[128]

In situ silica was as well formed in NR latex, observing better tensile and tear properties with respect to composites prepared with conventional mechanical mixing, with better results in the presence of a coupling agent such as TESPT.[129,130] Improved reinforcement effect by *in situ* silica was observed when γ-propyltrimethoxysilane was added.

ENR based nanocomposites. ENR was used to prepare *in situ* silica adopting the solution procedure[131,132] and chemical interactions between silica and the rubber were demonstrated by IR spectroscopy and by the insolubility of the rubber samples. Significant improvement in mechanical properties with increased TEOS loading were observed.

IR based nanocomposites. *In situ* silica was prepared in IR with the solution process.[133] Swelling experiments evidenced good polymer–filler adhesion, in the presence of coupling agents. The dynamic-mechanical behaviour was found to be increasingly non-linear for silica contents higher than 20 wt%.

2.10 Nano Metal Oxides

Nano zinc oxide. Zinc oxide (ZnO) nanoparticles were used as curing activators, with the aim to improve the performances of conventional ZnO. Nano ZnO was synthesized by homogeneous precipitation and calcination method preparing nanoparticles with an average diameter of about of 50 nm.[134] These nanoparticles were found to be more uniformly dispersed in NR (and also in NBR) based compounds with respect to conventional ZnO and led to the increase of the maximum torque value. The tensile strength was enhanced by 80% with ZnO nanoparticles and the glass transition temperature (T_g) showed a shift to higher temperatures, as a consequence of the increase of crosslinking density. In line with these observations, the swelling ratio decreased and the volume fraction of rubber in swollen gel increased.

Nano magnesium hydroxide and magnesium oxide. In recent years, increasing attention has been paid to nanocrystalline magnesium hydroxide (MH) as a flame retardant filler.[4,135] Specific morphologies, such as nanoneedles and nanolamellas, have been developed and they could be used as reinforcing agents or halogen-free flame retardants. Moreover, MH nanorods can be used as precursors for the synthesis of MgO nanorods,[136] which are expected to give novel mechanical, catalytic and electronic properties in consideration of the extremely small sizes, large anisotropy and perfect crystallinity. Examples in isoprene rubbers are not yet available.

2.11 Nano Calcium Carbonate

Micron-sized calcium carbonate ($CaCO_3$) has been used for long time to lower the cost of polymers. In fact, due its low surface area and low surface activity, it does not act as reinforcing filler. The interest for nano-$CaCO_3$ is thus due to its relatively high surface area, higher than 40 m^2/g (as BET surface area), that

allows to establish a larger interfacial area with the polymer. Moreover, nano-$CaCO_3$ is the cheapest commercially available nanofiller.

Nano-$CaCO_3$ was prepared by *in situ* deposition: water solutions of polyethylene glycol and of calcium chloride were first mixed, then calcium carbonate was added and, after a digestion of 12 hours, nano-$CaCO_3$ was isolated by filtration, washing and drying.[137]

Composites with butadiene based rubbers. This type of nano-$CaCO_3$ was added to butadiene rubber,[137] observing improvement of elongation at break and tear strength and a reduction of rate of burning, with respect to the composites with micron-sized $CaCO_3$.[137] When added to SBR,[138] this type of nano-$CaCO_3$ gave higher glass transition temperature, better flame retardancy and higher values of Young's modulus, tensile strength and elongation at break, particularly when nano-$CaCO_3$ with the smallest size (9 nm) was used. Precipitated nano-sized calcium carbonate is often coated with stearic acid to increase its dispersion in the polymer matrix. Thermal stability, tear strength and mechanical interfacial properties of BR were improved when nano-$CaCO_3$[139] with about 3 wt% of stearic acid on its surface was added.

Composites with NR. nano-$CaCO_3$ coated with some chemical reagents (among them phosphatidates) was added to NR latex before sulfuration[140] achieving a homogeneous dispersion. The thermo-oxidative aging resistance of the composites was significantly improved and better tear strength and elongation at break were observed.

2.12 Nano Carbon Black

In the previous paragraphs, carbon nanofillers such as nanotubes and graphite nanoparticles were examined. An intriguing carbon nanofiller is undoubtedly nano-CB. A preliminary crucial aspect is to define the meaning of nano-CB. By considering the diameter of primary particle, most carbon blacks could be classified as nano-CB,[84] as it is shown in Table 2.7. In fact, as mentioned in the Introduction, according to the acknowledged definition, a nanoparticle should have at least one dimension "of the order of 100 nm or less".[1] However, it was

Table 2.7 ASTM numbers and primary particle diameters of carbon blacks.

ASTM numbers	*Primary particle diameter (nm)*
900–999	201–500
800–899	101–200
700–799	61–100
600–699	49–60
500–599	40–48
400–499	31–39
300–399	26–30
200–299	20–25
100–199	11–19
000–099	1–10

also mentioned that fillers are considered to be 'nano' essentially when they can be dispersed as individual particles in the polymer matrix. In the case of nano-CBs of Table 2.7 they are present in the polymer matrix as aggregates, that can be however of dimensions lower than 100 nm.

CB of Table 2.7 are largely applied for important applications such as the one for tyre: thus, are largely applied in polyisoprene matrices. However, only few scientific investigations on nano-CB, particularly those with the lowest sizes of primary particles, are available. Conductive CB were in particular investigated. CB with high conductivity (Printex XE2, Degussa), with a primary particle diameter of about 30 nm, was used, at 10 phr level, in polyisoprene matrix,[141] observing a strong reversible tensoresistive effect of electrical resistance, by applying an uniaxial tension deformation. CB with larger size of primary particle such as N326 from Cabot was used in IR, also in the presence of other nanofillers such as clays, CNT and nano-G. As reported in Section 2.6.4.1 for the CB/OC filler systems and in Section 2.8.2.1 for the CB/CNT filler systems, CB is able to form hybrid networks with the nanofillers. It was also observed that this type of CB achieved the percolation threshold in the neat IR matrix at a content of about 30 phr, appreciably higher than the one observed for nanofillers: 5.9 phr for OC, 7.2 phr for CNT. This finding seems to indicate that the dispersion of nanofillers as individual particles actually plays a key role.

A synergistic effect was also found between clay and CB N330 from Cabot, in NR based nanocomposites prepared by emulsion compounding.[142] It was observed that both fillers were dispersed at nanoscale and randomly in the NR matrix: the space between the clay layers was filled with CB particles. The mechanical properties of the nanocomposites, such as moduli at 100% and 300% elongation, tensile strength and tear strength were much improved, at the same total filler level, by the hybrid filler system, with respect to composites containing only one filler.

References

1. British Standards Institute. *Vocabulary. Nanoparticles*, PAS 71:2005 [withdrawn].
2. M. Galimberti (ed.), *Rubber-Clay Nanocomposites: Science, Technology, Applications*, Wiley and Sons, New York, 2011, p. 601.
3. F. A. Bergaya, *Microporous Mesoporous. Mater.*, 2008, **107**, 141.
4. M. Maiti, M. Bhattacharya and A. K. Bhowmick, *Rubber Chem. Technol.*, 2008, **81**, 384.
5. B. Chen, J. R. G. Evans, H. C. Greenwell, P. Boulet, P. V. Coveney, A. A. Bowden and A. Whiting, *Chem. Soc. Rev.*, 2008, **37**, 568.
6. S. S. Ray and M. Okamoto, *Prog. Polym. Sci.*, 2003, **28**, 1539.
7. L. Bokobza, *Polymers*, 2007, **48**, 4907.
8. K. S. Novoselov, A. K. Geim, S. V. Morozov, D. Jiang, Y. Zhang, S. V. Dubonos, I. V. Grigorieva and A. A. Firsov, *Science*, 2004, **306**, 666.
9. B. Li and W.-H. Zhong, *J. Mater. Sci.*, 2011, **46**, 5595.

10. M. Galimberti, M. Coombs, V. Cipolletti, L. Giannini, L. Conzatti, T. Riccò, M. Mauro and G. Guerra, in *ACS Rubber Division - Proceedings of the Fall 180th Technical Meeting*, Session A: Advances in Materials and Tire Technology, Cleveland, Ohio, 11–13 October, 2011.
11. M. Messori, in *Recent Advances in Elastomeric Nanocomposites*, ed. V. Mittal, J. K. Kim and K. Pal, Springer-Verlag, Berlin Heidelberg, 2011, pp. 57–88.
12. M. Galimberti, V. Cipolletti and M. Coombs, in *Handbook of Clay Science*, 2nd ed., Part B: Techniques and Applications, eds. F. Bergaya and G. Lagaly, Elsevier, Amsterdam, 2013, Chapter 4.4., in press.
13. F. Bergaya, M. Jaber and J.-F. Lambert, in *Rubber-Clay Nanocomposites: Science, Technology, Applications*, ed. M. Galimberti, Wiley and Sons, New York, 2011, pp. 3–44.
14. F. Bergaya, M. Jaber and J.-F. Lambert, in *Rubber-Clay Nanocomposites: Science, Technology, Applications*, ed. M. Galimberti, Wiley and Sons, New York, 2011, pp. 45–86.
15. Y. Xi, Z. Ding, H. Heb and R. L. Frost, *Spectrochim. Acta, Part A*, 2005, **61**, 515.
16. R. A. Vaia, R. K. Teukolsky and E. P. Giannelis, *Chem. Mater.*, 1994, **6**, 1017.
17. H. Heinz, R. A. Vaia, R. Krishnamoorti and B. L. Farmer, *Chem. Mater.*, 2007, **19**, 59.
18. M. A. Osman, M. Ernst, B. H. Meier and U. W. Suter, *J. Phys. Chem. B*, 2002, **106**, 653.
19. M. A. Osman, M. Ploetze and P. Skrabal, *J. Phys. Chem. B*, 2004, **108**, 2580.
20. X. Yang, L. Li, S. Shang and X. Tao, *Polymer*, 2010, **51**, 3431.
21. Z. P. Sun, D. Popa, T. Hasan, F. Torrisi, F. Q. Wang, E. J. R. Kelleher, J. C. Travers, V. Nicolosi and A. C. Ferrari, *Nano Res.*, 2010, **3**(9), 653.
22. R. Zboril, F. Karlicky, A. B. Bourlinos, T. A. Steriotes, A. K. Stubos, V. Georgakilas, K. Saferova, D. Jancik, C. Trapalis and M. Otyepka, *Small*, 2010, **6**, 2885.
23. M. Mauro, V. Cipolletti, M. Galimberti, P. Longo and G. Guerra, *J. Phys. Chem. C*, 2012, **116**, 24809.
24. M. S. Dresselhaus, A. Jorio, M. Hofmann, G. Dresselhaus and R. Saito, *Nano Lett.*, 2010, **10**, 751.
25. A. Jorio, M. A. Pimenta, A. G. Souza Filho, R. Saito, G. Dresselhaus and M. S. Dresselhaus, *New J. Phys.*, 2003, **5**, 139/1.
26. R. Graupner, *J. Raman Spectrosc.*, 2007, **38**, 673.
27. A. Cuesta, P. Dhamelincourt, J. Laureyns, A. Martínez-Alonso and J. M. D. Tascón, *Carbon*, 1994, **32**, 1523.
28. A. M. Rao, J. Chen, E. Richter, U. Schlecht, P. C. Eklund, R. C. Haddon, U. D. Venkateswaran, Y.-K. Kwon and D. Tománek, *Phys. Rev. Lett.*, 2001, **86**, 3895.
29. C. Thomsen and S. Reich, *Phys. Rev. Lett.*, 2000, **85**, 5214.

30. S. D. M. Brown, A. Jorio, M. S. Dresselhaus and G. Dresselhaus, *Phys. Rev. B*, 2001, **64**, 073403.
31. A. K. Sood, R. Gupta and S. A. Asher, *J. Appl. Phys.*, 2001, **90**, 4494.
32. N. G. Sahoo, S. Rana, J. W. Cho, L. Li and S. H. Chan, *Prog. Polym. Sci.*, 2010, **35**, 837.
33. C.-M. Chang and Y.-L. Liu, *Carbon*, 2010, **48**, 1289.
34. N. Karousis, N. Tagmatarchis and D. Tasis, *Chem. Rev.*, 2010, **110**, 5366.
35. P.-C. Maa, N. A. Siddiqui, G. Marom and J.-K. Kim, *Composites, Part A*, 2010, **41**, 1345.
36. P. Singh, S. Campidelli, S. Giordani, D. Bonifazi, A. Biancoa and M. Prato, *Chem. Soc. Rev.*, 2009, **38**, 2214.
37. H. Fairbrother, B. Smith, J. Yang, J. Bitter, D. Goodwin, K. Marsh, Bouwer and B. Bill, in *244th ACS National Meeting & Exposition*, Philadelphia, PA, 19–23 August 2012, ENVR-342.
38. K. A. Wepasnick, B. A. Smith, J. L. Bitter and D. H. Fairbrother, *Anal. Bioanal. Chem.*, 2010, **396**, 1003.
39. T. I. T. Okpalugo, P. Papakonstantinou, H. Murphy, J. McLaughlin and N. M. D. Brown, *Carbon*, 2004, **43**, 153.
40. Y. L. Lu and L. Q. Zhang, in *Rubber-Clay Nanocomposites: Science, Technology, Applications*, ed. M. Galimberti, Wiley and Sons, New York, 2011, pp. 147–179.
41. M. Galimberti, V. Cipolletti and S. Giudice, in *Rubber-Clay Nanocomposites: Science, Technology, Applications*, ed. M. Galimberti, Wiley and Sons, New York, 2011, pp. 181–240.
42. B. Chuong, D. V. Hung, T. T. T. Huong, D. T. Y Oanh and T. T. P. Hoa, *Kautsch. Gummi Kunstst.*, 2012, **65**, 30.
43. L. Conzatti, P. Stagnaro, G. Colucci, R. Bongiovanni, A. Priola, A. Lostritto and M. Galimberti, *Appl. Clay Sci.*, 2012, **61**, 14.
44. A. A. Yehia, A. M. Akelah, A. Rehab, S. H. El-Sabbagh, D. E. El Nashar and A. A. Koriem, *Mater. Des.*, 2012, **33**, 11.
45. S. Rooj, A. Das, K. W. Stoeckelhuber, U. Reuter and G. I. Heinrich, *Macromol. Mater. Eng*, 2012, **297**, 369.
46. M. Galimberti, S. Giudice, V. Cipolletti and G. Guerra, *Polym. Adv. Technol.*, 2010, **21**, 679.
47. M. Galimberti, S. Senatore, L. Conzatti, G. Costa, G. Giuliano and G. Guerra, *Polym. Adv. Technol.*, 2009, **20**, 135.
48. D. J. Lowe, A. V. Chapman, S. Cook and J. C. Busfield, *Macromol. Mater. Eng.*, 2011, **296**, 693.
49. M. Galimberti, M. Coombs, V. Cipolletti, L. Giannini, T. Riccò, S. Pandini, L. Conzatti, M. Mauro and G. Guerra, in *ACS Rubber Division – Proceedings of the 181th Technical Meeting*, Session: Nanocomposites, San Antonio (TX), Apr. 22–25, 2012.
50. L. Bokobza and J. Zhang, *eXPRESS Polym. Lett.*, 2012, **6–7**, 601.
51. M. Galimberti, *Rubber Clay Nanocomposites*, *Advanced Elastomers – Technology, Properties and Applications*, ed: A. Boczkowska, Ch. 4,

http://dx.doi.org/10.5772/51410, http://www.intechopen.com/articles/show/title/rubber-clay-nanocomposites.
52. M. Galimberti, S. Giudice, V. Cipolletti and G. Guerra, *Polym. Adv. Technol.*, 2010, **21**, 679.
53. M. Galimberti, S. Senatore, L. Conzatti, G. Costa, G. Giuliano and G. Guerra, *Polym. Adv. Technol.*, 2009, **20**, 135.
54. M. Galimberti, A. Lostritto, A. Spatola and G. Guerra, *Chem. Mater.*, 2007, **19**, 2495.
55. Y. Ma, Q.-F. Li, L.-Q. Zhang and Y.-P. Wu, *Polymer*, 2007, **39**, 48.
56. S. Rooj, A. Das, K. W. Stoeckelhuber, De-Yi Wang, V. Galiatsatos and G. Heinrich, *Soft Matter*, 2013, **9**, 3798.
57. S. Rooj, A. Das, K. W. Stoeckelhuber, N. Mukhopadhyay, A. R. Bhattacharyya, D. Jehnichen and G. Heinrich, *Appl. Clay Sci.*, 2012, **67**, 50.
58. S. Rooj, A. Das, K. W. Stöckelhuber, U. Reuter and G. Heinrich, *Macromol. Mater. Eng.*, 2011, **297**, 369.
59. Z. Peng, C. Feng, Y. Luo, Y. Li and L. X. Kong, *Carbon*, 2010, **48**, 4497.
60. H. X. Jiang, Q. Q. Ni and T. Natsuki, *Adv. Mater. Res.*, 2009, **79-82**, 417.
61. G. Sui, W. H. Zhong, X. P. Yang, Y. H. Yu and S. H. Zhao, *Mater. Sci. Eng.*, 2008, **A485**, 524.
62. G. Sui, W. Zhong, X. Yang and S. Zhao, *Macromol. Mater. Eng.*, 2007, **292**, 1020.
63. Z. Peng, C. Feng, Y. Luo, Y. Li, Z. Yi and L. X. Kong, *J. Appl. Polym. Sci.*, 2012, **125**, 3920.
64. H. X. Jiang, Q. Q. Ni and T. Natsuki, *Polym. Compos.*, 2011, **32**(2), 236.
65. P. M. Ajayan, L. S. Schadler, C. Giannaris and A. Rubio, *Adv. Mater.*, 2000, **12**, 750.
66. V. G. Hadjiev, M. N. Iliev, S. Arepalli, P. Nikolaev and B. S. Files, *Appl. Phys. Lett.*, 2001, **78**, 3193.
67. L. Bokobza, *J. Inorg. Organomet. Polym. Mater.*, 2012, **22**, 629.
68. M. A. López-Manchado, J. Biagiotti, L. Valentini and J. M. Kenny, *J. Appl. Polym. Sci.*, 2004, **92**, 3394.
69. A. A. Azira, D. H. A. Hassim, A. B. Suriani and M. M. Rusop, *Nano Hybrids*, 2012, **1**, 81.
70. C. Nah, J. Y. Lim, B. H. Cho, C. K. Hong and A. N. Gent, *J. Appl. Polym. Sci.*, 2010, **118**, 1574.
71. J. R. Austin and M. Kontopoulou, *Polym. Eng. Sci.*, 2006, **46**, 1491.
72. H. S. Jeon, J. K. Rameshwaram and G. Kim, *J. Polym. Sci., Part B: Polym. Phys.*, 2004, **42**, 1000.
73. H. S. Jeon, J. K. Rameshwaram, G. Kim and D. H. Weinkauf, *Polymer*, 2003, **44**, 5749.
74. Y. T. Vu, J. E. Mark, L. H. Pham and M. J. Engelhardt, *Appl. Polym. Sci.*, 2001, **82**, 1391.
75. M. Tian, C. Qu., Y. Feng and J. Zhang, *J. Mater. Sci.*, 2003, **38**, 4917.
76. S. Sadhu and A. K. Bhowmick, *J. Polym. Sci., Part B: Polym. Phys.*, 2005, **43**, 1854.

77. M. Maiti, M. Bhattacharya and A. K. Bhowmick, *Rubber Chem. Technol.*, 2008, **81**, 384.
78. R. Stephen, R. Alex, T. Cherian, S. Varghese, K. Joseph and S. J. Thomas, *Appl. Polym. Sci.*, 2006, **101**, 2355.
79. R. Verdejo, M. Hernandez, N. Bitinis, J. M. Kenny and M. A. Lopez-Manchado, in *Rubber-Clay Nanocomposites: Science, Technology, Applications*, ed. M. Galimberti, Wiley and Sons, New York, 2011, pp. 275–303.
80. L. Giannini, A. Citterio and M. Galimberti, in *Rubber-Clay Nanocomposites: Science, Technology, Applications*, ed. M. Galimberti, Wiley and Sons, New York, 2011, pp. 127–144.
81. F. Avalos, J. C. Ortiz, R. Zitzumbo, M. A. López-Manchado, R. Verdejo and M. Arroyo, *Eur. Polym. J.*, 2008, **44**, 3108.
82. S. Takahashi, H. A. Goldberg, C. A. Feeney, D. P. Karim, M. Farrell, K. O'Leary and D. R. Paul, *Polymer*, 2006, **47**, 3083.
83. D. R. Paul and L. M. Robeson, *Polym. Nanotech.: Nanocomp. Polym.*, 2008, **49**, 3187.
84. J. B. Donnet and E. Custodero, in *The Science and Technology of Rubber*, ed. J. E. Mark, B. Erman and F. R. Eirich, Elsevier Academic Press, Amsterdam, 3rd edn, 2005, p. 367.
85. Y. Wu, Q. Jia, D. Yu and L. Zhang, *Polym. Test.*, 2004, **23**, 903.
86. M. Galimberti, M. Coombs, V. Cipolletti, P. Riccio, T. Riccò, S. Pandini and L. Conzatti, *Appl. Clay Sci.*, 2012, **65–66**, 57.
87. G. Ramorino, F. Bignotti, S. Pandini and T. Riccò, *Compos. Sci. Technol.*, 2009, **69**, 1206.
88. G. Huber and T. A. Vilgis, *Kautsch. Gummi Kunstst.*, 1999, **52**, 102.
89. A. R. Payne, *J. Appl. Polym. Sci.*, 1962, **21**, 368.
90. G. Ramorino, F. Bignotti, L. Conzatti and T. Riccò, *Polym. Eng. Sci.*, 2007, **47**, 1650.
91. M. Galimberti, S. Senatore, A. Lostritto, L. Giannini, L. Conzatti, G. Costa and G. Guerra, *e-Polymers*, 2009, **57**, 1.
92. M. A. Osman., M. Ploetze and P. Skrabal, *J. Phys. Chem. B*, 2004, **108**, 2580.
93. M. Galimberti, S. Giudice, V. Cipolletti and G. Guerra, *Polymer*, 2010, **21-47**, 672.
94. L. F. Valadares, C. A. P. Leite and F. Galembeck, *Polymer*, 2006, **47**, 672.
95. Y. Wu, Y. Wang, H. Zhang, Y. Wang, D. Yu, L. Zhang and J. Yang, *Compos. Sci. Technol.*, 2005, **65**, 1195.
96. J. Hrachová, P. Komadel and I. Chodák, *J. Mater. Sci.*, 2008, **43**, 2012.
97. P. L. Teh, M. Z. A. Ishak, A. S. Hashim and J. Karger-Kocsis, *Eur. Polym. J.*, 2004, **40**, 2513.
98. M. Arroyo, M. A. Lopez-Manchado and B. Herrero, *Polymer*, 2003, **44**, 2447.
99. B. Jurkowska, B. Jurkowski, M. Oczkowski, S. S. Pesetskii, V. Koval and Y. A. Olkhov, *J. Appl. Polym. Sci.*, 2007, **106**, 360.

100. M. Galimberti, L. Giannini, F. D'Oria, A. Lostritto, T. Ponta, P. Riccio and S. Senatore, in *ACS Rubber Division – Proceedings of the Fall 174th Technical Meeting*, Louisville, KY (USA), October 14–16, 2008.
101. M. Galimberti, S. Giudice, M. Coombs, L. Giannini, A. Buttafava, D. Dondi, A. Faucitano, S. Pandini, T. Riccò, S. Bracco, A. Cattaneo, P. Sozzani, L. Conzatti and V. Cipolletti, in *ACS Rubber Division – Proceedings of the Fall 178th Technical Meeting*, Milwaukee (WI) October, 12–14, 2010.
102. F. Cataldo, *Macromol. Symp.*, 2007, **247**, 67.
103. P. K. Chattopadhyay, N. C. Das and S. Chattopadhyay, *Composites, Part A*, 2011, **42**, 1049.
104. G. Sui, W. H. Zhong, X. P. Yang, Y. H. Yu and S. H. Zhao, *Polym. Adv. Technol.*, 2008, **19**, 1543.
105. A. M. Shanmugharaj, J. H. Bae, K. Y. Lee, W. H. Noh, S. H. Lee and S. H. Ryu, *Compos. Sci. Technol.*, 2007, **67**, 1813.
106. C. Nah, J. Y. Lim, B. H. Cho, C. K. Hong and A. N. Gent, *J. Appl. Polym. Sci.*, 2010, **118**, 1574.
107. A. Fakhru'l-Razi, M. A. Atieh, N. Girun, T. G. Chuah, M. El-Sadig and D. R. A. Biak, *Compos. Struct.*, 2006, **75**, 496.
108. L. Bokobza and M. Kolodziej, *Polym. Int.*, 2006, **55**, 1090.
109. P. S. Thomas, A. A. Abdullateef, M. A. Al-Harthi, A. A. Basfar, S. Bandyopadhyay, M. A. Atieh and S. K. De, *J. Appl. Polym. Sci.*, 2012, **124**, 2370.
110. M. Galimberti, M. Coombs, P. Riccio, T. Riccò, S. Passera, S. Pandini, L. Conzatti, A. Ravasio and I. Tritto, *Macromol. Mater. Eng.*, 2012, **298**, 241.
111. S. Kohjiya, A. Kato and Y. Ikeda, *Carbon*, 2008, **46**, 1037.
112. C. F. Matos, F. Galembeck and A. J. G. Zarbin, *Carbon*, 2012, **50**, 4685.
113. A. A. Aziz, D. H. A. Hassim, A. B. Suriani and M. R. Mahmood, *Nano Hybrids*, 2012, **1**, 81.
114. P. S. Thomas, A. A. Abdullateef, M. A. Al-Harthi, M. A. Atieh, S. K. De, M. Rahaman, T. K. Chaki, D. Khastgir and S. Bandyopadhyay, *J. Mater. Sci.*, 2012, **47**, 3344.
115. T. McNally, P. Poetschke, P. Halley, M. Murphy, D. Martin, S. E. J. Bell, G. P. Brennan, D. Bein, P. Lemoine and J. P. Quinn, *Polymer*, 2005, **46**, 8222.
116. M. A. Lopez-Manchado, J. Biagiotti, L. Valentini and J. M. Kenny, *J. Appl. Polym. Sci.*, 2004, **92**, 3394.
117. A. Boonmahitthisud and S. Chuayjuljit, *Adv. Mater. Res. (Durnten-Zurich, Switz.)*, 2012, **347**, 3197.
118. Y. H. Zhan, G. Q. Liu, H. S. Xia and N. Yan, *Plast., Rubber Compos.*, 2011, **40**, 32.
119. F. Deng, M. Ito, T. Noguchi, L. Wang, H. Ueki, K. Niihara, Y. A. Kim, M. Endo and Q. S. Zheng, *ACS Nano*, 2011, **5**, 3858.

120. O. A. Al-Hartomy, A. A. Al-Ghamdi, F. Al-Salamy, N. Dishovsky, R. Shtarkova, V. Iliev and F. El-Tantawy, *Plast., Rubber Compos.*, 2012, **41**, 408.
121. C. Brinker, G. Scherer, *Sol–Gel Science: The Physics and Chemistry of Sol–Gel Processing*, Academic Press, Boston, 1990.
122. L. Bokobza and J. P. Chauvin, *Polymer*, 2005, **46**, 4144.
123. L. Bokobza, *Compos. Interfaces*, 2006, **13**, 345.
124. S. Poompradub, B. Chaichua, C. Kanchanaamporn, T. Boosalee and P. Prasassarakich, *Kautschuk Gummi und Kunststoffe*, 2008, **61**, 152.
125. B. Chaichua, P. Prasassarakich and S. Poompradub, *J. Sol–Gel Sci. Technol.*, 2009, **52**, 219.
126. Y. Ikeda, S. Poompradub, Y. Morita and S. Kohjiya, *J. Sol–Gel Sci. Technol.*, 2008, **45**, 299.
127. Y. Ikeda and Y. Kameda, *J. Sol–Gel Sci. Technol.*, 2004, **31**, 137.
128. K. Murakami, S. Iio, T. Tanahashi, S. Kohjiya, K. Kajiwara and K. Ikeda, *Kautsch. Gummi Kunstst.*, 2001, **54**, 668.
129. V. Tangpasuthadol, A. Intasiri, D. Nuntivanich, N. Niyompanich and S. Kiatkamjornwong, *J. Appl. Polym. Sci.*, 2008, **109**, 424.
130. J. Siramanont, V. Tangpasuthadol, A. Intasiri, N. Na-Ranong and S. Kiatkamjornwong, *Polym. Eng. Sci.*, 2009, **49**, 1099.
131. A. Bandyopadhyay, M. De Sarkar and A. K. Bhowmick, *Rubber Chem. Technol.*, 2004, **77**, 830.
132. A. Bandyopadhyay, M. Maiti and A. K. Bhowmick, *Mater. Sci. Technol.*, 2006, **22**, 818.
133. M. Messori, F. Bignotti, R. De Santis and R. Taurino, *Polym. Int.*, 2009, **58**, 880.
134. S. Sahoo, M. Maiti, A. Ganguly, J. J. George and A. K. Bhowmick, *J. Appl. Polym. Sci.*, 2007, **105**, 2407.
135. D. An, X. Ding, Z. Wang and Y. Liu, *Colloids Surf., A*, 2010, **356**, 28.
136. M. McKelvy, R. Sharma, A. G. Chizmeshya, R. W. Carpenter and K. Streib, *Chem. Mater.*, 2001, **13**, 921.
137. S. Mishra, S. H. Sonawane, N. Badgujar, K. Gurav and D. Patil, *J. Appl. Polym. Sci.*, 2005, **96**, 6.
138. S. Mishra, N. G. Shimpi and U. D. Patil, *J. Polym. Res.*, 2007, **14**, 449.
139. F. L. Jin and S. J. Park, *Mater. Sci. Eng.*, 2008, **A478**, 406.
140. C.-M. Deng, M. Chen, N.-J. Ao, D. Yan and Z.-Q. Zheng, *J. Appl. Polym. Sci.*, 2006, **101**, 3442.
141. S. Varghese (for Rubber Research Institute of India), Indian Patent Appl. IN2005CH00562 A, 2007.
142. Q. Jia, Y. Wu, X. Ping, Y. Xin, Y. Wang and L. Zhang, *Polym. Polym. Compos.*, 2005, **13**, 709.

CHAPTER 3

Theory and Mechanisms of Filler Reinforcement in Natural Rubber

AZEMI BIN SAMSURI

Department of Polymer Technology, Faculty of Applied Sciences, Universiti Teknologi MARA, 40450 Shah Alam, Selangor, Malaysia
Email: azemi.sam@gmail.com; azemi@salam.uitm.edu.my

3.1 A General Introduction to Fillers

Vulcanized rubber, which contains ingredients necessary for the vulcanization process, is called unfilled or gum vulcanizate. Gum mix rubber compounds generally show poor processing characteristics such as giving high extrudate swell and high calender shrinkage. Pure natural rubber (NR) vulcanizates, although high in physical strength, are suitable for relatively few commercial applications, mainly dipped latex goods such as condoms, and surgical and examination gloves. Copolymer synthetics without reinforcing materials are too weak to be considered. For most types of service, relatively large amounts of materials known to increase hardness, stiffness, strength and abrasion must be present in any given formulation. These include materials such as carbon blacks, silicone materials such as calcium silicate, fine particle precipitated calcium carbonates and hard clays, to name a few examples. These materials are commonly known as fillers. The use of fillers overcomes the shortcomings of poor processability, and improve and modify both the mechanical strength and physical properties of the vulcanized rubber. Apart from these two roles,

RSC Polymer Chemistry Series No. 8
Natural Rubber Materials, Volume 2: Composites and Nanocomposites
Edited by Sabu Thomas, Hanna J. Maria, Jithin Joy, Chin Han Chan and Laly A. Pothen

Published by the Royal Society of Chemistry, www.rsc.org

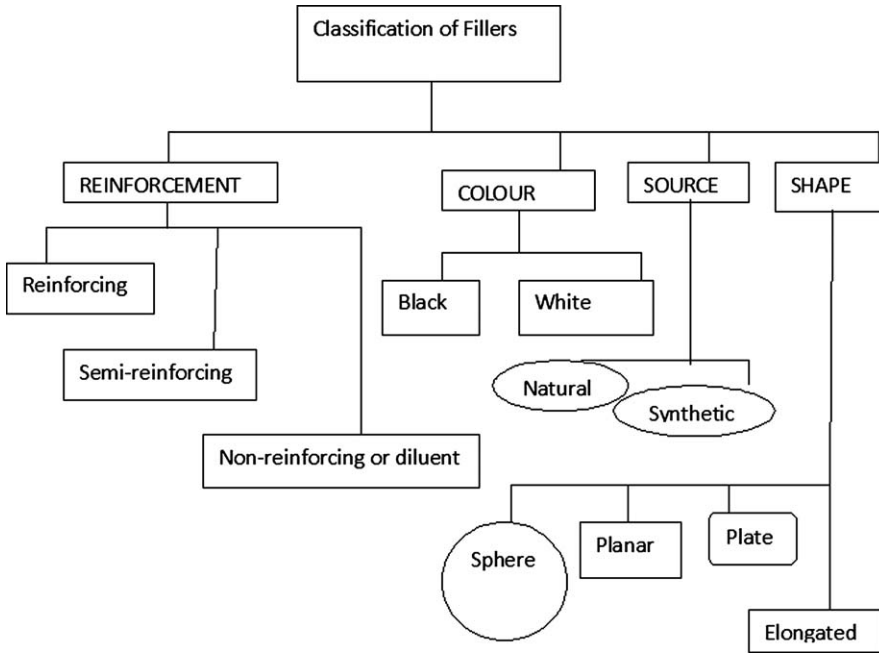

Figure 3.1 A schematic showing the common methods of classifying fillers.

fillers are incorporated into rubbers to reduce cost. Fillers are usually incorporated into rubber to meet the properties and specifications required in service. Among these fillers, carbon black is the most popular. Indeed carbon black is second only to rubber as the most critical and widely used raw material in the rubber industry.[1] When fine particles of carbon black are incorporated into rubber, physical properties and resistance to mechanical failure are greatly improved. Particulate fillers that enhance mechanical properties such as tensile strength, tear strength and abrasion resistance are called reinforcing fillers. Those particulate fillers that do not enhance mechanical properties, but instead reduce them, are classified as diluents or non-reinforcing fillers. Some of the common methods of classifying fillers are shown in Figure 3.1.

3.2 Reinforcing Fillers

The subject of filler reinforcement on vulcanized rubber is very wide and complex. Fillers can be classified as reinforcing, semi-reinforcing and non-reinforcing. All fillers increase the hardness, modulus and stiffness of vulcanized rubber whether or not they are reinforcing or non-reinforcing. It has been established for a very long time that the term reinforcement has been widely used by the rubber technologist to denote the enhancement in the tensile

strength, tear strengths and abrasion resistance of the vulcanized filled rubber. These three mechanical properties are often used as quality control tests by the tyre industry to judge the quality of the tread tyre compound.[2] The rubber that gains the most benefit of reinforcing filler would be those of non-strain-crystallizing rubbers. For example, the gum strength of vulcanized unfilled (gum) styrene butadiene rubber (SBR) is about 2.0–3.0 MPa. But when reinforcing carbon black is added (40–60 pphr) into the rubber, the tensile strength increases by a factor of 10 to 27–30 MPa. In the case of strain-crystallizing rubber such as NR, the benefit of reinforcing filler is less marked compared with SBR. This is because NR has high gum strength of about 27 MPa since NR can crystallize on straining because of its regular micro-structure. The crystals act as self-reinforcing filler to enhance the tensile strength of this unfilled vulcanized rubber. Obviously NR has a technical advantage in the sense that it does not rely on reinforcing filler since it already inherits high mechanical strength. The use of non-reinforcing filler is adequate for NR for most of its applications.

The subject of filler reinforcement of rubbers has been an area of interest to the rubber industry for more than a century. Various models had been proposed in the past to explain the filler reinforcement in vulcanized rubber. The use of modern finite element analysis (FEA) and various mathematical models have made further progress to understand the mechanisms of reinforcement in filled vulcanized rubber. But this does not imply that a complete understanding of the subject has been achieved. The detailed effects of filler properties such as surface area and shape on the filler reinforcement are still not completely understood. A detailed understanding of the filler reinforcement should provide an insight into the increase in modulus and strength.

The extent of reinforcement produced by the carbon black is affected by factors such as (i) particle size, (ii) structure, (iii) physical nature of the surface and (iv) degree of filler dispersion in the rubber matrix.

3.2.1 Particle Size

The particles of carbon black are not discrete but are fused clusters of individual particles.[3] The reinforcement conferred by the black is not influenced to any extent by the size of the unit but predominantly by the size of the particles within the unit. The primary particle typically has cross-sectional dimensions[4] of 5–100 nm. It is well established that the most appropriate way of describing the size of the primary particles is to express it as specific surface area/weight (m^2/g).[4,5] Particle size of itself has relatively little effect on the modulus. But tensile and tear strengths are affected by the particle size and both properties are normally enhanced as the surface area increases[2] (*i.e.* surface area increases with decreasing particle size). The high surface area enhances the ability of the filler to wet the rubber and thus enhances the interaction at the rubber–filler interface. It is the enhancement of the filler–rubber interface that provides the desired reinforcement in filled vulcanized rubber.

3.2.2 Aggregates

Aggregates of multiple primary particles are formed by chemical and physical–chemical interactions: typically they have dimensions of 100–500 nm.[4] The aggregate can be quantified by the number of primary particles and their geometrical arrangement. The aggregates are further condensed into agglomerates by van der Waals forces.[4] Typical dimensions of agglomerates are in the order of magnitude of 1–40 μm. Agglomerates disintegrate during rubber mixing – to about the size of aggregates. Figure 3.2 shows schematically the relative dimensions of primary particles, filler aggregates and filler agglomerates to that of polymer coils.[4] The tendency of individual filler particles, be it carbon black or silica, to aggregate under the effect of strong surface interactions has been said to be responsible for the change in mechanical properties of compounds prepared with a high filler loading (50 pphr).[6] The filler particles, here carbon black, have basically carbon surfaces. These interact directly with the monomers on their length scales. However, the aggregates and

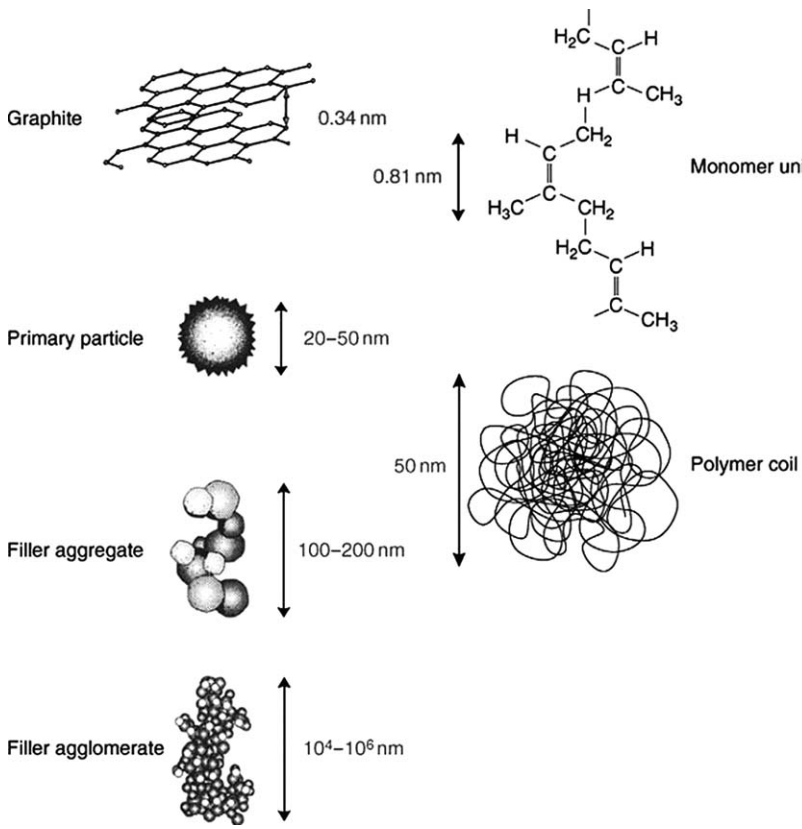

Figure 3.2 Comparison of the different length scales for the elements[4] (reproduced from reference 4).

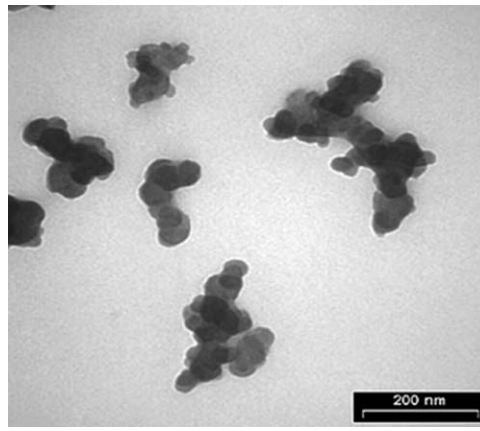

Figure 3.3 TEM of carbon black aggregates (N339) prepared from ready-mixed S-SBR composites with 40 pphr filler (in-rubber state)[4] (reproduced from reference 4).

agglomerates as shown in Figure 3.3 have dimensions similar to those of the polymer coils, so they can directly interact with them.[4]

3.2.3 Structure

The term structure refers to the joining together of carbon particles into long chains and tangled three-dimensional aggregates.[3] This aggregation of particles takes place in the flame during the manufacture of carbon black. The term 'structure' is commonly used to describe two arrangements: (i) low structure – linear arrangement; (ii) high structure – grape-like bundle. The 'structure' of the primary aggregates describes the amount of void volume and is measured by, for example, oil (dibutylphthalate, DBP) absorption. It typically varies between 0.3 cm^3/g and 1.7 cm^3/g for furnace blacks.[4] The characteristic shape of carbon black aggregates is illustrated in Figure 3.4, which shows transmission electron micrographs (TEM) of five different grades of furnace blacks (N220, N326, N330, N347, N550).[4]

Figure 3.4 shows that the size of the primary particles varies, increasing from top to bottom. It implies a decline in the specific surface[4] from 116 m^2/g for N220, 78 m^2/g for N326, 81 m^2/g for N330, 95 m^2/g for N347 to 41 m^2/g for N550. The 'structure' or amount of specific void of the five grades increases from left to right and varies between 0.72 cm^3/g and 1.2 cm^3/g. The N326 structure has relatively few voids. In contrast, it can be clearly seen that N347 has a structure with larger voids than N330 and N326. The higher the structure of the carbon black, the more irregular the shape of the aggregates, hence the less these aggregates are capable of packing together. The effect of structure is more noticeable on processing properties than on the properties of the vulcanizate.[3] In general, the higher the structure the stiffer the unvulcanized compound and the harder the vulcanized material.

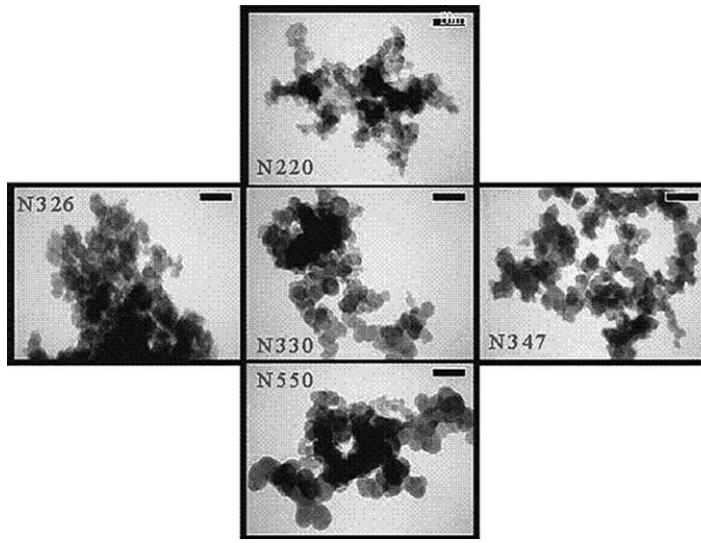

Figure 3.4 TEMs of five different grades of furnace blacks as indicated. The specific surface increases from top to bottom, the "structure" increases from left to right (bar length: 100 nm) (reproduced from ref. 4).

3.2.4 Physical Nature of the Surface

The carbon atoms in a carbon black are present in layer planes. In thermal blacks, the layers are highly oriented, parallel to the surface. Furnace blacks on the contrary, show less crystalline crystallite orientation than thermal blacks.[3,7] The geometry and activity of the filler surface play major roles in the polymer–filler interaction: the physical and chemical binding of polymers to the filler surfaces depends on the amount of surface disorder.[4] The role of the physicochemical nature of the surface in rubber reinforcement is not fully understood.[6] There were suggestions that the high modulus produced by the high structure blacks was not because the carbon black agglomerates restricted the crosslinked network, but because these aggregates when broken down during mixing produced active free radicals capable of reacting with rubber.[3] This black–rubber interaction is evident by the existence of the so-called 'bound rubber' which gives a measure as the amount of rubber insolubilized by the presence of filler when the mix is exposed to a solvent (toluene) in which the rubber alone is readily soluble.[8] It was reported by Brennan[8] that when a carbon black was progressively graphitized by heat treatment, tensile and tear strengths progressively decreased, indicating that the physicochemical nature of the surface is important.

3.2.5 Degree of Filler Dispersion in the Rubber Matrix

Apart from the three factors discussed above, another factor which affects reinforcement is the degree of filler dispersion. It is necessary that during mixing of filler with the rubber, the filler aggregates are broken down to

individual particle size and disperse uniformly within the rubber matrix. Aggregates that are not broken down and filler particles that are not well dispersed provide sites for high stress concentration because they act like flaws that initiate failure. In order to achieve a high degree of reinforcement the particulate must be well dispersed and uniformly distributed within the rubber matrix.

3.3 Theory and Mechanisms of Reinforcement

The enhancement of strength properties by fine particles of particulate filler provides an interesting paradox. It is well known that the presence of small amounts of impurities in the rubber, for example sand and grit, will reduce the strength of the vulcanized rubber because such impurities act as local stress concentrations and thereby initiate failure. It is therefore at first sight difficult to envisage how the introduction of these rigid particles can result in the enhancement of strength properties. Reinforcement of elastomers by colloidal fillers, like carbon black or silica, plays an important role in improving the mechanical properties of high-performance rubber materials. The reinforcing potential is mainly attributed to two effects: (i) the formation of a physically bonded flexible filler network and (ii) strong polymer–filler couplings.[4] Both of these effects arise from a high surface activity and the specific surface of the filler particles. The principal factors that determine the reinforcement capability are:

1. The van der Waals forces between the carbon black and the polymer.
2. The chemical crosslinks or chemisorptions of the polymer on to the filler surface due to free radical reaction between carbon atoms in the filler and in the rubber.
3. The mechanical interlocking of the polymer on to the filler surface.

Some theories and postulations by previous investigators are discussed below regarding the mechanisms of reinforcement of carbon black in rubbers.

3.3.1 Blanchard and Parkinson Model of Weak and Strong Linkage

Blanchard and Parkinson[9] proposed a model where in a vulcanized filled rubber, the filler particles are linked to rubber chains by combinations of strong and weak linkages. When the rubber is stressed, the weak linkage would fail before the strong linkage. This progressive failure of the weak linkages can be used to explain cyclic stress softening or the Mullins effect. Under cyclic loading the softening depends upon the maximum stress applied. Blanchard and Parkinson suggested that different stresses cause different weak linkages to break and contribute to softening. The Blanchard and Parkinson model was also applicable to explain modulus and tear strength of filled vulcanized rubber. The increase in modulus with filler content is attributed to an increase in

linkages of the filler to rubber chains. In the case of tear strength,[10] they suggested that when a rubber is strained the short linkages are tightened and the polymer chains align along the direction of the applied stress. Molecular chains can slip around the filler and align in the direction of the applied stress. These factors would increase tear strength in a filled rubber as slippage of molecular chains would distribute stress.

3.3.2 Bueche Model of Load-Sharing Mechanism

According to Bueche,[11] the fillers are connected with the molecular network chains. The reinforcement is due to a load-sharing effect arising from the attachment of several molecules to one filler particle. When a highly stressed molecular chain breaks, the tension it carried is believed to be distributed over a substantial number of other chains *via* the filler particle, instead of being imposed upon its immediate neighbours. Thus a catastrophic failure is avoided. The increase in strength is attributed to the filler particles acting effectively as a means of distributing the load more equitably. The stress is distributed to a much larger number of chains attached to filler particles. Except for the emphasis on chain breakage and omission of chain alignment, the Bueche reinforcement process is similar to the molecular slippage model as described in Dannenberg's slipping model.

3.3.3 Dannenberg Model of Slippage at Interface

Dannenberg[12] suggested that the rubber matrix can slide over the filler surface. Some slipping of molecular chains occurs over the surface of the filler particles, thus allowing highly stressed chains to relieve their tension. Polymer chains under applied stress would distribute stress by slipping and this could avoid chain breakage. This would result in energy dissipation and increase the strength of the filled elastomer. This model was used by Dannenberg to explain the hysteresis and cyclic stress softening observed in a filled vulcanized rubber. The model suggested that the hysteresis observed can be attributed to the loss of the strain energy as frictional heat occurring during the relative motion between molecular chains and the filler. The Dannenberg model shows similarities to the Bueche model.

3.3.4 Bound Rubber

When an uncured but well dispersed filled rubber is subjected to solvent extraction, not all of the elastomer is recovered. The portion of rubber that is not extracted is called the bound rubber. The bound rubber layer results from a complex combination of physical adsorption, chemi-adsorption and mechanical interlocking. The surface activity of carbon black is related to the bound rubber. Wolff *et al.*[13] have investigated the existence of the bound rubber layer and studied its characteristics. They measured the bound rubber layer for SBR filled with carbon black using NMR and the thickness of the bound rubber

layer was found to be 0.5–5 nm. They found at a constant carbon black volume fraction the bound rubber increases as the surface area of carbon black increases, indicating that the degree of reinforcement depends on a specific surface area and degree of structure.

3.3.5 Detachment of Filler Particles

Andrews and Walsh[14] suggested that the detachment of rubber from filler particles in the highly strained region around an advancing tear is an important source of energy dissipation which can contribute to an enhancement in strength. They studied the fractured surfaces of black-filled rubbers by means of replica electron microscopy. The rupture process was deduced from the micrograph of the replica, because it reflected an exact copy of the rupture path through the material. The amount of extracted filler lifted out by the replicating material (gelatin) reflected the relative strength of the adhesion of filler particles to the rubber matrix. Poor adhesion is reflected by a large amount of filler extracted. They found that the adhesion between rubber and filler particles must be neither too strong nor too weak. If the adhesion is too strong, as was the case with the peroxide-cured rubbers, then breakdown occurs in the matrix near the particle and the latter remains attached to the rubber. If the adhesion is too poor, then breakdown occurs at low stresses. Thus the importance of good adhesion is necessary only to a level where it could withstand stresses high enough to develop the necessary hysteresis to enhance strength.

However, the models in Sections 3.3.1 to 3.3.5 are not able to describe all the observed phenomena such as stress softening or the hysteresis behaviour completely. Hence, there is a need to understand the effect of size, shape, particle distribution and the interfacial boundary conditions on filler reinforcement. The modern approaches to modelling and studying the behaviour of filled rubber composites involve finite element microstructural modelling, molecular modelling, mathematical modelling, TEM and SEM imaging, and tomography, as well as measuring the changes in electrical and mechanical properties with strain. All these new approaches can be used to examine these various theories of filler reinforcement more closely. FEA is a mathematical means of solving a complex problem with the help of a generalized theory developed for a material, which can be utilized in the FEA model for simulating the actual material behaviour. The actual loading conditions are simulated by applying appropriate boundary conditions. Some of the current models are described below.

3.3.6 Theory of Reinforcement by Rigid (Fractal) Aggregates and Agglomerates of Filler Particles

This is the recent theory developed by Vilgis *et al.*[4] The theory involves very rigorous mathematical treatment. According to Vilgis *et al.*,[4] there are two different hydrodynamic regimes of reinforcement mechanisms elastomer.

The first hydrodynamic regime consists of randomly dispersed particulate filler in a rubber matrix, which gives an elastic reinforcement of the form given by Equation (3.1):

$$G = G_{\mathrm{m}}[1 + 2.5c] \tag{3.1}$$

This is the well-known Einstein–Smallwood equation, where c is the volume fraction of the filler and G_{m} is the elastic modulus of the rubber matrix. The equation is obtained based on three idealized assumptions, such as (i) freely dispersed particles, *i.e.* low volume fraction, (ii) a spherical shape (leading to the constant 2.5) and (iii) entirely non-elastic filler particles, *i.e.* their elastic modulus has to be infinitely large. The reinforcement term contains two factors: one is a simple number related only to the geometry of the particles, the other is linear in the volume fraction of the filler particles.

The second hydrodynamic regime is to generalize the dispersion of the filler particles. As mentioned above, the linear dependence in Equation (3.1) stems basically from the assumption of free dispersion of the filler particles. If the filler particles form clusters, two different regimes must be distinguished. First, small clusters may be dispersed freely without contact between them. In this situation the reinforcement was given by Equation (3.1) is expected to hold. The only changes to be expected are in the geometry factor, which may become size dependent. The second regime comes into play when the clusters begin to overlap. Then a different behaviour as a function of the volume fraction c is to be expected. By assuming that the clusters may have some 'fractal' geometry, Vilgis *et al.*[4] derived some scaling relations. They envisage a stronger reinforcement in the overlap regime than in the first simple regime.

The next step they have to generalize the mathematical formulation of the statistics of linear polymer to general fractal objects by assuming that the clusters formed by the filler particles can be described by a fractal shape. This assumption allows them to predict certain specific forms of the reinforcement, such as to work out the probability distribution for the filler clusters. By appropriate modelling of the filler structure they arrive at the generalization distribution to calculate the self-energy function which corresponds directly to the reinforcement factor. They then derive a new form of the Green function **G** which contains the effects of the filler particles. In this way, they are able to take into account of all the effects: the shape of the filler particles, the spatial distribution of the particles, *etc.*

The last step in their approach is the computation of the screening length, which introduces the cluster concentration (or volume fraction). The overlap concentration for the clusters c^* is given by Equation (3.2):

$$c^* = \frac{b^3 L^D}{R^3} = \frac{b^3 L^D}{b^3 L^{dv}} = L^{D-3v} \tag{3.2}$$

where L is the mean (linear) cluster diameter. The spectral dimension D describes the connectivity of the filler particles, ν is the excluded volume exponent, b is the size of primary particles and R its average extension.The results for the

screening length yield the reinforcement factor as a function of the volume fraction $\varphi = b^3 c$. To bring the results into a more useful form they replace the linear cluster size L by its spatial dimension $R = bL^{\nu}$. Then using this and $G_0(\mathbf{k}) \sim \mu^{-1} k^{-2}$ they obtain the general result:

$$\frac{G - G_m}{G_m} \overset{k \to 0}{\sim} (kb)^{(2-2\nu-D)/\nu} \times \begin{cases} \left(\frac{R}{b}\right)^{(2+\nu-2D)/\nu} c & \text{below overlap concentration} \\ \left(\frac{R}{b}\right)^{(2-D)/\nu} c^{\frac{2\nu}{3\nu-D}} & \text{above overlap concentration} \end{cases}$$

or alternatively using $\nu = D/d_f$ (3.3)

$$\frac{G - G_m}{G_m} \overset{k \to 0}{\sim} (kb)^{2(d_f/D)-d_f-2} \times \begin{cases} \left(\frac{R}{b}\right)^{2(d_f/D)-2d_f+1} \phi & \text{no overlap } \phi \leq \left(\frac{R}{b}\right)^{d_f-3} \\ \left(\frac{R}{b}\right)^{2(d_f/D)-d_f} \phi^{2/(3-d_f)} & \text{with overlap } \phi \gg \left(\frac{R}{b}\right)^{d_f-3} \end{cases}$$

For a realistic modelling of primary carbon black aggregates by ballistic cluster–cluster aggregation with $d_f = 1.9$ and $D = 1.3$, they came out with the following mathematical expression:

$$\frac{G - G_m}{G_m} \sim \begin{cases} R^{0.1}\phi & \text{for } \phi < \phi_{crit} \quad \text{(a)} \\ R^{0.1}\phi^{1.8} & \text{for } \phi > \phi_{crit} \quad \text{(b)} \end{cases} \tag{3.4}$$

$\varphi_{crit} = (R/b)^{1.1}$ denotes the critical overlap volume fraction for the branched filler aggregates. Thus the two different regimes correspond to (a) non-overlapping clusters and (b) overlapping clusters, depending on filler volume fraction. In the non-overlapping regime, the behaviour is similar to Equation (3.1) as they predicted, *i.e.* the reinforcement is proportional to the volume fraction, whereas in regime (b) the hydrodynamic reinforcement sensitively depends on the universal aggregate structure. In the non-overlapping regime (a), the filler contribution to the modulus is always proportional to the filler concentration itself and a geometrical factor.

Vilgis *et al.*[4] commented that the disadvantages of this model are the small range of application and the idealizations which they introduced in order to make the calculations tractable. The advantages are the successful derivation of a structure–property relationship, the possibility of explicitly including the fractal filler structure, and the universality (transfer to all types of branched aggregates). Refinements of the present model require the inclusion of local properties, such as particle–particle binding between the primary filler particles.

3.3.7 Theory of Filler Reinforcement in Elastomers Based on Uniform Soft-Sphere Model

This theory was introduced by Vilgis *et al.*[4] The simplest model consists of randomly dispersed uniform soft spheres. There are two limiting cases: if the modulus of the soft filler particles is zero, the matrix contains holes (resembling a Swiss cheese) and thus becomes softer. On the other hand, in the case of a very large modulus of the filler particles, the Einstein–Smallwood formula (Equation (3.1)) will be reproduced. For uniform soft filler particles with elastic modulus $G_f > G_m$ the intrinsic modulus $[\mu]$, is given by

$$[\mu] = 5\frac{1 - G_m/G_f}{2 + 3G_m/G_f}. \tag{3.5}$$

where G_f is the elastic modulus of the filled system and G_m is the elastic modulus of the rubber matrix. Inserting Equation (3.5) into the effective shear modulus Equation (3.6) gives Equation (3.7):

$$\frac{G}{G_m} = 1 + \frac{[\mu]\phi}{1 - \frac{2}{5}[\mu]\phi}. \tag{3.6}$$

$$\frac{G}{G_m} = 1 + \frac{5}{2}\phi\frac{G_f/G_m - 1}{G_f/G_m + 3/2 - \phi(G_f/G_m - 1)}. \tag{3.7}$$

For a hard core/soft shell, the intrinsic modulus can be calculated for filler particles with a totally rigid core (with an infinitely large modulus) and a soft shell. If the shell modulus G_{shell} is assumed to be larger than the matrix modulus G_m, this system resembles a carbon black-filled rubber, where the carbon black particles are surrounded by a bound rubber layer. Here the algebraic expression for the intrinsic modulus reads

$$\begin{aligned}[\mu] = \frac{5}{2} - 25\tilde{\mu} \times \{&(1 - \tilde{r}^3)(8\tilde{\mu} + 19/2) + (\tilde{\mu} - 1)(-42\tilde{r}^3 \\ &+84\tilde{r}^5 - 50\tilde{r}^7 + 8\tilde{r}^{10})\}\{(3\tilde{\mu} + 2)(16\tilde{\mu} + 19) \\ &+(\tilde{\mu} - 1) \times [-300(\tilde{\mu} + 3/4)\tilde{r}^3 + 168(3\tilde{\mu} + 2)\tilde{r}^5 \\ &-100(3\tilde{\mu} + 2)\tilde{r}^7 + 48(\tilde{\mu} - 1)\tilde{r}^{10}]\},\end{aligned} \tag{3.8}$$

where $\tilde{\mu} = G_m/G_{shell}$ and $\tilde{r}^{-1} = r_{shell}/r_{core}$.

Most interesting is the large increase in reinforcement even for small bound rubber thicknesses. Let us briefly discuss the advantages of the model. They find that the results obtained are realistic for small as well as intermediate filler concentrations, *i.e.* they are in accordance with experiments at least qualitatively. For the core–shell systems they have provided exact calculations of intrinsic moduli for various special forms of core–shell elasticity, *i.e.* soft spheres, hard spheres with soft surfaces, *etc.* These results contain no fit parameters and in principle both compressible and incompressible media are accessible.

Reinforcement is thus a multiscale problem. For example, the geometry and activity of the filler surface play major roles in the polymer–filler interaction: the physical and chemical binding of polymers to the filler surfaces depends on the amount of surface disorder. Aggregate structure is expected to be dominant at intermediate length scales and agglomerate structure at large length scales.[4] Considerable reinforcement can only be achieved if the length scales of the filler and the polymer matrix as shown in Figure 3.2 coincide. Figure 3.2 shows the possible interplay between the length scales. The small scales defined by the structure and the interactions need to be of the same order of magnitude in order to get a significant rate of adsorption and sticking, which will contribute to the reinforcement.[4]

3.3.8 Mathematical and Computer Models

Sen *et al.*[15] investigated the elastic properties of the polymer filled with spherical shaped fillers. They were able to verify the conformational and deformational properties of the polymer chains as a function of chain length, temperature and filler size.

Coveney *et al.*[16] modelled a carbon black-filled NR composite using a standard triboelastic solid (STS). The STS consisted of a leading spring, a parallel spring and a triboelastic assemblage (columbic frictional sliders). This STS model gave good correlation with behaviour of filled elastomer at low strains. Later, Coveney and Johnson[17] used STS to model behaviour of NR filled with variety of carbon blacks at different loading fillers. They show STS gave good agreement with the experimental data for dynamic stiffness for shear strain amplitudes down to 0.01. In another case, Coveney and Johnson[18] introduced two variants of the STS model, a four parameter rate dependent triboelastic (RT) model and five parameter viscous modified standard triboelastic solid (TVS) model. The RT model included a rate dependent frictional slider in series with a triboelastic assemblage. The TVS model had a combination of a STS and a parallel (dashpot) Maxwell body. The RT model showed a good correlation with the dynamic stiffness and a reasonable correlation with loss angle and stress relaxation. The behaviour of TVS model was similar to the RT model. However, TVS model did not show good correlation with stress relaxation behaviour.

3.3.9 Kluppeland–Schramm Tube Model

Most researchers have assumed that the rubber matrix can be represented as either single or multiple polymer chains with fillers that are spherical or have a simple shape factor that models the rubber elasticity. Kluppel and Schramm[19] have proposed a generalized tube model for the polymer network and rigid filler clusters. They used this model to explain the hyperelasticity and stress softening of filled vulcanized rubber. Breakdown of the aggregates by the applied stress causes stress softening under cyclic loading or pre-strain. The model produces fair agreement between theory and experiment for a filled SBR polymer and an

unfilled NR in uniaxial tensile loading. The application of this model to different filler materials along with varying load condition was verified by Kluppel and Meier.[20] This model showed a reasonable correlation in uniaxial loading for SBR filled with either silica or carbon black. However, there were significant deviations for filled rubber simulation of stress softening under equi-biaxial loading.

3.3.10 Fukahori and Seki Model

FEA has been used to model the microstructural behaviour of filled rubbers. Fukahori and Seki[21] used FEA to study the stress distribution around a circular filler particle in a cubical and a cylindrical rubber matrix at small strains and large strains. They analysed the stress around a filled particle using two different geometrical models. Their first model assumed a filler particle at the centre of a cylinder and used axial symmetric elements for the simulation of the behaviour. This model showed a poor correlation with the experimental data. Their second model assumed filler particle at the centre of a cube and an extra layer of rubber around the filler which they referred to as a glassy layer. The layer was assumed to be 1000 times stiffer than the matrix rubber. This approach can be considered to model the bound rubber layer around filler. Fukahori[22] proposed a filler rubber interface model consisted of two layers namely the glassy layer, that extends couple of nanometres and the sticky layer around 3–8 nm. Glassy layers have restricted chain mobility and increase the stresses at small strains. The sticky layer extends from the glassy layer into the polymer and contributes an increase to the stress at larger extensions. However, experiments have not yet identified any distinction between these two layers.

3.3.11 Bergstrom and Boyce Model

Bergstrom and Boyce[23] used a range of filled rubber models to investigate the mechanical behaviour at small deformations under compressive loading conditions. They considered a range of filler shapes and mesh representation. They showed that the Young's modulus of the material can be predicted by using a FEA model having representative volume element of many filler particles. Their study compared the effect on modulus of using one (unit) filler particle model and a multiple filler particle of a same shape. They also studied effect of the area to volume ratio of the filler particle on the mechanical behaviour. The models used do not accurately represent the filler shapes used in their experiments.

3.3.12 Hon *et al.* Micromechanical Model

Hon *et al.*[24] introduced a micromechanical model to predict the stiffness of a filled elastomer. They evaluated a range of 2D and 3D models to predict the stiffness of both medium thermal (MT) and high abrasion furnace (HAF)-filled elastomers. They used a simple Mooney stored energy function to characterize

the rubber elasticity. For MT carbon black-filled elastomer the models were able to predict the stiffness of the filled elastomers at low to moderate strains for filler volume fraction up to 10%. A 3D simulation of the elastomers filled with MT carbon black showed a good correlation with the Guth and Gold equation. HAF carbon black (filled elastomers) was modelled as simple rod-like particles in a cubic matrix. Simulation of the HAF black-filled elastomers did not correlate well with the experimental data. However, they were able to study the effect of the orientation of the rod-like particles in a cubic matrix.

3.3.13 Jha *et al.* Microstructural Finite Element Model

Jha *et al.*[25] studied the reinforcement of rubber by carbon black fillers over a wide range of strains using finite element microstructural models. They evaluated a range of microstructural finite element models and used two boundary conditions namely plane surface and free surface boundary conditions. They chose stored energy function as suggested by Gent[26] to model the finite extensibility effects at strains above 100%. Models using a plane surface boundary showed an unrealistic increase in modulus due to the geometric limitation of the models. Models using free surface boundary conditions were found to be suitable for prediction of stiffness of elastomer at higher strains. Their model shows that the predicted stiffening effect at a constant filler volume fraction increases as the number of fillers present in the unit cell increase, with a final stiffness being reached at a large number of fillers in the unit cell.

Later Jha *et al.*,[27] still using finite element microstructural models, investigated the effect of filler number, shape and position in the rubber matrix on the stiffness of filled elastomer. Two different types of microstructural model were used where they were examined under strain with a range of up to 36 filler particles present. The first type having smooth spherical surfaces and the second type having a more irregular surface constructed out of cubes. The first type of model, containing spherical fillers, became progressively stiffer as the number of fillers was increased. This resulted from an increase in the volume of rubber in the unit cell being constrained between the fillers as the filler number increased even if the volume fraction of fillers remained the same between the different models. Comparisons at up to 50% strain in shear and tension showed that an eight filler particle model of this type was essentially isotropic. The second modelling uses a perfect cubic lattice where only some of the elements, in regions to give the approximate shape of the filler and of the appropriate number to give an accurate representation of the filler volume fraction. The second model overcomes the problems encountered in the first model. The first model encountered problems of meshing and modelling difficulties associated with creating models with a totally random arrangement of smooth surface. They found that their second model made with basic cubic elements was stiffer than the real materials, as within the model there was a considerable amount of additional 'occluded' rubber that increased the effective filler volume fraction.

3.3.14 Electrical and Mechanical Behaviour of Filled Elastomers under Strain

Finite elements analysis has shown that filler properties such as surface area, shape and structure have strong influence on the filler reinforcement and filler rubber properties. Another approach to understand the filler network and the filler–rubber interactions more closely is to study the electrical and mechanical behaviour of the filled elastomer under strain for various different conditions. Jha *et al.*[28,29] have investigated the effect of surface area and structure of filler on the electrical changes of filled NR measured under strain. They used three different grades of carbon black ranging from the non-reinforcing MT, reinforcing HAF and very high surface area black such as Printex-XE2.

MTN990 carbon black has the lowest surface area and has very low structure among the three types of black chosen. MTN990 is essentially having primary particles which are approximately spherical in shape. They found that for a N990 filled rubber sample with a filler volume fraction of 56%, the resistivity initially increased by an order of magnitude by the application of a 10% strain during the first loading cycle. It increased 100 fold up to 60% strain. They attributed the increase in resistivity to the breakdown of the filler network structure.

In the case of HAF N330 filler in its virgin first cycle that the resistivity increased up to 20% strain. They have attributed this initial increase in resistivity to the breakdown of the filler network structure in the rubber. They observed that when the applied tensile strain increases above this 20% strain, the resistivity with strain graph reaches a plateau. They suggested the occurrence of this phenomenon is a consequence of the orientation effects of filler under strain and also the effect of the reformation of some of the conduction paths. When the load is removed, the resistivity does not return to its original value but increases further. This indicates that some of the breakdown of the filler agglomerate structure is permanent.

Jha *et al.*[29] reported that the electrical resistivity behaviour of a NR compound filled with Printex XE2 carbon black showed contrasting behaviour to that of HAF blacks. For Printex-XE2, the resistivity behaviour is virtually reversible with strain, suggesting that the filler network is not permanently altered. They attributed the reversibility in resistivity came from the high structure and large surface area of the carbon black. They found that after the first cycle there was no further breakdown in filler aggregate structure under cyclic loading. According to Jha *et al.*[29] the occurrence of this reversibility might be associated with the difficulties for the rubber to slide over the surface of the filler under strain because of the large surface area of the filler and the hollow hemispherical shape of the filler. Therefore, the weak van der Waal forces that hold the filler network structure might be able to reform each time that the rubber is relaxed. The discovery of reversibility in the electrical resistivity behaviour of Printex-XE2 by Jha *et al.* is very significant because devices can be made that will be able to measure forces and strains from the changes to the electrical resistivity. This might allow a whole new generation of smart rubber devices to be developed.

3.4 Mechanism of Reinforcement in Modulus

According to Mullins,[30] carbon black-filled vulcanized rubbers consist of a rigid hard phase and an extensible soft phase. The rigid hard phase is associated with the carbon black and the soft extensible phase is the rubber. When carbon blacks are loaded into rubbers, the stiffness of the rubber increases markedly. The stiffness of the black-filled vulcanizate can be expressed quantitatively in terms of the volume fraction of the filler in the vulcanized rubber by the Guth and Gold equation:[30,31]

$$E = E_o\left[1 + 2.5c + 14.1c^2\right] \tag{3.9}$$

where E is the modulus (whether in tension, compression or shear) of the filled rubber and E_o is the modulus of unfilled rubber and c is the volume fraction of the filler, *i.e.* the fraction of the total volume of the vulcanizate which is occupied by the filler. Equation (3.10) assumes that the filler is spherical in shape, but according to Mullins and Tobin,[30] for reinforcing black fillers, the assumption that the filler is spherical does not hold because the inherent nature of the filler is not spherical. Thus they introduced the so-called shape factor, f, having the empirically determined value of 6.5 for HAF black.[30] For reinforcing filler the Young's modulus can be predicted by Equation (3.11) below.[30]

$$E = E_o\left[1 + 0.67fc + 1.62f^2c^2\right] \tag{3.10}$$

Figure 3.5 shows a plot of hardness against volume fraction of filler [ISAF (intermediate super abrasion furnace) black] in the vulcanizate base on the rubber compound formulations shown in Table 3.1. Hardness is defined as the resistance to surface indentation as measured under specified conditions. It is a non-destructive test that measures the reversible deformation when an

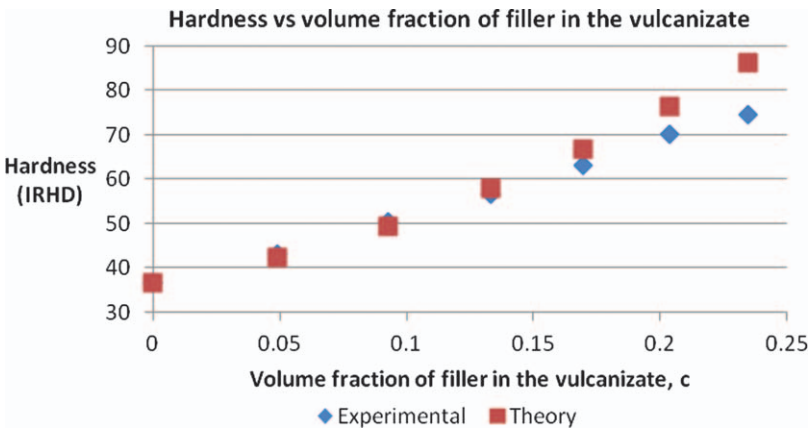

Figure 3.5 Effect of ISAF loading on hardness. Comparison between theory and experimental values.

Table 3.1 Black-filled NR compound formulations to investigate the effect of filler loading on hardness and tensile properties.

Mix no.	*1*	*2*	*3*	*4*	*5*	*6*	*7*
NR (SMR10)	100	100	100	100	100	100	100
Zinc oxide	5	5	5	5	5	5	5
Stearic acid	2	2	2	2	2	2	2
ISAF	0	10	20	30	40	50	60
6PPD	1	1	1	1	1	1	1
Sulfur	2.5	2.5	2.5	2.5	2.5	2.5	2.5
CBS	0.5	0.5	0.5	0.5	0.5	0.5	0.5

indenting force is applied on the rubber surface at a specified time. Hardness tests are widely used in quality control because hardness is sensitive to filler loading and also the state of cure. The indentation of a rubber is a rather complicated deformation and the depth of indentation is dependent on the shape and dimensions of the indenter. For a perfectly elastic material, the approximate empirical relationships for the spherical shape indenter, the hardness is related to Young's modulus[32] of the vulcanized rubber by Equation (3.11):

$$P = k_1(F/E)^{0.74}R^{0.48} \tag{3.11}$$

where P is the depth of indentation, F is the indenting force, E is the Young's modulus of the rubber, R the radius of the indentor, and k_1 is a constant.

In the unfilled state, the hardness of the vulcanized rubber was 36.5 International Rubber Hardness Degree (IRHD), which is a typical value for gum rubber. Once filler is added into the rubber compound, the hardness increased progressively in accord with Equation (3.9). If the Young's modulus E in Equation (3.9) is replaced by the hardness one can calculate to predict the hardness of vulcanized filled rubber as a function of volume fraction of filler in the vulcanizate. It is interesting to note that the agreement between the calculated value (theory) and the experimental value was fortuitously good. The theoretical value was calculated by using Equation (3.9) where E_o was replaced by the hardness of unfilled vulcanized rubber (36.5 IRHD). Indeed at volume fraction of filler, $c \leq 0.1697$ (40 pphr of ISAF), the agreement was excellent. But, at higher filler loading ($c > 0.1697$) there is a significant departure of the experimental value from the theoretical value.

The deviations might be attributed to other factors such filler interaction and fractal surface which are not taken into account in Equation (3.9). But Equation (3.9) is simple as compared to Equation (3.8), which takes into account of the filler interaction and fractal surface of the filler, but the computation of the mathematical expression is not simple.

It is quite common practice in the rubber industry that rubber technologists refer to M100 and M300 as the 'modulus' of the vulcanized rubber. Strictly speaking it is not scientifically correct because modulus is defined as stress over strain. Actually M100 denotes the tensile stress at 100% strain and M300

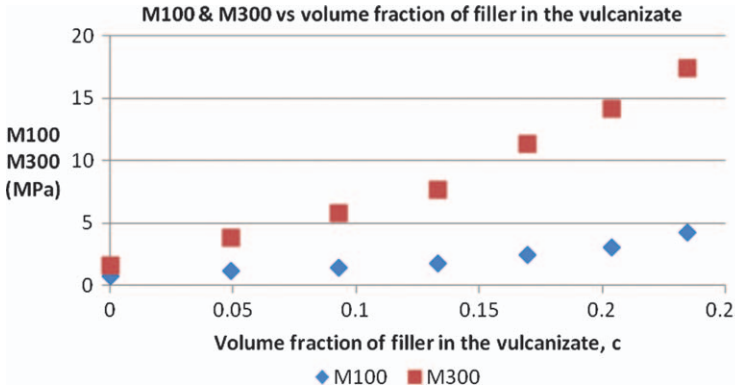

Figure 3.6 The effect of filler loading on M100 and M300 of vulcanized ISAF black-filled NR.

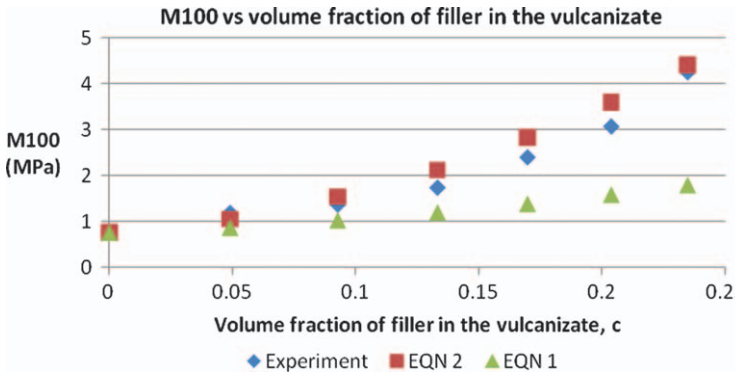

Figure 3.7 Comparison of Equation (3.10) (EQN 1) and Equation (3.11) (EQN 2) to predict M100 obtained from tensile test (ISO37).

denotes the tensile stress at 300% strain. Figure 3.6 shows the plot of M100 and M300 against volume fraction of filler in the vulcanizate. The results were obtained from tensile tests at 23 °C base on ISO37. The results represent the mean value taken from five dumbbell test pieces prepared from a vulcanized rubber sheet base on compound formulations shown in Table 3.1. Like hardness, the M100 and M300 increased progressively as the volume fraction of filler was increased. Figure 3.7 shows a comparison between theoretical prediction and experimental values. The theoretical values of M100 were calculated using Equations (3.9) and (3.10), and are shown in Table 3.2. The E_o value was replaced by the M100 value for vulcanized unfilled NR.

There are two important observations here. First, at low filler loading, the agreement between theory and experiment was good. Second, at a filler loading of more than 40 pphr of ISAF, theoretical values predicted by Equation (3.9) show marked deviation from the experimental value. However, the theoretical

Table 3.2 Effect of filler (ISAF) loading on tensile modulus M100 – comparison between theoretical and experimental values.

ISAF (pphr)	*0*	*10*	*20*	*30*	*40*	*50*	*60*
Volume fraction of filler, c	0	0.049	0.0927	0.1332	0.1697	0.2037	0.2347
M100 (experiment) (MPa)	0.76	1.19	1.37	1.74	2.40	3.07	4.25
$E = E_o\,[1 + 2.5c + 14.1c^2]$ (MPa)	0.76	0.87	1.03	1.20	1.39	1.59	1.8
$E = E_o\,[1 + 0.67fc + 1.62f^2c^2]$ (MPa)	0.76	1.05	1.54	2.12	2.82	3.59	4.4

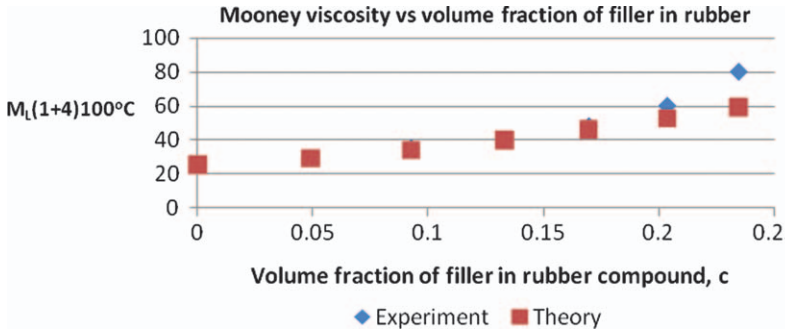

Figure 3.8 Influence of filler loading on Mooney viscosity of ISAF black-filled NR compounds.

values predicted by Equation (3.10) were fortituously in excellent agreement with the experimental values. The use of a shape factor is necessary to predict the tensile modulus, but does not seem to be necessary when predicting the hardness. The difference might be associated with the nature of the stress–strain distributions in compression and in tension. In tension, the stress–strain relationship is non-linear at moderate strain. In compression, the stress–strain relationship is still linear because the imposed strain is very low.

The mechanism by which fillers enhance the hardness and modulus is reasonably well understood, at least in qualitative terms. The stiffening is in part attributed to the absence of deformation within the rigid filler particles, and in part with the immobilization[33] of the rubber at the interface between the rubber matrix and the filler particles, plus the hydrodynamic effect.[34–36] For black-filled vulcanized rubber, this immobilization is attributed to the strong physisorption of the rubber in the filler structure and is often called occluded rubber.[37]

The effect of filler loading on Mooney viscosity of the rubber compound is a good indication of the immobility and hydrodynamic effect caused by the filler in the unvulcanized rubber. Figure 3.8 shows a plot of Mooney viscosity against volume fraction of filler in the vulcanizate base for data shown in Table 3.3. The theoretical value was calculated using Equation (3.12). This equation is an extension of Einstein's equation. Einstein studied colloidal suspensions and emulsions by hydrodynamic analysis.[38] The viscosity of the

Table 3.3 Effect of filler (ISAF) loading on Mooney viscosity of NR compounds – comparison between theoretical and experimental values.

ISAF (pphr)	*0*	*10*	*20*	*30*	*40*	*50*	*60*
Volume fraction of filler, c	0	0.049	0.0927	0.1332	0.1697	0.2037	0.2347
M_L (1 + 4)100 °C (experiment)	25.2	29.3	35.1	40.4	48.1	60.2	80.3
$\eta = \eta_o [1 + 2.5c + 14.1c^2]$	25.2	29.1	34.1	39.9	46.1	52.8	59.6

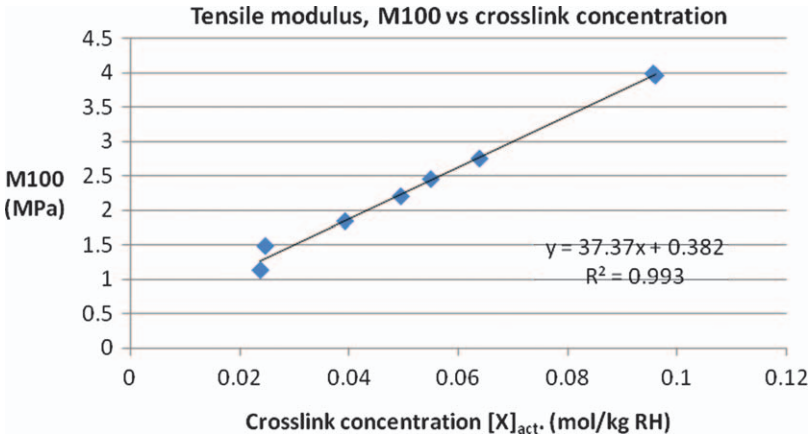

Figure 3.9 Effect of actual crosslink concentration $[X]_{act}$ on the tensile modulus, M100 of vulcanized HAF black-filled NR.

suspension, η, is related to the volume fraction of the particles in the liquid, c, by Equation (3.12):

$$\eta = \eta_o [1 + 2.5c + 14.1c^2] \tag{3.12}$$

where η_o is the viscosity of the liquid. In the calculation here, η_o was taken as the Mooney viscosity of unfilled NR compound. The agreement between experiment and theory was excellent at each filler loading, except at 60 pphr of ISAF where the experimental value was 35% higher than the theoretical value. The increase in Mooney viscosity of black-filled NR compound with increasing filler loading provides experimental evidence that the hydrodynamic effect contributed to the increase in modulus of vulcanized filled NR.

Apart from the filler, the stiffening effect can also arise from the rubber network itself such as the crosslink concentration, as shown in Figure 3.9. The results shown here are based on compound formulations given in Table 3.4. The tensile modulus M100 increased linearly with increasing crosslink concentration of the rubber network. The crosslink concentration was calculated by the Flory–Rehner[39] equilibrium swelling equation:

$$\ln(1 - \upsilon_r) - \upsilon_r - \Psi \upsilon_r{}^2 = 2\rho V_o [X]_{phys} \upsilon_r{}^{1/3} \tag{3.13}$$

Table 3.4 Compound formulations – base mix: SMR L 100, zinc oxide 5, stearic acid 2, Flectol H 2*, HAF black 50 in parts per hundred of rubber (pphr).

Sulfur (pphr)	*1.0*	*1.5*	*1.6*	*1.75*	*2.0*	*2.5*	*3.5*	*4.0*
MBS (pphr)	0.2	0.3	0.32	0.35	0.4	0.5	0.7	0.8
Cure time at 150 °C (minutes)	35	34	29	30	28	27	25	24
M100 (MPa)	1.13	1.48	1.84	2.20	2.45	2.75	3.99	3.96
Tensile strength (MPa)	18.8	19.5	21.7	25.6	26.8	25.6	27.8	27.6
Elongation at break (%)	575	550	511	525	526	481	433	447
$[X]_{act} \times 10^{-2}$ mol/kg Rubber Hydrocarbon (RH)	2.38	2.47	3.93	4.95	5.50	6.39	9.57	9.61

*Flectol H, polymerized 2,2,4-trimethyl-1,2 dihydroquinoline.

where v_r is the volume fraction of rubber in the swollen sample, and was corrected for the volume occupied by the carbon black and zinc oxide[40,41] particles using the relationship given by Equation (3.13). Ψ denotes the rubber–solvent interaction parameter, ρ is the density of the rubber, V_o is the molar volume of solvent and $[X]_{phys}$ is the physically manifested crosslink concentration.

$$v_r = (V_{RN})/(V_{RN} + V_s) \tag{3.14}$$

where V_{RN} is the volume of rubber network formed from the rubber hydrocarbon and curative by the vulcanization process, including any atoms or groups introduced in crosslinks or as modifications of the main chains.[41] The volume of solvent absorbed, V_s, was calculated from the difference in the weights of the swollen and dried deswollen samples. In this experiment the solvent used was *n*-decane. The actual concentration of crosslink in any NR vulcanizate containing a known volume of HAF black was calculated using the empirical formula used by Porter[40] and given by Equation (3.15):

$$[X]_{act} = [X]_{phys}/(1 + kc) \tag{3.15}$$

where k is a constant characteristic of the filler and has a value of 2.6 for HAF black,[40] and c is the volume fraction of carbon black in the vulcanizate. The increase in M100 with increasing crosslink concentration is in accord with the statistical theory of rubber elasticity[42] given by Equation (3.16):

$$G = Nk\theta = \rho R\theta/M_c \tag{3.16}$$

where G is the shear modulus, N represents the number of molecules per unit volume, k is the Boltzmann constant, θ is the absolute temperature, ρ is the density of rubber, R is the molar gas constant and M_c is molecular weight between crosslinks. The crosslink concentration $[X] = 1/(2M_c)$. Equation (3.16) shows that the shear modulus G increases proportionately with the crosslink concentration.

3.4.1 Effect of Pre-Stressing on Young's Modulus of Silica-Filled Vulcanized NR

One of the factors affecting the modulus of filled vulcanized NR is the immobilization caused by the strong physisorption of the rubber in the filler structure. It was reported by Luginsland *et al.*[43] that silica-filled vulcanized rubber exhibited higher degree of immobilization than that of carbon black-filled vulcanized rubber. They explained that the increase in immobilization in silica-filled vulcanized was attributed to chemical bonding that formed two network structures during vulcanization, viz; (i) the silica–rubber network resulting in the 'in-rubber structure' and (ii) the matrix network by the sulfur crosslinking of the polymer chains. This two-network formation is believed to be associated with the presence of silane coupling agent to enhance the rubber–silica surface interaction. Azemi *et al.*[44] investigated the effect of pre-stressing on the Young's modulus of vulcanized NR filled with 50 pphr of precipitated silica. However, the quantity of silane coupling agent [Si69, bis(3-triethoxysilylpropyl)tetrasulfide, abbreviated to TESPT] was varied from 1 pphr to 6 pphr in order to vary the extent of immobilization at the rubber–filler interface.

Simple extension measurement at low strain (below 50%) was done on a parallel strip of vulcanized rubber having dimensions of 150 mm × 3 mm × 0.5 mm. The cross-sectional area of the test piece was determined from the density measurement. The Young's modulus of the vulcanizate was estimated from the slope of the straight line of the stress–strain plot as shown in Figure 3.10. The mean value from two measurements was reported. Figure 3.11 shows the influence of coupling agent on Young's modulus where the Young's modulus increases progressively as the amount of Si69 is increased from 1 pphr to 3 pphr. At 4–6 pphr, the influence of Si69 on the Young's modulus appears to level off. Since the measurement of Young's modulus was done at very low

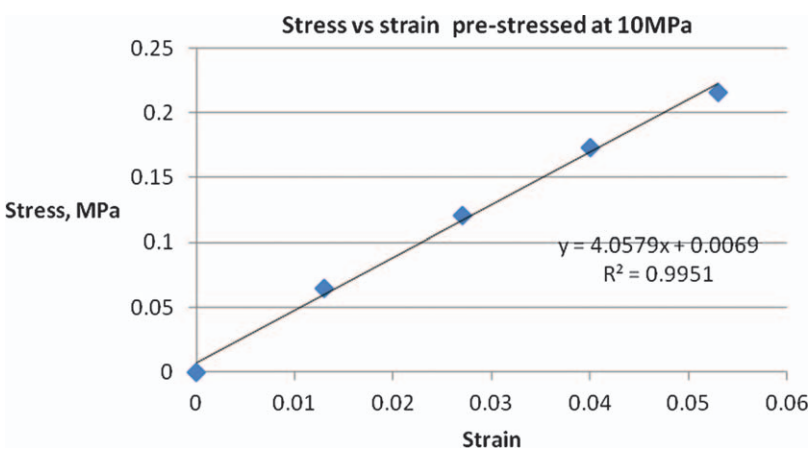

Figure 3.10 Stress–strain plot of pre-stressed silica-filled vulcanized NR containing 3 pphr of silane coupling agent (reproduced from reference 44).

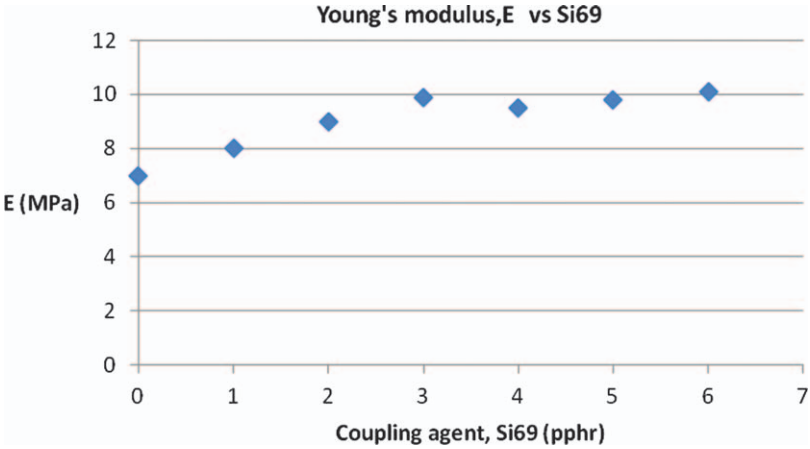

Figure 3.11 Influence of coupling agent TESPT (Si69) on Young's modulus *E* of silica-filled NR vulcanizates (reproduced from reference 44).

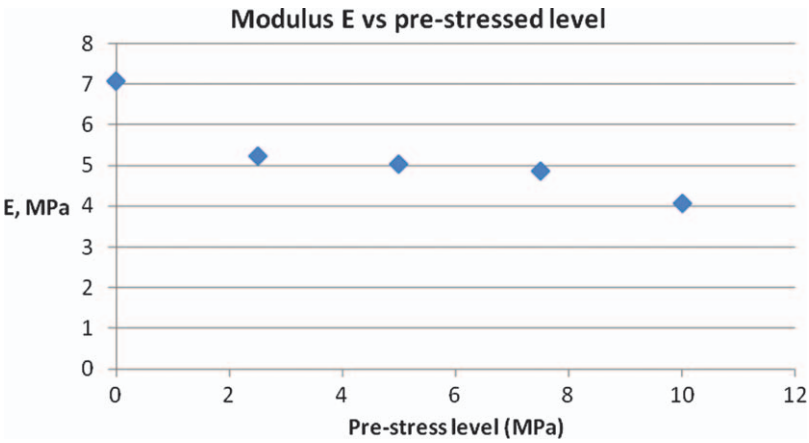

Figure 3.12 Effect of pre-stressing on the Young's modulus of silica-filled vulcanized NR containing 4 pphr Si69 (reproduced from reference 44).

strain level, it might be that the measurement was not sensitive enough to detect when the vulcanizate was too stiff.

Simple extension measurements were also done on test pieces subject to pre-stressing at different stresses by hanging dead loads on the test piece for 3 minutes, after which time the load was removed. This was done to assess the strength of the rubber–filler interaction. Simple extension measurements were done immediately after unloading. Figure 3.12 shows that the Young's modulus *E* decreased progressively with increasing level of pre-stressing, which might be associated with the breaking of bonds at the rubber–filler interface, as

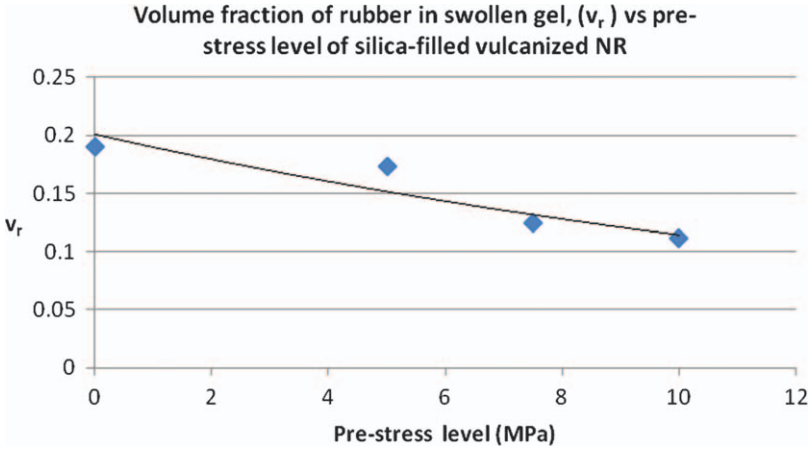

Figure 3.13 Effect of pre-stressing (static loading) on the volume fraction of rubber in the swollen gel of silica-filled vulcanized NR containing 4 pphr Si69 (reproduced from reference 44).

well as the effect of stress softening, because simple extension measurements were done immediately after unloading. In this test, the sample containing 4 pphr of Si69 was chosen because it gave the highest tensile strength (see Section 3.5.4, Figure 3.21) indicating the optimum level to achieve maximum reinforcement for this particular compound.

To verify that chemical links joining the silica surface to rubber chains *via* coupling agent were broken during pre-stressing, a separate experiment was done where the pre-stressed samples were swollen in toluene in a glass bottle until equilibrium swelling was attained. Generally, volume fraction of rubber in the swollen gel v_r decreased progressively with increasing level of pre-stressing as shown in Figure 3.13. The decrease in v_r with increasing stress level indicates that high number of chemical linkages joining silica filler to rubber molecules was broken during pre-stressing. Consequently more solvent diffused into the rubber network as the number of broken chemical linkages was high. Thus this result provides experimental evidence that chemical linkages joining silica filler to rubber molecules was relatively weak since they were broken at moderately low stresses (5–10 MPa). This result supports the findings of Luginsland *et al.*[43] who suggested that the silica–rubber interaction was weak. Apart from static loading, the effect of repeated stressing on the strength of rubber–silica interaction *via* coupling agent was investigated by Azemi *et al.*[44] In this experiment, cyclic pre-stressing was applied to thin strip of vulcanized silica-filled NR containing different amounts of Si69. The samples were pre-stressed to ten cycles before doing the equilibrium swelling measurement. The stress applied was 10 MPa. The samples were swollen in toluene until equilibrium swelling was attained before and after pre-stressing. The results are shown in Figure 3.14. The effect of coupling agent Si69 on v_r was very marked, where before applying cyclic loading v_r increased as the quantity of Si69 was

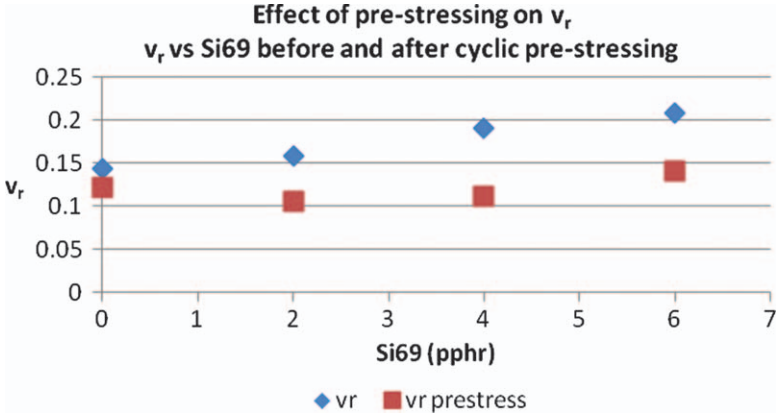

Figure 3.14 Effect of cyclic pre-stressing (10 cycles at 10 MPa) on volume fraction of rubber in the swollen gel of silica-filled vulcanized NR containing different amounts of coupling agent, Si69.

increased. This might be associated with the development of chemical linkages at the rubber–filler interface *via* Si69 which might restrict or slow down the diffusion of the solvent into the rubber matrix. But when the sample was pre-stressed dynamically to ten cycles, v_r decreased markedly at each level of Si69 loading, indicating that the quantity of solvent absorbed was more than for the unstressed sample. Probably the chemical linkages at the rubber–filler interface might be broken to some extent during cyclic pre-stressing, which consequently provided easy passage of solvent to diffuse into the rubber. The results in Figure 3.14 complement those in Figure 3.13.

3.4.2 Effect of Oil Extraction on Elastic Constant

In practice, oil is added into rubber compounds containing appreciable amount of fillers to facilitate mixing. These include to ease the incorporation of filler into the rubber, reduce heat generation during mixing and subsequent processes, and improve the flow of the rubber compound to ease fabrication processes. It is important to know how the process oil affects the reinforcement of the modulus of filled vulcanized rubber. Apart from that, the oil initially present in the rubber components may be loss by slow evaporation if exposed at elevated temperatures. Equally true the oil may be loss if immerse in liquid or solvent that can extract the oil. A rubber seal that is in contact with the oil may encounter this problem. This section discusses the work done to investigate the effect of acetone extraction on the elastic constant C_1 and tensile modulus (M100) of black-filled vulcanized NR[45,46] base on the compound formulations shown in Table 3.5. Simple extension measurement was done by using vulcanized parallel rubber strip having dimensions of 100 mm $\times$ 3 mm $\times$ 1 mm. In simple extension,[42] the force–extension relationship is given by Equation (3.17):

$$f = 2A_o\left(\lambda - \lambda^{-2}\right)\left[C_1 + C_2\lambda^{-1}\right] \tag{3.17}$$

Table 3.5 Compound formulations to investigate the effect of process oil on elastic constant before and after acetone extraction.

Paraffinic oil (pphr)	*0*	*5*	*25*	*35*
Cure time at 150 °C (minutes)	10	10	10.5	11
M100 (MPa) (before acetone extraction)	2.4	1.53	0.90	0.73
M100 (MPa) (after acetone extraction)	2.6	2.32	1.68	1.49
C_1 (kPa) (before acetone extraction)	162.3	140	96.3	86.8
C_1 (kPa) (after acetone extraction)	206.7	172.2	122.0	107.5

Base mix: NR (SMR CV60) 100, zinc oxide 5, stearic acid 2, Santoflex 13[a] 3, HAF black 50, sulfur 1.5 and *N*-cyclohexyl-2-benzothiazyl sulphenamine (CBS_ 0.75. All in parts per hundred of rubber (pphr).
[a]Santoflex 13, *N*-1,3-dimethyl butyl phenyl paraphenylene diamine.

where f is the force required to maintain at equilibrium, a strip of vulcanized rubber of cross-sectional area A_o at extension ratio λ. C_1 and C_2 are constants. However, for black-filled vulcanized rubber, the deformation on the rubber is no longer affine.[30] There is a further complication associated with stress softening, thus black-filled vulcanizate does not obey Equation (3.17). Mullins and Tobin[30] have suggested to use the strain-amplification factor to take into account of the strain at the vicinity of the particulate filler. They have assumed that the strain in the rubber matrix of a reinforced vulcanizate is a factor X times greater than the overall strain and have calculated the actual extension ratio, Λ, of the rubber matrix by Equation (3.18):

$$\Lambda = 1 + Xe \tag{3.18}$$

where e is the measured strain in the vulcanizate as a whole. For a reinforcing HAF black, they used:

$$X = 1 + 0.67fc + 1.62f^2c^2 \tag{3.19}$$

where f and c carry the same meaning as in Equation (3.10).

The load-extension behaviour of black-filled vulcanized NR is represented by plotting load/$(\Lambda - \Lambda^{-2})$ against Λ^{-1} as shown in Figure 3.15 after taking into account of the strain-amplification factor as suggested by Mullins.[30,45] In another experiment the samples were subject to hot acetone extraction for 48 h. After 48 h they were dried under vacuum at room temperature until their dried weight was constant. These dried samples were again immersed in a hot acetone for further 24 h to extract further any remaining acetone extractable materials. After the second extraction the samples were dried under vacuum until the weight of each sample was constant. Simple extension measurement was done on each sample and the results are shown in Figure 3.16. The straight line portion of the plot was extrapolated to intercept the load/$(\Lambda - \Lambda^{-2})$ axis. The C_1 value was calculated from the intercept. Figure 3.17 shows the effect of process oil on elastic constant C_1 before and after acetone extraction. The C_1 value decreased linearly with increasing amount of oil due to dilution effect.[46] It

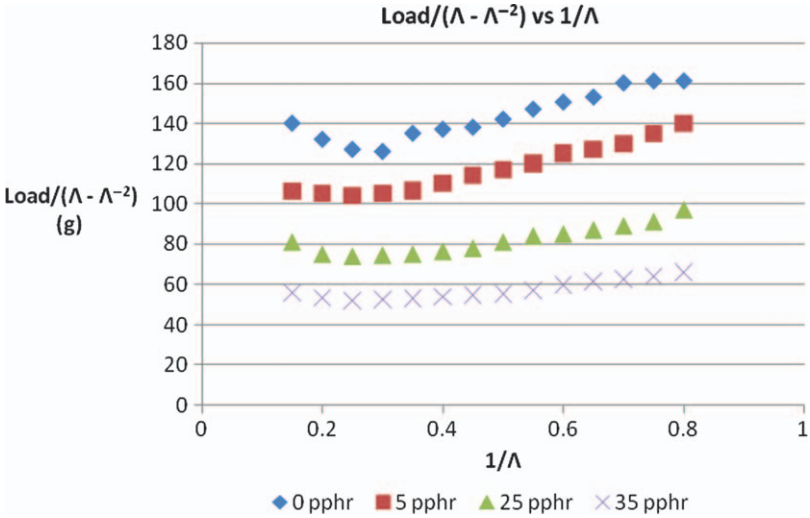

Figure 3.15 Mooney–Rivlin plot of vulcanized black-filled (50 pphr of HAF black) NR containing different amounts of paraffinic oil (before acetone extraction).

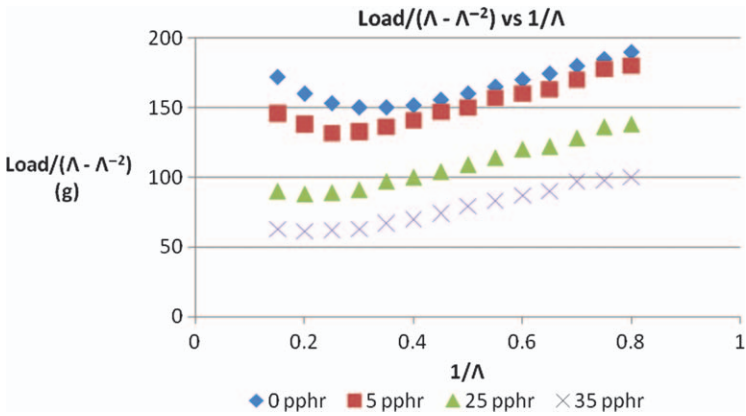

Figure 3.16 Mooney–Rivlin plot of vulcanized black-filled (50 pphr of HAF black) NR containing different amounts of paraffinic oil (after acetone extraction).

is interesting to note that even after the process oil was removed from the vulcanizate by hot acetone treatment, the C_1 value still decreased linearly with increasing oil initially present in the vulcanizate. This phenomenon is known as supercoiled network that formed when unvulcanized rubber diluted with oil or solvent is crosslinked in the diluted state and the diluent is then removed by extraction (or by evaporation).[41] As the rubber chains are unconstrained when being crosslinked it is assumed that the chains are then in their random configuration, and when the diluent (solvent) is removed the crosslinks move

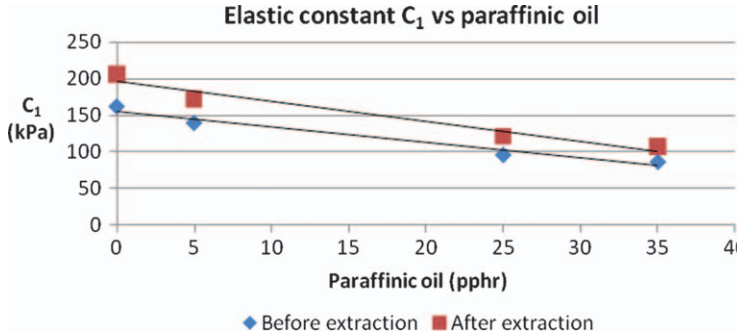

Figure 3.17 Comparison between elastic constant C_1 before and after acetone extraction.

towards each other, and so the end-to-end distance between the chain ends (at crosslinks) is less than it would be for the rubber crosslinked to the same extent in the dry state in the usual way. According to the statistical theory, as the free energy of a single chain varies as the square of the end-to-end distance, the modulus will vary similarly as the initial end-to-end distance.[42] The reinforcement in the modulus of in vulcanized black-filled NR is affected by the presence of diluent such as low molecular weight liquid or oil.

3.5 Mechanism of Reinforcement in Tensile Strength

3.5.1 Influence of Types of Crosslink and Crosslink Concentration

Apart from all the mechanisms discussed in Section 3.3, there are other factors that affect tensile strength of vulcanized filled rubber. These other factors include the geometrical structure of the rubber, the types of crosslink and the crosslink concentration of the rubber network as illustrated in Figure 3.18. At low crosslink concentration (below 0.04 mol/kg), the tensile strength of both CV and efficient vulcanizatrion system (EV) vulcanized black-filled NR was lower than that of vulcanized black-filled SBR. This phenomenon can be discussed in the light of the explanation put forward by Gee[47] for the dependence of the tensile strength of unfilled NR upon crosslink concentration. At very low crosslink concentration, portions of the uncrosslinked molecular chains can flow during extension. It is easy for the network to response to deforming stress by flow. As a result, the stress is dissipated before the critical stress necessary to effect reorientation and crystallization is attained. As the crosslink concentration increases, more chain segments are introduced which enable to support higher tensile force. Thus the tensile strength increases progressively with increasing crosslink concentration until it reaches its optimum value indicating that a complete network has been formed and viscous flow is no longer feasible. Over this region appreciable molecular orientation occurs during extension, and a large rise in degree of crystallization which enhances further the tensile

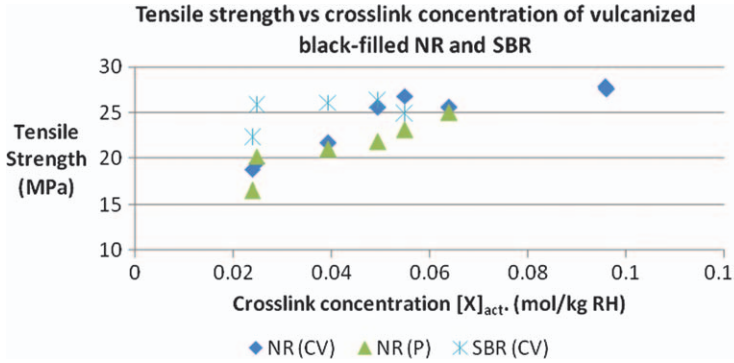

Figure 3.18 Effect of crosslink concentration and types of crosslink on tensile strength (TS) of vulcanized black-filled (50 pphr of HAF, N330) NR and SBR. CV, conventional sulfur system; EV, efficient sulfur vulcanization system.

strength. The crystallites consist of many chains aligned closely together and provide some form of reinforcement. The stress is now transferred to the crystals which are made up of lumps of chains. This is the same as if the stress is transferred to hundreds of chains knitted closely together.

The chain segments are made of short and long chains which are distributed randomly in the network. When the vulcanizate is pulled the chain segments are stretched and become taut. The shortest chain will break first and the stress will be transferred to neighbouring chains. As the shortest chain segments are being broken, the high stress is now supported by a less number of crosslink and finally complete rupture occurs.

At optimum value, the network structure is already completed, and further insertion crosslink can only result in the tightening of the network. This in turn imposes an increasing number of restrictions on any molecular segment attempting to orientate and aligned with neighbouring segments. The overall effect is that the degree of oriented crystallization falls and consequently the tensile strength decreases. In the case of a non-strain-crystallizing rubber, increasing the crosslink concentration makes the chain segments become shorter. The rubber vulcanizate now becomes less extensible and becomes stiffer and needs larger force to stretch than vulcanizate with low crosslink concentration. The large applied forces lead to its rupture since the network reaches its finite extensibility before appreciable elongation of the network as a whole takes place.

It is interesting to note that vulcanized black-filled SBR gives higher tensile strength than that of vulcanized black-filled NR at low crosslink concentration ($[X]_{act} \leq 0.04$ mol/kg Rubber Hydrocarbon (RH)). However, when ($[X]_{act} \geq 0.04$ mol/kg RH, the tensile strength of vulcanized black-filled NR is higher than that of vulcanized black-filled SBR. This phenomenon can be explained in the light of the theories discussed in Section 3.3. One common feature of these theories is that the enhancement in strength is associated with energy

dissipation or hysteresis. In the case of filled system, apart from viscous drag there are other sources of heat generation as follows: first is the friction between the filler particles. Secondly, is the friction between rubber chains and filler surface. Thirdly, is the detachment or debonding of filler from rubber chains. Last, but not least is the breaking of the filler structure. In addition to filler, two other factors that contribute to energy dissipation (hysteresis) are strain crystallization and the glass transition temperature (θ_g) of the rubber. At low crosslink concentration, the extent of strain crystallization in NR might be low thus producing low hysteresis. Indeed Hamed and Park[48] reported that up to 250%, wholesale crystallinity of the NR does not occur. In this region SBR gives higher tensile strength than that of NR since the former produces higher hysteresis than the latter because SBR has higher θ_g (−63 °C) than θ_g that of NR (−72 °C). As explain above at optimum crosslink concentration, it allows strain crystallization to develop fully. In this situation, NR gives higher hysteresis than that of SBR and hence the tensile strength of NR is higher than that of SBR in the regions where crosslink concentration is optimum. The high tensile strength produced by black-filled SBR indicates clearly that reinforcing filler enhances mechanical strength. The enhancement in the tensile strength of vulcanized black-filled SBR is very substantial because vulcanized unfilled SBR can produce tensile strength in the range of 1.0–3.0 MPa.

It is interesting to discuss recent work by Hamed and Rattanasom[49] who investigated the effect of crosslink density on vulcanized black-filled NR. Their results indicated that at low crosslink concentration, the gum (unfilled) strength NR vulcanizate was very low and incapable of inducing strain crystallization for the same reasons given earlier. However, in the case of black-filled NR, the vulcanizate is able to induce strain crystallization presumably because of the strain-amplification effect. Hamed and Rattanasom[49] commented that crystallization transforms some of the elastomeric network to hard domains, thereby increasing the effective volume fraction of filler. For example a vulcanized black-filled NR containing 50 pphr of carbon black corresponding to volume fraction filler, $c \approx 0.2$. Assuming that 20% of crystallization occurs, the effective filler volume fraction of reinforcement is about 0.38. The effect is the same as if we are putting 122 pphr of reinforcing carbon black into non-strain-crystallizing rubber. Such high filler loading is difficult to mix and to achieve uniform dispersion in the rubber matrix.

As far as the type of crosslink is concerned, it well established that the conventional sulfur (CV) system that produces predominantly polysulfidic crosslinks would give higher tensile strength than peroxide-cured NR. The same load transfer mechanism theory has been used widely to explain the effect of types of crosslink on tensile strength of vulcanized unfilled NR.[50] In a vulcanized rubber network, particularly if the crosslinks are polysulfidic type, the lengths of the crosslink are not uniform but vary from 3 to 6 sulfur atoms bridging the two polymer chains. Thus when the shortest link breaks, the stress is transferred to neighbouring longer links and the cycles repeat themselves until complete rupture is fulfilled. But during the cycles of transferring the stress to neighbouring links, it allows energy dissipation process to take place which

enables the network to support higher stress level. Thus when polysulfidic crosslink breaks and slips under the localized high stress concentrations, it relieves these stress concentrations by causing the load to be shared over neighbouring chains and thereby permitting the deformed network as a whole to bear a high stress. This stress-relieving mechanism does not take place in peroxide vulcanization system.

3.5.2 Effect of Filler Loading on Tensile Strength

Unfilled NR has a high tensile strength because of its ability to crystallize on straining. The crystals act as a reinforcing filler to enhance the tensile strength. Addition of reinforcing filler increased the tensile strength significantly but not substantially as shown in Figure 3.19. At the optimum filler loading (30–40 pphr) the increase is only about 20%. This shows that much of the enhancement in the strength comes from induced strain crystallization inherent in NR. In contrast the reinforcement in non-strain-crystallizing rubber like SBR is very substantial where the tensile strength increases by a factor of 9 or 10 as discussed in Section 3.5.1. In the case of filled system, apart from viscous drag there are other sources of heat generation as follows: first is the friction between the filler particles. Second is the friction between rubber chains and the filler surface. Third is the detachment or debonding of filler from rubber chains. Last but not least is the breaking of the filler structure. Indeed Medalia[51] attributed to breakage of carbon black structure that resulted increase in hysteresis with increasing black loading. The hysteresis of black-filled vulcanized rubber is also dependent on the particle size and filler loading.[51] Medalia[51] found that hysteresis increased almost linearly with the carbon black interfacial area A_b. The interfacial area of the carbon black is given by Equation (3.20):

$$A_b = \rho Sc \tag{3.20}$$

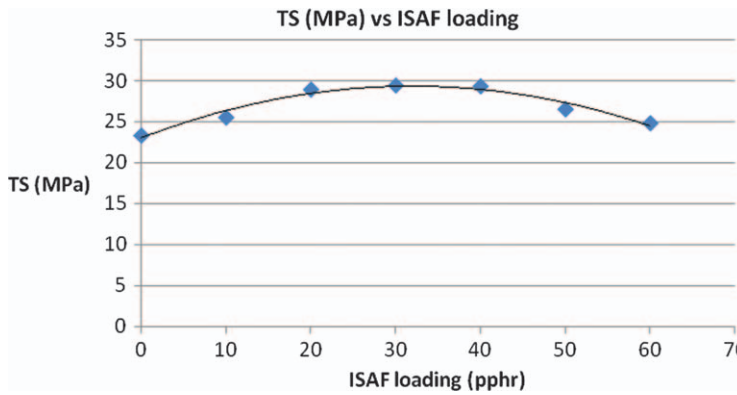

Figure 3.19 Effect of filler loading on tensile strength of vulcanized ISAF black-filled NR.

where ρ is the true density of carbon black, c is the volume fraction of carbon black in rubber, and S is the specific surface area of the black. Medalia[51] found that there was a linear function of $A_b c$ with that of the loss tangent (a quantitative measure of hysteresis) indicating that the hysteresis is expected to increase with filler loading. The increase in tensile strength with increasing filler loading is attributed to increase in the hysteresis until its optimum loading. Beyond the optimum loading, the tensile strength decreases because the volume occupied by the filler exceeds the volume made available in the rubber phase.

3.5.3 Dependence of Tensile Strength of Vulcanized Black-Filled Rubber on Particle Size

Apart from filler loading, the tensile strength of black-filled rubber is also dependent on the particle size. The tensile strength of vulcanized black-filled NR decreases gradually with increasing particle size as shown by the histogram in Figure 3.20. One of the factors affecting reinforcement is the particle size. Assuming that if the particle is spherical in shape having radius r, it can be shown that the surface area (SA) per unit volume (V) is given by $SA/V = 3/r$. From this simple relationship, the surface area increases as the particle size decreases. Consequently the high surface area enhances the immobilization of the molecular chains that leads to the enhancement in the rubber–filler interaction. High surface areas provide more contact points at the rubber–filler interface. Consequently, the extent of linkages or bonding at the rubber–filler interface increases, thus enabling the rubber matrix to support high stresses. The amount of energy dissipation would also increase when these particles are detached from the rubber chains during deformation. Indeed Medalia[51] found

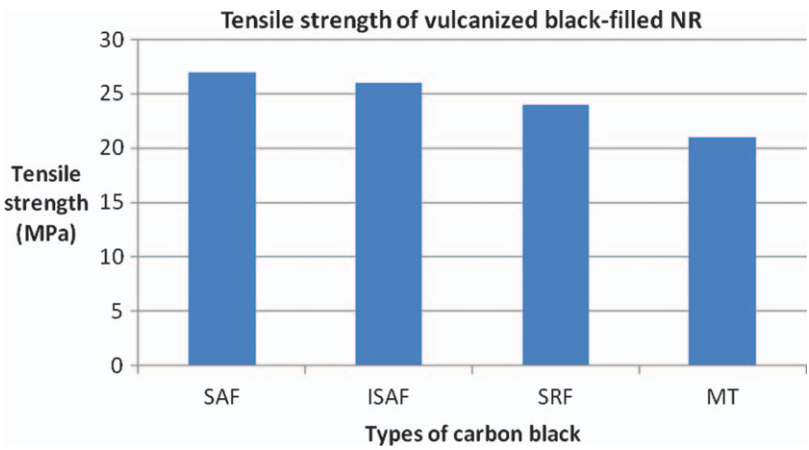

Figure 3.20 A histogram showing the dependence of tensile strength on particle size of carbon black (average particle sizes in μm: SAF, 20–25, ISAF, 24–33, SRF, 70–96, MT, 250–350[52]).

that hysteresis increased almost linearly with the carbon black interfacial area A_b as given in Equation (3.20) earlier.

The dependence of the reinforcement on particle size can be viewed in two ways, first is the surface area, and second is particle mass.[53] The surface area of a particle is inversely proportional to its particle size. If all particles are spheres of the same size, the surface area A_s per gram of filler is given by Equation (3.21):

$$A_s = \pi d^2/(1/6\pi d^3\rho) = 6/d\rho \qquad (3.21)$$

where d is the diameter and ρ is density. The difference between micron-sized and nanoscale filler surface area can be a factor of 10 to 100.

3.5.4 Effect of Filler–Rubber Interaction on Tensile Strength

One of the important factors affecting reinforcement is the extent of the bonding at filler–rubber interface.[11] This is particularly true in the case of silicas and silicates. Although their average particle size is smaller (18–25 nm)[52] than the average particle size of reinforcing ISAF carbon black (25–33 nm),[52] but silica filler on its own fails to enhance mechanical strengths of vulcanized NR unless coupling agent is included in the rubber formulation. The coupling agent is used to couple or bond a filler to the rubber molecule. This approach is necessary because the hydrophilic surfaces of the silica are basically incompatible with the hydrophilic rubber surface. The use of a coupling agent enables compatibility to be attained on a 'like-for-like' basis.[54]

The influence of silane coupling agent on the tensile strength of vulcanized silica-filled NR is shown in Figure 3.21, based on the same compounds discussed in Section 3.4.1. As the loading of Si69 in the formulation is raised, the tensile strength also increases until it reaches the optimum level. In the absence of coupling agent, the tensile strength is 11.2 MPa, markedly lower than mixes

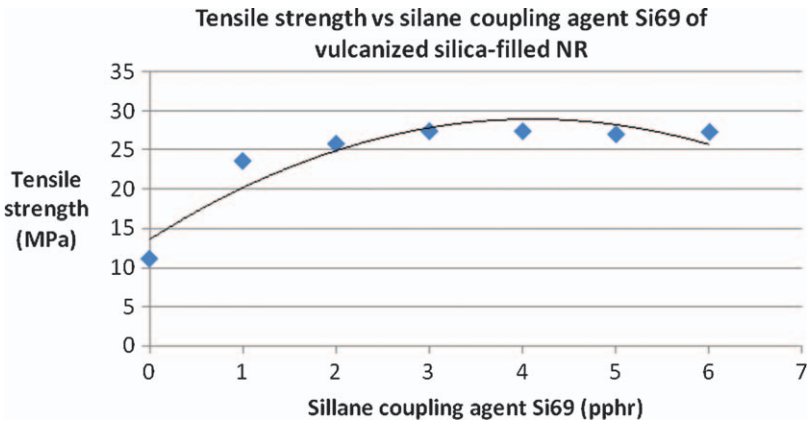

Figure 3.21 Influence of silane coupling agent on tensile strength of vulcanized silica-filled NR.

that contained the coupling agent. This indicates clearly that even if the particle size is very small, which provides high surface area for many contact points between filler and rubber, but in the absence of strong bonding or interaction at the rubber–filler interface, the desired reinforcement is not achieved. However, in the presence of coupling agent the tensile strength increases progressively with increasing amount of coupling agent, until it reaches an optimum value above which increasing the quantity of coupling agent decreases the tensile strength. This optimum value occurs at 4 pphr of coupling agent. Referring to Figure 3.14, the volume fraction of rubber in the swollen gel, v_r, increases progressively as the quantity of coupling agent increases indicating development of chemical bonding at the silica–rubber interface *via* coupling agent.[43] This additional chemical linkages has the same effect as if the chemical crosslink concentration in the rubber network has increased. When the crosslink network becomes tight tensile strength decreases as discussed in Section 3.5.1 above.

3.5.5 Influence of Filler Dispersion on Tensile Strength

The reinforcement in the strength of vulcanized rubber by particulate filler is affected not only by the characteristics of the filler as listed in Section 3.2, but also influenced by the quality of filler dispersion in rubber matrix. Azemi *et al.*[55] has investigated the effect of filler in NR latex film. They reported that black-filled vulcanized NR latex film produced lower tensile strength than unfilled NR latex film. The former gave tensile strength 10.5 MPa, in contrast the latter gave 28.3 MPa. In the case of black-filled NR vulcanizate prepared from SMR20, the tensile strength was 28.2 MPa. The effect of HAF black loading on tensile strength of vulcanized NR latex film post-vulcanized for 30 min at two different temperatures, 100 °C and 140 °C, respectively, is shown in Figure 3.22. The results are in contrast with Figure 3.19 for NR base on SMR10. The low tensile strength in filled NR latex film might be attributed to poor dispersion of the black. Although the carbon black dispersion was prepared by ball milling for 24 h, dispersion of the black into the latex might not be as efficient as in the

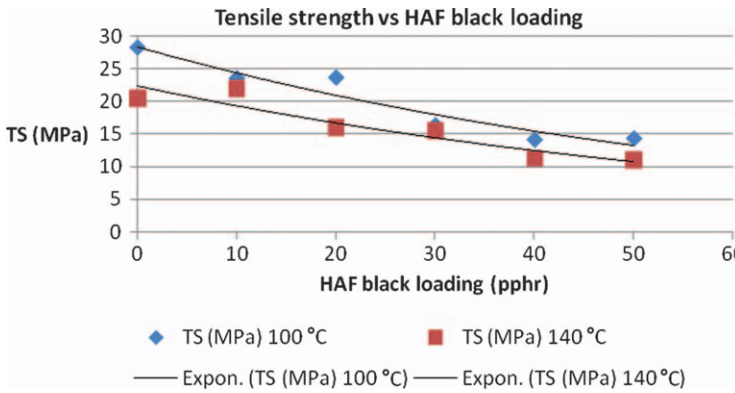

Figure 3.22 Influence of HAF black loading on tensile strength of post-vulcanized NR latex film.

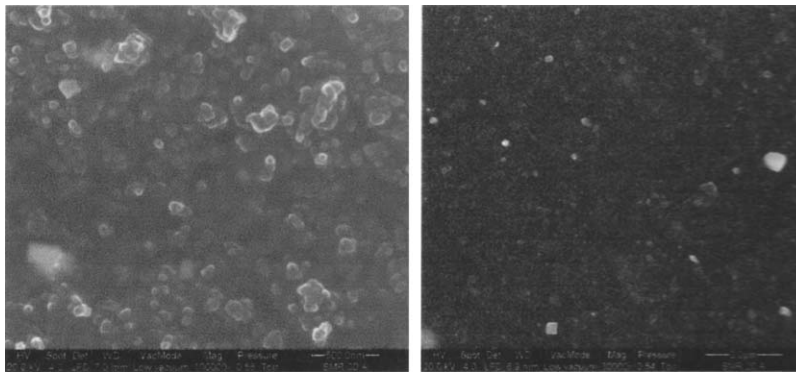

Figure 3.23 NR black-filled (SMR20 + 50 pphr HAF) with good black dispersions.

dry rubber. In the latter case, it is subject to high mechanical shear forces during mixing on the two-roll mill. This shearing action breaks down black aggregates and disperses them uniformly within the rubber matrix. This shearing action is not available in the case of latex compounding. The SEM micrograph tends to support this suggestion. Thus the results indicate that tensile strength is very sensitive to flaws. In tensile tests, the poorly dispersed black acts as flaws, giving rise to stress concentration and initiating failure around the flaws.

The SEM micrograph in Figure 3.23 shows good dispersion of carbon black in the rubber matrix, in contrast to that in Figure 3.24, which shows poor dispersion and large agglomerates in a NR latex film.

The high gum strength of NR latex film is attributed to at least four factors. First is the ability of NR latex film to strain crystallize as a consequence of its regular microstructure (100% *cis*-1,4 configuration). The crystallites consist of many chains aligned closely together and provide some form of reinforcement, thus enhancing the tensile strength. Secondly, NR latex has a very high molecular weight ($\sim 10^6$ g mol^{-1}) because compounding of NR latex does not involve a mastication process where long molecular chains are converted to short molecular chains by high mechanical shearing actions. It is well established that molecular weight affects mechanical strength. Mechanical strength increases with increasing molecular weight. Thirdly, NR latex films are viewed as having a reinforced structure consisting of hard domains of protein molecules held together by hydrogen bonds.[56] The domains arise during evaporation of water from the film by agglomeration of the protein present on the surface of the individual rubber particles of the latex. The fourth factor is associated with a high concentration of polysulfidic crosslinks. It is well established that low-temperature vulcanization produces more polysulfidic crosslinks than at high temperature.[57] Polysulfidic crosslinks have low bond energy ($\sim$ 268 kJ/mol), thus they are more stable at low temperature than at high temperature.[57] Polysulfidic crosslinks are well known for their enhancement in tensile strength because of their ability to relieve local stresses through

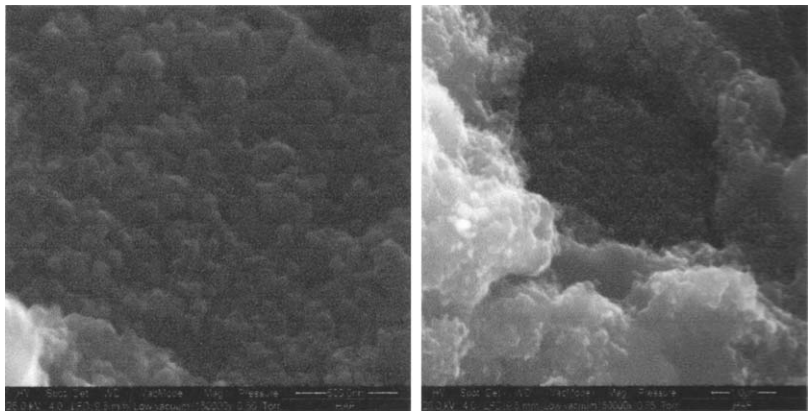

Figure 3.24 NR latex film filled with 50 pphr HAF. Poor black dispersion. Black aggregates are not broken up and dispersed uniformly in the rubber matrix.

'yielding'. The rubber itself does not yield, but yielding occurs within the polysulfidic crosslinks when they break and slip under the localized high stress concentrations, since they are weak and labile.[57]

Acknowledgements

The author is very grateful to Professor Dr Sabu Thomas for trusting in him and giving him the opportunity to write a book chapter. He would also like to thank Professor Dr Ri Hanum Yahaya Subban, Dean of the Faculty of Applied Science of the Universiti Teknologi MARA, Shah Alam Malaysia, for her encouragement and permission to publish some of the experimental data on some of the current research work conducted by the author and the students under his supervision.

The author would like to express his sincere appreciation and thanks to Cambridge University Press for giving permission to reproduce figures and data from their publications.

Last but not least, to Miss Siti Aisyah Jarkasi and Miss Rasyiqah Abdul Rahim for their kind assistance in formatting the chapter.

References

1. E. M. Danenberg, Carbon black, in *Vanderbilt Rubber Handbook*, R. T. Vanderbilt Company, Inc., Norwalk, CT, 1978, pp. 408–424.
2. D. Barnard, C. S. L. Baker and I. R. Wallace, *Rubber Chem. Technol.*, 1985, **58**, 740.
3. J. B. Horn, in *Rubber Technology and Manufacture*, Butterworths, London, 1971, pp. 174–190.
4. T. A. Vilgis, in *Reinforcement of Polymer Nano-Composites, Theory, Experiments and Applications*, 2009, pp. 1–209.

5. J.-P. Donnet, R. C. Bansal and M. J. Wang (ed.), *Carbon Black: Science and Technology*, New York, Marcel Dekker, 1993, p. 89.
6. J. B. Donnet, Elastomeric matrix and carbon black interactions in rubber compounds, in *Proceedings International Rubber Conference 1997*, Rubber Research Institute of Malaysia, Kuala Lumpur, pp. 323–327.
7. M. Gerspacher and C. P. O'Farrel, Filler–filler and filler–polymer interactions as a function of in-rubber carbon black dispersion, in *Proceedings International Rubber Conference 1997*, Rubber Research Institute of Malaysia, Kuala Lumpur, pp. 184–193.
8. J. J. Brennan, T. E. Jerymyn and B. B. Boonstra, *J. Appl. Polym. Sci.*, 1964, **8**, 2687.
9. A. F. Blanchard and D. Parkinson, in *Proceedings of the Second Rubber Technology Conference*, 23–25 June 1948, London, 1948, pp. 615–624.
10. A. F. Blanchard and D. Parkinson, *Ind. Eng. Chem*, 1952, **44**, 799.
11. F. Bueche, *J. Polym. Sci.*, 1958, **33**, 259.
12. E. M. Dannenberg, *Trans. Inst. Rubber Ind.*, 1966, **42**, T26.
13. S. Wolff, *Rubber Chem. Technol.*, 1996, **69**, 325.
14. E. H. Andrews and A. Walsh, *J. Polym. Sci.*, 1958, **33**, 39.
15. T. Z. Sen, M. A. Sharaf, J. E. Mark and A. Kloczkowski, *Polymer*, 2005, **46**, 7301.
16. V. A. Coveney, D. E. Johnson and D. M. Turner, *Rubber Chem. Technol.*, 1995, **68**, 660.
17. V. A. Coveney and D. E. Johnson, *Rubber Chem. Technol.*, 1999, **72**, 779.
18. V. A. Coveney and D. E. Johnson, *Rubber Chem. Technol.*, 2000, **73**, 779.
19. M. Kluppel and J. Schramm, in *An Advanced Micro-Mechanical Model of Hyperelasticity and Stress Softening of Reinforced Rubbers*, Proceedings of Constitutive Models for Rubber, Balkema, Rotterdam, 1999.
20. M. Kluppel and J. Meier, in *Modeling of Soft Matter Viscoelasticity for FE-Applications*, Proceedings of the First European Conference on Constitutive Models for Rubber, Hannover, Germany, 2001.
21. Y. Fukahori and W. Seki, *J. Mater. Sci.*, 1993, **28**, 4471.
22. Y. Fukahori, *Rubber Chem. Technol.*, 2007, **80**, 701.
23. J. S. Bergström and M. C. Boyce, *Rubber Chem. Technol.*, 1999, **72**, 633.
24. A. A. Hon, J. J. C. Busfield and A. G. Thomas, *Filler reinforcement in rubber carbon black systems, Constitutive Models for Rubber III*, Lisse:Balkema, 2003, 300.
25. V. Jha, J. J. Busfield and A. G. Thomas, in *Constitutive Models for Rubber IV*, Proceedings of the ECCMR Conference, London, UK, 2005, pp. 459–464.
26. A. N. Gent, *Rubber Chem. Technol.*, 1996, **69**, 59.
27. V. Jha, A. A. Hon, A. G. Thomas and J. J. C. Busfield, *J. Appl. Polym. Sci.*, 2007, **107**, 2572.
28. V. Jha, *Carbon Black Filler Reinforcement of Elastomers*, PhD Thesis, Dpt. of Materials, Queen Mary, University of London, 2008, pp. 159–206.
29. V. Jha, A. G. Thomas, M. Bennett and J. J. C. Busfield, *J. Appl. Polym. Sci.*, 2008, **116**, 541–546.

30. L. Mullins and N. R. Tobin, *J. Appl. Polym. Sci.*, 1965, **9**, 2993.
31. E. Guth and R. Simha, *Kolloid-Z*, 1936, **74**, 266.
32. J. G. Sommer and O. H. Yeoh, *Tests and Specifications, In Engineering with rubber: how to design rubber components*, Ed. A. N. Gent, Hanser-Gardner Publications, Cincinnati, OH, 2001, pp. 307–366.
33. M. J. Wang, *Rubber Chem. Technol.*, 1998, **71**, 520.
34. A. R. Payne and R. E. Whittaker, *Rubber Chem. Technol.*, 1971, **44**, 440.
35. E. Guth and O. Gold, *Phys. Rev.*, 1939, **53**, 322.
36. H. M. Smallwood, *J. Appl. Phys.*, 1944, **15**, 758.
37. A. I. Medalia, *J. Colloid Interface Sci.*, 1970, **32**, 115.
38. A. Einstein, *Ann. Physik*, 1911, **34**, 591.
39. P. J. Flory and J. Rehner, *J. Chem. Phys.*, 1943, **11**, 521.
40. M. Porter, *Rubber Chem. Technol.*, 1967, **40**, 866.
41. G. M. Bristow and M. Porter, *J. Appl. Polym. Sci.*, 1967, **11**, 2215.
42. L. R. G. Treloar, *The Physics of Rubber Elasticity*, Clarendon Press, Oxford, 3rd edn, 1975, pp. 42–58.
43. H. D. Luginsland, J. Frohlich and A. Wehmeier, *Influence of Different Silanes on the Reinforcement of Silica-filled Rubber Compounds*, paper No. 59 presented at the ACS Meeting, Rhode Island/USA, April 24–27; Rhode Island/USA, 2001.
44. A. B. Samsuri and C. M. S. Said, *J. Rubber Res.*, 2013, **16**, 101.
45. A. B. Samsuri, in *Meeting of the Rubber Division, American Chemical Society Chicago*, Illinois, USA, 1995, pp. 1–20.
46. A. B. Samsuri, *J. Nat. Rubber Res.*, 2012, **15**(1), 1–18.
47. G. Gee, *J. Polym. Sci.*, 1947, **2**, 451.
48. G. R. Hamed and B. H. Park, *Rubber Chem. Technol.*, 1999, **72**, 946.
49. G. R. Hamed and N. Rattanasom, *Rubber Chem. Technol.*, 2002, **75**, 935.
50. L. Mullins, in *Proceedings of the Natural Rubber Producers' Research Association Jubilee Conference, Cambridge*, Maclaren and Sons Ltd, London, 1964, pp. 136–169.
51. A. I. Medalia, *Rubber Chem. Technol.*, 1991, **64**, 481.
52. B. B. Boonstra, *Fillers: Carbon Black and Non-Black*, Ed. C. M. Blow, VNR, London, Toronto, Melbourne, 2nd edn, 1973, pp. 227–259.
53. Y. Wang, L. Zhang, C. Tang and D. Yu, in *Rubber Nanocomposites. Preparation, Properties and Applications*, *J. App. Polymer Sci.*, 2000, **78**, 1879–1883.
54. C. Hepburn, *Plast. Rubber Int.*, 1984, **9**, 12–13.
55. A. Samsuri, S. Sudin and N. Y. Saleh, in *PRIM Golden Jubilee International Polymer Conference GJIPC*, Sunway Resort Hotel and Spa, Kuala Lumpur, 2010, 1–23.
56. K. L. Chong and M. Porter, in *International Conference on Structure Property Relation of Rubber*, Kharagpur, India, 1980, p. 1.
57. P. S. Brown, M. Porter and A. G. Thomas, Influence of crosslink structure on properties in crystallizing and non-crystallizing polyisoprenes, in *Proceedings International Rubber Conference 1985*, Rubber Research Institute of Malaysia, Kuala Lumpur, pp. 20–45.

CHAPTER 4

Preparation and Properties of Natural Rubber Composites and Nanocomposites

DONGZHI CHEN,*[a] MINGJIE HU,[b] CHI HUANG[b] AND RUIWEN ZHANG[c]

[a] School of Materials Science and Engineering, Wuhan Textile University, No. 1 Yangguang Road, Jiangxia District, Wuhan, 430200, Hubei Province, China; [b] College of Chemistry and Molecular Sciences, Wuhan University, Luojiashan, Wuhan, 430072, Hubei Province, China; [c] School of Materials and Chemical Engineering, Zhongyuan University of Technology, No. 41 Zhongyuan Road (M), Zhenzhou, 450007, Henan Province, China
*Email: chdozh_2008@163.com

4.1 Introduction

Natural rubber (NR) is a high molecular weight polymer of isoprene (2-methyl-1,3-butadiene), the most important and the oldest known polymeric material. Over past decades, considerable attention has been paid to NR materials due to their excellent elasticity, flexibility, antivirus permeation, good formability and biodegradability.[1] NR materials have been widely used to produce pneumatic tyres for the automotive industry. Although NR has a wide range of properties, it still has some shortcomings that affect its application. For example, NR is susceptible to breakdown by oxidative and thermal degradation due to an unsaturated backbone, especially when it is presented in virgin form without

RSC Polymer Chemistry Series No. 8
Natural Rubber Materials, Volume 2: Composites and Nanocomposites
Edited by Sabu Thomas, Hanna J. Maria, Jithin Joy, Chin Han Chan and Laly A. Pothen

Published by the Royal Society of Chemistry, www.rsc.org

any modification, and mechanical properties of products made from NR latex cannot meet the requirements of industrial applications. The above disadvantages further limit widespread applications of NR. In recent years, great efforts have been made to improve properties of NR such as mechanical properties, thermal stability, electrical conductivity, and so on.

NR composites and nanocomposites can be fabricated by three main techniques, namely latex compounding, solution mixing and melt blending. A variety of nanofillers, such as carbon black, silica, carbon nanotubes, graphene, calcium carbonate, organomodified clay, reclaimed rubber powder,[2] recycled poly(ethylene terephthalate) powder,[3] cellulose whiskers, starch nanocrystals, *etc*. have been used to reinforce NR composites and nanocomposites over the past two decades. In this chapter, we discuss the preparation and properties of NR composites and nanocomposites from the viewpoint of nanofillers. We divide nanofillers into four different types: conventional fillers, natural fillers, metal or compound fillers and hybrid fillers, and the following discussion is based on this classification.

4.2 NR Composites and Nanocomposites based on Conventional Fillers

4.2.1 NR Composites and Nanocomposites Reinforced with Carbon Black

To date, carbon black (CB) continues to be one of the most important reinforcing agents in the rubber industry. About 5 million metric tons of CB is consumed globally each year. However, due to its polluting nature, the ubiquitous black colour of the compounded rubber material, and its dependence on petroleum resources caused researchers to look for white reinforcing agents to replace CB.[4] In rubber tyre applications, CB is widely used as reinforcing filler to improve tensile and tear strength, modulus and hardness, abrasion and thermo-oxidative resistance, *etc*.[5] The reinforcing effect of CB on properties of NR composites and nanocomposites mainly depends on both physical interactions and chemical linkages between the filler and NR molecular chains. The specific surface area and structure of CB also affect the level of entanglement with NR molecular chains and the reinforcement effect.

The selection of a suitable amount of CB and a feasible preparative method are very important to the design of NR materials with desired comprehensive properties. The uniform dispersion of CB throughout the polymer matrix is also essential to achieve optimum vulcanized properties, and hence the degree of CB dispersion is a factor which ultimately controls the physical properties of the NR composites.[6] With good dispersion, NR composites can be imparted superior mechanical properties, tear strength, electric conductivities and wear resistance. In order to obtain good dispersion, the mixing is done in two stages by melt blending. Drying NR latex, CB and other ingredients are first mixed by melt blending, and then the curing agents are added in the premixed compound,

and the obtained mixture is mixed sequentially by melt blending until uniform dispersion phases are achieved.

Nakason *et al.*[7] prepared CB-filled NR composites by melt blending and a compression moulding technique, and subsequently investigated the curing characteristics, mechanical, morphological and electrical properties of CB-filled NR composites. It was found that the presence of polar functional groups in NR molecules and the different structures of CB significantly affected the curing characteristics and mechanical properties of NR composites. That is, polar functional groups combined with finely structured CB had a high crosslink density, high dielectric constant, high AC conductivity and high mechanical strength such as Young's modulus and tensile strength.

CB is often used together with other fillers to get hybrid fillers, and the NR composites reinforced with hybrid fillers will be discussed in the next section.

4.2.2 NR Composites and Nanocomposites Reinforced with Silica

In the rubber industry, silica is widely used as a non-black reinforcing filler to improve the mechanical properties of NR composites due to its high specific surface area, particularly tensile strength, tear resistance, abrasion resistance and hardness. Silica can be obtained by various methods, such as precipitated silica by precipitation of an aqueous sodium silicate solution, fumed silica by pyrogenic process, silica from natural resources (*e.g.* rice husk ash and fly ash),[8,9] and *in situ* silica[10] or silica sol by the sol–gel process.

However, a major problem with silica-reinforced NR is the incompatibility between the hydrophilic silica and hydrophobic NR, resulting in the formation of a strong silica–silica network caused by the low polymer–filler and high filler–filler interaction. A well-known method for improving the reinforcement effect is to treat the silica surface with silane coupling agents to promote interaction between silica and polymer chains. Most of researches are focused on *in situ* silica reinforcing filler because its dispersion is easy to control, and be treated by silane coupling agents. The treated *in situ* silica-reinforced NR nanocomposites could show good mechanical properties and thermal stabilities. The preparation of NR nanocomposites reinforced with *in situ* silica was mainly discussed in this section.

The *in situ* silica can be synthesized by two different ways. In the first way, the crosslinked polymer is swelled with tetraethoxysilane (TEOS) which is hydrolysed *in situ*. In the second way, the polymer is swelled with TEOS before crosslinking. In this case, the incorporation of silica by TEOS may be carried out in the presence or absence of coupling agent, but this *in situ* silica could depress crosslinking reaction of NR during the process of vulcanization. In general, the first method has widely been used to prepare the polymer composites with *in situ* silica.

Bokobza *et al.*[11] prepared NR composites containing *in situ* silica by the sol–gel process. The sol–gel processing was conducted before and after the crosslinking reaction. They found that small and well-dispersed *in situ* silica particles

were generated when the sol–gel reaction was conducted after curing. Meanwhile, silica particles generated before vulcanization seemed to inhibit the crosslinking reaction of NR compound by sulfur and form a silica–silica network *via* the silanol groups present on the silica surface. But the use of a silane coupling agent led to a substantial extent of reinforcement.

Peng *et al.*[1,12] reported a novel process to prepare NR/SiO_2 nanocomposites by combining latex compounding and self-assembly techniques. They found that the SiO_2 nanoparticles were homogenously distributed throughout NR matrix as nanoclusters with an average size ranged from 60 to 150 nm when the SiO_2 loading was less than 6.5 wt%. When more SiO_2 was loaded, secondary aggregations of SiO_2 nanoparticles were gradually generated, and the size of SiO_2 cluster dramatically increased. The thermal/thermo-oxidative resistance and mechanical properties of NR/SiO_2 nanocomposites were enhanced when the SiO_2 nanoparticles were uniformly dispersed.

Tangpasuthadol *et al.*[13] reported that silica-reinforced NR composite was prepared by using TEOS as a precursor to generate silica particles inside the rubber. The preparative procedures were as follows. The silica was generated *in situ* by the sol–gel process of TEOS that was mixed directly into commercial-graded NR latex having 60% dry rubber content and 0.7% ammonia. The *in situ* silica-filled NR composites were mixed with vulcanizing chemicals by a two-roll mill, and the mixture was vulcanized to produce cured NR/SiO_2 composites. They found that the silica particles dispersed evenly with sizes between 100 and 500 nm. The mechanical properties were significantly affected by the amount of TEOS added into the latex. The presence of bis(3-triethoxysilylpropyl)tetrasulfide (Si69) resulted in increases of the mechanical properties and the rate of sulfur cure. Kiatkamjornwong *et al.*[14] studied the effects of methyl methacrylate (MMA) grafting NR latex and *in situ* formation of silica particles on the morphology and mechanical properties of NR nanocomposites. MMA grafting on NR latex was carried out using cumylhydroxy peroxide/tetraethylenepentamine as a redox initiator couple. The silane was converted into silica particles by a sol–gel process which was induced during film drying at 80 °C. They found that PMMA (poly MMA) grafted NR particles were presented as a core/shell structure from which the NR particles were the core seed and PMMA was a shell layer. The silica particles were fairly evenly distributed in the ungrafted NR matrix but were agglomerated in the grafted NR matrix. The *in situ* silica particles in the grafted NR matrix slightly increased both the modulus and the tear strength of the composite film.

Chuayjuljit *et al.*[15] reported on the nanocomposites of NR and polystyrene (PS)-encapsulated nano-silica prepared by latex compounding method. The synthetic processes were described as follows: the nanolatex of PS-encapsulated silica was synthesized *via in situ* differential microemulsion polymerization. The resultant hybrid nanoparticles had a core–shell morphology with an average diameter of 40 nm. The silica hybrid nanoparticles were subsequently used as a filler for the NR nanocomposite. The mechanical properties and flammability of NR were found to be improved by the incorporation of PS-encapsulated nano-silica. A similar investigation was carried out by Prasassarakich *et al.*[16] The nano-SiO_2 was initially treated with organosilane coupling agents of

3-methylacryloxypropyltrimethoxysilane and vinyltrimethoxysilane. Therefore a nano-core (SiO_2) with a shell polyisoprene (PIP) was synthesized by a differential microemulsion polymerization of isoprene on silane-treated nano-silica. PIP-SiO_2 nanoparticles were produced at about 20–60 nm with a narrow size distribution. They found that the PIP-SiO_2 nanocomposite had been used as an effective nanofiller in NR latex, and the NR filled with PIP-SiO_2 pre-vulcanizate clearly showed an improvement in storage modulus, tensile strength, tensile modulus and anti-ageing properties.

De *et al.*[2] prepared NR/reclaimed ground rubber nanocomposites with *in situ* silica by sol–gel technology. The preparative processes were described as follows: the NR/reclaimed ground rubber composites were first prepared by conventional mechanical blending. After vulcanization, the sol–gel vulcanizates were prepared by soaking the cured sheets in TEOS for 48 h at various temperatures (30, 50 and 70 °C). The swollen sheets were then immersed in a 10% aqueous solution of *n*-butylamine for 24 h at the same temperature with the swelling. The catalyst solution was then removed, and the sheets were heated at 50 °C for 72 h for drying and further dried in a vacuum oven at 50 °C to constant weight to produce NR/reclaimed ground rubber nanocomposites with *in situ* silica. They found the mechanical properties and thermal stabilities of NR/reclaimed ground rubber nanocomposites were improved by adding *in situ* silica.

4.2.3 NR Composites and Nanocomposites Based on Carbon Nanotubes

Carbon nanotubes (CNTs) have attracted the attention of scientists since their initial discovery in 1991.[17,18] CNTs possess high flexibility, low mass density and large aspect ratio, and some experimental data indicate extremely high tensile moduli and strengths for these materials.[19] There are two kinds of CNTs, single-walled (SWCNTs) and multi-walled (MWCNTs). SWCNTs consist of single layers of graphite lattice rolled into perfect cylinders with a diameter usually in the range of 0.7 to 2 nm. However, MWCNTs consist of sets of concentric cylindrical shells, each of which resembles a SWCNT.[20] SWCNTs can potentially be used as conductive materials – they can transport electrons over long distances without significant interruption, which make them more conductive than copper. For this reason, CNTs have been widely used as nanofillers to prepare new functional polymeric nanocomposites.[21]

In polymer composites, filler dispersion as well as interfacial interaction has been shown to be a crucial parameter for the enhancement of mechanical properties. In fact, one of the biggest challenges is to obtain a homogeneous dispersion of CNTs in a polymer matrix because van der Waals interactions between individual tubes often lead to significant aggregation or agglomeration, thus reducing the expected property improvements of the resulting composite.[21] This problem can be gradually overcome by introduction of functional groups such as carboxylic, carbonyl or hydroxyl groups, onto the CNT surface. These

pre-treated CNTs can be completely dispersed in solution. In principle, CNTs can be introduced into the NR matrix by three different methods, such as mechanical mixing, solution mixing and melting blending.[22,23]

Solution mixing is probably the most common method for preparing CNT-reinforced polymer composites because it needs mild conditions, unsophisticated equipment, and it is easy to control. The large majority of the NR/CNT composites described in the literature were prepared by solution mixing, in which the CNTs were previously dispersed in either a solvent or polymer solution, and then further mixed with NR latex to produce a homogeneous NR/CNT mixture; the mixture was then cast in a mould, and the solvent was finally evaporated to produce a composite film.[24]

Peng *et al.*[25] reported on the preparation of NR/MWCNT composites by a self-assembly process and latex compounding technique. After two steps of assembly, the strong self-aggregation of MWCNTs was greatly depressed and MWCNTs were homogeneously distributed throughout the NR matrix as individual nanotubes, due to the excellent interfacial adhesion between MWCNTs and the NR phase. The introduction of acid-modified MWCNTs into the NR matrix contributed to a significant improvement in tensile strength, tensile modulus at different elongations, and inner thermogenesis or thermal stability for NR host while the flexibility of the NR matrix was still maintained. Compared to that of the pure NR, the T_g values of NR/MWCNT composites are higher. A typical method of preparing CNT-reinforced NR composites using latex compounding is shown in Figure 4.1.

Salvetat *et al.*[26] manufactured NR/MWCNT nanocomposites according to the following steps: the first step is the carboxylation of MWCNTs in the presence of nitric acid. The activated MWCNTs were dispersed by sodium dodecyl sulfate (SDS) in water, and the dispersion was then added to the ammonia solution containing pre-vulcanized NR, the mixture was stirred, sonicated, and dried to obtain the composite films. The NR nanocomposites showed a very large increase in both tensile strength and storage modulus in the rubbery region at room temperature.

Carolina *et al.*[24] also prepared novel multifunctional iron/iron oxide-filled NR/CNT composites through the direct mixing of NR latex and two different CNT aqueous solutions. They found that the mechanical, thermal, chemical and electrical properties of the NR nanocomposites were improved, and the NR composites also exhibited magnetic properties due to the specific family of CNTs used in their preparation. Atieh *et al.*[27] prepared NR nanocomposites with MWCNTs using toluene as solvent by solution mixing. The MWCNTs were added into the NR solution without any further treatment, and the mixed solution was cast and the solvent evaporated to produce the NR nanocomposites. They found that, by increasing the amount of CNTs in the NR, the ductility decreased and the NR material became stronger and tougher but at the same time more brittle.

Sui *et al.*[28] reported on NR/CNT nanocomposites prepared using pre-treated CNTs with a blended acid and HRH (hydrated silica, resorcinol and hexamethylenetetramine with a weight ratio 15 : 10 : 6) bonding system through

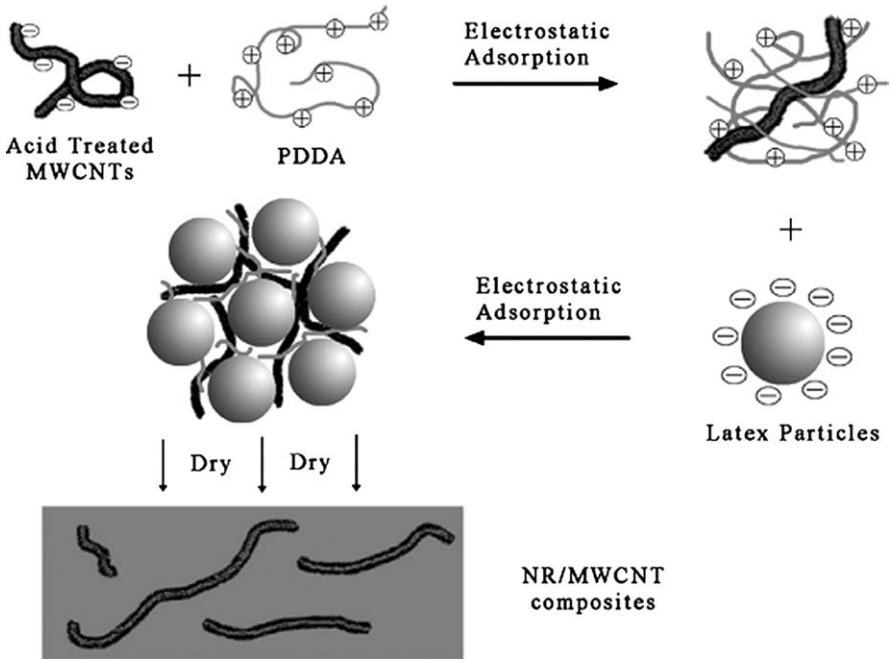

Figure 4.1 The self-assembly process of manufacturing CNT/NR composites.[25] (Reprinted with permission from ref. 25. Copyright 2010 Elsevier.)

mechanical mixing. They also prepared NR nanocomposites reinforced with pre-treated CNTs by solution mixing, using toluene as solvent.[29,30] Subsequently, the preparation of NR/CNT nanocomposites was accomplished by adding and mixing other ingredients including vulcanizing agent in an open two-roll mill at room temperature. The results showed that the crystallization melting peak in differential scanning calorimetry (DSC) curves of NR weakened and the curing rate of NR slightly decreased. Meanwhile, the over-curing reversion of NR/CNT nanocomposites was alleviated. The dispersion of the treated CNTs in the NR matrix and interfacial bonding between them were rather good. The mechanical properties (rebound resilience, dynamic compression properties and storage modulus) and thermal stability of NR were also greatly improved by adding the treated CNTs, compared to the neat NR and traditional CB/NR composite.

However, NR composites and nanocomposites reinforced with CNTs are seldom prepared *via* melt blending because it is difficult to disperse CNTs into the NR matrix.

4.2.4 NR Composites and Nanocomposites Based on Graphene

Graphene is considered as two-dimensional carbon nanofiller with an atomically thick planar sheet composed of sp^2 carbon atoms that are densely packed in a honeycomb crystal lattice.[31] Defect-free graphene presents outstanding

physical properties, such as high thermal conductivity (5000 W/m K), Young's modulus (1 TPa) and ultimate strength of 130 GPa. Furthermore, graphene possesses a large specific area (theoretical limit: 2630 m^2/g), gas permeability and high electron mobility.[31,32] Thus, considerable attention has been paid to graphene and its potential application as reinforcing filler for polymeric nanocomposites.

Recently, it has been used as a nanofiller to impart good mechanical, thermal and electrical properties of NR nanocomposites. Ozbas *et al.*[33] fabricated NR/functionalized graphene sheets (FGS) nanocomposites by solution mixing. The detailed procedure was stated as follows: NR compounds were completely dissolved in THF with the aid of a magnetic stirring bar. Then, the required amount of FGS suspended in THF was added to the NR solution with stirring. After mixing the FGS-NR-THF solution for an hour with a stir bar, THF was removed by evaporation at room temperature under vacuum. The uncured NR/FGS nanocomposites were further vulcanized by hot compression moulded technique.

Ruoff and coworkers[34] reported on the reduced graphene oxide (RG-O)/NR nanocomposites prepared by two different routes to incorporate curing agent following the co-coagulation procedure: solution treatment or mechanical mixing. They found that the processing approach had a tremendous impact on the NR composite morphology and properties. Solution treatment preserved the segregated filler network morphology produced by the co-coagulation procedure, whereas the milling process destroyed this network and generated a homogeneous dispersion of RG-O platelets in the NR matrix. The segregated network morphology was shown to be advantageous for conductivity properties and greatly increased the stiffness of the composite versus neat NR, but also significantly sacrificed the elongation to break the samples. The milled nanocomposites also exhibited enhanced stiffness and strength while maintaining a high elongation to break. The preparative procedures were depicted as follows: After the co-coagulation procedure, the composites were processed by two different routes to incorporate curing agent. The first processing route to prepare RG-O/NR composites was performed on a two-roll mill. Dicumyl peroxide (DCP) was used as the curing agent and added during mixing process. In the second route, the coagulated solids were soaked in a solution of DCP in toluene to swell the NR and implant DCP into the matrix. DCP was added to the minimal amount of toluene which immersed the solids completely. After the NR was completely swollen by the DCP/toluene mixture, the toluene was then removed by vacuum drying for 1 week at room temperature. All the cured (RG-O)/NR nanocomposites were produced by hot compression moulded technique.

Kong *et al.*[35] prepared graphene/NR by solution mixing using diluted ammonia solution as the stabilizer. It was found that the tensile strength and the T_g value and the crosslink density of NR nanocomposites were improved by incorporation of graphene, which was due to strong interfacial interaction originated from the π–π interactions and hydrogen bonds between graphene and NR matrix.

Ruoff *et al.*[36] reported that thermally expanded graphite oxide (TEGO)/NR nanocomposites were prepared by melt blending on a two-roll mill. They found that the improvements in properties of NR prepared by direct melt blending of TEGO into NR were not pronounced, however, by pre-mixing TEGO with NR latex followed by melt blending (L-TEGO/NR nanocomposites), substantial property enhancements were achieved. They attributed these improvements in the L-TEGO/NR nanocomposites to a more uniform dispersion of TEGO platelets, coupled with a larger accessible interfacial surface area. While ultrasonic treatment of TEGO in water did not produce a stable suspension of exfoliated TEGO platelets, it did serve to break down the particles and facilitated the dispersion of high aspect ratio platelets into the NR matrix during mixing.

Xia *et al.*[37] fabricated graphene (GE)/NR composite by ultrasound-assisted latex mixing and *in situ* reduction. The preparative procedures were described as follows: the GE oxide powder was dispersed in NR latex using an ultrasonic field and was then reduced *in situ* followed by latex coagulation to obtain the GE/NR masterbatch. Then the GE/NR masterbatch was mixed with common NR and other ingredients including crosslinking agent (sulfur) on an open twin roll mill at room temperature. Then the mixture was hot pressed and vulcanized to offer GE/NR composites. This approach produced a much better dispersion and exfoliation of GE in the rubber matrix and contributed to an increase in the tensile strength of NR composites.

4.3 NR Composites and Nanocomposites Based on Natural Fillers

4.3.1 Fibre-Reinforced NR Composites and Nanocomposites

Short fibres of glass, rayon, aramid, asbestos and cellulose as reinforcing fillers, have been broadly used in rubber industries due to their high modulus, high strength and low creep. In recent years especially, natural fibres such as jute fibre,[38] cellulose fibre,[39,40] coir fibre,[41,42] sisal fibre,[43,44] *etc.* have been also widely used in NR composites because they are environmental friendly, cheap, abundant and renewable. However, natural fibres also have some disadvantages such as moisture absorption, quality variations, low thermal stability and poor compatibility with the hydrophobic polymer matrix.

In order to improve compatibility in polymeric matrices, natural fibre was treated by alkali and silane coupling agents. Silane coupling agents present three main advantages: (i) they are commercially available on a large scale; (ii) at one end, they bear alkoxysilane groups capable of reacting with OH-rich surface, and (iii) at the second end, they have a large number of functional groups which can be tailored as a function of the matrix to be used. The last feature ensures, at least, a good compatibility between the reinforcing element and the polymer matrix or even covalent bonds between them.[40]

Thomas *et al.*[45] and Joseph *et al.*[46] reported that the short coir fibre or isora fibre reinforced NR composites were prepared by conventional blending and

vulcanizing process, and the effects of fibre length, orientation, alkali treatment and bonding agent on properties of new NR composites were studied. They found that the mechanical properties of the NR composites in the longitudinal direction were superior to those in the transverse direction. The optimum lengths for coir fibre and isora fibre were found to be 10 mm in order to achieve good reinforcement in NR composites. Adhesions between alkali-treated coir fibres or isora fibre and NR matrix were improved by using bonding agent.

Adhikari *et al.*[47] prepared the NR composites reinforced with grass fibre by mechanical mixing, and studied the mechanical properties of grass fibre filled NR composites. They found that 400 mesh grass fibre loaded NR composites showed superior mechanical properties, therefore continued to study the effect of silane coupling agent (Si69) on mechanical properties of this particular NR composite. Results showed that moduli at 200 and 300% elongation and hardness increased in the presence of Si69, but tensile strength was less compared to that of the NR composite without Si69.

Joseph *et al.*[48] had also prepared the oil palm microfibril-reinforced NR composites by conventional mechanical blending. The used microfibrils were separated from the oil palm fibres by using the steam explosion method, and were subsequently subjected to treatments such as mercerization, benzoylation, and silane treatment. They found that the storage modulus value of untreated and treated microfibril-reinforced NR composites was higher than that of macrofibre-reinforced composites. The T_g values of microfibril-reinforced composites were slightly higher than that of macrofibre-reinforced composites. The treated microfibril-reinforced NR composites displayed better adhesion between fibre and NR matrix.

Pasquini *et al.*[49] reported that cellulose whiskers with high aspect ratio extracted directly from cassava bagasse were used to prepare NR nanocomposite films by mixing with the NR latex emulsion. The mixtures were cast on Teflon plates and dried overnight to obtain composite films. These NR nanocomposite films were not vulcanized by standard process. They found that a significant increase of the storage tensile modulus was observed upon filler addition by dynamic mechanical analysis.

Visakh *et al.*[50,51] used cellulose nanowhiskers or nanofibres isolated from bamboo pulp residue of newspaper production as reinforcing phase to prepare NR nanocomposites. The prepared process of these novel NR composites was divided into two steps. In the first step, cellulose nanowhiskers or cellulose nanofibres and NR latex were mixed uniformly, and masterbatch was obtained after the mixture was coagulated and powered. In the second step, compounding of the masterbatch with solid NR and vulcanizing agents was carried out using a two-roll mill, cured by a standard procedure. The addition of cellulose nanowhiskers or nanofibres had a positive impact on the tensile strength, E-modulus, storage modulus, tan delta peak position and thermal stability of the NR composites. The obvious improvement in thermal stabilities and mechanical properties of NR composites were attributed to the possible restriction of polymer chain mobility of NR phase in the vicinity of cellulose

nanowhiskers or nanofibres. Meanwhile, the NR matrix also played an important role in nano-reinforcements.

Abraham *et al.*[52] reported that films of pre-vulcanized NR nanocomposite were fabricated by casting and evaporating a mixture of NR latex and aqueous suspension of cellulose nanofibrils (CNF). By this method, the CNF were evenly distributed in the NR composites. The increase of CNF content in the NR matrix caused the increasing the Young's modulus and tensile strength of materials, but the decreasing characteristic rubber elongation. The enhancements in mechanical and dynamic mechanical properties were attributed to the formation of a Zn–cellulose complex and the three dimensional network of the CNF in the NR matrix as a result of the deprotonation of the cellulose.

However, synthetic fibres, such as nylon fibre, have also been used in NR composites as reinforcing filler. Kutty *et al.*[53] reported on a novel method for the preparation of NR/short nylon fibre composites. The short fibres chopped to approximately 6 mm were incorporated in the latex stage and processed into sheet form. This method was found to reduce the mixing cycle time and fibre breakage during mixing without compromising the fibre dispersion. The new composites compounded with a dry bonding system based on hexamethylenetetramine, resorcinol and hydrated silica showed improved modulus, tensile strength and abrasion resistance compared to conventional composites. Tear strength, resilience, and compression set were similar to the conventional composites. SEM analysis indicated good interaction between matrix and fibres in the case of latex master batch. Subsequently, Kutty *et al.*[54] reported that polypyrrole (PPy) and PPy coated short nylon-6 fibre (F-PPy) based on NR composites were prepared by *in situ* polymerization method. The pre-mixtures were coagulated out, dried, compounded on a two-roll mill and cured by compression moulded technique. It was found that incorporation of PPy to NR retarded the cure reaction whereas addition of fibre accelerated the cure reaction. Higher direct current conductivity and better mechanical properties were attained for NR/PPy/F-PPy system as compared to NR/PPy systems.

4.3.2 Starch-Reinforced NR Composites and Nanocomposites

Starch is a natural polymer available in large quantities from various sources. It can be obtained from different plants for which it is the most common source of polysaccharides of energetic reserve. In its native state, starch consists of semi-crystalline granules insoluble in water. It is composed of two polysaccharides, branched amylopectin and essentially linear amylose.[49] Starch is cheap, environmentally friendly and a completely biodegradable biopolymer, which has been also used to reinforce NR composites as filler.

Preparation of starch nanocrystal-reinforced NR nanocomposites is often by the solution mixing method. The general steps are depicted as follows: the first step is preparation of starch nanocrystals. Starch nanocrystals were usually extracted from natural starch crops (such as maize,[55,56] cassava,[49] potato,[57,58] wheat,[59] *etc.*) by hydrolysis in the presence of strong acids (such as sulfuric acid or hydrochloric acid).The second step is the mixing of the starch nanocrystal

suspension and the NR latex. The starch nanocrystals are usually dispersed in water to produce a suspension, and this suspension is mixed with the NR latex. After homogeneously mixing, the mixtures of NR nanocomposites are prepared. The last step is the preparation of nanocomposite films, the mixture of the suspension of starch nanocrystals and NR were cast onto a mould and then dried to produce the composite films. These uncured NR nanocomposites reinforced with starch usually show good properties.

Angellier *et al.*[60–62] reported that NR nanocomposites reinforced with waxy maize starch nanocrystals were prepared by casting and evaporating a mixture of NR latex and aqueous suspension of waxy maize starch nanocrystals. SEM observations confirmed that the filler was evenly distributed within the NR matrix. By adding starch nanocrystals in NR, the swelling degree of NR composites decreased in toluene, but increased in water. It was assumed that these phenomena were due to the formation of a starch nanocrystal network through hydrogen linkages between starch nanoparticle clusters, and also to favourable interactions between the matrix and the filler. The platelet-like morphology of starch nanocrystals seemed to be responsible for the decrease in both the permeability to water vapour and oxygen of NR filled films. The surface chemical modification of starch nanocrystals resulted in a favoured swelling behaviour with toluene and a diminution of water uptake. They also found that up to a content of 20 wt% this new filler had the advantage of effectively reinforcing NR without sacrificing its elongation at break. The relaxed modulus at room temperature of nanocomposite films containing 20 wt% of filler was found to be 75 times higher than that of the unfilled matrix. All the results showed that particle interactions played a crucial role in the properties of starch nanocrystal filled NR.

Thomas *et al.*[58] prepared NR latex/potato starch nanocrystal nanocomposites by solution mixing. The detailed procedures were described as follows. Firstly, potato starch nanocrystals were prepared by hydrolysis of potato starch powder in the presence of sulfuric acid. Then the synthesized potato starch nanocrystal suspensions were mixed with NR latex by a latex stage mixing process using a magnetic stirrer. In this way, NR composites containing up to 20% (w/w) of fillers have been obtained. Morphological studies indicated a relatively uniform dispersion of starch nanocrystals in the NR nanocomposites until 15% (w/w) filler loading. Dielectric measurements confirmed the existence of a threshold at a composition close to 15% (w/w) of filler at which the fillers become agglomerated. One of the consequences of the electrical insulator nature of these nanofillers was the increase in the electrical barrier at the percolation threshold.

4.3.3 NR Composites and Nanocomposites Reinforced with Natural Mineral Fillers

Generally, NR composites are mainly synthesized by four different methods, namely simple mechanical blending,[63] solution mixing, melt blending and sol–gel technology. Clays are important natural mineral fillers, widely used as

reinforcing agents to minimize polymer consumption and reduce the cost. However, the reinforcing abilities of the natural mineral fillers are poor due to their large particle size and low surface activity. In addition, these natural mineral fillers are not compatible with polymer matrices, and the mineral fillers can only be dispersed on the micro-scale in the polymeric matrices. Thus the reinforcing effect of these mineral fillers in polymeric matrices is unremarkable.

Clays such as montmorillonite,[64] saponite,[65] hectorite,[66,67] bentonite,[67,68] vermiculite,[69] kaolin,[70] rectorite,[71] *etc*., have also been used to reinforce NR because of their low cost. From a structural perspective, the clays are composed of silicate layers 1 nm thick and about 200–300 nm in lateral dimensions. It is hard to exfoliate the individual layers by simple mechanical blending. A recent method to improve the reinforcing ability is by changing the hydrophilic nature of clay to organophilic. The internal and external cations can be exchanged by other inorganic or by organic ions, for example quaternary alkyl ammonium or alkyl phosphonium ions. Introduction of organic groups into clays makes the silicate compatible with polymeric matrices. These entering guest molecules can either simply increase the distances between the still parallel layers in an intercalation process or randomly entirely disperse the separate layers in an exfoliation.[72] Upon addition of small amount of organically modified clays, NR composites can achieve similar mechanical properties as compared with the NR composite with higher CB loading.

Arroyo research group[72] prepared organomodified clay by modifying Na^+-MMT with octadecylamine, and then blended NR with this modified montmorillonite to prepare new NR composites. They found that the organoclay (OC) could accelerate the vulcanization of NR to a greater extent than CB. Meanwhile, mechanical characterization showed the strong reinforcing effect of both fillers up to 350% in strength in relation to NR. The mechanical properties of NR with 10 phr of OC were comparable to the composite with 40 phr of CB. Moreover, the addition of OC improved the strength of the NR composites without reducing the elasticity of the material. López-Manchado *et al*.[73,74] prepared NR nanocomposites reinforced with organomodified bentonite by a similar method. Subsequently, they corroborated that organically modified bentonite behaved as an effective vulcanizing agent by swelling measurements, cure-meter testing and DSC under dynamic and isothermal conditions. This OC could accelerate the vulcanization reaction of the NR, and improve the crosslinking density. The thermal stability of the NR/OC nanocomposite was enhanced in comparison with the neat NR, which could be attributed to the clay nanolayers preventing diffusion out of the volatile decomposition products. The values for T_g of the NR were improved by adding the OC, due to confinement of the elastomer segment into the OC nanolayers, which restricted the mobility of the chains. In 2008, López-Manchado *et al*.[75] prepared NR/Na^+-MMT nanocomposites by mechanical blending using poly(ethylene glycol) (PEG) as dispersing agent. They found that the mechanical properties of NR nanocomposites were remarkably improved by adding small amounts of dispersing agent (PEG). Jia *et al*.[76] prepared NR

nanocomposites with solid-state organomodified montmorillonite (OMMT) by a traditional mechanical mixing and vulcanizing process. They found that the OMMT was homogeneously dispersed in the NR matrix with some orientation. Apart from accelerating the curing process, addition of OMMT to NR was found to improve the mechanical properties, ageing resistance and T_g value of NR.

Wirasate *et al.*[77] also prepared NR nanocomposites using pristine Na^+-MMT or OMMT as reinforcing agent by a conventional mechanical mixing method. They found that both Na^+-MMT and OMMT could accelerate the vulcanization reaction of NR. The abrasion resistance of NR was improved by the addition of either Na^+-MMT or OMMT. OMMT-filled NR composites showed better abrasion resistance than those of Na^+-MMT filled NR composites. Meanwhile, they had also found that the addition of Si69 to NR resulted in improvement of the abrasion resistance of the NR/Na^+-MMT composites due to the reduction in Na^+-MMT particle size. Particle size and dispersion of OMMT remained the same by the addition of Si69, thus the abrasion resistance, abrasion pattern and mechanical properties were not affected.

Crespo *et al.*[78] prepared NR nanocomposites with OC as a substitute for silica by conventional mechanical mixing. The results revealed that the OC was homogeneously dispersed in the NR matrix. The mechanical properties of NR indicated that 50 phr of silica can be replaced by 4 phr of OC without adversely affecting the tensile properties of the final material, even after ageing.

Meanwhile, NR composites and nanocomposites reinforced with OC were also prepared by solution mixing. López-Manchado *et al.*[79] reported that NR nanocomposites were synthesized by two different methods using octadecylammonium-modified saponite, namely mechanical blending and solution mixing methods. They found that both methods gave rise to an optimal dispersion of the filler into the NR matrix. Nevertheless, the compatibility between the filler and the rubber was improved by solution mixing. The mechanical and dynamic mechanical properties of the NR nanocomposites prepared by solution mixing were found to be better than those of the nanocomposites synthesized *via* mechanical blending. Meanwhile, adding a silane coupling agent was found to improve the adhesion between the OC and NR, and hence the NR nanocomposites with silane coupling agent had good mechanical properties. The preparation of NR nanocomposites by both methods is shown in Figure 4.2. The solution mixing prior to compounding was carried out as follows. NR was swollen in toluene under continuous stirring, and while the OC was dispersed in toluene. This dispersion was poured into the rubber/toluene solution and maintained under vigorous stirring for 24 h, and the solvent was then evaporated under vacuum at room temperature.

Galembeck *et al.*[80] prepared NR/Na^+-MMT nanocomposites by the solution method. The detailed procedures were as follows: the Na^+-MMT was dispersed in water with continuous stirring using a Turrax mixer for 1 min at 13,500 rpm. The NR latex was added to the clay dispersion and stirred for 1 min at 24,000 rpm. The samples were then concentrated in a spinning

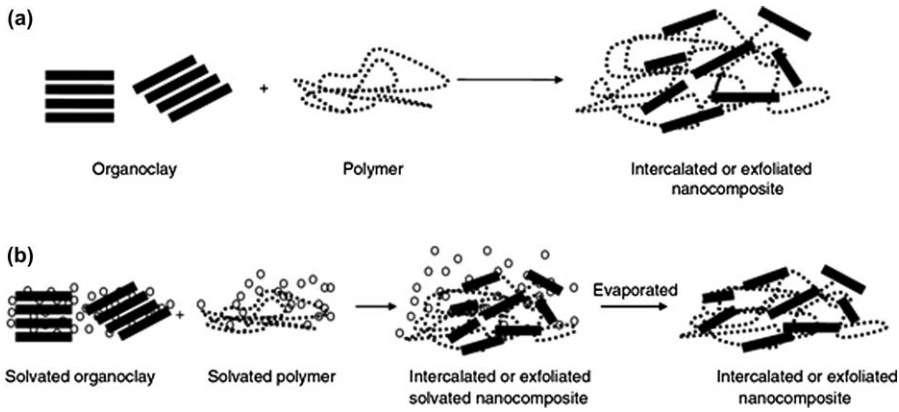

Figure 4.2 Preparations of NR nanocomposites *via* (a) mechanical blending (b) solution mixing.[68]
(Reprinted with permission from ref. 68. Copyright 2004 John Wiley and Sons.)

evaporator to remove water under reduced pressure. These produced thick slurries that were cast on flat plastic moulds, and were dried in an oven under air to produce NR/Na^+-MMT nanocomposites. They found that clay particles were well dispersed in the dry latex and the platelets had a preferential orientation, forming translucent nanocomposites. The tensile properties of NR/clay nanocomposites were analogous to those obtained with vulcanized rubber as well as an increased solvent resistance, which was expected considering that there was significant adhesion between clay lamellae and rubber.

Wu *et al.*[81] prepared NR/clay nanocomposites by directly co-coagulating the rubber latex and clay aqueous suspension. This preparative process is very simple, convenient and effective. SEM showed good dispersion of clay in the NR matrix, and these novel NR/clay nanocomposites exhibited excellent mechanical and gas barrier properties.

Although NR/OC nanocomposites can be made by solution blending, a drawback of this method is the need to remove large quantities of solvent to produce the NR nanocomposite. A more direct way of preparing NR/OC nanocomposites is *via* melt blending.[82–84] From an industrial standpoint, melt blending is the most direct, most cost effective and environmentally friendly method because no organic solvents are involved in the mixing process.

Sharif *et al.*[85] reported that NR/OC nanocomposites were prepared by melt blending using electron beam irradiation as a substitute for sulfur. It was found that the physical and mechanical properties of radiation-induced crosslinking of NR composites with OC were improved due to the presence of nanosize intercalated silicate layers in the NR matrix. Replacing sulfur with radiation-induced crosslinking of NR/OC nanocomposites was not significantly affected by the amount of OC up to 10 phr. Meanwhile, the thermal stability of NR/OC nanocomposites improved with an increase in clay content up to 10 phr.

Wu *et al.*[69] reported that a new kind of NR/organo-vermiculite (OVMT) nanocomposite was prepared *via* a melt process in a HAAKE mixer. The resultant mixtures were further pressed to vulcanize at 140 °C, and vulcanized sheets were obtained. The vermiculite (VMT) was intercalated by cetyltrimethylammonium bromide with a ball mill method to obtain used OVMT. The results showed that the intercalation led to an increase in the $d_{(001)}$ of VMT from 1.46 nm to 4.51 nm. Meanwhile, they found that the tensile strength and the elongation at break of the NR/OVMT nanocomposites loading 15 phr of the OVMT reached 28.4 MPa and 623.2%, respectively. The 300% modulus, tear strength and hardness (Shore A) of the nanocomposites increased with the increase in OVMT loading. The thermal properties of the NR/OVMT nanocomposites were also improved.

Das *et al.*[86] further used a series of long chain fatty acids to modify OMMT, and subsequently utilized them as reinforcing fillers to prepare NR nanocomposites by melt blending. They found that mechanical properties of NR nanocomposites with modified OMMT were remarkably improved. Thomas *et al.*[87] reported that NR nanocomposites with outstanding gas barrier properties had been prepared with OMMT *via* a melt mixing technique. They found that the permeability decrease of the NR nanocomposites had a good qualitative correlation with the volume of the constrained region.

4.4 NR Composites and Nanocomposites Based on Metal or Metallic Compound Fillers

Metal nanoparticles and metallic compound powders are most widely used in polymers to strengthen the polymers, and improve their thermal stability and gas barrier properties. NR is often reinforced with various kinds of metal nanoparticles and metallic compound powder.

Ismail *et al.*[88] reported that NR/silver nanocomposites were prepared by photo-reduction of film cast from NR latex containing silver salt. The preparative steps were described as follows: clean NR latex was diluted with deionized water before adding $AgNO_3$. The latex–salt mixture was homogenized for 30 min followed by casting on a microscope glass substrate and drying overnight in an oven at 50 °C. The resultant films were exposed to a UV light under atmospheric conditions. Unfortunately, the mechanical and thermal stability properties of these NR/silver nanocomposites were not characterized further.

Huang *et al.*[89] prepared NR/alumina nanocomposites using Si69 as treated agent by solution mixing. The preparative processes of NR/alumina nanocomposites were described as follows. Firstly, alumina nanoparticles were dispersed in absolute ethanol using ultrasonic vibration for 10 min to break up agglomerates. The required Si69 was added into absolute ethanol. The solution was then added drop-wise to the alumina nanoparticle solution in a water bath at room temperature under constant ultrasonic vibration for 10 min in order to provide a uniform distribution of the coupling agent on the nano-alumina

particle surfaces. This mixed solution was treated further at 140 °C for 30 min to ensure sufficient reaction. Then the treated nano-alumina was dispersed in the distilled water under vigorous stirring at 60 °C. The NR latex was added to the suspension slowly and sonicated for 20 min. Subsequently, the emulsion was coagulated by freezing and dried under vacuum to produce a masterbatch. Finally, all of the NR ingredients were mixed with the masterbatch on a two-roll mill at room temperature, and the mixed compound was cured by a hot compression moulding technique. They found that the mechanical properties of NR composites were enhanced by the inclusion of nano-alumina. Fu *et al.*[90] also prepared NR/Al_2O_3 composites using γ-methacryloxypropyltrimethoxy-silane as interface treated agent by the similar method. They also found that mechanical properties (such as tensile strength, elongation at break, modulus and tearing strength), chemical (acid and alkaline) and ageing resistance of NR composites were improved by incorporation of nano-Al_2O_3.

However, TiO_2 is also used to fabricate NR nanocomposites. Typical NR/rutile-TiO_2 (n-TiO_2(R)) nanocomposites were prepared as follows:[91] concentrated NR latex was diluted with water to 20% dry rubber content. The prepared n-TiO_2(R) suspension was mixed with NR latex and vigorously stirred for 30 min. After that, the mixture was co-coagulated with 2.5% formic acid. The coagulum was washed with water several times until its pH was about 7 and dried in an oven at 70 °C for 24 h to give the uncured NR/n-TiO_2(R) compounds. The NR nanocompounds were mixed with vulcanizing ingredients by mechanical mixing according to a standard procedure, and the compounds were vulcanized by a compression moulding technique. It was found that the mechanical performance of NR/n-TiO_2(R) composites was enhanced with an increase in n-TiO_2(R) content up to the optimum content at 5 phr and then declined. The addition of n-TiO_2(R) into NR also improved the resistance to UV irradiation.

Calcium carbonate is also used to manufacture NR composites because of its low cost and performance at high loading level. Cai *et al.*[92] prepared NR latex films reinforced with ultrafine calcium carbonate by solution mixing. They found that calcium carbonate was well dispersed in the NR latex. It was found that the tensile strength, modulus and tear strength of NR composite films were improved by a relatively low loading of calcium carbonate (15 wt%).

4.5 NR Composites and Nanocomposites Based on Hybrid Fillers

The combination of reinforcing fillers is one of the most promising tendencies in elastomer reinforcement, where a synergic effect between them is desired.[93] Recently, a lot of attention has been focused on the preparation of NR composites with hybrid fillers.[59,94–99] NR composites reinforced by one type of filler are insufficient to satisfy increasingly complicated industrial applications which usually demand these materials that synchronously have various outstanding properties. Therefore, hybrid systems are an alternative to conventional reinforcing systems, which have opened up a promising field on developing novel

NR composites with excellent properties. A few efforts have been devoted to preparing NR nanocomposites using two or even more different kinds of fillers. The synergistic effect of hybrid fillers can be used to design high-performance NR nanocomposites.

NR composites filled with hybrid fillers possess outstanding mechanical properties that are not caused by only one filler. Liu *et al.*[100] fabricated NR nanocomposites based on the hybrid fillers of CB and two poly(ethylene glycol) (PEG) modified clay by melt mixing. They found that NR with hybrid filler exhibited superior mechanical properties over that with CB as single phase filler. The hybrid filler had a good synergistic reinforcing effect on NR. They also found that the inclusion of nanoclay (NC) could induce a stronger and more developed filler network. Because of the anisotropy of NC layers would depress the reconstruction of filler network, and to some extent lower the reformation rate of the filler network. So, decreased loss factor was observed in CB/NC-filled NR.

Jong *et al.*[101] prepared NR composites reinforced with hybrid filler consisting of defatted soy flour (DSF) and CB. Aqueous dispersions of DSF and CB were first mixed, and then blended with NR latex and sulfur dispersion, respectively. The homogenous composite mixtures were quickly freeze-dried and compression moulded to offer the NR composites. They found that the NR composites reinforced with 40% of hybrid filler (the ratio of DSF to CB was 1 : 1) exhibited a 90-fold improvement in the rubber plateau modulus compared with unfilled NR, showing a significant reinforcement effect by the hybrid filler.

Mondragón *et al.*[102] reported that unmodified and modified NR latex were used to prepare thermoplastic starch/NR/MMT nanocomposites by twin-screw extrusion. After drying, the nanocomposites were injection moulded to produce test specimens. SEM of fractured samples revealed that chemical modification of NR latex enhanced the interfacial adhesion between NR and thermoplastic starch (TPS), and improved their dispersion. X-ray diffraction (XRD) showed that the nanocomposites exhibited partially intercalated/exfoliated structures. Surprisingly, transmission electron microscopy (TEM) showed that clay nanoparticles were preferentially intercalated into the rubber phase. Elastic modulus and tensile strength of TPS/NR blends were dramatically improved from 1.5 to 43 MPa and from 0.03 to 1.5 MPa, respectively, as a result of rubber modification.

Rattanasom *et al.*[103] used silica/CBas hybrid filler to manufacture NR nanocomposites by mechanical mixing and conventional vulcanized process. They also studied the effect of different ratios of the filler on the properties of the NR nanocomposites. The results revealed that the vulcanizates containing 20 and 30 phr of silica in hybrid filler exhibited the better overall mechanical properties. Huang *et al.*[104] prepared the NR/NC/CB nanocomposites by solution mixing and conventional vulcanized process. They found that synergistic reinforcement was achieved by adding hybrid filler consisting of CB and NC, and the tensile strength of NR nanocomposites increased by 147%. Zhang *et al.*[95] also found that the incorporation of nano-dispersed clay can greatly improve the crack growth resistance of NR/CB.

Bendahou *et al.*[105] also prepared a series of nanocomposite films based on NR, pristine Na^+-MMT, and cellulose whiskers by solution method. They found that the simultaneously introduced MMT and cellulose whiskers into NR could greatly improve the rubbery tensile modulus. Moreover, the strong decrease of the magnitude of the loss factor upon addition of whiskers was attributed to strong adhesion between the filler and the matrix. A similar result was reported by Mariano *et al.*[106]

Zhang *et al.*[83] prepared highly filled NR composites based on silane-modified kaolin (SMK), precipitated silica (PSi) and their mixed-compound additions (SMK + PSi) by melt blending. It was found that these highly filled NR/SMK composites exhibited outstanding mechanical properties, excellent gas barrier properties and much higher thermal stability, compared to the pure NR. The gas barrier properties of NR composites with SMK and PSi were much higher than those of NR/PSi composites, and better than those of NR/SMK.

Lopattananon *et al.*[107] prepared NR composites using hybridized reinforcing fillers consisting of short cellulose fibres and silica by conventional mechanical blending. They found that the tensile modulus of the NR incorporated with cellulose fibre was higher than that of NR filled with silica by about 1.5 times. The introduction of more cellulose fibre also increased the tensile modulus but decreased the tensile strength and elongation at break. Si69 was used in order to modify the surface properties of the cellulose fibre and silica fillers. They found that the silane treatment of both fillers had significant benefit on the processability but little benefit on NR reinforcement.

Zhao *et al.*[96] prepared NR nanocomposites using nanobarite (NB) and CB as hybrid filler by mechanical blending, and studied the synergistic effect of NB and CB fillers in the NR matrix. They found that the reinforcement of NB was influenced by the organic treatment method. In comparison with unmodified NB (U-NB) and NB modified by sodium stearate (SA-NB), NB modified by sodium aluminate and sodium stearate (SA-Al_2O_3-NB) exhibited outstanding reinforcement due to its homogenous dispersion in the NR matrix and the stronger polymer–filler interactions. Incorporating 2 wt% of SA-Al_2O_3-NB into the control NR containing 45 wt% of CB resulted in an obvious synergistic effect, including accelerating the curing process, improving the mechanical properties and enhancing the thermo-oxidative resistance and corrosion resistance.

Heinrich *et al.*[99] prepared NR/OMMT/CB composites. During preparation, mixing was accomplished in two steps. In the first step CB was mixed with NR matrix in the internal mixer together with ZnO and stearic acid (mechanical blending). Second step mixing was carried out in an open two-roll mill at 90 °C (melt blending). This temperature was selected to ensure the melting of docosanoic acids during the course of mixing. Clays and curatives were added in this step. The following vulcanizates were obtained by compression mould. The influence of OMMT nanoparticles on the microstructure and fracture mechanical behaviour of CB-filled NR composites was investigated. Tear fatigue analysis tests confirmed the dramatic improvement in fracture behaviour of NR-CB composites in the presence of OMMT. The incorporation of OMMT

also altered the viscoelastic behaviour of the resulting composites. A synergy in reinforcement between OMMT and CB was attested by the remarkable enhancement in mechanical properties. Finally, it was observed that at least approximately 30–40% reduction in CB loading without sacrificing the other physical properties like tensile strength, modulus, and hardness could be obtained.

4.6 Summary

In this chapter, all methods for preparation of NR composites and nanocomposites were summarized and discussed in detail based on the classification of reinforcing agents. The NR composites and nanocomposites were commonly prepared by conventional mechanical blending, solution mixing and melting blending. With regards to industrial applications, melt blending is the most direct, most cost effective and environmentally friendly method compared to solution mixing because no organic solvents are involved in mixing process.

However, different methods should be adopted to fabricate NR composites and nanocomposites with expected thermal and mechanical properties according to different properties of reinforcing fillers. Conventional fillers, natural fillers and inorganic metal particles or metallic compound powder fillers without any modification were seldom used to reinforce NR composites because of the bad compatibility between fillers and NR matrices. The compatibility between fillers and NR chains can be improved by treating these fillers using chemicals (silane coupling agents, mixed acid and intercalator) before mixing with NR. However, silane coupling agents were usually added to promote the adhesions between fillers and NR matrix, and to enhance the thermal and mechanical properties of NR composites.

Another promising approach to preparation of novel NR composites and nanocomposites with excellent properties is to adopt hybrid fillers because each reinforcing agent can retain its inherent advantages, which imparts a synergistic effect between hybrid fillers to reinforce NR nanocomposites.

References

1. Z. Peng, L. X. Kong, S.-D. Li, Y. Chen and M. F. Huang, *Compos. Sci. Technol.*, 2007, **67**, 3130.
2. D. De, P. K. Panda, M. Roy, S. Bhunia and A. I. Jaman, *Polym. Eng. Sci.*, 2013, **53**, 227.
3. H. Nabil, H. Ismail and A. A. Rashid, *J. Vinyl Addit. Technol.*, 2012, **18**, 139.
4. R. Sengupta, S. Chakraborty, S. Bandyopadhyay, S. Dasgupta, R. Mukhopadhyay, K. Auddy and A. S. Deuri, *Polym. Eng. Sci.*, 2007, **47**, 1956.
5. G. Kraus, in *Fortschritte der Hochpolymeren-Forschung*, Springer, Berlin Heidelberg, 1971, **8**, p. 155.
6. L. Karásek and M. Sumita, *J. Mater. Sci.*, 1996, **31**, 281.

7. S. Salaeh and C. Nakason, *Polym. Compos.*, 2012, **33**, 489.
8. S. Thongsang and N. Sombatsompop, *Polym. Compos.*, 2006, **27**, 30.
9. N. K. On, A. A. Rashid, M. M. M. Nazlan and H. Hamdan, *J. Appl. Polym. Sci.*, 2012, **124**, 3108.
10. D. Fragiadakis, L. Bokobza and P. Pissis, *Polymer*, 2011, **52**, 3175.
11. L. Bokobza and J.-P. Chauvin, *Polymer*, 2005, **46**, 4144.
12. Y. Chen, Z. Peng, L. X. Kong, M. F. Huang and P. W. Li, *Polym. Eng. Sci.*, 2008, **48**, 1674.
13. V. Tangpasuthadol, A. Intasiri, D. Nuntivanich, N. Niyompanich and S. Kiatkamjornwong, *J. Appl. Polym. Sci.*, 2008, **109**, 424.
14. P. Satraphan, A. Intasiri, V. Tangpasuthadol and S. Kiatkamjornwong, *Polym. Adv. Technol.*, 2009, **20**, 473.
15. S. Chuayjuljit and A. Boonmahitthisud, *Appl. Surf. Sci.*, 2010, **256**, 7211.
16. A. Kongsinlark, G. L. Rempel and P. Prasassarakich, *Chem. Eng. J.*, 2012, **193–194**, 215.
17. S. Iijima, *Nature*, 1991, **354**, 56.
18. M. Moniruzzaman and K. I. Winey, *Macromolecules*, 2006, **39**, 5194.
19. J. C. Grunlan, A. R. Mehrabi, M. V. Bannon and J. L. Bahr, *Adv. Mater.*, 2004, **16**, 150.
20. N. Grossiord, J. Loos and C. E. Koning, *J. Mater. Chem.*, 2005, **15**, 2349.
21. L. Bokobza, *Polymer*, 2007, **48**, 4907.
22. J. N. Coleman, U. Khan and Y. K. Gun'ko, *Adv. Mater.*, 2006, **18**, 689.
23. Z. Spitalsky, D. Tasis, K. Papagelis and C. Galiotis, *Prog. Polym. Sci.*, 2010, **35**, 357.
24. C. F. Matos, F. Galembeck and A. J. G. Zarbin, *Carbon*, 2012, **50**, 4685.
25. Z. Peng, C. Feng, Y. Luo, Y. Li and L. X. Kong, *Carbon*, 2010, **48**, 4497.
26. S. Bhattacharyya, C. Sinturel, O. Bahloul, M.-L. Saboungi, S. Thomas and J.-P. Salvetat, *Carbon*, 2008, **46**, 1037.
27. A. Fakhru'l-Razi, M. A. Atieh, N. Girun, T. G. Chuah, M. El-Sadig and D. R. A. Biak, *Compos. Struct.*, 2006, **75**, 496.
28. G. Sui, W. Zhong, X. Yang and S. Zhao, *Macromol. Mater. Eng.*, 2007, **292**, 1020.
29. G. Sui, W. H. Zhong, X. P. Yang and Y. H. Yu, *Mater. Sci. Eng.*, 2008, **485**, 524.
30. G. Sui, W. H. Zhong, X. P. Yang, Y. H. Yu and S. H. Zhao, *Polym. Adv. Technol.*, 2008, **19**, 1543.
31. H. Kim, A. A. Abdala and C. W. Macosko, *Macromolecules*, 2010, **43**, 6515.
32. M. Hernández, M. d. M. Bernal, R. Verdejo, T. A. Ezquerra and M. A. López-Manchado, *Compos. Sci. Technol.*, 2012, **73**, 40.
33. B. Ozbas, S. Toki, B. S. Hsiao, B. Chu, R. A. Register, I. A. Aksay, R. K. Prud'homme and D. H. Adamson, *J. Polym. Sci., Part B: Polym. Phys.*, 2012, **50**, 718.
34. J. R. Potts, O. Shankar, L. Du and R. S. Ruoff, *Macromolecules*, 2012, **45**, 6045.

35. C. Li, C. Feng, Z. Peng, W. Gong and L. Kong, *Polym. Compos.*, 2013, **34**, 88.
36. J. R. Potts, O. Shankar, S. Murali, L. Du and R. S. Ruoff, *Compos. Sci. Technol.*, 2013, **74**, 166.
37. N. Yan, H. Xia, Y. Zhan and G. Fei, *Macromol. Mater. Eng.*, 2013, **298**, 38.
38. V. M. Murty and S. K. De, *J. Appl. Polym. Sci.*, 1982, **27**, 4611.
39. A. M. Dessouki, N. H. Taher and H. H. El-Nahas, *Polym. Int.*, 1998, **45**, 339.
40. M. Abdelmouleh, S. Boufi, M. N. Belgacem and A. Dufresne, *Compos. Sci. Technol.*, 2007, **67**, 1627.
41. V. G. Geethamma, L. A. Pothen, B. Rhao, N. R. Neelakantan and S. Thomas, *J. Appl. Polym. Sci.*, 2004, **94**, 96.
42. V. G. Geethamma and S. Thomas, *Polym. Compos.*, 2005, **26**, 136.
43. S. Varghese, B. Kuriakose and S. Thomas, *J. Appl. Polym. Sci.*, 1994, **53**, 1051.
44. M. Jacob, K. T. Varughese and S. Thomas, *J. Appl. Polym. Sci.*, 2006, **102**, 416.
45. V. G. Geethamma, R. Joseph and S. Thomas, *J. Appl. Polym. Sci.*, 1995, **55**, 583.
46. L. Mathew and R. Joseph, *J. Appl. Polym. Sci.*, 2007, **103**, 1640.
47. D. De, D. De and B. Adhikari, *Polym. Adv. Technol.*, 2004, **15**, 708.
48. S. Joseph, S. P. Appukuttan, J. M. Kenny, D. Puglia, S. Thomas and K. Joseph, *J. Appl. Polym. Sci.*, 2010, **117**, 1298.
49. D. Pasquini, E. d. M. Teixeira, A. A. d. S. Curvelo, M. N. Belgacem and A. Dufresne, *Ind. Crops Prod.*, 2010, **32**, 486.
50. P. M. Visakh, S. Thomas, K. Oksman and A. P. Mathew, *Composites, Part A*, 2012, **43**, 735.
51. P. M. Visakh, S. Thomas, K. Oksman and A. P. Mathew, *J. Appl. Polym. Sci.*, 2012, **124**, 1614.
52. E. Abraham, B. Deepa, L. A. Pothan, M. John, S. S. Narine, S. Thomas and R. Anandjiwala, *Cellulose*, 2013, **20**, 417.
53. B. P. K and S. K. N. Kutty, *J. Appl. Polym. Sci.*, 2008, **109**, 1484.
54. D. S. Pramila Devi, P. K. Bipinbal, T. Jabin and S. K. N. Kutty, *Mater. Des.*, 2013, **43**, 337.
55. H. Angellier, S. Molina-Boisseau, P. Dole and A. Dufresne, *Biomacromolecules*, 2006, **7**, 531.
56. D. S. LeCorre, J. Bras and A. Dufresne, *Macromol. Mater. Eng.*, 2012, **297**, 969.
57. A. Dufresne, J.-Y. Cavaillé and W. Helbert, *Macromolecules*, 1996, **29**, 7624.
58. E. Bouthegourd, K. R. Rajisha, N. Kalarical, J. M. Saiter and S. Thomas, *Mater. Lett.*, 2011, **65**, 3615.
59. O. A. Al-Hartomy, A. A. Al-Ghamdi, F. Al-Salamy, N. Dishovsky, R. Shtarkova, V. Iliev and F. El-Tantawy, *Plast., Rubber Compos.*, 2012, **41**, 408.

60. H. Angellier, S. Molina-Boisseau and A. Dufresne, *Macromolecules*, 2005, **38**, 9161.
61. H. Angellier, S. Molina-Boisseau, L. Lebrun and A. Dufresne, *Macromolecules*, 2005, **38**, 3783.
62. H. Angellier, S. Molina-Boisseau and A. Dufresne, *Macromol. Symp.*, 2006, **233**, 132.
63. A. Jacob, P. Kurian and A. S. Aprem, *J. Appl. Polym. Sci.*, 2008, **108**, 2623.
64. T. Pojanavaraphan and R. Magaraphan, *Eur. Polym. J.*, 2008, **44**, 1968.
65. D. J. Lowe, A. V. Chapman, S. Cook and J. J. C. Busfield, *Macromol. Mater. Eng.*, 2011, **296**, 693.
66. R. Stephen, R. Alex, T. Cherian, S. Varghese, K. Joseph and S. Thomas, *J. Appl. Polym. Sci.*, 2006, **101**, 2355.
67. R. Stephen, S. Varghese, K. Joseph, Z. Oommen and S. Thomas, *J. Membr. Sci.*, 2006, **282**, 162.
68. A. A. Yehia, A. M. Akelah, A. Rehab, S. H. El-Sabbagh, D. E. El Nashar and A. A. Koriem, *Mater. Des.*, 2012, **33**, 11.
69. Y. Zhang, W. Liu, W. Han, W. Guo and C. Wu, *Polym. Compos.*, 2009, **30**, 38.
70. R. Sukumar and A. R. R. Menon, *J. Appl. Polym. Sci.*, 2008, **107**, 3476.
71. Y. Wang, H. Zhang, Y. Wu, J. Yang and L. Zhang, *Eur. Polym. J.*, 2005, **41**, 2776.
72. M. Arroyo, M. A. López-Manchado and B. Herrero, *Polymer*, 2003, **44**, 2447.
73. M. A. López-Manchado, M. Arroyo, B. Herrero and J. Biagiotti, *J. Appl. Polym. Sci.*, 2003, **89**, 1.
74. M. A. López-Manchado, B. Herrero and M. Arroyo, *Polym. Int.*, 2003, **52**, 1070.
75. J. Carretero-González, J. L. Valentín, M. Arroyo, K. Saalwächter and M. A. Lopez-Manchado, *Eur. Polym. J.*, 2008, **44**, 3493.
76. Y. Sun, Y. Luo and D. Jia, *J. Appl. Polym. Sci.*, 2008, **107**, 2786.
77. N. Tabsan, S. Wirasate and K. Suchiva, *Wear*, 2010, **269**, 394.
78. L. N. Carli, C. R. Roncato, A. Zanchet, R. S. Mauler, M. Giovanela, R. N. Brandalise and J. S. Crespo, *Appl. Clay Sci.*, 2011, **52**, 56.
79. M. A. López-Manchado, B. Herrero and M. Arroyo, *Polym. Int.*, 2004, **53**, 1766.
80. L. F. Valadares, C. A. P. Leite and F. Galembeck, *Polymer*, 2006, **47**, 672.
81. Y.-P. Wu, Y.-Q. Wang, H.-F. Zhang, Y.-Z. Wang, D.-S. Yu, L.-Q. Zhang and J. Yang, *Compos. Sci. Technol.*, 2005, **65**, 1195.
82. B. Jurkowska, B. Jurkowski, M. Oczkowski, S. S. Pesetskii, V. Koval and Y. A. Olkhov, *J. Appl. Polym. Sci.*, 2007, **106**, 360.
83. Y. Zhang, Q. Liu, Q. Zhang and Y. Lu, *Appl. Clay Sci.*, 2010, **50**, 255.
84. C. Bendjaouahdou and S. Bensaad, *J. Vinyl Addit. Technol.*, 2011, **17**, 48.
85. J. Sharif, W. M. Zin Wan Yunus, K. Z. H. Mohd Dahlan and M. H. Ahmad, *Polym. Test.*, 2005, **24**, 211.

86. S. Rooj, A. Das, K. W. Stöckelhuber, N. Mukhopadhyay, A. R. Bhattacharyya, D. Jehnichen and G. Heinrich, *Appl. Clay Sci.*, 2012, **67–68**, 50.
87. A. P. Meera, S. P. Thomas and S. Thomas, *Polym. Compos.*, 2012, **33**, 524.
88. N. H. H. Abu Bakar, J. Ismail and M. Abu Bakar, *Mater. Chem. Phys.*, 2007, **104**, 276.
89. Y. Nie, G. Huang, L. Qu, P. Zhang, G. Weng and J. Wu, *Polym. Adv. Technol.*, 2011, **22**, 2001.
90. J.-F. Fu, L.-Y. Chen, H. Yang, Q.-D. Zhong, L.-Y. Shi, W. Deng, X. Dong, Y. Chen and G.-Z. Zhao, *Polym. Compos.*, 2012, **33**, 404.
91. B. Seentrakoon, B. Junhasavasdikul and W. Chavasiri, *Polym. Degrad. Stab.*, 2013, **98**, 566.
92. H.-H. Cai, S.-D. Li, G.-R. Tian, H.-B. Wang and J.-H. Wang, *J. Appl. Polym. Sci.*, 2003, **87**, 982.
93. I. Mora-Barrantes, L. Ibarra, A. Rodriguez, L. Gonzalez and J. L. Valentin, *J. Mater. Chem.*, 2011, **21**, 17526.
94. J. Sapkota, M. Poikelispää, A. Das, W. Dierkes and J. Vuorinen, *Polym. Eng. Sci.*, 2013, **53**, 615.
95. X. Wu, Y. Wang, J. Liu, S. He and L. Zhang, *Polym. Eng. Sci.*, 2012, **52**, 1027.
96. G. Zhao, L. Shi, D. Zhang, X. Feng, S. Yuan and J. Zhuo, *Mater. Des.*, 2012, **35**, 847.
97. M. Galimberti, M. Coombs, P. Riccio, T. Ricco, S. Passera, S. Pandini, L. Conzatti, A. Ravasio and I. Tritto, *Macromol. Mater. Eng.*, 2013, **298**, 241.
98. M. Poikelispaa, A. Das, W. Dierkes and J. Vuorinen, *J. Appl. Polym. Sci.*, 2013, **127**, 4688.
99. S. Rooj, A. Das, I. A. Morozov, K. W. Stoeckelhuber, R. Stocek and G. Heinrich, *Compos. Sci. Technol.*, 2013, **76**, 61.
100. Y. Liu, L. Li and Q. Wang, *J. Appl. Polym. Sci.*, 2010, **118**, 1111.
101. L. Jong, *J. Appl. Polym. Sci.*, 2007, **106**, 3444.
102. M. Mondragón, E. M. Hernández, J. L. Rivera-Armenta and F. J. Rodríguez-González, *Carbohydr. Polym.*, 2009, **77**, 80.
103. N. Rattanasom, T. Saowapark and C. Deeprasertkul, *Polym. Test.*, 2007, **26**, 369.
104. L. Qu, G. Huang, P. Zhang, Y. Nie, G. Weng and J. Wu, *Polym. Int.*, 2010, **59**, 1397.
105. A. Bendahou, H. Kaddami, E. Espuche, F. Gouanvé and A. Dufresne, *Macromol. Mater. Eng.*, 2011, **296**, 760.
106. R. M. Mariano, P. H. d. S. Picciani, R. C. R. Nunes and L. L. Y. Visconte, *J. Appl. Polym. Sci.*, 2011, **120**, 458.
107. N. Lopattananon, D. Jitkalong and M. Seadan, *J. Appl. Polym. Sci.*, 2011, **120**, 3242.

CHAPTER 5

Strength and Durability of Natural Rubber and Chemically Modified Natural Rubber

AZEMI BIN SAMSURI

Department of Polymer Technology, Faculty of Applied Sciences, Universiti Teknologi MARA, 40450 Shah Alam, Selangor, Malaysia
Email: azemi.sam@gmail.com; azemi@salam.uitm.edu.my

5.1 Introduction

The strength of a material can be defined as its ability to resist fracture. Fracture involves the creation of new free surface area within a solid. For fracture to occur in a solid body the energy to create this new surface must be equal to or greater than the surface energy and other dissipative processes involved. Durability is defined as the resistance to any change in properties due to the service environment. In the laboratory, these changes in properties are usually measured in terms of strength. For this reason, strength and durability are very closely related.

It is well established that fracture of rubber, like that of all other materials, is initiated from imperfections or flaws inadvertently present or introduced into the body of the material or on its surface. These imperfections act as sites for the initiation of crack growth. The cracks may grow under an applied load, often slowly at first, until one or more of them reaches sufficient size for complete fracture to occur. Thus the crack growth characteristics of a rubber constitute the main factor determining its strength. To study these

RSC Polymer Chemistry Series No. 8
Natural Rubber Materials, Volume 2: Composites and Nanocomposites
Edited by Sabu Thomas, Hanna J. Maria, Jithin Joy, Chin Han Chan and Laly A. Pothen

Published by the Royal Society of Chemistry, www.rsc.org

characteristics and to use them to determine the failure of rubber components, it is necessary to define them in a fundamental manner. For this purpose, a fracture mechanics approach is usually applied.

Fracture mechanics is a useful tool for studying fracture of a material. The mechanics of failure of a solid body containing a flaw or other imperfections dates back to 1920, when Griffith[1] carried out a classic work on the fracture of glass. Griffith was curious when he observed that the actual strength of the material was substantially lower than predicted by theoretical calculation. One can calculate the theoretical strength of the material from the bond energies which hold the atoms/molecules together, intermolecular forces between the molecules and London's dispersion of forces. The main reason for the large discrepancy between theoretical strength and experimental value is associated with the imperfections of the material. The imperfections may be in the form of impurities, cracks, micro-voids and flaws, which act as stress raisers. Failure occurs at these flaws because the stress concentration at the tip of these flaws is substantially higher than the stress in the bulk of the material.

Griffith's fracture criterion[1] can be stated as follows: a pre-existing crack in an elastic body will grow if in so doing the elastic stored strain energy released at the instant of rupture is equal to or greater than the amount of surface energy required to create new surfaces. This can be expressed in mathematical form by Equation (5.1):

$$-(\partial U/\partial A)_l \geq 2S \tag{5.1}$$

where U is the elastic strain energy stored in the body, A is the new interfacial area of the fractured surface, and S is the surface energy of the material. The minus sign indicates that there is a reduction in the stored energy as A increases. U continues to decrease until the strain energy is zero, which is when the crack has spread across the body. A factor of 2 appears on the right-hand side of the equation because there are two surfaces to a crack. The suffix l of the partial differentiation denotes that the crack spreads under conditions such that the external forces on the test-piece do not move and do no work.

The term $-(\partial U/\partial A)$ is defined as the strain energy release rate, or the fracture energy. The word 'rate' normally means rate with to time. However in this context, the word rate refers to the rate of releasing elastic strain energy in propagating a fracture over an increment of area δA, and not the time.

Equation (5.1) implies that all the mechanical work appears as surface energy. Griffith's fracture criterion is only applicable to perfectly elastic materials where all the elastic strain energy released is converted into fracture energy whose value is about the value of the free surface energy (7–10 J m^{-2}). However, the theory is not applicable for materials that are not perfectly elastic such as polymers, because other energy dissipative processes are involved. It is easy to correct for energy lost by dissipation in the main bulk of the test specimen (from the area under the stress–strain curve), but it is difficult to deal with energy dissipated near the crack tip, where the strains are very high. If it is assumed that no energy has been dissipated in the bulk of the test-piece

(or that has corrected for), then all the energy dissipation requirement for fracture relate to the crack tip, *i.e.* additional to the surface energy requirement, and in fact usually overwhelms it.

5.2 Tearing Energy Theory of Rivlin and Thomas

In conventional tear tests, the force required to tear the test-piece is noted and the tear strength is computed by dividing the tearing force with the mean nominal thickness of the test-piece. The tear strength is defined as the tearing force per unit thickness of the test-piece.

There are three types of test-piece commonly used in tear tests, namely, trouser test-piece, crescent tear test-piece and Die-C (angled test-piece). Conventional tear tests often produce different ratings of tear strength for the same set of rubber vulcanizates because the tearing force is dependent on the geometry of the test-piece and the way the forces are applied. Thus conventional tear tests do not measure the true tear resistance or a characteristic of the rubber itself. To circumvent this problem, Rivlin and Thomas[2] introduced the tearing energy theory similar to Griffith's theory of fracture, but taking into consideration the energy dissipation.

The driving force for crack propagation in rubber is the stored elastic energy in the bulk of the rubber. When this becomes equal to the energy required to create the new surface plus the energy required by the viscoelastic dissipation processes near the crack tip, the crack will propagate. The rubber near the tip of the crack experiences a stress–strain cycle as the crack grows, and hence dissipates energy as viscoelastic hysteresis, H.

This tearing energy is given by Equation (5.2):

$$-(1/t)(\partial U/\partial c)_l \geq T \tag{5.2}$$

where $\boldsymbol{T}$ is the tearing energy, U is the total elastic energy in the test-piece considered, c is the crack length and t is the nominal thickness. Because $\boldsymbol{T}$ is defined as energy per unit initial crack area whereas fracture energy, $\boldsymbol{G}$, is defined in terms of energy per unit crack surface, because a crack has two surfaces then clearly tearing energy is twice the fracture energy ($T = 2\boldsymbol{G}$).

It does not matter whether tearing energy $\boldsymbol{T}$ or fracture energy $\boldsymbol{G}$ is used. However, it is generally accepted that for fracture of rubber which involves viscoelastic energy dissipation, $\boldsymbol{T}$ is used because it distinguishes from rigid fracture, which involves ductile energy dissipation.

Tearing is a localized process where the strain at the crack of the tip is at its breaking strain. When a crack grows, irreversible processes occur in the vicinity of the moving tip, leading to energy losses that must be made up for by the available elastic energy. The magnitude of these losses is determined by the properties of the rubber and the strain in the crack tip region, and the rate of growth of the crack. Thus the energy necessary to propagate a crack at a particular rate is likely to be a characteristic of the rubber itself, and may

therefore be independent of the overall shape of the test-piece. Thus tearing energy ***T*** is the sum of hysteretic loss and surface energy. Because tearing energy greatly exceeds the thermodynamic surface free energy, this indicates that hysteresis plays a predominant role in enhancing the tear strength of the rubber.

5.2.1 Experimental Verification of Tear Criterion

To verify that tearing energy is a material property independent of test-piece geometry and the way the forces are applied, Thomas made some tear measurements on the same vulcanized rubber but using different shaped test-pieces.[3] Values of ***T*** computed from the results should be the same for each test-piece at a given rate and temperature of testing. Figure 5.1 shows a plot of tearing energy versus rate using different test-piece geometries.[3] It can be seen that the results are consistent with a single relation, independent of the test-piece geometry, as implied by the fracture mechanics approach. Thus tearing energy measures the true tear resistance of the vulcanized rubber.

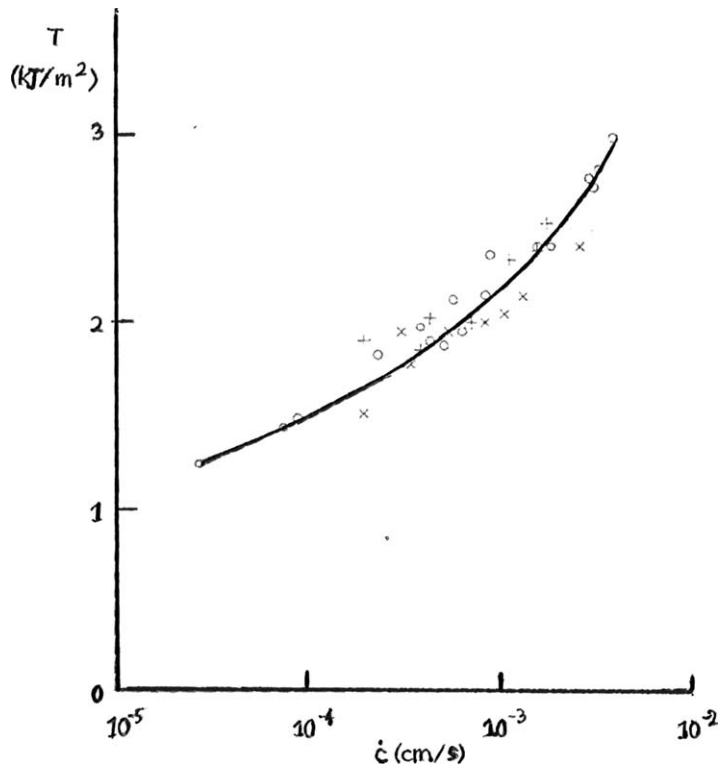

Figure 5.1 Tearing energy vs rate for different test-piece geometries.[3] Trouser test-piece, + pure shear test-piece, o split test-piece.
(Reproduced from ref. 3.).

5.2.2 Types of Test-Pieces

Figure 5.2 shows different types of test-pieces which can be used to measure the tear strength. The tearing energy, T, can be calculated from easily measurable applied forces or strains, which make them convenient for experimental purposes.

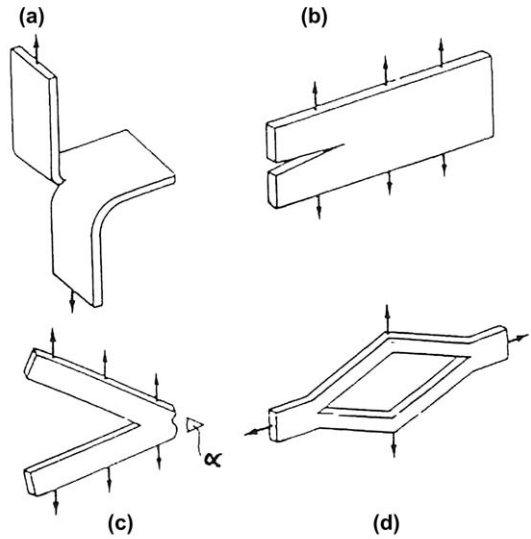

Crack growth test pieces for which T can readily be calculated: (a) "trousers," (b) pure shear, (c) "angled," and (d) "split."

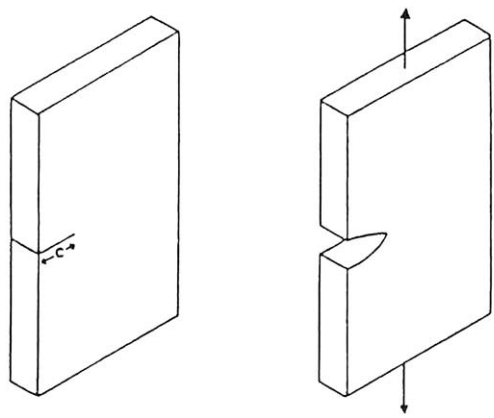

Tensile strip test piece with an edge crack of length c.

Figure 5.2 Different types of tear test-piece geometry: (a) trouser, (b) pure shear, (c) angle and (d) split tear test-pieces.

5.2.2.1 Trouser Test-Piece

The trouser test-piece is also known as the simple extension test-piece, and its tearing energy is given by:

$$\boldsymbol{T} = 2F\lambda/t - wU \tag{5.3}$$

where F is the applied tearing force, λ is the extension ratio in each leg, t is the thickness, w is the total width of the test piece, and U is the strain energy density in the legs of the test-piece that are in simple extension. At small strain, that is when λ is not much greater than unity, the stress–strain relation is linear. In this region, Equation (5. 3) can be reduced to:

$$\boldsymbol{T} = F(\lambda + 1)/t \tag{5.4}$$

A useful approximation is obtained when the legs of the test-piece are not extensible, for example by using a test-piece with wider legs or bonded to an inextensible material such as metal shim so that $\lambda = 1$ and $U = 0$. When this is the case, Equation (5.3) reduces to:

$$\boldsymbol{T} = 2F/t \tag{5.5}$$

5.2.2.2 Pure Shear Test-Piece

The tearing energy of a pure shear test-piece is given by Equation (5.6):

$$\boldsymbol{T} = Ul_0 \tag{5.6}$$

where U is the strain energy density in that region of the test-piece which is in a state of pure shear, and l_0 is the distance between the two parallel clamps.

5.2.2.3 Split Tear Test-Piece

For the split tear test-piece, the tearing energy is given by:

$$\boldsymbol{T} \approx \lambda t^{-1}\left[\left({F_\mathrm{A}}^2 + {F_\mathrm{B}}^2\right)^{1/2} - F_\mathrm{B}\right] \tag{5.7}$$

where λ is the average extension ratio in regions A and B, and F_1 and F_2 are the two forces applied.

5.2.2.4 Angled Test-Piece

For the angled test-piece, the tearing energy is given by:

$$\boldsymbol{T} = 2Ft^{-1}\sin\alpha \tag{5.8}$$

where α is the angle between the clamps.

5.2.2.5 Edge Crack Test-Piece

For this test-piece, the tearing energy is given by:

$$\boldsymbol{T} = 2kcU \tag{5.9}$$

where k is a constant, c is the crack length and U is the elastic stored energy in the test-piece having no cut.

5.3 Types of Failure

There are two types of tear failure that may affect the magnitude of the tearing energy of a particular vulcanizate. These have been classified qualitatively as steady (smooth) and stick–slip tearing, respectively.[4] Steady tearing is controlled by a basic tear process that is predominantly viscoelastic in nature. In this case, the tearing energy increases continuously with the rate of crack propagation. Stick–slip tearing is a secondary tear process where the tearing energy increases as the tear rate decreases. This is attributed to the development of strengthening structures, for example crystallization and strength anisotropy induced by the carbon black at the tip of a tear.

The most convenient way to distinguish between the two types of tear process is to do tear measurements at a constant rate separation using a trouser test-piece. The fluctuations of tearing force with rate will reflect the nature of the tear process. Typical tearing force–time curves for this type of tear measurement are illustrated in Figure 5.3.

In the case of steady or smooth tearing, the tearing force and rate of separation remain essentially constant apart from random fluctuations, once tearing has commenced. Curve (a) denotes negligible or no fluctuations of tearing force with rates and curve (b) denotes marked fluctuations of tearing force with rates. The appearance of the torn surface depends on the degree of fluctuation, which in a way reflects the nature of the tearing process.[4] If the fluctuations are relatively small, smooth torn surfaces are produced; otherwise

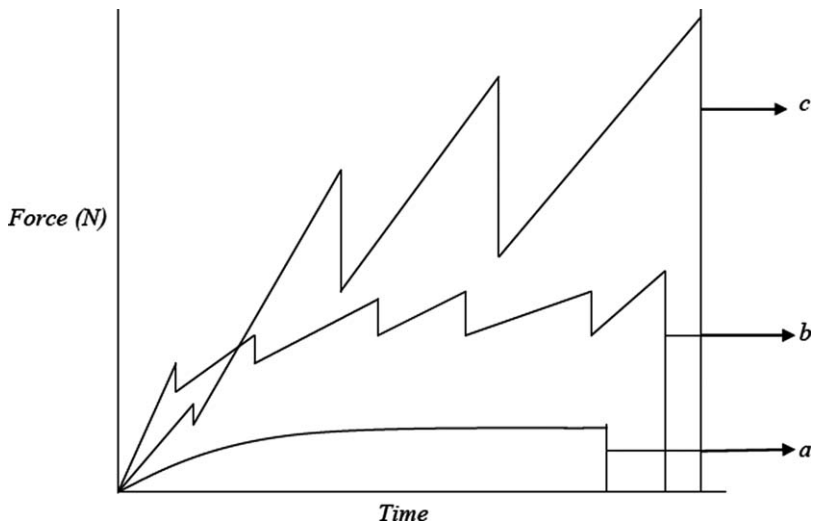

Figure 5.3 Schematic tearing force–time curves for constant rate of separation of trouser test-piece: (a) steady (smooth) tearing, (b) stick–slip tearing, (c) knotty tearing.

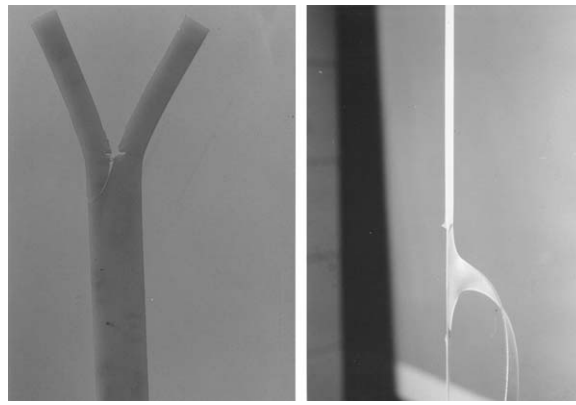

Figure 5.4 Knotty tearing of NR latex film.[11] Photo on LHS shows the crack of the torn sample, which approximates to a semi-circular arc. Photo on the RHS shows the deviation of the crack from the intended path during tearing.
(Reproduced from ref. 11.)

rough and irregular torn surfaces are produced. In the case of stick–slip tearing, a tear does not propagate continuously but rather arrests and reinitiates at fairly regular intervals. This would result in a more pronounced fluctuation of the tearing force with the rate of propagation (curve (c)). The torn surface appears to have both smooth and rough regions. The rough surface corresponds to the stick period (tear arrests) where the force is building up, and the smooth surface corresponds to tear moving (tear initiates).

There is another type of tear failure known as knotty tear,[5–10] where the tear tends to deviate from the intended tear path and circles around almost perpendicularly, as shown in Figure 5.4. The tearing force–time chart corresponds to curve (c) in Figure 5.3.

Knotty tear occurs in vulcanized rubbers filled with reinforcing fillers. The occurrence of knotty tear is associated with the strength anisotropy due to the development of strengthening structures such as strain crystallization and black structure. Knotty tear causes blunting of the tear tip and thus enhances the tear resistance of the rubber.

5.4 Dependence of Tearing Energy on Rate and Temperature

Tearing energy is not a constant quantity but depends on the rate and temperature of tear measurement. The effects are best described by three-dimensional plots of tearing energy versus tear rate and temperature,[12] as shown in Figures 5.5(a) and (b) for unfilled natural rubber (NR) and black-filled styrene butadiene rubber (SBR), respectively. In the case of unfilled SBR, the tearing energy increases either when tear rate increases or temperature decreases, *i.e.* the conditions where viscoelastic energy dissipation are high. In the case of

strain-crystallizing rubber like NR, the dependence of tearing energy on rate and temperature becomes less marked. This could be associated with the strain-crystallization effect, which outweighs the dependence of the viscous component on rate and temperature of tearing. The high tearing energy displayed by NR over a relatively wide range of temperature and rate could be associated with the high energy dissipation (hysteresis) which appears as heat of crystallization. Figure 5.5(b) shows the effect of loading carbon black particles into SBR. The flat plateau surface in Figure 5.5(b) represents knotty tearing regions where there is a marked increase in the tearing energy. Outside this range, where knotty tearing does not operate, carbon black produces a relatively small increase in strength. This suggests that the development of knotty tearing is dependent on rate or test speed, implying that a finite time is required for the strength anisotropy to form at the crack tip.

The tearing energy–tear rate relationship works well under conditions of steady (smooth) tearing because the crack-growth rate is easy to measure. However, in cases when stick–slip tearing or knotty tearing occurs, the tearing energy–tear rate relationship is harder to interpret because it is not clear what the actual crack-growth rate is because the fluctuations are very great – from a very rapid tear rate and a zero velocity tear rate.

Recently Sakulkaew *et al.*[13] attempted to characterize the rate of increase in the strain energy at the crack tip immediately before the onset of tearing in a trouser test-piece. They developed a new technique to characterize the tear behaviour where it is useful to measure the rate increase in strain at the tip of the crack, which can then be related to the critical strain energy release rate for the material. They then derived the relationship between the rate of change in the strain energy release rate with time $\dot{T}$ and the rate of change of the strain energy with time $\dot{E}$ at the tip of the crack as given by Equation (5.10):

$$\dot{T} \approx \mathrm{d}\dot{E} \tag{5.10}$$

This equation shows that a measure of the rate of change of strain energy release rate with time can be used as an equivalent measure of the increase in strain energy at the tip of the crack with time, assuming that the crack tip diameter, d, does not change significantly during tearing. They were able to examine all types of non-steady tearing such as stick–slip and knotty tearing, observed for a wide range of rubbers. With this new technique, they were able to plot critical tearing energy, T_c against $\dot{T}$ (where $\dot{T} = \mathrm{d}T/\mathrm{d}t$) to calculate data points. They determined $\dot{T}$ and T_c from the measured force–time curve as shown schematically in Figures 5.3(b) and (c) for stick–slip and knotty tearing. To obtain $\dot{T}$, they took the three points on the initial part of the force versus time curve, one at the peak force (critical tearing force) and another two near to, but just before, the peak force, because this is the portion of the curve that corresponds to the maximum strain at the tear tip before the new crack surface is introduced. They then transformed the three tearing forces to the strain energy release rate using Equation (5.10). They obtained the value of $\dot{T}$ from the slope of the resulting plot of tearing energy at the first tear versus time.

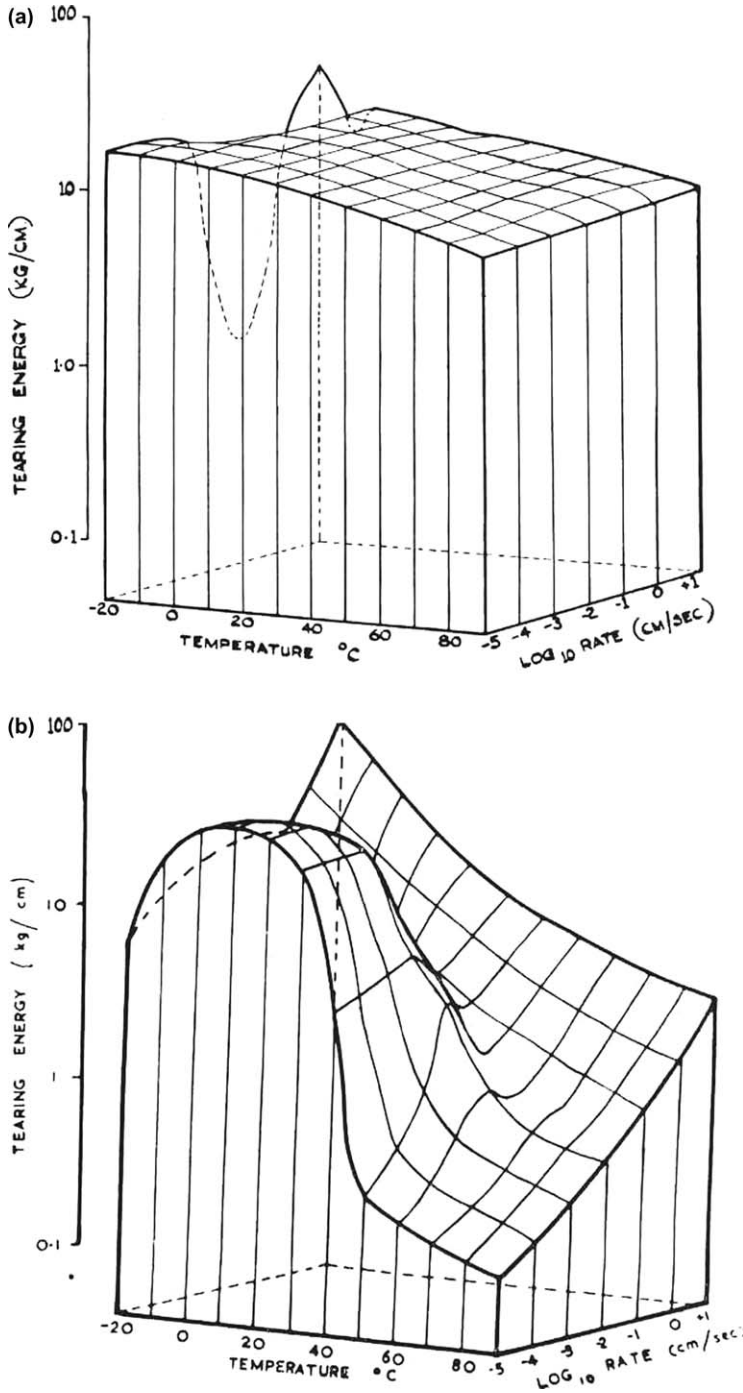

Figure 5.5 Effects of tear rates and temperatures on tearing energy: (a) unfilled vulcanized NR, (b) black-filled vulcanized SBR.
(Reproduced from ref. 12.).

From these data points the tearing energy–tear rate relation is obtained, where critical tearing energy $\boldsymbol{T_c}$ is plotted against the strain energy release rate with time $\dot{\boldsymbol{T}}$. They found that NR samples exhibited characteristic tearing at the slower rates that represents failure after the samples have been strain crystallized. At the fastest rates, the kinetics of crystallization was beaten and the behaviour was more typically associated with the viscoelastic strengthening alone.

5.5 Mechanism of Reinforcement in Tear Strength

The principal mechanism of reinforcement of tear resistance of vulcanized filled rubber is associated with the phenomenon of knotty tearing.[5–10] In knotty tearing the tear deviates almost perpendicularly from the intended tear path and the 'knot' looks approximately like a semi-circular arc on the torn test-piece (in the unstrained state) as shown in Figure 5.4.

Azemi[8] measured the size of each 'knot' by means of an eye-piece lens scale and the corresponding tearing energy was calculated from the tearing force chart. The relationship between knot diameter and tearing energy is shown in Figure 5.6. The results show that the tearing energy increases with size of 'knot' diameter in accordance with the approximate relation[14] given by Equation (5.11):

$$\boldsymbol{T} \approx W_b d \tag{5.11}$$

where W_b is the work done to break per unit volume of rubber and d is the size of the unstrained tear tip diameter. In fact the agreement between the measured and calculated values is fortuitously good, considering that W_b was not determined at the same rate as in the tear measurement. The results shown in Figure 5.6 provide experimental evidence that blunting of the tear tip appears to be the principal mechanism by which knotty tearing enhances the tear strength. The size of the 'knot' diameter reflects the degree of blunting of the tear tip. The larger the 'knot' diameter the blunter the tear tip. The blunting of the tear tip reduces the stress concentration at the tear tip. Therefore a large 'knot' diameter reduces the stress concentration more effectively than a small 'knot' diameter.

The size of the 'knot' diameter is influenced by the rate and temperature of tear measurement as shown by the photographs in Figures 5.7 and 5.8 at temperatures of 23 °C and 100 °C, respectively. The average knot diameter measured on the torn test-pieces was relatively big ($\sim$ 2.0–6.0 mm) either at a low rate or at a high temperature. At a fast rate and low temperature the average knot diameter measured on the torn test-pieces was relatively small ($\sim$0.5–1.2 mm). The strengthening structures require an appreciable time to form, as suggested by Greensmith.[6]

At a slow test speed (low rate) it gives sufficient time for the strengthening structure to develop. For this reason the knot diameter is bigger at slow test speed than at fast test speed. The temperature also plays a part in facilitating the development of this strengthening structure. The development of strengthening structures is not favoured either at low or very high

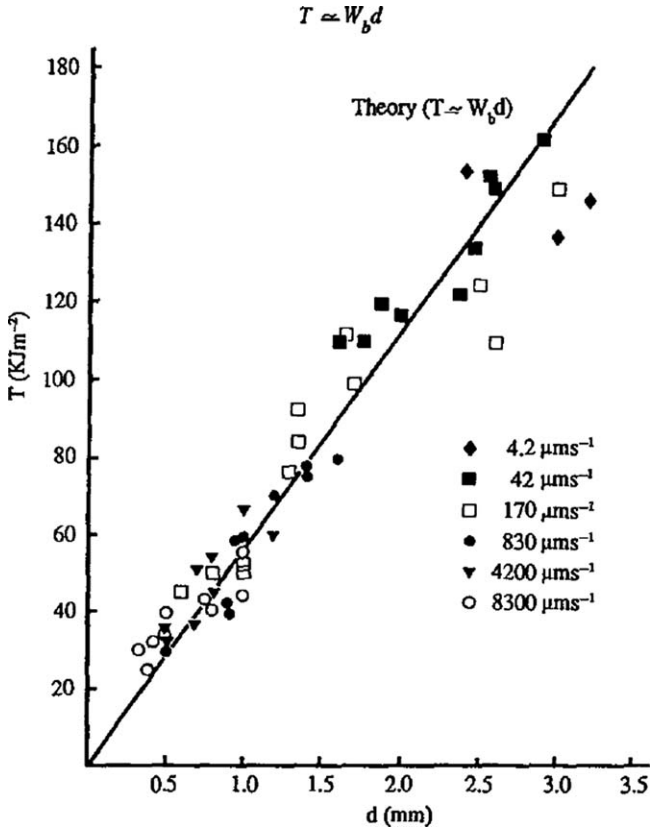

Figure 5.6 Tearing energy T vs knot diameter d showing the effect of tear rates on the size of knot diameter formed at 23 °C. The straight line shows the tearing energy–tip diameter relationship obtained from $T \approx W_b d$. (Reproduced from ref. 8.)

temperatures. At low temperatures the development of oriented structures is opposed by the very sluggish molecular mobility. At high temperatures the molecular mobility is very fast and it can destroy the initial development of strengthening structures. Knotty tearing normally occurs readily when the temperature gives the right molecular mobility. The flat plateau surface in Figure 5.5(b) (refer to Section 5.4) represents knotty tearing regions where the rates and temperatures are right for the development of knotty tearing.

Azemi and Thomas[8] suggested that in knotty tearing, additional energy must be applied to propagate the tear either through or around the strengthening structures. Thus a large knot diameter reflects large regions of strengthening structures forming at the tip of the tear.

Azemi and Thomas[8] used a split tear test-piece to model the strain energy release rate for a crack propagating along the molecular orientation as shown in Figure 5.9. Thus tearing energy in split tear test-pieces gives a quantitative measure of the energy to propagate tearing in the direction of molecular

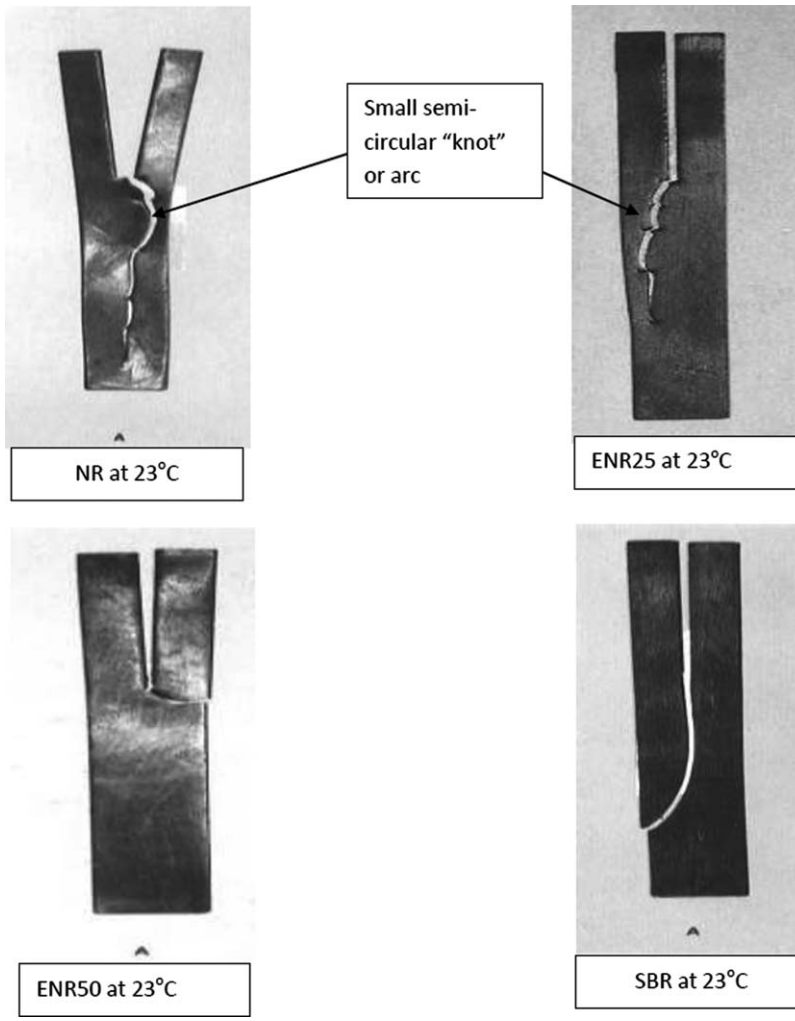

Figure 5.7 Photos showing the torn samples failed by knotty tearing at 23 °C at crosshead speed of 100 mm/min.

orientation, parallel to the direction of pre-strain that is applied. First, the split tear test-piece is pre-strained by applying a tensile force F_B. The crack is made to propagate in the direction of molecular orientation parallel to F_B, by applying a pair of transverse forces F_A. This is done by applying a dead load to each side of the test-piece. One of the interesting features is the time-dependent crack growth observed here. It is well established that both unfilled and filled vulcanized NR do not show time-dependent crack growth in conventional tear test-pieces because of the crystalline region at the tear tip.[8] Time-dependent crack growth is the term used to describe the increment in crack length as a function of time when the test-piece is subjected to constant load.

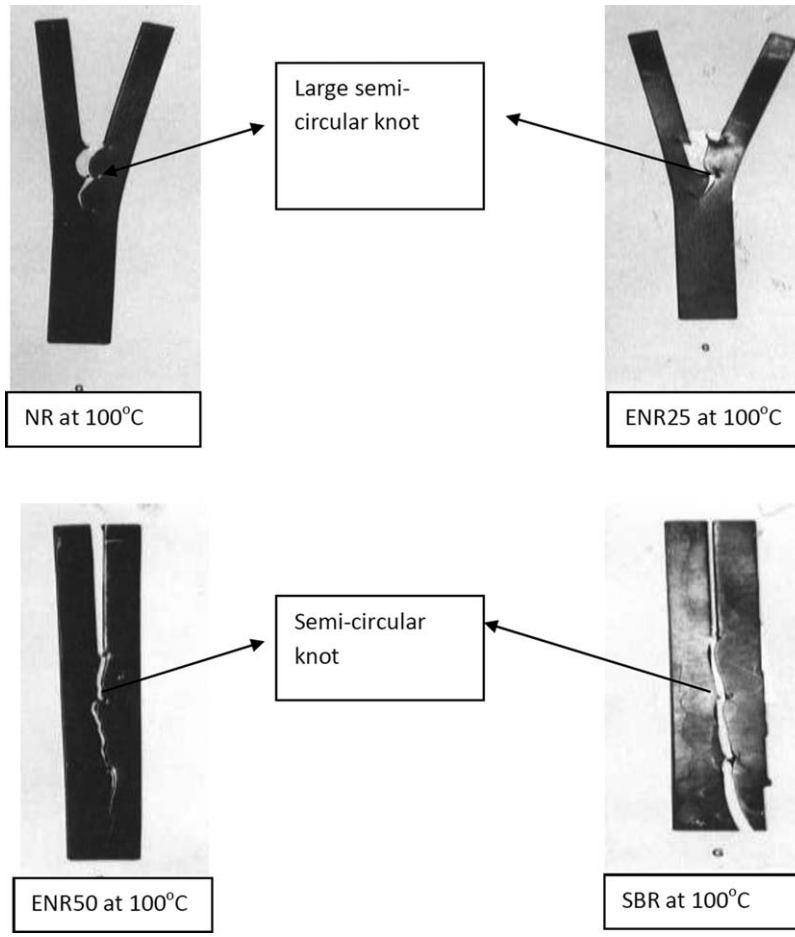

Figure 5.8 Photos showing the torn samples failed by knotty tearing at 100 °C at crosshead speed of 100 mm/min.

The occurrence of time-dependent tearing in a split test-piece can be explained as follows: in split tearing crystallization occurs in the bulk of the vulcanizate when the test-piece is pre-strained. Because the stress giving the orientation is maintained during the test, the crystals would remain in the bulk and would not melt. When the tearing forces F_A were applied, possibly few crystallizable units were available to induce further crystallization at the tip of the tear.

As a consequence of the absence of strain crystallization at the tip of the tear, time-dependent tearing occurred. The effect of pre-straining on the tearing energy of vulcanized HAF (high abrasion furnace) black-filled NR for a crack propagating in the direction parallel to molecular orientation is shown in Figure 5.10.[8] The tearing energies obtained from split tear test-pieces which produced steady tearing were very low, ranging from 1.0 to 4.0 kJ m^{-2} over the strain range covered. The tearing energy decreases as the amount of

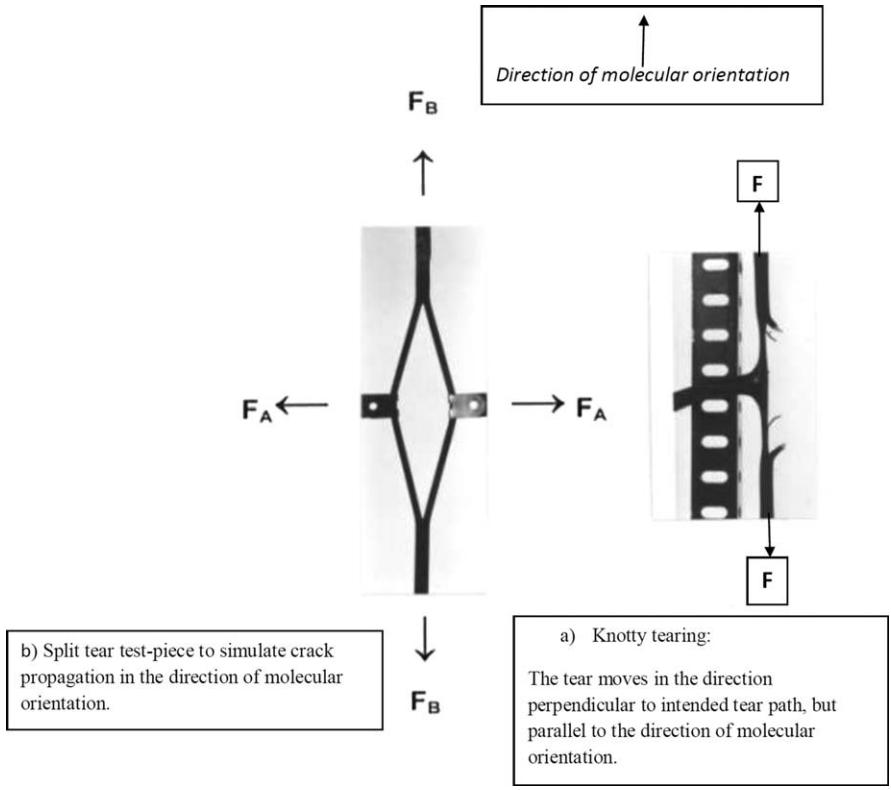

Figure 5.9 Photos showing split tear test-piece to simulate crack propagation in the direction of molecular orientation in knotty tearing.

pre-straining imposed on the test-piece increases. The tearing energy increases as the rate of tearing increases. In contrast, the tearing energy of trouser test-pieces that produces knotty tearing decreases with increasing rate, as shown in Figure 5.11. The experimental results shown in Figures 5.10 and 5.11 provide experimental evidence that the strain energy release rate (tearing energy) in the direction of molecular orientation is very low. This is the reason why the tear in black-filled vulcanized rubber deviates from the intended tear path and propagates in the direction parallel to molecular orientation because the energy in this direction is very low. This is consistent with the theory proposed by Gent.[15] Indeed Gent *et al.*[15] developed model cracks and used FEA to calculate the tearing energy both in the forward and sideways directions. They found that a crack will turn or split sideways if the strength in that direction was about 40% less than that of the forward direction. Indeed in Figure 5.11, at rates ranging from 1.0 to 10.0 μm/s, the trouser test-pieces that produced knotty tearing gave a tearing energy of about 100 kJ/m^2 compared to split tear test-pieces that produced smooth tearing, which gave a tearing energy of about 1.0 kJ/m^2; the strength of the latter is just 1/100 of the strength of the former.

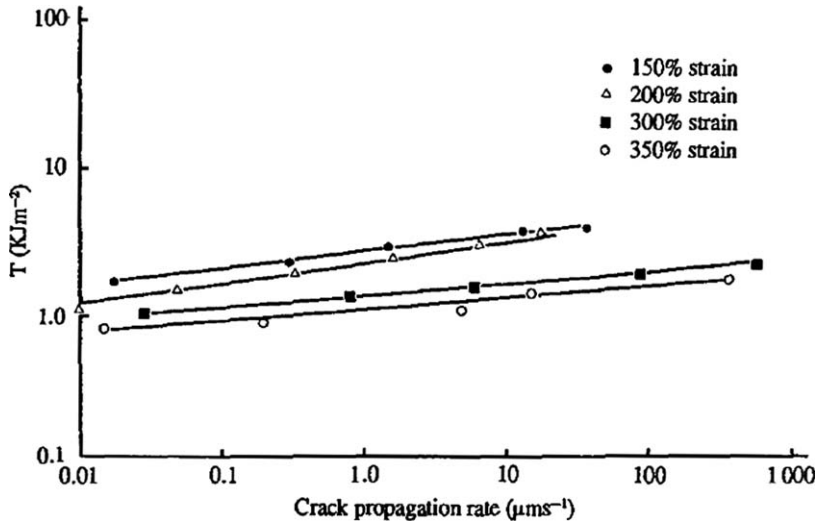

Figure 5.10 Influence of pre-straining on tearing energy for crack propagating in the direction parallel to the direction of molecular orientation. Vulcanized HAF black-filled (50 pphr) NR. Split test-piece was used. (Reproduced from ref. 8.)

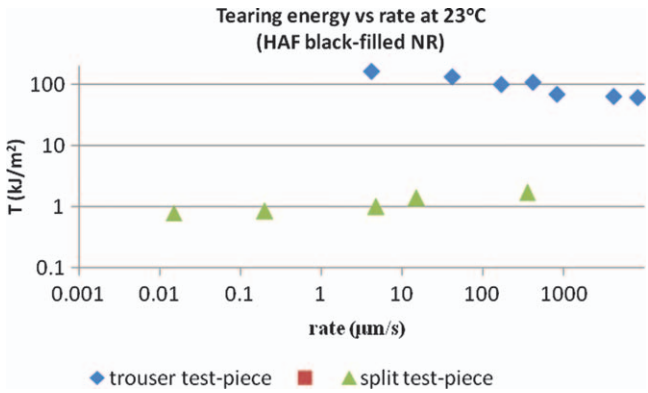

Figure 5.11 Comparison between tearing energy of trouser test-piece that produced knotty tearing and that of tearing energy of split test-piece that produced smooth tearing. Both test-pieces were prepared from the same vulcanized HAF (50 pphr) black-filled NR. (Reproduced from ref. 8.)

5.5.1 Factors Affecting the Development of Knotty Tearing

5.5.1.1 Degree of Crystallinity and Glass Transition Temperature of the Rubber

Azemi and Thomas[8] investigated the effect of the degree of crystallinity and the glass transition temperature of the rubber on the development of knotty

tearing. They used NR, ENR 25, ENR 50, SBR and INR. ENR 25 and ENR 50 are chemically modified NR to provide good swelling resistance towards hydrocarbon oil and to improve the resistance towards air permeability.[16] The former contains 25 mol% of epoxy groups and the latter contains 50 mol% of epoxy groups. These epoxidized natural rubbers can still crystallize on straining because the small oxygen atom can still fit into the crystal lattice,[17] although the degree of crystallinity is lower than pure NR.[17] Isomerized natural rubber (INR) containing 64 mol% of *trans*-1,4-isoprene was also used in their investigation. All the rubber compounds were prepared by mixing in a laboratory internal mixer (batch volume about 1400 cm^3) based on the same basic formulation. Each rubber compound was filled with 50 pphr of HAF black (N330) and the semi-EV system was used in each case. Tear measurements were done by using trouser test-pieces where the legs of the test-piece were pulled at various constant separation rates using a tensile machine. Figure 5.12 shows the effect of degree of crystallinity and glass transition temperature on the development of knotty tearing. The range of tear rates at which knotty tearing (shown by full line) occurs are different for each vulcanized rubber, depending on the degree of crystallinity and molecular mobility. Both NR and ENR 25, which crystallize readily on straining, produce

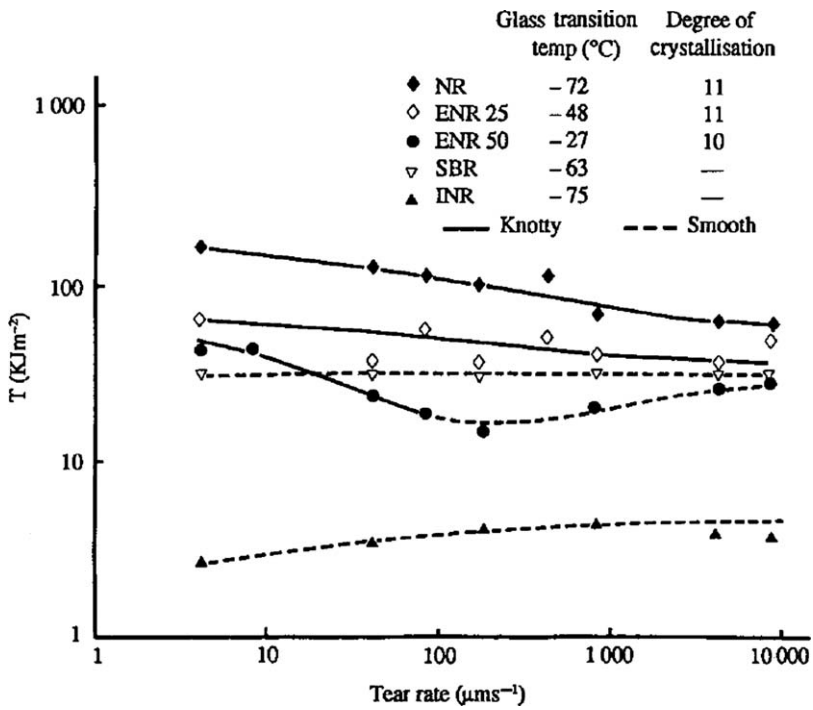

Figure 5.12 The effect of degree of crystallinity and glass transition temperature on development of knotty tearing energy as a function of tear rate at 23 °C. (Reproduced from ref. 8).

knotty tearing over the whole range of tear rates. In contrast, SBR and INR, which do not strain crystallize, do not produce knotty tearing, but instead produce smooth tearing over the whole range of tear rates. ENR 50, which strain crystallizes less readily than NR and also has lower molecular mobility associated with its high glass transition temperature, produces knotty tearing at a narrow range of tear rates, from 4.2 μm/s to 83 μm/s. This latter point also indicates that a finite time is required for the black structure to develop and produce the anisotropy necessary for the occurrence of knotty tearing. The comparison between NR and INR clearly illustrates the importance of crystallization. Both rubbers have about the same glass transition temperature and hence molecular mobility indicates that crystallization plays an important role in promoting knotty tearing. It may be that crystallization helps to enhance further the anisotropy already produced by the carbon black.

The effect of strain crystallization on the development of knotty tearing is clearly noticeable when all the tear measurements are done at relatively the same molecular mobility as NR. The legends in Figure 5.12 show the glass transition temperature and the degree of crystallinity of each rubber. The legends in Figure 5.13 show the required temperature of tear measurements for each rubber in order to get about the same molecular mobility as NR. It is

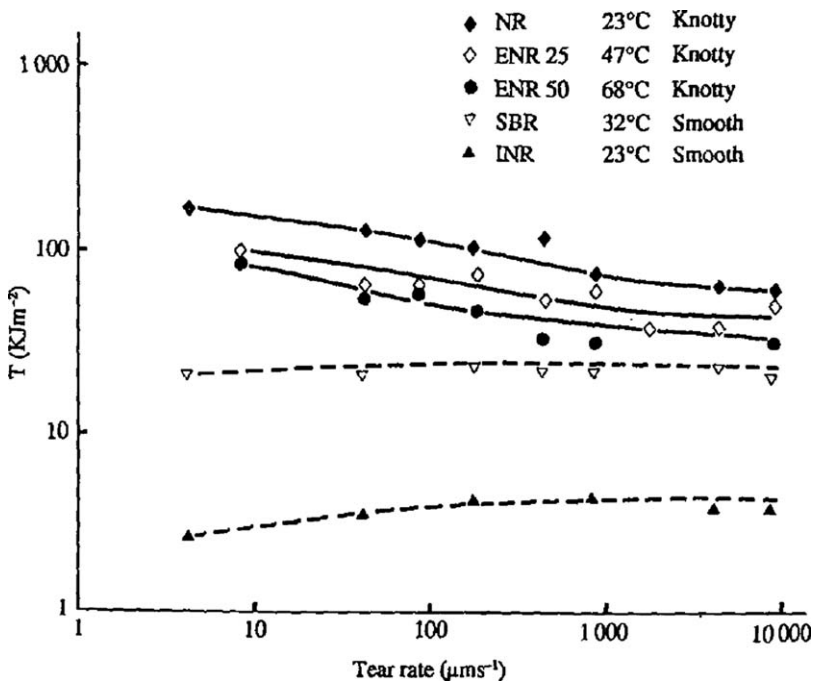

Figure 5.13 The effect of degree of crystallinity and glass transition temperature on development of knotty tearing energy as a function of tear rate at temperatures to equalize the molecular mobility of each rubber. (Reproduced from ref. 8.)

interesting to note that ENR 50 produces knotty tearing over the whole range of tear rates, and also between tear rates of 42 μm/s and 83 μm/s its tearing energy is more than a factor of two higher than previously at 23 °C. In the case of ENR 25, there is an increase of about 50% in the tearing energy. In the case of SBR, it still does not produce knotty tearing, again implying the importance of crystallization to promote knotty tearing. The comparison of tearing energy between SBR and INR sheds some light on the enhancement of tear strength of black-filled vulcanized rubber. In the absence of knotty tearing, the enhancement of tear strength is influenced by energy dissipation or hysteresis. In this case SBR produces higher tearing energies than that produced by INR over the whole range of tear rates because the former has a higher glass transition temperature than the latter.

5.5.1.2 *Anisotropy Associated with Permanent Set*

If the reinforced black-filled NR rubber is pre-stressed to a large strain for a short time, after which the stress is removed completely, the tearing energy to propagate tear in the direction of the previously applied pre-stressing is very low.[8] The tearing energy correlates strongly with the amount of set, where tearing energy decreases progressively with increasing amount of set,[8] as shown in Figure 5.14. The set is believed to be introduced during pre-stressing itself due to the ability of the broken crosslinks to recombine to form a new network consistent with the two-network theory of Green and Tobolsky.[18] The application of such a theory gives a quantitative measure of the proportion of crosslinks that break and recombine under the influence of the applied

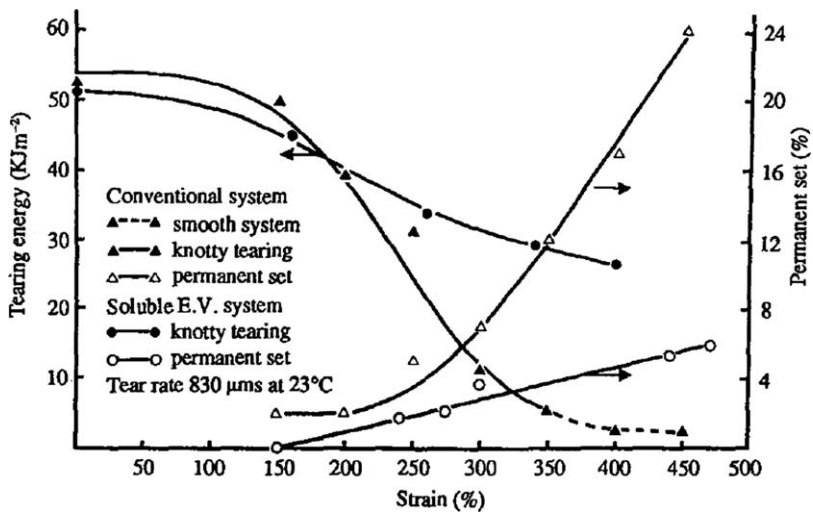

Figure 5.14 Effect of pre-stressing on tearing energy and permanent set. (Reproduced from ref. 8).

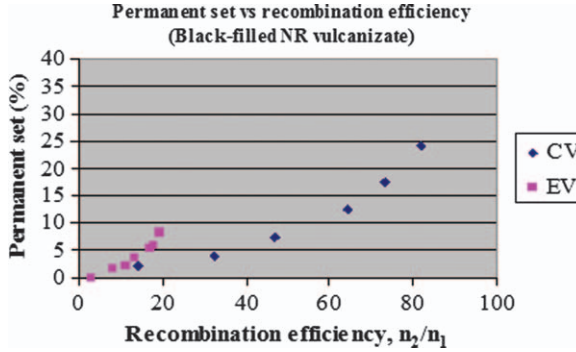

Figure 5.15 Plot of permanent set against recombination efficiency n_2/n_1 of conventional vulcanization system (CV) and efficient vulcanization system (EV) black-filled (50 pphr HAF) NR vulcanizates.
(Reproduced from ref. 24.)

stress.[19,20] The relationship between permanent set and the recombination efficiency n_2/n_1 is shown in Figure 5.15.[19]

The amount of set produced is very dependent on the type and nature of the crosslink network. The type of crosslinks produced in turn relies on the type of vulcanization system employed in the rubber mix formulation. There are two main sulfur vulcanization systems, namely conventional vulcanization (CV) and efficient vulcanization (EV). The former employs a higher sulfur to accelerator ratio than the latter. The CV system produces a predominantly polysulfidic type of crosslink, where the two rubber chains are bridged by three to six sulfur atoms. In contrast, the EV system produces a predominantly monosulfidic type of crosslink where the two rubber chains are bridged by one sulfur atom. It is well established that polysulfidic type crosslinks are weak and labile.[21] Such weak crosslinks usually give higher tensile strength than do stable crosslinks such as the monosulfidic type, because of their ability to relieve local stress through 'yielding', thereby permitting a more uniform distribution of stress.[21] This hypothesis has been supported by an independent investigation into the breaking and reforming of crosslinks during stressing.[19] Here, the permanent set provides an indication of the number of bonds that have recombined while in the deformed state, and the changes in equilibrium volume swelling indicate the fraction of crosslinks that break.[19] The earlier findings by Azemi *et al.*[8,20] are very significant because they implies that, in the vulcanizates produced by the conventional sulfur system, once the set has occurred during pre-stressing, it is no longer necessary to maintain the stress giving the molecular orientation because the anisotropy associated with the set is adequate to cause crack propagation in the direction of molecular orientation.[22,23] This is clearly an undesirable feature because it can lead to premature failure of the product. Figure 5.16 shows the effect of anisotropy produced by a permanent set after pre-stressing, and compares with that where the stress giving the orientation is maintained during the test.[8] The former uses the trouser test-piece

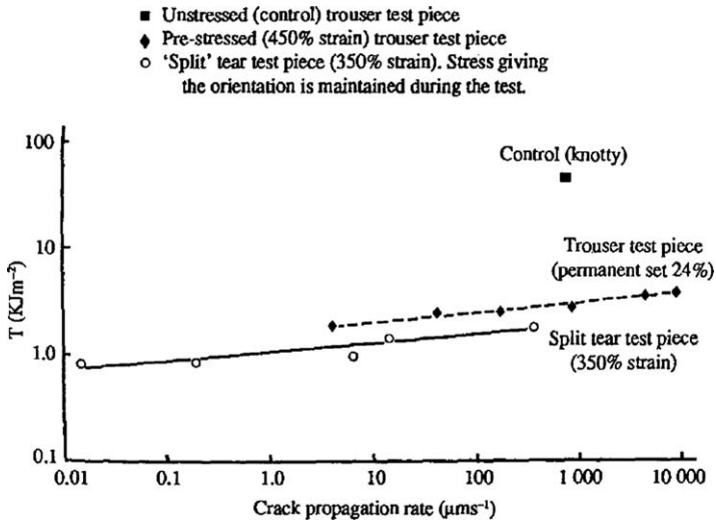

Figure 5.16 Tearing energy versus crack propagation rate of vulcanized (conventional sulfur cure system) HAF (N330) black-filled (50 pphr) NR at 23 °C. (Reproduced from ref. 8.).

and the latter uses the split tear test-piece. In both cases, tearing proceeded steadily with a smooth torn surface, followed by a substantial drop in the tearing energy. When the sample is pre-stressed, the tearing energy reduces by a factor of 15. However, when the stress giving the orientation is maintained, the tearing energy drops further, by a factor of two. Thus, this indicates that pre-stressing introduces substantial anisotropy into the material. Such a condition of vulcanized rubber is no longer durable since it is susceptible to premature failure in the presence of flaws and impurities, because such flaws may initiate crack growth to propagate tearing in the weak zone (parallel to the direction of molecular orientation).

It is well established that the EV sulfur system produces low set, and its tearing energy after pre-stressing is relatively high, as shown in Figure 5.14. In order to introduce a high set into the EV vulcanizate network, it is necessary to conduct vulcanization in two stages. The first-stage vulcanization involves curing the rubber up to 95% of its maximum state of cure. The second-stage vulcanization involves curing the rubber (held in a strained state) fully to its maximum state of cure. Thus the second network is formed in a strained state. This study also has some practical applications, for example in continuous vulcanization and in injection moulding. In these cases, vulcanization is carried out at high temperature, say at 190 °C and above, using a very fast accelerator system. Because of the very short vulcanization time (less than a minute), vulcanization may take place before the rubber completely fills the mould. The effect is analogous to the formation of two networks in the vulcanizates investigated in this work. It is not surprising that the strength properties, such as tensile and tear strengths of injection-moulded test-pieces, show a strong

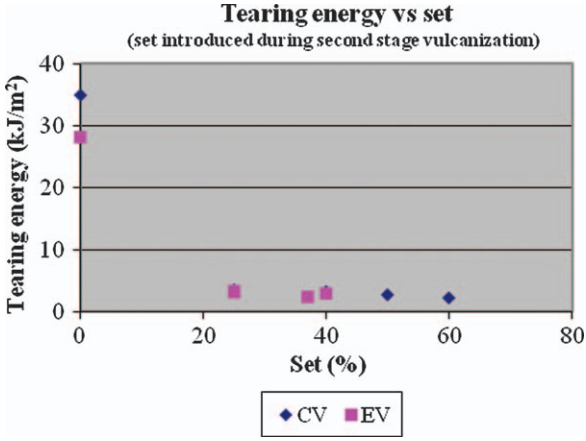

Figure 5.17 Effect of set introduced during second-stage vulcanization on tearing energy of vulcanized black-filled NR.
(Reproduced from ref. 24.)

dependence on the direction of orientation.[24] The results are shown in Figure 5.17, where tearing energy is plotted against set.

The amount of set introduced into the EV black-filled NR vulcanizate ranged from 23% to 40%. The tearing energy is very low, comparable with that of pre-stressed CV black-filled NR vulcanizate. Thus the results obtained from this work indicate that the tearing energy to propagate tear in the direction parallel to applied pre-stressing is low, provided that the amount of set is relatively high. The tearing energy is not dependent on the method of introducing the set, but relies on the magnitude of the set produced.

A similar effect is obtained if the vulcanized black-filled NR is subject to repeated (cyclic) stresses. In fact the effect of cyclic stresses is very detrimental to the durability of rubber products because under cyclic deformation the applied stress is much lower than a large stress applied in a single loading. In practice, rubber products such as tyres, conveyors and v-belts, and rubber mounts are subject to repeated stresses (dynamic deformation). Thus this approach is more relevant to practical situations than applying the stress in a single cycle. The parallel-sided test-piece measuring 75 mm × 10 mm × 0.5 mm was prepared by stamping a die on a flat 150 mm × 130 mm × 0.5 mm vulcanized black-filled NR sheet. This test-piece is pulled to a stress level of 12.4 MPa, and then relaxed to zero stress before pulling it again to the same stress level for the desired number of cycles. The apparent set was measured 1 min after completion of all the cycles. The apparent tension set was calculated using Equation (5.12):

$$\text{Apparent tension set} = (l_e - l_0)/l_0 \tag{5.12}$$

where l_e is the length of the gauge mark in the central region of the test-piece measured 1 min after completion of the cycle, and l_0 is the original gauge mark

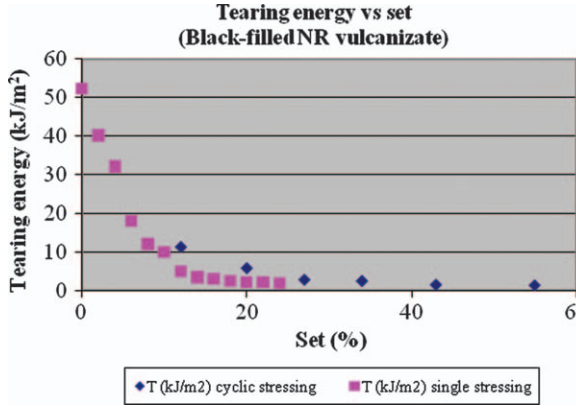

Figure 5.18 Effect of set on tearing energy of conventional cured black-filled NR vulcanizate at 24 °C and crosshead speed 100 mm/min. (Reproduced from ref. 24.)

before pre-stressing. A cut was introduced parallel to the direction of cyclic pre-stressing. The tear tests are done by separating the legs of the trouser test-piece using a tensile machine at test speeds ranging from 5 mm/min to 1000 mm/min. A temperature cabinet is used for measurements at temperatures outside 24 °C. The effect of set on tearing energy of black-filled NR in the direction of pre-stressing is shown in Figure 5.18. The tearing energy decreases progressively as the amount of set is increased. The decrease in the tearing energy is associated with the set, which introduces anisotropy as a consequence of the formation of a second network during pre-stressing.[20,22,23] According to Rivlin and Thomas, if the number of links per chain segment in the second network is much less than that in the first network, the tearing energy is much less for tearing parallel to the direction of pre-stressing than for tearing perpendicular to it.[22,23] The Rivlin and Thomas theory[22,23] is in line with Gent's theory[15] discussed in Section 5.5. Azemi[24] observed that below 10% set, knotty tearing still took place. However, when the set was more than 15%, steady or smooth tearing took place. Thus it appears that 15% set is adequate to provide the 40% less energy for the tear to split and propagate in the direction parallel to pre-stressing imposed to meet the anisotropic requirements as proposed by Gent *et al.*[15]

5.5.1.3 The Influence of Temperature and Rates on the Tearing Energy of Pre-Stressed Black-Filled Vulcanized NR

The strength and durability of rubber products are also affected by the rate and temperature at which they are subjected to different types of deformation. In this context, we are concerned with tearing of vulcanized black-filled NR after it is pre-stressed to 23 MPa in order to obtain high set. The samples were swollen, de-swollen and dried to constant weight before doing the tear measurements.

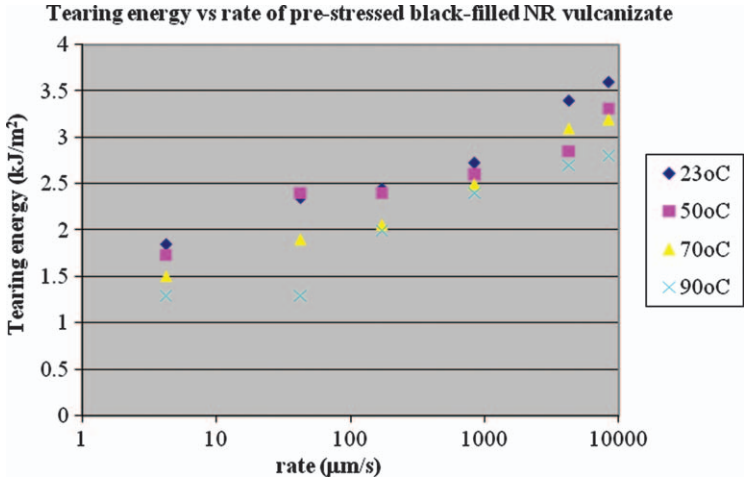

Figure 5.19 Tearing energy vs rate at four different temperatures. (Reproduced from ref. 24.)

Figure 5.19 shows the tearing energy versus rate at four different test temperatures. All test-pieces produced smooth tearing. The tearing energy increased with increasing tear rate at each test temperature. At any tear rate, the tearing energy also increased as the temperature was decreased. This is a clear manifestation of the viscoelastic behaviour of the rubber. At low temperatures and high tear rates, tearing energy increased because energy dissipations were higher than either at low tear rates or high temperatures. An attempt was made to construct a master curve of the data shown in Figure 5.19 using the WLF (William, Landel and Ferry) equation (Equation (5.13)):

$$\log a_\theta = -8.86(\theta - \theta_s)/(101.6 + \theta - \theta_s) \qquad (5.13)$$

where a_θ is the shift factor by which the rate must be multiplied to shift the points to a master curve, θ is the temperature of measurement, θ_s is a reference temperature. The two temperatures were expressed in degrees Kelvin. Figure 5.20 shows the tearing energy master curve obtained by plotting tearing energy against reduced rate. The former used a linear scale because the range of tearing energy values was small. In contrast, the latter used a log scale because of the wide range of tear rates covered. All the points lay satisfactorily around the master curve. The results show that tearing energy increased progressively with rate, implying that energy dissipation is an important factor in affecting the strength.

It should be noted that the tearing energy reduced rate relationship at the very low rate of 10^{-6} μm/s is obtained from constant load measurement.[24] This method of tear measurement is suitable only for non-strain-crystallizing rubbers that exhibit time-dependent tearing. Indeed, pre-stressed black-filled NR vulcanizate showed time-dependent tearing where the crack length increased with time when subject to constant load. This is more clear evidence indicating

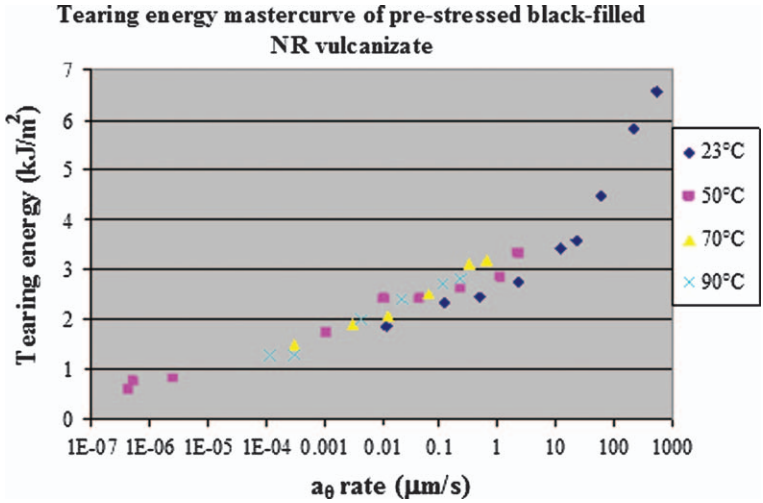

Figure 5.20 Tearing energy master curve of pre-stressed black-filled NR vulcanizate. (Reproduced from ref. 24.)

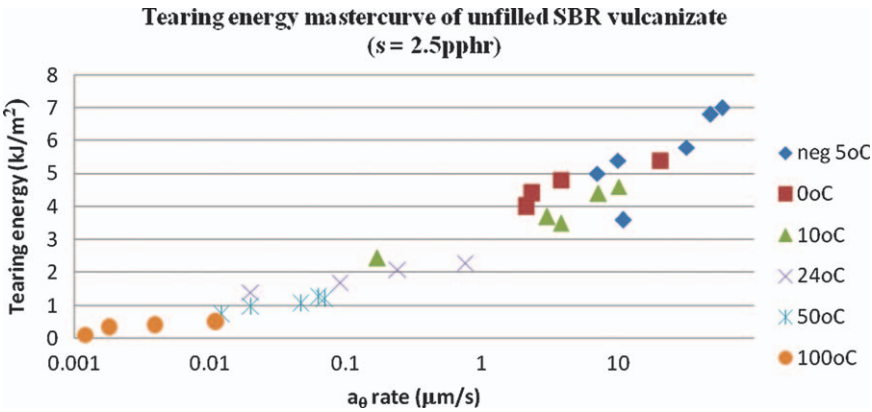

Figure 5.21 Tearing energy master curve of unfilled SBR with sulphur content of 2.5 pphr.
(Reproduced from ref. 24).

that the tearing process involved was controlled by the viscous behaviour of the material.

It would be useful to see whether pre-stressed black-filled NR vulcanizate shows similar behaviour to that of unfilled SBR vulcanizate. Figure 5.21 shows the tearing energy master curve for unfilled SBR where tearing energy is plotted against reduced rate. The result is very similar to that of pre-stressed black-filled NR. Comparing the two master curves, at reduced rates from 0.01 µm/s to 100 µm/s, the tearing energy of pre-stressed black-filled NR vulcanizate produced tearing energy ranging from 2.0 kJ/m^2 to 4.5 kJ/m^2,

while that of unfilled SBR gave tearing energy ranging from 1.0 kJ/m^2 to 7.0 kJ/m^2. At very low reduced rates, the tearing of pre-stressed black-filled NR gives marginally higher tearing energy than unfilled SBR. This effect might be associated with the presence of filler in pre-stressed NR. However, at moderate and high rates, the unfilled SBR vulcanizate gives significantly higher tearing energy than pre-stressed black-filled NR vulcanizate. This result indicates that, if black-filled vulcanized NR is subjected to a large stress, and then the stress is removed immediately, NR becomes a very weak material, weaker than unfilled non-strain-crystallizing SBR. The effect of pre-stressing on vulcanized black-filled NR is very detrimental to strength and durability of the rubber. At high rates unfilled SBR vulcanizate gives higher tearing energy than that of pre-stressed black-filled NR, which might be attributed to high energy dissipation associated with its glass transition temperature θ_g, SBR has higher θ_g than NR, and dissipates more energy than NR. It appears that the carbon black in the black-filled NR vulcanizate, after being pre-stressed, did not contribute much energy dissipation.

5.5.1.4 Tearing of Silica-Filled Vulcanized Rubber

It is common practice to add a small quantity (10–15 pphr) of silica to conventional carbon black-filled (35–45 pphr) tread compound formulations to reduce heat build-up while maintaining other properties such as tear resistance.[25] Evans *et al.*[26] found that incorporation of 9 pphr of silica in black-filled (42 pphr N330 HAF black) NR/BR (50 : 50) sidewall compound reduced the hysteresis (G'' at 30 °C) by about 27%. Silica has different surface activity to carbon black. It requires a coupling agent to enhance the rubber–filler interaction because silica is polar in nature and NR is non-polar. Azemi[27] investigated the effect of coupling agent on the tearing energy of silica (50 pphr)-filled NR, ENR 25 and ENR 50, respectively. The amount of coupling agent Si69 (bis[3-triethoxysilylpropyl] tetrasulfide), abbreviated as TESPT) is varied from 1 pphr to 6 pphr. Tear measurements are conducted by separating the legs of the trouser test-piece at various separation rates using a tensile machine. The tearing energy is computed by Equation (5.4). Figure 5.22 shows the influence of coupling agent on the tearing energy of silica-filled vulcanized NR. Without coupling agent the tearing energy of silica-filled vulcanized NR is relatively low, especially at low tear rates. In the absence of coupling agent there is no knotty tearing. Instead the crack propagates in a steady (smooth) manner and the tearing energy is strongly dependent on the tear rate. The tearing energy increased with increasing tear rate because the energy dissipation increases with rate as well. However, in the presence of coupling agent knotty tearing is produced. The tearing energy is about a factor of ten higher than that without coupling agent, in particular in regions of low tear rate. The results here indicate clearly that in silica-filled vulcanized NR, coupling agent is essential to induce the strength anisotropy necessary for the occurrence of knotty tearing. Without coupling agent the rubber–filler interaction is so weak that the stress is dissipated before it is high enough to cause orientation of filler structure. In the

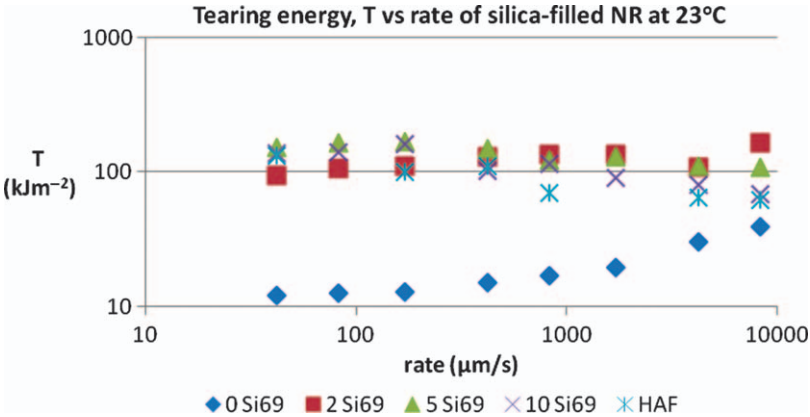

Figure 5.22 Influence of coupling agent (Si69, TESPT) on tearing energy of silica-filled vulcanized NR.

presence of coupling agent, the rubber–filler interaction is strong enough to support high stresses to cause orientation of filler structure and hence the strength anisotropy necessary for the occurrence of knotty tearing. Figure 5.22 indicates that 5 pphr appears to be the optimum quantity of coupling agent to produce high tearing energy over a whole range of tear rates.

At 10 pphr of coupling agent the tearing energy decreases markedly. This might be attributed to the immobilization caused by the strong physisorption of the rubber in the filler structure.[28] When this happens, the extent of strengthening structures developing around the tear tip regions might be small, because the high concentration of chemical linkages around the silica–rubber network might interfere with the molecular orientation and development of strengthening structures. This is in line with work by Azemi *et al.*,[29] who observed that the volume fraction of rubber in the swollen gel, v_r, increases as the quantity of coupling agent increases. This might be associated with the development of chemical linkages at the rubber–filler interface *via* coupling agent, which might restrict or slow down the diffusion of the solvent into the rubber matrix. Another possible explanation is as follows: Andrews and Walsh[30] put forward a hypothesis on the role of rubber–filler interaction in enhancing the tear resistance of the filled vulcanizate. They suggested that the adhesion between rubber and filler particles must be neither too strong nor too weak. If the adhesion between the rubber and filler is too weak, then breakdown occurs at low stresses. This might be the case for low tearing energy of silica-filled NR without coupling agent. If the adhesion is too strong, then breakdown occurs in the matrix near the particle and the latter remains attached to the rubber. Thus the importance of good adhesion is necessary only to a level where it could withstand stresses high enough to develop the necessary hysteresis to enhance strength, and also to obtain the orientation of the filler particles to induce the strength anisotropy necessary for the occurrence of knotty tearing.

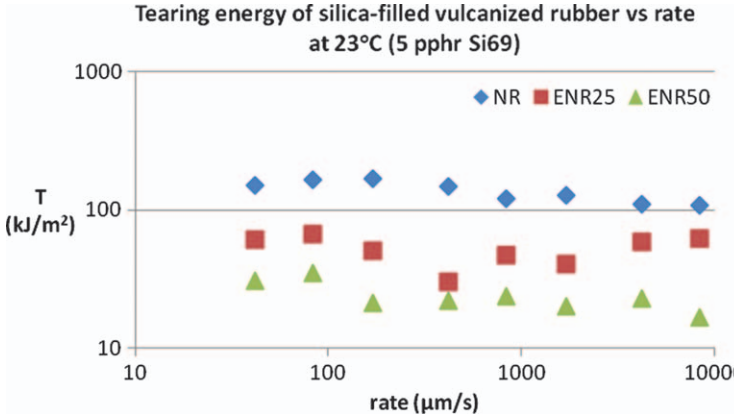

Figure 5.23 Comparison of tearing energy of silica-filled NR, ENR 25 and ENR 50 as a function of tear rate at 23 °C. All vulcanizates are filled with 50 pphr of precipitated silica (VN3) and 5 pphr coupling agent.

It is well recognized that silica filler interacts with polar rubber more readily than non-polar rubber. It is interesting to see whether this holds true for the case of epoxidized NR, which is considered to be polar because of the epoxy group. Figure 5.23 shows a comparison of the tearing energy–rate relationship for silica-filled vulcanized NR, ENR 25 and ENR 50. All the rubbers are filled with 50 pphr of precipitated silica (VN3) and 5 pphr of coupling agent.[27] Tearing measurements are done by pulling the legs of the trouser test-pieces at constant rate of separation by a tensile machine at 23 °C. Azemi[27] reported that all the rubbers produced knotty tearing. However, the difference in the magnitude of the tearing energy is influenced by the extent of strength anisotropy developed around the tear tip as reflected by the size of the knot diameter.

The reasons are not clearly understood but there are three possible factors. The first factor is the degree of strain crystallization. At any tear rate, the tearing energy increases in increasing order of the degree of strain crystallization, NR > ENR 25 > ENR 50. The second factor is the glass transition temperature of the rubber, which affects molecular mobility for the development of strength anisotropy. As discussed in Section 5.5.1.1 when the temperature of the tear test of black-filled ENR 50 was raised to 68 °C to match the molecular mobility of NR, black-filled vulcanized ENR 50 produced knotty tearing over a whole range of tear rates. The third factor is the strength of the chemical linkages at the rubber–filler interface *via* coupling agent. If the polarity of the rubber further enhances the rubber–filler interaction, in addition to the enhancement provided by the coupling agent, the net effect would be equivalent to increasing the 'crosslink concentration', giving a very tight network at the rubber–filler interface. Consequently, the molecular orientation and the orientation of filler structure are difficult to achieve for the development of strengthening structures necessary for the occurrence of knotty tearing.

5.6 Tearing of Vulcanized NR Latex Film

Latex products such as gloves and condoms are made from very thin latex film. The thickness is about 0.02 mm in the case of condoms, and about 0.1–0.4 mm in the case of surgical gloves. Such thin films are susceptible to tearing during stripping from the former. Thus the ability of NR latex film to produce knotty tearing as shown in Figure 5.4 is a highly desirable feature, to minimize rejects associated with tearing during stripping of the gloves from the former. The phenomenon of knotty tearing in NR latex film is not new and was reported by Kirchhof and Talalay[31,32] as far back as 1933. Figure 5.24 shows that unfilled peroxide pre-vulcanized NR latex film produces high tearing energy associated with knotty tearing[11] over the whole range of tear rates. The tearing energies of NR latex film are higher than sulfur-cured black-filled NR (SMR L). However, peroxide-cured unfilled NR prepared from SMR L does not produce knotty tearing but produces stick–slip tearing.[11] The reasons why unfilled NR latex produces knotty tearing, but not unfilled NR prepared from dry rubber, are not entirely clear. However, Azemi[11] suggested that the anisotropy in NR latex film necessary for the occurrence of knotty tearing might be attributed to one or a combination of these factors:

- ability of NR latex to strain crystallize
- hard protein domains which may act as reinforcing fillers
- high concentration of polysulfidic crosslinks
- presence of weak zones between the rubber particles inherited in the latex film

5.6.1 Effect of Filler Loading on Tearing Energy

Figure 5.25 is a histogram showing the variation of tearing energy as a function of filler loading base on reinforcing HAF black. All the latex films in this case

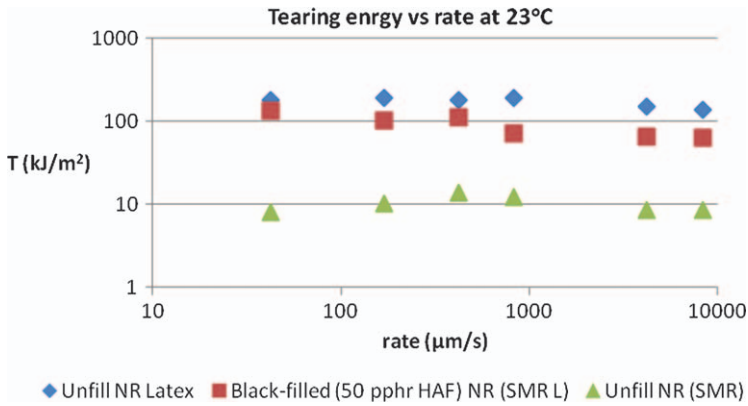

Figure 5.24 Tearing energy versus tear rate at 23 °C of vulcanized NR latex film(peroxide pre-vulcanized), black-filled NR (semi-EV sulfur system) and peroxide-cured unfilled NR (SMR L).
(Reproduced from ref. 11.)

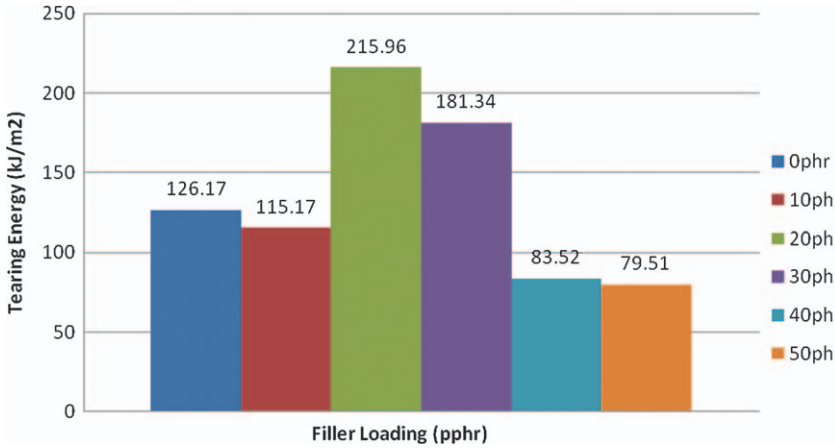

Figure 5.25 Histogram showing the influence of filler loading on tearing energy. (Reproduced from ref. 32.)

are post-vulcanized using sulfur as the crosslinking agent. The unfilled post-vulcanized NR latex film produced knotty tearing with high tearing of an average value 126.17 kJ m^{-2}. The tearing energy increased markedly to its optimum value of about 216 kJ m^{-2} at 20 pphr of HAF loading before decreasing to about 83.5 kJ m^{-2} and 79.5 kJ m^{-2} at 40 pphr and 50 pphr of loading, respectively. The magnitude of tearing energy is affected by the extent of tear deviation from the intended crack path as reflected by the size of the average knot diameter, which can be measured by means of an eye-piece lens scale. Azemi *et al.*[31] reported that at 20 pphr of HAF black, the average knot diameter was about 10 mm. In contrast, at 50 pphr filler loading, the diameter was about 8 mm. This indicates that the strengthening structure is greater at 20 pphr loading than at 50 pphr loading. This observation is very different from vulcanized black-filled NR based on SMR 5.

In the case of black-filled (HAF) vulcanizate from SMR 5, the optimum tearing energy occurred at 50 pphr loading.[19] This difference is associated with the efficiency of black particles being dispersed and distributed in the rubber particles during compounding. At low filler loading, the viscosity of the compounded latex was less viscous so that carbon black particles can diffuse easily into the rubber particles. As the filler loading is increased, the viscosity of the compounded latex increased, thus slowing down the diffusion rate into rubber particles. This latter condition favoured filler agglomeration. In the case of dry rubber, the shearing action during mixing facilitated incorporation of black particles into the rubber phase. The shearing action also helped to break the black particles agglomeration and dispersed them uniformly within the rubber phase.

5.6.2 Influence of Particle Size on Tearing Energy of Filled (at 30 pphr) NR Latex Film

The influence of particle size on tearing energy of filled NR latex film is shown in Figure 5.26, based on the data shown in Table 5.1.

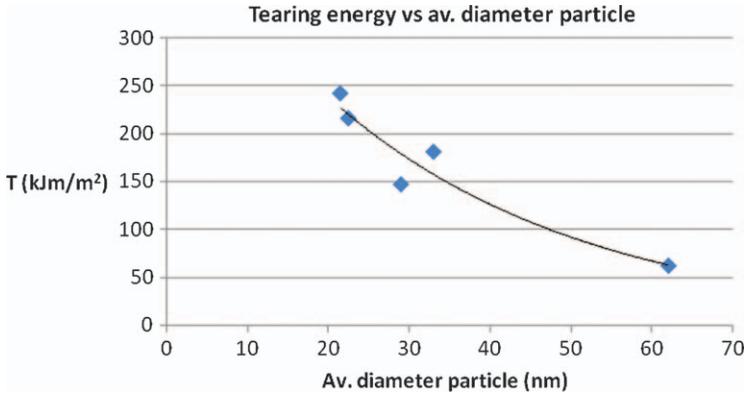

Figure 5.26 Tearing energy vs average particle size.

Table 5.1 Tearing energy of filled NR latex film at 30 phhr of different types of filler.

Filler	*Unfilled*	*SAF*	*ISAF*	*HAF*	*GPF*	*Silica*
Average particle size (nm)	–	20–25	25–33	30–36	50–73	18–25
T (kJ m^{-2})	126.2	216.3	146.8	181.3	62.3	241.9

Tearing energy decreases progressively as the average particle size increases. The result is consistent with the theoretical expectation where fine particulate filler provides higher reinforcement than large particulate fillers. This is because fine particles provide higher surface area than large particles. High surface area provides efficient interaction between filler and rubber chains because the rubber chains are able to wet the filler surface.

5.7 Crack Growth Resistance

One of the most important changes that can limit component durability is the growth of cracks in the material. Cracks may grow in any mode of deformation, and growth rates may be either slow and stable or catastrophic. Fracture mechanics has successfully been used to study crack growth behaviour of rubber vulcanizates. What is crack growth? Crack growth is an increment in crack length as a function of the number of repeated (cyclic) loading imposed on the rubber vulcanizate. It should not, however, be confused with time-dependent crack growth.[33] In the case of time-dependent crack growth, the crack grows as a function of time under a constant load. This type of crack growth behaviour is only observed with non-strain-crystallizing rubbers, but not with strain-crystallizing rubbers. With strain-crystallizing rubbers, tearing occurs catastrophically at or above their critical tearing energy, $\boldsymbol{T_c}$. The tear does not propagate at all below $\boldsymbol{T_c}$. However, under cyclic or repeated loading, the crack still grows even though the maximum tearing energy at each cycle is below $\boldsymbol{T_c}$.

The cyclic crack growth dc/dn is related to maximum tearing energy $\boldsymbol{T}$ attained during the cycle by Equation (5.14):

$$dc/dn = f(\boldsymbol{T}) \tag{5.14}$$

where c is crack length measured (referred to the unstrained dimension) at a particular number of cycles, n. Measurements of crack growth behaviour under repeated stressing using various test-pieces may be expressed as the crack growth per cycle (dc/dn) as a function of $\boldsymbol{T}$. The results for the crack growth under repeated stressing is independent of the test-piece geometry. Hence it is a true strength property of the material. The rate of crack growth per cycle can be determined from the gradient of the straight line obtained by plotting crack length versus number of cycles, as shown in Figure 5.27.

Azemi and Bijarimi[34,35] investigated the phenomenon of forking or deviation of the crack tip from the intended tear path in cyclic crack growth. The phenomenon of forking of the crack tip in cyclic crack growth is actually the same phenomenon as that of knotty tearing in conventional tear measurement. Like knotty tear, forking occurs in vulcanizates containing an appreciable amount of reinforcing fillers. When forking occurs at the crack tip, interpretation of the results is made difficult because the initially single crack tip branches into two or three new tips. In order to circumvent this problem, split tear test-pieces are preferred to other test-pieces.

Crack growth measurements using the split tear test-piece provide further experimental evidence that tearing energy is a measure of true crack growth

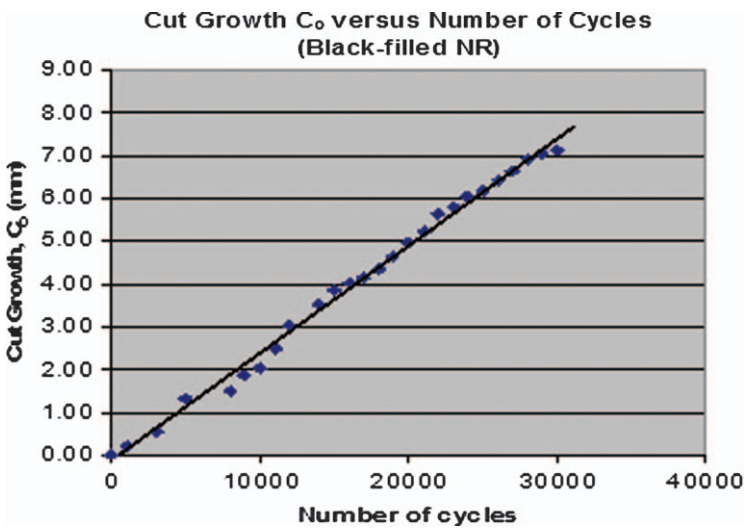

Figure 5.27 Crack length vs number of cycles.
(Reproduced from ref. 34.)

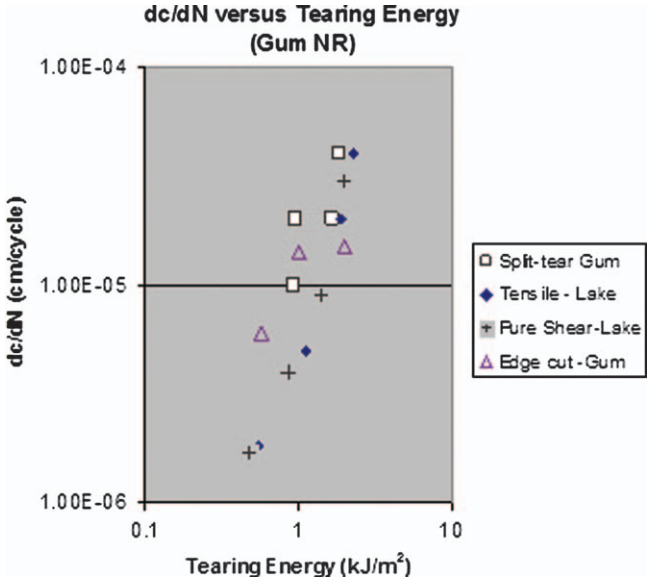

Figure 5.28 Comparison between split-tear and other test-piece, dc/dN vs tearing energy, T. The strain imposed on the split-tear test-pieces ranged from 25% to 60%.
(Reproduced from ref. 34.)

resistance independent of test-piece geometries. The split tear test-piece has a few advantages over other test-pieces, such as:

- It reduces the problems of forking as experienced with other common test-pieces such as parallel tensile strip, pure shear and trouser tear.
- It can relate crack-growth propagation rate to the anisotropy introduced at different strain levels.

The tearing energy of a split tear test-piece is computed using Equation (5.7), discussed in Section 5.2.

Figure 5.28 shows the crack growth characteristics of unfilled NR obtained from split tear test-pieces and compared with the results published by Lake *et al.*[36,37] The results are presented in the form of crack growth per cycle (dc/dN) versus tearing energy T using log–log scales. At a low tearing energy of about 0.9 kJ m^{-2}, the results obtained from split tear produced faster crack-growth rate (1×10^{-5} cm s^{-1}) than the result (4×10^{-6} cm s^{-1}) published by Lake. However, at tearing energies between 1.5 and 1.8 kJ m^{-2}, the crack-growth rates are comparable (dc/d$N = 4 \times 10^{-5}$ cm s^{-1} produced from split tear; and dc/d$N = 3.6 \times 10^{-5}$ cm s^{-1}, produced from pure shear (Lake)). In the case of an edge crack test-piece, close agreement was observed at a tearing energy of about 2 kJ m^{-2} where the current result matches the value produced by Lake. At tearing energy below 1.0 kJ m^{-2} the agreement was not that close.

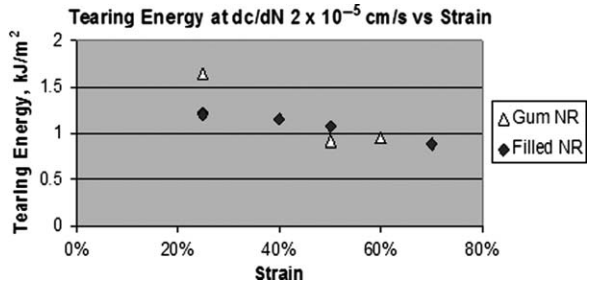

Figure 5.29 Effect of pre-straining on tearing energy at the same crack-growth rate, $dc/dN = 2 \times 10^{-5}$ cm/s.
(Reproduced from ref. 34.)

This disagreement may be attributed to the differences between the gum mix formulation used by Azemi *et al.*[34] and that used by Lake *et al.*[36] Nevertheless, the close agreement of crack-growth rate produced by split tear and those of pure shear and edge crack test-pieces at tearing energies of 1.5–1.8 kJ m^{-2} provides more experimental evidence to show that crack-growth rate is independent of the test-piece geometry when results are expressed in terms of tearing energy. Thus the split tear test-piece can be used both in conventional tear as well as in cyclic crack growth measurement.

The effect of anisotropy on the tearing energy measured at about the same crack growth rate ($dc/dN = 2 \times 10^{-5}$ cm s^{-1}) is shown in Figure 5.29, where tearing energy is plotted against applied strain for unfilled and black-filled vulcanizates. The tearing energy decreases progressively as the applied strain increases. The tearing energy decreases by about 30% as the applied strain is increased from 20% to about 70%. This indicates that as the amount of anisotropy increases with the applied strain, the energy to propagate tearing in the direction of the applied strain decreases. Just like the phenomenon of knotty tear in conventional tear tests using a trouser test-piece, the problem of forking of black-filled vulcanizates in cyclic crack growth measurements observed in conventional test-pieces is also associated with the splitting of the crack tip in the direction of the applied strain because the energy to propagate crack in this direction is lower than the intended path. At high strain levels, the tearing energy of black-filled vulcanizates is marginally higher than that of the unfilled vulcanizates.

The results indicate clearly that the effect of pre-straining is to weaken the vulcanized NR.

5.8 Environmental Factors Affecting Strength and Durability of Rubber

Apart from mechanical deformation imposed on the rubber, the strength and durability of the vulcanized rubber is affected by other environmental factors discussed in the subsequent sections.

5.8.1 Oxidation of Rubber

The service life and durability of rubber products are influenced by their resistance to outdoor exposures such as oxygen, ozone, UV light and heat. Corrosion of rubbers is associated with an ageing process known as degradation. The resistance of rubber to degradation depends on the chemical structure, the vulcanization system, and the protective agents used in the compound formulations. All unsaturated rubbers are subject to degradation due to the attack of heat, light (UV), oxygen, ozone, *etc*. The higher the amount of unsaturation the more it is susceptible to degradation. It is well established now that ageing of rubbers at elevated temperatures in air causes chain scission and/or crosslinking.[38,39] Chain scission will soften the vulcanizates and reduce the physical properties of rubber and rubber vulcanizates, whereas crosslinking will tend to harden and consequently the vulcanizate becomes brittle. The oxidation of rubber vulcanizate is technologically important because the absorption of only a small amount of oxygen (1%) by rubber vulcanizate results in a considerable change in the physical properties.

In the case of sulfur-vulcanized NR the oxidation reaction is much more complex than in raw NR because the various different types of crosslink (*e.g*. polysulfidic, disulfidic, monosulfidic, cyclic sulfides, conjugated dienes and trienes, *etc*.) present in the network structure may affect oxidation in some way or another.[38,39] Most types of sulfur vulcanizates initially harden on ageing before degradation occurs. This hardening is associated with the crosslinking associated with oxidative reactions of sulfur species in the network taking place before chain scissions take place.

5.8.2 Heat Ageing

Almost all technical specifications of elastomeric products require them to pass a heat ageing test. The use of ageing tests is extremely important in assessing the service life of elastomeric products because the properties of vulcanizates could change during service. The basic principle of the test is to expose rubber testpieces to air at an elevated temperature (70 or 100 °C) for a specified period (7 or 14 days or longer). This so-called accelerated ageing test causes deterioration of rubber in air due to the combined effects of oxidative and thermal ageing. The tensile properties, set and hardness are measured on these samples before and after ageing. If minor changes in these properties result, a long service life may be expected; if appreciable changes occur, service life may be short. However, it must be stressed here that the accelerated ageing test is a useful quality control and specification test. There are significant difficulties in predicting service life from an accelerated ageing test. Use of test temperatures much above the anticipated service temperature is not advisable because the correlation between the results of such tests and service performance becomes increasingly tenuous.

5.8.3 Ozone Cracking of Rubber

Apart from oxygen, all unsaturated elastomers are also susceptible to ozone attack, although ozone concentration in the outdoor atmosphere at ground level is

only about 1 pphm (parts per hundred million of air by volume).[40–42] However, this can be significant because the reaction of ozone with the double bond is extremely fast and causes cracking of strained rubber. The cracks appear slowly at right angles to the direction of the strain applied, which grow slowly and consequently lead to a break in the vulcanizate. Ozone, being very reactive, attacks the double bonds of the rubber and produces ozonide, which cleaves to produce zwitterions[43] as shown in Scheme 5.1. The zwitterions are unstable and will break

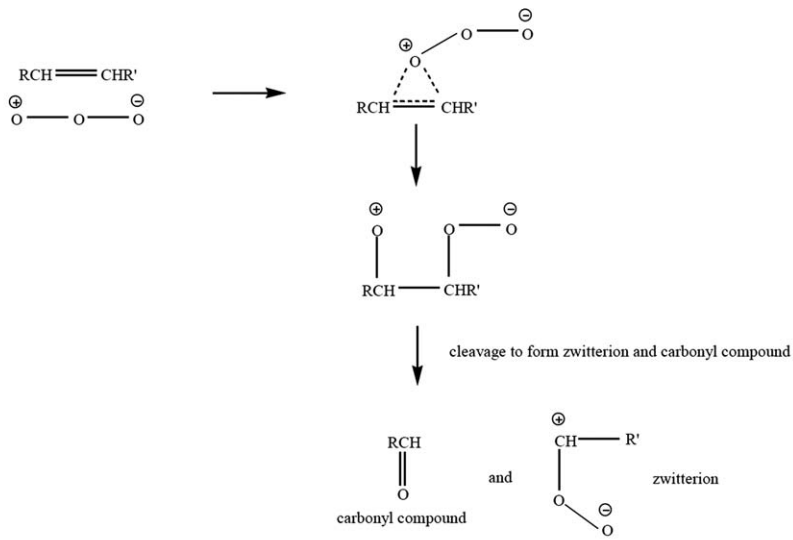

The zwitterion may react with

(a) other zwitterion to give diperoxide compound

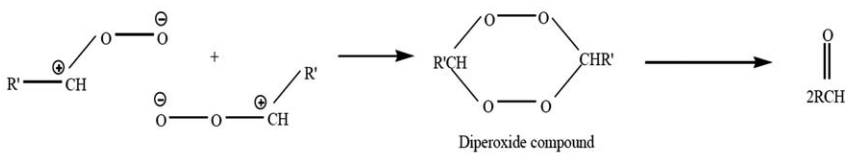

(b) or with carbonyl compound to give ozonide

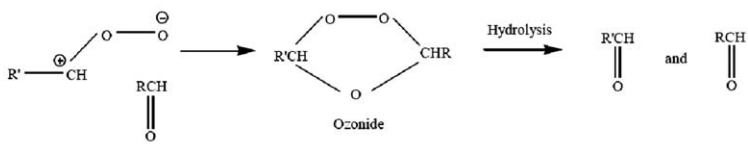

Reaction scheme 30. 1 mechanism of ozone attack on olefins

Scheme 5.1

down to form other zwitterions. These zwitterions may react with other zwitterions to produce diperoxide compounds, or react with carbonyl compounds to produce ozonide. In both cases, the ultimate result is chain scission.

However, ozone cracking occurs only in elastomers subject to tensile stresses. Elastomeric components used in compression will crack only in the regions of the surface where tensile stresses are induced. These cracks are unable to penetrate very far because they soon encounter compressive rather than tensile stresses. Thus ozone cracking is not a serious problem for large elastomeric components such as rubber bearings which are used in compression. Nevertheless, ozone cracks are unsightly and may initiate fatigue crack growth, which ultimately leads to mechanical failure. In view of this deleterious effect, it is necessary to carry out tests on ozone resistance. The test involves exposing the stretched test-pieces (20% strain) in an ozone-rich atmosphere at a fixed temperature (23 or 40 °C) and inspecting the surfaces for cracks with the aid of a magnifying glass at intervals of time. If cracks are not observed after completion of the test, the vulcanizate is said to have good resistance to ozone cracking.

5.8.4 Effect of Water Absorption on Physical Properties of Vulcanized Elastomers

Elastomers find widespread uses in marine and offshore engineering applications. The application of elastomers in water management is attributed to its high impermeability to water. Rubber sheet is used to line reservoirs and ponds, while rubber inflatables are used as water dams. Rubber dock fenders rely on the energy absorption capacity of the rubber. Inevitably, the rubber will absorb a quantity of water because these rubber products spend a considerable time under water. It is therefore a great concern as to whether the absorption of water would impair the strength properties of the rubber.

The true solubility of water in rubber is very low.[44] Nonetheless, relatively large amounts of water can be absorbed during prolonged immersion, as shown in Figure 5.30. The diffusion of water in elastomers is not straightforward, but complicated by the presence of hydrophilic materials. In the case of NR it is mainly proteinaceous. When water diffuses into the rubber, the water-soluble hydrophilic materials dissolve, forming droplets of solution within the rubber. An osmotic pressure gradient would exist between watery domains in the rubber and that of the external solution immersing the rubber. This results in more water diffusing into the internal solution droplet. Water absorption reaches equilibrium when the elastic stresses acting on the droplets balance the osmotic pressure difference. Muniandy and Thomas[44] proposed a mathematical model for water absorption to derive equations for the equilibrium water uptake and to evaluate the kinetics of water absorption and desorption. From the model, they calculated the equilibrium water uptake and the apparent diffusion coefficient. They found very good agreement between theory and experimental results.

Later, Lake[45] investigated the kinetics of water (tap water) absorption in elastomers and their effects on properties. He reported that when the absorption

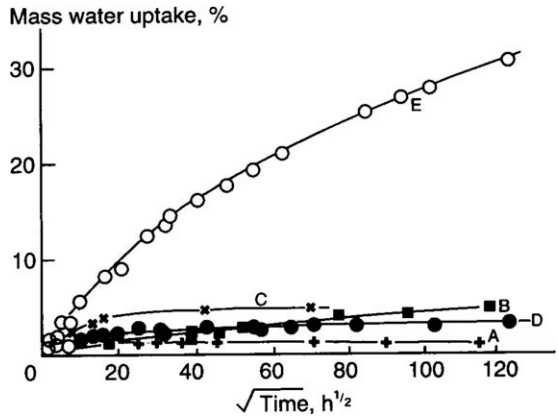

Figure 5.30 Corrected mass uptake measurements for engineering rubbers in sea water at 23 °C. A, deproteinized NR; B, lead oxide cured polychloroprene; C, nitrile rubber; D, conventional NR; E, conventional polychloroprene.
(Reproduced from ref. 44.)

was large (50% or more), the rubber test-piece degraded. Severe degradation leads to porosity of the surface layer, and when pressed, water exudes out. However, at low levels of absorption, Lake observed the formation of droplets similar to the blisters that occur in plastics or under protective coatings consistent with an osmotic diffusion mechanism. In salt water, water absorption reached a steady state at much lower levels than in fresh water, again consistent with an osmotic pressure mechanism. Thus sea water is less damaging than fresh water and may not have any serious consequences for many elastomers. This latter point is consistent with the findings of Ab-Malek and Stevenson,[46] who evaluated the physical properties of a rubber tyre recovered from sea water at a depth of 80 feet, as shown in Figure 5.31. They found that rubber tyres absorbed about 5% of sea water after 42 years of immersion. They found no evidence of microbiological attack. What is more interesting is that the physical properties of the tyre rubber were within normal specifications for new rubber of the same type. They even suggested storing elastomers in deep sea water in view of its inert nature. Indeed elastomers are a very suitable material to coat metal surfaces against corrosion in deep sea water. The photograph in Figure 5.31 shows clear evidence that the steel cords making up the bead of the tyre are corrosion-free after 42-year immersion in sea water.

5.8.5 Effect of Heat Ageing, Oil and Water on Rubber-to-Metal Bonding

Nor Ashikin and Azemi[47] evaluated the performance of bond strength in rubber-to-metal bonded products. The main focus is on observing the effect of heat ageing and diffusion of liquids or oils on bond strength.

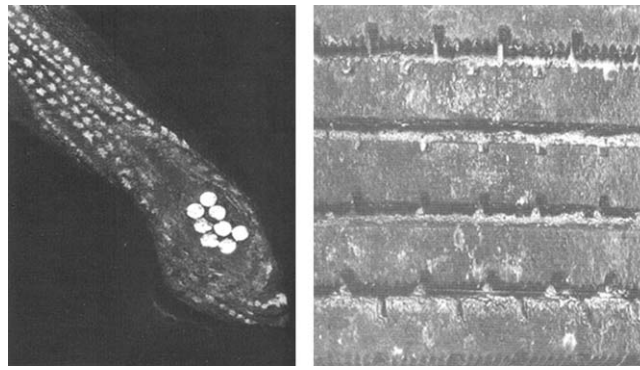

Figure 5.31 Natural rubber tyre after 40 years' exposure to sea water. (Courtesy of the publisher: Tun Abdul Razak Research Centre, Brickendonbury, Hertford, England.)
(Reproduced from ref. 46.)

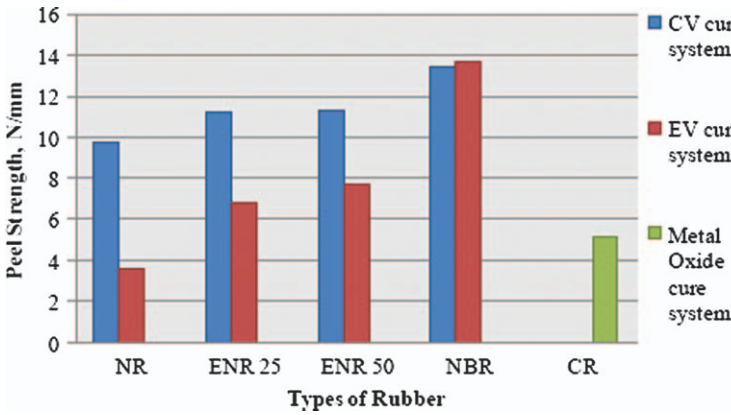

Figure 5.32 Effects of different types of cure system on peel strength for unaged samples.

5.8.5.1 Heat Ageing Tests

Rubber-to-metal bonded test-pieces are exposed to air at atmospheric pressure in either the usual single chamber type of oven or a multi-cell oven. The samples were aged for 7 days at 100 °C and 14 days at 70 °C, respectively. Figure 5.32 shows the peel strength of unaged samples for rubbers of different polarity such as NR, ENR 25, ENR 50, NBR and CR. They were vulcanized with different cure systems so that the effect of polarity and cure system on the peel strength before and after ageing could be evaluated. The result shows that the conventional sulfur system (CV) gives a higher peel strength value than the efficient sulfur system (EV) and metal oxide cure system. During the vulcanization process, it is believed that sulfur reacts with the bonding agent to form chemical

links to the metal surface. The results also show that peel strength increases in increasing order of polarity of the rubber for a particular cure system, thus NBR > ENR 50 > ENR 25 > NR. It is well established that high polar rubber adheres more effectively to the metal surface than non-polar rubber because metals are polar in nature.

Figure 5.33 shows the effects of heat ageing for 7 days at 100 °C on the peel strength of rubber vulcanizates. Surprisingly the results show that the CV cure system on this ageing condition gives higher peel strength than the EV cure system. It is well established that the EV cure system gives monosulfidic crosslinks that are more thermally stable than polysufidic crosslinks produced by the CV system. However, bond formation at the rubber–metal interface *via* bonding agents is stronger in the CV system than the EV system because of the presence of more sulfur atoms forming chemical linkages at the metal surface than that of the EV system. Consequently the CV cure system produces cohesive failure as shown in Figure 5.34. This latter point may outweigh the

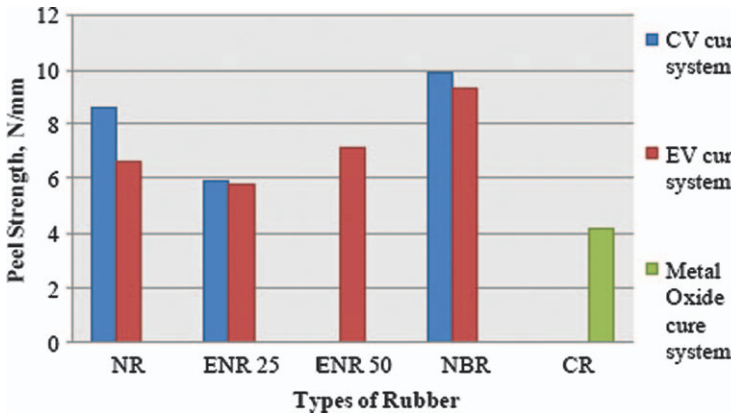

Figure 5.33 Effects of heat ageing condition (7 days/100 °C) on peel strength.

Figure 5.34 Photographs of samples which failed by cohesive failure based on CV system.

thermal stability of the EV system. In the case of the EV system, it produces R–C failure where the bond fails at the rubber–cement interface, as shown in Figure 5.35. The effect of polarity of the rubber still persisted even after ageing, where the peel strength increases in the order of polarity of the rubber.

Figure 5.36 shows the effects of ageing for 14 days at 70 °C on peel strength of rubber vulcanizates. The CV cure system shows a higher peel strength than the EV cure system for each type of rubber, except polychloroprene rubber (CR). It is rather surprising that the bond strength is higher after heat ageing than that of unaged samples. It might be possible that further crosslinking at the rubber–metal interface might have occurred during this heat ageing. It can be said here that the cure system is the predominant factor affecting bond strength. Even after heat ageing, the bond strength is not much affected, although the EV cure system is known to produce better heat ageing and thermal stability but it turns out that the CV cure system outweighs the heat stability of the EV system. The results provide a clear indication that the CV system, which produces predominantly polysulfidic types of crosslink, gives higher strength and durability than the EV sulfur system, which gives a predominantly

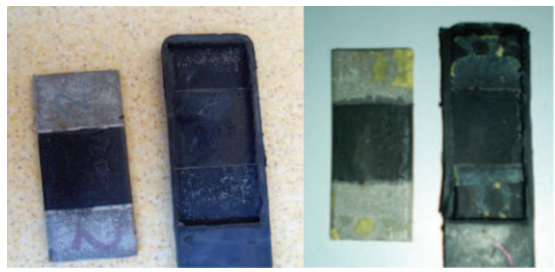

Figure 5.35 Photographs of samples which failed by R–C failure based on EV system.

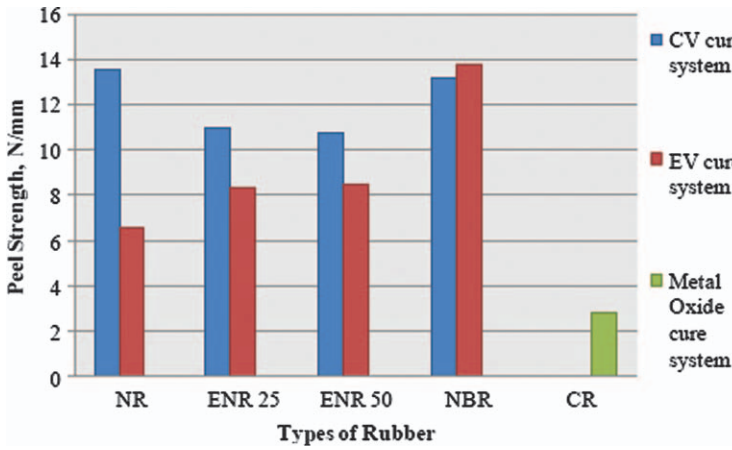

Figure 5.36 Effects of heat ageing condition (14 days/70 °C) on peel strength.

monosulfidic type of crosslink. The role of sulfur in enhancing the bond strength at the rubber–metal interface is very clear when CR gives very low peel strength, because sulfur is less effective at vulcanizing CR because of the chlorine atom which withdraws electrons at the double bonds. Zinc oxide and related metallic oxides are effective crosslinking agents for CR.

5.8.5.2 *Effect of Water Immersion on Bond Strength*

The test consists of immersing rubber-to-metal bonded test-pieces in distilled water and salt water for 30 days at ambient temperature. The changes in weight before and after the test are noted.

Figure 5.37 shows the effects of the water immersion test (distilled and salt water) on peel strength of NR and CR rubbers for 30 days at ambient temperature. The result is then compared with the dry sample of NR and CR rubbers. Within the 30-day period there is no sign of deterioration of the peel strength. The amount of water absorbed is relatively negligible and for this reason the peel strength is relatively unaffected. This is consistent with the findings of Ab-Malek *et al.*,[46] who reported that the rubber tyre had absorbed about 5% of sea water after 42 years of immersion.

5.8.5.3 *Effects of Oil Immersion Condition on Peel Strength*

Figure 5.38 shows the effects of oil immersion on peel strength. All of the samples were immersed in engine oil for 7 days at ambient temperature. This test was done only for the CV cure system. The histogram shows that as the polarity increases, the peel strength increases for both dry and oil immersion

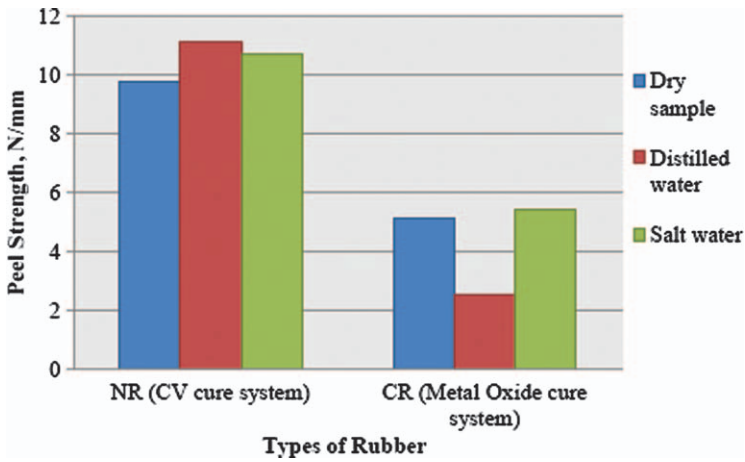

Figure 5.37 Effects of water immersion test of rubber vulcanizates on peel strength for 30 days at ambient temperature.

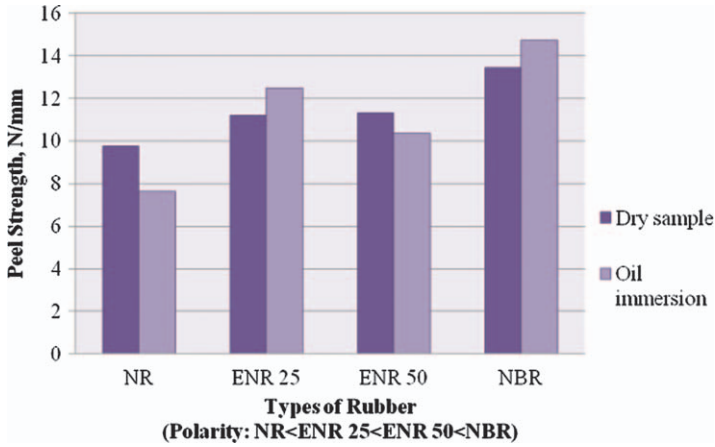

Figure 5.38 Effects of oil immersion test of rubber vulcanizates on peel strength for 7 days at ambient temperature.

samples. Greater polarity gives higher bond strength because metal is polar and it provides better interaction with the polar rubber.

The vulcanization system and polarity of the rubber have a great influence on the strength and durability of rubber-to-metal bonded products. The CV sulfur system is the preferred system to give high peel strength and durability. Rubbers with high polarity are preferred to rubbers with low polarity for the enhancement of peel strength and durability, especially when in contact with hydrocarbon oil.

Acknowledgements

The author is very grateful to Professor Dr Sabu Thomas who has given him the opportunity and trust to write a book chapter. The author would like to thank Professor Dr Ri Hanum Yahaya Subban, the Dean of the Faculty of Applied Science of the Universiti Teknologi MARA, Shah Alam Malaysia for her encouragement and permission to publish some of the experimental data on some of the current research work conducted by the author and the students under the supervision of the author.

It gives me great pleasure to thank the Publication Divisions of the Malaysian Rubber Board (MRB) (formerly Rubber Research Institute of Malaysia), and the Tun Abdul Razak Research Centre (TARRC) for permission to reproduce data and figures from their respective Publication Divisions. The author would like to express his sincere appreciation and thanks to Cambridge University Press for giving permission to reproduce figures and data from their publications.

Last but not least, to Miss Siti Aisyah Jarkasi and Miss Rasyiqah Abdul Rahim for their kind assistance in formatting the chapter.

References

1. A. A. Griffith, *Philos. Trans. R. Soc., A*, 1920, **A221**, 163.
2. R. S. Rivlin and A. G. Thomas, *J. Polym. Sci.*, 1953, **10**, 291.
3. A. G. Thomas, *J. Appl. Polym. Sci.*, 1960, **3**, 168.
4. H. W. Greensmith and A. G. Thomas, *J. Polym. Sci.*, 1955, **18**, 189.
5. W. F. Busse, *Ind. Eng. Chem.*, 1934, **26**, 1194.
6. H. W. Greensmith, *J. Polym. Sci.*, 1956, **21**, 175.
7. A. I. Medalia, *Rubber Division Meeting*, ACS: New York, NY, 1986, pp. 1–36.
8. A. Samsuri and A. G. Thomas, in *Proceedings International Rubber Technology Conference*, Rubber Research Institute of Malaysia Publication, Kuala Lumpur, 1988, pp. 147–165.
9. A. N. Gent, in *Proceedings of the International Rubber Conference & Exhibition 2008*, KLCC, Kuala Lumpur, 20–23 October 2008, p. 3.
10. G. R. Hamed and B. H. Park, *Rubber Chem. Technol.*, 1999, **72**, 946.
11. A. Samsuri, in *Proceedings of the International Rubber Technology Conference 1993*, Rubber Research Institute of Malaysia Publication, Kuala Lumpur, 1993, p. 137.
12. H. W. Greensmith, L. Mullins and A. G. Thomas, *Trans. Soc. Rheol.*, 1960, **4**, 179.
13. K. Sakulkaew, A. G. Thomas and J. J. C. Busfield, *J. Sci. Direct*, 2011, **30**, 163.
14. A. G. Thomas, *J. Polym. Sci.*, 1955, **18**, 177.
15. A. N. Gent, M. Razzaghi-Kashani and G. R. Hamed, *Rubber Chem. Technol.*, 2003, **76**, 122.
16. C. L. S. Baker, I. R. Gelling and A. Samsuri, *J. Nat. Rubber Res.*, 1986, **1**, 135.
17. C. K. L. Davies, S. V. Wolfe, I. R. Gelling and A. G. Thomas, *Polymer*, 1983, **24**, 107.
18. M. S. Green and A. V. Tobolsky, *J. Chem. Phys.*, 1946, **14**, 80.
19. A. Samsuri, *Tear Strength of Filled Rubbers*, PhD thesis, The Polytechnic of North London, London, 1989.
20. A. G. Thomas, *J. Polym. Sci.*, 1974, **48**, 145.
21. P. S. Brown, M. Porter and A. G. Thomas, in *Proceedings of the International Rubber Technology Conference*, Rubber Research Institute of Malaysia, Kuala Lumpur, 1985, pp. 20–46.
22. R. S. Rivlin and A. G. Thomas, *J. Polym. Sci., Part B: Polym. Phys*, 1983, **21**, 1807.
23. R. S. Rivlin and A. G. Thomas, *Eng. Fract. Mech.*, 1983, **18**, 389.
24. A. Samsuri, *J. Nat. Rubber Res.*, 2010, **11**, 44.
25. L. White, *European Rubber Journal*, 1999, **181**(6), pp. 30–33.
26. L. R. Evans, J. C. Hope and W. H. Waddle, in Proceedings of the 145th Meeting of the Rubber Division, American Chemical Society, Chicago, Illinois, 21 April 1994, American Chemical Society, Chicago, IL, 1994, pp. 1–20.

27. A. Samsuri, *Tearing of Silica-Filled Vulcanizate, PED Internal Report No. 72*, Rubber Research Institute of Malaysia, Kuala Lumpur, 1991.
28. H. D. Luginsland, J. Froelich and A. Wehmeier, *J. ACS Rubber Division*, 2001, 819.
29. A. Samsuri and C. M. S. Said, *J. Rubber Res.*, 2013, **16**(2), 101–117.
30. E. H. Andrews and A. Walsh, *J. Polym. Sci.*, 1958, **33**, 39.
31. W. F. Busse, *Industrial and Engineering Chemistry*, 1934, **26**, 1194–1199.
32. A. Samsuri, S. Sudin and N. Y. Saleh, *in PRIM Golden Jubilee Int. Polymer Conf. GJIPC*, Kuala Lumpur, 2010, pp. 1–23.
33. J. J. Busfield, K. Tsunoda, C. K. L. Davies and A. G. Thomas, *Rubber Chem. Technol.*, 2002, **75**, 643.
34. A. Samsuri and M. B. M. Piah, *J. Rubber. Res.*, 2004, **7**, 115.
35. M. Bijarimi, A. Samsuri and H. Zulkafli, in *Advances in Material Science, Polymer Processing and Characterization*, ed. S. Thomas, D. Ponnamma, A. K. Zachariah, Apple Academic Press, Toronto, New Jersey, 2012, Vol. 1, pp. 67–71.
36. G. J. Lake and A. G. Thomas, *Strength Properties of Rubber*, Natural Rubber Science and Technology, Oxford University Press, Oxford, 1988.
37. G. J. Lake, A. Samsuri, S. C. Teo and J. Vaja, *Polymer*, 1991, **32**, 2963.
38. J. L. Bolland and H. Hughes, *J. Chem. Soc.*, 1949, 492.
39. D. Barnard and P. M. Lewis, in *Natural Rubber Science and Technology*, ed. A. D. Roberts, Oxford University Press, Oxford, 1988, pp. 621–673.
40. M. Braden and A. N. Gent, *J. Appl. Polym. Sci.*, 1960, **3**, 90.
41. G. J. Lake and A. G. Thomas, *International Rubber Confernce*, Maclarens, London, 1967, 103.
42. G. J. Lake and P. G. Mente, *J. Nat. Rubber Res.*, 1992, **7**, 1.
43. R. W. Keller, *Rubber Chem. Technol.*, 1985, **58**, 637.
44. K. Muniandy, E. Southern and A. G. Thomas, in *Natural Rubber Science and Technology*, ed. A. D. Roberts, Oxford University Press, Oxford, 1988, pp. 820–851.
45. G. J. Lake, in *Conf. on Polymers in a Marine Environment*, London, 31 Oct.–2 Nov.; London, 1984; pp. 157–160.
46. K. Ab-Malek and A. Stevenson, *J. Mater. Sci.*, 1986, **21**, 147.
47. S. N. Jamal and A. Samsuri, *Rubber to Metal Bonding: The Effect of Oil Immersion, Heat Aging and Water Absorption on Peel Strength, Final Year Project Report FSG 660*, UPENA Publication, Kuala Lumpur, 2010, pp. 1–50.

CHAPTER 6

Carbon Black Reinforcement in Natural Rubber in Micro and Nano Length

GORDANA MARKOVIĆ,*[a] MILENA MARINOVIĆ-CINCOVIĆ,[b] VOJISLAV JOVANOVIĆ,[c] SUZANA SAMARŽIJA-JOVANOVIĆ[c] AND JAROSLAVA BUDINSKI-SIMENDIĆ[d]

[a] Tigar, Nikole Pašića 213, 18300 Pirot, Serbia; [b] University of Belgrade, Vinča Institute of Nuclear Science, Belgrade, Serbia; [c] Faculty of Natural Science and Mathematics, University of Priština, Kosovska Mitrovica, Serbia; [d] University of Novi Sad, Faculty of Technology, Novi Sad, Serbia
*Email: gordana1markovic@gmail.com

6.1 Introduction

Even though the expressions 'nanomaterials' or 'nanocomposites' are recent (and very successful), these industrial materials have existed for at least a century and apparently always existed in nature (in minerals and vegetables). These small particles range in size from a few to several tens of nanometres and are called quasi zero-dimensional mesoscopic systems, quantum dots, quantized or Q particles, *etc.*[1] According to Jordan *et al.*,[2] nano-sized inclusions are defined as those that have at least one dimension in the range 1–100 nm. In materials research, the development of polymer nanocomposites is rapidly emerging as a multidisciplinary research activity whose results could broaden the applications of polymers to the great benefit of many different industries.

RSC Polymer Chemistry Series No. 8
Natural Rubber Materials, Volume 2: Composites and Nanocomposites
Edited by Sabu Thomas, Hanna J. Maria, Jithin Joy, Chin Han Chan and Laly A. Pothen

Published by the Royal Society of Chemistry, www.rsc.org

Polymer nanocomposites (PNCs) are polymers (thermoplastics, thermosets or elastomers) that have been reinforced with small quantities (less than 5% by weight) of nano-sized particles having high aspect ratios ($L/h > 300$).[3] In contrast to conventional composites, where the reinforcement is in the order of microns, PNCs are exemplified by discrete constituents in the order of a few nanometres. PNCs contain substantially less filler (1–5 vol%), thus enabling greater retention of the inherent processibility.[4] According to Wagner and Vaia, development of PNCs, as with any multicomponent material, must simultaneously balance four interdependent areas: constituent selection, cost-effective processing, fabrication and performance.[4] For PNCs, a complete understanding of these areas and their interdependencies is still in its infancy, and ultimately many perspectives will develop, dictated by the final application of the specific PNC. To convey the origin and interrelation of these distinguishing characteristics, Figure 6.1 compares the dominant morphological scale of a classic filled polymer containing 1 μm×25 μm fibres in an amorphous matrix to that of a nano-filled system at the same volume fraction of filler, but containing 1 nm×25 nm fibres.

The internal 'graphitic-like' organization of carbon black (CB) particles has been progressively elucidated and we proposed[5] a model illustrated in Figure 6.5, which resulted from the systematic examination at the 'nanoscale' by STM microscope. This model shows 'scales' of carbon graphitic organization and it points out the existence of 'active sites' at the edges. Our recent work reveals the existence of a 'fullerene-like' structure at the surface of the 'particles'

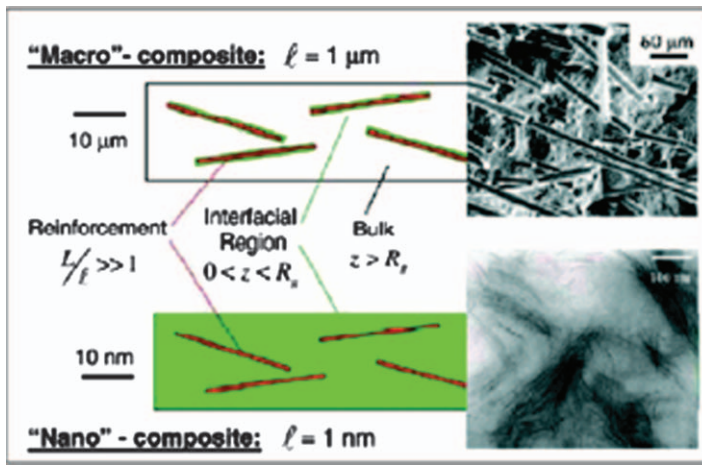

Figure 6.1 Schematic comparison of a macrocomposite containing 1 μm×25 μm fibres in an amorphous matrix to that of a nanocomposite at the same volume fraction of filler, but containing 1 nm×25 nm fibres. Constituents in any composite: the matrix (white), the reinforcement (fibre, red) and the so-called interfacial region (green). Scanning electron micrograph shows E-glass reinforced polyolefin (15 mm) and transmission electron micrograph shows montmorillanite-epoxy nanocomposite (1 nm thick layers).[4]

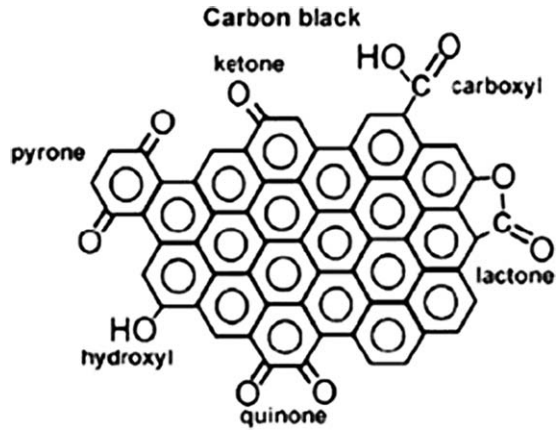

Figure 6.2 Bonded group of carbon black surface.

(Figure 6.2), and the formation of fullerenes in flames was confirmed recently.[6] On the other hand, the roughness of the carbon particles, as measured by STM microscopy, could also be related to the compound properties.

The influence of the filler surface and in the case of CB the proven presence of an active site, with a surface energy directly proportional to the specific surface of the filler,[7] tends to show also the importance of the interactions between the surface and the elastomeric chains. However, theories of reinforcement have been diverging and recall the main proposals and in the last years there is a strong trend to accept the Payne[8] proposals the carbon surface–elastomer interaction being a part of a total phenomenon, at the nanoscale.

6.2 Nanocomposites

There are three main material constituents in any composite: the matrix, the reinforcement (fibre), and the so-called interfacial region. The interfacial region is responsible for communication between the matrix and filler and is conventionally ascribed properties different from the bulk matrix because of its proximity to the surface of the filler.

In almost every case, nanoparticles are added to the matrix or matrix precursors as 1–100 μm powders, containing an association of nanoparticles. The overwhelming majority of the nanoparticles summarized in Figure 6.3 can be grouped into two categories based on this association: low-dimensional crystallites and aggregates.

Layered silicates, single-wall nanotubes (SWNTs), and other extreme aspect ratio, very thin (0.5–2 nm) nanoparticles, exhibit translational symmetry within the powder.[4] Polymer/layered nanocomposites in general can be classified into three different types, namely: intercalated nanocomposites, flocculated nanocomposites and exfoliated nanocomposites (see Figure 6.4).[9]

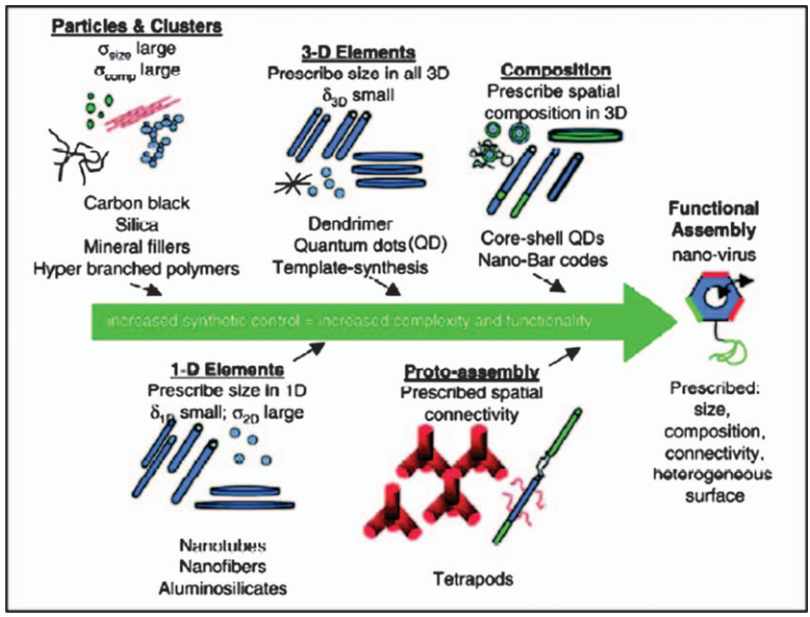

Figure 6.3 Categorization of nanoparticles based on increasing functionality and thus potential to increase functionality of the polymer matrix.[4]

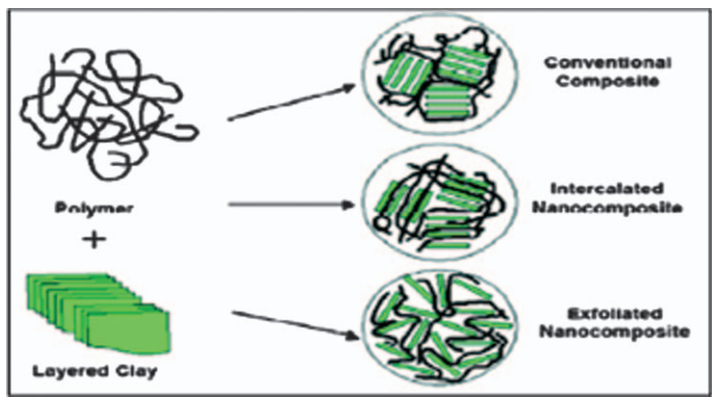

Figure 6.4 Polymer/layered nanocomposites.[3]

In the first case polymer chains are inserted into layered structures such as clays, which occur in a crystallographically regular fashion, with a few nanometres repeat distance, irrespective of the ratio of polymer to layered structure. In the second case, flocculation of intercalated and stacked layers to some extent takes place due to the hydroxylated edge-to-edge interactions of the clay layers. Finally, separation of the individual layers in the polymer matrix occurs in the third type by average distances that depend only on the loading of layered material such as clay. In this new family of composite materials, high

storage modulus, increased tensile and flexural properties, heat distortion temperature, decrease in gas permeability, and unique properties such as self-extinguishing behaviour and tunable biodegradability are observed, compared to matrix material or conventional micro- and macrocomposite materials. Table 6.1 lists some examples of layered host crystals used in this type of composite.

There is a general agreement in the literature that exfoliated systems lead to better mechanical properties, particularly higher modulus, than intercalated nanocomposites.[2] Figure 6.5 shows a plot of the function describing the ratio of surface area to volume (A/V) vs aspect ratio for cylindrical particles with a given volume.

The A/V value increases much quicker with respect to the aspect ratio for sheets compared to rods.[10] The exfoliation of layered minerals and hence the preparation of a homogeneous nanocomposite material is seriously hindered by the fact that sheet-like materials display a strong tendency to agglomerate due to their large contact surfaces.

Table 6.1 Example of layered host crystals susceptible to intercalation by a polymer.[9]

Chemical nature (element)	*Examples (graphite)*
Metal chalcogenides	PbS $(TiS_2)_2$ MoS_2
Carbon oxides	Graphite oxide
Metal phosphates	$Zn(HPO_4)_2$
Clays and layered silicates	Montmorillonite, hectorite, saponite, fluoromica, fluorohectorite, vermiculite, kaolinite, magadite
Layered double hydroxides	$Mg_6Al_2(OH)_{16}CO_3$ nH_2O; M = Mg, Zn

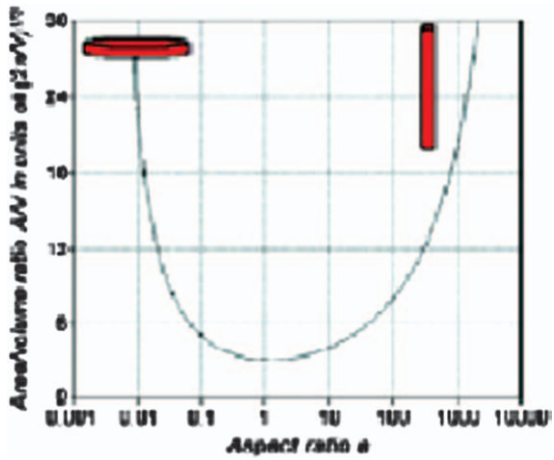

Figure 6.5 Plot of the function describing the ratio of surface area to volume (A/V) vs aspect ratio for cylindrical particles with a given volume.

6.2.1 Nanoparticles (Methods and Preparation)

Nanoparticles are obtained from available natural resources and generally they need to be treated because the physical mixture of a polymer and layered silicate may not form a nanocomposite; in this case a separation into discrete phases takes place. The poor physical interaction between the organic and the inorganic components leads to poor mechanical and thermal properties. In contrast, strong interactions between the polymer and the layered silicate nanocomposites lead to the organic and inorganic phases being dispersed at the nanometre level. As a result, nanocomposites exhibit unique higher properties than conventional composites.[11] Solids with nanoparticle size cannot be prepared or treated by traditional methods simply because the reactants are not mixed on the atomic scale. All the alternative methods, *e.g.* hydrothermal, sol–gel, Pechini, chemical vapour deposition and microwave, address this problem by achieving atomic scale mixing of reactants, in gas, liquid or even solid phases. Most of these are low-temperature methods, although final firing may be required at high temperatures, especially for ceramic-type products. These methods enable a final product with the following characteristics:[1] nano-size particles, narrow particle size distribution, high surface area, homogeneous, pure, improved properties.

6.2.1.1 Techniques for Characterization

Experimental techniques used for the characterization of nanocomposites include NMR for materials behaviour (giving greater insight into the morphology, surface chemistry, and to a very limited extent the quantification of the level of exfoliation in polymer nanocomposites), X-ray diffraction (due to ease and availability), transmission electron microscopy (TEM), allows a qualitative understanding of the internal structure, spatial distribution of the various phases, and direct visualization of defect structure), differential scanning calorimetry (DSC, to understand the nature of crystallization taking place in the matrix), FTIR (to detect functional groups and understand the structure of the nanocomposites), dynamic mechanical analysis (DMA, response of a material to oscillatory deformation as a function of temperature, giving storage modulus [corresponds to elastic response to deformation], loss modulus [corresponds to plastic response to deformation], and tan δ [ratio of the previous two and an indicator of occurrence of molecular mobility transitions]), and resonance Raman spectroscopy (for structural studies).[12] On the Figures 6.6 and 6.7 are show schematic illustration of nanocomposite synthesis.

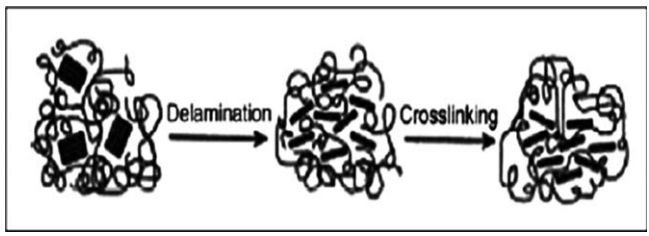

Figure 6.6 Schematic illustration of nanocomposite synthesis.[14]

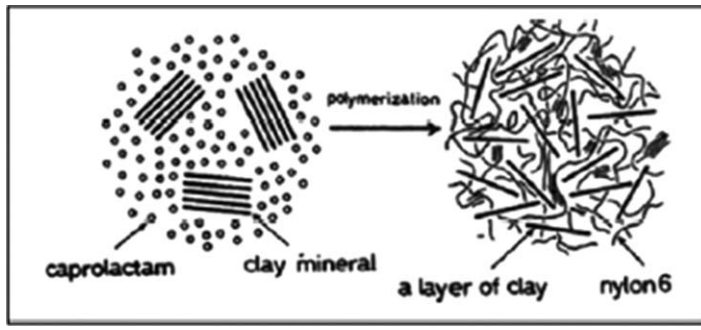

Figure 6.7 Schematic illustration for synthesis of nylon-6/clay nanocomposites.[14]

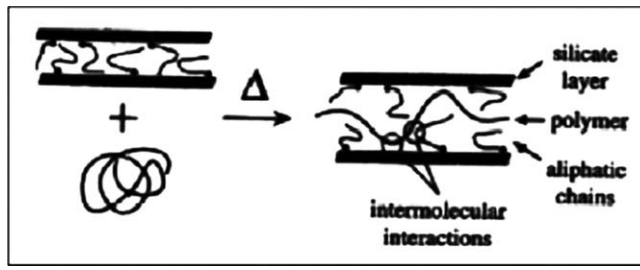

Figure 6.8 Schematic depicting the intercalation process between a polymer melt and an organic-modified layered silicate.[14]

Atomic force microscopy (AFM) is another technique used to characterize nanocomposites.[13] AFM can provide information about the mechanical properties of a surface at a length scale that is limited only by the dimensions of the AFM tip. AFM tips with 10 nm radius of curvature are readily available from commercial suppliers. When probing mechanical properties, the attractive and repulsive force interactions between the tip and sample are monitored. Schematic depicting the intercalation process between a polymer melt and an organic-modified layered silicate is shown on Figure 6.8.

6.3 Micro Carbon Black as a Filler in Rubber

Carbon black (CB) is unquestionably the most widely used reinforcing filler in elastomeric formulations, owing to the physicochemical characteristics and performances it gives to cured rubbers, it has the ability to strength the properties of rubber vulcanizates compared to the non-filled ones. However instability of the price of petroleum has been resulted in increasing interest for other mineral fillers such as precipitated silica. Adding CB to raw rubbers causes viscosity of resulted compound to increase for several reason such as the hydrodynamic effect of CB loading, the structure of CBs which is associated with anisometry of the filler aggregates, the occlusion of rubber within the aggregates, and adsorption of rubber molecules on the filler surface which is treated as shell of immobilized rubber or as bound rubber. The latter case seems

sensible, once a segment is anchored on the filler surface, because movement of whole molecules in the flow field is restricted.[15]

Filler morphologies such as particle size, structure, and essentially surface characteristics have a drastic effect on the physical performance of the elastomeric material. The most important of these parameters however, are the surface characteristics and the chemical active sites which determine the interaction between filler and polymer chains.[16]

Particle diameters can range from less than 20 nm in some furnace grades to a few hundred nanometres in thermal blacks. A discrete rigid colloidal entity of coalesced particles is the smallest dispersible unit of CB. Carbon black particle size and structure comparison are show on Figures 6.9 and 6.10.

Aggregate dimensions measured by the Feret diameter method can range from as small as 100 nm to a few micrometres (a cluster of physically bound and entangled aggregates). Agglomerates can vary widely in size, from less than a micrometre to a few millimetres in the pallet. Figure 6.11 shows the distinction between a particle and an aggregate in CB.

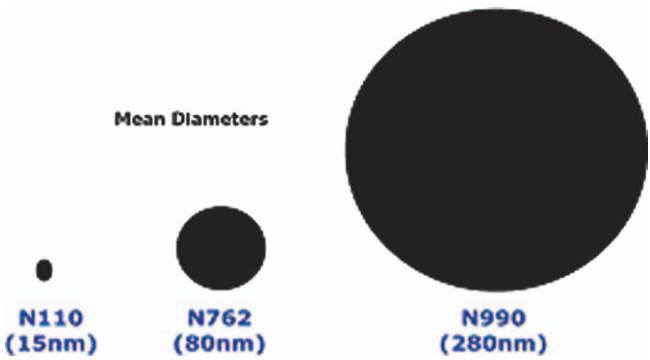

Figure 6.9 Carbon black particle size comparison.

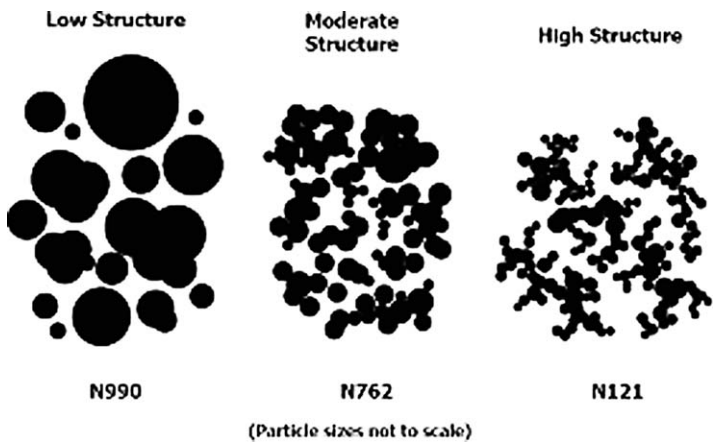

Figure 6.10 Carbon black structure comparison.

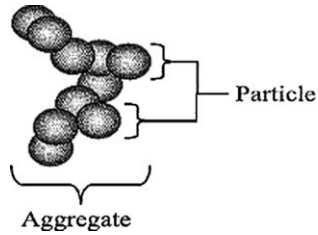

Figure 6.11 A schematic showing the distinction between carbon black particles and an aggregate.

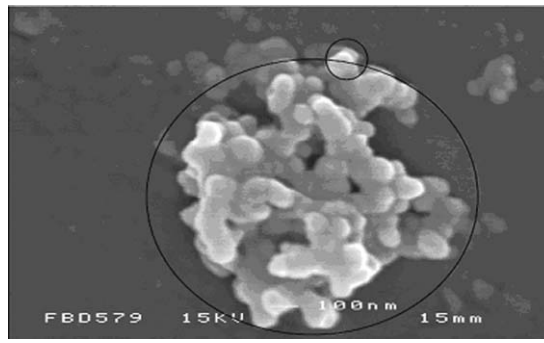

Figure 6.12 Carbon black aggregate showing the primary particle (small circle) and aggregate (larger circle).

Table 6.2 Summary of information about particle size.

Carbon black	*Surface area (m^2/g)*	*Approximate diameter of primary particle size (nm)*	*Diameter of aggregate (nm)*	*Size of agglomerate*
Oil furnace	11/30/40	09/30/00	50–400	Large (< 2 mm)
Thermal	06/15/12	120–500	400–600	Large (< 2 mm)
Impingement (channel)		10/30/12	50–200	Large (< 2 mm)
Lamp black	15–25	60–200	300–600	Large (< 2 mm)
Acetylene black	15–70	30–50	350–400	Pelletizes poorly

Different types of CB have a wide range of primary particle sizes, large surface areas per unit mass, low contents of ash and solvent-extractable materials and varying degrees of particle aggregation. A CB with a high degree of aggregation is said to have a high 'structure'. Structure is determined by the size and shape of the aggregated primary particles, the number of primary particles per aggregate and their average mass (Figure 6.12).

Table 6.2–6.5 present a summary of surface area and primary particle size, aggregate diameter and agglomerate size for different types of CB, particle range of rubber-grade CBs; grades, production process, selected properties and

Table 6.3 Range of particle sizes of rubber-grade carbon blacks.

Group number	*Typical average primary particle size (nm)*	*Average surface area (m^2/g)*
0	0–10	> 150
1	11/19/12	121–150
2	20–25	100–120
3	26–30	70–99
4	31–39	50–69
5	40–48	40–49
6	49–60	33–39
7	61–100	21–32
8	101–200	11/20/12
9	201–500	0–10

uses of CB, ASTM designations for furnace blacks used in rubber, three typical measures of surface area (iodine adsorption, nitrogen absorption and statistical thickness) and one measure of the degree of aggregation (dibutylphthalate absorption).

The reinforcing effect of finely divided particles when added to elastomer compounds is well known. However, it is not clear whether specific bonds are required at the elastomer/particle interface or if van der Waals bonds alone can produce a satisfactory level of reinforcement. Attempts to measure the strength of bonding between elastomers and filler particles directly have been described previously.[17] One of the sources of reinforcement between the CB surface and the rubber matrix is the van der Waals attraction. Also, rubber chains are grafted onto the CB surface by covalent bonds. The interaction is caused by a reaction between the functional group at the CB particle surface and free radicals on polymer chains. Hence, filler–rubber interface is made up of complex physical–chemical interaction. The adhesion at the rubber–filler interface also affects the reinforcement of rubber. The degree of adhesion was measured using an adhesion index. Thin cross-sections of filled rubber were observed using TEM.

From ASTM international NSA, nitrogen surface area, STSA, statistical thickness surface area, dibutylphthalate absorption.

There are many reviews of filler reinforcement by authors such as Kraus[18] and Leblanc[19] (Tables 6.6 and 6.7). The principal factors that determine the reinforcement capability are:

1. The van der Waal forces between the CB and the polymer.
2. The chemical crosslinks or chemisorptions of the polymer onto the filler surface due to free radical reaction between carbon atoms in the filler and in the rubber.
3. The mechanical interlocking of the polymer onto the filler surface.

Dannenberg[21] proposed a model of filler reinforcement that includes slippage at the interface between the molecular chains and the filler. Slippage of the

Table 6.4 Grades, production processes, selected properties and uses of carbon black.

Type	*Designation*		*Production process and feedstock*	*Average primary particle size (nm)*	*Iodine absorption number*[a] *(g/kg)*	*Primary rubber processing properties and use*
	Acronym	*ASTM*				
Super-abrasion furnace black	SAF	N110	Oil furnace	17	145	High reinforcement; used in special and off-road tyre products for which high abrasion resistance is required.
Intermediate super-abrasion carbon black	ISAF	N220	Oil furnace	21	121	High reinforcement and tear strength, good processing, used in passenger, off-road and special tyres for which good abrasion resistance is required.
High abrasion furnace black	HAF	N330	Oil furnace	31	82	Medium high reinforcement, low modulus, high elongation, good flex, tear and fatigue resistance, used in tyre broad, carcass and sidewall compounds, motor mounts, weather-stripping and bicycle tyres.
Fast extruding furnace carbon black	FF	N550	Oil furnace	53	43	Medium high reinforcement, high modulus and hardness, low die swell and smooth extrusion, used in tyre inner lines, carcass and sidewall compounds and hose and other extruded goods
General-purpose furnace carbon black	GPF	N660	Oil furnace	63	36	Medium reinforcement and modulus, good flex and fatigue resistance, low heat build-up, used in tyre carcass, inner lines and sidewalls, sealing rings, cable jackets, hose and extruded goods.
Semi-reinforcing carbon black	SRF	N762	Oil furnace	110	27	Medium reinforcement, high elongation and resilience, low compression set, used in mechanical goods, footwear, inner tubes and floor mats.
Medium thermal carbon black	MT	N990	Natural gas	320	9	Low reinforcement, low modulus, hardness, hysteresis and tensile strength, high elongation and loading capacity, used in wire insulation and jackets, mechanical goods, footwear, belts, hose, gaskets, O-rings and tyre inner lines.

[a]Used as a measure of surface area, which is an indication of reinforcement ability.

Table 6.5 Typical properties of rubber-grade carbon black.

ASTM classification	*Iodine absorption (g/kg)*	*NSA (m^2/g)*	*STSA (m^2/g)*	*DBPA (ml/100 g)*
N110	145	127	115	113
N115	160	137	124	113
N120	122	126	113	114
N121	121	122	114	132
N125	117	122	121	104
N134	142	143	137	127
N135	151	141	–	135
S212	–	120	107	85
N219	118	–	–	78
N220	121	114	106	114
N231	121	111	107	92
N234	120	119	112	125
N293	145	122	111	100
N299	108	104	97	124
S315	–	89	86	79
N326	82	78	76	72
N330	82	78	75	102
N335	92	85	85	110
N339	90	91	88	120
N343	92	96	92	130
N347	90	85	83	124
N351	68	71	70	120
N356	92	91	87	154
N358	84	80	78	150
N375	90	93	91	114
N539	43	39	38	111
N550	43	40	39	121
N582	100	80	–	180
N630	36	32	32	78
N642	36	39	–	64
N650	36	36	35	122
N660	36	35	34	90
N683	35	36	34	133
N754	24	25	24	58
N762	27	29	28	65
N765	31	34	32	115
N772	30	32	30	65
N774	29	30	29	72
N787	30	32	30	80
N907	–	9	9	34
N908	–	9	9	34
N990	–	8	8	43
N991	–	8	8	35

Table 6.6 Effect of particle size on reinforcement.[20]

Size (nm)	*Strength*
1000–5000	Low reinforcement
< 1000	Medium reinforcement
< 100	Strongest reinforcement

Table 6.7 Effect of carbon black on rubber properties.

Rubber property	*Effect of carbon black on rubber properties*		
Uncured properties	*Surface area*	*Structure*	*Loading*
Mixing temperature	Increases	Increases	Increases
Die swell	Decreases	Decreases	Decreases
Mooney viscosity	Increases	Increases	Increases
Dispersion	Decreases	Increases	Decreases
Loading capacity	Decreases	Decreases	–
Cured properties			
300% modulus	Insignificant	Increases	Increases
Tensile strength	Increases	Insignificant	Increases[a]
Elongation	Insignificant	Decreases	Decreases
Hardness	Increases	Increases	Increases
Tear resistance	Increases	Decreases	Increases[a]
Hysteresis	Increases	Insignificant	Increases
Abrasion resistance	Increases	Insignificant	Increases[a]
Low strain dynamic modulus	Increases	Insignificant	Increases
High strain dynamic modulus	Insignificant	Increases	Increases

[a]Increases to an optimum and then decreases.

molecular chains under strain also redistributes the stress. The redistribution of stress again inhibits a molecular rupture. The model suggested that the hysteresis observed can be attributed to the loss of the strain energy as frictional heat occurring during the relative motion between molecular chains and the filler.

6.4 Carbon Nanotube-Filled Natural Rubber

Elastomers such as natural rubber (NR) are of great importance in manufacturing industries. However, they possess properties which are less than that required for practical applications. This has led to the use of fillers for reinforcement of their properties. For practical applications, the physical and mechanical properties of elastomers are reinforced with mineral fillers such as silica, CB, clay fibre, short fibre and layered silicate.[22]

Although some advances have been recorded in the use of mineral fillers as reinforcement aids in elastomers such as NR, there are still some shortfalls in their application. These shortfalls include the fact that large amounts of mineral fillers are required, which often leads to heavy final products.[23] It has been reported by several authors that for a material to bestow any reinforcement to a matrix, it must have good surface area for effective load transfer.[24] In view of this, nanomaterials which are touted to have small size, high surface area, and excellent aspect ratio can be said to be good replacements for mineral fillers like silica and CB. Due to these assertions, nanocomposites have become a promising area in the field of polymer research. Polymeric nanocomposites have gained importance in the manufacture of products of high performance properties like light weight, material transparency, enhanced stiffness and toughness as well as decreased flammability for different industries.[25] NR composites are of special importance in nanocomposites. This is because of their extensive use in the industrial and societal field due to their high and

reversible deformability.[26] Since the essential modulus and strength of NR is, however, low, an additional reinforcing phase is necessary.[27] The use of CNTs as reinforcement phase in nanocomposite has been on the rise since its discovery in the early 1990s. This is not surprising as CNT has been reported to have tensile strength greater than steel but only one sixth of its weight[28] with an aspect ratio that can reach over 1000.[29]

6.4.1 NR/Carbon Nanotube Composites

Carbon nanotubes (CNTs) have chemical stability, good mechanical properties and high surface area, making them ideal for the design of sensors and provide very high surface area due to its structural network. Because CNTs are also suitable supports for cell growth, electrodes of microbial fuel cells can be built using them. In recent years, a great deal of attention has been paid to CNTs, which consist of rolled up graphite sheets built from sp2 carbon units, because CNTs possess outstanding electrical, thermal, and mechanical characteristics.[30] As ideal reinforcing fillers in polymer composites, CNTs are expected to provide a better reinforcement effect compared to other nanofillers due to their inherent superior properties. As a consequence, CNTs have been widely exploited in different kinds of polymers, and considerable enhancements of electrical conductivity and mechanical properties have been achieved in some instances.[31] However, very little work has been done on incorporating CNTs into rubber[32] because a large loading is needed for reinforcement due to material characteristics of rubber, *i.e.* the framework of the reinforcement phase must be formed in rubber for enhancing the low modulus and strength of a neat rubber. At present, the batch production of CNTs is available because of the progress in developing synthetic methods.[33] So further study and development of CNT-reinforced rubber nanocomposites are now feasible.

Some research on the pre-treatment of CNTs and interfacial modification techniques have been reported, which is helpful to the preparation of CNT-filled rubber composites.[34] But the dispersion of CNTs into rubber materials is still problematic due to possible entanglement of the high aspect ratio CNTs and the high viscosity of rubbers.

Although some studies on CNT-reinforced rubbers have been performed, presently the overall performance of these rubber nanocomposites has not reached the expected potential.[35]

The CNTs used in the experiments were prepared by chemical vapour deposition (CVD) of propylene gas at 700 °C using Ni as a catalyst. The diameters of raw nanotubes vary from 20 to 50 nm, and lengths vary from 100 to 1 mm. A TEM image of raw CNTs is shown in Figure 6.13.

The raw CNTs were purified in hydrofluoric acid (HF) for 24 h, and then cleaned continuously with deionized water until chemically neutral. The purified CNTs were obtained after drying for 24 h in a vacuum oven to remove moisture. To create some functional groups on the surface of the CNTs and improve the bonding between the CNTs and NR matrix, the purified CNTs

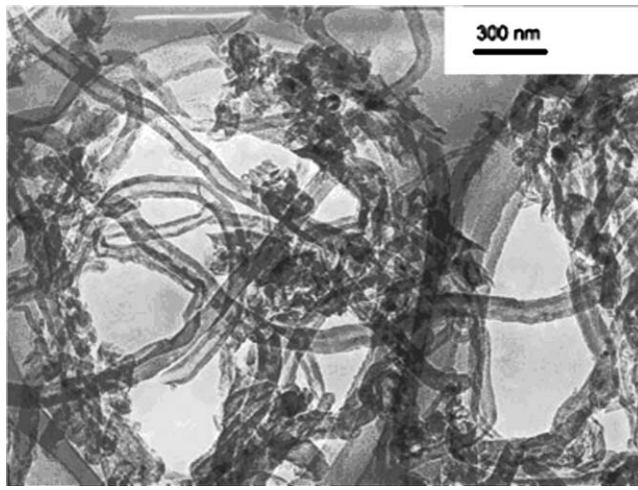

Figure 6.13 TEM image of raw CNTs.

were further treated with blended acid and HRH (hydrated silica, resorcinol and hexamethylene tetramine with a weight ratio 15:10:6) bonding systems. The dry tricomponent system comprising hydrated silica, resorcinol and hexamethylene tetra amine, popularly known as HRH, was used as the bonding system to achieve improved bonding between the fillers and the rubber matrix.[36] This effective and economical silica-containing bonding system was introduced in CNT/NR nanocomposites in this study. The dry HRH bonding system was prepared in the experiment. The purified CNTs were dipped in a blended acid solution with a volume ratio between nitric acid and sulfuric acid of 1 : 3.

The loading of CNTs was 1 g for 10 ml of blended acid solution. The mixing solution was boiled and refluxed for 0.5 h, and then the CNTs were carefully washed and filtered with deionized water until chemically neutral.

According to the analysis of previous infrared spectroscopy,[37] some functional groups such as hydroxyl, carboxyl and carbonyl were loaded on the CNT surface after the blended acid treatment. The dry acid-treated CNTs were blended with the HRH bonding system with a weight ratio of 25:3. To untie the entanglement of CNTs and facilitate the co-mixing of CNTs and HRH bonding systems, the mixture was milled for 0.5 h in a ball-milling machine. Dry ball milling was undertaken in a purified argon protect atmosphere on a planetary ball mill. Steel balls with diameters of 4 and 6 mm were used as a grinding medium. Ball milling was conducted with the disk revolution speed of 180 rpm. A scanning electron microscope (SEM) image of the ball-milled CNTs is shown in Figure 6.14.

It can be found that after the ball-milling treatment, the CNTs were loose in bulk, which was beneficial to the dispersion and penetration of CNTs inside the rubber macromolecular chains. Furthermore, there was no drastic decrease in the aspect ratio of the CNTs due to the short milling time (0.5 h), which can

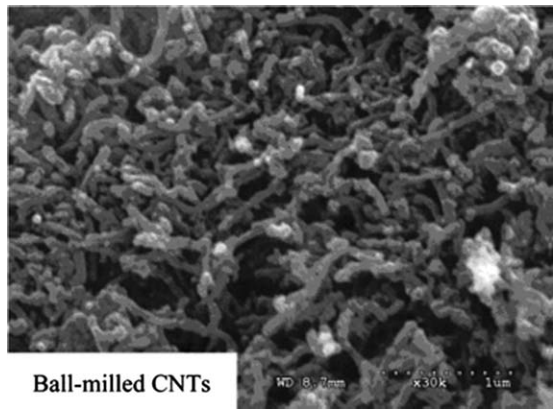

Figure 6.14 SEM image of ball-milled CNTs.

Table 6.8 The composition of NR composites.

Constituent	*Neat NR*	*CNT/NR*	*CB/NR*
NR	100 phr	100 phr	100 phr
Zinc oxide	5.0 phr	5.0 phr	5.0 phr
Stearic acid	3.0 phr	3.0 phr	3.0 phr
Sulfur	2.8 phr	2.8 phr	2.8 phr
N-cyclohexyl-2-benzothiazole-sulfenamide	1.3 phr	1.3 phr	1.3 phr
2-Mercaptobenzothiazole	0.1 phr	0.1 phr	0.1 phr
Ball-milled CNTs	–	25 phr	–
CB	–	–	25 phr

ensure stress transfer ability in the composites. The chemical properties of the ball-milled CNTs and the interaction between the CNTs and NR are reported in another of our papers.[38] CB (N326) was supplied by the Tianjin Carbon Black Factory, China. The NR used in this study was a Standard Malaysian Rubber 5, provided by Beijing Academy of Rubber Industry, China. The ball-milled CNTs and CB were mixed with NR (Figure 6.14). TEM micrographs of raw CNTs. in experiment, respectively.

Preparation of the CNT/NR nanocomposites

The formulation of NR composites used in experiments is shown in Table 6.8.

The incorporation of treated CNTs into NR was carried out by a solvent mixing method. Firstly, a certain quantity of CNTs and NR was added into the toluene solution, respectively. The solution of CNTs was sonicated using a Brasonic1 Ultrasonic cleaner 1210 (Branson Ultrasonics Corporation) for 2 h. Meanwhile, the solution of NR was stirred and kept for certain duration until the rubber was uniformly dissolved in the toluene. The toluene solution of CNTs was subsequently dispersed into the solution of NR with stirrer and ultrasonication simultaneously for 2 h. Then the dry CNT/NR mixture was obtained by evaporating the solvent off at 80 °C under vacuum. Subsequently,

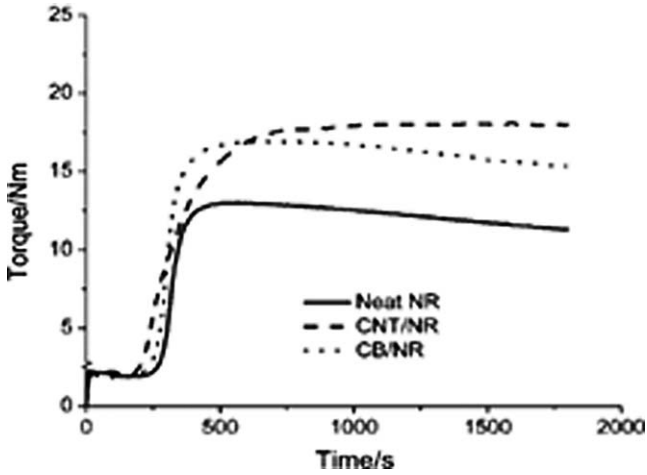

Figure 6.15 Vulcanization curves of neat NR and NR composites.

the preparation of CNT/NR nanocomposites was accomplished by adding other ingredients including vulcanizing agent in the formulation of composites in an open two-roll mill (160×320 mm^2) at room temperature with a nip gap of about 1 mm. At the same time, the neat NR and CB/NR composites were prepared in an open two-roll mill (160×320 mm^2) at room temperature by the traditional mechanical mixing method. Vulcanization curves of the neat NR and NR composites are shown in Figure 6.15.

It can be seen that the scorch time of NR, which is the measurement of premature vulcanization of rubber, showed a slight reduction after addition of the fillers. Although some studies indicated that the addition of CNTs could delay the onset of vulcanization,[39] the addition of the CNTs could improve the thermal conductivity of the NR material because of their superior thermal conductivity, and could promote the occurrence of vulcanization. Therefore, the effect of CNTs on the scorch time might depend on the composition and microstructure of rubber composites. During the curing reaction period, the torque of rubber specimens gradually increased. The time to reach the maximum torque of the nanocomposite containing treated CNTs was a little longer than the other two specimens, which reflected that the vulcanizing rate of CNT/NR nanocomposites is lower. Meanwhile, the maximum torque of the CNT/NR nanocomposite specimen was the highest among the materials. This is because the CNTs with ultra-high modulus effectively restricted the changes in polymer molecular configuration, and then enhanced the modulus of the rubber composites. In the last region of the vulcanization process, the over-curing reversion of NR reduced due to the addition of CNTs, when compared to the neat NR and CB/NR composites. It would be an advantage to eliminate the difference in crosslinking degree between the surface and inside of the thick rubber product arising from the low thermal conductivity of the rubber materials.

Several important physical and mechanical properties of the neat NR and NR composites are tested and listed in Table 6.9.

Compared to the neat NR and CB/NR composites, the addition of the CNTs brought about remarkable increase in hardness, tensile modulus and tensile strength to the rubber material. The rebound resilience and dynamic compression properties of the CNT/NR nanocomposites are better than that of CB-filled NR composites, which is beneficial for the actual application such as tire, *etc*., under a dynamic condition. The fracture morphology of the cured CNT/NR nanocomposites is shown in Figure 6.16.

It is noted that no obvious aggregates of treated CNTs in rubber matrix were found. A few outcrops of the CNTs existed on the fracture surface, which indicated that the strong interaction between the CNTs and the rubber macromolecules in the NR composites was formed. Therefore, the CNTs could carry stress throughout the rubber matrix, and play an effective reinforcement role in the resulting nanocomposites. Predictably, the NR composites containing the CNTs possessed the best mechanical properties among these specimens. This CNT/NR nanocomposite exhibited great enhancements in Shore A hardness, tensile modulus and tensile strength by 16, 32 and 10%, respectively, compared to NR composites reinforced with the same loading level of CB. The theoretical modelling studies on the mechanical properties of CNT/NR composites will be the subject of future work.

Table 6.9 The mechanical properties of NR composites.

Samples	*NR*	*CNT/NR*	*CB/NR*
Hardness (Shore A)	41 ± 2	63 ± 2	34 ± 2
Modulus at 300% (MPa)	1.8 ± 0.2	12.5 ± 0.3	9.5 ± 0.3
Tensile strength (MPa)	7.2 ± 0.6	24.8 ± 20	22.5 ± 1.8
Elongation at break (%)	680 ± 20	495 ± 15	480 ± 20
Rebound degree (%)		73 ± 2	54 ± 3
Goodrich compression permanent set (%)		12.5 ± 0.3	13.5 ± 0.5
Goodrich compression heat accumulation (C)		32 ± 0.3	4.4 ± 0.3

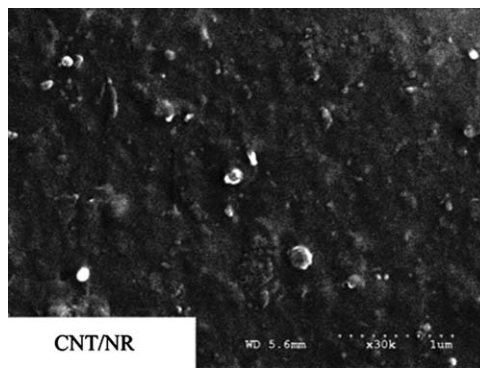

Figure 6.16 SEM image of CNT/NR nanocomposite.

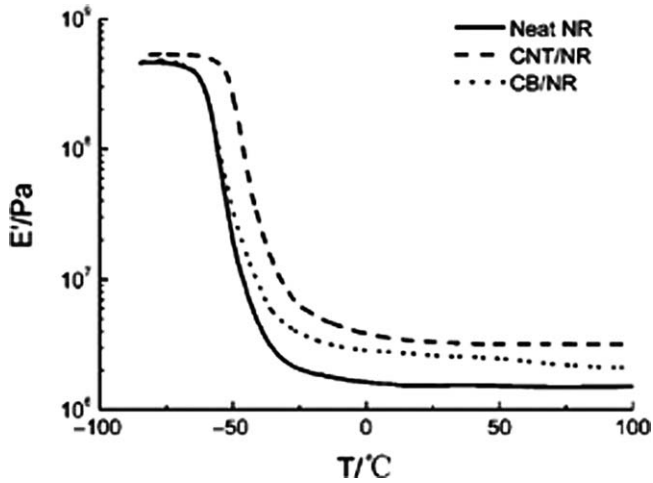

Figure 6.17 The dynamic storage modulus as a function of temperature for neat NR and NR composites.

The effect of the fillers on the dynamic mechanical property of NR material was analysed by DMA in this work. The elastic modulus (E') and the loss factor (tan δ) of the neat NR and NR composites were characterized as functions of temperature. Under an oscillating force, the resultant strain in specimen depends upon both elastic and viscous behaviour of materials. The storage modulus reflects the elastic modulus of the rubber materials which measures t recoverable strain energy in a deformed specimen, and the loss factor is related to the energy damped due to energy dissipation as heat.

The storage modulus of the neat NR and NR composites versus temperature curves is shown in Figure 6.17. It is found from Figure 6.17 that the storage modulus of the CNT/NR nanocomposites is higher than that of the neat NR and CB/NR composites from low-temperature to high-temperature regions. The high modulus and specific surface areas of CNTs enhance the stiffness of the NR, which results in an increment of storage modulus of the CNT/NR nanocomposite.

At low temperature, the modulus of the neat NR exhibits a high value due to the semicrystalline characteristic of NR, and a small variation of modulus of NR appeared after the addition of fillers. With the increase in temperature, although the E_0 of all specimens manifested declining trends, it is evident that stiffness of NR increases as a result of addition of fillers. A shift of rapid decreasing region of E' towards higher temperature can be seen for NR after adding the CNTs and the reinforcing effect is more obvious above the T_g of NR. The storage modulus of CNT/NR nanocomposites in the rubbery region is the highest among all specimens and keeps the steady value within the testing temperature.

Figure 6.18 shows the temperature dependence of tan δ of neat NR and NR composites. The position of the tan δ peak in the tan δ–temperature curve can

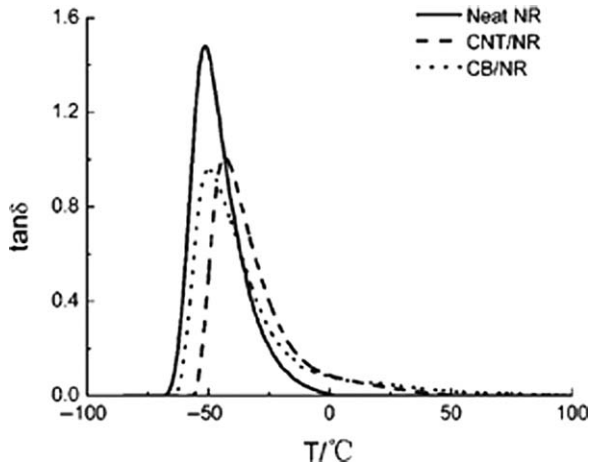

Figure 6.18 The loss factor as a function of temperature for neat NR and NR composites.

also be used to identify the T_g of the rubber materials. It can be seen that the peak of tan δ of the NR composite slightly shifts to a higher temperature compared to that of the neat NR. It denotes that the mobilization of rubber macromolecules is restricted due to the addition of fillers. The enhancement of tan δ peak position of NR composites corresponds to the DSC experiment results. The tan δ value of NR composites is related to both NR and fillers material characteristics. The adding of CNTs reduces the percentage of the NR in composites, which lowers hysteresis loss of the rubber under an oscillating force. Therefore, the height of the tan δ peak of NR decreases after the adding of fillers. In general, the higher tan δ value of a rubber from −20 to 10 °C can be used to predict the preferable anti-skid properties of rubber material under wet conditions, and the small tan δ value of a rubber in the region of 50–60 °C implies the low rolling resistance of rubber material.[39] Therefore, it can be deduced from Figure 6.17 that compared to CB, the CNTs can offer rubber materials significantly better anti-skid properties and low rolling resistance, which is of great value for ideal tire materials.

6.4.2 Thermal Stability of NR/CNT Vulcanizates

Figure 6.19 shows TGA curves of the neat NR and NR composites. By comparing the weight loss as a function of temperature, the effect of CNTs on the thermal stability of NR can be analysed. Although there is no obvious variation at the onset temperature of thermal degradation for different specimens, a shift of rapid degradation region towards higher temperature can be seen for NR after adding the fillers, especially adding the CNTs. Meanwhile, the weight loss of CNT/NR nanocomposites at the same temperature is the smallest among all studied specimens. The reason is that CNTs can impose the restriction on the mobilization of rubber macromolecules and conduct heat homogeneously and

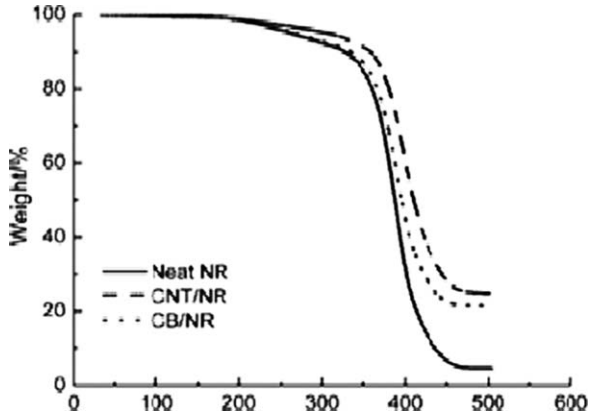

Figure 6.19 TGA curves of neat NR and NR composites.

avoid the heat concentration. Therefore, the thermal stability of NR was further improved by adding CNTs compared to CB/NR composites.

However, inconsistent results had been reported by Puglia *et al.*,[40] where they found the thermal degradation rate increased and the onset temperature of thermal degradation decreased for epoxy resin after the addition of CNTs. It was attributed to the high thermal conductivity and specific surface areas of CNTs which can accelerate the transfer of heat. This interpretation is not completely substantiated. The improved thermal stability of PMMA was also proved in thermal degradation experiment of CNT/PMMA.[41] A study by Troitskii *et al.* indicated that C60 can combine with free radicals produced in the thermal degradation process of PMMA, and form relative steady macro-free radicals.[42]

Therefore, the CNTs can also combine with free radicals produced in the thermal degradation process of NR, forming relative steady-free radicals, which then delay the progression of thermal degradation. Because the thermal degradation of epoxy usually proceeds according to a cation mechanism and the thermal degradation of PMMA and NR proceeds according to a free radical reaction, the different chemical mechanism during the thermal degradation process of polymer materials affects the thermal stability of CNT composites.

The CNT/NR nanocomposites were fabricated through solvent mixing assisted with a two-roll mill. Compared to the neat NR and traditional CB/NR composite, the over-curing reversion of CNT/NR nanocomposite abated. The dispersion of the treated CNTs in the rubber matrix and interfacial bonding between them were satisfactory.

6.5 Conclusions

This work has studied the reinforcement of NR by nano- and micro-CB fillers. It has also investigated the resulting mechanical and thermal behaviour of these

filled NRs. Significant research is needed into the behaviour of nano-interfaces, and this field can still be considered to be in its infancy. In particular, the development of accurate nanomechanical models, and understanding the properties of the polymer at the interface are required to address the outstanding issues of the polymer–nanoparticle interface and thus optimize the mechanical performance of NR polymer nanocomposites. It is believed that one of the main issues in preparing good NR polymer matrix nanocomposite samples is the good dispersion of the nanoparticles in a polymer matrix. Carbon nanoparticles have great potential to make NR nanocomposites.

The mechanical properties of the CNT/NR nanocomposites showed great improvement compared to the neat NR and CB/NR composite. The rebound resilience and dynamic compression properties of NR loaded with CNTs are better than those of CB/NR composites. The storage modulus and thermal stability of NR were also markedly improved by adding treated CNTs. In conclusion, the NR nanocomposites loaded with the treated CNTs exhibited excellent overall performance improvements due to the reinforcement effect of the high aspect ratio functionalized CNTs. Furthermore, advanced rubber nanocomposites with improved comprehensive performance have demonstrated the potential for expanded future industrial applications in bulk scenarios through a facile technique which improves the industrial processing, a requirement for high quality industrial-scale production. In summary the results indicate improved performance for the eventual NR products, and improved processing for production (less complicated procedures, higher quality, new manufacturing efficiencies).

Acknowledgements

Financial support for this study was provided by the Ministry of Science and Technological Development of the Republic of Serbia (Project Numbers 45022 and 45020).

References

1. P. Sharma, W. Miao, A. Giri and S Raghunathan, in *Dekker Encyclopedia of Nanoscience and Nanotechnology*, ed. J. A. Schwarz, C. I. Contescu and K. Putyera, Marcel Dekker, New York, 2004, 2nd ed., pp. 2799–2814.
2. J. Jordan, K. J. Tannenbaumc, M. Sharafb and I. Jasiukd, *Mater. Sci. Eng*, 2005, **393**, 1.
3. J. Denault and B. Labrecque, *Technology Group on Polymer Nanocomposites, PNC-Tech. Industrial Materials Institute*, National Research Council Canada, Québec, 2004.
4. D. Wagner and R. Vaia, *Mater. Today*, 2004, **7**, 38.
5. J. B. Donnet, *Carbon*, 1994, **32**, 1305.
6. Third International Conference on Carbon Black Mulhouse (October 2000), *Carbon* (special issue), 2000, **40**, 137.
7. J. B. Donnet and C. Lansinger, *Kautsch. Gummi Kunstst*, 1992, **45**, 45.

8. A. R. Payne, *Polym. Sci.*, 1962, **6**, 57.
9. F. Wypych and K. Satyanarayana, *J. Colloid Interface Sci.*, 2005, **285**, 532.
10. H. Fischer, *Mater. Sci. Eng.*, 2003, **23**, 763.
11. M. Biswas and R. S. Sinha, *Adv. Polym. Sci.*, 2001, **155**, 167.
12. T. Ellis and J. D'Angelo, *J. Appl. Polym. Sci.*, 2003, **90**, 1639.
13. M. Greene, C. Kinser, D. Kramer, L. Pingree and M. Hersam, *Microsc. Res. Tech.*, 2004, **64**, 415.
14. S. S. Ray and M. Okamoto, *Prog. Polym. Sci.*, 2003, **28**, 1539.
15. J. B. Donnet, R. C. Bansal and M. J. Wang, *Carbon Black Science and Technology*, Marcel Dekker, New York, 2nd ed., 1993, p. 284.
16. L. Bokobza and O. Rapoport, *J. Appl. Polym. Sci.*, 2002, **85**, 2301.
17. J. Frohlich, W. Niedermeier and H. D. Luginsland, *Composites, Part A*, 2005, **36**, 449.
18. G. Kraus, *Angew. Makromol. Chem.*, 1976, **60**, 215.
19. J. L. Leblanc, *Prog. Polym. Sci.*, 2002, **27**, 627.
20. J. B. Donnet and A. Voet, *Carbon Black, Physics, Chemistry, and Elastomer Reinforcement*, Marcel Dekker, New York, 1976.
21. E. M. Dannenberg, *Rubber Chem. Technol.*, 1986, **59**, 512.
22. A. A. L. Adedigba, M. Al-Harthi and M. A. Atieh, *Arabian J. Sci. Eng.*, 2010, **35**, 49.
23. J. Carretero-Gonzalez, H. Retsos, R. Verdejo, S. Toki, B. S. Hsiao, E. P. Giannelis and M. A. Lopez-Manchado, *Macromolecules*, 2008, **41**, 6763.
24. S. Kar, K. Pradip and M. A. K. Bhowmick, *J. Mater. Sci.*, 2010, **45**, 64.
25. K. S. Shah, R. C. Jain, V. Shrinet and A. K. Singh, *IEEE Trans. Dielectr. Electr. Insul.*, 2009, **16**, 853.
26. G. Nazlia, A. Fakhru'l-Razi, A. R. Suraya and A. A. Muataz, *Fullerenes, Nanotubes Carbon Nanostruct.*, 2007, **15**, 207.
27. A. A. Muataz, N. Nazif, Y. Faridah, F. Mohammed, T. R. Chantara, A. Mamdouh, A. A. Faraj, M. Khalid and M. Adnan, *Fullerenes, Nanotubes Carbon Nanostruct.*, 2010, **18**, 56.
28. M. D. Frogley, D. Ravich and H. D. Wagner, *Compos. Sci. Technol.*, 2003, **63**, 1647.
29. W. Zhang, J. K. Sprafke, M. A. Minglin, E. Y. Tsui, S. A. Sydlik, G. C. Rutledge and T. M. Swager, *J. Am. Chem. Soc.*, 2009, **131**, 8446.
30. P. M. Ajayan, L. S. Schadler, C. Giannaris and A. Rubio, *Adv. Mater.*, 2000, **12**, 750.
31. C. Stephan, T. P. Nguyen, M. L. Chapell, S. Lefrant, C. Journet and P. Bernier, *Synth. Met.*, 2000, **108**, 139.
32. A. M. Shanmugharaj, J. H. Bae, K. Y. Lee, W. H. Noh, S. H. Lee and S. H. Ryu, *Compos. Sci. Technol.*, 2007, **67**, 1813.
33. M. Endo, Y. A. Kim, Y. Fukai, T. Hayashi, M. Terrones and H. Terrons, *Appl. Phys. Lett.*, 2001, **79**, 1531.
34. P. C. Ma, J. K. Kim and B. Z. Thang, *Carbon*, 2006, **44**, 3232.

35. X. W. Zhou, Y. F. Zhu and J. Liang, *Mater. Res. Bull.*, 2007, **42**, 456.
36. V. G. Geethamma, M. K. Thomas, R. Lakshminarayanan and S. Thomas, *Polymer*, 1998, **39**, 1483.
37. Y. H. Li, J. Ding, J. F. Chen, C. L. Xu, B. Q. Wei, J. Liang and D. H. Wu, *Mater. Res. Bull.*, 2002, **37**, 313.
38. G. Sui, W. H. Zhong, X. P. Yang and Y. H. Yu, *Mater. Sci. Eng.*, 2008, **485**, 524.
39. S. H. Zhao, H. Zou and X. Y. Zhang, *J. Appl. Polym. Sci.*, 2004, **93**, 336.
40. D. Puglia, L. Valentini and J. M. Kenny, *J. Appl. Polym. Sci.*, 2003, **88**, 452.
41. Z. X. Jin, K. P. Pramoda, G. Q. Xu and S. H. Goh, *Chem. Phys. Lett.*, 2001, **337**, 43.
42. B. B. Troitskii, L. S. Troitskaya and A. S. Yakhnov, *Eur. Polym. J.*, 1997, **33**, 1587.

CHAPTER 7

Silica Reinforcement in Natural Rubber in Micro and Nano Length Scales

AZANAM S. HASHIM* AND S. K. ONG

Universiti Kuala Lumpur, Malaysian Institute of Chemical and Bioengineering Technology, Lot 1988, Vendor City, Taboh Naning, 78000 Alor Gajah, Melaka, Malaysia
*Email: azanam@unikl.edu.my

7.1 Silica and Silica Reinforcement of Rubbers

Silica is also known as white filler. It is in amorphous form and consists of silicon and oxygen arranged in tetrahedral structure of three-dimensional lattice. The particle size ranges from 10 to 30 nm.[1] Its surface has silanol groups which influence the degree of surface hydration. The silanol concentration depends on the number of silicon atoms per unit area at the surface and the number of hydroxyl group presence at each silicon atom. At high surface hydration, it can adversely affect the rubber composite's performance as it leads to formation of aggregates, agglomerates or clusters of silica.[1–3]

The hydrophilic nature of silica also affects the cure characteristics of rubber compounds, the properties of vulcanized rubber and also the compatibility with non-polar rubber such as natural rubber (NR). Silica retards the vulcanization as it reacts with zinc-accelerator-sulfur complex.[4] These drawbacks can be overcome through the use of silane coupling agents. The most common silane coupling agent used is bis(3-triethoxysilylpropyl) tetrasulfide (TESPT). A silane

RSC Polymer Chemistry Series No. 8
Natural Rubber Materials, Volume 2: Composites and Nanocomposites
Edited by Sabu Thomas, Hanna J. Maria, Jithin Joy, Chin Han Chan and Laly A. Pothen

Published by the Royal Society of Chemistry, www.rsc.org

coupling agent is a bifunctional molecule; one end has the capability to react chemically with silica forming silica–silane coupling agent intermediate and the other end with the rubber. The reaction with rubber is either direct or indirect participation during vulcanization process.[3] The silica–silane coupling agent intermediate will then take part in the vulcanization process. This improves the degree of compatibility between silica and non-polar rubber and subsequently enhances the reinforcing efficiency of silica.

Another key factor in governing the reinforcement efficiency of filler is its surface area. Ideally, the dispersion of silica in NR–silica composite should be as homogeneous as possible and less silica–silica interaction. This chapter will focus on NR–silica nanocomposites obtained through various approaches as reported in the literature. It is worth noting that from the aspect of sustainable development, NR–silica nanocomposite provides the opportunity for greener products where carbon black is either totally or partially replaced by silica.

7.2 NR/Silica Nanocomposites *via* the *in situ* Sol–Gel Silica Process

The *in situ* sol–gel silica process is an alternative method of incorporating silica into rubbers. The *in situ* sol–gel approach, in preparing silica-reinforced rubber, is considered a novel technique.[5] In principle, a rubber is swollen in a silica precursor, *e.g.* tetraethyl orthosilicate (TEOS) and the TEOS-swollen rubber is then subjected to hydrolysis and condensation reactions which could be acid- or base-catalysed. Subsequently, silica particles are generated in the rubber or rubber network.[6–8] The chemical reactions involved in the formation of silica particles are shown in Scheme 7.1 where the overall reaction indicates that 1 mole of TEOS requires 2 moles of water to be converted into anhydrous silica.

One of the earlier works of *in situ* silica generation in a rubber network was carried out by Mark and coworkers[10] involving polydimethylsiloxane (PDMS). It was observed by transmission electron micrograph that the *in situ*-filled PDMS has an average silica particle diameter of 25 nm. Although 50 wt% or more of silica could be incorporated into the PDMS network, the highest tensile strength observed was about 2.8 MPa. Other similar works have also been reported for butadiene rubber[11,12] and styrene-butadiene rubber[13–15] with a similar observation of low tensile strength. One significant work, which is frequently cited, was the study of TEOS-based sol–gel silica–SBR using TESPT as coupling agent.[16] Depending on the formulations, silica content ranging from 15 to 22 wt% could be incorporated into the rubber. With the use of TESPT, finer particle size of silica could be obtained. Compared to the conventional vulcanizate with the same silica content, the sol–gel vulcanizate was significantly stiffer and stronger reaching a tensile strength of 24 MPa. Based on dynamic mechanical analysis (DMA), the TESPT was also observed to reduce the heat build-up of the sol–gel vulcanizate in the rubbery region.

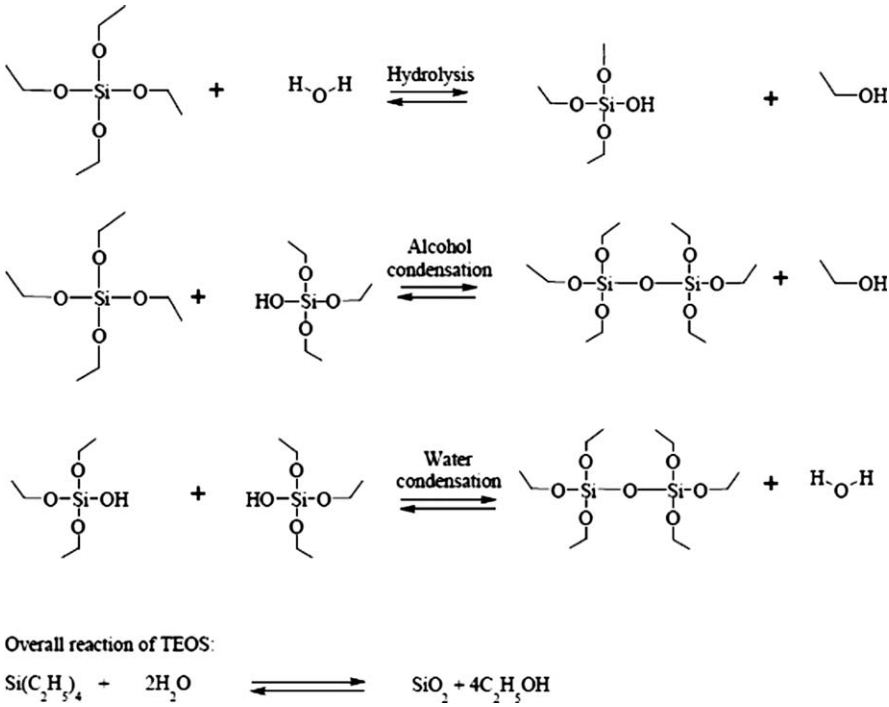

Scheme 7.1 Hydrolysis and condensation reactions of TEOS.

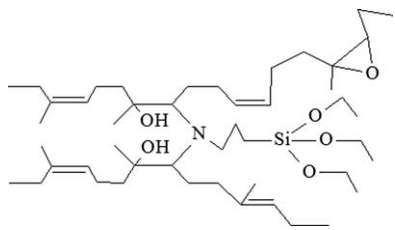

Scheme 7.2 The ENR–APS network.

Silica reinforcement using the sol–gel technique on epoxidized natural rubber 25 mol% (ENR 25) has been reported.[9,17] ENR was first pre-cured with 3-aminopropyltriethoxysilane (APS). APS was mixed into ENR and the ENR–APS mixture was cured at 180 °C to produce pre-cured rubber sheets with tensile properties much lower than those of normally cured rubber vulcanizates. The crosslinking of ENR utilizing the epoxy groups as crosslinking sites using amine functional groups catalysed by bisphenol A has been established.[18] The ENR–APS network is shown in Scheme 7.2.

The ENR–APS network was then subjected swelling in TEOS followed by immersion in 5% butylamine aqueous solution (pH 12.5) at room temperature followed by proper drying to a constant weight. Scheme 7.3 shows how the silica particles are formed and chemically bonded in the ENR–APS network.

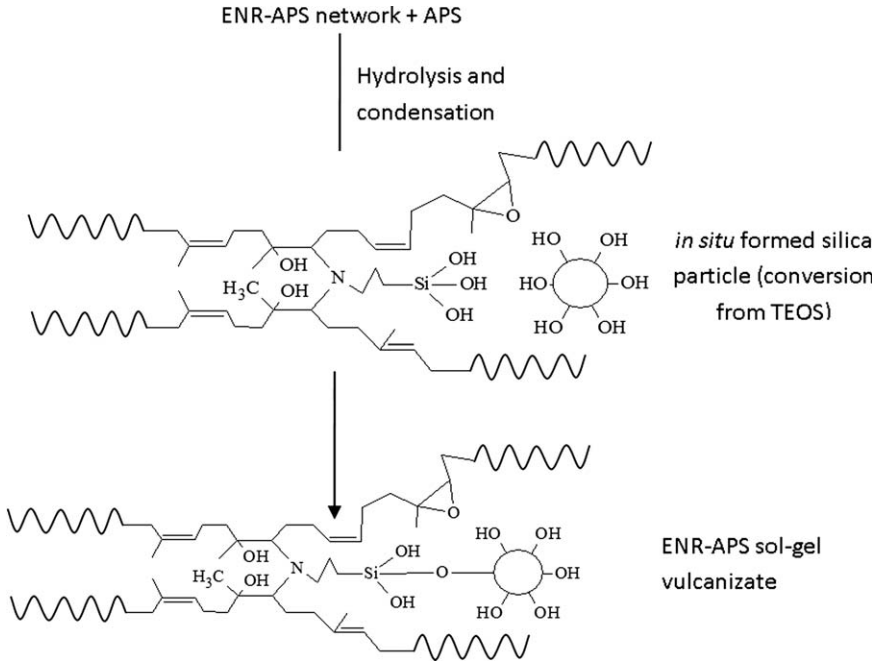

Scheme 7.3 Reaction between silica particles and the ENR–APS network during the sol–gel process.

Table 7.1 Tensile properties of ENR–APS sol–gel silica vulcanizates.

	EMR-APS-sol gel (28%)[a]	*ENR-APS-sol gel (27%)*[b]	*ENR-sulphur (27%)*[c]
TS, MPa	~19	~16	~12
Elongation at break (EB), %	~290	~300	~390
Modulus at 100% elongation (Ml00), MPa	~7	~5	~2

[a]ENR-APS-sol gel system with 28 % sol-gel silica (reaction and drying temperature are 30 °C and 100 °C, respectively).
[b]ENR-APS-sol gel system with 27 % sol-gel silica (reaction and drying temperature are room temperature and 60 °C, respectively).
[c]ENR-sulphur system with 27 % commercial grade silica.

Based on normal weight deduction and TGA, 27–36 wt% of silica could be attained for the final vulcanizates. The amount of silica incorporated depends mainly on the pre-cure time, amount of APS used and drying temperature. When compared to a conventional ENR-sulfur-cured silica vulcanizate (at 27% commercial silica content, no silane coupling agent), the ENR–APS sol–gel vulcanizate at the same amount of silica has higher tensile properties as shown in Table 7.1. Comparative DMA on the two vulcanizates observed that the storage modulus in the rubbery region up to 50 °C is significantly higher for the sol–gel vulcanizate supporting the chemical bonding between silica and the rubber network.

Similar works on another grade of ENR, *i.e*. ENR 50, have also been carried out at various pH covering both acidic and basic conditions.[19–21] The rubber was first dissolved in various solvents (THF, $CHCl_3$ and CCl_4) and the solvated rubber was subjected to the sol–gel reaction, at the appropriate pH, at TEOS to water ratio of 1:2 and 45% weight of TEOS in relation to the rubber. Both uncured and cured systems were investigated. Depending on the processing conditions, about 11–18 wt% silica could be incorporated into the rubber. pH 2 gave nanoparticles of <100 nm in the resultant ENR–silica composites. A maximum tensile strength of about 5 MPa was obtained when THF was used while the elongation at break was found to be $>900\%$. A more detailed study by the same authors[19] using DMA indicated that the sol–gel silica-filled ENR has higher filler–matrix interaction in the form of polymer-coated silica particles, as shown in Scheme 7.4.

Using pre-cured rubber for the *in situ* sol–gel silica process limits the thickness of the samples for homogeneous loading of *in situ* silica. It is also not practical for industrial applications in terms of forming and shaping the desired products. An alternative and practical method in preparing *in situ* sol–gel silica–rubber composites was introduced where uncured rubbers were used.[22] In this approach, the sol–gel reaction of TEOS introduced the silica nanoparticles in the unvulcanized rubbers by swelling gum NR sheets in TEOS, followed by sol–gel reaction in aqueous *n*-butylamine solution and appropriate drying. Finally, the *in situ* silica–rubber was compounded using a typical sulfur recipe, but without any silane coupling agent, and subsequently heat pressed to prepare the rubber vulcanizates as usual.

Scheme 7.5 summarizes the preparation method of sol–gel silica-filled NR vulcanizate as described. Compared to conventional NR–silica at 30 phr of silica, the sol–gel silica–NR compound has a much shorter Mooney scorch and cure time (t_{90} at 150 °C). It is also noticeable that the NR sol–gel vulcanizate has a lower hysteresis and is stiffer showing higher M100, M300 and Shore A hardness but lower tensile strength and elongation at break as expected. Scanning electron microscope (SEM) and atomic force microscope (AFM) observations suggest that although the average particle size is larger, the NR sol–gel vulcanizate has a better dispersion of silica particles.

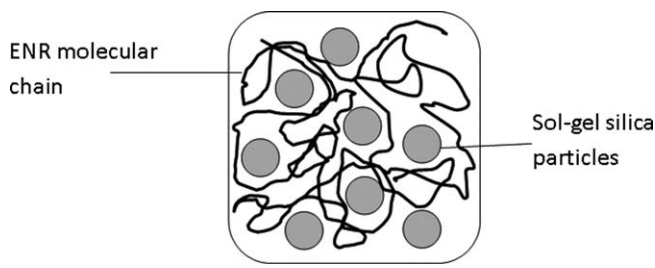

Scheme 7.4 Schematic diagram of filler–matrix interaction in the polymer-coated silica particles (adapted from ref. 20).

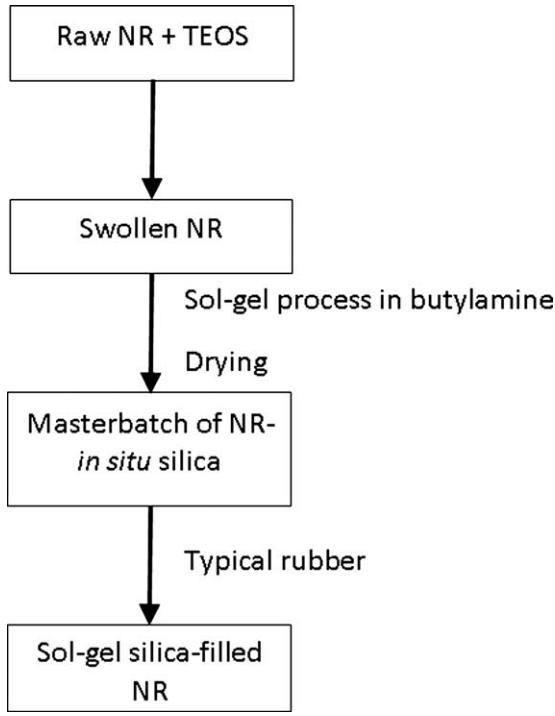

Scheme 7.5 Preparation of sol–gel silica-filled NR (adapted from ref. 22).

An extended study by the same research group[23] investigated the effect of γ-mercaptopropyltrimethoxysilane (γ-MPS) on the NR sol–gel vulcanizates also in comparison with conventional NR-silica. The *in situ* sol–gel silica was also found to be more homogenously dispersed in its matrix, ca. 20–45 nm in diameter of the silica particles, as substantiated by morphology analysis obtained from transmission electron microscopy (TEM) and AFM. Compared to the conventional NR–silica at 21% of silica content, the NR sol–gel silica is quite comparable in terms of the tensile properties. Its hardness, compression set hysteresis loss and storage modulus, however, are lower. Other similar works have been reported with similar findings.[24–26] By controlling the NR-TEOS's degree of swelling and the concentration of *n*-butylamine solution, different amount of sol–gel silica, up to 42 phr, could be incorporated into the rubber with particle size ranging from 10 nm to 40 nm. Compared to conventional NR–silica with the same silica content, the sol–gel silica–NR can achieve comparable tensile modulus at lower degree of deformation, higher tensile modulus at higher degree of deformation and comparable tensile strength. Consistently, the latter has more homogenous silica dispersion regardless of the amount of silica and significantly lower hysteresis loss.

The effect of three different amine catalysts, *i.e.* *n*-hexylamine, *n*-heptylamine and *n*-octylamine and their concentration on sol–gel silica–NR vulcanizate using uncrosslinked NR matrix has also been investigated.[27] *n*-hexylamine was found to

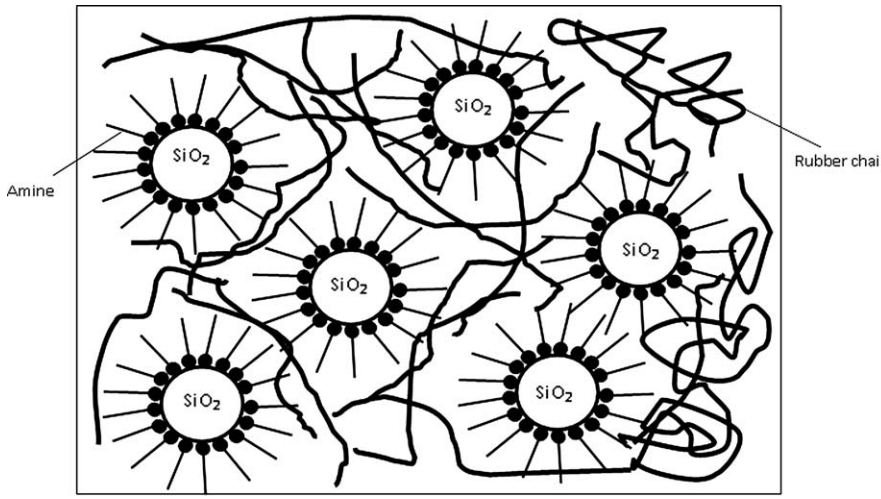

Figure 7.1 Schematic diagram representing sol–gel silica-NR in the presence of *n*-hexylamine (adapted from ref. 27).

the most effective due to its higher solubility in water. The amount of silica content increases with the increase in concentration of the amine giving a more homogeneous dispersion, compared to conventional silica–NR. Up to 78 phr of silica could be incorporated into the matrix with an average particle size of lower than 50 nm. The effectiveness of *n*-hexylamine can be visualized in Figure 7.1 in terms of achieving less filler–filler interaction and homogeneous dispersion. The amine is postulated to act as 'surfactant', separating the silica particles from each other.

A similar sol–gel process method, via NR rubber solution, was also conducted to study the effect of *in situ* silica content, which was varied from 15 to 65 phr, on the cure characteristics and mechanical, dynamic mechanical and thermal properties of the silica–NR nanocomposite.[28] Both the Mooney viscosity and cure time of the sol–gel silica–NR compound increased with increasing silica contents and were lower than those of the commercial silica-filled NR compound at the same amount of silica. This is attributed to the fewer amounts of silanol groups in the sol–gel silica as compared to the commercial silica. Better reinforcement of the *in situ* silica, compared to the normal silica, was confirmed when higher moduli and improved compression set were observed for the sol–gel silica–NR vulcanizate. This observation is consistent with the Guth and Gold equation as well as the TEM micrographs results. The sol–gel silica vulcanizate has lower storage modulus but better thermal stability then the commercial silica vulcanizate.

7.3 NR/Silica Nanocomposites *via* the Latex System

As previously described, silica can be incorporated into NR by sol–gel process where the solid rubber (cured or uncured) is immersed in TEOS followed by the sol–gel reaction. Alternatively, TEOS could be added directly into NR latex.[29]

This method allows the sol–gel silica–NR latex compound to be moulded into the desired shape. TESPT was co-mixed with TEOS and concentrated NR latex. Ammonia which functioned as base catalyst was added into the concentrated NR latex. The silica–TESPT–NR latex compound was then subjected to heat to complete the sol–gel silica conversion process. The dried sol–gel silica–NR mixture was compounded as per normal mixing procedure. A good dispersion of silica particles of the size between 100 and 500 nm was achieved. Using the two-level factorial design, it was concluded that the mechanical properties, *i.e.* tensile properties and tear strength, were significantly affected by the TEOS loading. It was also found that the amount of ammonia present in the concentrated latex, *i.e.* 0.7% (w/w) was sufficient to convert TEOS into silica.

Kiatkamjornwong and coworkers[30] later used a similar method to study the effect of the mixture of TEOS and non-sulfur-containing alkyltriethoxysilanes, *i.e.* vinyltriethoxysilane (VTOS), ethyltriethoxysilane (ETOS) and iso-butyltriethoxysilanes (BTOS) on the cure characteristics, swelling and mechanical properties of the sol–gel silica-filled NR latex. The study showed that only VTOS–TEOS mixture of 20/80 gave the highest silane–TEOS to silica conversion compared to the other two mixtures; the vinyl group in VTOS, which is more polarized than the ethyl in ETOS, resulted in better compatibility with the system while the presence of an iso-butyl group in BTOS partially inhibits the sol–gel process resulting in the lowest silane–TEOS to silica conversion. SEM and TEM revealed the *in situ* formed silica was well dispersed and the size as measured by TEM was less than 100 nm. The size of the *in situ* formed silica was not affected by using the three alkyltriethoxysilanes. Combination of TEOS and alkyltriethoxysilanes used showed no impact on the swelling index measured. However, the TEOS–VTOS combination showed better tensile modulus and tear resistance compared to the other two alkyltriethoxysilanes.

Recently, NR latex reinforced with silica aerogel was studied by Hamdan and coworkers,[31] focusing on thermal and mechanical properties; the silica aerogel was prepared from rice husk. In preparing the film, the silica aerogel was synthesized from rice husk by calcination of rice husk at 700 °C to obtain rice husk ash (RHA). Sodium silicate, the silica precursor was then obtained from the mixture of RHA, sodium hydroxide and water after 2-day stirring. The sodium silicate was then subjected to a gelation process for 48 h in the presence of sulfuric acid as catalyst. The aquagel obtained was then washed with distilled water and adjusted to pH 6 prior to conversion to alcogel. The alcogel was then subjected to supercritical drying in ethanol at 239 °C and 1200 psi. The silica aerogel obtained was then ground and dispersed in a ball mill. The synthesis of silica aerogel is summarized in Scheme 7.6. Curatives and the silica aerogel, loading 0 to 6 phr, were then compounded via a typical latex compounding method. In general, better tensile strength, tensile modulus and tear strength were reported for the NR latex–silica aerogel due to better interaction between the silica aerogel and NR latex molecular chains. The optimum loading reported was at 4 phr based on the mechanical properties studied. Thermal analysis revealed that the glass transition of silica aerogel filled-NR latex film was elevated by 3.78 °C compared to the unfilled version.

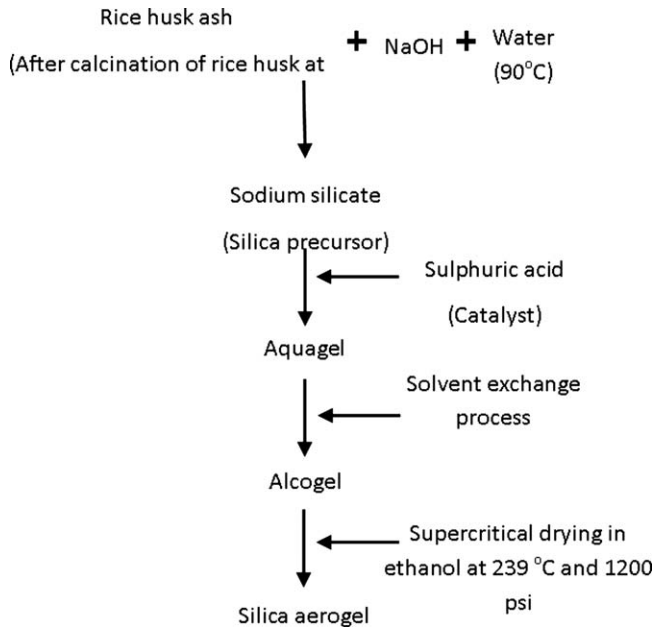

Scheme 7.6 Summary of silica aerogel synthesized from rice husk.

The thermogravimetric analysis suggested that the presence of the silica aerogel increased the absorption of energy during decomposition. Its noteworthy that the silica aerogel produced is in the range of 10–30 nm with the surface area of 402 $m^2/g \pm 5\%$ and the TEM micrgraph showed the existence of a core–shell structure of NR latex-silica aerogel.

Prasertsri and Rattanasom[32,33] used an innovative approach in compounding precipated and fumed silica to obtain silica-reinforced NR composites. In their study, precipated and fumed silica were added into NR latex to make silica–latex suspensions. A good dispersion of fumed silica was obtained by using either ultrasonic bath or agitator bead mill, *i.e.* 210 nm and 200 nm, respectively, in particle size. For precipitated silica, only agitator bead mill gave a well dispersed silica suspension where the particle size was noted to be 200 nm. After drying, SEM analysis of the dried silica–NR masterbatches showed the silica particles were still well distributed and dispersed. The losses of silica in the master batches were reported to be less than 1 phr even at silica loading of 30 phr. The dried precipated silica–NR and dried fumed silica–NR masterbatches were then compounded with curatives via a typical dry rubber compounding method. The study also showed that, by increasing the silica content from 10 to 30 phr, the compound viscosity and onset of crosslinking, and the stiffness of the silica–NR vulcanizate, tend to increase. Comparatively, the fumed silica resulted in higher surface area which leads to higher tear strength and thermal ageing resistance of the vulcanizates but, adversely, higher compound viscosity, heat build-up, compression set, rolling resistance and lower resilience. The dynamic properties, however, can be further improved with the addition of TESPT.

Peng and coworkers[34,35] developed a novel NR–silica nanocomposite by combining self-assembly and latex-compounding techniques. Here the negatively charged silica nanoparticles which act as template adsorb the positively charge poly (diallyldimethylammonium chloride) (PDDA). The negatively charged NR latex particles then assembled onto the surface of silica/PDDA nanoparticles. Finally the NR/silica nanocomposite was formed by post drying where the silica average size ranged from 60 to 150 nm at silica loading of less than 6.5 wt%. It is interesting to note that when the silica contents were ≤ 4 wt%, core shell structure was formed and only primary aggregations of silica were reported. However, at higher silica loading, secondary aggregation of silica was observed and the size of silica cluster increased dramatically. As the silica loading increased up to 4 wt%, better thermal and thermo-oxidative ageing resistance, tensile properties and tear strength were reported.

7.4 NR/Silica Nanocomposites *via* Modified Silica

For NR nanocomposite filled with silica, it has always been known that the hydrophilicity–hydrophobicity issue is a challenge since silica is hydrophilic and NR is hydrophobic. The usual method to overcome this issue is by adding coupling agent. In 1987 Wu and coworkers[36] introduced admicellar polymerization where a thin polymeric film will be formed on the silica's surface. This process yields a thin film of polymer on the silica which can further enhance the adhesion between the surfaces of silica and rubber.[37–39] The steps involved in admicellar polymerization are outlined in Scheme 7.7. In principle, a bilayer of surfactant, *i.e.* the admicelle, is first formed on the surface of the silica. Monomer will then penetrate the admicelle, *i.e.* the adsolubilization of monomer. Upon addition of initiator to the reaction system, *in situ* polymerization occurs in the admicelles. Finally, the surfactant is removed by washing with water and an ultrathin polymer layer is formed on the surface of the silica. The polymerization of the monomer in the admicelles can be induced by thermal process, chemical initiators or radiation.[40–42]

Table 7.2 summarizes recent works reported on silica admicellar polymerization of polyisoprene. The silica modified by admicellar polymerization was reported by researchers as having superior performance compared to those reinforced with unmodified silica or silica modified with typical silane coupling agents.[43] Studies also showed that the use of surfactant can influence performance of the rubber composite.[41]

Another approach of chemical modification of silica for rubber nanocomposite for the same aim, *i.e.* to reduce the filler–filler interaction, is differential microemulsion polymerization. In general, the process involves two main continuous steps: (i) pre-treatment/chemical bonding of silica particles with coupling agent, and (ii) polymerization of the monomer in a reaction medium containing the pre-treated silica. The resultant product is a core–shell structure where nano-silica is the core encapsulated by a nanopolymer shell.

Polystyrene (PS)-encapsulated nano-silica has been prepared via the microemulsion polymerization technique.[44] The PS-encapsulated silica was blended with NR, both in latex form, to finally prepare the NR nanocomposite sheets.

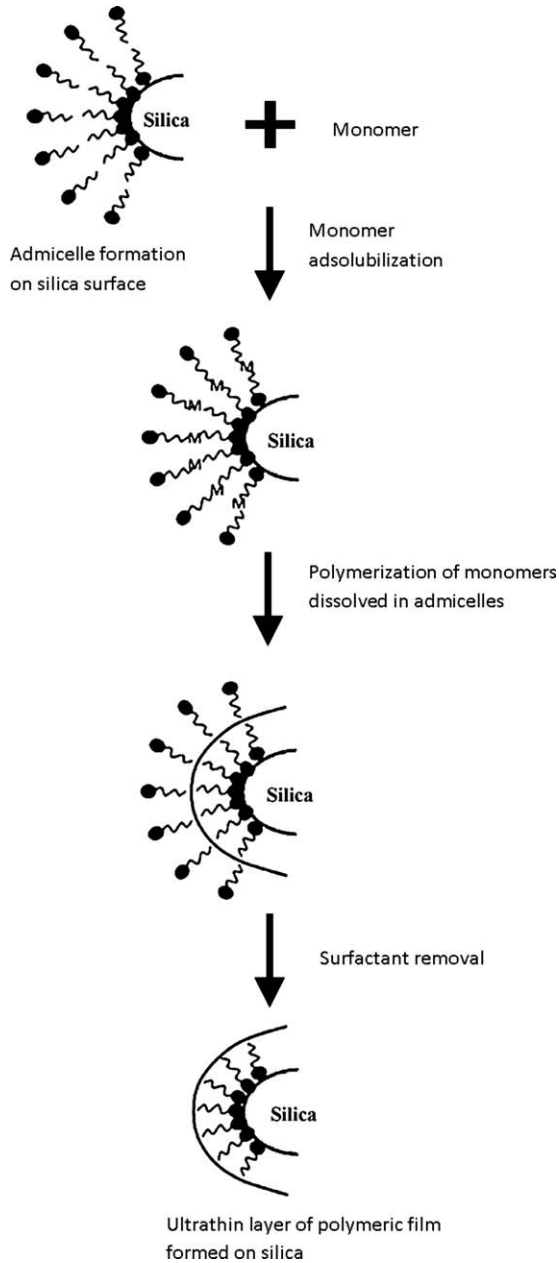

Scheme 7.7 Schematic diagram representing steps involved in admicellar polymerization (adapted from ref. 41).

The silica particles formed had an average diameter of 40 nm. Improvements in tensile strength, modulus at 300% strain and flammability as well as higher elasticity near the glass transition temperature were observed. The elongation

Table 7.2 Summary of some silica modified via admicellar polymerization in NR- or polyisoprene-based nanocomposites.

No.	*Focus of the study*	*Key findings*
1	1. A comparative studied on the radiation-induced admicellar polymerization with the traditional thermal process.[41] 2. Influence of hydrocarbon chain length in 3 types of surfactants; dodecyl trimethyl ammonium bromide (DTAB), tetradecyl trimethyl ammonium bromide (TTAB) and cetyl trimethyl ammonium bromide (CTAB)	1. The results showed that with an optimum dose of radiation; *i.e.* 8 kGy can lead to a better film formation on silica as compared to the thermal method. 2. Sample modified by CTAB showed highest degradation rate, followed by those modified with DTAB and TTAB for both thermal- and radiation-induced admicellar polymerization. 3. TEM revealed that the unmodified silica agglomerated in polyisoprene; better dispersion was observed in both thermal- and radiation-induced admicellar polymerization. The silica prepared in both thermal- and radiation-induced admicellar polymerization using the 3 types of surfactants are smaller than 100 nm. 4. CTAB is shown to be the most effective surfactant for modifying the silica surface via admicellar polymerization.
2	1. Effects of silica modified by radiation- and thermal-induced admicellar polymerization on the mechanical properties; *i.e.* tensile properties and tear strength of the reinforced polyisoprene were compared with those of the typical silica filled polyisoprene with and without TESPT.[41] 2. Effect of 3 different type of surfactants; cetyltrimethyl ammonium bromide (CTAB), dodecyltrimethyl ammonium bromide (DTAB) and tetradecyltrimethyl ammonium bromide (TTAB); to silica modified by both thermal admicellar polymerization and radiation induced admicellar polymerization.	1. Tensile properties and tear strength are superior in polyisoprene reinforced with modified silica modified by both admicellar were superior to those of typical silica filled polyisoprene with and without TESPT. 2. SEM carried out before and after mechanical test also revealed that the both silica modified with radiation- and thermal-induced admicellar polymerization showed no separation of the silica particles from the matrix which suggest that good adhesion between the matrix and filler. 3. CTAB proved to be the most effective surfactant, compared to DTAB and TTAB in polyisoprene filled with silica modified by admicellar polymerization.
3	1. Polyisoprene-coated silica was prepared by admicellar polymerization technique.[42] 2. The polyisoprene-coated silica was then function as filler in NR vulcanizate. 3. The abrasion resistance, tensile properties, tear strength and hardness was determined.	1. SEM, FTIR and TGA characterization on the modified silica confirm the success of the modification process. 2. Shorter cure time was obtained from NR vulcanizate filled with polyisoprene-coated silica as compare to the unmodifed silica. This is because the silica surface had been coated with polyisoprene and thus making it surface less chemical reactive and subsequently reduce the amount of the trapped accelerators and activator. 3. NR filled polyisoprene-coated silica showed better tensile strength, 300 % modulus and abrasion resistance due to better filler-rubber interation which was confirmed by SEM. However lower elongation at break, tear strength, hardness and specific gravity were also observed.

at break, however, was poor. The higher elasticity reported was due to the semi-interpenetrating nanostructure in the NR nanocomposites.

A recent study on the synthesis of polyisoprene–silica nanoparticles, based on pre-treated silica with some coupling agents, via differential microemulsion polymerization should be noted.[45] The core–shell morphology was confirmed with particle size ranging from 20 to 60 nm by TEM observation. The polyisoprene–silica latex was added into NR latex while stirring followed by the addition of curatives. The final polyisoprene–silica NR nanocomposites were obtained by casting and appropriate drying. The composites displayed significant improvement in tensile strength, tensile modulus, storage modulus and anti-ageing properties.

7.5 Opportunities in NR and Natural Resource-Based Silica Nanocomposites

NR is one of the world's important natural resources and silica is considered environmentally friendly upon disposal. Thus, in terms of sustainability development, development of silica-filled NR nanocomposites opens new opportunities for producing green materials/products such as tyres. Traditionally, carbon black is preferred over silica as filler in tyres due to the challenge in dispersing silica in rubber compounds. With the new development, *e.g. in situ* sol–gel silica, admicellar polymerization and polymer-encapsulated silica, the applications of nano-silica in NR and modified NRs are widened.

In terms of green composite or bio-composite, the sol–gel silica can be applied to natural fibres. An earlier work reports the generation of silica into the voids of kenaf fibre[46] about 20% of nano-silica could be incorporated into the fibre. Figure 7.2 showed the incorporation of sol–gel silica in the void of kenaf fibres. The kenaf sol–gel silica mixture could be used to prepare bio-composites or green composites by choosing the right polymer matrices.

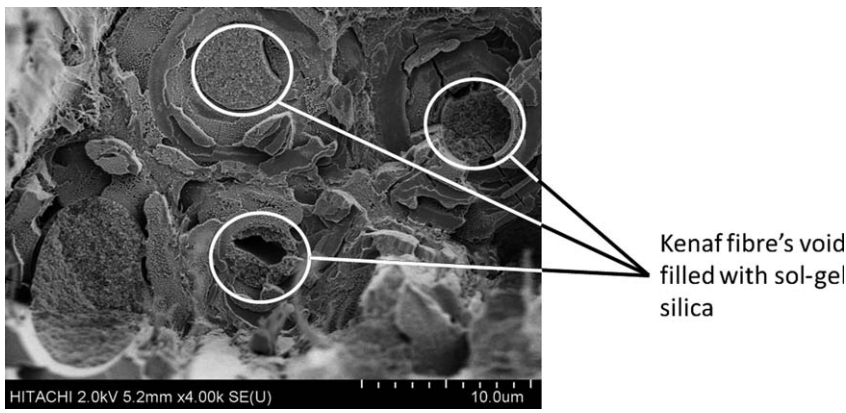

Figure 7.2 SEM showing the presence of sol–gel silica in the void of kenaf fibre.

References

1. M. Wagner, *Rubber Chem. Technol.*, 1976, **49**, 703.
2. N. Hewitt, in *Compounding Precipitated Silica in Elastomers*, N. Hewitt, William Andrew Publishing, New York, 2007, Chapter 2, pp. 25–167.
3. B. Rodgers and W. Waddell, in *The Science and Technology of Rubber*, ed. J. E. Mark, B. Erman and F. R. Eirich, Elsevier Academic Press, New York, 3rd ed., 2005, Chapter 9, pp. 421–427.
4. C. Hepburn, *Plast. Rubber Int.*, 1984, **9**, 11.
5. J. E. Mark, *J. Appl. Polym. Sci.: Appl. Polym. Symp.*, 1992, **50**, 273.
6. J. E. Mark, in *Science of Ceramic Chemical Processing*, ed. L. L. Hench and D. Ulrich, Wiley-Interscience, New York, 1986, Chapter 47, pp. 434–454.
7. J. E. Mark and C-C. Sun, *J. Polym. Sci., Part B: Polym. Phys*, 1987, **25**, 1561.
8. A. Yajima, Y. Ikeda, J. R. Yoon and S. Kohjiya, Paper presented at the *6th Meeting of the Society of Rubber Industry*, The Society of Rubber Industry, Japan, 1992.
9. A. Hashim, N. Kawabata and S. Kohjiya, *J. Sol-Gel Sci. Technol.*, 1995, **5**, 211.
10. J. E. Mark and S. J. Pan, *Makromol. Chem,: Rapid Commun.*, 1982, **3**, 681.
11. Y. Ikeda and S. Kohjiya, *Polymer.*, 1997, **38**, 4417.
12. M. Sugiya, K. Terakawa, Y. Miyamoto, S. Tomono, S. Kohjiya and Y. Ikeda, *Kautsch. Gummi Kunstst*, 1997, **50**, 538.
13. S. Kohjiya, A. Yajima, J. Yoon and Y. Ikeda, *Nippon Gomu Kyokaishi*, 1994, **67**, 859.
14. Y. Ikeda, A. Tanaka and S. Kohjiya, *J. Mater. Chem.*, 1997, **7**, 455.
15. Y. Ikeda, A. Tanaka and S. Kohjiya, *J. Mater. Chem.*, 1997, **7**, 1497.
16. A. Hashim, B. Azahari, Y. Ikeda and S. Kohjiya, *Rubber Chem. Technol.*, 1998, **71**, 289.
17. A. Hashim, S. Kohjiya and Y. Ikeda, *Polym. Int.*, 1995, **38**, 111.
18. A. Hashim and S. Kohjiya, *Polym. Gels Networks*, 1994, **2**, 219.
19. A. Bandyopadhyay, M. De Sarkar and A. K. Bhowmick, *J. Mater. Sci.*, 2005, **40**, 53.
20. A. Bandyopadhyay, M. De Sarkar and A. K. Bhowmick, *J. Polym. Sci., Part B: Polym. Phys.*, 2005, **43**, 2399.
21. A. Bandyopadhyay, M. De Sarkar and A. K. Bhowmick, *J. Mater. Sci.*, 2006, **41**, 5981.
22. K. Murakami, S. Lio, T. Tanahashi, S. Kohjiya, K. Kajiwara and Y. Ikeda, *Kautsch. Gummi Kunstst.*, 2001, **54**, 668.
23. K. Murakami, S. Lio, Y. Ikeda, H. Ito and M. K. S. Tosaka, *J. Mater. Sci.*, 2003, **38**, 1447.
24. Y. Ikeda and Y. Kameda, *J. Sol-Gel Sci. Technol.*, 2004, **31**, 137.
25. Y. Ikeda, *Kautsch. Gummi Kunstst*, 2005, **58**, 455.
26. S. Poompradub, S. Kohjiya and Y. Ikeda, *Chem. Lett.*, 2005, **43**, 672.
27. Y. Ikeda, S. Poompradub, Y. Morita and S. Kohjiya, *J. Sol-Gel Sci. Technol.*, 2008, **45**, 299.

28. B. Chaichua, P. Prasassarakich and S. Poompradub, *J. Sol-Gel Sci. Technol*., 2009, **52**, 219.
29. V. Tangpasuthadol, A. Intasiri, D. Nuntivanich, N. Niyompanich and S. Kiatkamjornwong, *J. Appl. Polym. Sci*., 2008, **109**, 424.
30. J. Siramanont, V. Tangpasuthadol, A. Intasiri, N. Na-Ranong and S. Kiatkamjornwong, *Polym. Sci. Eng*, 2009, **49**, 1099.
31. K. Ng, A. Abdul Rashid, M. Mohd Nazlan and H. Hamdan, *J. Appl. Polym. Sci*., 2011, **124**, 3108.
32. S. Prasertsri and N. Rattanasom, *Polym. Test*., 2011, **30**, 515.
33. S. Prasertsri and N. Rattanasom, *Polym. Test*., 2012, **31**, 593.
34. S. Li, Z. Peng, L. Kong and J. Zhong, *J. Nanosci. Nanotechnol*., 2006, **6**, 541.
35. Z. Peng, L. Kong, S. Li, Y. Chen and M. Huang, *Compos. Sci. Technol*, 2007, **67**, 3130.
36. J. Wu, J. Harwell and E. O'Rear, *J. Phys. Chem*., 1987, **91**, 623.
37. B. Kitiyanan, J. H. O'Haver, J. H. Harwell and S. Osuwan, *Langmuir*, 1996, **12**, 2162.
38. V. Thammathadanukul, J. O'Haver, J. Harwell, S. Osuwan, N. Na-Ranong and W. H. Waddell, *J. Appl. Polym. Sci*., 1996, **59**, 1741.
39. P. Nontasorn, S. Chavadej, P. Rangsunvigit, J. O'Haver, S. Chaisirimahamorakot and N. Na-Ranong, *Chem. Eng. J*, 2005, **108**, 213.
40. A. Bhattacharya, *Prog. Polym. Sci*., 2000, **25**, 371.
41. N. Yooprasert, T. Pongprayoon, P. Suwanmala, K. Hemvichian and G. Tumcharern, *Chem. Eng. J*, 2010, **156**, 193.
42. T. Pongprayoon, N. Yooprasert, P. Suwanmala and K. Hemvichian, *Radiat. Phys. Chem*., 2012, **81**, 541.
43. C. Poochai, P. Pae-on and T. Pongpayoon, *World Acad. Sci., Eng. Technol*, 2010, **65**, 969.
44. S. Chuayjuljit and A. Boonmahitthisud, *Appl. Surf. Sci*., 2010, **256**, 7211.
45. A. Kongsinlark, G. Rempel and P. Prasassarakich, *Chem. Eng. J*, 2012, **193-194**, 215.
46. M. Zulkifli, in 6th MPMA International Plastics Conference 2012, Malaysian Plastic Manufacturers Association (MPMA), Kuala Lumpur, 2012.

CHAPTER 8

Clay Reinforcement in Natural Rubber on Micro and Nano Length Scales

SANDIP ROOJ,*[a,b] AMIT DAS,[a]
KLAUS WERNER STÖCKELHUBER[a] AND
GERT HEINRICH[a,b]

[a] Leibniz-Institut für Polymerforschung Dresden e.V., Hohe Straße 6, D-01069 Dresden, Germany; [b] Technische Universität Dresden, Institut für Werkstoffwissenschaft, D-01069 Dresden, Germany
*Email: rooj@ipfdd.de; gheinrich@ipfdd.de

8.1 General Introduction

Rubber–clay nanocomposites have been of particular importance to several research groups during recent years because of their unique properties.[1–3] However, to achieve the excellent mechanical properties necessary for end-use application, rubbers have to be reinforced with some conventional filler such as carbon black (CB) or silica. In principle, 40–60% conventional filler (like CB, silica) is required to get the satisfactory level of reinforcement according to their final application. There are certain difficulties associated with these conventional filler reinforced rubbers for instance, mixing at such a high loading and final weight of the product, *etc*. Therefore, the concept of nanotechnology is highly relevant for rubber compounds since their application needs filler reinforcement.

RSC Polymer Chemistry Series No. 8
Natural Rubber Materials, Volume 2: Composites and Nanocomposites
Edited by Sabu Thomas, Hanna J. Maria, Jithin Joy, Chin Han Chan and Laly A. Pothen

Published by the Royal Society of Chemistry, www.rsc.org

However, commercial applications of rubber nanocomposites are yet to gain real momentum, since there are a few unresolved issues that necessitate to be resolved in order to the successful conversion of these novel materials into commercial artifacts. The biggest problem in the preparation of rubber–clay minerals nanocomposites is the difficulty of dispersion at higher loadings (above 5–7 phr), because beyond such critical loading most of the properties incline due to agglomeration of the nanoparticles. Nevertheless, since the layered silicates typically exist as aggregates due to strong attractive van der Waals forces, improvements in various physical properties do not attain theoretical expectations. Achieving nanocomposite with a highly exfoliated structure in which each individual nanolayer has been separated from its initial stack and dispersed uniformly throughout the polymer matrix is the key to grasp the full potential of the nanoclay to enhance various physical properties of a polymeric matrix.[4] Various studies have revealed that via appropriate surface chemistry design, it is possible to achieve excellent clay minerals dispersion as well as improved bonding between clay and polymer matrix.[5]

8.2 Clays and Layered Silicates

Of all clays, montmorillonite (MMT) is the most commonly used layered silicate in nanocomposite preparation due to its high cation exchange capacities, large surface area, good surface reactivity and surface adsorptive properties.[6] MMT belongs to the 2 : 1 family of phyllosilicate clay minerals, where each crystal layer is composed of a silica tetrahedral layer sandwiched between two octahedral sheets of aluminum and magnesium hydroxides. In MMT, the isomorphous substitution of Al^{3+} by Mg^{2+}, Fe^{2+}, *etc.* in the octahedral sheets results in a net negative charge in the sandwiched layers (Figure 8.1). As a result, cations (Na^{+}, K^{+}, *etc.*) and water molecules are intercalated in the interlayer region of MMT. The layer thickness is around 1 nm and the lateral dimensions of these layers may vary from 300 Å to several microns and even larger depending on the particular silicate.

8.2.1 Modified Clay

Addition of a small amount of nanofiller (for instance MMT) into the polymer matrix can improve various physical properties. But it is not an easy task. When polar nanofillers are mixed together with a non-polar polymer matrix one can certainly come up with a physical mixture of them. The physical mixture of a polymer and MMT may not form a nanocomposite. This situation is comparable to polymer blends, and in most cases separation into discrete phases takes place.

In this chapter we have divided modified clays in two different types namely organomodified montmorillonite (OMt) and expanded organomontmorillonite (EOMt). The effect of these clay particles in NR matrix will be discussed elaborately in the forthcoming section.

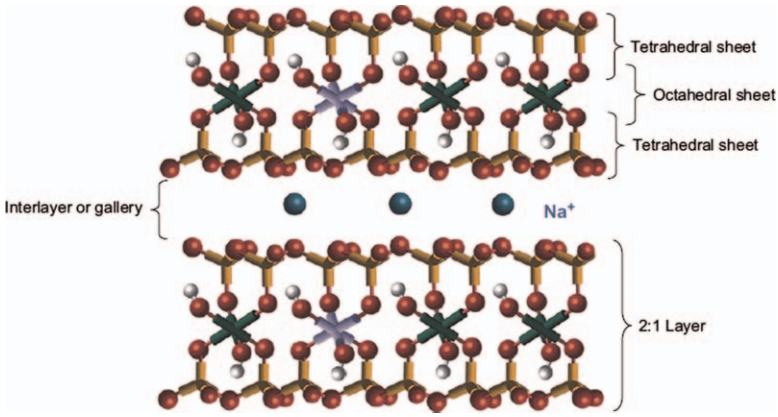

Figure 8.1 Crystalline structure of montmorillonite (MMT) clay.[6] (Reproduced with permission of Elsevier Ltd.)

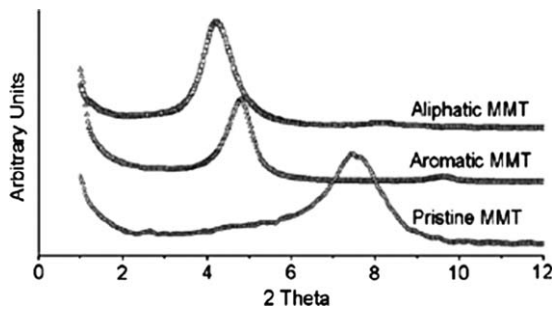

Figure 8.2 XRD spectra of different MMTs.[7] (Reproduced with permission of Elsevier Ltd.)

8.2.1.1 Organomodified Montmorillonite

In general, pristine MMT contains hydrated Na^+ or K^+ ions. Therefore, they are only miscible and compatible with polar polymers. In order to make it compatible with hydrophobic polymers, the interlayer cations are exchanged with quaternary alkylammonium cations through ion-exchange reaction. Ion-exchange reactions can be done with several cationic surfactants including primary, secondary, tertiary, and quaternary alkylammonium or alkylphosphonium cations.[6]

Two quaternary phosphonium salts (aromatic and aliphatic) have been used as intercalants for Na^+-MMT, as reported by Avalos *et al.*,[7] and the effect of intercalant structure on clay morphology and natural rubber (NR) vulcanization kinetics was investigated. A higher interlayer space was achieved with aliphatic intercalant and the corresponding diagram is given in Figure 8.2.

Di Gianni *et al.*[8] have reported the modification of commercial clay containing a hydroxylated ammonium ion (commercially known as Cloisite® 15)

Table 8.1 Data obtained from XRD and contact angle measurement.[8] (Reproduced with kind permission of John Wiley & Sons.)

Sample	$d_{001}(nm)$	*Contact angle of* H_2O (°)
Cloisite® 30B	1.8	60
A3	14.0	102
A4	6.9	107

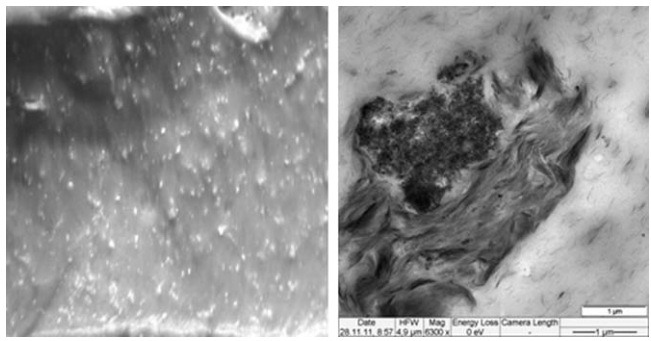

Figure 8.3 (a) Photomicrograph of NR-OMt nanocomposites. (b) TEM image of NR-OMt nanocomposites.
(Reproduced with permission of John Wiley and Sons.)

with maleinized polybutadienes (PBs, Lithene N4-5000-2.5 MA and Lithene PM-7.5 MA, labelled PB3 and PB4). Modification of clay was confirmed with the help of XRD, contact angle measurement and TGA study. Table 8.1 shows the different characteristics of MMT and OMt. The values of contact angles indicate a strong enhancement of the hydrophobicity of the clay after the maleinization treatment.

The interlayer distance in the pristine silicate (1.8 nm) remarkably increases, reaching a value of 14 nm for A3 (PB3 modified Cloisite® 30B) and about 7 nm for A4 (PB4 modified Cloisite® 30B). These values indicated the intercalation of the maleinized PB chains between the clay galleries and also support the presence of nearly exfoliated structures. In particular, the higher interlayer distance observed in sample A3 with respect to sample A4 was attributed to its higher content of PB.

8.2.1.2 Expanded Organo-Montmorillonite

Most of the earlier efforts have been paid in changing the surface character of clay minerals. Albeit the modified clay minerals are fairly compatible with the polar rubber like acrylonitrile butadiene rubber (NBR), carboxylated nitrile rubber (XNBR), chloroprene rubber (CR), *etc*., its dispersion in non-polar rubbers like NR, styrene butadiene rubber (SBR), ethylene propylene diene rubber (EPDM), butadiene rubber (BR), *etc*. is rather unsatisfactory.[9–15] Figure 8.3(a) and (b) display the state of dispersion of organomodified

montmorillonite (OMt) in a non-polar NR matrix. Large agglomerates of OMt can be observed with the naked eye throughout the matrix, which is shown in the photomicrograph. Even in the transmission electron microscopy (TEM) micrographs, highly agglomerated structures of clay particles can be clearly observed.

It has been reported by Das *et al.*[16,17] that an additional amount of stearic acid has a beneficial effect on the intercalation/exfoliation process of MMT in different rubbers. They have revealed that stearic acid has a profound effect on the intercalation/exfoliation process of the OMt in the NBR matrix when a sulfur-curing package is chosen for the vulcanization of NBR. Stearic acid is a small molecule and it can easily move to the gallery gap in between two clay layers, and as a result it promotes the dispersion of the clay.

A representative scheme has been given in Figure 8.4 according to the common perception for exfoliation of OMt in a polymer matrix during the course of melt blending. The exfoliation of OMt takes place when the attraction (designated as f_1) between the OMt layers, generally known as the van der Waals force of attraction, is minimized. There are another two important factors, namely the interaction (designated as f_2) between polymer and OMt and the melt viscosity (labelled η_m) of the polymer matrix, respectively.

The former is related to the chemical structures of polymers and the modifiers, and the modifier content in the OMt subsequently has no importance in our study as we will be dealing with only one non-polar rubber matrix. Therefore, the prime goal was to develop a novel way to disperse such clay minerals in the non-polar rubber matrices by minimizing the van der Waals force (a type of electrostatic force) between the OMt layers. It is believed that in the case of short interlayer spacing the van der Waals forces are the predominant factor.[18] Therefore, it is essential to reduce the high electrostatic force (f_1) between the clay layers in preparing polymer nanocomposites. Many large molecules are not directly intercalated into the interlayer space but can be introduced by the 'propping-open approach'. A schematic illustration is given in Figure 8.5. This method was first introduced by Brindley and Ray in 1964.[19] Brindley and Ray were able to enhance the interlayer spacing of Ca^{2+}-Mt to a considerable extent by stepwise swelling with ethanol, hexanol and then octadecanol. Although this method was well known in the field of clay science it had

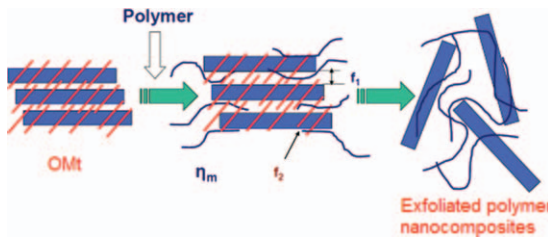

Figure 8.4 Scheme of exfoliation of OMt in polymers.

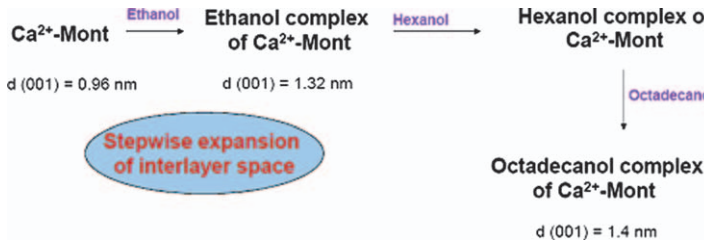

Figure 8.5 Schematic of the 'propping-open' procedure.

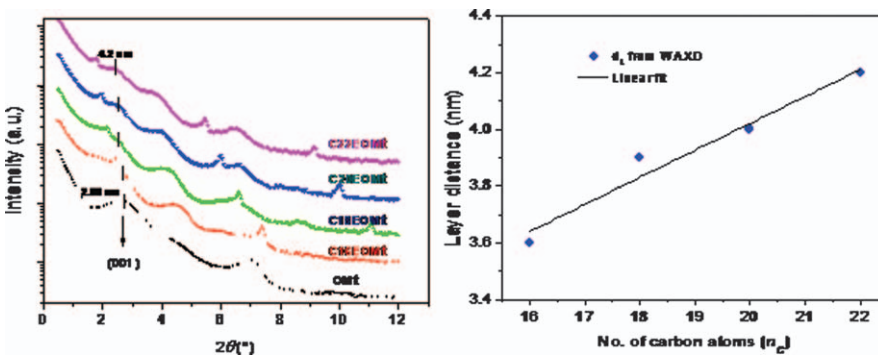

Figure 8.6 (a) WAXD patterns of EOMt. (b) Basal spacing as a function of the alkyl chain length of different fatty acids.
(Reproduced with permission of John Wiley and Sons and Elsevier Ltd.)

never been utilized in the field of polymer nanocomposites. Therefore, to utilize such nanostructured clay materials efficiently in a rubber matrix, this novel 'propping-open approach' was adopted.

Preparation and characterization of EOMt was first reported by Das *et al.*[20] Pre-intercalation of OMt was done by stearic acid. Stearic acid and OMt were taken in a porcelain mortar at a ratio of 1 : 1 by mass and well mixed by a pestle. The mixture was kept in an oven at 110 °C for 15 min. The mass was then cooled to room temperature and ground up again. This step was done several times to obtain a homogeneous mass. The resulting product was called 'expanded organo-montmorillonite' (EOMt).

Later, Rooj *et al.*[21,22] observed the effect of different long alkyl chain fatty acids on the intercalation behaviour of OMt. The wide-angle X-ray diffraction (WAXD) patterns of different EOMt are represented along with pure OMt in Figure 8.6(a). It was observed from Figure 8.6(a) that the *d*-basal spacing of the EOMt shifted to lower reflection angles compared to OMt. The highest extent of intercalation corresponding to the largest interlayer distance of 4.2 nm in C22-EOMt (compared to 3.6 nm for C16-EOMt) was obtained with C22 fatty acid. This indicated that the fatty acid with longer alkyl chains was beneficial to expand the interlayer space of MMT. A similar observation was reported by

Lagaly *et al.*[23] for organoclays modified with alkyl ammonium compounds of different alkyl chain length (C6-C18).

The shifting of all the diffraction maxima to lower 2θ was proportional to the size of alkyl chain of the fatty acids and indicated a linear relationship between basal spacing and the number of carbon atoms in the fatty acid alkyl chain, which is depicted in Figure 8.6(b). A rather good linear correlation ($R^2 = 0.94$) was observed between basal layer distance and the number of carbon atom (n_C) of the fatty acid. It is also interesting to note that the slope of the linear fit (0.10 nm) was very close to the expected value of the C–C bond length of fatty acids (0.15 nm). The small deviation was possibly attributed to the tilted structure of the fatty acid in the interlayer space of clay minerals.

A sharp peak appeared in the case of all EOMt at lower angles associated with the basal reflection of the clay layers. They attributed this observation to the crystallites of the corresponding fatty acids in the dimer form.[24] The size of the crystallites increased with the increase in chain length of the corresponding fatty acids. The quaternary ammonium compound (QUAT) previously present in the silicate nanogalleries of OMt, propping open the silicate layers further and paving the way for long chain fatty acids during melting. Furthermore, the presence of the long alkyl chains in the interlayer galleries reduces the hydrophilic character of these domains and draws the host fatty acid alkyl chains inside the clay galleries owing to the van der Waals force of attraction. It has been reported by Lagaly *et al.*[25] that in dried alkylammonium vermiculites the alkyl chains in paraffin-type arrangement are tilted to the silicate layer.

The interaction between OMt and different fatty acids was proved by FTIR spectroscopy. A new peak appeared at 1730 cm^{-1} (Figure 8.7), attributed to the strong interaction between the C=O group and interlayer cations via a water bridge, shown in Figure 8.7(b). A similar observation was reported by Yariv *et al.*[26] This indicates that fatty acid molecules intercalate the interlayer space of OMt and again supports the results obtained from WAXD patterns.

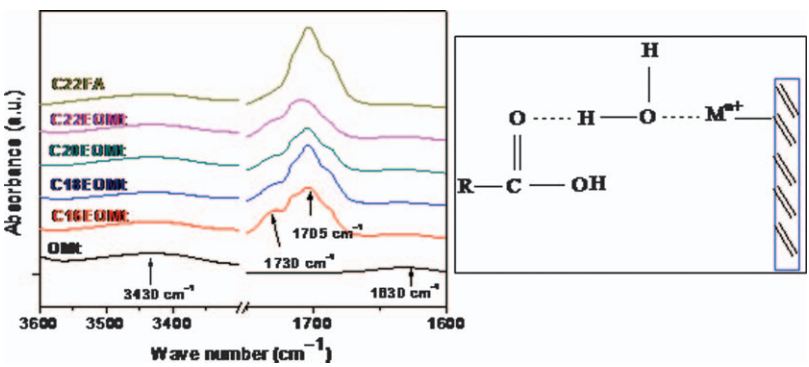

Figure 8.7 (a) FTIR spectra of EOMt in the region of 1780–1600 cm^{-1}. (b) Interaction between the C=O group of the fatty acid and interlayer cations via a water bridge.
(Reproduced with permission of John Wiley and Sons and Elsevier Ltd.)

8.3 Natural Rubber–Clay Nanocomposites

8.3.1 Natural Rubber–Organo-Montmorillonite Nanocomposites

8.3.1.1 Method of Preparation

At present there are four principal methods of producing NR–clay nanocomposites: melt mixing or compounding, *in situ* polymerization, latex blending and solution intercalation. Among the aforesaid methods, melt intercalation and *in situ* polymerization are considered as commercially attractive approaches for preparing so-called rubber–clay nanocomposites. The latex blending route is also promising for some rubbers available in aqueous dispersions (*e.g.* NR, because in this case pristine layered silicates can be used).[27–32] But the problem comes when considering many synthetic rubbers, because latex of these synthetic rubbers is not available commercially. There are also few reports on the preparation of rubber–clay nanocomposites and can be found based on solution intercalation technique.[33,34] Melt intercalation, in particular, is of particular practical interest because it presents significant advantages. The advantages of forming nanocomposites by melt processing are rather appealing, rendering this technique a promising new approach that would greatly expand the commercial opportunities for nanocomposite technology. If technically possible, melt compounding would be significantly more economical and simpler than *in situ* polymerization. It minimizes capital costs because of its compatibility with existing processes. That is, melt processing allows nanocomposites to be formulated directly using ordinary compounding devices such as extruders or mixers. Therefore, it shifts nanocomposite production downstream, giving end-use manufacturers many possibilities with regard to final product specifications (*e.g.* selection of polymer grade, choice of organoclay, level of reinforcement, *etc.*). At the same time, melt processing is environmentally friendly because no solvents are required; and it enhances the specificity for the intercalation of polymer, by eliminating the competing host–solvent and polymer–solvent interactions. The melt compounding method used for the preparation of rubber–clay nanocomposites is similar to that used for conventional polymer–clay nanocomposites. The organically modified clay is a suitable precursor for this process, which are mixed with molten polymer in the typical rubber processing equipment. Due to several advantages, most of the rubber–clay nanocomposites were prepared utilizing melt blending technique. The first effort was paid by Varghese *et al.*[35] who prepared NR–MMT nanocomposites using a melt blending technique in a two-roll mixing mill. Arroyo *et al.*[36] have also reported the preparation of NR–clay nanocomposites using a melt blending method. Carretero-Gonzalez *et al.* have reported the preparation of NR–clay nanocomposites using a melt-mixing technique in a two-roll mixing mill.[37] Very recently Chodak *et al.* have prepared NR–clay composites following a melt blending technique.[38]

8.3.1.2 Morphology and Physical Properties

Unlike polymer–clay nanocomposites, in rubber–clay nanocomposites complete exfoliation of clay layers results in disappearance of the diffraction maxima in their XRD patterns. However, this can also occur due to other reasons, like extremely low concentration of clay materials in the composites, crystal defects, *etc*. The majority of the reports on rubber–clay nanocomposites display the intercalated or swollen nature of the clay structures. The presence of the basal reflections in the XRD patterns of such type of nanocomposites indicates that the clay crystal structure is not destroyed completely. But, shifting of their positions to lower 2θ values is interpreted as an expansion of the interlayer region by the macromolecular rubber chains. Besides, broadening of the characteristic reflections in nanocomposites is often related to the defects in the crystal layer stacking caused by the interlayer polymeric species.

The first effective effort of the preparation of rubber–clay nanocomposites was paid by Vu *et al.*[33] which have attracted tremendous interest among the scientific community. They have prepared nanocomposites based on synthetic polyisoprene and epoxidized natural rubber (ENR) with the help of both melt mixing and solution intercalation technique. The clay was either a Na^+-MMT or OMt to make the galleries more hydrophobic and thus more compatible with the non-polar rubbers. The chemical modifications were carried out using an ion-exchange reaction with alkyl ammonium cations. The organically modified clays used in this work were bis-(2-hydroxyethyl) methyl tallow ammonium montmorillonite (C1), dimethyl dihydrogenated tallow ammonium montmorillonite (C2), and dimethyl hydrogenated tallow (2-ethylhexyl) ammonium montmorillonite (C3). X-ray diffraction results indicated intercalation of NR and ENR into the silicate interlayers, followed by exfoliation of the silicate layers into the elastomer matrices. But unfortunately, they did not show any morphological evidence to visualize the dispersion of clay minerals in rubber matrices by scanning electron microscopy (SEM) or transmission electron microscopy (TEM). They have also reported that NR vulcanizates with organically modified clay exhibits better tensile properties compared to the silica-filled vulcanizates attributed to the better polymer–filler interactions and weaker filler–filler interactions in the case of the modified clays. It has been observed that 10 phr loading; the C2 compound had better tensile properties than those of C1. The effect of dynamic strain amplitude on the storage modulus revealed that storage modulus of the compound ENR50 (50 mol% epoxidation) with Na^+-MMT was higher in comparison to that of the compound with Hi-Sil (silica) possibly due to a greater hydrodynamic reinforcement as a result of melt intercalation of the rubber in the Na^+-MMT galleries. Further, with an identical Na^+-MMT loading, storage modulus of ENR50 was greater than that of ENR25 (25 mol% epoxidation) and this can be attributed to the stronger rubber–filler interactions in the more polar ENR50. The storage modulus increased with increasing filler loading. However, the storage modulus of NR and the cited

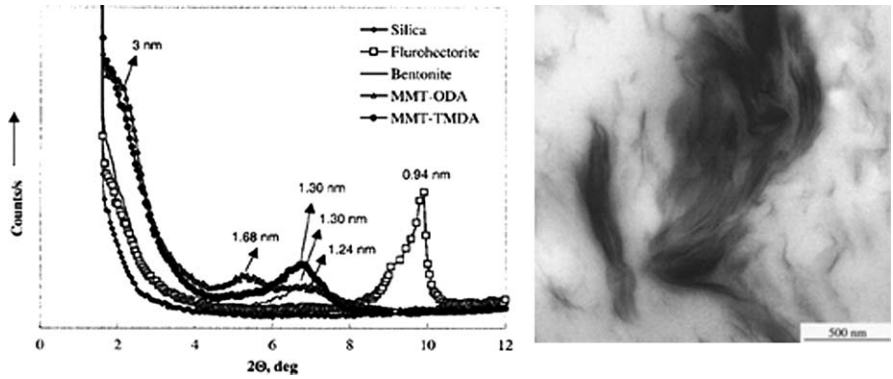

Figure 8.8 XRD and TEM of different NR nanocomposites. (Reproduced with permission of John Wiley and Sons.)

networking effects were much smaller than were those for the polar epoxidized rubber compounds.

Composites based on NR and organoclay were produced and reported by Varghese *et al.*[35] adopting melt compounding technique. Clay surfaces were modified using primary amine (denoted as MMT-ODA) and quaternary amine (denoted as MMT-TMDA). The organoclay content was 10 phr. The partial intercalation of macromolecular NR chains into the interlayer space of MMT was evidenced by XRD and TEM (Figure 8.8). The interlayer spacing of NR/MMT-ODA was higher than that of NR/MMT-TMDA. The property improvements caused by the fillers were ranked as follows: organophilic clays > pristine synthetic layered silicate (sodium fluorohectorite) > pristine natural clay (purified sodium bentonite) > precipitated non-layered silica (used as a reference).

In a study by Modhusoodanan *et al.*,[39] nanocomposites based on NR and organomodified clay were produced by melt-mixing technology. The dispersion of these silicates was studied by XRD and TEM (Figure 8.9). The greatest interlayer distance (3 nm) was observed in the case of OMt-filled NR nanocomposites.

The addition of OMt into the NR decreased both cure time and scorch time of the compounds, while much change is not observed compared to NR gum compound in the case of bentonite and English Indian clay (EIC). High Mooney viscosity values revealed that intercalation occurred during mixing of the silicate into the rubber. Mechanical properties such as tensile strength, modulus, hardness, abrasion resistance, tear strength, *etc.* of NR improved in the presence of organoclays, even at low loading. The improvements in the mechanical properties of the organosilicates are due to the exfoliation of the silicates, which causes a several-fold increase in surface area.

Very recently, the influence of nanoclay on the morphological and microstructural changes of NR networks has been reported by Carretero-Gonzalez *et al.*[37] The molecular structure of the polymer network and its morphological

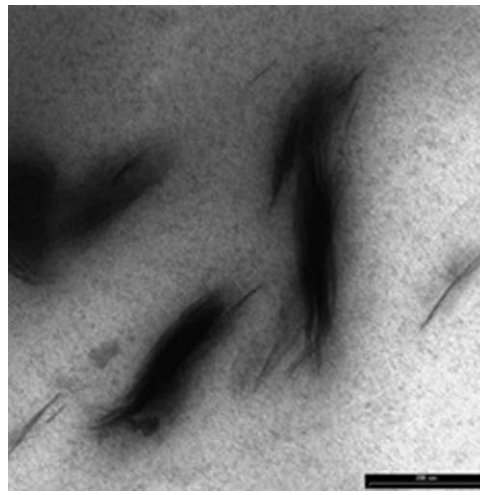

Figure 8.9 Morphological analysis of NR–OMt nanocomposites.[39] (Reproduced with permission of John Wiley and Sons.)

changes during deformation were characterized using broadband dielectric spectroscopy and *in situ* synchrotron WAXD, respectively. It was found that the presence of nanoclay introduces a dual crystallization mechanism due to the alignment of nanoparticles during stretching. The improved properties in NR–nanoclay nanocomposites can be attributed to both microstructural and morphological changes induced by nanoclay as well as to the nanoclay mobility in the NR matrix during crystallization.

Carretero-Gonzalez *et al.*[40] have also studied the effects of nanoclay on the microstructural network, topological constraints and non-elastically active components of NR with the help of broadband dielectric spectroscopy. In this study *cis*-poly(isoprene) was viewed as a model system to study the dynamics of relaxation modes of entangled or dilute NR and dry crosslinked rubber networks since *cis*-poly(isoprene) exhibits two relaxations (Figure 8.10). One is related to the segmental motion (known as segmental mode) and a slower one related to the relaxation of whole chains (known as normal mode). In general, the normal mode disappears after crosslinking attributed to the suppression of large-scale motions of the dipole oriented parallel to the polymer backbone. It is interesting to observe that the vulcanized NR exhibits an intense relaxation $\sim$237.5 K, associated with the segmental mode, accompanied at lower temperatures by another relaxation though of lower intensity. No substantial changes in the relaxation behaviour were observed in the presence of organoclay. This shows that the segmental motion of *cis*-poly(isoprene) is not hindered in the presence of organoclay and consequently, both samples retain similar glass transition temperature. However, the NR organoclay nanocomposite exhibits a slower relaxation at higher temperatures ($T \sim 325$ K) due to rubber–organoclay interaction which they termed as Maxwell–Wagner–Sillars (MWS) process. In this study the appearance of slower relaxation was conjectured as a

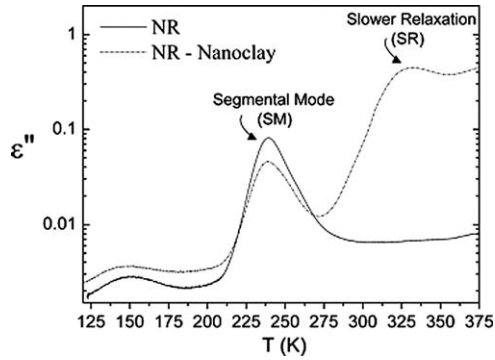

Figure 8.10 The temperature dependence of ε'' (at 1×10^3 Hz) for the unfilled and nanocomposite NR samples after crosslinking. For vulcanized NR the main process is associated with the segmental mode (SM). For the nanocomposite an additional slower relaxation (SR) appears at higher temperatures.

consequence of the interaction of the rubber chains with the clay surfaces inducing a slower segmental mode with a new effective T_g of $\sim$90 K higher than in the neat polymer (*i.e.* in the absence of the clay).

The effectiveness of organoclay in NR was observed and reported by Carli *et al.*[41] They evaluated the technical feasibility of NR nanocomposites with Cloisite® 15A, a commercial organoclay to substitute conventional silica (SiO_2) filler. TEM analysis indicated that the OMt was homogeneously dispersed in the rubber matrix. A shift of the characteristic peaks to lower angles was observed in XRD, attributed to the intercalation of the OMt by macromolecular rubber chains. Based on the mechanical properties of the compounds they concluded that 50 phr of silica can be replaced by 4 phr of OMt with a reduction in the filler content by 12.5 times, without adversely affecting the tensile properties of the final material even after ageing.

8.3.2 Natural Rubber–Organo-Montmorillonite Nanocomposites in the Presence of External Compatibilizers

Much effort has gone into preparing rubber–clay nanocomposites based on NR as described in the earlier section. However, the dispersion of such nanoclays in non-polar NR matrices was very poor. In this section we would like to outline the preparation and characterization of NR–clay nanocomposites in the presence of certain compatibilizers added into the system externally. For instance, Teh *et al.*[42] prepared NR–OMt nanocomposites by a melt compounding method. ENR 25 and ENR 50 were used as compatibilizers. Pristine MMT was modified with octadecyltrimethylamine and abbreviated as MMT–ODTMA. The amount of organoclay was only 2 phr while the amount of ENR was varied. NR–MMT-ODTMA showed mostly intercalated structure of the

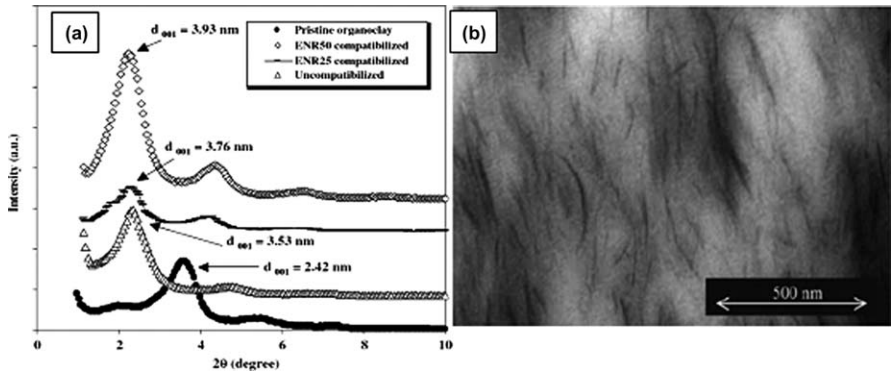

Figure 8.11 (a) XRD of the MMT–ODTMA, ENR 25 and ENR 50 compatibilized and uncompatibilized NR–OMt nanocomposites. (b) TEM image of ENR 50 compatibilized NR–OMt nanocomposites.
(Reproduced with permission of John Wiley and Sons.)

organoclay given in Figure 8.11. The best dispersion of organoclay in NR nanocomposites was achieved in the presence of ENR 50. This was attributed to the incorporation of ENR 50 in NR facilitating the penetration of both molecules into the interlayer space of MMT. The organoclay-filled NR vulcanizates showed the lowest torque values in rheometric experiment compared to CB- and silica-filled compounds. However, the improvements in tensile strength, elongation at break and tear properties in organoclay-filled NR compounds were considerably higher compared to CB- and silica-filled compounds.

Arroyo *et al.*[36] have prepared NR nanocomposites with the help of melt blending technology. The nanocomposites were prepared by blending NR with ENR 25 and ENR 50. Clay was modified with two different organomodifiers, namely dimethyl dihydrogenated tallow (MMT-2M2HT) and methyl tallow bis-2-hydroxyl quaternary ammonium (MMT-MT2EtOH). Exfoliated structure of NR–OMt nanocomposite was observed in the presence of ENR attributed to its polarity which further favours the intercalation of long rubber chains in the interlayer space of clay. Unmodified clay slightly changed the cure characteristics of NR as observed in the rheometric study and they attributed this fact to the poor compatibility between the unmodified clay and hydrophobic polymer. Nevertheless, the optimum cure time was reduced steeply in the presence of the organoclay. A similar observation was also noted in the case of CB, but the extent of decrement was smaller compared to the organoclay. NR filled with 10 phr of OMt exhibited higher torque compared to the NR with 40 phr CB, attributed to the higher crosslink density, which was further confirmed by swelling and differential scanning calorimetry (DSC) experiments. The mechanical behaviour of NR with 10 phr organoclay was comparable with the compound with 40 phr CB.

Knowledge of rheological behaviour of elastomers is of considerable importance in predicting and understanding their processing characteristics. The

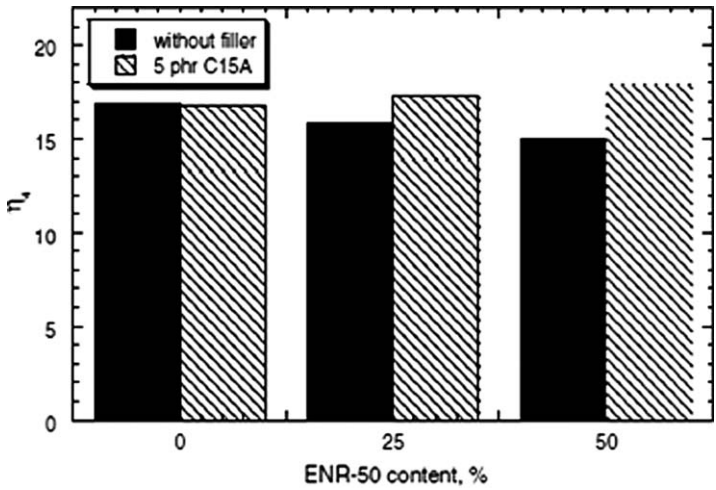

Figure 8.12 Variation of Mooney viscosity as a function of ENR 50 content in the blend reinforced with C15A (5 phr).

effect of ENR and filler treatment on the rheological behaviour of NR nanocomposites was observed and reported in another study by Arroyo *et al.*[43] The rheological behaviour of the nanocomposites was investigated through Mooney viscosity measurements. At very low shear rates ($\sim$1–2 s^{-1}), the Mooney viscosity has been shown to be directly proportional to the true shear viscosity.

The variation in Mooney viscosity versus time (of shearing) for NR and NR/ENR 50 blends and their nanocomposites containing C15A as organoclay is represented in Figure 8.12. It can be seen from Figure 8.12 that the viscosity of the NR compound barely varies with the inclusion of the organoclay. Although this behaviour does not correspond to that of other conventional fillers, for instance CB or silica, which usually give rise to enhanced viscosity and modified rheological properties of the elastomer. In general, the organic modifiers present in the clay interlayer space can act as plasticizer which further reduces the viscosity of the rubber compound. The viscosity enhancement is more significant in the presence of the organoclays and as both ENR content and epoxy units in the ENR increase. The enhanced rubber–clay compatibility with the incorporation of ENR not only causes a better dispersion of the clay in the rubber with an increase of interphase but also upsurges the rubber–clay interactions. As a result of all these factors, an increment in the final viscosity was observed.

The existence of a glassy layer or of a glassy interphase had already been suggested by many authors.[44,45] It has been proposed that dynamics of adsorption/desorption of the polymer chains at the filler interface might be responsible for numerous linear and non-linear effects.[46] Such dynamics is even more pronounced when polymer chains are anchored through covalent bonds at the filler interface. NMR measurements have confirmed the glassy nature of

the polymer chains near the particles surface. Montes *et al*. showed that the precocious non-linear mechanical behaviour of these filled systems is related to the strain softening of the glassy polymer shell surrounding the particles surfaces.[47] Very recently Merabia *et al*.[48] developed a microscopic model and pointed out that the strong reinforcement is achieved when such glassy layers between fillers overlap each other. It was also proposed that the dynamics of yield and resurgence of glassy bridges can account for the non-linear Payne effect and Mullins effect. In general, filled rubber compounds invariably exhibit a reduction in stress on the second and subsequent extensions under tensile strain, a phenomenon that has come to be known as the Mullins effect.

Nanocomposites based on (70/30) blends of NR, SBR and OMt have been prepared successfully via a melt-mixing process by Tavakoli *et al*.[49] Maleated EPDM (EPDM-*g*-MAH) and ENR50 were employed as compatibilizer. EPDM-*g*-MAH showed more potential in enhancing dispersion of the clay nanolayers and their interaction with rubber phases. More potential for separating and dispersing the clay nanoplatelets with better interface enhancement was exhibited by EPDM-*g*-MAH as compatibilizer. Both XRD and TEM examinations verified that the two rubber phases of the rubber blend compatibilized by both EPDM-*g*-MAH and ENR50 could be intercalated into the galleries of OMt and high extent of clay intercalation/exfoliation could be obtained in these nanocomposites. They have also studied the effectiveness of EPDM-*g*-MAH as an interfacial compatibilizer in enhancing the extent of interaction between NR and OMt nanolayers.[50] Microstructural characterizations revealed better interfacial compatibilization by EPDM-*g*-MAH compared to ENR50, which is attributed to the lower polarity of the EPDM-*g*-MAH and hence more affinity for the NR matrix to be diffused onto the galleries of OMt. The above observation was confirmed with the help of TEM analysis and higher elasticity exhibited by the unvulcanized NR/OMt/EPDM-*g*-MAH nanocomposites in melt rheological measurements. There is little literatures describing the effect of compatibilizers in NR based rubber blend–clay nanocomposites prepared by solution mixing technology.[51,52]

Finally, it can be concluded that the incorporation of OMt in NR by mechanical mixing leads to very poor dispersions with larger aggregates as discussed earlier. The dispersion of OMt in NR was rather unsatisfactory and could be observed in the respective TEM image, except they were prepared in the presence of external compatibilizers.

8.3.3 Natural Rubber–Expanded Organo-Montmorillonite Nanocomposites

The effect of EOMt, as already mentioned above, on the properties of different rubbers/Mt composites were studied and reported by Das *et al*.[20] A good correlation, which is shown in Figure 8.13, was observed between the area of the (001) basal reflections and the area of the tan δ–temperature curve from dynamic mechanical analysis (DMA) study. A small basal reflection was related

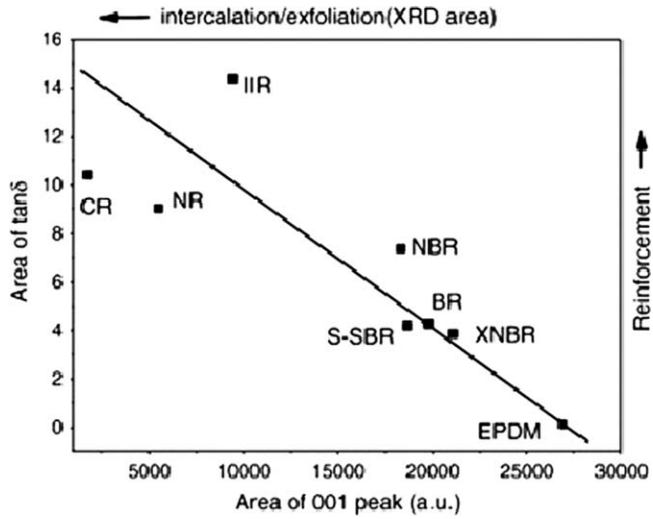

Figure 8.13 Area of the 001 reflection versus the area difference (gum-filled) of the tan δ–temperature peaks.
(Reproduced with permission of Elsevier Ltd.)

to a large difference (filled sample-gum rubber) tan δ peak area in good agreement with the improved physical properties in the presence of such clay particles. Better improvement in different physical properties was reported for the non-polar rubbers like NR, EPDM and BR compared to polar rubbers like NBR, CR and XNBR.

A high degree of exfoliation of MMT was achieved and reported by Rooj *et al.*[21] in NR utilizing the so-called 'propping-open approach', where stepwise expansion of the interlayer space of MMT took place (Figure 8.5).

The nanostructure was characterized by WAXD and TEM, which indicated different extents of the clay dispersion depending on the fatty acid chain length. The WAXD patterns of different nanocomposites are depicted in Figure 8.14 in the range of $2\theta = 1$–12°. It can be seen from Figure 8.14 that the measured $d(001)$ basal spacing of OMt is 2.98 nm, whereas in NR–OMt nanocomposites the basal spacing was 4.3 nm. However, the total dispersion as well as distribution of the OMt was found to be very poor as the big agglomerated particles of the OMt could be found in the rubber compound by simple visual examination and also in electron microscopy. The $d(001)$ basal spacing was found to be increased with increasing length of the fatty acid chain. A low angle broad halo in the WAXD pattern of NR-C22-EOMt was noticed. Such broadening of the $d(001)$ peak in a low 2θ region indicated the extensive layer separation associated with the clay lamellae intercalation and exfoliation. The TEM images obtained from different NR nanocomposites are compared in Figure 8.15. It was found from Figure 8.15 that the numbers of dark phase indicating the presence of clay sheets were higher in the case of C22-EOMt as compared to other EOMt.

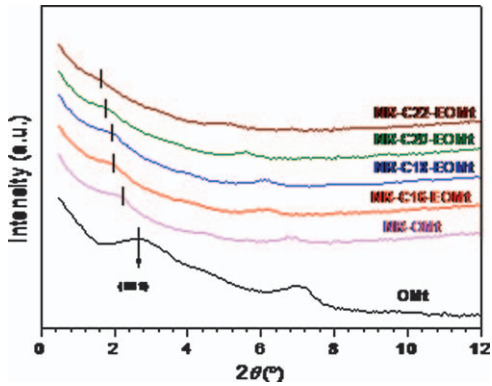

Figure 8.14 WAXD patterns of various NR–EOMt nanocomposites. (Reproduced with permission of John Wiley and Sons.)

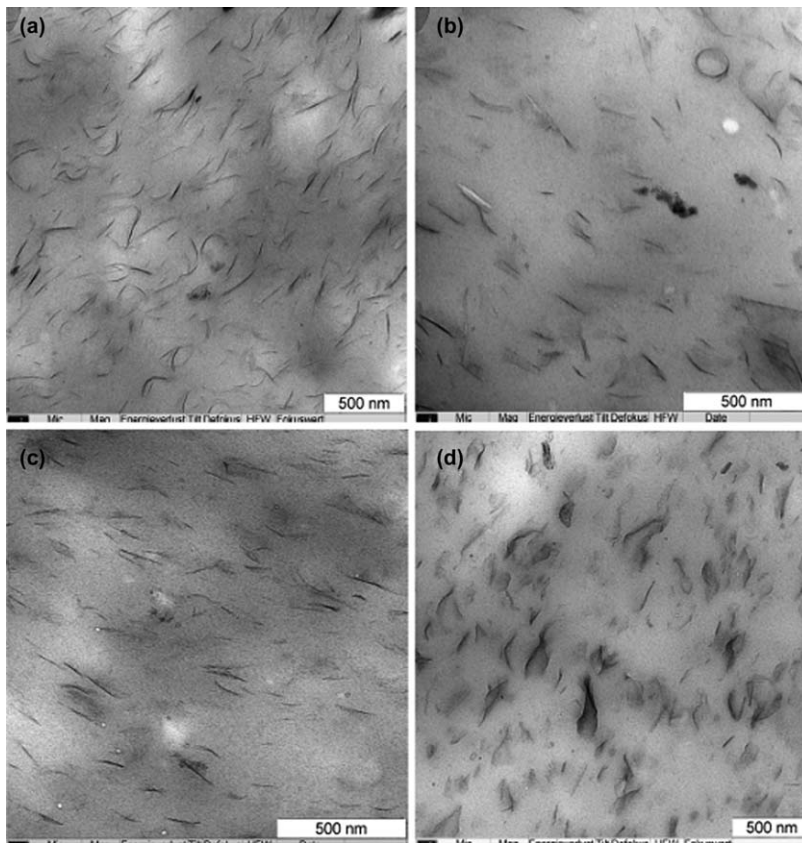

Figure 8.15 TEM micrographs: (a) NR-C22-EOMt, (b) NR-C20-EOMt, (c) NR-C18-EOMt, and (d) NR-C16-EOMt nanocomposites. (Reproduced with permission of John Wiley and Sons.).

Table 8.2 Cure characteristics of the EOMt-filled NR at 150 °C. (Reproduced with kind permission of Elsevier Ltd.)

Sample	*Maximum torque* (M_H) *(dNm)*	*Delta torque (dNm)*	*Cure time* (t_{90}) *(min)*	*Cure rate index* (CRI) (min^{-1})
NR gum	6.19	5.86	17.8	7.2
NR-EOMt-2	6.43	6.07	9.2	13.3
NR-EOMt-4	6.48	5.84	8.7	15
NR-EOMt-6	6.29	5.72	8.6	17.4
NR-EOMt-10	6.07	5.53	7.8	18.1

Since the fatty acid with 22 carbon atoms was found to offer the greatest interlayer distance among the fatty acids under consideration, this fatty acid intercalated OMt was selected further as reinforcing fillers in NR matrix and reported very recently in another study by Rooj *et al.*[22] C22-EOMt was successfully dispersed in the NR matrix, as confirmed by XRD and TEM. As a result, the mechanical properties were found to be remarkably improved. An improvement of ~114% in tensile strength and ~203% in modulus at 300% elongation was observed. They correlated these results with the morphological data obtained from WAXD and TEM. The various curing parameters are also summarized in Table 8.2. They observed that cure time (t_{90}) and scorch time (t_2) decreased gradually with the addition of EOMt. This behaviour indicated an accelerated curing process in the presence of EOMt compared to unfilled gum compound. It has been reported[53–56] that the amine used for the modification of clay minerals and sulfur-containing compounds participated in the formation of a Zn complex, which accelerated the rubber curing process. For all NR nanocomposites, the lower minimum torque (M_L) values signify lower viscosity and, therefore, an improvement in material processability. Interestingly the above-mentioned behaviour was independent of clay mineral content. On the other hand, the maximum torque (M_H) decreased with increasing amounts of EOMt loading. Generally, the M_H obtained during rheometric study depends on the degree of crosslinking. It is mentioned in the literature[57–59] that clay minerals adsorbed curatives onto their surface and inhibited the curing process. Hence, the decline in torque values could be associated with the intercalation of rubber chains into the interlayer space, which further prevented the formation of crosslinks. This lowering of M_H was an indication of improved filler dispersion in the NR matrix. There was an insignificant effect of an additional amount of C22FA on the curing behaviour of the NR compound.

WAXD patterns of pure OMt, EOMt and nanocomposites with various EOMt contents are shown in Figure 8.16. The mean interlayer spacing of the $d(001)$ plane for the OMt obtained by WAXD measurements was ~2.98 nm ($2\theta = 2.78°$). The interlayer distance of OMt was further expanded to 4.42 nm after successful intercalation with long alkyl chain C22 fatty acid. In the scattering pattern three sharp peaks appeared at $2\theta = 2.1°$, 5.4° and 9.4°, respectively. These were in addition to three broad peaks of Mt. These sharp

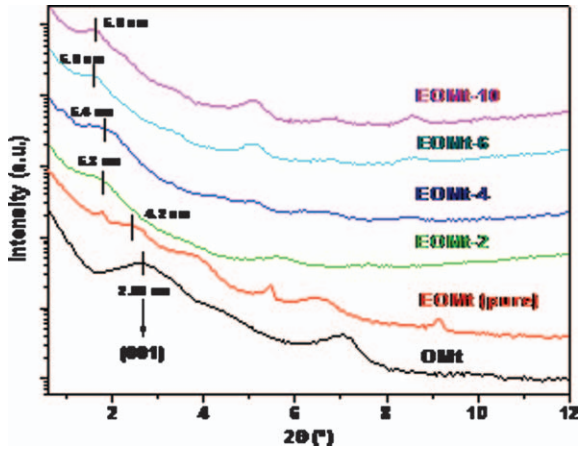

Figure 8.16 XRD patterns of different NR–EOMt nanocomposites. (Reproduced with permission of Elsevier Ltd.)

peaks indicated the presence of crystalline C22 fatty acid. For the sake of simplicity they considered only the small peak at $2\theta = 2.0^\circ$ (~ 5.3 nm), which corresponds to the (001) plane of the intercalated silicate layers in the NR matrix. With increasing EOMt content, this peak becomes stronger and gradually shifted towards the smaller diffraction angle $2\theta = 1.78^\circ$ at (~ 5.6 nm). They assumed that after the addition of large amounts of EOMt the intercalation of the rubber chains becomes more facile due to the plasticization effect of the fatty acid.

TEM investigation was carried out to examine directly the intercalation of rubber chains and the state of dispersion of the EOMt into the NR matrix. Figure 8.17 shows TEM micrographs of NR nanocomposites with both OMt and EOMt. The thickness of most EOMt tactoids was 7–8 nm and the length about 80–200 nm and these numbers were invariant to the EOMt loading.

In a recent study by Rooj *et al.*[60] strain sweep measurements were performed in order to investigate the polymer–filler and filler–filler interactions. At low EOMt loading (for instance 2 phr), the observed variation in the amplitude of the Payne effect was weak. However, pronounced variation was observed as the EOMt concentration increases. This behaviour was attributed to the breakdown of the filler–filler networks at higher strains. When comparing the magnitude of the Payne effect (for equivalent volume fractions) 10 phr OMt has an extremely low value compared to that of 10 phr EOMt (Figure 8.18).

The occurrence of mechanical percolation behaviour was also investigated by Rooj *et al.*[60] in both NR/OMt and NR/EOMt nanocomposites using the Huber–Vilgis approach.[61] The mechanical percolation threshold (φ_p) was obtained in a log–log plot (Figure 8.19) where the experimental data are linearly interpolated according to the two different straight lines. It was observed from Figure 8.19 that the φ_p of EOMt particles is decreased (~ 6 phr) when

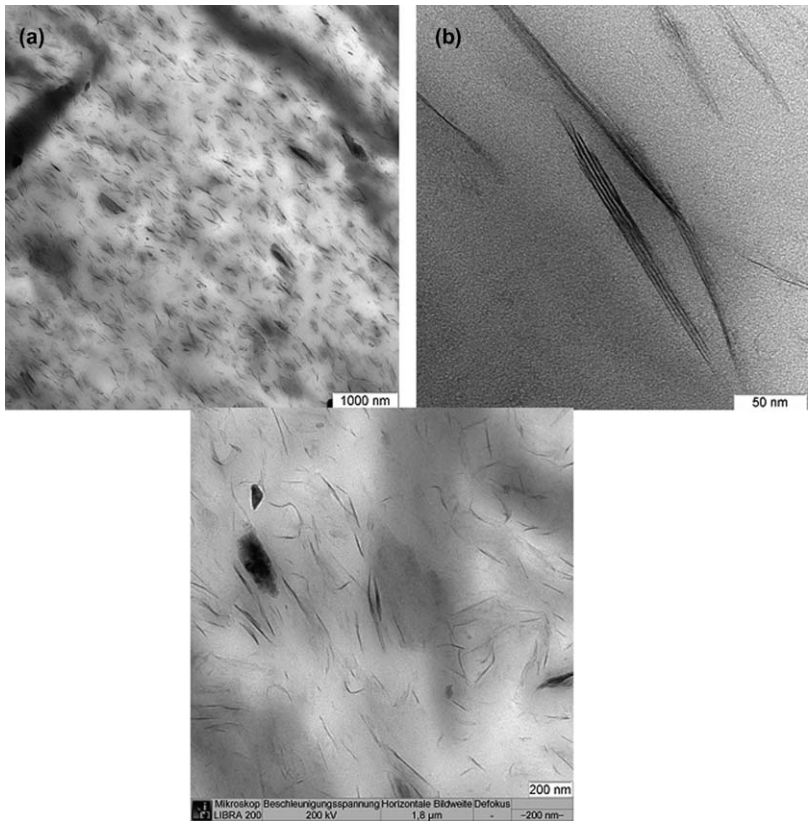

Figure 8.17 Different TEM images of NR nanocomposites with 10 phr of EOMt; different scale length.
(Reproduced with permission of Elsevier Ltd.)

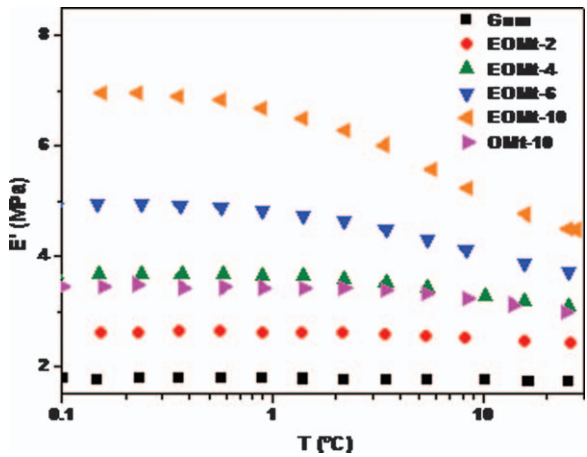

Figure 8.18 Dependence of amplitude sweep on E' of different NR–clay nanocomposites.

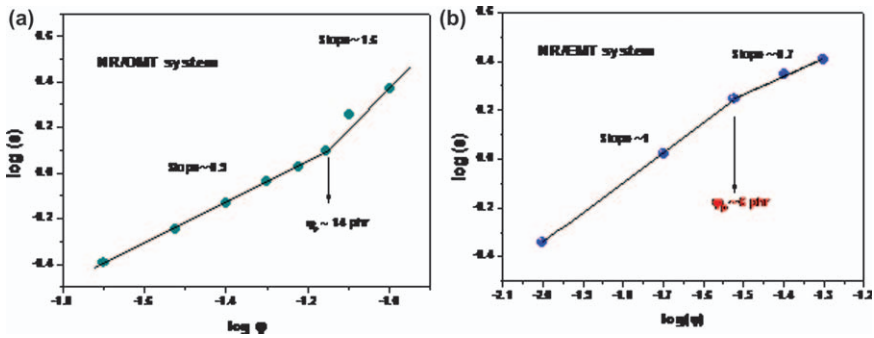

Figure 8.19 Percolation threshold predicted from Huber–Vilgis model. (a) NR–OMt system, (b) NR–EOMt system.

compared to OMt (~14 phr). This was attributed to the formation of highly networked structures of the EOMt. Therefore, filler–filler networks were formed even at very low loading of EOMt particles.

The fractal dimension of OMt and EOMt in the NR matrix was also calculated using an expression proposed by Huber and Vilgis[61] for CB-filled rubbers. Fractal dimension of $d_f \approx 1.75$ for OMt was found simply by applying the Huber–Vilgis approach. Such clusters are less compact than diffusion-limited aggregation (DLA). A suitable visualization for it would be the cluster–cluster model (CCA)[62] with $d_f = 1.78$ in three (Euclidean) dimensions. In CCA, one starts with a low concentration of particles diffusing on a lattice. When two particles meet, they form a cluster of two, which can also diffuse. When this cluster meets another two particles or another cluster, a larger cluster is formed. A further reduction in compactness of the filler clusters was observed in the case of EOMt in the rubber matrix. Such reduction in compactness may be attributed to the shaded diffuse spatial regions observed in the TEM micrograph. A nearly vanishing fractal dimension $d_f \sim 0.1$ was found in the case of EOMt, which indicates lower or even vanishing compactness of filler clusters. It is also interesting to note that even negative fractal dimensions have been introduced to help understand self-similar fractal measures called multifractals.[63]

8.4 Natural Rubber with Hybrid Filler System (Carbon Black and Clay)

Two or more different filler types are utilized in the case of multi-component compounding, which produces very famous hybrid structures where effects of the different materials or components are combined.[64–67] Recent investigations on composites having multi-component filler systems have focused mainly on thermoplastic and thermoset polymers and not so familiar with rubbery materials. In most of the applications, CB and silica have been used

together as a hybrid filler system to optimize the advantages and disadvantages of the individual filler system. When CB is compounded with rubbers many of the properties like tensile strength, tear strength, modulus hardness and abrasion resistance are increased. For this reason, CB has been extensively exploited in numerous rubber engineering products. In general, a CB-reinforced rubber has a higher modulus than a silica-reinforced one. In tyre treads, silica yields a lower rolling resistance at equal wear resistance and wet grip than CB. Like silica, nowadays clay has been utilized in rubber compounding along with CB to overcome certain negative aspects of CB such as tyre tread wear, *etc*.

Only very few rubber nanocomposites with a hybrid clay/CB filler system and different types of rubber can be found in the literature.[64–75] These works show, in particular, a remarkable enhancement of material dynamic-mechanical properties obtained by combining the two fillers, which were also commented to give rise to a synergistic effect. The combined effect of clay and CB in an NR matrix was reported by Qing-xiu *et al*.[75] using an emulsion polymerization technique. They characterized the nanomorphology in terms of XRD and TEM. A phase-separated structure was observed in the XRD and it was further supported by TEM analysis. Mechanical properties of the NR–clay/CB composites were remarkably enhanced. In a study by Liu *et al*., NR nanocomposites based on CB and two poly(ethylene glycol) (PEG)-modified clays were fabricated.[74,76] An intercalated and exfoliated structure was dominant in the case of OMt and ORD-filled rubber and was further confirmed by WAXD and DSC. Tensile tests and DMA showed that the two phase fillers have a significant synergistic reinforcing effect on NR, which was believed originate from the filler network. A pronounced interaction between OMt and CB has been reported in the scientific literature.[72–75] On the basis of TEM micrographs authors hypothesized the formation of 'nano-units', speculating synergy between the two fillers and proposing a 'reinforced intercalated structure', with polymer chains intercalated in the interlayer space and CB adsorbed on the clay mineral. Recently Das *et al*.[71] have reported the utilization of EOMt in truck tyre formulations based on NR–CB composites. They found that EOMt seems to dominate reinforcing capabilities compared to OMt. It was also found that the model truck tyre compounds can be formulated with 40% less fossil fuel resources without sacrificing various physical properties. It is also shown that the truck tyre formulation made with hybrid fillers offers better rolling resistance performance as compared with a conventional standard compound.

Figure 8.20 shows the XRD patterns for CB- and clay-filled NR composites. A broad peak is apparent for OMt-filled NR–CB composites. This peak disappears completely in the case of EOMt-filled NR–CB composites. Although the NR composites are filled with significant amounts of CB the absence of any peak indicates a complete exfoliation of the clay minerals when they are mixed in expanded form. Strain-induced filler–filler network breakdowns by dynamic tension mode at constant frequency and temperature was carried out and the

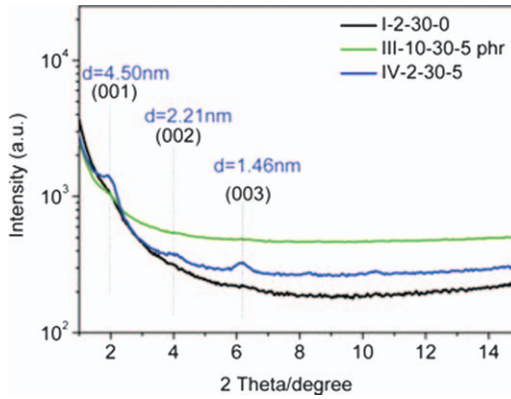

Figure 8.20 XRD patterns for CB- and clay-filled NR composites.

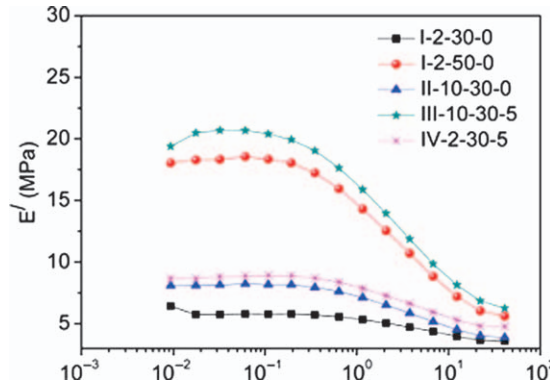

Figure 8.21 Filler–filler network (Payne effect) in hybrid filler filled NR composites.

corresponding storage modulus (E') versus dynamic strain (%) was established in Figure 8.21.

The storage modulus (E') decreases monotonically with increasing strain amplitude for all the NR composites during dynamic deformation. Generally, the absolute value of E' at low strain regimes indicates the degree of filler–filler networking. It was observed that the NR composites with 30 phr CB and 5 phr EOMt (designated as IV-2-30-5) acquires a higher E' value, implying that the degree of filler–filler networking is stronger compared to NR composites with 50 phr CB. The stronger filler–filler interaction with such a small amount of filler indicates the possibility of the existence of a new kind of filler–filler interaction between the silicate particles. Exfoliated layered clay minerals possess free hydroxyl groups at the edges and these hydroxyl groups interact with each other to form a new kind of silicate–silicate network in the rubber matrix. Tear fatigue analysis (TFA) tests were carried out and reported in another study by Rooj *et al.*[70] using pure-shear test specimens under cyclic

conditions to explicate the crack growth behaviour of CB-filled NR in the presence of EOMt. A significant reduction in crack growth rate was noticed in the presence of only 5 phr of EOMt.

8.5 Conclusions

The achievement of a high degree of exfoliation of layered clay minerals in non-polar rubber matrices, such as NR, is still a major issue. This chapter presents a brief overview of studies of clay reinforcement in NR both in micro and nano scale. Although quite a lot of studies have been reported in the field of NR reinforcement with simple organoclay (OMt), plenty of scope still exists to improve the dispersion of MMT followed by property enhancement. Better dispersion and improvement in different properties was observed in the case of EOMt-filled NR nanocomposites.

References

1. R. Stephen and S. Thomas, in *Rubber Nanocomposites: Preparation, Properties and Applications*, ed. S. Thomas and R. Stephen, John Wiley & Sons, Chichester, 2009, Chapter 2, pp. 1–12.
2. S. D. Sadhu, M. Maiti and A. K. Bhowmick, Current Topics in *Elastomer Research*, ed. A. K. Bhowmick, CRC Press, 2008, pp. 24–51, Boca Raton, Florida.
3. M. Galimberti, *Rubber–Clay Nanocomposites*, John Wiley & Sons, Hoboken, NJ, 2011.
4. J. Ma, Z.-Z. Yu, H.-C. Kuan, A. Dasari and Y. W. Mai, *Macromol. Rapid Commun.*, 2005, **26**, 830.
5. P. Kiliaris and C. D. Papaspyrides, *Prog. Polym. Sci.*, 2010, **35**, 902.
6. D. R. Paul and L. M. Robeson, *Prog. Polym. Sci.*, 2008, **49**, 3187.
7. F. Avalos, J. C. Ortiz, R. Zitzumbo, M. A. Lopez-Manchado, R. Verdejo and M. Arroyo, *Eur. Polym. J.*, 2008, **44**, 3108.
8. A. Di Gianni, G. Colucci, A. Priola, L. Conzatti, M. Alessi and P. Stagnar, *Macromol. Mater. Eng.*, 2009, **294**, 705.
9. A. A. Yehia, A. M. Akelah, A. Rehab, S. H. El-Sabbagh, D. E. El Nashar and A. A. Koriem, *Mater. Des*, 2012, **33**, 11.
10. A. Das, K. W. Stoekelhuber and G. Heinrich, *Macromol. Chem. Phys.*, 2009, **210**, 189.
11. M. Bhattacharya and A. K. Bhowmick, *Polymer*, 2008, **49**, 4808.
12. M. Krajnc, J. Karger-Kocsis and U. Šebenik, *J. Appl. Polym. Sci.*, 2013, **127**, 950.
13. M.-S. Kim, D.-W. Kim, S.-R. Chowdhury and G.-H. Kim, *J. Appl. Polym. Sci.*, 2006, **102**, 206.
14. Q.-X. Jia, Y.-P. Wu, Y.-L. Xu, H.-H. Mao and L.-Q. Zhang, *Macromol. Mater. Eng.*, 2006, **291**, 218.
15. S. Rooj, A. Das and G. Heinrich, *Polym. J.*, 2011, **43**, 285.

16. A. Das, R. Jurk, K. W. Stöckelhuber and G. Heinrich, *Macromol. Mater. Eng.*, 2008, **293**, 479.
17. A. Das, R. N. Mahaling, K. W. Stöckelhuber and G. Heinrich, *Compos. Sci. Technol.*, 2011, **71**, 276.
18. M. Bousmina, *Macromolecules*, 2006, **39**, 4259.
19. G. W. Brindley and S. Ray, *Am. Mineral.*, 1964, **49**, 106.
20. A. Das, K. W. Stöckelhuber, R. Jurk, D. Jehnichen and G. Heinrich, *Appl. Clay Sci.*, 2011, **51**, 117.
21. S. Rooj, A. Das, K. W. Stöckelhuber, U. Reuter and G. Heinrich, *Macromol. Mater. Eng.*, 2012, **297**, 369.
22. S. Rooj, A. Das, K. W. Stöckelhuber, N. Mukhopadhyay, A. R. Bhattacharyya, D. Jehnichen and G. Heinrich, *Appl. Clay Sci.*, 2012, **67**, 50.
23. G. Lagaly, M. F. Gonzalez and A. Weiss, *Clay Miner.*, 1976, **11**, 173.
24. E. Moreno, R. Cordobilla, T. Calvet, M. A. Cuevas-Diarte, G. Gbabode, P. Negrier, D. Mondieig and H. A. J. Oonk, *New J. Chem.*, 2007, **31**, 947.
25. G. Lagaly, R. M. Barrer and K. Goulding, *Philos. Trans. R. Soc., A*, 1984, **311**, 315.
26. S. Yariv, *Thermochim. Acta*, 1996, **274**, 1.
27. S. Varghese and J. Karger-Kocsis, *Polymer*, 2003, **44**, 4921.
28. Y. P. Wu, Y. Q. Wang, H. F. Zhang, Y. Z. Wang, D. S. Yu and L. Q. Zhang, *Compos. Sci. Technol.*, 2005, **65**, 1195.
29. L. F. Valadares, C. A. P. Leite and F. Galembeck, *Polymer*, 2006, **47**, 672.
30. A. K. Bhowmick, M. Bhattacharya and S. Mitra, *J. Elastomers Plast.*, 2010, **42**, 517.
31. A. K. Bhowmick, M. Bhattacharya, S. Mitra, K. Dinesh Kumar, P. K. Maji, A. Choudhury, J. J. George and G. C. Basak, *Adv. Polym. Sci.*, 2011, **239**, 1.
32. C. A. Rezende, F. C. Braganca, T. R. Doi, L. T. Lee, F. Galembeck and F. Boue, *Polymer*, 2010, **51**, 3644.
33. Y. T. Vu, J. E. Mark, L. H. Pham and M. Engelhardt, *J. Appl. Polym. Sci.*, 2001, **82**, 1391.
34. S. Joly, G. Garnaud, R. Ollitrault and L. Bokobza, *Chem. Mater.*, 2002, **14**, 4202.
35. S. Varghese and J. Karger-Kocsis, *J. Appl. Polym. Sci.*, 2004, **91**, 813.
36. M. Arroyo, M. A. Lopez-Manchado and B. Herrero, *Polymer*, 2003, **44**, 2447.
37. J. Carretero-Gonzalez, H. Retsos, R. Verdejo, S. Toki, B. S. Hsiao, E. P. Giannelis and M. A. Lopez-Manchado, *Macromolecules*, 2008, **41**, 6763.
38. J. Hrachová, P. Komadel, D. Jochec-Mošková, J. Krajči, I. Janigová, M. Šlouf and I. Chodák, *J. Appl. Polym. Sci.*, 2013, **127**, 3447.
39. K. N. Madhusoodanan and S. Varghese, *J. Appl. Polym. Sci.*, 2006, **102**, 2537.
40. J. Carretero-González, H. Retsos, E. P. Giannelis, T. A. Ezquerra, M. Hernández and M. A. López-Manchado, *Soft Matter*, 2009, **5**, 3481.

41. L. N. Carli, C. R. Roncato, A. Zanchet, R. S. Mauler, M. Giovanela, R. N. Brandalise and J. S. Crespo, *Appl. Clay Sci.*, 2011, **52**, 56.
42. P. L. Teh, Z. A. M. Ishak, A. S. Hashim, J. Karger-Kocsis and U. S. Rshiaku, *J. Appl. Polym. Sci.*, 2006, **100**, 1083.
43. M. Arroyo, M. A. López-Manchado, J. L. Valentin and J. Carretero, *Compos. Sci. Technol.*, 2007, **67**, 1330.
44. D. C. Edwards, *J. Mater. Sci.*, 1990, **25**, 4175.
45. M. J. Wang, *Rubber Chem. Technol.*, 1998, **71**, 520.
46. P. G. Maier and D. Göritz, *Kautsch. Gummi Kunstst.*, 1996, **49**, 18.
47. H. Montes, F. Lequeux and J. Berriot, *Macromolecules*, 2003, **36**, 8107.
48. S. Merabia, P. Sotta and D. R. Long, *J. Polym. Sci. Part B: Polym Phys.*, 2010, **48**, 1495.
49. M. Tavakoli, A. Asghar Katbab and H. Nazockdast, *J. Appl. Polym. Sci.*, 2012, **123**, 1853.
50. M. Tavakoli, A. Asghar Katbab and H. Nazockdast, *J. Macromol. Sci., Part B: Phys.*, 2011, **50**, 1270.
51. K. Pal, R. Rajasekar, S. K. Pal, J. K. Kim and C. K. Das, *J. Nanosci. Nanotechnol.*, 2010, **10**, 3022.
52. K. Pal, R. Rajasekar, D. J. Kang, Z. X. Zhang, J. K. Kim and C. K. Das, *Mater. Des.*, 2009, **30**, 4035.
53. M. A. Lopez-Manchado, M. Arroyo, B. Herrero and J. Biagiotti, *J. Appl. Polym. Sci.*, 2003, **89**, 1.
54. G. O. Piloyan, I. D. Ryabchikov and O. S. Novikova, *Nature*, 1966, **212**, 1229.
55. A. Mousa and J. Karger-Kocsis, *Macromol. Mater. Eng.*, 2001, **286**, 260.
56. M. Ganter, W. Gronski, H. Semke, T. Zilg, C. Thomann and R. Mühlhaupt, *Kautsch. Gummi Kunstst.*, 2001, **54**, 166.
57. S. S. Choi and I.-S. Kim, *Eur. Polym. J.*, 2002, **38**, 1265; *Polym. Adv. Technol.*, 2004, **15**, 400.
58. S. Rooj, A. Das, V. Thakur, R. N. Mahaling, A. K. Bhowmick and G. Heinrich, *Mater. Des.*, 2010, **31**, 2151.
59. S. Rooj, A. Das, K. W. Stöckelhuber, D. Y. Wang, V. Galiatsatos and G. Heinrich, *Soft Matter*, 2013, **9**, 3798.
60. G. Huber and T. A. Vilgis, *Kautsch. Gummi Kunstst.*, 1999, **52**, 102.
61. G. Heinrich and M. Klüppel, *Adv. Polym. Sci.*, 2002, **160**, 1.
62. B. B. Mandelbrot, *Physica*, 1990, A163, 306.
63. N. Nugay and B. Erman, *J. Appl. Polym. Sci.*, 2001, **79**, 366.
64. P. A. Jarvela and P. K. Jarvela, *J. Mater. Sci.*, 1996, **31**, 3853.
65. N. Chand and K. K. S. Gautam, *J. Mater. Sci. Lett.*, 1994, **13**, 230.
66. M. F. Uddin and C. T. Sun, *Compos. Sci. Technol.*, 2010, **70**, 223.
67. M. Galimberti, Materials Innovation for Tires, Presentation at 169th Technical Meeting of the Rubber Division, American Chemical Society, May 8–10, 2006, Akron, Ohio, p. 643. Available from: http://toc.proceedings.com/02596webtoc.pdf.
68. A. Malas and C. K. Das, *J. Mater. Sci.*, 2012, **47**, 2016.

69. S. Rooj, A. Das, I. A. Morozov, K. W. Stöckelhuber, R. Stocek and G. Heinrich, *Compos. Sci. Technol.*, 2013, **76**, 61.
70. A. Das, K. W. Stoeckelhuber, S. Rooj, D. Y. Wang and G. Heinrich, *Kautsch. Gummi Kunstst.*, 2010, **63**, 296.
71. P. K. Chattopadhyay, N. C. Das and S. Chattopadhyay, *Composites, Part A*, 2011, **42**, 1049.
72. F. Cataldo, *Macromol. Symp.*, 2007, **247**, 67.
73. M. Galimberti, M. Coombs, V. Cipolletti, P. Riccio, T. Riccò, S. Pandini and L. Conzatti, *Appl. Clay Sci.*, 2012, **52**, 65.
74. M. Bhattacharya and A. K. Bhowmick, *J. Mater. Sci.*, 2010, **45**, 6126.
75. Q. X. Jia, Y. P. Wu, P. Xiang, X. Ye, Y. Q. Wang and L. Q. Zhang, *Polym. Polym. Compos.*, 2005, **13**, 709.
76. Y. Liu, L. Li and Q. Wang, *J. Appl. Polym. Sci.*, 2010, **118**, 1111.

CHAPTER 9

Long and Short Glass Fibre Reinforced Natural Rubber Composites

QUAZI T. H. SHUBHRA

Research Institute of Chemical and Process Engineering, Faculty of Information Technology, University of Pannonia, Egyetem u. 10, H-8200 Veszprem, Hungary
Email: shubhro.du@gmail.com

9.1 Introduction

Composites were first used near the time 1500s B.C. when early Egyptians and Mesopotamian settlers used a mixture of mud and straw to create strong and durable buildings. Straw continued to provide reinforcement to ancient composite products including pottery and boats. The Mongols invented the first composite bow in 1200 AD. A combination of wood, bone, and 'animal glue', were used in bows and were pressed and wrapped with birch bark. These bows were not only powerful, but also accurate. Composite Mongolian bows provided Genghis Khan with military dominance. Because of the composite technology, this weapon was the most powerful weapon on earth until the invention of gunpowder.

The modern era of composites began after the developed of plastics by scientists. Until then, the only source of glues and binders were natural resins derived from plants and animals. In the early 1900s, various plastics like

RSC Polymer Chemistry Series No. 8
Natural Rubber Materials, Volume 2: Composites and Nanocomposites
Edited by Sabu Thomas, Hanna J. Maria, Jithin Joy, Chin Han Chan and Laly A. Pothen

Published by the Royal Society of Chemistry, www.rsc.org

polyester, polystyrene, vinyl, and phenolic were developed and became superior to natural resins. But plastics alone could not provide sufficient strength for structural applications. Reinforcement was needed to improve the strength, rigidity and other properties. In 1935, Owens Corning introduced the first glass fibre, fibreglass. Fibreglass was made almost by accident in 1930, when an engineer became intrigued by a fibre that was formed during the process of applying lettering to a glass milk bottle. Fibreglass, when combined with plastic polymers results incredibly strong, lightweight structure. This is the beginning of the fibre-reinforced polymers (FRPs) industry as we know it today.

Many of the greatest advancements in composite materials were incubated by war. Like the development of the composite bow by Mongols, World War II brought the FRP industry from the laboratory into actual production. For lightweight applications in military aircraft, scientists started using composites. It was observed that fibreglass composites were transparent to radio frequencies and the material was soon preferred for using in sheltering electronic radar equipment (Radomes). Later, boats were made from composites and the first commercial boat hull was introduced in 1946. By 1948 several thousand commercial boats had been made using fibreglass-reinforced polyester composites. At that time Brandt Goldsworthy who is often referred to as the 'grandfather of composites', developed new manufacturing processes for composites. He was the first person who used fibreglass in a surfboard which revolutionized the sport. Goldsworthy also invented a manufacturing process known as pultrusion and products being manufactured using this process include pipes, ladder rails, tool handles, arrow shafts, armour, train floors, medical devices, *etc*. In the 1970s the composite industries began to mature due to the development of better plastic resins and improved reinforcing fibres. DuPont developed an aramid fibre known as Kevlar and due to its high tenacity, this fibre has become the standard in armour. Another important fibre named 'carbon fibre' was also developed around this time. This fibre has some special advantages and replacing other fibres for composite manufacture as the new material of choice. The composites industry is now growing with its focus around renewable energy. Wind turbine blades are now made of composites and are requiring advanced materials, designs, and manufacturing.

In future, development of nanocomposites will bring additional improvement in the properties of composites offering a wider range of applications. Composites are on the path towards being more environmental friendly. Composites will continue to make the world stronger, lighter and more durable.

Today, FRCs are in use in a variety of structures, ranging from spacecraft and aircraft to buildings and bridges. FRCs find applications in construction industries, decking, window and door frames,[1] sports equipment such as bicycle frames, baseball bats, exercise equipment, *etc*. They are also suited for many automotive applications.[2] This wide use of composites has been facilitated by the introduction of new materials, improvements in manufacturing processes and developments of new analytical and testing methods.

9.2 Fibre Reinforced Composites (FRCs)

A typical composite material is a system of materials consisting two or more materials (mixed and bonded) on a macroscopic scale with two or more distinct phases having recognizable interfaces between them.[3] Proper combinations of materials into composite materials give rise to properties which transcend those of the constituents, as a result of the principle of combined action. Composites are produced to optimize various material properties like mechanical (mainly strength), chemical and/or physical properties. Since the early 1960s, there has been an increasing demand for stiffer and stronger materials, yet lighter in aeronautic, energy, civil engineering and in various structural applications. Unfortunately, no monolithic engineering material available is able to satisfy them. This need and demand certainly led to the concept of combining different materials in an integral composite structure.

Composites usually consist of a reinforcing material embedded in various matrices (binder). The effective method to increase the strength and to improve the overall properties of composites is to incorporate dispersed phases into the matrix which can be an either polymer or engineering materials such as ceramics or metals. Hence, metal matrix composites (MMCs), ceramic matrix composites (CMCs) and polymer matrix composites (PMCs) are obtained. Besides, hybrid composites, metal/ceramic/polymer composites and carbon matrix composites can also be obtained. MMC and CMC composites are developed to withstand high temperature applications. MMCs are also used in heat dissipation/electronic transmission applications due to the conductive nature of metals (electrically and thermally).

In fibre-reinforced composites (FRCs), fibres embedded in or bonded to a matrix with distinct interfaces (boundaries) between them. The matrix holds the fibres to form the desired shape while the reinforced fibres improve the overall mechanical properties of the matrix. In such composites, fibres are the main source of strength and principal load-carrying members while the matrix acts as a load transfer medium between them and keeps them in the desired location and orientation and protect them from environmental damages. The most common form in which FRCs are used in structural applications is called a laminate. Laminates are made by stacking number of thin layers of fibres and matrix and consolidating them into the desired thickness. Fibre orientation in each layer as well as the stacking sequence of various layers in a composite laminate can be controlled easily which helps to generate a wide range of physical and mechanical properties for the composite laminate.

Natural fibres such as flax, hemp, silk, jute, sisal, kenaf, cotton, etc are being used to reinforce matrices mainly thermoplastics and thermosets by many researchers. The principal synthetic fibres in commercial use are various types of glass, carbon, or aramid although other fibres, such as boron, silicon carbide, and aluminium oxide, are used in limited quantities. All these fibres can be incorporated into a matrix either in continuous lengths or in discontinuous (short) lengths. Both these fibres have some advantages and disadvantages.

Natural fibres have low abrasion resistance, low density, high toughness, acceptable specific strength properties, good thermal properties, enhanced energy recovery, biodegradability, *etc*.[4] Natural fibres produce composites offering advantages like environmental friendliness, renewability of the fibres, good sound abatement capability and improved fuel efficiency resulted from the reduced weight of the components.[5] On the other hand, synthetic fibres reinforced composites attracted much attention due to their high strength, better durability and moisture resistance properties.[6]

9.2.1 Different Types of FRCs

FRCs can be classified based on matrix and fibres. Based on fibre source, FRCs may be natural fibre reinforced and synthetic fibre reinforced. Based on fibre length, they can be continuous fibre reinforced and discontinuous fibre reinforced. But FRCs are generally classified based on matrix component. Thus according to the types of matrices stated earlier, composites are of three types: (i) ceramic matrix composites (CMCs), (ii) metal matrix composites (MMCs) and (iii) organic matrix composites (OMCs). Organic matrix is subdivided into two classes, namely polymer matrix and carbon matrix. A short description of all these types of composites are discussed below.

9.2.1.1 Metal Matrix Composites (MMCs)

A metal matrix composite (MMC) is a material that consists of a metallic base with a reinforcing constituent which is usually non-metallic and is commonly a ceramic. MMCs are a new range of advanced materials used in applications where conventional materials and alloys are not suitable for use. Metal matrix has the advantage over polymeric matrix in applications requiring a long-term resistance to severe environments, for example high temperature. The properties of MMCs depend on the nature of the two components. For example, the reinforcement of light metals opens up the possibility of application of these materials in areas where weight reduction is given the first priority. The precondition here is the improvement of the component properties. Metals have some excellent characteristics for which they are chosen as the matrix material in MMC structures. The advantages of MMCs are:

a) Fire resistance.
b) No outgassing.
c) No moisture absorption.
d) Higher temperature capability.
e) Better radiation resistance.
f) Higher transverse stiffness and strength.
g) Higher electrical and thermal conductivities.
h) They can be fabricated with conventional metal working equipment.

However, MMCs have the following disadvantages:

a) MMCs usually have high fabrication costs.
b) Most metals are heavy. So, MMCs comparatively possess heavy weight.

MMCs can be classified in various ways. One classification is based on the type of reinforcement. According to reinforcement, MMCs are of two different types:

a) Continuous reinforcement composites in which reinforcements are continuous fibres or filaments (continuous fibres in a composite are usually called filaments).
b) Discontinuous reinforcement composites in which reinforcements are short fibres, whiskers or particles.

The two most commonly used metal matrices are based on aluminium and titanium. These two metals have comparatively low densities and are available in a variety of alloy forms. Magnesium is lighter but it is less suitable for many applications due to its great affinity towards oxygen which promotes atmospheric corrosion. Although beryllium is the lightest of all structural metals and has a tensile modulus higher than that of steel, it suffers from extreme brittleness which is the reason for its exclusion as a potential matrix material. Aluminium and its alloys have been used widely as matrix material in MMCs. Aluminium alloys, such as 201, 6061 and 1100, have been used for their higher tensile strength–weight ratios. When carbon fibre is used with aluminium alloys, carbon reacts with aluminium to form aluminium carbide (Al_4C_3) at typical fabrication temperatures of 500 °C or higher which severely degrades the mechanical properties of the composite. A more common reinforcement for aluminium alloys is SiC.

Graphite/aluminium and graphite/magnesium systems were developed more recently which show significant potential in structural applications. The low coefficient of thermal expansion of these two material systems makes them particularly attractive in space structures. Other MMC systems of interest include alumina/magnesium, beryllium/titanium, boron/stainless steel/aluminium, silicon carbide/aluminium, boron/titanium/aluminium, borsic/aluminium, borsic/titanium, copper/graphite, graphite/lead, graphite/a1uminum, tungsten/nickel, *etc*.

MMC systems are being used for superconducting electrical applications. These include hydrofoils, missiles, Navy weapon systems, assault bridges and battle tanks, and spacecraft components such as deployable antennas and booms.

9.2.1.2 Ceramic Matrix Composites (CMCs)

Ceramics are solid materials which generally exhibit very strong ionic bonding and in few cases covalent bonding. Ceramics are known for their high

temperature stability, high modulus, high hardness, high thermal shock resistance, high corrosion resistance and low density. The main characteristics of ceramics for which they are chosen as the matrix material are:

a) They have low densities.
b) Elastic modulus values of ceramics are very high.
c) They can withstand very high temperature (> 2000 °C); hence they can be used in advanced heat engines.

On the other hand, the major disadvantages of ceramic matrix materials are their brittleness and low resistance to crack propagation which makes them easily susceptible to flaws. This is why the existence of even minor surface flaws, scratches or internal defects (pores, microcracks) can result in disaster. The primary reason for reinforcing a ceramic matrix is to increase its fracture toughness. Moreover they usually lack uniformity in properties. They also have low thermal and mechanical shock resistances, as well as low tensile strengths. CMCs are non-brittle refractory materials designed for applications in severe environments (often combining high temperatures, high stress levels and corrosive atmospheres). Naturally, ceramic matrices are preferred for high temperature applications.

Ceramic matrix materials can be classified in different ways. Structural ceramics used as matrix materials can be categorized into two main groups:

a) Oxides: Common oxide ceramics are alumina (Al_2O_3) and mullite (Al_2O_3–SiO_2).
b) Nonoxides: Common nonoxide ceramics are silicon carbide (SiC), silicon nitride (Si_3N_4), boron carbide (B_4C), and aluminium nitride (AlN). According to another classification, ceramic matrix materials can be categorized in the following four main groups:
c) Glass ceramics (*e.g.* lithium aluminosilicate),
d) Oxides (*e.g.* alumina and mullite),
e) Nitrides (*e.g.* silicone nitride), and
f) Carbides (*e.g.* silicone carbide, SiC).

Silicon carbide matrix can withstand high temperature and found wider applications, particularly where high modulus is desired. Silicone nitride matrices are specifically used for the production of ceramic matrix composite systems where tough, strong, oxidation resistant and very high temperature or high heat flux resistant materials are needed, *e.g.* for advanced heat engines. For these kinds of applications, high temperature resistant fibres are being employed (30% aligned SiC, *i.e.* 'SiCS6' fibres) in ceramic matrices. AlN is of interest because of its high thermal conductivity and Si3N4 is considered for applications requiring high strength.

The reinforcements used in CMCs are those fibres that can withstand relatively high temperatures required for the production of ceramics, without significant damage. Other desired requirements are long-term high-temperature stability, creep resistance and oxidation stability. The importance of each of

these demands depends on the type of application. Organic, polymeric fibre materials cannot be used in CMCs because of their degradation at temperatures below 500 °C. Conventional glass fibres having melting or softening points below 700 °C cannot be used for this purpose. Possible candidates for the reinforcement of ceramic materials are polycrystalline or amorphous inorganic fibres or carbon fibres. Commonly used fibres for CMCs are SiC, Si3N4, AlN and other ceramic fibres. Of these, SiC has been the most commonly used reinforcement because of its thermal stability and compatibility with a broad range of both oxide and nonoxide ceramic matrices. Carbon fibres can also be used under certain conditions in CMCs. Although carbon fibres degrade in an oxidizing atmosphere above 450 °C, they are stable under non-oxidizing conditions up to temperatures of 2800 °C.

The forms in which the reinforcement is used in CMCs include whiskers (with length to diameter ratio as high as 500), particulates, and both monofilament and multifilament continuous fibres.

9.2.1.3 Carbon Matrix Composites

Carbon matrix composites are composed of a carbon matrix into which reinforcing carbon fibres are embedded. They are commonly referred to as carbon–carbon (C–C) composites. Fibres in the C–C composites can be either continuous or discontinuous.

Carbon fibre reinforced carbon is a high strength composite material and it is also resistant to high temperature in a non-oxidizing atmosphere. Such composites are thermally stable up to 3000 °C in a non-oxidative environment. But they oxidize and degrade in presence of oxygen, even at 400–500 °C. That's why they need to be protected by a surface coating or must be chemically modified to prevent oxidation. Such a material was first used under extreme thermal and mechanical loads in space technology.

The main application of C–C composites is as braking material. It is used as aircraft brakes, brake system for high-speed trains and racing cars. Its application as braking material is due to high-energy absorption capacity and low specific weight. Some other examples of its use include heavy-duty clutches, tools for high-temperature production of alloys like titanium, *etc*. Lightweight, high-performance brake systems based on carbon–carbon (C–C) materials for brake discs and pads have been known in the aviation industry and car or motorcycle racing field for quite some time. It is also known that this system has some disadvantages such as low friction coefficient at temperatures below 450 °C and high wear of brake pads and discs at elevated operating temperature which can be improved by introducing silicon carbide (SiC) into the carbon fibre reinforced carbon base material.

9.2.1.4 Polymer Matrix Composites (PMCs)

Polymer matrix composites (PMCs) are very popular due to their low cost, simple fabrication methods, lightweight and desirable mechanical properties.

But the main drawbacks of PMCs are their low thermal resistance and high coefficient of thermal expansion. PMCs are the most developed composite materials group and they have found widespread applications. Polymers are long chain molecules containing one or more repeating units of atoms joined together by covalent bonds. Strong fibres reinforced PMCs are characterized by some properties such as high strength, high stiffness, high fracture toughness, good corrosion resistance, abrasion resistance, *etc*. In fibre-reinforced PMCs, fibres may be arranged in different forms such as unidirectional, rovings, woven, short, *etc*. Properties of fibre-reinforced PMCs depend on: (i) properties of the fibres, (ii) orientation of the fibres, (iii) concentration of fibres and (iv) properties of the polymer matrix. Glass fibre reinforced/NR composites fall in this class.

9.3 Reinforcing Agents

Reinforcing agents are special classes of fillers that have better 'reinforcement' properties than the matrix and after incorporation into the matrix, influence the matrix properties. Usually composites consist of a reinforcing material embedded in a matrix. In the broadest sense, composites are the result of a combination of substantial volume fractions of high strength, high stiffness reinforcing components with a lower modulus matrix. Generally, the reinforcing component in a composite structure can be divided into two classes:

(a) Discontinuous: It can be in the form of dispersions/particles, flakes, whiskers and discontinuous short fibres with different aspect ratios.
(b) Continuous: It can be long fibres and sheets.

In practice, the most commonly employed reinforcing component is in particulate or in fibrous form. On the basis of these two types of reinforcing agents, sometimes composites are divided into two groups: particulate reinforced composites and fibre reinforced composites. In addition to these two types of composites, existence of another group of composite system should be noted which is called 'laminar composites (or simply laminates)'. In lamina composites, the reinforcing agents are in the form of sheets bonded together and are often impregnated with more than one continuous phase in the system.[7]

Particulate (or particle) reinforcing agents have aspect ratios around '1' and possess similar length and breadths. They cover particulates of both regular shapes (such as spheres) and irregular shapes that may have extensive convolution and porosity. Particulate reinforcing agents are the most common and the cheapest reinforcing agent. They are divided into two groups: organic (*e.g*. powdered cellulose, powdered rubber, a wide variety of starches and particulate carbon[8] and inorganic (*e.g*. silica and some simple metal oxides like alumina, glass, *etc*.).

Fibres are stronger and stiffer materials than any other form of reinforcements which is the main reason for the overwhelming attraction for fibrous

reinforcements. Fibres are the important class of reinforcements, as they satisfy the desired conditions with strengthening the matrix constituent influencing and enhancing their properties as desired. Generally fibre means a continuous single material whose length is at least 200 times of its width or diameter and filaments are endless or continuous fibres. Fibre reinforcing agents can be either natural or synthetic. Fibres can be used in as woven, non-woven fabrics, yarn or rovings.

9.3.1 Fibres

Fibres are a class of material that are continuous filaments or are in discrete elongated pieces, similar to lengths of thread. They can be spun into filaments, rope or string. Fibres are of two types: natural and synthetic. Figure 9.1 shows a general classification of fibres.

All of the different fibres used in composites have different properties and so affect the properties of the composite in different ways. The mechanical properties of most reinforcing fibres are considerably higher than those of unreinforced resin systems. The mechanical properties of the fibre/resin composites are therefore dominated by the contribution of the fibre to the composite. The four main factors that govern the fibre's contribution are (i) the basic mechanical properties of the fibre itself; (ii) the surface interaction of fibre and resin (the 'interface'); (iii) the amount of fibre in the composite ('fibre volume fraction') and (iv) the orientation of the fibres in the composite.

9.3.1.1 Natural Fibre

Natural fibre-reinforced polymers have created interest in the recent years in the automotive industry. Besides, other applications of natural fibre composites include door inner panel, seat back, roof inner panel, and so on. Natural fibres are being used in automotive industry due to the following reasons:

a) Natural fibres are comparatively of very low cost than glass and carbon fibres.
b) They are biodegradable and environment friendly. Unlike glass and carbon fibres, the energy consumption to produce them is very small.
c) The density of natural fibres is in the range of 1.25–1.5 g/cm^3 whereas that of E-glass fibres and carbon fibres is 2.54 g/cm^3 and 1.8–2.1 g/cm^3, respectively.
d) Natural fibre composites provide higher acoustic damping than glass or carbon fibre composites that makes natural fibres more suitable for noise attenuation which is an increasingly important requirement in automotive applications.
e) The modulus–weight ratio of some natural fibres is greater than that of E-glass fibres indicating that they can be very competitive with E-glass fibres in stiffness-critical designs.

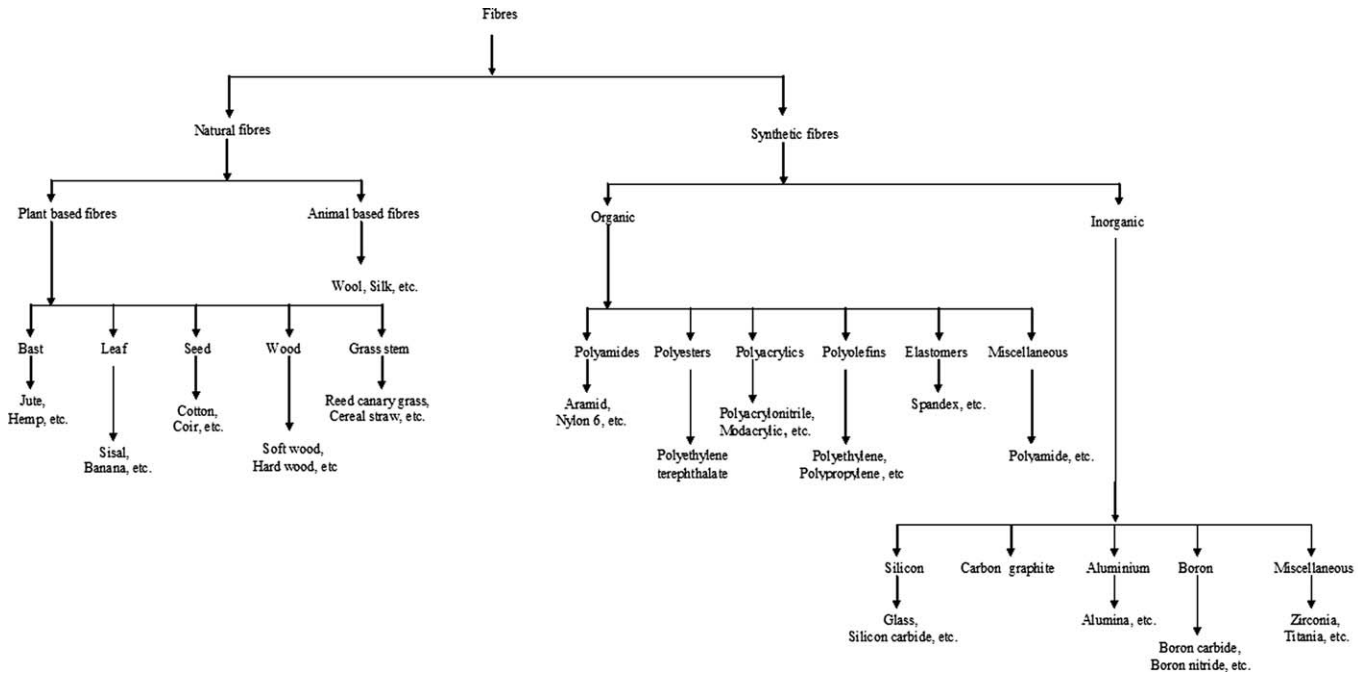

Figure 9.1 General classification of fibres.

However, there are several limitations of natural fibres such as:

a) The strength of natural fibres is relatively low.
b) They absorb moisture.
c) They start to degrade at a comparatively lower temperature than synthetic fibres like glass or carbon fibres.

The two main sources of natural fibres are plants and animals. The main component of animal based fibres is various proteins[9]: examples include mohair, wool, silk, alpaca, angora, *etc*. The components of plant fibres are cellulose microfibrils dispersed in an amorphous matrix of lignin and hemicellulose[10]: examples include cotton, jute, flax, ramie, sisal, hemp, *etc*.

9.3.1.2 Synthetic Fibre

Synthetic fibres are usually more uniform in size, more economical to use and behave in a more predictable manner. For engineering applications the most commonly employed significant fibres are synthetic fibres which includes glass fibres, metallic fibres, organically derived synthetic fibres, *etc*. Most strong and stiff fibres (*e.g*. ceramic, fibres of glass, graphite–carbon, boron carbide and silicone carbide) are usually difficult to use as structural materials in bulk. However, embedding such materials in a ductile matrix (such as a polymer or metal) enables them to behave as a stronger, stiffer, tougher material.

9.3.1.2.1 Glass Fibre. Glass is well known to all of us because the history of glass is ancient although its engineering and scientific development is not ancient. Glass was first produced thousands years ago probably in Egypt (about 4000 years ago) in the furnaces used to produce pottery. But glass in fibre form was invented in the early seventeenth century when the Venetians utilized it to create specialized gowns. However, commercial fibreglass was made in last century. Commercially it was made in 1939 due to the outcome of the joint research efforts of Owen-Illinois and Corning Glass Works. Later, Pittsburgh Plate Glass (now PPG), Pilkington of UK, Libby–Owens–Ford and Vetrotex (a division of St. Gobain) of France, all acquired the licenses from Owens Corning. Interesting reviews can be found in the two books specifically written on this subject.[11,12] In the last decade, Owens Corning, PPG, and Vetrotex International have expanded their production worldwide. In these days, glass fibres are produced in every corner of the world.[13]

Glass fibre production starts with the dry mixing of silica sand and limestone, boric acid and a number of other products such as clay, coal and fluorspar. In a high-refractory furnace, these materials are melted. Although the temperature of the melt being dependent on the glass composition, generally it is about 1260 °C (2300 °F). Molten glass then directly flows to the fibre-drawing furnace in a direct melt flow process or into a marble making machine. These marbles can be either sorted or remelted and drawn into fibres. Continuous glass fibres are produced when molten glass from the fibre-drawing furnace is gravity fed through numerous tiny openings in a platinum alloy tank known as bushing.[14]

Glass fibres are the most common of all reinforcing synthetic fibres for polymeric matrix composites (PMCs). The basic commercial form of continuous glass fibres is strand roving. Strand is a collection of parallel filaments numbering 204 or more. Chopped strands are also used for PMCs which is produced by cutting continuous strands into short lengths. Roving is a group of untwisted parallel strands (also known as ends) wound on a cylindrical forming package and are used in continuous moulding operations like filament winding and pultrusion. They can also be pre-impregnated with a thin layer of polymeric resin matrix to form prepregs. Prepregs are subsequently cut into required dimensions, stacked, and cured into the final shape in batch moulding operations for example compression moulding and hand layup moulding. Glass fibres are also available in woven form (like woven roving or woven cloth). Woven roving looks like a coarse drapable fabric in which continuous rovings are woven in two mutually perpendicular directions. On the other hand, woven cloth is weaved using twisted continuous strands called yarns. Both woven roving and cloth provide bi-directional properties that depend on the style of weaving as well as relative fibre counts in the length (warp) and crosswise (fill) directions. The principal advantages of glass fibres are low cost, high tensile strength, high chemical resistance, and excellent insulating properties. The disadvantages are relatively low tensile modulus and high density (among the commercial fibres), sensitivity to abrasion during handling (which frequently decreases its tensile strength), relatively low fatigue resistance, and high hardness (which causes excessive wear on moulding dies and cutting tools).[15]

9.3.1.2.1.1 Types. Different types of glass fibres are available depending on the properties desired from the resulting fibres. For example: A-glass fibre, C-glass fibre, D-glass fibre, E-glass fibre, Low K fibre, R-glass fibre, S-2 glass fibre, Te glass fibre, Hollow fibre, *etc.*[14] A-glass fibre is a high alkali or soda glass fibre and used in applications where good chemical resistance is needed. C-glass fibre is a material based on soda borosilicate and offers excellent chemical resistance. D-glass fibre is a low dielectric fibre having low density, low dielectric constant and low dielectric loss. It is an ideal reinforcement for making light weight and high-performance radar masks with high wave permeability and wide frequency band and print circuit board. E-glass fibre is a low alkali glass fibre, based on aluminium borosilicate. This glass possesses excellent electrical insulation properties and is the exclusive glass fibre used in the majority of textile fibreglass production. S-2 glass fibre is made up of aluminium silicate and magnesium and offers higher physical strength. R-glass fibre is alkali resistant and is used in reinforcing concrete. Hollow glass fibres are tube-like or hollow fibres and have specific applications in reinforced aircraft parts where weight could be significant. Te glass having high strength is a Japanese manufactured S-glass for higher strength structural application. Table 9.1 shows composition of some glass fibres.

9.3.1.2.1.2 Properties of Glass Fibres. Composition of the original glass melt has significant role in determining the properties of the glass fibres. The widespread use of glass fibres which is continuing in numerous and diverse

Table 9.1 Compositions of various glass fibres (wt%).

	Grade of glass			
Components	*A (high alkali)*	*C (chemical)*	*E (electrical)*	*S (high strength)*
Silicon oxide	72.0	64.6	54.3	64.2
Aluminium oxide	0.6	4.1	15.2	24.8
Boron oxide	–	4.7	8.0	0.01
Barium oxide	–	0.9	–	0.2
Ferrous oxide	–	–	–	0.21
Sodium oxide	14.2	7.7	0.6	0.27
Potassium oxide	–	1.7	–	–
Calcium oxide	10.0	13.2	17.2	0.01
Magnesium oxide	2.5	3.3	4.7	10.27
Miscellaneous	0.7	–	–	–

applications can be directly related to its inherent unique properties. Some important properties are mentioned below[14]:

High tensile strength: Glass fibre has exceptionally high tensile strength compared with other textile fibres. Its strength to weight ratio exceeds steel wire in some applications.

Heat and fire resistance: Being inorganic, glass fibre does not burn or support combustion.

Chemical resistance: Glass fibre has excellent resistance to lots of chemicals. It is impervious to bacterial, fungal or insect attack.

Moisture resistance: Glass fibre does not absorb water. It neither swells or stretches nor disintegrates. Glass fibre does not readily rot. It can maintain its mechanical strength in humid environments.

Thermal properties: Glass fibre has low coefficient of thermal linear expansion and high coefficient of thermal conductivity. So it can exhibit excellent performance in thermal environments.

Electrical properties: Glass fibre is nonconductive and is an ideal choice for electrical insulation, where designers can make use of the high dielectric strength and low dielectric loss properties.

In manufacturing glass fibre reinforced composites, we may take advantage of one or more of the above properties. For example, aircraft industry has found glass fibre an excellent reinforcement for radome applications due to its high strength and excellent electrical properties. For various applications glass fibre is chosen as reinforcement because it allows composites to retain maximum properties in high moisture environments. E-glass fibres are the material of choice because of their excellent water resistance. It is interesting to know that E-glass fibres exhibit only a 1–7% weight loss when exposed to boiling water for 60 min. It is well known that water resistance helps maintaining physical and electrical characteristics of the composite over prolonged time exposure to aqueous atmospheres.

A comparison of properties between E-glass fibre and different natural fibres are shown in Table 9.2.[16]

Table 9.2 A comparison of the properties of E-glass fibre and various natural fibres.[16]

Parameter	*Unit*	*Flax*	*Jute*	*Hemp*	*Cotton*	*Kenaf*	*Ramie*	*Sisal*	*E-glass*
Diameter	m	11–33	200	15–50	–	200	40–80	50–200	5–25
Fineness	dtex	1–7	2–3	2–6	1–4	5–6	5–13	–	–
Length	mm	10–40	1–5	15–28	10–60	2–6	60–260	1–5	–
Maximum stress	cN/tex	30–62	30–34	35–70	25–50	34.5–50	40–70	30–45	–
Tensile strength	Mpa	345–1035	393–773	690–1000	330–585	930	400–1050	511–635	1800
Young's modulus	Gpa	27.6–45.0	26.5	50.0	4.5–12.6	53.0	61.5	9.4–15.8	69.0–73.0
Density	g cm^{-3}	1.43–1.52	1.44–1.50	1.47–1.50	1.5–1.54	1.5	1.5–1.6	1.16–1.5	2.5
Maximum strain	%	2.7–3.2	1.5–1.8	1.0–1.6	7–8	1.6	3.6–3.8	2.0–2.5	2.5–3.0
Specific tensile strength	km	73.8	52.5	69.3	39.2	63.2	71.4	43.2	73.4
Specific stiffness	km	3.21	1.80	3.47	0.85	3.60	4.18	1.07	2.98

9.4 Matrix

As stated earlier, the matrix holds the reinforcement in a composite. Matrix supports the fibres and keeps them together in the composite material. If load is applied to composite, matrix transfers that to the fibres, thereby keeping the fibres in their position and chosen orientation. The matrix also gives the composite environmental resistance. Some important functions of the matrix in FRCs are: (1) to hold the fibres in place in the structure, (2) to protect the fibres from environment, (3) to help to distribute or transfer loads, (4) to enhance transverse properties of a laminate, (5) to improve impact and fracture resistance, (6) to avoid propagation of crack growth through the fibres by providing alternate failure path along the interface between the fibres and the matrix, (7) to carry interlaminar shear, *etc*.

Matrix must have some desired properties which are important for a composite structure. Some of these properties are:

a) Matrix must wet the fibres with bonding.
b) Minimization of moisture absorption.
c) Easily processable into the desired composite shape.
d) Must flow to penetrate the fibre bundles completely and eliminate voids.
e) Must have reasonable strength, modulus and elongation (elongation should be greater than fibre).
f) Have low shrinkage and coefficient of thermal expansion.
g) Must be elastic to transfer load to fibres.
h) Have dimensional stability to maintain its shape.

There are many matrix choices available and different types have different impact on the processing techniques, physical and mechanical properties and environmental resistance of the finished composites. In selecting matrix material, some factors may be taken into consideration like: (1) the matrix must be easy to use in the selected fabrication process, (2) the resultant composite should be cost effective, (3) the matrix is be able to withstand service conditions, viz., temperature, humidity, exposure to ultraviolet environment, exposure to chemical atmosphere, abrasion by dust particles, *etc*.

Matrix can be classified in different ways. Generally it can be divided into three classes: ceramic, metal and organic. As we have mentioned, organic matrix is subdivided into two classes, namely polymer matrix and carbon matrix. Natural rubber (NR) is one of the widely used biodegradable polymeric matrices.

9.4.1 Natural Rubber

Rubber is an elastomer, *i.e*. a polymer that has the ability to regain its original shape after being deformed. Rubber is also tough and resistant to weathering and chemical attack. Rubbers have high elastic properties and can be stretched near about 300%.[17] The unstretched rubber is amorphous and the polymer

chains are in a coiled state. Unstretched rubber on stretching gets aligned causing crystallization. In releasing the stress the chains revert back to their original coiled state. NR is polymerized isoprene, which occurs in the latex (a milky colloid) of various trees. One of these plants is the tree *Hevea brasiliensis* species of the family *Euphorbiaceae*, native to Brazil. The molecular weight of raw rubber is about 100,000–150,000.[17]

9.4.1.1 History

Early 'rubber technologists' were found among the Aztecs and Mayas of South America well over 2,000 years ago who used rubber for coated fabrics, shoe soles and playballs. An article of Malaysian Rubber Producers' Research Association mentions that the Aztec king, Montezuma was paid tribute by the lowland tribes in the form of 16,000 rubber balls, and that ball courts have been excavated in Snaketown in the south-western United States dating back to AD 600–900.

Charles Marie de La Condamine is credited with introducing samples of rubber to the Académie Royale des Sciences of France in 1736 and his paper published in 1755 described many of the properties of rubber. This has been referred to as the first scientific paper on rubber. In 1770 English chemist Joseph Priestley, the discoverer of oxygen, proposed the name 'rubber' for the substance because it could be used to erase pencil marks by its rubbing on paper in lieu of previously used bread crumbs. In 1791 rubber was first used commercially when English manufacturer Samuel Peal patented a method of making waterproofing cloth by treating it with a solution of rubber in turpentine. In 1820 the modern rubber industry began when English coach maker and inventor Thomas Hancock established the first rubber factory. He was the first to compound rubber with other materials to be shaped into moulds, a common modern industrial practice. In 1823 Scottish chemist and inventor Charles Macintosh started manufacturing double-textured rainproof garments known as 'mackintoshes'. He made these by introducing a coal tar naphtha solution of rubber between two pieces of fabric, thus circumventing the sticky (when warm) and brittle (when cold) surfaces associated with single-textured rubber-containing garments.

South America remained the main source of the limited amounts of latex rubber that were used during much of the 19th century. In 1876, Henry Wickham gathered thousands of para rubber tree seeds from Brazil, and these were germinated in Kew Gardens, England. The seedlings were then sent to Ceylon (Sri Lanka), Indonesia, Singapore and British Malaya. Malaya (now Malaysia) was later to become the biggest producer of rubber. About 100 years ago, the Congo Free State in Africa was also a significant source of NR, mostly gathered by forced labour. Liberia and Nigeria also started production of rubber. In India, commercial cultivation of NR was introduced by the British planters, although the experimental efforts to grow rubber on a commercial scale in India were initiated as early as 1873 at the Botanical Gardens, Calcutta. The first commercial *Hevea* plantations in India were established at Thattekadu

in Kerala in 1902. In the 19th and early 20th century, it was often called 'India rubber'. Nowadays, Indonesia, Malaysia, Thailand, China and India currently produces more than 80% of NR.

9.4.1.2 Sources of NR

NR is *cis*-1,4-polyisoprene and is present as latex in a large variety of plants in many regions of the world. Latex containing appreciable quantities of rubber occurs in certain plant species belonging to the *Moraceae, Euphorbiaceae, Apocynaceae* and *Compositae* families as listed in Table 9.3. The most important source is the tree *Hevea brasiliensis*. Latexes from the other sources suffer from disadvantages such as low rubber content, high resin content and difficulties in extraction. However, *Parthenium argentatum*, which yields guayule rubber has gained some importance in the last two decades. This is because this shrub can be cultivated in the semi-arid regions of South-Western USA and Mexico.[18]

9.4.1.3 Structure and Composition of NR

Structure:
Chemically, NR is a polymer of 2-methyl-1,3-butadiene, also known as isoprene (Figure 9.2). Isoprene is a conjugated diene containing double bonds at alternate positions.

Like substituted ethylene, isoprene undergoes free radical polymerization. Polymerization of isoprene results in the polymer polyisoprene, which is a simple alkene having one double bond in each unit (Figure 9.3). Polymerization of isoprene may follow one of two pathways: *cis*-polymerization or *trans*-polymerization.

Figure 9.4 shows *cis*- and *trans*-polyisoprene. The rubber formed from *cis*-polymerization is called *cis*-polyisoprene and is the main constituent of NR.

It is presumed that NR is a pure *cis*-1,4-polyisoprene, containing no detectable amounts of *trans*-1,4 and 3,4 units as indicated by ^{1}H-NMR at

Table 9.3 Major plant sources of NR.

Family	*Popular name*	*Species*
Euphorbiaceae	Para rubber	*Hevea brasiliensis*
Euphorbiaceae	Ceara rubber	*Manihot glaziovii*
Compositae	Guayule rubber	*Parthenium argentatum*
Moracea	India rubber	*Ficus elastica*
Moracea	Panama rubber	*Castilla elastica*
Apocynaceae	Lagos silk rubber	*Funtumia elastica*

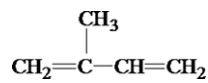

Figure 9.2 Structure of isoprene (monomer of natural rubber).

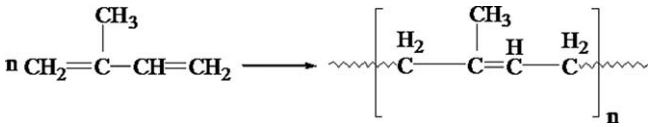

Figure 9.3 Polymerization of isoprene to *cis*-polyisoprene, the main constituent of natural rubber.

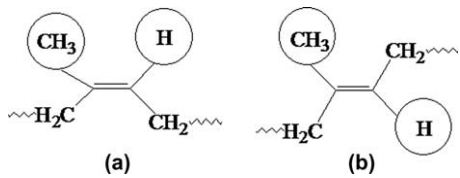

Figure 9.4 Structure of (a) *cis*- and (b) *trans*-polyisoprene.

100 MHz.[19] Oligomers of natural isoprene that consist of 9–23 isoprene units, referred to as polyprenol, can be a good model for structural analysis of naturally-occurring polyisoprenes. Polyprenol is categorized into three classes: all-*trans* (Solanesol-type), two-*trans* and poly-*cis* (Betulaprenol-type), and three-*trans* and poly-*cis* (Ficaprenol-type). Surprisingly, a polyprenol of all-*cis* configuration has not been reported.[20]

The sequence distribution of both *cis*- and *trans*-isoprene units in polyprenol can be analysed by ^{13}C-NMR using acyclic terpenes of all the arrangements of both *cis*- and *trans*-isoprene units. The chemical shifts of signals reflect independent sequence distribution. It is independent of the degree of polymerization for polyprenols, longer than 10-mer.[21,22] In this case, the dimethylallyl group and hydroxylated isoprene unit are referred to as ω and α terminals, respectively. In all the polyprenols, *cis–trans* linkage is absent and only one *trans–cis* linkage is present per chain indicating that the *trans–cis* polyprenols are diblock copolymer, aligned in order of ω-$(trans)_2$ or $_3$-$(cis)_n$-OH. Solanesol is a homologue of every *trans*-acyclic terpenes.

NR produced from *Hevea brasiliensis* showed clear ^{13}C-NMR signals because of *trans*-isoprene units in the *trans–trans* linkage, the relative intensity of which decreases with increasing the molecular weight of fraction. It can be presumed that these *trans*-isoprene units are derived from an initiating species of rubber formation and not isomerisation of *cis* isoprene units. This can be presumed because the *trans*-isoprene units were in the *trans–trans* linkage and not in the *cis–trans* linkage.[23] At 500 MHz, the ^{1}H-NMR spectrum of polyprenols gives isolated signals for the methyl protons of *trans*-isoprene units in *trans–trans* and *trans–trans–trans* sequences.[24] The methyl proton signals of NR shows striking resemblance to two-*trans* polyprenol. However the signal from dimethylallyl group itself is not detected. Accordingly, the structure of NR was postulated to be a kind of two-*trans* and poly-*cis* rubber as found in literature.[25,26]

Composition:
The composition of *Hevea* latex varies with age of tree, condition of soil, climatic conditions, season, *etc*. An average composition is shown in Table 9.4.

9.4.1.4 Properties

The physical and chemical properties of the rubber are influenced by the presence of the non-rubber substances. NR is a natural polymeric substance having high molecular weight, possessing viscoelastic properties. As we have already discussed and shown in Figure 9.3, structurally it is *cis*-1,4-polyisoprene, *i.e*. a diene, and 1,4-addition leaves a double bond in each of the isoprene units in the polymer. Because of this, it shows all the reactions of an unsaturated compound. It gives addition compounds with hydrogen chloride, halogens, ozone and several other reactants that combine with olefins. An interesting reaction of NR is its combination with sulfur, called 'vulcanization'. This reaction converts the raw rubber into an elastic material. Vulcanized rubber possesses high tensile strength, hardness and abrasion resistance. Because of the unique combination of these properties, NR finds application in the manufacture of various types of products. Some physical properties of NR are shown in Table 9.5.

9.4.1.5 Preservation and Coagulation of Latex

After tapping a small amount of a preservative is mixed with the rubber latex because the latex is unstable. It undergoes putrefaction and tends to coagulate

Table 9.4 Average composition of *Hevea* latex.[27]

Ingredients	*Composition*
Rubber hydrocarbon	30–40%
Proteins	1.9–2.5%
Fats and other related compounds	0.9–1%
Sugars (carbohydrates)	1–1.5%
Ash	0.4–0.6%
Water	55–65%

Table 9.5 Physical properties of NR.

Specific gravity	0.92
Heat of combustion	10547.084 cal/g
Thermal conductivity	0.00032 cal/s/cm/°C
Refractive index	1.52
Cohesive energy density	63.7 cal/cm^3
Coefficient of cubal expansion	0.00062/°C
Power factor (at 1000 cycles)	0.15–0.2
Dielectric constant	2.37
Dielectric constant	3937 V/mm
Volume resistivity	1015 ohm.cm

at different rates on standing, depending on storage conditions. Preservation is possible over longer period of time using ammonia with or without sodium pentachlorophenate as the preservative. The *Hevea* rubber latex globules are about 0.2 micron in diameter.[27] These latex are usually constituted of three characteristic layers: the core consisting of lower molecular weight, sol rubber with an immediate outer layer or skin of higher molecular weight and gel rubber. The outermost layer (surface) is sorbed layer consisting mainly of soaps and proteins. They impart a negative electrical charge to the globules upon ionization. On arrival at the factory, the *Hevea* latex is somewhat diluted and strained through a sieve (60–80 mesh) to remove foreign particles and dirt. Most *Hevea* rubber reaches the user industry in the form of pale crepe or smoked sheet. The dilution level of the latex before coagulation and creaming depends on what type of rubber is desired to be made. The coagulation is done by the addition of acetic or formic acid. The coagulum contains nearly 80% of water. Much of the serum is removed from the rubber hydrocarbon by washing with water and squeezing through rollers. For crepe rubber manufacture, the wet strip is heavily milled and the sheets formed are finally dried before packing. If smoked sheet is desired to produce, light milling of the wet strips is allowed on the rollers and final drying of the ribbed sheets is accomplished in a smoke house. Spray dried 'whole-latex' rubber may be produced which will contain all the solid impurities present in the latex.[27]

9.4.1.6 Vulcanization

Raw and unvulcanized rubbers are entangled high molecular weight viscoelastic liquids. They are generally not very sticky, strong, brittle when cold, easily deformed when warm and incapable of maintaining their shape after a large deformation. Raw rubbers are completely soluble in solvents and have a consistency similar to chewing gum. They give rise to inelastic deformation being made of long polymeric chains that can move independently to each other. It is not possible to use uncured rubbers to make articles with a good level of elasticity. The transformation of rubbers to useful articles such as tires and mechanical goods is due to the discovery of the vulcanization process by Goodyear.[28] During 1839, this American inventor developed the method of vulcanization of rubber by which the properties of NR can be improved to a large extent. Vulcanization is a process of compounding rubber with different chemicals.

Vulcanization increases the overall elasticity of rubbers significantly by locking the chains to each other which greatly decreases the amount of slipping, the chains can undergo. This is the process of crosslinking. Cured rubber is heat resistant and much more dimensionally stable material.[29] Vulcanization reaction is an irreversible process that gives rise to the formation of a three-dimensional network structure of polymer chains. These chains are chemically bonded to one another converting a plastic material into an elastic one. This transformation can occur through various chemical mechanisms such as

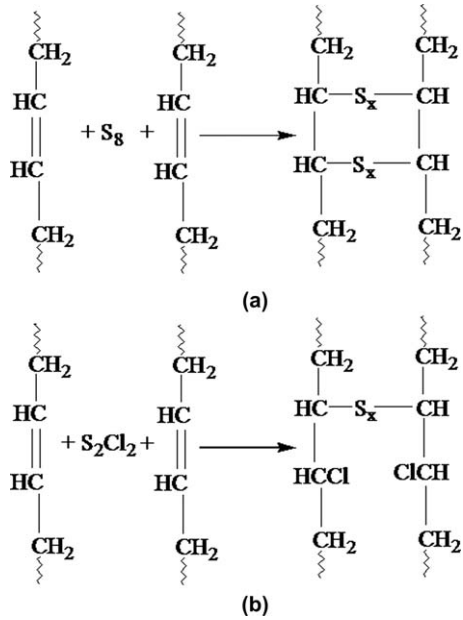

Figure 9.5 Vulcanization of NR with (a) sulfur and (b) disulfur dichloride.

addition or condensation, nucleophilic substitution, free radical coupling and ring opening reactions, end linking, *etc*. Several crosslinking systems such as sulfur, sulfur donors, organic peroxide, silane, amino acids, phenolic resins, bismaleimides, azide compounds, benzenoquinone, aldehydes, electron beams, UV radiation, gamma rays, ultrasonic waves, microwave, *etc*. have been used for the rubber vulcanization. Among these, sulfur vulcanization is the most widely used in the rubber industry.[30]

In sulfur vulcanization, the rubber is heated with sulfur or sulfur compounds at a temperature of 150 °C for a few hours. It converts rubber into a tougher product giving the rubber better elasticity over a wide range of temperature. Sulfur and sulfur compounds react with rubber molecules to effect crosslinking during vulcanization, as shown in Figure 9.5.

The vulcanization process converts the NR into either soft rubber, which contains about 5% sulfur, or hard rubber, containing about 30–35% sulfur. A comparison of the properties of natural and vulcanized rubber is given in Table 9.6.

Properties of vulcanized rubber can be further enhanced by the addition of certain organic substances (also known as accelerators) and certain inorganic compounds (also known as activators).[31] Commonly used accelerators are tetramethyl thiouran disulfide and diphenylguanidine. Commonly used activators are oxides and salts of calcium, zinc and lead. To prevent the oxidation of rubber, a little amount (1–2%) of antioxidant such as hydroquinone monobenzyl ether, phenyl β-naphthylamine, *etc*. are added.[31]

Table 9.6 Comparative study between natural and vulcanized rubber.[17,31]

Property	*Raw rubber*	*Vulcanized rubber*
1. Resilience	good	much better
2. Quality	inherent	can be controlled by vulcanization
3. Elasticity	very high	low, depending on percentage of sulfur
4. Tackiness	marked	low
5. Resistance to organic solvents	low	much higher but swells
6. Tensile strength	200 kg/cm^2	2000 kg/cm^2
7. Durability	less	better
8. Insulation property	good	much better
9. Useful temperature range	10 °C to 60 °C	−40 °C to 100 °C
10. Chemical resistance	very bad	very good
11. Water absorption tendency	large	small

Vulcanized rubber has some advantages. Some of them are as follows:

1. Vulcanized rubber has good tensile strength and extensibility.
2. It is better electrical insulator than NR.
3. It shows low water absorption tendency.
4. It possesses higher resistance to oxidation and abrasion.
5. It is resistance to organic solvents such as benzene, petrol, CCl_4, oils and fats.
6. It has excellent resilience *i.e.*, articles made from it regains original shape after the removal of the deforming load.
7. It has higher resistance to wear and tear as compared to raw rubber.

9.4.1.7 *Advantages of Rubber as a Matrix over Metals*

In lots of applications for rubber products, it is not possible to find alternative materials except other rubbers. Rubbers have very high deformability and consist of molecules of very high molecular mass. These molecules present in rubber, can be crosslinked together to form a network. In the case when crosslink density is not too high, the material keeps a memory of its original unstressed state. As a result it will return to its original dimensions when external forces are removed (even after strains as high as 1000%). This ability to recover its original dimensions leads to many applications.[18]

The main advantage of rubber as a matrix over metals is that rubber does not 'corrode' like metals (*e.g.* iron). This makes rubber in applications such as bridge bearing effectively 'maintenance free'. Engineers are familiar with metals. It might be interesting for them to get a brief comparison between metals and rubber. For convenience steel can be compared with rubber which is an alloy of iron. One of the most important things to be considered is that rubber can be thought of as an energy storage device. It converts kinetic energy and storing it as potential energy. It is capable of storing 150 times more energy than steel.[32]

If we compare a tall block of rubber with a short block, the tall one can be compressed more per unit thickness, even though the cross-sectional area and load on that area is the same for both blocks. The short block is apparently 'harder' than the tall block. But for steel, all blocks (no matter tall or short) will deflect to the same extent per unit thickness. This property makes rubber extremely versatile since stiffness of a rubber product can be altered by a simple change in its shape.[29]

If we consider tensile strength at break, we can find that rubber at its best has a value around 35 MPa, while that of carbon steel is about 500 MPa. It would appear that steel is vastly stronger than rubber. But according to Lindley,[33] if we take the cross-section of the rubber at the point when it breaks (since it is still elastic up to this point) rather than the original cross-section, and then recalculate the tensile strength (force/area), it begins to approach that of steel.

Steel can only be stretched to about 2% of its original dimension, while still remaining elastic. On the other hand, while possibly not being as resilient, rubber can keep most of its elasticity when stretched anywhere from one hundred to several hundred percent. When an elastic material is stressed, then upon release of the stress, no permanent strain remains. Many engineers would like to consider the property 'elastic modulus'. For steel this is the same as Young's modulus.[29] For steel it can be considered as constant and can be relied on like the sun coming up each morning. For rubber, the case is not like this. Due to stretching, the modulus changes as it is stretching. If rubber is heated or cooled, it stretches quickly or slowly, it keeps changing and it even changes from one stretch cycle to the next.[29]

9.5 Glass Fibre/NR Composites

Glass fibres are the most common of all reinforcing synthetic fibres for polymeric matrix composites (PMCs). The major advantages of glass fibres are high tensile strength, low cost, high chemical resistance and excellent insulating properties. The disadvantages are relatively low tensile modulus and high density (among the commercial fibres), high hardness which causes excessive wear on moulding dies and cutting tools, sensitivity to abrasion during handling which tends to decrease its tensile strength, relatively low fatigue resistance, *etc*. For fibre-reinforced polymers (FRPs), two types of glass fibres commonly used: E-glass and S-glass.[15] The letter 'E' stands for 'electrical' as the composition has a high electrical resistance and 'S' stands for strength. Another type, known as C-glass, provides greater corrosion resistance to acids than is provided by E-glass fibre and is used for chemical applications. S-glass was originally developed for aircraft components and missile casings and has the highest tensile strength among all the glass fibres in use. E-glass has very low cost of all commercially available synthetic reinforcing fibres, which is the reason for its widespread use in the FRP industry. Due to compositional difference and higher manufacturing cost, S-glass fibre is more expensive than E-glass fibre. A lower cost version of S-glass, called S-2 glass, is also available.

Long fibre reinforced thermoplastics have attracted huge interest in automotive industry because of their better structural performance like high strength, higher elastic moduli, durability, *etc*. However, in order that long fibre reinforced composites can be efficiently used for automotive applications, there is a tremendous need to develop process and constitutive models as well as computational tools to predict the microstructure of the formed composites and its resulting properties and macroscopic responses from processing to the final product. Reinforcement of short fibre affect the mechanical properties of rubber composites. The primary effects include decreased elongation at failure, increased modulus, greatly improved creep resistance over particulate-filled rubber, increased hardness and a substantial improvement in cut, tear and puncture resistance. Fatigue strength of the composites are also improved. Tensile strength develops a characteristic drop with increasing fibre volume content when fibres are aligned parallel to the stress direction and it develops until a critical fibre level is reached. The critical concentration level at which the unreinforced matrix strength is recovered is directly related and varies with the critical fibre aspect ratio. With fibre concentration, the stiffness and modulus of short fibre composite increase though it may not be necessarily linear. With the increase in concentration, tear strength also increases as it is highly dependent on fibre loading.

The major ingredient of glass fibre is silica which is mixed with varying amounts of other oxides. Glass fibres are used successfully for reinforcing the plastics and therefore, the suitability of this fibre as a reinforcing material for rubbers has been studied. Glass fibres can provide high initial aspect ratio but brittleness causes breakage of the fibres during processing. Czarnecki and White[34] have studied the mechanism of glass fibre breakage. They also studied severity of breakage with time of mixing. Gregg *et al.*[35] studied glass fibre/rubber composites and found that the tensile strength of glass fibre/NR composites decreases with the increase in atmospheric humidity during the glass fibre storage. Marzocchi *et al.*[36] studied the development of glass fibre–elastomer composites with improved strength and wear resistance to be used in V-belts, conveyor belts and auto tires. Derringer[37] studied the advantages of short glass fibre-reinforced rubber composites, which included high modulus, low creep and high resilience. Murty and coworkers studied physical properties and the extent of fibre–matrix adhesion of short glass fibre-reinforced NR and synthetic rubber composites.[38–40] Murty added to NR matrix up to 75 phr of short glass fibre. The resulted composites showed anisotropy in technical properties only when added at >25 phr.[39] Lee[41] studied the mechanical properties along with morphology of short glass fibre-reinforced polychloroprene composites. The author developed a set of constitutive equations for predicting the anisotropic stress–strain properties and also developed a thermodynamic mixing rule.

Strain-induced crystallization is the property that makes NR a very strong matrix because of its. It has been observed that generally the tensile strength shows initial drop down to a certain amount of fibre and then increases. The fibre reinforces the matrix above critical volume which is the minimum volume

of fibre needed for reinforcing. The nature of matrix and fibre, fibre aspect ratio and fibre /matrix interfacial adhesion strongly affect critical volume.[42] At low fibre concentrations, the fibre acts as a flaw in the rubber matrix and the matrix is not restrained by enough fibres. This phenomenon cause highly localized strains to occur in the matrix at low stress and makes the bond between fibre and rubber to break leaving the matrix diluted by non-reinforcing debonded fibres.[42] With the increase in the fibre concentration, strength of composite increases because stress is more evenly distributed. The incorporation of fibre into rubber matrix increases the hardness of the composite, which is related to toughness and strength. The close packing of fibres in the compounds increases the density but decreases the resilience.[42]

9.5.1 Fabrication of Glass Fibre/NR Composites

Fibre-reinforced NR composites are manufactured by various processes, the most common being extrusion, injection moulding and compression moulding (Figure 9.6). To fabricate glass-reinforced NR composites with unidirectional long fibres, extrusion is not used because this process can only result in short fibre-reinforced polypropylene composites (a few millimetres at most).

9.5.1.1 Extrusion Moulding

Extrusion process is a continuous process by which many products like pipes, sheets, fibre, *etc*. can be manufactured. Extrusion of thermoplastics is a process in which the material is melted by external heat/frictional heat and conveyed forward by a screw to the opening of the die. The die gives shape of the required product. Extruders mainly comprise of three parts: hopper, barrel/screw and dies. A principal function of the extruder for rubbers and plastics is to pump material in a fluid state against the back pressure created by the resistance of the die. This flow is complex, helps mixing and energy is transformed into heat by shearing, leading to temperature changes and distribution.[43] In an extruder, a screw pushes mixture of fibre and rubber through a heated cylinder, changing rubber from solid to liquid and mixing with the fibres as it moves through the barrel followed by the die which will give the mixture a constant cross-sectional area. Extruder can be either single screw or twin screw type. Extrusion method is widely used to fabricate short fibre reinforced rubber composites.

9.5.1.2 Injection Moulding

Injection moulding refers to a process that generally involves forcing or injecting a fluid plastic material into a closed mould of desired shape. The moulding compound is fed into injection chamber through the feed hopper. In the injection chamber, the moulding compound is heated wherein it changes into liquid form. It is forced into the injection mould by the plunger. This method is normally used for high-volume and low-cost component manufacturing. Both thermoplastic and thermoset are subjected to injection

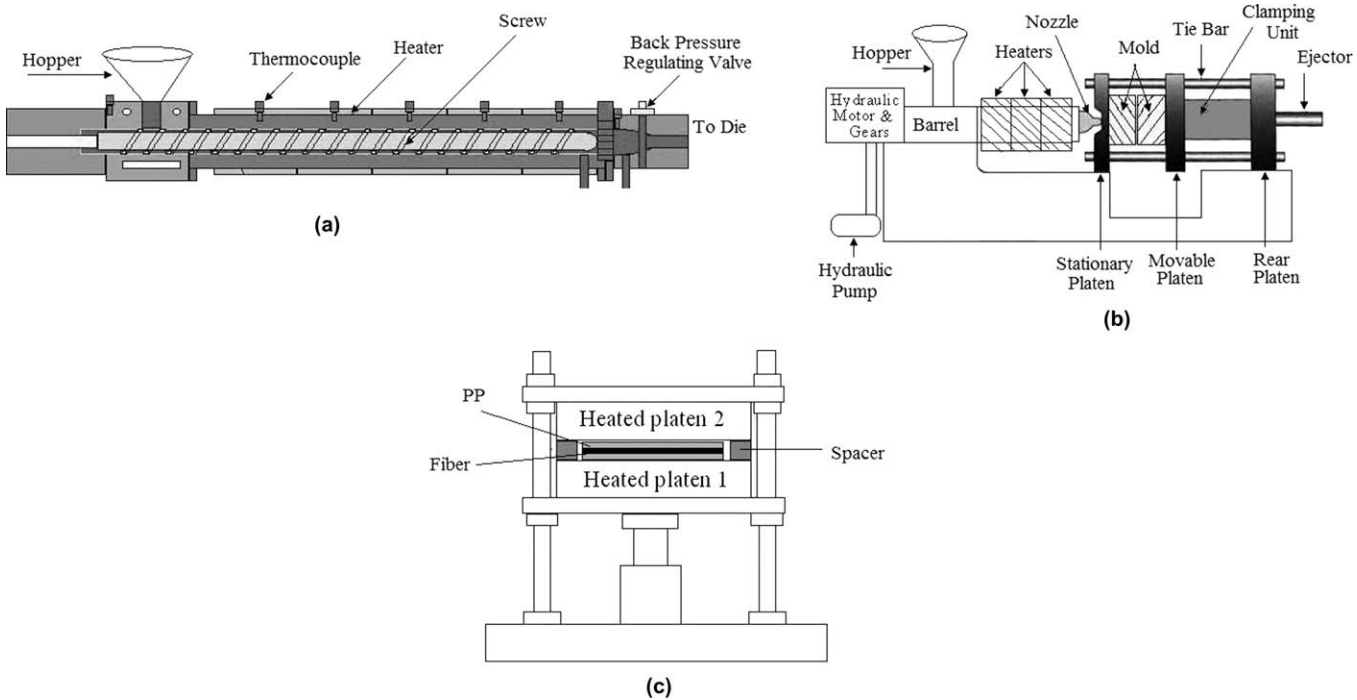

Figure 9.6 (a) Extrusion, (b) injection and (c) compression moulding machines.

moulding.[44] A thermoplastic material is first melted and then forced through an orifice into the mould which is kept relatively cool. The material solidifies in the mould from which it can then be removed. But in thermoset injection moulding, high temperature is required for solidification. Therefore, a reaction material is forced into a generally warm mould in which the material further polymerizes into a solid part. This method is suitable for high-volume and low-cost component manufacturing. But the method is limited to materials with short fibres.

9.5.1.3 Compression Moulding

Compression moulding is one of the oldest manufacturing techniques that use large presses to compress the prepreg material between two matched steel dies.[45] The recent development of high strength, fast cure, sheet moulding compounds and advancement in press technology has made this process very popular for mass production of composite parts. In comparison with the injection moulding process, better physical and mechanical properties can be obtained in compression moulding. This process utilizes large tonnage presses wherein the curing occurs between two matched steel dies under pressure and high temperature. Compression moulding basically involves the pressing of a deformable materials charged between the two heated mould, and its transformation into a solid product under the effect of the elevated mould temperature. After placing the laminate to be cured, the cavity is closed. The moulds are heated to a high temperature which causes the charge viscosity to be reduced. With increasing mould pressure, the charge flows towards the cavity extremities, forcing air out of the cavity. High pressure helps to eliminate the problem of development of voids. The primary advantage of the compression moulding is its ability of producing large number of parts with little dimensional variations. Various shapes, sizes and complexity can be achieved by compression moulding. This process has high tooling cost and not practical for low volume production. It is very important to control the cure time otherwise cracking, blistering or warping may occur.

9.5.1.4 Transfer moulding

Transfer moulding is sometimes used to fabricate glass fibre/NR composites. Transfer moulding is a form of injection moulding. Rubber to be cured is held in a heated reservoir, the amount of rubber to fill the mould is subjected through sprues or a runner system and into the mould cavities by a piston by applying force. Pressure is maintained by the piston and a mould closure system. The mould must be hot enough to ensure sufficient temperature for curing of the rubber although the reservoir has to be at a lower temperature.

9.5.2 Mechanical Properties of Glass Fibre/NR Composites

As in the case of other fibres, glass fibres also exhibit a minimum concentration of fibre[45,46] below which no reinforcement can be achieved using glass fibres.[39]

Table 9.7 Tensile properties of different glass fibres.

	Grade of glass			
Mechanical properties	*A*	*C*	*E*	*S*
Tensile strength (MPa)	3033	3033	3448	4585
Tensile modulus of elasticity at 22 °C (GPa)	–	69	72.4	85.5

For glass fibre reinforced NR composites, mechanical properties are of major concern as reinforcement affects the mechanical properties of glass fibre/NR composites. Tensile, bending, impact strength, elongation at break and hardness are some mechanical properties that are considered significantly for FRCs. The mechanical properties of glass fibre/NR composites strongly depend on properties of glass fibres. Tensile properties of some glass fibres are listed in Table 9.7.[14] It is seen from the table that E-glass fibre has better tensile properties than A-glass fibre. So, it is expected that E-glass/NR composites will show better tensile properties than A-glass/NR composites.

It is often observed that increase in fibre content leads to an increase in the strength and modulus of a fibre reinforced polymer matrix composite.[47–52] Joseph *et al*.[53] have studied the influence of interfacial adhesion on the mechanical and fracture behaviour of short sisal fibre reinforced polymer composites of several thermoset resin matrices and a thermoplastic matrix with respect to fibre length and fibre loading. He observed that all the composites showed a general trend of increasing properties with fibre loading. Generally with the increase in fibre content, strength of fibre reinforced polymer composites increases up to a certain limit and then decreases with further increase in fibre content. Mechanical properties also depend on fibre orientation. It varies for unidirectional and non-unidirectional arrangements and for long and short fibres also.

The strength of a unidirectional FRC, in the direction of fibres is given by the rule of mixture as shown by Equation (9.1):

$$\sigma_{cL} = \sigma_f V_f + \sigma'_m (1 - V_f) \tag{9.1}$$

where V_f is the volume fraction of fibres, σ_f is the tensile strength of fibres and σ'_m is the stress developed in the matrix. For composites with long parallel fibres, the Young's modulus (E_c) in the fibre direction is calculated using Equation (9.2):

$$E_c = E_f V_f + E_m V_m \tag{9.2}$$

where E_c, E_f, E_m are the Young's moduli of the composite, fibre and matrix, respectively, and V_f and V_m are the volume fractions of the fibre and matrix, respectively.

Tensile strength[54,55] is the maximum stress that a material can withstand without tearing apart. It is a measurement of the ability of a material to withstand forces that tend to pull it apart. Tensile strength is measured in unit of force per unit area. Tensile properties of fibre reinforced polymer composites (FRPCs) can be determined according to ASTM D638[56–59] or according to

DIN 53455 method.[60] Tensile strength of FRPCs is determined by Equation (9.3):

$$\sigma_{fu} = F_u / A_f \tag{9.3}$$

where F_u is the force at failure, A_f is the average cross-sectional area of filament.

The tensile strength (σ_c) of short-fibre reinforced polymer composites (SFRPs) can be predicted using the modified rule of mixtures equation which is given by Equation (9.4):[61]

$$\sigma_c = \lambda_\sigma \sigma_{fu} V_f + \sigma_m(1 - V_f) \tag{9.4}$$

where λ_σ is the fibre efficiency factor for the composite strength taking into account the effects of fibre length and orientation. V_f is the fibre volume fraction. σ_m is the stress of the matrix at the failure of the composite. Similarly, the tensile modulus (E_c) of SFRP composites can be predicted by the modified rule of mixtures equation as shown by Equation (9.5):[62]

$$E_c = \lambda_E E_f V_f + E_m(1 - V_f) \tag{9.5}$$

where λ_E is the fibre efficiency factor for the composite modulus considering the effects of fibre length and orientation. E_m and E_f are the modulus of matrix and fibre, respectively.

Bending strength,[63] also known as flexural strength, is defined as a material's ability to resist deformation under load. Bending strength represents the highest stress experienced within the material at its moment of rupture. There are two methods that cover the determination of bending properties of material: three-point loading system and four-point loading system. Prior to 1997, one ASTM standard covered both loading modes, which was ASTM D 790. However since 1997, only three-point loading is included in ASTM D 790 and a new ASTM standard has been created for four-point loading, ASTM D 6272. Without ASTM standards, DIN 53452 method[60] can be used also to determine bending properties of FRPCs. For a rectangular sample of FRPCs under load in a three-point bending set-up, the bending strength is calculated by Equation (9.6):

$$\sigma = 3FL / 2bd^2 \tag{9.6}$$

where F is the load (force), L is the length of the support span, b is width and d is thickness. For a rectangular sample under a load in a four-point bending set-up where the loading span is one-third of the support span, bending strength is calculated by Equation (9.7):

$$\sigma = FL / bd^2 \tag{9.7}$$

where F, L, b and d have the same meaning as indicated above.

But if the loading span is one-half of the support span, bending strength is calculated by Equation (9.8):

$$\sigma = 3FL / 4bd^2 \tag{9.8}$$

where F, L, b and d have the same meaning as indicated above.

Impact strength[64,65] is the ability of a material to resist suddenly applied loads. In most cases, impact test of FRPCs are carried out using two different types of testing method: Charpy test and Izod test. Izod impact strength of FRPCs can be determined according to ASTM D256[66] or DIN EN IS0 180 and Charpy impact strength can be determined according to ASTM D 6110 or DIN EN IS0 179.[60]

Zaman *et al*. studied the mechanical properties of unidirectional glass fibre reinforced NR composites.[67] The same author also reported jute fibre/NR composites in another study.[68] The author fabricated rubber sheet by a compression moulding method. Solid NR was subjected to hot press at 140 °C to make the rubber sheets. GF–NR composites were prepared by the author using the same press at 140 °C for 5 minutes applying 5 bar pressure. The author maintained thickness of the composites using shims. The tensile strength (TS), bending strength (BS), tensile modulus (TM) and elongation at break (Eb; %) were studied by the author. Significant effect of fibre loading on TS, BS and TM of the composites were observed. Different fibre loadings were investigated, *e.g*. 5, 10, 15 and 20% (by weight). The TS and BS increased with the increase in the percentage of fibre content in the composites. Tensile and bending properties of their NR-GF composites were measured according to DIN 53455 and DIN 53452 standard methods, respectively.

TS and TM of the solid NR sheets were found quite low and BS could not be determined. The NR used in that study was non-vulcanized and during hot press at 140 °C (for making sheets), TS loss can be expected. The composites with 20% (by weight) glass fibre showed best mechanical strength and lowest elongation at break. For NR matrix the author found that tensile strength, tensile modulus and elongation at break were 1.2 MPa, 1.8 MPa and 697%, respectively. The author found that with the increase in glass fibre content mechanical properties of glass fibre/NR composites increases. For 5% (by weight) glass fibre and 95% (by weight) NR tensile strength, bending strength, tensile modulus and elongation at break were 8.3 MPa, 12.1 MPa, 9.2 MPa, 118%, respectively. For 10% (by weight) glass fibre and 90% (by weight) NR, strength of composites increased more but elongation at break decreased. The tensile strength, bending strength, tensile modulus and elongation at break for glass fibre/NR (10:90) were 12.6 MPa, 18.2 MPa, 14.4 MPa, 93%, respectively. When the author increased the fibre content from 10% to 20% *i.e*. double increase in fibre content (glass fibre:NR = 20:80) increased the strength of composites remarkably with remarkable decrease in elongation at break. The tensile strength, bending strength, tensile modulus and elongation at break for glass fibre/NR (20:80) were 18.3 MPa, 23.6 MPa, 19.3 MPa, 72%, respectively.

Murty studied short glass fibre/NR composites.[39] The author studied effect of glass fibre concentration on the physical properties such as elongation at break, tensile strength, tear strength, heat build-up, flexing resistance, permanent set, compression set, resilience, hardness and ageing resistance of short glass fibre/NR composites.[39] The same author also studied short jute fibre/NR composites[45] and found that the minimum concentration of glass fibres was

higher than that for jute fibres. According to the author, this high value of the minimum loading for glass fibre may be due to severe breakage and poor bonding of glass fibre with rubber matrix. As a short fibre, glass fibre is inefficient because of high modulus which leads to breakage during mixing in case of rubber matrix.[34,46] It is known that short fibres act as reinforcing fillers only when they are added beyond a certain volume loading. It is also important that the fibres to be used must have some critical aspect ratios for reinforcing the rubber matrix. Vulcanization was carried out at 150 °C. Different glass fibre loadings were studied (*e.g.* 25 phr G_{25}, 75 phr G_{75}). Tensile testing was done according to ASTM methods D412-52T. For G_{75} the tensile strength was 11.73 MPa. Tear testing was done according to ASTM D624-54 method. For G_{75} the tear strength was 41.76 kN/m. Although tear strength improved by the addition of fibre but it was mostly independent of fibre concentration and orientation. According to the author, the improvement in tear strength was because fibres obstruct tear paths from proceeding straight. Elongation at break was found to drop down with the increase in fibre concentration. Flexing was carried out at 70 °C in a De-Mattia flexing machine according to ASTM D430-73. Flex resistance for G_{75} was 1.0 (kilo cycles) and was found to drop down with the increase in fibre loading. In the transverse direction flex resistance is higher since the stiffness becomes higher in the longitudinal direction. Heat build-up and permanent set measurements were made with a Goodrich flexometer according to ASTM D623-61, method A. For G_{75} heat build-up was found 29 (ΔT °C) which increases with the increase in fibre loading. Heat build-up is lower in the case of composites with fibres oriented transversely. Compression set measurements were made according to ASTM D395-61 method B and for G_{75} it was 33.6%. Shore A hardness was determined according to ASTM D676-57 and for G_{75} it was 75 Shore A. Resilience was measured at 35 °C using a Dunlop Tripsometer for G_{75} it was 59.7 %. Abrasion resistance was measured with a Croydon Akron Abrader and the samples were abraded for 500 cycles for G75 abrasion loss was 1.41 cc/500 revolution.

9.5.3 Fibre–Matrix Adhesion

For FRCs, the stress transfer at the interface between the matrix and fibre phases is determined by the degree of adhesion. Effective transfer of stress and load distribution throughout the interface is possible when strong adhesion exists at the interfaces. The adhesion phenomenon is described in several theories including mechanical interlocking, absorption, primary bonding, interdiffusion, electronic theories, *etc.*

9.5.3.1 Testing of Adhesion in Glass Fibre/NR Composites: Micromechanical Characterization

Interfacial shear strength (IFSS) is measured by the pullout test. In the first step of this test, one end of the fibre is embedded in a block of a polymer matrix and

in the second step a force is applied to the free end to pull it out of the matrix. Applied force is continuously monitored and recorded and the force at which debonding occurs is obtained. The average IFSS can be calculated using Equation (9.9):

$$\tau = F / \pi \times d \times l \tag{9.9}$$

Here, F = maximum load measured prior to debonding of the fibre, d = diameter of used fibre, and l = length of embedded portion of fibre.

Single-fibre fragmentation test (SFFT) is also used to calculate the IFSS. A single fibre is embedded in the matrix which is then converted to a dog bone-shaped tensile coupon using appropriate method (*e.g.* cutting). The specimen is then subjected to a tensile load and tensile forces are transferred from the matrix to the fibre. Depending on the level of fibre–matrix adhesion, build-up of tensile stresses occur within the fibre. After certain level of tensile strength, stress concentration reaches to a certain high level at which debonding occurs resulting fracture. This loading process continues until the fibre fragmentation process ceases. The final fibre fragment length is termed as the fibre critical length and denoted by l_c. The critical length (l_c) can be measured using the following formula:

$$l_c = 4 / 3 l_f$$

where l_f indicates average fragment length.[69] Critical length is a good indicator of the ability of the interphase to transmit loads between the matrix and fibre. Kelly and Tyson[70] developed Equation (9.10), by which IFSS is calculated, using this length:

$$\tau_i = d \times \sigma_f / 2 \times l_c \tag{9.10}$$

In Equation (9.10), d is the diameter of fibre used, σ_f is the tensile strength of a single fibre at the critical length. The ratio (l_c/d) can be used as an indicator of the fibre–matrix bond strength.

Drzal *et al.*[71] altered the above equation reflecting Weibull statistics and rearranged the Kelly and Tyson's equation, proposing the following modification to calculate the IFSS:

$$\tau_i = \sigma_f \times \Gamma \times [1 - 1 / \alpha] / 2\beta \tag{9.11}$$

In Equation (9.11), β is the scale, α is the shape parameters in the Weibull distribution and Γ is the gamma function. The strength of fibre can be calculated from the extrapolation gauge length using Weibull chart.[72] At the critical fragment length, the strength of fibre is found by Equation (9.12):[69]

$$\sigma_f = \sigma_{f0}(l_c / l_0)\exp - 1 / \rho \tag{9.12}$$

In Equation (9.12), σf_0 is the fibre strength at gauge length l_0 and ρ is the shape parameter of the Weibull distribution for the tensile strength of fibre.

Karlsson *et al.*[73] used the Wilhelmy plate method to measure the apparent perimeter of regenerated cellulose. He used this parameter to calculate the IFSS. Due to inherent variability of the henequen fibres (*Agave fourcroydes*),

Equations (9.10) and (9.11) were rearranged to use the perimeter P_f instead of the diameter to calculate the IFSS. Following this approach the calculation of IFSS for the pullout test was done using Equation 9.13:

$$\tau_i = F_f / P_f \times l_e \tag{9.13}$$

In Equation (9.13), F_f is the debonding force, P_f is the measured perimeter of the henequen fibre and l_e is the fibre-embedded length. In the case of the single fibre fragmentation test the IFSS is calculated with Equation 9.14:

$$\tau_i = 2F_f / \beta \times \Gamma \times P_f \times [1+1 / \alpha] \tag{9.14}$$

In Equation (9.14), F_f is the tensile load at break for the henequen fibre, P_f, α, β and Γ have the same meaning as indicated above.

Zaman *et al.*[67] studied IFSS of glass fibre/NR composites. The author prepared single-fibre composite samples using one single filament of fibre between two sheets of NR. Fragmentation test was performed using universal testing machine and the number of fragments were counted by microscope. NR matrix is quite transparent, which facilitates the counting of the number of fibre fragments in the specimen. The critical length (l_c) was measured using the formula mentioned above. From number of fragments, the critical length was counted. Fibre tensile properties were obtained by tensile testing filaments following international standard ISO 11566. A single fibre was mounted on a paper frame with a gauge length of 25 mm. The interfacial shear strength (IFSS) of the composites was calculated from both the Kelly–Tyson and Drzal equations mentioned above. The critical length of the glass fibre/NR system was found to be 9438.7 mm, TS of the fibre at critical length was reached at 435.1 MPa, and the diameter of the single glass fibre was found to be 46 μm. The IFSS calculated was 1.1 MPa for glass fibre/NR system.

9.5.4 Improvement in Strength of Glass Fibre/NR Composites

Strength of glass fibre/NR composites can be improved by modification of NR and glass fibre. Modified NR can also give higher strength and better adhesion properties. Modification of glass fibre helps to improve the fibre/matrix adhesion. It is discussed very shortly in this section.

9.5.4.1 Chemical Modification of NR

NR will provide better properties if modified chemically. Chemical modification of NR can be categorized into three main categories[42]:

(1) Modification by attachment of new chemical groups for example chlorine, epoxy, *etc*. Attachment of these groups will result addition or substitution reactions at the olefinic double bonds and format chlorinated NR, hydrochlorinated NR and epoxidized NR (ENR). Chlorination and hydrochlorination of NR can be carried out in dry, solution or latex form. Due to its resistance against alkalis and acids, and its wear

resistance, ageing resistance and corrosion resistance in sea water, chlorinated NR (CNR) is used as raw material for paint.

(2) Modification by bond rearrangement without introducing new atoms for example cyclization, carbon–carbon crosslinking, *cis*, *trans*-isomerisation, depolymerisation, *etc*. If NR is treated with a proton donor such as sulfonic acid, sulfuric acid, stannic chloride or if NR is heated, cyclized NR is formed. Cyclized NR is reported to be hard, tough and brittle having little elastic behaviour and being used in adhesives and in printing ink. It is also being blended with NR to give high hardness, high modulus and low specific gravity.

(3) Grafting a second polymer onto the NR backbone which is mostly carried out using vinyl monomers like methyl methacrylate (MMA) and styrene. The commercial available grafted copolymer of NR with poly(methyl methacrylate) (PMMA) is Heveaplus MG which is available in two different grades: 30% (MG 30) and 49% (MG 49) of PMMA. The grafted products have degrees of grafting in the range of 60–80% and some free PMMA. Heveaplus MG has superior properties like abrasion, hardness, modulus, electrical resistance, light colour, *etc*. It improves the impact properties of polystyrene, in blends with NR and also used as reinforcing agent.

9.5.4.2 *Treatment of Glass Fibre*

Glass fibre can be treated by various chemical agents to improve the adhesion between glass fibre and NR. Glass is an inorganic material, whereas the NR is a polymer and organic. These two materials are naturally incompatible and hydrolytically stable bonds are not formed between them. A coupling agent is necessary for the chemical reaction to occur between NR and glass fibre. Coupling agents contain chemical functional groups that can react with silanol groups on glass. At the other end of coupling agent, the organofunctional group is to react with NR polymer. Covalent bonds that assumed to happen lead to the strongest interfacial bond. In the dawn of the fibreglass-reinforced plastics industry, chromium complex, Volan, showed most effectiveness as a coupling agent. In the late 1950s and 1960s, organofunctional silanes began to displace Volan in many applications. Various silanes were developed for specific resin systems for much more superior composite properties over Volan.[74] A complete review of adhesion promoters, including non-silanes, was written by Sathyanarayana and Yaseen.[75]

Silanes are well recognized and very efficient coupling agents extensively used in composites and adhesive formulations.[76] They have been successfully applied in inorganic filler reinforced polymer composites for years and extensively used for glass fibre reinforced polymer composites.[77–79] In this chapter, only silane treatment is discussed in short which is as follows:

Monomeric silicon chemicals are known as silanes. A silane that contains at least one silicon–carbon bond (*e.g.* Si-C_2H_5) is an organosilane. The carbon–silicon bond is very stable and non-polar. In the presence of an alkyl group it

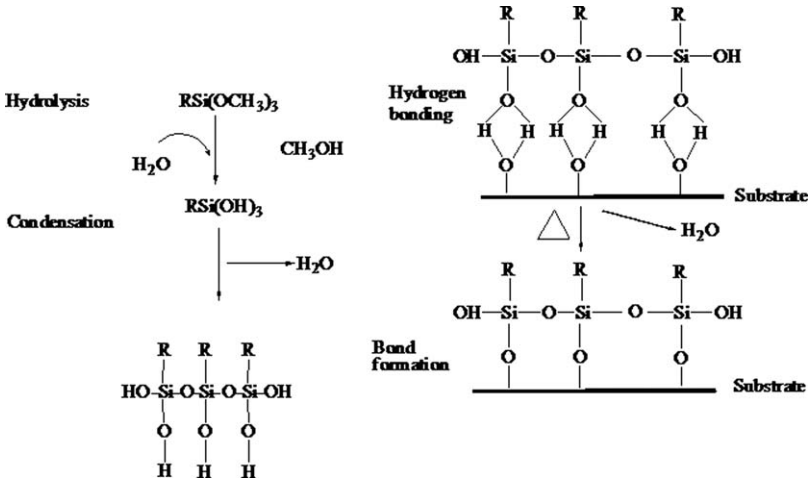

Figure 9.7 Organofunctional silane hydrolysis, condensation and covalent bonding with inorganic substrate (*e.g.* glass fibre).

gives rise to low surface energy and hydrophobic effects. For organofunctional silanes, many combinations are possible. But these are characterized by the fact that they contain two different types of reactive groups (OR and X groups). The OR groups are hydrolysable groups such as methoxy, ethoxy or acetoxy groups. The Si–OR bonds hydrolyse readily with water or even with little moisture adsorbed on the surface, to form silanol Si-OH groups. These silanol groups can then condense with each other forming polymeric structures with very stable siloxane Si–O–Si bonds. Condensation with metal hydroxyl groups on the surface of glass, minerals or metals to form stable Si–O–M bonds (M = Si, Al, Fe, *etc.*) is also possible. This allows surface treatment, coupling and assembling of very dissimilar surfaces chemically, as between inorganic and organic materials (Figure 9.7).

9.5.5 Biodegradation Characteristics of the Matrix

NR is biodegradable whereas inorganic glass fibre is non-biodegradable. Biodegradation is nothing but the biological breakdown of organic compounds by microorganisms into cell biomass and less complex compounds, and ultimately to water, and either carbon dioxide (aerobically) or methane (anaerobically). Compounds having a molecular structure to which microorganisms have not been exposed to (*i.e.* xenobiotic compounds) are usually resistant (recalcitrant) to biodegradation. The extent and rate of this natural process depends on several things: interactions between the environment, the number and type of microorganisms present and the chemical structure of the compound(s) being degraded. Secretion of enzymes from microorganisms catalyse the degradation of polymers. Oxygen, microorganisms and nutrients are very often the limiting factors in soils. Bioremediation can be enhanced when the rate of

biodegradation is increased by adequate supply of required nutrients to an indigenous microbial population (biostimulation) and by inoculating the site with microorganisms capable of degrading the target pollutant (bioaugmentation).

Degradation of NR by microorganisms

Most natural polymers commonly used *e.g.* NR, gelatin, starches, *etc.* are inherently biodegradable under proper conditions. The extent of degradation decreases with increasing molecular weights of the polymers. NR is not only a photosynthetically-renewable resource but also an environmentally degradable material. This unsaturated high molecular weight polymer is expected to degrade very slowly in nature in comparison with other natural polymers. NR degrading bacteria are widely distributed in water, soil, and sewage and interestingly, with some exceptions, belong to the actinomycetes.[80] As a group, the actinomycetes are significant decomposers in soils. Some early reports on the biodeterioration of NR rubber goods had been reviewed by Cundell and Mulcock[81] and Zyska.[82] Different results from the several rubber-degrading microorganisms may be obtained under various test conditions.

According to Shaposnikov,[83,84] pure strains of some bacteria are able to cause up to a 55% loss in weight of thin rubber sheets in 70 days, and 43% loss in 45 days for pure cultures of actinomycetes. If fungi are present, the weight loss due to actinomycetes increases to 52%.

Low *et al.* also studied degradation of latex and used fungi and actinomycetes to degrade diluted latex for 6 weeks.[85] The author found reduction of 17 and 24% in molecular weights due to a fungus (*Fusarium* sp.) and an actinomycete, respectively. Tsuchii and Takeda later found that a crude enzyme from a bacterium, *Xanthomonas* sp. strain 35Y have the ability to biodegrade NR in the latex state to produce two fractions of reaction products.[86] This work was the first evidence for the existence of an extracellular polyisoprenoid oxygenase in a Gram-negative bacteria. Vulcanized NR shows resistance to degradation. In looking at this question, Cundell and Mulcock[87] observed that dicumyl peroxide-cured NR was most susceptible and a TMTD sulfurless-cured NR was least susceptible to microbial deterioration. Antioxidants and antiozonants have both sensitive and fungitoxic properties. Most plasticisers, softeners and extenders are not fungicidal. Tsuchii *et al.* further studied NR vulcanizates containing various amounts of sulfur and an accelerator (CBS) to degradation by Nocardia sp. strain 835A[88] and found that the higher the sulfur or CBS content, the less was the weight loss of the vulcanizates after microbial attack. Keursten *et al.*[89] studied biodegradation of rubber particles in rubber–soil mixtures at different rubber contents by the carbon dioxide production and modelled cumulative carbon dioxide production modelled according to a two parameter exponential function. According to the author, the cumulative production can be modelled according to Equation (9.15):

$$Y = Y_{max}[1 - e^{(-\alpha t}] \tag{9.15}$$

where Y is the cumulative CO_2 concentration in ml per jar (the incubation study was carried out by the author with 1 litre standard mason jars), Y_{max} the maximum CO_2 production (also in ml per jar), t is the time in days and α is a degradation parameter and can be obtained by Equation (9.16):

$$\alpha = \frac{\ln 2}{T_{1/2}} (day^{-1}) \tag{9.16}$$

where $T_{1/2}$ is the half-life (in days) of the degrading material. For the controls the degrading material was soil organic matter whereas for the mixtures of soil and rubber, the degrading material was the soil organic matter and the rubber. According to Keursten, the degradation of rubber particles in soil could be described by first order kinetics and the parameter α probably depends on the degree of contact between soil and rubber.[89]

Zaman *et al.* performed degradation of glass fibre/NR composites in soil at ambient condition for 120 days.[67] The author found remarkable decrease in tensile properties (TS and TM) of glass fibre/NR composites. For the first month, the decrease rate was very sharp. Weight loss of glass fibre/NR composites was also studied over the same period of time (120 days). After 7 and 120 days of soil burial, glass fibre/NR composites lost 2.8%and 7.2% of weight. A comparison of weight loss was shown in that study and was found that after 120 days glass fibre/NR composites lose 94% higher weight than that of glass fibre/polypropylene composites under the same condition of experiment.[67]

Shubhra *et al.* studied loss of mechanical properties of fibre/NR based composites due to biodegradation. The matrix contained mixture of NR and polypropylene (PP). Since PP is non-biodegradable, according to the author, the degradation was due to degradation of NR and fibre. The author kept the fibre (20% by weight) constant for all composites studied by them. It was found that strength of composites sharply decreases with the increase in ratio of NR in the matrix which is due to biodegradation of NR.

The loss of TS observed by Shubhra *et al.* is shown in Figure 9.8.[90] It was found that TS values of the composites decreased slowly. For silk fibre/PP composites the TS value was 54.7 MPa whereas after 24 weeks of soil burial test it was 49.1 MPa. So, after 24 weeks of soil burial, silk fibre reinforced PP composite lost 10.2% TS, whereas silk-reinforced PP and NR blend (50:50) composite lost 24.3% TS. For silk-reinforced PP and NR blend (50:50) composites the TS value was 39.9 MPa whereas after 24 weeks of soil burial test it was 30.2 MPa. The author mentioned that this 14.1% higher loss of TS is due to incorporation of NR in the PP matrix. The author found that if NR is low (25% instead of 50%), the composite loses less TS value after 24 weeks of degradation test (from 42.4 MPa to 34.3 MPa, which is 19.1%).

The loss of BS observed by Shubhra *et al.* is shown in Figure 9.9.[90] It was found that BS values of the composites decreased more rapidly than TS values. For silk fibre/PP composites the BS value was 58.3 MPa whereas after 24 weeks of soil burial test it was 50.7 MPa. So, after 24 weeks of soil burial, silk fibre reinforced PP composite lost 13% BS whereas silk-reinforced PP and NR blend

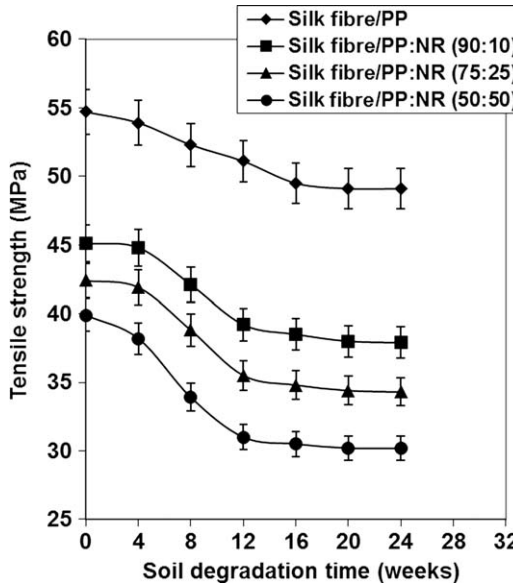

Figure 9.8 Loss of tensile strength of rubber composites during soil burial test. (Reprinted from T. H. Quazi *et al.*, *Composites: Part A*, 2010, xx, 1587–1596, with permission from Elsevier.)

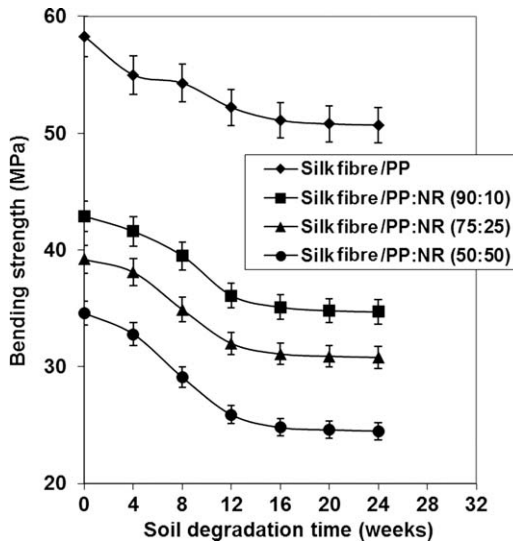

Figure 9.9 Loss of bending strength of rubber composites during soil burial test. (Reprinted from T. H. Quazi *et al.*, *Composites: Part A*, 2010, xx, 1587–1596, with permission from Elsevier.)

(50:50) composite lost 29.2% TS. For silk-reinforced PP and NR blend (50:50) composites the BS value was 34.6 MPa whereas after 24 weeks of soil burial test it was 24.5 MPa. The author mentioned this 16.2% higher loss of BS is due to incorporation of NR in the PP matrix. The author found that if NR is low (25% instead of 50%), the composite losses less BS value after 24 weeks of degradation test (from 39.2 MPa to 30.8 MPa, which is 21.4%).

9.6 Applications

Glass fibre with natural NR is one of the most promising routes to create natural–synthetic polymer composites. Glass fibre is a very strong synthetic fibre. NR is a highly valuable biomaterial. In contrast with most other biopolymers, it is essential for many applications and cannot be replaced by other synthetic materials. For example, heavy-duty tyres for trucks, buses and airplanes, as well as many latex products for the medical profession, cannot be made with synthetic rubber, or only at great cost. NR is a general purpose elastomer. Its high resilience, low heat build-up and excellent dynamic properties coupled with outstanding processability, make it an ideal material for automotive tyres. Therefore, it is no surprise that around 55% of all the NR is used in making automotive tyres. Apart from tyres a modem automobile has more than 300 components made out of rubber. The major non-tyre applications include beltings, hoses, cycle tyres, footwear, engineering products, latex products such as dipped goods, rubber-backed carpets and adhesives. Recent attention has been focused on the suitability of such composites in high-performance applications. One of the most important recent applications of short fibre–rubber composites is as thermal insulators, intended to protect the metallic casing by undergoing a process called ablation, which is described in a broad sense as the sacrificial removal of material to protect structures subjected to high rates of heat transfer.[36] In automotive and truck tires fibre/NR composites find application and provide better abrasion resistance for the chafer strip and in improved cut resistance to treads, especially for trucks and OTR vehicles. Better interfacial bonding between the glass fibre and NR is needed to get better mechanical properties of the composites which will increase their versatile applications. Future research must emphasize the reduction in the production cost.

9.7 Conclusions

Composite materials are now well established all over the world and used in almost every type of advanced engineering structure, with their usage ranging from aircraft, helicopters and spacecraft through to ships, boats and offshore platforms and to automobiles, sports goods, chemical processing equipment and civil infrastructure such as bridges and buildings. Among different types of reinforcements, fibres are stronger and stiffer materials than any other form which is the main reason for the overwhelming attraction for fibrous reinforcements. Different types of fibres used in composite have different

properties and so affect the properties of the composite in different ways. The mechanical properties of most reinforcing fibres are considerably higher than those of unreinforced resin systems. The mechanical properties of the fibre/resin composite are therefore dominated by the contribution of the fibre to the composite. Between synthetic and natural fibres, synthetic fibres are usually more uniform in size, more economical to use and behave in a more predictable manner. For engineering applications the most commonly employed significant fibres are synthetic fibres and the first priority is given to glass fibre. Polymer matrix composites (PMCs) are very popular due to their low cost, simple fabrication methods, lightweight and desirable mechanical properties. In most applications for rubber products there are no alternative materials except other rubbers. It has very high deformability. NR is biodegradable, so environment friendly. For automotive tyres, fibre/NR composites are the only material in use and cannot be replaced by other materials. The development of FRCs has not only been a great motivating factor for scientists, but also an important provider of opportunities to improve the standard of living of people around the world. Along with researchers and entrepreneurs, we also expecting the expansion of research for new glass fibre reinforced NR composite materials with high performance at affordable costs.

References

1. S. K. Rai and S. P. Priya, *J. Reinf. Plast. Compos*, 2006, **25**, 565.
2. Y. Chen, O. Chiparus, L. Sun, I. Negulescu, D. V. Parikh and T. A. Calamari, *J. Ind. Text*, 2005, **35**, 47.
3. H. E. Peply, in *Engineered Materials Handbook,* ed. T. J.Reinhart, ASM International, Ohio, 1987, Volume 2, Chapter 2.3.
4. T. A. Bullions, R. A. Gillespie, J. Price-O'Brien and A. C. Loos, *J. Appl. Polym. Sci.*, 2004, **92**, 3771.
5. A. Nick, U. Becker and W. Thoma, *J. Polym. Environ.*, 2002, **10**, 115.
6. Haydaruzzaman, A. K. Ruhul, A. K. Mubarak and M. A. Hossain, *Radiat. Phys. Chem.*, 2009, **78**, 986.
7. L. Hollaway, *Polymer Composites for Civil and Structural Engineering*, Chapman and Hall, Glasgow, 1993.
8. R. P. Sheldon, *Composite Polymeric Materials*, Applied Science Publishers, London, 1982.
9. Q. T. H. Shubhra, A. K. M. M. Alam, M. A. Gafur, S. M. Shamsuddin, M. A. Khan, M. Saha, D. Saha, M. A. Quaiyyum, J. A. Khan and M. Ashaduzzaman, *Fibres Polym.*, 2010, **11**, 725.
10. D. N. Saheb and J. P. Jog, *Adv. Polym. Technol.*, 1999, **18**, 351.
11. K. L. Loewenstein, *The Manufacturing Technology of Continuous Glass Fibres*, 3rd ed., Elsevier Science Publishers, Amsterdam, 1993.
12. J. G Mohr and W. R. Rowe, *Fibre Glass*, 1st ed., Van Nostrand Reinhold Company, New York, 1978.
13. T. F Starr, *Glass-Fibre Databook*, 1st ed., Chapman & Hall, London, 1993.

14. D. J. Vaughan, in *Handbook of Composites*, S. T. Peters, Chapman & Hall, London, 1998, p. 131.
15. P. K. Mallick, *Fibre-Reinforced Composites: Materials, Manufacturing, and Design*, 3rd ed., CRC Press, New York, 2007.
16. Q. T. H. Shubhra, in *Fibre-Reinforced Composites*, 1st ed., Q. Cheng, Nova Science Publishers, Inc., New York, 2012, p. 6.
17. R. Mukhopadhyay and S. Datta, *Engineering Chemistry*, New Age International Pvt. Ltd, New Delhi, 2007.
18. N. M. Mathew, in *Rubber Technologist's Handbook*, ed. J. R. White and S. K. De, Rapra Technology Limited, Shropshire, 2001, p. 12.
19. H. Y. Chen, *J. Polym. Sci., Part B: Polym. Lett*, 1966, **4**, 891.
20. F. W. Hemming, in *Natural Substances Formed Biologically from Mevalonic Acid*, ed. T. W. Goodwin, Academic Press, London, 1970, p. 105.
21. Y. Tanaka, H. Sato and A. Kageyu, *Polymer*, 1982, **23**, 1087.
22. Y. Tanaka, in *Methods in Plant Biochemistry*, ed. P. M. Dey and J. B. Harborne, Academic Press, London, 1991, p. 519.
23. A. H. Eng, S. Kawahara and Y. Tanaka, *Rubber Chem. Technol.*, 1994, **67**, 159.
24. Y. Tanaka and H. Hirasawa, *Chem. Phys. Lipids*, 1989, **51**, 183.
25. Y. Tanaka, A. H. Eng, N. Ohya, N. Nishiyama, J. Tangpakdee, S. Kawahara and R. Wititsuwannakul, *Phytochemistry*, 1996, **41**, 1501.
26. V. M. Litvinov and P. D. Prajna, *Spectroscopy of Rubbers and Rubbery Materials*, Rapra Technology Limited, Shropshire, 2002.
27. P. Ghosh, *Polymer Science and Technology: Plastics, Rubbers, Blends and Composites*, 2nd ed., Tata-McGraw-Hill, New Delhi, 2002.
28. C. Goodyear, *Gum-Elastic and its Varieties, with a Detailed Account of its Applications and Uses*, New Haven(published by the author), 1853.
29. A. Ciesielski, *An Introduction to Rubber Technology*, 1st ed., Rapra Technology Limited, Shropshire, 1999.
30. R. Verdejo, M. Hernandez, N. Bitinis, J. M. Kenny and M. A. Lopez-Manchado, in *Rubber-Clay Nanocomposites: Science, Technology, and Applications*, M. Galimberti, John Wiley & Sons, Inc., Hoboken, NJ, 2011, pp. 275–303.
31. A. K. Pahari and B. S. Chauhan, in *Engineering Chemistry*, 1st ed., Laxmi Publications (P) Ltd, New Delhi, 2007, p. 70.
32. A. Syrotiuk and P. G. Howgate, *Prog. Rubber Plast. Technol*, 1986, **2**, 24.
33. P. B. Lindley, in *Engineering Design with Natural Rubber, The Malaysian Rubber Producers' Research Association*, Brickendonbury, Hertford, 1992, p. 9.
34. L. Czarnecki and J. L. White, *J. Appl. Polym. Sci.*, 1980, **25**, 1217.
35. R. A. Gregg, *Rubber Chem. Technol.*, 1972, **45**, 49.
36. R. S. Rajeev, in *Current Topics in Elastomer Research*, ed. A. K. Bhowmick, CRC Press, New York, 2008, pp. 354–364.
37. G. C. Derringer, *J. Elastomers Plast*, 1971, **3**, 230.
38. V. M. Murty and S. K. De, *J. Appl. Polym. Sci.*, 1984, **29**, 1355.
39. V. M. Murty, *J. Polym. Mater*, 1983, **10**, 149.

40. V. M. Murthy, A. K. Bhowmick and S. K. De, *J. Mater. Sci.*, 1982, **17**, 709.
41. M. C. H. Lee, *J. Polym. Eng.*, 1988, **8**, 257.
42. M. J. John, R. D. Anandjiwala and S. Thomas, in *Natural Fibre Reinforced Polymer Composites: From Macro to Nanoscale*, ed. S. Thomas and L. A. Potha, Old City Publishing, Inc., Philadelphia, PA, 2008, pp. 257–259.
43. M. J. Stevens and J. A. Covas, in *Extruder Principles and Operation*, 2nd ed., Chapman & Hall, London, 1995, pp. 127–129.
44. M. A. Khan, J. Ganster and H. P. Fink, *Composites, Part A*, 2009, **40**, 846.
45. Q. T. H. Shubhra, M. Saha, A. K. M. M. Alam, M. D. H. Beg and M. A. Khan, *J. Reinf. Plast. Compos.*, 2010, **29**, 3338.
46. V. M. Murty and S. K. De, *Rubber Chem. Technol.*, 1982, **55**, 287.
47. J. E. O'Connor, *Rubber Chem. Technol.*, 1977, **50**, 945.
48. L. Biolzi, L. Castellani and I. Pitacco, *J. Mater. Sci.*, 1994, **29**, 2507.
49. S. R. Doshi and J. M. Charrier, *Polym. Compos.*, 1989, **10**, 28.
50. M. Joshi, S. N. Maiti and A. Misra, *Polym. Compos*, 1994, **15**, 349.
51. M. L. Shiao, S. V. Nair, P. D. Garrett and R. E. Pollard, *J. Mater. Sci.*, 1994, **29**, 1739.
52. T. Vu-Khanh, J. Denault, P. Habib and A. Low, *Compos. Sci. Technol.*, 1991, **40**, 423.
53. K. Joseph, S Varghese, G. Kalaprasad, S. Thomas, L. Prasannakumari, P. Koshy and C. Pavithran, *Eur. Polym. J.*, 1996, **32**, 1243.
54. P. Wambua, J. Ivens and I. Verpoest, *Compos. Sci. Technol.*, 2003, **63**, 1259.
55. K. Oksman, *Appl. Compos. Mater.*, 2000, **7**, 403.
56. N. A. Thomas and K. E. George, *J. Thermoplast. Compos. Mater.*, 2009, **22**, 5.
57. M. R. Rahman, M. Hasan, M. M. Huque and M. N. Islam, *J. Reinf. Plast. Compos*, 2010, **29**, 445.
58. M. Haque, S. Islam, S. Islam, N. Islam, M. Huque and M. Hasan, *J. Reinf. Plast. Compos.*, 2010, **29**, 1734.
59. M. Haque, R. Rahman, N. Islam, M. Huque and M. Hasan, *J. Reinf. Plast. Compos.*, 2010, **29**, 2253.
60. A. H. Haydaruzzaman, M. A. Khan, M. A. Hossain, R. A. Khan, Khan and M. A. Hakim, *J. Compos. Mater.*, 2010, **44**, 1945.
61. S. Y. Fu and B. Lauke, *Compos. Sci. Technol.*, 1996, **56**, 1179.
62. S. Y. Fu and B. Lauke, *Compos. Sci. Technol.*, 1998, **58**, 389.
63. M. J. A. van den Oever, H. L. Bos and M. J. J. M. van Kemenade, *Appl. Compos. Mater.*, 2000, **7**, 387.
64. M. N. Nahas, *J. Mater. Sci.*, 1987, **22**, 657.
65. M. J. A. van den Oever, H. L. Bos and K. Molenveld, *Die Ang. Makrom. Chem.*, 1999, **272**, 71.
66. Y. Qiang, W. Donglyang, G. Januar and B. Stuart, *J. Thermoplast. Compos. Mater.*, 2008, **21**, 195.
67. H. U. Zaman, M. A. Khan and R. A. Khan, *J. Elastomers Plast*, 2012, **44**, 499.
68. H. U. Zaman, M. A. Khan, R. A. Khan and M. D. H. Beg, *Int. J. Polym. Mater*, 2011, **60**, 303.

69. R. A. Khan, M. A. Khan, S. Sultana, M. N. Khan, Q. T. H. Shubhra and F. G. Noor, *J. Reinf. Plast. Compos*, 2010, **29**, 466.
70. A. Kelly and W. R. Tyson, *J. Mech. Phys. Solids*, 1965, **13**, 329.
71. L. T. Drzal, M. J. Rich, M. F. Koeng and P. F. Lloyd, *J. Adhes.*, 1983, **16**, 133.
72. H. F. Wu and A. N. Netravali, *J. Mater. Sci.*, 1992, **27**, 3318.
73. J. O. Karlsson, P. Gatenholm, J. F. Blachot and A. Peguy, *Polym. Compos.*, 1996, **17**, 300.
74. E. P. Plueddemann, *Silane Coupling Agents*, 2nd ed., Plenum Press, New York, 1991, pp. 17–18.
75. M. N. Sathyanarayana and M. Yaseen, *Prog. Org. Coat*, 1995, **26**, 275.
76. A. N. Rider and D. R. Arnott, *Int. J. Adhes. Adhes.*, 2000, **20**, 209.
77. H. F. Wu, D. W. Dwight and N. T. Huff, *Compos. Sci. Technol*, 1997, **57**, 975.
78. H. A. Clark and E. P. Plueddemann, *Mod. Plast.*, 1963, **40**, 133.
79. Y. Xie, C. Callum, A. S. Hill, Z. Xiao, H. Militz and C. Mai, *Composites, Part A*, 2010, **41**, 806.
80. D. Jendrossek, G. Tomasi and R. M. Kroppenstedt, *FEMS Microbiol. Lett.*, 1997, **150**, 179.
81. A. M. Cundell and A. P. Mulcock, *Int. Biodeterior. Bull.*, 1972, **8**, 119.
82. B. J. Zyska, in *Microbial Biodeterioration, Economic Microbiology*, A. H. Rose, Academic Press, London, 1981, vol. 6 , pp. 323–385.
83. V. N. Shaposhnikov, I. L. Rabotnova, G. A. Yarmola and V. M. Kuznetsova, *Mikrobiologiya*, 1952, **21**, 280.
84. V. N. Shaposhnikov, I. L. Rabotnova, G. A. Yarmola, V. M. Kuznetsova and N. N. Mozokhina-Porshnya-kova, *Mikrobiologiya*, 1952, **21**, 146.
85. F. C. Low, A. M. Tan and C. K. John, *J. Nat. Rubber Res*, 1992, **7**, 195.
86. A. Tsuchii and K. Takeda, *Appl. Environ. Microbiol.*, 1990, **56**, 269.
87. A. M. Cundell and A. P. Mulcock, *Mater. Org.*, 1973, **8**, 165.
88. A. Tsuchii, K. Hayashi, T. Hironiwa, H. Matsunaka and K. Takeda, *J. Appl. Polym. Sci.*, 1990, **41**, 1181.
89. G. T. G. Keursten and P. H. Groenevelt, *Biodegradation*, 1996, **7**, 329.
90. Q. T. H. Shubhra, A. K. M. M. Alam, M. A. Khan, M. Saha, D. Saha and M. A. Gafur, *Composites, Part A*, 2010, **41**, 1587.

CHAPTER 10

Micro and Nano TiO_2 Reinforced Natural Rubber Composites

JIJI ABRAHAM,[a] SABU THOMAS[a] AND SONEY C. GEORGE*[b]

[a] Centre for Nanoscience and Nanotechnology, Mahatma Gandhi University, Kottayam, Kerala, India; [b] Department of Basic Science and Technology, Amal Jyothi College of Engineering, Kanjirappally, Kerala, India
*Email: soneygeo@gmail.com

10.1 Introduction

Natural rubber (NR) is widely used in various applications and products for its excellent properties such as elasticity, low hysteresis, high resilience, toughness, *etc*.[1] NR is the basic constituent of many products in the consumer goods, health and medical sectors, and it is widely used in transportation. The properties of NR can be improved by the addition of fillers. The inclusion of inorganic fillers in polymers usually results in improvement in strength, toughness, processability, dimensional stability, wear and lubrication properties, and in some cases resistance to thermal and UV radiation of the matrix.

Titanium dioxide (TiO_2) is an example of a versatile inorganic filler with many interesting properties. It is an inexpensive, non-toxic and photostable inorganic material that has good optical and photocatalytic properties for many applications.[2] Due to its high refractive index and ability to reflect and refract or scatter light more effectively than any other pigment, TiO_2 has for

RSC Polymer Chemistry Series No. 8
Natural Rubber Materials, Volume 2: Composites and Nanocomposites
Edited by Sabu Thomas, Hanna J. Maria, Jithin Joy, Chin Han Chan and Laly A. Pothen

Published by the Royal Society of Chemistry, www.rsc.org

many years served and is still serving as a white pigment. It is also used to provide protection against the effects of UV, because it is capable of absorbing UV light.

By combining the properties of NR and TiO_2, we can make composites with enhanced properties and applications. This chapter covers the synthesis and characterization of TiO_2, and the fabrication of TiO_2/NR composites, their properties and applications.

10.2 Composites

A composite material can be defined as a material in which two or more distinct structurally complementary substances are combined to produce structural or functional properties which are different from the individual components. Composites may be either synthetic or natural. Polymer matrix composites are much easier to produce than other composites, because of their low cost, low density and ease of processing. Composites have two phases, a continuous matrix phase and a dispersed phase or reinforcement phase. Polymer composites can be classified according to the nature of the dispersed phase as micro- or nanocomposites.[3]

In a nanocomposite, the dispersed phase has at least one dimension in the nanometre range, while in a microcomposite, the dispersed phase has at least one dimension in the micrometre range. In both cases the matrix may be a metal, a ceramic or a polymer. Nanocomposites have several advantages over microcomposites. Nanoparticles have high surface area-to-volume ratio, especially when the size is below 100 nm. Because of this high surface area-to-volume ratio for the same particle loading, nanocomposites will have a much greater interfacial area than microcomposites. Because the interfacial area is higher for nanocomposites it can have a significant impact on properties.[4]

Another advantage of nanocomposites over microcomposites is the reduced filler content in nanocomposites, perhaps ten times lower than in microcomposites. This big difference in filler content and interfacial area will cause significant changes in various properties of polymer composites. It is reported that mechanical properties, heat resistance, thermal conductivity, flame retardancy, gas barrier properties, electrical and dielectric properties are much improved if polymers are so nanostructured.[5]

10.3 Fillers

Fillers are those materials added to a matrix in order to improve its properties. The filler characteristics that affect the composite's properties are particle size, size distribution, specific surface area and particle shape and interfacial interactions. The shape of most mineral filler particles can be approximated as a sphere, cube, block, plate, needle or fibre. Some fillers contain a mixture of shapes.[6]

Fillers are very often introduced into the polymer to create new functional properties not possessed by the matrix polymer at all. Properties which are

improved by the addition of fillers include stiffness, heat deflection temperature, appearance, heat conductivity, flame retardancy, conductivity. *etc*.[7]

There are two types of fillers: reinforcing and extending. Reinforcing type fillers improve tensile strength, modulus, tear strength and abrasion resistance. Common reinforcing fillers are fused silica, aerogel silica and carbon black. Extending fillers are semi-reinforcing or non-reinforcing materials used to impart some desirable properties and also to extend the formulation. Common extending fillers are ground quartz, TiO_2, clay, whiting, alumina trihydrate (ATH) and zinc oxide.[8]

Based on the size, fillers can be broadly classified into two categories, micro and nano sized fillers. Lighter, thinner, stronger and cheaper structures are the goals of material science and engineering applications today.[9] Nanoparticles satisfy these requirements. The use of nanofillers improves mechanical and physical polymer properties. The added cost of the nanofilled matrix can be low due to the small amounts of filler necessary for a significant improvement. Nanofillers can significantly improve or adjust the properties of the materials into which they are incorporated, such as optical, electrical, mechanical, thermal or fire-retardant properties.

Compared to traditional additives, the advantage of nanoparticles over conventional fillers is their low loading requirements. The disadvantage of microsized fillers is their light scattering tendency, thus reducing light transmittance and optical clarity.[10] Efficient nanoparticle dispersion combined with good polymer–particle interfacial adhesion eliminates scattering and allows the exciting possibility of developing strong yet transparent films, coatings and membranes.

10.4 Micro and Nano TiO_2

TiO_2 has emerged as one of the most fascinating and interesting materials of the present era. It captures the attention of physical chemists, physicists, material scientists and engineers in exploring many of its wonderful properties such as semiconducting and catalytic properties.[11]

Titania exists in two tetragonal forms, a metastable phase, anatase, and a stable form, rutile. The volume free energy of the rutile phase is always lower than that of anatase. Therefore, upon heat treatment, the anatase phase transforms to the stable rutile form. The transformation is non-reversible, and is from metastable to stable; the transition temperature ranges from 450 to 1200 °C. Factors that affect the physical and chemical properties of TiO_2 crystals include intrinsic electronic structure, size, shape, organization, and surface properties of particles.[12]

TiO_2 is a wide band gap (3.2 eV) semiconductor that exhibits high photocatalytic efficiency. With its combined features, low cost and stable properties, TiO_2 makes a good candidate for polymeric material protection. Many researchers are interested in studying how to control the nanostructure of TiO_2, because the high surface area resulting from nanostructure control improves the properties of the TiO_2. Because of the high refractive index of TiO_2, which is

higher than that of diamond (rutile TiO_2, 2.76; anatase TiO_2, 2.52; and diamond, 2.42), it can be used as an optical material for applications such as ultraviolet emitters, lasers and prisms.

TiO_2 is found being used in various fields including photovoltaic cells, photo/electrochromics, photocatalysis, photonic crystals, smart surface coatings, rechargeable lithium batteries, sensors, and so on.[13–17] In recent years, TiO_2 has been extensively utilized in environmental applications such as self-cleaning, antibacterial and waste water purification.[18] By combining low cost and stability, TiO_2 makes a good candidate for polymeric material protection. The use of TiO_2 as a filler in polymeric materials also improves the thermal and electrical properties. So TiO_2 is a useful filler for achieving higher thermal conductivity and relative permittivity for polymers.[19]

TiO_2 particles are widely used, mainly because of their semiconducting and photocatalytic properties[2] (Figures 10.1 and 10.2). Opportunities for TiO_2 now

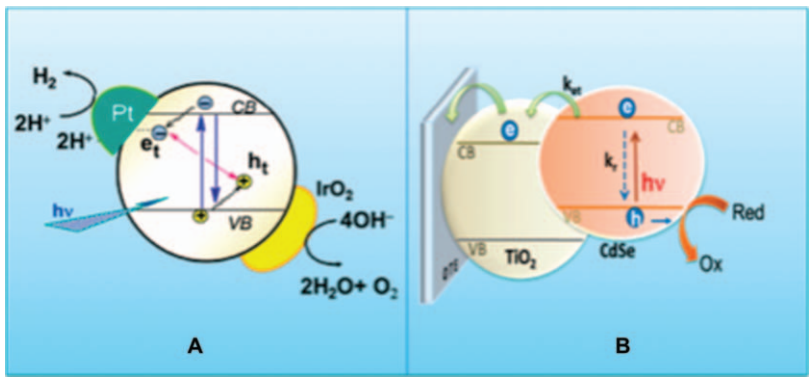

Figure 10.1 Photocatalytic activation using TiO_2 nanoparticles: (A) direct band gap (UV) excitation and (B) sensitized charge injection using a visible light absorber.
(Reproduced with permission from ref. 20.)

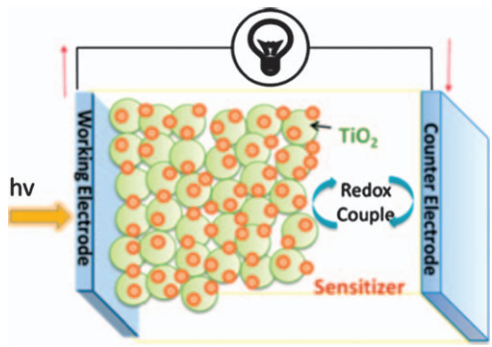

Figure 10.2 Principle of operation of liquid junction dye or quantum dot sensitized solar cell using mesoscopic TiO_2 films.
(Reproduced with permission from ref. 20.)

lie in more challenging areas, such as energy conversion and storage. TiO_2 nanostructures have recently shown promise in designing Li and Na ion storage batteries. Shape- and size-controlled TiO_2 nanostructures will continue to provide the base architecture to construct light harvesting assemblies and facilitate photoinduced charge separation processes.

10.5 Synthesis of TiO_2 Particles

Several processing methods, including sputtering, sol–gel processes, vapour deposition and thermal spraying, have been developed to deposit nanocrystalline and microcrystalline TiO_2 powders.

10.5.1 Synthesis of Nano TiO_2 Particles

Nanophase TiO_2 particles, with typical particle sizes in the range of 20–50 nm, have been synthesized by using a microemulsion-mediated process. In this process, the aqueous cores of water/Triton X-100/hexanol/cyclohexane microemulsions have been used as constrained micro-reactors for the precipitation of precursor TiO_2. The hydroxide particles thus formed were separated, dried and calcined at different temperatures to form nanoparticles of TiO_2.[21]

Titanium tetraisopropoxide $Ti(O\text{-}iPr)_4$ (TIP) was hydrolysed in an ethanol solution of glacial acetic acid at room temperature. TIP was added drop-wise in ethanol and acetic acid solvent under vigorous stirring until a clear solution was formed. Water (0.05% v/v) was added under stirring and the solution became white. This solution was stirred for 6 h. TIP, ethanol and acetic acid were maintained in the ratio of 1 : 100 : 0.05, respectively. The solution was filtered and washed with deionized water twice. The filtrate was dried at 60 °C for 12 h under reduced pressure. Dry powder was calcined at 600 and 900 °C for 2 h and will be referred to as A (anatase) and R (rutile).

Single-crystal anatase TiO_2 was synthesized by hydrothermal treatment of aqueous titanium trichloride ($TiCl_3$; 0.15 mol dm^{-3}) solutions with sodium dodecyl sulfate (SDS; 0–0.133 mol dm^{-3}. The solution of $TiCl_3$ in dilute aqueous HCl was supplied by Wako Pure Chemicals. The precursor solution (40 mL) was placed in a Teflon-lined autoclave. Glass slides were used as substrates and were immersed in the solutions. The solutions were then heated at 200 °C for 3 h in a dry oven. The TiO_2 deposited on the substrates was rinsed with deionized water and dried at room temperature.[22]

10.5.2 Synthesis of Micro TiO_2 Particles

The oil phase consisted of 36 g of kerosene with 530 wt% of surfactant. The surfactant was sorbitan monooleate (Span 80®) and sorbitan monostearate (Span 60®) with a weight ratio of Span 80®/Span 60® = 3 : 1. The water phase consisted of TTIP, diethanolamine, methanol and water. DEA was used as a stabilizer to control the hydrolysis rate of TTIP, and methanol was used to increase the compatibility between water and TTIP. The molar ratio of

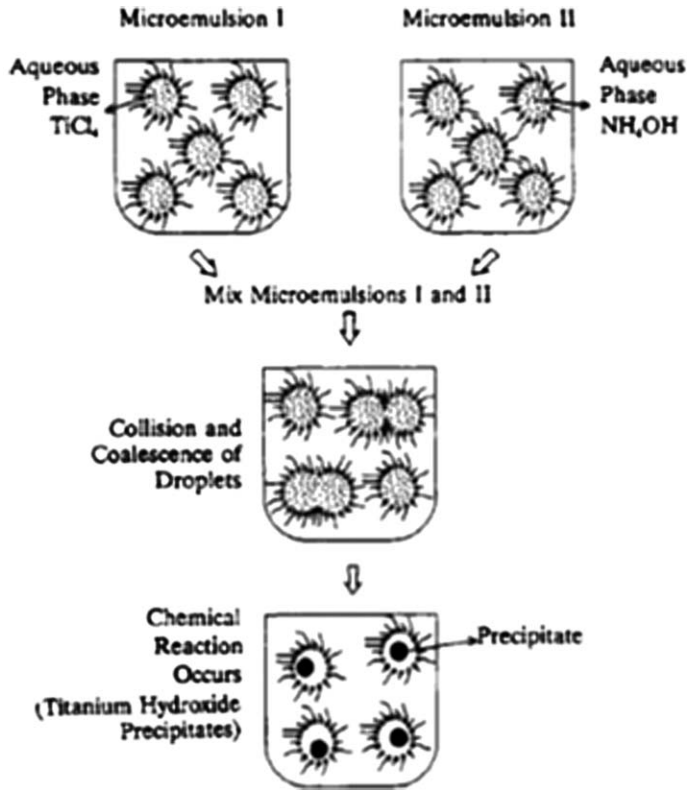

Figure 10.3 Schematic diagram showing the preparation of TiO_2 particles in microemulsions.
(Reproduced with permission from ref. 21.)

TTIP/DEA/CH_3OH/H_2O was 1 : X : Y : 22. The X was varied from 1.3 to 2.1 and the Y was changed from 4.2 to 12.5 to control the particle size as well as the dispersibility of microspheres (Figure 10.3).[23]

A novel atmospheric pressure plasma jet (APPJ) was used to synthesize micro TiO_2 particles. This was achieved by controlling the operating parameters in a low temperature, capacitive radiofrequency plasma jet in which TTIP precursor was vaporized with an argon/oxygen carrier gas, and then exposed to ambient air. The influence of plasma power and oxygen gas flow rate, which result in control of surface morphology, microstructure and chemical composition, has been investigated.[24]

10.6 Characterization of TiO_2

There are different ways to synthesize TiO_2 particles and different routes often produce different results. Even for the same route, the powder size obtained is different using different amounts of the starting materials. Consequently, phase

and particle size are the important parameters that influence the physical properties of the material. The particle size can be determined from direct observation of particles by transmission electron microscopy (TEM) or scanning electron microscope (SEM) techniques. Important information on the shape of particles can also be determined. It is important to note that TEM and XRD methods allow not only the measurement of particle size, but also identification of crystalline phases. Apart from TEM, XRD and SEM there are several techniques to characterize TiO_2 particles including Raman spectroscopy, FTIR, EDX, UV-vis spectroscopy, *etc*.

10.6.1 XRD

XRD patterns of nano TiO_2 and micro TiO_2 in rutile and anatase phases are shown in Figures 10.4.1 and 10.4.2, respectively. In Figure 10.4.1, strong diffraction peaks at 27°, 36° and 55° indicate TiO_2 in the rutile phase. In Figure 10.4.2, strong diffraction peaks at 25° and 48° indicate TiO_2 in the anatase phase. From the two figures it is clear that diffraction pattern peak intensity of the TiO_2 increases with increasing particle size. These results suggested that the nano TiO_2 powder is composed of irregular polycrystalline material. Amorphous material revealed a broad pattern with low intensity.

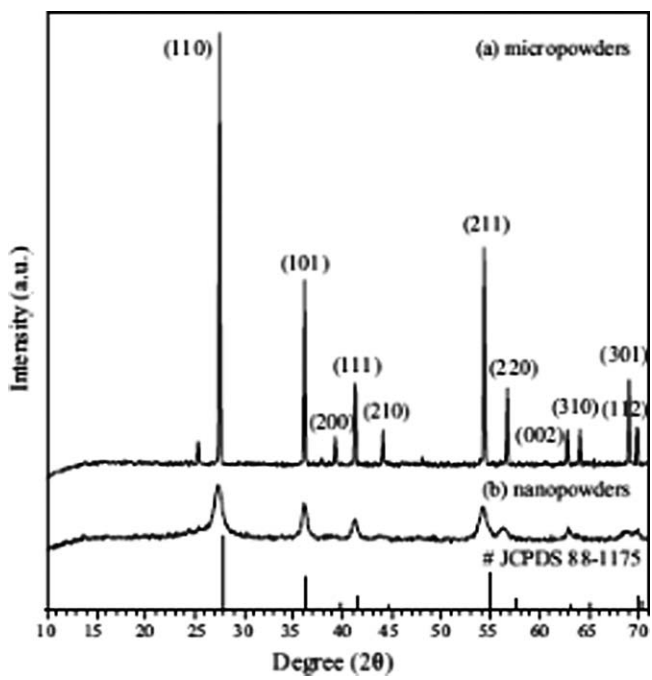

Figure 10.4.1 X-ray diffraction pattern of rutile TiO_2.

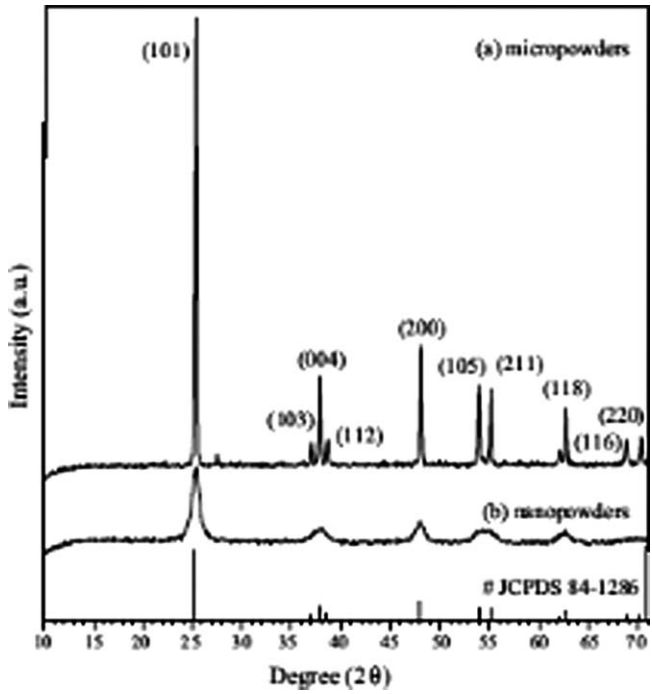

Figure 10.4.2 X-ray diffraction pattern of anatase TiO_2.

10.6.2 TEM

TEM was used to investigate the particle size, crystallinity and morphology of samples. TEM bright field images of TiO_2 micro powders in rutile and anatase phases are shown in Figure 10.5.1. TiO_2 powders in the rutile phase consist of both spherical and rod shapes but the particles of TiO_2 powders in the anatase phase consist only of spherical shapes.[25] Furthermore, it can be estimated that the particle size of samples in Figure 10.5.1 are microscale, with a grain size about 0.3–0.7 μm. TEM bright field images of TiO_2 nanopowders in rutile and anatase phases are shown in Figure 10.5.2. It can be estimated that the particle size of powders in Figure 10.5.2 are nanoscale, with a grain size below 10 nm.

In Figure 10.6.1 the SAED patterns of nano TiO_2 powders in the rutile phase show spotty ring patterns without any additional diffraction spots and rings of second phases, revealing their very crystalline structure. On the other hand, the SAED patterns of nano TiO_2 powders in the anatase phase (Figure 10.6.2) show that the brightness and intensity of the polymorphic ring is weak, so they are poorly crystallized and partly amorphous.

10.6.3 FTIR

FTIR spectra of TiO_2 nanoparticles exhibiting the transmittance band at 1624 cm^{-1} present in the anatase phase only was assigned to the bending

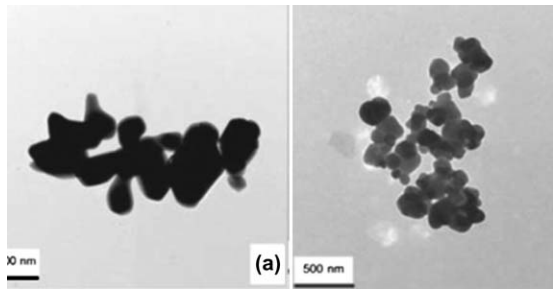

Figure 10.5.1 TEM images of TiO_2 micro powders in rutile and anatase phases.

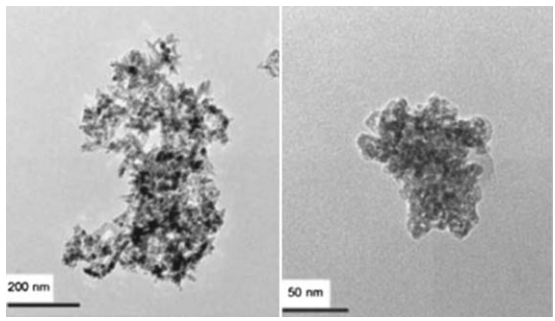

Figure 10.5.2 TEM images of TiO_2 nano powders in rutile and anatase phases.

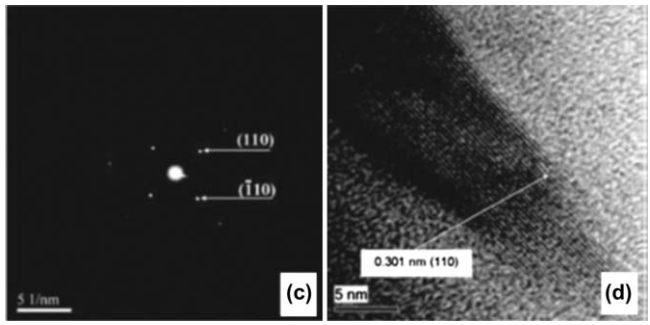

Figure 10.6.1 SAED pattern of rutile nano TiO_2 powder and HRTEM image of nano TiO_2 powder.

vibration of coordinated H_2O as well as from the Ti–OH bond.[26] The intensity of the IR absorption band decreases with increasing temperature.

10.6.4 Raman Spectroscopy

The anatase phase has six Raman active modes: $A1g + 2B1g + 3Eg$. For a single crystal, Ohsaka determined the following allowed bands at 144 cm^{-1}

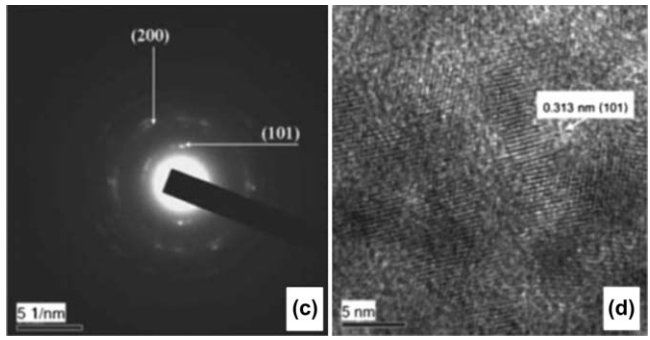

Figure 10.6.2 SAED pattern of anatase nano TiO_2 powder and HRTEM image of nano TiO_2 powder.

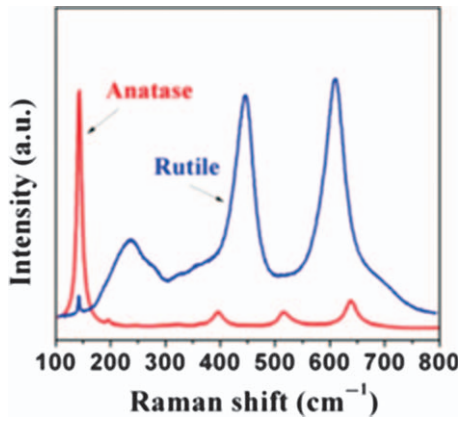

Figure 10.7 Raman spectrum of images of TiO_2 nano powders in rutile and anatase phases.

(Eg), 197 cm^{-1} (Eg), 399 cm^{-1} (B1g), 513 cm^{-1} (A1g), 519 cm^{-1} (B1g) and 639 cm^{-1} (Eg). In contrast, the rutile phase has four Raman active modes assigned to A1g, B1g, B2g, and Eg. From a single crystal, the allowed modes were at 143 cm^{-1} (B1g), 447 cm^{-1} (Eg), 612 cm^{-1} (A1g) and 826 cm^{-1} (B2g). A wide mid-intensity peak at about 235 cm^{-1} appeared, which is assigned to the B1g, two phonon scattering of the rutile phase. However, Raman spectra confirm the pure phase of anatase and rutile of the nanocrystals prepared using the sol–gel route (Figure 10.7).[27]

10.6.5 Energy-Dispersive X-Ray (EDX) Analysis

An APPJ with a power of 13.56 MHz could be used to synthesize micro TiO_2 particles. The EDX spectrum of the particles has indicated the formation of micro TiO_2 structures. The chemical composition of micro TiO_2 particles was investigated by energy-dispersive X-ray (EDX) analysis.

10.7 Fabrication of TiO_2–NR Composites

10.7.1 Preparation of TiO_2 Film–NR Composites

Latex (16 g) was taken into a beaker and various pre-weighed TiO_2 dispersions were added respectively with vigorous stirring so as to yield composites. Amounts of 2, 4 and 6 pphr (parts of the solid pigment per hundred parts of rubber) were used, giving a total number of 12 preparations. The mixing process was carried out under rapid stirring adjustment with a magnetic hot plate/stirrer (FMH Instruments) at ambient temperature ($\sim$25 °C) until a visually homogeneous phase was obtained. Thin films were then prepared from this mixture by casting on non-sticky transparent polyester sheets pasted on rectangular glass sheets. Immediately afterwards, the glass sheets with the wet films were transferred into a convection oven set at 50 °C to dry for about 18 h. At the end of this time, the resulting dry films were allowed to cool to ambient temperature.[28]

10.7.2 Preparation of TiO_2–NR Composites

10.7.2.1 Latex Mixing Method

Industrial grade micron-TiO_2(R) was used as a starting material for the preparation of n-TiO_2(R) by ultrasonication. The suspension was sonicated for 30 min. After the reaction finished, the prepared n-TiO_2(R) suspension was obtained. NR/n-TiO_2(R) composites were prepared as follows: concentrated NR latex was diluted with water to 20% dry rubber content. The prepared n-TiO_2(R) suspension was mixed with NR latex and vigorously stirred for 30 min. After that, the mixture was co-coagulated with 2.5% formic acid. The coagulum was washed with water several times until its pH was about 7 and dried in an oven at 70 °C for 24 h to give the NR/n-TiO_2(R) compounds (uncured nanocomposites). To obtain NR vulcanizates, the NR nanocompounds were mixed with vulcanizing ingredients.

10.7.2.2 Two-Roll Mixing Method

Compounding was performed in an open two-roll mixing mill (laboratory size). NR was first masticated on the two-roll mill for about 2–3 min followed by addition of the ingredients. Cure characteristics were analysed using an oscillating disk rheometer (Monsanto R-100) at a temperature of 150 °C. The composites were cured at their respective cure times in a hydraulic press under a pressure of about 120 bar at 150 °C. Aged samples were prepared by keeping the samples in a hot air oven at 70 °C for 7 days.[29]

10.8 Properties of NR–TiO_2 Composites

By incorporating TiO_2 into NR, there is an improvement in mechanical properties up to a certain filler content and then it decreases. An improvement in both elongation at break and tensile strength data at low filler concentration (2 phr), and thereafter a decrease in the trend can be observed. The affinity

between the filler and matrix was examined using the composite theory of Einstein. Theoretical prediction of Young's moduli from this was compared against experimental data and it was found that there was a certain level of interfacial interaction. Mechanical properties depend on filler–matrix interactions. The above results indicate that the filler and the matrix have some interaction and a TiO_2 content of 2 phr represents the optimum amount of filler for the best performing composites.

The stress relaxation behaviour of the TiO_2/NR composites under tension was studied by Meera *et al.*[29] with reference to the filler loading and strain level. An increase in rate of stress relaxation with increase in filler loading can be observed. This is due to the breakdown of filler–filler and weak polymer–filler networks during the course of the relaxation process. At low loading, the chances of forming aggregates are comparatively less and hence good dispersion of the filler is achieved. So the rate of stress relaxation is almost comparable with that of the unfilled rubber. But at higher loading, due to the breakdown of the aggregates, the relaxation becomes faster.

The effect of strain level on the relaxation behaviour has also been investigated and is shown in Figure 10.8. It was observed that the increase in strain level from 20 to 200% does not have any effect on the rate of relaxation of the unfilled rubber and the composites. The effect of ageing on the stress decay was also investigated and the rate of stress relaxation was found to decrease after ageing and is shown in Figure 10.9.

The thermophysical properties of NR filled with TiO_2 composites have been investigated at room temperature for several filler concentrations by Meera *et al.*[30]

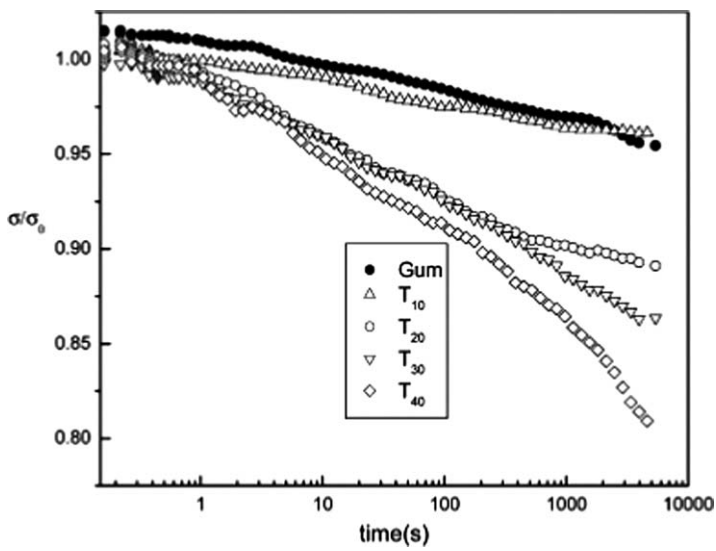

Figure 10.8 Stress relaxation curve of TiO_2-filled natural rubber. (Reproduced with permission from ref. 29.)

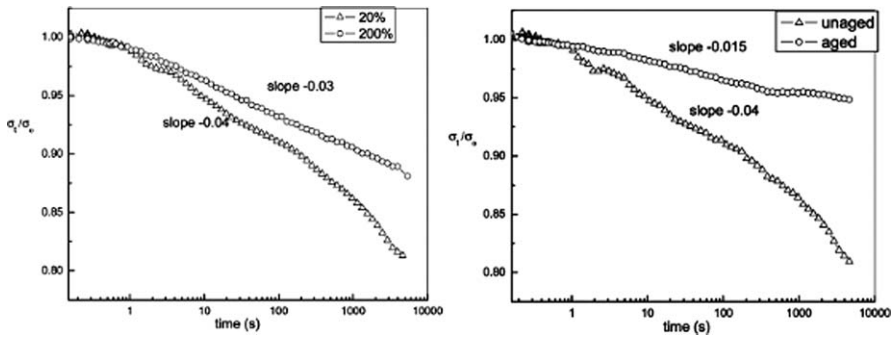

Figure 10.9 Effect of strain level for NR filled with 40 phr TiO_2. Effect of ageing on the stress decay T40.
(Reproduced with permission from ref. 29.)

The incorporation of fillers can induce modifications in the thermal properties of the polymers. Factors that affect the thermal conductivity of composites are the dispersion and orientation of the filler particles, the filler aspect ratio, and the relative ratio of thermal conductivity of the filler and the matrix. The thermal conductivity was found to be increased when the TiO_2 volume fraction increases. The measured values of thermal conductivity have been compared to different theoretical models.

The addition of n-TiO_2(R) into NR improves the resistance to UV irradiation. The addition of n-TiO_2(R) into NR improves not only the mechanical properties, but also the resistance to UV irradiation. ATR-FTIR spectra are used to explain the UV-protection property of the prepared NR nanocomposites. When the unfilled NR is exposed to UV, various chemical reactions take place, and as a result some changes may occur in the ATR-FTIR spectra. Some new peaks can be observed, the strong peak at 1715 cm^{-1} being assigned to C=O stretching vibration, which means the formation of carbonyl groups due to photo-oxidation at the main NR chain. On comparing the spectrum of the unfilled NR before and after UV irradiation, the evolution of the absorption peaks within the carbonyl region is crucial. Hence, the absorption band at 1715 cm^{-1} in the ATR-FTIR spectrum is a measure of degradation.

The UV-protection property of NR/micron-TiO_2(R) composites with 5 phr of micron-TiO_2(R) compared with the NR/n-TiO_2(R) composites were also examined. The carbonyl index of NR/n-TiO_2(R) composite is higher than that of NR/micron-TiO_2(R) composite at the same 5 phr of TiO_2(R) content. The results confirm that the NR nanocomposites incorporating n-TiO_2 possess effective UV-protection properties.

10.9 Photocatalytic Study of TiO_2–NR Composites

TiO_2 is generally one of the most widely used photocatalysts due to its chemical stability, non-toxicity, low cost and high efficiency in the photocatalysis process. But it has many disadvantages, including (i) it is difficult and expensive to

separate and recover the catalyst from suspension, (ii) the catalyst is not re-usable, (iii) the suspended particles readily aggregate, (iv) it is difficult to apply to continuous flow systems, and (v) there is the possibility that the loose power could cause adverse human health problems. There are many ways to avoid these problems, of which the most interesting is the fabrication of TiO_2 film on substrates with low thermal stability, such as plastics and hydrocarbon polymers.

A new method for preparing thin rubber sheet embedded with TiO_2 from NR latex has been developed by ChavalSriwong *et al.*[31] The characteristics of this thin and flexible TiO_2 sheet were studied by X-ray diffraction (XRD) and scanning electron microscopy/energy-dispersive X-ray spectrometer (SEM/EDS) techniques.

The SEM images of the pristine rubber sheet and the TiO_2-strewn sheet are shown in Figure 10.10. The surface morphology of the pristine rubber sheet is very smooth, without any particles adhering to the surface. On the contrary, for the strewn sheet, TiO_2 particles can be seen spread evenly over the sheet surface, causing high surface unevenness and roughness.

EDS analysis is used to determine the presence of elements in the TiO_2-strewn sheet. From the EDS spectrum (Figure 10.11) it is clear that the elements present in the sheet are carbon, oxygen and titanium, as evidenced from their corresponding K lines.

The photocatalytic activity of TiO_2 sheet was evaluated using indigo carmine (IC) dye as a model for the organic dye pollutant in water.[32] Photocatalytic activity is related to the surface roughness. As surface roughness increases, photocatalytic activity increases. A 5 wt% sheet showed higher photodegradation efficiency than the 10 wt% and 15 wt% sheets because surface roughness is higher for NR composites with 5% TiO_2. The effects of pH and initial concentration on the photocatalytic activity of composites have also been studied. Even though rubber sheets embedded with TiO_2 have less activity than powdered TiO_2, it has one clear advantage over the loose powder in that it can be easily recovered after having been used and can be reused many times.

According to Ming Jin *et al.*, TiO_2 can act as an anti-ageing layer on the surface of NR.[33] One of the major problems with NR is its short lifetime. Because of some special characteristics such as the ability of TiO_2 film to absorb

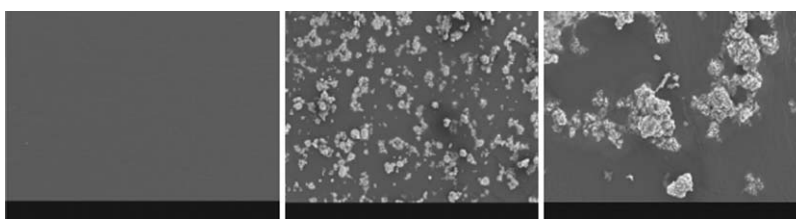

Figure 10.10 (a) SEM images of surface morphology of pristine rubber sheet, (b) TiO_2-strewn sheet at 35× magnification, and (c) TiO_2-strewn sheet at 150× magnification.
(Reproduced with permission from ref. 32.)

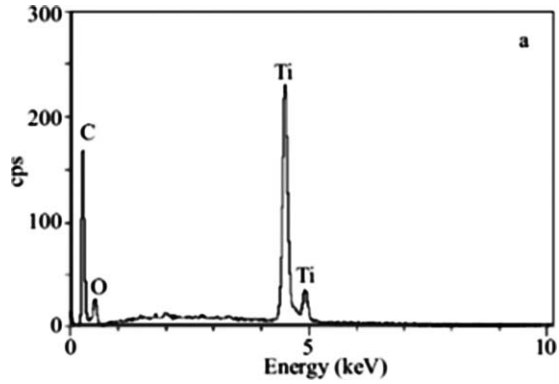

Figure 10.11 EDS spectrum of TiO_2-strewn sheet. (Reproduced with permission from ref. 32.)

UV light below 380 nm, photoinduced hydrophilic conversion and photocatalytic properties, it can be used as an anti-ageing agent for NR and can increase its lifetime.

Effects of coating thickness and TiO_2 dosage in polyurethane (PU) coatings on near infrared (NIR) reflectance, adhesion, crack resistance to bending, and thermal conductivity for wood/natural rubber (WNR) composite sheet before and after a prolonged UV ageing condition has been studied. The experimental results suggested that the solar reflectance slightly increased with increasing amounts of TiO_2 powder. Increasing TiO_2 powder in the PU coating resulted in a slight increase in thermal conductivity of TiO_2/PU coated WNR composite layer.

10.10 Applications of TiO_2–NR Composites

NR is a flexible raw material in the sense that it has the ability to be easily modified by the addition of fillers, while retaining its characteristic processing ease, to yield materials suitable for various applications.

TiO_2 is an inexpensive, non-toxic and photostable inorganic material, which has good optical and photocatalytic properties for many applications:

1. NR/TiO_2 composites are used to manufacture packaging materials meant to protect substances against the effect of UV prior to their use, as well as development of surface coatings and related products.
2. NR/TiO_2 nanocomposites can be used as antibacterial materials.
3. TiO_2-strewn rubber sheet can be used as a photocatalyst and is used to identify organic pollutants in waste water.
4. TiO_2-coated NR has increased lifetime, so this composite can be used in many applications.
5. TiO_2 impregnated in the rubber surface promote accumulation of dye molecules onto the surface and so it can be used to purify waste water.

10.11 Conclusions

By combining the properties of NR and TiO_2, we can make composites with enhanced properties and applications. Several processing methods, including sputtering, sol–gel processes, vapour deposition and thermal spraying, have been used to deposit nanocrystalline and microcrystalline TiO_2 powders. Other than TEM, XRD and SEM, there are several techniques to characterize TiO_2 particles including Raman spectroscopy, FTIR, EDX, UV-vis spectroscopy, *etc*. Composites can be fabricated by a latex mixing method or by two-roll mixing. Improving the properties of NR by the addition of TiO_2 particles is investigated. NR/TiO_2 composites can find application in various fields.

References

1. P. L. Teh, Z. A. Mohd-Ishak, A. S. Hashim, J. Karger-Kocsis and U. Sishiaku, *Eur. Polym. J.*, 2004, **40**, 2513.
2. A. L. Linsebigler, G. Lu and J. T. Yates, *Chem. Rev.*, 1995, **95**, 735.
3. D. Hull and T. W. Clyne, *An Introduction to Composite Materials*, 2nd ed., Cambridge University Press, Cambridge, 1996.
4. W. Peukert, H. C. Schwarzer, M. Götzinger, L. Günther and F. Stenger, *Adv. Powder Tech.*, 2003, **14**, 426.
5. T. Imai, F. Sawa, T. Nankano, T. Ozaki, T. Shimizu, M. Kozako and T. Tanaka, *IEEE Trans. Dielectr. Electr. Insul.*, 2006, **1**, 319.
6. J. Moczo and B. Pukanszky, *J. Ind. Eng. Chem. (Amsterdam, Neth.)*, 2008, **14**, 535.
7. R. N. Rothon, *High Performance Fillers 2007: Hamburg, Germany*, Smithers Information Ltd., 2007, pp. 10–15.
8. G. Momen and M. Farzaneh, *Rev. Adv. Mater.*, 2011, **27**, 1.
9. J. Njuguna, K. Pielichowski and S. Desai, *Polym. Adv. Technol.*, 2008, **19**, 947.
10. G. Schmidt and M. Malwitz, *Curr. Opin. Colloid Interface Sci.*, 2003, **8**, 103.
11. P. N. K. Kumar, PhD thesis, University of Twente, Enschede, the Netherlands, 1993.
12. G. Liu, L. Z. Wang, H. G. Yang, H. M. Cheng and G. Q. Lu, *J. Mater. Chem.*, 2010, **20**, 831.
13. A. Fujishima and K. Honda, *Nature*, 1972, **238**, 37.
14. M. Gratzel, *Nature*, 2001, **414**, 338.
15. A. L. Linsebigler, G. Lu and J. T. Yates, *Chem. Rev.*, 1995, **95**, 735.
16. J. S. Chen and X. W. Lou, *Electrochem. Commun.*, 2009, **11**, 233.
17. S. W. Liu, J. G. Yu and M. Jaroniec, *J. Am. Chem. Soc.*, 2010, **132**, 119.
18. S. Liu, J. Yu and M. Jaroniec, *Chem. Mater.*, 2011, **23**, 4085.
19. A. Laachachi, A. M. Cochez, M. Ferriol, J. M. Lopez-Cuesta and E. Leroy, *Mater. Lett.*, 2005, **59**, 36.
20. P. V. Kamat, *J. Phys. Chem. C*, 2012, **116**, 11849.

21. V. Chhabra, V. Pillai, B. K. Mishra, A. Morrone and D. O. Shah, *Langmuir*, 1995, **11**, 3307.
22. E. Hosono, S. Fujihara, H. Imai, I. Honma, I. Masaki and H. Zhou, *ACS Nano*, 2007, **4**, 273.
23. Z. Li, M. Kawashita and M. Doi, *J. Ceram. Soc. Jpn.*, 2010, **118**, 467.
24. C. Huang, Y. Chang and S. Wu, *J. Chin. Chem. Soc. (Weinheim, Ger.)*, 2010, **57**, 1204.
25. K. Thamaphat, P. Limsuwanand, B. Ngotawornchai and Kasetsart, *J.: Nat. Sci.*, 2008, **42**, 357.
26. M. M. Viana, V. F. Soares and N. D. S. Mohallem, *Ceram. Interfaces*, 2010, **36**, 2047.
27. K. K. Gupta, A. Kundan, P. K. Mishra, P. Srivastava, S. Mohanty, N. K. Singh, A. Mishrad and P. Maiti, *Phys. Chem. Chem. Phys.*, 2012, **14**, 12844.
28. S. S. Ochigbo and A. S. Luyt, *Int. J. Composite Materials*, 2011, **1**, 7.
29. A. P. Meera, S. Said, Y Grohens, A. S. Luyt and S. Thomas, *Ind. Eng. Chem. Res.*, 2009, **48**, 3410.
30. A. P. Meera, R. Tlili, A. Boudenne, L. Ibos, V. Poornima, S. Thomas and Y. Candau, *J. Elastomers Plast.*, 2012, **44**, 369.
31. C. Sriwonga, S. Wongnawaa and O. Patarapaiboolchaib, *Chem. Eng. J*, 2012, **191**, 210.
32. C. Sriwonga, S. Wongnawaa and O. Patarapaiboolchaib, *J. Environ. Sci.*, 2012, **24**, 464.
33. M. Jin, X. Zhang, A. V. Emeline, T. Numata, T. Murakami and A. Fujishima, *Surf. Coat. Technol.*, 2008, **202**, 1364.

CHAPTER 11

Micro and Nano Metal Particle Filled Natural Rubber Composites

JITHIN JOY,[a,c] ANU TRESA SUNNY,[b] LOVELY MATHEW P.,[c] LALY A. POTHEN[d] AND SABU THOMAS*[a,b]

[a] Centre for Nanoscience and Nanotechnology, Mahatma Gandhi University, Kottayam, Kerala, India; [b] School of Chemical Science, Mahatma Gandhi University, Kottayam, Kerala, India; [c] Department of Chemistry, Newman College, Thodupuzha, Kerala, India; [d] Bishop Moore College, Mavelikara, Alappuzha, Kerala, India
*Email: sabupolymer@yahoo.com

11.1 Introduction

Polymers are well known for their insulating properties. However, addition of certain metal or metalloid materials enhances both the electrical and thermal conductivity of composites.[1] These metal powder filled polymer composites have emerged as a new-generation material and are of interest to many fields of engineering. Recently, conductive polymer composites (CPCs) have become of great interest because of their unique properties. CPCs find unlimited applications in various fields such as high-capacity information storage devices, integrated circuits, magneto-optical media,[2] micro-electromechanical systems (MEMS)[3] and micro-sensors. MPNCs are also finding uses in biomedical applications in cell separation, enzyme immunoassay, bioprocessing, medical

RSC Polymer Chemistry Series No. 8
Natural Rubber Materials, Volume 2: Composites and Nanocomposites
Edited by Sabu Thomas, Hanna J. Maria, Jithin Joy, Chin Han Chan and Laly A. Pothen

Published by the Royal Society of Chemistry, www.rsc.org

diagnosis and controlling targeting drug delivery.[4,5] Various metal particles, such as Al, Zn, Cu, Fe, stainless steel, Ag, Au and Ni are incorporated into different polymer matrices. The main aim of adding inorganic fillers into polymers is to reduce the cost of the product.

11.2 Nanocomposites

Recent research in composite materials containing a polymeric matrix reinforced with various inorganic fillers had led to the development of 'nanocomposites'. In polymeric nanocomposites, inorganic particles having a size of 10–100 Å in at least one dimension are incorporated into an organic polymer matrix. The advantages of nanocomposites over virgin polymers or their conventional microcomposites are they exhibit excellent barrier, mechanical, thermal, optical and physicochemical properties. This is due to the nanometric size effect, *i.e*. the greater exposed surface of nano-sized filler particles towards the polymer.[6] Depending upon the dimensions of the dispersed particles, nanocomposites can be categorized into three types. When all the dimensions of the dispersed particles are in the order of nanometres, for example spherical nano-sized particles of silica, various metals, metal oxides, *etc*., they are referred to as iso-dimensional nanocomposites. In the second category, filler particles with two dimensions in the nanometre scale are employed, *e.g*. nanotubes, whiskers, *etc*. The third type of nanocomposite use particles with only one dimension in the nanometre range, *e.g*. various layered silicates. The history of polymer nanocomposites began in 1990, when Toyota first used clay/nylon-6 nanocomposites to produce timing belt covers for its cars. Following Toyota's lead, General Motors and Mitsubishi, among others, started to use composites for various automotive applications.[7–10] As the size of nanoparticles decreases, specific surface area increases, and this distinguishes nanocomposites from conventional composites. Consequently, smaller amounts of nanoparticles are needed to achieve improved properties.

11.3 Metal Particle–Polymer Composite Materials

CPCs are very useful materials in various applications such as self-regulated heating, heat conduction, conversion of mechanical to electrical signals, vapour sensing and bipolar plates in fuel cell electromagnetic interference shielding, discharging static electricity, *etc*.[11] Addition of conductive fillers such as carbon nanotubes (CNTs), silica, synthetic diamond (SND), silicon nitride, boron nitride (BN), copper (Cu), nickel, iron (Fe), aluminium, ferrite, bronze and aluminium nitride to the polymers can satisfy the required characteristics of CPCs.[12–16] Nano-sized conductive fillers in polymer composites give better thermal conductivity and stability compared to micro-sized particles, due to the better interaction of smaller particles leading to the formation of a good conductive path. Thus, CPCs offer an alternative economical and effective solution to thermal problems.[2] The other factors that affect the conductivity of CPCs are the geometry and volume fraction of the metal particles in the polymer.

However, a higher amount of metal particles is required to achieve the desired properties of composites. Higher amounts of metal particles in a polymer matrix affect the unique properties of the matrix, such as processability, appearance, density and ageing performance.[17] CPCs made by incorporating powdery metal fillers into polymers have the combined properties of metals and polymer, with cost effectiveness and a rapid fabrication rate, light weight and non-corrosiveness.

11.4 Metal Particle Natural Rubber Composite Materials

Magnetic fillers such as metal particles or magnetic oxides like ferrites have the ability to impart magnetic properties to the natural rubber (NR) matrices.[18,19] Because of the low density of metal oxides in comparison to metals, large amounts of magnetic oxides are necessary to obtain the required magnetization. Large amounts of filler can negatively affect the expected properties of the polymer material. To overcome this difficulty metal particles are used as fillers. A reasonable number of studies are reported on the magnetic properties of MPNCs with various magnetic fillers and several polymeric matrices.[20,21] The dielectric properties of an insulating medium can be modified by incorporating electrically conducting particles into the matrix.[22] The insulating polymer can be made conducting or semiconducting, depending on the amount of filler particles dispersed in the medium. The NR–metal composites can easily be shaped into various complicated shapes.[23] The major advantages of these materials are that they are inexpensive, offer better corrosion resistance than metals, and only require one-step processing in most cases, compared to the many steps involved in metal processing. Additionally, the conductivity level can be fixed in order to satisfy the various requirements of the end user. The filling of NR with metallic particles leads to increased density of composites. The incorporation of magnetic fillers in NR leads to the formation of a composite with improved mechanical, magnetic and electrical properties.

Ferromagnetic (Fe), nickel (Ni) or cobalt particles are the main metallic magnetic filler materials. Ni particles are chemically more stable than other magnetic fillers and therefore are a better choice than other magnetic fillers. Due to the flexibility and mouldability of composites obtained by incorporating metal particles into elastomers, they have many useful technological applications. NR is a commonly available elastomer and reports are available on studies of the electrical properties of composites based on NR with metal particles as fillers.[24]

11.4.1 Metal Particles Employed in Composite Fabrication

Jamal *et al.*[25] synthesized Ni particles by a modified sol–gel combustion process[26] and then reduced the size to below 100 nm by high-energy ball milling. The average particle size of the Ni metal particles was found to be

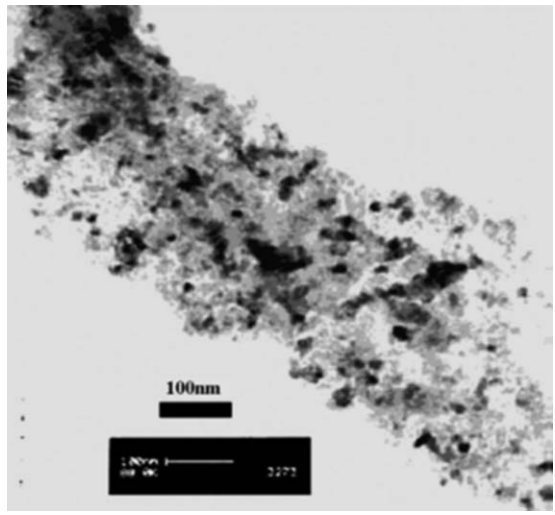

Figure 11.1 TEM image of nickel nanoparticles.
(Reproduced with permission from ref. 25.)

26 nm. Figures 11.1 shows the TEM image of Ni particles in the range of 25–40 nm. The Ni particles synthesized are ferromagnetic with a coercivity of 68 Oe and a remnant magnetization of 8.5 emu/g; saturation magnetization was found to be 47.5 emu/g. Figures 11.2 shows the X-ray diffraction pattern of the Ni particles obtained and it exactly matches the reported result (ICDD data file no. 03–1051).

Vinod *et al.*[27] used aluminium particles having a specific gravity of 2.7 and a particle size of 127–300 nm to prepare NR–aluminium composites. Nasher *et al.*[28] prepared NR composites incorporating different ratios of Fe with average particle size varying between 26 and 45 nm and Ni particles with an average particle size of between 22 nm and 50 nm.

11.5 Property Analysis of NR–Metal Composites

11.5.1 Structural Properties

11.5.1.1 Positron Annihilation Study

Positron annihilation lifetime spectroscopy (PALS) can be used to measure the free volume in various materials.[29] Jean *et al.*[30] discussed the application of positron annihilation spectroscopy (PAS) in the detailed study of polymers and polymers with fillers. The primary experimental PAS technique used in this research is PALS, one of the three techniques in the PAS family and a powerful tool for measuring the free volume in various materials.[31] The free volume has a great role in polymer research and is widely used to explain the behaviour of physical properties such as glass transition temperature, viscosity and physical ageing. Free volume is affected by the blending of polymers, ageing and addition

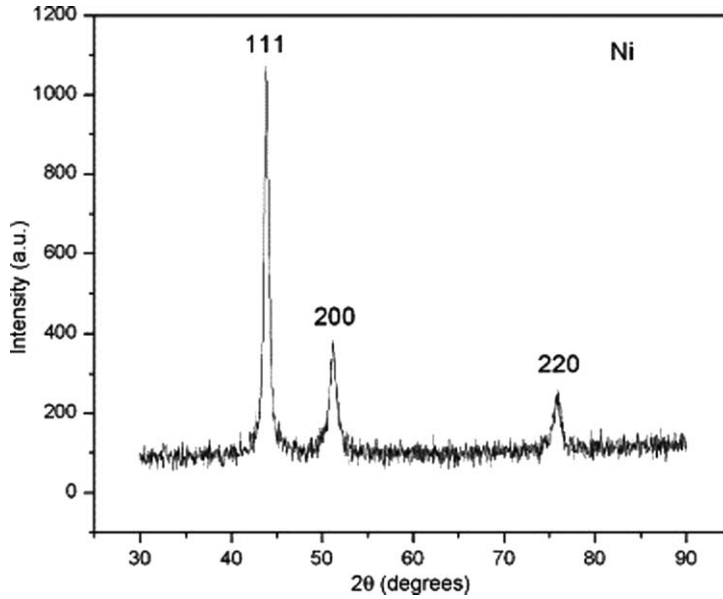

Figure 11.2 XRD pattern of nickel particles.
(Reproduced with permission from ref. 25.)

of various fillers. PALS is an effective method of detecting the free volume space considering the fact that the positronium (Ps) atoms are formed and localized in the nanometre-scale holes in various materials. PALS measures the ortho-Ps (o-Ps) lifetime distribution in the sample, which is particularly related to the free volume on the scale of 1–10 nm. Additionally, the intensity of Ps annihilation is connected to the amount of free volume or the number of voids.

Aly *et al.*[32] studied the PAS of NR–Ni and NR–Fe composites. They observed that the size of free-volume holes of NR–Ni composites tends to decrease by increasing the filler content (ranging from 159 $Å^3$ to 155 $Å^3$). In contrast, the free-volume hole size of NR–Fe composites is found to increase at about 159 $Å^3$ and then decreases (about 154 $Å^3$) at a higher filler loading of Fe. This behaviour is due to the magnetic properties of the Fe filler. The addition of filler, Ni or Fe ions changes the crosslinking density of the composites and inhibits o-Ps formation; therefore, the fraction of free-volume holes decreases by increasing the filler content in NR. A positive correlation is observed between the size of free-volume holes and tensile strength for both NR–Ni and NR–Fe composites. However, this correlation is found to be negative with respect to permittivity ε', dielectric loss ε'' and conductivity σ. The decrease in τ_2 and increase in I_2 in the case of Ni–rubber composites indicate that the created defects in the crystalline regions and amorphous–crystalline interfaces are definitely affected by the addition of Ni. The addition of Fe leads to the creation of certain defects with constant size and low fraction. The oxidative stability of NR decreases dramatically when large amounts of Fe particles are

incorporated into the matrix. This is probably due to the catalytic effect of Fe ions on the decomposition of hydroperoxides, and the large amounts of oxygen on the surface of the particles.[33]

11.5.2 Mechanical Properties

Conductive metal–NR composite materials are widely used instead of metallic conductors because they possess the obvious advantages of flexibility, light weight and ability to absorb mechanical shocks.[34] NR composites filled with metals have properties close to those of metals, whereas the mechanical properties and processing methods are typical of elastomers.

Vinod *et al.*[27] prepared NR–Al composites by using Al particles as the filler. They observed an increase in tensile strength with Al powder-filled samples at all loadings. The NR composite with 40 phr of Al shows a maximum tensile strength of 22.5 MPa from 20.5 MPa. Ageing of NR–Al powder composites at 70 °C for 7 days slightly increased the tensile strength due to the continued crosslinking in the composite, but degradation predominates on prolonged ageing, resulting in a decreased tensile strength. The maximum elongation is found to decrease after prolonged ageing. The hardness (Shore A) of the composites shows a similar trend to that of tensile strength. The hardness increases from 42 to 53 by the incorporation of 40 phr of Al powder. The elongation at break values decrease from 800 to 555% on incorporation of 40 phr of Al powder. The limiting oxygen index (LOI) value increased with Al powder loading. The LOI is defined as the volume fraction of oxygen in an oxygen–nitrogen atmosphere that will just support steady candle-like burning of a material. It is widely applied as a measure of polymer flammability. Gamma irradiation of the composite caused a decrease in tensile strength, but the extent of the decrease is a minimum for Al powder-filled compounds, whereas in other cases, a sharp fall in tensile strength was observed. Although gamma irradiation can cause crosslinking and polymer degradation, the reduction in tensile value shows that chain scission leading to polymer degradation is the main reaction here. The Al powder-filled NR composites showed better retention of mechanical properties after thermal ageing compared to other fillers like high abrasion furnace black (HAF), silica and acetylene black. These composites also have better resistance to ozone exposure, heat and gamma radiation. Gamma radiation leads to a decrease in tensile strength of the composites, but in the case of Al-filled NR the decrease is minimized. Table 11.1 shows the properties of NR–Al composites at various filler loadings.

El-Nashar *et al.*[28] prepared NR–Ni and NR–Fe nanocomposites by using various amounts of metal particles. Table 11.2 shows the properties of NR–Ni composites at various filler loadings. They observed that for all strains the stress increased with the filler loading from 0.5 (50% elongation of the original length) to 3 (300% elongation). The incorporation of Ni nanoparticles in the NR matrix enhanced its elasticity. But the breaking stress decreases with increasing filler percentage. This may be due to the presence of the metal particles or the agglomerates of the particles by microscopic discontinuities introduced

Table 11.1 Properties of the NR–Al composites.

Sample (phr of Al particle)	t_{90} *(min)*	*Tensile strength (MPa)*	*Hardness (Shore A)*	*Elongation at break (%)*	*LOI (n%)*
100NR	18.0	20.1	42	800	16.4
10	17.5	20.8	43	790	17.3
20	16.0	21.4	49	750	17.4
30	15.0	22.0	51	660	17.8
40	14.0	22.2	53	550	18.2

Table 11.2 Effect of different masses of nickel on the mechanical properties of vulcanized NR.

Concentration of nickel (phr)	*Magnetization (emu/g)*	*Tensile strength (MPa)*	*Elongation at break (%)*	*Strain modulus at 100% (MPa)*
0	–	28.9	1210	0.75
20	7	26.7	1102	0.80
40	11	22.8	930	0.91
60	14	21.6	858	1.1
80	18	20.5	858	1.1
100	20	19.2	764	1.4

in the matrix material. The tensile strength of these composites increases with increasing the magnetic filler up to 30 phr and then it decreases with increased filler loading. The increase in tensile strength at a filler loading of 30 phr was due to the good filler-NR interaction as a result of better filler dispersion in the NR matrix. Strong NR–filler interaction would increase the effectiveness of the stress transfer from the NR matrix to filler particles dispersed in the NR matrix. However, the reduction in strength at filler loading >30 phr is due to the reduction in the stress-induced crystallization of the NR matrix by loading of magnetic filler. The Young's modulus also exhibits the same behaviour. For the elongation at rupture no significant changes were observed. The hardness increases with increasing filler loading. NR with 30 phr of magnetic fillers improves the rheometric characteristics. It was observed that the Fe filler enhances the physico-mechanical properties more than Ni.

Jamal *et al.*[25] prepared NR–Ni composites by using Ni particles. It can be observed that the stress developed for strains from 50 to 300% enhances as the loading increases. However, there is a steady decrease in breaking stress with the increase in filler loading. This phenomenon may be due to the formation of agglomerates of filler particles within the NR matrix. The chances of agglomerates forming are higher with Ni particles compared to other metal particles because of the magnetic properties of nickel.

The hardness of the composite samples increases, whereas the resilience decreases, with an increase in filler concentration. The hardness is a measure of elastic modulus at small strains. The increase in hardness is due to the drop in the mobility of the elastomer chains due to the distribution of metal particulate filler. The decrease in resilience is due to a decrease in damping properties of the composite caused by a decrease in NR content in the samples.[35]

11.5.3 Dielectric Properties

The conducting and dielectric properties of insulator polymer-metal composites are dependent upon many factors.[36] The most important of these is the ratio of the filler particles to the host material. At lower volume ratios, the composites are good dielectric materials, but the conductivity of the material can increase sharply at some critical value of the volume ratio. The composites made with an insulating matrix change to a conductor over a very narrow range of metal filler concentration. This is due to the development of conductive paths at the percolation threshold of the filler particles[37] and this critical metal volume fraction is called the percolation threshold (φ_c). At this point the conductivity of the composite is σ_c.[38] When a continuous network is established between the fillers, then only the percolation condition occurs. Below the percolation threshold, the conductivity change is negligible and the conductivity of the composites is equal to the polymer conductivity (σ_p) or slightly higher. This is due to absence of contact between the metal particle fillers. As the filler concentration increases from φ_c to the filling limit, *F*, the conductivity increases rapidly from the value of σ_c at the percolation threshold to the maximum value σ_m. An increase in filler loading results in 'close proximity' of conductive filler particles, allowing the electron to travel across the polymeric gap in between the conductive particles, permitting current to flow.[39]

According to Bigg,[40] the percolation behaviour is primarily affected by the particle size, the shape of the filler, filler particle distribution, *etc*. Many researchers have proposed equations to calculate the conductivity of insulating polymers filled with conductive fillers, such as metal. For example, the conductivity (σ_{comp}) of a composite consisting of a homogeneous polymeric matrix with a conductivity of σ_{pol} and a volume fraction of σ_{pol} as well as conducting particulate filler with a conductivity of σ_{filler} and a volume fraction of σ_{filler} can be calculated with Equations (11.1):[41]

$$\sigma_{comp} = \sigma^{HS-}$$

$$\sigma_{comp} = \sigma_{pol}\left(\frac{2\sigma_{pol} + \sigma_{filler} - 2X_{filler}(\sigma_{pol} - \sigma_{filler})}{2\sigma_{pol} + \sigma_{filler} - X_{filler}(\sigma_{pol} - \sigma_{filler})}\right) \quad (11.1)$$

where σ^{HS-} is the Hashin-Shtrikman lower boundary.[41]

Due to the negligible electrical conductivity of the polymer matrix, the electrical conductivity of the composite holds the lower bound equation found by Hashin and Shtrikman assuming a high conducting phase (metal) surrounded by an insulator (polymer).

Figures 11.3[42] shows the methods of packing metal particles in a polymer matrix, such as random and segregated distributions. Figure 11.3(a) and (b) refer to the random distribution, below and above critical volume percentage (φ_c) of metal filler. In the random packing method, no network formation of metal particles occurs between contiguous sites. In contrast, in the segregated distribution, a network is formed. Figures 11.3(c) and (d) refer to the segregated

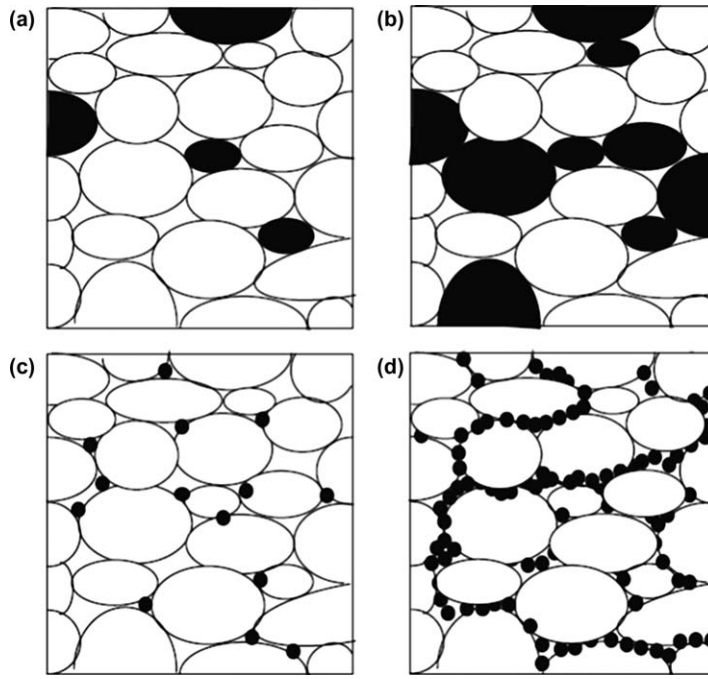

Figure 11.3 Schematic illustration of random (a) and (b) and segregated (c) and (d) particle distributions.
(Reproduced with permission from ref. 37.)

distribution, below and above φ_c. The critical volume loading (φ_c) in the random distribution is found to be higher than that of the segregated distribution.

For dielectric studies circular discs with a diameter of 12 mm were cut out from the cured sheets of composites. These studies were carried out using a HP impedance analyser model 4285 A in the frequency range of 100 kHz to 8 MHz by varying the temperature from 30 °C to 120 °C. The samples were inserted between two copper plates of the same diameter to form a capacitor in a home-made dielectric cell. The dielectric permittivity of the sample was calculated using the relation:[43,45]

$$\varepsilon' = \frac{Cd}{A\varepsilon_o} \tag{11.2}$$

and the dielectric loss by the relation:

$$\varepsilon'' = \varepsilon' \tan \delta \tag{11.3}$$

where ε' is the dielectric permittivity of the sample (the real part), C is the capacitance of the capacitor formed by inserting the sample between two metal plates, d is the thickness of the sample, ε_o is the permittivity of free space, A is the area of cross-section of the sample and d is the loss tangent.[44] The dielectric

permittivity decreases almost linearly with frequency. The drop in dielectric permittivity with increasing applied frequency is understood on the basis of the Debye model of dielectric relaxation.[40]

In Figure 11.4 the variation in dielectric permittivity (ε') with the Ni content in the composite is plotted for four different frequencies at a temperature of 40 °C. Permittivity increases with filler loading almost linearly for all frequencies. Metallic inclusions in any insulating material enhance the dielectric permittivity of the material. The increase in permittivity in NR–Ni nanocomposites is nearly linear with the increase in percentage loading of the Ni particles. It is possible to tune the dielectric permittivity to a desired value, and the dielectric loss in the material with Ni loading is small, and this material can be a potential candidate for making capacitors, owing to the possibility of moulding NR as very thin sheets or films.

Figures 11.5 shows the variation in dielectric permittivity of the composites with temperature. The plots are of composites of NR with Ni content of 0–100 phr. The segmental mobility of the polymer material increases with temperature and this can lead to an increase in the dielectric permittivity. But on the other hand, the thermal expansion of the elastomer material can cause an increase in volume and this can affect the measurement condition as the thickness of the capacitor increases. This can be the cause of the measured decrease in the dielectric permittivity at higher temperatures. The average decrease in the dielectric permittivity over a temperature range of 90 °C is around 7% of the value at room temperature. Differential thermal expansion between the metallic inclusions and the NR matrix and the resulting disruption of metal clusters had been suggested as a possible reason for the drop in the dielectric permittivity

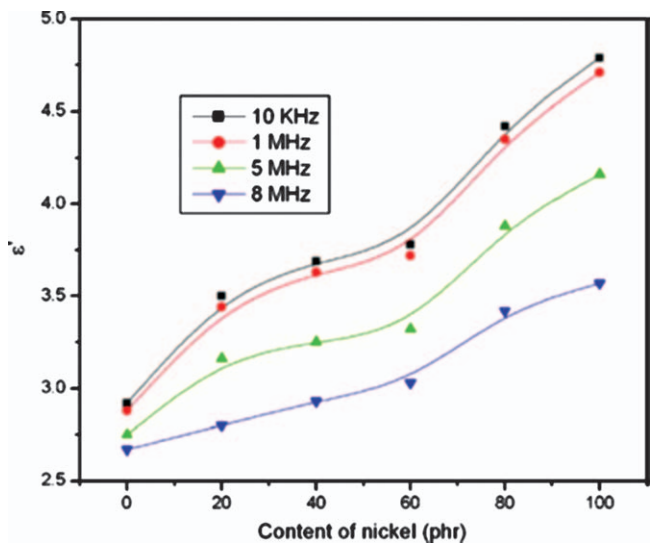

Figure 11.4 Variation in permittivity with nickel content in the NR–Ni composites. (Reproduced with permission from ref. 25.)

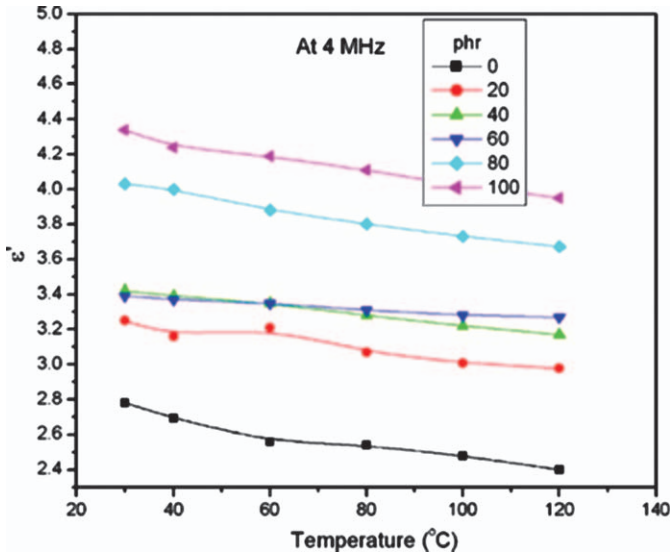

Figure 11.5 Variation in dielectric permittivity of the NR–Ni composites with temperature.
(Reproduced with permission from ref. 25.)

with temperature. The dielectric loss of the samples was measured and was found to increase with temperature.[25]

Nasher *et al.* studied the permittivity and dielectric loss value of NR–Fe and NR–Ni composites. They observed that these values increased as the filler content increased at room temperature and at constant frequency $f = 100$ Hz Hz. The values of permittivity are higher for NR–Ni composites than for NR–Fe composites. These higher values are due to the higher loss values of Ni–NR composites compared to NR–Fe composites. This is due to formation of iron oxide during the process. The conductivity of the composites increased by increasing filler content in both cases. The conductivity (σ) was calculated from the measured resistance R using the equation $(\sigma) = L/RA$ where A is the area of the sample in cm^2 and L its thickness in cm.[45] The conductivity σ are found to be $0.59 - 11.9 \times 10^{-11}\Omega^{-1}cm^{-1}$ for the samples containing different concentrations of Fe, while it ranges from 0.76 to $35.9 \times 10^{-11}\Omega^{-1}cm^{-1}$ for the different concentrations of nickel.[28] Figures 11.6 shows the variation in conductivity with filler content of Ni and Fe particles.

Jamal *et al.*[46] determined the complex dielectric permittivity and magnetic permeability of NR–Ni nanocomposites in the X band of microwave frequencies from 7 to 12 GHz. The real part of dielectric permittivity does not change with the frequency but shows a steady increase with the increase in loading of Ni nanoparticles. The dielectric loss shows an increase with the frequency in general and for NR–based composites there is a shallow relaxation peak around 8.25 GHz. In both type of composites, the dielectric loss increases

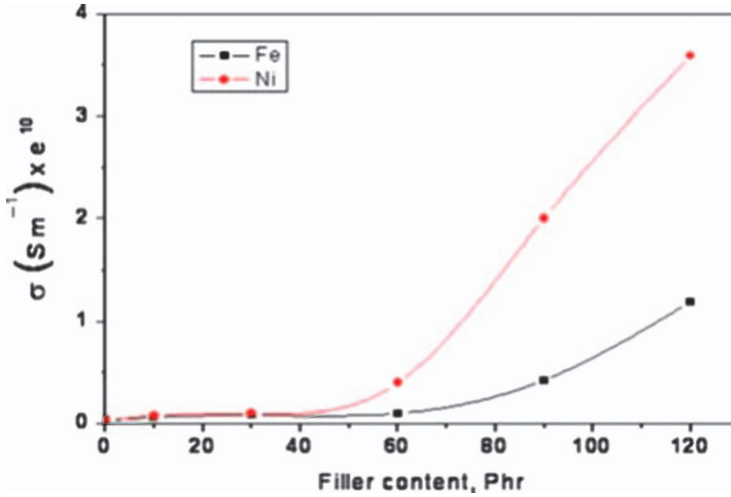

Figure 11.6 Variation in conductivity with various fillers. (Reproduced with permission from ref. 28.)

with the increase in the concentration of filler and a conductance loss is attributed to this observation. The magnetic loss shows a small relaxation at 8 GHz and then decreases. Magnetic resonance of ferromagnetic Ni particles is attributed to the observed peak in magnetic loss. Figures 11.7 shows the variation in dielectric permittivity of NR–Ni composites with frequency at different loadings and Figures 11.8 the dielectric loss of NR–Ni composites at different loadings.

11.5.4 Thermal Properties

The effective thermal conductivity of two-phase materials can be predicted by various models (empirical or theoretical). Using the potential theory, Maxwell and Eucken[47] obtained a simple relationship for the conductivity of randomly distributed and non-interacting homogeneous spheres in a homogeneous medium:

$$K_c = K_p\left[\frac{K_m + 2K_p + 2\theta(K_m - K_p)}{K_m + 2K_p - \theta(K_m - K_p)}\right] \tag{11.4}$$

where K_c, K_p and K_m are, respectively, the thermal conductivity of the composite (metal particle-filled polymer), continuous phase (polymer) and discrete phase (metal particles), and θ is the volume fraction of filler (discrete phase). This model can predict the effective thermal conductivity at low filler concentrations. For high filler concentrations, particles begin to touch each other and form conductive chains in the direction of heat flow, so this model underestimated the value of effective thermal conductivity in this region. Starting with Tsao's probabilistic model,[48] Cheng and Vachon[49] assumed a parabolic distribution of the discontinuous phase. The equivalent thermal conductivity of

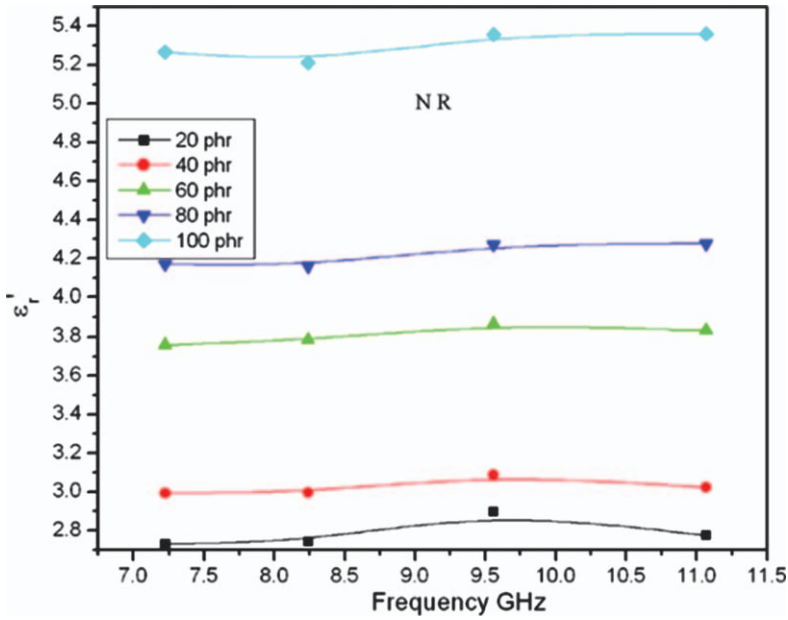

Figure 11.7 Dielectric permittivity of NR–Ni composites with frequency at different loadings.
(Reproduced with permission from ref. 41.)

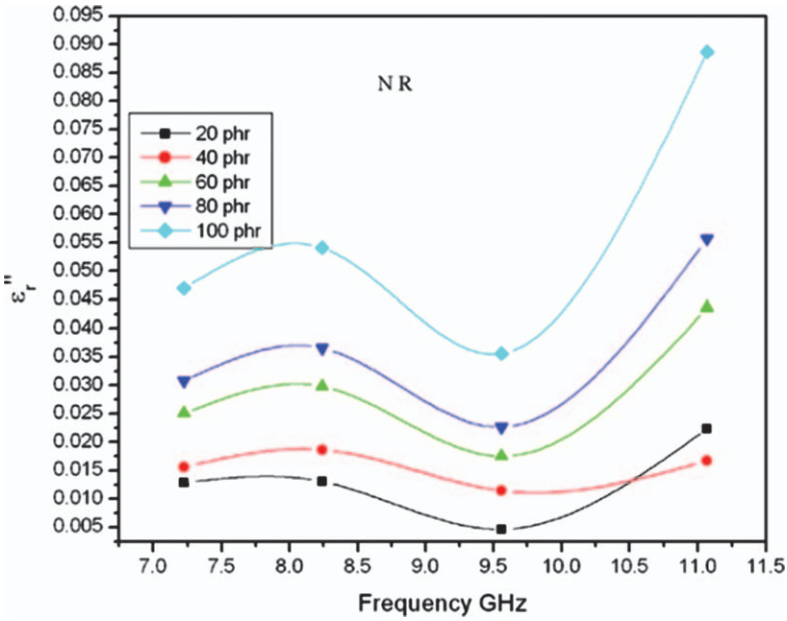

Figure 11.8 Dielectric loss of NR–Ni composites at different loadings.
(Reproduced with permission from ref. 41.)

a unit cube of the mixture is derived in terms of the distribution function and the thermal conductivity of the constituents.

For two-phase materials for which the thermal conductivity of the continuous phase is much smaller than the thermal conductivity of the discrete phase, $K_p \ll K_m$ or $K_m/K_p > 100$:

$$K_c \approx \frac{K_p}{1 - B} \tag{11.5}$$

where $B = \sqrt{3\theta/2}$.

The thermal characteristics of NR–metal composites are close to the properties of metals, whereas the mechanical properties and the processing methods are typical of polymers.[50,51] Thermally conducting, but electrically insulating, polymer-matrix composites are increasingly important for electronic packaging because the heat dissipation ability limits the reliability, performance and miniaturization of electronics.[52,53] Thermal properties such as thermal conductivity, thermal diffusivity and specific heat of metal (copper, zinc, Fe and bronze) powder-filled polymer composites are investigated experimentally in the range of filler content 0–24% by volume.[15]

11.5.5 Magnetic Properties

El-Nashar *et al.*[28] observed that the hysteresis loops of the magnetic nanoparticles distributed in the NR (which is a non-magnetic medium) have a super paramagnetic behaviour. The magnetic nanoparticles of Fe with 30 phr loading show a switching field (H_s) of 0.007728 T, and the magnetization saturation (M_s) is 22.75 emu/g, while for Fe with 120 phr loading the switching field is 0.005049 T, and M_s is 60.67 emu/g. It is clearly shown that by increasing the concentration of Fe nanoparticles in NR samples, the magnetization (emu/g) increases while the switching field (H_s) decreases. Increasing the concentration of magnetic nanoparticles in the NR medium leads to a decrease in the distance between the magnetic nanoparticles. Decreasing the distance leads to magnetic coupling between the nanoparticles. This coupling decreases the switching field because once one particle is switched, the other particles started to switch earlier due to the magnetic coupling. This leads to a decrease in the switching field and increases the magnetization in the NR medium.

In NR–Ni samples, the switching field (H_s) for 30 phr Ni is 0.00438 T, and M_s is 18.96 emu/g while the H_s for 120 phr is 0.003620 T, and M_s is 25.03 emu/g. The Ni samples show the same behaviour as Fe samples, apart from the switching field which is higher for Fe nanoparticles (hard magnet) than for Ni nanoparticles (soft magnet). Increasing the concentration of magnetic particles has an influence on the magnetic properties (due to the coupling between the magnetic nanoparticles, which affects the switching field) rather than the electrical properties. From the magnetic measurements, it is clear that the samples show a super paramagnetic behaviour for all samples. The hysteresis loops show a switching dependence on the particles percentage and on the type of magnetic particles. Figure 11.9(a) and (b) shows the

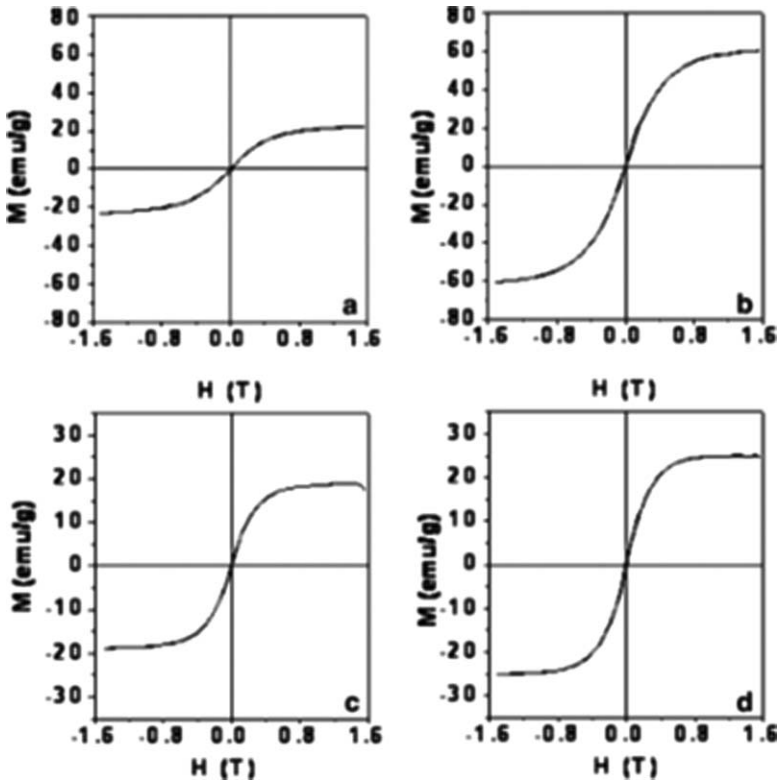

Figure 11.9 Hysteresis loops of NR–Ni and NR–Fe composites. (Reproduced with permission from ref. 28.)

hysteresis loops for NR samples containing 30 phr and 120 phr of Fe, respectively, and Figure 11.9(c) and (d) shows the hysteresis loops for rubber samples with 30 phr and 120 phr Ni nanoparticles, respectively.

Jamal *et al.*[35] observed that magnetic properties of cured NR samples clearly indicate that the ferromagnetic characteristics of Ni particles are retained in the NR. A steady increase in saturation magnetization with increase in filler fraction can be observed in both composite samples from the magnetization curves and the magnetic properties are identical in both types of composites. The remnant magnetization keeps a linear variation with the increase in concentration of Ni nanoparticles, again keeping exactly the same characteristics in both composite types. The coercivity of the samples did not show any variation with the concentration of Ni particles in the composites. Figure 11.10 shows magnetic hysteresis of NR–Ni composites with various filler loadings.

11.6 Applications of NR–Metal Composites

NR–metal composites have many important properties such as non-linear optical properties, electronic conductivity and luminescence, and have been

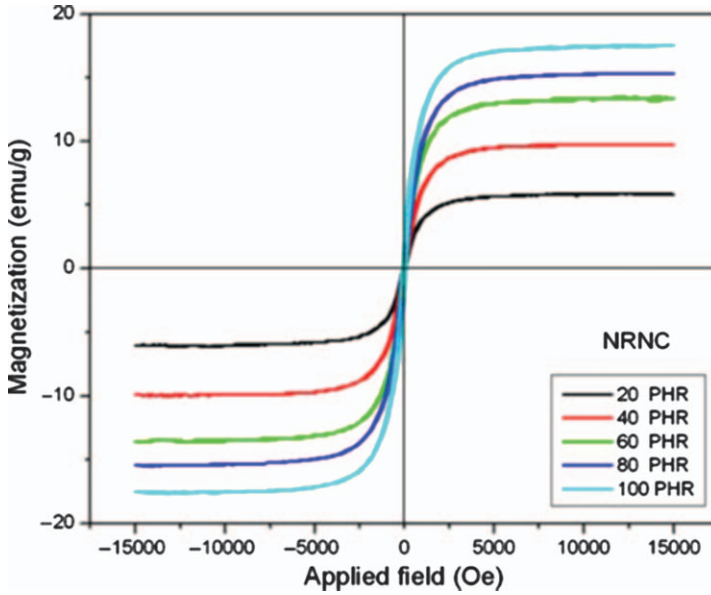

Figure 11.10 Magnetic hysteresis of NR–Ni composites. (Reproduced with permission from ref. 41.)

proposed for use in various applications including chemical sensors, electroluminescent devices, electrocatalysis, batteries, smart windows and memory devices. They weigh less than metals and are also cheaper. The physical properties and the percentage of filler must be known in order to determine the usefulness of the materials. It is therefore important, from a scientific and practical point of view, to understand the effects of metallic fillers on the properties of a polymer matrix.[54] They are also used as microwave absorbers and flexible magnets. Such applications are increasing because both radio frequency (RF) and microwaves in telecommunication are causing electromagnetic interference (EMI). The mouldability of these composites into complex shapes is another advantage. Ternary composites of NR filled with particulate carbonaceous and metal fillers were developed for electro-mechanical sensing purposes, while maintaining good elasticity and loading capability.[55]

11.7 Conclusions

The insulating host NR material can be turned into a conducting or semiconducting material, depending on the amount of metal particles dispersed in the medium. Ferromagnetic iron, nickel and cobalt particles are the choices as metallic magnetic fillers. The composites show a ferromagnetic behaviour and the saturation magnetization is found to increase with the metal content. The dielectric permittivity increases with an increase in the concentration of filler and decreases with rise in temperature. The oxidative stability of NR decreases

dramatically when large amounts of iron particles are incorporated into the matrix. The magnetic properties of the composites can be tailored by incorporating appropriate amounts of metal particles. The LOI values are increased by the incorporation of various fillers. They are also used as microwave absorbers and flexible magnets.

References

1. Y. P. Mamunya, V. V. Davydenko, P. Pissis and E. V. Lebedev, *Eur. Polym. J.*, 1887, **2002**, 38.
2. J. Sláma, A. Grusková, R. Vícen, S. Vícenová, R. Dosoudil and J. Franek, *J. Magn. Magn. Mater.*, 2003, **254**, 642.
3. A. Voigt, M. Heinrich, C. Martin, A. Llobera, G. Gruetzner and F. P. Murano, *Microelectron Eng.*, 2007, **84**, 1075.
4. S. Sindhu, S. Jegadesan, A. Parthiban and S. Valiyaveettil, *J. Magn. Magn. Mater.*, 2006, **296**, 104.
5. M. Rusu, N. Sofian and D. Rusu, *Polymer Test.*, 2001, **20**, 407.
6. Y. Kozima, A. Usuki, M. Kawasumi, A. Okada, Y. Fukushima, T. Kurauchi and O. J. Kamigaito, *J. Mater. Res.*, 1993, **8**, 1185.
7. A. Usuki, Y. Kojima, M. Kawasumi, A. Okada, Y. Fuku-shima and T. Kurauchi, *J. Mater. Res.*, 1993, **8**, 1179.
8. Z. Wang and T. J. Pinnavaia, *Chem. Mater.*, 1998, **10**, 1820.
9. S. Varghese, J. Karger-Kocsis and K. G. Gatos, *Polymer*, 2003, **44**, 3977.
10. K. Haraguchi, M. Ebato and T. Takehisa, *Adv. Mater.*, 2006, **18**, 2250.
11. G. Droval, P. Glouannec, J. F. Feller and P. Salagnac, *J. Thermophys Heat Transfer*, 2005, **19**, 375.
12. R. Kochetov, A. V. Korobko, T. Andritsch, P. H. F. Morshuis, S. J. Picken and J. J. Smit, *J. Phys. D: Appl. Phys.*, 2011, **44**, 395.
13. R. Kotsilkova, *J. Appl. Polym. Sci.*, 2005, **97**, 2499.
14. L. Huang, R. Zhan and Y. Lu, *J. Reinf. Plast. Compos.*, 2006, **25**, 1001.
15. N. M. Sofian, M. Rusu, R. Neagu and E. Neagu, *J. Thermoplast. Compos. Mater.*, 2001, **14**, 20.
16. J. Gu, Q. Zhang, J. Dang, J. Zhang and Z. Yang, *Polym. Eng. Sci.*, 2009, **49**, 1030.
17. C. L. Wu, M. Q. Zhang, M. Z. Rong and K. Friedrich, *Compos. Sci. Technol.*, 2002, **62**, 1327.
18. S. Sindhu, M. R. Anantharaman, B. P. Thampi, K. A. Malini and P. Kurian, *Bull. Mater. Sci.*, 2002, **25**, 599.
19. B. Zhang, Y. Feng, J. Xiong, Y. Yang and H. Lu, *IEEE Trans. Magn.*, 2006, **42**, 1778.
20. H. Nathani and R. D. K. Misra, *Mater. Sci. Eng., B*, 2004, **113**, 228.
21. K. H. Wu, T. H. Ting, C. I. Liu, C. C. Yang and J. S. Hsu, *Compos. Sci. Technol.*, 2008, **68**, 132.
22. G. C. Psarras, *Composites, Part A*, 2006, **37**, 1545.

23. D. M. Kalyon, E. Birinci, R. Yazici, B. Karuz and B. Karuz, *Polym. Eng. Sci.*, 2002, **42**, 1609.
24. M. R. Anantharaman, S. Sindhu, S. Jagatheesan, K. A. Malini and P. Kurian, *J. Phys. D: Appl. Phys.*, 1999, **32**, 1801.
25. E. M. A. Jamal, P. A. Joy, P. Kurian and M. R. Anantharaman, *Mat. Sci. Eng., B*, 2009, **156**, 24.
26. R. K. Sahu, A. K. Ray, S. K. Das, A. J. Kailath and L. C. Pathak, *J. Mater. Res.*, 2006, **21**, 1664.
27. V. Vinod, S. Varghese and B. Kuriakose, *Polym. Degrad. Stab.*, 2002, **75**, 405.
28. D. E. El-Nashar, S. H. Mansour and E. Girgis, *J. Mater. Sci.*, 2006, **41**, 5359.
29. T. L. Dull, W. E. Frieze, D. W. Gidley, J. N. Sun and A. F. Yee, *J. Phys. Chem. B*, 2001, **105**, 4657.
30. Y. Xu, D. D. L. Chung and C. Mroz, *Composites, Part A*, 2001, **32**, 1749.
31. G. Kalaprasad, P. Pradeep, G. Mathew, C. Pavithran and S. Thomas, *Compos. Sci. Technol.*, 2000, **60**, 2967.
32. E. H. Aly, *Am. J. Appl. Sci.*, 2011, **8**, 147.
33. M. Lokander, T. Reitberger and B. Stenberg, *Polym. Degrad. Stab.*, 2004, **86**, 467.
34. A. M. Y. EI-Lawindy, K. M. Abdel-Kader, W. E. Mahmoud and H. H. Hassan, *Polym. Int.*, 2002, **51**, 601.
35. E. M. A. Jamal, P. a. Joy, P. Kurian and M. R. Anantharaman, *Polym. Bull.*, 2009, **64**, 907.
36. Z. M. Elimat, A. M. Zihlif and G. Ragosta, *J. Phys. D: Appl. Phys.*, 2008, **41**, 165408.
37. Z. M. Dang, C. W. Nan, D. Xie, Y. H. Zhang and S. C. Tjong, *Appl. Phys. Lett.*, 2004, **85**, 97.
38. Y. P. Mamunya, V. V. Davydenko, P. Pissis and E. V. Lebedev, *Eur. Polym. J.*, 2002, **38**, 1887.
39. D. M. Kalyon, E. Birinci, R. Yazici, B. Karuz and B. Karuz, *Polym. Eng. Sci.*, 2002, **42**, 1609.
40. D. M. Bigg, *Metal Filled Polymers (Properties and Application)*, Marcel Dekker, Inc., New York, 1986, pp. 165–222.
41. Z. Hashin and A. Shtrikman, *J. Appl. Phys.*, 1962, **33**, 3125.
42. S. K. Bhattacharya and A. C. D. Chaklader, *Polym-Plast Technol*, 1982, **19**, 21.
43. S. Sindhu, M. R. Anantharaman, B. P. Thampi, K. A. Malini and P. Kurian, *Bull. Mater. Sci.*, 2002, **25**, 599.
44. E. M. Mohammed and M. R. Anantharaman, *J. Instrum. Soc. India*, 2002, **32**, 165.
45. I. I. Perepechko, *An Introduction to Polymer Physics*, Mir Publishers, Moscow, 1981.
46. E. M. A. Jamal, P. Mohanan, P. A. Joy, P. Kurian and M. R. Anantharaman, *Appl. Phys. A: Mater. Sci. Process.*, 2009, **97**, 157.
47. J. C. Maxwell, *A Treatise on Electricity and Magnetism*, 3rd ed., Dover Inc., New York, 1954, Chapter 9.

48. S. C. Cheng and R. I. Vachon, *Int. J. Heat Mass Transfer*, 1969, **12**, 249.
49. T. Lewis and L. Nielsen, *J. Appl. Polym. Sci.*, 1970, **14**, 1449.
50. D. M. Bigg, *Polym. Compos.*, 1986, **7**, 125.
51. D. Hansen and G. A. Bernier, *Polym. Eng. Sci.*, 1972, **12**, 204.
52. Y. Xu, D. D. L. Chung and C. Mroz, *Composites, Part A*, 2001, **32**, 1749.
53. G. Kalaprasad, P. Pradeep, G. Mathew, C. Pavithran and S. Thomas, *Compos. Sci. Technol.*, 2000, **60**, 2967.
54. A. S. Luyt, J. A. Molefi and H. Krump, *Polym. Degrad. Stab.*, 2006, **91**, 1629.
55. M. Pardavi-Horvath, *J. Magn. Magn. Mater*, 2000, **315**, 171.

CHAPTER 12

Micro and Nano Zinc Oxide Filled NR Composites

SHAJI P. THOMAS*[a] AND E. J. MATHEW[b]

[a] Postgraduate Department of Chemistry, B. A. M. College, Thuruthicad, Kerala, India; [b] Retired Head of Department of Chemistry, S. B. College, Changanacherry, Kerala, India
*Email: shajiparel@gmail.com

12.1 Introduction

Natural rubber (NR) is a high molecular weight polymer of isoprene (2-methyl-1,3-butadiene). The high tensile properties of NR make it an industrially important substance. However, its initial modulus and durability are low and an additional reinforcement is required for practical applications.

Zinc oxide (ZnO) is a widely used chemical in the rubber industry owing to its excellent property which enables it to act as activator during sulfur vulcanization. The tire industry remains the largest single market for ZnO, consuming more than half of the total worldwide demand of 1.20×10^6 tonnes.[1] Traditionally, ZnO is used in rubber compounds in dosages of 3–8 parts per hundred parts of rubber (phr). Heavy-duty pneumatic tyres carry high loadings of ZnO for heat conductivity as well as reinforcement, since heat build-up is critical at their higher operating speeds compared with their solid rubber counterparts.

In spite of its superior characteristics, there is more concern about the environmental effects of higher dosages of ZnO. Different techniques have been taken into consideration for reducing ZnO levels. Among all the approaches, the use of nano-sized ZnO particles with high surface area proves to be the

RSC Polymer Chemistry Series No. 8
Natural Rubber Materials, Volume 2: Composites and Nanocomposites
Edited by Sabu Thomas, Hanna J. Maria, Jithin Joy, Chin Han Chan and Laly A. Pothen

Published by the Royal Society of Chemistry, www.rsc.org

significant and promising one. A number of studies comparing different metal oxides as vulcanization activators, in order to find out substitutes for ZnO, are available. Metals oxides like that of Mg, Cu, Pb, Ni, Ca, *etc*. have been tried by researchers and found that the oxide of Mg was most promising candidate, since it is a non-heavy metal oxide that helps the breakdown of the accelerator to be faster than when ZnO is used and it is able to form active sulfonating agents. But the crosslink level achieved when MgO was used during rubber vulcanization is lower than that obtained with ZnO, making a limitation on its industrial application. Active researches are going on to synthesize variously modified nano-ZnOs to serve as potential ingredient in rubber vulcanization. In this chapter, a summary of methods of synthesis and characterization variously modified nano-ZnO is included. Additionally, a comparative discussion on the various physico-mechanical properties of micro and nano-ZnO filled NR composites is also presented.

12.2 General Functions of ZnO in Rubber Vulcanization

- As an activator
- As a filler
- As a processing aid

In the curing process of natural and most types of synthetic rubbers, the chemical reactivity of ZnO enables it to accelerate the activity of organic accelerators. The high activity of ZnO can be explained on the basis of its ability to form complex with accelerators (zinc being a d-block element can easily form complex). ZnO reacts with stearic acid forming rubber hydrocarbon soluble zinc stearate and liberates water prior to the onset of crosslinking.[2] Furthermore, ZnO is a precursor of zinc-derived accelerators.[3] It also solubilizes insoluble accelerators to form the actual catalyst. Complex formation of the zinc ion with different accelerators is critical for efficient curing.[4] The Zn^{2+} ion functions as a Lewis acid in the complex formation and the cleaved accelerator as a Lewis base. The basicity of a metal ion is dependent on its size and the charge, according to Equation (12.1):[5]

$$\textit{cation acidity} = \frac{kz^2}{r} \tag{12.1}$$

where k is a constant, z is the charge and r is the radius of the cation.

Molecules of accelerators, sulfur and fatty acids diffuse through the rubber matrix and are adsorbed on to the ZnO surface with the formation of intermediate complexes. Nieuwenhuizen[3] proposed a mechanism in which the ZnO surface functions both as a reactant and as a catalytic reaction template, activating and bringing together the reactants. The unreacted portion of the ZnO remains available as a basic reserve to neutralize the sulfur-bearing acidic decomposition products formed during vulcanization. Sufficient quantity of ZnO contributes markedly to chemical reinforcement, scorch control, and resistance to heat ageing and compression fatigue. ZnO acts as a heat sink, which accepts

frictional energy without a large increase in internal temperature.[6] In the bonding of rubber to brass, ZnO reacts with copper oxide on the brass surface to form a tightly adhering zinc-copper salt. Duchacek[7] found that increasing the ZnO concentration increased the rate and extent of crosslinking up to a certain concentration of ZnO, which is believed to be the minimum level of ZnO needed for complete conversion of accelerator to the zinc–accelerator–sulfur complex. It was also noted that the optimum ZnO content to minimize reversion was slightly greater than this minimum. Coran[8] also showed that the induction time had a dependence on the ZnO concentration. The efficiency of ZnO during vulcanization can be enhanced by the maximizing the contact between the ZnO particles and the accelerators in the compound. This particle–particle contact is dependent on the size of the particle, their shape and the specific surface area. The main parameter that determines activity of ZnO is its specific surface, which is affected by different factors, among which particle size is more significant. The conventional ZnO has average particle size 0.6 μm approximately with 6 m^2/g of specific surface, while nano-ZnO particles have a specific surface equal to 30–70 m^2/g, which causes higher activity in comparison to conventional ZnO.

12.3 Additional Advantages of ZnO

12.3.1 Biochemical Activity

ZnO is useful in the preservation of plantation latex as it reacts with the enzyme responsible for the decomposition. The oxide is also a fungi stat, inhibiting the growth of such fungi as mould and mildew.

12.3.2 Dielectric Strength

ZnO improves the resistance to corona effects by virtue of its dielectric strength. In high-voltage wire and cable insulation and at elevated operating temperatures it contributes to the maintenance of the physical properties of the rubber compound by neutralization of acidic decomposition product.

12.3.3 Light Stabilization

ZnO is outstanding among the white pigments and extenders for its absorption of ultraviolet rays. Thus, it serves as an effective stabilizer of white and tinted rubber compounds under prolonged exposure to the destructive rays of the sun.

12.3.4 Pigmentation

Through its high brightness, refractive index, and optimum particle size, ZnO provides a high degree of whiteness and tinting strength for such rubber products as tire sidewalls, sheeting and surgical gloves.

12.3.5 Heat Stabilization

ZnO imparts thermal stability thereby retarding devulcanization of many types of rubber compounds operating at elevated temperatures.

12.3.6 Latex Gelation

ZnO is especially effective in gelation of the latex foam with sufficient stability making it to be useful in the production of latex foam rubber products.

12.3.7 Reinforcement

ZnO provides reinforcement in NR, and in some synthetic elastomers such as polysulfide and chloroprene rubbers. The degree of reinforcement seems to depend upon factors like the particle size of the oxide (the finest size being the most effective), the reactivity of the oxide with the rubber *etc*.

Under such service condition involving rapid flexing or compression, ZnO also provides heat conduction to more rapidly dissipate the heat and thereby provides lower operating temperatures. Additionally, it imparts heat stabilization by reacting with acidic decomposition products.

12.3.8 Rubber–Metal Bonding

In the adhesive mechanism of rubber to metal surface, ZnO plays an important role. In the bonding of rubber to brass, ZnO reacts with copper oxide on the brass surface to form a tightly adhering zinc–copper salt.

12.3.9 Tack Retention

One of the unique properties of ZnO is its ability to retain the tack of uncured rubber compounds over many months of shelf–storage for adhesive tapes.

12.3.10 Application of ZnO in the Plastics Industry

Zinc compounds have the ability to provide a variety of properties in the plastics field. ZnO is efficient in imparting heat resistance and mechanical strength to acrylic composites. It is also known to be efficient in contributing to the curing of epoxy resins. Epoxy resins cured with aliphatic polyamines acquire higher tensile strength and water resistance when ZnO is also added during the curing process. ZnO imparts fire resistance to nylon fibres and mouldings. The presence of ZnO during the formation of polyesters imparts higher viscosity and strength. It reacts with unsaturated polyesters to form higher viscosity and a thixotropic body. The dyeability of polyester fibres is improved by the presence of ZnO particles. ZnO mixtures stabilize polyethylene against ageing and ultraviolet radiation. It increases the transparency of poly(chlorofluoroethylene) moulding resin. The presence of ZnO in polyolefins has proved to improve the colour, tensile strength and vulcanization properties.

Thermal stability of PVC is found improved by adding ZnO during its manufacture. The antistatic, fungi static and emulsion stability of vinyl polymers are also improved by the addition of ZnO. ZnO-stabilized polypropylene and high-density polyethylene are used in the production of safety helmets, insulation, pallets, bags and filaments, and also agricultural and recreational equipment.

12.4 Advantages of Nano-ZnO over Micro-ZnO

The International Programme on Chemical Safety (IPCS) under the auspices of the World Health Organization (WHO) constituted a Task Force on Zinc to establish Environmental Health Criteria for zinc. The Task Force states: ''Zinc is an essential element in the environment. The possibility exists for both a deficiency and excess of this metal. For this reason it is important that regulatory criteria for zinc, while protecting against toxicity, are not set as low as to drive zinc levels into the deficiency area.''[9]

The task of effective control of the performance of ZnO activator with respect to processing and final properties of rubbers, is important both for environmental and economic reasons. One of the strategies for achieving the goal of reducing the dosage of zinc is by developing and using nanomodified ZnO. The efficiency of ZnO during vulcanization is dependent up on the contact between the ZnO particles and the accelerators in the compound. This contact is again dependent on the size of the particle, their shape and the specific surface area, and these factors are most favourable in nanomodified ZnOs. The major difference between nano- and micro-ZnOs is the level of opacity. ZnO particles that are bigger than 150 nm are used as a white pigment in paints and cosmetics. This whitening effect vanishes when the particles size is smaller than 100 nm creating an invisible but highly effective broad spectrum UV barrier. Therefore, nano-ZnO is advantageously used in:

- sunscreens and sunblock
- lipstick
- antibacterial lotions
- rubber emulsions
- UV stabilizer in plastics
- as a catalyst in the chemical industry

Also, nanomodified ZnO is found to improve photocatalytic properties compared to micro-sized ZnO. Sebastian *et al.*[10] showed that the intensity of blue colour of methylene blue dye reduced at a faster rate in presence of nano-ZnO due to the enhanced rate of photo decomposition of the dye.

ZnO nanoparticles are found excellent in imparting higher durability to treated fabrics due to the large surface area and surface energy possessed by the nanoparticles compared to the micro counterparts.[11] The higher surface to volume ratio of the nanoparticles enhances their ability to block UV rays and offer better affinity to fabrics. Thus by virtue of peculiar properties of

nano-ZnO, it has a wide range of applications like that in electronic, optoelectronic, electrochemical, and electromechanical devices.[12–17]

12.5 Strategies for Synthesizing Micro and Nano-ZnO

12.5.1 Synthesis of Micro-ZnO

French Process

The metallic zinc is melted, evaporated and the vapours are oxidized with air to get ZnO after purifying the zinc by evaporation and condensation. The size and shape of the ZnO crystals can be controlled by the oxidation conditions. After combustion, the ZnO is precipitated from the ZnO/air mixture in settling chambers, in which classification of the ZnO particles takes place according to their size.

American Process

The roasted zinc ores and zinc hydroxides or carbonate obtained from the scrap are reduced with coal and directly re-oxidized to ZnO in the same reaction chamber. The purity of the ZnO is normally a little inferior to that obtained from the 'French' process. Grades of various purities can be produced by fractionation.

Wet Chemical Process

Zinc is precipitated from purified zinc salt solutions as hydroxide, or basic carbonate, which is washed, filtered and dried. The resulting compound is subsequently calcined. By varying the precipitation and calcination conditions, different grades of ZnOs are prepared. At low calcination temperatures transparent ZnO, which is actually the basic carbonate, is obtained. ZnOs produced by wet chemical methods are particularly pure, since very pure zinc salt solutions can be obtained.

12.5.2 Synthesis of Surface-Modified Micro-ZnO

Ganjeli *et al.*[18] prepared surface-modified micro-ZnO by preparing an aqueous suspension of 25 g of micro-ZnO in 100 ml of water followed by ultrasonication, and addition of solution of 1.25 g polyethylene glycol (PEG) in 100 ml water. The mixture was stirred for 24 h and centrifuged for removing unreacted PEG. The product was dried at 120 °C. The surface modification was confirmed by SEM and IR analysis. The peak around 1110 cm^{-1} was due to C–O stretching, the peaks in the region 2800–3000 cm^{-1} were due to C–H stretching and the broad peak in the region 3200–3600 cm^{-1} was due to O–H stretching. The TEM images (Figure 12.1)[18] show that surface-modified ZnO particles are not aggregated as the unmodified ZnO. Surface modification was also done using polypropylene glycol (PPG) also, but less efficient than PEG due to larger size of PPG.

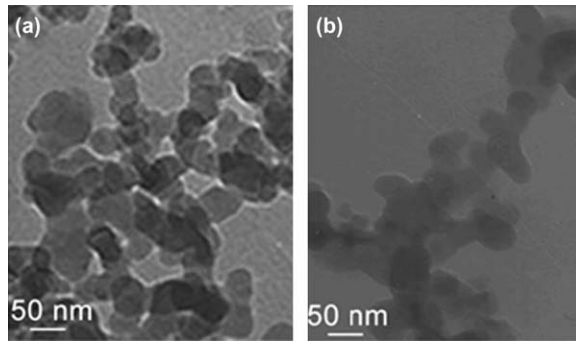

Figure 12.1 (a) TEM image of unmodified ZnO (b) TEM image of modified ZnO. [Reused with permission from *J. Appl. Polym. Sci.*, 2011, **122**, 249.]

12.5.3 Synthesis of Nano-ZnO

One-dimensional (1D) ZnO nanostructures have been synthesized by various techniques, such as solution method, physical vapour deposition, metal–organic chemical vapour deposition (MOCVD)], molecular beam epitaxy (MBE), pulsed laser deposition, sputtering, flux methods, electrospinning, *etc.*[19–29] Among these, physical vapour deposition and flux methods usually require high temperature and catalysts and there is chance of impurities getting incorporated into the ZnO nanostructures. Therefore, they are less apt to be able to integrate with flexible organic substrates for future foldable and portable electronics. MOCVD and MBE methods can yield superior quality ZnO nanowire arrays. But the factors like low sample uniformity, low product yield, limited choices of substrate and high cost put a limitation on the application of these methods on a wider range. Pulsed laser deposition, sputtering and top-down approaches have less controllability and repeatability compared with other techniques. Electrospinning gives polycrystalline fibres. Compared to other methods, solution methods appear to be attractive and promising owing to low cost, less hazards, and the high ease of scaling up.[30,31] In these methods growth of nanoparticles occurs at a relatively low temperature without the involvement of metal catalysts, making the particles compatible with flexible organic substrates and thus it can be integrated with well-developed silicon technologies.

Several researchers have synthesized ZnO nanostructures by using various chemical precursors and different processing methods such as the preparation of ZnO nanostructures on SiO_2-buffered Si substrates.[32] Variation in pH value of the solution was effected to synthesize rod and platelet using the sol–gel method. Pal *et al.*[33] presented the synthesis of various types of ZnO nanostructures by using ethylenediamine, zinc acetate dihydrate, sodium hydroxide and water at two different pH values by the hydrothermal method. Bai *et al.*[34] reported the rose like ZnO nanostructures by using $ZnCl_2$ and ammonia (25%) synthesized through a hydrothermal decomposition method on a copper plate substrate. Rizwan *et al.*[35] prepared nano-ZnOs with

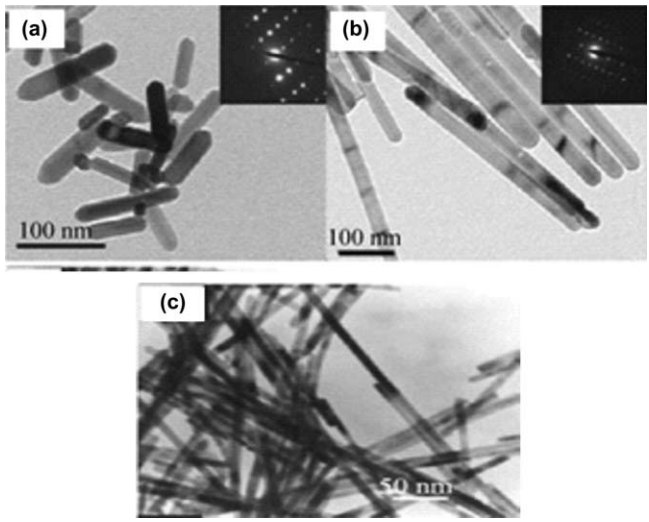

Figure 12.2 ZnO nanostructures formed in different solvents: (a) methanol, (b) ethanol, (c) butanol.
[Reused with permission from *J. Am. Chem. Soc.*, 2003, **125**, 4430.]

different morphologies using zinc nitrate hexahydrate, NaOH and hydroxyl amine hydrochloride. The microscopic images of the different nanostructures are given in Figure 12.2. Heideman *et al.* synthesized modified nano-ZnO using glycerol.[36]

An alkaline solution is required for the formation of ZnO nanostructures because normally divalent metal ions do not undergo hydrolysis in acidic environments.[37] KOH is preferred to NaOH because of the chance of incorporation of K^+ into ZnO lattice is minimized by virtue of its larger size. Generally, the solubility of ZnO in an alkali solution increases with the alkali concentration and temperature. The main reactions involved in the growth mechanism are given in the following equations:[38–40]

$$Zn^{2+} + 2OH^- \longleftrightarrow Zn(OH)_2 \quad (1)$$

$$Zn(OH)_2 + 2OH^- \longleftrightarrow [Zn(OH)_4]^{2-} \quad (2)$$

$$[Zn(OH)_4]^{2-} \longleftrightarrow ZnO_2^{2-} + 2H_2O \quad (3)$$

$$ZnO_2^{2-} + H_2O \longleftrightarrow ZnO + 2OH^- \quad (4)$$

$$ZnO + OH^- \longleftrightarrow ZnOOH^- \quad (5)$$

Because the O^{2-} required for the formation of ZnO is not taken from water, organic solvents, such as methanol, ethanol, butanol or even ionic liquids can be used.[41–43] Since the growth of polar inorganic nanocrystals is sensitive to the reaction solvents, their morphologies can be tuned and controlled by the

crystal–solvent interfacial interactions.[44] The aspect ratio of the ZnO nanostructures increases on going from the more polar solvent methanol to the less polar solvent 1-butanol.[45] The morphologies of ZnO nanostructures formed in different solvents are shown in Figure 12.2.

One of the most commonly used hydrothermal methods reported in literature is using zinc salt and aqueous solution of hexamethylenetetramine (HMTA).[46] Here O^{2-} is thought to be provided by water and HMTA acts as bidentate ligand for Zn^{2+}.[47,48]

12.5.3.1 Seeded Growth

One of the key advantages of wet chemical methods is that, using ZnO seeds in the form of thin films or nanoparticles, ZnO nanowires can be grown on arbitrary substrates.[49–51] Green *et al.*[50] demonstrated that ZnO nanocrystal seeds prepared by thermal decomposition of a zinc acetate precursor could give vertically well-aligned ZnO nanowire arrays as shown in the SEM (Figure 12.3).[51]

12.5.3.2 Electrodeposition

Electrochemical deposition is a very powerful technique for producing uniform and large area ZnO nanostructures since it exerts a strong external driving force to help the reactions take place, even if they are non-spontaneous.[52,53] Konenkamp *et al.* used mixed solution of zinc chloride and potassium chloride to grow vertically aligned ZnO–nanowire arrays on a SnO_2 glass substrate, as shown in Figure 12.4.[54]

12.5.3.3 Templated Growth

ZnO nanowires can be synthesized by electrodeposition method using suitable templates. AAO is found the most widely used template owing to the ease of

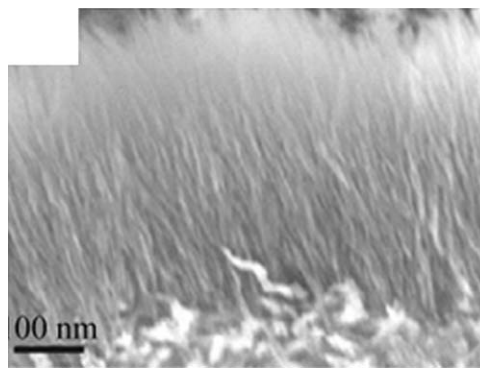

Figure 12.3 Cross-section SEM image of ultrathin ZnO nanofibres grown on a Zn metal substrate.
[Reused with permission from *Small*, 2006, **2**, 612.]

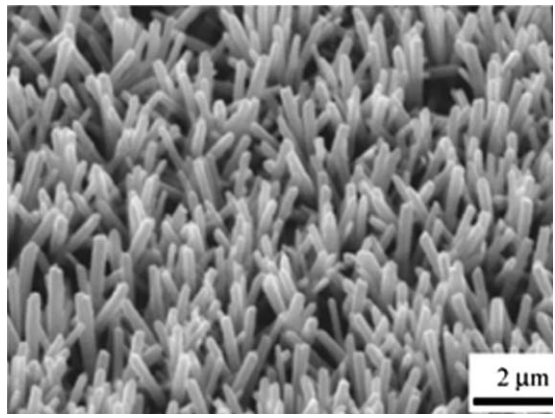

Figure 12.4 SEM image of ZnO nanowires formed on a SnO_2 substrate by electrodeposition.
[Reused with permission from *Appl. Phys. Lett.*, 2000, **77**, 2575.]

fabrication.[55] The template is attached to the surface of a flat or curved, flexible or rigid substrate.

12.5.3.4 Epitaxial Growth

Epitaxial growth is also considered to involve a heterogeneous nucleation and growth process. The energy gain from satisfying the interfacial dangling bonds provide the driving force for the epitaxial growth. Different substrates have different isoelectric points. So, positive or negative charge polarities is considered as appropriate at different reaction pH values for an epitaxial substrate.[56]

12.5.3.5 Capped Growth

Capping agents can be added in the solution to modify the growth habits of the ZnO nanostructures.[28] Commonly used capping agents for hydrothermal growth of ZnO nanostructures are of two types; those that adsorb onto the side surfaces and enhance the vertical growth, such as amines like polyethylenimine (PEI), ethylenediamine and those that cap onto the basal plane of the ZnO nanostructures and promote lateral growth, such as Cl^- and citrate ions.[57–60]

12.5.4 Synthesis of Surface-Modified Nano-ZnO

With a view to modify the hydrophilic surface of ZnO to hydrophobic surface so as to improve the dispersion of the particles in the nonpolar polymer like NR matrix and also to reduce the agglomeration of the nanoparticles of ZnO, Taghvaei-Ganjeli *et al.*[18] modified the surface of nano-ZnO by treating its aqueous suspension with PEG and PPG as discussed in Section 12.5.2. He

showed that the surface area of the nanoparticles was enhanced from 39.7 to 46.52 m^2/g by surface modification using PEG. The authors[61] have also synthesized stearic acid-coated, and accelerator BIAT-capped nano-ZnO using zinc acetate and NaOH in 2-propanol–DCM–water ternary solution.

12.6 Characterization of Micro and Nano-ZnO

12.6.1 X-Ray Diffraction

The primary tool for the nanostructure determination is the use of XRD techniques. Faal *et al.*[62] determined the particle size of the nano-ZnO prepared by microwave irradiation of the solution containing zinc acetate and triethanolamine (TEA) from XRD patterns (Figure 12.5) using Scherrer formula. The lattice strain and crystalline size was calculated using Equation (12.2):

$$\frac{\beta \cdot \cos\theta}{\lambda} = \frac{1}{\varepsilon} + \frac{\tau \cdot \sin\theta}{\lambda} \tag{12.2}$$

where β is the measured FWHM (full width at half maximum), θ the Bragg angle of the peak, λ is the wavelength of X-ray used, ε is the effective particle size and τ the strain. The average particle size was obtained (as 35 nm) from the intercept of the plot (Figure 12.5). The XRD pattern was identical to the hexagonal phase with wurtzite structure with unit cell parameters $a = b = 3.248$ Å and $c = 5.2$ Å.

Liu *et al.*[63] investigated the crystalline structure of ZnO nanowires and nanorods using XRD (Figure 12.6). The easy growth axis of one-dimensional

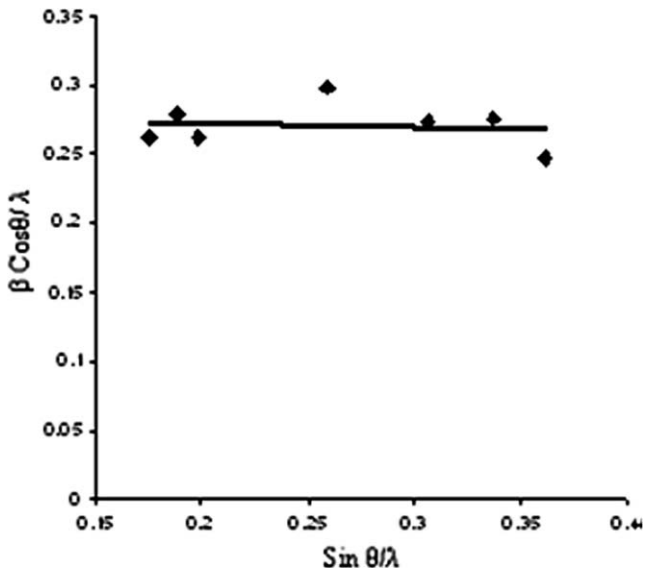

Figure 12.5 βcos θ/λ *vs.* sin θ/λ for ZnO nanocrystals.
[Reused with permission from *J. Sci., Islamic Repub. Iran*, 2006, **17**, 231.]

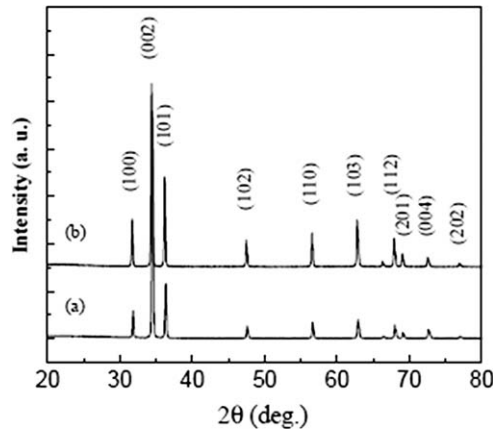

Figure 12.6 XRD of (a) ZnO nanowires, (b) ZnO nanorods.
[Reused with permission from Elsevier, *J. Cryst. Growth*, 2005, **274**, 126.]

ZnO nanomaterials is [0 0 0 1] and as the alignment of ZnO arrays improves, the diffraction peaks other than (0 0 0 1) begin to vanish.[64] From Figure 12.6, one can infer that the diffraction peaks other than (0 0 0 1) of ZnO nanowires show higher relative intensity than those of the ZnO nanorods, indicating that the alignment of the nanorods is better than that of nanowires. According to the standard XRD pattern, both the ZnO nanowires and the ZnO nanorods have wurtzite structure.

Rizwan Wahab *et al.*[35] determined crystallinity and crystal phases of the ZnO nanostructures synthesized at different pH. All the diffraction peaks were indexed as the hexagonal ZnO with lattice constants $a = 0{:}3249$ and $c = 0{:}5206$ nm. Additionally, higher intensity and narrower spectral width of ZnO peaks in the spectrum proved that the obtained products have good crystallinity. In another study Singh *et al.* also determined the particle size of nano-ZnO (synthesized by controlling the flow of nascent oxygen) from XRD peaks.[65] Their result is also in the range of the earlier results.

12.6.2 FTIR Spectroscopy and Electron Microscopy

The FTIR spectrum of the particles enables one to get a primary structure of the compound synthesized. Wahab *et al.*[35] conducted compositional analysis of as grown ZnO nanostructures at different pH (6–12) by FTIR measurement at room temperature in the range of 4000–400 cm^{-1} (Figure 12.7). The band at 3200–3600 cm^{-1} corresponds to O–H stretching vibration. The position of the peak changes from sharp (pH = 6) to broad peak at (pH = 12), indicating that in acidic condition (at pH = 6) grown sheets were undeveloped, as evident from the FESEM images (Figure 12.8). But as the pH changes to basic, the structures change into micro flowers. The strong bands at 1566–1547 cm^{-1} is assigned to asymmetric stretching vibration of C=O. As the pH was increased, the C=O

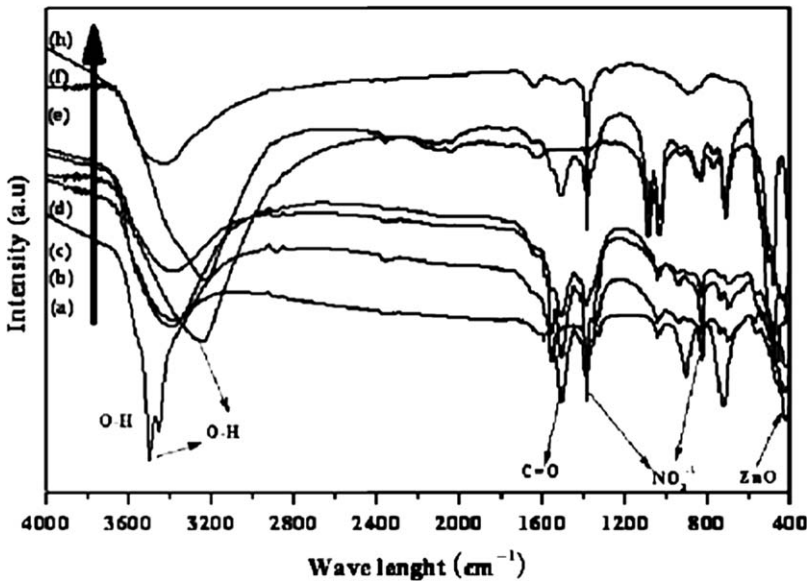

Figure 12.7 FTIR spectra of grown ZnO nanostructures under different pH conditions (pH 6–12) (a) to (h).
[Reused with permission from *Mater. Trans.*, 2009, **50**, 2092, Japan Institute of Metals.]

peak was also shifted to up and down due to the morphological changes. The standard peak of ZnO nanostructures appeared in the range 475–424 cm^{-1}. As the solution pH increases the vibration band of ZnO decreases from 475 to 424 cm^{-1}. This change indicates the changes in morphology of ZnO, as seen in the FESEM (Figure 12.8).

Faal *et al.*[62] also analysed ZnO nanostructures using IR spectrum .They observed broad band with very low intensity at 3493 cm^{-1} corresponding to the O–H stretching vibration indicating the presence of small amount of water adsorbed onto the ZnO nanocrystal surface. The band at 1628 cm^{-1} is due to O–H bending. A strong band at 500 cm^{-1} is attributed to Zn–O stretching. The TEM image (Figure 12.9) reveals that the product consists of spherical particles with the average size of 35–45 nm.

12.6.3 Optical Studies

Lieu *et al.* investigated the optical properties of nano-ZnOs.[63] The PL spectra of ZnO nanowires and nanorods are given in Figure 12.10. The absorption peak at 381.2 nm in the case of nanowires gets shifted to lower frequency for nanorods. This is attributed to the intensive tensile strain in the nanorods having more diameter than the nanowires.[66]

Wahab *et al.*[35] also studied the optical properties of nanostructured ZnO synthesized at different pH values. They observed broad peak (Figure 12.11) in

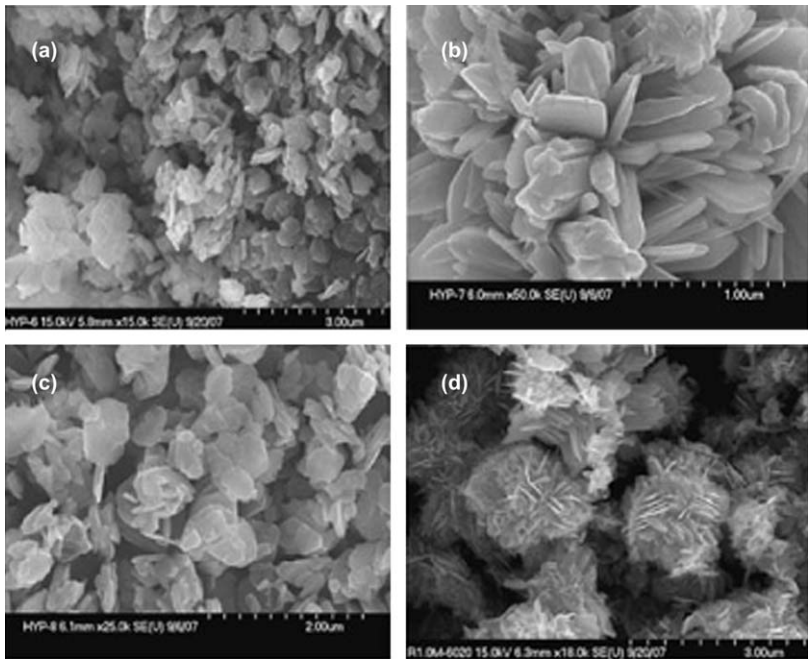

Figure 12.8 FESEM images of spherical disk-like grown ZnO nanostructures (a) at pH 6, (b) at pH 7, (c) at pH 8, (d) at pH 9.
[Reused with permission from *Mater. Trans.*, 2009, **50**, 2092, Japan Institute of Metals].

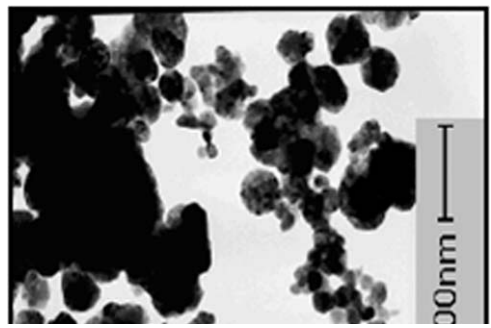

Figure 12.9 TEM image of ZnO nanocrystals produced by microwave irradiation.
[Reused with permission from *J. Sci. Islamic Repub. Iran*, 2006, **17**, 231.]

362–375 nm range for the ZnO synthesized at different pH values. This peak is a direct evidence for the wurzite hexagonal phase.[67,68]

From the PL spectra of the nanomaterials, it is clear that the intensity of the green emission (492.8 nm) decreases while the UV emission increases from nanowire to nanorod. The higher intensity of the green luminescence indicates more oxygen vacancies, and hence the observed decrease of the green emission

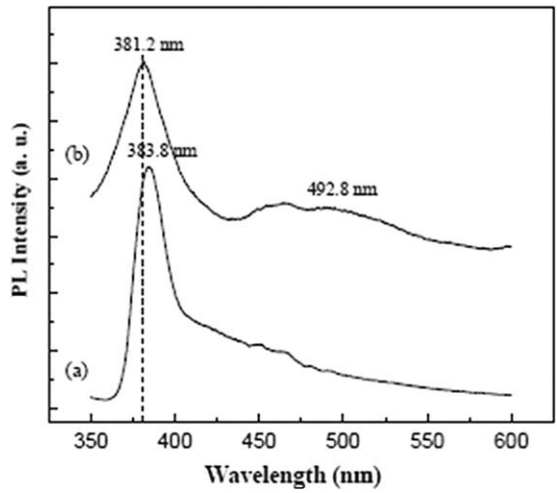

Figure 12.10 PL spectra of (a) ZnO nanorods, (b) ZnO nanowires.
[Reused with kind permission from Elsevier, *J. Cryst. Growth*, 2005, **274**, 126.]

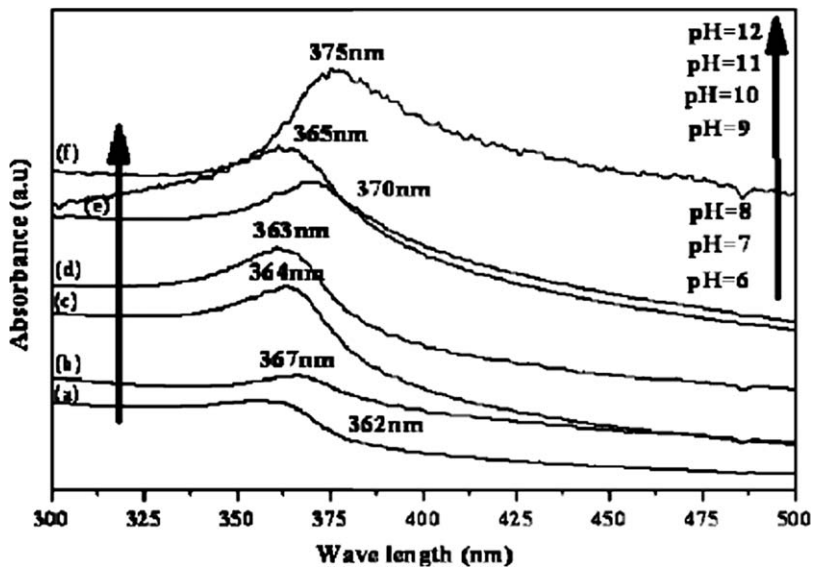

Figure 12.11 UV-vis spectra of ZnO nanostructures produced under different pH conditions (pH 6 to 12).
[Reused with permission from *Mater. Trans.*, 2009, **50**, 2092, Japan Institute of Metals.]

relative to the UV emission shows that the ZnO nanorods have higher crystallization and less oxygen vacancy concentrations than the ZnO nanowires. Thus the optical property of the ZnO nanostructures can be tuned to the

requirements by controlling the morphology, paving for their applications in nanolaser technology.

Zhang *et al*. also investigated the optical properties of ZnO nanostructures dispersed in ethanol.[68] The band at 375 nm corresponds to ZnO nanoparticles. Compared with bulk ZnO, the blue shift observed in the ZnO nanostructures, is due to size effect. This band is also attributed to the band gap of semiconductor ZnO nanoparticles.

12.7 Studies of NR Composites Containing Micro and Nano-ZnO

Taghvaei-Ganjeli[18] prepared NR/SBR (75:25) compounds containing 50 phr carbon black (CB), 10 phr oil, 0.75 phr N-cyclohexyl benzothiazyl sulfenamide (CBS), 1.5 phr PPD, 1.5 phr S, 1 phr TMQ, 2 phr stearic acid, 2 phr unmodified nano-ZnO and the dosage of PEG-modified nano-ZnO and investigated its cure and other technological properties and compared with that of the rubber compound containing 2 phr unmodified and modified micro-ZnO. They observed that optimum cure time t_{90} was increased by nano-ZnO compared to micro form, which was attributed to agglomeration of nanoparticles causing delay in formation and disappearance of crosslink precursors. But t_{90} was reduced by surface modification due to the enhancement of its activity by virtue of the acquired hydrophobicity which could increase the rubber–activator interaction. Cure rate index (CRI) also enhanced when modified ZnOs were used indicating faster curing. PEG-modified ZnO and nano-ZnO constituted faster curing systems due to the finer dispersion and less number of agglomerates resulting faster zinc ion release for the zinc–accelerator complex.

Modified ZnO filled rubber compounds showed minimum abrasion loss (118 cm^3), compared to that containing unmodified ZnO (170 cm^3) due to efficient dispersion in the rubber matrix. Fatigue was increased by the use of nano-ZnO (>300 KC) and also by the surface modification. There was no track on the dumbbells up to 300 KC. Tensile strength was enhanced by the use of surface-modified micro- and nano-ZnO, compared to the unmodified ZnO (18 MPa for surface-modified micro-ZnO against 9 MPa for unmodified micro form). 300% modulus was increased from 2.8 to 7.4 MPa by surface modification of micro-ZnO, and from 4.9 to 5.3 MPa by surface modification of nano-ZnO. Due to the increase in tensile strength, elongation at break % decreased on surface modification. All these observations can be attributed to the improvement in dispersion of ZnOs by the incorporation PEG on the ZnO surface, which could increase adhesion of ZnO to the rubber matrix. The finer, uniform and efficient dispersion of the surface-modified micro and nano forms of ZnO in the rubber matrix is evident from the SEM images (Figure 12.12.a–d). Large number of agglomerates is seen in the SEM image of the rubber composite containing unmodified micro-ZnO (Figure 12.12(a)). The surface modification reduces agglomeration tendency by decreasing the surface energy of the ZnO particles. Agglomerates are rarely present in the

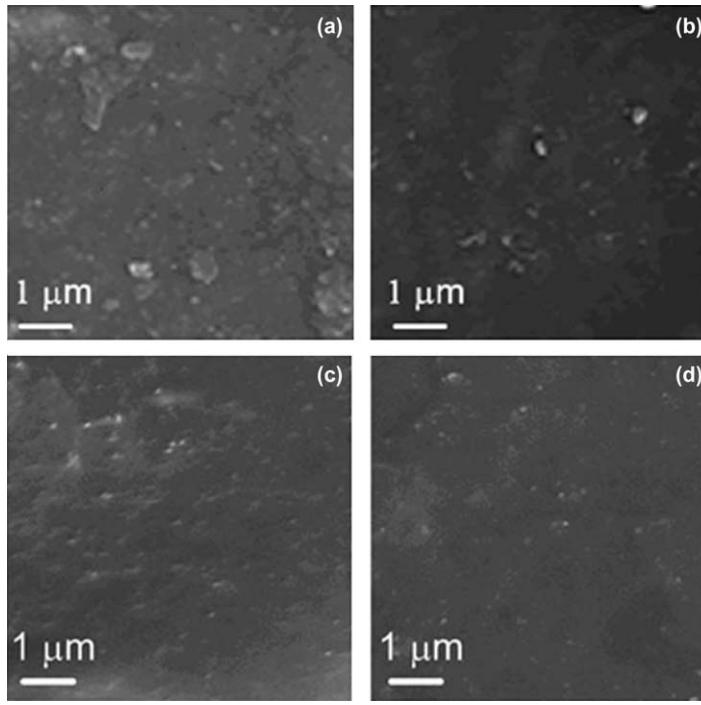

Figure 12.12 SEM images of NR composites containing (a) unmodified micro ZnO, (b) surface modified micro ZnO, (c) nano ZnO (d) modified nano ZnO. [Reused with permission from *J. Appl. Polym. Sci.*, 2011, **122**, 249.]

SEM image of the composite containing surface-modified nano-ZnO (Figure 12.12(d)).

Oneagoro[69] conducted studies on the effect of concentration of micro-ZnO on the technological properties of NR composites. He prepared NR compounds taking 100/100 NR and NBR, 2 phr stearic acid,4 phr wax, 0.5 phr of MBT, 1 phr of TMTD, 55 phr of CB, 3 phr of sulfur and varying amounts of micro-ZnO starting from 2 to 8 phr of ZnO. They observed that tensile strength and modulus of elasticity increased with the dosage of ZnO up to 5 phr due to increase in crosslink density. Further increase in the dosage of ZnO reduced the tensile strength and modulus due to the over cure. Compression set showed an increasing trend with increase in the dosage of ZnO due to the reduction in chain mobility which is again attributed to the increase in crosslink density. Hardness and abrasion resistance increased with increase in dosage of ZnO up to 5 phr due to the increase in crosslink density. Further increase of ZnO addition caused reversion and hence abrasion resistance also decreased beyond 5 phr of ZnO.

In another study,[70] it was reported that NR gum and CB filled compounds containing nano-ZnO have been prepared on a laboratory size two-roll mixing mill at a friction ratio of 1 : 1.25 as per ASTM D 3184-89 and the samples were

vulcanized at 150 °C, up to the optimum cure time (previously determined on Rubber Process Analyzer, RPA 2000, Alpha technologies, USA, as per ASTM D 2084-01). The various technological properties were determined as per ASTM standards. The rubber formulations, the cure properties and other technological properties are given in Tables 12.1, 12.2 and 12.3, respectively.

The investigators observed superior cure properties for the nano-ZnO filled NR compounds, compared with the micro-ZnO-filled samples. The mix containing 2 phr of nano-ZnO (prepared by the investigators by sol–gel process) N_2

Table 12.1 NR formulations containing micro/nano ZnO.[70]

	Rubber compound no.			
Ingredients (phr)	N_1	N_2	N_3	N_4
NR	100	100	100	100
Micro-ZnO	0	2	0	2
Nano-ZnO	2	0	2	0
Stearic acid	2	2	2	2
HAF	0	0	40	40
Aromatic oil	0	0	8	8
HS	1	1	1	1
CBS	0.6	0.6	0.6	0.6
TMTD	0.1	0.1	0.1	0.1
S	2.5	2.5	2.5	2.5

Table 12.2 Cure properties of NR formulations containing micro-/nano-ZnO.[70]

	Rubber compound no.			
Cure properties	N_1	N_2	N_3	N_4
Minimum torque (M_L) dNm	0.03	0.04	0.06	0.02
Maximum torque (M_H) dNM	2.79	2.44	6.19	4.01
Scorch time (ts_2) min	5.74	4.33	2.56	2.44
Optimum cure time (t_{90}) min	7.79	7.27	4.48	5.46
Cure rate index (CRI)	48.78	34.01	52.08	33.11

Table 12.3 Mechanical properties of NR formulations containing micro-/nano-ZnO.[70]

	Rubber compound no.			
Cure properties	N_1	N_2	N_3	N_4
Tensile strength (MPa)	22.94	20.80	32.26	26.03
300% modulus (MPa)	1.46	1.04	7.76	4.75
Elongation at break (%)	1591	1899	826	946
Tear strength (N/mm)	40	33	107	80
Hardness (Shore A)	45	40	66	53
Compression set (%)	41.05	49.25	40.15	46.92
Abrasion loss (cm^3)	4.75	5.80	3.50	4.54

exhibited higher delta torque value (by 11.3%) compared with the corresponding mix containing micro-ZnO (N_4). Optimum cure time (t_{90}) for the nanocomposite was almost comparable with that of the micro counterpart (7.79 min for nano and 7.27 min for microcomposite). Scorch safety (ts_2) was 32.6% higher for the nanocomposite. The NR nanocomposite exhibited 43% more CRI ($(100/t_{90} - ts_2)$, indicating improved activation of the cure process. The improvement of the cure properties of the nanocomposites is a direct evidence of the superior power of nano-ZnO in the vulcanization of NR when compared with micro-ZnO. The superior and efficient action of nano-ZnO in cure process compared to micro form is due to the smaller particle size and the resultant larger specific surface area available to the accelerator particles for its faster action. Also, the increased surface area enhanced the rubber–particle interaction.[70,71]

The investigators also reported that the mix containing 2 phr of nano-ZnO exhibited enhanced tensile strength (10% more) compared to the mix containing micro-ZnO (Table 12.3). The enhancement of tensile strength was attributed to the increase in crosslink density. Similarly, 300% modulus (tensile modulus at 300% elongation) was also higher for the nanocomposite by 40%. The increased stiffness of the nanocomposite resulted lower elongation at break. The nanocomposites also exhibited improved tear strength (21% increase). Hardness of the nanocomposite increased by 12.5% compared to the microcomposite.

The CB filled composites containing nano-ZnO also showed improved technological properties (Tables 12.2 and 12.3). The filled mix containing 2 phr of nano-ZnO (N_6) was superior in delta torque, scorch safety and optimum cure time, compared to the filled mix N_8 containing 2 phr of conventional micro-ZnO. The nanocomposite showed 53.6% increase in delta torque value (6.13 against 3.99 dNm). About 5% increase was observed for scorch safety and 18% decrease for optimum cure time of the nanocomposite. Similarly, the investigators observed improved mechanical properties for the filled mix N_6 containing 2 phr of nano-ZnO. About 24% increase was observed in tensile strength and about 63% increase in 300% modulus for the nanocomposite N_6 when compared with the microcomposite N_8. This is also attributed to the combined reinforcing action of nano-ZnO and CB, compared with the micro-ZnO. The higher modulus of the filled mix N_6 caused a reduction in elongation at break % (about 12.6% reduction). The increased crosslink density resulted in higher tear strength (about 34% increase), hardness (about 24% increase) and smaller abrasion loss (about 23% decrease) for the mix N_6 compared with N_8. The lower compression set observed for N_6 is due to its higher elasticity. Heat build-up was also lower for the filled mix N_6 (3.4^0 against 4.8^0). This is because of its higher elasticity which results in only a smaller loss of heat during dynamic stress. Demattia flex testing is an important measure of the flex resistance, especially in tire industry. The number of flex cycles required for crack initiation was determined and it was higher for N_6 (46.28 cycles against 28.31 cycles) due to strong crosslinks between chains.

The observed improvement in the technological properties of the NR mix containing 2 phr of nano-ZnO is attributed to its larger surface area of the nanoparticles which enable better dispersion and rubber–nanoparticle interaction.

The researchers also conducted swelling studies. From the swelling measurements (conducted in toluene) they obtained crosslink densities of vulcanized NR samples, using Flory–Rehner equation.[72] The crosslink density values were maximum for the filled samples containing nano-ZnO, compared to the micro counterpart. The swelling index values for solvents like cyclohexane, petrol and diesel were also calculated and minimum values were obtained for the vulcanized sample containing nano-ZnO. These results indicate higher crosslink density of the nanocomposite. In the DSC analysis, they obtained the glass transition temperature T_g of the composites approximately as −61 °C, indicating that chain flexibility is not affected by the ZnOs.

The authors[61] conducted similar studies on NR using as synthesized nanomodified ZnOs like stearic acid-coated nano-zinc oxide (ZOS) and stearic acid-coated-BIAT-coated nano-zinc oxide (ZOBS). They observed that the capping process helped to reduce the surface energy of the nanoparticles of ZnO, and thereby to reduce the agglomeration of nanoparticles. The authors prepared NR compounds containing micro and nano secondary accelerator N-benzylimine aminothioformamide (BIAT), nano-ZnO, and silicate-coated nano calcium carbonate (SCC). In one study they prepared NR compounds using 100 phr of NR, 1.32 phr of CBS, 1.5 phr of sulfur and varying quantities of ZOBS from 3 to 7 phr. Delta torque values increased with increase in dosage of ZOBS from 4.54 MPa and the value reached maximum for 7 phr of ZOBS (6.78 MPa). The total amount of nano-ZnO, stearic acid, and the accelerator BIAT was less than that was present in the microcomposite , which contained 5 phr of micro-ZnO, 2 phr of stearic acid, and 1.3425 phr of BIAT. This type of capping of ZnO reduced the mixing time and mill loss as is common in the separate addition of ZnO, stearic acid and accelerators. The optimum cure time decreased with increase in dosage of ZOBS and the value was minimum for the mix containing 7 phr of ZOBS (4.5 min), which was much less than that of the microcomposite (9.4 min).The scorch safety was better for the nanocomposites, around 3 min against 1 min for the microcomposite. The improvement of cure properties in the case of nanocomposites containing capped ZnO.

ZOBS is due to higher interparticle interactions on the surface of ZnO which activate them further.[73,74] The extra time and energy required for the diffusion of BIAT and stearic acid particles on to the surface of ZnO was saved by capping ZnO with BIAT and stearic acid.[74] In other words, the capping technique increased the activities of BIAT and stearic acid particles on the catalytic surface of ZnO, and made easy path for the formation of Zn–accelerator complex. The improvement of scorch safety (ts_2) could be due to the delayed release of BIAT for its synergic action with CBS. The authors claimed that the delayed release of BIAT was due to the previously established interactions between the sulfur of BIAT and zinc ions.

Other technological properties were also superior for the nanocomposites. Tensile strength increased with increase in dosage of ZOBS from 12.98 to 20.98 MPa for the mix containing 7 phr of ZOBS. The 300% modulus also showed increasing trend from 2.1 to 3.73 MPa. But elongation at break exhibited a decreasing trend as expected when there is an increase in modulus. The nanocomposites were superior in tear strength and abrasion resistance. The nanocomposite exhibited tear strength of 34.8 N/mm against 30.97 N/mm for the microcomposite and 221 mm^3 of abrasion loss against 342 mm^3 for the micro counterpart. The improvement in technological properties of the nanocomposites compared with the micro was due to the improved dispersion of BIAT, stearic acid and zinc ions in the NR matrix by capping mechanism as evidenced by the SEM image (Figure 12.13).

In another study the authors reported the effect of stearic acid-coated nano zinc oxide (ZOS), nano secondary accelerator (BIAT) and silicate-coated nano-$CaCO_3$ (SCC) in NR vulcanization. They prepared NR gum compounds containing 100 phr of NR, 5 phr of ZOS, 1.32 phr of CBS (5 mmol) and varying amounts of nano-BIAT, from 2.5 to 7.5 mmol. The nanocomposites exhibited increase in delta torque value (from 4.85 dNm to 7.69 dNm) as the dosage of nano-BIAT increased from 2.5 to 7.5 mmol. They observed almost a regular decrease in optimum cure time as the dosage of nano-BIAT was increased. Corresponding CRI was obtained for the nanocomposites. Thus the nanocomposites showed better cure properties than those for the microcomposite containing 5 phr of micro-ZnO, and 7.5 mmol of micro-BIAT (delta torque-7.37 dNm, t_{90} – 9.4 min, CRI- 11.90).Scorch safety was also a little better for the nanocomposites. Here also, the capping of ZnO with stearic acid helped to reduce its surface energy and hence agglomeration. The nano form of the accelerator BIAT also was well dispersed along with the ZOS, thus effecting superior rubber–nanoparticle interaction.

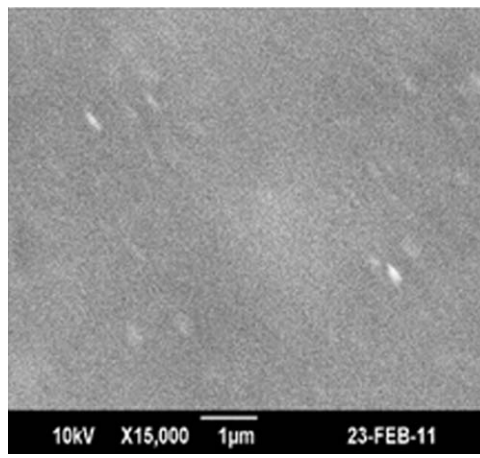

Figure 12.13 SEM image of NR nanocomposite containing 7 phr of ZOBS. [Reused with permission from *J. Appl. Polym. Sci.*, 2012, **124**, 3099.]

The mechanical properties of the gum nanocomposites were also superior to the microcomposite containing 5 phr of micro-ZnO. The nanocomposite containing 7.5 mmol nano-BIAT and 5 phr of nano-ZOS exhibited higher tensile strength (20.81 MPa) than the micro counterpart containing 5 phr of micro-ZnO and 7.5 mmol of BIAT (18.64 MPa). The nanocomposite containing 5 phr of nano-ZOS and 5 mmol of nano-BIAT exhibited about 17% increase in tear strength, when compared with the microcomposite. Hardness of this nanocomposite was a little higher than that of the microcomposite. The nanocomposites containing more than 2.5 mmol of nano-BIAT showed higher abrasion resistance and lower compression set values.

The filled composites containing 5 phr of nano-ZOS and 10–15 phr of SCC exhibited comparable tensile properties , tear strength and hardness as that of the microcomposite containing 5 phr of micro-ZnO and 30 phr of precipitated silica. These observations also support the findings that stearic acid-coated nano-ZnO (ZOS), nano-BIAT and SCC are better dispersed due to the small size of the particles as well as the higher specific surface area as already discussed in this chapter.

Kim *et al.*[75] conducted studies on the effect of nano-ZnO in the vulcanization of NR/BR/HSR blend. They prepared both gum and silica filled NR/BR/HSR compounds on a two-roll mill at a roll speed ratio of 1 : 1.4 and the compounds were moulded up to optimum cure time at 160 °C. The unfilled compounds contain 20 NR,10 HSR, 70 BR, 1 antioxidant (Naugard 445), 1 oil, 1 S,1.5 MBTS, 0.5 TMTM (all in phr)and varying amounts of ZnO (from 0.3 to 3 phr) and stearic acid (0.1 and 1 phr). The cure properties were determined using ODR cure meter, Tensile properties and tear strength were measured using UTM. Other properties were determined as per ASTM standards. They observed that the compound containing 1.5 phr of nano-ZnO and 0.1 phr of stearic acid exhibited comparable tensile strength, 300% modulus, elongation at break, swelling ratio and tear strength with that containing 5 phr of conventional ZnO and 1 phr of stearic acid. Though the maximum torque values were almost the same, the minimum torque of the nanocomposite was higher than the micro counterpart (47 Nm and 0.60 Nm, respectively, for micro and nanocomposite). This is because of the lower dosage of stearic acid (0.1 phr) in the nanocomposite, which caused only a lower lubrication effect. There was about 12.5% reduction in cure time for the nanocomposite when compared with the microcomposite (1318 to 1153 s respectively). All these are due to the size effect and dispersion of the nano-ZnO. The smaller size (30–40 nm) and larger specific surface area (25–50 g/m^2) of the nano-ZnO particles increased dispersion in the polymer matrix and enhanced the accelerator–activator as well as nanoparticle–rubber interactions.[69] On further reducing the dosage of nano-ZnO to 0.3 phr, scorch time and optimum cure time considerably decreased to about 18% and 23.5% respectively when compared with the composite containing 5 phr of micro-ZnO (895 to 736 s and 1318 to 1009 s, respectively, for the micro- and nanocomposite).This is due to the fact that the decomposition time of ZnO decreased during combination between rubber and sulfur–accelerator as the Zn^{2+} content decreases.[74–76] But due to the reduction

in modulus for the nanocomposite containing 0.3 phr of nano-ZnO, it showed 85% increase in elongation at break compared to that of the microcomposite. This compound also exhibited about 63.7 % increase in tear strength because the well dispersed nanoparticles prevented the crack growth.

The silica filled NR/BR/HSR compounds were prepared with 35 phr of silica (Zeosil-155) along with other ingredients as in the case of unfilled compounds. The dosage of stearic acid was varied from 0.1 to 0.3 phr and nano-ZnO from 0.1 to 3 phr. The reference compound was prepared using 5 phr of micro-ZnO. Among the compounds, that containing 1 phr of nano-ZnO and 0.1 phr of stearic acid exhibited superior tensile and tear properties. The minimum and maximum torque increased by 16 and 2% respectively of that of the microcomposite containing 5 phr of micro-ZnO (1.55 to 1.81 and 4.78 to 4.87 Nm). The scorch time and optimum cure time decreased by 15% and 11% respectively, compared to that containing 5 phr of micro-ZnO (163 to 148 and 256 to 227 s.).Tensile strength and tear resistance of this nanocomposite increased by 14.6 and 8%, respectively. The 300% modulus of the nanocomposite was increased by 30%.

The various properties of the silica filled compounds were improved compared to the unfilled compounds. The torque values of the filled compounds were increased due to the increase in viscosity. The scorch time and optimum cure time significantly decreased due to the heat conduction of filler particles. Tear and tensile properties of the silica filled compounds were considerably higher because of the effects of strain amplification and hysteresis of the silica filled vulcanizates.[77,78]

Sahoo *et al.* reported the effect of nano-ZnO (70 nm size) on the cure and mechanical properties of CB filled NR/NBR blends.[71] 1.0 phr of nano-ZnO in the CB filled compounds showed comparable properties as that containing 5.0 phr of micro-ZnO. But maximum torque was lower due to low degree of dispersion of ZnO in CB filled system. But Wang *et al.* used nano-ZnO masterbatch to improve the dispersion and consequently 1.0 phr of nano-ZnO in the CB filled SBR compounds produced equivalent maximum torque as that containing 5.0 phr of micro-ZnO.[76–78] Elongation at break and tensile strength of the nanocomposites were increased by 60 and 50%, respectively. Compared to the use of nano-ZnO in CB filled compounds, the use of 1.0 phr of nano-ZnO in silica filled rubber compound (in presence of dispersing agent PEG) improved the cure and mechanical properties due to the improvement in dispersion of nano-ZnO in rubber matrix in presence of PEG. Thus the surface area available to accelerator and rubber increased.[69]

12.8 Comparison of the Properties of Nano- and Microcomposites of NR

The aforesaid studies make it more evident that the dosage of ZnO in rubber compounds can be conveniently reduced to a lower dosage from 5 phr of micro form to even 1 phr of nano to obtain almost comparable or even better technological properties as obtained with 5 phr of micro-ZnO. This reduced dosage

is more advantageous in environmental terms. Nano-ZnO gets better dispersed in silica when a dispersing agent like PEG is used during the preparation of NR compounds than in CB. Stearic acid in lower amount as 0.1 phr along with 1 phr of nano-ZnO is very efficient in improving the technological properties of NR, whereas higher dosages like 2 phr of stearic acid is required in the case of micro-ZnO to bring about good curing of NR. No separate addition of stearic acid is required if nano-ZnO capped with stearic acid is used in the preparation of rubber compounds. Since higher dosages of stearic acid is used along with micro-ZnO, the wearing rate of the NR compound decreases with decrease in the dosage of ZnO.[73] This is attributed to the lubrication effect of stearic acid which dominates when the ZnO content is low. But when nano-ZnO is used along with lower dosages of stearic acid such as 0.1 phr, the lubrication effect of stearic acid is not dominating but the reinforcing effect of nano-ZnO dominates and as a result as ZnO content decreases, wearing rate of the NR increases.[73]

12.9 Conclusions

- Capping is an efficient method for the synthesis of nano-ZnO by sol–gel method.
- The capping process reduces the surface energy of ZnO nanoparticles and thus prevents agglomeration.
- ZnO can be suitably capped with accelerators, stearic acid *etc*.
- Accelerator and stearic acid capped ZnO can improve the cure properties and other mechanical properties of NR.
- Such capped nano-ZnO reduces the time and energy needed for the diffusion of these particles on to the catalytic surface of ZnO nanoparticles, which is advantageous in industry in respect of both energy and environmental issues.
- The larger surface area of nano-ZnO particles enables better dispersion of the particles in the rubber matrix and improves the rubber–nanoparticle interaction. This results in the improvement of technological properties of NR compounds containing nano-ZnO.
- Nano-ZnO is required only in smaller dosages like 1 phr to produce comparable/better technological properties of NR vulcanizates compared to micro-ZnO. This also is environmentally advantageous.

References

1. J. Walter, *Tire Technol. Int*., 2009, March, 18.
2. A. B. Sullivan, C. J. Hann and G. H. Kuhls, *Rubber Division Meeting*, American Chemical Society, Toronto, Canada, 1991.
3. P. J. Nieuwenhuizen, *Thesis*, Rijksuniversiteit Leiden, 1998.
4. R. F. Ohm, in *Kirk-Othmer Encyclopedia of Chemical Technology*, John Wiley & Sons Inc., New York, 1997, p. 460.

5. J. E. Huheey, E. A. Keiter and R. L. Keiter, *Inorganic Chemistry, Principles of Structure and Reactivity*, Harper-Collins, New York, 1993.
6. L. Domka, *Int. Pol. Sci. Techn.*, 1980, **7**, 18.
7. V. J. Duchacek, *J. Appl. Polym. Sci.*, 1978, **22**, 227.
8. A. Y. Coran, *Rubber Chem. Technol.*, 1964, **37**, 689.
9. Zinc in the Environment – An introduction, 2nd edition, International Zinc Association (IZA), Belgium, 1997, pp. 1–24.
10. S. Wille, Y. K. Mishra, D. Gedamu, I. Paulowicz, X. Jin and R. Adelung, *SPIE Newsroom*, DOI: 10.1117/2.1201111.003944, 2011.
11. A. Becheri, M. Durr, P. L. Nostro and P. Baglioni, *J. Nanopart. Res.*, 2008, **10**, 679.
12. J. Zeller and T. Manzur, *Proceedings of SPIE*, 7833,783313 (2010).
13. Aga and Mu, *Nanowires Science and Technology*, Lupu N., Ed. In Tech, 2010, 402.
14. Z. L. Wang, D. L. Polla, N. K. Dhar, T. Manzur and A. F. M. Anwar, in *ZnO Nanostructures for Optoelectronic Applications, Optoelectronic Devices and Properties*, ed. O. Sergiyenko, In Tech, 2011, 174.
15. Z. L. Wang, *ACS Nano*, 2008, **2**, 1987.
16. Z. L. Wang, *Mat. Sci. Eng. R*, 2009, **64**, 33.
17. Z. L. Wang, *Chinese Sci. Bull*, 2009, **54**, 4021.
18. S. T. Ganjal, M. Malekzadeh, M. Farahani, A. Abbasian and M. Khosravi, *J. Appl. Polym. Sci.*, 2011, **122**, 249.
19. A. Umar, S. Lee, Y. S. Lee, K. S. Nahm and Y. B. Hahn, *J. Cryst. Growth*, 2005, **277**, 479.
20. J. Y. Park, H. J. Oh, J. Kim and S. S. Kim, *J. Cryst. Growth*, 2006, **287**, 145.
21. Y. Li, G. W. Meng and L. D. Zhang, *Appl. Phys. Lett.*, 2000, **76**, 2011.
22. S. Y. Li, C. Y. Lee and T. Y. Tseng, *J. Cryst. Growth*, 2003, **247**, 357.
23. W. Z. Pan, R. Z. Dai and Z. L. Wang, *Science*, 2001, **291**, 1947.
24. J. Y. Lao, J. Y. Huang, D. Z. Wang and Z. F. Ren, *Nano Lett.*, 2003, **3**, 235.
25. S. A. Studenikin, N. Golego and M. Cocivera, *J. Appl. Phys.*, 1998, **84**, 2287.
26. Y. J. Xing, Z. H. Xi, Z. Q. Xue, X. D. Zhang, J. H. Song, R. M. Wang, J. Xu, Y. Song, L. Zhang and D. P. Yu, *Appl. Phys. Lett.*, 2003, **83**, 1689.
27. J. Q. Hu and Y. Bando, *Appl. Phys. Lett.*, 2003, **82**, 1401.
28. H. Zahang, D. Yang, D. Li, X. Ma, S. Li and D. Que, *J Cryst. Growth Design*, 2005, **5**, 547.
29. K. Haga, F. Katahira and H. Watanabe, *Thin Solid Films*, 1999, **343**, 145.
30. H. Zhang, D. R. Yang, X. Y. Ma, N. Du, J. B. Wu and D. L. Que, *J Phys Chem B*, 2006, **110**, 827.
31. P. C. Chang and G. J. Lu, *TIEEE Electron Dev*, 2008, **55**, 2977.
32. J. Li, S. Srinivasan, G. N. He, J. Y. Kang, S. T. Wu and F. A. Ponce, *J Cryst Growth*, 2008, **310**, 599.
33. U. Pal, J. G. Serrano, P. Santiago, G. Xiong, K. B. Ucer and R. T. Williams, *Opt Mat*, 2006, **29**, 65.

34. W. Bai, K. Yu, Q. Zhang, X. Zhu, D. Peng, Z. Zhu, N. Dai and Y. Sun, *Phys E*, 2008, **40**, 822.
35. R. Wahab, Y. S. Kim and H. S. Shin, *Materials Transactions*, 2009, **50**, 2092.
36. G. Heideman, J. W. M. Noordermeer and R. N. Datta, *Rubber Chem Technol*, 2005, **78**, 245.
37. L. N. Demianets, D. V. Kostomarov, I. P. Kuz'mina and S. V. Pushko, *Crystallogr. Rep.*, 2002, **47**, S86.
38. L. N. Demianets and D. V. Kostomarov, *Ann. Chim. Sci. Mat.*, 2001, **26**, 193.
39. L. N. Demianets, D. V. Kostomarov, I. P. Kuz'mina and S. V. Pushko, *Inorg. Mater.*, 2002, **38**, 124.
40. A. Kawska, P. Duchstein, O. Hochrein and D. Zahn, *Nano Lett*, 2008, **8**, 2336.
41. B. Liu and H. C. Zeng, *J. Am. Chem. Soc.*, 2003, **125**, 4430.
42. H. L. Cao, X. F. Qian, Q. Gong, W. M. Du, X. D. Ma and Z. K. Zhu, *Nanotechnology*, 2006, **17**, 3632.
43. T. Alammar and A. V. Mudring, *Mater. Lett.*, 2009, **63**, 732.
44. B. Cheng and E. T. Samulski, *Chem. Commun.*, 2004, 986.
45. S. Xu and Z. L. Wang, *Nano Res.*, 2011, DOI: 10.1007/s12274-011-0160-7-2011.
46. L. Vayssieres, *Adv. Mater.*, 2003, **15**, 464.
47. I. S. Ahuja, C. L. Yadava and R. Singh, *J. Mol. Struct.*, 1982, **81**, 229.
48. K. Govender, D. S. Boyle, P. B. Kenway and P. O'Brien, *J. Mater. Chem.*, 2004, **14**, 2575.
49. S. H. Jung, E. Oh, K. H. Lee, W. Park and S. H. Jeong, *Adv Mater*, 2007, **19**, 749.
50. L. E. Greene, M. Law, D. H. Tan, M. Montano, J. Goldberger, G. Somorjai and P. D. Yang, *Nano Lett.*, 2005, **5**, 1231.
51. Y. P. Fang, Q. Pang, X. G. Wen, B. N. Wang and S. H. Yang, *Small*, 2006, **2**, 612.
52. J. Liu, J. C. She, S. Z. Deng., J. Chen and N. S. Xu, *J Phys Chem C*, 2008, **112**, 11685.
53. H. B. Zeng, J. B. Cui, B. Q. Cao, U. Gibson, Y. Bando and D. Golberg, *Sci Adv Mater*, 2010, **2**, 336.
54. R. Konenkamp, K. Boedecker, M. C. Lux-Steiner, M. Poschenrieder, F. Zenia, C. Levy-Clement and S. Wagner, *Appl Phys Lett*, 2000, **77**, 2575.
55. M. J. Zheng, L. D. Zhang, G. H. Li and W. Z. Shen, *Chem Phys Lett.*, 2002, **363**, 123.
56. J. H. Kim, E. M. Kim, D. Andeen, D. Thomson, S. P. DenBaars and F. F. Lange, *Adv. Funct. Mater*, 2007, **17**, 463.
57. W. B. Wu, G. D. Hu, S. G. Cui, Y. Zhou and H. T. Wu, *Cryst. Growth Dec.*, 2008, **8**, 4014.
58. Y. Zhou, W. B. Wu, G. D. Hu, H. T. Wu and S. G. Cui, *Mater. Res. Bull.*, 2008, **43**, 2113.

59. J. F. Zang, C. M. Li, X. Q. Cui, J. X. Wang, X. W. Sun, H. Dong and C. Q. Sun, *Electroanal.*, 2007, **19**, 1008.
60. P. C. Hidber, T. J. Graule and L. J. Gauckler, *J Am Ceram Soc*, 1996, **79**, 1857.
61. S. P. Thomas, E. J. Mathew, C. V. Marykutty and J Appl Polm, *Sci*, 2012, **124**, 3099.
62. N. Faal Hamedani and F. Farzaneh, *J. Sci. I R Iran*, 2006, **17**, 231.
63. F. Liu, P. J. Cao, H. F. Zhang, C. M. Shen, Z. Wang, J. Q. Li and H. J. Gao, *J. Crystal Growth*, 2005, **274**, 126.
64. M. H. Huang, Y. Wu, H. Feick, N. Tran, E. Weber and P. Yang, *Adv Mater*, 2001, **13**, 113.
65. N. Singh, S. Mittal, K. N. Sood and P. K. Rashmi, Gupta, *Chalcogenide Letters*, 2010, **7**, 275.
66. J. S. Lee, K. Park, M. I. Kang, I. W. Park, S. W. Kim, W. K. Cho, H. S. Han and S. S. Kim, *J. Crystal Growth*, 2003, **254**, 423.
67. S. G. Wahab, Y. S. Ansari, H. K. Kim, G. S. Seo, G. Kim and H. S. Khang, Shin, *Mater Res Bull*, 2007, **42**, 1640.
68. H. Zhang, D. Yang, S. Li, X. Ma, Y. Ji, J. Xu and D. Que, *Mater. Lett.*, 2005, **59**, 1696.
69. G. N. Oneagoro, *Academic res. International*, 2012, **3**(1), 499.
70. P. M. Sabura Begum, Studies on the use of nano zinc oxide and modified silica in NR, CR and SBR, PhD thesis, Cochin University of Science and Technology, India, 2010.
71. A. Sahoo, M. Maiti, A. Ganguly, J. J. George and A. K. Bhowmick, *J. Appl. Polym. Sci.*, 2007, **105**, 2407.
72. P. J. Flory and J. Rehner, *J Chem Phys.*, 1943, **11**, 512.
73. P. Nieuwenhuizen and J Appl Catal, *A: General*, 2001, **207**, 55.
74. P. Arjunan, U. S. Patent, 5,352739, 1994.
75. I. J. Kim, W. S. Kim, D. H. Lee, W. Kim and J. W. Bae, *J Appl Polym Sci*, 2010, **117**, 1535.
76. W. Wilson, in *The Vanderbilt Rubber Handbook*, 13th ed., R. E. Ohm, Ed., Vandervilt: Norwalk, CT, 1990, 281.
77. A. E. Medalia and G. Kraus, In *Science and Technology of Rubber*, 2nd ed., J. E. Mark, B. Erman and F. R. Eirich, Eds., Academic Press, New York, 1994, p. 408.
78. J. Wang and Y. Chen, *J. Appl. Polym. Sci.*, 2006, **101**, 922.

CHAPTER 13

Green Natural Fibre Reinforced Natural Rubber Composites

SA-AD RIYAJAN

Department of Materials Science and Technology, Faculty of Science, Prince of Songkla University, Thailand
Email: sa-ad.r@psu.ac.th; saadriyajan@hotmail.com

13.1 Introduction

Natural rubber (NR) is a main biopolymer and it widely used in many fields such as medical fields, tire and glove due to theirs good physical properties. Since NR can crystallize upon stretching. However, the mechanical and biodegradable of NR are improved to the optimal some application and environmental friendly. The physical properties of NR were improved by addition of filler, chemical modification and blending with other polymers such as polyethylene (PE),[1] propylene (PP)[2] and nitrile rubber (NBR).[3] At present, we are still actively studying these blends, especially those filled with natural fibres. This chapter is focused on the improving mechanical properties of NR by addition of green fibre. The green fibre and 'natural fibre' covers broad ranges of vegetable fibre such as wood fibre and plant-based bast, leaf, seed and stem fibre and animal fibres such as collagen, keratin and fibroin. Recently, they are used in plastics polymer composites to help theirs mechanical properties providing significantly reinforcement. Considering to NR, the natural fibre was blended with NR to improve its modulus and biodegradability.[4–12] In the

RSC Polymer Chemistry Series No. 8
Natural Rubber Materials, Volume 2: Composites and Nanocomposites
Edited by Sabu Thomas, Hanna J. Maria, Jithin Joy, Chin Han Chan and Laly A. Pothen

Published by the Royal Society of Chemistry, www.rsc.org

previous work, the raw materials were obtained from many natural sources such as sugar beet pulp,[4] eucalyptus kraft pulp[5] as H_2SO_4, HCl, $HClO_4$, NaOH which is capable to react with these functional groups can react with cellulose fibre. The problem of the NR composite is poor adhesion between NR and cellulose fibre. The factors affecting the properties of the polymer composite are fibre type, fibre amount chemical treatment, shape of fibre, adhesion and arrangement of fibre in polymer composite.[6]

13.2 Basic Information about Natural Fibre

At present, synthetic fibres are durable and difficult to degrade in nature leading to the pollution or environmental problem after their use. Therefore, the synthetic fibre replace with natural fibre due to its low cost, non-toxic, renewable and recyclable material. Cellulose is widely used in various applications, *e.g.* cloth, paper, food packaging, fibre and biomedical materials depending on their composition and physical properties. It composes of a linear polymer of anhydroglucose units linked at the one and four carbon atoms by a β-glycoside bond including three hydroxyl groups with different polarities containing secondary OH at the C2 and C3 positions, and primary OH at the C6 position.[12–14] Besides cellulose, natural fibre consists of non-cellulose, *i.e.* fatty acid, wax and hemicellulose. The hemicellulose contains xyloglucan which binds to the surface of cellulose microfibrils and may link them together.[15] The sources of natural fibre are made from vegetable fibre and animal fibre. Agricultural waste is a major source of natural fibre, for example maize leaves, sugar cane leaves and coconut waste, as shown in Figure 13.1. In addition, cotton, jute, flax, ramie, sisal and hemp are important materials in the manufacture of paper and cloth. Natural fibres consist of cellulose, hemicellulose and lignin, as shown in Figure 13.2. The compositions of cellulose, hemicellulose and lignin vary depending on different plants, location and season, as shown in Table 13.1.[16]

Natural fibres consist of cellulose and non-cellulose components such as lignin, hemicellulose, wax and fatty acid. The cellulose is a crystalline region and exhibits high strength and stiffness. The natural cellulose fibres are prepared by chemical treatment through addition of acid, alkali, enzymes or a combination of these chemicals. Natural cellulose is widely used in various applications, *e.g.* cloth, paper, food packaging, fibre and biomedical materials, depending on its composition and physical properties. The chemical structure of cellulose fibre is made up of a linear polymer of anhydroglucose units linked at the one and four carbon atoms by a β-glycoside bond, including three hydroxyl groups with different polarities containing secondary OH at the C2 and C3 positions, and primary OH at the C6 position. In the case of lignin, it is an amorphous structure that consists of an irregular array of variously bonded hydroxyl- and methoxyl-substituted phenylpropane units. The functions of lignin in natural fibre are to act as a chemical adhesive within and between fibres.

Figure 13.1 Digital photographs of natural fibre from sugar cane leaves (author's experiment).

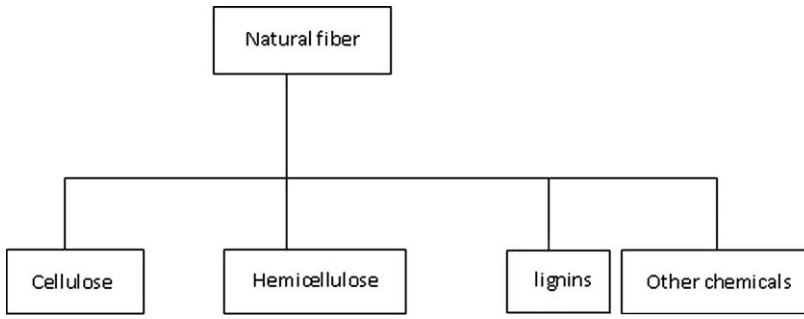

Figure 13.2 Components of natural fibre (author's experiment).

Table 13.1 Chemical compositions of different types of natural fibre.[16]

Natural fiber types	*Cellulose*	*Lignin*	*Pectin*
Flax	65–85	1–4	5–12
Kenaf	45–57	8–13	3–5
Sisal	50–67	–	3
Jute	45–63	12–25	4–10
Hardwood	40–50	20–30	0–1
Softwood	40–45	36–34	0–1

The composition including cellulose, hemicellulose, pectin, lignin, water soluble and water of cotton were 82.7, 5.7, 7.5, no data, 1.0, 0.65 and 10.0%, respectively.[17] While the amounts of cellulose, hemicellulose, pectin, lignin, water soluble and water in jute were 64.4, 12.0, 0.2, 11.8, 1.1, 0.5 and 10.0%, respectively.[18]

The cellulose fibres from sugar cane bagasse after employing octadecanoyl and dodecanoyl chloride/supercritical carbon dioxide pulping process were then blended with low-density polyethylene (LDPE).[18] The results showed the improvement of compatibility between the cellulose fibres and PE matrix. However, the mechanical performances of the modified fibre-based composites when compared to the unmodified fibres did not improve due to the strong degradation of cellulose fibre after chemical treatment despite using the mild conditions. Chemical modification of sugar cane leaves is yet to be reported, so this present study aims to prepare and characterize cellulose obtained from sugar cane leaves. The hydrogen bonding between the hydroxyl groups of cellulose is shown in Figure 13.3.[18]

Natural fibres can be obtained from various parts of a plant, as shown in Table 13.2. Natural fibres can be continuous fibres, short fibres, whiskers or particles, as shown in Figure 13.4. Types of polymer composite based on shape and structure are divided into particle, fibre and structural.

The highest strength of fibre was found in flax samples, as shown in Table 13.3. Generally, the mechanical properties of natural fibres are lower than those of synthetic fibres, but their mechanical performance is good for some applications. The properties of natural fibres vary depending on species

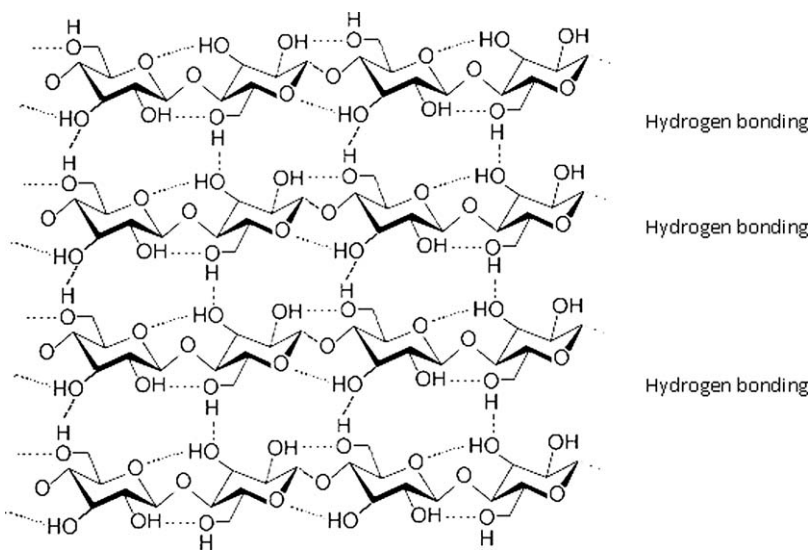

Figure 13.3 Model of a strand of cellulose (conformation I_{α}), showing the hydrogen bonds (dashes) within and between cellulose molecules.[18]

Table 13.2 Types of plant fibre classified according to the part of a plant they come from.[18]

Types	*More detail*
Seed fiber	Fibers collected from seeds or seed cases, *e.g.* cotton and kapok
Leaf fiber	Fibers collected from leaves, *e.g.* fique, sisal, banana and agave
Skin fiber	Fibers are collected from the skin or bast surrounding the stem of their respective plant. These fibers have higher tensile strength than other fibers. Therefore, these fibers are used for durable yarn, fabric, packaging, and paper. Some examples are flax, jute, kenaf, industrial hemp, ramie, rattan. and vine fibers.
Fruit fiber	Fibers are collected from the fruit of the plant, *e.g.* coconut (coir) fiber.
Stalk fiber	Fibers are actually the stalks of the plant. For example, straws of wheat, rice, barley, and other crops including bamboo and grass. Tree wood is also such a fiber

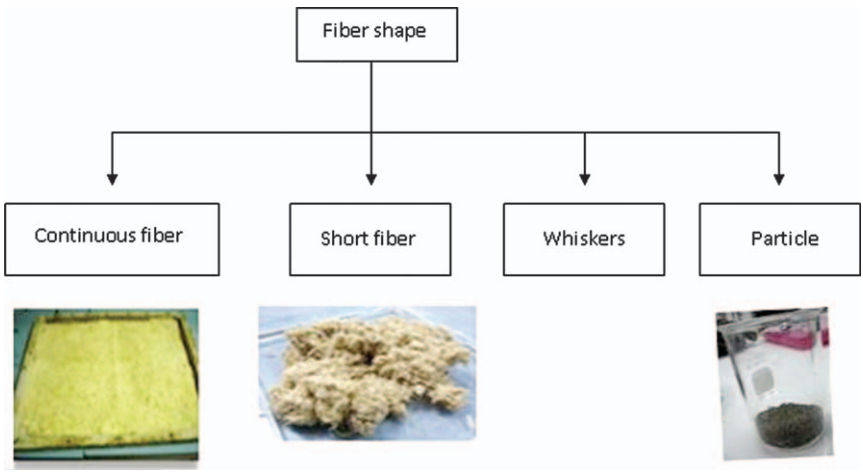

Figure 13.4 Various shapes of natural fibres (author's experiment).

Table 13.3 Mechanical properties of different types of natural fibre.[16]

Type	*Density (g/cm^3)*	*Stiffness (GPa)*	*Strength (MPa)*	*Elongationat break (%)*
Flax	1.4–1.5	50–70	500–900	1.5–4.0
Hemp	1.48	30–60	300–800	2–4
Jute	1.3–1.5	20–55	200–500	2–3
Sofwood	1.4	10–50	100–170	–
Hardwood	1.4	10–70	90–180	

types, growing conditions and processing methods. Considering performance application, the balance of significant reinforcing potential, low cost and low density is part of the reason they are attractive to polymer industries.

13.3 Preparation of Natural Fibre

The natural raw material such as sugar cane leave, bagasse, oil palm ash, palm fibre, coir fibre, coconut fibre and jute fibre are treated with NaOH, H_2O_2, H_2SO_4/HCl or $HClO_4$.

The natural raw fibres were submitted to chemical treatments as described below. After this, modified fibres were thoroughly rinsed with distilled water and dried under vacuum for 2 h. Figure 13.5 shows the procedure for preparing cellulose from sugar cane leaves.

Treatment with NaOH: 500 g of sugar cane fibre was immersed in basic medium (10 g NaOH) at 32 °C for 24 h.

Treatment with H_2O_2: the natural raw material was soaked in 500 mL of 0.9% H_2O_2 for about 2 h at 32 °C.

Treatment with a mixture of HCl and H_2SO_4 at different ratios: performed by soaking 200 g of fibres in 500 mL of a mixture of 1 : 1 or 1 : 2 or 1 : 3 or 1 : 4 HCl : H_2SO_4 for 2 h at 32 °C and, after that, the fibres were washed with water.

Treatment with perchloric acid: 200 g of the natural fibres was immersed in 1 L of 10% perchloric acid for 2 h at 32 °C.

ATR-FTIR, solid state ^{13}C-NMR and XRD results showed the composition of the fibre surface and the relationship of its characteristic with thermal resistance. The crystalline content of the natural fibre remarkably increased after chemical treatment, which was confirmed by XRD and solid-state ^{13}C-NMR. $HClO_4$ is the most efficient chemical in terms of wax and fatty acid residue removal in our work. Hence, the dynamic mechanical properties of the natural fibre after $HClO_4$ treatment were improved. It was reported that the acidolysis lignins were isolated from sugar cane bagasse and curaua fibres by adding a mixture of dioxane and 0.1 N aqueous HCl (8.5 : 1.5, v/v) at 100 °C for 2 h under N_2.[20] ATR-FTIR and TGA of the oxidized lignins revealed a decrease in

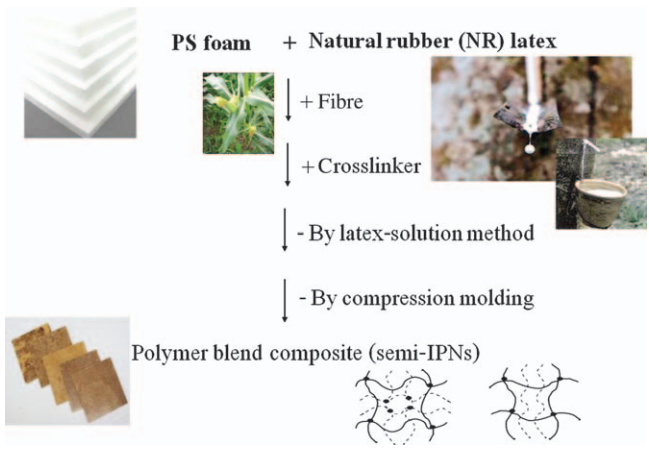

Figure 13.5 Procedure for preparing rubber composites based on latex (author's experiment).

the aromatic and methoxy content due to the partial degradation of the polymer. Results showed that the decomposition exothermal temperature of lignin oxidized with furfuryl alcohol (2-furyl methanol) was lower than that of both curaua and sugar cane bagasse lignins. In order to limit the chemical modification to the substrate surface, the microcrystalline cellulose and cellulose fibres derived from different sugar cane bagasse pulping processes were treated with small amount of octadecanoyl and dodecanoyl chloride.[21] It was found that the chemical modification. The raw leaves were treated with sodium hydroxide (NaOH), hydrogen peroxide (H_2O_2), perchloric acid ($HClO_4$) or mixture of sulfuric acid and hydrochloric acid (H_2SO_4/HCl). Sugar cane leaves are the waste obtained from local farming in Southern Thailand. They were cut into small pieces (2–3 cm), washed with distilled water five times and dried at 60 °C for 24 h before being chemically treated.

The procedure for preparing cellulose from sugar cane leaves is shown in Figure 13.5. After each treatment, the modified fibres were thoroughly rinsed with distilled water three times.

The partial wet natural fibres were poured into a glass tray ($10\times10\times0.2$ cm^3) to form a dried sheet having 0.1 mm in thickness. After drying at 50 °C in an oven for 24 h, the natural fibre sheet was kept in a desiccator before characterization. The average particle size of coconut waste before and after the milling process was about 350 and 950 μm, respectively, as shown in Figure 13.6.

ATR-FTIR was used to identify the chemical structure of the sugar cane leaves before and after chemical treatment. The spectra of pristine sugar leaves and chemical treated natural fibre are presented in Figure 13.7, while Table 13.4 shows the summary of the main peaks.

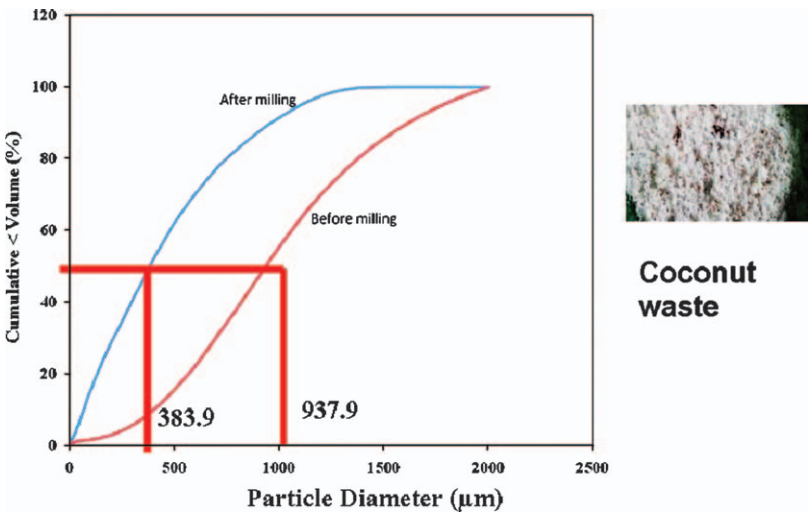

Figure 13.6 Cumulative particle size of coconut fibre showing particle size measurement (author's experiment).

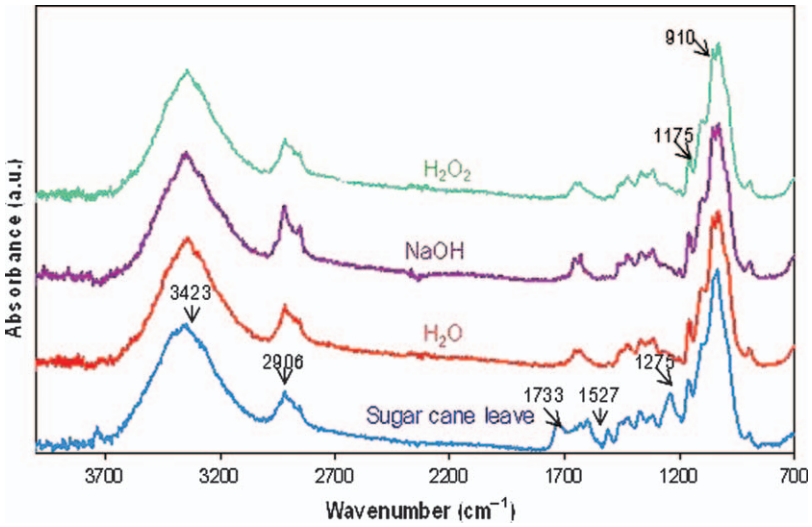

Figure 13.7 ATR-FTIR spectra of sugar cane leaves and their cellulose fibres obtained by chemical treatment (author's experiment).

Table 13.4 Summary of ATR-FTIR bands of cellulose fibre.

Wave number (cm^{-1})				
Sugar cane leave	*H_2O*	*NaOH*	*H_2O_2*	*Peak assignments*
910	910	910	910	C–H stretching and O–H stretching of β-glycosidic linkages
1275	–	–	–	C–O–C stretching of pectin and hemicellulose
1334	1334	1334	1334	C–O stretching
1454	1454	1454	1454	CH_2-symmetric stretching
1527	–	–	–	Aromatic group of lignin
1640	1640	1640	1640	O–H stretching of water
1733	–	–	–	C=0 stretching of methyl ester and carboxylic acid
2906	2906	2906	2906	C–H stretching
3423	3423	3423	3423	O–H group of cellulose

It was observed that the chemical structures of the pristine sugar cane leaves and the treated samples of cellulose fibres were generally similar. However, the absorption bands at 1733 cm^{-1} relating to stretching carbonyl group from methyl ester and carboxylic acid and at 1527 cm^{-1} corresponding to stretching of the aromatic skeletal vibration in residue lignin were observed in the fibres after treatment with H_2O_2, mixture of HCl/H_2SO_4 and $HClO_4$. In addition, the absorption band at 1275 cm^{-1} derived from stretching of –C–O–C– in pectin and hemicellulose appeared only in the pristine sugar cane leaves.

The main absorption bands of the treated cellulose were observed at 3423, 2906, 1640, 1500, 1454, 1387, 1334, 1175 and 910 cm^{-1}.[22] The bands at 3423, 2906

and 1640 cm^{-1} correlate to stretching of OH, C–H groups and water molecules absorbed in the cellulose, respectively. Moreover, the peak at 1500 cm^{-1} is assigned to the deformation of internal coordinates of a hydrogen glucopyranose as a cyclic form of glucose residues. The peaks at 1454, 1334 and 1175 cm^{-1} are the stretching C–C, C–O skeletal vibration and C–O antisymmetric bridge stretching, respectively. In addition, the small peak at 910 cm^{-1} relates to the glycosidic C_1–H deformation with ring vibration contribution and OH bending from β-glycosidic linkages between glucose in natural fibre. The chemical composition and ATR-FTIR analyses, therefore, revealed the reduction of hemicellulose content in the fibres treated with NaOH, HCl/H_2SO_4 or $HClO_4$.

The ^{13}C NMR signal of pristine sugar cane leaves was broad because of the presence of crystalline and amorphous portions, *i.e.* cellulose and non-cellulose (lignin, wax, fatty acid and carbohydrate). There was no optimum relaxation time in the pristine sample. After chemical treatment, the NMR signal of the fibres was, therefore, sharp due to the removal of non-cellulose. Moreover, the sharpest signal was observed in the fibres treated with $HClO_4$. It was, therefore, assumed that $HClO_4$ was the most efficient chemical in terms of non-cellulose residues removal compared to the others. In all cases, the region of 60–70 ppm is assigned to C6 of the primary alcohol group. The next cluster of resonance at 70–81 ppm is attributed to C2, C3 and C5 of cellulose fibre. The region of 81–93 ppm is associated with C4 and that between 102 and 108 ppm with C1, the anomeric carbon as the centre of a hemiketal functional group.[23] The signals at 99–100 ppm are assigned to xylose (C1) of xyloglucan 5 and at 80 ppm to glucose (C4) of xyloglucan indicating that xyloglucan is associated with the cellulose.[22] Other signals from xyloglucan are presumed to overlap with the dominant signal strengths from the cellulose fibre, both in the C1 and C4 regions of the solid state ^{13}C-NMR spectra. The broader C1 resonance associated with the disordered chains dominates the shape of all spectra. Figure 13.8 shows the region between 86 and 92 ppm correlating to the crystalline portion in cellulose. The intensity of this region increased with further removal of non-cellulose. It is clear that the intensity of C4 (86–92 ppm) in natural fibres remarkably increased after the chemical treatment.

X-ray diffraction patterns were used to analyse the crystalline content of the treated fibres and results are shown in Figure 13.9.

It is clear that the XRD pattern of the modified cellulose exhibited diffraction peaks at the 2θ angles of 17 and 22°. The position of the peak at 17° indicated an increase in interplanar distance of the treated fibres when compared to the pristine sugar cane leaves. The results indicated the formation of order in cofibres after chemical treatment. The crystalline content of the modified cellulose was calculated from Equation (13.1):[24]

$$\%\,\text{crystalline content} = \frac{A_c}{(A_c + A_a)} \tag{13.1}$$

where A_c and A_a are areas of crystalline and amorphous peaks in cellulose, respectively.

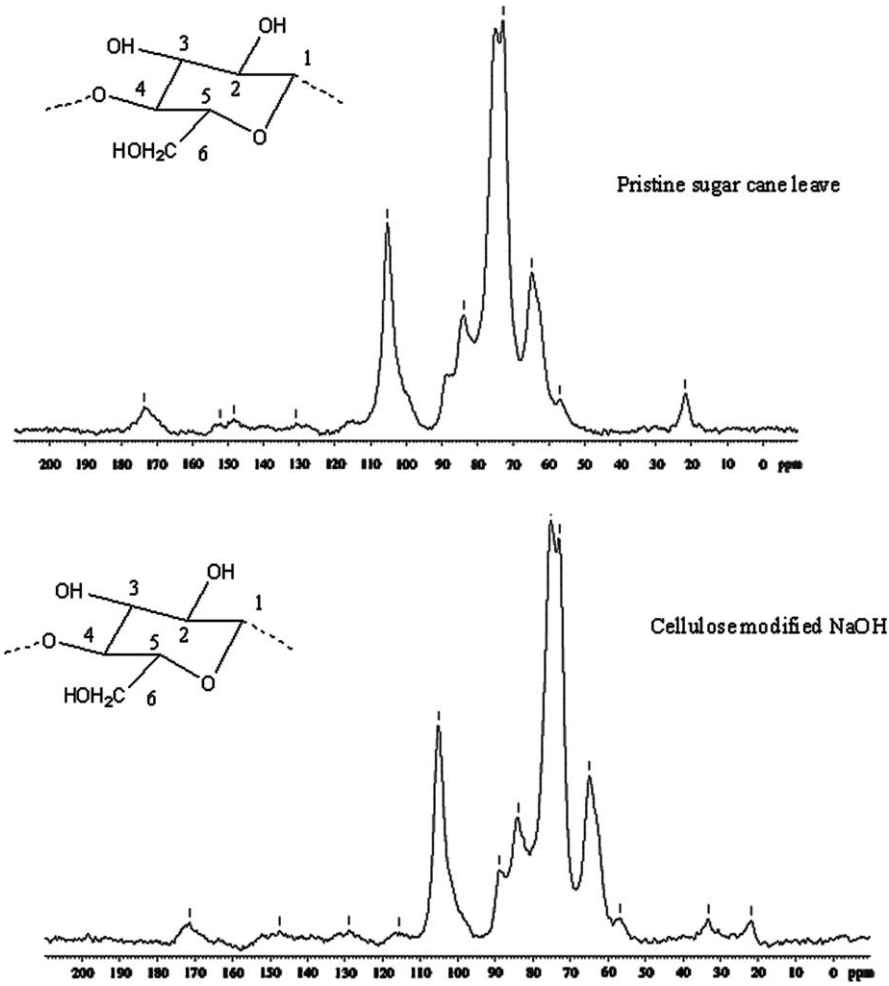

Figure 13.8 Solid-state ^{13}C-NMR spectra of sugar cane leaves and modified cellulose fibre (author's experiment).

It was found that the crystalline content of the treated fibres increased because of the removal of remaining fatty acid. The crystalline content of the pristine sugar cane fibres was ~40% while that of the fibres after chemical treatments was ~70%. The XRD results, therefore, agreed well with those obtained from the solid-state ^{13}C-NMR. The effect of chemical treatment on the morphology of sugar cane fibres investigated under SEM is shown in Figure 13.10.

SEM micrographs show that the pristine sugar cane fibres differ considerably from the fibres treated with H_2SO_4/HCl and $HClO_4$. The removed non-cellulose was responsible for the smooth surface of the treated fibres. The diameter of fibres after NaOH, 4 : 1 of H_2SO_4/HCl and $HClO_4$ treatments was

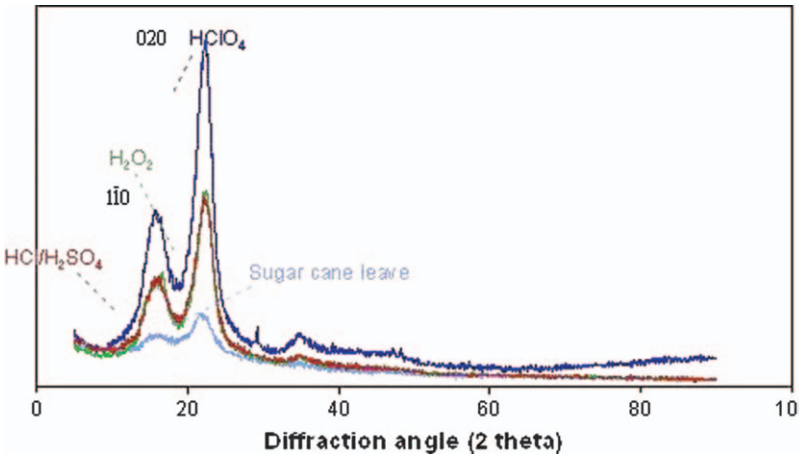

Figure 13.9 XRD patterns of sugar cane leaves and their cellulose fibre (author's experiment).

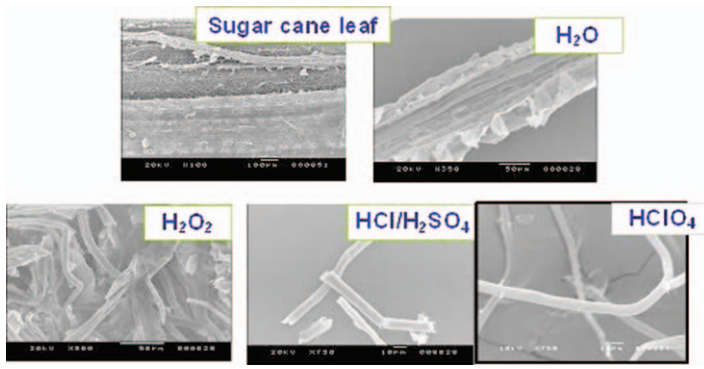

Figure 13.10 SEM images of unmodified and modified cellulose (author's experiment).

10, 12 and 8 μm, respectively. The diameter of all treated fibres was smaller than that of the untreated fibres (150 μm) due to the oxidation of non-cellulose.[25] From the size of fibres, it was assumed that all chemical agents removed the non-cellulose from natural fibre. The explanation involved the strength of acid, *i.e.* $HClO_4$ which is stronger than H_2SO_4 and HCl, was the most efficient chemical for removing non-cellulose from the fibres. In the case of H_2O_2, it exhibits strong oxidizing properties and is a powerful bleaching agent. However, its oxidizing ability is lower than that of $HClO_4$.

From ATR-FTIR, solid-state ^{13}C NMR, XRD and SEM, it was concluded that the sugar cane fibre consists of cellulose and non-cellulose (fatty acid, wax and hemicellulose). A schematic of a natural cellulose fibre from a sugar cane leaf is shown in Figure 13.11.

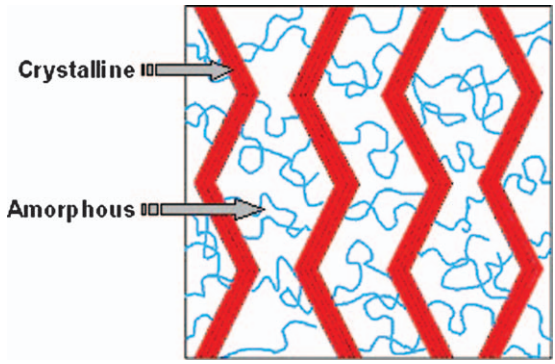

Figure 13.11 Schematic of natural fibre consisting of crystalline and amorphous regions (author's experiment).

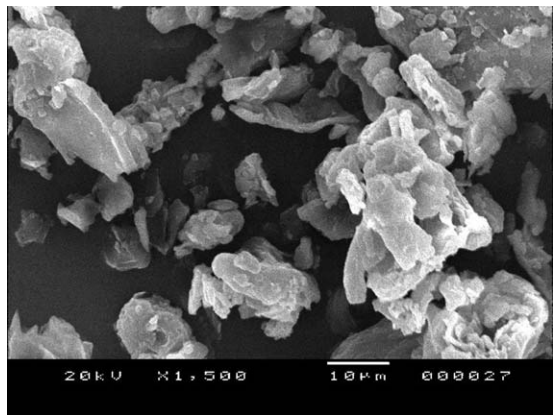

Figure 13.12 Length of cellulose fibre from sugar cane leaves and treated with $HCl:H_2SO_4$ at 1 : 1, 1 : 2, 1 : 3 and 1 : 4 as observed by a particle size analyser (author's experiment).

In this schematic, the natural fibre consists of a cellulose part, represented as a zigzag line, and a non-cellulose part, shown as a wavy line. The cellulose or crystalline region embedded in the matrix of non-cellulose which is amorphous region containing wax, fatty acid hemicellulose and lignin by taking into account the different spiral angles and layer thickness of each of the layers. The amorphous region is easily decomposed by chemical while the crystalline portion is more resistant to the reagent. This model is well supported by the results obtained from ATR-FTIR, solid-state ^{13}C-NMR, XRD and SEM. The average length of fibre was about 100 µm, observed by a particle size analyser as shown in Figure 13.12.

The characterization of modified sugar cane bagasse was investigated by SEM, AFM and FTIR. The ester linkage or OC=O stretching of modified bagasse was observed at 1085 and 1238 cm^{-1}. In addition, the wavelength at

1321 cm^{-1} of modified bagasse indicates the stretching C–O. The new peak of modified sugar cane observed at 1180 and 1225 cm^{-1} referred to Si–O–Si and Si–O–cellulose. This result responds with this reference.[26] They reported that the broad band around 1200 and 1180 were assigned to the stretching of the Si–O–cellulose and –Si–O–Si– bonds. The spectra of unmodified bagasse and modified bagasse represent wavenumber around 2500 and 4000. The new peak with high intensity of modified bagasse appears at 3300 cm^{-1} which are presented the stretching hydroxyl group occurring from chemical reaction between silane and moisture. In addition, the new peak of modified bagasse observed at 2885 and 2973 cm^{-1}, presented the CH and CH_2 of silane. Two peaks are different with result of unmodified bagasse. These results are revealed that the successfully modified surface of bagasse. It is clear that the surface of unmodified bagasse exhibited lower roughness comparing to sample with modified with sodium hydroxide treatment. This result explained that the fatty acid on surface of sugar cane was removed by sodium hydroxide and silane treatment. The diameter of sugar cane was roughly 0.1 mm. Results showed that the surface of unmodified sugar cane showed more roughness than that modified sugar cane observed from different colours. This result is responding to SEM results.[27] The adhesion force of unmodified sugar cane, modified sugar cane with sodium hydroxide and silane were 142, 58 and 233 Nm observing by AFM. This result confirmed that the surface of modified bagasse with sodium hydroxide is more hydrophobic behaviour than that of unmodified bagasse observed from adhesion forces. These results are explained that the lipid and fatty acid on surface of bagasse are removed after sodium hydroxide treatment. After bagasse was modified with silane, the adhesion force of bagasse increased from 58 to be 233 due to hydroxyl group from reaction between moisture and silane.[28] These results respond with ATIR-FTIR results. Riyajan and his coworkers[27] have worked on chemical medication of surface of bagasse with silane. For example, the preparation of polymer composite was successfully derived from NR, bagasse and plaster. The chemical stretching of the modified bagasse exhibited the occurrence of Si–CH_3 group after chemical modification. The roughness of bagasse modified with sodium hydroxide was observed from SEM, in which it leads to removing fatty acid from bagasse. Figure 13.13 shows the morphology of tea waste observed by SEM, which shows that it is not spherical. It was found that the particle size of tea waste was about 20–30 μm, and decreased after the milling process.

The cellulose fibres from bagasse after employing octadecanoyl and dodecanoyl chloride/supercritical carbon dioxide pulping process were then blended with LDPE.[19] The results showed an improvement in compatibility between the cellulose fibres and PE matrix. However, the mechanical performance of the modified fibre-based composites when compared to the unmodified fibres did not improve due to the strong degradation of cellulose fibre after chemical treatment despite using the mild conditions. Since the chemical modification of the sugar cane leaves has not yet been reported, this present study aims to prepare and characterize cellulose obtained from sugar cane leaves. The coupling agents for rubber composite are zirconium, titanate, zirconium

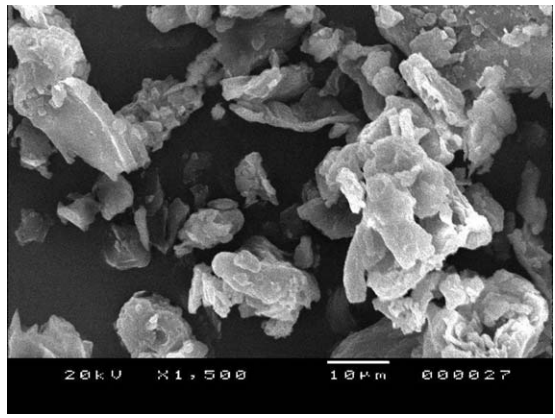

Figure 13.13 SEM images of milled tea waste fibre (author's experiment).

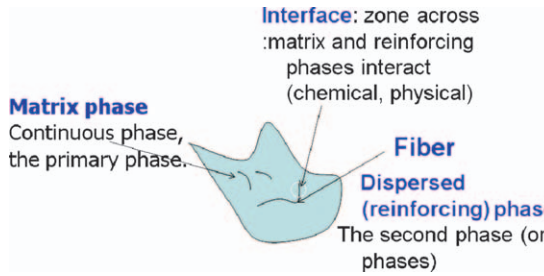

Figure 13.14 Schematic of polymer composite at the interphase.

aluminates and chromium complex. The coupling agent can improve adhesion between matrix and reinforcing phases or natural fibre as shown in Figure 13.14.

13.4 Preparation of Natural Rubber Composites

In general, the techniques of preparing polymer composites are hand lay-up moulding, spray-up moulding, compression moulding, transfer moulding, resin transfer moulding, injection moulding, plunger-type injection moulding, reaction injection moulding, pultrusion and filament winding.

Hand lay-up is the simplest and oldest open moulding for manufacturing polymer composite fabrication processes.[29,30] It is a low volume, labour intensive method suited especially for large components, such as boat hulls. Glass or other reinforcing mat or woven fabric or roving is positioned manually in the open mould, and resin is poured, brushed, or sprayed over and into the glass plies. Entrapped air is removed manually with squeegees or rollers to complete the laminates structure. For a high quality part surface, a pigmented gel coat is first applied to the mould surface.

Fibre glass spray lay-up process is very different from the hand lay-up process which comes from the application of the fibre and resin material to the mould.[31] Spray-up is an open-moulding composites fabrication process where resin and reinforcements are sprayed onto a reusable mould. The resin and glass may be applied separately or simultaneously 'chopped' in a combined stream from a chopper gun. Workers roll out the spray-up to compact the laminate. Wood, foam, or other core material may then be added, and a secondary spray-up layer embeds the core between the laminates. The part is then cured, cooled, and removed from the mould. Compression moulding is a method of moulding in which the moulding material, generally preheated, is first placed in an open, heated mould cavity.[32,33] The mould is closed with a top force or plug member, pressure is applied to force the material into contact with all mould areas, while heat and pressure are maintained until the moulding material has cured. Compression moulding is a high-volume, high-pressure method suitable for moulding complex, high-strength fibreglass reinforcements. Advanced composite thermoplastics can also be compression moulded with unidirectional tapes, woven fabrics, randomly oriented fibre mat or chopped strand.

Reaction injection moulding (RIM) is different with injection moulding to raw material.[34] In case of RIM, thermosetting polymers are used, in which it requires a crosslinking reaction to occur within the mould. First, the two parts of the polymer are mixed together. The mixture is then injected into the mould under high pressure using an impinging mixer. The mixture is allowed to sit in the mould long enough for it to expand and crosslinking. In case of polymer composite, the reinforcing agents such as glass fibres and mica and natural cellulose are added to the mixture then the process is known as reinforced reaction injection moulding (RRIM). This process is usually used to produce rigid foam automotive panels.

There are two methods including latex blending and dried rubber for this chapter in detail as shown in Figure 13.15.

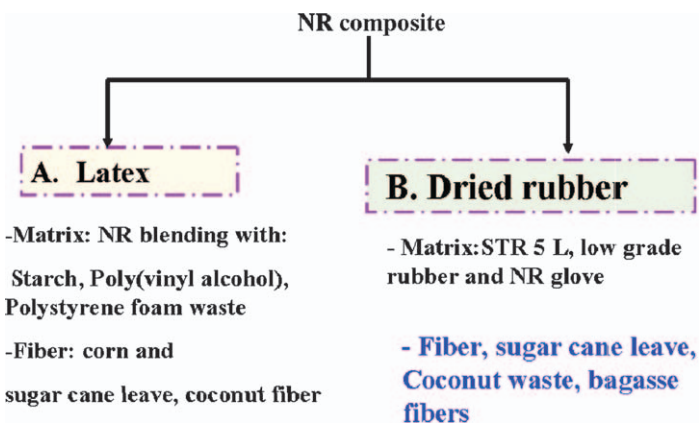

Figure 13.15 Method of preparing rubber composite obtained from original.

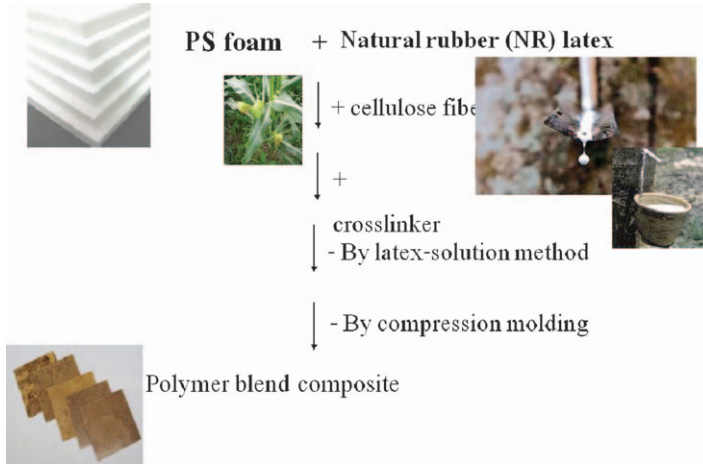

Figure 13.16 Preparation of rubber composite reinforced with cellulose fibre (author's experiment).

13.4.1 Latex Blending

The PS solution (10% w/v) was blended with different NR latex (60% w/v) contents containing 5 g of 10% w/w of PVA at room temperature while being continuously stirred by homogenizer as shown in Figure 13.16. Then, the 0.5 benzoyl peroxides (BPO) and different of divinylbenzene (DVB) were added in mixture at ambient temperature with the help of a mechanical stirrer. The mixture was poured onto a glass surface in the form of a sheet 0.55 mm thick, which was dried at ambient temperature and then at 80 °C for 6 h. The dried polymer blend was compressed by compression moulding at 150 °C for 10 h and the resulting sample was kept at ambient temperature overnight.

13.4.2 Mechanical Blending

In dry blending, the rubber composite was prepared using equipment including a two-roll mill, Brabender mixer and extruders. For example, melt blending of polymer PP and NR dust was carried out in a Brabender Plasti-Corder®. Then, cellulose fibre was added in polymer blend during mixing in a Brabender Plasti-Corder®. The conditions are a temperature; rotor speed and residential time are found. The natural rubber gloves (NRG) were segregated from municipal solid waste, cleaned, washed with detergent powder mechanically and dried. Then, the masticated NRG was immersed in toluene for 2 days at ambient temperature and then stirred for 5 h. After stirring with a mechanical stirrer for 1 h, the size and size distribution of the NRG suspended in toluene was measured by a laser particle size analyser. The NRG suspension with various contents was blended with 10% w/v of PSF in toluene at room temperature by using a homogenizer. 0.5% BPO, 5% glycerol and different maleic anhydride

Figure 13.17 Preparation of rubber composite using a two-roll mill (author's experiment).

(MA) concentrations were added into the blend under stirring. In order to form a sheet 0.45 mm thick, the mixture was poured onto a glass plate ($10 \times 10 \times 0.5$ cm^3) at ambient temperature. The polymer blend was mixed with cellulose fibre using a two-roll mill as shown in Figure 13.17. Under a hot press, the rubber composite was preheated to 150 °C for 6 min and then compressed for 4 min before being cooled under 3 MPa at 30 °C for 4 min. In addition, NR and plastic are blended using an extruder. Then, the cellulose fibre was added in mixture at high temperature under continuous mechanical stirring. The parameters such as output rate of rubber composite, barrel temperatures, screw configuration on the properties of rubber composite are investigated.

13.5 NR Composites Reinforced with Natural Fibre

Natural fibres derived from waste renewable resources have received tremendous attention during the past decade. Examples of natural fibres include jute, sugar cane leaves, bagasse and tea waste. In previous work, the different natural fibre types obtained from different sources are blended with NR and more details are given in Table 13.5.[35–41]

The properties of NR composites are controlled by natural fibre content, natural fibre orientation and adhesion between green fibre and NR matrix.[42] The mechanical property of the polymer composite increased. The modulus and hardness and oil resistance of the resulting NR increased with increasing tea leave waste but the tensile strength and elongation at break of the NR compound decreased as a function of tea leave waste. In addition, the NR compound with tea leave and carbon black exhibits excellence in thermal properties. The polymer composite possesses the best properties at 30 phr of modified tea leave with MMA and 30 phr of carbon black.

Table 13.5 Summary of NR composites obtained from different natural fibre types and coupling agents.

Fiber type	*Coupling agent/ coating*	*References*
Bagasse cellulose whiskers (84–102 nm in particle size)	No coupling agent	Bras *et al*., 2010[36]
Sugar cane 1eave fiber	Maleic anhydride	Riyajan *et al*., 2012[35]
Cellulose xanthate	No coupling agent	Ortiz-Serna *et al*., 2011[37]
Nanocellulose jute fibre (5–40 nm)	No coupling agent	Abraham *et al*., 2012[38]
Cellulosenanowhiskers (CNWs) bamboo pulp	No coupling agent	Visakh *et al*., 2012[39]
Cellulose whiskers from cassava bagasse	Silane	Pasquinief *et al*., 2010[40]
Alia pulps and pine fibres	No coupling agent	Abdelmouleh *et al*., 2007[41]
Surface -a cetylated cellulose	No coupling agent	Zhang *et al*., 2008[42]
Bagasse cellulose fiber	Silane	Riyajan & Intharit, 2010[28]

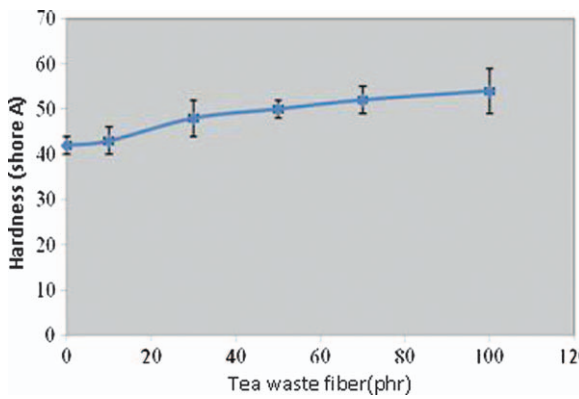

Figure 13.18 Influence of tea waste fibre content on the hardness of a rubber composite (author's experiment).

13.5.1 Tea Waste Fibre

Figure 13.18 shows the effect of tea waste fibre on the hardness of NR composites, showing that the hardness increases as a function of tea waste fibre content.

The modulus and hardness and oil resistance of the resulting NR increased with increasing tea leaf waste but the tensile strength and elongation at break of the NR compound decreased as a function of tea leaf waste. In addition, the NR compound with tea leaves and carbon black exhibits excellence in thermal properties.[43] The polymer composite possesses the best properties at 30 phr of modified tea leave with MMA and 30 phr of carbon black. After the tea leaf waste was modified with PMMA, higher adhesion between NR and tea leaf waste was observed. In addition, the dispersion of tea leaf waste is greatly

improved and the phase interface interaction between rubber and tea leaf waste is markedly enhanced.[43] In case of non-treatment, there are some apparent holes on the fracture surface of the composites, which suggests that the interfacial interaction between the tea leaf waste and rubber is weak.[43]

13.5.2 Oil Palm Ash/Palm Fibre

Cellulose fibre made from palm trees was used to improve the properties of NR and other polymers through blending.[44–51] Asia is the world's largest producer of palm oil. The production of palm oil leads to millions of tons of oil palm waste.[52] At present, the use of solid waste is alternative fuel for steam generation in oil palm mill. The by-product of this process is oil palm ash. The palm as a raw material is used to produce the cellulose nanoparticles. After that, they are used to reinforce with NR matrix.[53,54] For example, Zulkifli and coworkers[44] reported that the stiffness of the NR was significantly increased above its glass–rubber transition temperature upon nanoparticle addition. Jacob and coworkers[45] describe the NR composites from palm obtained by casting/evaporation. They concluded that the stiffness of the NR was significantly increased over the T_g and the favourable interactions between the polymeric matrix and the cellulosic nanoparticles were also found. In addition, the properties of NR composite significantly increased after adding fibre having range 4–12 nm in width. SEM is a common method to analyse the level of fibre/matrix adhesion in polymer composite to evaluate the bonding between matrix and fibre. In addition, SEM is a vital tool for revealing the surface morphology of fibres, the cause of crack initiation and the failure process in composites. The interfacial adhesion as a function of fibre loading of sisal–oil palm hybrid reinforced NR composites was analysed by Jacob *et al.*[45] The authors found that at low and high levels of fibre loading the interfacial adhesion was quite poor while at intermediate levels of loading interfacial adhesion was found to be good as the population of fibres was just right for uniform stress transfer. Alkali treatment increased the tensile strength of the composites compared to untreated composites and the maximum tensile strength was observed for composites prepared with 4% NaOH treated fibres.[52] Composites prepared from fluorosilane-treated fibres exhibited better mechanical among the other silane treated composites. This suggest that for composites treated with 4% NaOH there exists a strong interface due to better adhesion between rubber and fibre and this prevents the entry of solvent and results in minimum swelling. Surface characterization by XPS showed the presence of numerous elements on the surface of the fibre. Anisotropic swelling studies revealed that composite containing fluorosilane treated fibre reinforced composites has the highest degree of fibre alignment.

13.5.3 Bagasse Whiskers and Baggage Fibre

Bras and coworkers[36] studied the composite from NR and the bagasse whiskers which resulted in an increase in moisture sorption of rubber films up to 5%

whiskers loading while at higher whiskers fibre loading the moisture sorption tended to decrease. The mechanical properties of the NR composite increased as a function of cellulose whiskers. The advantage of the composite is well biodegradable in nature. The achievement in the preparation of polymer composite was obtained from NR, bagasse and plaster. The chemical stretching of the modified bagasse showed the occurrence of Si–CH_3 group after chemical modification. The roughness of bagasse modified with sodium hydroxide was higher than that of unmodified bagasse while the adhesion forces of modified bagasse decreased after sodium hydroxide modification, leading to remove fatty acid from sugar cane. The techniques for evaluation between fibre and matrix are pull-out test, indentation test and single-fibre fragmentation test. But the adhesion between fibre and rubber matrix was investigated by SEM and swelling behaviour for this work. The torque of the polymer composite increased with increasing both plaster content and bagasse. The modulus of the polymer composite increased as a function of the both sugar cane bagasse and plaster contents in polymer composite. But the both tensile strength and elongation at break of the polymer composite decreased dramatically with increase in both plaster and sugar cane bagasse. When the addition of both bagasse and plaster in NR matrix was subjected to this system, curing time at t_{c90} of sample decreased as a function of cellulose fibre as shown in Figure 13.19(a). In addition, the torque of the polymer composite increased with increasing bagasse content, as shown in Figure 13.19(b). When the sugar cane bagasse kraft pulp was digested into cellulose whiskers with a length of 84–102 nm and a width of 4–12 nm.[53] They were then used as reinforcing elements for NR composites. Significant improvement in Young's modulus and tensile strength was observed as a result of addition of whiskers to the rubber matrix, especially at high whisker loadings. DMTA results showed no change in the glass transition temperature (T_g) of the rubber matrix upon addition of cellulose whiskers but at softening of rubber, cellulose whiskers have reinforcing effect on the rubber. At low temperature, the modulus remains roughly constant and the addition of the whiskers does not increase it significantly. This could be ascribed to the fact that in this temperature range NR is in the glassy state and the difference between the modulus of the host matrix and the reinforcing phase is not high enough to generate a significant reinforcing effect. Then a sharp decrease of log (E') is observed around -55 °C, corresponding to the main relaxation phenomenon of the matrix, associated to its glass transition.

13.5.4 Coir Fibre/Coconut Fibre (Cofibre)

In the previous work, the coir fibres which is obtained from the coconut husks, they may be classified according to the peeled off time from the husks are used as reinforced filler in NR compound.[55–58] The properties of brown cofibre show highly resistance to abrasion. Usually, they are primarily used in brushes, floor mats and upholstery padding. In case of white cofibre, it is made from the husks of coconuts shortly before they ripen. The white fibre is softer and less strong

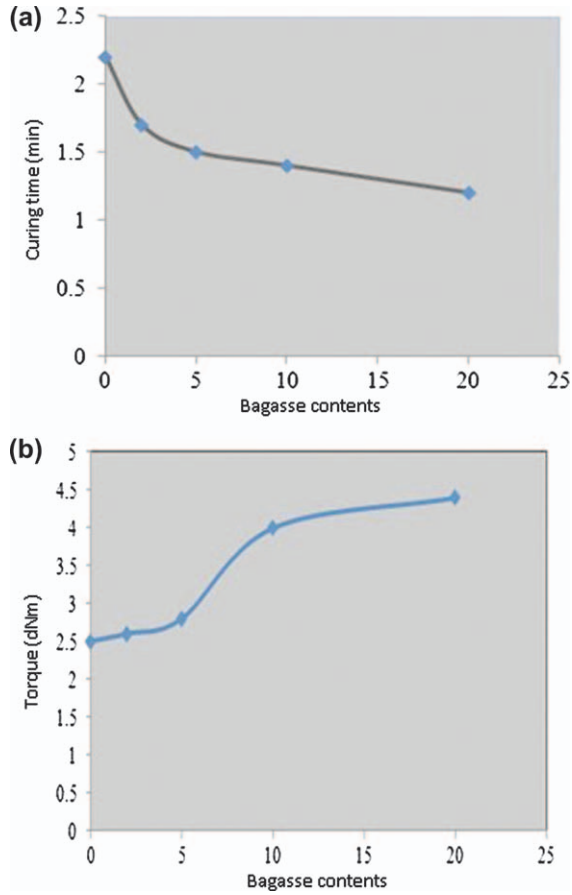

Figure 13.19 Effect of sugar cane content on (a) curing time and (b) torque of a composite (author's experiment).

comparing to brown fibre. The application of white cofibre was mats or twisted into twine or rope. About 60 billion coconuts are harvested annually in the world; roughly 20% of the husk fibres is actually recovered for use.[56] The effect of cofibre on the tensile strength of polymer composites is shown in Figure 13.20. The highest tensile strength was observed in a sample containing 10% cofibre. After adding 5% cofibre, the tensile strength of the rubber composite decreased. This result explained that the reduction of the tensile strength can be attribution to the more de-wetting of NR matrix at the interface between NR and filler and more agglomeration of plaster, leading to the generation of a weak structure because stress concentrations are created.[27,28] The highest tensile strength was observed in a sample containing 10% cofibre, which generates an improvement of tensile strength of up to 5 MPa. This result explains that this composite possess a good dispersion of cofibre in polymer matrix, leading to a more effective transfer of stress from NR matrix to bagasse

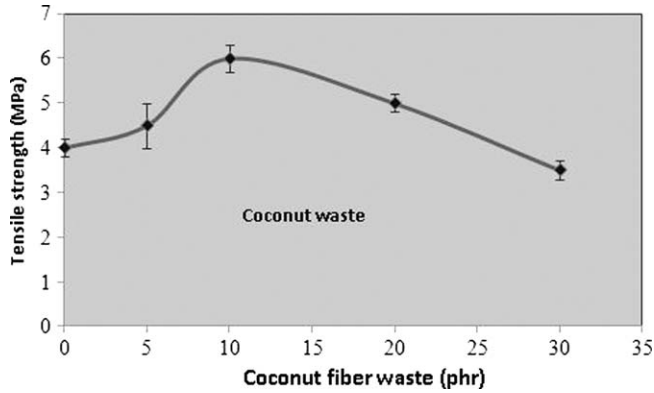

Figure 13.20 Effect of coconut fibre content on tensile strength of a NR composite (author's experiment).

and plaster. When cofibre increases from 10 phr to 20 phr in a rubber composite, the tensile strength of the rubber composite dramatically decreased because of the formation of voids in the rubber composite.

13.5.5 Jute Fibre

Jute is a shiny vegetable fibre obtained from Corchorus. It can be spun into coarse, strong threads. Many jute sources are found in Asia. Jute fibres consist of cellulose (major component of plant fibre) and lignin (major components of wood fibre). It is thus a lignocellulosic fibre that is partially a textile fibre and partially wood. The jute fibre was used to improve the mechanical properties of NR.[59–64] First, the jute fabrics (hessian cloth) reinforced NR matrix composites (30% fibre by weight) were prepared by compression moulding. Tensile strength and percentage elongation at break of the composites were found to be 14 MPa and 94%, respectively. In addition, the degradation of the composites were performed in aqueous medium and it was found that jute/NR composites lost much of its original strength and modulus compared to that of the jute/PP composites for 6 weeks. The interfacial shear strength of jute/PP and jute/NR systems appeared to be 2.16 and 0.89 MPa, respectively. In addition, after adding jute fibre in NR matrix, its composite for noise reduction in household appliances, automotive and architectural applications was done observing from acoustical and fibre-retardant properties.[60] Results showed that the low density jute is a better sound absorber as compared to high density jute material. Moreover, NR composite reinforced with jute gives higher sound transmission class value than jute felt/cloth. Considering to fire retardant tests, it was found that composite's high limiting oxygen index value as compared to fibreboard and low light absorption with respect to glass fibre as well as self-extinguishing ability.

The biodegradation of the composites of NR reinforced with nano-cellulose from jute fibre by steam explosion was studied by vermicomposting method

with reference to the crosslinking of the matrix.[61] The rate of biodegradation of the NR composite increased as a function of nano-cellulose. The rate of biodegradation of the NR composites indicates that the cellulose has to be hydrolysed before microorganisms can utilise it as a nutrient source. In addition, after jute fabric was coated with NR, it was developed to use double-texture rubberized waterproof fabric and fabric-reinforced rubber sheeting for hospitals.[62,63] Results showed that the jute/NR composite was much superior to a conventional polyester/NR composite for producing such double-texture rubberized fabric with respect to the fabric-to-NR adhesion, breaking strength, tear strength, abrasion resistance, puncture resistance and biodegradability.

13.5.6 Chemistry of the Interface Modification and Characterization

The possible mechanism of grafting maleated sulfur pre-vulcanized NR (M-SPNR) with cellulose fibre by using benzyl peroxide (BPO) and $K_2S_2O_8$ at 80 °C is shown in Figure 13.21. Free radicals from BPO activate the carbon–carbon double bonds of MA, which then react with carbon–carbon double bonds of SPNR molecules activated by $K_2S_2O_8$ to form the M-SPNR. When the M-SPNR reacts with cellulose fibre, the M-SPNR-*g*-cellulose fibre is

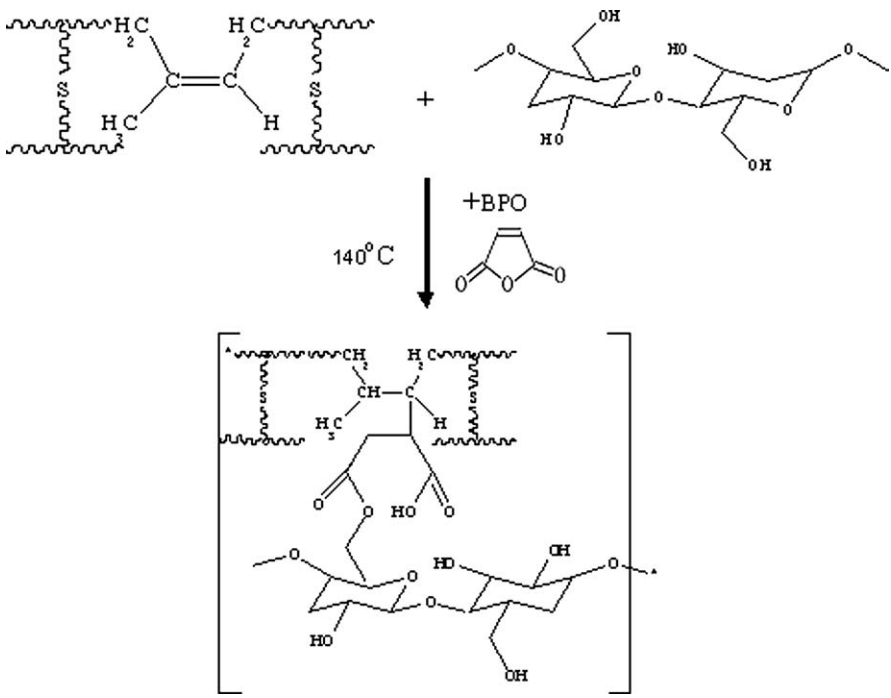

Figure 13.21 Possible mechanism of grafting M-SPNR with cellulose fibre in the presence of potassium persulfate.

obtained. The crosslink between M-SPNR and cellulose fibre may also occur through MA bridging. FTIR was used to investigate the chemical reaction at the interface between fibre and polymer matrix.[35] The presence of grafted anhydride on SPNR molecules was confirmed by a broad and intense characteristic band at 1780–1784 cm^{-1} and a weak absorption band at 1854 cm^{-1} assigned to symmetric (strong) and asymmetric (weak) C=O stretching vibrations of succinic anhydride rings, respectively. The grafted MA was also deduced from the absorbance ratio of FTIR peaks at 1780–1784 cm^{-1} and 1854 cm^{-1} to 835 cm^{-1} (–C–H stretch on *cis* C=C bonds of *cis*-1,4-polyisoprene). The weak band at 3045 cm^{-1} was attributed to an intramolecular hydrogen stretching bond from the maleate conformation. After chemical modification of M-SPNR with cellulose fibre, the new functional group was formed. It was expected to be the carboxylic group corresponding to the bands at two bands 2530 and 3450 cm^{-1} and 1734–1724 cm^{-1} assigned to ester group in SPNR-*g*-cellulose fibre.

Abdelmouleh and coworkers[64] studied the chemical reaction between cellulose fibres modified with three silane coupling agents, namely methacryloxypropyltrimethoxy (MPS), c-mercaptopropyltrimethoxy (MRPS) and hexadecyltrimethoxysilanes (HDS) and NR matrix, as shown in Figure 13.22. The modified cellulose reacted with free radicals at the C–C double bonds of

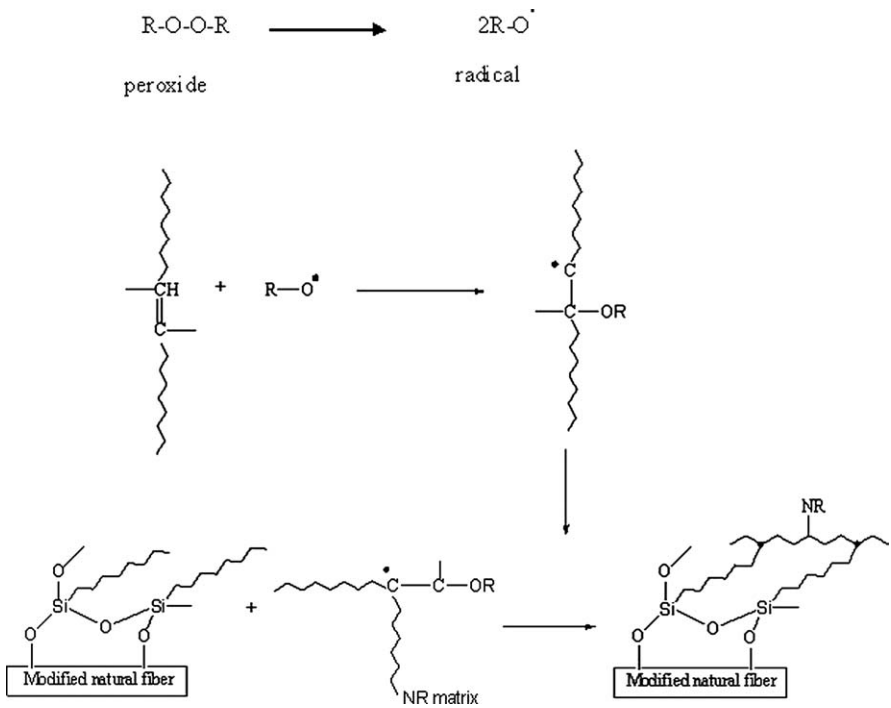

Figure 13.22 Possible mechanism of NR containing the modified cellulose fibre with silane (modified from ref. 11).

NR, which are activated with peroxide through a radical grafting reaction between the –C=C– unsaturation of NR and terminal acrylic moieties of MPS or –SH groups of MRPS. The radical species could be generated from peroxy (or similar) formed during the evaporation period. These results confirm again that reactive silane coupling agents are suitable for the modification of cellulose fibres, as reinforcing elements for non-polar thermoplastic polymeric matrices, leading to good mechanical properties.

Evidence of a better enhancement of the fibre–NR adhesion is also confirmed by SEM.[63] This reveals that the fibres are totally fractured under at the surface level when they are treated with MPS or MRPS. But in case of non-treatment, some pulling out occurs observing from SEM. The reactive MPS and MRPS reactive silane is related to their ability to react with the matrix during the curing process and their capacity to establish covalent bonds between the fibres and the matrix through the interface, thus enhancing the adhesion between the two phases. Recently, Abraham and coworkers studied the mechanism between NR matrix, nano-cellulose and crosslinking agent.[62] No crystalline peak of the cellulose is observed. This is due to NR make chemical bonds with nano-cellulose through Zn–cellulose complex which will result in the loss of its crystallinity. The nano-cellulose and the crosslinking agents enter in between the layers of NR bonds with each other. Moreover, cellulose units react with zinc to form a Zn–cellulose complex. This phenomena results a good dispersion of nano-cellulose in NR matrix which will leads to the loss of crystallinity of cellulose in polymer composites.

13.6 ENR/Biodegradable Polymers Reinforced with Cellulose Fibre

In the case of epoxidized natural rubber (ENR), its properties were improved by adding natural fibre.[65,66] For example, the effect of oil palm empty fruit bunch (OPEFB) and poly(methyl acrylate) grafted OPEFB fibre on the properties of poly(vinyl chloride)/ENR (PVC/ENR) blends under irradiation were studied.[65] The grafting of the OPEFB fibre with methyl acrylate did not cause any appreciable effect on the tensile properties and gel fraction of the composites upon irradiation. The adhesion between the fibre and the matrix was achieved upon grafting of the fibre with methyl acrylate was observed from SEM. The water resistance of the green blend was improved by addition of sugar cane leaf fibre observing from swelling ratio. The swelling ratios of the polymer blend decrease as a function of cofibre, as shown in Figure 13.23. The swelling index, which is a measure of the swelling resistance of the rubber compound, is calculated using Equation (13.2):

$$\text{Swelling ratio} = (W_2 - W_1) / W_1 \tag{13.2}$$

where W_1 = original weight of the sample and W_2 = weight of swollen sample.

Figure 13.24 represents the influence of cofibre on the tensile strength of rubber composites. Results showed that the tensile strength of rubber blend

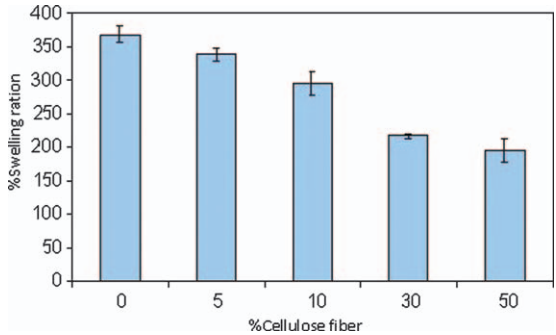

Figure 13.23 Effect of cofibre content on swelling ratio of PVA/starch/ENR blends (author's experiment).

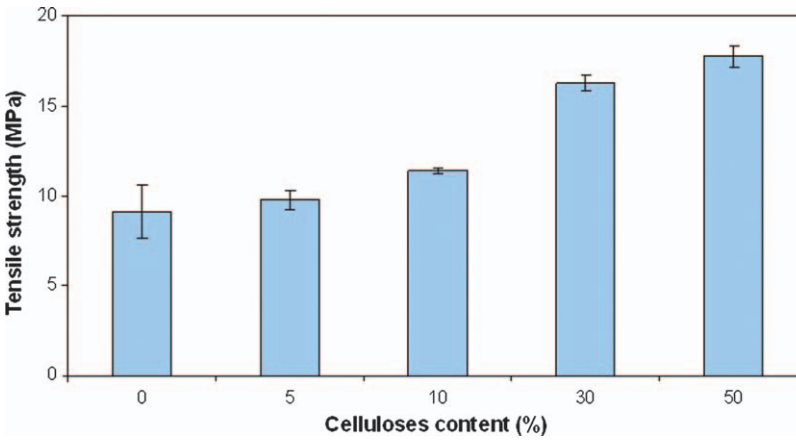

Figure 13.24 Effect of cellulose fibre content on tensile strength of PVA/starch/ENR (8/2/3) blend (author's experiment).

increased as a function of the cellulose fibre. The tensile strength of rubber composite was higher than that of rubber blend due to reinforcement of fibre.

The fibre dispersed in polymer blend matrix was confirmed by SEM. The effects of ENR content on the swelling ratio of composite beads immersed in water for 12 h and the Pb^{2+} adsorption are presented in Figure 13.25. With increasing ENR content, the swelling ratios of composite beads decreased because of the hydrophobicity of ENR as shown in Figure 13.23. In the present work, the novel adsorbent in the form of bead composing of NaAlg blended with ENR before being crosslinked with $CaCl_2$ was prepared. Since ENR displays high elasticity, high strength and high water resistance, it would help to reduce the swelling ratio of NaAlg beads in water and increase the bead stability.[67] The composite beads could be easily used for metal ion adsorption due to the convenient separation from waste water by filtration.

The effects of % cofibre in composite beads and bead dosage on the Pb^{2+} adsorption are shown in Figure 13.26. The data showed that the Pb^{2+}

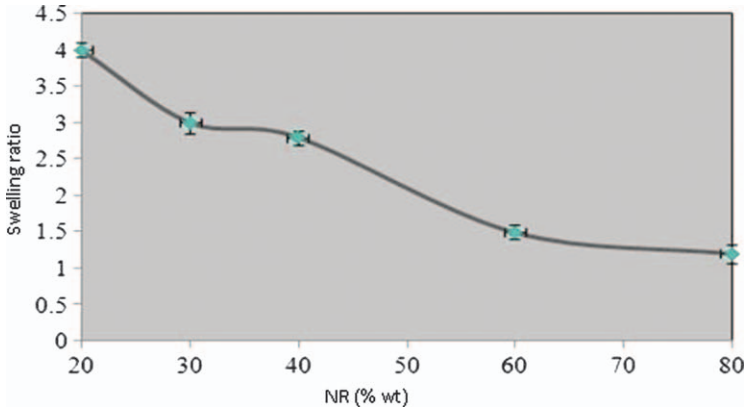

Figure 13.25 Effect of NR content on swelling ratio of bead containing 7.5% cofibre (author's experiment).

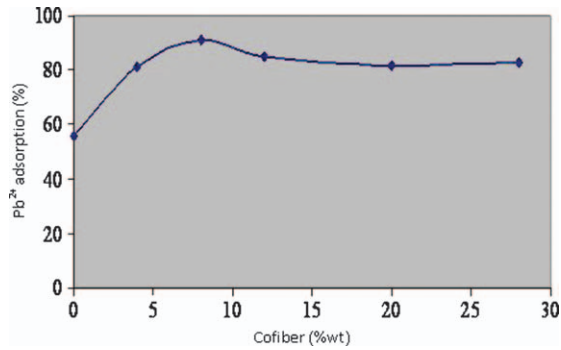

Figure 13.26 Effect of cofibre content on Pb^{2+} adsorption of bead at Pb^{2+} concentration of 40 mg/L, at 25 °C (author's experiment).

adsorption increased when increasing cofibre until 7.5% and then nearly constant. This was resulted from the increase in the roughness of bead, *i.e.* adsorbed site, as mentioned above.[68] At $>7.5\%$ cofibre, the Pb^{2+} adsorption slightly decreased due to encapsulated cofibre in matrix. Since the maximum Pb^{2+} adsorption of 92% was obtained when using 7.5% cofibre, this cofibre content was used for further study.

13.7 NR/Synthetic Polymer Blends Reinforced with Natural Fibre

13.7.1 NR/Polystyrene Foam Waste (PSf) Blends

The phase morphology of NR/PSf blends depends on blend ratio, crosslinker level and initiating systems.

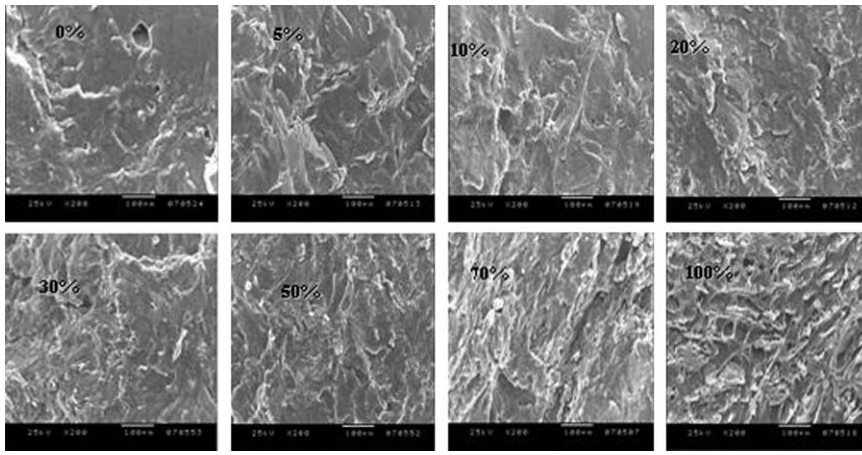

Figure 13.27 SEM images of 40/60 NR/PSf 6% MA with different cofibre content (author's experiment).

SEM micrographs of fracture surfaces of NR/PSf blend and NR/PS blends are shown in Figure 13.27. The cofibres are homogeneously distributed in the NR matrix. The adhesion between SPNR with cofibers at less than 50 phr appears to be good. These results support swelling ratio. But at higher than 50 phr of cofibre, the adhesion between SPNR and cofibre was poor, as observed from voids in the SPNR-*g*-cofibre. The properties of a blend depend on the crosslink density of the elastomer, the crosslink density of the plastic, and the elastomer/plastic ratio as well as filler (cofibre) in detail as follows.

Swelling Behaviour and Solvent Resistance

The diffusion mechanism in rubbers is essentially connected with the ability of the polymer to provide pathways for the solvent to progress in the form of randomly generated voids. The swelling ratio of blend sample was estimated by Equation (13.2). As the void formation decreases with addition of cofibre, the solvent uptake also decreases, as shown in Figure 13.28. But when adding over 70 phr cofibre, the swelling ratio of the polymer blend slightly decreased due to excess void. The presence of bonding agent binds the alkali treated fibre and rubber so that swelling is highly restricted in the composite.

The influence factors of SPNR/PSf ratio on swelling ratio of blend were investigated as shown in Figure 13.29. The lowest swelling ratio of the polymer blend was observed at 40/60 SPNR/PSf.

The influence of NRG/PSf blend ratio on toluene resistance is shown in Figure 13.30. At high NRG content, good dimensional stability was recorded due to more NRG portion in blend. The optical micrographs of PSf blended with 5% cofibre and various amounts of MA (0, 5, 10 and 15%) after immersion in toluene are shown in Figure 13.30(e). The good dimensional stability of PSf/cofibre added with MA especially of 15% was observed in

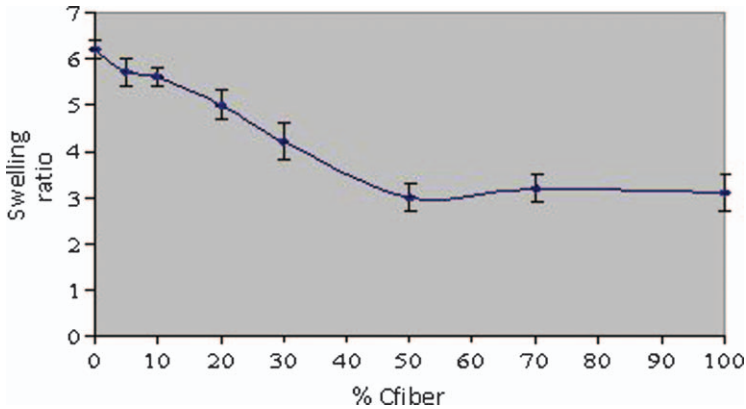

Figure 13.28 Effect of cofibre content on the swelling ratio of the polymer composite at different cofibre contents (author's experiment).

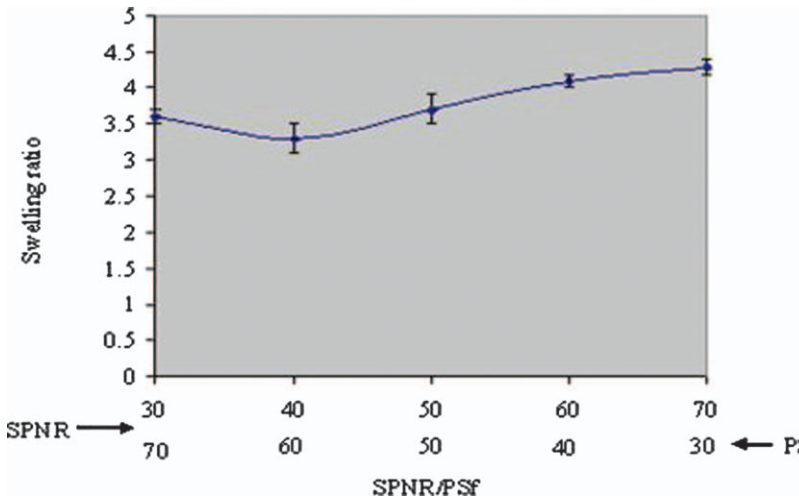

Figure 13.29 Effect of blend ratio on swelling ratio of the polymer composite at 50% cofibre (author's experiment).

Figure 13.30(e). This result indicated the occurrence of chemical interaction between PSf and MA or between cofibre and MA during blending process. The swelling ratio of the polymer composite film immersed in toluene at ambient temperature for 5 days was used to confirm the chemical reaction between MA and SPNR/PSf as well as cofibre. The swelling ratio of the polymer composite dramatically decreased as a function of the cofibre. The effect of MA content on the swelling of the polymer blend is shown in Figure 13.31. The swelling ratio of the polymer decreases with increasing MA. The swelling ratio of the polymer blend 50/50 sulfur pre-vulcanized NR (SPNR)/NR containing 0, 2.5, 6 and 9 MA% was 3.8, 3.6, 3.4 and 3.2, respectively.

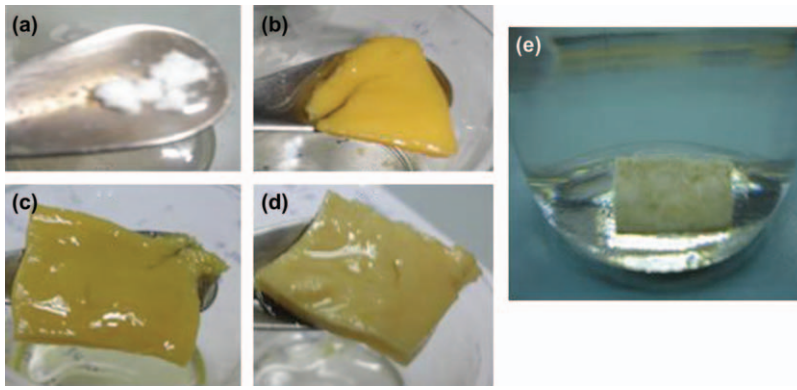

Figure 13.30 IPN sample resistances in organic solvent (a) 20 : 80, (b) 30/70, (c) 50/50 and (d) 30/70 NRG/PS blend, as well as (e) 50/50 NRG/PS in the presence of 40% cofibre (author's experiment).

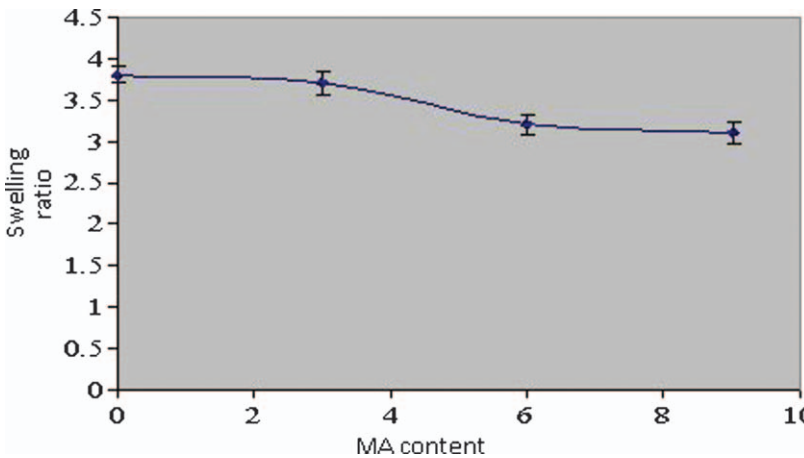

Figure 13.31 Effect of MA content on the swelling ratio of the polymer composites at 50/50 SPNR/PSf (author's experiment).

In order to develop novel materials, PSf was simply blended with NRG in this present study. The effect of cassava starch (Cs) or gelatinized Cs (GCs) and its content on swelling ratio of the polymer blend was investigated. With increasing the starch contents from 0, 5, 10, 15 to 20%, the swelling ratio of the polymer blend having Cs decreased from 2.7, 2.4, 2.3, 1.8 to 1.7 while that containing GCs decreased from 2.2, 2.1, 1.6 to 1.4, respectively, as shown in Figure 13.32. The swelling ratio of GCs was lower than that of Cs because the gelatinization process broke down the intermolecular bonds of Cs granules containing both linear amylose and branched amylopectin. Hence, the hydrogen bonding sites (hydroxyl hydrogen and oxygen) engaged more water and irreversibly dissolves Cs granules. Penetration of water at high temperature

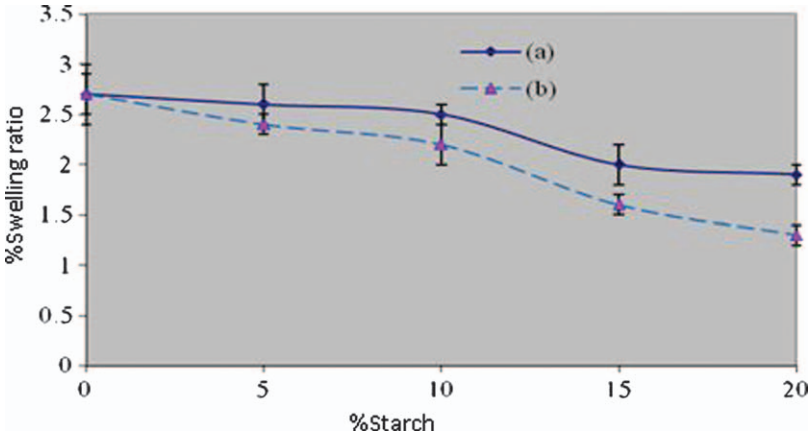

Figure 13.32 Effect of (a) Cs and (b) GCs on the swelling ratio of NRG/PSf blends (author's experiment).

increased randomness in the granule structure and decreased the number and size of crystalline regions. Therefore, the swelling ratio of the polymer blend in the presence of GCs in toluene was lower than that of sample containing Cs. The linear amylose and branched amylopectin chains from starch might migrate to the surface of polymer blend sheet and prevented the adsorption of the non-polar solvent.

Tensile Strength

The tensile strength of SPNR/PS blends was improving by adding carbon black. At 30 phr, the highest tensile strength of NR/PS blend was achieved. The values of tensile strength of the SPNR/PS blend sheets at various cofibre contents are illustrated in Figure 13.33. The tensile strength of the blend increased as a function of cofibre content. The highest tensile strength of the polymer blend was found at 50% cofibre. Since the cofibre exhibits reinforcement filler in polymer blend. In addition, the tensile strength of blend increase is due to the interaction and interlocking of SPNR and PSf networks, which result in the reinforcement of the SPNR phase. However, the tensile strength of the blend sample dramatically decreased after adding over 50 phr due to void formation in sample. The tensile strength of the samples having 5, 10, 20, 30, 50, 70 and 100% w/w of natural cofibre were 3.0, 3.8, 4.0, 4.8, 6.5, 6.0 and 5.5 MPa, respectively, while that of the SPNR/PSf without cofibre was 1.0 MPa.

Figure 13.34 represents the influence of MA on the tensile strength of the NR/PSf blend. It was clear that the tensile strength of the IPN sample dramatically increased as a function of the MA.

These results agree with the tensile results. The possible grafting reaction between NR/PSf, MA and cofibre is reported in Figure 13.35. BPO decomposed into free radicals which then react with carbon–carbon double

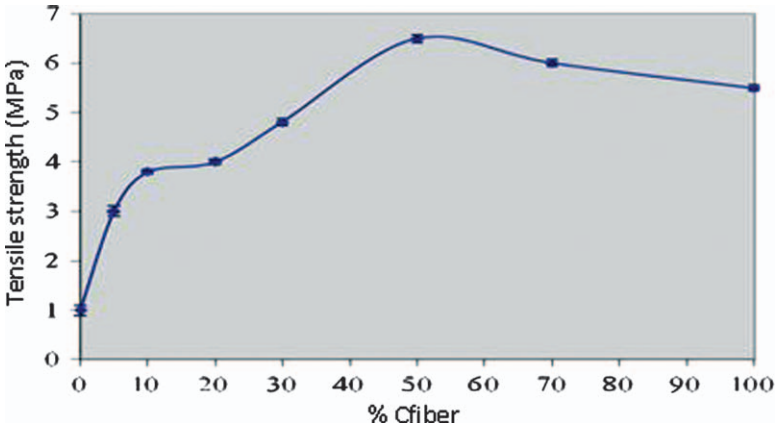

Figure 13.33 Effect of cofibre content on the tensile strength of the 50/50 SPNR/PSf blend (author's experiment).

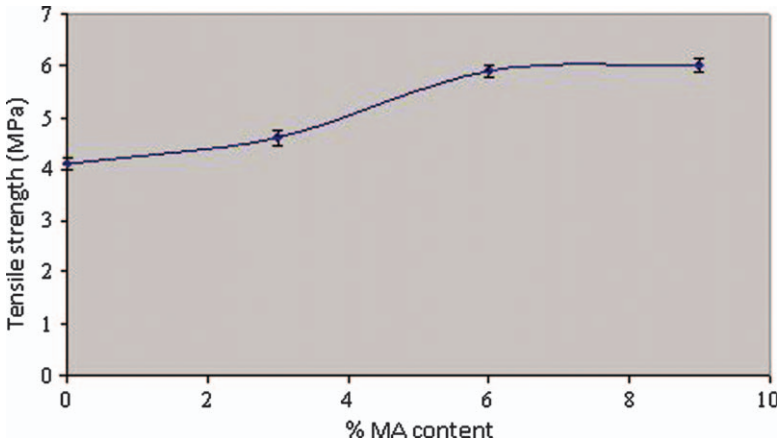

Figure 13.34 Effect of MA content on the tensile strength of the 50/50 NSPR/PSf blend (author's experiment).

bonds of MA and NR molecule.[28] Besides the grafting of MA on both *cis*-1,4-polyisoprene of rubber and cofibre. In addition, the crosslink product from NR molecules through MA bridging or cellulose and MA could be also obtained. The maleated SPNR continued to react with cellulose. The detailed reaction of the maleated SPNR grafted with cofibre is presented in Figure 13.35.

The elongations at break of the polymer blend increase with increasing cofibre up to 50%w/w of cofibre as shown in Figure 13.36. After that, the elongation at break of the polymer blend decreased after adding over 50%w/w PSf because phase separation occurs. In addition, this is due to the plastic nature and lower elongation of PSf in comparison with SPNR. The effect of SPNR/PS on the elongation at break of the rubber composite is presented in

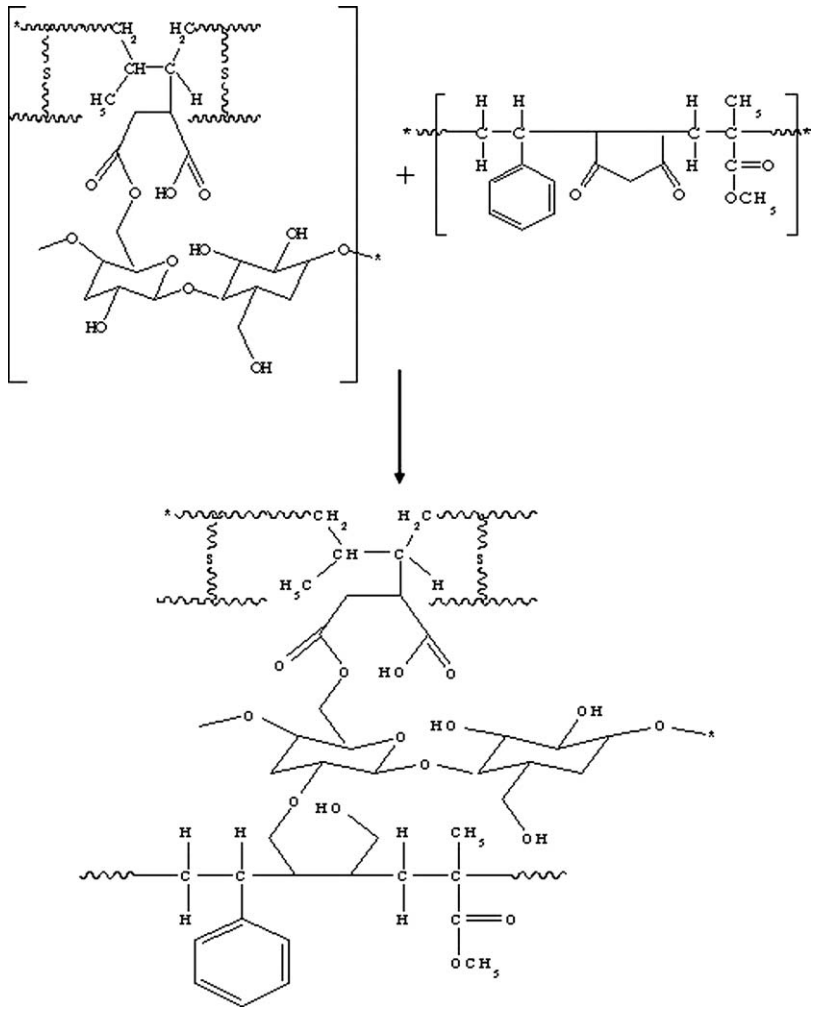

Figure 13.35 Possible reaction of IPN made from SPNR latex and polystyrene foam.

Figure 13.37. It is clear that the elongation at break of the polymer blend increases as a function of SPNR content of the sample. But at high PS content and high extent of PS crosslinking, the agglomeration of plastic phase was observed, which resulted in reduced phase mixing to reduce the elongation at break.

Modulus

The influence of the cofibre of the modulus of polymer blend is shown in Figure 13.38. It is clear that the modulus of the polymer blend increased as a function cofibre until to reach 50% cellulose. This result agrees with tensile strength and elongation at break. After that, it decreased after adding over

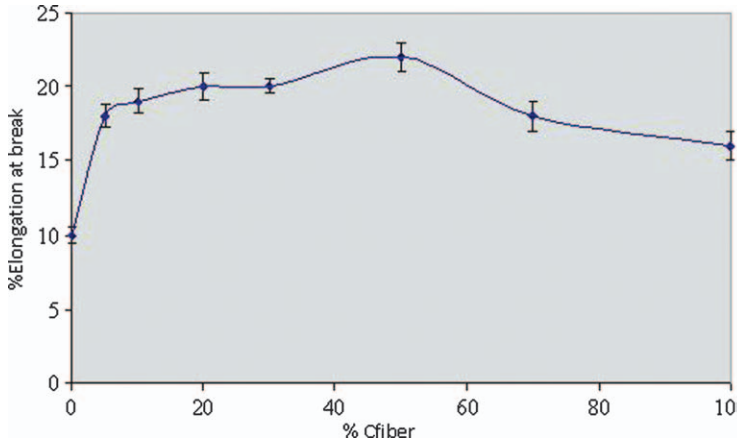

Figure 13.36 Effect of cofibre content on the elongation at break of the 50/50 SPNR/PS blend (author's experiment).

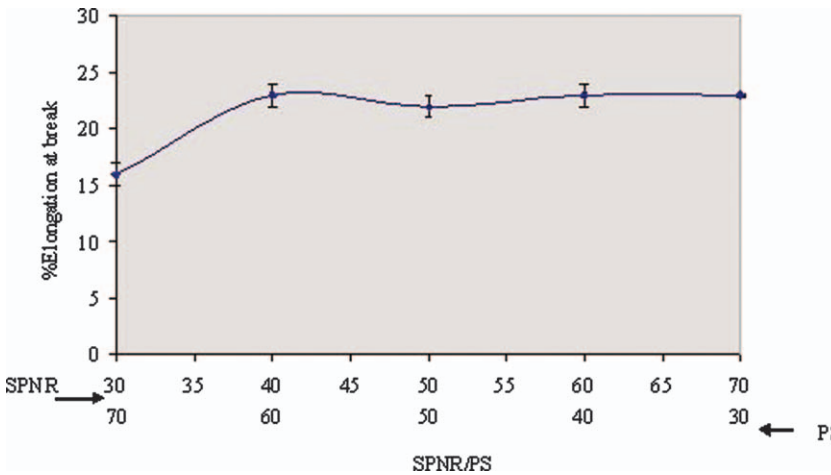

Figure 13.37 Effect of SPNR/PS ratio on elongation at break of the 50/50 SPNR/PS blend (author's experiment).

50%. The influence of SPNR/PS blend ratio on the modulus of the rubber composite is shown in Figure 13.39. The highest modulus was observed at 60/40 SPNR/PSf.

Hardness

Figure 13.40 shows the hardness of SPNR and semi-SPNR/PSf. It was found that the hardness of NR/PSf was 78 Shore A, whereas that of the SPNR/PSf containing different amounts of cofibre was ~79–88 Shore A. The results indicate the change in composition of the IPN sample after addition of cofibre. This result agreed well with that of the tensile strength.

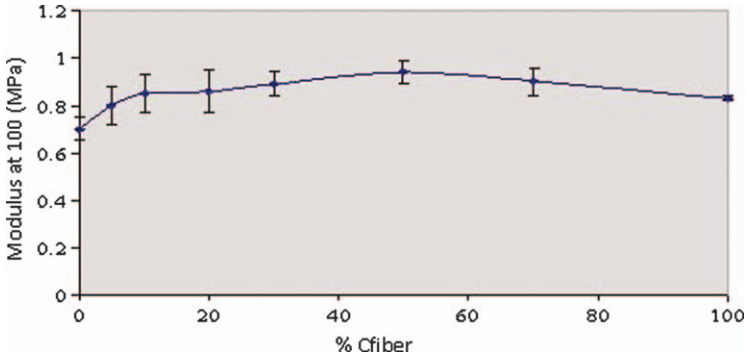

Figure 13.38 Effect of cofibre on elongation at break of the 50/50 SPNR/PS blend (author's experiment).

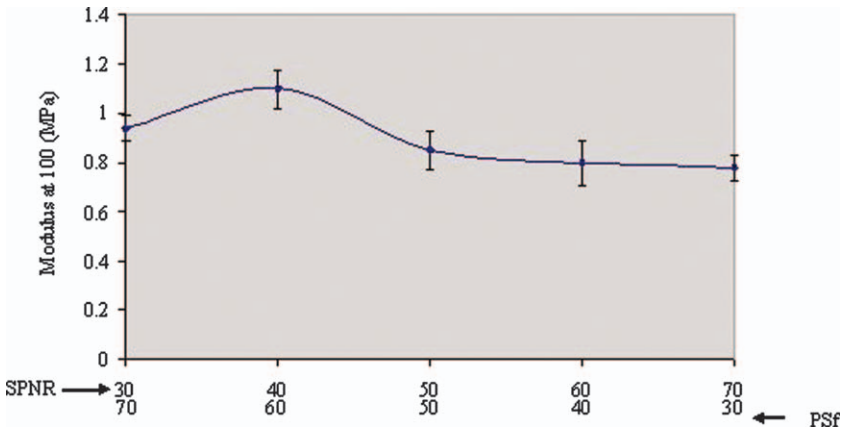

Figure 13.39 Effect of SPNR/PSf ratio on elongation at break of the SPNR/PSf polymer blend (author's experiment).

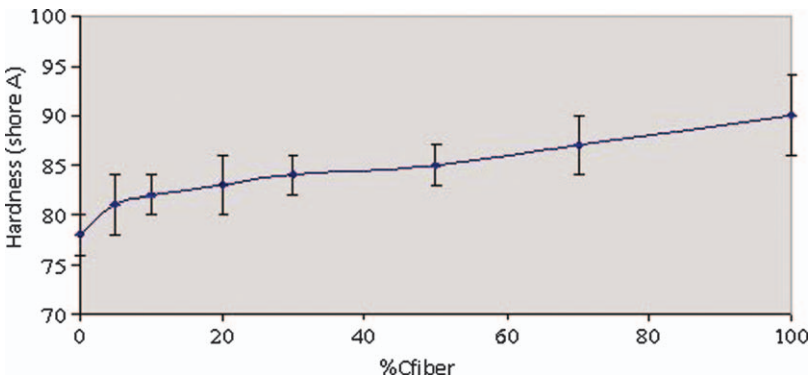

Figure 13.40 Effect of cofibre content on hardness of the 50/50 SPNR/PS blend (author's experiment).

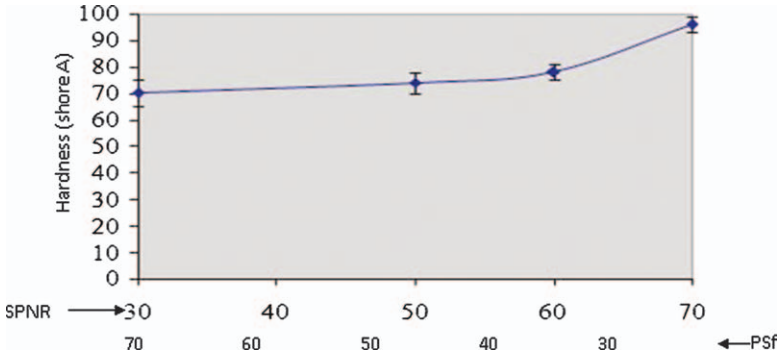

Figure 13.41 Effect of SPNR/PSf ratio on the hardness of the semi-IPN samples (author's experiment).

The effect of SPNR/PSf on the hardness of the polymer blend is shown in Figure 13.41. The hardness of the polymer blend decreases as a function of SPNR content in the sample due to the nature of SPNR. These results agree with those of Sabu and coworkers.[69] They found that samples with high plastic content have a tendency to undergo ductile deformation. As PS content decreases and NR content increases the elastic nature of the specimen also increases, thus resulting in a low set value. The PSf sample undergoes brittle fracture without undergoing any elongation. So the set is zero. In pure NR, due to elasticity, the sample after elongation recovers almost fully, and the set is zero when the crosslinking of the samples increases. However the brittleness increases as PSf crosslinking increases, *i.e.* set tend to decrease with increase in crosslinker level. The tear strength and hardness increase with increase in PS content.

In addition, the hardness of the rubber composite was improved by the addition of plaster, as shown in Figure 13.42. The hardness of the sample increased as a function of plaster content, with the highest hardness occurring with 100 wt% plaster.

Impact Strength

An impact-15 resilience test pendulum impact tester was applied to determine impact resistance at 25–28 °C. The impact strength of the IPN increased when PSf crosslinker level increases up to 4%. In addition, 30/70 SPNR/PS blend exhibits the maximum impact strength values. The effect of cofibre on the impact strength of the polymer blend is presented in Figure 13.43. It is clear that the impact strength of rubber composite increased with increasing cofibre to reach a 50% cofibre. After that, when adding over 50 phr cofibre, the impact strength of rubber composite dramatically decrease due to occurrence of void in IPN sample. The influence of SPNR/PS blend ratio on the impact strength is presented in Figure 13.44. Results showed that the impact strength of rubber composite increase with increasing the amount of NR due to from the ductile fracture initiated by the shear yielding mechanism.[70] Due to the low T_g of

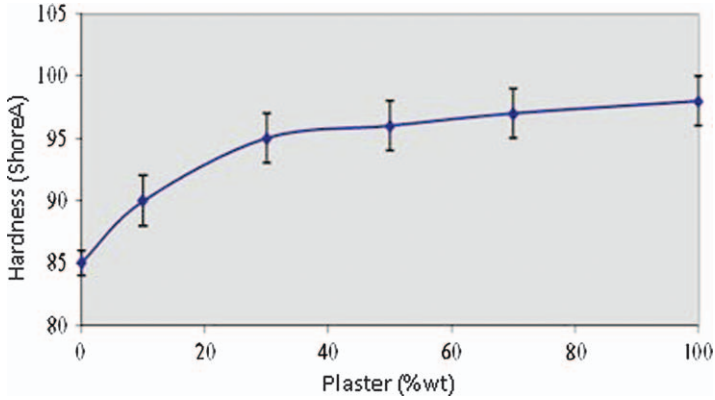

Figure 13.42 Effect of plaster content on the hardness of the semi-IPN 50/50 SPNR/PSf blend containing 50% cofibre (author's experiment).

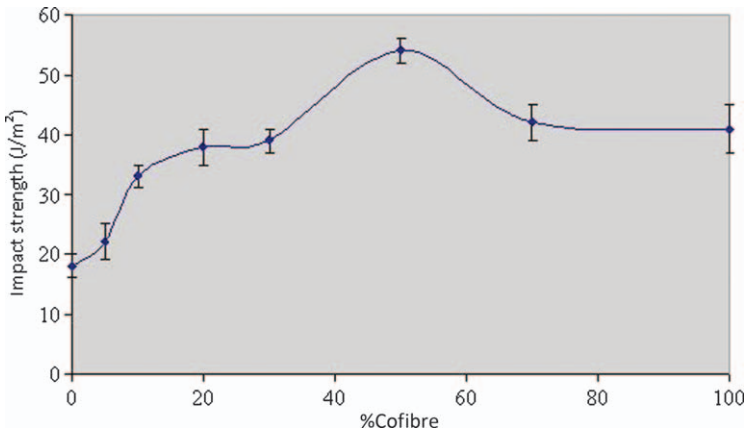

Figure 13.43 Effect of cofibre content on impact strength of the 50/50 SPNR/PSf blend (author's experiment).

SPNR (−78 °C), the SPNR chains easily moved at room temperature and played the role of toughening agent. The dual phase continuity and phase interpenetration might also enhance the impact resistance. It was reported that the co-continuous blend structure exhibited high impact strength of polymer composite because the uniform rubbery phase allowed the energy to be dissipated into the whole sample.[70] This effective dissipation of energy was the principal role of rubbery phase in impact resistant materials. When adding SPNR was over 50% in rubber composite the impact strength of polymer blend decreased. This results are explained that the poor miscibility between SPNR and PSf. The highest impact strength was observed in 40/60 SPNR/PSf blend.

Figure 13.45 shows schematic representations of two characteristic fracture failure profiles of a sample including brittle and ductile behaviour.

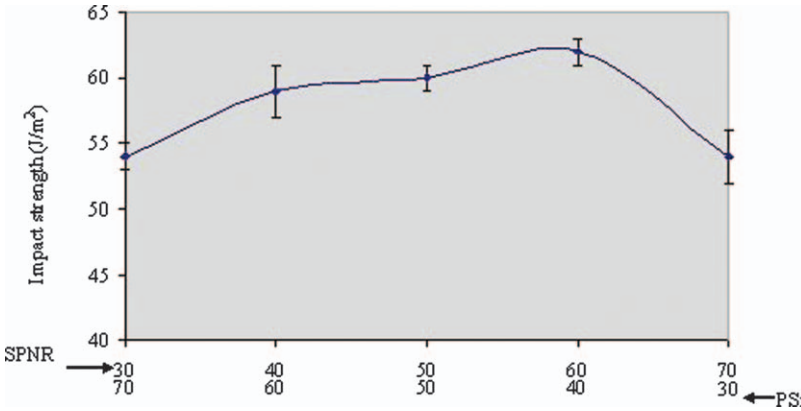

Figure 13.44 Effect of SPNR/PS and MA on impact strength of the SPNR/PS polymer blend (author's experiment).

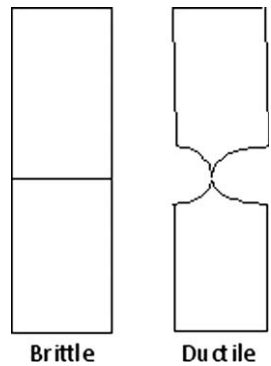

Figure 13.45 (a) Brittle fracture of IPN sample without any plastic deformation and (b) ductile fracture of IPN sample in which the specimen necks down to a point.

After a hard sample (high PSf) receives a load, brittle fracture occurs without any appreciable deformation and by rapid crack propagation, as shown in Figure 13.45(a). In addition, the direction of crack motion is very nearly perpendicular to the direction of load tensile stress. In the case of a ductile sample (high SPNR), it is shown to neck down to a point fracture, showing almost 100% reduction in area.

Tear Strength

Figure 13.46 shows that the tear strength of SPNR/PSf blends increases as a function of cofibre content. The lower tear strength of SPNR/PSf blends containing over 50%w/w cofibre was observed comparing to SPNR/PSf blend containing 50 cofibre. The effect of SPNR/PSf and MA on the tear strength is shown in Figure 13.46. The highest tear strength of the polymer blend was found to be 20/80 SPNR/PSf. The reason for this trend may be the brittleness

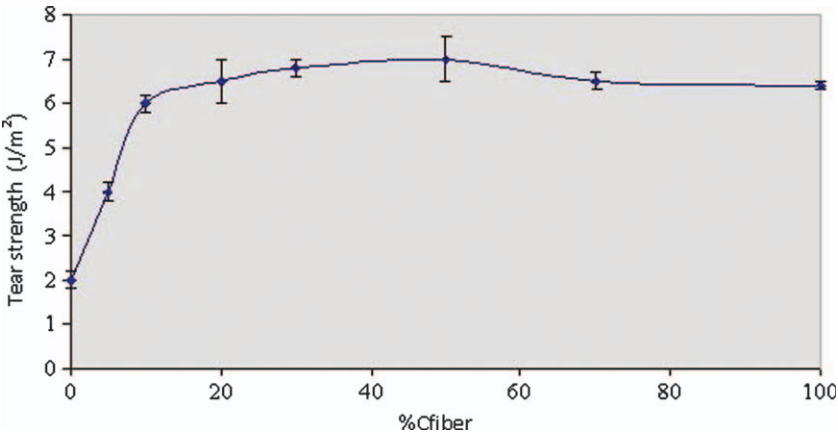

Figure 13.46 Effect of cofibre content on tear strength of the 50/50 SPNR/PSf polymer blend (author's experiment).

Table 13.6 Parameters affecting mechanism failure types of polymer composites.

Factor	*Failure type*
Low crosslinker High NR Low filler	Ductile behavior
High crosslinker High PS High Filler	Brittle behavior

of the samples caused by high crosslinking of PSf, which forms the major phase. This will nullify the elastic effect of the SPNR phase. This is due to the yielding of the NR phase. The increase in crosslinking of PSf phases also results in an increase in load and decrease in displacement. The enhanced intermixing and interpenetration leads to higher strength and low displacement. In tear failure microfracture take places in the regions of high strain.[70] Therefore the dissipation of the stress near the tip of the sample determines the resistance to tearing. This may be accomplished by slippage or breakage of crosslinks or chain entanglements, deviation of fracture path or complete arresting of crack growth by filled particles. The parameters including crosslinker, polymer blend ratios and fillers affecting on the properties of sample are presented in Table 13.6. For example, a good improvement is observed in tear strength and hardness on increasing the crosslinker content of PS.

Creep Properties

After preparing the IPN sample, it was analysed by creep test, as shown in Figure 13.47(a). Figure 13.47(b) shows the influence of plaster content on the creep properties of the SPNR/PSf blend. It is clear that the creep time of the

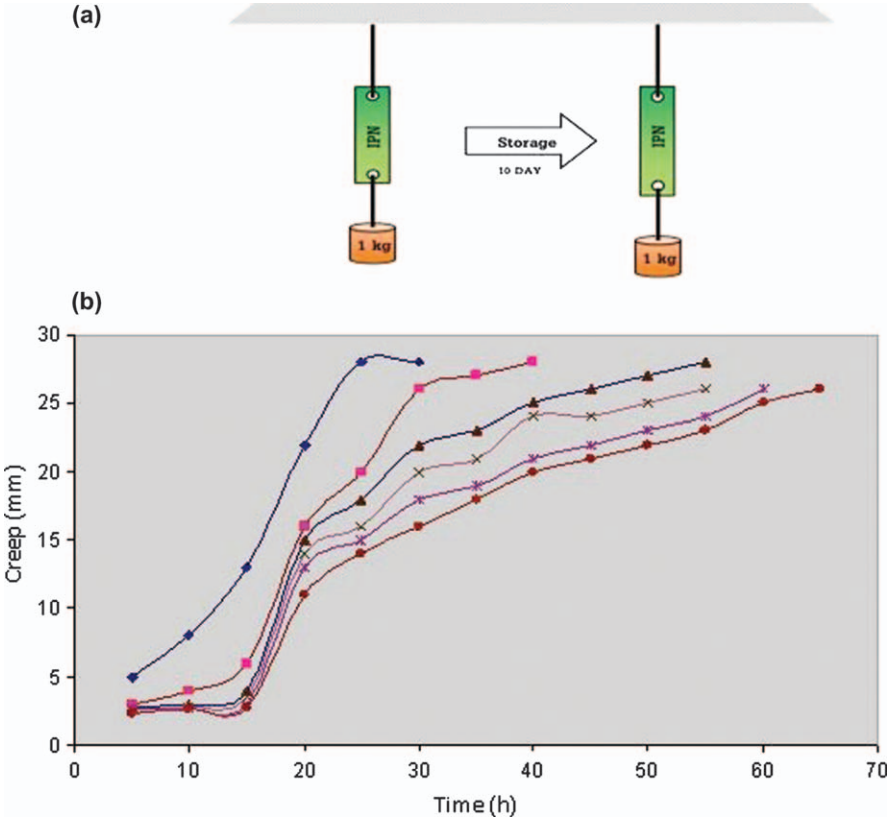

Figure 13.47 (a) Creep experiment and (b) effect of plaster on the creep of an IPN sample (author's experiment).

NR/PSf increases with increasing plaster content. This is due to the elastic modulus of the plaster in the polymer blend.

The influence of ageing at 90 °C on the tensile strength of the SPNR/PSf containing 50% cofibre is shown in Figure 13.48. The tensile strength of the SPNR/PSf containing 50% cofibre decreased with ageing time at 90 °C.

Viscoelastic Properties

Riyajan and coworkers studied the viscoelastic properties of polymer composites from 30/70, 50/50 and 70/30 NRG/PSf blends using dynamic mechanical thermal analysis (DMTA) as shown in Figure 13.49. The storage moduli of polymer blends decreased with decreasing amount of amorphous PSf having high T_g (100 °C). As formerly observed, the storage moduli of polyurethane and PS blend increased as function of PS content.[71] With increasing volume fraction of PS, the rubbery plateau between the T_g of polyurethane and of PS increased to higher moduli, reflecting the change in composition. It was not surprising that the storage modulus of the polymer composite in (d) increased after addition of 3% cellulose fibre in Figure 13.49.

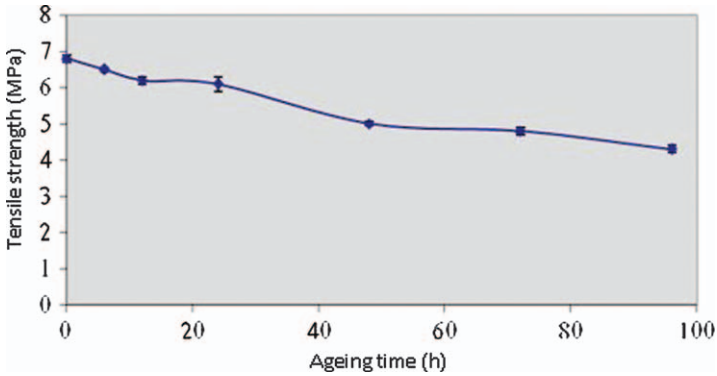

Figure 13.48 Effect of ageing time at 90 °C on the tensile strength of SPNR/PSf containing 50% cofibre (author's experiment).

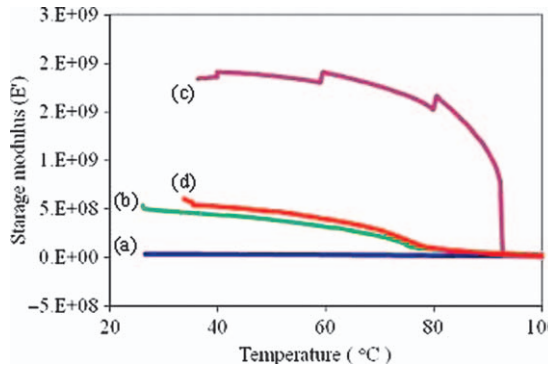

Figure 13.49 DMTA of (a) 30/70, (b) 50/50 and (c) 70/30 NRG/PSF blends and of (d) polymer composite consisting of 50/50 NRG/PSF and 3% cellulose (author's experiment).

The tan δ values of (a) 30/70, (b) 50/50 and (c) 70/30 NRG/PSF blends and of (d) polymer composites containing 50/50 NRG/PSF and 3% cellulose are shown in Figure 13.50. The tan δ of each polymer blend in Figure 13.50(a) to (c) shows two separate loss factor peaks at 100 and 230 °C indicating an immiscible system. Comparing the IPNs to the homopolymer networks, the T_g of the immiscible polymers shifted when their composition was changed. The T_g of PS consistently shifted to lower temperature with increasing PSF content. In addition, two T_gs at 100 and 290 °C were observed in the polymer composite, as shown in Figure 13.50(d). The cellulose fibre that shifted the T_g from 270 to 285 °C might be due to the restriction of chain mobility caused by the steric effect and chemical interaction between MA grafted to cellulose and polymer blend.[6] It was observed that the peaks at lower T_g broadened when PSF content was low (30%). The result confirmed the chemical interaction between cellulose fibre and the polymer matrix.

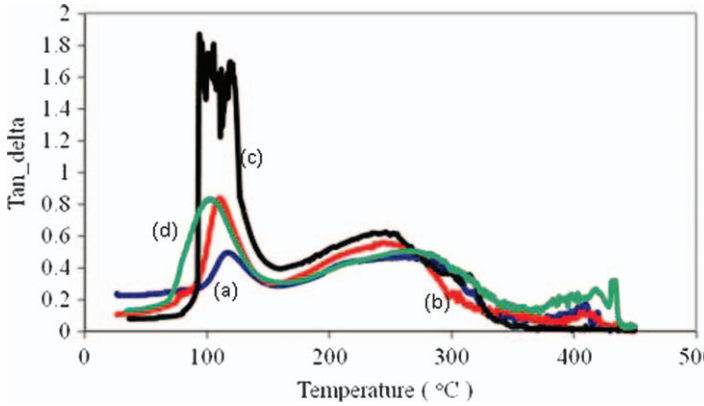

Figure 13.50 Tan δ of (a) 30/70, (b) 50/50 and (c) 70/30 NRG/PSF blends and of (d) polymer composite containing 50/50 NRG/PSF and 3% cellulose (author's experiment).

Crosslinked NR nanocomposites were prepared from cellulose nanowhiskers (CNWs) that were extracted from bamboo pulp residue of newspaper production and NR latex.[39] In this process, NR in presence of bamboo nanowhiskers (master batch) was compounded with solid NR and vulcanizing agents using a two-roll mill and subsequently cured to introduce crosslinks in the NR phase. The addition of CNWs into the polymer composite had a positive impact on storage modulus, and tan δ peak position of the crosslinked NR 39. When the amount of CNWs increased in composite, the values of storage modulus in all the nanocomposites also increased compared to the NR matrix. This sort of enhancement in modulus even below T_g is good evidence of the reinforcing tendency of CNWs in the NR matrix. The storage modulus, however, increased with the addition of CNWs only up to 5 wt% and then decreased slightly for 10 wt%. The modulus drop corresponds to an energy dissipation phenomenon displayed during the relaxation process where it passes through a maximum. This relaxation process involves cooperative motions of long chain sequences. The rubbery modulus is known to depend on the degree of crystallinity of the material. The crystalline CNW particles act as physical crosslinks for the elastomer and increase the modulus substantially.

Biodegradation

Biodegradable SPNR/PSf containing cofibre was studied in soil and it was investigated by reduction of weight; results are shown in Figure 13.51. Material scientists have reported on the degradation of cellulose in previous work. It is clear that the biodegradation of SPNR-*g*-cofibre dramatically decreased as a function of cellulose in the SPNR-*g*-cofibre. The cofibre highly degrades to bacteria and fungi in water, soil and air, which, in the presence of moisture, heat and dirt, form a biofilm on the surface of the cofibre during their growth and development. SPNR obtained from the latex of *Hevea brasiliensis* is a high

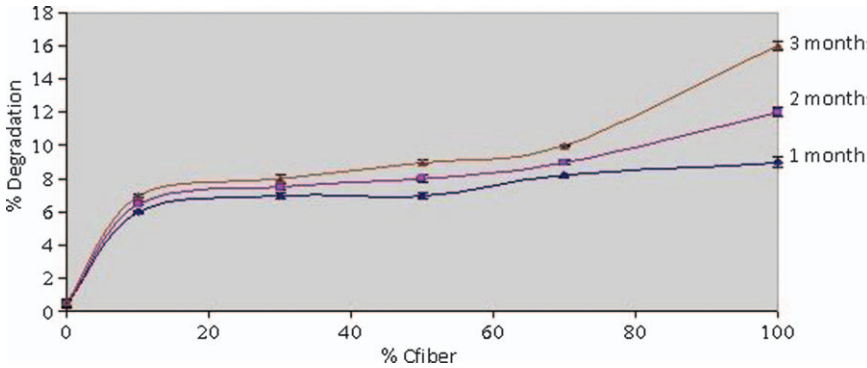

Figure 13.51 Relationship between % degradation and polymer blends containing different cofibre contents (0–100 wt%) (author's experiment).

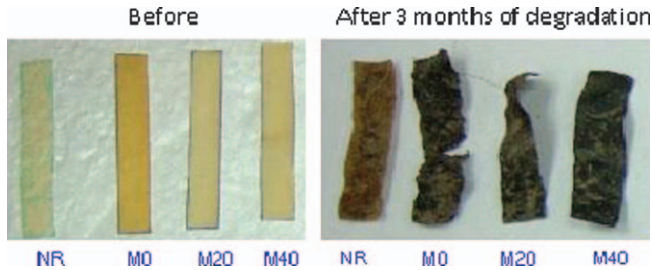

Figure 13.52 Digital photographs of NR/PVA blends containing different MA contents (author's experiment).

polymer of *cis*-1,4-polyisoprene (molecular weight $\approx 10^6$). NR is subjected to vulcanization (crosslinking of the linear *cis*-1,4-polyisoprene chains) for commercial applications and crosslinking in NR molecule difficulty leads to the biodegradation due to the presence of sulfur bridges, reducing to accessibility sites for cleavage.[72,73] It is clear that the degradation of SPNR/PSf containing cofibre increased with increasing cofibre content observing from weight loss and colour change. The rate of degradation of SPNR/PSf containing cofibre was dramatically increased within 1 month. After that, the rate of degradation of this sample slowly decreased due to the low amount of cofibre in the polymer blend. The SPNR degrades in nature by specific microorganisms by a slow process and the growth of bacteria.

In the case of NR/PVA blends, their colour changed from yellow to black when they were left in soil for 3 months as a result of their biodegradation, as shown in Figure 13.52.

13.7.2 PP/NR Blends Reinforced with Cellulose Fibre

PP/NR blends reinforced with jute fibre were prepared by compression moulding.[74] It was found that tensile strength, tensile modulus, percentage

Figure 13.53 Photographs of polymer composite products from NR and PS (author's experiment).

elongation at break, bending strength, bending modulus, impact strength and hardness of the composites were decreased with the increase of NR in PP, while the impact strength and elongation at break % were improved significantly.

13.8 Possible Applications of Rubber Composites

Rubber composites made from NR are used in adhesives.[24] This investigation is concerned with the preparation of rubber blends based on NR and PMMA because incorporation of PMMA into the NR phase may lead to materials with improved strength, clarity and weather resistance and could be used in automotive and other applications.[71] Rubber composites from NR and PSf containing cofibre could be expected to find use in artificial wood applications, cups and picture frames,[6] as shown in Figure 13.53.

13.9 Conclusions

Modification in the properties of NR with natural fibre has been extensively studied over recent decades. The natural fibres were prepared from sugar cane leaves treated with base catalysts such as NaOH, H_2O_2, or acid catalysts such as H_2SO_4/HCl or $HClO_4$. There are two methods such as latex blending and dried rubber. The properties of rubber varied depending on main parameter such as natural fibre types, natural fibre content, shape and size of natural fibre and coupling agent as well as rubber matrix. The property of the rubber composite sample shows outstanding in tensile strength, creep, thermal resistance and damping properties. The parameters controlling the properties of polymer blend are crosslinker content, crosslinker types, polymer blend ratio, nature polymer and fillers. The tensile strength, tear strength and hardness increased with increase in green fibre content. The increase in phase mixing with increased

plastic content is the reason for this enhancement in mechanical performance. The tensile strength, impact strength, %100 modulus of the resulting composite sample as well as swelling in toluene increased as a function of curing agent and cofibre content. In addition, the tensile strength of the polymer blend was also improved by addition of cofibre in sample. This observation was supported by swelling ratio, impact strength, tear strength and hardness. The adhesion between natural fibre and NR matrix are confirmed by SEM, AFM and swelling behaviour. Moreover, the obtained polymer blend containing cofibre exhibits good biodegradable in nature. The possible of the simple could be expected to use in membrane, ion adsorption, electric application, adhesive artificial wood application, cup and picture frame.

Acknowledgements

The authors are grateful for the fundamental research grant from The Thailand Research Fund/Commission on Higher Education: Grant No: (MRG5380190), (RTA 5480007) and Prince of Songkla University (SCI 540032S) that supported this work.

References

1. W. Pechurai, C. Nakason and K. Sahakaro, *Polym. Test.*, 2008, **27**, 621.
2. A. Bahruddin, A. Ahmad and R. Prayitno, Satoto, *Procedia Chem.*, 2012, **4**, 146.
3. A. A. Yehia, A. M. Akelah, A. Rehab, S. H. El-Sabbagh, D. E. El Nashar and A. A. Koriem, *Mater. Des.*, 2012, **33**, 11.
4. F. Guillon, A. Auffret, J. A. Robertson, J.-F. Thibault and J.-L. Barry, *Carbohyd. Polym.*, 1998, **37**, 185.
5. W. Han, C. Zhao, T. Elder, K. Chen, R. Yang, D. Kim, Y. Pu, J. Hsieh and A. J. Ragauskas, *Carbohyd. Polym.*, 2012, **88**, 719.
6. S. Riyajan, I. Intharit and P. Tangboriboonrat, *Ind. Crops Prod.*, 2012, **36**, 376.
7. S. Kanking, P. Niltui, E. Wimolmala and N. Sombatsompop, *Mater. Des.*, 2012, **41**, 74.
8. S. Riyajan, I. Intharit and P. Tangboriboonrat, *J. Polym. Mater., Accept.*, 2013.
9. E. Abraham, P. A. Elbi, B. Deepa, P. Jyotishkumar, L. A. Pothen, S. S. Narine and S. Thomas, *Polym. Degrad. Stab.*, 2012, **97**, 2378.
10. S. J. Tan, A. G. Supri and P. L. Teh, *Appli. Mech. Mater.*, 2013, **284–287**, 87.
11. E. Abraham, B. Deepa, L. A. Pothan, M. John, S. S. Narine, S. Thomas and R. Anandjiwala, *Cellulose*, 2013, **20**, 417.
12. J. X. Sun, F. Xu, X. F. Sun, B. Xiao and R. C. Sun, *Polym. Degrad. Stab.*, 2005, **88**, 521.

13. M. F. Rosa, E. S. Medeiros, J. A. Malmonge, K. S. Gregorski, D. F. Wood, L. H. C. Mattoso and G. Glenn, *Carbohyd. Polym.*, 2010, **81**, 83.
14. S. Mohanty, S. K. Verma and S. S. Nayak, *J. Appl. Polym. Sci.*, 2004, **94**, 1336.
15. S. M. Bociek and D. Welti, *Carbohyd. Res.*, 1975, **42**, 217.
16. H. Lilholt and J. M. Lawther, in *Natural Organic Fibres*, T.-W. Chou, Elsevier, New York, 2000, vol. 1, ch. 1.10, p. 303.
17. http://en.wikipedia.org/wiki/Natural_fiber#Vegetable_fibers (accessed 11 September 2013).
18. A. K. Bledzki and J. Gassan, *Prog. Polym. Sci.*, 1999, **24**, 221.
19. D. Pasquini, E. D. Morais Teixeira, A. D. Silva Curvelo, M. N. Belgacem and A. Dufresne, *Comp. Sci. Technol.*, 2008, **68**, 201.
20. W. Hoareau, W. G. Trindade, B. Siegmund, A. Castellan and E. Frollini, *Polym. Degrad. Stab.*, 2004, **86**, 567.
21. A. D. S. Curveloa, *J. Colloid Interface Sci.*, 2006, **295**, 79.
22. J. F. Kadla and R. D. Gilbert, *Cellul. Chem. Technol.*, 2000, **34**, 197.
23. E. L. Hult, P. T. Larsson and T. Iversen, *Cellulose*, 2000, **7**, 35.
24. K. Ruel, Y. Nishiyama and J. P. Joseleau, *Plant Sci.*, 2012, **193–194**, 48.
25. S. Ouajai and R. A. Shanks, *Polym. Degrad. Stab.*, 2005, **89**, 327.
26. S. M. Luz, J. Del Tio, G. J. M. Rocha, A. R. Gonçalves and A. P. Del'Arco Jr, *Composites, Part A*, 2008, **39**, 1362.
27. S. Riyajan and I. Intharit, *J. Elastomers Plast.*, 2011, **43**, 513.
28. M. Abdelmouleh, S. Boufi, M. N. Belgacem and A. Dufresne, *Compos. Sci. Technol.*, 2007, **67**, 627.
29. M. Jawaid, H. P. S. Abdul Khalil, A. Hassan, R. Dungani and A. Hadiyane, *Composites, Part B*, 2013, **45**, 619.
30. B. Suresha, R. M. Devarajaiah, T. Pasang and C. Ranganathaiah, *Mater. Des.*, 2013, **47**, 750.
31. W. X. Wang, Y. Takao, T. Matsubara and H. S. Kim, *Compos. Sci. Technol.*, 2002, **62**, 767.
32. J. H. Lee, J.-S. Lee, T. Kuila, N. H. Kim and D. Jung, *Composites, Part B*, 2013, **51**, 98.
33. H. N. Dhakal, Z. Y. Zhang, R. Guthrie, J. MacMullen and N. Bennett, *Carbohyd. Polym.*, 2013, **96**, 1.
34. P. Rytlewski, *Electrochim. Acta*, 2012, **61**, 191.
35. S. Riyajan, I. Intharit and P. Tangboriboonrat, *Polym. Bull.*, 2012, **69**, 635.
36. J. Bras, M. L. Hassan, C. Bruzesse, E. A. Hassan, N. A. El-Wakil and A. Dufresne, *Ind. Crops Prod.*, 2010, **32**, 627.
37. P. Ortiz-Serna, R. Díaz-Calleja, M. J. Sanchis, E. Riande, R. Nunes, A. Martins and L. Viscontem, *J. Non-Cryst. Solids*, 2011, **357**, 598.
38. E. Abraham, P. A. Elbi, B. Deepa, P. Jyotishkumar, L. A. Pothen, S. S. Narine and S. Thomas, *Polym. Degrad. Stab.*, 2012, **97**, 2378.
39. P. M. Visakh, S. Thomas, K. Oksman and A. P. Mathew, *Composites, Part A*, 2012, **43**, 735.

40. D. Pasquini, E. de Morais Teixeira, A. Aprígio da Silva Curvelo, M. Naceur Belgacem and A. Dufresne, *Ind. Crops. Prod.*, 2010, **32**, 486.
41. M. Abdelmouleh, S. Boufi, M. N. Belgacem and A. Dufresne, *Compos. Sci. Technol*, 2007, **67**, 1627.
42. W. Zhang, X. Zhang, M. Liang and C. Lu, *Compos. Sci. Technol.*, 2008, **68**, 2479.
43. S. Riyajan and W. Sukhlaaied, *Kautsch. Gummi Kunstst.*, 2012, **64**, 20.
44. R. Zulkifli, L. K. Fatt, C. H. Azhari and J. Sahari, *J. Mater. Process. Technol.*, 2002, **128**, 33.
45. M. Jacob, S. Thomas and K. T. Varughese, *Compos. Sci. Technol.*, 2004, **64**, 955.
46. A. Bahruddin, A. Ahmad, Prayitno and R. Satoto, *Procedia Chem.*, 2012, **4**, 146.
47. S. Shinoj, R. Visvanathan, S. Panigrahi and M. Kochubabu, *Ind. Crops Prod.*, 2011, **33**, 7.
48. H. Ismail, H. D. Rozman, R. M. Jaffri and Z. A. M. Ishak, *Eur. Polym. J.*, 1997, **33**, 1627.
49. C. T. Ratnam, G. Raju and W. M. Z. Wan Yunus, *Nucl. Instrum. Methods Phys. Res., Sect. B*, 2007, **265**, 510.
50. M. J. John, B. Francis, K. T. Varughese and S. Thomas, *Composites, Part A*, 2008, **39**, 352.
51. D. Shanmugam and M. Thiruchitrambalam, *Mater. Des.*, 2013, **50**, 533.
52. M. Jacob John, B. Francis, K. T. Varughese and S. Thomas, *Composites, Part A*, 2008, **39**, 352.
53. J. Bras, M. L. Hassan, C. Bruzesse, E. A. Hassan, N. A. El-Wakil and A. Dufresne, *Ind. Crops Prod.*, 2010, **32**, 627.
54. H. Ismail and H. P. S. Abdul Khalil, *Polym. Test.*, 2000, **20**, 33.
55. K. Sathya Prabha, P. Ravindran and N. Ilavarasan, *Indian J. Environ. Prot.*, 2012, **32**, 147.
56. V. G. Geethamma, K. T. Mathew, R. Lakshminarayanan and S. Thomas, *Polymer*, 1998, **39**, 1483.
57. W. Wang and G. Huang, *Mater. Des.*, 2009, **30**, 2741.
58. S. Oda, J. Leomar Fernandes Jr and J. S. Ildefonso, *Const. Build. Mater.*, 2012, **26**, 13.
59. R. A. Khan, M. E. Haque, T. Huq, M. A. Khan, H. U. Zaman, K. J. Fatema, M. D. Al-Mamun and M. A. Ahmad, *J. Compos. Mater.*, 2010, **23**, 665.
60. S. A. R. Mohanty, *Appl. Acoust.*, 2011, **72**, 108.
61. M. Mushfequr Rahman, N. Sharmin, R. A. Khan, K. Dey and M. E. Haque, *J. Thermoplast. Compos. Mater.*, 2012, **25**, 249.
62. E. Abraham, P. A. Elbi, B. Deepa, P. Jyotishkumar, L. A. Pothen, S. S. Narine and S. Thomas, *Polym. Degrad.Stab.*, 2012, **97**, 2378.
63. D. Das, M. Datta, R. B. Chavan and S. K. Datta, *J. Appl. Polym. Sci.*, 2005, **98**, 484.
64. M. Abdelmouleh, S. Boufi, M. N. Belgacem and A. Dufresne, *Compos. Sci. Technol.*, 2007, **67**, 1627.

65. C. T. Ratnam, G. Raju and W. M. Z. Wan Yunus, *Nucl. Instrum. Methods Phys. Res., Sect. B.*, 2007, **265**, 510.
66. H. Ismail, H. D. Rozman, R. M. Jaffri and Z. A. Mohd Ishak, *Eur. Polym. J.*, 1997, **33**, 1627.
67. S. Riyajan and J. T. Sakdapipanich, *Polym. Bull.*, 2009, **63**, 609.
68. H. Baker and F. Khalili, *Anal. Chim. Acta*, 2004, **516**, 179.
69. A. P. Mathew, S. Packirisamy and S. Thomas, *J. Appl. Polym. Sci.*, 2000, **78**, 2327.
70. A. P. Mathew, S. Packirisamy, H. J. Radusch and S. Thomas, *Eur. Polym. J.*, 2001, **37**, 1921.
71. D. J. Hourston, F. U. Schäfer, M. H. S. Gradwell and M. Song, *Polymer*, 1998, **39**, 5609.
72. H. Ismail, A. Rusli and A. A. Rashid, *Polym. Test.*, 2005, **24**, 856.
73. S. Riyajan, I. Intharit and P. Tangboriboonrat, *J. Polym. Mater.*, 2013, **30**, 159.
74. H. U. Zaman, R. A. Khan, M. E. Haque, M. A. Khan, A. Khan, T. Huq, N. Noor, M. Rahman, K. M. Rahman, D. Huq and M. A. Ahmad, *A.A. J. Reinf. Plast. Comp.*, 2010, **29**, 3064.

CHAPTER 14

Synthesis of Natural Rubber-Based Completely Green Bionanocomposites

SONAL I. THAKORE

Department of Chemistry, Faculty of Science, The Maharaja Sayajirao University of Baroda, Vadodara 390002, Gujarat, India
Email: drsonalit@gmail.com

14.1 Introduction

Natural rubber (NR) is the most attractive and insdustrially appropriate rubbery material. It also has unique mechanical properties (high elasticity) due to its highly stereoregular microstructure.[1] NR is a versatile raw material with usnique chemical and physicomechanical properties that make it ideal for many dynamic applications.[2] It is a macromonomer isoprenoid [poly(*cis*-1,4-isoprene)] and is synthesized by more than 2000 plant species mostly belonging to the Euphorbiaceae family and by some fungi. The NR latex, which is a stable colloidal dispersion of *cis*-1,4-polyisoprene of high molecular mass in an aqueous medium, is obtained from the tree *Hevea brasiliensis*. The latex can be stabilized with ammonia and water content is reduced by concentration, then coagulated and dried.

Most of the rubbers, including NR, are available in the form of an aqueous dispersion of rubber particles, known as latex. Natural and synthetic rubbers in vulcanized form are used to prepare various rubber products such as mechanical goods, hoses, soles, V-belts, seals, gaskets, tyre treads, *etc*. NR in its

RSC Polymer Chemistry Series No. 8
Natural Rubber Materials, Volume 2: Composites and Nanocomposites
Edited by Sabu Thomas, Hanna J. Maria, Jithin Joy, Chin Han Chan and Laly A. Pothen

Published by the Royal Society of Chemistry, www.rsc.org

original uncured form has low strength, softens in warm weather and is brittle in cold weather and is practically of limited use.[3] Vulcanization, a chemical process where long chains of rubber molecules are crosslinked, transforms the soft, weak plastic-like material into a strong elastic product with high and reversible deformability and good mechanical properties owing to strain-induced crystallization, low hysteresis, excellent dynamic properties and fatigue resistance. After vulcanization, rubber loses its tackiness, becomes insoluble in solvent and becomes more resistant to heat, light and ageing processes.[2]

14.1.1 Fillers used in Natural Rubber

For practical uses, reinforcing phases like carbon black and silica particles have been extensively used for obtaining improved initial modulus and durability.[4,5] They are normally used up to 50 phr. In spite of being well known for their capabilities as reinforcements, *i.e.* they impart strength and stiffness to the vulcanized rubber, these fillers are relatively expensive. While maintaining their desired properties. Moreover, C-black is produced by the incomplete combustion of heavy petroleum products and hence causes pollution and gives black colour to the rubber. Recently, International Agency for Research on Cancer (IARC) evaluated that, it is possibly carcinogenic to humans. Hence research was focused on the development of other reinforcing agents to replace C-black in rubber compounds. Silica and other types of fillers have a weaker polymer–filler interaction and are extensively used where a high degree of reinforcement is not essential.[6,7] Therefore, considerable R & D efforts are being carried out to investigate the possibility of replacing these fillers with the target to reduce the cost of rubber products.

14.1.2 Synthetic and Natural Fibres

In certain cases, rubber products require stiffness along with flexibility, often in specific directions. This can be achieved by reinforcing rubbers with long or short fibres to form composites.[8,9] NR inherently possesses high strength due to strain-induced crystallization. When fibres are incorporated into NR, the regular arrangement of rubber molecules is disrupted and hence the ability for crystallization is lost. Synthetic fibres of reinforcing agents like carbon, aramid, and glass, rayon, nylon, aramid, asbestos, in natural and synthetic rubbers have been studied by many researchers.[10] Synthetic fibre-reinforced polymer matrix composites are intensively used both in end-use applications and the area of research and development. These composites exhibit the combined behaviour of the soft, elastic rubber matrix and the stiff, strong fibrous reinforcement. The development of fibre-reinforced rubber composites has made available polymers that are harder than aluminium and stiffer than steel. They have some additional advantages such as ease of installation, good processability, relatively good resistance to environmental agents and fatigue. A good number of matrices and fibres such as polyester, nylon, carbon, Kevlar, glass and asbestos with a wide range of properties are being used for processing composites. But

these are very expensive compared to natural fibres. Environmental preservation, pollution control, and emphasis on the use of energy efficient materials and processing in the industrial sector have renewed interest in agro-based lignocellulosic (LC) fibres such as wood pulp, jute, sisal, flax, pineapple and oil palm fibres as a means to produce environmentally friendly materials. Research efforts are currently being harnessed in developing a new class of fully biodegradable 'green' composites by combining (natural/bio) fibres with biodegradable resins.[11] The major attractions about green composites are that they are environmentally friendly, fully degradable and sustainable, *i.e.*, they are truly 'green' in every way. At the end of their life, they can be easily disposed of or composted without harming the environment.

14.1.3 Biocomposites

Biocomposites are composite materials comprising one or more phase(s) derived from a biological origin. In terms of the reinforcement, this could include plant fibres such as cotton, flax, hemp and the like, or fibres from recycled wood or waste paper, or even by-products from food crops. During the last decade of the 20th century, lignocellulosic fibre-reinforced composite materials have become popular for low cost as well as high volume engineering markets such as automotive, military, aeronautic and building industries.[12,13] Derived from a renewable resource[14] the favourable aspects about plant fibres are their high aspect ratio, high tensile strength and bending modulus, low density, low cost, processing economy, high stiffness, greater deformability, less abrasive to equipment, design flexibility, high low strain moduli, damping, and biodegradability.[15–17] The advantage of elongated, fibrous structures over the spherical ones has been emphasized, and the networking ability of natural fibres is particularly interesting for increasing the modulus at low filler content.[18–20] As indicated from the literature most of the research work involving biocomposites has been devoted to the combination of lignocellulosic fillers and/or fibres. Many researchers have reported the processing advantages and improvements in the mechanical properties of the short fibre-reinforced rubber composites.[21–30] A number of reviews discuss the reinforcement of elastomers with biofibres[31] their applications[32] as well as their comparison with carbon black.[33]

The properties of a hybrid composite mainly depend on the fibre content, length of individual fibres, orientation, extent of intermingling of fibres, fibre-to-matrix bonding, and arrangement of both the fibres. The strength of the hybrid composite is also dependent on the failure strain of individual fibres. Maximum hybrid results are obtained when the fibres are highly strain-compatible.[34] The extent of reinforcement is found to depend on the fibre–matrix adhesion, aspect ratio of the fibre in the vulcanizate, fibre dispersion and orientation, nature of matrix, and type of fibres.[35–37] This is the reason why fibre-reinforced NR composites possess lower tensile strength than gum compounds. When fibre-reinforced rubber composites is subjected to load, the fibres act as carriers of load and stress is transferred from matrix along the

fibres leading to effective and uniform stress distribution which results in a composite having good mechanical properties. The uniform distribution of stress is dependent on two factors: (a) population of fibres, (b) orientation of fibres. At low levels of fibre loading, the orientation of fibres is poor and the fibres are not capable of transferring load to one another and stress gets accumulated at certain points of composite leading to low tensile strength. At high levels of fibre loading the increased population of fibres leads to agglomeration and stress transfer gets blocked. At intermediate levels of loading (30 phr) the population of the fibres is just right for maximum orientation and the fibres actively participate in stress transfer.

14.2 Polysaccharides as Reinforcing Agents

Polysaccharides such as starch, cellulose and chitin, are interesting renewable resources for non-food applications. Indeed, as they are obtained from biomass, they are available in large quantities, renewable and biodegradable and have a low cost. Among the huge amount of different polysaccharides available, the most significant polysaccharides are starch, cellulose and chitin.

14.2.1 Starch

Starch is a natural, renewable and biodegradable polymer produced by many plants as a source of stored energy. It is the second most abundant biomass material in nature and is found in plant roots, stalks, crop seeds, and staple crops such as rice, corn, wheat, tapioca and potato.[38,39] Depending on their botanic origin, starch raw materials have different conversion factors, size, shape and chemical content. It consists of mainly two glucosidic macromolecules: amylose and amylopectin.

14.2.2 Cellulose

Cellulose is the most abundant renewable organic material produced in the biosphere, having an annual production over 7.5×1010 tons.[40] Cellulose is widely distributed in higher plants, in several marine animals (for example, tunicates). In general, cellulose is a fibrous, tough, water-insoluble substance that plays an essential role in maintaining the structure of plant cell walls. Regardless of its source, cellulose can be characterized as a high molecular weight homopolymer of 1,4-linked anhydro-D-glucose units in which every unit is corkscrewed 180° with respect to its neighbours, and the repeat segment is frequently taken to be a dimer of glucose, known as cellobiose. Each cellulose chain possesses a directional chemical asymmetry with respect to the termini of its molecular axis: one end is a chemically reducing functionality (*i.e.* a hemiacetal unit) and the other has a pendant hydroxyl group, the nominal non-reducing end.

14.2.3 Chitin

Chitin is the other polysaccharide used extensively. It constitutes the structure of the external skeleton in shellfish and insects and is one of the major components of the fibrous material of cellular walls in mushrooms and algae.[41] In terms of structure, chitin may be compared to the polysaccharide cellulose and, in terms of function, to the protein keratin. It has also proven useful for several medical and industrial purposes. It is a modified polysaccharide that contains nitrogen; it is synthesized from units of *N*-acetylglucosamine (to be precise, 2-(acetylamino)-2-deoxy-D-glucose). These units form covalent β-1,4 linkages (similar to the linkages between glucose units forming cellulose). Therefore, it may be described as cellulose with one hydroxyl group on each monomer substituted with an acetylamine group. This allows for increased hydrogen bonding between adjacent polymers, giving the chitin–polymer matrix increased strength. In its pure form, chitin is leathery, but in most invertebrates it occurs largely as a component of composite materials.

The use of these three polysaccharides as reinforcing fillers in their native form was evaluated and their performance compared with carbon black.[42] The results showed that the optimum loading of biofillers was 20 phr up to which they showed better mechanical properties than carbon black (Figure 14.1). Among all fillers, chitin exhibited exceptional mechanical strength even at minimum loading. The SEM images of the biocomposites at 20 phr loading (Figure 14.2) showed a uniform morphology like a single phase with no distinction between the matrix and the dispersion phase, while composites of C-black showed the presence of holes formed during fracture. Probably the polysaccharides form a polymer blend with NR with a certain degree of compatibility at these compositions. At higher ratios their hydrophilic nature leads to immiscibility and hence poorer mechanical strength.

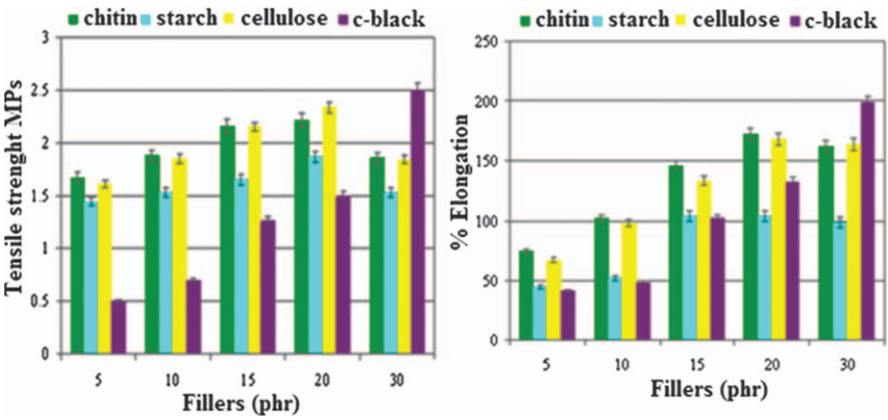

Figure 14.1 Variation in tensile strength and elongation at break with polysaccharide loading.
(Reproduced from reference 43 with permission from Wiley.)

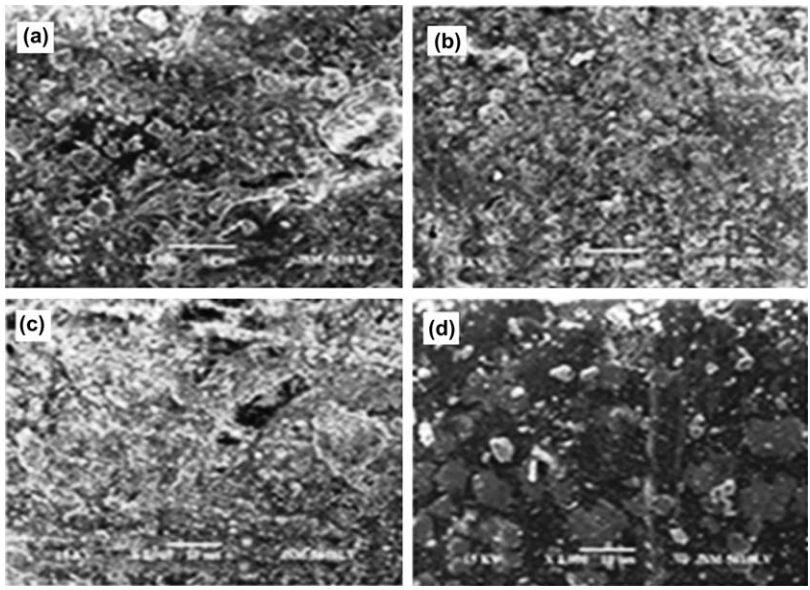

Figure 14.2 SEM of NR composite containing (a) starch, (b) chitin, (c) carbon black and (d) cellulose.
(Reproduced from reference 43 with permission from Wiley.)

Chitosan is a deacetylated product of chitin, also classified as a natural polymer because of the presence of a degradable enzyme, chitosanase. Biodegradable blends of NR latex/chitosan (NR=CS) have been developed by solution casting followed by compression.[43] X-ray diffraction study shows a decrease in crystallinity in NR with addition of chitosan.

14.3 Disadvantages of Polysaccharides as Fillers

Despite these attractive properties, natural fillers are used only to a limited extent in industrial practice due to difficulties associated with surface interactions. The inherent polar and hydrophilic nature of polysaccharides and the nonpolar characteristics of most of the thermoplastics result in difficulties in compounding the filler and the matrix and, therefore, in achieving acceptable dispersion levels, which results in inefficient composites.[44] Moreover, the processing temperature of composites is very low because these biofillers start to degrade at high temperature (around 230 °C). Another drawback of biofillers is their high moisture absorption and the resulting swelling and decrease in mechanical properties. Moisture absorbance and corresponding dimensional changes can be largely prevented if the hydrophilic filler is thoroughly encapsulated in a hydrophobic polymer matrix and there is good adhesion between both components. However, if the adhesion level between the filler and the matrix is not good enough, a diffusion pathway can pre-exist or can be

created under mechanical solicitation. The existence of such a pathway is also related to the filler connection and therefore to its percolation threshold.

To overcome these bottlenecks and to enhance their performance further by improved dispersion the following strategy has been adopted.

1. Reduction in particle size to obtain nanofillers which can result in more uniform distribution within the polymer matrix.
2. Organic modification of the nanofillers to obtain hydrophobic derivatives having improved compatibility with the hydrophobic rubber.

14.4 Polysaccharides for Nanoreinforcement

Polysaccharides are good candidates for renewable nanofillers because they have partially crystalline structures conferring interesting properties.[45,46] Two important types of nanofillers have been developed from cellulose, namely whiskers and nanocrystals. Whiskers have also been developed from chitin while starch has been used for preparation of nanocrystals.

14.4.1 Chitin Whiskers

Nanometric monocrystals of chitin, commonly referred to as whiskers, are prepared by acid hydrolysis of chitin obtained from various sources such as squid pen chitin,[47] riftia tubes,[48] crab shells[49,50] and shrimp shells.[51,52] The surface of crab shell whiskers was chemically modified with alkenyl succinic anhydride (ASA) and phenyl isocyanate (PI).[53] TEM images in Figure 14.3 show that after surface chemical modification the chitin fragments seem to be entangled, and individual whiskers are difficult to observe.

14.4.2 Cellulose Whiskers

Whiskers of cellulose can be obtained from various sources including Syngonanthusnitens (Capim Dourado), rachis of palm tree, sisal and bagasse[54,55] and an animal cellulose called tunicin.[56] Cellulose whiskers are of particular interest

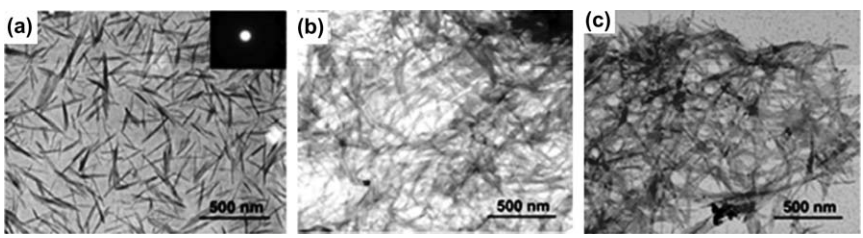

Figure 14.3 TEM images of a dilute suspension of (a) unmodified, (b) ASA-modified and (c) PI-modified chitin whiskers.
(Reproduced from reference 54 with permission from the American Chemical Society.)

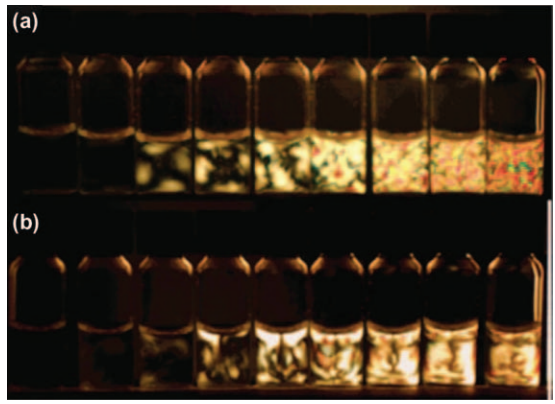

Figure 14.4 Photographs of sulfate-functionalized tunicate whiskers: (a) dispersions of as-prepared in water and (b) freeze-dried redispersed in water, viewed through crossed polarizers. Concentrations are from left to right: 0.1, 0.5, 1.0, 2.0, 3.0, 4.0, 5.0, 6.0 and 7.0 mg/mL.
(Reproduced from reference 64 with permission from the American Chemical Society.)

because of their rod-like shape. Conventional bright-field (BF) TEM has frequently been applied to study cellulose whiskers based on various sources such as wood and sugar beet,[57] tunicin,[58] ramie,[59] cotton, wheat straw, bacterial cellulose.[60] The formation of this rigid network, resulting from strong interactions between whiskers, was assumed to be governed by a percolation mechanism.[61] This hydrogen-bonded network induced a thermal stabilization of the composite up to 500 K, the temperature at which cellulose starts to decompose.

Cellulose whiskers without surface modification display strong interactions and have been reported as difficult to disperse in water. Sulfate-functionalized tunicate whiskers were prepared by sulfuric acid hydrolysis of cellulose pulp derived from tunicates (*Styelacla*V*a*). These high aspect ratio nanoparticles formed colloidal suspensions in water (Figure 14.4).[61] A stable suspension of tunicin whiskers was obtained in an organic solvent (*N*,*N*-dimethylformamide) without surfactant addition or chemical surface modification.[62] Both the high value of the dielectric constant of DMF and the medium wettability of tunicin whiskers were supposed to control the stability of the suspension (Figure 14.5).

Recently bionanowhiskers have been extracted from jute by acid hydrolysis.[63] Initially cellulose microfibrils were formed by alkali treatment then addition of an acid to the microfibrils triggered the formation of cellulose nanowhiskers.

14.4.3 Cellulose and Starch Nanocrystals

It has been known for a long time how to obtain nanocrystals from cellulose and starch, by carrying out an acid hydrolysis.[19,64] During the last 10 years,

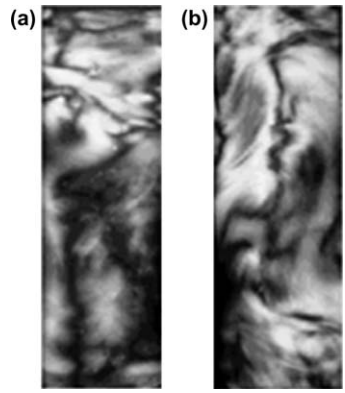

Figure 14.5 Photographs of suspension of tunicate whiskers (0.5 wt%) in (a) water and (b) DMF observed between cross nicols, showing the formation of birefringent domains.
(Reproduced from reference 65 with permission from the American Chemical Society.)

mainly cellulose, has been used to prepare nanoreinforcements that can be used to prepare nanocomposite materials. Recent reviews have been published on cellulose nanoparticles[65,66] which is by far the most studied polysaccharide for such application. The literature in this field is growing very fast, and it is now a commercial product. However, there is no doubt that increasing works will be done in the near future on starch nanoparticles (SNPs).

14.4.3.1 Preparation of Cellulose Nanocrystals

In the 1950s, Ranby reported for the first time that colloidal suspensions of cellulose can be obtained by controlled sulfuric acid-catalysed degradation of cellulose fibres.[67–69] The main process for the isolation of cellulose nanocrystals from cellulose fibres is based on acid hydrolysis. Disordered or paracrystalline regions of cellulose are preferentially hydrolysed, whereas crystalline regions that have a higher resistance to acid attack remain intact.[70,71] Thus, following an acid treatment that hydrolyses the cellulose rod-like nanocrystals are produced. The obtained cellulose nanocrystals have a morphology and crystallinity similar to the original cellulose fibres; examples of such elements are given in Figure 14.6.[6]

The main difference between the preparation of cellulose microfibrils (MFC) and cellulose whiskers is the last step, in which the bleached cellulose is disintegrated by pumping through a microfluidizer processor instead of submitting it to an acid hydrolysis treatment. The slurry was passed through valves that applied a high pressure (Figure 14.7).[72] In a recent study the derivation and structures of cellulose nanocrystals from grape skins were reported.[73] Pure cellulose was isolated from chardonnay grape skins by a process involving organic extraction, acid and base dissolutions, and basic and acidic oxidation.

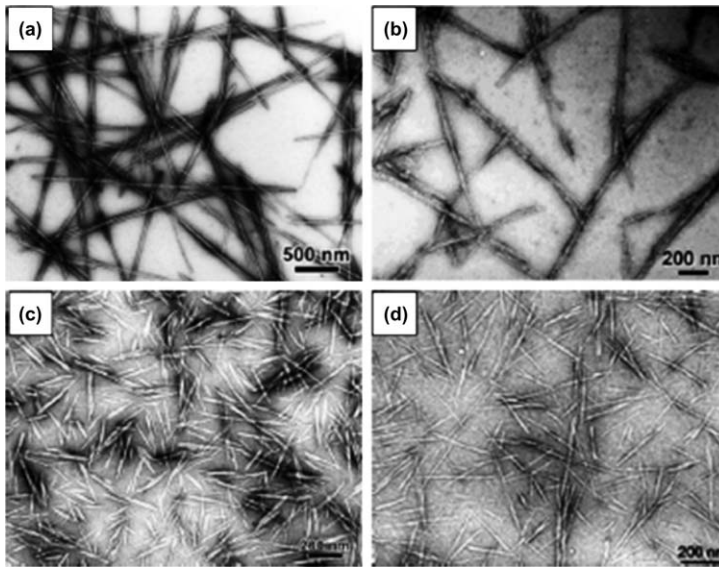

Figure 14.6 TEM images of dried dispersions of cellulose nanocrystals derived from (a) tunicate, (b) bacterial, (c) ramie and (d) sisal.
(Reproduced from reference 76 with permission from the American Chemical Society.)

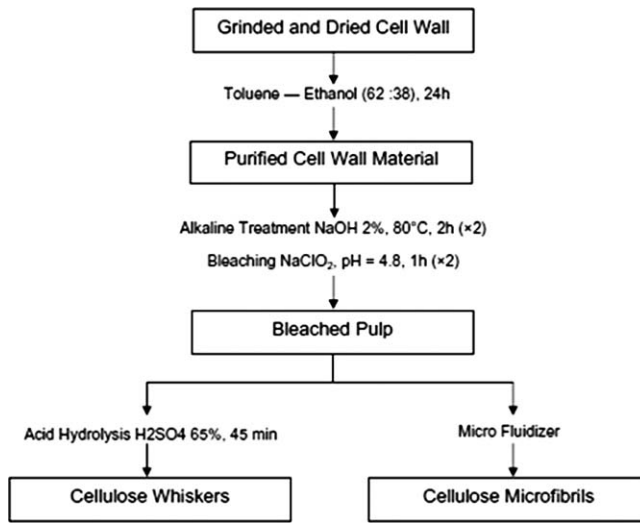

Figure 14.7 Extraction of cellulose whiskers and microfibrillated cellulose from the date palm tree.
(Reproduced from reference 77 with permission from Elsevier.)

14.4.3.2 Preparation of Starch Nanocrystals

Starch has a multiscale structure, as shown in Figure 14.8.[74] Amylose molecules are thought to occur in the granule as individual molecules, randomly interspersed among amylopectin molecules and in close proximity with one another, in both the crystalline and amorphous regions. Depending on the botanic origin of starch, amylose is preferably found in the amorphous region interspersed among amylopectin clusters in both the amorphous and the crystalline regions, in bundles between amylopectin clusters, or co-crystallized with amylopectin.

Dufresne *et al.*[75] reported a method for producing 'microcrystalline starch' by acid hydrolysis using HCl. His group revealed the morphology of nanocrystals resulting from the disruption of the waxy maize starch granules by acid hydrolysis.[76] TEM observations (Figure 14.9) showed (a) a longitudinal view of lamellar fragments consisting of a stack of elongated elements with a width of 5–7 nm and (b) a planar view of an individualized platelet after hydrolysis.[75]

In most recent studies, new processes have been tried out to produce starch nanoparticles by (i) precipitation of amorphous starch by Ma *et al.*[77] and Tan *et al.*,[78] (ii) combining complex formation and enzymatic hydrolysis by Kim and Lim,[79] yielding nanocrystals (*i.e.* complexed with lipids), and

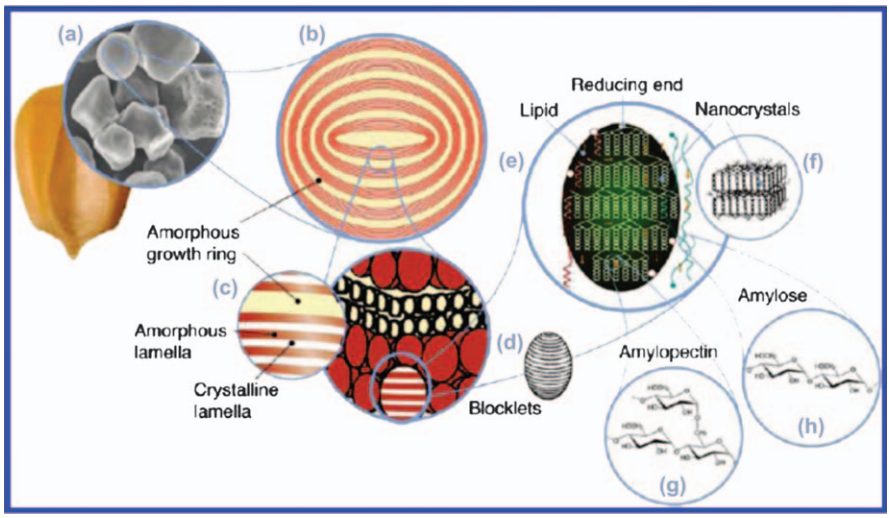

Figure 14.8 Starch multiscale structure: (a) starch granules from normal maize (30 μm), (b) amorphous and semicrystalline growth rings (120–500 nm), (c) amorphous and crystalline lamellae (9 nm), magnified details of the semicrystalline growth ring, (d) blocklets (20–50 nm) constituting a unit of the growth rings, (e) amylopectin double helixes forming the crystalline lamellae of the blocklets, (f) nanocrystals: other representation of the crystalline lamellae called starch nanocrystals when separated by acid hydrolysis, (g) amylopectin's molecular structure, and (h) amylose's molecular structure (0.1–1 nm).
(Reproduced from reference 79 with permission from the American Chemical Society.)

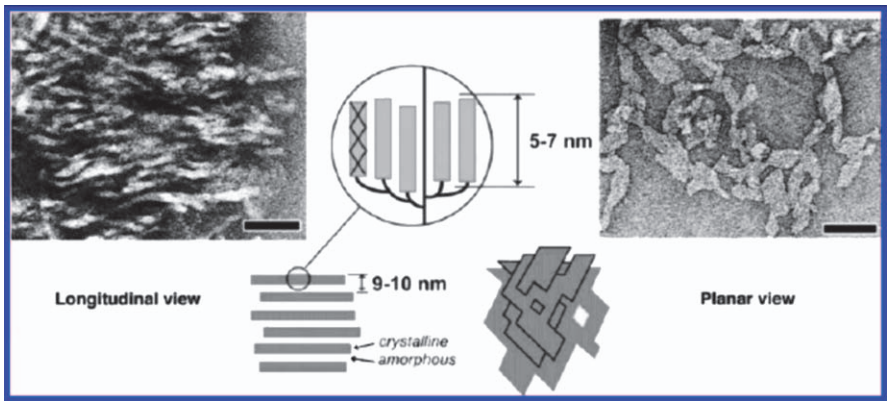

Figure 14.9 TEM observations of starch nanocrystals: longitudinal view and planar view. (Reproduced from reference 79 with permission from the American Chemical Society.)

(iii) microfluidization by Liu *et al.*[80] It is worth noting that such starch nanoparticles have different properties, crystallinity and shape (Figure 14.10).

To allow the processing of composite materials from an organic solvent instead of aqueous suspensions and to achieve maximum interaction and adhesion between the filler and the matrix, the surface chemical modification of starch nanocrystals was carried out.[81–84] Contact angle measurements have shown that the surface chemical modification of waxy maize starch nanocrystals with isocyanate and anhydride functions enhanced the non-polar nature of original starch nanocrystals.

14.5 Nanocomposites and Bionanocomposites

Polymer nanocomposites have emerged as a new class of materials largely due to their new and often much improved mechanical, thermal, electrical and optical properties as compared to their macro- and micro-counterparts.[85] In general, polymer nanocomposites are made by dispersing inorganic or organic nanoparticles into either a thermoplastic or thermoset polymer. Nanoparticles can be three-dimensional spherical and polyhedral nanoparticles (*e.g.* colloidal silica), two-dimensional nanofibres (*e.g.* nanotube, whisker) or one-dimensional disc-like nanoparticles (*e.g.* clay platelet). Such nanoparticles offer enormous advantages over traditional macro- or micro-particles (*e.g.* talc, glass, carbon fibres) due to their higher surface area and aspect ratio, improved adhesion between nanoparticle and polymer, and lower amount of loading to achieve equivalent properties. There is a huge interest in the processing of packaging materials filled with nanoscale components.[86] Therefore, there is a growing interest in bionanocomposites, *i.e.* nanocomposites for which at least one, or preferably both, of the components are derived from renewable resources. Rubber-based bionanocomposites have been studied to a limited

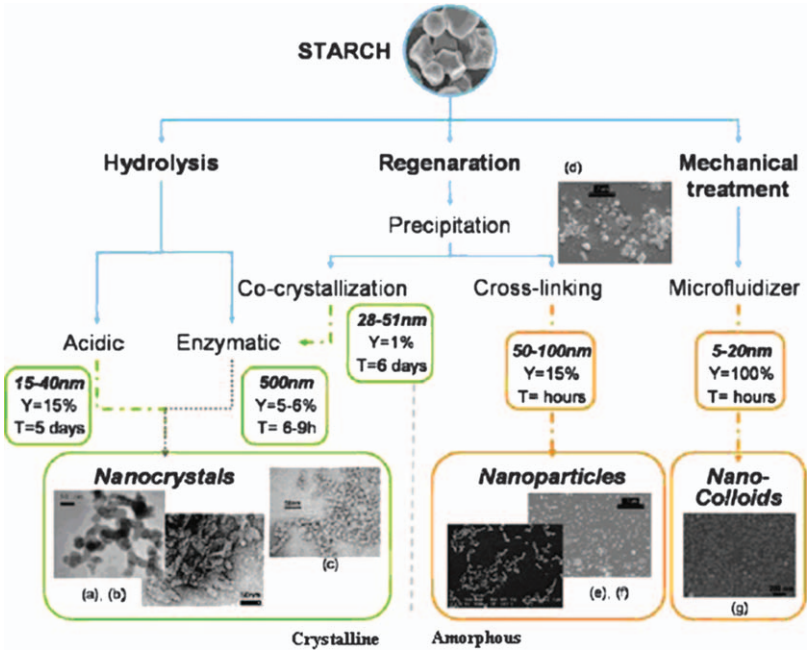

Figure 14.10 Different approaches to producing crystalline and amorphous starch nanoparticles.
(Reproduced from reference 79 with permission from the American Chemical Society.)

extent as compared to plastic-based ones with most of the research focusing on the use of either nanoclays or carbon nanotubes as reinforcements.[87,88]

14.6 Preparation of Bionanocomposites

To obtain a uniform dispersion in the rubbery matrix, different processing methods like solution casting, latex blending, two-roll mill mixing, melt mixing *etc*. have been attempted.[89,90] However, two methods are popularly used to prepare nanocomposites of NR and have been discussed in detail in a recent review on chitin whiskers.[55]

14.6.1 Casting and Evaporating

Polysaccharide whiskers can homogenously dispersed in water and are usually obtained as aqueous suspensions. In the preparation, as shown in Figure 14.11, NR latex or dispersion was first mixed with an aqueous suspension of whiskers to obtain a homogeneous dispersion, which was then cast onto a container, followed by evaporation of water (solvent).

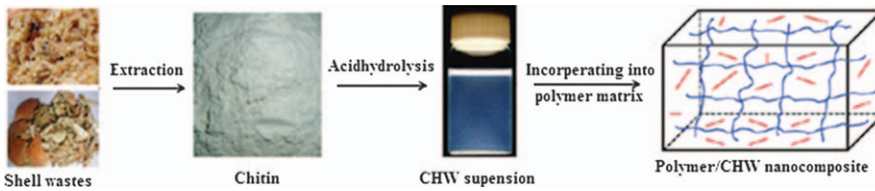

Figure 14.11 Preparation of nanocomposite films from natural rubber and chitin whiskers (CHW).
(Reproduced from reference 96 with permission from the American Chemical Society.)

14.6.2 Freeze Drying and Hot Pressing

Another method called freeze drying and hot pressing can also be used to prepare nanocomposites but only for unvulcanized NR matrix. In this method, the blends of polymer and chitin whiskers were prepared in water medium to prepare well-dispersed aqueous mixtures, which were then freeze dried to give nanocomposite powders, and the powders were consequently processed into specimen by hot pressing.

Polymer/chitin whiskers nanocomposites produced by the two techniques usually showed different physical properties due to the different morphology of the composite and the fact that different interactions between whiskers can be established.[50]

14.6.3 Non-Aqueous Solvent Dispersion

This technique is also a kind of casting and evaporating technique which is used for polysaccharides modified by various surface chemical reactions.[91,92] With improved hydrophobicity, these nanocrystals can disperse in non-aqueous solvents and be more compatible with hydrophobic polymers.[93] Therefore, non-aqueous solution mixing techniques are possible for preparing well-dispersed polymer/polysaccharide nanocrystals nanocomposites.

14.6.4 Dry Mixing

This is a more commercially viable process, carried out on a two-roll mixing mill in accordance with the method described by ASTM D 3184-80.[94] The NR is masticated on the mill followed by addition of the ingredients until homogenous mixing occurs. The nip gap, mill roll, speed ratio, time of mixing and the sequence of addition of the ingredients were kept constant for a certain set of composites. The samples have to be milled for sufficient time to disperse the fibres in the matrix. The fibres are generally added at the end of the mixing process, taking care to maintain the direction of compound flow, so that the majority of fibres followed the direction of the flow. The fibres are also processed prior to mixing.

This is followed by vulcanization to obtain vulcanized composite sheets using a compression moulding in hydraulic press. The cure time for the vulcanization is generally determined using a Monsanto rheometer and optimum curing times (t_{90}) is calculated. The sheeted rubber compounds are conditioned at a temperature of 25 °C for 24 h in a closed container before cure assessment.

In a recent reference nanocomposites of cellulose nanowhiskers with NR as a matrix were also prepared in a two-step process.[1] The first step was master batch preparation wherein NR latex and whiskers in aqueous medium were stirred together for 12 h to obtain a uniform dispersion. This was coagulated using 1% formic acid and dried in an oven to yield the powdered master batch. The second step was compounding of the master batch with solid NR and vulcanizing agents using a two-roll mill followed by curing. Nanocomposite compositions were adjusted during this process by diluting the master batch with appropriate amount of solid NR.

14.7 Natural Rubber–Polysaccharide Nanocomposites

Some NR-based nanocomposites with bio-based nanoreinforcements like chitin whiskers, starch nanocrystals, cellulose whiskers. A lot of work on bionanocomposites of NR has been reported by Alain Dufresne and coworkers.[19,54,79,95] But most of these studies use latex blending technique without vulcanization, for the bionanocomposites preparation. There are less reports available on vulcanized rubber-based bionanocomposites prepared by master batch processing and two-roll mill mixing, which have the potential to be adapted for commercial use.[96–99]

14.7.1 Mechanical and Morphological Investigations

14.7.1.1 NR–Chitin Nanocomposites

Dufresne *et al.* studied stress vs strain curves (nominal data) for the chitin whiskers/unvulcanized NR evaporated composites, shown in Figure 14.12.[100] The polymeric matrix is in the rubbery state and its elasticity from entropic origin is ascribed to the presence of numerous entanglements due to high molecular weight chains. They further observed that the incorporation of anhydride and isocyanate modified chitin whiskers into NR lead to composite materials with improved mechanical properties. The study of the morphology of these nanocomposites leads to the conclusion that the various chemical treatments improve the adhesion between the filler and the matrix (Figure 14.13).[53] However in some cases there is loss of performance, which could be due to the partial or total destruction of the three-dimensional network of chitin whiskers assumed to be present in the unmodified composites.

14.7.1.2 NR–Starch Nanocomposites

Waxy maize starch nanocrystals appeared to be an effective reinforcing agent for NR at temperatures higher than the glass transition temperature of the

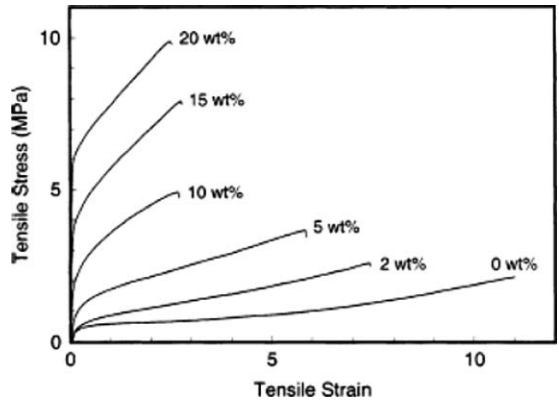

Figure 14.12 Typical stress *vs* strain curves of chitin whisker/unvulcanized NR composites obtained by evaporation ($T = 25$ °C, $d\epsilon/dt = 8.3 \times 10^{-3} s^{-1}$). The crab shell chitin whisker contents are indicated in the figure.
(Reproduced from reference 107 with permission from the American Chemical Society.)

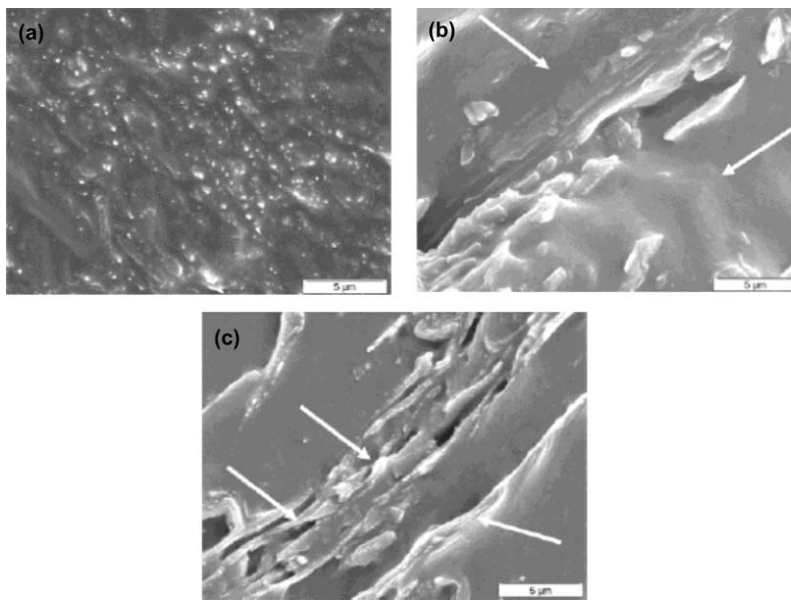

Figure 14.13 SEM of the cryofractured surfaces of 10 wt% (a) unmodified, (b) ASA-modified and (c) PI-modified chitin whisker filled NR films.
(Reproduced from reference 54 with permission from the American Chemical Society.)

matrix.[54] Figure 14.14 displays the evolution of the nominal stress at break vs elongation at break. Considering the ultimate properties, a good compromise between the increase in strength and the decrease in elongation at break seems

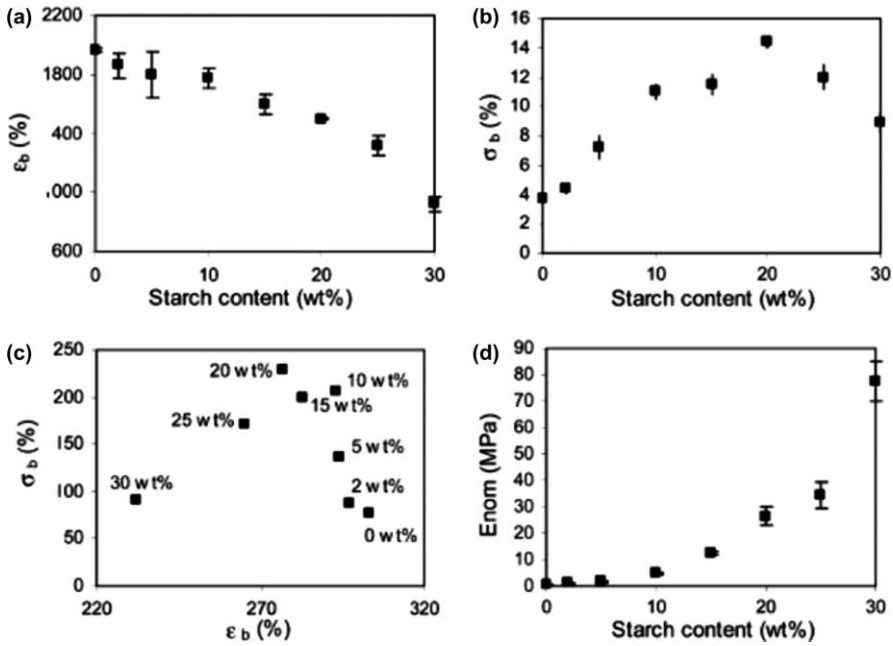

Figure 14.14 Nominal (a) elongation at break, (b) strength, (c) nominal strength *vs* nominal elongation at break (the starch nanocrystal contents are indicated in panel) and (d) tensile modulus for waxy starch nanocrystals/NR nanocomposite films *vs* starch content.
(Reproduced from reference 102 with permission from the American Chemical Society.)

to be reached for a starch content around 20 wt%.[94] The tensile modulus increases nearly exponentially with starch content. Furthermore, high starch nanocrystal contents seem to preserve the elastic behaviour of NR-based composites, contrarily to carbon black (Figure 14.5).[54] Results showed that particle–particle interactions play a crucial role in the properties of starch nanocrystals filled NR. Any deterioration of these interactions results in a dramatic decrease in the mechanical performances of the resulting composites.

The SEMs in Figure 14.16 show the surface of unfilled NR and films filled with 5 wt% and 30 wt% of nanocrystals. The freshly fractured surface of the unfilled NR film is smooth and uniform.[100] By comparing these with the micrographs showing the surface of fractured composites, it is easy to identify the filler. Starch nanocrystals appear like white dots, whose concentration is a direct function of the starch content in the composite. The distribution of the filler among the matrix is homogeneous for both compositions. It is a key property for expecting good mechanical properties. Furthermore, no particular sedimentation phenomenon of starch nanocrystals within the thickness of the films was observed.

The nanocomposite materials were also developed from acetylated and hexamethylenediisocyanate (HMDI) modified starch nanoparticles by a commercial milling process.[85] The bionanocomposites showed superior strength

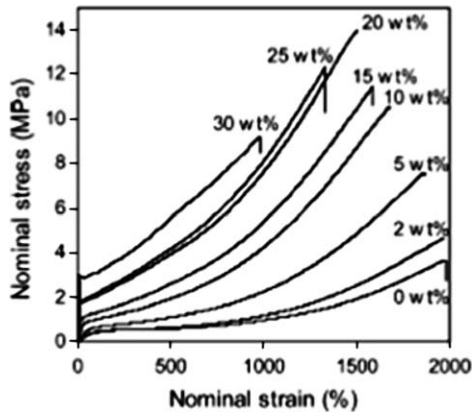

Figure 14.15 Typical nominal stress *vs* nominal strain curves of waxy maize starch nanocrystals/NR nanocomposite films. The starch nanocrystal contents are indicated in the figure.
(Reproduced from reference 102 with permission from the American Chemical Society.)

and elongation to conventional carbon black/NR composites up to 40 phr loading (Figure 14.17). The modified starch nanoparticles showed better compatibility with the NR matrix, as per SEM and XRD studies which revealed the uniform morphology and nearly exfoliated structure. HMDI-modified starch nanoparticles imparted the highest strength, increased the T_g and decreased solvent sorption, probably due to formation of additional crosslinks during the vulcanization process.

14.7.1.3 NR–Cellulose Nanocomposites

Cellulose whiskers and microfibrillated cellulose were used as the reinforcing phase to prepare nanocomposite films using NR latex as the matrix. The nanoparticle content for which the behaviour change is between 5 and 10 wt% for nanocomposite films reinforced with cellulose whiskers and 1 and 2.5 wt% for MFC (Table 14.1).[72] As expected, and for both sets of nanocomposites, the elongation at break decreases and both the tensile modulus and the strength increase drastically when increasing the nanoparticle content. Entangled MFC provides a higher stiffness than cellulose whiskers but induces brittleness into the material. It means that the behaviour of the material is mainly governed by the NR matrix over a broader composition range for cellulose whiskers compared to MFC. The higher aspect ratio and possibility of entanglements of the latter could probably explain this different behaviour. Also, the higher compatibility of MFC with the hydrophobic NR matrix, and the ensuing higher filler/matrix adhesion could explain this difference.

The development of nanocomposites highly filled (>50 phr) with acetylated cellulosic fillers has also been attempted. A comparison of mechanical properties

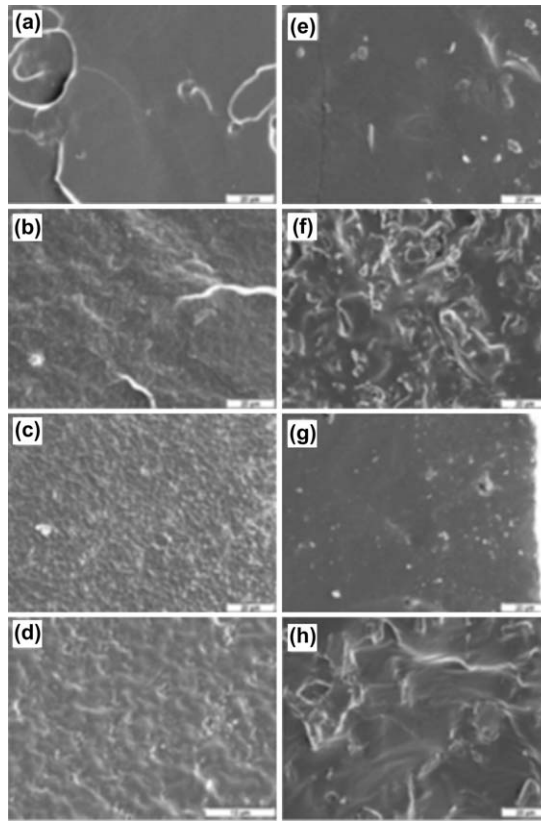

Figure 14.16 SEM of the fractured surfaces of (a) unfilled NR, NR filled with (b) 5 and (c, d) 30 wt% of starch nanocrystals, NR filled with (e) 5 and (f) 30 wt% of ASA-modified particles, and NR filled with (g) 5 and (h) 30 wt% of PI-modified starch nanoparticles.
(Reproduced from reference 108 with permission from the American Chemical Society.)

with unmodified cellulose fillers and carbon black revealed that these fillers exhibit promising reinforcement even at higher loadings (Figure 14.18).[101]

14.7.2 Dynamic Mechanical Analysis (DMA)

There are quite a few reports on the dynamic-mechanical properties of NCs of NR.[19,53,57,61] As seen from the results shown in Figure 14.19,[103] starch nanocrystals displayed a significant reinforcing effect, in particular on the rubbery plateau of the non-vulcanized NR polymer. This reinforcing effect was attributed to the formation of a percolating starch nanocrystal network through hydrogen linkages between starch nanoparticle clusters.

DMA results of NR/chitin whiskers[57] revealed that above T_g, the modulus of all chemically modified whisker-based composites was found to be much lower than that of the unmodified one and more similar to that of the unfilled matrix.

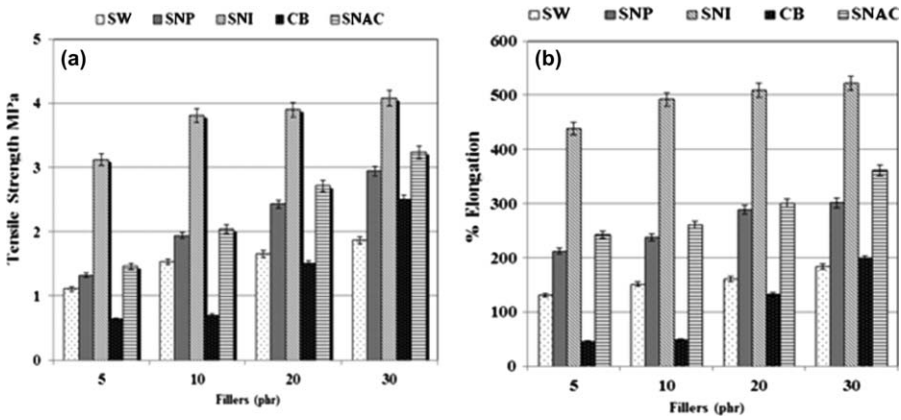

Figure 14.17 Effect of various fillers on (a) tensile strength and (b) % elongation of nanocomposites at 30 phr loading of waxy starch (SW), starch nanoparticles (SNP), HMDI-modified SNP (SNI), acetylated SNP (SNAC). (Reproduced from reference 89 with permission from Elsevier.)

Table 14.1 Mechanical properties of NR films reinforced with cellulose nanocrystals and microfibrils (MF) cellulose extracted from the date palm tree obtained from the tensile tests: Young's modulus (E), strain at break (€R) and strength.

Sample	*E (MPa)*	σ_R *(MPa)*	ε_R *(%)*
NR	0.5 ± 0.15	0.56 ± 0.12	575 ± 35
NR-W1	1.75 ± 0.5	0.86 ± 0.06	408 ± 49
NR-W5	8.4 ± 1.1	2.71 ± 0.10	231 ± 53
NR-W10	118 ± 6	8.93 ± 1.23	16 ± 3
NR-W15	187 ± 0.5	12.15 ± 1.48	14 ± 1
MF-W1	1.27 ± 0.0	0.70 ± 0.13	209 ± 29
MF-W2.5	10.52 ± 0.66	0.80 ± 0.26	14.6 ± 4.5
MF-W5	35.46 ± 5.79	2.17 ± 0.38	13.8 ± 2.3
MF-W7.5	121.2 ± 8.8	4.15 ± 0.71	8.18 ± 1.65
MF-W10	172 ± 62	5.99 ± 2.56	6.65 ± 2.08
MF-W15	233 ± 57	6.26 ± 2.70	3.95 ± 1.14

(Reproduced with permission from ref. no. 72 copyright 2010 Elsevier).

The thermal stability of the composites is also very much reduced after chemical modification. It could be mainly attributed to the negligible presence or absence of the rigid network of chitin as a result of chemical modification.

14.7.3 Sorption Properties in Water and other Organic Solvents

One interesting area of study in the case of composites is the moisture uptake of fibre-reinforced composites.[103] Pure hydrocarbon rubber absorbs very little water, less than 1 ppt. This limited uptake takes place because of the small amount of protein that is present in the polymer. A major drawback of vegetable fibre-reinforced composites is their affinity toward moisture, leading to

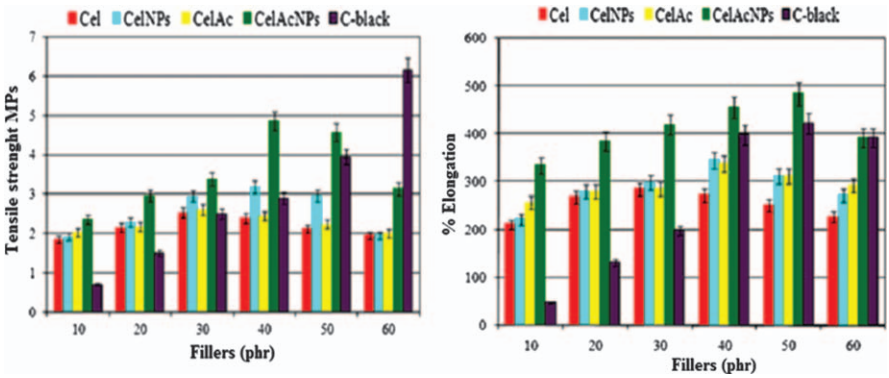

Figure 14.18 Mechanical properties of NR composites at 40 phr loading of cellulose (Cel), cellulose NPs (CelNPs), cellulose acetate (CelAc), cellulose acetate NPs (CelAcNPs) and carbon black.
(Reproduced from reference 101 with permission.)

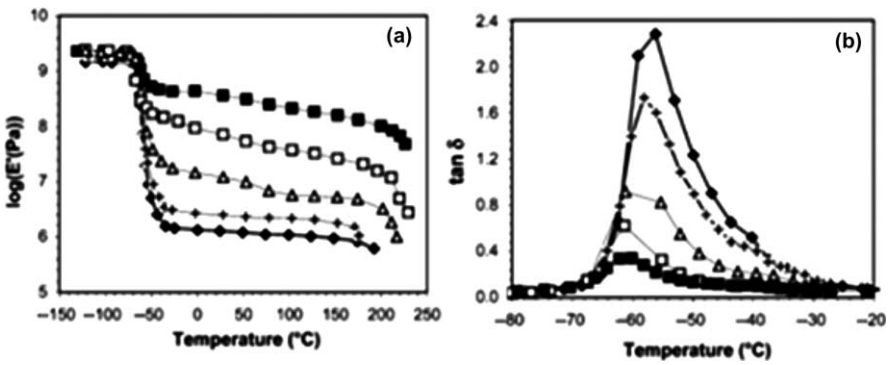

Figure 14.19 (a) Logarithm of the storage tensile modulus E_0 and (b) tangent of the loss tangent angle tan δ vs temperature at 1 Hz for NR filled with different waxy maize starch nanocrystal contents: (■) 5, (Δ) 10, (+) 20 and (▲) 30 wt%.
(Reproduced from reference 103 with permission from the American Chemical Society.)

low degrees of adhesion between fibre and matrix. Incorporation of natural fibres into polymeric composites thus generally increases the rates of water sorption ability. Moisture absorption takes place by three types of mechanisms, namely, diffusion, capillarity, and transport *via* microcracks. Among the three, diffusion is considered to be the major mechanism. Water absorption largely depends on the water-soluble or hygroscopic components embedded in the matrix, which acts as a semipermeable membrane. The water penetration and diffusion are mainly through the fibre matrix interfacial region and the cross-sectional portions of the fibres by capillary mechanisms. The porous structure of the fibre facilitates the water absorption by capillary action. This mechanism involves the flow of water molecules along the fibre–matrix interface followed

by diffusion from the interface into the matrix and the fibre. Microcracks can also pave the way for moisture transport involving the flow and storage of water within the cracks. Thus, fibre/matrix adhesion is an important factor in determining the sorption behaviour of a composite. Moreover, fibre architecture has also been found to affect the moisture absorption. Moisture diffusion in polymeric composites has been shown to be Fickian as well as non-Fickian in character. The main factors which affect the diffusion process in a polymeric composite are as follows:

(1) The polarity of the molecular structure, *i.e.* the presence of chemical groups capable of forming hydrogen bonds.
(2) The degree of crosslinking.
(3) The presence of residual monomers or other water attacking groups.
(4) Crystallinity and diffusivity.
(5) Free hydroxyl groups.
(6) Temperature and humidity.
(7) Area of exposed surfaces.
(8) Surface protection.

In general, moisture diffusion in a composite depends on factors such as volume fraction of fibres, void volume, additives, orientation of reinforcement, nature of fibre (that is permeable or impermeable).

In nanocomposites of starch it was shown that above 10 wt% starch nanocrystals form a continuous network within the NR matrix supposed to be held through hydrogen bonding forces between nanoparticles. The existence of this network results in decreasing and increasing the diffusivity of toluene and water in composites, respectively.[87] Compared to unmodified nanoparticle-based composites, the resulting decrease of particle–particle H-bond interactions induced an increase of the toluene uptake and a decrease of the water uptake of NR/modified starch nanocrystals composite films.[104] Furthermore, the morphological nature of SNPs confers to the materials barrier properties to water vapour and oxygen.

Figure 14.20 shows photographs of unvulcanized NR/chitin whisker nanocomposites before and 24 h after swelling in toluene.[105] It clearly appears that swelling of the material systematically decreases with increasing amount of chitin whiskers within the NR matrix. Similarly, adding chitin whiskers within the pre-vulcanized NR matrix results in a progressive decrease of D value (Table 14.2).[105] The increasing stiffness of the hydrogen-bonded chitin network and strong filler–matrix interactions limits the toluene diffusivity within the entangled polymer matrix.

14.7.4 Gas Permeability

14.7.4.1 Permeability to Water Vapour

The same authors based on the results of water uptake, predicted that the permeability to water vapour would also increase by adding starch nanocrystals

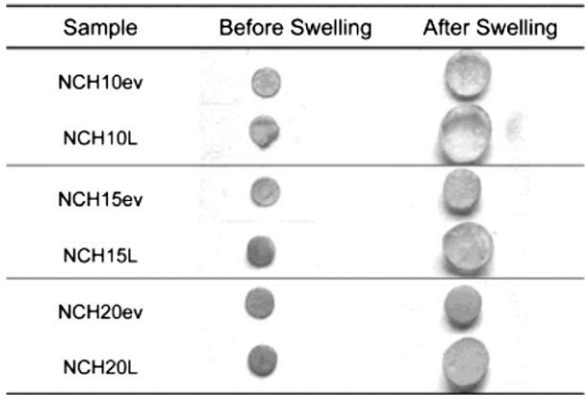

Figure 14.20 Photographs of unvulcanized samples of NR–chitin composites (prepared by evaporation (ev) and hot-pressing methods (L)) before and just after swelling in toluene for 24 h at room temperature (25 °C). The diameter of all samples before swelling was $d_0 = 7.5$ mm.
(Reproduced from reference 105 with permission from the American Chemical Society.)

Table 14.2 Toluene uptake at equilibrium and toluene diffusion coefficients in chitin whiskers/vulcanized NR composites immersed in toluene.

Sample	*Toluene uptake at equilibrium (%)*	*Toluene diffusion coefficient ($cm^2.s^{-1} \times 10^8$)*
PNRev	488	14.1
PCH5ev	413	8.1
PCH10ev	331	5.0
PCH15ev	282	4.6
PCH20ev	239	4.4

P indicates prevulcanized natural rubber and ev indicates rubber obtained by water evaporation technique
(Reproduced with pemission from ref. no. 105 copyright 2003 American Chemical Society).

due to their interconnection and thereby the most likely formation of a continuous starch pathway.[86] However, the water vapour transmission rate (WVTR) decreases continuously upon starch nanocrystals addition (Table 14.3). The hydrophilic nature of starch nanocrystals does not affect the permeability of NR to water vapour. The morphological nature and platelet-like structure of starch particles have most probably an incidence on this result.

14.7.4.2 Permeability to Oxygen

Starch nanocrystals also reduced the oxygen diffusion through the nanocomposite films as shown from the decrease of diffusion coefficient values upon filler content increase in Table 14.3.[72] It is believed that the platelet-like low permeable structures of the starch stand in the way of the oxygen molecules (O_2 diameter 3.47 Å), increasing the tortuosity of the diffusion path. The

Table 14.3 Water vapour transmission rate (WVTR), diffusion coefficient (D), permeability coefficient (P) and solubility (S) of oxygen for starch nanocrystal/NR nanocomposite films.

Sample	*WVTR* *(g m^{-2} day^{-1})*	*D* *(cm^2 $s^{-1} \times 10^7$)*	*P* *(barrer)*[a]	*S* *(cm^2 STP cm^{-1} Hg $cm^{-3} \times 10^3$)*
L100	0.078	16.3	25.7	1.58
L95	0.055			
L90	0.054	15.2	21.1	1.39
L80	0.043	10.2	16.8	1.65
L70		7.2	8.9	1.23

[a]1barrer = 10^{-10} cm^3 STP cm $s^{-1}cm^{-2}$ $cmHg^{-1}$. L100 indicates the unfilled NR.
(Reproduced with permission from ref. no. 108 copyright 2005 American Chemical Society).

addition of starch nanocrystals also reduces the oxygen permeability (Table 14.3). The large decrease in permeability of NR filled with 30 wt% of starch nanocrystals is due to a large decrease in sorption coefficient, which adds to the barrier effect. The platelet-like morphology of starch nanocrystals seems to be responsible for the decrease in both the permeability to water vapour and oxygen of NR filled films.

14.8 Reinforcing Mechanisms

The use of high aspect ratio whiskers induces a mechanical percolation phenomenon leading to outstanding and unusual mechanical properties through the formation of a rigid filler network. In addition to some practical applications, the study of such model systems can help to understand some physical properties as geometric and mechanical percolation effects. According to a recent review[74] the reinforcing effect of starch and cellulose nanocrystals is generally ascribed to the formation of a hydrogen-bonded percolating filler network above a given starch content corresponding to the percolation threshold. However, this assumption is difficult to prove because the connecting particles should be starch clusters or aggregates with ill-defined size and geometry. Later the same authors[102] developed phenomenological modelling approach to understand the reinforcing mechanism of starch nanocrystals in a non-vulcanized NR matrix.

14.8.1 Payne Effect

Filler–matrix and filler–filler interactions are generally associated with the decrease of the dynamical modulus with the strain amplitude, which is known as the Payne effect.[106] The typical features generally associated with the Payne effect, that is, strain dependence of the viscoelastic properties of filled NR are illustrated in Figure 14.21. Unfilled NR displayed a linear viscoelastic behaviour, with no change in dynamic moduli with strain amplitude, whereas the storage modulus of nanocomposites decreased with increasing deformation from a maximum value, G'_0, down to a value, G'_1, corresponding to the storage

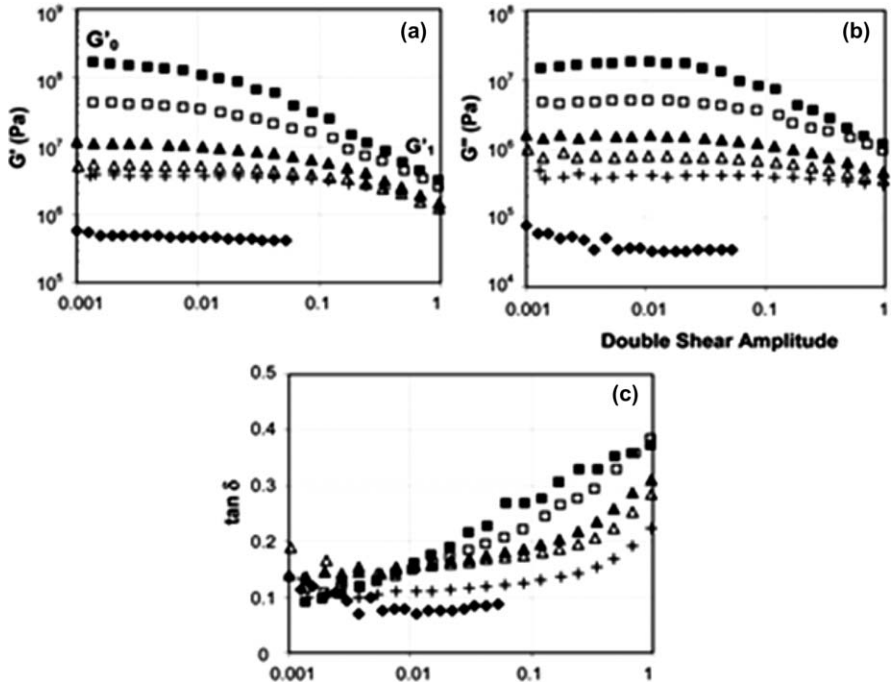

Figure 14.21 Variation of (a) the storage shear modulus G', (b) the loss shear modulus G'' and (c) tan δ as a function of the double shear amplitude γ, at 25 °C, for NR filled with different waxy maize starch nanocrystal contents: (◆) 0, (+) 5, (Δ) 10, (▲) 15, ( ) 20 and (■) 30 wt%.

modulus at 100% of deformation.[103] The magnitude of the Payne effect increased with increasing filler content, as already shown by many authors for vulcanized elastomers.[103]

14.8.2 Mullins Effect

The Mullins effect is characterized by stress softening. In order to demonstrate the presence of the Mullins effect in NR nanocomposites, three successive tensile cycles were performed for each sample. For the unfilled NR matrix, curves corresponding to the successive cycles were perfectly superposed, to a few per cent (6–8%) (Figure 14.22(a)).[103] For nanocomposites, a significant decrease in G'_0 can be observed between the first and the second cycle, for films reinforced with 30 wt% starch nanocrystals (Figure 14.22(b)).[103] Similar to the Payne effect, the magnitude of the Mullins effect also increases with filler content. Furthermore, this increase was almost proportional to the filler content.

14.9 Commercial Avenues

Recently Novamont (Novara, Italy), working in partnership with Goodyear Tire and Rubber, has developed tyres using nanoparticles derived from corn

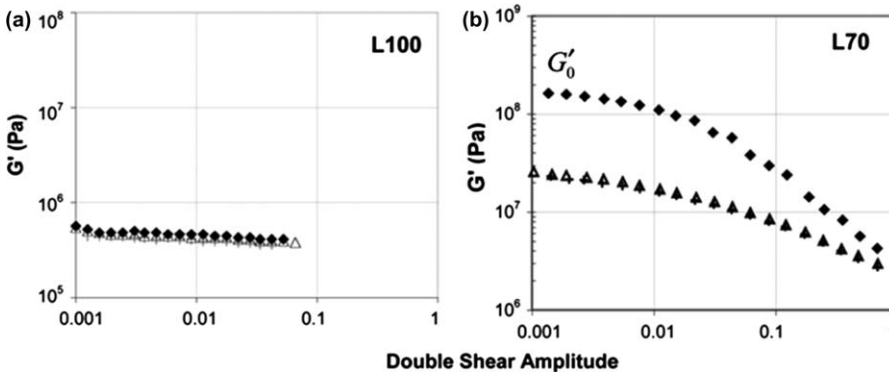

Figure 14.22 Variation in the storage shear modulus G' as a function of the double shear amplitude γ for (a) unfilled NR (L100) and (b) NR filled with 30 wt% waxy maize starch nanocrystals (L70), at 25 °C, for three successive cycles: (◆) cycle no. 1, (Δ) cycle no. 2 and (+) cycle no. 3.

starch, partially replacing the conventional carbon black and silica used in making tyres.[13] This patented innovation, called Biotred, presents environmental advantages but also allows the rolling resistance of tyres to be reduced. In this approach, waxy maize starch nanocrystals constitute another possible filler for NR.

SEM observations confirmed that the filler was evenly distributed within the NR matrix, which is a key property for expecting good mechanical properties. Wide-angle X-ray diffraction analysis showed that the processing did not affect the crystallinity of the starch nanocrystals. By adding starch nanocrystals in NR, the swelling by toluene decreases and the swelling by water increases. It was assumed that these phenomena were due to the formation of a starch nanocrystals network through hydrogen linkages between starch nanoparticles clusters and also to favourable interactions between the matrix and the filler. The formation of the network of starch nanocrystals was assumed to be governed by a percolation mechanism. The platelet-like morphology of starch nanocrystals seemed to be responsible for the decrease of both the permeability to water vapour and oxygen of NR filled films. The surface chemical modification of starch nanocrystals results in a favoured swelling behaviour with toluene and a diminution of the water uptake.

14.10 Comparison of Properties: Bionanocomposites *vs* Micro- and Nanocomposites

The reinforcing effect of starch nanocrystals was compared to the one of other fillers for NR published in the literature such as clays, organoclays, carbon black, fly ash and chitin whiskers.

The relative values of the conventional tensile modulus at 100% elongation, strength, and elongation at break, which correspond to the ratio of a given

Table 14.4 Comparison of relative mechanical properties of NR filled with different types and contents of fillers: relative conventional tensile modulus at 100%, elongation (ER100%), relative strength (σRb), and relative elongation at break (εRb).

Sample	*ER100%*	*σRb*	*εRb*
NR-5 wt % of starch nanocrystals	1.6	1.95	0.91
NR-10 wt % of starch nanocrystals	2.5	2.97	0.9
NR-20 wt % of starch nanocrystals	5	3.89	0.76
CNR-14.2 vol % of flyash	0.97	2.68	~1
CNR-8.3 wt % of carbon black	1.41	1.16	0.66
CNR-26.6 wt % of carbon black	2.71	2.42	0.62
CNR-8.3 wt % of unmodified clay	0.90	0.85	0.79
CNR-8.3 wt % of organoclay	2.92	3.53	~1
NR-5 wt % of chitin whiskers	2.78	1.76	0.53

CNR indicates crosslinked NR.
(Reproduced with permission from ref. no. 102 copyright 2005 American Chemical Society).

property divided by the one of the unfilled NR matrix, are collected in Table 14.4.[94] Except for films reinforced with chitin whiskers, the NR matrix is systematically crosslinked (labelled CNR in Table 14.4) whereas it is unvulcanized. This difference can have an importance mainly for ultimate properties. Starch nanocrystals present better mechanical properties than flyash.[107] They are clearly a good substitute for carbon black since the addition of only 10 wt% of starch nanoparticles to NR induces a reinforcing effect similar, in terms of stiffness, to the one observed with 26.6 wt% carbon black.[96] In addition, high starch nanocrystals contents seem to preserve the elastic behaviour of NR-based composites, contrarily to carbon black. Indeed, the decrease of the elongation at break is more progressive for the starchy filler than for carbon black, which induces a high brittleness of the material with only a few per cent. However, starch nanocrystals are not as competitive as organoclays. This could be ascribed to the higher aspect ratio of exfoliated organoclay nanoplatelets. Compared to chitin whiskers, starch nanocrystals based nanocomposites display a lower tensile modulus but higher ultimate properties (both higher strength and elongation at break) for 5 wt% filler content. This is due to the higher aspect ratio and completely different geometry of rod-like chitin nanocrystals and thus a lower percolation threshold.

14.11 Summary and Future Challenges

State of art on the subject reveals that considerable efforts have been devoted to develop completely green nanocomposites of NR. Much of the synthesis of bionanofillers has been attempted with polysaccharides obtained from numerous sources. The combined effect of size reduction and organic modification improves filler–matrix adhesion and in turn the performance of polysaccharides. Due to simplicity of process, nanosized derivatives of polysaccharides can be synthesized in bulk and can be used for the development of

bionanocomposites. They can be promising substitutes for carbon black and organoclays for reinforcement of NR. Such completely green bionanocomposites may also be suitable for certain biomedical applications. However, various other aspects such as thermal stability, ageing and long-term stability need to be investigated.

References

1. P. M. Visakh, S. Thomas, K. Oksman and A. P. Mathew, *Composites, Part A*, 2012, **43**, 735.
2. S. Riyajan, I. Intharit and P. Tangboriboonrat, *Ind. Crops Prod.*, 2012, **36**, 376.
3. S. Mohapatra and G. B. Nando, *Ind. Eng. Chem. Res.*, 2013, **52**, 5951.
4. E. Guth, *J. Appl. Phys.*, 1945, **16**, 20.
5. A. Zhang, L. Wang, Y. Lin and X. Mi, *J. Appl. Polym. Sci.*, 2006, **101**, 4933.
6. Y. Liu, L. Li and Q. Wang, *J. Appl. Polym. Sci.*, 2010, **118**, 1111.
7. N. Rattanasom, T. Saowapark and C. Deeprasertkul, *Polym. Test.*, 2007, **26**, 369.
8. J. W. Rogers, *Rubber World*, 1981, **21**, 183.
9. L. A. Goettler, A. J. Lambright, R. I. Leib and P. J. Dimauro, *Rubber Chem. Technol.*, 1981, **54**, 274.
10. H. Ismail, N. Rosnah and H. D. Rozman, *Eur. Polym. J.*, 1997, **33**, 1231.
11. A. N. Netravali and S. Chabba, *Mater. Today*, 2003, **6**, 22.
12. H. Ismail, H. D. Rozman, R. M. Jaffri and Z. A. Mohdishak, *Eur. Polym. J.*, 1627, **1997**, 33.
13. W. Pichayakorn, J. Suksaeree, P. Boonme, T. Amnuaikit, W. Taweepreda and G. C. Ritthidej, *Ind. Eng. Chem. Res.*, 2012, **51**, 8442.
14. G. R. Lightsey, *Polymer Sci. Technol.*, 1981, **17**, 19.
15. W. G. Glasser, R. Taib, R. K. Jain and V. Kander, *J. Appl. Polym. Sci.*, 1999, **73**, 1329.
16. L. A. Goettler and J. S. Shen, *Rubber Chem. Technol.*, 1983, **56**, 620.
17. D. K. Setua and S. K. De, *J. Mater. Sci.*, 1984, **8**, 8.
18. V. Favier, J. Cavaille, G. Canova and S. Shrivastava, *Polym. Eng. Sci.*, 1732, **1997**, 37.
19. M. A. S. A. Samir, F. Alloin and A. Dufresne, *Biomacromolecules*, 2005, **6**, 612.
20. N. Ljungberg, C. Bonini, F. Bortolussi, C. Boisson, L. Heux and J. Y. Cavaille, *Biomacromolecules*, 2005, **6**, 2732.
21. J. Bicerano and J. L. Brewbaker, *J. Chem. Soc., Faraday Trans.*, 1995, **91**, 2507.
22. V. P. Silva, M. C. Gonçalves and I. V. P. Yoshida, *J. Appl. Polym. Sci.*, 2006, **101**, 290.
23. M. Jacob, F. Bejoy, S. Thomas and K. T. Varughese, *Polym. Compos.*, 2006, **27**, 671.
24. K. Boustany and P. Hamed, *Rubber World*, 1974, **171**, 39.

25. A. Y. Coran, *Rubber Chem. Technol.*, 1974, **47**, 396.
26. K. Boustany and R. L. Arnold, *J. Elastoplast.*, 1976, **8**, 160.
27. H. Ismail and R. M. Jaffri, *Polym. Test.*, 1999, **18**, 381.
28. L. A. Goettler and K. S. Shen, *Rubber Chem. Technol.*, 1983, **56**, 619.
29. V. G. Geethamma, K. T. Mathew, R. Lakshminarayanan and S. Thomas, *Polymer*, 1998, **39**, 1483.
30. G. C. Derringer, *Rubber World*, 1975, **165**, 45.
31. A. Y. Coran and P. Hamed, *Additives for Plastics*, Academic Press, New York, 1978, p. 1.
32. S. Joseph, M. Jacob and S. Thomas, *Natural Fibers, Biopolymers and their Biocomposites*, Eds. A. K. Mohanty, M. Misra and L. T. Drzal, CRC Press, Oxford, 2005.
33. J. E. O'Connor, *Rubber Chem. Technol.*, 1977, **50**, 945.
34. M. S. Sreekala, J. George, M. G. Kumaran and S. Thomas, *Compos. Sci. Technol.*, 2002, **62**, 339.
35. S. R. Moghe, *Rubber Chem. Technol.*, 1976, **49**, 1160.
36. V. M. Murty and S. K. De, *J. Appl. Polym. Sci.*, 1984, **29**, 1355.
37. V. M. Murty and S. K. De, *Rubber Chem. Technol.*, 1982, **55**, 287.
38. A. Buleon, P. Colonna, V. Planchot and S. Ball, *Int. J. Biol. Macromol.*, 1998, **23**, 85.
39. R. L. Whistler and E. F. Paschall, *Starch: Chemistry and Technology*, Academic Press: New York, 1965.
40. A. D. French, N. R. Bertoniere, R. M. Brown, H. Chanzy, D. Gray, K. Hattori and W. Glasser, 'Cellulose', In The Encyclopedia of Polymer Science and Technology, Ed. J. I. Kroscwitz, 3rd Ed. Vol. 5, John Wiley & Sons, New York, pp. 473–507.
41. D. R. Rathke and S. M. Hudson, *J. Macromol. Sci., Rev. Macromol. Chem. Phys.*, 1994, **34**, 375.
42. M. Valodkar and S. Thakore, *J. Appl. Polym. Sci.*, 2012, **124**, 3815.
43. J. Johns and V. Rao, *Int. J. Polym. Anal. Charact.*, 2008, **13**, 280.
44. M. Valodkar and S. Thakore, *Carbohydr. Res.*, 2010, **345**, 2354.
45. E. Bouthegourd, K. R. Rajisha, N. Kalarical, J. M. Saiter and S. Thomas, *Mater. Lett.*, 2011, **65**, 3615.
46. M. Valodkar and S. Thakore, *Int. J. Polym. Anal. Charact.*, 2010, **15**, 1.
47. A. Morin and A. Dufresne, *Macromolecules*, 2002, **35**, 2190.
48. M. Paillet and A. Dufresne, *Macromolecules*, 2001, **34**, 6527.
49. Y. S. Lu, L. H. Weng and L. N. Zhang, *Biomacromolecules*, 2004, **5**, 1046.
50. X. Wu, F. G. Torres, F. Vilaseca and T. J. Peijs, *J. Biobased Mater. Bioenergy*, 2007, **1**, 341.
51. J. Sriupayo, P. Supaphol, J. Blackwell and R. Rujiravanit, *Carbohydr. Polym*, 2005, **62**, 130.
52. J. D. Goodrich and W. T. Winter, *Biomacromolecules*, 2007, **8**, 252.
53. K. G. Nair and A. Dufresne, *Biomacromolecules*, 2003, **4**, 1835.
54. Y. Bendahou, H. Habibi, A. Kaddami and A. Dufresne, *J. Biobased Mater. Bioenergy*, 2009, **3**, 81.

55. J. B. Zeng, Y. S. He, S. L. Li and Y. Z. Wang, *Biomacromolecules*, 2012, **13**, 1.
56. R. H. Marchessault, F. F. Morehead and N. M. Walter, *Nature*, 1959, **184**, 632.
57. J. F. Revol, L. Godbout, X. M. Dong, D. G. Gray, H. Chanzy and G. Maret, *Liq. Cryst.*, 1994, **16**, 127.
58. J. Sugiyama, H. Chanzy and J. F. Revol, *Planta*, 1994, **193**, 260.
59. L. Heux, E. Dinand and M. R. Vignon, *Carbohydr. Polym.*, 1999, **40**, 115.
60. M. A. S. A. Samir, F. Alloin, M. Paillet and A. Dufresne, *Macromolecules*, 2004, **37**, 4313.
61. O. Berg, J. R. Capadona and C. Weder, *Biomacromolecules*, 2007, **8**, 1353.
62. M. A. S. A. Samir, F. Alloin, J. Y. Sanchez, N. E. Kissi and A. Dufresne, *Macromolecules*, 2004, **37**, 1386.
63. N. Kasyapi, V. Chaudhary and A. K. Bhowmick, *Carbohydr. Polym.*, 2013, **92**, 1116.
64. Y. Habibi, L. A. Lucia and O. Rojas, *J. Chem. Rev.*, 2010, **110**, 3479.
65. M. A. Hubbe, O. J. Rojas, L. A. Lucia and M. Sain, *BioResources*, 2008, **3**, 929.
66. L. Sir and D. Plackett, *Cellulose*, 2010, **17**, 459.
67. H. Chanzy, K. Imada, A. Mollard, R. Vuong and F. Barnoud, *Protoplasma*, 1979, **100**, 303.
68. W. Helbert, J. Sugiyama, M. Ishihara and S. J. Yamanaka, *Biotechnol. J*, 1997, **57**, 29.
69. B. G. Rånby, *Acta. Chem. Scand.*, 1949, **3**, 649.
70. M. N. Angles and A. Dufresne, *Macromolecules*, 2001, **34**, 2921.
71. P. Ortiz-Serna, R. Díaz-Calleja, M. J. Sanchis, E. Riande, R. Nunes, A. Martins and L. Visconte, *J. Non-Cryst. Solids*, 2011, **357**, 598.
72. A. Bendahou, H. Kaddami and A. Dufresne, *Eur. Polym. J.*, 2010, **46**, 609.
73. P. Lu and Y. L. Hsieh, *Carbohydr. Polym.*, 2012, **87**, 2546.
74. D. L. Corre, J. Bras and A. Dufresne, *Biomacromolecules*, 2010, **11**, 1139 and references cited therein.
75. A. Dufresne, J. Y. Cavaille and W. Helbert, *Macromolecules*, 1996, **29**, 7624.
76. J. L. Putaux, S. Molina-Boisseau, T. Momaur and A. Dufresne, *Biomacromolecules*, 2003, **4**, 1198.
77. X. Ma, R. Jian, P. R. Chang and J. Yu, *Biomacromolecules*, 2008, **9**, 3314.
78. Y. Tan, K. Xu, L. Li, C. Liu, C. Song and P. Wang, *ACS Appl. Mater. Interfaces*, 2009, **1**, 956.
79. J.-Y. Kim and S.-T. Lim, *Carbohydr. Polym.*, 2009, **76**, 110.
80. D. Liu, Q. Wu, H. Chen and P. R. Chang, *J. Colloid Interface Sci.*, 2009, **339**, 117.
81. H. Namazi and A. Dadkhah, *Carbohydr. Polym.*, 2010, **79**, 731.
82. W. Thielemans, M. N. Belgacem and A. Dufresne, *Langmuir*, 2006, **22**, 4804.

83. X. Fan, Z. T. Liu and Z. W. Liu, *J. Hazard. Mater*., 2010, **177**, 452.
84. M. Valodkar and S. Thakore, *Carbohydr. Polym*., 2011, **86**, 1244.
85. Q. H. Zeng, A. B. Yu, G. Q. Max and D. R. Paul, *J. Nanosci. Nanotechnol*., 2005, **5**, 1574.
86. M. Labet, W. Thielemans and A. Dufresne, *Biomacromolecules*, 2007, **8**, 2916.
87. A. K. Anand, S. T. Jose, R. Alex and R. Joseph, *Int. J. Polym. Mater*., 2010, **59**, 33.
88. Y. Wang, H. Zhang, Y. Wu, J. Yang and L. Zhang, *J. Appl. Polym. Sci*., 2005, **96**, 318.
89. P. Hajji, J. Y. Cavaille, V. Favier, C. Gauthier and G. Vigier, *Polym. Compos*, 1996, **17**, 4.
90. J. Bras, M. L. Hassan, B. Cecile, E. A. Hassan, N. A. El-Wakil and A. Dufresne, *Ind. Crops Prod*., 2010, **32**, 627.
91. H. H. Yuan, Y. Nishiyama, M. Wada and S. Kuga, *Biomacromolecules*, 2006, **7**, 696.
92. W. Thielemans, M. N. Belgacem and A. Dufresne, *Langmuir*, 2006, **22**, 4804.
93. C. Gousse, H. Chanzy, G. Excoffier, L. Soubeyrand and E. Fleury, *Polymer*, 2002, **43**, 2645.
94. H. Ismail, M. N. Nasaruddin and H. D. Rozman, *Eur. Polym. J*., 1999, **35**, 1429.
95. H. Angellier, S. Molina-Boisseau and A. Dufresne, *Macromolecules*, 2005, **38**, 9161.
96. M. Arroyo, M. A. Lopez-Manchado and B. Herrero, *Polymer*, 2003, **44**, 2447.
97. L. E. Yahaya, K. O. Adebowale, A. R. R. Menon, S. Rugmini, B. I. Olu-Owolabi and J. Chameswary, *African J. Pure Appl. Chem*., 2010, **4**, 198.
98. Z. F. Wang, Z. Peng, S. D. Li, H. Lin, K. X. Zhang, X. D. She and X. Fu, *Compos. Sci. Technol*., 2009, **69**, 1797.
99. K. G. Nair and A. Dufresne, *Biomacromolecules*, 2003, **4**, 666.
100. H. Angellier, S. Molina-Boisseau, L. Lebrun and A. Dufresne, *Macromolecules*, 2005, **38**, 3783.
101. M. Valodkar, PhD thesis, M.S. University of Baroda, India.
102. M. Patrice, H. A. Coussy, S. M. Boisseau and A. Dufresne, *Biomacromolecules*, 2011, **12**, 1487.
103. M. Jacob, K. T. Varughese and S. Thomas, *Biomacromolecules*, 2005, **6**, 2969.
104. G. Cantero, A. Arbelaiz, R. Llano-Ponte and I. Mondragon, *Compos. Sci. Technol*., 2003, **9**, 1247.
105. K. G. Nair and A. Dufresne, *Biomacromolecules*, 2003, **4**, 657.
106. S. Bhattacharyya, C. Sinturel, O. Bahloul, M. L. Saboungi, S. Thomas and J. P. Salvetat, *Carbon*, 2008, **46**, 1037.
107. D. G. Hundiwale, U. R. Kapadi, M. C. Desai and S. H. Bidkar, *J. Appl. Polym. Sci*., 2002, **85**, 995.

CHAPTER 15

Magnetic Filler-Reinforced Natural Rubber Macro- and Nanocomposites

ALDO ELOIZO JOB,*[a] FELIPE SILVA BELLUCCI,[a] FLÁVIO CAMARGO CABRERA,[a] ALEXANDRE FIORAVANTE DE SIQUEIRA,[a] EDUARDO ROQUE BUDEMBERG[b] AND LEANDRA OLIVEIRA SALMAZO[a]

[a] Departamento de Física, Química e Biologia, Faculdade de Ciências e Tecnologia - FCT, Univ Estadual Paulista - UNESP, Roberto Simonsen St., 305, Postal Code 19060-900, Presidente Prudente, SP, Brazil; [b] Escola de Engenharia de Lorena - EEL, Universidade de São Paulo - USP, Postal Code 12.602-810, Lorena, SP, Brazil
*Email: job@fct.unesp.br

15.1 Introduction

Natural rubber (NR) currently presents a set of consolidated scientific, technological and industrial applications, being of fundamental significance for several sectors of the global economy. Such applications derive from its distinguished mechanical and thermal properties, obtained through thermal and chemical processes (*e.g.* the vulcanization process).[1,2] In contrast, new fields of application are pursued mainly in sectors traditionally occupied by materials with a nature distinct from polymers, such as ceramic and metallic materials.

RSC Polymer Chemistry Series No. 8
Natural Rubber Materials, Volume 2: Composites and Nanocomposites
Edited by Sabu Thomas, Hanna J. Maria, Jithin Joy, Chin Han Chan and Laly A. Pothen

Published by the Royal Society of Chemistry, www.rsc.org

Vulcanized NR is widely used as a polymeric matrix due to its particular capacity to disperse fillers and nanofillers in concentrations greater than 100 parts per hundred of rubber (phr). It is interesting to note the NR capacity of disperse various kinds of fillers, regardless of the existence of chemical or physical interactions between matrix and filler.

In general, one can insert one or more types of fillers in polymeric matrices aiming for a unique combination of properties, and these fillers may present different chemical and physical properties, and also broad dimensional range: these fillers can present no dimension (*i.e.* nanoparticles), be unidimensional (nanotubes), bidimensional (coatings and lamers) or tridimensional (tridimensional nets or macroparticles).[3,4] The inclusion of these fillers in vulcanized NR, generating composite or nanocomposite materials, gives to these materials different structural, chemical, physical, thermal, electric, electrochemical, optical and magnetic properties.[5,6]

Currently, researches are developed to improve the control over the dispersion of nanometric components and comprehension of the role of interfaces between chemically different structures. Incorporation of nanoparticles in piezoelectric, pyroelectric or ferroelectric phases in a polymeric matrix induces the composite to provide the electric properties of the nanoparticles.[7,8] Some electrical applications may be restricted due to heating caused by the great dielectric loss in electric fields of high magnitude or in some specific frequencies for alternating electric fields. Magnetic nanocomposites in which magnetic species are dispersed within magnetic or non-magnetic matrices present technological applications in the areas of magnetic recording, giant magnetoresistances and magnetic refrigeration. Magnets made of nanocomposite materials have gained academic and industrial attention, because they may have high remanence and considerable capacity to store energy when compared to conventional magnetic materials.[9,10]

15.2 Magnetic Fillers used in Natural Rubber Matrices

Due to the distinguished capacity of inserting amounts greater than 100 phr of inorganic fillers in NR matrices, composites with magnetic properties are formed by embedding inorganic particles which exhibit magnetic properties.

This section is aimed to the study of ceramic phases with magnetic properties for incorporation into matrices of NR, forming magnetic composites and nanocomposites.

15.2.1 Ceramic Fillers: Ferrite

Ceramic materials can present a wide set of physical properties (*e.g.* ferroelectricity, pyroelectricity, piezoelectricity and ferromagnetism). The main class of ceramic material which exhibits magnetic properties is the class of ferrites.

Ferrites are oxide materials whose main phase component is iron (Fe). In general, iron has valence +3, although ferrite structures are also composed by divalent materials (*e.g.* magnesium (Mn), zinc (Zn), copper (Cu), cobalt (Co) or

nickel (Ni)), composing a cubic packing structure of oxygen atoms. This ceramic material class presents the crystallographic structure known as spinel, whose general formula is DE_2O_4. D and E are divalent and trivalent metals, respectively. The unit cell is composed of 56 ions in this structure, of which 32 are anions (O^{2-}) and 24 are cations (8 cations D^{2+} and 16 cations E^{3+}).

In the spinel structure, divalent cations occupy tetrahedral sites, being coordinated by four oxygens and trivalent cations occupy octahedral sites, being coordinated by six oxygens. Typical materials that share this structure include $ZnAl_2O_4$, $ZnFe_2O_4$ and $NiAl_2O_4$.[11] Spinel structure presents a derivation, known as inverse spinel, which differs from the original for a different cation distribution in the crystallographic net.

Most magnetic ceramics possess inverse spinel structure due to a greater net stability when D and E are transition metals. The difference between the structures consists only in a different form of distribution of cations in the atomic sites. In the inverse spinel structure, divalent (D) and half of trivalent (E) cations occupies the octahedral sites, and the tetrahedral sites are occupied by the other half of D metal cations. One must note that, due to trivalent cation division between the two kinds of sites, the contribution of these elements for the magnetic dipole moment of the material while this is only formed by divalent cations is null.[12]

15.2.2 Inverse Spinel Structure and the Nickel–Zinc Ferrite

Among the materials with inverse spinel structure, the paramagnetic or superparamagnetic phasis of Ni–Zn ferrite must be highlighted. This phasis has cubic symmetry and spatial group Fd3m, with unit cell displaying a occupation represented by $(Zn_x^{2+}Fe_{1-x}^{3+})[Ni_x^{2+}Fe_{1+x}^{3+}]O_4^{2-}$.[13] In this formulae the metallic transition cations in parenthesis occupies the tetrahedral site D and metallic cations in brackets occupies the octahedral site E.[14]

If one considers the inexistence of Zn^{2+} cations in ferrite, the amount of iron in both atomic sites would be equal and their contribution for the magnetic dipole moment would be cancelled; this formation would become a responsibility of Ni^{2+} cations. Doping ferrite with Zn^{2+} cations, there is a compulsory migration of Fe^{3+} cations, then there is an abrupt increase in magnetic dipole moment magnitude, because Fe^{3+} and Zn^{2+} cations begin to contribute for the material dipole moment. Thereby it is possible to produce a great number of ferrites with intrinsic magnetization, for appropriate substitution of the metallic ions.

Figure 15.1 shows the $Ni_{0.5}Zn_{0.5}Fe_2O_4$ ferrite structure with octahedral sites in red and tetrahedral sites in dark yellow. This ferrite is formed by a solid solution of Ni_2O_3 (nickel oxide), ZnO (zinc oxide) and iron oxide (Fe_2O_3) in haematite form (α-Fe_2O_3), where this last oxide contains about 70% by weight of ferrite composition.

Ni–Zn ferrites are remarkable scientifically and technologically because of their high electrical resistivity, magnetic properties and several technological

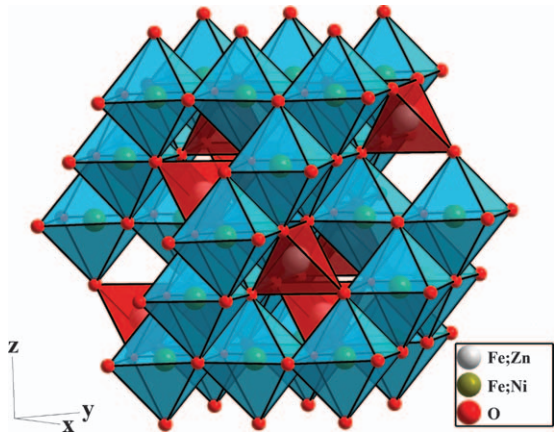

Figure 15.1 Inverse spinel structure representation of the nickel–zinc ferrite with stoichiometry $Ni_{0.5}Zn_{0.5}Fe_2O_4$.

Table 15.1 Relative magnetic permeability values of some Ni–Zn ferrites at 25 °C.

Material	*μr (25 °C)*
$Ni_{0.24}Zn_{0.65}Fe_{2,04}O_4$	1400
$Ni_{0.3}Zn_{0.7}Fe_2O_4$	3422
$Ni_{0.35}Zn_{0.65}Fe_2O_4$	1202
$Ni_{0.4}Zn_{0.6}Fe_2O_4$	1665
$Ni_{0.5}Zn_{0.5}Fe_2O_4$	304
$Ni_{0.65}Zn_{0.35}Fe_2O_4$	415
$Ni_{0.7}Zn_{0.3}Fe_2O_4$	185
$Ni_{0.8}Zn_{0.2}Fe_2O_4$	47

applications in electronics and telecommunications. In general, they are used in core transformers and high-frequency inductors, electronic equipments, microwave devices, telecommunication systems and radars, magnetic read and write heads of high speed.[15] They are also used in digital information processing, energy distribution networks, cellular telephony, prevention of signal interference in television devices, microwave ovens security, hospital equipment, and represents the larger market slice for electromagnetic radiation absorber materials in civil applications.

In the context of magnetic ceramics, Ni–Zn ferrite awakens much interest of scientific community for its high permeability and high resistivity. This fact constitutes a reason for the application of this material in microwave devices. This absorption capacity may be generated or potentiated by changing material magnetic and dielectric properties.

Table 15.1 lists the magnetic permittivity values of some Ni–Zn ferrites in room temperature. It is worth mentioning that variations in these values due to differences in morphological parameters, processing and structure are expected.[12]

The spinel formula can be modified to distinguish between normal and inverse kinds:

Normal spinel: $[A]^{tet}[B_2]^{oct}O_4$
Inverse spinel: $[B]^{tet}[A,B]^{oct}O_4$

Commercially, ferrite-type ceramic materials can be subdivided into three classes, depending on the specific crystal structure. The first class consists of soft ferrite with spinel structure of cubic type (*e.g.* manganese–zinc ferrite (MnZnFeO), nickel–zinc ferrite (NiZnFeO), nickel–magnesium ferrite (NiMgFeO), magnesium–manganese–zinc ferrite (MgMnZnFeO)). The second class is also composed of soft ferrites, but with garnet-type structure, as the microwave ferrites. The third class is composed of hard ferrites with hexagonal structure.

Soft ferrites such as nickel–zinc (Ni–Zn) are composed of spinel type with cubic structure, isomorphic to mineral $MgAl_2O_4$, exhibiting a permanent magnetization called ferrimagnetism. The material of soft ferrite is used in inductors, antenna rods, charging coils and blockers, deflection yokes, recording heads, magnetic amplifiers, on electromagnetic interference (EMI) and power transformers, meeting basic requirements at areas of high technology.

Ferrites have been embedded in matrices under suitable preparation conditions for obtaining a performance required from the final composite.[16,17] In ferrite and rubber composites, the magnetic properties depends on the fraction of ferrite in the matrix.

15.2.3 Preparation of Magnetic Fillers for use in Natural Rubber Matrices

Magnetic materials are widely used in industrial sector, that seeks innovative applications (*e.g.* magnetic composites based in NR), and also the enhancement of already consolidated applications (*e.g.* the use of magnetic particles in cores of transformers and electronic devices). Likewise, this material class is investigated in academic sector to optimize production processes making them economically viable and also seeking new properties and applications.

The preparation of structured materials, powders and ceramic particles in micrometric and nanometric scales need refined forms of processing to obtain materials on adequate dimensional scale and desired magnetic properties. Currently, it is known that it is possible to architect, design, estimate, and add specific characteristics or properties to materials through use of specific preparation routes. The preparation methods of magnetic ceramic materials are classified in physical and chemical routes.

15.2.4 Processing of Materials using Physical Routes

The main advantage of using physical routes is the possibility to prepare greater quantities of material. However, the obtainment of materials with a high degree of purity and complex structure is difficult. Among the physical routes, the

methods based on solid-state reactions, precipitation and mechanical milling are most used.

15.2.4.1 Processing by Solid-State Reaction

A conventional ceramic method, known as solid-state reaction, consists of a diffusional process for obtaining the ceramic phase from the mechanical mixture of oxides, in pre-set stoichiometric amounts. This process is followed by suitable thermal treatment, generally at high temperature (800–1300 °C). After the thermal treatment, calcining and sintering methods lead to a crystalline and homogeneous product.

Employed reactants typically have high melting point and low vapour pressure, then to exceed the diffusion barrier may involve very long reaction times. To increase the diffusion rates in solid–solid reactions, most common features are the use of temperatures near the melting point of the constituents and to reduce the particle size to maximize the contact area between the reactants.

This route is widely used in industry because it is relatively inexpensive and simple, and enables the production of materials in larger quantities, although can present some disadvantages, such as: (a) the need for milling of the obtained oxide or reactant oxides due to the high relative particle size, (b) high processing temperatures, (c) low relative control of the formed phase stoichiometry and (d) the need of washing the products in some cases.[18]

15.2.4.2 Processing by Milling

Three types of mills are used in materials processing by milling: planetary mill, vibratory mill and mechanical attrition mill, also known as an attritor. The first two classes are generally used on an industrial scale because they present less purchase/deployment cost and increased processing capacity. The third class is most frequently used in the production of finest materials, at laboratory scale. Independent of type of mill selected, the energy used to promote the reaction between the elements of the ceramic phase is mechanical in nature and comes from the collision between the milling spheres, or milling rods, and the reactants from the desired ceramic phase. This process of energy transfer is efficiently low, and milling may require times up to 12 hours.

An important point to be evaluated before selecting the physical route is the superficial disorder that materials processed by this route usually present. The processing by mechanical milling produces, in most cases, materials with severe change in surface area and a high degree of structural disorder, which may be interesting (or not) depending of the desired application for the material. In contrast, it is possible to obtain materials in micrometre and nanometre scales, depending on the selected type of milling. The main disadvantage of this method is the greater difficulty to obtain single-phase materials with micrometre or nanometre dimensions.[19]

15.2.5 Processing of Materials by Chemical Routes

Using chemical routes for the preparation of ceramic phases, it is possible to obtain materials with high purity and chemical homogeneity, single phase and greater complexity degrees. However, cost, complexity of the process and amount of produced material are considerable drawbacks. Among the chemical routes, the methods known by polyol, combustion reaction, Pechini, micelles and sol–gel are most used.

15.2.5.1 Polyol Method

Polyol method[20] basically consists in the reduction of metal ions (*e.g.* Co^{2+}, Ni^{2+} and Fe^{3+}) in an alcoholic environment (typically a polyalcohol such as ethylene glycol). Polyol acts in the reaction environment simultaneously as solvent, reducing agent, passivating and means for particle growth.

The advantages of this method are the increasing of chemical homogeneity, possibility of crystalline material production at low temperatures depending on the complexity of phase, possibility of obtaining monophasic, nanosized ($\approx$30 nm) or sub-micrometric ($\approx$250 nm) powders depending on the thermal calcination cycle used, and a large portion of material (10 to 100g) produced in a single synthetic process, when compared to another chemical syntheses.

This chemical route is widely used in the academic environment, because it enables the processing of more complex magnetic phases and allows the precise control of a large set of process variables.[21] Industrially its use is restricted by the high cost compared with the physical processing routes.

15.2.5.2 Pechini Method

The Pechini method, or method of polymeric precursors,[22] is one of the first processing techniques to yield materials with high purity, chemical homogeneity and surface area. The basic methodology consists in dissolve the metals of interest in deionized water at temperatures between 50 and 80 °C. Acid is added (*e.g.* citric acid, $C_6H_8O_7$) in order to form metallic citrate and polyalcohol, such as ethylene glycol. The suitable molar amount of acid and polyalcohol to be added must meet the chemistry reaction of esterification responsible for the formation of the ceramic phase. Thermal treatments of calcination and sintering generally are required for removal of organic material and water.

The main advantages associated with this method are the use of low temperatures, the possibility of obtaining phases and complex ceramics with high purity and the ability to obtain nanosized powders, while the main drawbacks are the high cost of some reactants, the formation of agglomerated powders and low efficiency of synthesis cycles.

15.2.6 Methods of Preparing Magnetic Macro- and Nanocomposites

Academic and industrial environment employs a large set of techniques for preparation of magnetic composites based in vulcanized NR and other

composites. In general, preparation methods for magnetic composite materials do not differ greatly from classical methods for preparation of composites based on NR. It should be emphasized that the main difference between the preparation methods for magnetic and non-magnetic composite materials consists of an additional set of procedures to be followed primarily with respect to preferred orientation and adequate dispersion of the dispersed magnetic phase and cares to not contaminate the preparation equipment.

The main methods of preparing magnetic composite materials are essentially:

i. Mixing in a Banbury mixer, which is the most used industrially where the goal is to obtain larger amounts of material. This equipment is formed basically by one closed chamber with two or more rotating cylinders inside. The mixing and plasticization processes are realized in the same time and the energy for those processes comes from the rotation movie of the cylinder;
ii. Mixing using an open chamber mixer that it is adequate to prepare samples in smaller amounts and because of this, the method is more referenced in scientific literature at an academic level. In this kind of equipment, there are two hot rollers that spinning with different speeds.

In the next section is presented the method of preparation through open chamber mixer, commonly known as a calender, for magnetic composites, emphasizing the key points for processing this class of material.

15.2.7 Method: Dry Mechanical Mixing

The method of dry mechanical mixing[23] using an open chamber mixer is widely used in industry and academia, due to ease in adjusting formulation and external parameters, as processing temperature, thermal treatment time and geometric parameters of the final product, besides the possibility of preparing material in amounts ranging from laboratory to industrial scales. Magnetic composites can be obtained by mechanical mixing and subsequent thermoconformation of dry NR, magnetic ceramic particles in concentrations up to 100 phr and vulcanization system.

Currently, the most used vulcanization systems are based on sulfur. Such systems are composed of an activating system and an acceleration system. The activating system generally contains between 2 and 5 parts of zinc oxide (ZnO) and from 1 to 5 phr of stearic acid ($CH_3(CH_2)_{16}COOH$) that react with each other, as shown in the reaction below, forming zinc stearate ($Zn(C_{18}H_{35}O_2)_2$), responsible for activating the vulcanization process through the generation of active sites mainly in methyl radicals, contained in the main chain of NR. At this stage the samples are named 'activated samples' and should be stored at room temperature without exposure to light for 24 hours.

$$2(C_{17}H_{35}COOH) + ZnO \rightarrow (C_{17}H_{35}COO^-)_2Zn^{2+} + H_2O$$

The acceleration system usually contains between 1.5 and 2.5 parts of octagonal sulfur (S_8) and 0.5 to 2.5 phr of accelerator as, for example, 2-mercaptobenzothiazol. In such a system the temperature is responsible for fragmenting the sulfur chain into smaller segments, responsible together with the sulfurs donated by the accelerator by generating crosslinks between chains of NR. In this step the samples are termed 'accelerated samples'.

The accelerated samples may be thermo-conformed under pressure in thicknesses that can vary between 100 μm and 100 mm in presses, heated rollers or heated jets of air between 120 and 170 °C for predetermined time intervals via rheometric tests. The optimum temperature for vulcanization of NR is of 150 °C, and changes in this temperature imply in inversely proportional changes to the thermo-conformation time. The final geometric shape of the magnetic part determines the vulcanization device. In general, presses are used for closing uniaxial pressures between 1 and 5 MPa.[24]

Rheological studies must be carried out to obtain information about the optimal time to vulcanization process, adjusting the vulcanization system to get the best mechanical properties or thermal properties and to estimate the cure rate index of the vulcanization process. Equipments like the rubber process analyser (RPA), a dynamic mechanical rheological tester, is a common equipment in the rubber industry.

One may note that insertion of the ceramic charge with magnetic properties can occur at any processing step before the thermo-conformation of the composite since, due to their inorganic nature, this filler is inert and does not react or interact chemically with the components of the vulcanization system or the chain of NR. Agents to improve dispersion of the ceramic filler in the polymeric matrix can be used to increase the homogeneity of the dispersion and increase properties that depend on the best structural organization of the material.

Specific fillers may be added to add or enhance specific properties in magnetic materials. Alumina, antimony trioxide or magnesium carbonate may be added to improve the flame retardant properties of the composite. The addition of lead oxide or carbide lead is suggested for improve resistance to nuclear radiation. To improve thermal conductivity, alumina, aluminium powder or silicates can be added. Silica, talc, mica or kaolin are indicated to increase the electrical resistance. The inclusion of metal powders, metal oxides or silicates are suggested to thermal absorption improvement. To increase the tensile strength in NR-based materials, carbon black in general, fibres or polymeric materials may be added.

Figure 15.2 shows images of films that are 200 μm thick and membranes with a thickness of 6 μm of vulcanized NR and nanocomposites formed by ferrite-type paramagnetic nanoparticles of nickel zinc with stoichiometric composition $Ni_{0.5}Zn_{0.5}Fe_2O_4$ (NR/NZF) dispersed in an NR matrix at concentrations of nanoparticles equal to 5 and 50 phr.

Nanocomposites shown in Figure 15.2 were obtained using mechanical mixing, calendering, dry NR, various concentrations of nanoparticles ceramic type nickel–zinc ferrite (NZF) and vulcanization system

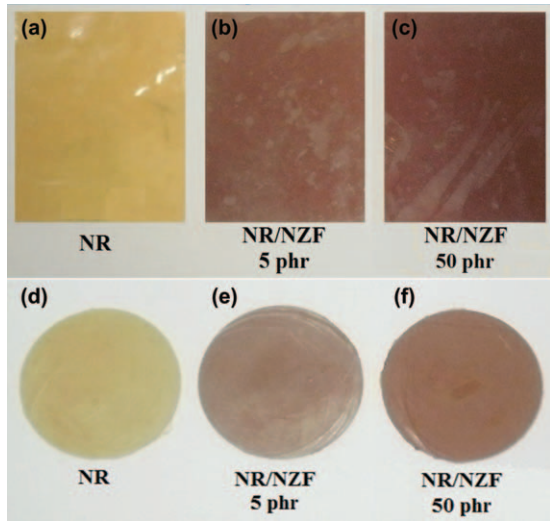

Figure 15.2 (a), (b) and (c): Image of thin films with a thickness of 200 μm, and (d), (e) and (f): membranes with a thickness of 6 mm from vulcanized NR and nanocomposites formed by paramagnetic nanoparticles of nickel–zinc ferrite type dispersed in NR matrix at concentrations of 5 and 50 phr.

compound of 4 phr of zinc oxide, 3 phr of stearic acid, 2 phr of sulfur and 1 phr of 2-mercaptobenzothiazole. The samples were then thermo-conformated in a press with heating system at 150 °C for a period of 8 min 30 s and uniaxial closing pressure of 2.5 MPa. In general, it is not expected to observe magnetic filler/magnetic filler network formation because the mechanical energy transmitted by the preparation process is more than the magnetic attraction. However, small local networks can be formed utilizing other kinds of inorganic fillers like carbon black and silicates.

15.3 Morphological and Spectroscopic Studies of Magnetic Composites

The morphological and spectroscopic studies of magnetic composites and nanocomposites based on NR is widely performed using microscopic techniques, being possible to evaluate, from the micrometre scale to the nanometre scale, the uniformity of surface and volume of materials, homogeneity of the dispersion of magnetic charge, formation and distribution of agglomerates, defect formation, adequacy of the vulcanization system used among other morphological characteristics of this class of materials. The microscopy techniques most commonly used to evaluate the morphology of this class of materials are optical microscopy (OM), scanning electron microscopy (SEM), transmission electron microscopy (TEM) and atomic force microscopy (AFM). In the next item the SEM and AFM techniques are shown, applied to magnetic nanocomposites.

15.3.1 Scanning Electron Microscopy

Scanning electron microscopy (SEM) is widely used in surface and volumetric analysis of composites and nanocomposites based on NR, allowing the analysis of the homogeneity of the dispersion of fillers into the matrix, filler/matrix compatibility, formation of defects, and mainly analysing the formation or absence of aggregate fillers. In magnetic composites, the preparation process is significant for filler dispersion, once the charge magnetism itself may influence the process of formation of agglomerates.

Figure 15.3 shows SEM images of the cross-section of cryogenically fractured samples for vulcanized NR and magnetic nanocomposites formed by paramagnetic nanoparticles of nickel–zinc ferrite at concentrations of 5, 20 and 50 phr, respectively embedded in matrices of NR. The magnification used was 5000 times. The inset is the percentage of nanoparticles with diameter less than 75 nm (black column), between 75 and 250 nm (red column) and greater than 250 nm (green column).

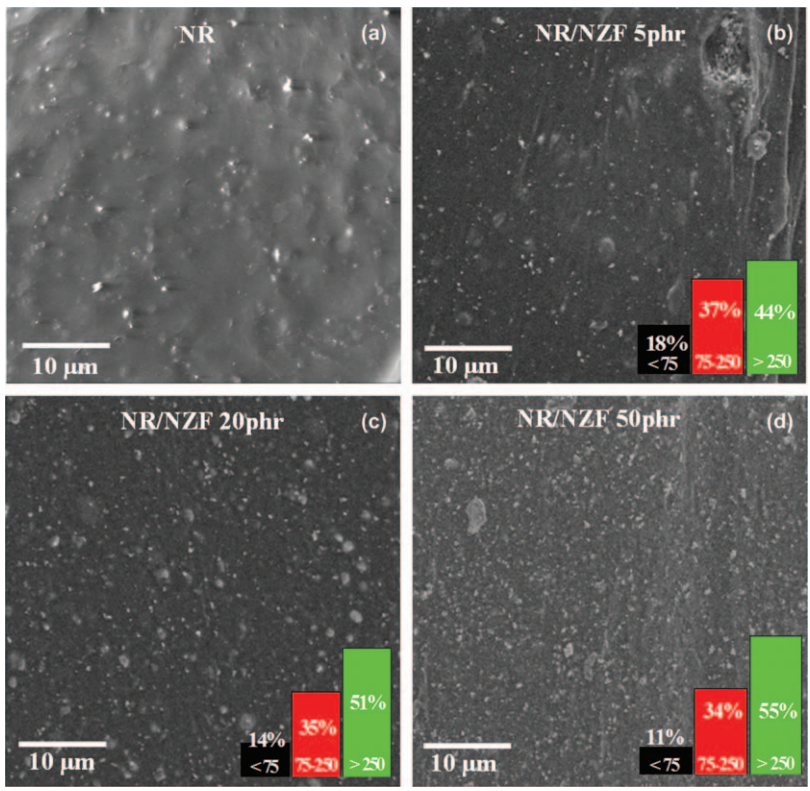

Figure 15.3 (a) SEM images of vulcanized NR and (b), (c) and (d) nanocomposites with 5, 20 and 50 phr of ceramic nanoparticles of type nickel–zinc ferrite embedded in NR.

As one can see in Figure 15.3, an acceptable volumetric homogeneity was obtained for all samples, indicating that the preparation method, system and vulcanization parameters used were appropriately selected. As might be expected, the density of points in the sample volume increases with the increase in concentration of ceramic filler. Particles with nanometric dimensions ($\leq$75 nm) and small agglomerates ($>$75 nm and $\leq$250 nm) are identified in the ceramic phase used. Sub-micrometre particles ($>$250 nm) are also found and are possibly associated with the vulcanization system particles and agglomerates of nanoparticles with greater dimensional magnitude. There is a reduction in the particles with size percentage smaller than 75 nm for both ceramic phases investigated as a function of concentration increasing, indicating a reduction in the dispersibility of nanoparticles and preference for interactions nanoparticle/nanoparticle opposite to interactions nanoparticle/polymer. For particles with sizes between 75 nm and 250 nm, the particle percentage is approximately independent of the concentration of nanoparticles in the polymer matrix. For particles and aggregates with size larger than 250 nm, there is a directly proportional trend between the percentage of occurrence and concentration of nanoparticles. This observation is in agreement with the calculated percentage with particles smaller than 75 nm.

To complement the information obtained from the images of scanning electron microscopy, one can identify and estimate what the components are in a composite or nanocomposite magnetic based on NR conducting energy-dispersive X-ray spectroscopy (EDX) tests. Figure 15.4 shows SEM images performed on the sample surface, a representation of the polymer chain and the EDX spectrum for the vulcanized NR and magnetic nanocomposites.

According to Figure 15.4(a), there is a good surface homogeneity, indicating that a vulcanization system was used in appropriate amounts and an efficient system for preparing nanocomposites. White points were noted and marked with white arrows. Such points may be associated with the vulcanization system, in particular zinc and sulfur with submicron dimensions ($>$250 nm), which could be confirmed by X-ray diffraction assays, since sulfur and zinc oxide generally used are crystalline materials. According to Figure 15.4(b), it is possible to identify a large dispersion of particles and small agglomerates with sizes in the nanometre range between 20 nm and 80 nm, and particles with dimensions in the submicron range. It is suggested that particles and small agglomerates are magnetic nanoparticles. In the EDX spectra, C, O, S and Zn peaks were identified and are associated with the curing system and the polymer chains. Percentages of Fe, Ni and Zn were found for the magnetic samples, in accordance with the elements present in the paramagnetic phase type ferrite with stoichiometry $Ni_{0.5}Zn_{0.5}Fe_2O_4$ used in the preparation of nanocomposites. The values obtained are in agreement with the estimated quantities for stoichiometric calculations. The difference in surface roughness observed in Figure 15.4(a) and Figure 15.4(b) may be associated to the differences in mobility of NR chain due to the incorporation of nanoparticles, even in small quantities of mass.

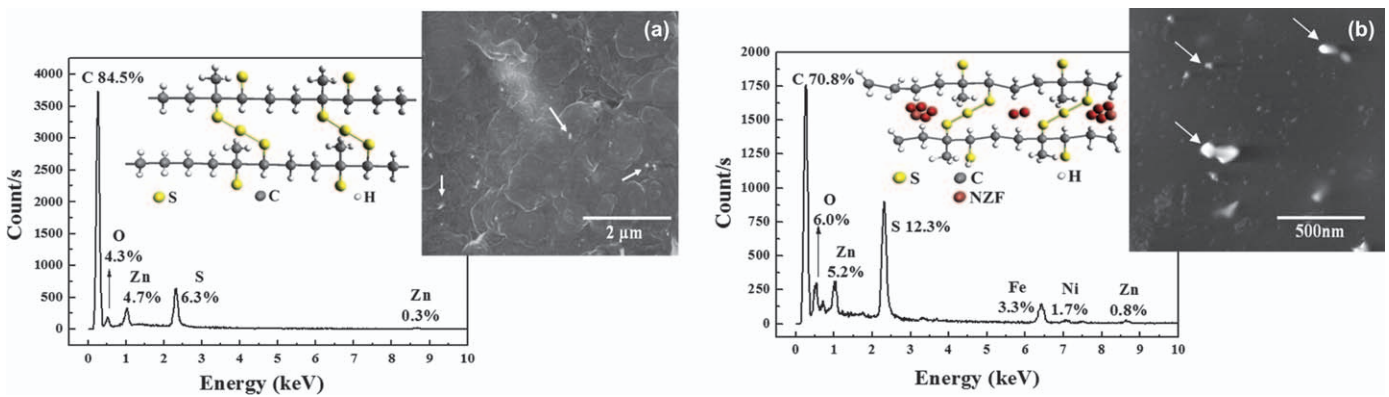

Figure 15.4 Images of (a) SEM of the sample surface representation of the polymer chain and EDX spectrum for the vulcanized NR and (b) magnetic nanocomposites.

15.3.2 Atomic Force Microscopy

Atomic force microscopy (AFM) is a technique designed primarily for the topographic mapping of the sample surface, where this mapping is generated from the interactions between a tip attached to the equipment and the surface to be analysed. The interactions between the tip and the material occur from Van der Waals forces, electrostatic, magnetic and frictional forces, depending on the type of material and the distance between the tip and the sample. The utilization of this morphological technique in magnetic composites and nanocomposites based on NR is higher in the academic environment, for allocating molecular level information of the material. This technique provides mainly information about the surface topography of the material, molecular ordering and defects, allowing direct measurement of the depth of valleys and hills on the molecular level, as well as its roughness. The AFM measurements are performed locally in areas ranging from nanometre scale to micrometric scale. One of the differences of this technique compared to other characterizing techniques of morphological characterization is that it is not necessary that the surface is electrically conductive, further expanding its potential applications.

Figure 15.5 shows images obtained directly over the surface of the samples and their respective three-dimensional projection by the technique of atomic force microscopy to vulcanized NR and the magnetic nanocomposite formed by the addition of 5, 20 and magnetic loading 50 phr in a matrix of vulcanized NR.

According to Figure 15.5, it is possible to observe a good surface homogeneity for both samples of vulcanized NR as for the investigated nanocomposites, indicating that the system and vulcanization parameters used were appropriate. Significant differences for surface roughness were identified only for the NR/NZF 5 phr nanocomposite, indicating that phenomena such as stress-induced crystalization[25,26] may be predominant, associated with insertion of low amounts of nanometric filler.

15.3.3 Infrared Spectroscopy

In general, infrared spectroscopy can be used to investigate the chemical bonds of the NR matrix and the chemical links of the inorganic filled added to the matrix. For infrared spectrum of composites and nanocomposites based on NR, it is possible to identify all of the vibration band characteristics of the poly(*cis*-1,4-isoprene) structure being principally two main sets of bonds. The first set around 3000 cm^{-1} and the second set around 1500 cm^{-1}. For the inorganic filler, it is expected to identify bands mainly between 800 and 200 cm^{-1} that it can be attributed mainly to the metal–oxygen bonds.

15.4 Mechanical and Thermal Analysis

The selection of a specific material for use in engineering projects must take into account a broad set of variables, involving from the search of a material that

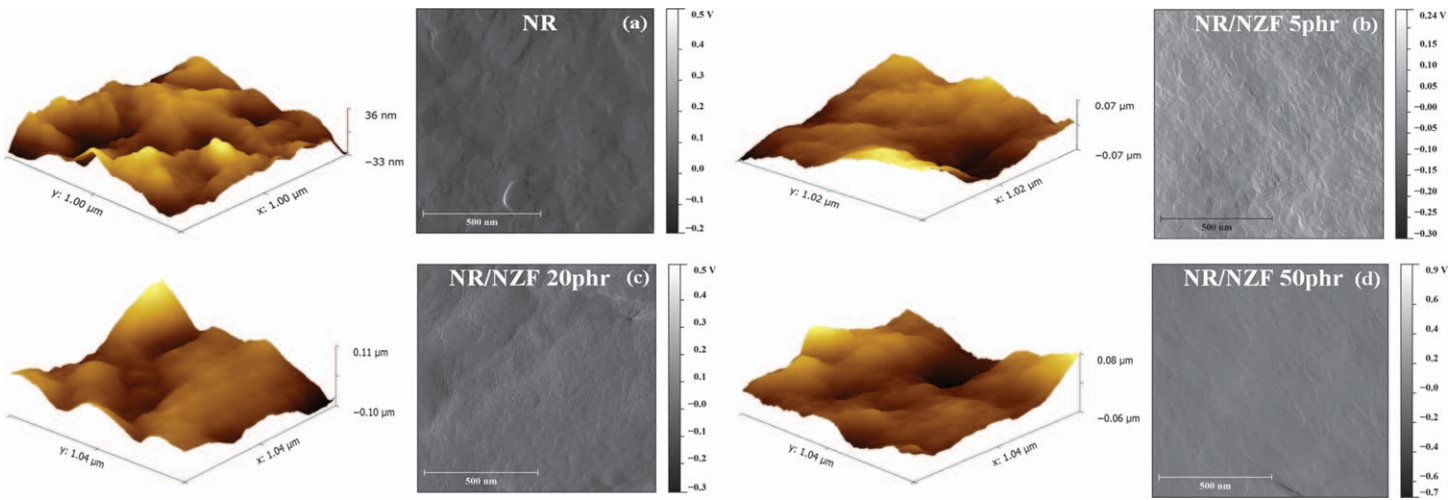

Figure 15.5 Images obtained using AFM for (a) vulcanized NR and (b), (c), (d) the magnetic nanocomposite with different concentrations of magnetic charge.

has a desirable property to its availability and commercial viability. The work of sorting options to make the ideal selection requires a systematic approach based on knowledge of the nature of engineering and material science. Among the variables to be considered, the thermal and mechanical behaviour of the material are unquestionably parameters to be considered. Especially for magnetic composites or nanocomposites based on NR, thermal parameters such as thermal stability and mechanical parameters such as resistance to compression must be properly selected so that there is a loss of composite properties during the life cycle of the material.

15.4.1 Thermal Properties

The thermoanalytical techniques comprise a set of flexible tools for characterization and development of new organic materials, which are relevant in the academic and technological developments. Such techniques are essentially based on the systematic provision of thermal energy and monitoring of physical/chemical of the samples, such as weight variation or change in enthalpy of the sample. The main techniques for thermal analysis are thermogravimetry (TGA), differential thermal analysis (DTA), differential scanning calorimetry (DSC), evolved gas analysis (EGA), evolved gas detection (EGD), dilatometry (DIL), thermomechanical analysis (TMA), dynamic thermomechanical analysis (DMA) and high temperature diffraction (DRXAT). For magnetic nanocomposites and composites such techniques are widely used for obtaining physical and chemical processing parameters, and presents a series of advantages such as the requirement of small amounts of samples, the variety of data in a single assay, the non-necessity of sample preparation and the relatively short time of the experiment.

15.4.1.1 Thermogravimetric Analysis

The thermogravimetric test is one of the most common ways to evaluate the thermal behaviour of materials and monitors, in particular, the mass loss of the sample as a function of the temperature. This technique is very useful technologically because it is capable to indicate what may be the working temperatures for which the material preserves unchanged mainly its mechanical properties and chemical composition. For NR-based composites vulcanized at working temperatures, generally are predominantly working temperatures of the elastomeric matrix and does not exceed 280 °C due to the organic nature of the polymeric materials, although inorganic fillers such as carbon black can be added to increase the thermal stability of the composites. The magnetic composites or nanocomposites follow the same thermal behaviour of composites in general, since the thermal treatment used to increase the NR viscosity during processing and the temperature and pressure used for thermoconformation do not alter the properties of the magnetic particles which are mostly ceramic materials. Due to the low interaction between the magnetic charge and the polymer matrix which is usually observed in this class of materials, inserting an

inorganic filler does not significantly alter the thermal properties of the composites.[27]

Figure 15.6(a) shows the thermogravimetric curves for magnetic nanocomposites (NR/NZF) with magnetic filler concentrations between 1 and 50 phr performed in a typical laboratory equipment in the temperature range of 50 to 850 °C, in a heating ratio of 20 °C/min in an inert atmosphere of N_2 with a flow of 60 mL/min. The mass of sample used in the measurements was of about 10 mg. Figure 15.6(b) shows the temperature evolution of work threshold or temperature of 'thermal stability', considered here with the temperature to which the mass loss is equal to 1% for the magnetic nanocomposites according to the concentration of nanoparticles.

As can be seen in Figure 15.6(a), all materials studied show similar trends in mass loss versus temperature, indicating that the elastomeric characteristics of NR are preserved. Fundamentally, for all materials shown, there is only a single intense mass loss between 300 and 490 °C, mainly associated with degradation of polyisoprene (≈50%), dipentene (≈35%) and p-methene (≈10%). Inset on Figure 15.6(a), as expected, there is a linearly increasing evolution of residual mass depending on the concentration of magnetic nanoparticles indicating that the obtained residue is fundamentally ceramic material. The working temperature or 'thermal stability' found for the vulcanized NR was equal to 215 °C, as seen in Figure 15.6(b). This value is approximately 79% higher than that published by Mathew *et al*. for NR[28] and approximately 43% higher than the thermal stability of silicone rubber studied by Li *et al*.[29] The average temperature of thermal stability for NR/NZF is equal to 232 °C, approximately 8% higher than for NR. For this class of materials an increasing temperature evolution of work threshold was identified due to a possible increase in the crosslinking process associated with the insertion of a second stable phase. The observed increase in the working temperature of the magnetic composites tends to be intensified in ceramic materials that have nickel in its composition, well

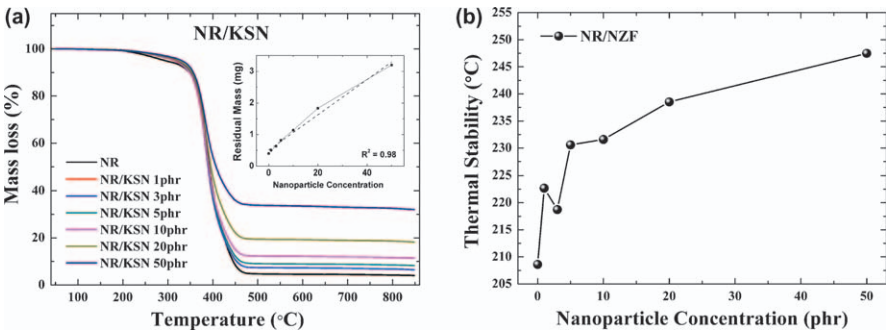

Figure 15.6 (a) Thermogravimetric curves for the magnetic nanocomposites (NR/NZF) as a function of nanoparticle concentration. Inset, the residual mass depending on the concentration of nanoparticles. (b) Evolution of 'thermal stability' of the nanocomposites according to the concentration of nanoparticles.

known to catalyse organic reactions. A decrease peak in 3 phr can be observed and probably attributed to the phenomenon of stress-induced crystalization[25] which reduces the thermal stability due to a local crystallization.

15.4.1.2 Differential Scanning Calorimetry (DSC) Analysis

Measurements of differential scanning calorimetry (DSC) are widely used in the investigation of magnetic composites and nanocomposites based on NR by allowing the determination and monitoring of a large number of parameters such as glass transition temperature, time and temperature of crystallization, curing reaction, specific heat, thermal stability and reaction kinetics.[30,31] Figure 15.7(a) and (b) shows DSC curves highlighting the glass transition region and the evolution of the glass transition temperature and dielectric permittivity, respectively, to vulcanized NR and for the magnetic nanocomposites based on NR (NR/NZF) with different concentrations of magnetic nanoparticles. DSC measurements were performed on typical laboratory equipment using an alumina crucible, approximately 10 mg of sample, heating rate of 10 °C/min with temperature between −130 °C and 270 °C, with an inert atmosphere of N_2 and stream of 50 mL/min. The dielectric permittivity measurements normalized by the geometric factor were performed at room temperature using a typical laboratory impedance analyser with sample submitted to an uniaxial compression equal to 0.0038 kgf/m, frequency of 100 kHz and applied potential between the electrodes of 500 mV.

As can be seen in Figure 15.7(a), the DSC curves associated with nanocomposites are similar to the DSC curve of NR, indicating that thermal characteristics of the polymeric matrix predominate, regardless of the concentration of nanoparticles. Only a discontinuity in the baseline of endothermic character is observed near −60 °C, whose point of inflection is attributed to the glass transition temperature (T_g) of the material. A combination of the degree of mobility of the molecules, the degree of crosslinking, intra and intermolecular interactions determine the T_g of the investigated material. A reaction

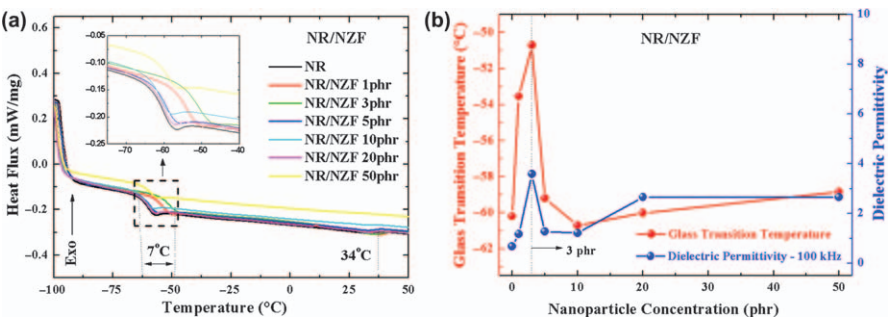

Figure 15.7 (a) DSC curves and (b) evolution of the glass transition temperature and dielectric permittivity at 100 kHz for NR and for the magnetic nanocomposite based on natural rubber (NR/KSN) with different concentrations of magnetic filler.

of low intensity and exothermic character is observed at 34 °C in both classes of nanocomposites and it is suggested that is an association with elimination of volatile elements adsorbed on the nanocomposite surface. In general, two peaks of exothermic character could be identified around 200 °C of lesser intensity, and 370 °C of greater intensity attributed to cleavage of NR and degradation of the polymer chains of isoprene, respectively. As can be seen in Figure 15.7(a), magnetic nanocomposites exhibit higher T_g values with respect to the NR for all concentrations of nanoparticles investigated indicating significant changes in the polymer matrix. The change observed in T_g for the magnetic nanocomposites NR/NZF was of 7 °C. An increase peak in the T_g is observed in 3 phr and attributed to the phenomenon of stress-induced crystallization, since a more crystalline polymer chain has less mobility and greater restriction on movement freedom. At concentrations greater than 3 phr there is a reduction followed by stabilization in the T_g. For the dielectric permittivity, it was found that this parameter is higher for the nanocomposites compared with NR, but with a small difference between them indicating the low connectivity between the nanoparticles in the polymer matrix.

No significant changes are observed in the dielectric properties of magnetic nanocomposites before the percolation concentration, which usually is near to 30% v/v. Analysing the evolution of the dielectric permittivity of magnetic nanocomposites as a function of concentration, one can say that there is a similarity with the evolution of T_g. For low concentrations the phenomenon of stress-induced crystallization predominates, since a crystallized polymer chain, and consequently more ordered, presents ease on filler separation. For higher concentrations, the values of the dielectric constant are practically constant. The same parameters that previously influenced T_g are responsible for the greater capacity of filler separation in the nanocomposites, with emphasis on the surface area and crystalline character of the NZF nanoparticles.

15.4.2 Mechanical Properties

Nowadays, there is an incessant search to understand the various mechanical properties of polymeric composites and nanocomposites, in particular those based on NR, in microscopic and macroscopic scopes in order to design, construct and modulate the characteristics of the final product. Many materials, when in service, are subject to forces or fillers, and such materials must be properly designed to not lose their initial characteristics. The mechanical behaviour of a material reflects the relationship between its response or deformation to a filler or strength applied. Some important mechanical properties are: tensile strength, elasticity, ductility, fluency, fatigue, toughness, hardness and rigidity. For magnetic composites or nanocomposites whose matrix is NR, usually mechanical properties of the matrix are preserved, but the suitable selection of the type and amount of magnetic filler added is required to avoid any excessive reduction of the mechanical properties, which would hamper its use in electromagnetic or mechanical magnetic devices.

15.4.2.1 Hardness Type Shore A

The hardness testing type Shore A represents parameters related to surface resistance of the material and are widely used in industry of artefacts, composites and nanocomposites based on NR to be rapidly applied tests, based on equipment of easy handling and transportation, and by being a suitable parameter of the crosslinking degree or crosslinking density of NR. The scale of hardness type Shore A type ranges from 0 to 100, where until 50 the rubber is seen between soft and medium soft. The inclusion of an inorganic filler such as ceramic in the NR matrix increases the hardness of the composite, because the material has a hardness much higher than the hardness of rubber, but this increase can be accentuated if the filler added interacts with the matrix or intensify the generation of step crosslinkings within the matrix.[32]

Figure 15.8 shows the evolution of the parameter of surface hardness type Shore A, depending on the concentration of nanoparticles for vulcanized NR and magnetic nanocomposites (NR/NZF). Dots represent the experimental data and the line represents the theoretical fit. Measurements were made using a typical laboratorial durometer in Shore A scale. The assay was performed in quintuplicate and measurement time equal to 1s, in accordance with the international standard ISO 868:2003. The hardness type Shore A was determined from Equation (15.1):

$$F = 550 + 75\,H_A \tag{15.1}$$

where F is the strength applied to the sample in mN, and H_A is the Shore hardness indicated on the durometer type A. Using the semi-empirical Equation (15.2) given by Gent[33] for elastomers, it is possible to estimate the value of

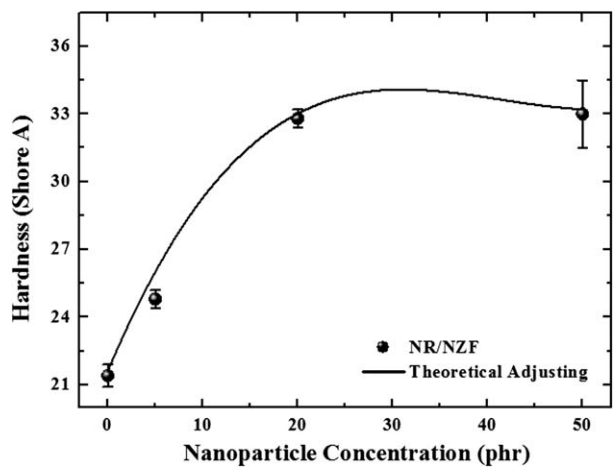

Figure 15.8 Hardness type Shore A for the magnetic nanocomposites based on vulcanized natural rubber (NR/NZF) depending on the nanoparticle concentration.

Young's modulus (E) in MPa, from the data of Shore A hardness (H_A) for magnetic nanocomposites:

$$E(H_A) = \frac{0.0981(56 + 7.66\,H_A)}{0.137505(254 - 2.54\,H_A)} \tag{15.2}$$

According to Figure 15.8, there is a good agreement between experimental data and theoretical fit. The parameter R^2 obtained for this fit was greater than 0.98. A non-linear increase in hardness type Shore A or surface rigidity with respect to vulcanized NR due to the increased concentration of nanoparticles was observed. The increase is marginal for low concentrations, but with differences close to 12 units ($\approx$54%) at higher concentrations, suggesting that such changes are not only due to the insertion of a component of greater hardness to the system. In general, the insertion of nanofillers in polymer matrices can promote alterations in the degree of crosslinking or mobility of the polymer chains[34] and in this case, as there is an increase in surface rigidity of the nanocomposites, it is suggested that there was a variation in the degree of crosslinking and a consequent reduction in mobility of polymer chains from the matrix. Using Equation (15.2), it was possible to estimate the value of E from the Shore A hardness data (H_A) for the materials cited above. The values of E (H_A) were 0.79, 0.92, 1.28 and 1.30 MPa for the vulcanized NR and magnetic nanocomposites with 5, 20 and 50 phr NZF, respectively.

15.4.2.2 Mechanical Testing Type Stress/Strain

The elastomer industry, in particular of vulcanized NR, uses mechanical testing stress/strain to evaluate sample preparation parameters, to define vulcanization systems, characterize new products and intend them to correct applications, for example. The parameters typically evaluated using this test are tension of rupture, deformation of rupture and Young's modulus, being that these parameters reflect mainly the surface characteristics of the material once that the ratio surface area/volume is high.[35,36] In magnetic composites or nanocomposites, inserting an inert filler tends to reduce the parameters mentioned above, but these reductions did not hinder the use of these materials in applied designs.

Figure 15.9(a) shows the results of the stress/strain mechanical traction tests for vulcanized NR and for the magnetic nanocomposites NR/KSN with different concentrations of ceramic nanoparticles. In detail the region of low deformation (0–300%). The evolution of the voltage parameters (UTS) in MPa and per cent strain (e_r) at break are shown in Figure 15.9(b). Mechanical tests were performed on a typical universal testing machine for laboratories, in accordance with the international standard ISO 37:2005. Test tubes that are tie-shaped type 2 automated cut and quintupled were used. The thickness of these test pieces was equal to 2 mm, the width was 4 mm and the speed of extension

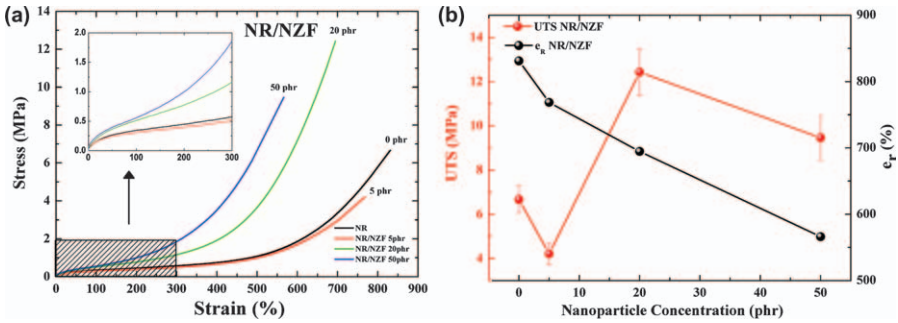

Figure 15.9 (a) Stress/strain curves and (b) evolution of the parameters stress (UTS) and deformation (e_r) at break to vulcanized NR and the magnetic nanocomposite (NR/NF).

50 mm/min. The average standard deviation obtained in the tests was less than 13.5%. The stress (σ) for a given deformation, expressed in MPa, can be calculated using Equation (15.3):

$$\sigma = F_e(Wt)^{-1} \tag{15.3}$$

where F_e is the strength of a given deformation, W is the test tube width and t is the thickness of the narrow section of the test tube.

As can be seen in Figure 15.9(a), the stress/strain curves presented by magnetic nanocomposites are typical curves of elastomeric materials indicating the insertion of nanofillers in these quantities do not change the overall characteristics of the materials. As expected, the addition of nanoparticles in the polymer chain reduces the levels of deformation at rupture at 31.9% for the NR/50 phr with respect to NR/NZF, indicating an increased rigidity of the polymer chain; see also the black curve of Figure 15.9(b). This increase in stiffness is possibly due to the variation of the degree of crosslinking of the polymer chains of the nanocomposites and insertion of the ceramic phase that involves the reduction in its mobility.

Contributing to reduction in deformation at rupture is the fact that by adding fillers with low chemical interaction with the polymer chain, the number of possible breaking points on the samples increases and there is a reduction in free space for the stretch of the polymer chains. It should be noted that in traditional applications, such material is not stretched to near its breaking point. Thus, the obtained values and the observed reduction are not considered a demerit for the material. In accordance with Figure 15.9(b), the evolution of the rupture tension parameter as a function of the fraction of nanoparticles exhibits a decrease in 5 phr for the nanocomposites. It is suggested that this decrease is related to phenomena of crystallization of the local polymer chain due to the inclusion of small quantities of nanometric filler, stress-induced crystallization. In this regard, a pre-filler chain would reduce the level of elongation of the material.

15.4.2.3 Mechanical Testing Type Stress/Compression

Mechanical tests of resistance to compression are commonly used in the field of composites and nanocomposites based on NR, to estimate the voltage necessary to achieve compression from 15 to 80%, and enables the testing of fatigue and mechanical hysteresis cycles, making it possible to estimate the elastic region of the material. Figure 15.10 shows the results of mechanical tests in compression mode for vulcanized NR and the magnetic nanocomposites NR/KSN with different concentrations of nanoparticles. Inset, the region of low deformation (0–50%). The compression tests between 0 and 75% were conducted in quintuplicated, in a typical laboratory mechanical testing machine, in accordance with international standard ISO 7743:1989, and the obtained average standard deviation was less than 7%. To this test class, the compression modulus (K) can be calculated using Equation (15.4):

$$K = F(A\varepsilon)^{-1} \tag{15.4}$$

where F is the strength applied to cause deformation by compression, A is the original cross-sectional area of the test tube and ε is the deformation by compression expressed as a per cent of the sample thickness.

As one can see in Figure 15.13 and in Table 15.2, the addition of the nanoparticles in NR polymeric chain in different concentrations does not significantly alter the evolution of the stress parameter as a function of compression. For all samples of nanocomposites investigated, higher compression stress values are identified when compared to NR, giving them greater rigidity than the NR, in agreement with the discussions of Figure 15.8. It is suggested that three factors significantly contribute to this increase in rigidity observed in

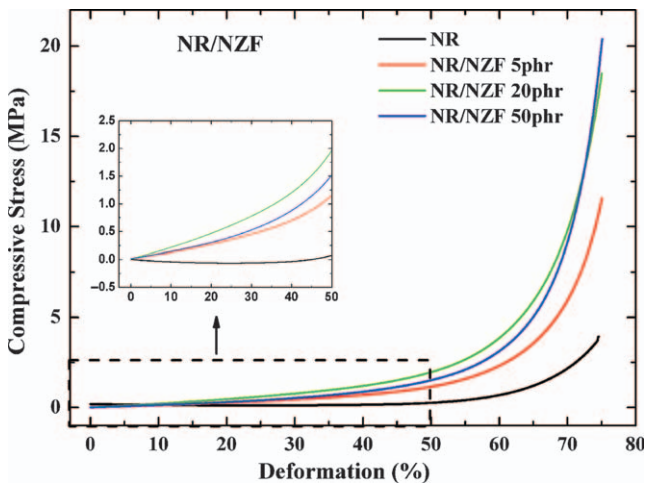

Figure 15.10 Mechanical tests of compression between 0 and 75% for NR and the magnetic nanocomposites (NR/KSN) with different concentrations of nanoparticles.

Table 15.2 Compression modules at 25%, 50%, 70% and 75% for vulcanized NR and magnetic nanocomposites NR/NZF with different concentrations of nanoparticles.

Fillers (phr)	*Modulus at 25% strain (MPa)*	*Modulus at 50% strain (MPa)*	*Modulus at 70% strain (MPa)*	*Modulus at 75% strain (MPa)*
0	0.1	0.3	2.2	3.9
5	0.4	1.2	6.0	11.4
20	0.6	2.1	10.4	19.0
50	0.4	1.6	9.6	20.4

both types of nanocomposites: adding nanoparticles to the system, a component of higher hardness, the reduction in mobility of polymer chains due to this insertion having favourable surface characteristics to a physical interaction with the polymer chains (crystallinity, particle sizes in the nanometre scale, surface activity, high surface area and micro-deformations) and the variation in the degree of crosslinking of the polymeric chains due to insertion of the nanofillers in the NR matrix, where the first factor mentioned is the most important among the three.

For tests of stress/strain shown in Figure 15.9(a) and (b), the influence of the sample surface, a region in which the thermal treatment is more severe since the thermal energy is transmitted by thermal conduction from the sample, on the studied properties is more evident as the ratio surface area/volume is about 1500 m^{-1}. For the mechanical testing of compression, Figure 15.10, the influence of the volume of samples is more evident and the ratio surface area/volume of the sample is approximately 600 m^{-1}.

15.5 Magnetic Analysis

Magnetism can be defined as the phenomenon by which materials impose an attractive or repulsive influence over other materials across a field. However, the principles and underlying mechanisms that explain the magnetic phenomena are complex and subtle, and their understanding has attracted research in this area. Many of the modern technological devices rely on magnetism and magnetic materials, which include electricity generators and transformers, electric motors, radio, television, telephones, computers, sound components and systems for video playback. Iron, some steels and the mineral magnetite, which occur naturally, are well-known examples of materials that exhibit magnetic properties. Not so familiar, however, is the fact that all substances interact to a greater or lesser degree with a magnetic field, and therefore being carriers of magnetic properties.

Ferrites represent the most widespread technological solution to reduce electromagnetic interference (EMI), because they allow the directly induced noise to be filtered. These ferrimagnetic ceramics produce magnetic flow density in response to small magnetization forces applied. Currently, ferrites used for EMI suppression above 30 MHz are composed of mixtures of oxides of iron,

nickel and zinc, which have high bulk density values (10^7 Ohm/cm^2) and a moderate initial permeability ($r = 100$ to 1500). Telecommunication systems, digital information processing, power distribution networks, cellular telephony, prevention of 'ghosts' in TV sets, microwave ovens, security and hospital equipment represent the largest share of the market for applications of absorbing materials of electromagnetic radiation in the civil field.

15.5.1 Vibrating Sample Magnetometer

Perhaps the magnetic characterization technique more widely used, vibrating sample magnetometry (VSM) is a technique based on magnetic induction law of Faraday. It is very versatile because it allows the characterization of materials in various states of matter, performs relatively fast measurement cycles and enables obtaining various relevant parameters from a single hysteresis cycle of the material. This type of testing enables the realization of a set of experiments, for example the classical magnetic hysteresis cycles, magnetization and demagnetization curves.

For magnetic composites and nanocomposites based on NR, this technique allows to determine the saturation magnetization (M_S), remnant magnetization (M_R), coercive field (H_C) and initial magnetic permeability (μ_i), and provides evidence about the interaction between the magnetic charge and the polymer matrix. It is common to perform the comparison between the data of experimental and theoretical saturation magnetization, calculated by Equation (15.5), as a parameter of the interaction filler/matrix, where the excellent agreement with the theoretical/experimental interaction is indicative of low chemical and/or physical interaction between magnetic filler and polymer matrix. The theoretical saturation magnetization of the nanocomposites can be calculated using the mixture equation given by Equation (15.5):

$$M_S(composite) = \frac{m_2}{m_1} M_S(ferrite) \tag{15.5}$$

where M_S (composite) is the saturation magnetization of the composite, M_S (ferrite) is the saturation magnetization of the ferrite nanoparticles, m_1 is the mass of the nanocomposite and m_2 is the mass of ferrite nanoparticles in the sample assuming that the other components are non-magnetic.

The hysteresis curves and their extension in the region of low magnetic field, obtained at room temperature, for nanoparticles of nickel–zinc ferrite with stoichiometry $Ni_{0.5}Zn_{0.5}Fe_2O_4$ (NZF) for vulcanized NR and magnetic ferrite nanocomposites (NR/NZF) with different concentrations of nanoparticles are shown respectively in Figures 15.11(a) and (b) and Figure 15.12. VSM tests were conducted in a typical magnetometer laboratory, with the sample vibrating at 80 Hz and applied magnetic field between 15 and 60 kOe.

According to Figure 15.11(a), the hysteresis curve for ferrite nanopowders at room temperature showed that the particles are ferrimagnetic above the blocking temperature of 50 K.[37] The hysteresis loop parameters, like saturation magnetization (M_S), coercivity field (H_C), magnetic remanence (M_R) and an

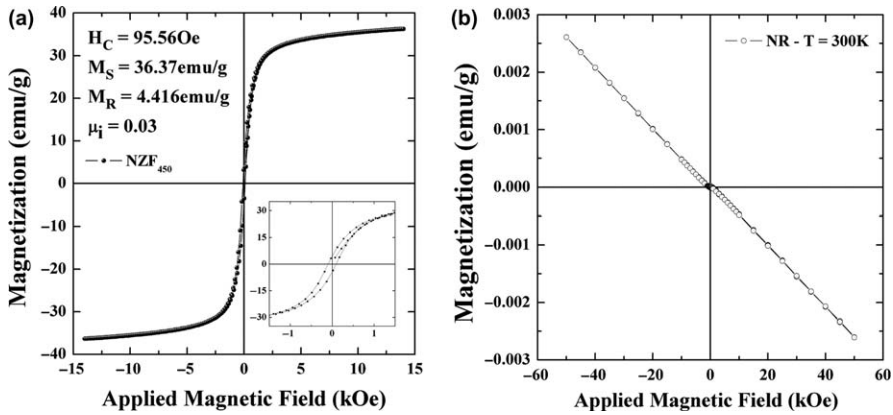

Figure 15.11 (a) Hysteresis cycle for $Ni_{0.5}Zn_{0.5}Fe_2O_4$ nanopowders calcinated at 450 °C for 2 h and (b) for vulcanized NR. The measurement was performed at room temperature.

initial magnetic permeability ($\mu_i = (dB(H)/dH)_{H=0}$) are found to be 36.37 emu/g, 95.56 Oe, 4.42 emu/g and 0.03, respectively.[37,38] The lower value of saturation magnetization of ferrite nanopowders was found when compared to the bulk or to the standard ceramic (70.3 emu/g[37] and 56 emu/g[39]). This saturation magnetization value, 36.37 emu/g, is about 77% of the magnetization of nickel nanoparticles with a particle size equal to 26 nm[40] and about 79% of the magnetization of magnetite (Fe_3O_4) with a particle size equal to 19 nm.[41] These differences can be associated with a low quantity of nickel and iron in the NZF phase and the greater complexity of NZF phase that makes the formation of magnetic domains difficult. These values are compatible with the finite size effects occurring at the nanoregime. The measured hysteresis loops show the remanence ratio (M_R/M_S) equal to 0.12. This result suggests that in the remanence state, the predominant dipolar interactions at these systems are negative which suppresses the remanence ratio below 0.5. Negative dipolar interactions arise when the dipolar field of neighbouring particles is acting in such a way as to destabilize the magnetization of the particle within the aggregate.[42] In Figure 15.11(b), one can observe the magnetic behaviour that at room temperature of NR can be classified into diamagnetic magnetization with maximum equal to 0.003 emu/g due to the opposite magnetic field produced by atomic structure.

Figure 15.12 shows the hysteresis cycles and its extension in the region of low magnetic fields obtained at room temperature for magnetic ferrite nanocomposites (NR/NZF) with different concentrations of nanoparticles.

According to Figure 15.12, the magnetic nanocomposites based on NR/NZF exhibit hysteresis cycles similar to that of ferrite nanoparticles calcined at 450 °C, ferrimagnetic in a predominantly paramagnetic state, indicating that the magnetic properties of the nanoparticles are retained in the NR/NZF samples, as the polymeric matrix of NR is originally a non-magnetic material. For the nanoparticles, the NR/NZF have narrow hysteresis cycles typical of soft magnetic

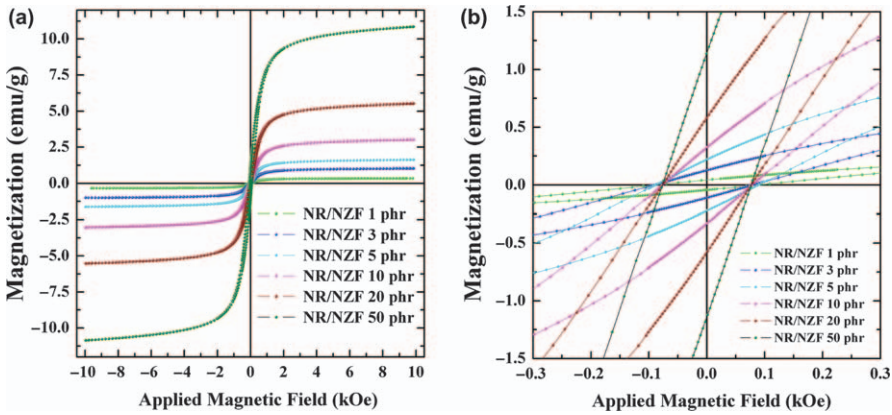

Figure 15.12 (a) Magnetic hysteresis curves and (b) amplification of magnetic hysteresis curves in the region of low fields at room temperature, for the magnetic ferrite nanocomposites with different concentrations of nanoparticles.

Table 15.3 Experimental and theoretical values of saturation magnetization (M_S), magnetic permeability and remnant magnetization (M_R) for the NR/NZF with different concentrations of ferrite nanoparticles.

Fillers (phr)	*Saturation Magnetization (emu/g)*			*Initial Magnetic Permeability*	*Remnant Magnetization (emu/g)*	*Coercive Field (Oe)*
	Experimental	*Theoretical*	*Δ%*			
1	0.34	0.33	−2.94	2.0×10^{-5}	0.1	98.5
3	1.02	0.97	−4.90	8.6×10^{-4}	0.1	79.7
5	1.63	1.58	−3.07	1.5×10^{-3}	0.2	89.1
10	3.02	3.03	+0.33	2.7×10^{-3}	0.3	76.4
20	5.52	5.60	+1.39	6.8×10^{-3}	0.6	77.3
50	10.85	11.37	−4.79	1.0×10^{-2}	1.2	77.3

materials, which causes low hysteresis losses. With increasing concentration of nanoparticles in the NR/NZF, significant changes are not observed in the coercive field, indicating low interaction between the nanoparticles in the agglomerate within the polymer matrix. According to the data listed in Table 15.3, there is a linear evolution of the experimental and theoretical data of saturation magnetization, as calculated by Equation (15.5), initial permeability and remnant magnetization with increasing concentration of nanoparticles. The linear evolution presented by the parameters is due to the low chemical nanoparticle/matrix interaction and dependent only on the amount of magnetic material in the matrix, which can be evidenced by the low percentage difference between experimental and theoretical saturation magnetization. It should be noted that the inclusion of nanoparticles in the matrix of vulcanized NR causes no significant reduction in mechanical properties of NR/NZF.[43]

15.6 Applications of Magnetic Composites

Bonded magnets are widely used today and can be produced using common industrial routes such as compression moulding, extrusion, injection moulding or calendering processes for their use as a final product or starting material for other applications. Such materials, when produced by compression moulding, have the magnetic filler added to a matrix, usually NR or epoxies, and the compound is compression moulded with the desired geometry and using the appropriate curing parameters. The raw materials, or polymeric matrix, such as NR, the magnetic charge and the vulcanization system for the production of composites or nanocomposites, when produced by injection moulding, extrusion and calendering processes, pass first through a process of severe mixing at low temperatures, around 50 °C, to ensure homogeneity of the mixture. Then this mixture may be again extruded, injection moulded or calendered, to obtain the final material ready for vulcanization or already vulcanized. It should be noted that the vulcanization system can be adjusted to obtention of rigid or flexible magnetic composites. Typical flexible magnetic materials are the rubber ferrite composites or nanocomposites, widely used technologies for absorption of electromagnetic radiation and magnetic memories. In the next two topics new applications for this technology, oriented intelligent systems to absorb impact and biological systems, will be presented and discussed.

15.6.1 Application 1: Intelligent Impact-Absorption Systems

Composites and nanocomposites formed by inserting particles or magnetic nanoparticles in a matrix of vulcanized NR can be used in intelligent, high-performance systems for the absorption or damping of impacts, by having the ability to amplify or reduce the mechanical response of the system when subjected to a magnetic field. Such variations are proportional to the amount of magnetic material inserted in NR and the intensity of externally applied magnetic field. Technological applications as more efficient damping systems for footwear and high-performance damping systems for intensive vehicles already have potential for industrial use.

To exemplify this type of application, compression tests between 0 and 75% assisted by magnetic field were performed in vulcanized NR nanocomposites with ferrite magnetic nanoparticles (NR/NZF). Tests were conducted in quintuplicate in a typical laboratory mechanical testing machine in accordance with international standard ISO 7743:1989, and the average standard deviation obtained was less than 7%. However, between the plates of the compression system were added commercial rare earth magnets (Ne–Fe–B), model N42, with cylindrical geometry, diameter of 30 mm, thickness of 20 mm, remnant magnetic field equal to 13,200 G, or 1.32 T, and $BH_{max} = 42$ MGOe, as shown in Figure 15.13.

With the aim of presenting only the effects of the sample subjected to the magnetic field, the effects of the magnetic force on the results were discounted

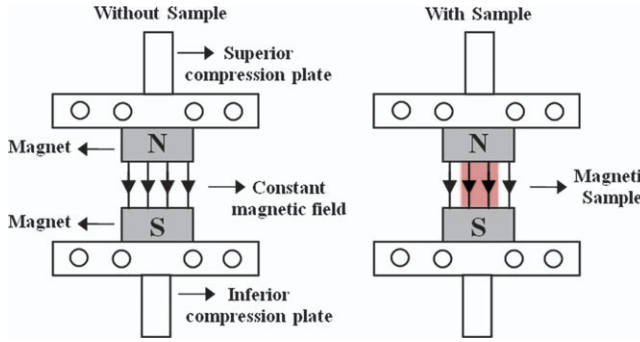

Figure 15.13 Flow chart for the mechanical tests of compression type assisted by magnetic field for rubber ferrite composites (RFC).

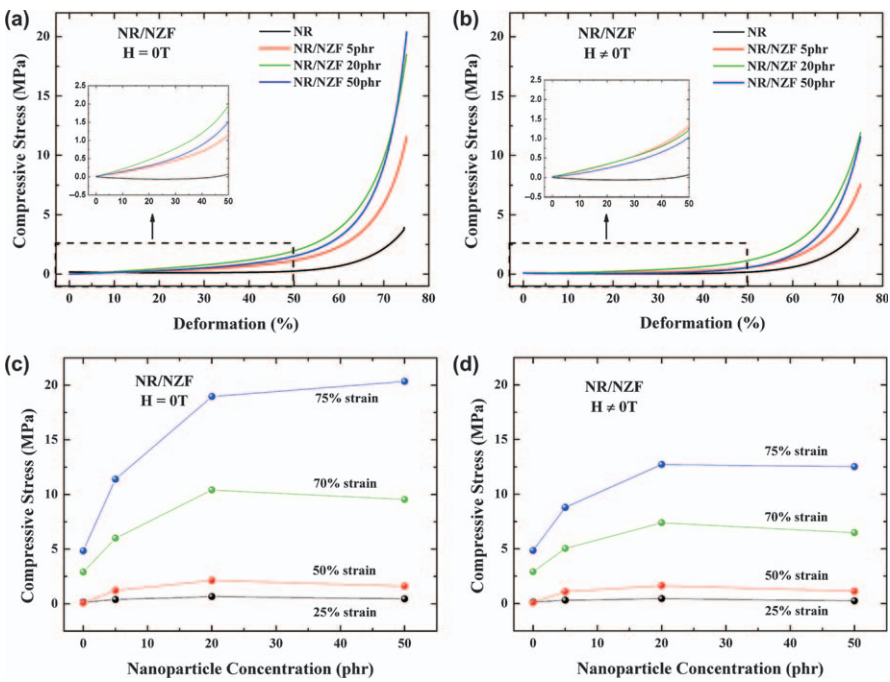

Figure 15.14 Stress/compression curves for NR/NZF (a) without magnetic field and (b) with magnetic field. Evolution of tension to constant compressions of 25, 50, 70 and 75%, depending on the nanoparticle concentration (c) in the absence and (d) in the presence of a constant magnetic field.

from the data obtained in a test performed without samples. An average standard deviation of less than 5% was obtained.

Figures 15.14(a) and (b) show the mechanical tests in the compression mode without magnetic field and assisted by a magnetic field, as previously described for the nanocomposite NR/NZF with different concentrations of

Table 15.4 Comparison of the compression modules at 50%, 70% and 75% for the NR/NZF nanocomposite with absence and presence of a constant magnetic field and different concentrations of nanoparticles.

	Mod ulus at 50% strain (MPa)				*Modiulus at 70% strain (MPa)*				*Modulus at 75% strain (MPa)*			
Filler loading (phr)	$H=0$	$H\neq0$	Δ	Δ %	$H=0$	$H\neq0$	Δ	Δ %	$H=0$	$H\neq0$	Δ	Δ %
5	1.22	1.09	−0.13	−10.66	6.00	5.04	−0.96	−16.00	11.40	8.79	−2.61	−22.90
20	2.14	1.64	−0.50	−23.36	10.41	7.39	−3.02	−29.01	18.96	12.72	−6.24	−32.91
50	1.61	1.13	−0.48	−29.81	9.55	6.48	−3.07	−32.15	20.35	12.52	−7.83	−38.48

nanoparticles. Evolutions of the compression modules to deformations of 25, 50, 70 and 75% depending on the concentration nanoparticles without and with constant magnetic field are shown in Figures 15.14(c) and (d), respectively.

In accordance with Figure 15.14(b), adding magnetic nanoparticles in the matrix of NR and the presence of the magnetic field does not alter the shape of the curve of evolution tension/compression, as compared to NR and vulcanized nanocomposites shown in Figure 15.14(a), but change the values of the compression module as seen in Table 15.4. For all investigated samples, independent of the concentration of NZF nanoparticles or compression amount, the presence of a constant magnetic field decreases the values of resistance to compression. NZF nanoparticles are ferrimagnetic materials in a paramagnetic state, and in the presence of a magnetic field, they undergo a magnetization process generating an induced magnetic field of same direction as the applied external field, which tends to amplify the external magnetic field. Thus, exerts an additional magnetic force in the same direction and sense of the external magnetic field, and in the same direction of the strength exerted by the compression plates, but with the opposite direction, thus justifying the reduction in compressive modulus values in the presence of a magnetic field.

As expected, there was a non-linear reduction of the resistance to compression for samples of NR/NZF with the increase of compression module. It is suggested that the nonlinear evolution of the resistance to compression is mainly attributed to two factors. The first and most significant factor is due to the inverse dependence of the magnetic field and hence of the magnetic force with the distance between the magnets. The second factor is the collaborative, or coupling, effect between neighbouring magnetic nanoparticles, which is favoured by the closeness between them in the compressed polymer matrix. So, with proper manipulation of the composition of the magnetic composites and magnetic field applied, it is possible to conveniently modulate the mechanical response of the system.

15.6.2 Application 2: Control of Colonies of Leishmaniasis Parasites

Multidisciplinary research have gained great strength in recent decades, aiming to increase the number of tools for addressing problems. Each day new materials and methodologies are tested in fighting diseases such as cancer and diseases neglected by the pharmaceutical industry, for example, malaria, leishmaniasis and Chagas' disease. Magnetic particles and nanoparticles coated with proteins and other biological materials emerge as major innovations in medicine by the ability to be distance-sensitized via external magnetic field, generating sufficient heat to kill specific cells by hyperthermia, or even release drugs in controlled times and amounts at specific locations of biological material. As a result of this innovation, magnetic nanocomposites and composites based in NR can be used in biological applications, aiming at development of devices such as intelligent bandages or agents of control and reduction of parasitic colonies.

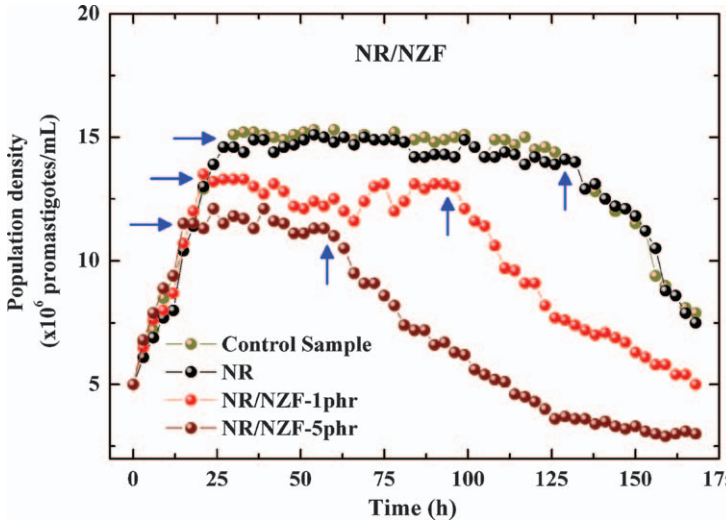

Figure 15.15 Population growth kinetics of promastigotes of *Leishmania braziliensis* (LB) exposed to samples of vulcanized NR and NR/NZF nanocomposites with different concentrations of nanoparticles.

As an example, magnetic nanocomposites based on NR (NR/NZF) were tested as control agents in colonies of the parasite *Leishmania braziliensis*, in order to investigate its population growth kinetics *in vitro*. In a BHI (brain heart infusion) environment supplemented appropriately, a sample of magnetic nanocomposites with an inoculum of parasites was introduced in the promastigote form. From this moment, for a week, the cell count was made on the supernatant portion of the colony using a Neubauer chamber. Control colonies, *i.e.* without the introduction of samples of NR or magnetic nanocomposites were also investigated. Throughout the test, temperature and pH parameters were maintained properly. All tests were performed in triplicate and the average standard deviation obtained was lower than 1%. Figure 15.15 show the kinetics of population development of the colonies of *Leishmaniasis* parasites exposed to samples of vulcanized NR and magnetic nanocomposites at different concentrations of nanoparticles.

According to Figure 15.15, there is an evolution of the population growth curve of LB promastigotes similar for all investigated samples, indicating that the presence of the samples did not change the overall behaviour of the colony. As expected, this development follows the standards of a colony of microorganisms grown in an artificial environment being composed of three well-defined stages. In the first stage, named logarithmic phase, in which the pathogen has provision of a large amount nutrient, conditions conducive to their physiological maturation and cell division, a linear increase in the number of promastigotes versus time is identified. In the second stage, called the continuous phase, which stabilizes the processes of cell division, where the parasites are mature and new members in the population does not arise, has identified a

constant number of promastigotes in function of time. In the third stage, called fall phase, in which the nutritional resources of the culture medium are reduced and the process of cell death by depletion of internal microorganism resources begins, a decreasing linear function of time is identified for control colony and for the colony exposed to the sample of vulcanized NR and an exponential decrease to the colonies exposed to the nanocomposite samples for both concentrations of nanoparticles.

Comparing the results obtained for the control colony and for the colony with a sample of vulcanized NR, there are not significant changes in the kinetics of population growth, thus keeping the stages of cell development and maturation unchanged. However, the colonies exposed to the magnetic nanocomposite samples have identified changes in the patterns of microbial growth. It was also observed that by increasing the concentration of nanoparticles, the differences between the growth curves were accentuated. A linear decrease in density and lifetime of leishmaniasis parasites is identified, as a function of increasing concentration of nanoparticles indicating that the presence of such magnetic nanoparticles would be difficult for the protein intake of culture and also limiting the cell division by the parasite. With fewer parasites in culture and limited nutritional intake in the middle, there is a smaller stationary phase and a fall phase greater than the control colonies and exposed to the NR sample. It should be noted that these observations are still being studied by the scientific community.

Acknowledgements

The authors would want to acknowledge the Brazilian research agencies FAPESP, CAPES and CNPq for financial support, the graduate program of Materials Science and Technology, Carlos Gomes Barbosa-Filho for the biological tests, Dr Marcos Augusto de Lima Nobre for the scientific discussions and also Dr Ricardo F. Aroca and Ariel Guerrero for the AFM measurements.

References

1. Q. H. Fang, S. L. Zhou, N. Wang, X. B. Zhang and Z. Wang, *Mat. Sci. Forum*, 2012, **704–705**, 541.
2. S. Amnuaypornsri, S. Toki, B. S. Hsiao and J. Sakdapipanich, *Polymer*, 2012, **53**, 3325.
3. M. Wilson, K. Kannangara, G. Smith, M. Simmons and B. Raguse, *Nanotechnology: Basic Science and Emerging Technologies*, ed. Chapman and Hall/CRC, 2002, 290.
4. C. T. Wu and M. Koishi, *Int. J. Numer. Meth. Engng*, 2012, **91**, 1137.
5. Q. Xu, Y. Yao, Z. Ma and Z. Xia, *Sci. Adv. Mater.*, 2012, **4**, 888.
6. C. H. Pearson, K. Cornish and D. J. Rath, *Ind. Crops Prod.*, 2013, **43**, 506.
7. C. Calebrese, L. Hui, L. S. Schadler and J. K. Nelson, *IEEE Trans. Dielectr. Electr. Insul.*, 2011, **18**, 938.

8. S. Lanfredi, G. Palacio, F. S. Bellucci, C. V. Colin and M. A. L. Nobre, *J. Phys. D. Appl. Phys.*, 2012, **45**, 435302.
9. S. Yuan, J. Wang, X. Zhong, F. Wang, B. Li and Y. Zhou, *J. Mater. Chem. C*, 2013, **1**, 418.
10. V. Sunny, P. Kurianb, P. Mohananc, P. A. Joyd and M. R. Anantharaman, *J. Alloys and Comp.*, 2010, **489**, 297.
11. A. Goldman, *Modern Ferrite Technology*, ed. Springer, 2006, **2**, 438.
12. A. R. West, *Solid State Chemistry and its Applications*, ed. John Wiley & Sons Ltd, 1995, 742.
13. S. Zahi, *J. Electromagn. Anal. App.*, 2010, **2**, 56.
14. A. N. Simões, D. A. Vieira, M. C. Silva, A. C. F. M. Costa, L. Gama and R. H. Kiminami, *Rev. Eletr. Mat. Proc.*, 2009, **4**, 15.
15. D. K. Pawar, J. S. Shaikh, B. S. Pawar, S. M. Pawar, P. S. Patil and S. S. Kolekar, *J. Porous Mater.*, 2012, **19**, 649.
16. M. R. Anantharaman, K. Malini, S. Sindhu, E. M. Mohammed, S. K. Date, S. D. Ulkarni, P. A. Joy and P. Kurian, *Bull. Mat. Sci.*, 2001, **24**, 623.
17. L. J. Yu, A. H. Sahrim, I. Kong and A. T. Mouad, *Adv. Mater. Res.*, 2012, **501**, 24.
18. D. Mandal, D. Sathiyamoorthy and V. G. Rao, *Fus. Eng. Des.*, 2012, **87**, 7.
19. V. Kazmiruk, *Scanning Electron Microscopy*, ISBN 978-953-51-0092-8, chapter 34, 2012, p. 830.
20. A. Daigle, J. Modest and A. L. Geiler, *Nanotechnol.*, 2011, **22**, 305708.
21. N. L. Tarwal, P. R. Jadhav, S. A. Vanalakar, S. S. Kalagi, R. C. Pawar, J. S. Shaikh, S. S. Mali, D. S. Dalavi, P. S. Shinde and P. S. Patil, *Powder Tec.*, 2011, **208**, 185.
22. M. Pechini, *U.S. Patent*, United States Patent Office, 1963, 3330 697.
23. S. J. Yaghmour, M. Hafez, K. Ali and W. Elshirbeeny, *Pol. Comp.*, 2012, **33**, 1672.
24. M. Morton, 2nd Ed., Van Nostrand Reinhold, New York, 1989.
25. S. Trabelsi, P. A. Albouy and J. Rault, *Macromol.*, 2002, **35**, 10054.
26. B. Ozbas, S. Toki, B. S. Hsiao, B. Chu, R. A. Register, I. A. Aksay, R. K. Prud'homme and D. H. Adamson, *J. Polym. Sci., Part B: Polym. Phys.*, 2012, **50**, 718.
27. P. Dallas, V. Georgakilas and D. Niarchos, *Nanotech.*, 2006, **17**, 2046.
28. A. P. Mathew, S. Packirisamy and S. Thomas, *Polym. Degrad. Stabil.*, 2001, **72**, 423.
29. Z. Li, W. Lin, K. S. Moon, S. J. Wilkins, Y. Yao, K. Watkins, L. Morato and C. Wong, *Carbon*, 2011, **49**, 4138.
30. X. Chen, S. Wei, C. Gunesoglu, J. Zhu, C. S. Southworth, L. Sun, A. B. Karki, D. P. Young and Z. Guo, *Macrom. Chem. and Phys*, 2010, **211**, 1775.
31. E. C. Montoya and C. Rinaldi, *J. App. Phys.*, 2010, **107**, 09B506.
32. H. Zou, S. Wu and J. Shen, *J. Chem. Rev.*, 2008, **108**, 3893.
33. A. N. Gent., *Int. Rub. Inst. Transact.*, 1958, **34**, 46.

34. F. S. Bellucci, L. O. Salmazo, E. R. Budemberg, M. R. da Silva, M. A. Rodríguez-Pérez, M. A. L. Nobre and A. E. Job, *J. Nanosci. Nanotechnol.*, 2012, **12**, 2691.
35. S. Varghese and J. Kocsis, *Polymer.*, 2003, **44**, 4921.
36. W. E. Mahmoud, A. A. Al-Ghamdi and F. R. Al-Solamy, *Polym. for Adv. Tec.*, 2012, **23**, 161.
37. S. A. Morrison, C. L. Cahill, S. Calvin, R. Swaminathan, M. E. McHenry and V. G. Harris, *J. Appl. Phys.*, 2004, **95**, 6392.
38. A. Chatterjeea, D. Dasa, S. K. Pradhana and D. Chakravorty, *J. Magn. Magn. Mater.*, 1993, **127**, 214.
39. V. Sepelák, K. Tkáová, V. V. Boldyrev, S. Wigmann and K. D. Becker, *Physica B*, 1997, **234**, 617.
40. E. M. A. Jamal, P. A. Joy, P. Kurian and M. R. Anantharaman, *Mater. Sci. Eng., B*, 2009, **156**, 24.
41. K. Woo, J. Hong, S. Choi, H.-W. Lee, J.-P. Ann, C. S. Kim and S. W. Lee, *Chem. Mater.*, 2004, **16**, 2814.
42. Y. Liu, D. J. Sellmyer and D. Shindo, *Tsinghua University Press*, Springer, 2006.
43. K. A. Malini, P. Kurian and M. R. Anantharam, *Mater. Lett.*, 2003, **57**, 3381.

CHAPTER 16

Micro and Nano Calcium Carbonate Filled Natural Rubber Composites and Nanocomposites

IMRAN KHAN*[a] AND A. H. BHAT[b]

[a] Centre for Research in Ceramics and Composites Materials (CICECO), Department of Chemistry, University of Aveiro, Campus Universitario de Santiago, Aveiro-3810-193, Portugal; [b] Department of Fundamental and Applied Sciences, Universiti Teknologi Petronas Malaysia, Bandar Seri Iskandar, 31750 Tronoh, Perak Darul Ridzuan, Malaysia
*Email: imran.pchr@gmail.com

16.1 Introduction

Natural rubber (NR) is one of the important elastomers and widely utilized to prepare many rubber products. NR is often reinforced by incorporation of filler to improve its mechanical properties: modulus, hardness, tensile strength, abrasion resistance and tear resistance, and so on.[1] For decades, fillers have been widely used in the rubber industry. They are incorporated into rubber compound for many purposes, *e.g.* to improve processability, reduce cost, and also to modify the physical properties of the vulcanizate. Generally, fillers can be classified into three main groups, *i.e.* reinforcing fillers, semi-reinforcing fillers, and non-reinforcing fillers. Efficiency of the reinforcing filler depends on several factors such as particle size, surface area and shape of filler. Recently, there has been a growing interest in the use of renewable resources such as bamboo[2] and wood[3] or products like rice husk,[4] chitin[5] and coir[6,7] as fillers for

RSC Polymer Chemistry Series No. 8
Natural Rubber Materials, Volume 2: Composites and Nanocomposites
Edited by Sabu Thomas, Hanna J. Maria, Jithin Joy, Chin Han Chan and Laly A. Pothen

Published by the Royal Society of Chemistry, www.rsc.org

polymers. Benefits of these fillers include low cost, light weight, biodegradability and so on.[8] Among commercial fillers, carbon black and precipitated silica (SiO_2) are the most important reinforcing fillers and these are extensively used when high strength is essential.[9,10] These fillers are added in order to get a substantial improvement in the physical and mechanical properties of the compound.[11] However, high concentrations of conventional fillers (above 40 phr, parts per 100 parts of rubber by weight) are required to attain the desired properties, which has a detrimental effect on the processability of the compound, increases the final weight and limits their applications. However, for some applications where cost and processability are of greatest concern, the use of non- or semi-reinforcing fillers such as clay, talc, and $CaCO_3$ is highly recommended.

$CaCO_3$ is one of the important inorganic powders and is widely used as filler in paints, plastics, and rubber industry.[12,13] Its regular and controlled crystalline shape and ultrafine particle size together with the hydrophobic surface coating are combined to the benefit for both rubber processing and subsequent physical properties. Generally, commercial $CaCO_3$ can be divided into two forms, *i.e.* ground $CaCO_3$ (GCC) and precipitated $CaCO_3$ (PCC). Compared to GCC, PCC possesses a smaller particle size and, thus gives higher reinforcement. However, the degree of reinforcement provided by PCC is still far below that of SiO_2 or carbon black. Many attempts have therefore been made to enhance the reinforcing efficiency of PCC. With modern technology, a new type of PCC, the particle size of which is reduced to the nanoscale, has been produced and commercialized, namely, nano-precipitated $CaCO_3$ (NPCC). In the past few years, polymer nanocomposites have aroused widespread interest because of the small particle size and surface activity of nanoparticles, allowing the required properties to be achieved at low filler loadings.[14,15] So, a nanocomposite is a nanostructured material consisting of a homogenous dispersion of nanoparticles inside a polymer matrix. Because of their nanometre filler size, nanocomposites show unique properties typically not shared by their more conventional microcomposite counterparts and, therefore, offer new technology and business opportunities. The main feature of a nanoparticle is that it has at least one dimension in the nanometric range.

The size of the (nano) particles for reinforcing substances plays an important role in the strengthening and toughening of rubber composites.[1,9,16] In order to improve the role of $CaCO_3$, acting as a reinforcing filler and an antioxidant, the surface of $CaCO_3$ should be modified. A fairly large amount of research has been reported on the surface modifications to $CaCO_3$[17–19] and the effects of different modified $CaCO_3$ preparations on the properties of rubber.[20] The most widely used methods for surface modification are surface grafting and coupling.[21–27] In addition, chemical decomposition is a relatively new method for modifying the surface of inorganic particles[28] and the novel technique,[29] developed to improve the properties of NR, is the modification of the $CaCO_3$ reinforcing filler surface with gallic acid, a natural phenolic compound that has potent antioxidant ability. Additionally, many kinds of rubber, such as NR,

styrene butadiene rubber (SBR), butadiene rubber (BR) and so on, have unsaturated carbon–carbon double bonds in the chemical structure.

NR nanocomposites have gained increased attention in both academic and industrial research in recent years because of their superior properties, such as good reinforcement, thermal stability, flame retardancy, obstructs property and other properties.[30–33] From the definition, a nanocomposite is considered as a polymer composite in which the occluded phase has at least one nanoscale dimension, that is, one measuring from 1 to 100 nm. As is well known, nano calcium carbonate (NCC) is an important inexpensive nanoscale inorganic filler (NIF) in preparing polymer nanocomposites. Good dispersion of NCC particles in polymer matrix can significantly improve the strength, stiffness and other properties of polymer/NCC nanocomposites.[12,34–36] However, hydrophilic (pristine) NCC (HNCC) particles are easily aggregated in polymer matrix, which usually induces the poor mechanical properties of polymer composites.[36] Therefore, organic reagent-treated HNCC (ONCC) particles are widely applied to prepare the polymer/ONCC nanocomposites.[35,37]

In materials research, the development of rubber nanocomposites is rapidly emerging as a multidisciplinary research activity whose results could broaden the applications of rubber to the great benefit of many different industries. This chapter covers the various parameters effecting material properties of micro and nano-$CaCO_3$ filled NR composites and nanocomposites.

16.2 Global Distribution of Rubber

NR is one of the most important agricultural products in Thailand which is currently the world largest NR producer, with the production capacity of 1.8 million tons per year (Rubber Research Institute, 1999) (Figures 16.1–16.3).

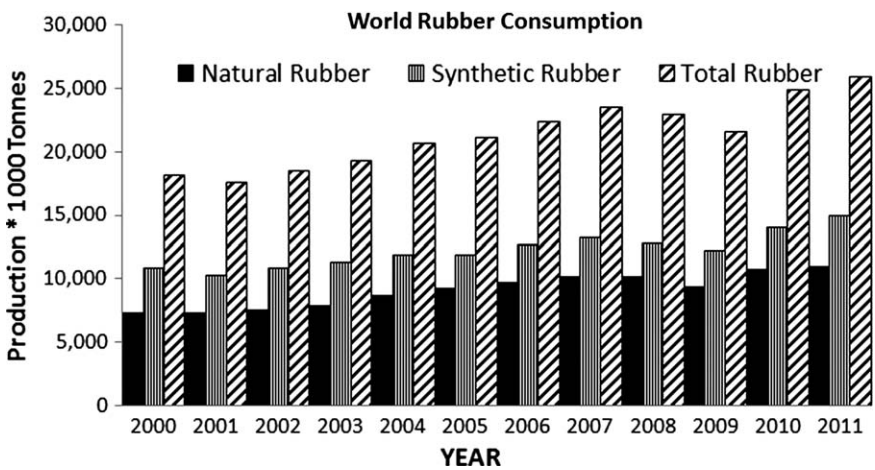

Figure 16.1 Global production of rubber according to Rubber Statistical Bulletin (April–June 2012 edition).

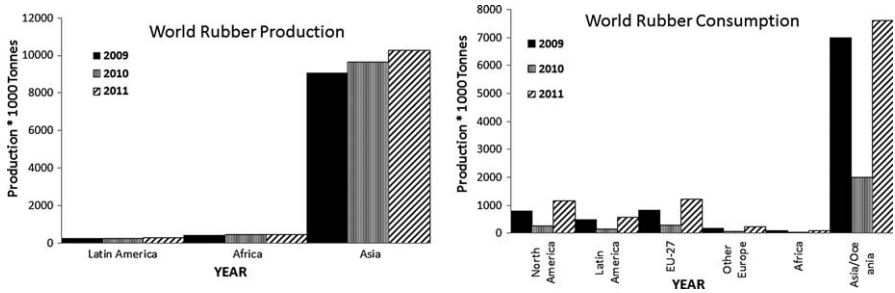

Figure 16.2 World rubber production/consumption in last 3 years according to Rubber Statistical Bulletin (April–June 2012 edition).

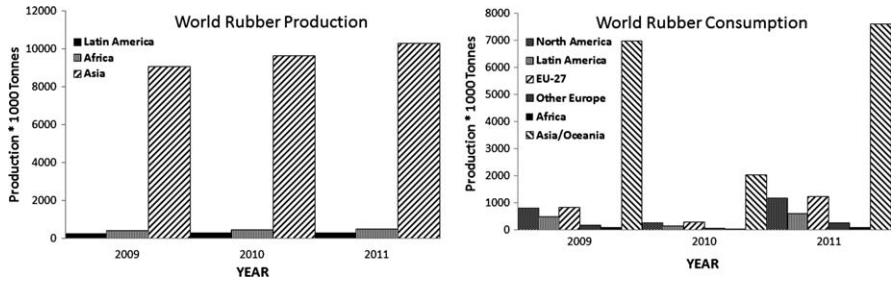

Figure 16.3 World rubber production/consumption according to Rubber Statistical Bulletin (April–June 2012 edition).

16.3 Calcium Carbonate

16.3.1 Nano Calcium Carbonate (NCC) vs Micro Calcium Carbonate (MCC)

Although a number of studies have been devoted to the analysis of SiO_2 or carbon black-filled elastomer networks, little work has been done on the reinforcement of $CaCO_3$-filled elastomer networks. With the development of nanotechnology, nanosized $CaCO_3$ have attracted more and more interest due to the abundance of these raw materials, low cost compared with fumed SiO_2, and the generation of activity by surface treatment. The nanosize, larger surface area and active sites of nano-$CaCO_3$ make it feasible for use as reinforcing agent, just like carbon black or SiO_2.

Fillers such as $CaCO_3$, clay, *etc.* with average particle size in the range 01 to 100 nm may be defined as nanofillers. Unlike traditional fillers, mainly used for cost reduction, nanofillers are performance-enhancing fillers used in relatively small amounts (5–10%) in order to provide substantial improvements in physical and other properties. Nanosized particles (average diameter around 40 nm) form a very fine and homogeneous distributed system in polymer matrix. As compared to micron size filler particles the nanosized filler particles are able to occupy substantially greater number of sites in the polymer matrix.

The significant increase in specific surface area of filler particles contributes to the enhanced physical property of the polymer matrix. Nanosized fillers increase barrier properties by creating a maze or 'tortuous path' that slows the progress of gas molecules through the polymer matrix, thereby substantially improving the gas/air permeability of the polymer. Nanosized fillers in a polymer matrix substantially improve surface properties like gloss, surface finish, grip (friction), *etc*.

16.4 Elastomer Nanocomposites

16.4.1 Filler Characteristics

Fillers, especially mineral fillers, have been widely used in many industries, particularly in the rubber and latex industries, for decades. These fillers function as reinforcing agents, which increase certain mechanical properties such as tensile strength, tear strength and abrasion resistance.[38,39] Carbon blacks, kaolinite clays, SiO_2 and $CaCO_3$ are examples of fillers that impart certain reinforcing effects to rubbers and latex films. Extensive work has been done on the reinforcing effects of carbon blacks in the rubber industry[40,41] and SiO_2 and kaolinite clays in the latex industry[42] and $CaCO_3$ in paints, plastics and rubber industry.[12,13] The importance of fillers in the rubber compounds is well known. Fillers are widely used to enhance the performance of rubbers and other polymeric materials. Filler characteristics such as size and shape of particles and aggregates, chemical nature and porosity of surface, dispersibility and tendency to agglomerate and form secondary filler networks determine its effect on rubber compounds. Fillers can be classified into black and non-black. Soon after carbon black was discovered to be active filler in rubber, at the beginning of this century, it became one of the most important components in the manufacture of rubber products, with consumption second only to rubber itself.

16.4.2 Filler Size

Size of filler plays an important role in the vulcanization of rubber and its improvement is directly related to the particle size of the filler.[43] The influence of $CaCO_3$ filler on composite properties is depicted in the Table 16.1. The increase of modulus and tensile strength is very much dependent on the

Table 16.1 The influence of calcium carbonate filler on composite properties.

Micro calcium carbonate filler	*Nano calcium carbonate filler*
Size < 1 μm	Size 1–100 nm
Loading percentage 10–50%	Loading percentage 5–10%
Low specific surface area	Significant increase in specific surface area
Gas/air permeability is not efficient	Enhanced barrier properties
Mechanical property improvement is comparably weaker	Substantial enhancement in mechanical properties

particle size of the filler; smaller particle size fillers imparting greater reinforcement to the rubber compound than the coarse ones. Since particle size is directly related to the reciprocal of surface area per gram of filler, an increase in surface area that is in contact with the rubber phase probably leads to the increase in reinforcement. And because of this reason from micro to nanosized filler is significantly take place over traditionally micro sized filler. Reducing particle size also simply results in a greater influence in polymer–filler interaction. In addition to average particle size, the particle size distribution also has a significant effect on reinforcement. Particulate fillers with a broad particle size distribution have better packing in the rubber matrix, which results in a lower viscosity than that provided by an equal volume of filler with a narrow particle size distribution. Another important concern in reinforcement is the presence of large particles or agglomerates in the rubber. These agglomerates not only reduce the contact between filler and rubber matrix but also function as failure initiation sites which would lead to premature failure of materials.

16.4.3 Particle Structure and Anisometry of Filler Aggregates

In addition to the surface area, the shape of the filler particle is an important factor that affects the performance of a rubber compound. Inorganic and mineral fillers possess considerable differences in particle geometry, depending on the crystal form of the mineral. The minimum anisometry is found with materials that form crystals with approximately equal dimension in the three directions, *i.e.* isometric particles. More anisometric are particles in which one dimension is much smaller than the two others, *i.e.* platelets. The most anisometric are particles which have two dimensions much smaller than the third, so that they are rod-shaped. In compounds containing fillers having identical surface area and chemical nature but differing in shape, modulus increases with increasing anisometry.[44] Particles with a high aspect ratio, such as platelets or fibrous particles have a higher surface-to-volume ratio, which results in greater reinforcement of the rubber compound. The greatest hardness is also provided by rod-shaped or plate-like particles, which can line up parallel to one another during processing, compared to spherical particles of similar diameter. Particle shape has a more pronounced effect on processing behaviour than on reinforcement potential and provides important benefits in processing. It can also significantly increase modulus due to occlusion or shielding of some of the rubber phase in highly structured fillers such as structural aggregates of carbon black or SiO_2.[45]

16.4.4 Surface Activity

The particle size of the filler as discussed earlier may be considered as a physical contribution to reinforcement, while filler surface activity provides the chemical contribution. The ability of the filler to react with the polymer results in chemical bonding, which increases strength significantly. In the absence of strong coupling bonds, the polymer is physically absorbed on the surface of the

filler, resulting in a reduced mobility of the rubber molecules near the surface of the filler. Polymer–filler bonding, particularly in the case of carbon black, develops through active sites on the filler surface resulting in 'bound rubber' attached to the filler surface. Bound rubber is regarded as the result of rubber to filler interactions which can be considered as a measure of the surface activity of the black or white filler. The surface activity of the filler is reflected in the mechanical properties of the rubber such as tensile strength, modulus, abrasion and tear resistance.[46] Adhesion between polymer and filler may also be induced by a coupling agent, which participates in the vulcanization reaction to form polymer–filler networks. This mechanism of increasing strength is well established with both mineral fillers and carbon blacks.[47] Both mechanisms interfacial adhesion and formation of networks between filler and polymer, lead to the formation of high modulus compounds, which is a very clear indicator that polymer filler bonding has taken place. The increased modulus occurs as a result of attachment of the rubber to the filler, which has the effect of reduced mobility of the polymer chain. Organosilane coupling agents have been successfully utilized to further increase the physical properties of a number of non-black fillers including calcium silicate, clay, mica, SiO_2 and talc.[48]

16.4.5 Surface Area

The most important single factor, which determines the degree of reinforcement, is the development of a large polymer–filler interface. It can be provided only by particle of colloidal dimensions. Spherical particles of 1 μm in diameter have a specific surface area of 6 m^2/cm^3. This constitutes approximately the lower limit for significant reinforcement. The upper limit of useful surface area is of the order of 300–400 m^2/cm^3 and it is decided on the basis of considerations of dispensability and processability of the uncured compound and serious loss of rubbery characteristics of the composite.[49] The surface area of particulate solid is related to its particle size. If all the particles are considered as spheres of the same size, the surface area A_s per gram of filler can be calculated from the equation where d is the diameter and p the density of the filler particle. In reality, particles have a distribution of size and are usually far from being spherical. Different fillers of the same particle size may not impart the same reinforcement, *e.g.* carbon black and SiO_2. The shape of particle also may be different for different fillers, viz., spheroidal, cubic/prismatic, tubular, flaky or elongated. Non-spherical particles can impart better reinforcement.[50]

16.4.6 Porosity

Porosity is a characteristic property of carbon black and can be seen with other particulate type of fillers. Filler porosity can affect the properties of the vulcanizate. However, its effect on reinforcement is secondary. In most cases, the pores are too small for the polymers to enter although some smaller molecules in the compound may do so. Particulate fillers used in rubber industry in general can be classified as 'black' and 'non-black', depending on their origin,

the former being mostly produced from petroleum feedstock and the latter from mineral sources. The most important particulate fillers being used in rubber industry are carbon black and SiO_2. Silicates, clays, whiting ($CaCO_3$) and other mineral fillers are used extensively where a high degree of reinforcement is not essential.[49]

16.4.7 Filler Surface Modification

Surface treatment to improve filler polymer interaction has become very common in rubber industry. The material used for surface modification is one which is compatible with chemical nature of both rubber and filler. Stearic acid and their metallic salts are good examples of surface active agents. For inorganic nanofillers a coating of the filler surface by stearic acid or silanes reduces the tendency to agglomerate and also increases compatibility with the rubber matrix. The surface energy of SiO_2 can be reduced by adding glycols or amines in rubber compound. Nano-zinc oxide is stabilized by hydroxyl functional oligomers. $CaCO_3$ is generally coated with stearic acid or even with (g-aminopropyl) triethoxysilane. There is a limitation for using a coating to increase compatibility with the rubber matrix. Even though the properties of polymers are improved by addition of surface active agents, the effect does not last in humid conditions or during a long storage period. This is solved by introducing suitable functional groups on the filler surface through chemical reactions. There are many coupling agents that can be used to enhance polymer–filler interaction and include silanes, phosphorous esters, titanate coupling agents and chromium acid complexes. Coupling agents may be added directly to polymers or may be fixed to the fillers prior to their addition to polymers. Silane coupling agents have dual reactivity since they are capable of reacting both with polymer and filler. Layered silicates used in production of nanocomposites are also polar and hydrophilic. The modifier may be associated with silicate by strong interactions (covalent or ionic bonds) so as to make it less hydrophilic. The most commonly used modifiers are alkyl ammonium salts. Other cationic surfactants like phosphonium, pyridinium and imidazolium salts are also used for modification. Generally it is very difficult to get a good dispersion of carbon nanotubes (CNTs) in a polymer matrix due to the tendency of nanotubes to form aggregates by van der Waals forces. The absence of functional groups also adversely affects dispersion. Grafting with suitable polymer chains increases compatibility with polymer matrix.[51,52] A breakthrough for the use of tubular nanofillers was achieved by chemical bonding of suitable functional groups onto the surface.[53,54] Under suitable conditions surfactants, polymers or aromatic compounds get adsorbed on surface of nanotubes and result in enhanced compatibility with polymer matrix.[55]

16.4.8 Carbon Black vs Silica

The effect of $CaCO_3$ content on NR compound does not significantly affect the rheological nature of the NR compounds while the addition of SiO_2 and carbon

black causes a sharply increase in the compound viscosity and Mooney viscosity (ΔM), especially for SiO_2 which may be attributed to the number of hydroxyl groups on the surface of SiO_2, which results in strong filler–filler interactions and thus it can aggregate more tightly as compared with carbon black.[56] Carbon black and precipitated SiO_2 which have comparable surface area and structure. The effect of filler surface energies on rubber reinforcement where the surface energies of SiO_2 are characterized by a lower dispersive component, γ_s^d, and higher specific component, γ_s^{sp}, also it was found that the high γ_s^{sp} of SiO_2 leads to strong inter-aggregate interaction, resulting in higher viscosity of the compounds, higher α_f, and higher moduli of the vulcanizates at small strain whereas the higher γ_s^d of carbon black causes strong filler–polymer interaction, which is reflected in a higher bound rubber content of the compounds and higher moduli of the vulcanizates at high elongation.[57] Many other authors have reported the effect of filler carbon black versus SiO_2 on the properties of rubber.[58–61]

16.5 Natural Rubber-Based Calcium Carbonate Nanocomposites

16.5.1 Swelling Properties

Effect of the acrylic dispersed nanosized $CaCO_3$ filler loading to a pre-vulcanized latex compound on the apparent swelling index (SI_{app}) of the aged and unaged pre-vulcanized latex films showed that the SI_{app} decreased as the filler loading was increased for both aged and unaged films, where in unfilled rubber systems the decrease is caused by the crosslinking between the curatives and the rubber molecules. However, aged films have lower SI_{app} values compared to those of unaged films which is attributed to vulcanization of the curatives present in the films.[62]

The influence of $CaCO_3$ addition to the swelling ratio values of the reinforced rubbers (NR and NBR) compounds against square root of time ($t_{1/2}$) at room temperature showed swelling curves exhibit a linear portion followed by a plateau region at longer time which again proved that rubber matrix due to the filler matrix effects during vulcanization where NBR matrix shows lower values than NR.[63] Addition of limestone dust waste (LDW), light precipitated calcium carbonate (PCC) and nano-precipitated calcium carbonate (NPCC) types of filler in NR results regardless of the filler type showed the swelling ratio declines whereas the number of elastically active chains per unit volume increases consistently with increasing filler loading.[64] These results indicate that the crosslink density of the rubber vulcanizate increases consistently with increasing filler loading which again might be attributable to the basic nature of all fillers used in this study.

Effect of $CaCO_3$ addition to NR on the swelling ratio and results showed that swelling curves exhibit a linear portion followed by a plateau region at longer time and the results seemed to be nearly dependent on the rubber matrix due to

the filler matrix effects during vulcanization where NBR matrix shows lower values than NR.[65]

16.5.2 Mechanical Properties

Effect of the acrylic dispersed nanosized $CaCO_3$ filler loading to a pre-vulcanized NR compound in different amounts on tensile strength and elongation at break (*Eb*) showed an increase up to 10 phr of filler loading and then decreased again.[62]

Addition of LDW, PCC and NPCC types of filler in NR, showed the reduction of tensile strength , it was found that the degree of reduction was less pronounced for NPCC-filled vulcanizate as compared to PCC-filled and LDW-filled vulcanizates[64] whereas tear strength tends to decrease slowly with increasing LDW and PCC loadings and some contrasting results were reported for the addition of NPCC; in this case, the tear strength does not significantly change on increasing filler loading up to 30 phr, but further increases in NPCC loading results in a noticeable increase in tear strength.[64] The increase in tear strength is mainly attributed to the reduction of stress concentration at the crack tips in the presence of fillers, particularly those with fine particles.[66]

Saad and Younan[67] investigated that when NR loaded with $CaCO_3$ at a level of 40 phr have been studied in the presence of various proportions of nylon 6 short fibres and reported that longitudinal (warp) and transversal (weft) tensile strength in both directions decreases sharply as the fibre concentration is increased up to 15 phr, then increases with further increasing fibre concentration up to 25 phr, the increase in the longitudinal direction being higher than in the transversal direction and the *Eb* sharply decreases with increase of fibre concentration up to 25 phr, and that the longitudinal elongation is slightly lower than the transversal elongation.

A potential application of cuttlebone as filler for NR was reported[68] and study proved that cuttlebone to be a biomass for new reinforcing filler for NR as the cuttlebone particles did not prevent a peroxide crosslinking reaction of NR, and mechanical properties of peroxide crosslinked NR filled with cuttlebone particles were found to be comparable with those of peroxide crosslinked NR filled with commercial $CaCO_3$ filler. Presence of chitin on the surface of the cuttlebone particles was speculated to result in a good interaction between cuttlebone particles and NR, which may be ascribed to the mechanical properties of cuttlebone filled NR samples.

For the tensile properties, the moduli of NR vulcanizates increased with increasing filler contents (0–60 phr) for both unmodified and modified $CaCO_3$ compared to the NR vulcanizate without any reinforcing filler, presumably due to the reinforcement effect of the $CaCO_3$ where T_B decreased more markedly with increasing modified $CaCO_3$ contents (20–60 phr) than that seen with increasing levels of unmodified $CaCO_3$ contents whereas E_B value declined slightly at a constant rate with increasing modified $CaCO_3$ contents[56] which resulted in values of T_B and E_B of modified $CaCO_3$ filled NR samples were lower than those of unmodified $CaCO_3$ filled NR ones, except for the inclusion

of modified $CaCO_3$ at 20 phr where they were higher. Effect of $CaCO_3$ addition to NR and NBR showed that the optimum concentrations of $CaCO_3$ are 20 phr and 40 phr for NR and NBR, respectively, while at higher filler contents, all the measured properties are decreased, resulting in a poor dispersion of the filler on the rubber matrix, filler agglomeration.[65]

16.5.3 Morphological Studies

Effect of the acrylic dispersed nanosized $CaCO_3$ filler loading to a pre-vulcanized latex compound in different amounts, the micrographs showed that agglomeration occurred as the filler content was increased which results in a decrease in tensile strength and Eb of films.[62]

SEM images of cross-sections of cuttlebone filled NR samples with different filler loadings[68] where the white/bright spots representing filler particles were dispersed in the NR matrix (black-toned colour). It is worth noting that many cuttlebone particles seem to be covered with NR, and the boundary between the cuttlebone and NR is not so sharp comparing with that between Silver W and NR. The interaction between cuttlebone and NR through the organic part on the surface of particles must be stronger than that between Silver W and NR to give the specific SEM images of cuttlebone filled samples.

The difference in the tensile properties between the unmodified $CaCO_3$ and the modified $CaCO_3$ filled NR vulcanizates may be attributed to the different surface properties of $CaCO_3$.[69] When the inorganic particles are introduced into the rubbery matrix, they decrease the effective load-bearing cross-sectional area, which would reduce the tensile strength of the composites as the inorganic particle content was increased.[70] On the other hand, the aggregation of inorganic particles in the rubbery matrix reduces the contact area and creates physical defects in the rubber composites, all of which will decrease the effective interfacial interaction, and the T_B of rubber composites. The authors has reported[29] that the SEM image of the rubber composite materials clearly supported why similar mechanical properties for both $CaCO_3$ and gallic acid modified $CaCO_3$ filled NR vulcanizates were obtained.

16.5.4 Dynamic Mechanical Analysis

NR has unique dynamic mechanical properties. The storage modulus (E′) decreases with an increase in temperature up to -10 °C. Below this temperature, the elastomer is in an enthalpy-dominant deformation regime. In this regime, the internal friction among the polymer chains during the deformation of the elastomer network structure is the controlling mechanism.[71] Consequently, a high damping characteristic of the elastomers is expected. Above -10 °C, the storage modulus increases with an increase in temperature. This defines the entropy-dominant deformation regime[71,72] in which the conformational change of polymer chains during the deformation of an elastomer network structure is the controlling mechanism. In other words, the elastomer network approaches

a perfect network deformation and the elastomers exhibit low damping characteristics.[72]

With increase of filler loading on the modulus at 100% elongation (M100) and modulus at 300% elongation (M300), before and after ageing is proportional to the increase in filler loading and increase in modulus with filler loading is explained by the stiffening effect caused by the interaction between the filler and rubber particles.[62] The good mechanical properties of peroxide crosslinked NR filled with cuttlebone particles were also detected in a dynamic mechanical analysis (DMA).[68] Variations of temperature dispersions of dynamic modulus (E′) at 25 °C and tan δ peak by the increase of filler were same in both series (commercial $CaCO_3$ (Silver W) filled NR samples). E′ at 25 °C increased and loss tangent (tan δ) peak decreased with the increase of the filler content. The temperatures of tan δ peak, which are ascribed to the glass transition temperatures, were almost equal among the samples. These observations mean that the effect of cuttlebone particles on dynamic mechanical properties of peroxide crosslinked NR is comparable with that of Silver W. Not only the size and surface properties but also the dispersion of cuttlebone particles would bring about the characteristics of the dynamic mechanical properties.[68]

16.6 Comparative Study of Acrylonitrile Butadiene Rubber (NBR) and Natural Rubber-Based Calcium Carbonate Nanocomposites

16.6.1 Mechanical Properties

The effect of filler $CaCO_3$ addition for reinforced rubbers (NR and NBR) compounds on tensile strength are more significant at optimum 20 phr and 40 phr are exhibited for NR and NBR respectively.[63] While at higher filler content, the tensile strength is decreased, resulting in a poor dispersion of the filler on the rubber matrix and this behaviour can be related to the probable tendency to form filler agglomerates. It is obvious that for the prepared rubber compounds, Eb% increases steadily, while it decreases gradually with increase in the filler loading but $CaCO_3$ shows an extra extension due to the increase of the dilution effect that imparted at higher loading.[63] For NBR matrix, Eb% exhibit lower values with $CaCO_3$ increase, in comparison with NR matrixes that are explained by the mutual reinforcement of the strain-induced crystallizable rubbers, which hinders the mobility of rubber chain molecules, on the other hand NBR matrix allows more rheological flow due to nearly good filler–rubber interaction and hence greater Eb% is obtained in this matrix, *i.e.* good toughening material.[63]

Chookaew *et al.*[73] described the effects of filler types and contents on the weld line strength of NBR, suggesting that an increased amount of $CaCO_3$ has little effect on the weld line strength, whereas in the case of SiO_2 the weld line strength of NBR is far lower than the values obtained for the samples absent of

weld line. With regard to the effects of thermal ageing, the aforementioned study also revealed that the weld-line strength of NBR does not significantly change after the ageing test. However, as for the compression moulding of NR products, knowledge of weld line strengths and microstructures and their dependencies on various process conditions remains elusive.

Effect of $CaCO_3$ addition to NBR on the cure characteristics and results seemed to be dependent mainly on the rubber matrix where cure time, t_{90} decreased with increasing $CaCO_3$ content and also observed that NBR matrix exhibits longer T_{C90} than those of NR compounds;[63] this result can be related to the fact that $CaCO_3$ particles are isotropic in nature, have small nucleation effect[74,75] and interact strongly with rubber especially with a polar rubber such as NBR.[65]

16.6.2 Morphological Studies

The morphologies of NR compounds that filled with different concentrations of $CaCO_3$ show finer dispersion at 20 phr, while aggregates are visible at higher loading whereas for the NBR matrix the critical dispersion appeared difficult to obtain where small particles are too high for sufficient dispersion at 40 phr.[63] From TEM and SEM images author[76] concluded that good dispersion of HNCC particles and UFPNBR particles in NBR matrix and so the corresponding NBR/UFPNBR/HNCC ternary nanocomposites have shorter vulcanization time, better properties of abrasive resistance, oil resistance, lower heat build-up in dynamic compression, and lower mass loss rate in fire compared with NBR/ONCC binary composites containing the same NCC loading level. However, with the HNCC loading increasing to 40 phr, too much aggregated HNCC particles and UFPNBR particles were formed in NBR matrix, which lead to worse abrasive resistance and dynamic compression properties of the NBR/UFPNBR/HNCC ternary composites (Figure 16.4).[76]

16.7 Comparative Study of SBR and NR Based Calcium Carbonate Nanocomposites

SBR is extensively used in elastomeric compounds for industrial applications. Regardless of the organic nature of an elastomer (polar or non0polar), using these materials without reinforcing agents cannot be justified. Among different types of inorganic fillers, CA is customary applied in almost polymeric compounds due to its abounding and also process ability at high level of loading in incorporation stage of mixing.[77–79] There are some approaches on polymer composites by employing the CA nanofillers in SBR nanocomposites.[80] Some studies have shown that employing the surface-modified fillers reduces the surface energy at filler–polymer interface and consequently reduces the probability of agglomerates being formed.[81] The modification procedure which is conducted by using stearic acid caused enhancing the adhesion properties toward polymer–filler interaction.[80,81] Nevertheless, nanosized CA has been

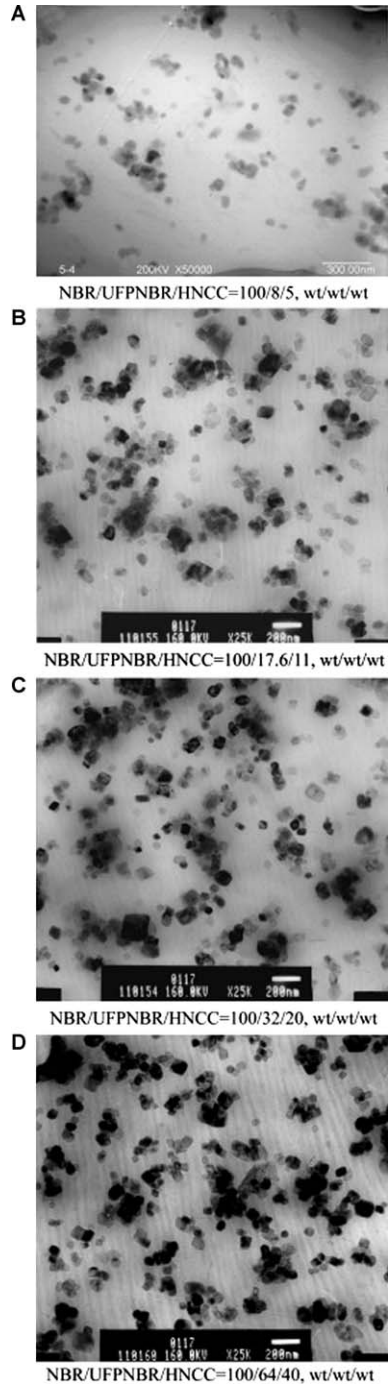

Figure 16.4 TEM images of several NBR/UFPNBR/HNCC ternary.

partially employed as reinforcing agent in SBR compounds, the resulting materials showed superior thermal and mechanical properties.[80] It must be considered that the shape, particle size, aggregate size, surface energy and the matrix properties have showed effective aspects.[81]

16.7.1 Swelling Index

It is observed that SI_{app} of nano-$CaCO_3$ is less than the commercial $CaCO_3$ filled SBR which is attributed to greater crosslinking of rubber, as the uniform dispersion of nano-$CaCO_3$ brings the chains closer and keeps them intact with nanoparticles.[80,82] Swelling depends on elastomer crosslinking density and solvent used. Solvent penetration is more in commercial micron size $CaCO_3$ than the nano-$CaCO_3$ rubber composites.

16.7.2 Mechanical Properties

The tensile strength of nano-$CaCO_3$ filled SBR (2.58 MPa for 9 nm $CaCO_3$) are higher than the commercial $CaCO_3$ (1.63 MPa) and the fly ash filled SBR (1.37 MPa)[82] which means nano-$CaCO_3$ provides higher tensile strength as compared to commercial $CaCO_3$ and fly ash filled SBR which is attributed to uniform dispersion of nanofiller into the rubber matrix that intercalates the rubber matrix, and so the degree of crosslinking of rubber chain increases.

In the nanocomposites having SBR as the matrix and $CaCO_3$ as filler were prepared and found that the ΔG increases in presence of commercial $CaCO_3$ and considerable decrease in energy (ΔG) and increase in ΔS are observed with reduction of nanosize and increase in amount of nano-$CaCO_3$ in SBR. It is assumed that ΔG is closely related to elastic behaviour of the material; the nano-$CaCO_3$ shows better elasticity than commercial $CaCO_3$.[80] In the nanocomposites having SBR as the matrix and $CaCO_3$ as filler were prepared and observed[80] that tensile strength increases with reduction in size of $CaCO_3$ filled SBR and results showed that the nanofillers are not appreciable above 8 wt% loading, because the nanoparticles get agglomerated at higher wt% of $CaCO_3$. Inorganic nanoparticles are strongly fixed by electrostatic forces in rubber, so it is necessary to add a hydrophobic layer with coupling agent to reduce the agglomeration problem. The E_b of nano-$CaCO_3$ and commercial $CaCO_3$ filled SBR increases with increase in the filler content but the increment in E_b in all nanosized of $CaCO_3$ is significantly greater than the commercial $CaCO_3$ filled SBR[80] which is due to very fine size of particles, which produce more interfacial bonding along with good dispersion and homogeneity in bonding as discussed earlier in the text. The tensile strength of the nano-$CaCO_3$ rubber composites with linseed oil as an extender was higher than that of the composites without an extender up to 8 wt% filler and beyond that and beyond that a reduction[83] which is attributed to the linseed oil used as an extender, which helped with the uniform dispersion of nano-$CaCO_3$ in the rubber matrix, which resulted in an intercalation phenomenon[84] whereas above an 8% composition, the results for the nanofiller were not appreciable because the nanoparticles agglomerated at a

higher percentage of $CaCO_3$ (*i.e.* filler–filler interaction).There was a continuous increase in the hardness with an increase amount of the filler for all compositions. The increase in the hardness was more pronounced for nano-$CaCO_3$ filled SBR than for commercial $CaCO_3$[83] SBR filled with nano-$CaCO_3$ showed an increase in the specific gravity and hardness is due to greater and uniform dispersion of filler into the matrix, which brings chains of matrix closer to reduce the free volume to the greater extent in crosslinking of chain.[82] The Eb of nano-$CaCO_3$ filled SBR are higher than the commercial $CaCO_3$ and the fly ash filled SBR which is because of uniform dispersion of nano into the rubber matrix particles and rubber–filler interaction.[82]

16.7.3 Morphological Studies

In order to study the interfacial adhesion, the micrographs at different concentrations of nano-$CaCO_3$ and commercial $CaCO_3$ were compared with SBR as the matrix. The nano-$CaCO_3$ showed good dispersion with the SBR matrix while commercial $CaCO_3$ filled showed agglomeration thereby weakens interfacial adhesion in case commercial or microsized $CaCO_3$.

In the X-ray analysis, the absence of peaks indicates that nano-$CaCO_3$ is dispersed throughout the matrix; whereas commercial $CaCO_3$ filled SBR composite showed a peak at 2.82° in the X-ray diffractograms of 8 wt% SBR/nano-$CaCO_3$ (21, 15 and 9 nm) composites which is attributed to micron size of filler and above 8 wt% of loading of filler in nano-$CaCO_3$ and commercial $CaCO_3$ presence of peaks indicate that nano- and commercial $CaCO_3$ get agglomerated.[80]

16.7.4 Flame Retardancy

The measuring principle of flammability is the oxygen consumption. The principle states that there is a constant relationship between the mass of oxygen consumed from the air and the amount of heat released. The flame retardancy of nano-$CaCO_3$ SBR composites observed significantly as compared to commercial $CaCO_3$. The nanoscale inorganic filler in the rubber nanocomposites promotes formation of the char layer, which acts as an excellent insulator and mass transfer barrier due which this effect drastically improves the burning resistance and absorbs the heat of burning. This insulating effect of char layer of nano-inorganic filler slows down the escape of the volatile products generated from decomposition of SBR. Also SBR nanocomposites are thermally more stable as compared to commercial $CaCO_3$ filled SBR as shown in TGA study.[80] The flammability rates showed that the absorption of energy by nanoparticles $CaCO_3$ is uniform (endothermic).[80] The literature suggests that the source of the improved flammability properties of these materials is due to difference in condensed phase decomposition processes and not a gas phase effect.[85] It is found that the crucial parameter responsible for lowering the heat release rate of the rubber nanocomposites is the mass loss rate during combustion, which is significantly reduced for nanocomposites compared to the

pure SBR and commercial filled SBR composites. The lowering of heat release rate is also due to the presence of nano-inorganic particles between the chains of rubber, which first hinder diffusion of volatile decomposition product from the nanocomposites and acts as a barrier to diffusion of oxygen into the nanocomposites at the same time. Together to this effect uniform dispersion of nano-inorganic filler into the rubber matrix provide a stronger barrier property.

SBR filled with nano-$CaCO_3$ with linseed oil as an extender showed a significant reduction in flammability in comparison with that without an extender.[83] The rate of flame retarding of nano-$CaCO_3$ was more than that of commercial $CaCO_3$ with linseed oil and the increase in flame retardancy with a decrease in the size was due to the uniform dispersion of the nanosized, which resulted in greater absorption of heat energy.[83] One of the other author[82] also investigated the SBR filled with nano-$CaCO_3$ and found that reduction in nanosize shows better improvement in flame retardancy which is attributed to nanofiller forms effective layer on the surface, which absorbs the heat of burning.

16.7.5 Applications

Application of $CaCO_3$ in industries has been significantly grown for over the last 30 years. $CaCO_3$ particles have been utilized as filler to give specific properties for rubber products and to reduce the costs of products in rubber industry.

Nano-$CaCO_3$ is one of the many emerging applications of nanotechnology that is already finding successful commercial application. Reinforcing effect of nano-$CaCO_3$ in different compounds – NR and NR/NBR blend used in sports goods (laminated sheet for inflated balls), NR based cycle tube, bromobutyl-based pharmaceutical closures and CPE/CSM blend used for coated fabric was studied with one characteristic in mind that is to improve barrier properties as all these products have requirement of one common property – air retention.

16.8 Conclusions

In this chapter, the study carried out on nanofillers reinforced natural/synthetic rubber has been discussed. After a description on the NR rubber and $CaCO_3$ as filler, the development of synthetic composites with the incorporation of micro and nano-$CaCO_3$ as a filler material has also been discussed for comparative study. In particular, the role of fillers on the property modification of rubber properties, such as surface properties, mechanical strength, thermal conductivity, and permittivity has been mentioned. The effectiveness of this coating was demonstrated. The importance of well-dispersed nanoparticles on the improvement of the mechanical and electrical properties of polymers is also emphasized. However, one of the problems encountered is that the nanoparticles agglomerate easily because of their high surface energy.

Nano-$CaCO_3$ is already finding successful commercial applications. Reinforcing effect of nano-$CaCO_3$ in different compounds – NR and NR/NBR

blend used in sports goods (laminated sheet for inflated balls. The addition of impermeable $CaCO_3$ particles to rubbery polymeric membranes reduces light gas and vapour permeability as particle loading increases. According to the researchers, the nano-$CaCO_3$ filler in NBR created a more extended tortuous path against gas penetration compared to conventional fillers, thus, lower permeation values.

Abbreviation

BR	Butadiene Rubber
$CaCO_3$	Calcium Carbonate
CV	Conventional Vulcanizing systems
DMA	Dynamic Mechanical Analysis
Eb	Elongation at Break
GCC	Ground $CaCO_3$
HNCC	Hydrophilic Nanoscale Calcium Carbonate
NCC	Nano Calcium Carbonate
NIF	Nanoscale Inorganic filler
NPCC	Nano-precipitated $CaCO_3$
PCC	Precipitated $CaCO_3$
SI_{app}	Swelling Index
UFPNBR	Ultrafine Full-Vulcanized Powder Nitrile Butadiene Rubber
γ_s^d	Lower Dispersive Component
γ_s^{sp}	Higher Specific Component
SI_{app}	Swelling Index
$t_{1/2}$	Square Root of Time

References

1. K. C. Baranwal and H. L. Stephens, *Basic Elastomer Technology*, The Rubber Division American Chemical Society Akron, 2001.
2. H. Ismail, M. R. Edyham and B. Wirjosentono, *Polymer Testing*, 2002, **21**, 139.
3. T. G. Vladkova, P. D. Dineff, D. N. Gospodinova and I. Avramova, *Journal of Applied Polymer Science*, 2006, **101**, 651.
4. H. M. Da Costa, L. L. Y. Visconte, R. C. R. Nunes and C. R. G. Furtado, *Journal of Applied Polymer Science*, 2002, **83**, 2331.
5. A. Yang and R. Wu, *Journal of Applied Polymer Science*, 2002, **84**, 486.
6. V. G. Geethamma, G. Kalaprasad, G. Groeninckx and S. Thomas, *Composites Part A: Applied Science and Manufacturing*, 2005, **36**, 1499.
7. M. M. Rahman and M. A. Khan, *Composites Science and Technology*, 2007, **67**, 2369.
8. M. Abdelmouleh, S. Boufi, M. N. Belgacem and A. Dufresne, *Composites Science and Technology*, 2007, **67**, 1627.

9. J. A. Brydson, *Rubber Materials and their Compounds*, Elsevier Applied Science, London, 1988.
10. W. Hofmann, *Rubber Technology Handbook*, Hanser Publishers, Munich, 1989.
11. J. B. Donnet, *Rubber Chemistry and Technology*, 1998, **71**, 323.
12. C.-M. Chan, J. Wu, J.-X. Li and Y.-K. Cheung, *Polymer*, 2002, **43**, 2981.
13. C. S. Gopinath, S. G. Hegde, A. V. Ramaswamy and S. Mahapatra, *Materials Research Bulletin*, 2002, **37**, 1323.
14. P. C. LeBaron and T. J. Pinnavaia, *Chemistry of Materials*, 2001, **13**, 3760.
15. S. Sinha Ray and M. Okamoto, *Progress in Polymer Science*, 2003, **28**, 1539.
16. G. Kraus, Reinforcement of elastomers by particulate fillers, *Eirich FR edn., Science and Technology of Rubber*. Academic Press, New York, 1978.
17. Z. Mao and J. Huang, *Journal of Solid State Chemistry*, 2007, **180**, 453.
18. K. Premphet and P. Horanont, *Journal of Applied Polymer Science*, 1999, **74**, 3445.
19. D.-g. J. Xun-qiu W., *J China Univ Min Technol*, 2008, **18**, 76.
20. M. Lipińska, M. Zaborski and L. Ślusarski, *Macromolecular Symposia*, 2003, **194**, 287.
21. T. Nakatsuka, H. Kawasaki, K. Itadani and S. Yamashita, *Journal of Colloid and Interface Science*, 1981, **82**, 298.
22. Y. N. Sharma, R. D. Patel, I. H. Dhimmar and I. S. Bhardwaj, *Journal of Applied Polymer Science*, 1982, **27**, 97.
23. Z. Deqin and S. Yu, *Acta Polymerica Sinica*, 2008, **08**, 813.
24. R. M. Ma C and M. Zhang, *Acta Polym Sin*, 2003, **3**, 381.
25. A. Tabtiang and R. Venables, *Composite Interfaces*, 1998, **6**, 65.
26. T. Nakatsuka and S. Yamashita, *Journal of Applied Polymer Science*, 1983, **28**, 3549.
27. F. Qiang, G. Wang and C. Liu, *Polymer*, 1995, **36**, 2397.
28. A. Hanprasopwattana, S. Srinivasan, A. G. Sault and A. K. Datye, *Langmuir*, 1996, **12**, 3173.
29. S. Poompradub, T. Luthikaviboon, S. Linpoo, R. Rojanathanes and P. Prasassarakich, *Polymer Bulletin*, 2011, **66**, 965.
30. M. Bhattacharya, M. Maiti and A. K. Bhowmick, *Polymer Engineering & Science*, 2009, **49**, 81.
31. S. Pradhan, F. R. Costa, U. Wagenknecht, D. Jehnichen, A. K. Bhowmick and G. Heinrich, *European Polymer Journal*, 2008, **44**, 3122.
32. M. Endo, T. Noguchi, M. Ito, K. Takeuchi, T. Hayashi, Y. A. Kim, T. Wanibuchi, H. Jinnai, M. Terrones and M. S. Dresselhaus, *Advanced Functional Materials*, 2008, **18**, 3403.
33. Y. Chen, Z. Peng, L. X. Kong, M. F. Huang and P. W. Li, *Polymer Engineering & Science*, 2008, **48**, 1674.
34. L. Jiang, Y. C. Lam, K. C. Tam, T. H. Chua, G. W. Sim and L. S. Ang, *Polymer*, 2005, **46**, 243.
35. L. Xiang, Y. Xiang, Z. G. Wang and Y. Jin, *Powder Technology*, 2002, **126**, 129.

36. X. H. Li, S. C. Tjong, Y. Z. Meng and Q. Zhu, *Journal of Polymer Science Part B: Polymer Physics*, 2003, **41**, 1806.
37. M. A. Osman, A. Atallah and U. W. Suter, *Polymer*, 2004, **45**, 1177.
38. D. C. Blackley, *Polymer Latices, Science and Technology*, Kluwer Academic, Dordrecht, The Netherlands, 1997.
39. H. Ismail, *Pengisi dan Penguatan Getah*, 2000.
40. D. Rivin, J. Aron and A. I. Medalia, *Rubber Chemistry and Technology*, 1968, **41**, 330.
41. J. Le Bras and E. Papirer, *Journal of Applied Polymer Science*, 1978, **22**, 525.
42. G. G. Winspear, *The Vanderbilt Latex Handbook*, ed. R. T. Vanderbilt, New York, 1954.
43. S. Chuayjuljit, A. Imvittaya, N. Na-Ranong and P. Potiyaraj, *Journal of Metals, Materials and Minerals*, 2002, **12**, 51.
44. M.-J. Wang, *Rubber Chemistry and Technology*, 1998, **71**, 520.
45. F. R. Eirich, *Science and Technology of Rubber*, Academic Press, New York, 1978.
46. S. Wolff, *Rubber Chemistry and Technology*, 1996, **69**, 325.
47. R. Rothon, *Particulate-Filled Polymer Composites*, Longman Scientific & Technical, New York, 1995.
48. M. Morton, *Rubber Technology*, Van Nostrand Reinhold Co, New York, 1987.
49. A. I. Medalia, G. Kraus, *Science and Technology of Rubber*, ed. J. E. Mark, B. Erman and R. F. Eirich, Academic Press, New York, 1994.
50. S. Blow, *Handbook of Rubber Technology*, Galgotia Publication Ltd, New Delhi, 1998.
51. G. L. Hwang, Y. T. Shieh and K. C. Hwang, *Advanced Functional Materials*, 2004, **14**, 487.
52. M. Wang, K. P. Pramoda and S. H. Goh, *Polymer*, 2005, **46**, 11510.
53. X. Zhang, T. Liu, T. V. Sreekumar, S. Kumar, V. C. Moore, R. H. Hauge and R. E. Smalley, *Nano Letters*, 2003, **3**, 1285.
54. A. Rasheed, M. D. Dadmun, I. Ivanov, P. F. Britt and D. B. Geohegan, *Chemistry of Materials*, 2006, **18**, 3513.
55. M. F. Islam, E. Rojas, D. M. Bergey, A. T. Johnson and A. G. Yodh, *Nano Letters*, 2003, **3**, 269.
56. S. Patcharaphun, W. Chookaew, T. Tungkeunkunt and N. Na-Ranong, *Polymer Engineering and Science*, 2011, **51**, 2353.
57. S. Wolff and M.-J. Wang, *Rubber Chemistry and Technology*, 1992, **65**, 329.
58. Y. Li, M. J. Wang, T. Zhang, F. Zhang and X. Fu, *Rubber Chemistry and Technology*, 1994, **67**, 693.
59. J. A. Ayala, W. M. Hess, A. O. Dotson and G. A. Joyce, *Rubber Chemistry and Technology*, 1990, **63**, 747.
60. J.-B. Donnet, *Rubber Chemistry and Technology*, 1998, **71**, 323.
61. P. Pasbakhsh, H. Ismail, M. N. A. Fauzi and A. A. Bakar, *Journal of Applied Polymer Science*, 2009, **113**, 3910.

62. S. Manroshan and A. Baharin, *Journal of Applied Polymer Science*, 2005, **96**, 1550.
63. M. S. Sobhy, D. E. El-Nashar and N. A. Maziad, *Egyptian Journal of Solids*, 2003, **26**, 241.
64. P. Sae-oui, C. Sirisinha and P. Thaptong, *J. Mater. Cycles Waste Manag.*, 2009, **11**, 166.
65. B. T. Poh, C. P. Kwok and G. H. Lim, *European Polymer Journal*, 1995, **31**, 223.
66. E. M. Dannenberg, *Rubber Chemistry and Technology*, 1975, **48**, 410.
67. A. L. G. Saad and A. F. Younan, *Polymer Degradation and Stability*, 1995, **50**, 133.
68. S. Poompradub, Y. Ikeda, Y. Kokubo and T. Shiono, *European Polymer Journal*, 2008, **44**, 4157.
69. J. B. Donnet and E. Custodero, in *The Science and Technology of Rubber*, ed. J. E. Mark, B. Erman and F. R. Eirich, Elsevier Academic Press, San Diego, 2005, p. 367.
70. S. Sun, C. Li, L. Zhang, H. L. Du and J. S. Burnell-Gray, *European Polymer Journal*, 2006, **42**, 1643.
71. H. E. Trexler and M. C. H. Lee, in *Research Publication GMR-4908*, The American Chemical Society, 1985, vol. Rubber Division Meeting.
72. P. J. Flory, *Principles of Polymer Chemistry*, Cornell Univ. Press, New York, 1953.
73. W. Chookaew, T. Tungkeunkunt, J. Mingbunjerdsuk, N. Na-Ranong and S. Patcharaphun, *International Conference on Materials Processing Technology*, Bangkok, Thailand, 2010.
74. B. T. Poh, H. Ismail, E. H. Quah and P. L. Chin, *Journal of Applied Polymer Science*, 2001, **81**, 47.
75. A. L. N. da Silva, M. C. G. Rocha, M. A. R. Moraes, C. A. R. Valente and F. M. B. Coutinho, *Polymer Testing*, 2002, **21**, 57.
76. Q. Wang, Q. Song, J. Qiao, X. Zhang, L. Zhang and Z. Song, *Polymer*, 2011, **52**, 3496.
77. F.-L. Jin and S.-J. Park, *Materials Science and Engineering: A*, 2008, **478**, 406.
78. H. Zhang, J. F. Chen, H. K. Zhou, G. Q. Wang and J. Yun, *Journal of Materials Science Letters*, 2002, **21**, 1305.
79. X. Xu, Y. Song, Q. Zheng and G. Hu, *Journal of Applied Polymer Science*, 2007, **103**, 2027.
80. S. Mishra, N. Shimpi and U. Patil, *Journal of Polymer Research*, 2007, **14**, 449.
81. S. Sahebian, S. M. Zebarjad, S. A. Sajjadi, Z. Sherafat and A. Lazzeri, *Journal of Applied Polymer Science*, 2007, **104**, 3688.
82. S. Mishra and N. Shimpi, *Journal of Scientific and Industrial Research*, 2005, **64**, 744.
83. S. Mishra and N. G. Shimpi, *Journal of Applied Polymer Science*, 2005, **98**, 2563.
84. M. Xiong, L. Wu, S. Zhou and B. You, *Polymer International*, 2002, **51**, 693.
85. J. W. Gilman, *Applied Clay Science*, 1999, **15**, 31.

CHAPTER 17

Preparation and Characterization of Natural Rubber Reinforced with Carbon Nanotubes

MOU'AD A. TARAWNEH* AND SAHRIM HJ. AHMAD

School of Applied Physics, Faculty of Science and Technology, Universiti Kebangsaan Malaysia, 43600 Bangi, Selangor, Malaysia
*Email: moaath20042002@yahoo.com

17.1 Introduction

Thermoplastic elastomer (TPE) blends have been broadly studied as a new class of materials. TPEs offer various advantages and require no state-of-the-art processing machinery, while scrap and rejects are recyclable.[1] Blends can be homogeneous, phase separated or both. TPEs are multi-phase polymer systems consisting of hard and soft domains that can be copolymers or mechanical blends. This phase separation leads to materials having unique and viable commercial physical properties. TPEs exhibit the thermoplastic characteristics of the hard thermoplastic phase, and resilience as a result of the rubbery domains.[2] TPEs based on natural rubber (NR) and thermoplastic blends are known as thermoplastic natural rubber (TPNR) blends. There are two types of TPNR, namely thermoplastic polyolefin (TPO) and thermoplastic vulcanizate (TPV).[3]

RSC Polymer Chemistry Series No. 8
Natural Rubber Materials, Volume 2: Composites and Nanocomposites
Edited by Sabu Thomas, Hanna J. Maria, Jithin Joy, Chin Han Chan and Laly A. Pothen

Published by the Royal Society of Chemistry, www.rsc.org

One of the most important aspects to be considered in the TPE blend is the components ratio. Processing parameters, involved temperature, rotor speed of the mixer and mixing time also play a significant role in producing good blends properties.[4] The processing is normally done at a temperature above the melting point of the thermoplastic. The quality of blend reflects its miscibility, where it exhibited better mechanical and thermal properties, and good homogeneity. The properties obtained can be further enhanced by introducing a variety of additives to promote miscibility by reducing interfacial tension such as compatibilizer agent, interfacial agent, crosslinking agent and fillers.

A pioneer group of researchers in UKM has extensively studied utilization of liquid natural rubber (LNR) as a compatibilizer on various NR/polyolefin blends. LNR was produced by photodegradation of NR in toluene and exposure to the ultraviolet for 6 h. The LNR has the same microstructure as NR but with a short polyisoprene chain (of different molecular weight, M_w). The M_w of LNR is around 50,000 whereas for NR is 900,000. The formation of new functional groups such as –OH, C–O and C=O via oxidation of photochemical sensitization of NR. The presence of the new functional groups is shown in Figure 17.1. The LNR with some active terminals like –OH is

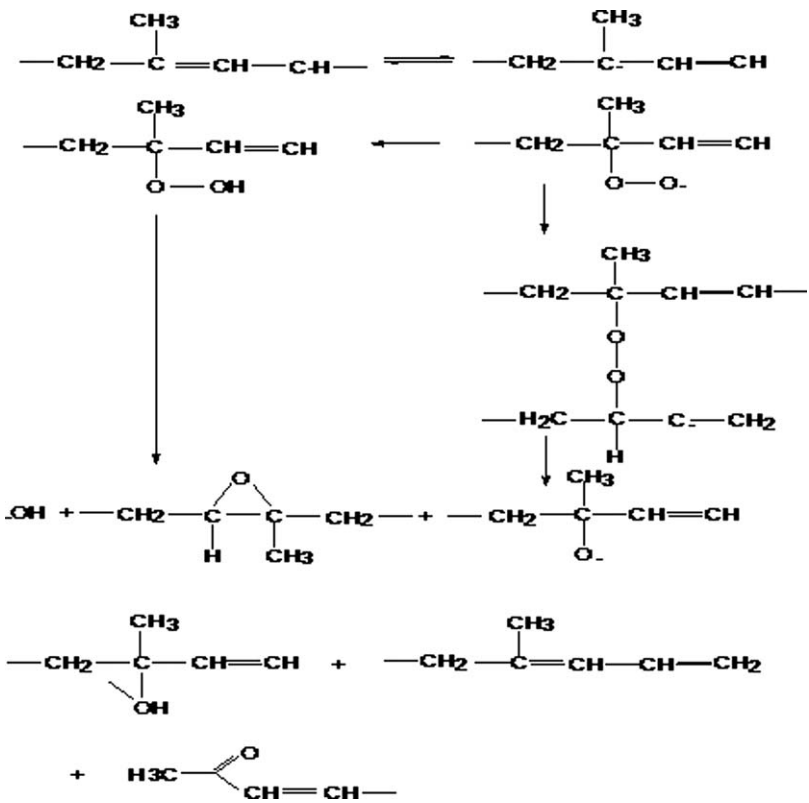

Figure 17.1 Schematic diagram of photochemical sensitization of natural rubber.

expected to react with the plastic particles and thereby bond the plastic particles to the NR matrix. There are also successful studies on NR and various PE with LNR as a compatibilizer.[5,6]

Mechanical blending of PP and NR with an addition of LNR as a compatibilizer was reported to be optimal at temperature of 175–185 °C and rotor speed of 30–60 rpm.[1] The percentage of LNR used depends on the ratio of NR to PP. For NR:PP ratio of 30:70 the best physical properties are obtained at 10% LNR.[7] The compatibilizer helps to induce interaction between the rubber and plastic interphase and thereby increases the homogeneity of the blend.

Carbon nanotubes (CNTs) exhibit a great range of remarkable properties, including unique mechanical and electrical characteristics. These remarkable high modulus and stiffness properties have led to the use of CNTs to reinforce polymers in the past few years. Both theoretical (*e.g.* molecular structural mechanics and tight-binding molecular dynamics) and experimental studies have shown SWCNTs to have extremely high elastic modulus ($\approx$1 TPa).[8,9] The tensile strength of SWCNTs estimated from molecular dynamics simulation is $\approx$150 MPa.[10] The experimental measurement of 150 MPa was found for the break strength of MWCNTs.[11]

The remarkable properties of CNTs offer the potential for improvement of the mechanical properties of polymers at very low concentrations. In practice, MWCNTs are preferred over SWCNTs as the reinforcing fillers for polymers due to their lower production cost. However, slippage between the shells of MWCNTs would undermine the capability of the fillers to bear the external applied load.

The effect of SWCNTs and carbon fibre additions on the tensile ductility of silicone rubber is shown that the strain to failure drops from 325 (RTV) to 275% upon loading with 1 wt% SWCNTs, corresponding to $\approx$ 15% reduction.[12]

When 1 wt% of CNTs were added to the rubber the stress level for the nanocomposite material increased from 0.2839 to 0.56413 MPa. At 10 wt% of CNTs the stress value obtained reached 2.55 MPa which is nine times that of pure NR.[13] Nanocomposites of NR reinforced with SiC nanoparticles and single-walled carbon nanotubes were synthesized and processed using toluene as the solvent.[14] Both types of nanocomposite showed an increase in initial modulus with increasing filler content, with a maximum initial modulus at 1.5% filler content. The tangent modulus at 200% strain further confirms the enhancement of reinforcement by the nanofillers at 1.5% content.

Pure NR and SWCNTs/NR composite sheets have been prepared by adding different amounts of sulfur and it was found that the resulting mechanical response of the samples changes with respect to the degree of vulcanization. It was also found that by adding 0.25 wt% of SWCNTs, the modulus of the SWCNTs/NR composites increase about 20% compared to the pure NR material at the same degree of vulcanization without losing their elastic properties, though strength and elongation to failure did not change.[15] NR/silane functionalized carbon nanotube composites exhibits higher modulus, tensile strength and elongation at break compared to NR vulcanizates due to the higher polymer–filler interaction between the silanized carbon nanotube and NR vulcanizates.[16]

The CNTs/NR nanocomposites were fabricated through solvent mixing on the basis of pre-treatment of CNTs.[17] The pre-treated CNTs reinforced NR composite showed enhanced tensile modulus and tensile strength which were nearly six times and three times higher, respectively, than that of neat NR. Correspondingly, the storage modulus of pre-treated CNTs/NR nanocomposites markedly exceeds that of neat NR under all temperature regions. Reinforcement of NR was achieved using carboxylated multi-walled carbon nanotubes (c-MWCNTs) dispersed with sodium dodecyl sulfate. The tensile and dynamic mechanical tests demonstrated a strong enhancement in the Young's modulus ($\sim$10-fold), tensile strength ($\sim$2-fold) and storage modulus ($\sim$60-fold) at low strain in the rubbery state with up to 8.3 wt% of MWCNTs, with a small reduction in elongation at break.[18]

A numerical tool capable of predicting the mechanical behaviour of SWCNTs reinforced rubber.[19] The formulation is based in a micromechanical, non-linear, multi-scale finite element approach and utilizes a Mooney–Rivlin material model for the rubber and takes into account the atomistic nanostructure of the nanotubes. The interfacial load transfer characteristics were parametrically approximated via the use of joint elements of variable stiffness. The SWCNTs improve significantly the composite strength and toughness especially for higher volume fractions.

The well-dispersed CNTs/elastomer composite was prepared by open roll mill mixer with high shear stress.[20] The mechanical interfacial regions formed around CNTs together with CNTs divided elastomer matrix into small 'cells' in which the elastomer matrix was occluded. Therefore, the greatly enhanced mechanical properties were considered to have arisen from the three-dimensional structure formed by CNTs and the mechanical interfacial regions bound to them.

A novel mixing method using a rotation–revolution mixer was applied to the preparation of CNTs/SBR composites.[21] The results indicate that mixing technique can reduce the amount of CNTs needed to provide high electrical conductivity to the SBR matrix. The mixing method can be applied to various types of CNTs with SBR. For all CNTs/SBR composites, the percolation thresholds were less than 1 phr and were largely dependent on the structural quality of CNTs used as the filler material.

The solvent resistance characteristics of non-crosslinked and crosslinked NR composites reinforced by multi-walled carbon nanotubes (MWCNTs).[22] All the MWCNTs were individually dispersed within the rubber matrix where a three-dimensional cellulation structure was created when the added amount of MWCNTs exceeded 16 wt%. The non-crosslinked MWCNTs-filled rubber composite was not soluble, but swelled in toluene. They found that a continuous three-dimensional structure at the interface between the MWCNTs and the NR was extremely tough and thus contributed to the improvement in the elastic modulus and thermal stability of NR composites.

Theoretical prediction showed an extremely high thermal conductivity (6000 W/mK) of an isolated SWCNTs.[23] High thermal conductivity of the CNTs may provide the solution of thermal management for the advanced

electronic devices with narrow line width. The thermal conductivity of epoxy-based composites reinforced with 1.0 wt% SWCNTs increased over 125% reaching a value of ~0.5 W/mK.[24] High thermal conductivity of 42 and ~18W/mK of the aligned and the random bucky paper mats, respectively. However, the thermal conductivity drops significantly by almost an order of magnitude when the aligned bucky paper mats were loaded with epoxy, the volume fraction of the aligned bucky paper composites is about 50%.[25]

The differences in the composite manufacturing methods, *i.e.* powder- (MWCNTs and ball milled SWCNTs) or liquid- (chemically treated SWCNTs) based approach, cannot account for the differences in the properties, since both methods were used for the SWCNTs composites and resulted in similar thermal behavior.[26] They concluded that in this case, there must be a very large interface resistance to the heat flow associated with poor phonon coupling between the stiff nanotubes and the (relatively) soft polymer matrix. Also, it is possible that the phonon vibrations in the SWCNTs are dampened by the matrix interaction, while in the MWCNTs the phonons can be carried in the inner walls without hindrance.

The elastomeric nature and thermoplastic processability of TPNR make it an important commercially viable material. Due to competition from other synthetic materials have led various research focuses on improving the properties of TPNR. This includes on initiatives to incorporate various fillers and reinforcement fibres to improve mechanical and thermal properties. TPNR composites with different amounts of MWCNTs were prepared and their thermal properties were investigated.[27] The higher thermal conductivity was achieved in the samples with 1 wt% and 3 wt% of MWCNTs compared to the pristine TPNR. The reinforcing effect of MWCNTs on the TPNR was also confirmed by DMA where the addition of nanotubes has increased the storage modulus, the loss modulus, and also the glass transition temperature (T_g).[28] Two types of MWCNTs reinforced thermoplastic NR and the tensile properties were measured.[29] The tensile strength and elongation at break of MWCNTs 1 increased by 23%, and 29%, respectively. The Young's modulus had increased by increasing the content of MWCNTs. For MWCNTs 2 the optimum result of tensile strength and Young's modulus was recorded at 3% which increased 39%, and 30%, respectively.

In this chapter, TPNRs reinforced with multi-walled carbon nanotube (MWCNTs) nanocomposites was prepared by the melt blending method. Using this method, (MWCNTs) will be dispersed homogeneously in the TPNR matrix in an attempt to increase the properties of these nanocomposites. The effect of MWCNTs on the mechanical and thermal properties of TPNR nanocomposites is reported in this chapter.

17.2 Experimental Details

Polypropylene, with a density of 0.905 g/cm^3, was supplied by Propilinas (M) Sdn. Bhd, NR was supplied by Guthrie (M) Sdn. Bhd, polypropylene (PP) with density of 0.905 g/cm^3 was supplied by Polipropilinas (M) Sdn. Bhd were used

in this research. Maleic anhydride–grafted–polypropylene (MAPP) with density of 0.95 g/cm^3 was supplied from Aldrich Chemical Co., USA. The maleic anhydride content in MAPP was about 0.57%. Chemicals used were sodium hydroxide and sulfuric acid (95–97) % supplied by MERCK, Germany. LNR was prepared by photochemical degradation technique. A multi-walled carbon nanotube was provided by Arkema (Graphistrength™ C100). The specification of MWCNTs is as follows: purity >90%, length 0.1–10 μm, diameter 10–15 nm.

Mixing was performed by internal mixer (Haake Rheomix 600P). The mixing temperature was 180 °C, with a rotor speed of 100 rpm and 13 min mixing time. The indirect technique (IDT) was used to prepare nanocomposites, this involved mixing the MWCNTs with LNR separately, before it was melt blended with PP and NR in the internal mixer. TPNR nanocomposites were prepared by melt blending of PP, NR and LNR with MWCNTs in a ratio of 70 wt% PP, 20 wt% NR and 10 wt% LNR as a compatibilizer and 2 wt%, 4 wt%, 6 wt% and 8 wt% MWCNTs.

Tensile properties were performed using Testometric universal testing machine model M350-10CT with 5 kN load cell according to ASTM 412 standard procedure using test specimens of 1 mm thickness and cross-head speed 50 mm min^{-1}. At least five samples were tested for each composition, and the average value was reported. Impact test was carried out using Ray Ran Pendulum Impact System according to ASTM D 256-90b. The velocity and weight of the hammer were 3.5 m/s and 0.898 kg, respectively.

The thermal conductivity was measured by a laser flash method. Disk-type samples (12.7 mm in diameter and 1mm in thickness) were set in an electric furnace. Specific heat capacities were measured with a differential scanning calorimeter. Thermal diffusivity (λ, Wm^{-1}K^{-1}) was calculated from thermal diffusivity (α, m^2 s^{-1}), density (ρ, g/cm^3) and specific heat capacity (C, J g^{-1}K^{-1}) at each temperature using the following:

$$\lambda = \alpha.\rho.\mathrm{C}. \tag{17.1}$$

The reference used for the heat capacity calculation was a 12.7 mm thick specimen of pyroceram. The reference sample also coated with thin layer of graphite before the measurement was performed. The thermal conductivity of MWCNTs reinforced TPNR matrix composites of all volume fractions studied from 30 °C to 150 °C. Morphology of the MWCNTs and the composite were examined by scanning electron microscope (Philips XL 30). The samples were coated with a thin layer of gold to avoid electrostatic charging during examination.

17.3 Results and Discussion

17.3.1 Mechanical Properties

The tensile strength of TPNR reinforced with two types of MWCNTs of different percentages (2, 4, 6 and 8 wt%) is shown in Table 17.1. Generally, the

Table 17.1 Mechanical properties of TPNR and TPNR/MWCNTs nanocomposites.

Sample	*Tensile Strength (MPa)*	*Young's Modulus (MPa)*	*Elongation at Break (%)*	*Impact Strength (KJ/m^2)*
TPNR	13	337	350	8.23
TPNR + 2wt%MWCNTs	15.46	384	120	11
TPNR + 4wt%MWCNTs	17.86	450	90	15
TPNR + 6wt%MWCNTs	16.46	403	70	14
TPNR + 8wt%MWCNTs	14.55	384	40	12.13

MWCNTs exhibited an increasing trend up to 4 wt% content. Further increments in MWCNTs content decreased the tensile strength compared to the optimum filler loading. From Table 17.1, TPNR with MWCNTs has optimum results at 4 wt%, which, compared with TPNR, increased by 37%. The tensile strength increased radically as the amount of MWCNTs concentration increased. The mechanical performance, such as tensile properties, strongly depends on several factors such as the properties of the filler reinforcement and matrix, filler content, filler length, filler orientation, and processing method and condition. The improvement in the tensile strength may be caused by the good dispersion of MWCNTs in the TPNR matrix, which leads to a strong interaction between the TPNR matrix and MWCNTs. These well-dispersed MWCNTs may have the effect of physically crosslinking points, thus, increasing the tensile strength.[30–35] A good interface between the MWCNTs and the TPNR is very important for a material to stand the stress. Under load, the matrix distributes the force to the CNTs, which carry most of the applied load. When the content of MWCNTs is higher (more 4 wt%), the MWCNTs cannot disperse adequately in the TPNR matrix and agglomerate to form a big cluster. This is because of the huge surface energy of MWCNTs as well as the weak interfacial interaction between MWCNTs and TPNR, which leads to inhomogeneous dispersion in the polymer matrix and negative effects on the properties of the resulting composites that causes a decrease in the tensile strength.[36]

Table 17.1 shows the effect of filler content on the tensile modulus of TPNR reinforced by MWCNTs. The same trend as for the tensile strength the tensile modulus clearly shows that the presence of MWCNTs has significantly improved the tensile modulus of the TPNR. As depicted in the table, the Young's modulus of MWCNTs increased with the increase in the amount of MWCNTs. The maximum result was achieved at 4 wt%, with an increase of about 34%, which was due to the good dispersion of nanotubes displaying perfect stress transfer.[37–39] As explained before, a reduction in performance occurred at higher filler contents. Initially it increases with filler content and then decreases when exceeding the filler loading limit due to the diminishing interfacial filler–polymer adhesion. It is assumed that aggregates of nanotube ropes effectively reduce the aspect/ratio (length/diameter) of the reinforcement.[40]

The elongation at the break of TPNR with MWCNTs is shown in Table 17.1. It can be deduced that the reinforcing effect of MWCNTs is very marked. As the MWCNTs content in the TPNR increases, the stress level gradually increases but at the same time the strain of the nanocomposites decreased. This is because the MWCNTs included in the TPNR matrix behave like physical crosslinking points and restrict the movement of polymer chains. This shows that the inclusion of MWCNTs makes the TPNR stronger but more brittle.

The effect of filler loading on the impact strength of TPNR/MWCNTs nanocomposites is given in Table 17.1. It shows that incorporation of MWCNTs into TPNR considerably affects the impact strength of TPNR nanocomposites. The results exhibited better impact strength for MWCNTs at 4 wt% with an increase of almost 82 %. This is due to the better dispersion of carbon nanotubes in the matrix, which generated a significant toughening effect on the TPNR/MWCNTs nanocomposite. However, when the load is transferred to the physical network between the matrix and the filler, the debonding of the chain segments from the filler surface facilitates the relaxation of the matrix entanglement structure, leading to higher impact toughness. The low impact energy was attributed to the filler content. This will reduce the ability of reinforced composites to absorb energy during fracture propagation. However, in the case of elastomer-toughened polymer, the presence of the elastomer basically produces stress redistribution in the composite, which causes micro cracking or crazing at many sites, thereby resulting in a more efficient energy dissipation mechanism.[41] Consequently, because of their higher surface energy and large aspect ratio, it will be difficult for the nanotubes to disperse in the TPNR when the MWCNTs content is higher. This will lead to less energy dissipating in the system due to the poor interfacial bonding and induces micro spaces between the filler and polymer matrix. This causes micro-cracks when impact occurs, which induces easy crack propagation. Therefore, the higher agglomeration of MWCNTs can cause the mechanical properties of the composites to deteriorate.[42]

17.3.2 Thermal Conductivity

Introducing MWCNTs (2–8 wt%) to TPNR can significantly enhance the thermal conductivity of the TPNR matrix, as shown in Figure 17.2, the thermal conductivity of TPNR/MWCNTs composites increased at 4 wt% compared to 2, 6 and 8 wt%, respectively, as compared to TPNR at 30 °C, as shown in Figure 17.2. Thermal transport in the CNT composites includes phonon diffusion in the matrix and ballistic transportation in the filler. The improvement in thermal conductivity in MWCNTs/TPNR may stem from the improved percolation because of the better dispersion and formation of a network.[43] The dispersion of 2 wt% and 4 wt% MWCNTs is better than 6 wt% and 8 wt% in TPNR, at 6 wt% and 8 wt% the MWCNTs agglomerated inside TPNR. Therefore, the large amounts of junctions among the carbon nanotubes form a single conducting path, which is believed to be the reason why the measured thermal conductivity is low.

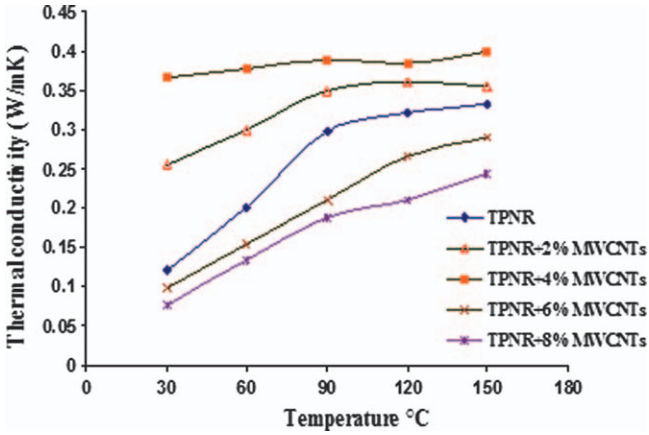

Figure 17.2 Glass transition temperature of TPNR reinforced with MWCNTs.

Two factors have been proposed to explain the significant enhancement of thermal conductivity with MWCNTs: (i) the rigid linkage between MWCNTs and TPNR matrix provides good interface compatibility, which may reduce interface thermal resistance; (ii) the good interface compatibility allows MWCNTs to disperse well in the matrix, consequently, the results of the SEM indicate that the MWCNTs possess good dispersion and compatibility in the TPNR matrix. The significant enhancement in the thermal conductivity of CNTs nanocomposites is possibly attributed to the kinks or twists of MWCNTs. When the phonon travels along the nanotubes, if it meets the kinks or twists it would be blocked at those sites. The existence of such kinks or twists in CNTs would lead to a decrease in the effective aspect ratio of the nanotubes.[44] When the amount of MWCNTs increases, and, thus, the thermal conductivity of TPNR/MWCNTs nanocomposites would be reduced.

The formation of the MWCNTs bundles restrict the phonon transport in composites, which may be attributed to two reasons: (i) the MWCNTs aggregation reduces the aspect ratio, consequently, decreasing the contact area between the MWCNTs and the TPNR matrix; (ii) the MWCNTs bundles cause the phenomenon of reciprocal phonon vector, which acts like a heat reservoir and restricts heat flow diffusion.[45–49]

The resistance to phonon movement from one nanotube to another through the junction will hinder phonon movement and, hence, limit the thermal conductivity. The low thermal conductivity could be partly due to the non-uniform diameter and size, as well as the defects in and the nanoscale dimension of MWCNTs. However, the numerous junctions between carbon nanotubes involved in forming a conductive path and the exceptionally low thermal conductance at the interface,[50] are believed to be the main reason for the low thermal conductivity. The effect of reducing the thermal conductivity is the transfer of phonons from nanotube to nanotube. This transition occurs by direct coupling between CNTs, in the case of the improper impregnated ropes,

CNT junctions and agglomerates, or via the matrix. In all these cases, the transition occurs via an interface, and, thus, the coupling losses can be attributed to an intense phonon boundary scattering. At the same time the thermal conductivity decreases with the increase in temperature (if the temperature is near the melting point of the matrix). This indicates that the thermal conductivity of the composites is dominated by the interface thermal transport between the nanotube/matrix or nanotube/nanotube interface. Thus, it is believed that the decreased effective thermal conductivity of the studied composites could be due to the high interface thermal resistance across the nanotube/matrix or nanotube/nanotube interfaces.[51]

17.3.3 Morphological Examination

Figure 17.3 shows MWCNTs as-received, with a large agglomeration of bundles of MWCNTs, the carbon nanotubes tend to aggregate to form bundles because of the strong van der Waals forces (many graphene layers wrapped into themselves). The SEM micrograph of TPNR is shown in Figure 17.4. This figure shows the TPNR without filler inside it, and so the surface is smooth. The homogeneous dispersion of MWCNTs in the composites is confirmed by SEM. Figures 17.5 and 17.6 show 2 wt% and 4 wt% of MWCNTs, respectively, they are well dispersed as individual tubes in the matrix, they also show that the nanotubes that had pulled out from the matrix were still coated with polymer. In addition, the bright spots inside the TPNR, suggestion a strong polymer nanotubes interfacial. The key parameter to improve the composites containing the nanotubes is their uniform dispersion.[52] This is often conducted in two

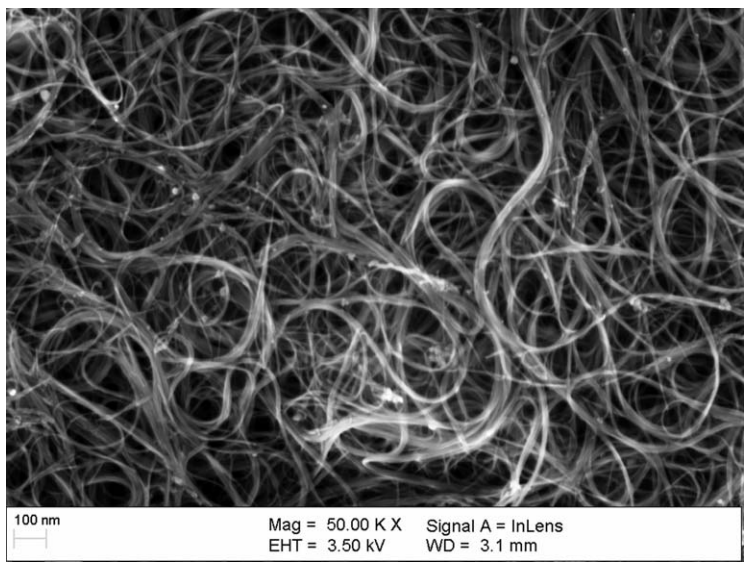

Figure 17.3 SEM micrograph of MWCNTs.

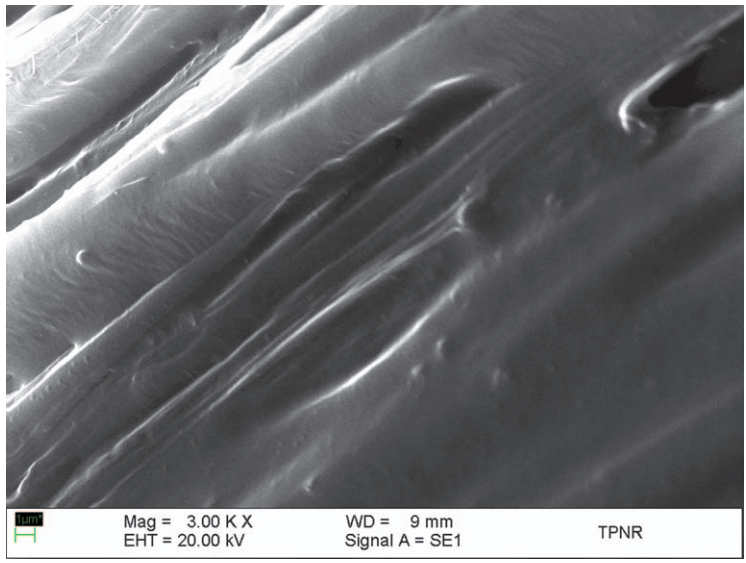

Figure 17.4 SEM micrograph of thermoplastic natural rubber (TPNR).

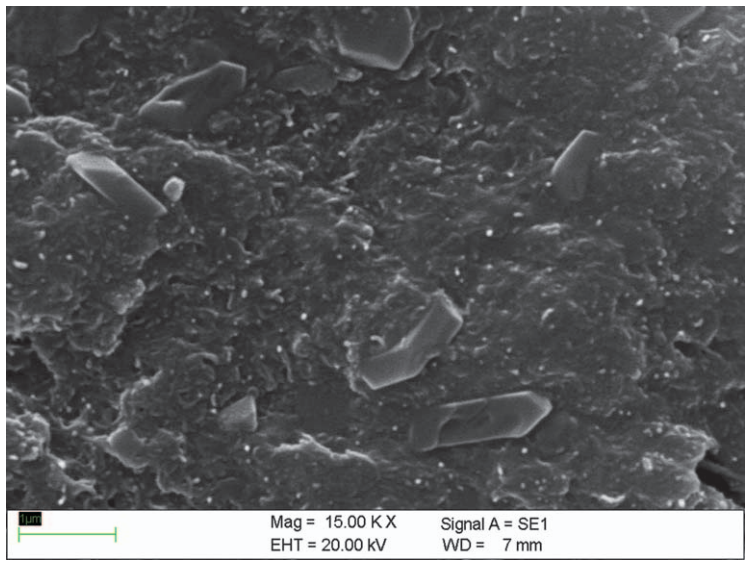

Figure 17.5 SEM micrograph of TPNR with 2 wt% MWCNTs.

steps. One is to reduce the aggregate (the tangled MWCNTs) size. The second is to homogenize the individual nanotubes and the aggregates in the matrix. Therefore, strong interfacial adhesion is essential for efficient stress transfer from the matrix to the nanotubes. This supports our observation of the higher efficiency of carbon nanotubes in enhancing the properties of TPNR

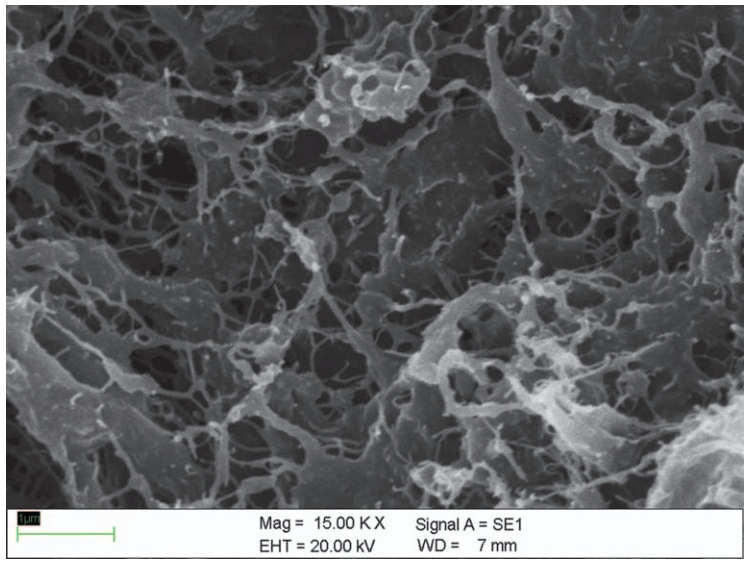

Figure 17.6 SEM micrograph of TPNR with 4 wt% MWCNTs.

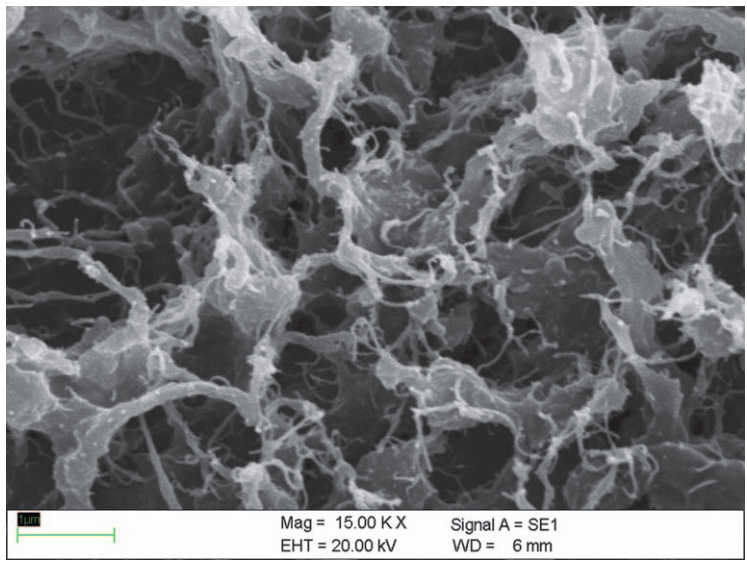

Figure 17.7 SEM micrograph of TPNR with 6 wt% MWCNTs.

nanocomposites. Figure 17.7 shows the SEM image of TPNR with 6 wt% of MWCNTs. They depict an aggregate in TPNR, which observes a large amount of MWCNTs that are self-organized in bundles. Low magnification was necessary in Figure 17.8 (8 wt% MWCNTs) to observe the poor dispersion of nanotubes in the TPNR. The figure clearly shows a large number of unbroken

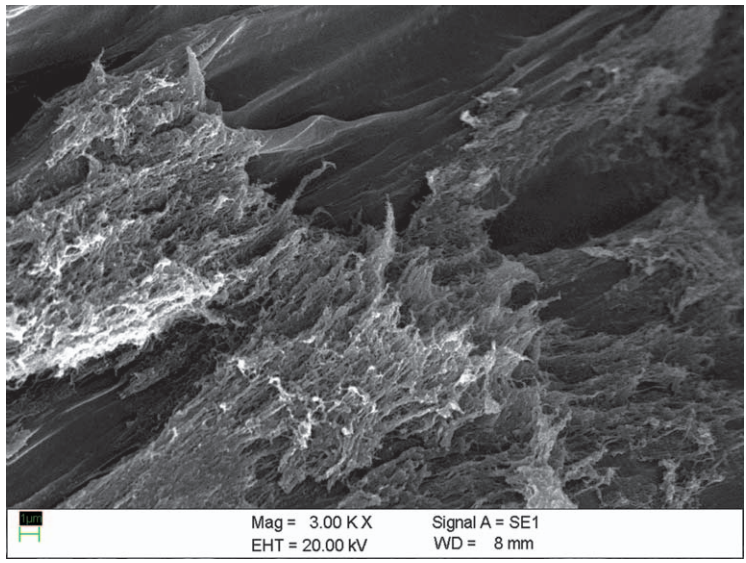

Figure 17.8 SEM micrograph of TPNR with 8 wt% MWCNTs.

carbon nanotubes (many zones with very high local MWCNTs concentrations), indicating a poor polymer/nanotube adhesion, which contributes to a reduction in the properties of TPNR/MWCNTs nanocomposites.

17.4 Conclusions

TPNR reinforced with multi-walled carbon nanotube (MWCNTs) nanocomposites was prepared by the melt blending method. Using this method, MWCNTs will be dispersed homogeneously in the TPNR matrix in an attempt to increase the properties of these nanocomposites. In this work, TPNR/MWCNTs nanocomposites were fabricated and the mechanical and thermal properties were measured. The addition of MWCNTs in the TPNR matrix improved the mechanical properties. The optimum result of tensile strength and Young's modulus was recorded at 4 wt% which increased 37%, and 34%, respectively. However, elongation of break decreased by increasing the amount of MWCNTs. The results exhibited better impact strength for MWCNTs at 4 wt% with an increase of almost 82 %. The reinforcing effect of MWCNTs was also confirmed by dynamic mechanical analysis where the addition of nanotubes have increased the glass transition temperature (Tg) with an increase in the amount of MWCNTs. The laser flash technique was used to measure the thermal conductivity from the results obtained. The high thermal conductivity was achieved at 4 wt% of MWCNTs compared with TPNR. The homogeneous dispersion of the MWCNTs throughout the TPNR matrix and strong interfacial adhesion between MWCNTs and matrix as confirmed by the SEM images are considered responsible for the significant mechanical and thermal enhancement.

Acknowledgements

The authors would like to thank the Malaysian Government and Universiti Kebangsaan Malaysia (UKM) under Science Fund Grant UKM-OUP-NBT-29-142/2011 and UKM-OUP-2012-135 for financial support.

References

1. I. Abdullah and M. Dahlan, *Prog. Polym Sci.*, 1998, **23**, 665.
2. A. Y. Coran and R. Patel, 116th Meeting of the Rubber Division, American Chemical Society, Cleveland, Ohio, 1980.
3. C. Nakason, P. Wannavilai and A. Kaesaman, *Polym Test.*, 2005, **25**, 34.
4. Li-Y. Yang, D. Bigio and T. G. Smith, *J. Appl. Polym. Sci*, 1995, **58**, 129.
5. I. Abdullah, S. Ahmad and C. S. Sulaiman, *J. Appl. Polym. Sci*, 1995, **58**, 1125.
6. C. S. Sulaiman, S. Ahmad and I. Abdullah, *Sains Malaysiana*, 1994, **23**, 29.
7. I. Abdullah and S. Ahmad, *Mater Forum*, 1992, **16**, 353.
8. C. Y. Li and T. W. Chou, *Int. J. Solids Struct.*, 2003, **40**, 2487.
9. E. Hernandez, C. Goze, P. Bernier and A. Rubio, *Phys. Rev. Lett.*, 1998, **80**, 4502.
10. B. I. Yakobson, M. P. Campbell, C. J. Brabec and J. Bernholc, *Comp. Mater. Sci*, 1997, **8**, 341.
11. B. G. Demcyzk, Y. M. Wang, J. Cumings, M. Hetman, W. Han, A. Zettl and R. O. Ritchie, *Mater. Sci. Eng. A*, 2002, **334**, 173.
12. M. D. Frogley, D. Ravich and H. D. Wagner, *Compos. Sci. Technol.*, 2003, **63**, 1647.
13. A. Fakhru'l-Razi., M. A. Atieh, N. Girun, T. G. Chuah, M. El-Sadig and D. R. A. Biak, *Composite Structures*, 2006, **75**, 496.
14. K. Kueseng and K. I. Jacob, *European Polymer Journal*, 2006, **42**, 220.
15. Qing Zhao, Rina Tannenbaum and Karl I. Jacob, *Carbon*, 2006, **44**, 1740.
16. A. M. Shanmugharaj, J. H. Bae, K. Y. Lee, W. H. Noh, Se Hyoung Lee and S. H. Ryu, *Composites Science and Technology*, 2007, **67**, 1813.
17. G. Sui, W. H. Zhong, X. P. Yang and Y. H. Yu, *Materials Science and Engineering A*, 2008, **485**, 524.
18. S. Bhattacharyya, C. Sinturel, O. Bahloul, Saboungi Marie-Louise, S. Thomas and Jean-Paul Salvetat, *Carbon*, 2008, **46**, 1037.
19. S. K. Georgantzinos, G. I. Giannopoulos and N. K. Anifantis, *Theoretical and Applied Fracture Mechanics*, 2009, **52**, 158.
20. D. Wang, S. Fujinami, K. Nakajima, Ken-ichi Niihara, S. Inukai, H. Ueki, A. Magario, T. Noguchi, M. Endo and T. Nishi, *Carbon*, 2010, **48**, 3708.
21. K. Tsuchiya, A. Sakai, T. Nagaoka, K. Uchida, T. Furukawa and H. Yajima, *Composites Science and Technology*, 2011, **71**, 1098.
22. T. Kinumotoa, J. Nakamura, K. Kikuchib and Z. Ogumic, *Carbon*, 2011, **49**, 378.
23. S. Berber, Y. K. Kwon and D. Tomanck, *Phys. Rev. Lett.*, 2000, **84**, 4613.

24. M. J. Biercuk, M. C. Llaguno, M. Radosavljevic, J. K. Hyun and A. T. Johnson, *Appl. Phys. Lett.*, 2002, **80**, 2767.
25. P. Gonnet, Z. Liang, E. S. Choi, R. S. Kadambala, C. Zhang, J. S. Brooks, B. Wang and L. Kramer, *Current Applied Physics*, 2006, **6**, 119.
26. Q. L. Moisala, I. A. Kinloch and A. H. Windle, *Composites Science and Technology*, 2006, **66**, 1285.
27. M. A. Tarawneh, S. Ahmad, R. Rasid, S. Y. Yahya and S. Y. Noum, *Journal of Reinforced Plastic and Composites*, 2011, **30**, 216.
28. M. A. Tarawneh1, S. Ahmad1, R. Rasid1, S. Y. Yahya and S. Y. Noum, *Journal of Reinforced Plastic and Composites*, 2011, **30**, 363.
29. M. A. Tarawneh, S. Ahmad, S. Y. Yahya, Carbon Nanotubes-Synthesis, Characterization, ed. S. Yellampalli, *InTech*, 2011, p. 443.
30. B. Zhang, R. Fu, M. Zhang, X. Dong, B. Zhao, L. Wang and C. U. Pittman, Composites, *Part A*, 2006, **37**, 1884.
31. W. D. Zhang, L. Shen, I. Y. Phang and T. Liu, *Macromolecules*, 2004, **37**, 256.
32. T. Liu, I. Y. Phang, L. Shen, S. Y. Chow and Y. D. Zhang, *Macromol*ecules, 2004, **37**, 7214.
33. W. D. Zhang, I. Y. Phang, L. Shen, S. Y. Chow and T. Liu, *Macromol* R*apid Commun*, 2004, **25**, 1860.
34. O. Meincke, D. Kaempfer, H. Weickmann, C. Friedrich, M. Vathauer and H. Warth, *Polymer*, 2004, **45**, 739.
35. J. Gao, M. E. Itkis, A. Yu, E. Bekyarova, B. Zhao and R. C. Haddon, *J Am Chem Soc*, 2005, **127**, 3847.
36. S. H. Jin and K. H. Young-Bin Park, Yoon, *Composites Science and Technology*, 2007, **67**, 3434.
37. P. Potschke, T. D. Fornes and D. R. Paul, *Polymer*, 2002, **43**, 3247.
38. R. Blake, J. N. Coleman, M. T. Byrne, J. E. McCarthy, T. S. Perova and W. J. Blau, *J Mater Chem*, 2006, **16**, 4206.
39. L. Xie, F. Xu, F. Qiu, H. Lu and Y. Yang, *Macromolecules*, 2007, **40**, 3296.
40. M. A. Lopez, L. Valentine, J. Biagiotti and J. M. Kenny, *Carbon*, 2005, **43**, 1499.
41. G. Canche-Escamilla, J. Rodriguez-Laviada, J. I. Cauich-Cupul, E. Mendizabal, J. E. Puig and P. J. HerreraFranco, *Compos.-Part(A):Appl.Sci.&Manufact*, 2002, **33**, 539.
42. J. Shen, W. Huang, L. Wu, Y. Hu and M. Ye, *Composites Scienc*e and Technology, 2007, **67**, 3041.
43. S. Kumar, M. A. Alam and J. Y. Murthy, *Appl Phys Lett.*, 2007, **90**, 104105–1.
44. C. W. Nan, Z. Shi and Y. Lin, *Chem Phys Lett.*, 2003, **375**, 666.
45. N. N. V. Sastry, A. Bhunia, T. Sundararajan and S. K. Das, *Nanotechnology*, 2008, **19**, 055704/1.
46. L. Chen, H. Xie, Y. Li and W. Yu, *Colloid Surf A: Physicochem Eng Aspects*, 2008, **330**, 176.
47. J. C. Grunlan, Y. S. Kim, S. Ziaee, X. Wei, B. Abdel-Magid and K. Tao, *Macromol Mater Eng*, 2006, **291**, 1035.

48. J. Koo, Y. Kang and C. Kleinstreuer, *Nanotechnology*, 2008, **19**, 375705/1.
49. G. Chen, J. Lu and D. Wu, *Mater Chem Phys*, 2007, **104**, 240.
50. X. Yunsheng, R. Gunawidjaja and Beckry Abdel-Magid, *Composites A*, 2006, **37**, 114.
51. S. Ramasamy, G. Shuqi, N. Toshiyuki and K. Yutaka, *Scripta Materialia*, 2007, **56**, 265.
52. J. Sandler, M. S. P. Shaffer, T. Prasse, W. Bauhofer, K. Schulte and A. H. Windle, *Polymer*, 1999, **40**, 5967.

CHAPTER 18

Metal Oxide Filled Micro and Nano Natural Rubber Composites

SUNEEL KUMAR SRIVASTAVA

Inorganic Materials and Nanocomposites Laboratory, Department of Chemistry, Indian Institute of Technology, Kharagpur-721302, India
Email: sunit@chem.iitkgp.ernet.in

18.1 Introduction

Depending on the distribution of micro/nanofiller in the polymer matrix, the composites may be classified as microcomposites or nanocomposites. These two types of composites differ significantly with respect to their properties. The nanocomposites show improved properties compared to pure polymer or that of microcomposites. It started only back in 1990, when Toyota research group showed that the use of montmorillonite can improve the mechanical, thermal, and flame retardant properties of polymeric materials without hampering the optical translucency behaviour of the matrix.[1] Since then, the majority of research has been focused in improving the physicochemical properties, *e.g.* mechanical, thermal, electrical, barrier *etc.* properties of polymer nanocomposites using cost effective and environmental friendly nanofillers with the aim of extending the applications of these materials in automotive, aerospace, construction, electronic, *etc.* as well as their day to day life use.[2–20] The improvements in the majority of their properties have invariably been attributed

RSC Polymer Chemistry Series No. 8
Natural Rubber Materials, Volume 2: Composites and Nanocomposites
Edited by Sabu Thomas, Hanna J. Maria, Jithin Joy, Chin Han Chan and Laly A. Pothen

Published by the Royal Society of Chemistry, www.rsc.org

to the increased interaction between the nanodimensional fillers and the polymeric chains enhancing the properties of the nanocomposites as a whole.

Natural rubber (NR) is an important unsaturated elastomer and a polymer of isoprene. About 93–95% of isoprene production is used to produce *cis*-1,4-polyisoprene (MW 100,000–1,000,00000). Some NR sources called gutta-percha constitutes high quality NR are composed of *trans*-1,4-polyisoprene, a structural isomer which has similar, but not identical properties. NR possesses numerous commendable properties including high strength, high tear resistance, low heat build-up, high resilience, retention of strength at elevated temperature, excellent dynamic properties and general fatigue resistance.[21–29] The special feature of NR is concerned with strain-induced crystallization, which lowers the crack initiation processes thereby making it more suitable for dynamic applications.[30] It is suggested that the stereoregular microstructure is responsible for such high mechanical properties of NR, however, due to high degree of unsaturation these properties are affected.[31] Also, substitution of these unsaturated bonds through hydrogenation, epoxidation, *etc.* severely affects the properties of the NR making it unsuitable for many desired applications. Because of its elasticity, resilience and toughness, NR is the basic constituent of many products used in the transportation (*e.g.* tyres), industrial (sealants), consumer (sports materials), hygienic and medical sectors.[21–29] However, NR, unlike many other polymers, is highly susceptible to many forms of degradation: light, ozone, radiation, humidity and heat, due to the presence of double bonds in the main chain. Furthermore, NR can be vulcanized with sulfur compounds, which can crosslink the chain because of the presence of reactive double bonds accounting for its many applications. In addition, its inherent high flammability restricts its usage in many otherwise critical products necessitating the way and means for reducing the flammability.[32] Therefore, the development of NR nanocomposites provided one of the best alternative by using various inorganic fillers, *e.g.* carbon black,[33–35] clay,[36–40] MMT aerogels,[41] modified starch,[42] bamboo fibres,[43] carbon nanotubes,[27,44] graphene,[45–47] hybrid filler,[48] SiO_2,[49–77] ZnO,[78–86] TiO_2,[87–106] Al_2O_3,[107–117] Fe_2O_3,[118–120] $BaTiO_3$,/$PbTiO_3$,[121–124] $Mn_{1-x}Zn_xFe_2O_4$, $BaFe_{12}O_{19}$ and $Ni_{1-x}Zn_xFe_2O_4$ ferrites.[125–131] These fillers are incorporated prior to its crosslinking by the usual techniques of blending resulting in the significant improvements in the properties of the corresponding NR nanocomposites. The present article makes an attempt to review the updated work dealing with the different morphology, mechanical, thermal, and other properties of micron/nano metal oxide reinforced NR nanocomposites.

18.2 Metal Oxides as Reinforcing Fillers in Natural Rubber

The extent of reinforcement of filler in a polymer matrix depends on the surface characteristics and morphology. Therefore, the different metal oxides have successfully been reinforced in SR.

18.2.1 SiO_2

Silica is one of the excellent reinforcing fillers being widely used as an alternative to carbon black in rubber products. It not only improves tear strength and abrasion resistance but also reduces rolling resistance in tires when compared to the traditional carbon black.[33–35] Synthetic amorphous silica can be mainly categorized into two types, precipitated silica also referred as conventional silica and pyrogenic silica or fumed silica, which differs from one another in terms manufacturing process and particle dimensions. The precipitated silica in the rubber matrix remains highly aggregated in the rubber matrix and is not favourable as reinforcing filler. In order to overcome this difficulty, the silica nanoparticles have been used in the preparation of NR nanocomposites.[63,49–77] Although, solid and latex forms of the rubber can be used to prepare silica/rubber masterbatch prior to compounding, the wet masterbatch method gives relatively low dust exposure and consumes lower compounding energy.[63] Wang *et al.*[57] suggested that latex compounding is more eco-friendly and low-pollutant processing. However, the addition of as-received silica into the latex leads to poor silica distribution due to its agglomerates. It is also reported that the major disadvantage of silicas is their acidity and polarity due to the presence of silanol groups on the silicas surfaces.[28] This causes unacceptably long cure times and slow cure rates and also loss of crosslink density in sulfur-cured rubbers. In addition, processing becomes more difficult in presence of highly loaded silica in NR. Therefore, it is desirable to improve the dispersion of nanoparticles and the interfacial adhesion between nano-silica and NR matrix in reinforcing the compatibility between SR matrix and SiO_2. As a result, several attempts have been made in enhancing the dispersion of silica in the natural rubber by using silane coupling agents.[50,51,57,59,61] For example, bis(3-triethoxysilylpropyl-tetrasulfide (TESPT) has been used as a coupling agent, while reinforcing NR with silica.[28] It consists of ethoxy reactive groups, which react with the silanol groups on the surfaces and facilitates the reinforcement of silica/NR composites through its improved dispersion.

Prasertsri and Rattanasom[77] prepared silica/NR masterbatches from a well-dispersed silica suspension obtained by using a bead mill before adding into NR. A self-assembly nanocomposite process has also been successfully used to prepare NR/silica nanocomposites.[63] Recently a sol–gel method, which can generate *in situ* reinforcing particles, has also been reported for the synthesis of silica-filled NR.[65–75] The process consists of hydrolysis and condensation of alkoxysilane, such as tetraethoxysilane (TEOS) as silica precursor.[65,66] According to the first method, raw rubber is crosslinked and swelled in TEOS and hydrolysed *in situ*. In the second one, silica particles are precipitated before the crosslinking process in presence or absence of coupling agent.

18.2.2 ZnO

Zinc oxide (ZnO) is one of the most cost effective inorganic pigments for the rubber industry over the past many decades.[78] It plays as an active rubber

active agent in rubber vulcanization processes acting as a crosslinking additive agent in activating the rate of sulfur cure with the accelerators.[79] The high loadings of zinc oxide are used for better heat conductivity and reinforcement in heavy-duty pneumatic tires. The particle size of conventional rubber grade ZnO varies from 0.1 to 0.4 mm and a corresponding specific surface area in the range of 10–20 m^2/g.[80] However, it is toxic for aquatic organisms US (Environmental Protection Agency) and hazardous chemical (The European Union). Therefore, it is desirable to decrease the zinc content in the formulation for its application in rubber technology. Recently, the ultra-fine ZnO is found as an alternate in the vulcanization process of rubber and is likely to improve the properties of rubber in machinery, heat consumption, the use of performance, to save a great amount of natural resources and to lower the production costs of rubber or tire industries.[81] The researches on nano-ZnO applied to light-coloured rubber product to promote anti-ageing ability are rare. Recently, ZnO has also been used in developments related to green tires.[19]

18.2.3 TiO_2

TiO_2 (anatase, rutile and brookite crystal forms) is whitish and a semi-conducting material and regarded as a safe material for human beings and animals.[87,88] The n-TiO_2 possesses high surface area per particle size ratio, which causes a significant increase in the effectiveness in protecting UV ir-radiation when compared to micron-size TiO_2 (micron-TiO_2).[89] TiO_2 also shows sustaining antimicrobial capability, biocompatibility, and self-cleaning functionality.[90,91] It is also an effective photocatalyst in the removal of en-vironmental pollutants and for antibacterial.[92,93] Recently, it has been reported that the TiO_2 nanoparticles prepared by ultrasonification, when used as filler in NR, could introduce UV protection and antibacterial property.[94] Sol gel method has also been used for the preparation of nano-TiO_2.[95] Recently, green tire moulding sheet involving TiO_2 has been patented.[20]

18.2.4 Al_2O_3

The most common form of crystalline alumina is corundum, which has a rhombohedral Bravais lattice with a space group R-3c.[96] These materials have been used in energy storage, alkali metal thermal-to-electric conversion cells, and gas sensors.[97] In recent years, it has been reported that alumina can also reduce heat, humidity, light, ozone and gamma radiation, flame resistance, and the crack growth in NR.[98]

18.2.5 Fe_2O_3

Fe_2O_3 better known as rust is a dark red substance, which occurs in nature as the mineral hematite, and is the principal ore for iron. It could be one of the economically feasible magnetic filler in the preparation of NR matrix.[109–111]

18.2.6 $BaTiO_3$ and $PbTiO_3$

Perovskite-like oxides exhibit high dielectric constant, piezoelectric properties and Curie temperature of approximately 120 and 490 °C.[124] They find applications in various fields, *e.g.* multilayer ceramics capacitors, piezoelectric sensors, transducers, actuators, and microelectromechanical systems. The combination of these ceramic with polymers forms composites with many advantages in terms of high dielectric constant, lightweight, high mechanical strength and good flexibility. Recently, the composites of $BaTiO_3$ and $PbTiO_3$ with NR (unmodified NR and epoxidized NR) have been developed.[121–124]

18.2.7 $Mn_{1-x}Zn_xFe_2O_4$, $BaFe_{12}O_{19}$ and $Ni_{1-x}Zn_xFe_2O_4$

Ferrites are other materials, which constitute predominantly oxides of Fe along other oxides of Ba, Sr, Mn, Ni, Zn, Li and Cd. According to the available literature, manganese zinc ferrite ferrites ($Mn_{1-x}Zn_xFe_2O_4$), barium ferrite ($BaFe_{12}O_{19}$), nickel zinc ferrite ($Ni_{1-x}Zn_xFe_2O_4$ ferrites have been embedded in the rubber to enhance its properties.[125–131] These rubber ferrite composites are increasingly used as microwave absorbers and in other devices, where flexibility and mouldability is an important criterion. NR is abundantly available in nature and could be used in the preparation of its composite.

18.3 Structure and Morphology of Metal Oxide Filled NR Composites

It is now well established that the extent of reinforcement highly depends on the filler characteristics, especially surface characteristics and morphology. In addition, the dispersion of the nanofillers is considered to be one of the most important determining factors of physical properties of the polymer composites. Therefore, it is desirable to investigate metal oxide filled micro/nanocomposites of NR for the structural analysis by XRD and morphology by TEM, SEM, FE-SEM and AFM.

Peng *et al.*[63] developed a novel NR/silica nanocomposite by combining self-assembly and latex compounding techniques. Figure 18.1 shows the SEM micrographs of NR/SiO_2 nanocomposites at 1.0, 4.0 and 8.5 wt% SiO_2 loadings. It is obvious that almost all SiO_2 nanoparticles (< 4 wt%) are homogeneously distributed throughout the NR matrixes as individual spherical nanoclusters. However, intensive aggregation of SiO_2 takes place at its higher loadings in NR. A novel NR/SiO_2 nanocomposite with a SiO_2 loading of 4 wt% has also been developed by incorporating latex compounding with self-assembly techniques.[64] The SiO_2 nanoparticles are homogeneously distributed throughout the NR matrix as spherical nanoclusters with an average size of 75 nm. In comparison with the host NR, the thermal resistance of the nanocomposite is significantly improved.

The different amount of *in situ* silica was generated by sol gel method to prepare NR nanocomposites.[65] Figure 18.2 shows TEM image of NR

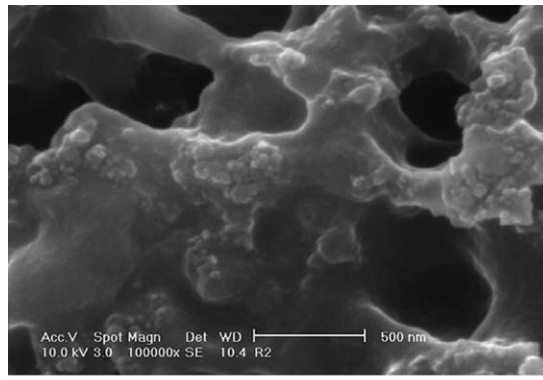

(a)

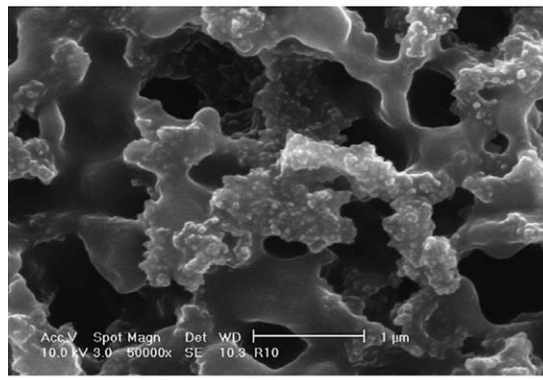

(b)

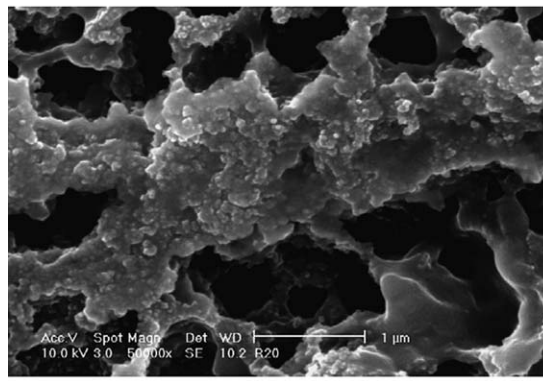

(c)

Figure 18.1 SEM micrographs of NR/SiO_2 nanocomposites: (a) 1.0 wt% SiO_2, (b) 4.0 wt% SiO_2 and (c) 8.5 wt% SiO_2.
(Reproduced from ref. 63 with permission from Elsevier.)

containing 11 phr of silica generated after the crosslinking process indicating the presence of small sized silica domains. They attributed the good dispersion to the steric limitation for cluster growth by the network chains. In case of NR

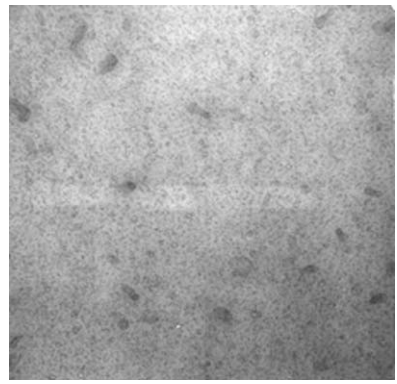

Figure 18.2 TEM of natural rubber containing 11 phr of silica generated after the crosslinking process.
(Reproduced from ref. 65 with permission from Elsevier.)

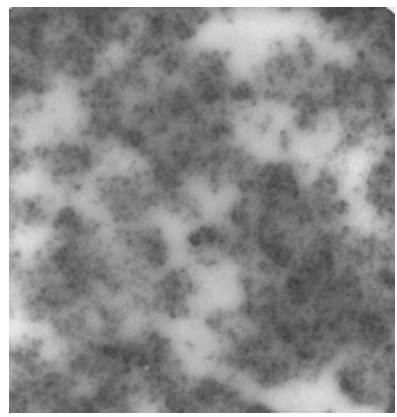

Figure 18.3 TEM of natural rubber containing 20 phr of silica generated before the crosslinking reaction and without the use of a silane coupling agent.
(Reproduced from ref. 65 with permission from Elsevier.)

containing 20 phr of *in situ* generated (before the crosslinking reaction and without the use of a silane coupling agent), TEM in Figure 18.3 revealed the tendency for silica particles to attach to each other via the active silanols present on their surface forming a strong silica network. However, TEM image of NR containing 20 phr of silica generated before the crosslinking reaction in the presence of a silane coupling agent in Figure 18.4 suggested less clustering. However, the dispersion was found to be more heterogeneous than that obtained in the case of a silica filling of an already formed network. Poompradub *et al.*[67] also reported the formation of NR nanocomposites filled with *in situ* generated silica via the sol–gel reaction using tetraethoxysilane

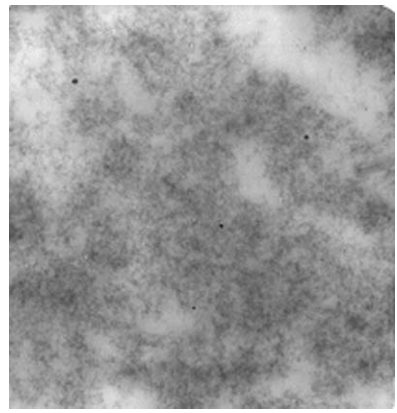

Figure 18.4 TEM of natural rubber containing 20 phr of silica generated before the crosslinking reaction in the presence of a silane coupling agent. (Reproduced from ref. 65 with permission from Elsevier.)

(TEOS). TEM micrographs of NR vulcanizates filled with 30 phr of *in situ* silica (50–60 nm) and commercial silica particles (40–60 nm) are displayed in Figure 18.5. It clearly shows that the *in situ* silica particles are homogeneously dispersed in the NR matrix with only some aggregates, while a much higher amount of aggregates of commercial silica was observed in the commercial silica vulcanizate at the same filler content. Ikeda and others[68] investigated the effects of amine catalyst and its reaction condition on the sol–gel reaction of TEOS in the uncrosslinked NR matrix to obtain a high *in situ* silica generation in NR. TEM in Figure 18.6 photographs of 71 phr filled *in situ* silica and commercial silica NR vulcanizates. It suggested relatively better dispersion of *in situ* silica particles than that of commercial silica-filled NR vulcanizate.

The alkylated silica particles filled NR latex composites have been prepared by sol gel process using alkyltriethoxysilanes [vinyltriethoxysilane (VTOS), ethyltriethoxysilane (ETOS), and i-butyltriethoxysilane (BTOS)] and studied morphology and distribution of silica in composites.[50] Siramanont *et al.*[73] reported SEM micrographs of NR vulcanizates filled with mechanically mixed silica and NR vulcanizates filled with *in situ* silica (Figure 18.7). It is concluded that the silica particles are aggregated and form clusters in case of mechanically mixed NR vulcanizates. On the contrary, *in situ* generated silica is well dispersed in NR matrix with low level of agglomeration. Transmission electron micrographs of the *in situ* silica-filled vulcanizates are also shown in Figure 18.8. This suggests that the type of alkyl group in alkyltriethoxysilane used in this system has no effect on the particle size. Kohjiya *et al.*[58] established a three-dimensional nanostructure of *in situ* silica in NR by using a 3D transmission electron microscope (3D-TEM), which is a TEM combined with electron tomography to reconstruct 3D structural images of NR consisting of *in situ* silica.

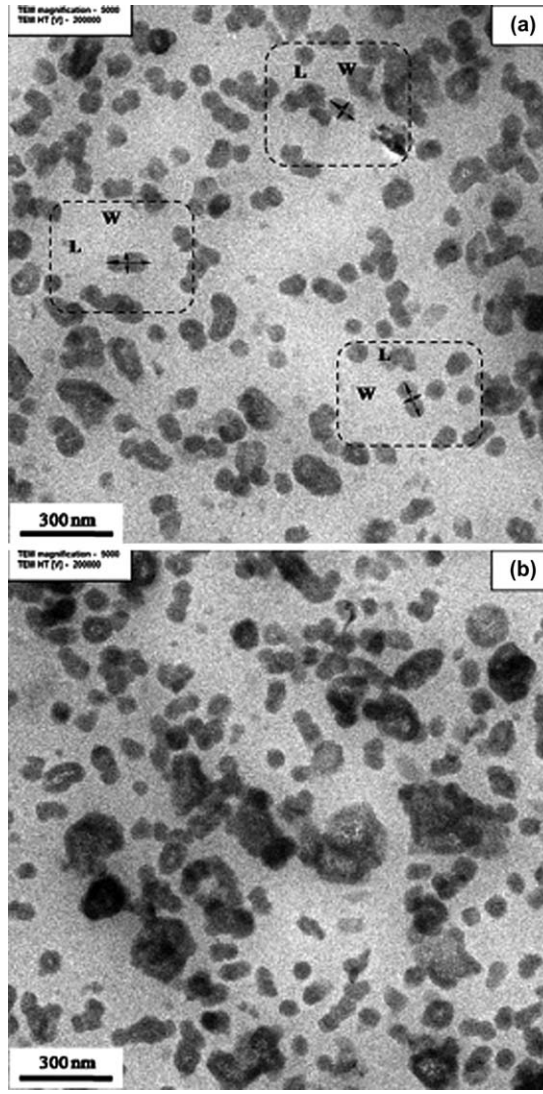

Figure 18.5 TEM photographs of NR vulcanizates with (a) *in situ* silica 30 phr, (b) commercial silica 30 phr.
(Reproduced from ref. 67 with permission from Elsevier.)

ZnO nanoparticles (average diameter 50 nm) have been synthesized and their effect studied as a cure activator in NR by Bhoumick *et al.*[86] The authors established that the dispersion of ZnO nanoparticles is more uniform in comparison with the conventional rubber grade ZnO. Because of reduction in size and increase in the surface area of the ZnO nanoparticles, they effectively form the complex with accelerator, sulfur, and rubber and get easily dispersed into the matrix instead of forming agglomerates on the surface, whereas some

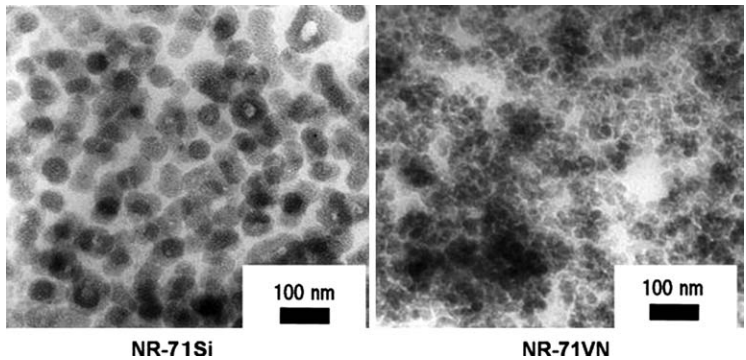

Figure 18.6 TEM photographs of *in situ* silica and commercial silica-filled NR vulcanizates.
(Reproduced from ref. 68 with permission from Elsevier.)

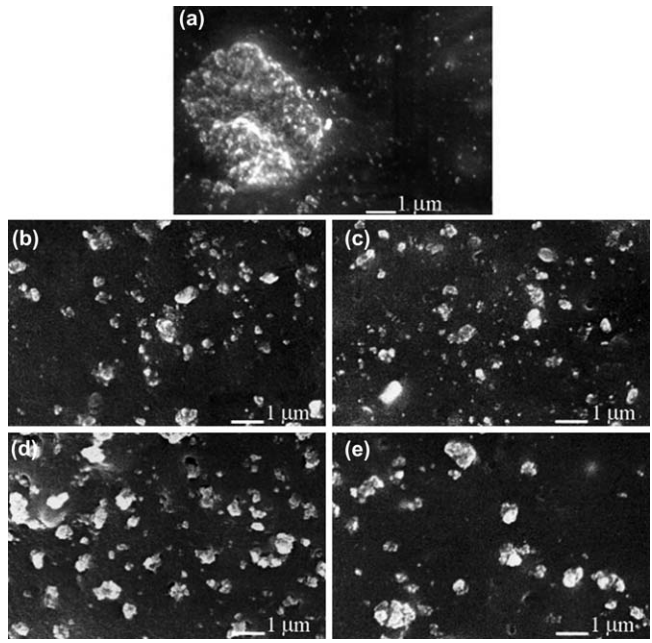

Figure 18.7 SEMs of NR vulcanizate filled with mechanically mixed silica (a) and NR vulcanizates filled with *in situ* silica (b) T100 (14.1 ± 0.4 phr silica), (c) V20T80 (14.1 ± 0.3 phr silica), (d) E20T8 (13.4 ± 0.4 phr silica) and (e) B20T80 (11.9 ± 0.3 phr silica) $\times$ 10,000 magnification.
(Reproduced from ref. 73 with permission from Wiley Interscience.)

agglomerations are observed in the case of conventional rubber grade ZnO. Li and Liu[79] studied the effect of nano-ZnO on the dispersion of NR. Figures 18.9 and 18.10 show TEM images of the NR before modification and nano-ZnO filled vulcanized NR. It is clearly evident that the ball shape and sizes of

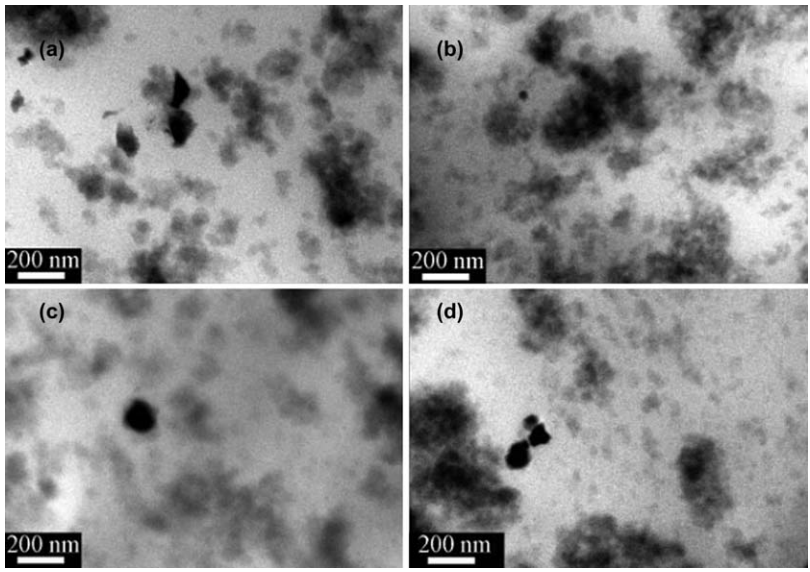

Figure 18.8 TEMs of the *in situ* silica-filled NR vulcanizates (a) T100, (b) V20T80, (c) E20T80 and (d) B20T80.
(Reproduced from ref. 73 with permission from Wiley Interscience.)

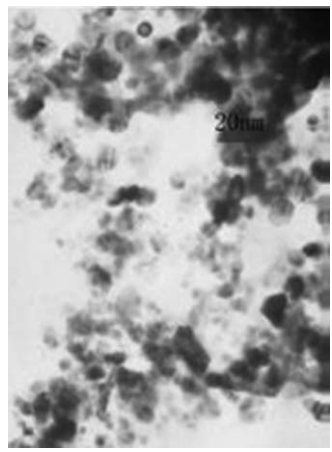

Figure 18.9 Photo of nano-ZnO without modification.
(Reproduced from ref. 79 with permission from Trans Tech Publications.)

nano-ZnO (~10–30 nm) remains unaltered. However, the dispersion of nano-ZnO (modified) is greatly improved and the surface area per gram is greatly increased, from 35.6 m^2/g (without modification) to 63.2 m^2/g (after modification).

Seentrakoon[94] successfully prepared *n*-TiO_2(R) with median particle size (d50) of 73 nm from commercial micron-TiO_2(R) by ultrasonication and filled

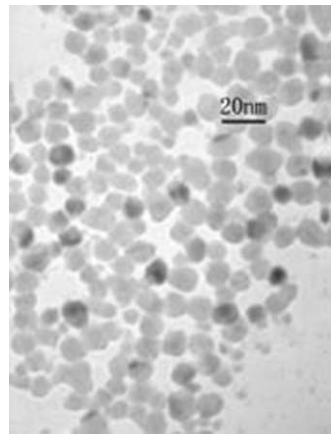

Figure 18.10 Photo of nano-ZnO with modification.
(Reproduced from ref. 79 with permission from Trans Tech Publications.)

its different content to prepare NR nanocomposite (NR/*n*-TiO_2(R); Figure 18.11 shows the corresponding SEM micrograph of the cross-sections. Figure 18.11 also shows that n-TiO_2(R) are separated from each other and effectively dispersed without aggregation in the NR matrix. A homogeneous distribution of n-TiO_2(R) is seen in the SEM images at 1,3 and 5 phr loadings in NR. An increased n-TiO_2(R) content create non-uniformity that was clearly seen in the NR/*n*-TiO_2(R) composites at 10 and 20 phr of n-TiO_2(R).

Atomic force microscopy (AFM) 3D images of T_{30} (7.57 vol% TiO_2 filled NR), T_{40} (9.84 vol% TiO_2 filled NR) and Ns_{10} (3.35 vol% silica-filled NR) composites are displayed in Figure 18.12.[102] It is apparent from Figures 18.12(a) and (b) that TiO_2 particles are aggregated in NR matrix. Figure 18.12(c) shows the agglomerates of SiO_2 nanoparticles.

18.4 Properties of NR and NR/Nanocomposites

18.4.1 Mechanical Properties

The mechanical properties of a polymer involve its behaviour under stress. These properties .of the polymers are often the guidelines for selecting a polymer for its multifaceted applications.

The effect of different preparation methods on the mechanical properties of micro/nano-SiO_2 filled NR composites have been studied by many workers. These findings show that the mechanical properties of SiO_2 nanocomposites of NR are enhanced in comparison to that prepared by traditional blending.

A novel NR/SiO_2 nanocomposite was developed by combining self-assembly and latex compounding techniques.[63] Table 18.1 lists the mechanical properties of the pure NR and NR/SiO_2 nanocomposites with different SiO_2 loadings. NR as a typical elastomer shows an excellent flexibility and low rigidity. The tensile

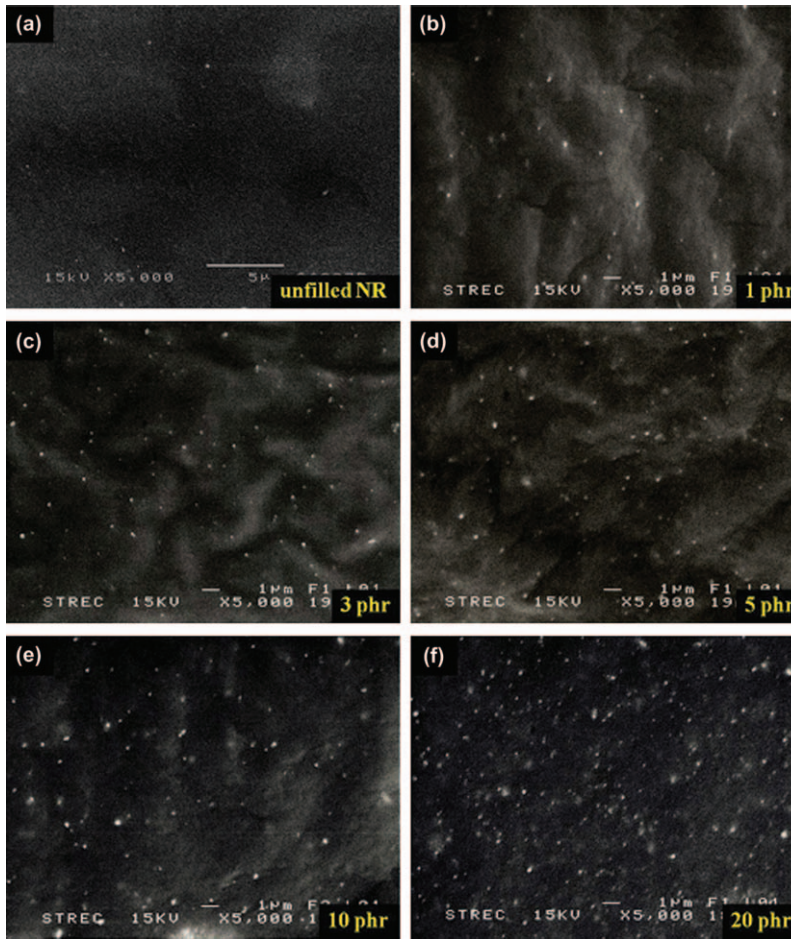

Figure 18.11 SEM micrographs of the cross-section of (a) unfilled NR and NR/n-TiO_2(R) composites with different n-TiO_2(R) contents: (b) 1 phr, (c) 3 phr, (d) 5 phr, (e) 10 phr, and (f) 20 phr at $\times 5000$ magnification. (Reproduced from ref. 94 with permission from Elsevier.)

strength and modules (at different elongations) of NR increases with SiO_2 loading. These properties are maximum enhanced at 4 wt% filler loading due to the better dispersion of SiO_2 in NR. However, the tensile strength and modules gradually decrease due to aggregation at higher loadings of SiO_2 in NR. In addition, tear resistance also increases significantly with the introduction of SiO_2 in NR. It is noted that the tear strength of NR/SiO_2 (6 wt%) is almost doubled that of the pure NR. The elongation at break of NR/SiO_2 nanocomposites is found to be lower compared to NR at 0.5–8.5 wt% SiO_2 loading. The presence of a coupling agent (c-mercaptopropyltrimethoxysilane, c-MPS) improved the reinforcement of NR filled with *in situ* generated silica.[70,71]

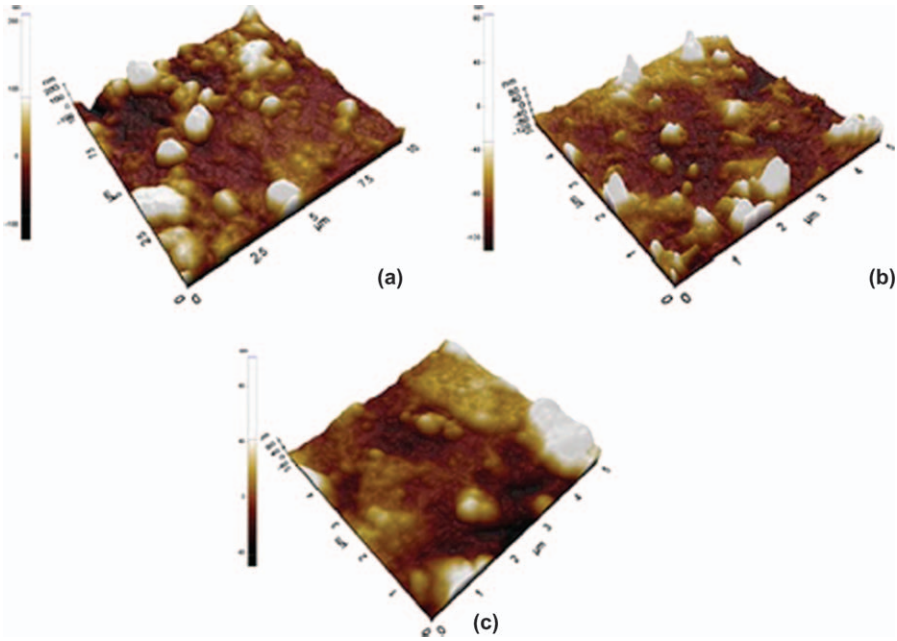

Figure 18.12 Atomic force microscopy (AFM) 3D images of (a) T_{30}, (b) T_{40} and (c) Ns_{10} composites.
(Reproduced from ref. 102 with permission from SAGE publications.)

Table 18.1 Mechanical properties of pure NR and NR/SiO_2 nanocomposites. (Reproduced from ref. 63 with permission from Elsevier.)

Tensile strength (MPa)	15.1	18.0	19.8	22.7	26.3	21.0	1.06
Tensile modulus (MPa)							
100% elongation	0.63	1.05	1.50	1.90	2.26	1.87	0.30
200% elongation	0.96	1.54	2.03	2.48	3.08	2.35	0.65
300% elongation	1.27	2.14	3.15	4.17	5.08	3.71	0.99
Elongation at break (%)	995	963	919	857	730	568	384
Tear strength (kN/m)	37.1	41.9	53.0	59.0	61.4	70.7	30.2

Xu *et al.*[54] used 3-aminopropyl-triethoxysilane modified nanocrystalline cellulose (MNCC) to partially replace silica in NR composites via coagulation to prepare NR/MNCC/silica and NR/nanocrystalline cellulose (NCC)/silica nanocomposites. Figure 18.13 show the variation of tensile strength, 300% modulus, elongation at break, tear strength and hardness (Shore A) of NR/NCC/silica and NR/MNCC/silica nanocomposites with NCC/silica (phr) content. It can be seen that the tensile strength, elongation at break and tear strength were almost kept constant with the increasing of NCC or MNCC, while the modulus at 300% increased significantly. This improvement may be explained by the high stiffness and rod-like structure of NCC, whereas a

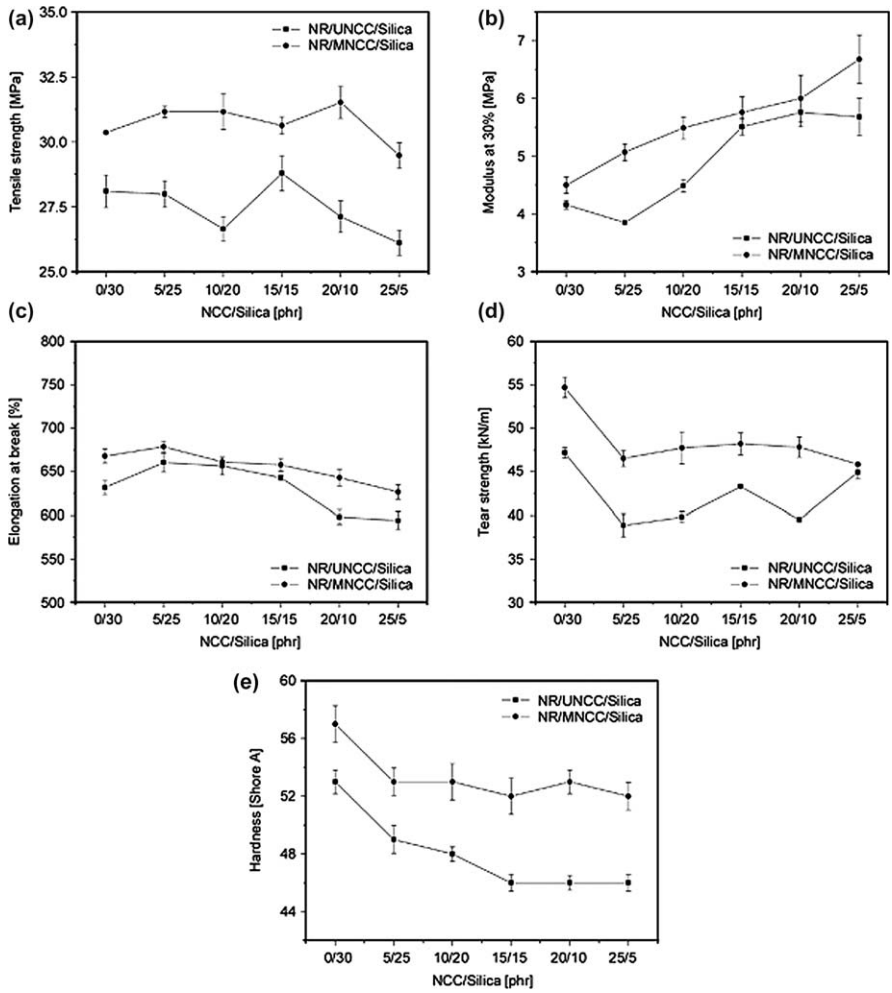

Figure 18.13 Variation of mechanical properties of NR/NCC/silica and NR/MNCC/silica nanocomposites via NCC/silica content. The values are given by average and the error ranges are given by standard deviation as evaluated by results from three to five parallel samples. (a) Tensile strength, (b) 300% modulus, (c) elongation at break, (d) tear strength and (e) hardness (Shore A). Lines are to guide the eye.
(Reproduced from ref. 54 with permission from MDPI.)

significant increase of Young's modulus was achieved by using NCC to reinforce nanocomposites. It can also be observed that the mechanical properties of nanocomposites were obviously improved by using MNCC compare to NCC, especially on 300% modulus, tear strength and hardness. The uniform distribution of MNCC particles in the NR matrix established by SEM as well as the stronger interfacial interaction between rubber and fillers account for the improvement in the mechanical properties of the nanocomposites.

Bokobza and coworkers[65,66] studied the mechanical properties of NR composites containing *in situ* generated silica particles (8 to 21 phr) before the vulcanization of the rubber matrix in solution and after the vulcanization of the rubber in presence/absence of a silane coupling agent (bis(3-triethoxysilypropyl) tetrasulfide)). Figure 18.14 shows the tensile stress–strain curves of the NR and NR films filled with silica after the crosslinking.[65] It is observed that the stress increases by increasing the silica content at a given strain, *i.e.* the NR is significantly reinforced in presence of *in situ* generated silica. The increase in the modulus is observed, which could be attributed to the hydrodynamic effect arising from the presence of rigid particles and increase in the crosslink density created by polymer–filler interactions. The first term is quantitatively taken into account using the Guth and Gold equation:[132,133]

$$G = G_0(1 + 2{:}\ 5\phi + 14.1\phi^2) = G_0X$$

where G_0 is the modulus of the unfilled matrix and ϕ is the volume fraction of filler. The authors compared their experimental curves of unfilled NR and NR/SiO_2 (21 phr) and calculated curve for NR/SiO_2 (21 phr) and inferred that the stress–stain curve calculated by Guth and Gold equation lies lower with respect to the experimental curve. These findings can only be explained in terms of filler–rubber interactions. The stress-strain behaviour when represented in the form of Mooney and Rivlin plots also led to the similar conclusion.

The formation of silica reinforced NR has been reported by the sol–gel process of tetraethoxysilane (TEOS) as precursor to generate silica particles inside the NR.[72] It was found that the mechanical properties are significantly

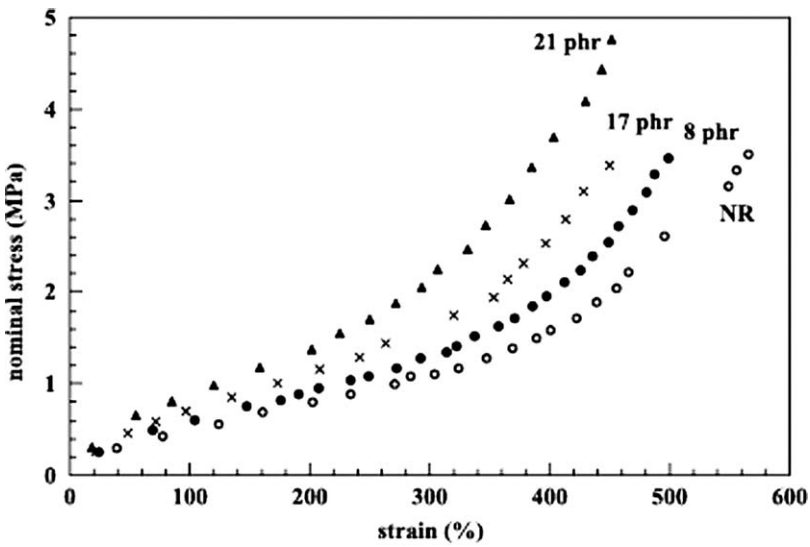

Figure 18.14 Stress–strain curves for the unfilled NR and NR films filled with silica after the crosslinking process.
(Reproduced from ref. 65 with permission from Elsevier.)

affected by the amount TEOS added into the latex. Sol–gel processes of alkyltriethoxysilanes (vinyltriethoxysilane, ethyltriethoxysilane and i-butyltriethoxysilane) in latex for alkylated silica formation NR have also been used to generate alkylated silica particles inside the rubber.[73] The measurement of hardness, tensile and tear confirmed the reinforcement by the *in situ* generated silica and alkylated silica better than the composites prepared by conventional mechanical mixing by adding silica in the rubber vulcanizates. It may be noted that the, vinyltriethoxysilane, among the different alkyltriethoxysilane investigated, seemed to be the most promising taking into account the high enhancement in tensile modulus and resistance to tear of the vulcanized rubber.

Ikeda and Poompradub[68,69] used TEOS to *in situ* generate silica particles and use it as filler in NR in the presence of amines as catalyst before the vulcanization. Figure 18.15 displays the stress elongation curves of *in situ* silica and commercial silica-filled NR vulcanizates.[68] It is observed that the *in situ* silica reinforced rubber showed the lower stress at the elongation up to about 200% and higher stress at the elongation beyond about 200%, for the same filler content (71 phr) and for comparable network chain densities. The high modulus at low elongation for conventional silica-filled rubber has been assumed to be due to the formation of larger aggregates of particles suggesting a

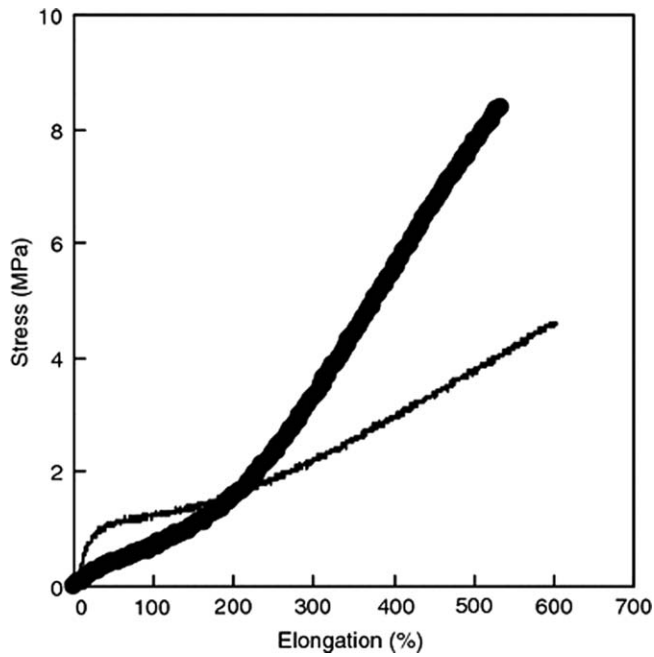

Figure 18.15 Stress–elongation curves of *in situ* silica and commercial silica-filled NR vulcanizates (● NR-71Si NR-71 referring to 71 phr of *in situ* silica-filled NR and – NR-71VN NR-71 referring to 71 phr of commercial silica-filled NR vulcanizates.
(Reproduced from ref. 68 with permission from Springer.)

better dispersion in the case of *in situ* silica reinforced rubber. On the other hand, the high modulus observed at higher elongation for *in situ* silica-filled rubber is attributed to a stronger interaction between NR matrix and *in situ* generated silica particles.

Prasertsri and Rattanasom[134] prepared fumed silica (FSi) and precipitated silica (PSi) suspensions for preparing silica/NR masterbatches via a latex system followed by dried silica/NR masterbatch mixing with other rubber chemicals on a two-roll mill. Figure 18.16 displays the variation of tensile strength of silica-filled NR vulcanizates, containing different types of silica contents. It is evident that tensile strength of all composites increases with increasing silica loading up to 20 phr. At 30 phr silica content in NR, tensile strength declines possibly due to the formation of larger aggregates acting as defects. SEM micrographs of silica/NR composites containing different silica types and contents confirmed that the state of dispersion of silica at its $\leq$20 phr loading is not much different in FSi- as well as PSi-filled NR. This accounts for the corresponding observations in their tensile strength.[77] However, the tensile strength of FSi-filled composite tends to be higher compared to PSi composite at the 30 phr silica loading due to its greater reinforcing ability and better dispersion of FSi. Figure 18.16 also shows that the tensile strength of MS30 samples for both silica types is higher in comparison with that of M30 samples.[115]

Core–shell morphology consisting of silica as the nano-core encapsulated by polyisoprene (PIP) was prepared as the nano-shell by a differential microemulsion polymerization of isoprene on silane treated nano-silica.[51] PIP–SiO_2 nanocomposite were used as an effective nanofiller in NR latex. NR filled with PIP–SiO_2 pre-vulcanizate clearly showed an improvement in the

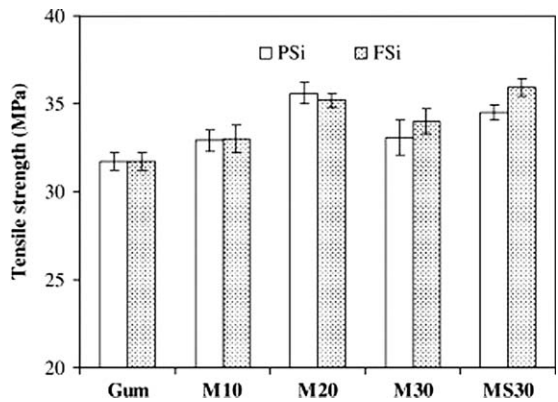

Figure 18.16 Tensile strength of silica/NR composites containing different silica types and contents. [M10, M20 and M30 refers to 10, 20 and 30 phr of silica (FSi and PSi) in presence of other formulations excluding the bis-(3-triethoxysilylpropyl) trisulfide; MS30 refers to 30 phr of silica in presence of formulations used in M10 to M30 including bis-(3-triethoxysilylpropyl) trisulfide].
(Reproduced from ref. 134 with permission from Elsevier.)

storage modulus, tensile strength and tensile modulus. Wang *et al.*[57] prepared high performance NR/SiO_2 (2 wt%) nanocomposites by latex compounding technique, when NR is reinforced with core–shell structure silica–poly(methylmethacrylate) (PMMA) nanoparticles. In their synthesis, double bonds were introduced onto the surface of the SiO_2 particles with the silane coupling agent before polymerization. Subsequently, the core–shell structure silica–poly(methyl methacrylate), SiO_2–PMMA, nanoparticles were formed by grafting polymerization of MMA on the surface of the modified SiO_2 particles via *in situ* emulsion, and then NR/SiO_2 nanocomposite was prepared by blending SiO_2–PMMA and PMMA-modified NR (NR–PMMA). TEM studies confirmed that the core–shell SiO_2–PMMA particles (60–100 nm) are well dispersed in latex at a suitable SiO_2/MMA ratio of 1 : 0.3, and the thickness of PMMA shell is about 25–35 nm. Table 18.2 records tensile properties of pure NR, NR/PMMA, NR–PMMA/SiO_2, and NR–PMMA/SiO_2–PMMA. It is evident that the tensile strength and tensile modulus of NR–PMMA/SiO_2–PMMA are superior compared to neat SR, NR–PMMA and NR–PMMA/SiO_2. It is suggested that PMMA as a bridge between the inorganic nanoparticles and polymer matrix improving the mutual compatibility, which in turn, results in excellent mechanical property.

Bhowmick *et al.*[86] for the first time carried out detailed investigations on effect of ZnO nanoparticles as cure activator on mechanical properties of NR and compared it with conventional ZnO; the corresponding data are tabulated in Table 18.3. These findings show that the tensile strength improved by 80%

Table 18.2 Tensile properties of pure NR and its nanocomposites (SiO_2/NR = 2/100 w/w). (Reproduced from ref. 57 with permission from Hindawi Publishing Corporation.)

Samples	*NR*	*NR–PMMA*	*NR–PMMA/SiO₂*	*NR–PMMA/SiO₂ – PMMA*
Tensile strength (MPa)	6.99	7.23	8.95	10.65
Elongation at break (%)	835	823	772	773
Tensile modulus (MPa)				
300% elongation	0.92	0.82	1.22	1.95
500% elongation	1.00	0.94	1.46	2.32
700% elongation	1.58	2.06	2.96	3.37

Table 18.3 Mechanical properties of NR vulcanizates. (Reproduced from ref. 86 with permission from Wiley Interscience.)

Compound	*Tensile strength (MPa)*	*Elongation at break (%)*	*Modulus (MPa)*		
			100%	*200%*	*300%*
NR-RG	6.7 ± 0.1	1000 ± 10	0.72 ± 0.01	1.15 ± 0.01	1.57 ± 0.02
NR-N3	7.6 ± 0.1	900 ± 10	0.83 ± 0.02	1.36 ± 0.03	1.89 ± 0.01
NR-N5	12.7 ± 0.2	1050 ± 20	0.81 ± 0.01	1.36 ± 0.02	1.92 ± 0.03

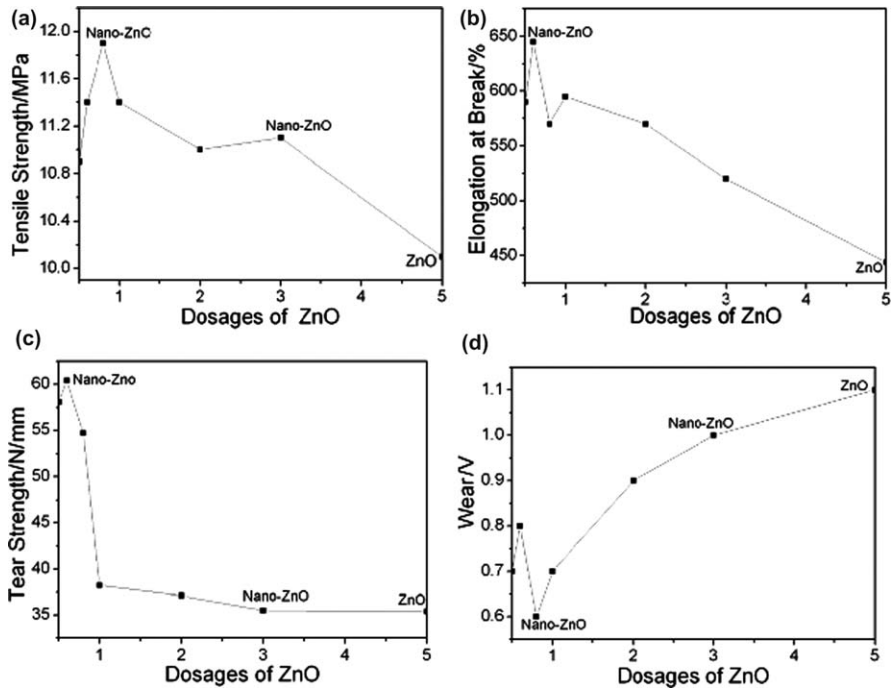

Figure 18.17 Dosage effects of ZnO on mechanical properties of rubber. (Reproduced from ref. 79 with permission from Trans Tech Publications.)

for NR-N5 and by 12% for NR-N3 in comparison with NR-RG (NR-N5, NR-N3 and NR-RG refers to NR filled with other ingredients and rubber grade ZnO and 5 and 3 wt% of ZnO nanoparticles respectively). The elongation at break remains almost unaltered in the case of conventional ZnO or ZnO nanoparticle filled NR. The modulus 300% shows a remarkable improvement by 20% both for NR-N5 and NR-N3 in comparison to NR-RG. The improvement in the mechanical properties is attributed to the increase in crosslink density, better dispersion of ZnO with NR vulcanizate as inferred through SEM and increased interfacial interaction.

Highly dispersed nano-ZnO has also been employed as an alternative to the ordinary ZnO in the vulcanization process of natural rubber.[79] Figure 18.17 shows the mechanical properties as a function of different dosages of nano- and ordinary ZnO in NR. It is noted that the tensile strength, elongation at break, tear strength of the specimens added with the highly dispersed nano-ZnO were higher than the ordinary ZnO specimens, but the wear became smaller. Further to add, the tensile strength, elongation at break and tear strength showed the maximum improvements at the nano-ZnO dosage of 0.8 compared to the ordinary ZnO specimens. These findings are confirmation that the highly dispersed nano-ZnO is evenly distributed into and dissolved completely in vulcanizing rubber.

Meera *et al.*[102] studied the mechanical properties of NR filled with titanium dioxide (TiO_2) and nano-silica composites at room temperature. It is inferred that the composites filled with silica exhibit higher tensile strength and dynamic modulus than the TiO_2-filled composites due to the strong interfacial interactions of nano-silica with the NR matrix.

Seentrakoon *et al.*[94] prepared nanocomposites of NR filled with nanocrystalline TiO_2 (referred as n-TiO_2(R)) and microcrystalline TiO_2 ((NR/micron-TiO_2(R)) and compared their mechanical properties with unfilled NR. It may be noted that n-TiO_2(R) and micron-TiO_2(R) contents in NR is filled with 1, 3, 5, 10, 20 phr and 5 phr, respectively, while other ingredients are maintained constant (ZnO, stearic acid, MBT and S equal to 5, 0.8, 1.0 and 1.8 phr, respectively). Table 18.4 displays the findings on tensile strength, elongation at break and tear strength of the NR and its corresponding nano- and micro-composites. As expected the addition of n-TiO_2(R) into NR increases the tensile strength and tear resistance compared to the unfilled NR suggesting the reinforcing of n-TiO_2(R) in NR matrix. This is due to a large surface of n-TiO_2(R), which tended to improve interfacial interaction between n-TiO_2(R) and NR matrix. It is also interesting to note that n-TiO_2(R) improves the elongation at break of the NR nanocomposites. Table 18.4 shows that the tear resistance of NR/n-TiO_2(R) composites also increases with increasing n-TiO_2(R).Such improved mechanical properties of NR/n-TiO_2(R) composites

Table 18.4 Mechanical properties of the unfilled NR, NR/micron-TiO_2(R) and NR/n-TiO_2(R) composites before and after UV irradiation. (Reproduced with permission from ref. 94 from Elsevier.)

		Mechanical properties					
		Tensile strength (MPa)		*Elongation at break (%)*		*Tear strength (kN/m)*	
Samples	*TiO_2 content (phr)*	*Before UV*	*% Retention*[b]	*Before UV*	*% Retention*	*Before UV*	*% Retention*
Unfilled NR	–	43.3 (0.4)[a]	51.2	688.1 (8.8)	84.0	11.6 (0.3)	73.7
NR/n-TiO_2(R)	1	62 (1.4)	73.3	725.2 (3.5)	88.4	17.5 (0.3)	83.3
	3	78.6 (0.8)	86.8	754.3 (5.9)	91.8	19.4 (0.3)	87.6
	5	81.2 (1.3)	90.6	792.4 (4.3)	92.9	20.6 (0.3)	89.8
	10	68.8 (0.5)	90.8	725.3 (2.4)	92.2	18.6 (0.3)	89.0
	20	62.5 (0.9)	78.2	701.8 (4.2)	89.0	16.8 (0.3)	87.8
NR/micron-TiO_2(R)	5	48.2 (1.2)	54.4	689.3 (9.7)	86.9	12.8 (0)	75.6

UV irradiations at 25 °C for 24h.
[a]Standard deviation values are given in parenthesis.
[b]% Retention = (Properties after UV irradiated/properties before UV irradiated)×100.

could be linked to the fine dispersion and homogeneous distribution of n-TiO_2(R) in the NR matrix leading to higher reinforcement.

Homogeneous dispersion and size reduction of TiO_2 has been achieved by ultrasonication and subsequently dispersed homogeneously in the NR matrix.[106] It is found that the nanocomposites exhibits improve mechanical properties. This may be due to the reduced particle sizes, owing to enhanced surface areas and aspect ratios. It is seen that both the TS and EB of the composites increase with the loss of moduli at low filler concentration (2 phr). Sikong *et al.*[107] also observed that the TS of the TiO_2 and Ni/B/TiO_2 coated NR films are significantly higher than that of pure NR film.

Lin and workers[93] prepared nano-TiO_2/NR composites by blending varying amounts of nano-TiO_2 (0–5 phr) with NR and studied the mechanical properties of the composites. According to this, the hardness, stress at 100% strain and tensile strength of the composites is not changed insignificantly with TiO_2 content. It is also noted that only tensile strength of NR gum vulcanizates exhibit dramatic enhancement by thermal ageing.

The stress relaxation behaviour of the TiO_2 and nano-silica-filled NR composites under tension has also been studied with reference to the filler loading and strain level.[103] It is observed that the rate of stress relaxation increases with increase in filler loading. These studies also show that rate of stress relaxation to be higher for silica-filled NR compared to TiO_2 filled NR. This is due to the high degree of agglomeration in silica compared to titanium dioxide filler. In addition, the effect of ageing on the stress decay was also investigated and the rate of stress relaxation was found to decrease after ageing.

Ji-Fan *et al.*[114] introduced Al_2O_3 nanoparticles in the NR and investigated its reinforcement effect on filled NR vulcanizates. These results show that nano-Al_2O_3/NR nanocomposites exhibit significantly improved tensile strength, elongation at break, modulus and tearing strength. After ageing test, tensile strength, tearing strength and modulus improved, and elongation at break decreased. This could be attributed to the crosslink maturation reactions, which result in the conversion of polysulfidic linkages into disulfidic and monosulfidic ones. The acid and alkaline resistances of nano-Al_2O_3 filled NR vulcanizates improved compared with that of unfilled NR systems. It was also noticed that the tensile strength and elongation at break improve, and modulus decreased after acid and alkaline test. According to Tangboriboon *et al.*,[110] the enhancement in mechanical properties of NR/Al_2O_3 composites crosslinked with dicumyl peroxide is caused by the strong C–C bond, the tunnelling phenomenon and the ionic polarization of the alumina particles acting as the dispersed phase in the elastomer matrix.

Ahmed and others[118] studied the relation between tensile strength as a function of volume fraction for 3 Fe_2O_3:1Al_2O_3, 1Fe_2O_3:1Al_2O_3, 1Fe_2O_3:3Al_2O_3 and compared with Al2O3 (reference) fillers in NR. These investigations reveal that the NR composites filled with 1Fe2O3:3Al2O3 exhibits better tensile strength owing to the uniform and efficient stress transfer through a strong interfacial bond between the filler and the polymer.[135] The tensile strength is found to be maximum at 10 phr of filler loading by composites filled

with α-Fe_2O_3. The variation of Young's modulus for NR composites containing different volume fraction of $1Fe_2O_3:3Al_2O_3$, $1Fe_2O_3:1Al_2O_3$, $3Fe_2O_3:1Al_2O_3$. These investigations show that Young's modulus increases with volume fraction of $1Fe_2O_3:3Al_2O_3$, $1Fe_2O_3:1Al_2O_3$ and $3Fe_2O_3:1Al_2O_3$ in NR. When α-Fe_2O_3 (10 phr) is used as filler NR, Young's modulus firstly increases with loading then decreases.

Ferroelectric ceramic material ($BaTiO_3$ and $PbTiO_3$) were used to prepare NR (air dried sheet, ADS) composites by melt mixing to study their influence on mechanical of NR vulcanizate.[124] Figure 18.18 shows stress–strain curves of gum and ceramics/rubber composites vulcanizates with different types of rubber and ceramic materials. It is observed that the ceramic/NR composites exhibit higher Young's modulus than those of the gum vulcanizates. This is due to incorporation of the ceramics particles that caused lower mobility of molecular chains and hence increasing stiffness of the materials. Stress-strain plots has been used to express variation of tensile strength and elongation at break of NR vulcanizate and its ceramics composites in Figures 18.19 and 18.20 respectively. It is noted that the tensile strength of NR gum is slightly improved in presence of $BaTiO_3$. The elongation at break NR and its ceramic filled composite followed the order: $NR > NR/BaTiO_3 > NR/PbTiO_3$. The higher elongation at break of unmodified NR vulcanizate could be attributed to the lower chemical interaction between ADS molecules.

Malini *et al.*[125–127] prepared rubber ferrite composites containing nickel zinc ferrite (NZF) and examined the variation of tensile strength, elongation at

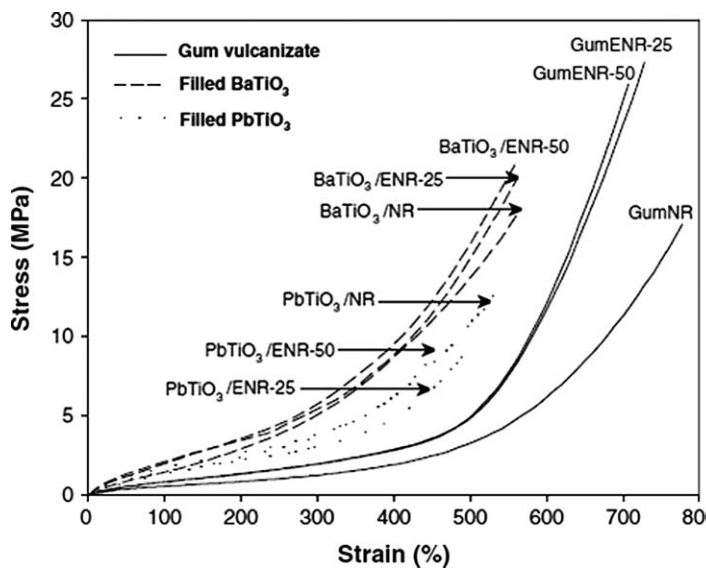

Figure 18.18 Stress–strain curves of gum and ceramic/rubber composite vulcanizates with different types of rubber and ceramic materials. (Reproduced from ref. 124 with permission from Springer.)

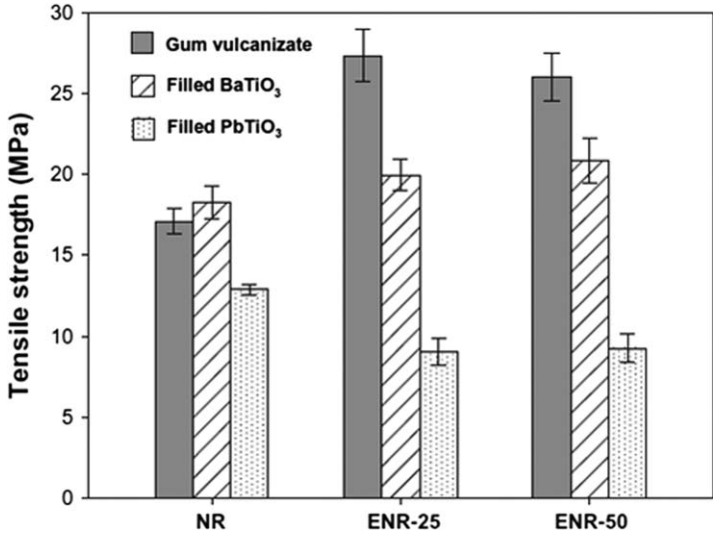

Figure 18.19 Tensile strength of gum and ceramic/rubber composite vulcanizates with different types of rubber and ceramic materials. (Reproduced from ref. 124 with permission from Springer.)

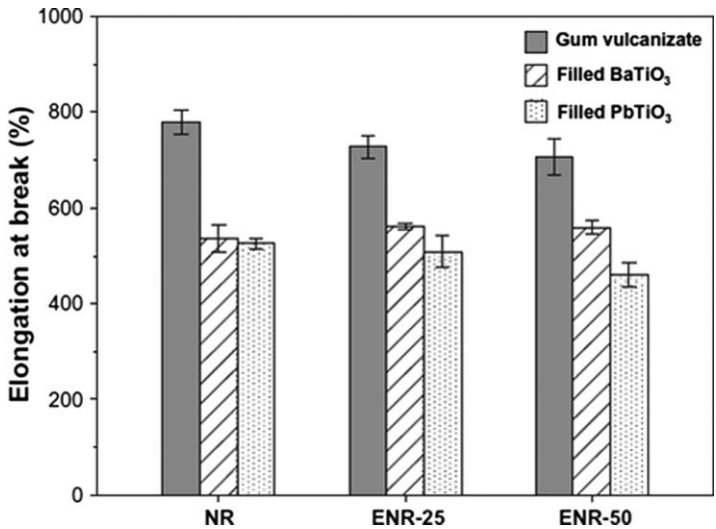

Figure 18.20 Elongation at break of gum and ceramic/rubber composite vulcanizates with different types of rubber and ceramic materials. (Reproduced from ref. 124 with permission from Springer.)

break and 100% modulus with loading and the corresponding findings are displayed in Figures 18.21 to 18.23.[127] It is evident that the tensile strength first decreases with initial loading up to 30 phr and thereafter it increases with

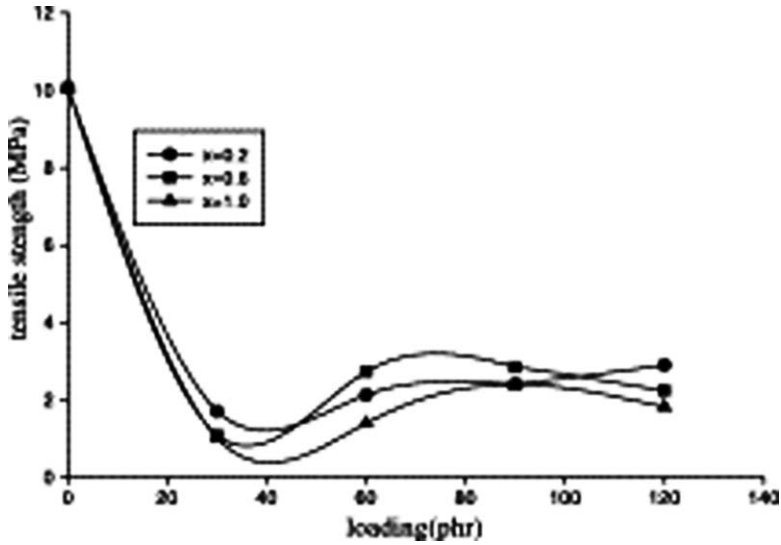

Figure 18.21 Variation of tensile strength with loading $Ni_{1-x}Zn_xFe_2O_4$ in NR. (Reproduced from ref. 127 with permission from Elsevier.)

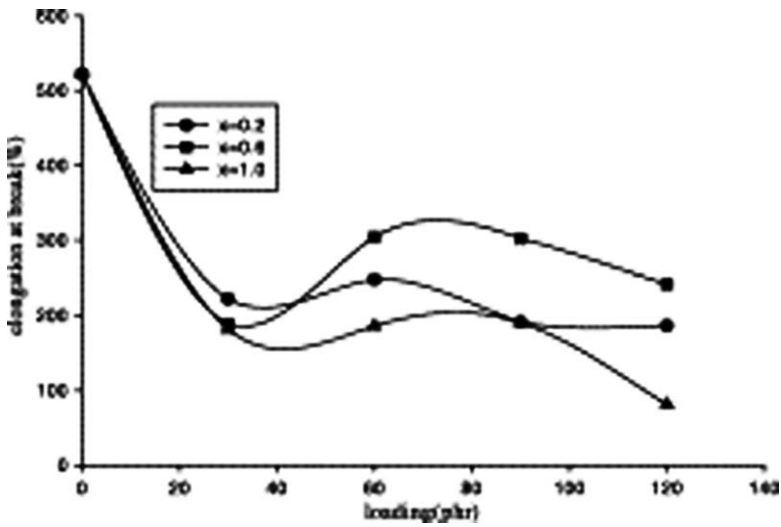

Figure 18.22 Variation of elongation at break with loading $Ni_{1-x}Zn_xFe_2O_4$ in NR. (Reproduced from ref. 127 with permission from Elsevier.)

loading. It is known that stress-induced crystallization will increase the tensile strength and hence blank NR has got a higher tensile strength. But the addition of filler inhibits the stress-induced crystallization, which in turn results in a decreased tensile strength for the initial filler loading of 30 phr. For further loadings of the filler, the tensile strength shows an increasing trend suggesting

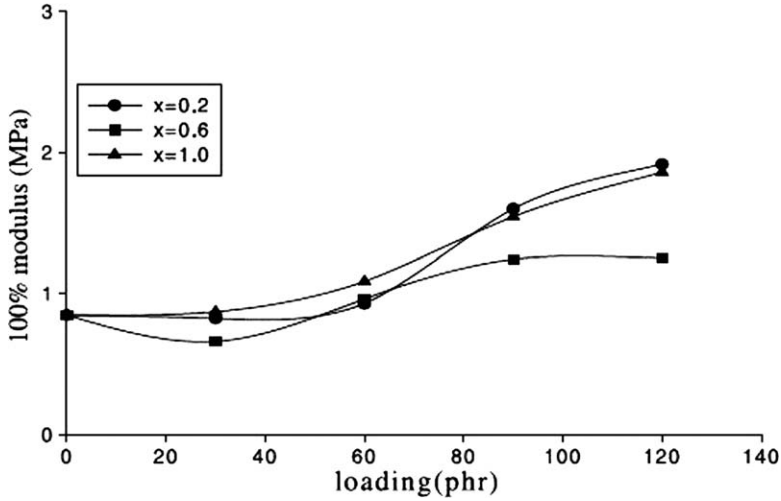

Figure 18.23 Variation of 100% modulus with loading $Ni_{1-x}Zn_xFe_2O_4$ in NR. (Reproduced from ref. 127 with permission from Elsevier.)

that the filler NZF acts as a semi-reinforcing filler. Elongation at break also shows a similar decrease for the initial loading and it remains by and large the same for higher loadings. One hundred per cent modulus shows an increasing trend with increase in loading.

18.4.2 Dynamical Mechanical Thermal Analysis (DMTA)

Dynamic mechanical thermal analysis (DMTA) is very useful for generating modulus versus temperature plots in rubber samples. The effect of temperature on this important property can be obtained over a wide range of temperature (−150 °C to +200 °C). It also helps in studying viscoelastic behaviour and the glass transition temperature (T_g) of the polymers.

DMTA studies have been reported on pure NR and its silica–PMMA (core/shell) reinforced nanocomposites (NR/PMMA, NR–PMMA/SiO_2 and NR–PMMA/SiO_2–MPS–PMMA). The corresponding data has been represented in the form of loss factor versus temperature in Figure 18.24.[57] It is observed that T_g of NR–PMMA/SiO_2–MPS–PMMA (−48 °C) is higher than either NR or its composites due to well-dispersed SiO_2–PMMA nanoparticles in NR–PMMA matrix. Figure 18.25 show the variation of storage modulus as a function of temperature for the corresponding samples. It is evident that NR–PMMA composite filled with core–shell SiO_2–PMMA nanoparticles has a higher storage modulus than the others at the temperature range from −100 °C to −50 °C. When the temperature is below T_g, the core–shell SiO_2–PMMA nanocomposites possess a high storage modulus, which is caused by introducing rigid nano-silica particles.[57]

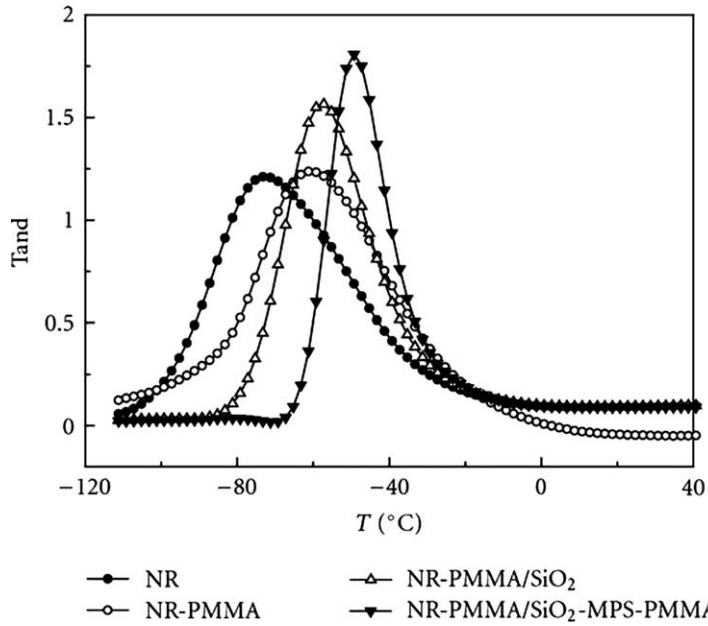

Figure 18.24 The loss factor as a function of temperature for pure NR and its nanocomposites.
(Reproduced from ref. 57 with permission from Hindawi Publishing Corporation.)

Chen *et al.*[60] reported DMA studied on NR and NR/SiO_2 nanocomposite the temperature dependence storage modulus (E') and loss tangent (tan δ) of the raw NR and nanocomposite under the scan frequency of 5 Hz. The E' of the raw NR is around 4200 MPa at −100 °C, while NR/SiO_2 (4 wt%) resulted in a significant increases to 7600 MPa. The corresponding glass transition temperature (T_g) are found to be −62.0 °C and −52.5 °C. The remarkable increase in T_g of NR/SiO_2 is largely due to the restriction of the NR molecular chain movement, namely, the SiO_2 is not just physically blended with NR, but strongly interacts with NR molecular chains.

The measurement of dynamic mechanical properties of NR vulcanizate without silica, NR vulcanizate with commercial silica, (20.1 silica content) NR vulcanizates with γ–MPS (20.1 silica content), *in situ* silica (21.4 % silica content) and γ-MPS (21.3% silica content) showed that the corresponding E′ values at 25 °C are found to be 1.81, 7.20 10.5, 7.08 and 3.91 MPa respectively.[70] According to Poompradub and coworkers,[67] the variation of storage modulus (E′) and tanδ of NR vulcanizates filled with 30 phr of *in situ* and commercial silica and NR vulcanizate in absence of filler show the temperature dependent behaviours with three distinct regions, *e.g.* glassy, transition and rubbery. The value of E′ (25 °C) in case of NR/commercial SiO_2 are found to be higher than the NR/*in situ* SiO_2 vulcanized. This suggests that the filler to filler interactions of NR/commercial SiO_2 vulcanized is high, resulting in an

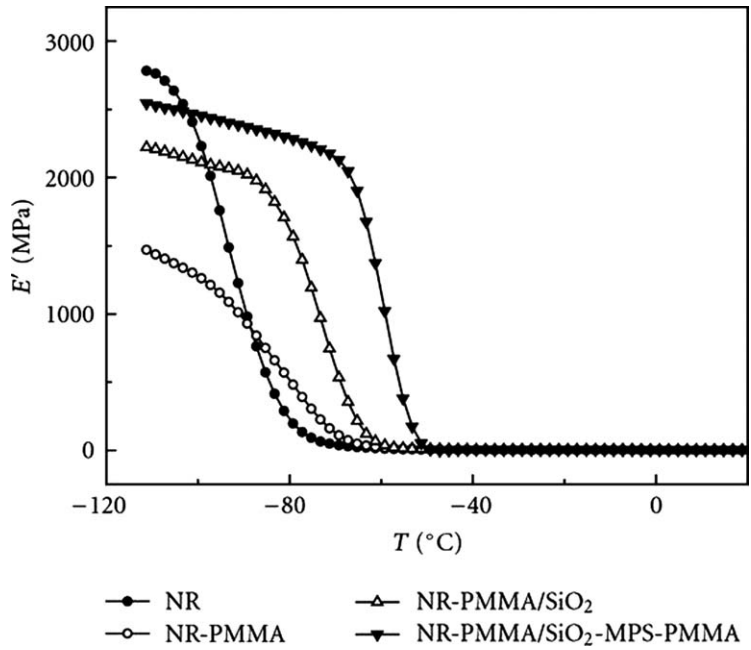

Figure 18.25 The storage modulus as a function of temperature for pure NR and its nanocomposites.
(Reproduced from ref. 57 with permission from Hindawi Publishing Corporation.)

impaired moments of rubber chain segments. In addition, the aggregated silica particles in NR/ commercial SiO_2 form a pseudo-network structure resulting in its higher E′ value compared to that of NR/SiO_2 *in situ* vulcanizate. The tan δ peaks also shifted towards higher temperature region compared to NR and follows the order: NR/30 phr commercial SiO_2 (−50.1 °C) > NR/30 phr *in situ* SiO_2 (−53.3 °C) > NR (−57.1 °C). Xu *et al.*[54] observed that the dynamic mechanical performance of NR/MNCC (modified nanocrystalline cellulose)/ silica nanocomposites was greatly improved due to reinforcement of MNCC and NR/silica. They noticed that the T_g was nearly unchanged and the tan δ peak of nanocomposites became much higher with the increasing of NCC or MNCC in NR/NCC/silica and NR/MNCC/silica nanocomposites.

Bhowmick *et al.*[86] carried extensive investigations on the effect of ZnO nanoparticles as cure activator on dynamical mechanical properties of NR and compared it with conventional ZnO. Figure 18.26 shows the plot of tan δ versus temperature for NR vulcanizates (Inset consists of storage modulus versus temperature plot) and the corresponding data for NR/5 phr rubber grade ZnO, NR/5 phr ZnO nanoparticles and NR/3 phr ZnO nanoparticles (with other formulations being identical) are tabulated in Table 18.5. It is observed that NR/ZnO nanoparticles (5 phr) (referred as NR-N5) shows a shift in T_g by 6 °C for NR/5 phr rubber grade ZnO (referred as NR-RG), which indicates an

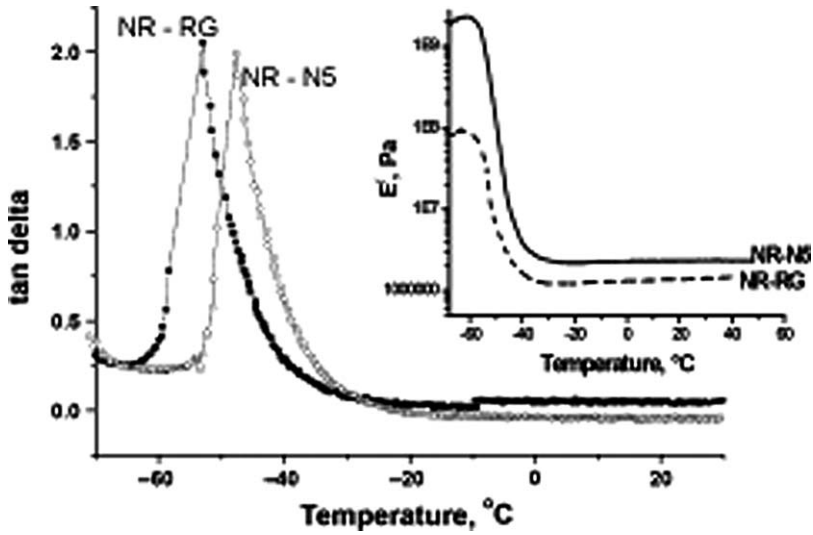

Figure 18.26 Plot of tan δ versus temperature for NR vulcanizates. (Inset: plot of storage modulus versus temperature (modified)).
(Reproduced from ref. 86 with permission from Wiley Interscience.)

Table 18.5 Dynamic mechanical properties of NR vulcanizates. (Reproduced from ref. 86 with permission from Wiley Interscience.)

Compound designation	*Tan δ at Tg*	*Storage modulus at 25 °C (MPa)*	*Tg (°C)*
Neat NR	2.70	0.98	−66.0
NR-RG	2.05	2.25	−53.0
NR-N5	1.95	2.58	−47.0

increase in crosslink density for the vulcanizates with ZnO nanoparticles. Further, Tan δ at T_g is reduced from 2.05 to 1.95, indicating better reinforcement. It further supports the improvement in mechanical properties. The storage modulus at 25 °C shows an improvement of 15% when ZnO nanoparticles are used as a cure activator.

DMA analysis of NR/TiO_2 nanocomposites prepared by latex blending showed that its Tg and activation energy are higher than the pure NR.[101] According to their dynamic model, the decomposition activation energy of blank sample (vulcanized rubber) and the samples which contained TiO_2 with 0.1%, 0.5%, 1.0%, 2.0% were 229.99, 231.085, 201.727, 219.107, 208.249 kJ mol^{-1} and their pre-exponential factor of dynamic model were found to be 5.07×10^{17}, 8.46×10^{17}, 2.94×10^{15}, 8.03×10^{16}, 1.04×10^{16} s^{-1}, respectively.

When micrometre-sized Al_2O_3 particles embedded in a NR, the Al_2O_3 particles are moderately dispersed within the NR matrix.[116] Without an electric field, the Al_2O_3 particles merely act as a filler to absorb or store an additional

stress. The storage modulus increases by nearly a factor of 4 as the alumina volume fraction is varied from 0 to 0 · 009. With an electric field on, the ionic and the orientation polarizations and induced dipole moments were generated, leading to interparticle interactions, and an additional increase in the storage modulus; the storage modulus sensitivity at the electric field strength of 2 kV mm^{-1} varied from 0 · 10 to 0 · 20 within the same volume fraction range.

Tangboriboon *et al.*[117] prepared Al_2O_3 (β-phase polytype)/NR composites and observed that the storage modulus (G′) of the composites, or the rigidity, increases by nearly two orders of magnitude, with variations in particle volume fraction and electrical field strength. The increase in the storage modulus causes the ionic polarization of the alumina particles and the induced dipole moments set up in the NR matrix. High coercivity barium ferrite ($BaFe_{12}O_{19}$) powders have been prepared by a co-precipitation method and incorporated them into a NR matrix with different loading levels up to 120 phr.[128]

18.4.3 Thermal Properties

Thermal decomposition of NR occurs in a single step in the range of 300–400 °C with maximum decomposition (around 95 mass loss of %). This is primarily initiated by thermal scission of the C–C chain bonds accompanied by a transfer of hydrogen at the site of scission.[136,137] The process is also sometimes associated with an initial small mass loss attributed to the elimination of volatile components, such as water, and ammonia residue (added to the latex to stabilize it during the transportation, and to avoid coagulation).[138] Though, NR has widely been used in the many medical products, the improvement in the thermal degradation at a high temperature (in presence of nitrogen/oxygen) is further desirable. Therefore, silica has invariably been used as fillers in NR to enhance the thermal stability of NR.[52,57,60,64,139,140] Figure 18.27 show the TG/DTG curves of NR and NR/SiO_2 nanocomposites in nitrogen atmosphere.[60] This clearly suggests that the thermal decomposition of NR and SR/SiO_2 (4 wt%) is one step decomposition and is in agreement with many other

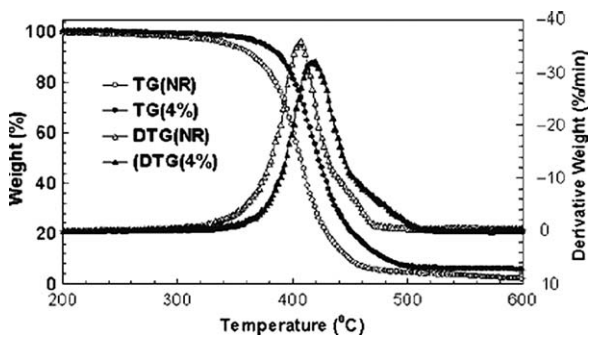

Figure 18.27 TG/DTG curves of pure NR and its nanocomposites in nitrogen. (Reproduced from ref. 60 with permission from Wiley Interscience.)

workers.[52,57,64,140] Thermograms also clearly indicate the marked increase in the thermal ageing resistance of SR/SiO_2 nanocomposite. However, Chaichua *et al.*[67] observed that the thermograms of neat NR as well as its composites with commercial and nano-silica follow two-step decomposition. The first stage of degradation (250–450 °C) of all the samples takes place due to the thermal decomposition of SR. The second mass loss peak (450–550 °C) is associated with the carbonaceous residues from the rubber.[136] These studies show that the thermal stability of the *in situ* silica-filled NR vulcanizate is better compared to commercial silica-filled NR (or NR). The thermal degradation kinetics of the SR/SiO_2 nanocomposites has also been investigated on the basis of the corresponding TG curves at different heating rates.[64] According to this, the reaction order of the NR thermal degradation is 2.3, while it increases to 3.2 with the addition of SiO_2. The activation energy for the nanocomposite is 270.8 kJ mol^{-1}, which is 73.9 kJ mol^{-1} higher than that of pure NR.

Table 18.6 records the initial thermal degradation temperatures of NR and its SiO_2 nanocomposite. The increase in the initial degradation temperature of nanocomposite with respect to neat NR clearly suggests the enhanced thermal stability of the nanocomposite. Peng *et al.*[60] suggested that SiO_2 and NR molecular chains strongly interact through various effects (branching, nucleation, size, and surface), which slow down the diffusion of decomposition products from the bulk polymer to gas phase. Alternatively, the migration of SiO_2 to the surface of the composites at elevated temperatures could result in the formation of a SiO_2/NR char, which acts as a heating barrier to protect the NR inside.

Wang *et al.*[57] studied the thermal stability behaviour of NR, NR–PMMA), NR–PMMA/SiO_2 and NR–PMMA/SiO_2-3-(trimethoxysilyl) propyl methacrylate (MPS)–PMMA in nitrogen environment. They observed that the degradation curve of NR–PMMA/SiO_2–PMMA is slightly shifted to a higher temperature, compared with other samples due to the intertwining between one PMMA chain on the surface of nano-silica and another PMMA chain grafted on NR molecules.

However, contemporarily, not much significant work has been reported dealing with the thermal stability behaviour of other metal oxide filled SR composites. Zhuang *et al.*[81] observed that the thermogram of nano-ZnO/NR

Table 18.6 Initial thermal decomposition temperature and corresponding enhancement in NR and its NR/SiO_2 composites.

Reference	*NR and NR/SiO_2 composite*	*T_i (°C)*
60	NR	385.0
	NR/4 wt% SiO_2	395.4
67	NR vulcanized	283.7
	NR vulcanized with *in situ* silica 30 phr	299.7
	NR vulcanized with commercial silica 30 phr	322.5
64	NR	382.6
	NR/SiO_2	400.5

(and general ZnO/NR) composites consist of first, second and third stages of degradations, in the temperature ranges of 200–440 °C (200–430 °C), 440–560 °C (430–550 °C) and 560–760 °C (550–760 °C), respectively. Thus it is clear that the ending temperature in the first stage is 10 °C higher in nano-ZnO/NR than that general ZnO/NR and the max reaction rate is lower and corresponding peak temperature is higher. In the second stage, the both starting and ending temperature of nano-ZnO/NR composite material are 10 °C higher than those of the general ZnO/NR composite material. The maximum reaction rate is lower and the peak temperature is higher also as same as the first stage. In the third stage, the beginning resolution temperature of nano-ZnO/NR composite material is 10 °C higher than that of the general ZnO/NR composite material too. In this stage, the maximum reaction rate of nano-ZnO composite material is lower and the peak temperature is higher.

18.4.4 Electrical Properties

Alumina is one of the potential materials existing as a dispersed phase in the NR matrix.[141–143] Vinod *et al.*[109] and Jakubowickz[144] reported that alumina can also reduce heat, humidity, light, ozone, and gamma radiations, flame resistance, and the crack growth in NR. Very recently, Tangboriboon *et al.*[108] reported the electrical and electrorheological properties of NR (XL)/Al_2O_3 composites Table 18.7 presents the corresponding data at room temperature and 500 Hz and its comparison with non-conducting NR and the insulating Al_2O_3. It is noted that the electrical conductivity and the dielectric constant increase gradually with increasing particulate volume fraction. The dielectric constant (and electrical conductivity) values are found to be 1.542 (6.517×10^{-9} $\Omega^{-1}.m^{-1}$), 11.811 (1.502×10^{-7} $\Omega^{-1}.m^{-1}$)), and 2.123 (2.683×10^{-8} $\Omega^{-1}.m^{-1}$) for NR, Al_2O_3, and 0.00968 volume fraction Al_2O_3 filled NR. The elec. properties of NR–β alumina (Al_2O_3) composites crosslinked with dicumyl peroxide (DCP) has also been investigated by Tangboriboon *et al.*[110] The electrical conductivity of the composites with DCP is found to be greater by nearly three orders of magnitude than that of NR–Al_2O_3 composites without DCP and pure NR. The observed increase in the elec. cond. is attributed to the strong C–C bond, the tunnelling phenomenon and the ionic polarization of the alumina particles acting as the dispersed phase in the elastomer matrix

18.4.5 Magnetic Properties

The magnetic properties of prepared fillers (α-Fe_2O_3, $Fe_2O_3:1Al_2O_3$, $3Fe_2O_3:1Al_2O_3$, $1Fe_2O_3:3Al_2O_3$ and rubber vulcanizates loaded with 40% of α-Fe_2O_3, $1Fe_2O_3:1Al_2O_3$, $3Fe_2O_3:1Al_2O_3$, $1Fe_2O_3:3Al_2O_3$ have been investigated.[118] The shapes hysteresis loops are found to be characteristic for antiferromagnetic particulates with canted domains ordering.[145] Saturation magnetizations and the remanance values are found to be higher for fillers and lower for the corresponding rubber composites. The values of specific saturation induction B_s and retentivity B_r in emu/g and the coercive force H_c in

Table 18.7 Electrical properties of XL/Al_2O_3 measured at room temperature and at 500 Hz. (Reproduced with permission from ref. 108 with permission from Wiley Interscience.)

Code	*Mass of XL (g)*	*Mass of Al_2O_3 (g)*	*Volume fraction of Al_2O_3 (Φ)*	*Dielectric constant ε' at 500 Hz*	*Dielectric loss factor ε'' at 500 Hz*	*Conductivity $(\Omega.m)^{-1}$, σ at 500 Hz*
Al_2O_3	0.0000	1.0000	1.00000	11.811	7.66E-03	1.502E-07
XL/Al_0	3.0000	0.0000	0.00000	1.542	6.84E-04	6.517E-09
XL/Al_1	3.0000	0.0069	0.00054	1.343	2.15E-04	7.685E-09
XL/Al_2	3.0000	0.0316	0.00284	1.357	1.44E-03	8.688E-09
XL/Al_3	3.0000	0.0572	0.00448	1.436	1.36E-03	1.235E-08
XL/Al_4	3.0000	0.0784	0.00613	1.518	1.52E-03	1.471E-08
XL/Al_5	3.0000	0.0961	0.00750	1.550	1.58E-03	1.594E-08
XL/Al_6	3.0000	0.1120	0.00873	1.575	1.96E-04	1.937E-08
XL/Al_7	3.0000	0.1243	0.00968	2.123	1.65E-04	2.683E-08

Measured at 27 °C; density XL is 0.92 g/cm^3; density Al_2O_3 powder is 3.90 g/cm^3; XL rubber has extra light colour.

Table 18.8 Magnetic properties of the prepared fillers and the corresponding rubber-based composites. (Reproduced with permission from ref. 118 with permission from Wiley Interscience.)

Materials	B_s *(emu/g)*	B_r *(emu/g)*	H_c *(Oe)*
α-Fe_2O_3	0.96	0.16	246
$1Fe_2O_3$:$1Al_2O_3$	0.40	0.1	3169
$3Fe_2O_3$:$1Al_2O_3$	0.44	0.13	1845
$1Fe_2O_3$:$3Al_2O_3$	0.35	0.13	3037
α-Fe_2O_3-rubber	0.46	0.027	109
$1Fe_2O_3$:$1Al_2O_3$-rubber	0.30	0.02	99
$3Fe_2O_3$:$1Al_2O_3$-rubber	0.37	0.01	61
$1Fe_2O_3$:$3Al_2O_3$-rubber	0.29	0.02	123

Orested for the prepared fillers and the corresponding composites in Table 18.8 exhibits the parasitic ferromagnetic characteristics indicating the antiferromagnetic ordering for the domains. It is also noted that the addition of the fillers to the rubber vulcanizates changes the properties of rubber from diamagnetic in pure rubber (without addition of magnetic fillers) to weak ferromagnetic with different specific saturation induction properties (B_s, B_r and H_c) depending on the concentration of the filler loaded within rubber vulcanizates. The specific saturation induction (B_s) was greater in case of rubber composites containing higher ratios of α-Fe_2O_3 powder than those containing greater ratio of Al_2O_3. The values of coercive force (H_c) and the retentivity (B_r) of the composites have lower values in case of rubber composites than in the powder filler due to the increase in magnetic interaction between the filler particles with each other than interaction between filler and rubber in the formed rubber composites. It is concluded that rubber vulcanizates filled with $3Fe_2O_3 : 1Al_2O_3$ showed better magnetic properties than those loaded with $1Fe_2O_3 : 1Al_2O_3$ and both are better than those loaded with $Fe_2O_3 : 3Al_2O_3$.

Magnetic properties of the iron/iron oxide filled carbon nanotubes/NR composites have been studied.[146] According to this, the interaction between the magnetization of the tip and the magnetic field of the sample causes an increase or decrease in the oscillation phase of the tip due to the attractive or repulsive force between the poles. The phase variation is used to create an image in which the different colours indicate the different magnetic domains in the sample.

Soloman *et al.*[126] investigated the effect of carbon black on the dielectric properties of NR composites containing barium ferrite ($BaFe_{12}O_{19}$) for several applications, such as microwave absorbers. The magnetic properties studies indicated that these composites possess suitable magnetization values. The coercivity of the composites remained almost the same as that of the ceramic barium ferrite. The preparation of ferrite composites (RFCs) containing powdered NZF ($Ni_{1-x}Zn_xFe_2O_4$) in a NR matrix has also been reported.[127] It is observed that was also observed that for $x = 0.4$ and for the maximum ferrite loading, the composite sample exhibits maximum magnetization and optimum flexibility.

18.4.6 Thermal Conductivity and Thermal Diffusivity

In the last decades, many experimental as well as theoretical studies have been focused to understand the thermophysical properties of polymers filled with nanoparticles.[147,148] However, not much work has been reported on the nanocomposites of NR. Meera *et al.*[102] for the first time reported room temperature variation of the thermal conductivity and thermal diffusivity of NR filled TiO_2 and nano-SiO_2 composites have been investigated as a function of filler volume fraction and findings are displayed in Figures 18.28 and 18.29, respectively. It is observed that the thermal conductivity and thermal diffusivity of the composites increase with filler loading. The NR/TiO_2 (and NR/nano-silica) composite showed an increase of 41% (37%) of the thermal conductivity with only 9.84 vol% of TiO_2 (6.48 vol% of nano-silica). It is also noted that the thermal diffusivity of NR/TiO_2 (9.84 vol%) and NR/nano-silica (6.48 vol%) composites increases by 28 and 26%, respectively. The dispersion and orientation of the filler particles, the filler aspect ratio, the relative ratio of thermal conductivity of the filler and the matrix could be major reasons for the observed enhancement in the thermal properties of the composites. Recent studies also confirmed that the nanosized zinc oxide (ZnO) and nano-alumina (Al_2O_3) filled NR composite possess excellent thermal conductivity.[112] Li *et al.*[149] prepared micro and nano-Al_2O_3 as the thermal filler in NR, compared their thermal conductivity. The results showed that the thermal conductivity of NR filled with micro-Al_2O_3 is better than the nano-Al_2O_3 filled NR at the same filler content.

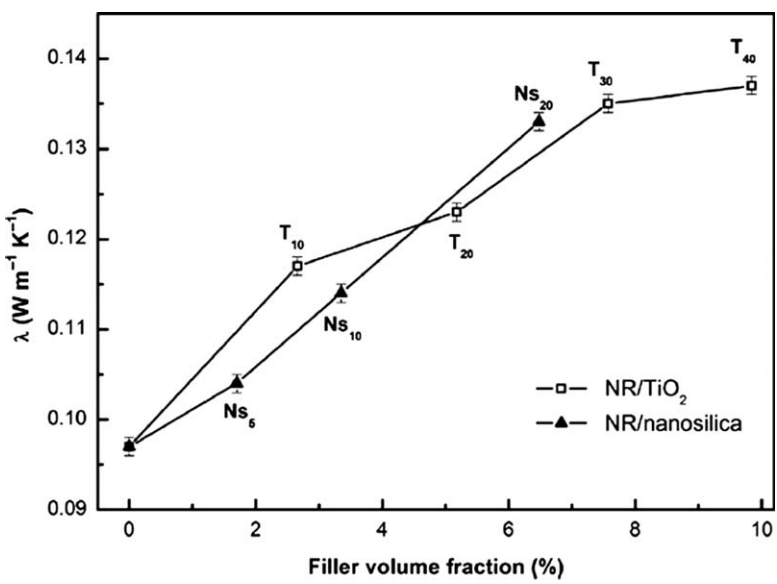

Figure 18.28 Thermal conductivity vs filler volume fraction for TiO_2- and nanosilica-filled natural rubber (NR) composites.
(Reproduced from ref. 102 with permission from SAGE.)

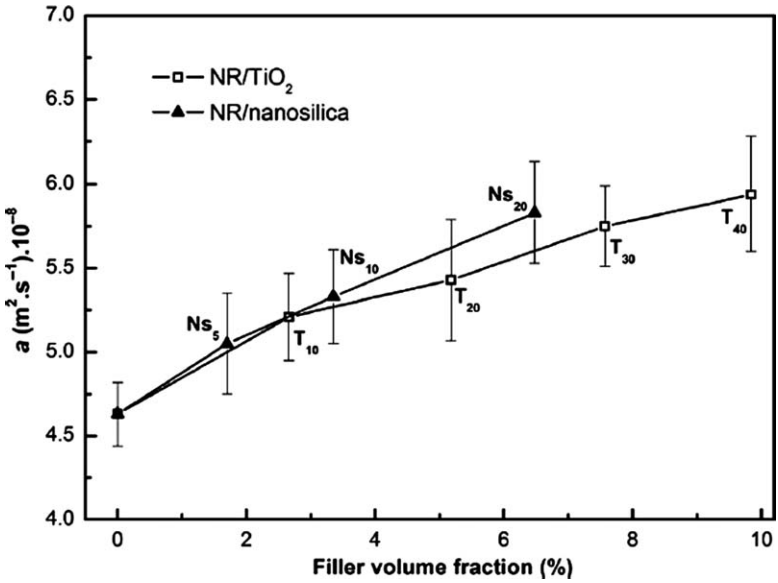

Figure 18.29 Thermal diffusivity versus filler volume fraction for TiO_2- and nanosilica-filled natural rubber (NR) composites.
(Reproduced from ref. 102 with permission from SAGE.)

18.4.7 UV Resistance Properties

NR, when exposed to UV radiation, undergoes extensive changes in macroscopic, microscopic and mechanical properties limiting its applications in outdoor applications. Although many commercially available antioxidants are added into the rubber formulations to guard the rubber products against UV degradations,[150–154] these are not desirable from the international regulatory authorities concern.[155] Therefore, rutile-TiO_2 is a chemically stable as well as safe for consumption and could be used as an filler in NR to obtain the enhanced UV-protection properties.[94] ATR-FTIR analysis suggested that a strong carbonyl adsorption band appeared in the unfilled NR after UV irradiation. However, the addition of n-TiO_2(R) into NR has led the effective reduction in its intensity. SEM observations of the fractured surface morphology of NR/n-TiO_2(R) composites and the retention values of mechanical properties of the NR nanocomposites after UV irradiation also confirmed the UV-protection ability of the prepared NR nanocomposites.

18.4.8 Antibacterial Properties

The smaller size of n-TiO_2 also exhibits sustaining antimicrobial capability, biocompatibility, and self-cleaning functionality.[156,157] This motivated Boonchai Seentrakoon *et al.*[94] to add n-TiO_2 in NR and study its effect of

Table 18.9 Inhibition zone diameter of the unfilled NR, NR/micron-TiO_2(R) and NR/n-TiO_2(R) composites against *E. coli* and *S. aureus* bacteria after 24 h under UV exposure. Reproduced from ref. 94 with permission from Elsevier.)

Samples	*TiO_2 (R) content (phr)*	*Inhibition zone diameter (mm)*	
		E. coli (G^-)	*S. aureus (G^+)*
Unfilled NR	–	0	0
NR/n-TiO_2(R)	1	16.0 (0.2)[a]	17.9 (0.5)
	3	15.3 (01.)	18.7 (0.1)
	5	17.5 (0.4)	18.5 (0.3)
	10	17.7 (0.3)	18.6 (0.4)
	20	18.8 (0.7)	19.1 (0.1)
NR/micron-TiO_2(R)	5	0	0

[a]Standard deviation values are given in parentheses.

formed nanocomposite on antibacterial properties against *Escherichia coli* (*E. coli*) and *Staphylococcus aureus* (*S. aureus*) under UV exposure and compare it with respect to unfilled NR and NR/micron-TiO_2(R) composite. Table 18.9 refers the corresponding data related the inhibition zone diameter of the unfilled NR, NR/micron-TiO_2(R), and NR/n-TiO_2(R) composites against *E. coli* and *S. aureus* bacteria after 24 h under UV exposure. The results show that NR/n-TiO_2(R) composites at different n-TiO_2(R) contents (1–20 phr) presented good antibacterial property against *E. coli* bacteria and against *S. aureus* bacteria. The results also display that the antibacterial property of NR nanocomposites against *S. aureus* was higher than that against *E. coli* bacteria.

NR/ZnO/Ag nanocomposites have been explored to investigate its antibacterial and anti-algae performance.[85] These findings have shown that the sedimentation rate of ZnO/Ag nanocomposites antibacterial agent modified by tri-Bu phosphate (TBP) decreased from nearly 1 to 0.2 below, and the lipophilic and dispersion of ZnO/Ag nanocomposites antibacterial agent increased significantly. The antibacterial properties of NR composites of titanium dioxide (20–40 nm diameter) are found to be greatly improved compared with those of the unfilled composites before and after ageing. Lin *et al.*[105] Huang *et al.*[95] also observed the excellent antibacterial and antifungal effects in TiO_2/NR nanocomposites.

18.5 Curing Characteristics of NR and Metal Oxide NR Composites

Cure time corresponds to the time required for optimum vulcanization of samples. NR filled with different silica types (precipitated silica, PSi and fumed silica, FSi) have been prepared and their cure characteristics features were analyzed.[134] The corresponding data related to the cure characteristics, scorch time (t_{s2}), cure time (t_{c90}), cure rate index (CRI) and minimum torque (M_L) are recorded in Table 18.10. It can be seen that compared to PSi/NR compounds, degree of reversion and viscosity are higher for FSi/NR compounds at the same

Table 18.10 Cure characteristics and crosslink density of silica/NR composites containing different silica types and contents. (Reproduced from ref. 134 with permission from Elsevier.)

Silica types	*Sample codes*	*Cure characteristics*				*Crosslink density 10^{-3} (mol/cm^3)*
		t_{s2} (min)	*t_{c90} (min)*	*CRI (min^{-1})*	*M_L (dN.m)*	
Without silica	Gum	1.87 ± 0.01	3.00 ± 0.01	88.1 ± 0.6	0.2 ± 0.00	8.7 ± 0.1
Precipitated silica (PSi)	M10_Psi	1.81 ± 0.02	3.01 ± 0.04	83.0 ± 1.5	0.41 ± 0.00	10.9 ± 0.2
	M20_Psi	1.50 ± 0.01	2.81 ± 0.08	79.2 ± 4.0	0.52 ± 0.00	13.5 ± 0.04
	M30_Psi	1.37 ± 0.02	2.90 ± 0.05	75.2 ± 0.7	0.83 ± 0.01	14.9 ± 0.2
	MS30_Psi	1.22 ± 0.01	3.21 ± 0.03	50.8 ± 0.4	0.78 ± 0.00	25.9 ± 0.3
Fumed silica (FSi)	M10_FSi	1.88 ± 0.06	3.08 ± 0.01	79.7 ± 0.5	0.71 ± 0.00	1.0 ± 0.1
	M20_FSi	1.75 ± 0.04	3.05 ± 0.01	76.9 ± 1.7	1.27 ± 0.00	13.9 ± 0.2
	M30_FSi	1.48 ± 0.01	2.97 ± 0.02	67.1 ± 0.6	2.92 ± 0.01	15.5 ± 0.8
	MS30_FSi	1.41 ± 0.02	3.27 ± 0.06	54.2 ± 0.6	1.34 ± 0.01	26.7 ± 0.3

silica loading. Furthermore, it is found that t_{s2} of both silica-filled systems gradually reduces with increasing silica loading while their t_{c90} is not significantly affected, when there is no Si-69 in the system. The results also show that CRI of both silica-filled compounds reduces with increasing silica loading. The crosslink density also progressively increased with increasing silica content in PSi and FSi.

Choi *et al*. studied the rheological behaviour of TBBS containing carbon black and silica-filled NR composites.[161] The maximum torque (T_{max}) value increases for the silica-filled NR composites without the silane coupling agent and the degree of the cure reversion also increases as the TBBS content increases. The T_{max} for both silica-filled and carbon black filled NR composites with silane coupling agent increases with increase in the TBBS content but no remarkable reversion occurs. It is seen that the viscosity decreases with the increase of TBBS content in the composites which is attributed to the peptizing effect of TBBS. The viscosities of the unmodified silica-filled composites are found to be much higher than those of the other composites. This is due to a poorer dispersion of silica in absence of silane coupling agent compared with the other compounds

ZnO loaded composites of NR have been studied for their curing characteristics.[86] It is inferred that the maximum torque value shows an improvement by $\sim$12% for both 5 and 3 phr loading of ZnO nanoparticles in comparison with the conventional rubber grade ZnO, which indicates a better state of cure because of better interaction of ZnO nanoparticles with the matrix.

Salaeh *et al*.[124] investigated the curing characteristics of the gum rubber compound and the ceramic/NR composites in terms of minimum, maximum and delta torques, scorch time, cure time, and cure rate index (CRI) are summarized in Table 18.11. This suggests that longer cure time but lower CRI in the $BaTiO_3$ composites compared with the $PbTiO_3$ composites. This indicated lower rate of vulcanization in the $BaTiO_3$ compounds. Furthermore,

Table 18.11 Cure characteristics of gum vulcanizate (NR) and its ceramic composites (MODIFIED). (Reproduced from ref. 124 with permission from Springer.)

Properties	*NR vulcanizate*	*NR filed $BaTiO_3$*	*NR filed $PbTiO_3$*
Min. torque (M_L) (dN m)	1.70	0.73	0.93
Max. torque (M_H) (dN m)	8.80	26.17	22.92
Delta torque (M_H-M_L)(dN m)	7.11	25.43	21.99
Scorch time (t_{s1}) (min)	1.00	0.51	0.51
Optimum cure time (t_{c90}) (min)	7.00	5.19	4.71
Cure rate index (min^{-1})	16.67	21.37	23.81

incorporation of $BaTiO_3$ caused higher delta torque than that of the incorporation of $PbTiO_3$. This may be attributed to higher reinforcing capability of the $BaTiO_3$ particles in the rubber matrix.

The variation of curing time for different loadings of $Ni_{1-x}Zn_xFe_2O_4$ in NR clearly shows that the curing time sharply decreases for initial filler loadings (30 phr).[127] Subsequently, the change in cure time is only marginal at further higher loading off the filler. These observations confirm that the processability of the composites is not significantly altered by the addition of the fillers. Makled *et al.*[159] investigated the variation of scorch time (t_{10}) and cure time (t_{90}) as a function of ferrite loading. They observed a significant decrease in scorch time with increasing ferrite content up to 160 phr followed by no further change at higher loadings. On the contrary, the total time required for optimum vulcanization of the samples (cure time) decreases sharply with increasing ferrite loading (at low ferrite content) because of the decreasing of scorch time. However, the cure time starts to increase sharply after 160 phr of ferrite loadings.

18.6 Conclusions and Future Direction of Work

NR which is nothing but *cis*-1,4-polyisoprene has proved its utility as a 'commodity polymer' as well as 'engineering elastomer' by virtue of its unique combination of physico-mechanical properties. Therefore, the introduction of micro/nanofillers into the NR matrix remains a high priority option. In this regard, inorganic metal oxides have demonstrated great potential as fillers in the preparation and property enhancement of NR. In this regards, metal oxides have been considered as another class of effective fillers in the enhancement of mechanical, thermal magnetic, electrical and UV resistance and antibacterial properties of the composites. However, there is enough room to work on the NR-based composites for potential and technological applications.

References

1. Y. Kojima, A. Usuki, M. Kawasumi, Y. Fukushima, A. Okada, T. Kurauchi and O. Kamigaito, *J. Mater. Res.*, 1993, **8**, 1185.

2. E. P. Giannelis, *Adv Mater*., 1993, **8**, 29.
3. M. Alexandre and P. Dubois, *Mater. Sci. Eng*, 1993, **28**, 1.
4. C. O. Oriakhi, *J. Chem. Educ*., 1993, **77**, 1138.
5. S. S. Ray and M. Okamoto, *Prog. Polym. Sci*., 1993, **28**, 1539.
6. F. R. Costa, M. Saphiannikova, U. Wagenknecht and G. Heinrich, *Adv. Polym. Sci*., 1993, **210**, 101.
7. S. Pavlidou and C. D. Papaspyrides, *Prog. Polym. Sci*., 1993, **33**, 1119.
8. M. Pramanik, S. K. Srivastava, B. K. Samantaray and A. K. Bhowmick, *J. Mat. Sci. Lett*., 1993, **20**, 1377.
9. M. Pramanik, S. K. Srivastava, B. K. Samantaray and A. K. Bhowmick, *J. Polym. Sci. Part B: Polym. Phys*., 1993, **40**, 2065.
10. M. Pramanik, S. K. Srivastava, B. K. Samantaray and A. K. Bhowmick, *J. Appl. Polym. Sci*., 1993, **87**, 2216.
11. H. Acharya, M. Pramanik, S. K. Srivastava and A. K. Bhowmick, *J. Appl. Polym. Sci*., 1993, **93**, 2429.
12. H. Acharya, S. K. Srivastava and A. K. Bhowmick, *Compos. Sci. Technol*., 1993, **67**, 2807.
13. T. Kuila, S. K. Srivastava, A. K. Bhowmick and A. K. Saxena, *Compos. Sci. Technol*., 1993, **68**, 3234.
14. B. Pradhan, S. K. Srivastava, A. K. Bhowmick and A. Saxena, *Polym. Int*., 1993, **61**, 458.
15. S. K. Srivastava, in *Barrier Properties of Polymer Clay Nanocomposites*, Ed. Vikas Mittal, NOVA Publishers, USA, 2010, p. 189.
16. M. Kotal, S. K. Srivastava and B. Pramanik, *J. Phys. Chem. C*, 2011, **115**, 1496.
17. M. Kotal and S. K. Srivastava, *J. Mater. Chem*., 1993, **21**, 18540.
18. T. Kuila, S. Bose, A. K. Mishra, P. Khanra, N. H. Kim and J. H. Lee, *Prog. Mater. Sci*., 1993, **57**, 1061.
19. Mafune, Toshiyuki, Jpn. Kokai Tokkyo Koho (2009), JP 2009113398 A 20090528.
20. Ogawa, Kenji, Jpn. Tokkyo Koho (2011), JP 4646385 B2 20110309.
21. H. Angellier, S. Molina-Boisseau and A. Dufresne, *Macromolecules*, 1993, **38**, 9161.
22. S. Sato, Y. Honda, M. Kuwahara, H. Kishimoto, N. Yagi, K. Muraoka and T. Watanabe, *Biomacromolecules*, 2004, **5**, 511–515.
23. K. Sanguansap, T. Suteewong, P. Saendee, U. Buranabunya and P. Tangboriboonrat, *Polymer*, 2005, **46**, 1373.
24. C. Sirisinha, P. Saeoui and J. Guaysomboon, *Polymer*, 1993, **45**, 4909.
25. P. B. Sulekha, R. Joseph and K. E. George, *Polym. Degrad. Stab*., 1993, **63**, 225.
26. V. V. Rajan, W. K. Dierkes, R. Joseph and J. W. M. Noordermeer, *Prog. Polym. Sci*., 1993, **31**, 811.
27. S. Kohjiya, A. Kato and Y. Ikeda, *Prog. Polym. Sci*., 1993, **33**, 979.
28. S. Ostad-Movahed, K. Ansar Yasin, A. Ansarifar, M. Song and S. Hameed, *J. Appl. Polym. Sci*., 1993, **109**, 869.

29. A. K. Bhowmick and Howard L. Stephens Eds. *Handbook of Elastomers* Anil K. Publishers Marcel Dekker, Inc. New York, Second edition, 2001.
30. C. M. Liauw, N. S. Allen, M. Edge and L. Lucchese, *Polym. Degrad. Stab*., 1993, **74**, 159.
31. S. K. Srivastava and T. Kuila, in *A Comprehensive Guide to Additives and Their Applications*, edited by C.D Papaspyrides and P. Kiliari, Degruyter Publishers, Gruyter Publisheres, Berlin 2, 2, 013, (In press).
32. S. K. Srivastava and H. Acharya, in *Rubber Nanocomposites: Preparation, Properties and Applications*, Sabu Thomas and Ranimol Stephen (Eds), John Wiley, 551, 2010.
33. Z. A. Mohd Ishak, P. Y. Wan, P. L. Wong, Z. Ahmad, U. S. Ishiaku, J. Karger-Kocsis, *Journal of Applied Polymer Science*, 2002, **84**, 2265–2276.
34. S. Salaeh and C. Nakason, *Polym. Compos*., 2012, **33**, 489.
35. S. Rooj, A. Das, I. A. Morozov, K. W. Stöckelhuber and R. Stocek, *Compos. Sci. Tech*., 1993, **76**, 61.
36. P. Bala, B. K. Samantaray, S. K. Srivastava and G. B. Nando, *J. Mat. Sci. Lett*., 1993, **20**, 563.
37. P. Bala, S. K. Srivastava, B. K. Samantaray and G. B. Nanda, *J. Appl. Polym. Sci*., 1993, **92**, 3583.
38. S. Varghese and J. Karger-Kocsis, *Polymer*, 2003, **44**, 4921.
39. A. K. Bhowmick, M. Bhattacharya and S. Mitra, *J. Elastomers Plast*., 1993, **42**, 517.
40. G. C. Psarras, K. G. Gatos and J. Karger-Kocsis, *J. Appl. Polym. Sci*., 1993, **106**, 1405.
41. K. G. Gatos and J. Karger-Kocsis, *KGK Kautschuk Gummi Kunststoffe Jahrgang*, 2004, **57**, 350.
42. Chi Liu, Yan Shao and Demin Jia, *Polymer*, 1993, **49**, 2176.
43. H. Ismail, S. Shuhelmy and M. R. Edyham, *Eur. Polym. J*., 1993, **38**, 39.
44. A. Fakhru'l-Razi, M. A. Atieh, N. Girun, T. G. Chuah, M. El-Sadig and D. R. A. Biak, *Compos. Struct*., 1993, **75**, 496.
45. M. Hernandez, M. de M. Bernal, R. Verdejo and T. A. Ezquerrs, *Compos. Sci. Technol*., 1993, **73**, 40.
46. J. R. Potts, O. Shankar, S. Murali, L. Du and R. S. Ruoff, *Compos. Sci. Technol*., 1993, **74**, 166.
47. M. Hernández, M. del Mar Bernal, R. Verdejo, T. A. Ezquerra and M. A. López-Manchado, *Compos. Sci., Tech*., 1993, **73**, 40.
48. H. S. Ghari and Z. Shakouri, *Rubber Chem. Technol*., 1993, **85**, 132.
49. M. Jarnthong, C. Nakason, N. Lopattananon and Z. Peng, *Polym. Compos*., 1993, **33**, 1911.
50. A. Intasiri, N. Na-Ranong and S. Kiatkamjornwong, *Polym. Eng. Sci*., 2009, 1099.
51. A. Kongsinlark, G. L. Rempel and P. Prasassarakich, *Chem. Engg. J*., 2012, **193–194**, 215.
52. C.-P. Li, S.-D. Li, J.-P. Zhong and L. Yang, *J. Polym. Mater*., 2011, **28**, 623.

53. S. Xu, J. Gu, Y. Luo and D. Jia, *Fuhe Cailiao Xuebao*, 1993, **28**, 39.
54. S. H. Xu, J. Gu, Y. F. Luo and D. M. Jia, *eXPRESS Polym. Lett*., 2012, **6**, 14.
55. L. Yang, H. Lin, Z.-F. Wang, Z. Peng and F. Xin, *Huaxue Gongchengshi*, 1993, **25**, 7.
56. L. Liu, D. Jia, Y. Luo, H. Lu and L. Yu, *Faming Zhuanli Shenqing*, 2008CN 101113216 A 20080130J.
57. Q. Wang, L. Yongyue, F. Chunfang, Y. Zhifeng, Q. Quanfang, L. X. Kong and Z. Peng, *J. Nanomater*., **2012**, Article ID 782986, DOI: 10.1155/2012/782986.
58. S. Kohjiya, A. Katoh, J. Shimanuki *et al*., *Polymer*, 2005, **46**, 4440.
59. S. Choi and S.-J. Choi, *Bull. Korean Chem. Soc*., 1993, **27**, 1473.
60. Y. Chen, Z. Peng, L. X. Kong, M. F. Huang and L. P. Wang, *Polym. Engg. Sci*., 2008, **48**, 1674.
61. W.-J. Chen, H.-X. Fang and X. Fu, *Huaxue Gongchengshi*, 1993, **22**, 62.
62. A. Kato, S. Kohjiya and Y. Ikeda, *Rubber Chem. Technol*., 1993, **80**, 690.
63. Z. Peng, L. X. Kong, S. D. Li, Y. Chen and M. F. Huang, *Compos. Sci. Technol*., 2007, **67**, 3130.
64. S.-D. Li, Z. Peng, L. X. Kong and J.-P. Zhong, *J. Nanosci. Nanotechnol*., 1993, **6**, 541.
65. L. Bokobzaa and J.-P. Chauvin, *Polymer*, 2005, **46**, 4144–4151.
66. L. Bokobzaa, *Compos. Interfaces*, 1993, **13**, 345.
67. B. Chaichua, P. Prasassarakich and S. Poompradub, *J Sol Gel Sci Technol*., 1993, **52**, 219.
68. Y. Ikeda, S. Poompradub, Y. Morita and S. Kohjiya, *J Sol Gel Sci Technol*., 1993, **45**, 299.
69. Y. Ikeda and Y. Kameda, *J Sol Gel Sci Technol*., 1993, **31**, 137.
70. K. Murakami, S. Iio, Y. Ikeda, H. Ito, M. Tosaka and S. Kohjiya, *J. Mater. Sci*., 1993, **38**, 1447.
71. S. Kohjiya and Y. Ikeda, *J Sol Gel Sci Technol*., 1993, **26**, 495.
72. V. Tangpasuthadol, A. Intasiri, D. Nuntivanich, N. Niyompanich and S. Kiatkamjornwong, *J. Appl. Polym. Sci*., 2008, **109**, 424.
73. J. Siramanont, V. Tangpasuthadol, A. Intasiri, N. Na-Ranong and S. Kiatkamjornwong, *Polym. Engg Sci*., 1993, **49**, 1099.
74. B. P. Kapgate, C. Das, A. Das, D. Basu, U. Reuter and G. Heinrich, *J Sol Gel Sci Technol*., 1993, **63**, 501.
75. M. Messori, in *Recent Advances in Elastomeric Nanocomposites, Advanced Structured Materials*, ed. V. Mittal *et al*., Springer-Verlag Berlin Heidelberg 2011.
76. N. M. Claramma, L. Varghese and N. M. Mathew, *J. Elastmers and Plastics*, 1993, **31**, 130–142.
77. S. Prasertsri and N. Rattanasom, *Polym. Testing*, 1993, **30**, 515.
78. C. Gao and G. Hu, *Yingyong Huagong*, 1993, **39**, 13394.
79. L. Li and L. Liu, *Materials Sci Forum*, 1993, **650**, 367.
80. W. George, *Handbook of Fillers*, 2nd ed., William Andrew: Toronto, 1999.

81. T. Zhuang, T. Shan and L. Zhou, *Adv. Mater. Res.*, 1993, **87–88**, 462.
82. S.-Y. Sun, Z.-L. Peng and S.-Q. Jiang, *Hecheng Xiangjiao Gongye*, 1993, **35**, 216.
83. Gr. Bakhshandeh, G. Naderi, A. Abolfathi, M. Barikani, A. Parvin and M. H. Astaraki, *Iranian J. Polym. Sci. Tech.*, 1993, **22**, 117.
84. A. Chaitanee, B. Junhasavasdikul and W. Chavasiri, *PMSE Preprints*, 1993, **101**, 1490.
85. Z. Li, W. Cen, F. Guo, A. Mengm and Z. Zhang, *Huagong Xinxing Cailiao*, 1993, **36**, 66.
86. S. Sahoo, M. Maiti, A. Ganguly, J. J. George and A. K. Bhowmick, *J. Appl. Polym. Sci.*, 1993, **105**, 2407.
87. K. Schilling, B. Bradford, D. Castelli, E. Dufour, J. F. Nash, W. Pape *et al.*, *Photochem Photobiol Sci.*, 1993, **9**, 495.
88. T. Faunce, K. Murray, H. Nasu and D. Bowman, *Nanoethics*, 2008, **2**, 231–240.
89. A.-W. Sing, M.-F. Huang, P.-W. Li, T.-M. Gao and Z.-Q. Zeng, *Anhui Nongye Kexue*, 1993, **37**, 16224.
90. A. Yadav, V. Prasad, A.A. Kathe, S. Raj, D. Yadav, C. Sundaramoorthy *et al.*, *Bull Mater Sci.*, 1993, **29**, 641.
91. R. M. Wang, B. Y. Wang, Y. F. He, W. H. Lv and J. F. Wang, *Polym. Adv. Technol.*, 1993, **21**, 331.
92. O. Legrini, E. Oliveros and A. M. Braun, *Chem. Rev.*, 1993, **93**, 671.
93. A. Ahmad, M. Y. Rahman, S. P. Low and H. Hamzah, *Mater. Sci.*, 2011, 401280, DOI: 10.5402/201/401280.
94. B. Seentrakoon, B. Junhasavasdikul and W. Chavasiri, *Polym. Degrad. Stabil.*, 2013, **98**, 566.
95. M. Huang, A. Ding, T. Gao, M. Lv, P. Li and A. Ding, *International Conference on Biomedical Engineering and Informatics*, ed. Yu, Weichuan, 3rd, Yantai, China, Oct. 16–18, 2010, **4**, 1714–1717.
96. JCPDS, 00-042-1458.
97. W. Taweepreda and K. Phatcharasit, *World J. Engg.*, 1993, **9**, 349.
98. S. P. Low, A. Ahmed, H. Hamzah and M. Y. A. Rahman, *J. Solid St Electrochem.*, 1993, **15**, 26110.
99. L. Sikong, M. Masae, K. Kooptarnond, W. Taweepreda and F. Saito, *Appl. Surf. Sci.*, 1993, **258**, 4436.
100. M. Lu, US 20080194736 A1 20080814.
101. A.-W. Ding, M.-F. Huang, P.-W. Li, T.-M. Gao and Z.-Q. Zeng, *Anhui Nongye Kexue*, 2009, **37**, 16224.
102. A. P. Meera, R. Tlili, A. Boudenne, L. Ibo, V. Poornima, S. Thomas and Y. Candau, *J. Elastomers Plast.*, 2012, **44**, 369.
103. A. P. Meera, S. Said, Y. Grohens, A. S. Luyt and S. Thomas, *Indust. Engg Chem. Res.*, 1993, **48**, 3410.
104. G. Lin, M. Tia, Y.-L. Lu, X.-J. Zhang and L.-Q. Zhang, *Polym. J*, 1993, **38**, 498.

105. G. Lin, Y. Qian, P. Zhang, R. Xu, L. Yu and L. Zhang, *Hecheng Xiangjiao Gongye*, 1993, **28**, 98.
106. S. S. Ochigbo and A. S. Luy, *Int J Compos Mater*, 1993, **1**, 7–13.
107. L. Sikong, M. Masae, K. Kooptarnonda, W. Taweepred and F. Saitoc, *Appl Surf Sci*, 1993, **258**, 4436.
108. N. Tangboriboon, N. Uttanawanit, M. Longtong, P. Wongpinthong, A. Sirivat and R. Kunanuruksapong, *Materials*, 1993, **3**, 656.
109. V. S. Vinod, S. Varghese and B. Kuriakose, *Polym. Degrad. Stab.*, 1993, **75**, 405.
110. N. Tangboriboon, S. Chaisakrenon, A. Banchong, R. Kunanuruksapong and A. Sirivat, *Plast. Rubber Compos.*, 1993, **42**, 26.
111. M.-Q. Li, J.-J. Zhang, H.-J. Niu and Z.-Y. Zhang, *Tanxingti*, 1993, **22**, 17.
112. Y.-L. Lu, L.-Q. Zhang, Y.-L. Feng, Z.-H. Wang and J.-B. Ding, *Technical Meeting-American Chemical Society*, Rubber Division, 180th, & Advanced Materials in Health Care, Cleveland, OH, United States, Oct. 11–13, 2011, 1, 390–415.
113. N. Tangboriboon, S. Chaisakrenon, A. Banchong, R. Kunanuruksapong and A. Sirivat, *J. Elastomers Plastics*, 1993, **44**, 21.
114. J.-F. Fu, L.-Y. Chen, H. Yang, Q.-D. Zhong, L.-Y. Shi, W. Deng, X. Dong, Y. Chen and G.-Z. Zhao, *Polym. Compos.*, 2012, **33**, 404.
115. W. Cui, Q. Cao, H. Jin, Y. Chen, Q. Ji and S. Zhang, *Hecheng Xiangjiao Gongye*, 2002, **25**, 300.
116. N. Tangboriboon, M. Longtong, A. Sirivat and R. Kunanuraksapong, *Mater. Technol: Adv. Performance Mater.*, 1993, **26**, 100.
117. N. Tangboriboon, N. Uttanawanit, M. Longtong, P. Wongpinthong, A. Sirivat and R. Kunanuruksapong, *Composites Materials*, 2010, **3**, 656–671.
118. S. H. El-Sabbagh, N. M. Ahmed and W. M. Daoush, *J. Appl. Polym. Sci.*, 2006, **102**, 494.
119. W. Xiao, *Faming Zhuanli Shenqing*, 2013, CN 102876242 A 20130116.
120. V. V. Havanoor, N. N. Mallikarjuna, A. K. Lagashetty, A. Kumar and A. Venkataraman, *Asian J. Chem.*, 1993, **15**, 79.
121. J. F. Chen, Z. G. Shen, F. T. Liu, X. L. Liu and J. Yun, *Scripta Mater*, 1993, **49**, 509.
122. P. Kumar, S. Singh, J. K. Juneja, C. Prakash and K. K. Raina, *Physica B*, 2009, **404**, 1752.
123. C. B. Carter and M. G. Norton, *Ceramic materials: Science and Engineering.*, Springer, New York, 2007.
124. S. Salaeh, N. Muensit, P. Bomlai and C. Nakason, *J. Mater. Sci.*, 2011, **46**, 1723.
125. E. M. Mohammed, K. A. Malini, Philip Kurian and M. R. Anantharaman, *Mater. Res. Bull.*, 1993, **37**, 753.
126. M. A. Soloman, Philip Kurian, M. R. Anantharaman and P. A. Joy, *J. Appl. Polym. Sci.*, 1993, **89**, 769.
127. K. A. Malinia, P. Kurianb and M. R. Anantharamana, *Mater. Lett.*, 1993, **57**, 3381.

128. M. H. Makled, T. Matsuib, H. Tsuda, H. Mabuchi, M. K. El-Mansy and K. Morii, *J. Mater. Processing Technol.*, 1993, **160**, 229.
129. L. Kantiyong, M.Sc (Chemistry) Thesis, Graduate School, Kasetsart University, 2009.
130. F. S. Bellucci, L. O. Salmazo, E. R. Budemberg, M. R. da Silva, M. A. Rodriguez-Perez, M. A. L. Nobre and A. E. Job, *J. Nanosci. Nanotechnol.*, 1993, **12**, 2691.
131. D. Puryanti, S. H. Ahmed and M. H. Abdullah, *Polym. Plastic Technol. Engg.*, 2006, **45**, 561.
132. E. Guth and O. Gold, *Phy Rev*, 1993, **53**, 322.
133. E. Guth, *J Appl Phys*, 1993, **16**, 20.
134. S. Prasertsri and N. Rattanasom, *Polymer Testing*, 1993, **31**, 593.
135. D. G. Hundiwale, U. R. Kapadi, M. C. Desai, A. G. Patil and S. H. Bidkar, *Polym. Plast . Technol. Eng.*, 1993, **43**, 615.
136. M. A. Martins, R. M. B. Morenoa, C. M. McMahanc, J. L. Birchtac, P. S. Goncalvesb and L. H. C. Mattosoa, *Thermochim. Acta*, 1993, **474**, 62.
137. A. R. R. Menon, C. K. S. Pillai and G. B. Nando, *Poly. Degrad. Stabil.*, 1993, **52**, 265.
138. L. C. S. Oliveira, De. E. J. de. Arruda, R. B. da. Costa, P. S. Goncalves and A. Delben, *Thermochim. Acta*, 1993, **398**, 259.
139. L. Li, S. Li and Z. Wang, *Tanxingti*, 2011, **21**, 70.
140. K. J. Arun, P. J. Joseph, Francis and R. Joseph, *Optoelecronics Adv. Mater.-Rapid Communications*, 2010, **4**, 1520–1525.
141. M. Parthasarathy and D. J. Klingenberg, *Mat. Sci. Eng.*, 1996, **17**, 57.
142. D. F. M. Rob, *Toxicology*, 1993, **113**, 242.
143. F. Wang and Hecheng, *Xiangjiao*, 1993, **32**, 493.
144. I. Jakubowickz, *Polym. Degrad. Stab.*,**2003**, 39.
145. Y. Deng, L. Wang, W. Yang, S. Fu and A. Elaıssari, *J. Magn. Magn. Mater.*, 1993, **257**, 69.
146. C. F. Matos, F. Galembeck and A. J. G. Zarbi, *Carbon*, 2012, **50**, 4685.
147. H. Zhang, X. Ge and H. Ye, *Model Simul Mater. Sci. Eng.*, 2005, **3**, 401.
148. R. Sivakumar, S. Guo, T. Nishimura and Y. Kagawa, *Scripta Mater.*, 2007, **56**, 265.
149. M.-Q. Li, J.-j. Zhang, H.-J. Niu and Z.-Y. Zhang, *Tanxingti*, 1993, **22**, 17.
150. S. A. Avirah and R. Joseph, *J. Appl. Polym. Sci.*, 1993, **57**, 1511.
151. M. N. Ismali, M. A. Abd El Ghaffar, K. A. Shaffei and N. A. Mohamed, *Polym Degrad Stab.*, 1993, **63**, 377.
152. B. T. Poh and C. S. Te, *J Appl. Polym. Sci.*, 1993, **77**, 3234.
153. M. N. Ismali, A. A. Yehia and A. A. Korium, *Polym Degrad Stab.*, 1993, **74**, 247.
154. Y. Zhao and Y. Dan, *J. Appl. Polym. Sci.*, 1993, **102**, 2203.
155. A. Charles, G. S. Andre, M. Ralph and L. Pual, *J. Biomat. Sci. Polym.*, 1993, **1**, 231.

156. R. M. Wang, B. Y. Wang, Y. F. He, W. H. Lv and J. F. Wang, *Polym. Adv. Technol.*, 2010, **21**, 331.
157. C. Chawengkijwanich and Y. Hayata, *Int. J. Food Microbiol.*, 2008, **123**, 288.
158. S. S. Choi, C. Nah and B. W. Jo, *Polym. Int*, 2003, **52**, 1382–1389.
159. M. H. M. Makled, H. Washiya, H. Tsuda and T. Matsui, *J Appl Polym Sci*, 2009, **113**, 3294–3299.

CHAPTER 19

Mechanical Properties of Natural Rubber Composites Filled with Macro- and Nanofillers

AZURA A. RASHID* AND SITI ROHANA YAHYA

School of Materials and Mineral Resources Engineering, Universiti Sains Malaysia, 14300 Nibong Tebal, Penang, Malaysia
*Email: azura@eng.usm.my

19.1 Introduction

Elastomers have many useful applications in engineering due to their special properties. Nowadays, many important products that meet high requirements are made of elastomers, such as tyres, vibration mounts, seals, bearings, *etc*. Natural rubber (NR) is an unsaturated elastomer containing 93–95% of *cis*-1,4-polyisoprene, characterized by its crystallinity and having excellent properties such as high green strength, outstanding resilience, high elasticity, hot tear resistance, excellent dynamic properties and good fatigue resistance; it is also economically available. However, NR has poor resistance to heat, oxygen and ozone, due to the presence of many double bonds in its chemical structure.[1–4]

The incorporation of fillers into NR leads to the formation of a composite with improved mechanical properties. For decades, fillers have been widely used in the rubber industry. They are incorporated into rubber compounds for

RSC Polymer Chemistry Series No. 8
Natural Rubber Materials, Volume 2: Composites and Nanocomposites
Edited by Sabu Thomas, Hanna J. Maria, Jithin Joy, Chin Han Chan and Laly A. Pothen

Published by the Royal Society of Chemistry, www.rsc.org

many purposes, for example, to improve processability, to reduce cost, and also to modify the physical properties of the vulcanizates.[5–8] Generally, fillers can be classified into two main groups, reinforcing fillers and non-reinforcing fillers. Reinforcing fillers such as carbon black and silica generally have a significant effect in terms of improving tensile strength, modulus, abrasion resistance, tear and flexural properties. However, for some applications where cost and processability are the greatest concern, the use of non-reinforcing fillers such as clay, talc and calcium carbonate is highly recommended. These types of fillers give advantages in the enhancement of stiffness and reduce the tackiness of unvulcanized vulcanizates. Non-reinforcing fillers also play role in the increment of hardness and the decrement of tensile strength, resilience, resistance to abrasion and tear properties. Normally, this type of filler is used to reduce the cost of final product.[6,9]

The use of novel nanosized rigid (essentially inorganic) particles as fillers in rubber compounding is one of the latest trends in the development of polymeric materials which is so-called nanocomposites. Nanocomposites exhibit markedly improved properties compared to their conventional macro- and microcomposite counterparts. The most common reinforcements currently used to make nanocomposites are carbon nanotubes (CNTs) and natural silicates, such as mica, montmorillonite, kaolinite, saponite and hectorite. The application of nanofillers in elastomers is restricted by both their limited availability and their strong tendency to aggregate preventing their homogeneous dispersion within a continuous matrix, which is the key step required for high mechanical performances.[10,11]

19.2 Macro- and Nanofiller Reinforcements in Rubber Composites

In the case of filled vulcanizates, the reinforcement efficiency depends on a complex interaction of several filler-related parameters including particle size, particle shape, particle dispersion, surface area, surface activity, structure of the filler, and interactions between the fillers and the rubber matrix.[12]

19.2.1 Particle Size and Surface Area of Fillers

Table 19.1 shows the particle sizes of filler greater than 10 μm act as degradant due to insignificant contribution on reinforcement but tend to alter the

Table 19.1 Role of fillers according to particle size measurement.

Particle Size (μm)	*Role of Filler*
>10	Degradants
1 to 10	Diluents
0.1 to 1	Semi-Reinforcing
0.01–0.1	Reinforcing

properties of rubber composites. Fillers with particle size in the range of 1–10 μm are generally used, primarily as diluents. The filler particle sizes, which range from 0.1 to 1 μm, can be categorized as semi-reinforcing fillers, while filler particle sizes from 0.01 to 0.1 μm (10–100 nm) generally is so-called reinforcing filler. As particle size becomes smaller, the surface area increases, providing more available contact between the rubber molecules and the filler particles.[13,14]

19.2.2 Structure of Filler Particles

Fillers are usually made up from primary particles at the smallest size scale, which are strongly bonded to other primary particles to form aggregate structures. The aggregates can interact with other aggregates through weaker secondary bonding to form agglomerates. High structure filler exhibits a high number of primary particles per aggregate, which is called a strong aggregation, whereas low structure filler show only a weak aggregation. These aggregates may form loose agglomerates linked by van der Waals interactions.[15–17]

19.2.3 Surface Activities

A filler can offer small particle size and high surface area but still provide relatively poor reinforcement if it has low specific surface activity. Filler which has chemically active surface that formed by various chemical groups such as hydroxyl, carboxyl, quinone, phenol and lactone groups provides good interaction between rubber and filler generally is related to the formation of strong covalent bonding. The physical surface such as porosity will increase the surface activities.[16]

For hydrophobic elastomers such as NR and styrene butadiene rubber, carbon black usually has been selected as filler due to the hydrophobic surface characteristics and special particle shapes of carbon black which provide good dispersion. However, the dispersion of polar filler in hydrophobic rubbers matrix is difficult because of its hydrophilic surface.[18,19] The hydroxyl groups exist on the surface of polar filler provide strong filler–filler interactions which resulted in poor filler dispersion. The polar surface of filler formed hydrogen bonds with polar materials in a rubber compound. As known, the silica surface is acidic and forms strong hydrogen bonds with basic materials.[20]

In general, the chemical treatment of polar filler surfaces is the most successful way of enhancing rubber–filler interactions and reducing filler–filler interactions. Among these chemical treatments, coupling agents are widely used to improve the adhesion of rubber to filler. The chemical modification of polar filler surfaces with coupling agent generally occurs during the rubber mixing process. This modification leads to a shielding of the polar surface, which leads to better rubber compatibility, hence reduced filler agglomeration.[21]

19.3 Effects of Macro- and Nanofillers on Mechanical Properties of Rubber Composites

Recently, there has been much interest in the effect of filler sizes in polymer composites. In this review, the effect of macro- and nanofillers such as palm ash, wood flour, CNTs, organoclay on mechanical properties of NR composites are discussed.

19.3.1 Effects of Macrosized Fillers on Mechanical Properties of Natural Rubber Composites

Polymer composites can be classified according to their particle size. Macrofilled composites contain filler particle size more than 10 μm. Midsize fillers are less than 10 μm and more than 1 μm while nanofillers have a particle size less than 1 μm and more than 0.1 μm. The micro-filled composite contains filler particle size less than 0.1 μm.[22] The macrofiller generally is non-reinforcing filler and generally used for cost reduction particularly.

19.3.1.1 Palm Ash

Palm oil industry is one of the biggest industries in Malaysia which contribute to a large amount of solid waste as an output. The palm ash is produced after burning the palm oil shells and fibres as boiler fuel for palm oil consumption.

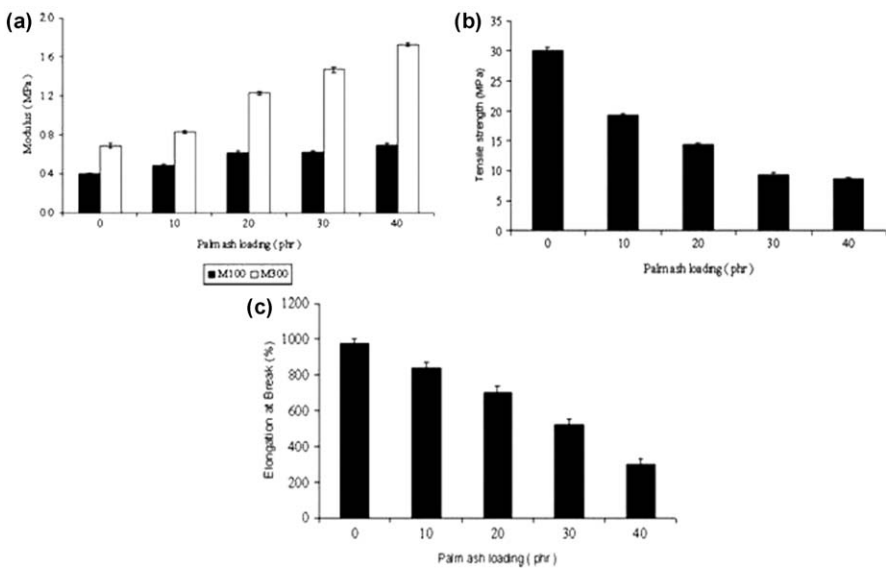

Figure 19.1 Effect of filler loadings on the (a) tensile modulus, (b) tensile strength and (c) elongation at break (%) of palm ash-filled natural rubber composites. (Reprinted from ref. 25 with permission from Wiley©.)

Most of the ashes are disposed of in landfill, which requires a relatively large area and affects the surrounding environment.[23,24]

Ismail and Haw[25] studied the effects of palm ash loading and maleated natural rubber as a coupling agent on the properties of palm ash-filled NR composites. The main materials used are Standard Malaysian Rubber Grade L (SMR L) natural rubber and palm ash with mean particle size 75 μm and the composites were carried out using a laboratory scale two-roll mill. Results indicated that the tensile modulus, M100 and M300 increased with filler loading as shown in Figure 19.1(a). This observation shows that the incorporation of palm ash into the rubber matrix improves the stiffness of the composites. Figure 19.1(b) and (c) show that the tensile strength and elongation at break percentages of the palm ash-filled NR composites decreased with filler loading. The reduction in strength of the composites is attributed to the irregularly shaped fillers, making the filler unable to support stress transferred from the polymer matrix. The use of high filler loadings in a rubber matrix tends to block the flow of the rubber chains, meaning the rubber composites break at lower elongation.[26]

19.3.1.2 Starch

Starch is available in large amounts from several renewable plant sources, inexpensive biopolymer, able to biodegrade, and economical to replace the mineral fillers. These advantages lead to the growing interest in the starch-based products either to be matrix or filler in polymer composites. Starch consists of two main structures: amylose and amylopectin. Amylose is principally linear with α-1,4-glucose units while amylopectin is highly branched unit with 1-4 linked α-D-glucosyl joined by 1-6 linkages.[10,27–29] For starch polymer only three hydroxyl groups of the cyclic glucose units are free and may rotate to one side of the molecule ring, make that side more hydrophilic. The opposite side is consequently slightly hydrophobic due to the exposed –CH groups. In fact in aqueous solutions amylose forms a helix with six glucose monomers per turn. The interior of the helix structure is hydrophobic, whereas the outer shell is hydrophilic.[30,31] Starch also has several significant disadvantages, such as poor mechanical properties, poor dimensional stability, and the fact that it is a hydrophilic material.[32] Schematically, the semicrystalline growth rings consist of a stack of repeated crystalline and amorphous lamellae[33,34] as shown in Figure 19.2.

Liu *et al.*[35] investigated chemically modified starch-reinforced NR latex composites. The natural starch used was common corn starch and butyl acrylate (BA) and ammonium persulfate (APS) were chemical reagents. About 6% starch aqueous suspension was gelatinized at 80 °C for 30 min under a nitrogen atmosphere. Graft copolymerization was conducted with the starch paste, BA and initiator APS at 80 °C for 2 h to give a modified starch paste (MST). Modified starch powders were obtained by precipitating the paste and then extracting the precipitate with acetone to remove ungrafted PBA. The grafting ratio of PBA was 21.6%, the ratio of ungrafted PBA was 2.4%

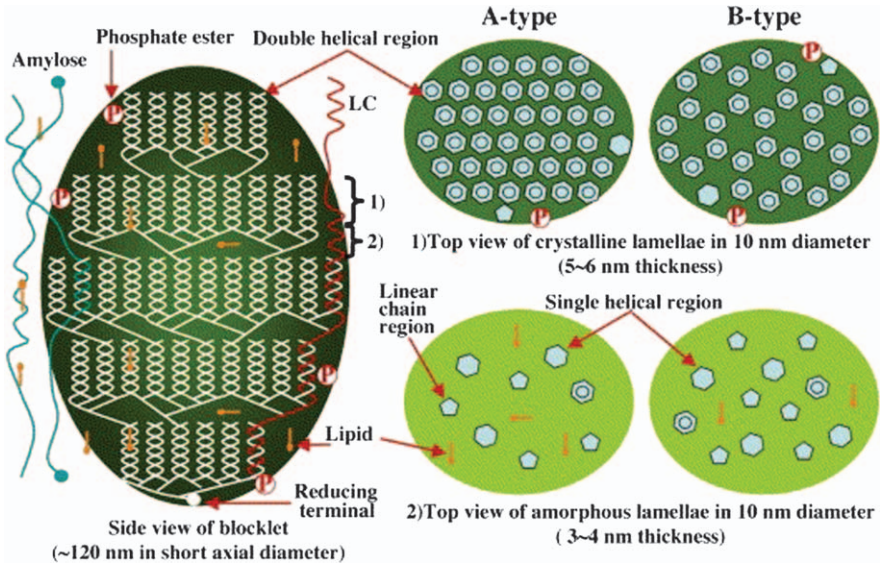

Figure 19.2 Stack of repeated crystalline and amorphous lamellae in blocklet structure of starch granules.
(Reprinted from ref. 34 with permission from Elsevier©.)

Table 19.2 Compounding formulation of neat natural rubber vulcanizates (NR), unmodified starch-filled natural rubber (NR/starch) composites and modified starch-filled natural rubber (NR/modified starch) composites. (Reprinted from ref. 35 with permission from Elsevier©.)

Conpounds	*NR*	*NR/starch*	*NR/modified-starch*
NR	100	100	100
Starch	0	7.5, 15, 22.5, 30	7.5, 15, 22.5, 30
PBA (grafted and ungrafted)	0	0	24% of starch
Sulphur	2	2	2
Stearic acid	1	1	1
Zinc oxide	5	5	5
Accelerator CZ	1	1	1
Accelerator DM	0.5	0.5	0.5
Antioxidant RD	1	1	1

and the grafting efficiency was 90%. The unmodified gelatinized starch paste was prepared at 80 °C and noted as PST. The starch paste was mixed with NR latex and stirred vigorously for 20 min, and then 10% calcium chloride solution was used to co-coagulate the mixture (NR/MST or NR/PST). The coagulum was washed with water and dried in an oven at 70 °C for 24 h. The starch composition was varied from 7.5, 15, 22.5 to 30 phr as shown in the formulation in Table 19.2. Compounding was carried out on a two-roll mill at 50–60 °C in a standard procedure. The rubber compound sheets were

compressed and vulcanized at 150 °C. The 15 phr starch powder filled NR composite also were carried out and labelled as NR/NST.

The mechanical properties of the unmodified starch paste (NR/PST) and the modified starch paste (NR/MST) composites with different MST loadings are examined as shown in Figure 19.3(a) to (e). NR/NST composites containing 15 phr starch powder are also shown in the diagrams as separate points. As expected, direct filling of natural starch powders caused a deterioration in the mechanical properties of NR with decreased tensile strength, tear strength and

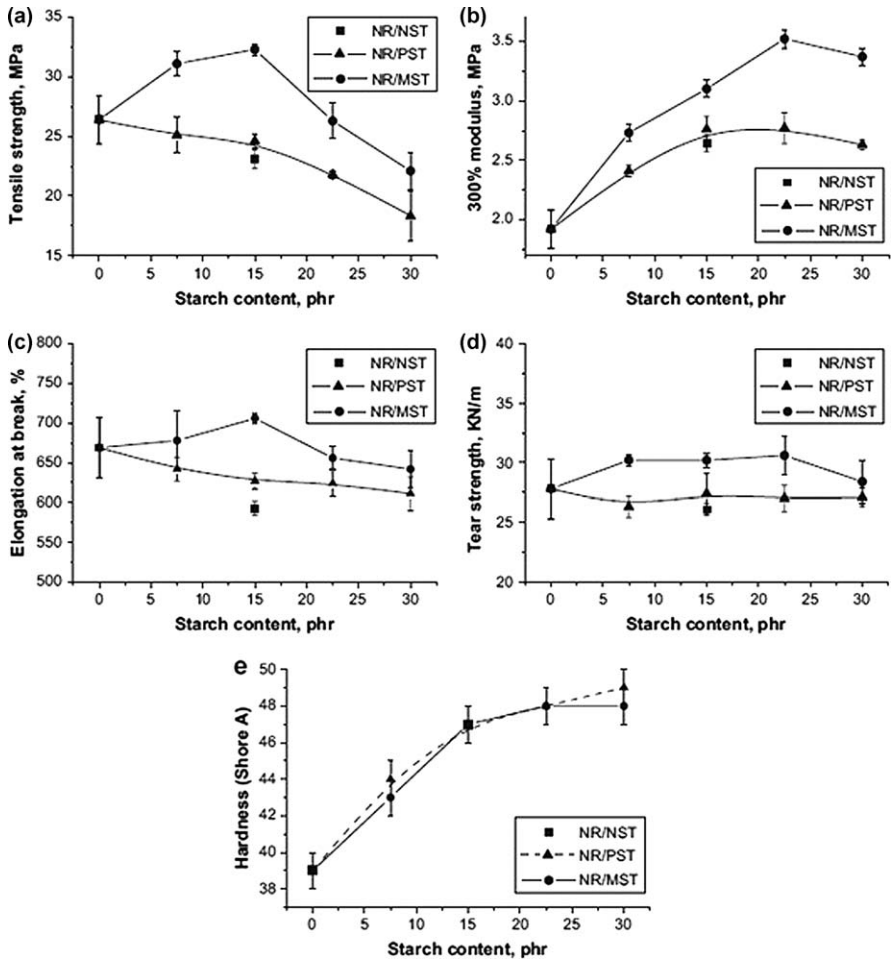

Figure 19.3 (a) Tensile strength, (b) 300% modulus, (c) elongation at break, (d) tear strength and (e) hardness (Shore A) of natural rubber composites filled with 15 phr starch powder (NR/NST), natural rubber composites filled with unmodified starch paste (NR/PST), and natural rubber composites filled with modified starch paste (NR/MST).
(Reprinted from ref. 35 with permission from Elsevier©.)

elongation at break. The NR macromolecule is hydrophobic, while starch is hydrophilic, and this phenomenon leads to the incompatibility of the two materials and hence a decrease in mechanical properties.

The addition of PST from 0 to 30 phr caused a decrease in tensile strength and elongation at break of NR composites. The addition of MST loadings up to 15 phr in NR/MST composites improved the tensile strength, 300% modulus, elongation at break and tear strength, and apart from Shore A hardness, is comparable compared to the NR/PST composites and NR/NST composites with similar amount of starch loadings. The utilization of MST improved the mechanical properties due to the addition of many PBA graft chains with partial hydrophilic carbonyl group and hydrophobic alkyl groups would distribute inside the expanded starch particles. Figure 19.4 shows the mechanism of starch grafting copolymerization with PBA. The PBA graft chains are larger and have a more irregular structure compared to the hydroxyl group and this could effectively prevent the agglomerations as well as regular packing of starch hence improving the compatibility between the NR matrix and starch.[36] NR/MST composites filled with 15 phr of modified starch showed the optimum mechanical properties compared to the unfilled NR vulcanizates. However, the mechanical properties of NR/MST composites decreased with the increase in MST filler loadings. The rapid decrease in tensile strength and elongation at break is generally ascribed to the increase in defects resulting from filler agglomerations due to their hydrophilic nature in the composites.

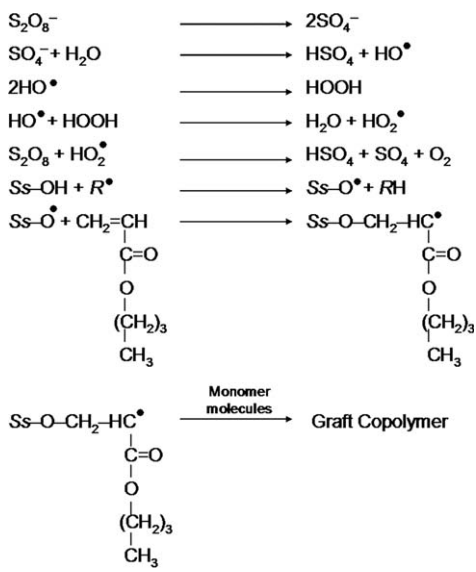

Figure 19.4 Mechanism of starch grafting copolymerization with PBA (where *Ss* indicates sago starch, $R^\bullet$ is a free-radical species such as $HO^\bullet$ and $HO_2^\bullet$).

Table 19.3 Physical properties of rice husk ash, silica and carbon black. (Reprinted from ref. 39 with permission from Wiley©.)

Properties	*BRHA*	*WRHA*	*Silica*	*Carbon Black*
Mean particle size (μm)	2.5	2.2	0.018	0.054
Surface area (m^2/g)	109	17	185	30
Density (g/cm^3)	1.9	2.0	2.0	1.9
pH	9.5	9.4	6.5	6.4

19.3.1.3 Rice Husk

Rice husk is the outer covering of paddy and accounts for 20–25% of its weight. Rice husk is characterized by low bulk density and high ash content (18–22% by weight). Silicon dioxide or so-called silica is the main component which is about 90–97% of the ash with trace amounts of CaO, MgO, K_2O and Na_2O. Therefore, rice husk ash has high potential as an alternative source for high specific area silica.[37,38]

Da Costa *et al.*[39] investigated the influences of rice husk ash loadings on the mechanical properties of NR composites. Table 19.3 shows the physical characterization of black rice husk ash (BRHA) and white rice husk ash (WRHA). The compounds were carried out using a laboratory-sized two-roll mill.

The effects of BRHA, WRHA, silica and carbon black loading on tensile properties, tear strength and hardness of NR composites were shown in Table 19.4. The addition of BRHA up to 20 phr resulted in the increased of tensile strength of NR composites. While the utilization of WRHA as filler gave a positive effect on the tensile strength of NR composites, up to 30 phr. The tear strengths of BRHA- and WRHA-filled NR composites decreased with the increasing of filler content. Despite higher silica content comparable to that of commercial silica, the utilization of rice husk especially WRHA-filled NR composite exhibited poorer tear resistance than silica- and carbon black-filled NR. The different performances resulted from the influence of surface activities, particle size, and surface area of the filler. Modulus at 300% and hardness which indicated stiffness for BRHA- and WRHA-filled NR composites were increased with increasing filler content, but the values was lower than silica-filled and carbon black-filled NR composites. Higher filler loadings are introduced into the rubber caused the decreased in elasticity of the rubber chains as shown from elongation at break values for all types of fillers in NR composites.

19.3.2 Effects of Nanosized Fillers on Mechanical Properties of Natural Rubber Composites

Nanocomposites are a relatively new class of materials, which exhibit ultra-fine phase dimensions, typically in the range 1–100 nm dispersed in the polymer matrix homogeneously.[40,41] In contrast to conventional composites, where the reinforcement is on the order of microns, polymer nanocomposites are

Table 19.4 Mechanical properties of NR composites filled with BHRA, WRHA, silica and carbon black. (Reprinted from ref. 39 with permission from Wiley©.)

Property	*Tensile Strength (MPa)*	*Elongation at Break (%)*	*Modulus at 300% (MPa)*	*Tear Strength Strength (kN/m)*	*Hardness (Shore A)*
Filler loading					
0	19.5	900	3.5	30.7	35
WRHA					
10	21.5	820	6.2	29.1	37
20	22.7	755	6.8	27.8	39
30	20.0	710	7.9	26.8	42
40	18.7	690	8.4	23.8	45
50	17.8	660	9.0	23.0	47
BRHA					
10	19.7	855	5.9	26.5	36
20	20.2	820	6.0	25.7	38
30	18.4	765	6.2	24.2	41
40	17.5	720	7.0	21.0	43
50	16.0	680	7.2	19.1	45
Carbon black					
10	23.5	750	6.0	32.7	39
20	25.2	675	8.7	35.5	44
30	23.0	620	10.4	38.9	48
40	22.4	575	11.6	42.5	52
50	21.0	530	12.5	48.7	56
Silica					
10	22.2	810	5.8	33.6	38
20	23.5	750	7.8	37.8	42
30	22.0	670	9.9	40.5	47
40	20.9	620	10.5	47.9	50
50	19.5	520	11.8	55.6	52

exemplified by discrete constituents on the order of a few nanometres. The low filler loadings can be used in polymer nanocomposites in order to retain or enhance the mechanical properties of neat polymer matrix or other polymer composites filled with conventional fillers.[42]

19.3.2.1 Carbon Nanotubes

Carbon nanotubes (CNTs) are made up of cylindrical graphite layers that are typically of nanometre diameter and many micrometres in length. CNTs have advantages in industrial applications due to the low loading required to achieve comparable conventional composite properties. CNTs are very promising for their outstanding mechanical properties along with high thermal and electrical conductivities. However, the neat CNT is its inherently weak interactions with the matrix polymers because the graphite does not have the functional groups required to promote filler–polymer interactions in the CNT/rubber composites.

CNT can be treated using purification process by exposing them to strong oxidizing acids to introduce hydroxyls and carboxyl groups on the CNT surface thus can interact with unsaturated carbon bonds of the elastomers.[43–45]

Sui *et al.*[46] investigated on the properties of NR composites reinforced with pre-treated CNTs. The CNT used in the experiments were prepared by chemical vapour deposition (CVD) of propylene gas at 700 °C using nickel as a catalyst. The diameters of CNT vary from 20 to 50 nm, and lengths vary from 100 to 1 μm. The incorporation of treated CNT into NR was carried out by a solvent mixing method. Several important physical and mechanical properties of the gum vulcanizates, CNT/NR, and CB/NR composites are listed in Table 19.5. Compared to the gum vulcanizates and CB/NR composites, the addition of 25 phr CNT loadings bring about remarkable increase in hardness, tensile modulus and tensile strength of NR nanocomposites. The rebound resilience and dynamic compression properties of the CNT/NR nanocomposites are better than that of CB-filled NR composites. From the fracture morphology of CNT/NR nanocomposites as shown in Figure 19.5, there are no obvious aggregates of treated CNT in the rubber matrix. A few outcrops of the CNT existed on the fracture surface, which indicated that the strong interaction

Table 19.5 The mechanical properties of NR composites filled with CNTs and carbon black as filler. (Reprinted from ref. 46 with permission from Wiley©.)

Samples	*NR*	*CNT/NR*	*CB/NR*
Hardness (Shore A)	41 ± 2	63 ± 2	54 ± 2
Modulus at 300% (MPa)	1.8 ± 0.2	12.5 ± 0.3	9.5 ± 0.3
Tensile strength (MPa)	7.2 ± 0.6	24.8 ± 2.0	22.5 ± 1.8
Elongation at break (%)	680 ± 20	495 ± 15	480 ± 20
Rebound degree (%)		73 ± 2	54 ± 3
Goodrich compression permanent set (%)		12.5 ± 0.3	13.5 ± 0.5
Goodrich compression heat accumulation (°C)		3.2 ± 0.3	4.4 ± 0.3

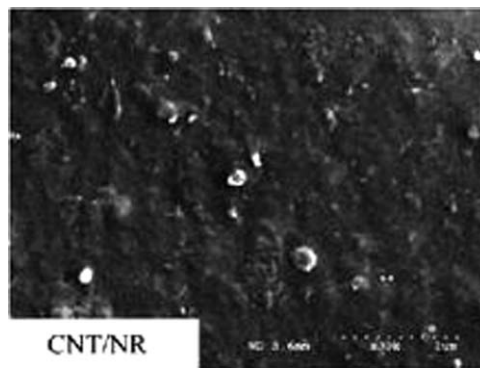

Figure 19.5 SEM micrograph of CNT/natural rubber nanocomposites. (Reprinted from ref. 46 with permission from Wiley©.)

between the CNT and the rubber macromolecules resulted in an increase of the mechanical properties of CNT/NR composites.

19.3.2.2 Halloysite Nanotubes (HNTs)

Halloysite is a unique and versatile nanomaterial composed of a double layer of aluminium, silicon, hydrogen and oxygen, which has a predominantly hollow tubular structure with the chemical composition $Al_2(OH)_4$-$Si_2O_5(2H_2O)$. It is a naturally occurring nanotube which is used as a reinforcing filler for polymer composites due to its rigidity and the unique crystal structure of HNTs resembles that of CNTs in terms of aspect ratio. However, HNTs are more cost-effective than CNTs and can be mined from deposits as a raw material.[47–49] HNTs contain two types of hydroxyl groups, inner and outer hydroxyl groups. Most of the hydroxyl groups are inner groups and only a few hydroxyl groups are located on the surface due to the multilayer structure of HNTs as illustrated in Figure 19.6.[50,51] Compared to other silicates such as kaolinite and montmorillonites, the density of surface hydroxyl groups of HNTs is much smaller. HNTs are readily obtainable, are much cheaper than other nanofillers such as CNTs and are biocompatible.[52] In addition, only traces of heavy metals were detected and can be classified as green, non-toxic and biocompatible material. It has a fine particle size, high surface area, good dispersion, high aspect ratio, high porosity and non-swelling.

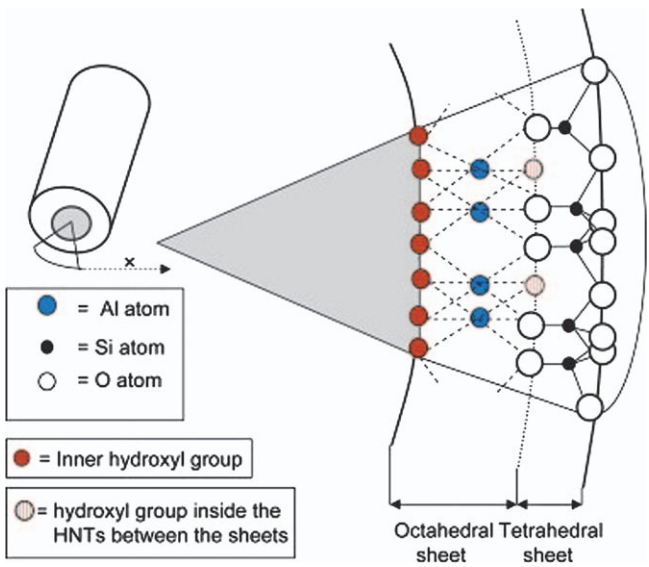

Figure 19.6 Crystalline structure of HNTs.
(Reprinted from ref. 50 with permission from Elsevier©.)

The mechanical properties of natural nanocomposites based on NR and naturally occurring HNTs were studied by Rooj *et al.*[53] NR, used in their study is Standard Malaysian Rubber. The halloysite used possessed an average tube diameter of 50 nm and inner lumen diameter of 15 nm. Typical specific surface area of this halloysite was 65 m^2/g; pore volume of 1.25 mL/g; refractive index 1.54; and specific gravity 2.53 g/cm^3. The HNT-filled NR composite was also treated with silane coupling agent, Si-69 to improve the compatibility with NR and compared to the silica-filled NR composites. All NR composites prepared containing 10 phr of filler loadings. The compounding of NR with HNT and silica including other ingredients such as zinc oxide, stearic acid, ZDMC and sulfur was done on a laboratory-sized two-roll mill (Polymix 110L, friction ratio was 1 : 1.25, roll temperature was 40 °C. The rubber samples were then cured until their optimum curing time (t_{90}) by a hot press at 160 °C.

The mechanical properties of the control NR composite, untreated HNT-filled NR nanocomposite, treated HNT-filled NR nanocomposite, and silica-filled NR composite are tabulated in Table 19.6. The addition of 10 phr HNT loading increased the tensile modulus and tensile strength compared to the neat NR vulcanizate. However, the values of elongation at break of the HNT filled rubber nanocomposite were decreased in comparison to the unfilled NR vulcanizate. The silica filled NR vulcanizate showed inferior properties as comparison to HNT filled nanocomposites. It is well known that the modulus of rubber vulcanizates is proportional to the degree of crosslink density. Therefore, modulus of rubber vulcanizates increased with the increased of crosslink density. In contrast, the elongation at break decreased with increasing crosslink density.

Figure 19.7 shows the proposed schematic of a chemical reaction between HNT and Si-69 as a coupling agent. Hydroxyl groups present on the surface of HNT can react with the silane coupling agent, typically known as a silanization reaction. It is well known that the S–S bond strength is quite low and can be broken during mixing, forming sulfur radicals. The sulfur radicals will further react with the unsaturation present in NR. Therefore, the silane coupling agent (Si-69) can form a bridge between the HNT and rubber molecules.

Table 19.6 Mechanical properties of HNT-filled NR nanocomposites. (Reprinted from ref. 53 with permission from Elsevier©.)

Sample	*200% modulus (MPa)*	*300% modulus (MPa)*	*Tensile strength (MPa)*	*Elongation at break (%)*	*Cross-link density (mol/cm^3)*
NR	0.83	1.12	14	1496	4.0×10^{-5}
NR-HNT	1.12	1.54	18	1270	5.1×10^{-5}
NR-HNT-Si69	1.24	2.18	15	1050	6.4×10^{-5}
NR-Sil-Si69	1.03	1.41	12	996	5.7×10^{-5}

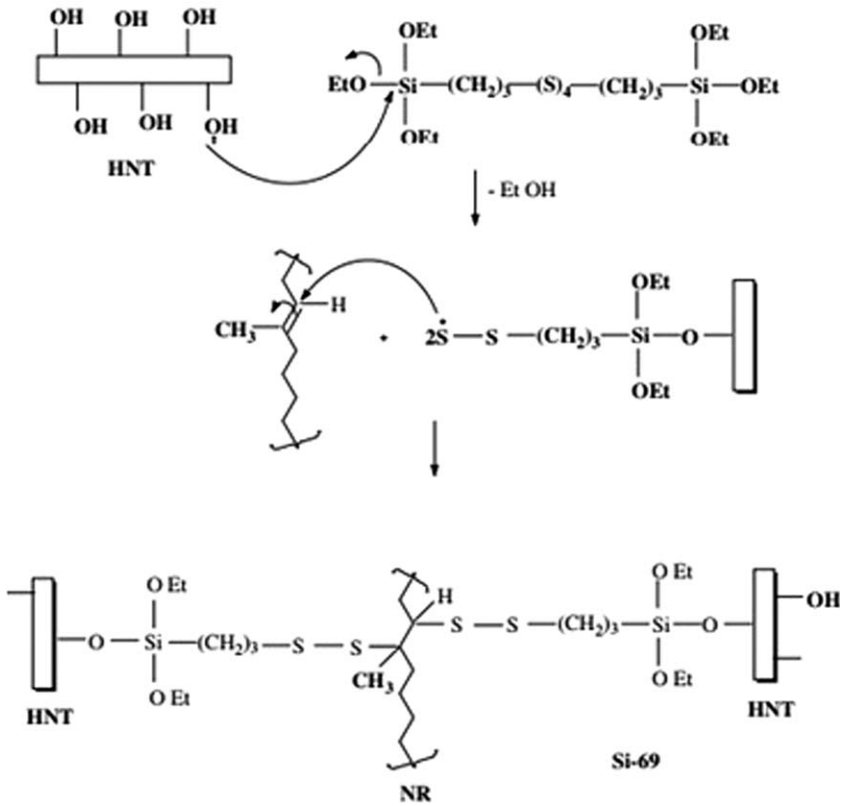

Figure 19.7 Schematic chemical reaction between halloysite nanotubes and natural rubber with bis(triethoxysilylpropyl)-tetrasulfide (Si-69) coupling agent. (Reprinted from ref. 53 with permission from Elsevier©.)

19.3.2.3 Nanoclays

The interest in clay–polymer nanocomposites has been developed and being incorporated into polymeric composites in order to enhance the performance of the materials. The clay minerals are the most abundant minerals on the surface of the earth. Their crystal structure consists of two-dimensional layers formed by fusing two silica tetrahedral sheets with an edge-shared octahedral sheet of either alumina or magnesia. The stacking of the platelets leads to a van der Waals gap orgallery between the platelets. There are generally two types of structures for polymer–clay composites, intercalated and exfoliated. In the intercalated structure, a single (sometimes more than one) extended polymer chain is intercalated between the clay platelets, resulting in a well-ordered multilayer morphology built up with alternating polymeric layer and clay platelet. In the exfoliated structure, the clays are completely and uniformly dispersed in a continuous polymer matrix. The most commonly used clay is montmorillonite (MMT) with a platelet thickness of approximately

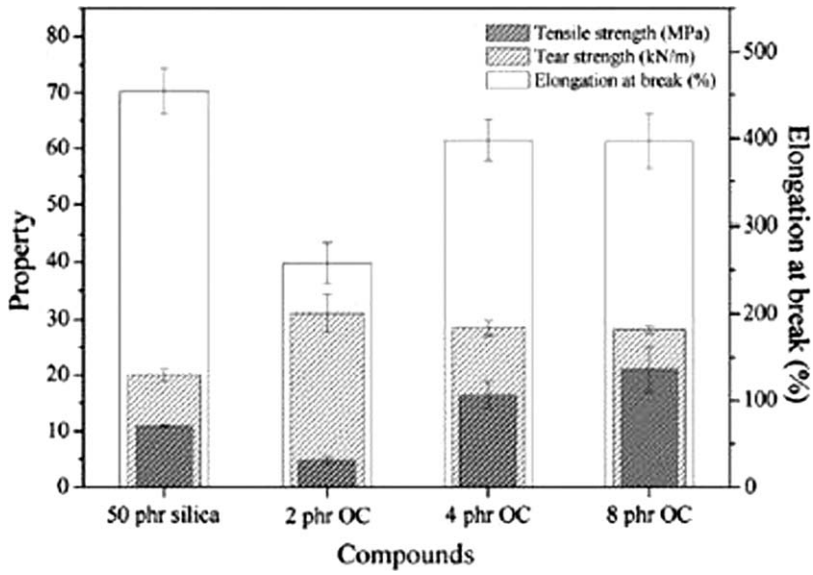

Figure 19.8 Mechanical properties of different filler loadings of organoclay and 50 phr silica-filled natural rubber composites.
(Reprinted from ref. 56 with permission from Elsevier©.)

1 nm which lead to the extremely large surface area, and a high aspect ratio.[41,54,55]

Carli *et al.*[56] investigated on the effect of organoclay (OC) as filler in NR nanocomposites. The NR and Cloisite 15A®, a natural montmorillonite modified with 30 wt% of a quaternary ammonium salt with a cation exchange capacity of 125 meq/100 g clay were used as main materials in OC filled NR nanocomposites. Three organoclay/NR nanocomposites were prepared while varying the loadings of OC (2, 4 and 8 phr). In addition, 50 phr of Zeosil® silica-filled NR composites were prepared to compare the properties with the rubber nanocomposites. All compounds were carried out using two-roll mill method. Figure 19.8 shows the mechanical properties of the NR compounds. The NR nanocomposites showed an increase in tensile strength and elongation at break percentages with the increasing in OC loadings in the rubber matrix.

For 4 and 8 phr of OC loadings, tensile strength values of rubber nanocomposites were higher than the compound containing silica. This effect could be related to good dispersion and a strong interaction between the clay interface and the elastomeric matrix. Notably, the increase in tensile properties by the addition of the OC occurred without any loss of elongation at the break of the material. All organoclay filled NR nanocomposites exhibited greater tear strength than the silica compound. This outcome was attributed from high loading silica which it tend to agglomerate in hydrophobic rubber matrix resulted in poor rubber–filler interactions as well as poor filler dispersion.

In addition, the layer structure of the clay in the nanocomposite can strongly restrict the motion of rubber molecules and hinders the propagation of the crack during tearing.[57] These results indicate that 50 phr of silica can be replaced by 4 phr of OC with a reduction of the filler content by 12.5 times without adversely affecting the final properties of the material. The enhancement of the mechanical properties is due to the better dispersion of OC in the NR matrix and strong rubber–filler interaction.

19.3.3 Effects of Hybrid Fillers on Mechanical Properties of Natural Rubber Composites

Recently, a method of incorporating combination different types of fillers simultaneously into the rubber matrix has been put forward. The hybrid filler composites were developed in manufacturing industry for various reasons including to meet specific processing and performance requirements which cannot be satisfied using single component, scientific interests to develop new materials with a unique material property characteristic; and financial or economic advantages.[58]

Hybrid filler composites can be undertaken using the combination of similar or different types of fillers. Each type of fillers consist different grades which provide their own advantages and disadvantages. The utilization of fillers combination with similar size will limits the qualities achieved in the rubber vulcanizates. The incorporation of the carbon black with different grades as hybrid fillers in rubber compounds have improve rubber product with good compression and resilience characteristics generally attributed from the use of large carbon black particles in a rubber while retaining the good elongation, modulus, tear and tensile strength attributable to the presence of small carbon black particles. The utilization of unique carbon black hybrid fillers can produce a rubber composition with a combination of the optimum qualities of the large and small particles.[59]

19.3.3.1 Carbon Black/Nanobarite

Recent work by Zhao *et al.*[60] investigated the reinforcement NR/carbon black/nanobarite nanocomposites (NR/CB/NB) prepared by mechanical compounding. The materials used basically is NR (SCR 5L), carbon black (N220), SA-Al_2O_3-NB refers to unmodified nanobarite with a specific surface area of approximately 35.69 m^2/g and an average primary particle size of 40–50 nm that was firstly modified by sodium aluminate to construct an inorganic Al_2O_3 layer and then modified by sodium stearate to form an organic layer to improve the surface hydrophobicity. 0, 2, 4, 6 and 8 phr of SA-Al_2O_3-NB loadings were added into the control NR containing with 45 wt% of carbon black. The rubber nanocomposites were prepared in open two-roll mill under room temperature. The compounds were left for 24 hours and then moulded in an electrically heated hydraulic press at 150 °C.

Figure 19.9 shows the tensile strength, tear strength, abrasion loss and 300% modulus of NR/CB/SA-Al_2O_3-NB with different SA-Al_2O_3-NB loadings. It was concluded that the optimum mechanical properties of CB/SA-Al_2O_3-NB filled NR composites at the ratio of 45/2. In comparison with NR/CB (100/45), the tensile strength, tear strength, 300% modulus and abrasion resistance of NR/CB/SA-Al_2O_3-NB (100/45/2) were increased by 10.5%, 5.9%, 2.5% and 26.1%, respectively. Among the static mechanical properties, the abrasion resistance of the NR nanocomposites was remarkable. When the SA-Al_2O_3-NB

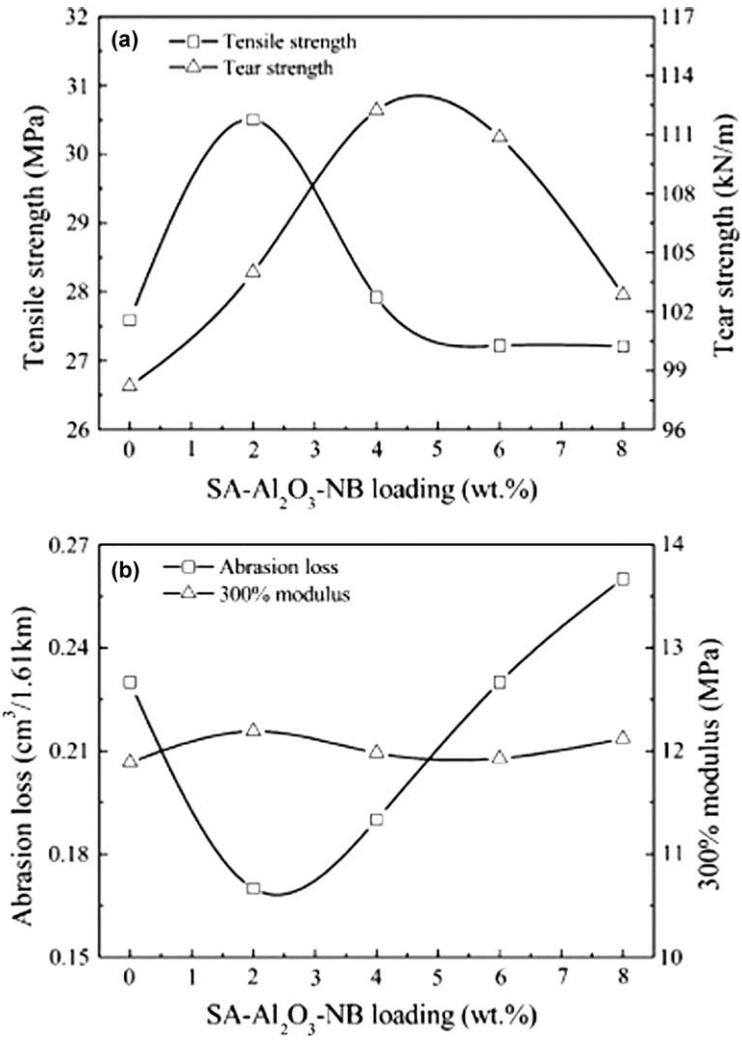

Figure 19.9 Mechanical properties of NR/CB/SA-Al_2O_3-NB with different SA-Al_2O_3-NB loadings: (a) tensile and tear strength and (b) abrasion loss and 300% modulus.
(Reprinted from ref. 60 with permission from Elsevier©.)

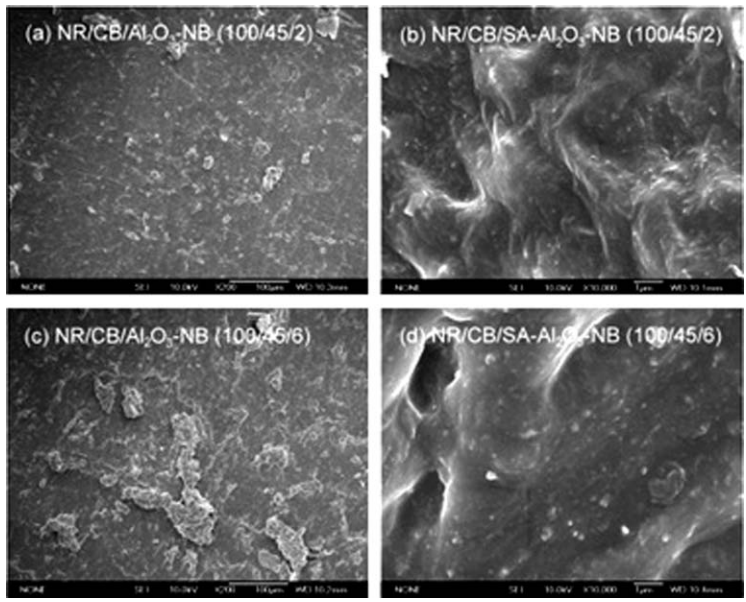

Figure 19.10 Morphology analysis (SEM) of abrasion surfaces of NR/CB/SA-Al_2O_3-NB with different SA-Al_2O_3-NB loadings: (a) NR/CB/SA-Al_2O_3-NB (100/45/2), (b) NR/CB/SA-Al_2O_3-NB (100/45/2), (c) NR/CB/SA-Al_2O_3-NB (100/45/6), (d) NR/CB/SA-Al_2O_3-NB (100/45/6). (Reprinted from ref. 60 with permission from Elsevier©.)

loading was 2 wt%, the abrasion loss reached its minimum value. Further addition of SA-Al_2O_3-NB increased the abrasion loss. Figure 19.10 shows the SEM results of the abrasion surfaces for NR/CB/SA-Al_2O_3-NB at high and low magnification. The NR/CB/SA-Al_2O_3-NB with ratio of 45/2 of carbon black and nanobarite loading exhibited a smooth abrasion surface (Figure 19.10(a)) and it was proved that at high magnification, the homogeneous dispersion of fillers in NR composites were observed (Figure 19.10(b)). During the abrasion test, uniformly dispersed SA-Al_2O_3-NB and CB particles were transmitted to the abrasion surface and contributed to a decrease in abrasion loss due to strong polymer–filler adhesion. While the NR/CB/SA-Al_2O_3-NB (100/45/6) exhibited a relatively coarse abrasion surface, loose fragments and grains worn away from the matrix (Figure 19.10(c)), and at high magnification, the holes and filler aggregates were found on the rubber composite surface (Figure 19.10(d)). In contrast, at higher filler loading, the filler aggregates were pulled out from the matrix and hence formed holes, which resulted in an increase in abrasion loss.

19.3.3.2 Silica/Clay

Ogbebor *et al.*[61] used clay which air dried at 49 ± 5 °C, pulverized and sieved through mesh size 300 μm and silica (Vulkasil S) with particle size around

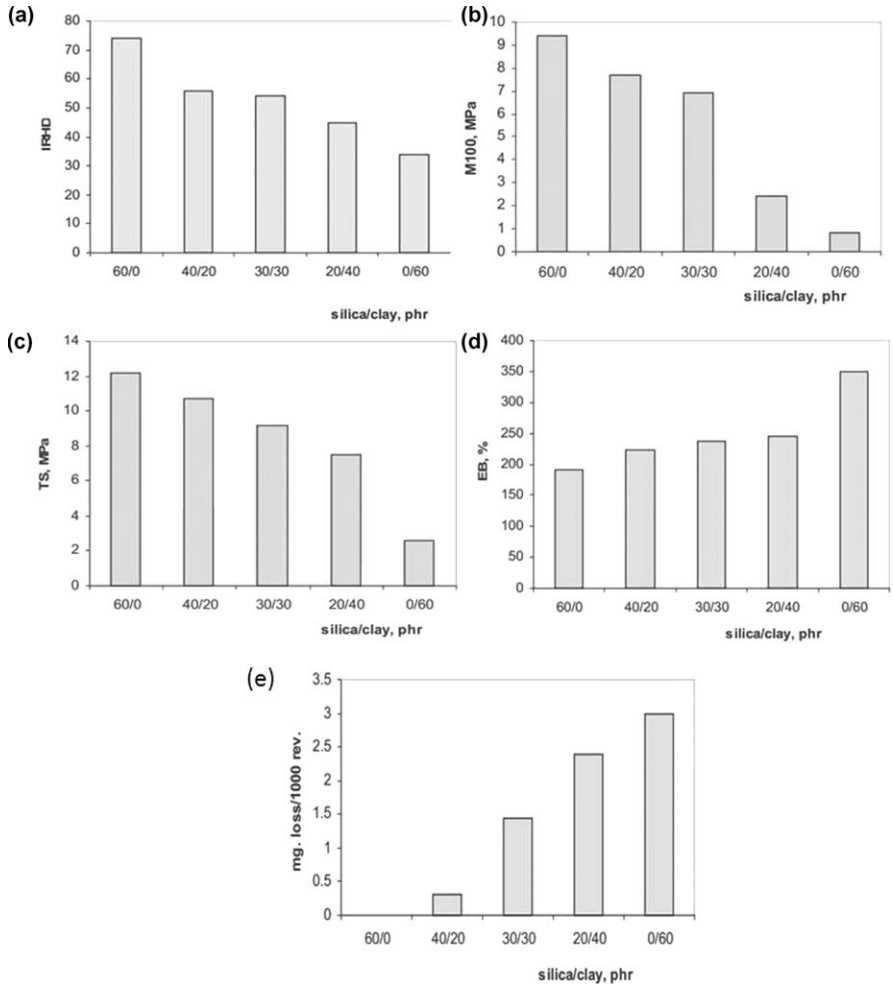

Figure 19.11 Effect of silica/clay filler loadings on (a) hardness, (b) tensile modulus, M100, (c) tensile strength, (d) elongation at break (%) and (e) abrasion loss of natural rubber composites.
(Reprinted from ref. 61 with permission from the Association of the Chemical Engineers of Serbia©.)

30 nm as hybrid fillers in NR mixed by a laboratory-sized two-roll mill. The mechanical properties which are hardness, tensile properties and abrasion resistance were carried out on silica/clay filled NR composites. The mechanical properties of silica/clay filled NR composites used in this investigation are shown in Figures 19.11(a) to (e). Initially, the silica acts as a reinforcing filler in NR composites. However, the partial replacement of clay in hybrid filler composites showed a decrease in hardness (Figure 19.11(a)), tensile modulus (Figure 19.11(b)) and tensile strength (Figure 19.11(c)). The reduction in the

reinforcing properties of silica/clay filled NR composites was due to the effect of particle size of filler. As mentioned earlier, clay has a larger mean particle size compared to silica. Therefore, a large mean particle size reduced the surface contact area, thus decreasing the surface activities of filler as well as the strength of the rubber composites. However, the addition of clay improved the extension of the rubber composites where the increased elongation at break of silica/clay filled NR composites were observed in Figure 19.11(d). The low rigidity of clay resulted in poorer abrasion resistance of silica/clay filled NR composites as the clay loadings increased, as shown in Figure 19.11(e).

19.3.3.3 Fly Ash/Silica

Thongsang *et al.*[62] examined the properties of fly ash/precipitated silica-filled NR vulcanizates. NR used is grade STR20. The silica hybrid filler in this work consisted of mixtures of fly ash silica (FASi) and precipitated silica (PSi). The major component of FASi was silicon dioxide, at 33.5%. The silica content of FASi added to the rubber compounds based on the fly ash chemical composition. Fly ash with the particle sizes of 25 mm and 45–74 mm were studied. The precipitated silica used was Hi-Sil 233-S which had a pH of 6.8, a bulk density of 0.235 g/cm^3, and a surface area of 128 m^2/g. The total silica contents filled into the NR compounds were 10 and 40 phr for low and high total silica loadings, respectively. The FASi:PSi ratios used were 100 : 0, 75 : 25, 50 : 50, 25 : 75 and 0 : 100.

Table 19.7 shows the mechanical properties of NR composites filled with varied PSi fractions in FASi/PSi hybrid filler. 100% of PSi showed better tensile modulus (M300), tensile strength, elongation at break, tear strength, and abrasion resistance compared to FASi. However, the utilization of 100% fly ash fraction gave improved the hardness of NR composites compared to PSi and this indicated that FASi has high rigidity. The increased of filler loading in NR composites enhanced the tensile modulus and the hardness values, but decreased the elongation at break percentages and abrasion resistance. The smaller particle size of FASi improved the mechanical properties of NR composites due to the increased in surface area and thus provided better interaction with rubber matrix. The additions of PSi in NR matrix basically increased the tensile strength, tear strength, and abrasion resistance of the composites, while the utilization of FASi showed the opposite behaviour. This phenomenon indicated that FASi is non-reinforcing filler and this limitation can be improved by incorporating both of PSi and FASi as hybrid filler in NR composites.

As expected, the addition of high PSi loadings and minimize the FASi content in hybrid filler system increased the tensile properties, tear strength, and abrasion resistance of NR composite. The incorporation of smaller particle size of FASi gave a slight increase in tensile modulus and hardness of NR composites filled with hybrid filler. Overall, the optimum mechanical properties of hybrid filler composites were obtained at 5/75 FASi/PSi of 40 phr filler loadings.

Table 19.7 Mechanical properties of FASi/PSi-filled NR composites with different PSi weight fractions. (Reprinted from ref. 62 with permission from Elsevier©.)

Properties	*Total silica content (phr)*	*FASi particle size (μm)*	*Weight fraction of PSi (%)*				
			0	*25*	*50*	*75*	*100*
Modulus at 300% elongation (MPa)	10	45–74	2.4 ± 0.1	2.6 ± 0.2	2.5 ± 0.1	3.0 ± 0.3	3.3 ± 0.1
	40	<25	5.5 ± 0.8	6.4 ± 0.1	6.8 ± 0.2	6.3 ± 0.1	5.9 ± 0.1
		45–74	4.1 ± 0.2	4.4 ± 0.1	5.5 ± 0.1	5.9 ± 0.1	5.9 ± 0.1
Tensile strength (MPa)	10	45–74	17.6 ± 0.7	17.5 ± 1.2	17.5 ± 0.3	19.9 ± 1.0	21.7 ± 1.1
	40	<25	10.4 ± 0.7	12.6 ± 0.5	15.3 ± 1.7	19.5 ± 0.4	24.0 ± 1.0
		45–74	8.2 ± 0.4	10.7 ± 0.1	14.0 ± 0.5	18.3 ± 0.5	24.0 ± 0.1
Elongation at break (%)	10	45–74	782.9 ± 17.4	776.2 ± 14.9	761.2 ± 3.4	794.3 ± 10.9	869.0 ± 29.0
	40	<25	527.7 ± 22.1	507.5 ± 8.4	556.9 ± 14.0	629.0 ± 22.0	711.1 ± 9.0
		45–74	515.7 ± 16.3	547.6 ± 14.8	553.5 ± 7.3	633.2 ± 6.4	711.1 ± 9.0
Tear strength (MPa)	10	45–74	26.3 ± 1.1	33.8 ± 3.0	35.0 ± 2.6	38.1 ± 2.1	40.0 ± 2.2
	40	<25	24.2 ± 1.9	26.6 ± 1.2	31.9 ± 2.0	59.8 ± 5.7	91.7 ± 8.4
		45–74	21.5 ± 1.0	30.2 ± 1.8	35.6 ± 1.9	57.9 ± 3.5	91.7 ± 8.4
Hardness shore A	10	45–74	45.5 ± 0.6	41.3 ± 0.3	42.2 ± 0.3	42.3 ± 0.3	41.3 ± 0.3
	40	<25	59.0 ± 2.0	60.4 ± 0.6	60.2 ± 1.5	63.7 ± 0.8	63.1 ± 0.7
		45–74	58.5 ± 0.6	57.5 ± 0.7	56.5 ± 0.7	62.8 ± 0.4	63.1 ± 0.7
Volume loss (mm^3)	10	45–74	49.6 + 2.5	39.4 + 2.0	39.8 + 2.0	33.8 + 1.7	22.0 + 1.1
	40	<25	65.1 ± 3.3	46.6 ± 2.3	44.2 ± 2.2	33.4 ± 1.7	30.0 ± 1.5
		45–74	78.6 ± 3.6	58.2 ± 2.9	43.4 ± 2.2	37.4 ± 1.9	30.0 ± 1.5

19.4 Conclusions

The mechanical properties of NR composites are strongly influenced by the particle size, surface area, and surface activities of fillers. Recently, many types of natural fillers such as palm ash, starch, rice husk, and clays were proposed in order to overcome the environmental issues. The rigid and macro particle size of fillers basically enhanced the tensile modulus and hardness of NR composites. However, the properties such as tensile strength, elongation at break, and tear strength decreased with the increased of filler loadings due to low surface area and surface activities. Several natural fillers are hydrophilic in nature thus contributed to the poor dispersion of filler in NR matrix which it has hydrophobic macromolecules. Some natural filler such as rice husk has potential to replace conventional silica where it showed the increment of tensile strength of composites although it still inferior compared to silica-filled NR composites. A few methods can be applied to reduce the hydrophilicity of fillers and it was reported that the modified filler could improve the tensile strength, elongation at break, tear strength, tensile modulus and hardness of NR composites due to better compatibility and dispersibility. Recent nanotechnology application gained interest for researchers to investigate the influences of nanosized filler on NR composites properties. Most researchers reported that the use of nanoparticle sized fillers improved the tensile properties, tear strength and set resistance with less loss of elasticity of materials compared to NR composites filled with macrosized filler. The main purpose of using at least two types of fillers in NR composites is not to increase the mechanical properties eventually but to obtain the optimum overall properties contributed from different fillers with reasonable production cost.

References

1. S. Burtscher, A. Dorfmann and K. Bergmeister, PhD Symposium, Vienna, 1998, 1–7.
2. C. A. Harper, *Handbook of Plastics, Elastomers and Composites*. 4th ed. New York, McGraw-Hill, 2002.
3. C. Nakason, A. Kaesaman and K. Eardrod, *Mater. Lett.*, 2005, **59**, 4020.
4. A. R. Azura and A. G. Thomas, *Elastomer and components: Service life prediction – progress and challenges*, Woodhead Publishing in Materials, 2006, 27–38.
5. W. Arayapranee, N. Naranong and G. L. Rempel, *J. Appl. Polym. Sci.*, 2005, **98**, 34.
6. P. Sae-Oui, C. Sirisinha and P. Thantong, *J. Mater. Cycles Waste Manage.*, 2009, **11**, 166.
7. M. A. Taha, A. M. El-Sabbagh and I. M. Taha, *Key Eng. Mater.*, 2010, **425**, 61.
8. A. R. Azura, G. Suriati and M. Mariatti, *J. Appl. Polym. Sci.*, 2008, **110**, 747.

9. Esposito, *Rubber Engineering*. India: McGraw-Hill, 1998.
10. H. Angellier, L. Choisnard, S. Molina-Boisseau, P. Ozil and A. Dufresne, *Biomacromolecules*, 2004, **5**, 1545.
11. D. E. El-Nashar, S. H. Mansour and E. Girgis, *J. Mater. Sci.*, 2006, **41**, 5359.
12. G. Marćovi, M. Marinović-Cinović, B. Radovanović and J. Budinski Simendić, *Chem. Ind. Chem. Eng. Q.*, 2007, **13**, 186.
13. P. A. Ciullo, *Industrial Minerals and Their Uses – A Handbook and Formulary*, Norwich, NY: William Andrew Publishing, 1996.
14. G. R. Hamed, in *Engineering with Rubber – How to Design Rubber Components*, ed. A. N. Gent, Hanser, New York, 1992, pp. xx–xx.
15. J. V. Accorsi, International Wire and Cable Symposium, 1999, 1–8.
16. J. Frohlich, W. Niedermeier and H. D. Luginsland, *Composites, Part A*, 2005, **36**, 449.
17. G. Heinrich and M. Klüppel, *Adv. Polym. Sci.*, 2005, **160**, 1.
18. J. Liu, C. Wu, P. Zhang and S. Zhao, *J. Macromol. Sci., Part B: Phys.*, 2008, **47**, 689.
19. P. Pasbakhsh, H. Ismail, M. N. Ahmad Fauzi and A. A. Bakar, *J. Appl. Polym. Sci.*, 2009, **113**, 3910.
20. C. Sung-Seen, *Polym. Adv. Technol.*, 2002, **13**, 466.
21. A. Hasse, A. Wehmeier and H. D. Luginsland, *Crosslinking and Reinforcement of Silica/Silane-Filled Rubber Compounds*, Rubber World Magazine's Electronic Publishing Division, Akron, Ohio, 2004.
22. D. Fortin and M. A. Vargas, *J. Am. Dent. Assoc.*, 2000, **131**, 268.
23. M. R. Ali, S. B. Jamaludin, A. Z. Nur Hidayah and C. M. Ruzaidi, *Aust. J. Basic Appl. Sci.*, 2011, **5**, 291.
24. A. R. Mohamed, K. T. Lee, N. Mohamed Nor and N. F. Zainudin, *Chem. Eng. Technol.*, 2005, **28**, 939.
25. H. Ismail and F. S. Haw, *J. Appl. Polym. Sci.*, 2008, **110**, 2867.
26. H. Ismail, N. Rosnah and H. D. Rozman, *Polymer*, 1997, **38**, 4059.
27. A. E. C. Peres and M. I. Correa, *Miner. Eng.*, 1996, **9**, 1227.
28. A. Buléon, P. Colonna, V. Planchot and S. Ball, *Int. J. Biol. Macromol.*, 1998, **23**, 85.
29. N. Lin, J. Huang, P. R. Chang, D. P. Anderson and J. Yu, *J. Nanomater.*, 2011, **20**, 1–13.
30. S. Pavlovic and P. R. G. Brandao, *Miner. Eng.*, 2003, **16**, 1117.
31. Q. Liu, Y. Zhang and J. S. Laskowski, *Int. J. Miner. Process.*, 2000, **60**, 229.
32. S. Taghvaei-Ganjali, F. Motiee, E. Shakeri and A. Abbasian, *J. Appl. Chem. Res.*, 2010, **4**, 53.
33. D. Le Corre, J. Bras and A. Dufresne, *Biomacromolecules*, 2010, **11**, 1139.
34. H. Tang, T. Mitsunaga and Y. Kawamura, *Polymer*, 2006, **63**, 555.
35. C. Liu, Y. Shao and D. Jia, *Polymer*, 2008, **49**, 2176.
36. Q. Qi, Y. P. Wu, M. Tian, G. H. Liang, L. Q. Zhang and J. Ma, *Polymer*, 2006, **47**, 3896.
37. A. Bharadwaj, V. S. Arunachalam, S. Sridhar and Y. Wang, *Curr. Sci.*, 2004, **87**, 981.

38. V. P. Della, *Mater. Lett.*, 2002, **57**, 818.
39. H. M. Da Costa, L. L. Y. Visconte, R. C. R. Nunes and C. R. G. Furtado, *J. Appl. Polym. Sci.*, 2002, **83**, 2331.
40. N. Salahuddin, A. Moet, A. Hiltner and E. Baer, *Eur. Polym. J.*, 2002, **38**, 1477.
41. J. M. Hwu, G. J. Jiang, Z. M. Gao, W. Xie and W. P. Panthe, *J. Appl. Polym. Sci.*, 2002, **83**, 1702.
42. E. W. Gacitua, A. A. Ballerini and J. Zhang, *Cienc. Tecnol.*, 2005, **7**, 159.
43. M. S. Dresselhaus, G. Dresselhaus, J. C. Charlier and E. Hernández, *Philos. Trans. R. Soc., A*, 2004, **362**, 2065.
44. S. Agnelli, G. Ramorino, S. Passera, J. Karger-Kocsis and T. Riccò, *Polym. Lett.*, 2012, **6**, 581.
45. L. D. Perez, M. A. Zuluaga, T. Kyu, J. E. Mark and B. L. Lopez, *Polym. Eng. Sci.*, 2009, **49**, 866.
46. G. Sui, W. H. Zhong, X. P. Yang, Y. H. Yu and S. H. Zhao, *Polym. Adv. Technol.*, 2008, **19**, 1543.
47. W. O. Yah, A. Takahara and Y. M. Lvov, *J. Am. Chem. Soc.*, 2012, **134**, 1853.
48. K. Prashantha, M. F. Lacrampe and P. Krawczak, *Polym. Lett.*, 2011, **5**, 295.
49. P. Pasbakhsh, H. Ismail, M. N Ahmad Fauzi and A. Abu Bakar, *Appl. Clay Sci.*, 2010, **48**, 405.
50. P. Pasbakhsh, H. Ismail, M. N. Ahmad Fauzi and A. Abu Bakar, *Polym. Test.*, 2009, **20**, 548.
51. M. Du, B. Guo and D. Jia, *Polym. Int.*, 2010, **59**, 574.
52. V. Vergaro, E. Abdullayev, Y. M. Lvov, A. Zeitoun, R. Cingolani, R. Rinaldi and St. Leporatti, *Biomacromolecules*, 2010, **11**, 820.
53. S. Rooj, A. Das, V. Thakur, R. N. Mahaling, A. K. Bhowmick and G. Heinrich, *Mater. Des.*, 2010, **31**, 2151.
54. N. Gupta, T. C. Lin and M. Shapiro, *J. Miner. Met. Mater. Soc.*, 2007, **59**, 61.
55. L. Zhu and K. A. Narh, *J. Appl. Polym. Sci.: Polym. Phys.*, 2004, **42**, 2391.
56. L. N. Carli, C. R. Roncato, A. Zanchet, R. S. Mauler, M. Giovanela, R. N. Brandalise and J. S. Crespo, *Appl. Clay Sci.*, 2011, **52**, 56.
57. Y. Liang, W. Cao, Z. Li, Y. Wang, Y. Wu and L. Zhang, *Polym. Test.*, 2008, **27**, 270.
58. M. B. A. Bakar, Y. W. Leong, A. Ariff and Z. A. Mohd Ishak, *J. Appl. Polym. Sci.*, 2007, **104**, 434.
59. D. W. Carlson and W. D. Breach, *Carbon Black Pair with Different Particle Size and Improved Rubber Stock*, US Patent 5430087, 1995.
60. G. Zhao, L. Shi, D. Zhang, X. Feng, S. Yuan and J. Zhuo, *Mater. Des*, 2012, **35**, 847.
61. O. J. Ogbebor, U. N. Okwu, F. E. Okieimen and D. Okuonghae, *Chem. Ind. Chem. Eng. Q*, 2010, **16**, 373.
62. S. Thongsang, W. Vorakhan, E. Wimolmala and N. Sombatsompop, *Tribol. Int.*, 2012, **53**, 134.

CHAPTER 20

Linear and Non-Linear Viscoelastic Behaviour of Natural Rubber Composites from Micro- to Nanoscales

ROBERT A. SHANKS

Applied Sciences, RMIT University, GPO Box 2476 Melbourne, Victoria 3001, Australia
Email: Robert.shanks@rmit.edu.au

20.1 Introduction

The linear viscoelastic range of stress is where the strain response is incremented in the same ratio as the stress, such as doubling the stress doubles the strain. Linear viscoelastic polymers will have low internal friction corresponding to weak intermolecular interactions, asymmetrical molecular configuration to resist crystallizing under strain and absence of molecular motion restricting components.

Non-linear viscoelasticity begins at strains where generally an increasing stress is required for each increment in strain. Strain increases involve more variables than uncoiling of macromolecules. Rigid groups in the molecular chain or pendant from it may interrupt reversible extension of random coils. Strain hardening due to fully extended chain segments between crosslinks and crystallization of extended chain segments creates non-linearity at higher extensions. The term crosslinks specifically refers to intermolecular chemical

RSC Polymer Chemistry Series No. 8
Natural Rubber Materials, Volume 2: Composites and Nanocomposites
Edited by Sabu Thomas, Hanna J. Maria, Jithin Joy, Chin Han Chan and Laly A. Pothen

Published by the Royal Society of Chemistry, www.rsc.org

bonds forming a continuous network. The crosslink term can be generalised to include physical crosslinks from a hard phase of a block copolymer, interactions with a blended polymer hard phase, or filler. The latter is the concern of this chapter, although natural rubber (NR) must still have chemical crosslinks since its hydrocarbon structure means intermolecular interactions are weak. Increasing interactions, constrained polymer chains and dispersed or clustered filler create a time-dependent reversible response.

Polymer molecules may have rigid groups such as aromatics, bulky groups that restrict motion by steric hindrance, polar groups that can force intra- and intermolecular dipolar interactions or hydrogen bonds. Fillers can produce a non-linear behaviour because they adsorb and bind molecular segments that impart time dependence upon molecular motion.

NR has a precisely defined molecular structure and so some of the aforementioned factors are not present. However NR blends with other polymers and filled compositions can bring about non-linear viscoelasticity. In particular when nanofillers are included due to their large surface area for polymer adsorption, and tendency for percolation networks and agglomerates.

Specialty rubbers are elastomers that require a low modulus and high reversible elongation, utilizing principles learnt from study of NR. They require properties ranging from high ultimate strength, high break strain, low permanent set, toughness, durability to cyclic strain, abrasion resistance, thermal resistance, and solvent or corrosive chemical resistance. Low hysteresis and high damping are characteristic of linear viscoelastic response. Fillers are added to contribute to many of these properties and nanofillers can be most effective because of large surface area to volume ratio. The nanosized fillers contribute to the performance via specialized mechanisms such as resisting crack propagation, forming agglomerates, or edge bridging; having fibrous, platelet, or particulate shape; and maybe forming specific bonds with the polymer. However, the use of nanofillers increases and extends performance of NR for specialty applications.[1]

Elastomers require a mechanism to provide reversible deformation. Only the elastic component of the four-element viscoelastic model must be active for linear response. The viscous contributions resulting from molecules sliding past each other resulting in irreversible flow, is eliminated by crosslinking in a network elastomer. Physical crosslinks are present in a thermoplastic elastomer as a second vitrified or crystalline phase. However NR is dependent upon chemical crosslinking that may be supplemented by filler or blended polymers. The viscoelastic component can be reduced by minimizing chain stiffness and intermolecular interactions in the continuous elastic phase. Thermoplastic elastomers offer ease of processing the same as thermoplastics without the need for a separate curing reaction. Upper application temperature limitations exist dependent upon the glass transition or melting temperature of the hard phase. Stress resistance is limited to the yield stress of the hard phase since permanent deformation will follow distortion or flow of the hard phase. Fillers enhance thermoplastic elastomers with nanofillers having particular relevance when

small amounts can support the hard phase. In the soft phase, fillers will modify the elastic response.[2]

The aim is to review the linear viscoelastic behaviour of NR and components that can be added to compositions to impart non-linear viscoelastic behaviour. Non-linear viscoelastic behaviour enhances mechanical damping properties. Damping can be bought about by use of alternate chemical structures to NR, however often it is convenient to enhance properties of existing materials.

20.2 Theory

20.2.1 Viscoelasticity

Viscoelasticity is a time-dependent reversible response. It is described by the analogy of the four-element model where the viscoelastic response is represented by a spring and dashpot in parallel. An extended analogy would be a distribution of parallel springs and dashpots representing a distribution of relaxation times. For a linear response, strain must be proportional to stress, which is applicable at small strain, of about 1%, producing a linear region in the stress–strain response. Figure 20.1 shows a comparison of stress–strain hysteresis curves for NR and poly(styrene-*co*-butadiene) rubber (SBR). NR has a much greater linear region, which is a broader linear viscoelastic region, than SBR. Hysteresis is extremely low for NR compared with SBR, which would be reflected in heat build-up during strain cycles.

Creep and recovery tests are another way of distinguishing elastic, viscoelastic and viscous flow. These mechanical phenomena are represented by a

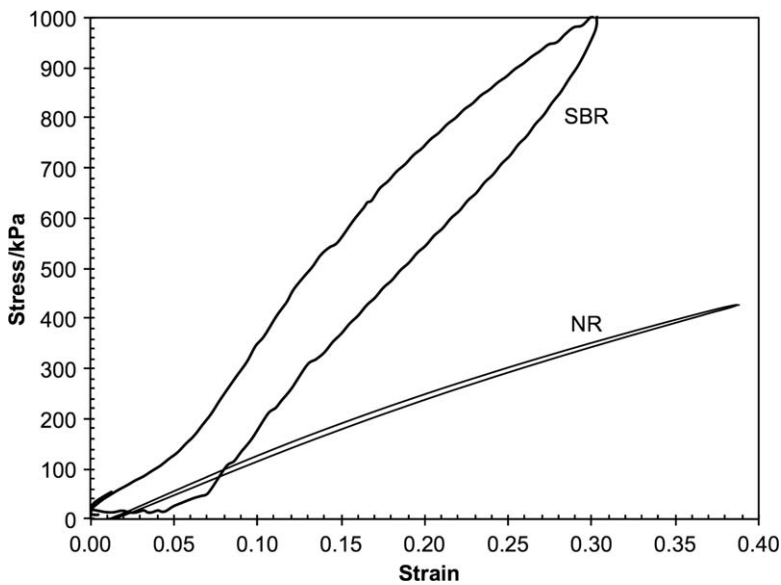

Figure 20.1 Comparison of stress–strain response and hysteresis for NR and SBR.

group of parameters including elastic modulus, viscoelastic modulus, relaxation time and viscosity. A more realistic distribution of relaxation times can be modelled using a Weibull function of the time-dependent recovery region. Other similar relationships between the time-domain properties are the Kohlrausch–Williams–Watts (KWW) and the frequency-domain properties in the Havriliak–Negami (HN) relaxation functions.[3] The recovery is used because viscous flow only occurs in the extension or creep part of the test, at the same time as the viscoelastic response. The Weibull function, or KWW, is a stretched exponential function of time (t) where an exponent (β) represents the non-exponentiality or the breadth of the distribution of relaxation times (τ):

$$E = k \cdot e^{\{t/\tau\}^{\beta}} \tag{20.1}$$

A modulated force thermomechanical response (dynamic mechanical analysis) with frequency dependence must be performed at low strain, in the linear viscoelastic region to be valid. Strain beyond the linear viscoelastic region would result in permanent deformation during each frequency cycle, thus the test specimen would be continuously changing from its original dimensions. The distinction between linear and non-linear viscoelasticity depends upon the frequency of the test as well as the characteristic response time of the material; thus the experimental conditions impinge upon the observed properties of the material. Under these conditions the data would not be characteristic of the original specimen across the test curve. A valid test curve must have only a small reversible strain applied over each frequency cycle. Within the frequency (time response) some deformation modes will be independent of frequency (time) and be in-phase while other modes will be frequency (time) dependent and be in-phase or out-of-phase depending on the frequency. These responses give the storage (E') and loss (E'') modulus, respectively, and the magnitudes and ratio of these moduli will be frequency-dependent (Figure 20.2). The ratio of the moduli $(E''/E') = \tan\,\delta$, the loss tangent or damping factor.

An addition to the standard viscoelastic four-element spring and dashpot models is through time-dependent latch elements. Latches describe incremental jumps to the time dependence of stress or strain. Stress relaxation, creep and recovery are correlated by stretched exponential functions such as Weibull and KWW as already discussed. Weibull is used to describe the distribution of failures occurring in discrete elements and KWW approximates overcoming a potential energy barrier where additional degrees of freedom for molecular motion are released. In stress relaxation, creep and recovery all molecular segments do not begin motions simultaneously, some modes must wait for others to suitably relax before commencing. The release of modes of motions are analogous to opening a latch in the potential energy. Figure 20.3 illustrates the viscoelastic properties by a standard four-element model showing the elastic element (E_1, spring contribution), viscoelastic element (E_2, η_2 spring and dashpot in parallel) and viscous element (η_3, dashpot contribution).

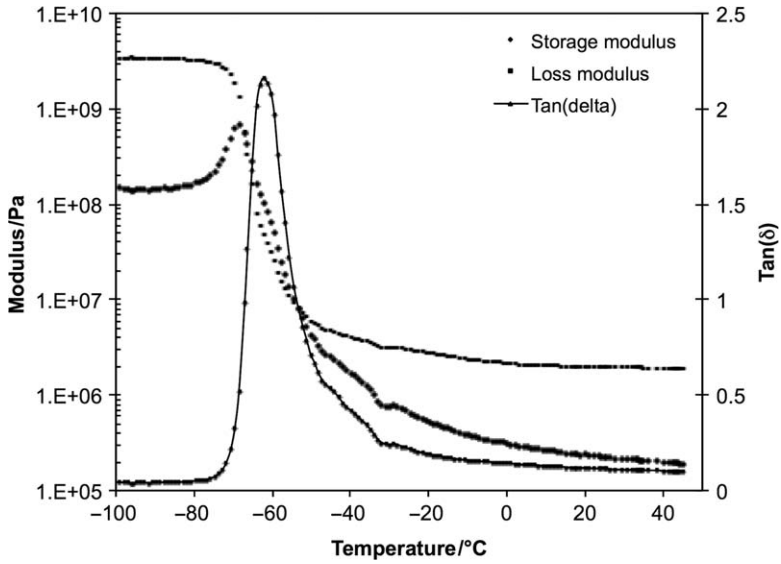

Figure 20.2 Modulated force thermomechanical response for NR with temperature.

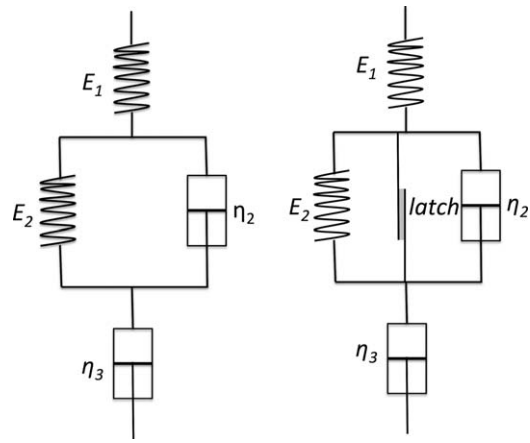

Figure 20.3 Viscoelastic models showing standard (left) and latched (right) mechanical analogy models.

The latched model has a constraining latch or adhesive joint analogy that will release at a critical stress allowing extension or recovery, depending on whether the spring is being stressed or the stress is being removed, based on Fancey.[4] The concept of the model is simplified in Figure 20.3 because there should be a distribution of each type of element. A distribution of latches means that as extension or relaxation takes place a distribution of latches is released as described by the shape parameter, β, in the Weibull equation.

Energy dissipation from a perfect elastomer may be due to a discontinuous deformation mechanism. An elastomer may be stretched through a continuous stress or an instantaneous stress that causes a sudden increase in strain. Stretching an elastomer is thermodynamically analogous to compression of a gas. In both cases the stored energy is recovered on removing the stress. Excess work is dissipated as heat. This heat is not due to a viscoelastic mechanism associated with molecular friction because the elastomer has been defined as perfect. The energy is independent of the stress–strain path, but only depends upon the initial and final states of the elastomer.[5] A perfect elastomer can dissipate much energy through cyclic deformations. Many applications of elastomers require energy dissipation and/or storage, such as in tension or shear when used in automotive systems. Many steps in the deformation cycle can eliminate dissipation leaving storage as the main thermodynamic response. By analogy with compression–decompression of a gas, stretching and compression of an elastomer creates a thermomechanical heat engine that converts heat input into mechanical output.[6]

20.3 Time–Temperature Superposition

Time–temperature superposition (TTS) assumes a linear viscoelastic response that is modulated force thermomechanical properties must be measured over a frequency range at a series of incrementing temperatures within the linear viscoelastic region of stress–strain. Figure 20.4 shows a modulated force thermomechanical (DMA) curve for the damping factor (tan δ) of NR measured at frequencies from 0.01 to 100 Hz. The time for segmental motions is reduced by higher frequency and therefore a higher temperature is required as indicated by the increasing temperature and decreasing damping of the peaks in the curves.

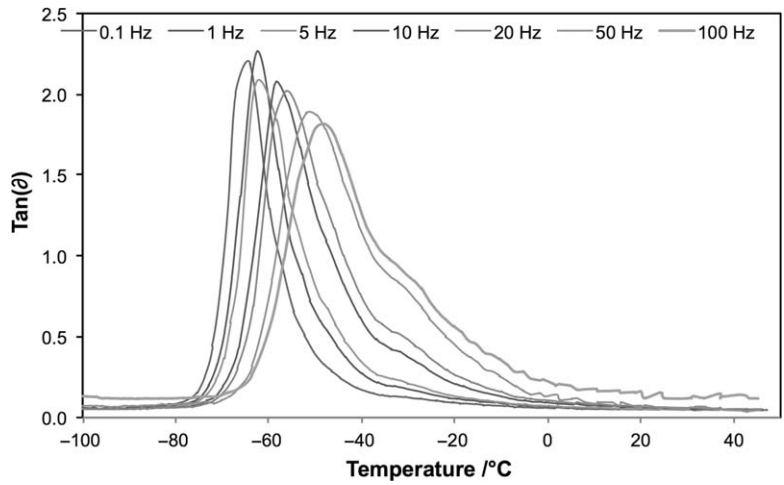

Figure 20.4 Modulated force thermomechanical response for NR with frequency and temperature.

Again the linear viscoelastic region must be maintained because the test specimen must return to its original dimensions after each frequency cycle otherwise the specimen being measured would gradually change while the measurements were being performed. TTS requires that linear viscoelasticity be maintained throughout the temperature range being measured so that the superposition of the data will be valid.

SBR elastomer with known crosslinking densities was studied in dynamic shear and tensile creep and data collected from −30 to 70 °C used to construct TTS master curves. In addition to a temperature shift factor a vertical shift factor was required from 10 to 30 °C to account for changes in density. Linear viscoelastic properties were observed in accordance with the classical theory of rubber elasticity. Standard vertical shift factors were required in a comparative TTS test with uncrosslinked polybutadiene and poly(ethylene-*co*-propylene-*co*-diene monomer) (EPDM).[7]

20.4 Creep and Recovery

Creep is measured beyond the linear viscoelastic stress–strain region. However as described above elastic and viscoelastic parameters are separated from the irreversible viscous flow component by considering both the creep and recovery curves. After an initial elastic response, the material undergoes creep as molecules uncoil and slide past each other in a time-dependent response. The uncoiling of chains, elongating of crosslinks and inter-crystalline tie molecules leads to a viscoelastic response. Sliding and slippage of molecules past each other leads to a permanent set or irreversible response that does not recover upon removal of the force even after long times. Creep rate has been correlated with constant stress to calculate activation energy and relaxation time or retardation time using a temperature jump technique, though the contribution is negligible over longer relaxation time distributions. The method has been applied to polypropylene where measurement of creep activation energy at 40 °C by single and double temperature jumps agreed with theory. This indicated that the temperature jump method was precise enough for changes in activation energy with retardation time to be measured.[8]

Polymers undergo deformation under an applied stress over their lifetime; some deformations which are irrecoverable once the source of stress is removed are referred to as creep. An understanding of the mechanical response of a polymer can be obtained by investigating the viscoelastic properties using creep experiments, where the behaviour is monitored under small deformational stress. Creep behaviour is an important consideration if the properties and dimensions are to be maintained. Experimental creep behaviour can be quantified using the four-element model with some limitations evident in the viscoelastic transitional region.[9]

Creep, stress relaxation and deformation under constant strain rate can be described assuming a viscoelastic response. Application of a constant strain can give rise to yield in thermoplastic materials. At yield the viscoelastic behaviour is non-linear, though the transition to non-linear is likely to occur prior to yield.

A model has been proposed to describe three phases of creep (primary, secondary and tertiary), stress relaxation and yielding under constant strain rate because they are manifestations of the same phenomena. Figure 20.5 shows a stress relaxation curve for NR that follows a KWW or Weibull model as described for creep. The model could describe transition between these modes without stress or strain discontinuities.[10]

20.5 Thermodynamics

Polymers possess a distribution of strain energy dissipation modes that are exhibited as relaxation spectra. The relaxation modes are coupled to conformational rotations of molecular segments that require carbon–carbon bond rotations occurring at the picosecond timescale. The required rotational cooperativity is limited in the crowded condensed state and becomes increasingly so as the temperature is lowered. Cooperativity leads to the concept of a domain size and hence the Vogel equation, analogous to Williams–Landel–Ferry (WLF) and free volume equation descriptions. The Vogel equation allows construction of a master relaxation curve from single frequency data over a temperature range.[11]

20.6 Non-Linear Viscoelasticity

Non-linearity is introduced due to time-dependent but reversible deformation events. Molecular motions may include uncoiling with release of entanglements, overcoming steric crowding and interlocking while elongating, limited mobility of chain segments due to rigid chemical groups, release of intra- and

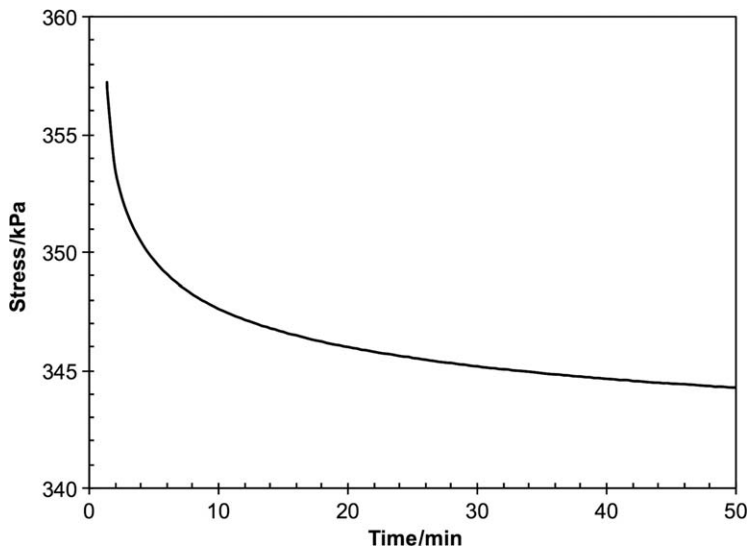

Figure 20.5 Stress relaxation of NR.

intermolecular interactions. Crosslinking, either through chemical bonding or physical constraints is necessary for reversibility. Irreversibility arises from relative translational motion of molecules due to chains slipping past each other such that there is no return force memory of original conformation.

Deformation time dependence is exhibited as a difference in the loading and unloading stress–strain curves known as hysteresis. The area between the curves is a measure of hysteresis. The energy lost or gained due to non-linear events results in a temperature increase upon extension and decrease upon contraction. In an ideal elastomer, which NR approaches, there would be no temperature change and no hysteresis. Elastomer compositions that are used for mechanical energy damping do so by converting mechanical energy to temperature gain or loss. Overall energy is conserved during elastomeric and viscoelastic processes.

The time dependent response of high-density polyethylene was represented by a one-dimensional integral including recoverable viscoelastic strain and irrecoverable viscoplastic strain. The response was represented by an effective time concept. Creep, recovery, two-step creep, and constant stress loading and unloading rates. The concept can also model preconditioning of semicrystalline polymers.[12]

Entanglements of flexible polymer chains contribute to non-linear viscoelastic response. Motions hindered by entanglements are a contributor to dielectric and diffusion properties since they constrain chain dynamics. Macromolecular dynamics are theoretically described by the reptation model. Reptation includes fluctuations in chain contour length, entanglement release, tube dilation, and retraction of side chains as the molecules translate using segmental motions, through a theoretical tube. The reptation model shows favourable comparison with experimental data from viscoelastic and dielectric measurements. The model reveals much about chain dynamics, relaxation times and molecular structures of individual macromolecules.[13]

A phenomenological model has been proposed for the non-linear viscoelastic behaviour of thermorheologically complex polymer glasses prior to and including yield. The approach was based upon stress additivity. A linear viscoelastic material will exhibit stress–strain additivity. The molecular processes modelled were resolved into two parallel processes, each with a characteristic relaxation time spectrum. The model described the yield behaviour and creep experiments at increasing stress.[14]

Conformational relaxation of polymers at temperatures below their glass transition temperature is retarded by lack of segmental motions. The conformation and free volume at the glass transition temperature continues at lower temperatures since equilibrium cannot be attained over typical experimental times. Cooperative relaxation towards conformational equilibrium depends upon temperatures, relaxation time spectrum, and the disparity between the actual and equilibrium states. The approach of the vitrified polymer to equilibrium is called thermal aging. Aging is both non-linear and non-exponential and several descriptions and models have been proposed. One model is based on a concept of temporary networks where the viscoelastic

medium is a network of active chains under Brownian motion. Formation and disruption of the temporary network is dependent on temperature and conformational entropy. Compressibility of the vitrified polymer was included as the model structure was subjected to finite strains. The model was tested with high-density polyethylene and poly(vinyl chloride) where some parameters were set using experimental data. The model demonstrated that physical aging could be described as a non-linear viscoelastic phenomenon occurring under small strains.[15]

20.7 Natural Rubber

20.7.1 Structure

NR (*Hevea*) is a hydrocarbon structure (poly(*cis*-1,4-isoprene)) with weak intermolecular forces leading to rapidly reversible stress–strain response. Irregularity is caused by *cis* double bonds in each repeat unit. While the double bonds produce a local rigidity they are geometrically asymmetric. The *trans* isomer, gutta-percha rubber, (poly(*trans*-1,4-isoprene)) can crystallize due to the regular zigzag configuration of the chains although intermolecular interactions are weak between the elongated chains. Removal of the elongating stress results in rapid entropy driven contraction with consequent melting of the crystals. The crystallization is consistent with crystallization of other polymers in that enthalpy of fusion is released upon elongation. Contraction is accompanied by an endotherm as the crystals melt. The enthalpy and entropy associated with straining of rubber was observed as the Gough–Joule effect and theoretically interpreted as conformational analysis of macromolecules advanced.

NR is a hydrocarbon with low intermolecular forces and low energy for rotation about chain bonds. C=C double bonds present do not allow rotation, however they do inhibit conformations favouring crystal growth. Without C=C NR would be like high-density polyethylene and hence readily crystallizable. The pendant methyl groups further constrain chain packing though they will reduce segmental rotation ability. Facile conformational changes with some modification by crosslinking mean that NR displays a broad linear viscoelastic response. Further modifications and formulation will tend to contribute non-linear viscoelastic response.

20.7.2 Crosslinking

A reversible crosslinked system forms a transient network that when placed under a macrodeformation shear rate exhibited shear flow. The properties depended on disruption and recombination of the reversible network.[16] The linear response to oscillatory deformations has been determined for the reversible network with uniform chains with reversible crosslinking at end groups. Where molar mass (M) was less than the critical M for entanglements the dynamic moduli were related to temperature, M and crosslink bond

lifetime. In this system with physical crosslinks the Cox–Merz rule did not apply. Crosslink bond lifetime dominated normal temperature, frequency and frequency–temperature superposition shift-factor influences, when compared with stationary viscosity measurements.[17]

Oscillatory shear rheology of EPDM plasticized with resol was used to determine an equilibrium shear modulus (*Ge*), relaxation in compression and strain recovery. *Ge* was analysed with consideration of crosslink density and permanent entanglements, including evaluation of plasticizer and soluble polymer fraction. Relaxation data were modelled with the empirical Chasset–Thirion equation and it was proposed that longer relaxation times were associated with chains pendant from the network. Relaxation times increased with crosslink density. When the crosslink density was low and pendant chains were longer and more numerous, relaxation times were increased and elastic recovery diminished.[18]

20.7.3 Natural Rubber Non-Linearity

NR exhibits some initial non-linearity as entangled chains uncoil and loosen entanglements. This is why a first stress–strain cycle is different from repeated subsequent cycles. A linear response then occurs until relatively high strain. A non-linear region then follows at high strain when crosslinks become taught and chains between crosslinks become fully extended. Note that in order for a considerable elastic response to occur crosslinks must be present to provide a network molecular structure. The extended NR will return to almost its original state upon decreasing the stress. Low hysteresis will be observed because there is little molecular friction and hence damping behaviour.

Non-linear, time-dependent characteristics of viscoelastic materials such as polyethylene have been mathematically modelled and the model compared with experimental results.[19] Mechanical properties such as creep and stress relaxation are non-linear because they include time-dependent and irreversible components. The time-dependent component is non-linear when relaxation time is longer than the timeframe of the experiment. This becomes increasingly so at high stress. Low stress will act on faster responding deformation modes and as stress increases slower modes will respond. The slower modes will be non-linear relative to the timescale of the experiment. Some slower modes such as relative translation of molecules are irreversible. Stress relaxation is complementary to creep in that strain is applied creating a stress that may relax according to the relative times of the experiment and molecular processes.

Non-linear viscoelastic response of polymers and composites has been studied with preloading prior to creep and recovery evaluation. When high preloading stress was applied the response became non-linear. The mode of the preloading was important in determining non-linear viscoelastic behaviour. This may have been due to damage to the specimen in the preloading stage.

This effect was investigated for the viscoelastic/viscoplastic response using a test program where the preload was applied at varying stress levels. Variation of viscoplastic strain was observed with change in preloading mode.[20]

Pre-strain was included in modulated stress testing of rubber and the dimensions of the pre-strained specimens used in calculation of the loss modulus. The loss modulus was independent of pre-strain for filled and unfilled rubbers. A test specimen geometry was chosen where pure shear could be superimposed with a small strain imparted with a shear oscillation. Again. loss modulus was mostly independent of pre-strain for filled and unfilled rubbers, including those filled with carbon black. The results enable understanding of energy dissipation mechanisms in rubber composites.[21]

NR and SBR blends including carbon black were subjected to large pre-strain while storage and loss modulus were measured. The loss modulus was independent of pre-strain except at high carbon black loading of 50% where an increase was found at extension ratio of less than 2. The increase of loss modulus was interpreted as due to elastomer orientation and slip at the polymer–filler interface.[22] Both events are non-linear, with orientation transient crystals formed, while interfacial rupture is an irreversible event for the original structure.

The transition from linear to non-linear viscoelastic behaviour and the transition threshold has been investigated with time and temperature. Thermal and mechanical tests were applied followed by isothermal creep tests at temperature steps and with differing stress levels. Isochronal creep curves were constructed to reveal the non-linearity threshold at different times and temperatures. The study was important for design and performance of elastomeric components.[23]

20.8 Natural Rubber Blends

Viscoelasticity of polymer blends and specifically NR blends with other elastomers is dependent on miscibility. Where blends are miscible they are likely to retain linear viscoelasticity to moderate strains. However when the blends are immiscible though compatible non-linear viscoelasticity may be observed due to a two-phase morphology. Latex blends of unvulcanized NR with carboxylated poly(styrene-*co*-butadiene) rubber (CSBR) were investigated. Blends were prepared with variation of blend ratio, while experimental temperature and frequency were varied. Tensile strength, modulus and elongation at break were measured. Tensile strength increased with CSBR fraction and then decreased as a result of self-curing of CSBR. Viscoelasticity was characterized using dynamic mechanical analysis, which showed two glass transition temperatures confirming that the blends consisted of two discrete phases that corresponded to the transitions of the individual elastomers. Thus the blends were immiscible though compatible. Time–temperature superposition was used to construct a master curve. Cole–Cole analysis of the master curve further demonstrated the two-phase structure of the blend. The storage moduli were

interpreted using Kerner model and Halpin–Tsai[24] (an approximate version of the Kerner equations, Equation (20.2)) model for aligned filler composites:[25]

$$E = \frac{E_0(1 + 2f\beta V)}{(1 + \beta V)} \tag{20.2}$$

where E = tensile modulus of composite, E_0 = tensile modulus of unfilled polymer, V = filler volume fraction, E_f = tensile modulus of the filler, and β is given by Equation (20.3).

$$\beta = \frac{(E_f/E_0) - 1}{(E_f/E_0) + 2f} \tag{20.3}$$

20.9 Natural Rubber Composites

20.9.1 Mineral Fillers (Kaolin, Calcite, Talc)

Particulate and platelet mineral fillers bind polymer molecules through adsorption. The fillers can exhibit a critical concentration where non-linear response commences, depending on the experiment and conditions used to measure the viscoelasticity. The filler contribution will increase with increased interfacial attraction or bonding. Fillers retard segmental motions of the elastomer molecules. While the pure elastomer has rapid response with its relaxation modes, the presence of filler constrains motions both by its occupying volume and binding polymer segments. The fillers thus described (kaolin, calcite, talc and others in this category) are general purpose fillers mainly used to extend the polymer.

20.9.2 Silica

Silica is an important filler for elastomers due to particle flocculation, ability to be surface modified with alkysilanes, alkytitanates and long chain carboxylic acids. Silica readily imparts non-linear viscoelasticity due to its strong binding effect especially when surface treated. Silica aggregates and agglomerates create physical networks throughout the matrix and flocculate into clusters that often include immobilised elastomer. The latter clusters cause an apparent increase in filler volume fraction due to the included elastomer essentially becoming part of the filler phase. Silica has become increasingly important in automotive tyre formulations for energy dissipation and abrasion resistance.

20.9.3 Carbon Black

Carbon black is the most important filler for elastomers and in particular NR. It can bind strongly with hydrocarbons. Carbon black gives protection from ultraviolet radiation that would otherwise cause chemical degradation. Carbon black in common with other fillers will reduce gas permeation that is critical for

applications where the rubber product must be inflated with air. Carbon black adsorbs elastomers strongly and can form conductive physical networks throughout the matrix increasing non-linear viscoelasticity. Some carbon blacks consist of nanoparticles and these are categorised separately in the next section. Non-linear viscoelasticity is advantageous in many elastomer applications, such as automotive tyres, since energy dissipation is required for high performance mechanical damping. A compromise must be reach to limit heat build-up with potential failure. A typical tyre will contain 25–30% carbon black together with 10% hydrocarbon oil plasticizer.

Carbon black physical networks within a rubber matrix have been rearranged or thermally disrupted by heat treatment under vacuum. Disruption of the network increased electrical resistivity in NR vulcanizates. Dynamic mechanical properties and thermal expansion coefficient were a function of carbon–carbon network structures in addition to rubber–carbon interactions. Disruption of carbon black networks was revealed using three-dimensional transmission electron microscopy (3D-TEM). Some carbon blacks were observed to form stronger networks within the rubber. The stronger networks were a function of the purity of the carbon black since prolonged heating for 3 h or more at 110 °C under vacuum disrupted the aggregates, observed as increased volume resistivity. Structural change of carbon black NR vulcanizate is reflected in the dynamic viscoelastic behaviour. Physical interaction between rubber chain segments and carbon causes the Payne effect, dependence of storage and loss modulus on frequency and stress. Storage modulus increases with carbon black volume fraction, specific surface area and surface activity, resulting in a carbon black gel or network.[26]

20.10 Natural Rubber Nanocomposites

20.10.1 Nanolayered Clay

Crosslinked NR nanocomposites were prepared with montmorillonite. Morphology was characterized using transmission electron microscopy (TEM), wide-angle X-ray scattering (WAXS), and dynamic mechanical analysis (DMA). X-ray scattering patterns revealed clay intercalation and TEM showed dispersion with partial delamination. The loss modulus peak broadened with clay content, while T_g remain constant. Montmorillonite reinforced the rubber. The DMA exhibited non-linear behaviour typified as a Payne effect (see Section 20.11) that increased with clay content and was more pronounced for this type of nanocomposite. Viscoelastic behaviour was observed under large strains via recovery and stress relaxation.[27]

20.10.2 Nano-Silica and Carbon Black

NR blends with SBR were prepared, using a two-roll mill, containing carbon black and silica. The composites were tested in tensile modes using specimens with varying widths, and heat build-up measurements were performed.

The elastic behaviour was described by hyperelastic models. The viscoelastic behaviour was modelled with a Prony series linear model and a Bergstrom–Boyce non-linear model, including estimation of parameters using finite element analysis. The mechanical deformation had a significant viscoelastic contribution. At large strain and with wider specimens the linear viscoelastic model was unsatisfactory. However the non-linear hyperviscoelastic models described behaviour under these conditions of medium and large strain. Both models described hysteresis of the rubber blend composites and these could be extended to evaluate rolling resistance of tyres.[28]

The curing and dynamic properties of precipitated nano-silica on NR without and with the sulfur addition (NR with S), synthetic polyisoprene (IR), polybutadiene (BR) and SBR was investigated. Silica was treated with bis(3-triethoxysilylpropyl)tetrasulfane (TESPT) to form bonds at interfaces. Cure, Mooney viscosity, glass transition temperature, bound rubber, crosslink density and DMA were measured. The properties of silica-filled SBR and BR correlated with highest rolling resistance and SBR–silica correlated with best skid resistance. A Payne effect was observed in the loss modulus under some experimental conditions. In addition to possible filler de-agglomeration and network disruption, the nanoscale of the filler may have further contributed to the non-linear response typified by the Payne effect.[29]

The linear viscoelastic behaviour of silica and organoclay nanocomposites has been evaluated for the limits of viscoelasticity evident as a critical strain and the strong non-viscoelastic behaviour referred to as the Payne effect. Two mechanisms are in operation, particle–particle interactions (Payne effect) is the predominant mechanism, whereas particle–polymer interactions predominate in systems with larger particle sized silica (colloidal silica). Such interactions are moderated by silica surface treatments such as silane coupling or polymer grafting. Flow history in transient shear experiments were important for organoclay orientation that may provide a weakly agglomerated network of clay tactoids making interparticle interactions dominate in the non-linear viscoelastic response.[30]

A dual phase filler consisting of silica and carbon black was used in rubber vulcanizates along with separate silica and carbon black. DMA was performed on the filled elastomers and the data used to construct a pseudo master curve, which has a feather-like appearance due to lack of shifting of higher frequency data to the master curve. This feathering was due to filler network formation and polymer–filler interactions dominating the properties. The dual phase silica–carbon filler was more similar to silica with its strong interparticle networking.[31]

Non-linear viscoelastic behaviour of NR filled with surface-modified nano-silica was prepared with a range of silica compositions. Non-linear viscoelastic properties were measured with change in temperature. A Payne effect was observed at higher silica loadings and evaluated with filler particle size, specific surface area and surface characteristics that were found to be the source of the Payne effect. Storage modulus decreased non-linearly with increasing strain even for unfilled NR. The mechanism included disruption of networks such as

filler – filler network, weak polymer–filler network, chemical network and entanglement network. A model of variable network density proposed by Maier and Goritz was used to interpret the non-linear behaviour. Activation desorption energy was calculated and within that expected for van der Waals interaction energy.[32]

20.10.3 Nano-Cellulose and Starch

NR can be combined with cellulose and its derivatives for low performance materials. Celluloses may consist of wood flour, microcrystalline cellulose (MCC) or various forms of nano-cellulose. These composites have low interfacial strength and potential for filler agglomeration. NR reinforced with short fibre cellulose and carbon black were prepared and water absorption, crosslink density, tensile strength, and dynamic storage modulus with variation of strain amplitude were characterized revealing viscoelastic behaviour consistent with interfacial bonding of cellulose and elastomer. Cellulose fibres were shown to be adequately bonded to the matrix.[33] NR has been filled with bamboo fibres, with and without surface modification. Tensile strength, tensile modulus, tear strength, elongation at break and hardness were measured. Increase in tensile strength and SEM demonstrated that interfacial bonding was enhanced by surface modification of the bamboo fibre.[34]

Cellulose nanowhiskers with high aspect ratio were prepared from palm rachis and leaflets. The nanofibres were incorporated into NR and nanocomposite films were prepared by casting followed by evaporation. The NR nanocomposites were characterized using differential scanning calorimetry (DSC), DMA and tensile testing. The modulus of the NR was increased by the nanowhiskers, implying favourable interactions between rubber and cellulose, and hence linear viscoelastic behaviour.[35] Cellulose whiskers were formed from bleached sugar cane bagasse kraft pulp, with dimensions 4–12 nm diameter and 84–102 nm length. The whiskers were used to reinforce NR. Tensile properties, thermal properties, moisture sorption, water vapour permeation, and soil biodegradation was characterized. Modulus and tensile strength were increased by the cellulose nanowhiskers and these properties increased with filler content. The glass transition temperature of the rubber measured by DMA and DSC was found to not change. The bagasse whiskers increased moisture sorption and barrier properties to water vapour decreased, except at high filler content where sorption decreased and barrier properties increased. Bagasse increased degradation of the nanocomposites in soil.[36]

Enzyme hydrolysis and bleaching of sisal fibres was used for preparation of cellulose nanocrystals. The nanocrystals were dispersed in NR to form nanocomposites that exhibited increased modulus. Enzyme treatment provided nanoparticles that could be specifically prepared for varying thermomechanical properties.[37]

MCC was prepared by hydrolysing waste cotton fabric with hydrochloric acid. The MCC was characterized by measurement of laser light scattering particle size, WAXS morphology, SEM and thermogravimetric properties.

The crystal structure was type I. MCC was dispersed in concentrated NR latex, cast into sheets, air dried and then heat cured. Tensile properties overall decreased for MCC composites compared with pure NR sheets. However at 20 pphr a maximum tensile strength and break strain was obtained. Water absorption and biodegradability were enhanced by presence of MCC.[38]

Starch nanocrystals were used to reinforce a non-vulcanised NR matrix. The NR was not vulcanised to enhance biodegradability of the total biocomposite. Non-linear dynamic mechanical experiments demonstrated a strong reinforcement by starch nanocrystals, with the presence of Mullins and Payne effects. The Payne effect was able to be predicted using a filler–filler model (Kraus model) and a matrix–filler model (Maier and Göritz model). The Maier and Goritz model showed that adsorption–desorption of NR onto the starch surface contributed the non-linear viscoelasticity. The Kraus model confirmed presence of a percolation network.[39]

Nanocomposites formed from a NR latex were filled with an aqueous suspension of waxy maize starch nanocrystals and morphology, structure and barrier properties characterized. The materials were measured in linear and non-linear viscoelastic regions. Starch nanocrystals reinforced the NR to a content of 20 $\% \cdot w/w$ without significant loss of ultimate strain. The NR modulus was greatly increased when nano-starch was present. Starch–starch interactions were important for enhancing the composite properties. Moisture and starch nanocrystal surface chemistry were important influences on properties.[40]

20.10.4 Carbon Nanotubes

Carbon nanotubes (CNTs) have nanodiameter with large surface area, moderated by extended length that can give network formation and hence conductivity at low volume fractions. The physical CNT network and entanglements superimposes on the elastomer morphology. Mechanical properties of CNT–NR composites are thus more complex than those of particulate composites. This complexity can contribute to non-linear behaviour at relatively low strains due to the co-continuous nature of the matrix elastomer and the physical CNT network. Single-walled carbon nanotubes (SWNTs) were included in NR. DSC, DMA and Raman spectroscopy were used to characterize the SWNT nanocomposites and the results compared with analogous composites with carbon black. SWNTs demonstrated increased filler–matrix interaction with decreased damping factor and a shift of T_g to higher temperatures. Elastic modulus was enhanced by SWNTs. Raman spectroscopy was consistent with uniform dispersion that created residual strain on SWNT bundles, which indicated effective load transfer form matrix to SWNT.[41]

Functionalized multi-walled carbon nanotubes (MWNTs) were prepared by acid treatment followed by reaction with 3-aminopropyltriethoxysilane. Reaction of silane with oxidized nanotubes was confirmed by Fourier transform infrared (FTIR) spectroscopy and energy dispersive X-ray (EDX) analysis to confirm silicon on the surface of the MWNTs. Raman spectroscopy of the acid-treated MWNTs confirmed formation of surface defects due to carboxyl

groups. Thermogravimetry demonstrated additional mass loss in the silanized MWNTs confirming functionalization. Functionalization caused increased scorch time and cure time. Modulus and tensile strength increased because of enhanced interactions between the MWNTs and NR.[42] MWNTs were used to prepare NR nanocomposites via solution dispersion and solvent evaporation. TEM revealed efficient dispersion. Mechanical properties that were measured included tensile strength, tensile modulus, tear strength, elongation at break and hardness. Modulus increased significantly for the nanocomposites. Overall properties of the MWNT–NR composites were improved compared with those of carbon black or silica.[43]

Carboxylated multiwalled carbon nanotubes (C-MWNTs) dispersed with sodium dodecyl sulfate were included in NR latex and cast into films. Dispersion uniformity was confirmed using TEM and atomic force microscopy (AFM). Modulus enhancement, with small reduction of break strain, was confirmed by tensile and dynamic mechanical testing. A low percolation threshold was revealed from dielectric measurements. Large Payne and Mullins effects were observed in mechanical properties due to the physical nanotube network. Disruption of the network by strain increased electrical resistivity accompanied by stress softening.[44] Cure kinetics and vulcanizate properties of CNT–NR nanocomposites were investigated. CNT were treated with acid and ball milling prior to solution dispersion in NR. The NR vulcanizates were characterized using static and dynamic mechanical analysis and SEM. Cure kinetics were measured at temperature increments and activation energy calculated. Treatment of CNT improved dispersion and interaction with NR, as evidenced by improved physical and mechanical properties.[45] CNT–NR composites were developed with improved performance. The nanocomposites were prepared in NR solution after pre-treatment with acid and ball milling of the CNT. CNT–NR were compared with carbon black NR composites. Hydrated silica, resorcinol, and hexamethylene tetramine bonding agents were used to enhance the interface between CNT and NR. A considerable increase of modulus and strength was obtained, as well as improved rebound resilience and dynamic compression properties. Thermal stability of NR was improved with the addition of treated CNT.[46]

MWNTs were used to reinforce NR. Volume resistivity decreased with increase in filler content with a percolation threshold being reached at less than 1 pphr. Storage shear modulus decreased with strain amplitude, attributed to a Payne effect and a disruption of the MWNT network. This non-linear viscoelastic behaviour is consistent with many NR composites where fillers form clusters and/or networks. The high aspect ratio of MWNTs increased the tensile modulus, though tensile strength and ultimate strain were decreased. It was proposed that agglomerates increase with MWNT content and this decreased strength and ultimate strain. The explanation was confirmed by cyclic straining where ultimate strain was higher after a second repetition. Tip sonication and a solvent, cyclohexane, improved dispersion of MWNTs.[47] The increase in MWNT dispersion after sonication decreased the percolation threshold detected by measurement of electrical properties. A weak

NR–MWNT interface was confirmed using Raman spectroscopy while the composites were under strain, however deconvolution of NR chain orientation from MWNT orientation was obtained when the composites were subjected to uniaxial tension.[48]

20.10.5 Graphene

Graphene is a single carbon atom layer consisting of repeating aromatic structures formed by exfoliating graphite through several techniques. Exfoliation can be mechanical, facilitated by oxidation or other intercalation to reduce the interlayer adhesion. Graphene sheets are often folded or buckled that can create complex conformations within a surrounding rubber matrix. Dispersion of reduced graphene oxide (GO) into NR was found to enhance the mechanical, electrical, and thermal properties of the resulting nanocomposite, dependent upon processing history. When reduced GO was dispersed into NR latex and the latex then coagulated, a physical network of GO platelets between NR particles was formed, which required ball milling to disrupt. A physical network was found to enhance modulus, thermal and electrical conductivity.[49] Dispersion NR composites with graphene is assisted by ultrasonication, which may be performed directly in latex form. Sonication further assists exfoliation of the graphene since most graphenes contain multiple layered structures as well as a single layer. Increasing graphene content in NR increases physical network structures, modulus, tensile and tear strength, and thermal conductivity.[50]

Functionalized graphene sheets were dispersed in NR, SBR and polydimethylsiloxane (PDMS). The graphene sheets were mainly oxidized single crumpled sheets prepared by thermal exfoliation of GO. Mechanical properties and gas permeation resistance were enhanced with data for permeation fitting the Nielson model. Electrical conductivity commenced at a composition of 0.08 % graphene in PDMS.[51]

Functionalized graphene sheets were used to prepare nanocomposites with NR by two-roll shear mixing. NR–graphene interactions assisted crosslinking reactions of NR, and graphene networks created electrical conductivity and enhancement of mechanical performance.[52]

NR composites were prepared containing both carbon black and graphene. Dielectric and microwave absorption and reflection were characterized to access electromagnetic interference shielding effectiveness. Graphene was shown to be effective as a second filler in NR.[53]

A dispersion of graphene in NR latex was prepared in conjunction with ammonia solution as a stabilizer for the latex during dispersion. The latex was then used to cast films that were dried to obtain the NR composite. The method gave good dispersion and strong interfacial interaction due to π–π interactions, resulting in increased *Tg*, crosslink density, decreased free volume with enhanced tensile strength and retention of elongation of the NR.[54]

Functionalized graphene sheets and carbon black were used to prepare NR composites for comparison of properties. Strain induced crystallization was measured using WAXS in real time during elongation. The onset of strain

induced crystallization was detected to occur at lower strains with graphene filled NR compared with carbon black filled NR. Small angle X-ray scattering revealed that graphene sheets became aligned in the strain direction.[55]

20.11 Filler Aggregates and Agglomerates

Mechanical properties of nanoparticle filled elastomers are subject to the kinetics of rupture and reformation of glassy bridges linking adjacent nanoparticles and building of large rigid agglomerates with finite lifetimes. Filler–polymer interactions, temperature, interparticle distance and deformation history are factors determining this non-linear behaviour. The original mechanical properties are approached upon relaxation of the composites even after large deformations and while the composites are held continuously under large deformation when new glassy bridges are concluded to have formed.[56] This behaviour has been attributed to the Payne and Mullins effects discussed in the next sections.

20.11.1 Payne Effect

Non-linear mechanical properties were observed for rubber composites and referred to as the Payne effect. The Payne effect was interpreted as due to filler agglomeration where the filler clusters formed contained adsorbed rubber. The occluded rubber molecules within filler clusters could not contribute to overall elastic properties. The composites behaved similarly to rubber composites with higher filler loading. Uniform and stable filler dispersion is required for rubber composites to exhibit linear viscoelastic behaviour. Payne performed dielectric measurements on SBR vulcanizates containing silica or carbon black. The dielectric data were used to construct time–temperature superposition master curves. The reference temperature increased with crosslinking but not significantly with filler. Comparison of dynamic mechanical and dielectric results for the SBR blended with NR was made and interpreted.[57]

While elastomers tend to exhibit linear viscoelasticity due to weak interactions and flexible chain segments, reinforced elastomers exhibit non-linear effects at relatively low strains, which is the Payne effect. For example silica-filled SBR exhibit a Payne effect at silica content below the percolation threshold, with temperature, filler content and surface treatment contributing. Coupling agents lower the critical filler concentration for transition to non-linear viscoelasticity. The system has been modelled using a mechanical model, its evolution under stress with physical mechanisms such as polymer–filler debonding as the Payne manifestation.[58] Silica filled poly(ethylene-*co*-vinyl acetate) (EVA) was found to exhibit elasticity, a Payne effect, percolation threshold in both molten and solution states. Strain dependence of viscoelastic properties were interpreted as due to filler network disruption, however non-linearity was found at low silica concentrations when dynamic mechanical measurements were made. In addition to filler percolation, a mechanism involving trapped entanglements was considered. Gel-like behaviour was observed in the terminal zone. Liquid–solid transition to the gel due to formation

of a percolation network could also be described as due to a filler cluster–cluster agglomeration.[59]

Non-linear viscoelastic properties were observed for fumed silica–poly(vinyl acetate) (PVAc) composites, with varying PVAc molar mass and including a PVAc copolymer with vinyl alcohol. Dynamic mechanical moduli were measured at low strains and found to decrease with strain depending on surface treatment of the silica. The loss modulus decreased significantly with filler surface treatment and more so with lower molar mass polymer. Copolymers with vinyl alcohol presumably increased interactions with silica and decreased non-linearity. Percolation network formation or agglomeration by silica were less important than silica–polymer interactions. Silica–polymer interactions were proposed to form trapped entanglements. The reinforcement and non-linear viscoelastic characteristics of PVAc and its vinyl alcohol copolymer were similar to observations of the Payne effect in filled elastomers, characteristic of conformations and constraints of macromolecules.[60]

20.11.2 Mullins Effect

The Mullins effect was observed for filled rubber composites as a decrease in modulus at high extensions.[61] The contributing structural changes are complex, however they can be summarized as disaggregation or disagglomeration of filler clusters at high strain, thus this simple description is subject to challenge. The Mullins effect is dependent on filler concentration since at higher concentrations aggregates and agglomerates increase due to decreased efficiency in complete dispersion of filler. The Mullins effect has been subject of much research and the evidence and interpretations have been reviewed.[62] Investigations have provided some models, however the review found little predictive ability for the models since crucial parameters could not be experimentally measured in order to compare calculated and experimental physical quantities.

Non-linear viscoelastic mechanical behaviour of a crosslinked sealant was interpreted as due to a Mullins effect. The Mullins effect was observed for a series of sealants under tensile and compression tests. The Mullins effect was partially removed after a mechanical test, when a long relaxation time was allowed, that is the modulus increased over time. Non-linear stress relaxation was observed for pre-strained filler sealants. Time–strain superposition was used to derive a model for the filled sealants.[63] Relaxation over long periods demonstrates that the Mullins effect is caused by non-equilibrium with experimental conditions being faster than return to the initial state. If experiments were conducted over times of the order of a day there may be no Mullins effect. If a filled elastomer were only required to perform its function once per day then each response might be linear viscoelastic.

20.12 Applications

Many applications of elastomers formulations rely on non-linear as well as linear response. Two examples are mentioned to illustrate the need for extended

understanding of these materials beyond typical linear viscoelastic response. When tests are performed keeping within the linear viscoelastic regions is stressed if representative results are to be obtained. However the non-linear region needs to be explored since many products are exposed to such mechanical conditions during their life cycle or when in regular use.

20.12.1 Auto Tyre Performance

Knowledge of non-linear contributions to viscoelasticity is important for design of elastomer blends and composites for rolling resistance performance of tyres, hysteresis and heat build-up behaviour, and friction or grip characteristics. The importance extends beyond developing suitable blend and filler compositions, to the construction, geometry and tread pattern design of tyres to arrive at optimum performance.

20.12.2 Belt Drives and Conveyors

Belts and conveyors require strength, toughness and abrasion resistance. This complex set of properties includes choice of polymers, fillers and additives. However contribution of non-linear viscoelastic behaviours would lead to unpredictable performance.

20.13 Conclusions

NR nanocomposites have been commercialized for a long time since carbon black is a nanofiller that is ubiquitous. Fumed silica is another nanofiller that is known to enhance the exceptional properties of NR. Nanocomposites are extended through use of carbon nanotubes, graphene and nano-cellulose varieties. NR is almost a perfect elastomer when lightly crosslinked. However many applications require changes to basic elastomeric properties, such as increasing non-linear viscoelastic attributes. High strains, micro- or nanofiller contents, interactions and physical network formations generates complex mechanical properties. The complex mechanical properties are revealed by linear and non-linear viscoelastic characterization. Interpretation of this viscoelasticity has contributed much to morphology and theory of structure and structure development under strain.

References

1. R. A. Shanks and B. Rengarajan, *Recent Advances in Polymer Nanocomposites: Synthesis and Characterization*, ed. S. Thomas, S. V. Valsaraj, A. P. Meera and G. E. Zaikov. Brill NV, Leiden, The Netherlands, 2010, 216–232.
2. R. A. Shanks and I. Kong, *Thermoplastic Elastomers*, ed. A. Z. El-Sonbati, InTech, Rijeka, Croatia, 2012, 137–154.
3. F. Alvarez, A. Alegra and J. Colmenero, *Phys. Rev. B*, 1991, **44**, 7306.

4. K. S. Fancey, *J. Mater. Sci.*, 2005, **40**, 4827.
5. A. Raman and R. J. Farris, *Polym. Eng. Sci.*, 2007, **47**, 1511.
6. A. Raman and R. J. Farris, *Polym. Eng. Sci.*, 2007, **47**, 1521.
7. R. Prabhu, R. Klitkou, G. A. Medvedev and J. M. Caruthers, *J. Polym. Sci., Part B: Polym. Phys.*, 2013, **51**, 687.
8. F. C. Chen, N. G. McCrum and M. Pizzoli, *Polymer*, 1979, **20**, 488.
9. A. Genovese and R. A. Shanks, *Macromol. Mater. Eng.*, 2007, **292**, 184.
10. R. D. Sudduth, *J. Appl. Polym. Sci.*, 2001, **82**, 527.
11. S. Matsuoka, *J. Thermal Anal.*, 1996, **46**, 985.
12. J. Lai and A. Bakker, *Polym. Eng. Sci.*, 1995, **35**, 1339.
13. H. Watanabe, *Progr. Polym. Sci.*, 1999, **24**, 1253.
14. E. T. J. Klompen and L. E. Govaert, *Mechanics of Time-Dependent Materials*, 1999, **3**, 49.
15. A. D. Drozdov, *Computational and Theoretical Polym Sci*, 1999, **9**, 73.
16. F. Tanaka and S. F. Edwards, *J Non-Newtonian Fluid Mech*, 1992, **43**, 247.
17. F. Tanaka and S. F. Edwards, *J Non-Newtonian Fluid Mech*, 1992, **43**, 273.
18. G. Martin, C. Barres, P. Cassagnau, P. Sonntag and N. Garois, *Polymer*, 2008, **49**, 1892.
19. N. Heymans, *Progress and Trends in Rheology V, Proceedings of the European Rheology Conference*, 5th, Portoroz, Slovenia, 1998, 100.
20. S. P. Zaoutsos and G. C. Papanicolaou, *Compos. Sci. Tech.*, 2010, **70**, 922.
21. N. Suphadon, A. G. Thomas and J. J. C. Busfield, *Polym. Test.*, 2010, **29**, 440.
22. N. Suphadon, A. G. Thomas and J. J. C. Busfield, *J. Appl. Polym. Sci.*, 2010, **117**, 1290.
23. G. C. Papanicolaou, A. G. Xepapadaki, K. Karagounaki and S. P. Zaoutsos, *J. Appl. Polym. Sci.*, 2008, **108**, 640.
24. J. C. Halpi and J. L. Kardos, *Polym. Eng. Sci.*, 1976, **16**, 344.
25. R. Stephen, K. V. S. N. Raju, S. V. Nair, S. Varghese, Z. Oommen and S. Thomas, *J. Appl. Polym. Sci.*, 2003, **88**, 2639.
26. A. Kato, T. Suda, Y. Ikeda and S. Kohjiya, *J. Appl. Polym. Sci.*, 2011, **122**, 1300.
27. G. Ramorino, F. Bignotti, L. Conzatti and T. Ricco, *Polym. Eng. Sci.*, 2007, **47**, 1650.
28. M. H. R. Ghoreishy, M. Alimardani, R. Z. Mehrabian and S. T. Gangali, *J. Appl. Polym. Sci.*, 2012, **128**, 1725.
29. A. A. Saeed Ostad Movahed and M. Song, *Polym. Int.*, 2009, **58**, 209.
30. P. Cassagnau, *Polymer*, 2008, **49**, 2183.
31. M.-J. Wang, S. X. Lu and K. Mahmud, *J. Polym. Sci., Part B: Polym. Phys.*, 2000, **38**, 1240.
32. A. P. Meera, S. Said, Y. Grohens and S. Thomas, *J. Phys. Chem. C*, 2009, **113**, 17997.
33. P. Flink, B. Westerlind, M. Mikael Rigdahl and B. Stenberg, *J. Appl. Polym. Sci.*, 1988, **35**, 2155.
34. H. Ismaila, M. R. Edyhama and B. Wirjosentono, *Polym. Test.*, 2002, **21**, 139.

35. A. Bendahou, Y. Habibi, H. Kaddami and A. Dufresne, *J. Biobased Mater. Bioenergy*, 2009, **3**, 81.
36. J. Brasa, L. Mohammad, M. L. Hassanb, C. Bruzessea, E. A. Hassanb, N. A. El-Wakilb and A. Dufresne, *Ind. Crops Prod.*, 2010, **32**, 627.
37. G. Siqueira, S. Tapin-Lingua, J. Bras, D. da Silva Perez and A. Dufresne, *Cellulose*, 2011, **18**, 57.
38. S. Chuayjuljit, S. Su-Uthai, C. Tunwattanaseree and S. Charuchinda, *J. Reinf. Plast. Compos.*, 2009, **28**, 1245.
39. P. Mélé, H. Angellier-Coussy, S. Molina-Boisseau and A. Dufresne, *Biomacromolecules*, 2011, **12**, 1487.
40. H. Angellier, S. Molina-Boisseau and A. Dufresne, *Macromolecules*, 2005, **38**, 9161.
41. M. A. López-Manchado, J. Biagiotti, L. Valentini and J. M. Kenny, *J. Appl. Polym. Sci.*, 2004, **92**, 3394.
42. A. M. Shanmugharaj, J. H. Bae, K. Y. Lee, W. H. Noh, S. H. Lee and S. H. Ryu, *Compos. Sci. Tech.*, 2007, **67**, 1813.
43. A. Fakhru'l-Razia, M. A. Atieha, N. Giruna, T. G. Chuaha, M. El-Sadigb and D. R. A. Biak, *Compos. Struct.*, 2006, **75**, 496.
44. S. Bhattacharyyaa, C. Sinturela, O. Bahloula, M.-L. Saboungia, S. Thomas and J.-P. Salvetat, *Carbon*, 2008, **46**, 1037.
45. G. Suia, W. H. Zhong, X. P. Yanga and Y. H. Yu, *Mater. Sci. Eng.: A*, 2008, **485**, 524.
46. G. Sui, W. H. Zhong, X. P. Yang, Y. H. Yu and S. H. Zhao, *Polym. Adv. Technol.*, 2008, **19**, 1543.
47. L. Bokobza, *eXPRESS Polym Lett.*, 2012, **6**, 213.
48. L. Bokobza, *Polym. Adv. Technol.*, 2012, **23**, 1543.
49. J. R. Potts, O. Shankar, L. Du and R. S. Ruoff, *Macromolecules*, 2012, **45**, 6045.
50. Y. Zhan, J. Wu, H. Xia, N. Yan, G. Fei and G. Yuan, *Macromol. Mater. Eng.*, 2011, **296**, 590.
51. B. Ozbas, C. D. O'Neill, R. A. Register, I. A. Aksay, R. K. Prud'homme and D. H. Adamson, *J. Polym. Sci., Part B: Polym. Phys.*, 2012, **50**, 910.
52. M. Hernándeza, M. del Mar Bernala, R. Verdejoa, T. A. Miguel and A. López-Manchado, *Compos. Sci. Tech.*, 2012, **73**, 40.
53. O. A. Al-Hartomy, A. S. Al-Ghamdi, F. Al-Salamy, N. Dishovsky, R. Shtarkova, V. Iliev and F. El-Tantawy, *Int. J. Mater. Chem.*, 2012, **2**, 116.
54. C. Li, C. Feng, Z. Peng, W. Gong and L. Kong, *Polym. Compos.*, 2013, **34**, 88.
55. B. Ozbas, S. Toki, B. S. Hsiao, B. Chu, R. A. Register, I. A. Aksay, R. K. Prud'homme and D. H. Adamson, *J. Polym. Sci., Part B: Polym. Phys.*, 2012, **50**, 718.
56. S. Merabia, P. Sotta and D. R. Long, *J. Polym. Sci., Part B: Polym. Phys.*, 2010, **48**, 1495.
57. A. R. Payne, *SCI Monograph*, 1959, **5**, 273.

58. C. Gauthier, E. Reynaud, R. Vassoille and L. Ladouce-Stelandre, *Polymer*, 2004, **45**, 2761.
59. P. Cassagnau, *Polymer*, 2003, **44**, 2455.
60. S. S. Sternstein and A.-J. Zhu, *Macromolecules*, 2002, **35**, 7262.
61. L. Mullins, *Rubber Chem. Technol.*, 1969, **42**, 339.
62. J. Diani, B. Fayolle and P. Gilormini, *Eur. Polym. J.*, 2009, **45**, 601.
63. C. C. White and D. L. Hunston, *Polym. Eng. Sci.*, 2008, **48**, 2317.

CHAPTER 21

Rheological Behaviour of Natural Rubber Based Composites and Nanocomposites

RUNCY WILSON*[a] AND SABU THOMAS[b]

[a] School of Chemical Sciences, Mahatma Gandhi University, P.D. Hills, Kottayam, Kerala, 686 560, India; [b] Center for Nanoscience and Nanotechnology, Mahatma Gandhi University, P.D. Hills, Kottayam, Kerala, 686 560, India
*Email: runcy21@gmail.com

21.1 Introduction

Natural rubber (NR) is an elastomer (an elastic hydrocarbon polymer) that was originally derived from latex, a milky colloid produced by some plants (*Hevea brasiliensis*, a member of the spurge family, Euphorbiaceae). The plants are 'tapped' by making an incision in the bark of the tree and collecting the sticky, milk-coloured latex sap, which is refined into usable rubber. The purified form of NR is the chemical polyisoprene, which can also be produced synthetically. NR is used in many applications and products, as is synthetic rubber. It is normally very stretchy and flexible and extremely waterproof.

Rheology is a branch of physics that deals with the deformation and flow of matter under stress. The word **rheology** is defined as the science of deformation and flow, was coined by Prof Bingham in 1920s.[1] Rheology involves measurements in controlled flow, mainly the viscometric flow in which the velocity

RSC Polymer Chemistry Series No. 8
Natural Rubber Materials, Volume 2: Composites and Nanocomposites
Edited by Sabu Thomas, Hanna J. Maria, Jithin Joy, Chin Han Chan and Laly A. Pothen

Published by the Royal Society of Chemistry, www.rsc.org

gradients are nearly uniform in space. In these simple flows, there is an applied force where the velocity (or the equivalent shear rate) is measured, or vice versa. It is particularly concerned with the properties of matter that determine its behaviour when a mechanical force is exerted on it. Rheological properties have important implications in many and diverse applications. The applications of rheology are very important in the areas of industries involving metal, plastic, and many other materials. The rheological investigations will provide a mathematical description of the viscoelastic behaviour of material under study. The rheology of a material is very important in the processing of composites for injection moulded part or determining the curing behaviour of the materials.

Molecular weight distribution of a polymer is another level of complexity, as polymers are rarely synthesised in a sharp monodisperse population. This brings in the need to study the behaviour of polymeric liquid in simple flows and for simple systems, with the hope that the knowledge gained can be appropriately used in a complex flow pattern. They are called **viscometric** as they are used to define an effective shear viscosity η from the measurements,

$$\eta = \frac{\sigma_{xy}}{\dot{\gamma}} \tag{21.1}$$

where σ_{xy} is the shear stress (measured or applied) and is the shear rate (applied or measured), Viscosity is measured in Pa s (Pascal second).

Rheology is not just about viscosity, but also about another important property, namely the elasticity. Complex fluids also exhibit elastic behaviour. Similar to the viscosity defined above being similar to the definition of a Newtonian viscosity, the elasticity of a complex material can be defined similar to its idealised counterpart, the Hookean solid. The modulus of elasticity is defined as

$$G = \frac{\sigma_{xy}}{\gamma} \tag{21.2}$$

where γ is called the strain or the angle of the shearing deformation, G is measured in Pa (Pascal). G is one of the elastic moduli, known as the storage modulus, as it is related to the amount of recoverable energy stored by the deformation. G for most polymeric fluids is in the range 10–10^4 Pa, which is much smaller than that of solids ($>10^{10}$ Pa). This is why complex fluids, of which polymeric fluids form a major part, are also known as soft matter, *i.e.* materials that exhibit weak elastic properties.

Polymeric liquids have a microstructure that is like springs representing the linear chain. Restoration of these springs to their equilibrium state is through the elastic energy that is 'stored' during the deformation process. But polymeric fluids are not ideal elastic materials, and they also have a dissipative reaction to deformation, which is the viscous dissipation. For small deformations, the response of the system is linear, meaning that the response is additive: effect of sum of two small deformations is equal to the sum of the two individual responses.

This chapter mainly deals with the rheological behaviour of NR nanocomposites. In the following sections there will be a broad overview about the various rheological phenomena observed in NR nanocomposites.

21.2 Rheological Properties of Natural Rubber Composites

21.2.1 Mica-Filled Composites

Mica is widely distributed and occurs in igneous, metamorphic and sedimentary regimes. Large crystals of mica used for various applications are typically mined from granitic pegmatites. The mica group represents 37 phyllosilicate minerals that have a layered or platy texture. The commercially important micas are muscovite and phlogopite, which are used in a variety of applications. Mica's value is based on several of its unique physical properties. Mica filler has characteristics that entitle it as a processing aid for material rubber compositions. Viviane *et al.*[2] studied the rheology of NR–mica-filled composites in the rubber processing analyser. However, to function as a processing agent in NR compounds, the content of mica must be kept below 20 phr.

Figure 21.1 shows the log plots of rubber process analyzer (RPA) complex dynamic viscosity (η*) vs shear rate (from changes in frequency, in radians/second). The results characterize the rubber as a pseudoplastic material in

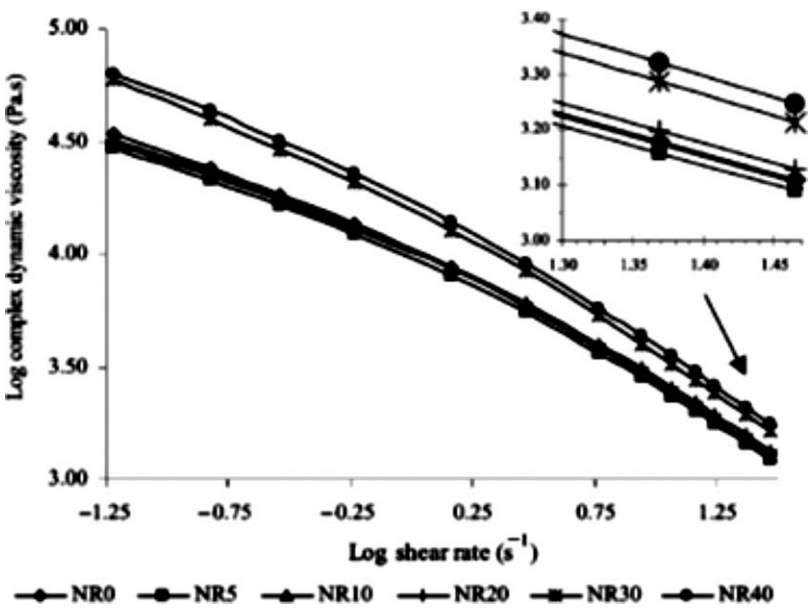

Figure 21.1 Complex dynamic viscosity as a function of shear rate (100 °C, 1 Hz) for the mica-filled NR composites.

which the viscosity decreases with the increase in shear rate. The curves show the same profile, non-Newtonian in character and independent of the presence of filler or its content. For the compositions with less than 20 phr of mica, the curves lie below that with no filler, indicating that at these low levels mica acts as a processing agent. The studies also revealed that the melt viscosity, total torque and mechanical energy (EM) show little increase with the addition of mica. This is a consequence of a weak rubber–filler interaction. The plate-like and crystalline form of mica makes processability easier and act as a good processing agent.

21.2.2 Silica-Filled Composites and Nanocomposites

Silica is a crystalline compound occurring abundantly as quartz, sand and many other minerals and is used to manufacture a variety of materials, especially glass and concrete. Natural silica is a non-reinforcing material and has been used as a filler, only to reduce the cost. The synthetic ones are reinforcing and nowadays have particle sizes as small as the carbon black besides an extremely reactive surface.[3] Important natural varieties are silica (amorphous), silica (crystalline), silica diatomaceous (fossil origin) and silica (microcrystalline). Types of synthetic silica are precipitated, pyrogenic, aerogels and hydrogels. Of these varieties, precipitated silica and pyrogenic (fumed) silica are being used for elastomer reinforcement.

Surface groups on fillers have a prominent role in the cure behaviour. Generally they tend to accelerate or retard cure. Silica contains substantial amounts of combined oxygen in the form of silanol (Si–OH) and siloxane (Si–O–Si), which retard sulfur vulcanization.[4] The silanol groups can interact with curatives through hydrogen bonding. Effect of these interactions can affect compound properties such as viscosity, scorch time, cure rate and cure efficiency and also the vulcanizate properties. Retardation of vulcanization was earlier attributed to the adsorption of curatives by the silica surface.[5] The studies claim that retardation is due to a deactivation mechanism involving interaction of the filler with the zinc–accelerator–sulfur complex.

The addition of silica to the elastomer results in a strong increase of the viscosity. Silanol groups, responsible for the strong inter particle forces, cover the silica surface. Silica particles tend to agglomerate, they are difficult to disperse and reagglomerate after mixing.[6] One of the effects of reagglomeration is the reduction of processability during storage. The viscosity of a compound increases during storage, with an increasing rate at higher temperatures. The viscosity increase follows a second order kinetic law, suggesting that the process is based either on coalescence of filler-bound rubber entities or reagglomeration of filler particles. The tendency of reagglomeration is influenced by the water content of the silica. A higher water content results in a lower rate of viscosity increase during storage due to a shielding effect of the water molecules on the surface of the silica, which reduces the inter particle forces. Highly developed filler networks of silica can give rise to compounds of high viscosities. The difference between types of filler became less pronounced as the average filler

particle size is increased.[7] At about 20 nm size silica produces significantly higher viscosity than carbon black of comparable size.[8] Viscosity modification studies of rubbers filled with smaller particle size silica was reported by Dunnom.[9]

Peng *et al.*[10] studied the morphology of the NR/SiO_2 nanocomposites with different SiO_2 contents. The SiO_2 nanoparticles are homogeneously (Figure 21.2) distributed throughout the NR matrix as nanoclusters with an average size ranging from 60 to 150 nm when the SiO_2 loading is less than 6.5 wt%.

In the SEM images of NR/SiO_2 nanocomposites, the dark phase represents the NR matrix and the bright phase corresponds to the SiO_2 particles, which are strongly embedded in the NR matrix (Figure 21.3). It can be seen that the higher the SiO_2 content the more severe the aggregation observed. At lower concentrations of SiO_2 (<1.0 wt%), most of the spherical clusters of nanoparticles are individually distributed among the NR matrices. When more SiO_2 nanoparticles are loaded, the density of the SiO_2 clusters increases and the SiO_2 clusters start to aggregate in some areas for the nanocomposite.

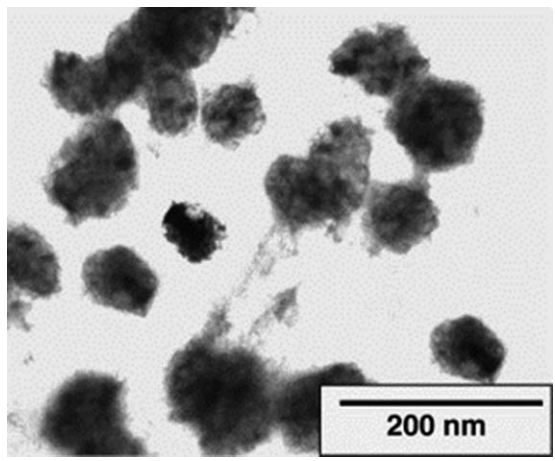

Figure 21.2 TEM image of nanoclusters (4 wt% SiO_2).

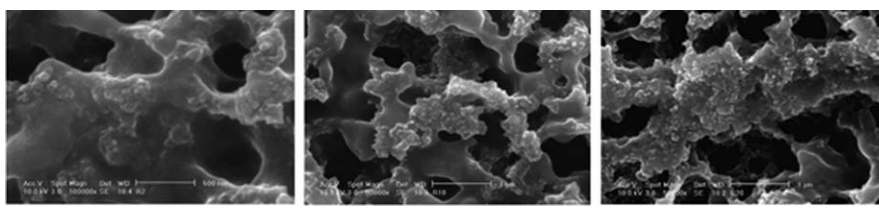

Figure 21.3 SEM images of NR/SiO_2 nanocomposites: (a) 1.0 wt% SiO_2, (b) 4.0 wt% SiO_2 and (c) 8.5 wt% SiO_2.[10]

Meera *et al.*[11] reported the non-linear viscoelastic behaviour of the composites of NR filled with surface-modified nano-silica. The effect of temperature on the non-linear viscoelastic behaviour has been investigated and it was observed that Payne effect becomes more pronounced at higher silica loading. The filler characteristics such as particle size, specific surface area, and the surface structural features were found to be the key parameters influencing the Payne effect. A non-linear decrease in storage modulus with increasing strain was observed for unfilled compounds also. The results reveal that the mechanism includes the breakdown of different networks namely the filler–filler network, the weak polymer–filler network, the chemical network, and the entanglement network. The model of variable network density proposed by Maier and Goritz has been applied to explain the non-linear behaviour. The activation energy of desorption was calculated and found to be within the range of van der Waals interaction energy. The model fits well with the experimental results.

The viscoelastic behaviour vs strain is investigated for silica-filled NR and the results show the qualitative features generally observed for the Payne effect. The effect of the strain amplitude on the storage modulus at various silica concentrations for the composites is shown in Figure 21.4. The storage modulus is the highest at small amplitude (referred to as E'_0) and gradually decreases to a minimum value (referred to as E'_∞). The magnitude of

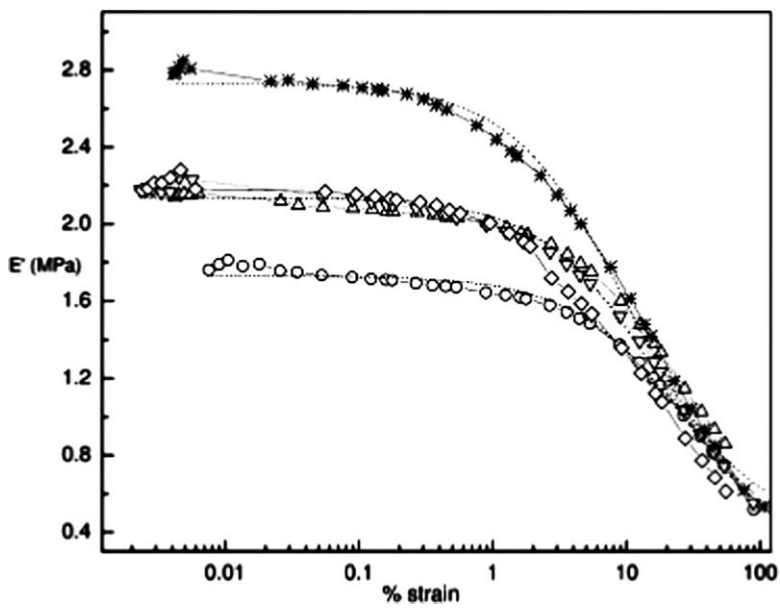

Figure 21.4 Strain dependence of the storage modulus for NR filled with nano-silica: (○) 0 phr, (△) 5 phr, (▼) 10 phr, (◇) 15 phr, (*) 20 phr. The dotted lines represent the curve fits according to the model.

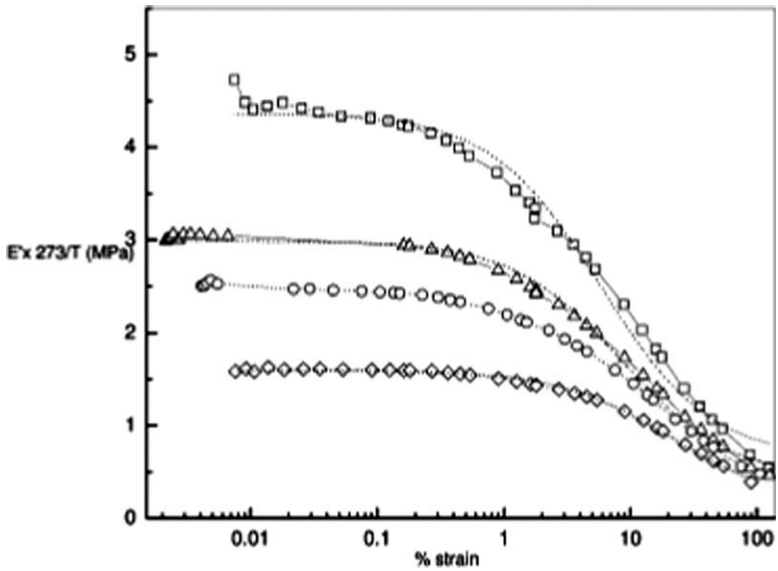

Figure 21.5 Effect of temperature on the Payne effect for NR filled with 20 phr silica: (□) 248 K, (△) 263 K, (○) 303 K, (◇) 373 K. The dotted lines represent the curve fits according to the model.

the Payne effect ($E'_0 - E'_\infty$) increases with the silica content. At low silica loading, the observed variation in the amplitude of the Payne effect is weak. But as the silica concentration increases, significant and pronounced variation is observed. This is principally due to the breakdown of the filler networks at high strains. At low filler loading, the chances of forming agglomerates are practically zero. But at higher loading, because of the small particle size (12–13 nm) and high specific surface area (25 m^2/g), silica particles tend to agglomerate to higher extent. The structure of filler particles within the rubber matrix, *i.e.* the state of dispersion and aggregation has a strong influence on the Payne effect. In the rubber matrix, the state of dispersion of spherical particles can vary from highly dispersed to totally aggregate depending on the thermodynamics of the system and kinetics of samples preparation. The clustering of filler particles is favoured by strong van der Waals forces.

Figure 21.5 shows the effect of temperature on the Payne effect for NR filled with 20 phr of nano-silica. As previously reported,[12] the amplitude of the Payne effect decreases dramatically with temperature. This is contrary to the theory of rubber elasticity, according to which the modulus should increase linearly with the temperature. In agreement with the former explanation given for the Payne effect, the temperature increases the rate of destruction of the network by weakening its cohesion. In the Kraus' model, the temperature affects the strength of the van der Waals forces between the particles. In the Merabia's vision, the thickness of the glassy layer decreases, diminishing as a consequence

the number of glassy bridges forming the network. For Maier and Goritz, the rate of the chains desorption increases with temperature.

21.2.2.1 Application of the Model of Variable Network Density

In the Maier and Goritz model,[13–15] it is assumed that the rubber molecules come in contact with the filler surface and get adsorbed. After forming the first link, the neighbouring segments have a high probability to attach to the next interaction position. These chains form stable bonds to the filler surface, whereas the remaining chains coming afterward form unstable bonds having very weak links to the particle. These can be easily removed by a tensile force or by raising the temperature. According to this model, the network density of a filled vulcanized elastomer (N) comes from the overall contribution of the chemical network density, N_c, the chains network density caused by stable bonds at the filler surface, N_{st}, and the density of unstable bonds between chains and filler, N_1

$$N = N_c + N_{st} + N_1 \tag{21.3}$$

Storage modulus $E' = Nk_BT$ where N is the network density, k_B is the Boltzmann constant, and T is the temperature in Kelvin. The strain dependent modulus can be described by means of the theory of entropy and elasticity with

$$E'(\gamma) = (N_c + N_{st} + N_1(\gamma)K_BT \tag{21.4}$$

By analogy with the Langmuir isotherm formation, it is assumed that the adsorption/desorption process reaches a balance after a certain time. On the assumption that the desorption rate is proportional to the strain amplitude, γ, the dependence of the modulus on γ can be written as

$$E'(\gamma) = E'_{st} + E'_1/(1 + c\gamma) \tag{21.5}$$

$$E'_{st} = (N_c + N_{st})k_BT \tag{21.6}$$

$$E'_1 = N_{10}K_BT \tag{21.7}$$

From the fit parameters, E'_{st} and E'_1 and the values of χ^2/DOF and R^2 to assess the quality of fit, both E'_{st} and E'_1 increase with an increase in silica content. The values characterizing the unstable part of the network are strongly influenced by the filler content. The model equally applies when no filler is added, suggesting that part of the entanglement network has a longer relaxation time than the experimental time defined as the inverse of the frequency.

The experimental curves obtained for NR filled with 20 phr silica and fitted to Equation 21.5[11] are shown in Figure 21.5. The dotted lines represent the curve fits according to the model. It is observed that both the number of the stable and unstable bonds of the network is identically reduced by roughly a factor of 5 when the temperature goes from 248 to 373 K.

21.2.3 Clay-Filled Nanocomposites

In recent years, polymer/clay nanocomposites (PCNs) emerged as a new class of material. Compared with their relative micro and macro scale counterparts and their pristine polymer matrices, PCNs exhibit significantly improved performances such as tensile strength, modulus, heat resistance, gas barrier properties, swelling resistance, *etc*. Very recently, increasing attention has been paid on rubber/clay nanocomposites (RCNs). According to reports, Several RCNs based on one or two elastomers has been prepared via solution intercalation, melt intercalation, and rubber-latex compounding.[16–18]

The most commonly used layered silicates are montmorillonite, hectorite and saponite. The important characteristics of layered silicates are its ability to disperse into individual layers and also their ability to fine-tune their surface chemistry through ion-exchange reactions with organic and inorganic cations. According to the strength of interfacial interactions between the polymer matrix and layered silicates, three different types of polymer layered silicates (PLS) nanocomposites can be thermodynamically achieved as shown in Figure 21.6; (a) microcomposite, (b) intercalated and (c) exfoliated nanocomposites. Because of the high contact surface area, exfoliated system exhibits better properties. There are reported studies on the mechanical properties of lattices with layered silicates.[19,20]

Clays compatibilized and evenly dispersed in a polymer matrix tend to build networks at low concentration. Rheological measurements, performed on RCN based on various types of rubbers, revealed the pronounced rubber–clay interaction, when measurements were taken at zero shear. The filler networking phenomenon was observed as well in matrices based on various other rubber systems.[21–23] At zero shear, the viscosity of RCN is thus higher than the one of

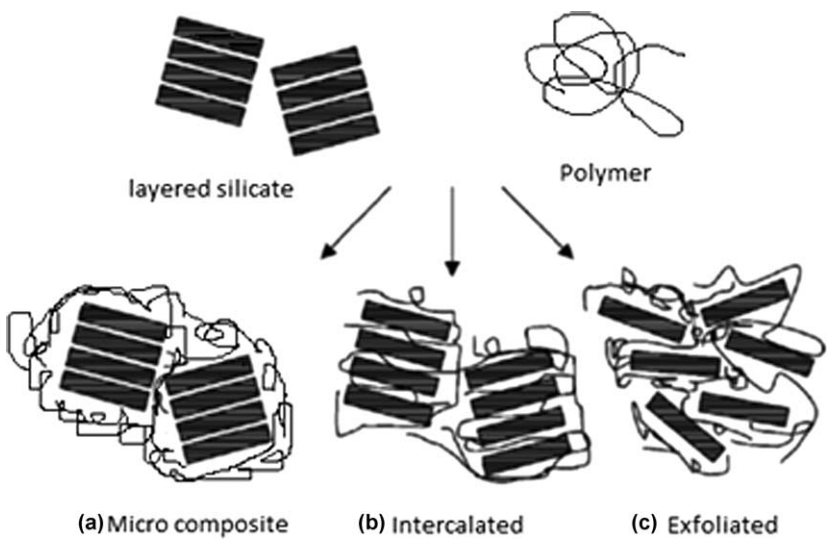

Figure 21.6 Three different types of polymer–clay nanocomposites.

the neat elastomer. However, organophilic clays were shown to reduce the steady shear viscosity of RCN. Most evident results were a pronounced shear-thinning behaviour, increasing with the clay content, a higher extent of extrudate, a lower swelling and a better surface smoothness, by increasing the shear rate. These findings are of great importance, as they indicate that organoclay have a positive effect on the processability of rubber compounds. A compensating cation with longer alkyl chains led to a reduction of Mooney viscosity, which was not observed with a short chain substituent.[24] This behaviour of organoclay, which is opposite to that of traditional fillers, is attributed to the orientation, occurring at high shear rates, of clay platelets along flow direction, and to the slippage of platelets on the chains.

Ranimol *et al.*[25] reported the impact of layered silicates such as sodium bentonite and sodium fluorohectorite on the rheological behaviour of NR, carboxylated styrene butadiene rubber and their blends. The rheological behaviour was analysed with special reference to shear rate, temperature, and filler loading. In their study it was found that the viscosity of the lattices with layered silicates increased as a function of concentrations of filler and also exhibited pronounced shear-thinning behaviour. The enhancement in viscosity upon the addition of nanofillers indicated a more uniform distribution of clay particles and higher extent of silicate exfoliation on nanoscale. As the temperature is increased the viscosity of all samples decreased because of the rupturing of network existed between rubber and filler. It was observed that the activation energy of layered silicates reinforced NR latex is higher than other samples because of the intercalation of polymer into the layers of silicates, thereby enhancing the temperature sensitivity of the material. Zero shear viscosity of layered silicate-filled latices was higher than unfilled samples due to the enhancement in contact surface area between polymer and the filler.

Teh *et al.*[26] studied the effect of compatibilizer and organophilic layered clay on NR as matrix, epoxidized natural rubber (ENR). By the analysis of cure characteristics, the addition of ENR in NR will decrease both scorch and cure times. This may be due to the activation effects of epoxy functional groups on the crosslinking. A further cure acceleration was observed when organoclay was introduced. This was traced again to changes in the sulfur curing owing to the onium intercalant present. The observed increase in the maximum torque, minimum torque and torque difference suggested an increment in stiffness, viscosity and crosslink density, respectively.

Manchado *et al.*[27] studied the effect of the incorporation of a bentonite on the vulcanization kinetics of NR by means of both cure meter testing and differential scanning calorimetry (DSC) under dynamic and isothermal conditions. The vulcanization curves showed that the modified clay behaved as an effective vulcanizing agent, accelerating the vulcanization reaction of the elastomer. A marked decrease in the induction time and optimum cure time of the elastomer were observed in the presence of the organoclay. Although the octadecylamine itself accelerated the vulcanization process, the octadecylamine-modified clay gave rise to a further noticeable increase in the vulcanization rate, which could be attributed to a synergetic effect between the filler and the amine. Moreover, in the

presence of the organoclay, a dramatic increase in the torque value was obtained because of the formation of a higher number of crosslinks, which could be attributed to the confinement of the elastomer chains within the silicate galleries and, consequently, to better interactions between the filler and the rubber. As was expected, the torque value gradually decreased as the cure temperature increased. However, an over-curing reversion reaction was easily observed. Above t_{97}, the rheometer curve tended to descend, which corresponded to a loss of the mechanical characteristics of the material. This was attributed to the breakdown of bonds, in particular, polysulfide bonds. In the same manner and to evaluate the effect of the incorporation of the clay (unmodified and organically modified) on the cure characteristics of NR, the vulcanization curves of all the studied materials at 160 °C were obtained. According to these results, it can be assumed that the organoclay behaved as a vulcanizing agent for NR, giving rise to a noticeable increase in the elastomer vulcanization rate. The increase in the vulcanization rate of the elastomer is attributed by the amine group of organo modified nanoclay.

21.2.4 Fly Ash-Filled Composites

Ash residues are wastes of coal-fired power plants; these include fly ash (FA) and bottom ash.[28,29] Fly ash material solidifies while suspended in the exhaust gases and is collected by electrostatic precipitators or filter bags. Since the particles solidify rapidly while suspended in the exhaust gases, FA particles are generally spherical in shape and range in size from 0.5 μm to 300 μm. FA is a relatively inexpensive by-product, and its usages have the benefit of decreasing environmental problems. Furthermore, FA has been used in industry as a consequence of such advantages as low cost, smooth spherical surface and good processability of the filled materials.[30] In a previous study,[31–37] it has been reported that FA particles consist of silicon dioxide similar to silica but with the lower content of silicon dioxide than silica. The use of FA is restricted because of its much lower structure and surface reactivity.

Reyad *et al.*[38] carried out surface modification of oil fly ash (OFA), a by-product generated by oil power plants, by chemical treatment. A mixture of sulfuric and nitric acids was used to modify the surface in order to attach a carboxylic functional group to the surface of OFA. The goal of surface modification of OFA is to make its surface more compatible with non-polar polymers in order to produce OFA/polymer composite materials with improved dispersion of OFA, and to increase OFA surface area in order to support its use as adsorbent materials in adsorptive separation and purification applications. Different acid compositions were used in their study for the treatment by gradually increasing the nitric acid concentration from 0 to 20%. They also examined the effect of oxidation on surface modification by introducing air to enhance the oxidation of OFA.

Thanunya *et al.*[39] reported the use of FA as filler in NR to reinforce and/or reduce product cost. In their study the viscoelastic properties of FA-filled NR composites with various FA loadings were investigated with the utilization of

two different modes of shear flow, namely, oscillatory and steady shear flow. It is found that the addition of FA to NR increases storage modulus (G_0) and shear viscosity under both oscillatory and steady shear flow. Moreover, the oscillatory test results exhibit the unexpected increase in magnitude of viscous response with increasing FA loading in FA-filled NR compounds. The explanation is proposed in terms of the ball-bearing effect of FA with spherical shape associated with the occurrence of molecular degradation induced by inorganic constituents particularly manganese, iron, and copper in non-rubber component of NR as well as the small amount of heavy metals including iron, copper in FA.

21.2.5 Other Inorganic Composites and Nanocomposites

Hard ferrite or ceramic permanent magnets are considered to be an important and sophisticated class of engineering materials, which are used extensively in various applications. Hexa-ferrite magnets have found acceptance in many electronic products, as a result of their superior cost efficiency, large coercivity, and specific magnetic saturation associated with their high magnetic and chemical stability.[40,41] Many sintered magnets are brittle, hard, and difficult to machine to their final form. The advantages of polymer-bonded magnets over their metallic and ceramic counterparts include low weight, resistance to corrosion, ease of machining and forming, and capability for high production rates.[42] The evaluation of the cure characteristics and dynamic properties helps to understand the processability and also provides valuable information about the matrix–filler interaction, percolation threshold, and filler dispersion. These essential characteristics play an important role in determining the overall physical properties of the composites. Furthermore, the filler parameters influence the dynamic and the physical properties of the composites in different ways.[43] For example, (i) particle–particle interactions become important above certain volume fractions, depending on the particle morphology;[44,45] (ii) the percolation limit can be achieved at different filler loadings, depending on the aspect ratio and the particle size of the fillers.[46,47] (iii) filler aggregation, especially at high loading, leads to chain-like filler structure or clusters, which affect rubber properties and viscoelastic behaviour. (iv) Filler increases the thermal conductivity of the composite matrix, consequently reducing the cure time for thick rubber articles and giving uniform curing throughout the material.[48] In other words, the dynamic properties of rubber products are influenced by many factors, such as the size, shape, nature, and state of distribution of filler; type of rubber; adhesion and thermal compatibility of the matrix; and so forth.[49,50] Thus, the overall effect of each of the variables on the final properties of the composites is complex.

Makled *et al.*[51] reported the influence of co-precipitated hexagonal barium ferrite $BaFe_{12}O_{19}$ phase on the cure characteristics and dynamic properties of NR–ferrite composites as a function of ferrite loading up to 2–20 phr (parts per hundred parts of rubber). The results showed that the scorch time decreased dramatically with increasing ferrite content until 160 phr BaF loading, this is because of the heat of mixing increases as the filler loading.

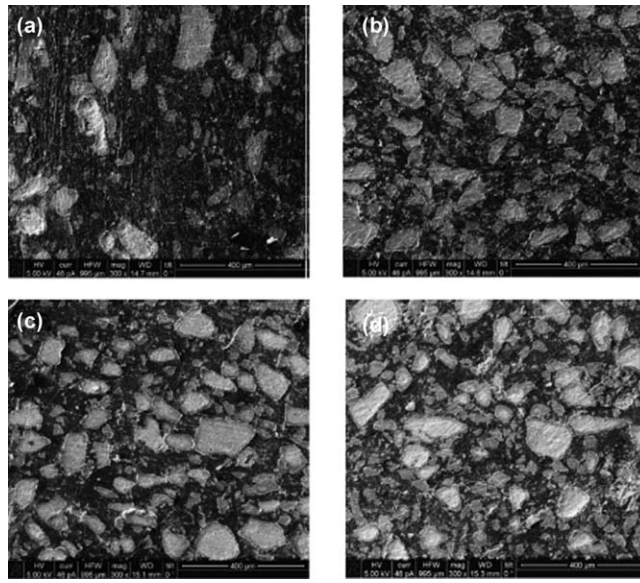

Figure 21.7 SEM images for the RFC samples with different ferrite loadings: (a) 90 phr, (b) 160 phr, (c) 180 phr and (d) 220 phr.

Figure 21.7(a) to (d) shows the distribution of ferrite particles in rubber matrices. The variation in particle size, the broad particle distribution and the homogeneous dispersion can be observed from the images. It is also interesting to note that there is no tendency to form agglomerates at high loading level. There is a formation of a cohesive network for the ferrite particles in the rubber matrix, leading to percolation above 180 phr. It was also found that there is a saturation of scorch time and this is attributed to the starting formation of a filler network inside the rubber matrix. Consequently, the heat of mixing becomes sufficient, saturated and independent of ferrite loading, leading to no change in t_{10}. On the other hand, cure time, which is the total time required for optimum vulcanization of the samples, decreases sharply with increasing ferrite loading at low ferrite content because of the decreasing of scorch time. This can be explained by the fact that $BaFe_{12}O_{19}$ particles are isotropic in nature, have a small nucleation effect, and interact strongly with rubber. Furthermore, the reduction of cure time of the filled vulcanizates can be attributed to the higher time the rubber compound remains on the mill during mixing. As the filler loading increases, the time of incorporation also increases consequently, generating more heat due to the fraction.

Ahmed *et al.*[52] studied the improved properties of rubber vulcanizates containing white molybdates. The fillers were incorporated into NR formulations indifferent ratios up to 40 phr to study the effect of filler loading on the properties of the vulcanizates. Molybdates can be used as reinforcing fillers in rubber compounds to replace carbon black. Molybdenum is unlike other heavy metals, in that it is non-toxic, has good whiteness, and is reasonably priced,

qualities that may ensure good commercial potential for these white molybdate pigments. Molybdates have controlled solubility. From the data, it was clear that the maximum torque (M_H), minimum torque (M_L) and optimum cure time (t_{90}) increased as filler content increased. It was also noted that the NR vulcanizates loaded with inorganic white molybdate fillers showed an increase in crosslinking (by swelling measurements), indicating an interaction or bonding between the rubber and fillers.

21.2.6 Carbon Nanotube-Filled Nanocomposites

Carbon nanotubes can be visualized as graphene layers rolled into cylinders consisting of a planar hexagonal arrangement of carbon–carbon bonds. Their outstanding properties are a consequence of this unique bonding arrangement combined with topological defects required for rolling up the sheets of graphite into cylinders. During growth, depending on the synthesis methods, they can assemble either as concentric tubes (multiwall nanotubes, MWNTs) or as individual cylinders (single-wall nanotubes, SWNTs). Their diameters range from about a nanometre to tens of nanometres with lengths ranging from several micrometres to millimetres or even centimetres (Figure 21.8).

Carbon nanotubes (CNTs) are useful in electronics, optics, and materials applications. The exceptional mechanical and transport properties of CNTs provide useful insight into the potential for nanoparticle additives in liquids and solid polymers to achieve significant improvements in bulk properties at low volume concentrations. The uniqueness of CNT properties arises from the structure and molecular arrangement of the carbon atoms. It is expected that the mechanical and physical properties of a rubber material may be improved through the addition of a lower amount of nanoscale fillers due to the higher specific surface area, and which will also retain the elasticity of the rubber. In the development of rubber nanocomposites, especially utilizing CNTs composite materials will have great significance and beneficial results for various industrial applications. There has been much research into CNT-reinforced rubber.[53–57]

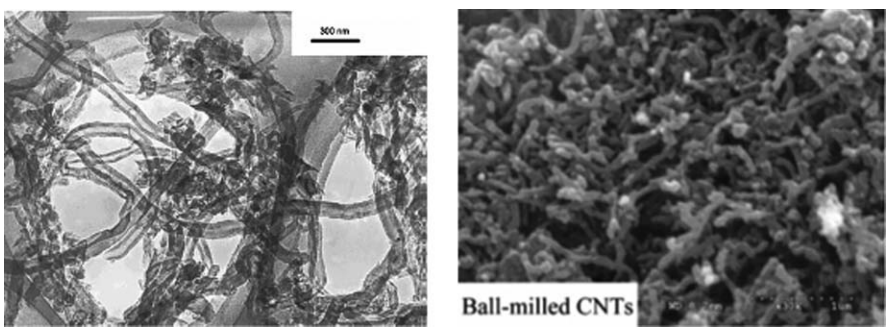

Figure 21.8 TEM images of raw CNTs and ball-milled CNTs.

Sui *et al.*[58] reported that the scorch time of NR, which is the measurement of premature vulcanization of rubber, showed a slight reduction after the addition of the fillers. The effect of CNTs on the scorch time might depend on the composition and microstructure of rubber composites. During the curing reaction period, the torque of rubber specimens gradually increased, which reflected that the vulcanizing rate of CNT/NR nanocomposites is lower. This is because the CNTs with ultra-high modulus effectively restricted the changes in polymer molecular configuration, and then enhanced the modulus of the rubber composites.

It was found from Figure 21.9 that the storage modulus of the CNT/NR nanocomposites is higher than that of the neat NR and carbon black/NR composites from low temperature to high temperature regions. The high modulus and specific surface area of CNTs enhance the stiffness of the NR, which results in an increment of storage modulus of the CNT/NR nanocomposite. At low temperature, the modulus of the neat NR exhibits a high value due to the semicrystalline characteristic of NR, and a small variation in the modulus of NR appeared after the addition of fillers. With the increase in temperature, although the E' of all specimens manifested declining trends, it is evident that stiffness of NR increases as a result of the addition of fillers. A shift of rapid decreasing region of E' towards higher temperature can be seen for NR after adding the CNTs and the reinforcing effect is more obvious above the T_g of NR. The storage modulus of CNT/NR nanocomposites in the rubbery region is the highest among all specimens and remains steady within the testing temperature.

The position of tan δ peak in tan δ – temperature curve can also be used to identify the Tg of the rubber materials. It can be seen from Figure 21.10 that the peak of tan δ of the NR composite slightly shifts to a higher temperature compared to that of the neat NR. It denotes that the mobilization of rubber

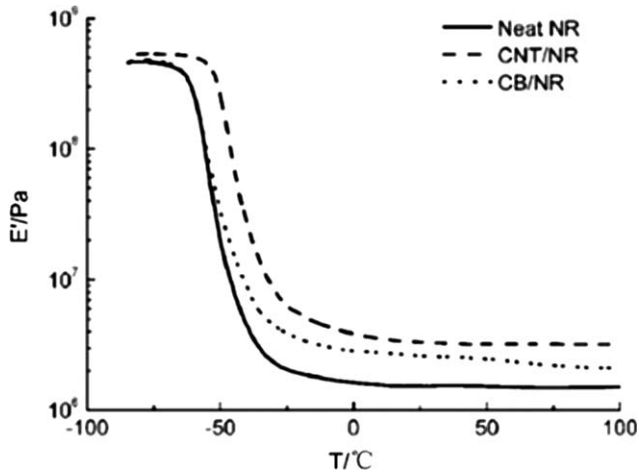

Figure 21.9 The storage modulus of the neat NR and NR composites vs temperature.

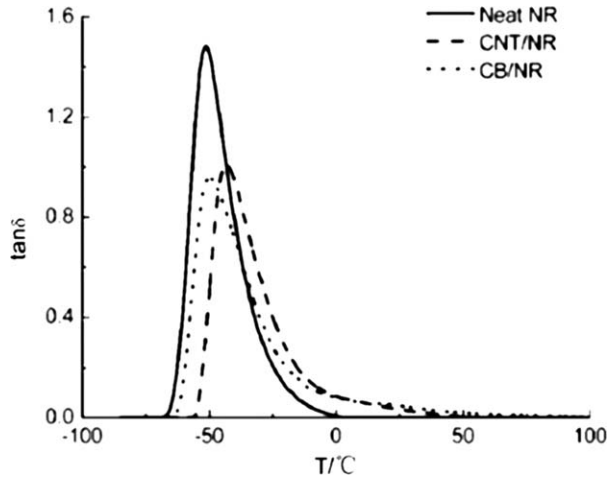

Figure 21.10 Temperature dependence of tan δ of neat NR and NR composites.

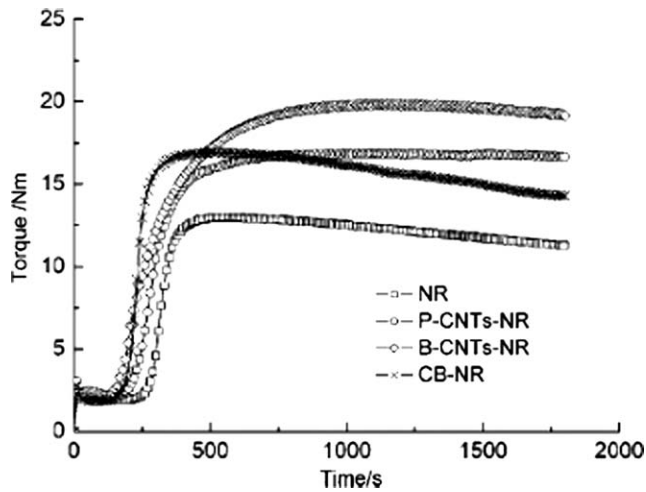

Figure 21.11 Vulcanization curves of neat NR and NR nanocomposites.

macromolecules is restricted due to the addition of fillers. The adding of CNTs reduces the percentage of the NR in composites, which lowers hysteresis loss of the rubber under an oscillating force. Therefore, the height of the tan δ peak of NR decreases after the adding of fillers.

Another study by Sui *et al.*[59] shows the vulcanization curves of the neat NR and NR composites. In Figure 21.11 it can be seen that the scorch time (measurement of premature vulcanization) decreased after adding CNTs or carbon black into the NR. This may be because when CNTs are added, they would absorb the basic accelerator species and delay the onset of vulcanisation. The reason for this is that the addition of the CNTs could improve thermal

conductivity of the NR material. The second region in the vulcanization curves is the curing reaction period, during which the crosslinking network was formed in the rubber and the stiffness of the rubber was increased. The maximum torque was found to be the nanocomposite specimen containing ball-milled CNTs was the highest among the materials. This may be due to that that the ball-milled CNTs effectively restricted the changes in polymer molecular configuration, and then enhanced the modulus of the rubber composites. In the last region of the vulcanization process, Comparing to the NR specimen filled with carbon black, the over-curing reversion of CNT-filled composites was reduced and processing security was enhanced. This would help eliminate the difference in the degree of crosslinking between the surface and the inside of thick rubber products, such as truck tires, *etc*., which arises from the low thermal conductivity of the rubber materials.

21.2.7 Bio-Based Composites

Biocomposites are defined as the materials made by combining natural fibre and petroleum-derived non-biodegradable polymer or biodegradable polymer. Biocomposites derived from natural fibre and crop/bioderived plastic (biopolymer/bioplastic) are likely to be more eco-friendly and such composites are termed as green composites.[60] Use of natural fibre as filler in polymeric matrix offers several advantages over conventional inorganic fillers with regard to their low energy cost, positive contribution to global carbon budget,[61] greater deformability, biodegradability,[62] combustibility, ease of recyclability,[63] good thermal and insulation properties,[64] lower density, less abrasiveness to processing equipment, environmentally friendly nature, lower cost,[65] renewable nature, non-toxicity, flexible usage, high specific strength, good electrical resistance, good acoustic insulation property, worldwide availability, *etc*. There is a growing interest on natural fibre composites in various fields due to these advantages.

Jacob *et al*.[66] reported that the storage modulus (E') of OPF–sisal fibre–NR hybrid composites increased when chemical treatments were done on fibres. Higher values of E′ were exhibited by the composite prepared from fibres treated with 4% NaOH. Improved interfacial adhesion and increased surface area of fibres on alkali treatment led to more crosslinks within rubber matrix–fibre network and thus the E' increased. The loss modulus increased from 634 to 655 MPa when fibres were treated with 0.5% NaOH (both contain 30 phr fibres). The loss modulus further increased to 801 MPa when fibres were treated with 4% NaOH. However, treated fibre composites exhibited low mechanical damping parameter (tan δ_{max}). The strong and rigid fibre–matrix interface due to improved adhesion reduces molecular mobility in the interfacial zone causing a decrease in tan δ_{max}. The presence of bonding agent results in more number of crosslinks being formed and alkali treatment on fibres leads to strengthening of these crosslinks. As a result, molecular motion along the rubber macromolecular chain was severely hindered, leading to low damping characteristics.

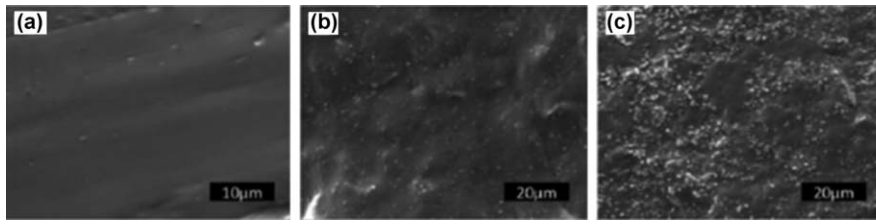

Figure 21.12 SEM images of the fractured cross-section of (a) NR100, (b) M27-NR95 (5 wt% of maize starch nanocrystal and 95 wt% of NR), and (c) M27-NR70 (30 wt% of maize starch and 70 wt% of NR).

Morphological analysis of the NR nanocomposites was done by Dufresne *et al.*[67] Figure 21.12 shows SEM images of the fractured cross-section of NR filled with 0, 5 and 30 wt% starch nanocrystals. The unfilled NR matrix (Figure 21.12(a)) shows a clearly smooth and uniform cross-section. The distribution of starch nanocrystals seems rather homogeneous throughout the matrix from the fact that starch nano crystals (SNC) can be spotted in these micrographs (Figure 21.12(b) and (c)).

In another work, Dufresne *et al.*[68] developed a phenomenological modelling approach to understand the reinforcing mechanism of starch nanocrystals in a non-vulcanized NR matrix. The NR was not crosslinked to maintain the biodegradability of the biosourced materials. Non-linear dynamic mechanical experiments highlighted the significant reinforcing effect of starch nanocrystals and the presence of the Mullins and Payne effects. Two models were used to predict the Payne effect considering that either filler–filler (Kraus model) or matrix filler (Maier and Goritz model) interactions are preponderant. The use of the Maier and Goritz model demonstrated that phenomena of adsorption and desorption of NR chains on the filler surface governed non-linear viscoelastic properties, even if the formation of a percolating network for filler contents >6.7 vol% was evidenced by the Kraus model. The non-linear dynamic mechanical experiments confirmed the significant reinforcing effect of waxy maize starch nanocrystals in a non-vulcanized NR matrix. The reinforcing of NR by 6.7 vol% of starch nanocrystals allowed us to increase the relaxed modulus at room temperature by a factor 10. The presence of both Mullins and Payne effects was highlighted for all nanocomposites, even for low filler contents. The phenomenological modelling approach was to understand the reinforcing mechanisms of starch nanocrystals and to discriminate the possible origins of the non-linear viscoelastic behaviour of NR/starch nanocrystal nanocomposites. Two models were used to predict the Payne effect: (i) the Kraus model considering that filler–filler interactions are preponderant and (ii) the Maier and Goritz model that is based on matrix–filler interactions. It was demonstrated that phenomena of adsorption/desorption or slippage of NR chains on the filler surface governed the non-linear viscoelastic properties of no vulcanized NR/starch nanocrystal nanocomposites, even if the formation of a percolating network for filler contents >6.7 vol% (10 wt%) was evidenced.

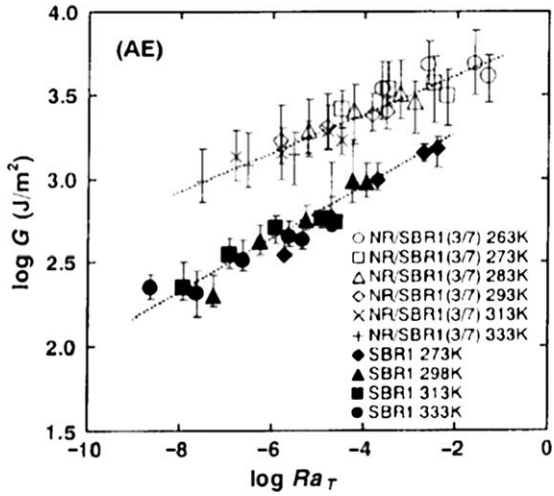

Figure 21.13 Plot of G for the acetone-extracted NR/SBR1 (NR/SBR1-AE) blend with respect to Ra_T, for which a_T for SBR1.

The approach proposed in this Article is now being applied to other nanocomposites to separate the relative contributions of filler–filler to filler–polymer interactions from their non-linear viscoelastic behaviour.

Tetsuji *et al.*[69] studied the effect of fatty acids on the rapid strain-induced crystallization of crosslinked NR. The factors influencing the rapid strain-induced crystallization have still remained unclear because of the difficulty of detecting the rapid crystallization reproducibly. In their study the blend samples NR/SBR1 and SBR2/SBR1 (30/70 w/w) were also prepared by the mixing of SBR1 and SBR2, respectively, with masticated NR on the roll mill. In their investigation they noticed about the tear energy (G) of the NR/SBR blend because the strain-induced crystallization of NR must play an important role in preventing crack growth of the blend under large deformation. G of a non-crystalline polymer is well known to depend on the rate of tear and the temperature, and a principle of time–temperature superposition according to the Williams–Landel–Ferry (WLF) equation.

From Figure 21.13 it can be noted that there is a single master curve for the SBR2/SBR1 blend. This was quite different from the two curves for G that appeared for the NR/SBR1 blend after superposition. The difference may be due to the effect of the fatty acid because the fatty acid was mainly removed by acetone extraction. This may suggest that the fatty acid promoted the strain-induced crystallization of NR.

21.3 Conclusions

Rheology has been used as a semi-quantitative tool in polymer science and engineering. The developments involving rheological properties of polymer, structure and morphology of molten polymer composites clearly specifies that

the field expands at unprecedented rates. The rheological measurements on polymers can reveal the variety of behaviour exhibited even in simple flows and provide useful insights to enthusiastic engineers on how to control the flow and feel of polymeric liquids. The leading progress behind the progress of rheological measurements is efficiency, functionality and precision of these materials. The effective implementation of morphology of molten polymer composites, morphology and its effects on rheology directly depends on the degree of understanding of their behaviour and properties. Rheology helps to mould advanced rubber composites with improved comprehensive performance and this is a potential technique for expanded future industrial applications in bulk scenarios for industrial processing and a requirement for high quality industrial-scale production.

21.4 Challenges

In the rheological measurements the main challenges arise due to the understanding of the polymers to variations in their manufacture, time and temperature-dependent effects and the non-linearity of their coupled mechanical, physical and chemical properties. The major problem with much priority is the morphology and the control of these materials. The basic properties of the polymers combined with their control functions tend to produce new and unexplored effects that should be fully understood. It is also important that polymers execute their functions over a wide range of temperatures and frequencies. Such conditions tend to accelerate their degradation and, consequently, alter their functional response through electromechanical couplings. Other than the experimental investigations the prediction of the end-use properties of polymeric products is faced with some daunting challenges. The current process simulation approach, which is based on the continuum mechanics of non-Newtonian fluids, must be combined with models describing macromolecular conformations, relaxation and polycrystalline morphologies.

References

1. H. A. Barnes, J. F. Hutton and K. Walters, *An Introduction to Rheology*, Elsevier, Amsterdam, 1989.
2. A. Viviane, E. Leila, L. Y. Visconte and R. C. R. Nunes, *Int. J. Polym. Mater.*, 2008, **57**, 374.
3. R. C. R. Nunes, J. L. C. Fonsecs and M. R. Pereira, *Polym. Test.*, 2000, **19**, 93.
4. C. Hepburn, *Plastics and Rubber International*, 1984, **9**, 11.
5. R. C. W. Moakes and J. R. Payne, *Proc. of IRI*, 1954, **1**, 151.
6. S. Wolff, U. Goerl and M. J. Wan, *Eur. Rubber J.*, 1994, **16**, 1619.
7. M. Q. Fetterman and M. P. Wagner, *Rubber Chem. Technol.*, 1972, **45**, 1161.
8. M. A. Schoenbeck, *Rubber Age*, 1962, **92**, 75.
9. D. Dunnom, *Rubber Age*, 1968, **100**, 49.

10. Z. Peng, L. X. Kong, S.-D. Li, Y. Chen and M. F. Huang, *Compos. Sci. Tech.*, 2007, **67**, 3130.
11. A. P. Meera, S. Said, Y. Grohens and S. Thomas, *J. Phys. Chem. C*, 2009, **113**, 17997.
12. M. Wang, *Rubber Chem. Technol.*, 1998, **71**, 520.
13. P. G. Maier and D. Goritz, *Kautsch. Gummi Kunstst.*, 1993, **46**, Jahrgang. Nr.11/93.
14. P. G. Maier and D. Goritz, *Kautsch. Gummi Kunstst.*, 1996, **49**, Jahrgang. Nr.1/96.
15. P. G. Maier and D. Goritz, *Kautsch. Gummi Kunstst.*, 2000, **53**, Jahrgang. Nr. 12/2000.
16. A. Alipour, G. Naderi, G. R. Bakhshandeh, H. Vali and Sh. Shokoohi, *Int. Poly. Pro.*, 2011, **XXVI**, 48.
17. S. Varghese, K. G. Gatos and A. A. Apostolov, *J. Appl. Polym. Sci.*, 2004, **92**, 54.
18. S. Varghese, J. Karger-Kocsis and K. G. Gatos, *Polymer*, 2003, **44**, 3977.
19. Y. Wang, H. Z. Zhang and Y. Wu, *J. Appl. Polym. Sci.*, 2005, **96**, 318.
20. R. A. Vaia, G. Price, P. N. Ruth and H. T. Nguyen, *J. Lichtenhan, J. Appl. Clay. Sci.*, 1999, **15**, 67.
21. K. Yano, A. Usuki, A. Okada, T. Kurauchi and O. Kamigaito, *J. Polym. Sci., Part A: Polym Chem.*, 1993, **31**, 2493.
22. Y. T. Vu, J. E. Mark, L. H. Pham and M. Engelhardt, *J. Appl. Polym. Sci.*, 2001, **82**, 1391.
23. M. Tian, C. Qu, Y. Feng and L. Zhang, *J. Mater. Sci.*, 2003, **38**, 4917.
24. J. T. Kim, T. S. Oh and D. H. Lee, *Polym. Int.*, 2003, **52**, 1203.
25. S. Ranimol, A. Rosamma, C. Treesa, S. Varghese, J. Kuruvilla and T. Sabu, *J. Appl. Polym. Sci.*, 2006, **101**, 2355.
26. P. L. Teh, Z. A. MohdIshak, A. S. Hashim, J. Karger-Kocsis and U. S. Ishiaku, *Eur. Polym. J.*, 2004, **40**, 2513.
27. M. A. López-Manchado, M. Arroyo, B. Herrero and J. Biagiotti, *J. Appl. Polym. Sci.*, 2003, **89**, 1.
28. N. Sombutsompop, S. Thongsang, T. Markpin and E. Wimolmala, *J. Appl. Polym. Sci.*, 2004, **93**, 2119.
29. J. Duchesne and E. Reardon, *J. Waste Manage*, 1999, **19**, 221.
30. P. Janos, M. Wildnerova and T. Loucka, *J. Waste Manage.*, 2002, **22**, 783.
31. J. Gu, G. Wu and Q. Zhang, *Mater. Sci. Eng.*, 2007, **614**, 452.
32. G. Wu, J. Gu and X. Zhao, *J. Appl. Polym. Sci.*, 2007, **105**, 1118.
33. U. Atikler, D. Basalp and F. Tihminlioglu, *J. Appl. Polym. Sci.*, 2006, **102**, 4460.
34. E. Cokca and Z. Yilmaz, *Waste Manage.*, 2004, **24**, 153.
35. N. Alkadasi, D. G. Hundiwale and U. R. Kapadi, *J. Appl. Polym. Sci.*, 2004, **91**, 1322.
36. D. G. Hundiwale, U. R. Kapadi, M. C. Desai and S. H. Bidkar, *J. Appl. Polym. Sci.*, 2002, **85**, 995.
37. J. G. S. Jaarsveld, J. S. J. Deventer and G. C. Lucky, *Chem. Eng. J.*, 2002, **89**, 63.

38. R. Shawabkeh, M. J. Khan, A. A. Al-Juhani, H. I. Al-Abdul Wahhab and I. A. Hussein, *Appl. Surf. Sci.*, 2011, **258**, 1643.
39. T. Saowapark, N. Sombatsompop and C. Sirisinha, *J. Appl. Polym. Sci.*, 2009, **112**, 2552.
40. J. Smit and H. P. J. Wijin, *Ferrites*; Philips Technical library: Tokyo, 1959–1965.
41. E. C. Milke, M. Rei, J. P. de Souze and L. Schaeffer, *Int. J. Powder Metall.*, 2001, **37**, 47.
42. J. U. Otaigbe, H. S. Kim and J. Xiao, *Polym. Compos.*, 1999, **20**, 697.
43. M. Wang, *J. Rubber Chem. Technol.*, 1998, **72**, 430.
44. T. J. Fiske, H. S. Gokturk and D. M. Kalyon, *J. Mater. Sci.*, 1997, **32**, 5551.
45. D. Puryanti, S. Hj Ahmad and M. Hj Abdullah, *Polym. Plast. Tech. Eng.*, 2006, **45**, 561.
46. W. George, *Handbook of Fillers*, William Androw Publisher, New York, 1999.
47. K. A. Malini, E. M. Mohammed, S. Sindhu, P. A. Joy, K. Date, S. D. Kulkarni, P. Kurian and M. R. Anantharaman, *J. Mater. Sci.*, 2001, **36**, 5551.
48. V. S. Vinod, S. Varghese and B. Kuriakose, *J. Adhes. Sci. Technol.*, 2000, **14**, 1105.
49. L. E. Nielsen and R. F. Landel, *Mechanical Properties of Polymer and Composites*, Marcel Dekker Inc: New York, 1974.
50. C. Sirisinha, S. Phoowakeereewiwat and P. Saeoui, *Eur. Polym. J.*, 2004, **40**, 1779.
51. M. H. M. Makled, H. Washiya, H. Tsuda and T. Matsui, *J. Appl. Poly. Sci.*, 2009, **113**, 3294.
52. N. M. Ahmed and S. H. El-Sabbagh, *Polym. Plast. Tech. Eng.*, 2006, **45**, 275.
53. A. M. Shanmugharaj, J. H. Bae, K. Y. Lee, W. H. Noh, S. H. Lee and S. H. Ryu, *Compos. Sci. Technol.*, 2007, **67**, 1813.
54. K. Kueseng and K. I. Jacob, *Eur. Polym. J.*, 2006, **42**, 220.
55. M. A. López-Manchado, J. Biagiotti, L. Valentini and J. M. Kenny, *J. Appl. Polym. Sci.*, 2004, **92**, 3394.
56. Y. A. Kim, T. Hayashi, M. Endo, Y. Gotoh, N. Wada and J. Seiyama, *Script Mater.*, 2006, **54**, 31.
57. A. Fakhru'l-Razi, M. A. Atieh, N. Girun, T. G. Chuah, M. El-Sadig and D. R. A. Biak, *Compos. Struct.*, 2006, **75**, 496.
58. G. Sui, W. H. Zhong, X. P. Yang, Y. H. Yu and S. H. Zhao, *Polym. Adv. Technol.*, 2008, **19**, 1543.
59. G. Sui, W. Zhong, X. Yang and S. Zhao, *Macromol. Mater. Eng.*, 2007, **292**, 1020.
60. M. J. John and S. Thomas, *Carbohydr. Polym.*, 2008, **71**, 343.
61. C. A. S. Hill and H. P. S. A. Khalil, *J. Appl. Polym. Sci.*, 2000, **78**, 1685.
62. H. D. Rozman, M. J. Saad and Z. A. M. Ishak, *Polym. Test.*, 2003, **22**, 335.

63. M. S. Sreekala, M. G. Kumaran, M. L. Geethakumariamma and S. Thomas, *Adv. Compos. Mater.*, 2004, **13**, 171.
64. A. B. A. Hariharan and H. P. S. A. Khalil, *J. Compos. Mater.*, 2005, **39**, 663.
65. G. Raju, C. T. Ratnam, N. A. Ibrahim, M. Z. A. Rahman and W. M. Z. W. Yunus, *J. Appl. Polym. Sci.*, 2008, **110**, 368.
66. M. Jacob, B. Francis, S. Thomas and K. T. Varughese, *Polym. Compos.*, 2006, **27**, 671.
67. D. S. LeCorre, J. Bras and A. Dufresne, *Macromol. Mater. Eng.*, 2012, **297**, 969.
68. P. Mele, H. Angellier-Coussy, S. Molina-Boisseau and A Dufresne, *Biomacromolecules*, 2011, **12**, 1487.
69. T. Kawazura, S. Kawahara and Y. Isono, *J. Appl. Polym. Sci.*, 2005, **98**, 613.

CHAPTER 22

X-Ray, Light and Neutron Scattering Studies on Natural Rubber Composites and Nanocomposites

JINI VARGHESE,[a] CINTIL JOSE CHIRAYIL,[b] LAKSHMIPRIYA SOMASEKHARAN[a] AND SABU THOMAS*[a,b]

[a] School of Chemical Sciences, Mahatma Gandhi University, Kottayam, Kerala, India; [b] Centre for Nanoscience & Nanotechnology, Mahatma Gandhi University, Kottayam, Kerala, India
*Email: sabupolymer@yahoo.com

22.1 Introduction

Natural rubber (NR) is a high molecular weight, linear polymer with repeating units of isoprene. It is extracted in the form of latex from the bark of Hevea tree. Major part of NR contains highly stereoregular 1,4-polyisoprene (94%) along with some non-rubber contents (6%). Its molecular weight ranges from 1.0 to 2.5 lakhs. The non-rubber contents in NR such as protein, phospholipids, fatty acids, carbohydrate and inorganic substances helps to promote sulfur curing and improve the mechanical properties. These parts often act as discrete microstructures. When NR is stretched or subjected to low temperatures, it tends to crystallize spontaneously due to its unique ordered structure.[1–3] Such strain-induced crystallites provide some additional crosslinking

RSC Polymer Chemistry Series No. 8
Natural Rubber Materials, Volume 2: Composites and Nanocomposites
Edited by Sabu Thomas, Hanna J. Maria, Jithin Joy, Chin Han Chan and Laly A. Pothen

Published by the Royal Society of Chemistry, www.rsc.org

and also carry the applied strain. The crystallization provides high tensile strength and resistant to tear and abrasion. An additional reinforcing phase is necessary for increasing the practical use of NR. The physical as well as the chemical properties of rubber is crucial when interacted with fillers.[4–7] Scattering is a powerful tool to determine the filler structure, morphology of the polymers, polymer–filler interactions, filler–filler interactions, crystallinity of rubber and structure and morphology of rubber composites in a non-destructive way.[8,9] In this chapter, a brief introduction to X-ray scattering, light scattering and neutron scattering techniques and illustrated examples from literature related to this methods are included.

22.2 X-Ray Scattering Studies

NR is a fascinating material in the rubber technological industry due to its high elasticity and mechanical properties. NR nanocomposites achieve enhancement in overall properties compared to pure NR. The nanometre scale dispersion of the reinforcement agent and high aspect ratio of fillers are the essential factors determining the properties of the nanocomposites. Reinforcement is a complex and a distinct mechanism related to the structure and morphology at the molecular level.[10–12] In this case, qualitative X-ray scattering study is an essential tool for predicting the role of the above-mentioned factors. X-rays have wavelengths in the order of atomic dimensions, which help them to interfere and extract information from crystal lattices and predict their structures. Elastomers due to their amorphous nature will appear to be indifferent to X-ray scattering or diffraction studies. But strain-induced crystallization and filler induced electron density fluctuations makes an elastomer composite to be prone to these studies. X-ray scattering technique is the collective name given to the techniques of small-angle X-ray scattering diffraction (SAXS) and wide-angle X-ray diffraction (WAXD). X-rays are elastically scattered from a sample due to the differences in densities of electrons. The analysis of the resulting scattered radiation as function of scattering angle provides information regarding the sample size, shape and orientation of the components in the sample. X-ray diffraction provides a non-destructive technique for analysing degree of dispersion and morphology of a specimen by sampling the whole bulk of the specimen.

22.2.1 Small-Angle X-Ray Scattering and Wide-Angle X-Ray Scattering

When X-rays are irradiated on a sample, the atoms inside the sample are scattered in all directions which results in background radiations. If the background radiation is occurring in the small-angle region, it is known as small-angle X-ray scattering (SAXS). On the other hand, if the background radiation is occurring in wide-angle region, it is known as wide-angle X-ray scattering (WAXS). SAXS can measure the particle in the size range 5–25 nm. So SAXS is often used for measuring the structure of lamellae. In the SAXS

analysis, the shape of the scattering curve in very small angles is known as Guinier region and at higher angles is known as Porod region. The Guinier region is useful for predicting the radius of gyration of any distinct structures. The Porod region gives information about the surface to volume ratio and dimensions of the scattering object.[13,14] WAXS is used for measuring the scattering intensity of scattering angles greater than 5°. The crystal structure at the atomic level could be identified by WAXS analysis.[15] In WAXS analysis the sharp peaks are formed by the various crystalline plane reflections. According to Bragg's law, the reflections obtained by various angles are:

$$n\lambda = 2d\sin\theta \tag{22.1}$$

where d is the distance between successive crystalline planes, θ is the diffraction angle produced by the incoming X-rays, λ is the wavelength of incoming X-ray beam and n is an integer having values 1,2,3 ....

A SAXS analysis provides an idea about the scattering vector (q), which is given by Equation (22.2):

$$q = (4\pi\lambda)\sin\theta \tag{22.2}$$

where λ is the incident radiation wavelength and θ is the half the angle through which radiation is scattered.

In a semi crystalline material, both sharp reflections for crystalline part (A_c) and amorphous halo (A_a) are formed. The weight fraction of the crystalline phase (W_c) is calculated by following equations:

$$W_c = \frac{A_c}{(A_c + A_\alpha)} \tag{22.3}$$

Both these methods could be used for differentiating amorphous and crystalline polymers. The amorphous material produce diffused but the crystalline sample shows sharp X-ray patterns.

22.2.2 Characterization of Rubber Nanocomposites

22.2.2.1 Strain-Induced Crystallization

NR shows high mechanical performance under the influence of an applied stress. When applying a stress, the coiled structure of polymer molecule is changed into an extended configuration simultaneously. Hence crystallization is induced during stretching process. During stretching, the orientation and alignment of polymer chains results in nucleation of crystallization. This phenomenon is Hookean and is linearly related to stress and strain. Vulcanized rubbers have an ability of self-reinforcement. In addition to this, vulcanized NR attains an additional physical crosslinking network by the help of an induced load. Hence NR attained strain-induced crystallization (SIC) behaviour by addition of an applied load. Several factors affect the orientation of the polymer and crystalline formation in NR such as number of crosslinks and distribution of crosslink junctions.[16,17] In unvulcanized NR, the dangling

groups and loops are the network imperfection factors which enhanced the number of crosslinks. The broad distribution of the chain length between the crosslink junction points and the non-uniform distribution of crosslink junctions are increasing the orientation and crystallinity of the vulcanized NR. The crystallization mainly occurs in the network rubbery region but not much inside the network domain region. Therefore upon stretching the crystallization is mainly seen on the rubbery phase. The SIC increases with increasing strain and decreases with increasing crosslink density. Compared to vulcanized NR, the NR microcomposites retard the local stress and SIC due to less interaction between micro sized fillers and rubber chains. The micro sized fillers are non-uniformly dispersed in the rubber matrix preventing the regular alignment of rubber chains and crystallization. In the case of NR nanocomposites, the SIC mechanism is entirely different. It depends on several factors such as filler–filler inter-networking and filler–rubber networking. The large interfacial surface area of nanofillers promotes the overall rubber chain orientation and total crystallinity. Due to SIC the material shows much more tensile strength, modulus properties and crack resistant properties than vulcanized rubber. Hence SIC is an important parameter for predicting the material quality. The SIC in NR was first reported by Katz *et al*. in 1920. Acken in 1932 was the first person to study SIC under dynamic load by spectroscopic techniques. But Kawai *et al*. observed the crystallization studies as function of stress. In 1967, WAXS study was first used for analysing the SIC of NR by Dunning *et al*.

Figure 22.1 shows the WAXS diffraction patterns of vulcanized NR at different strain ratios.[18] The amorphous rubber in the undeformed state exhibits a

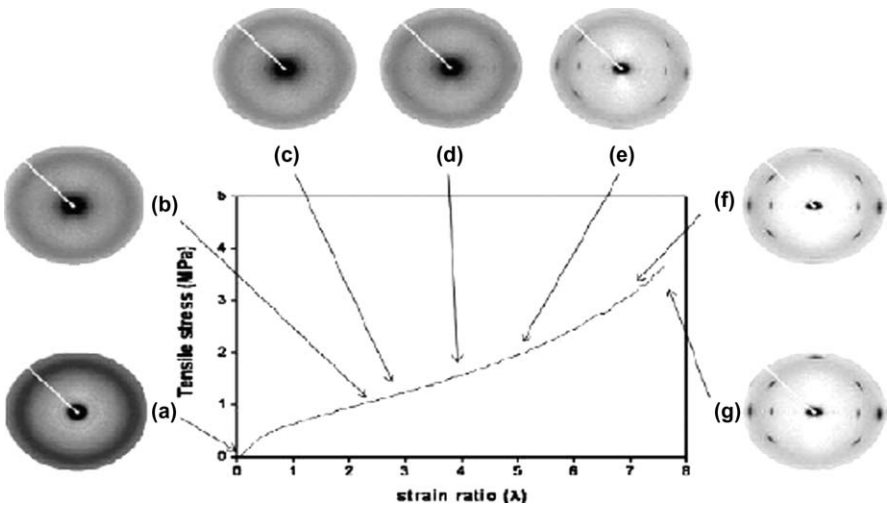

Figure 22.1 Tensile stress–strain curve of the vulcanized NR sample stretched up to $\lambda = 7.5$. Insets correspond to WAXS patterns of NR upon stretching at room temperature at $\lambda =$ (a) 0, (b) 2.5, (c) 3, (d) 4, (e) 5, (f) 7 and (g) 7.5. (Reprinted with permission from ref. 18.)

complete halo characteristic, which is represented in inset (a). If the strain ratio is at 3 ($\lambda = 3$), the presence of crystalline maxima can be seen due to the orientation of the rubber chains, shown in inset (c). If the strain rate is greater than 3 ($\lambda > 3$), the rubber chains are tied together strongly to form extra crosslinks, resulting in an oriented crystalline phase formation. The crystalline phase orientation increases with increasing strain ratios. This phenomenon can be clearly seen in inset figures (d) to (g).

The amorphous halos existing in the WAXS patterns reveal the significance of the amorphous phase in the orientation process. Due to this good orientation of the crystalline phase ($\lambda > 3$), NR exhibits SIC, which increases with increasing strain ratios, as clearly represented in Figure 22.2.

SAXS analysis reveals information about the morphology of the dispersed filler. Before applying a stress on the sample, the SAXS analysis pattern obtained was made up of isotropic rings, showing that the fillers are randomly dispersed in the rubber matrix. The perpendicular view of the unstretched sample by SAXS analysis clearly reveals the degree of morphological orientation induced by the process. The parallel view gives information on the degree of rotational disorientation. When rubber filled with aggregates is uniaxially stretched, the resulting stress–stain relationship shows the lateral compression of the fillers. The corresponding SAXS pattern represented an '8' or buckled shape with the major axis parallel to the stretching direction.[19] The butterfly patterns or anisotropy are not formed in the initial stage and are originated by further uniaxial stretching.

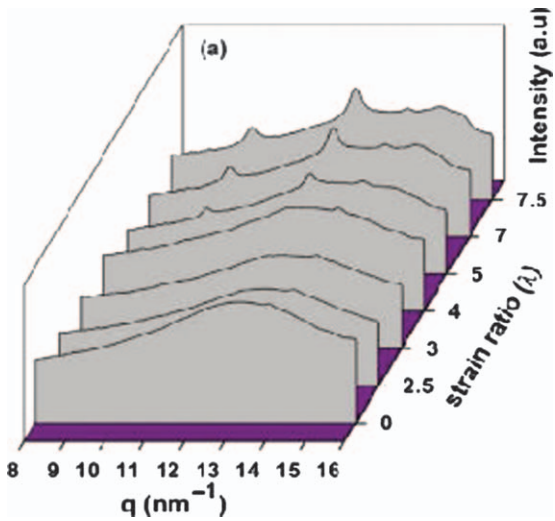

Figure 22.2 Azimuthally integrated intensity of the WAXS patterns as a function of the scattering vector q.
(Reprinted with permission from ref. 18.)

The distance between fillers in the stretching direction (D) is calculated by Equation (22.4):

$$D = \frac{d}{\cos \mu} \tag{22.4}$$

where μ is the azimuthal angle of the buckled structure.

(a) Carbon Nanotubes Natural Rubber Nanocomposites

Carbon nanotubes are one of the fascinating reinforcing materials in rubber industry owing to its high mechanical properties, high surface area and high aspect ratio. Two types of CNTs are most common in fabrications: single walled carbon nanotubes (SWCNTs) and multi walled carbon nanotubes (MWCNTs). In SWCNT, a single layer of graphite sheet is wrapped into a cylindrical tube. Several concentric graphite layers arranged like rings formed MWCNT. The XRD peaks of MWCNTs are represented in Figure 22.3. MWCNTs exhibit diffraction peaks at 26.5°, 42.4°, 54.7° and 77.4° corresponding to the graphite hexagonal structures at (002), (100), (004) and (110) reflections.[20]

The good dispersion of CNTs in the rubber matrix leads to enhancement of most of the properties of the rubber matrix. The SIC of NR filled with CNT (2 phr) was identified by WAXS analysis and is shown in Figure 22.4.

As the strain increases during the stretching process, the corresponding intensities of NR and CNT-filled NR composites also increase. The figure clearly shows that stearic acid, one of the vulcanizing ingredients itself, crystallizes and is highly oriented along the stretching direction. The equatorial diffraction patterns along the equator of SIC taken by WAXS analysis at different strains during stretching is shown in Figure 22.5.

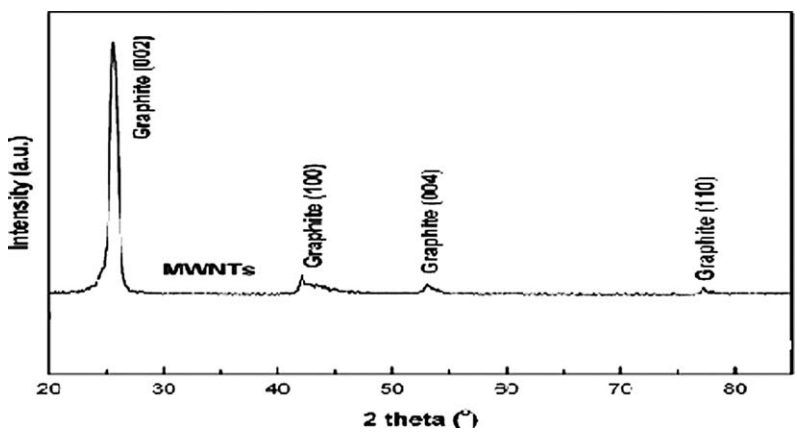

Figure 22.3 XRD peaks of MWCNTs.
(Reprinted with permission from ref. 20.)

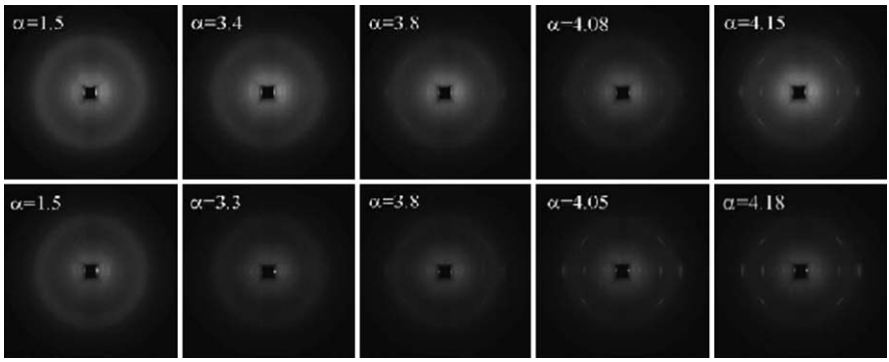

Figure 22.4 Sequential variation of WAXD patterns from (a) pure NR and (b) MWCNT–NR nanocomposites. Corresponding strain values are indicated at the top left in each pattern of panels a and b. [Reprinted with permission from ref. 21.)

The peak intensities of CNT-reinforced NR composites are greater than those of pure NR composites.[21] NR consists of short and randomly oriented long (amorphous) chains. The short chains contribute to the crosslinking in vulcanization process. During the vulcanization process these short chains are tied strongly together with long chains resulting in better orientation that strengthen the whole NR network. In the case of NR composites, the orientation and interaction between amorphous long chains and short chains are also increased with increasing stretching. Hence the resulting peak intensity of SIC also increases with increased stretching angle. In other words a high-level interaction occurs between the MWCNTs and NR chains due to the high surface area of the MWCNT (given as $400\,g^2\,m^{-1}$). The MWCNTs are aligned and oriented in the stretching directions. Hence a sub-network orientation (large-scale orientation) is induced in the rubber chains at an early stage. Hence the SIC intensity peaks of MWCNT-reinforced NR composites are higher than those of neat NR composites.

(b) Graphene–Natural Rubber Nanocomposites

A two-dimensional, single-layer carbon sheet having an sp^2 hybridized state is known as graphene. Graphene has remarkable physical properties such as high electrical conductivity, thermal stability, excellent mechanical strength, high aspect ratio and low density. Besides, the ease of processability and functionalization makes graphene a promising material for preparing nanocomposites. Graphene can be easily synthesized from graphite flakes. The graphite flakes are first modified with a suitable oxidizing agent to form graphite oxide. Graphite oxide is then reduced to form exfoliated graphene. All these modifications can be easily identified with the help of XRD analysis.[22] Figure 22.6 shows the exact XRD peaks of these modifications.

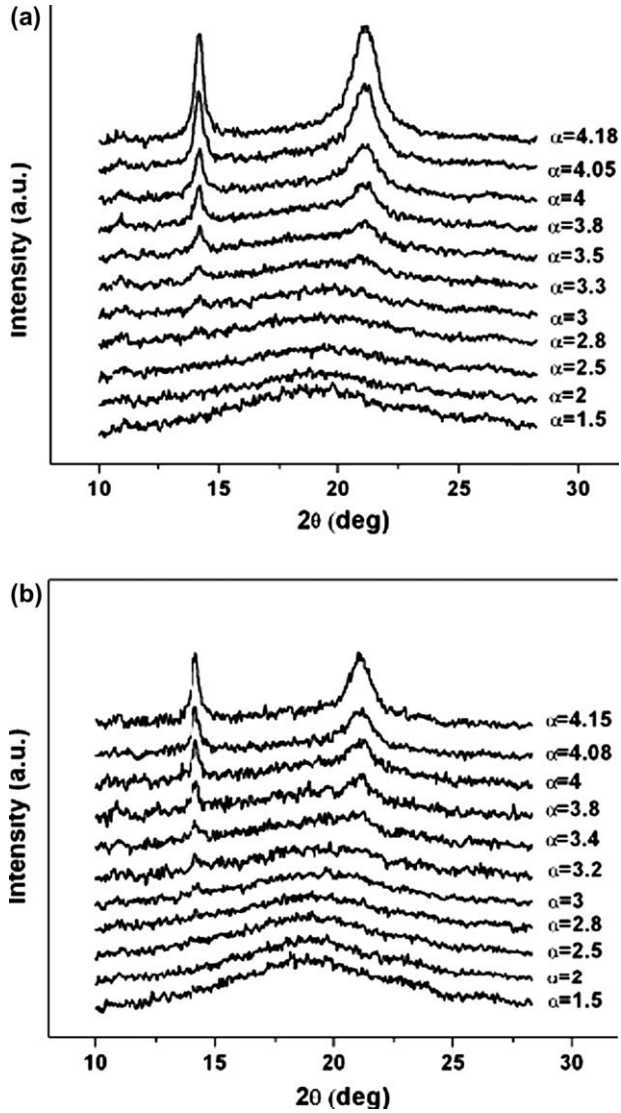

Figure 22.5 Equatorial diffraction profiles taken from 2D WAXD patterns at selected strain values of MWCNT–NR nanocomposites (a) and pure NR (b) as a function of strain under stretching at the 2θ angle range of 10–28.3°.
(Reprinted with permission from ref. 21.)

Graphite shows a sharp diffraction peak at 26°, and the corresponding interlayer distance is 3.36 Å, which reveals the crystalline nature of graphite. Modification of graphite to graphite oxide occurs mainly due to intercalation of some oxide functional groups. The XRD peak of graphite oxide appears at

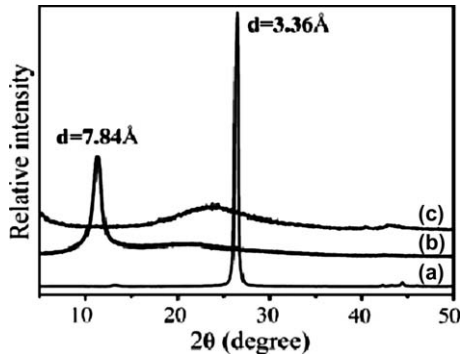

Figure 22.6 XRD pattern of (a) pristine graphite, (b) graphite oxide and (c) graphene. The interlayer distance is represented by *d*. (Reprinted with permission from ref. 22.)

11.3 Å, revealing intercalation of these epoxide groups. In the case of graphene, all the characteristic peaks disappeared, which shows that it has a new lattice structure by exfoliation into monolayers or a few layers. Figure 22.7 shows the WAXS diffraction pattern of functionalized graphene–NR composites.

The peaks show a sharp increase in intensity when compared to vulcanized NR during addition of small amounts of fillers (1 and 4 wt%). The origin of the halo is scattering from amorphous chains. Graphene is functionalized with an oxygenated species. The resulting graphene has polar functional groups such as hydroxyl and epoxy. When functionalized graphene is dispersed into the NR matrix, the polar functional groups enable the coupling interaction between NR and functionalized graphene.[23] The lateral dimension of the functionalized graphene is in the order of hundreds of nanometres. When arranged in the stretching direction, it results in a crystal orientation in the stretching direction.[24] Hence the intensities of the WAXS peaks increase sharply with increasing strain ratios.

(c) Clay–Natural Rubber Nanocomposites

Hydrous aluminium silicates having (two-dimensional) flat hexagonal sheet are commonly known as clay. SiO_4 and AlO_4 tetrahedra are arranged in the corners of the sheet. The tetrahedral sheets of SiO_4 clay are bonded with octahedral sheets of Al_2O_4. If these layers are charged, interlayer cations such as Na^+, K^+ are bonded to balance these charges. Montmorillonite (MMT) is a smectic type soft clay consisting of two tetrahedral sheets sandwiching a central octahedral sheet. In MMT, the cations inside its layers are hydrated and exchangeable. The MMT represented as Na-MMT indicates that it contains exchangeable cations of Na inside its interlayer space. In some cases MMTs are organically modified and are represented as O-MMT. The XRD peaks of Na-MMT and organically modified MMT are given in Figure 22.8.

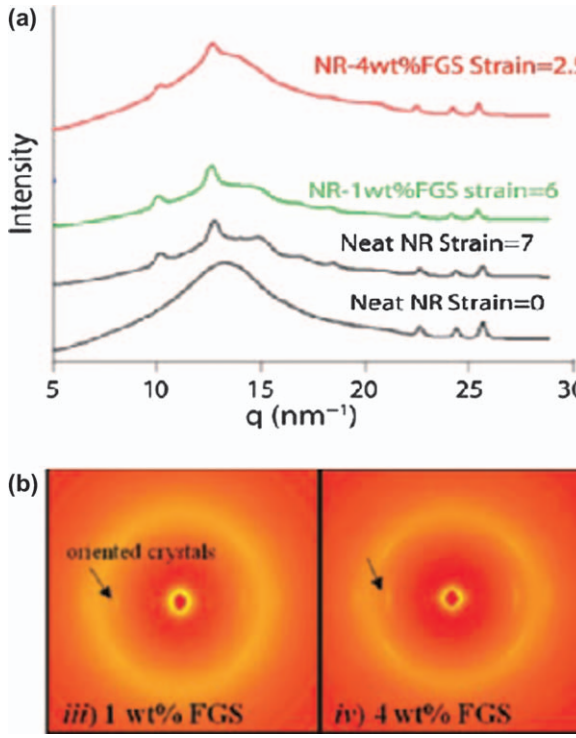

Figure 22.7 (a) 1D WAXD patterns for unstretched neat NR, and all samples shortly before failure in the tensile test. (b) 2D WAXD patterns at strain 1/4 2 (air scattering is subtracted as background). Stretch direction is vertical. (Reprinted with permission from ref. 24.)

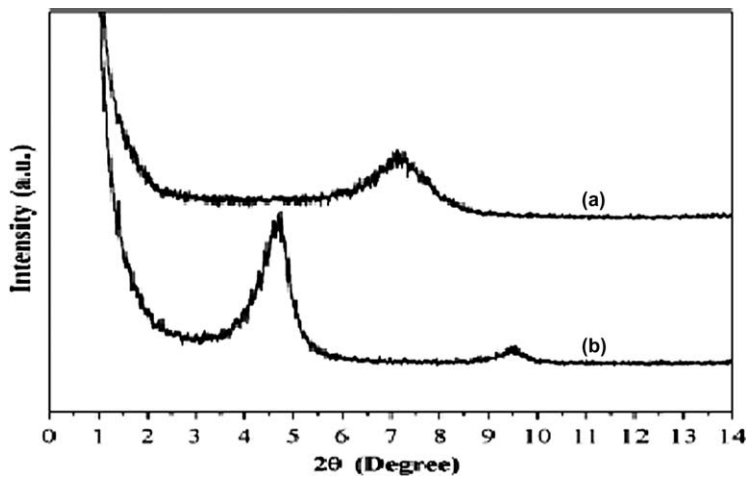

Figure 22.8 XRD patterns of (a) Na-MMT and (b) modified Na-MMT. (Reprinted with permission from ref. 25.)

The Na-MMT clay shows a diffraction peak at 2θ of 7.12°. But in the case of organically modified MMT the peaks are shifted lower, having a 2θ value of 4.7° which indicates the increase in the *d* value. The organically modified MMT shows a new peak at 2θ of 9.5° revealing the second-order reflections. But such reflections are absent in Na-MMT clay.[25] The increase in gallery height in modified MMT is due to the inclusion of organic groups inside the unmodified Na-MMT clay galleries.

A pronounced difference in stress–strain behaviour and SIC of various clay-reinforced NR nanocomposites are shown in Figure 22.9.

Figure 22.9(a) shows unfilled NR, (b) is for Na^+-MMT/NR and (c) is for NR/O-MMT. The dramatic variation in SIC with increasing strain is seen in the case of NR/O-MMT nanocomposites. Addition of nanoclay platelets in NR provides a regular polymer network microstructure.[26] The O-MMT and NR are hydrophobic in nature. Hence NR chains are interfacially adsorbed at the outer surface of O-MMT. But in Na-MMT, no such interaction is present due to the changes in dipole distribution. So in the SIC analysis, the NR/O-MMT nanocomposites show sharper crystalline peaks than the other clay nanocomposites.

The SAXS of unstretched and compressed patterns (A: face-on view, B and C: edge-on views) of O-MMT is shown in Figure 22.10.

Due to the platy character and high aspect ratio of O-MMT, the edge-on view measurements reveal that the particles are aligned in the plane of the sample. Hence it exhibits a highly anisotropic pattern. The face-on view analysis reveals the random distribution of particles with respect to the plane of directions resulting in an isotropic pattern.

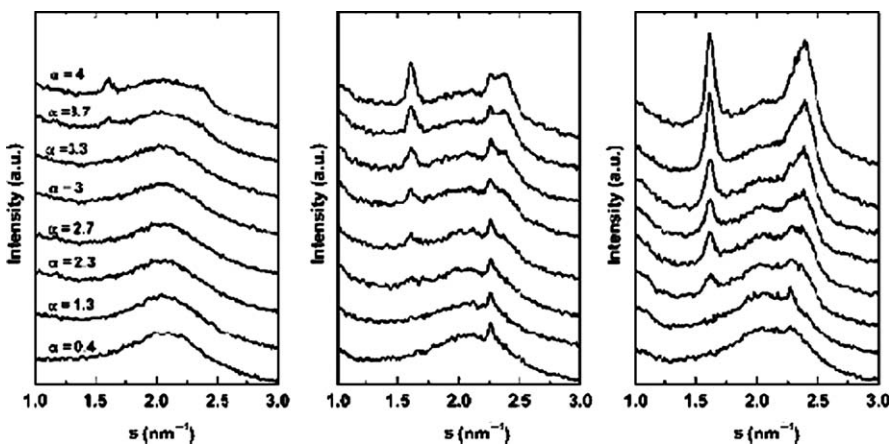

Figure 22.9 Normalized and corrected linear diffraction profiles for (a) unfilled NR, (b) NR/Na^+-MMT and (c) NR/O-MMT samples. (Reprinted with permission from ref. 26.)

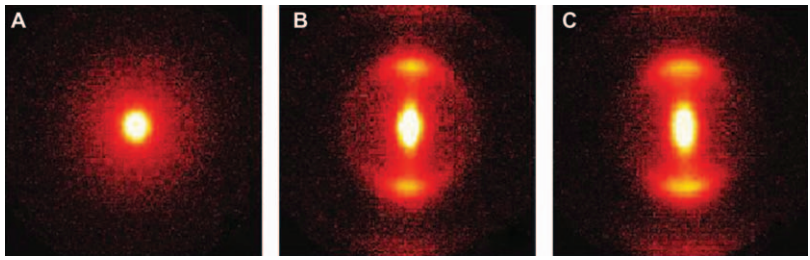

Figure 22.10 A2D SAXS patterns (A: face-on view; B and C: edge-on views) for the unstretched state of the nanocomposites NR/O-MMT loaded with 15 phr of nanoclay.
(Reprinted with permission from ref. 26.)

22.2.2.2 Defects in Rubber Nanocomposites

Rubbers undergo crack formation during a cyclic applied stress which leads to the complete fracture of the polymer materials. The cracks are micrometre or nanometre cavities or voids. In vulcanized NR, the nanoscale voids are observed at high temperature due to the destruction of crosslinking structure. In a rubber nanocomposite the non-rubber components, especially zinc sulfide particles detach each other to form free spaces known as nanovoids. The non-rubber components again move apart in the vicinity of these nanovoids leading to crack formation. Temperature and SIC are the two important factors affecting the nanovoid formation. At high temperature fatigue, elliptical and spherical cavities are also created. Small-angle X-ray scattering (SAXS) pattern is an important tool to identify the growth, mechanism and effect of strain on the nanocrack formation in polymer samples.[27] SAXS can also be used to measure the volume, size and shape of nanovoids. From the discernible scattering intensity, the nanovoid is identified by SAXS analysis.

(a) Void Volume Fraction

The nanovoid volume fraction (Q_{void}) is measured by Equation (22.5):

$$\frac{Q}{Q_0} = 1 + \left[\frac{\phi_R \rho_{R^2} + \phi_F \rho_{F^2}}{\phi_R \phi_F (\rho_R - \rho_F)^2} - 1\right] \phi_{void} \tag{22.5}$$

where Q and Q_o are the scattering invariant, ϕ_R and ϕ_F are volume fraction of rubber and fillers. The terms r_r and r_f are X-ray scattering densities of rubber and fillers.

(b) Void Size and Shape

According to the Poroid analysis combined with Wu's analysis the voids are considered as ellipsoids. The average values of scattering pattern of the semi

axis in the tensile axis (y axis) and in the transverse direction (x axis) are calculated with Equations (22.6) and (22.7):

$$\frac{\langle R_{y^3}\rangle}{\langle R_{y^2}\rangle} = \frac{3\lambda_{void}^{3}}{\pi(1-\phi_{void})}\frac{Q_{void}}{K_{py}} \tag{22.6}$$

$$\frac{\langle R_{x^3}\rangle}{\langle R_{x^2}\rangle} = \frac{3\lambda_{void}^{1.5}}{\pi(1-\phi_{void})}\frac{Q_{void}}{K_{py}} \tag{22.7}$$

where Q_{void} is the nanovoid's scattering invariant. The Porod constant is K_{py}. λ_{void} is calculated from the ratio of two Porods constants. λ_{void} is deformation from a sphere with preserved volume to the ellipsoid.[28] The ratio of the average size along the tensile direction [$\langle R_{y^3}\rangle$ $\langle R_{x^2}\rangle$] to the transverse direction [$\langle R_{y^2}\rangle$ $\langle R_{x^3}\rangle$] gives the shape of the voids (e).

$$e = \frac{\langle R_{y^3}\rangle}{\langle R_{y^2}\rangle}\frac{\langle R_{x^3}\rangle}{\langle R_{x^2}\rangle} = \lambda_{void}^{\frac{3}{2}} \tag{22.8}$$

In the SAXS analysis, the flame-like shape is obtained due to the scattering pattern obtained from nanovoids and butterfly shape is originated from scattering of fillers. Nano voids are initiated at a small strain range and grow perpendicular to the stretching direction as the strain attained a higher value.[29]

22.2.2.3 *Morphological Studies*

The art of filler dispersion in polymer matrix is easily determined by X-ray analysis especially WAXS analysis. The intensity and position of X-ray diffraction peaks reveals the exact idea regarding the morphological structure of polymer nanocomposites. Figure 22.11 compares reduced graphite oxide dispersions in NR matrix by different processes such as milling and solution casting methods.

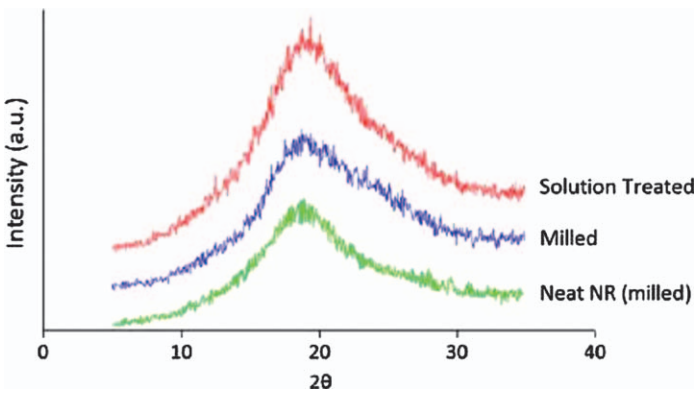

Figure 22.11 Comparison of WAXS spectra of neat NR, milled RG-O/NR, and solution-treated RG-O/NR nanocomposites with 5 wt% RG-O platelets. (Reprinted with permission from ref. 27.)

Vulcanized NR prepared by a milling process shows a diffraction peak (shoulder) of 2θ at about 20 Å. Comparison of reduced graphite oxide dispersion in NR by the WAXS analysis revealed that the shoulder of the diffraction peaks diminished following the mill mixing process.[30] That again proved that dispersion is more effective by milling than by solution mixing. Nanofillers when dispersed into the rubber matrix through mill mixing, produces some shear forces which reduces their agglomeration and enhances the dispersion.

22.3 Light Scattering

Scattering occurs when a beam of light encounters with matter. This phenomenon is known as light scattering. Light scattering methods are used in a wide spectrum of fundamental and applied optics problems.[30,31] Based on the study of Peter Debye, light scattering technology is utilized to characterize the microstructure of polymers like molecular weight and mean square radius of gyration.[32] The light scattering theory of solids, developed by Stein *et al*. is now widely used to study the structure of polymer crystal. For measuring the patterns of scattered light, the two experimental methods used are dynamic light scattering (DLS) and static light scattering (SLS). DLS is also called quasi-elastic light scattering (QELS) or photon correlation spectroscopy (PCS). Classical light scattering, also known as static or Rayleigh scattering[33] gives a direct measure of molecular mass and is very useful for determination of molar mass of polymers.

22.3.1 Dynamic Light Scattering

The dynamic light scattering (DLS) technique measures the time-dependent fluctuations in intensity of scattered light. It allows determination of the distribution of the particles and the diffusion coefficient. DLS is one of the most popular experimental techniques in the characterization of complex liquids like colloidal suspensions, polymer solutions, polymer melts, gels, etc. DLS make use of scattered light to measure the rate of particle diffusion.[34,35] A schematic representation of the DLS method is shown in Figure 22.12. Dynamic scattering could be very effectively used in sensing presence of small amounts of aggregated polymers and studying samples containing a very large range of particle masses. It is useful for real-time monitoring of size changes. Diffusion motion of the particles causes intensity fluctuations in colloidal particles and macromolecules. Now DLS is used as a non-destructive and convenient method for particle size analysis by using the correlation between diffusion coefficient and particle size. From the diffusion coefficient of micelle, the hydrodynamic radius RH of a macromolecule or block copolymer micellar system can be found. DLS gives a measure of the timescale for fluctuations in the index of refraction of complex liquids. Using this technique it is possible to characterize particles from nanometre to micrometre ranges. In undiluted scattering systems the interpretation of DLS experiment becomes difficult due to their very strong

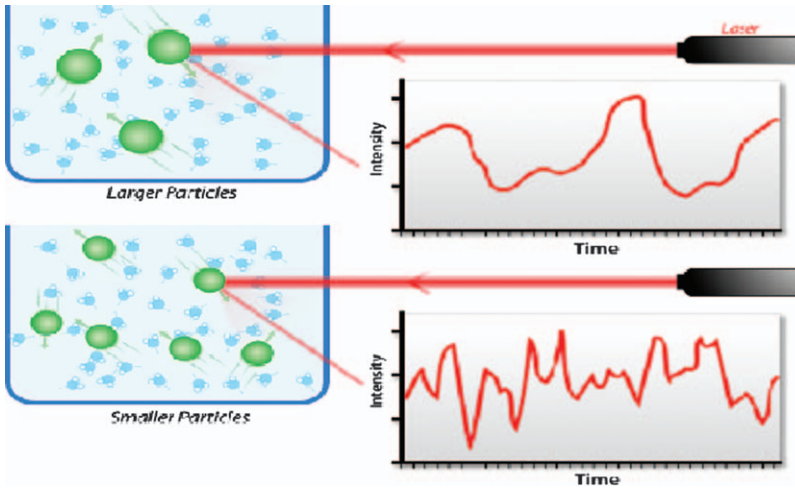

Figure 22.12 Hypothetical dynamic light scattering of two samples: larger particles on the top and smaller particles on the bottom.

multiple scattering. The multiple scattering effects in DLS experiments can be minimized by the use of cross-correlation scheme.

Based on the DLS measurements it is possible to find particle size distributions of polymers and proteins, particle aggregation phenomena, micellar systems and their stability, micro-emulsion technology, colloid behaviour, nucleation processes and protein crystallization. DLS is a non-destructive and convenient method and so it can find application in various branches of science. In chemistry it finds application in topics of colloids, polymers, emulsions, suspensions, nanoparticles, and in physics, applications such as in astrophysics and atmosphere physics and in biology it involves biophysics and biomedicine applications.

22.3.2 Static Light Scattering or Classic Light Scattering

Static light scattering (SLS) measures light intensity as function of sample concentration and scattering angle. It allows the study of average molecular weight, shape information and radius of gyration. The advantage of light scattering is that it is a non-destructive technique with rapid response to the density and orientation fluctuation of polymer systems. Its applications include the study of phase behaviour, crystallization and gelation of multiphase polymer systems, and *in situ* monitoring of the change in morphology of multiphase polymer system in processing condition. In light scattering experiments, a parallel laser beam scattered by the medium (colloidal suspensions, macromolecules in solution). The signal is usually averaged in terms of orientation and time and the detector area is much larger than the coherence area.

22.3.3 Phase Analysis Light Scattering and Forced Rayleigh Light Scattering

Phase analysis light scattering (PALS) is a technique that is very similar to laser Doppler electrophoresis (LDE) and is used to measure the electrophoretic mobilities of colloidal particles. This technique is particularly suited to measurements of charged particles suspended in nonpolar media and sensitivity of the method is far superior to that which could be obtained by LDE measurements. It makes use of a cross-beam technique and offsets one of the laser beams relative to the other by several kHz.[36,37]

Forced Rayleigh scattering (FRS) is used to measure diffusion of a substance through a liquid or solid material and most commonly for investigating diffusion of liquids through porous solids. In FRS, two excitation beams are crossed within the studied sample and it produces a band of bright and dark fringes. Molecules in the sample change their shape when they absorb light from the excitation beams and it also causes changes in optical properties, producing an RI profile in the sample that mimics the profile of the interference fringes. A second laser beam (probe beam) is also sent through the sample. As it passes through the region with varying RI, it diffracts just like light passing through a diffraction grating. By observing the intensity of the diffracted light change it is possible to determine how quickly the molecules are moving through their environment.

22.3.4 Resonance Light Scattering

Resonance light scattering (RLS) is a technique used to observe various biological processes on a single molecule based on light scattering spectroscopy of a single nanoparticle. It is highly intense, often being at least several orders of magnitude greater than fluorescence light when compared per label. In RLS, the analytes are bound to at least one detectable light scattering particle with the size smaller than the wavelength of the illuminating light and the scattered light detected under those conditions is a measure of presence of one or more analytes in a sample. Metal nanoparticles show a pronounced resonance in their scattering spectrum of visible light. By changing intrinsic parameters such as the nanoparticle material, its size, or its shape, this nanoparticle plasmon (NPP) resonance could be tuned over a wide spectral range and also the extrinsic parameters such as dielectric properties of the particle or charge distributions decisively influence the NPP resonance position.[38–40]

22.3.5 Light Scattering in Soft and Bulk Materials

For characterization of multiphase polymeric materials, various light scattering and optical techniques are potential candidates. Physical processes like crystallization, morphology of semi crystalline polymers, polymer mixtures, composite materials, aggregation, kinetics of phase separation and dissolution of polymer blends, stress whitening, photon migration in polymer composites[35] are studied by light scattering methods.

22.3.6 Technological Processes and Light Scattering

Technological processes like aggregation, phase separation, phase dissolution, crystallization, swelling and deswelling can be monitored by light scattering. The kinetics of coarsening of phase-separated immiscible polymers are studied using the time-resolved light scattering experiments. The blends studied were polystyrene/poly (methyl methacrylate) mixtures with diblock copolymer composed of the corresponding homopolymer blocks. The time evolution of the peak position qm (t,T) and the scattered intensity maximum Im (t,T) at qm compared with theoretically predicted values of exponents for distinct tie scales of phase separation at various annealing temperatures Figure 22.13.

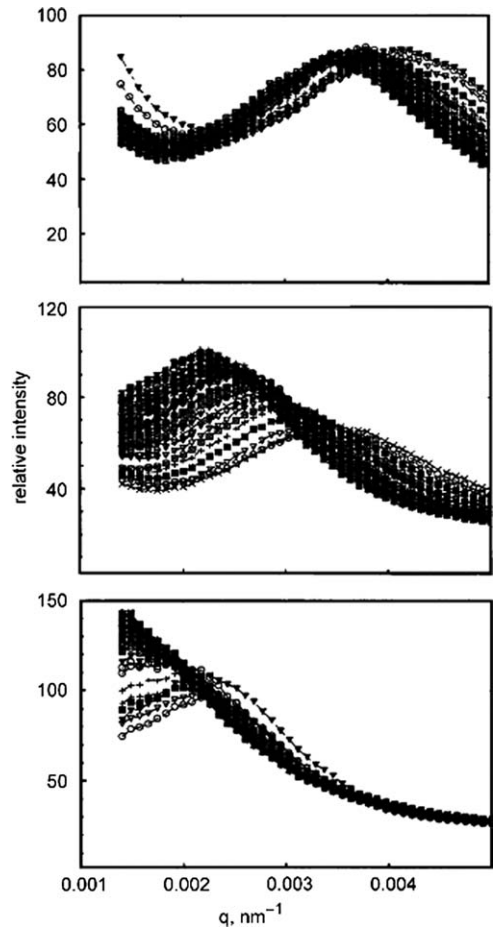

Figure 22.13 Experimental profiles of scattered intensity for blend of two immiscible polymers (PS/PMMA) with addition of a compatibilizing block copolymer. Total 30 intensity profiles with mutual time delay 90 s. Annealing temperatures 130, 160 and 180 1C (from top). The increasing temperature leads to enlargement of domains.

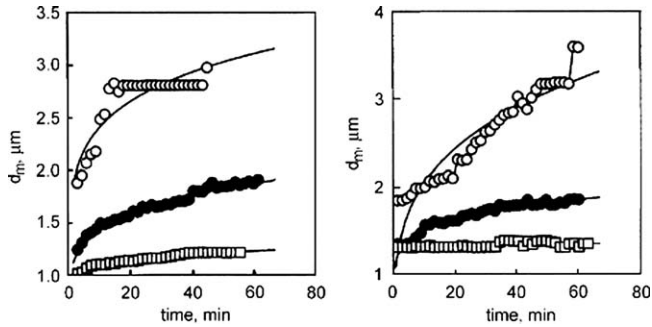

Figure 22.14 Time evolution of domain sizes for (a) blend with 4% of the copolymer, (b) blend without the copolymer. Annealing temperatures UT $\frac{1}{4}$ 130, _T $\frac{1}{4}$ 160, JT $\frac{1}{4}$ 180 1C.

The corresponding time evolution of domain sizes at various temperatures shown in Figure 22.14.

22.3.7 Use of Small-Angle Light Scattering in Phase Behaviour Studies

Different phase diagrams of polymer blends including lower critical solution temperature (LCST) and upper critical solution temperature (UCST) and the phase behaviour of polymer blends under equilibrium conditions could be determined using small-angle light scattering (SALS).[41] Earlier, the SALS technique was utilized to study the miscibility of polymer solutions and homopolymer blends. Those studies were based on miscibility and originated from dipole–dipole interaction and also the specific interactions such as hydrogen bonding.

The effect of molecular weight, component ratio and temperature on the miscibility was discussed.[42] The SALS technique has made a large contribution to the theoretical development and industrial application of polymer blends. The results of SALS were usually compared with Flory–Huggins theory. Tang *et al.*[43] investigated the thermodynamic phase behaviour of blends with random copolymers of polystyrene-co-methyl methacrylate (SMMA) and polystyrene co-acrylonitrile (SAN). The results indicated that SMMA and SAN are miscible within a certain copolymer composition range and exhibit LCST behaviour. Due to the real-time and non destructive nature of SALS, it has been widely utilized to study the kinetics of phase separation of polymer blends. Tang *et al.*[44] investigated the kinetics of phase separation for blends of the random copolymer poly (Styrene-co-Methyl Methacrylate) (SMMA) and poly (Styrene-co-Acrylonitrile) (SAN) by using SALS. It was found that the time evolution of q_m at the beginning of the late stages of spinodal decompositions phase separations followed the relationship $q_m \alpha t^{-1/3}$ corresponding to an evaporation condensation mechanism. Demyanchak *et al.*[45] investigated the

phase separation kinetics of an off-critical mixture of polystyrene and poly (Methyl Phenyl siloxane). The results from the light scattering experiments were correlated with the images obtained from the optical microscopic observation in order to find characteristic features of the scattering intensity during the percolation-to-droplets morphology transition. It was found that when the large bicontinuous network starts to break up into disjointed elongated domains a second peak in the scattering intensity appears.

Time resolved small angle light scattering (TR-SALS) is widely used to study the reaction-induced phase-separation behaviour and the structural development of thermoset/thermoplastic mixtures. The final properties and the morphology of the curing system were controlled by the competition between the curing reaction and the phase separation. Researches in this field revealed that the phase separation of these systems followed the spinodal decomposition (SP) mechanism by analyzing the scattering pattern evolution and the co-continuous morphology observed by optical microscopy. Tang *et al.*[46] studied the cure reaction induced phase separation in attapulgites (ATTS)/epoxy/poly (ether sulphone) (PES) ternary hybrid nanocomposite using TR-SALS. The phase morphologies, dependent on the curing condition, the composition, the molecular weights and distribution of thermoplastics. The incorporation of ATT particles did not affect the critical composition of the epoxy/PES blends but changes the final phase morphology which had a small phase domain and silk like PES-rich phase. Small angle light scattering (SALS) is the most widely-used approaches, due to its non-destructive well established theory and technique for measuring the change of size, shape, degree of order and orientation of polymer species in complex fluids.[47] Light scattering techniques are very efficient for characterizing the morphology of polymer blends under shear flow.[48] The main advantage of light scattering techniques is their immediate response obtained during shear flow without disturbing the samples measured.

22.4 Neutron Scattering Studies

Small-angle neutron scattering (SANS) technique measures the shape and the organization, averaged in time, of particles or aggregates dispersed in a continuous medium. It is used in analysing a wide variety of particles such as colloids (clay, ferrofluid, nanotube), surfactant aggregates, polymers, liquid crystals and proteins in solution. SANS was discovered by Guinier in 1930s while conducting X-ray diffraction studies.[49] and Guinier along with Fournet proposed its main principles and equations.[50] The difference of scattering length densities between isotopes and more precisely between hydrogen and deuterium atoms is at the basis of most of the experiments.[51] Also neutrons are non-destructive and do not alter the samples as X-rays from synchrotron sources can do.

Neutron scattering is used to study the structure of polymers including polymer chain dimensions, conformations, miscibility of blends structures of block copolymers,[52] semicrystalline polymers and biomacromolecules. The unique property of neutrality makes a neutron an excellent probing tool for

Table 22.1 Interaction of neutrons with matter.

Interaction	*Elastic scattering*	*Inelastic scattering*
Strong-force interaction (nuclear scattering)	Position of nuclei in solid (lattice structure)	Lattice vibrations (phonons)
Magnetic interaction	Position and orientation of electronic magnetic moments in solids (ferromagnetism, antiferromagnetism)	Spin excitations (magnons, spin waves)

micro and nanostructures. Neutron also possesses weak long-range magnetic moment which helps in finding out the magnetic interaction in materials. The strong short range nuclear force can penetrate matter much more deeply than that of electrons and X-rays and can even probe smaller atoms like hydrogen. Hence we can say that neutron scattering is a bulk probe. Interactions of neutrons with matter can produce both elastic and inelastic scattering (Table 22.1).

The wavelength of neutron can be comparable with the interatomic spacing and its kinetic energy can be compared with that of atoms in a solid. The bulk properties of the samples can be measured due to the penetrating effect of the neutrons. Neutrons are also sensitive to isotopes and unpaired electrons and offer a wide range of solvent selectivity. But this technique has certain disadvantages also. This is a very expensive technique and since neutron sources are weak, large samples are required. Some elements like Cd, B and Gd strongly absorb neutron signals and instrumental error often happens. Neutrons can probe the bulk of the sample ($\sim$ 1 cm) without damaging them. Scattering depends on Fourier transform of interaction potential and holds Born approximation.

In 1994, the Nobel Prize in physics was given to Bertram N Brockhouse and Clifford G Shull for their contributions to the development of neutron scattering for the study of condensed matter.[53] In neutron scattering the intensity of the scattered neutrons are measured, which is a function of momentum and energy transferred to the sample during scattering. The neutron scattering law is written as $I\,(Q, \epsilon)$ where $\hbar Q$ is the momentum transfer and ϵ is the energy transfer:

$$\epsilon = \frac{\hbar^2(\mathrm{k}'^2 - \mathrm{k}^2)}{2\mathrm{m}} \tag{22.9}$$

Here k and k' are incident wave vector and scattering wave vector and Q is an important vector proportional to momentum transfer vector. Nowadays neutron science is involved in many areas of science including chemistry, crystalline materials, complex fluids, disordered materials, magnetism and superconductivity, polymers and structural biology.

The greater amount of H-atoms in rubber–filler systems often makes it difficult to analyse the scattering due to incoherent scattering. The synthesis of deuterated polymers is not necessary in the case of NR/CB composites due to

the high degree of contrast between phases that allows collection of scattering function measurements.[54] The structure of filler aggregates, their morphologies and their dispersions in rubber can be clearly observed using SANS.

22.4.1 Natural Rubber Structure Analysis

Scattering data provides information on, for example, the weight average molecular weight of polymer molecules, their *z*-average radius of gyration, and in the case of mixtures, the inter-diffusion coefficient, the interpenetration depth, and the extent of polymer mixing.[55] Neutron scattering is a great tool in analysing the microstructure and dynamics of NR.[56] Neutron scattering of deuterated chains between crosslinks is a powerful tool for microscopic investigations. The scattered intensity of a deuterated chain in a network is proportional to form factor.[57] The form factor contains the microscopic details of the chain in the network. In general the form factor is defined as

$$S(k) = 1 / N^2 \sum_{n,m} (\exp(-ik(r_n - r_m))) \qquad (22.10)$$

Here N is the number of scattering elements, r_n and r_m are the positions of scattering atoms on the chain, and k is the wave vector.

Suzuki *et al*. studied the macroscopic structures of crosslinked NR using contrast-variation SANS (CV-SANS).[58] The various in homogeneities in rubber matrix were studied by 'visualization-by-swelling method' using deuterated solvent. These are mainly due to the presence of clusters of polyisoprene chains and large protein aggregates. The results showed that the addition of DCP crosslinker suppressed the network inhomogeneities. Also the crosslinking did not influence the structure of protein aggregates. Thus the structural aspects and its relation with the crosslinker provide better understanding of the elastic properties of NR.

Westermann *et al*. studied the phenomenon of rubber reinforcement and the effect of reinforcement on the matrix chains by the method of neutron scattering.[59] The stress–strain behaviours of unfilled rubbers are influenced by the presence of crosslinks and chain entanglements. For filled systems matrix–filler and filler–filler interactions are also to be considered. These effects were earlier studied using birefringence and light scattering methods.[60] Neutron scattering can shed light in this area. The study showed that the reinforcement factor is dependent on the filler concentration according to the overstrain picture and varies slightly with strain.

SANS is used in the determination of chain dimensions of polymers in the bulk amorphous state.[61–63] Here the isotopic difference in neutron scattering cross-sections of deuterium and hydrogen are made use of. Jeffrey *et al*. studied the chain dimensions of rubber by using SANS technique.[64]

Neutron scattering also provides information regarding polymer dynamics[65] and particularly in methyl group dynamics through studies of their relaxational behaviour.[66] It has been proved that there are distributions of local environment potentials for the methyl groups. Adams *et al*. measured the local

environment potential of the methyl groups with the help of incoherent inelastic neutron scattering.[67] It has certain advantages over optical techniques as it has large energy transfer range. It does not have any selection rules and almost all bands can be observed. In INS spectrum, the comparison of data and ab initio calculations is more straightforward as the intensities of normal mode vibrations are related to the vibration amplitudes. The dynamics of a system is often studied using a scattering law, $S(Q,\omega)$, which is related to the generalized vibrational density of states $G(\omega)$:[68]

$$G(\omega) = \frac{S(Q,\omega)\omega}{Q^2\,(n(\omega)+1)} \tag{22.11}$$

Karino *et al*. used SANS to study the microscopic structures of NR and deprotonized NR (DPNR).[69] The investigations led to conclusion that the SIC and excellent green strength of NR is due to the presence of phospholipids rather than proteins and also due to its stereoregular nature. The protein phase in NR acts not only as crosslinking sites but also reinforcing fillers thus accelerating the upturn of stress at low strain. SANS studies also revealed the role of proteins in causing inhomogeneities in the bulk polymer.

SANS along with other techniques like AFM allows the monitoring of latex particle coalescence and polymer chain inter-diffusion in greater and greater detail. Such fundamental understanding of film formation allows modification to polymerization reactions/ coating recipes and methods of film formation and the development of better quality films.[70]

22.4.2 Natural Rubber Composites

22.4.2.1 Carbon Black–Natural Rubber Composites

Koga *et al*. studied the hierarchical structures of the CB filler in the rubber matrices over a wide range of the reciprocal space by making use of three techniques: USANS (ultra-small-angle neutron scattering), USAXS (ultra-small-angle X-ray scattering) and SAXS (small-angle scattering).[71] The unified Guinier/power law[72] approach was used to analyse each structure level and hierarchical structures. From the scattering profiles, it was found that the smallest structure elements of CB were composed of several unbreakable units bound together by polymer chains ('dispersible units') and their sizes depends on the polymer structure. The mechanism of dispersion of fillers in a polymer matrix was thus studied with the help of these unified techniques. Figure 22.15 shows the various structures of carbon black filler when dispersed in the rubber matrix.

The dispersed CB particles had ellipsoidal shapes and they also calculated their approximate dimensions. The difference in size and shape of the ellipsoidal structures were due to the difference in attractive interactions and viscosity between the filler and polymer. They also found that the size of these aggregates increased after crosslinking and was unaffected by the nature of processing oils.

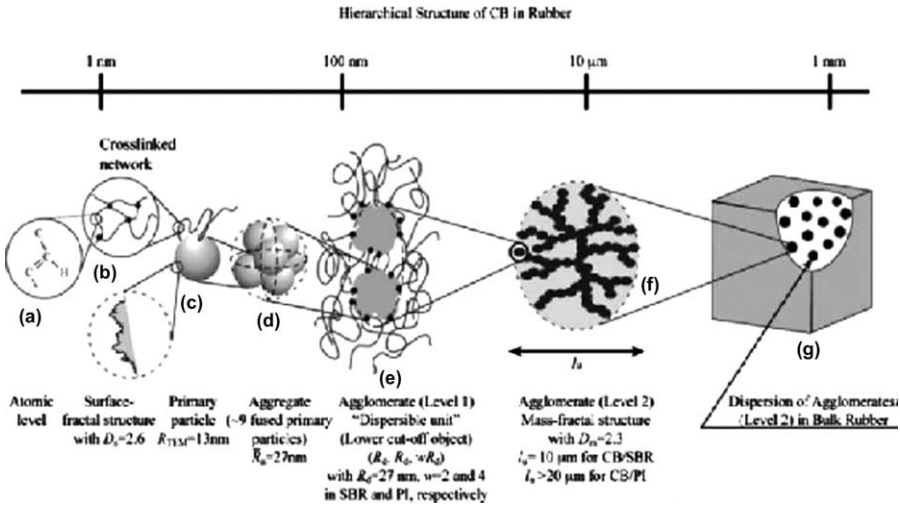

Figure 22.15 Schematic model for the hierarchical structure of the CB filler in the rubber matrices.

Yamauchi *et al*. investigated the structures of NR/high density polyethylene (HDPE) thermoplastic elastomers (TPEs) and their composites with carbon black using SANS. The extremely low contrast between crystalline and amorphous HDPE for SANS enabled us to measure the interface thickness between NR and HDPE in the TPE (5–6 nm) as well as that between NR and carbon black in the composite (2.4 nm).[73] The interface thickness and fractal dimension of the blends and composites were carefully analysed using SANS even though both polymers were not deuterated. It was revealed that NR and HDPE are immiscible blends.

22.4.2.2 Clay–Natural Rubber Composites

Rezende *et al*. studied the reinforcing effect of clay by studying the mechanical properties of non-vulcanized NR and dialysed NR by uniaxial deformations.[74] The reinforcing effect of clay can be increased by removing non-rubber molecules. The structure of clay components in the rubber matrix were also studied using SANS. It can scan a sample over 20 mm^3 sample volume with a thickness of 1 mm. Pristine rubber shows strong scattering due to non-rubber particles. By subtracting the spectrum of pure rubber matrix from that of the nanocomposite, we can obtain the scattering signal from clay particles. Clay particles are dispersed in the polymer matrix in the form of tactoids and this rough surface morphology helps in entrapping the polymer chains more efficiently. This eventually leads to a good reinforcement to the matrix.

Here clay is proved to be high-modulus lamellar particles that strongly adhere to the rubber latex leading to excellent reinforcement. A lot of scope exists

in the field of neutron scattering studies of NR nanocomposites. Very little work has been done in this field so far.

22.5 Conclusions

The effect of various fillers on NR based composites, nanocomposites and blends have been study by means of X-ray scattering, light scattering and neuron scattering. The morphology and structure of filler in rubber matrix, filler–filler interactions, filler–rubber interactions, morphology of the polymer rubber based nanocomposites are easily analysed by X-ray scattering methods. The origin of nanovoids in polymer nanocomposite and effect of nanovoids on creation of cracks are clearly studied by X-ray scattering techniques.

The molecular mass and particle size distribution of polymers, polymer blends, aggregates, are easily analysed by using light scattering techniques. The production and stability of micelles, miscibility of polymer blends and protein crystallization are also easily identified by light scattering methods. Using neutron scattering techniques the weight average molecular mass of polymers and polymer composites are easily measured. Creation of lamellae and formation and mechanism of tactoids are measuring by using SANS method.

References

1. K. Brüning, K. Schneider, S. V. Roth and G. Heinrich, *Macromolecules*, 2012, **45**, 7914.
2. Y. Ikeda, N. Higashitani, K. Hijikata, Y. Kokubo and Y. Morita, *Macromolecules*, 2009, **42**, 2741.
3. J. Che, S. Toki, J. L. Valentin, J. Brasero, A. Nimpaiboon, L. Rong and B. S. Hsiao, *Macromolecules*, 2012, **45**, 6491.
4. L. Bokobza, *Macromol. Mater. Eng.*, 2004, **289**, 607.
5. S. Toki, C. Burger, B. S. Hsiao, S. Amnuaypornsri, J. Sakdapipanich and Y. Tanaka, *J. Polym. Sci., Part B: Polym. Phys.*, 2008, **46**, 2456.
6. M. Hernández, T. A. Ezquerra, R. Verdejo and M. A. López-Manchado, *Macromolecules*, 2012, **45**, 1070.
7. P. V. Anil Kumar, K. T. Varughese and S. Thomas, *Ind. Eng. Chem. Res.*, 2012, **51**, 6697.
8. S. Murakami, K. Senoo, S. Toki and S. Kohjiya, *Polymer*, 2002, **43**, 2117.
9. T. A. Ezquerra, *Macromolecules*, 2011, **44**, 6574.
10. F. Deng, M. Ito, T. Noguchi, L. Wang, H. Ueki, K. Niihara, Y. A. Kim, M. Endo and Q.-S. Zheng, *ACS Nano*, 2011, **5**, 3858.
11. M. Hernandez, J. Carretero-Gonzalez, R. Verdejo, T. A. Ezquerra and M. A. Lopez-Manchado, *Macromolecules*, 2010, **43**, 643.
12. P. C. Song, C. H. Liu and S. S. Fan, *Appl. Phys. Lett.*, 2006, **88**, 153111.
13. C. Marega, V. Causin, R. Saini, A. Marigo, A. P. Meera, S. Thomas and K. S. Devi, *J. Phys. Chem. B*, 2012, **116**, 7596.
14. A. Marigo, C. Marega, R. Zannetti, G. Morini and G. Ferrara, *Eur.Polym. J.*, 2000, **36**, 1921.

15. M. Tosaka, D. Kawakami, K. Senoo and S. Kohjiya, *Macromolecules*, 2006, **39**, 5100.
16. J. Carretero-Gonzalez, R. Verdejo, S. Toki, B. S. Hsiao, E. P. Giannelis and M. A. Lopez-Manchado, *Macromolecules*, 2008, **41**, 2295.
17. Y. Ikeda, Y. Yasuda, K. Hijikata, M. Tosaka and S. Kohjiya, *Macromolecules*, 2008, **41**, 5876.
18. M. Hernandez, M. A. Lopez-Manchado, A. Sanz, A. Nogales and T. A. Ezquerra, *Macromolecules*, 2011, **44**, 6574.
19. Y. Ikeda, Y. Yasuda, S. Yamamoto and Y. Morita, *J. Appl. Crystallogr.*, 2007, **40**, s549.
20. W. Li, C. Liang, W. Zhou, J. Qiu, Z. Zhou, G. Sun and Q. Xin, *J. Phys. Chem. B*, 2003, **107**, 6292.
21. G. Weng, G. Huang, L. Qu, Y. Nie and J. Wu, *J. Phys. Chem. B*, 2010, **114**, 7179.
22. X. Zhao, Q. Zhang and D. Chen, *Macromolecules*, 2010, **43**, 2357.
23. F. Li, N. Yan, Y. Zhan, G. Fei and H. Xia, *J. Appl. Polym. Sci.*, 2013, DOI: 10.1002/app.38958.
24. B. Ozbas, S. Toki, B. S. Hsiao, B. Chu, R. A. Register, I. A. Aksay, R. K. Prud'homme and D. H. Adamson, *J. Polym. Sci., Part B: Polym. Phys.*, 2012, **50**, 718.
25. S. Suin and B. B. Khatua, *Ind. Eng. Chem. Res.*, 2012, **51**, 15096.
26. J. Carretero-Gonzalez, H. Retsos, R. Verdejo, S. Toki, B. S. Hsiao, E. P. Giannelis and M. A. Lopez-Manchado, *Macromolecules*, 2008, **41**, 6763.
27. G. Weng, G. Huang, H. Lei, L. Qu, Y. Nie and J. Wu, *Polym. Degrad. Stab.*, 2011, **96**, 2221.
28. H. Zhang, A. K. Scholz, F. Vion-Loisel, Y. Merckel, M. Brieu, H. Brown, S. Roux, E. J. Kramer and C. Creton, *Macromolecules*, 2013, **46**, 900.
29. J. Lipfert, L. Columbus, V. B. Chu, S. A. Lesley and S. Doniach, *J. Phys. Chem. B*, 2007, **111**, 12427.
30. J. R. Potts, O. Shankar, L. Du and R. S. Ruoff, *Macromolecules*, 2012, **45**, 6045.
31. J. Holoubek, *J. Quant. Spectrosc. Radiat. Transfer*, 2007, **106**, 104.
32. R. Ecora, B. J. Berne, and R. Pecora *Dynamic light scattering, with applications to chemistry, biology and physics*. DoverPublishers, New York Inc. 2000, p. 384.
33. R. Borsali and R. Pecora, *Scattering, imaging and manipulation*. Springer, Berlin 2007, p. 2003.
34. J. Holoubek *Light scattering methods and characterization of polymer systems and processes*. SPIE 1998, 3726, 438–49.
35. J. P. Wilcoxon and P. P. Provencio, *J. Phys. Chem. B*, 2005, **28**, 13461.
36. H. Wang, K. Shimizu, E. K. Hobbie and Z.-G. Wang, *Macromolecules*, 2002, **35**, 1072.
37. F. Moreno, E. Gonzalez and J. M. Saiz, *Opt. Lett.*, 2006, **31**, 1902.
38. M. Francoeur, P. G. Venkata, M. M. Aslan, and c- M. P. Mengu, *Ninth international conference ELS by non-spherical particles*, St. Petersburg, Russia, 2006, **47**, June 5–9.

39. E. A. Hawes, J. T. Hastings, C. Crofcheck, and M. P. Menguc, *ninth international conference ELS by non-spherical particles*, St. Petersburg, Russia, 2006, **67**, June 5–9.
40. N. Posharnowa, A. Schneider, M. Wunsch, V. Kuleznew and B. A. Wolf, *J. Chem. Phys.*, 2001, **115**, 9536.
41. D. R. Paul and C. B. Bucknall, *Polymer Blends*, Wiley, New York, 2000.
42. P. Tang, J. S. Higgins, V. Arrighi and J. T. Cabral, *Polymer*, 2002, **43**, 6661.
43. P. Tang, V. Arrighi, J. S. Higgins and G. X. Li, *Polym. Int.*, 2004, **53**, 1689.
44. I. Demyanchuk, S. A. Wieczorek and R. Holyst, *J. Chem. Phys.*, 2004, **121**, 1141.
45. L. Zhao, G. Zhan, Y. Yu, X. Tang and S. Li, *J. Appl. Polym. Sci.*, 2008, **108**, 953.
46. W. B. Ouyang, G. X. Li and Q. Yang, *Macromol. Theor. Simul.*, 2004, **13**, 178.
47. I. Demyanchuk, S. A. Wieczorek and R. Holyst, *J. Chem. Phys.*, 2004, **121**, 1141.
48. Y. Yang, Z. Xiao, X. Jiang and J. Sheng, *J. Macromol. Sci., Part B: Phys.*, 2006, **45**, 1083.
49. A. Guinier, *Ann. Phys. (Paris, Fr.)*, 1939, **12**, 161.
50. A. Guinier, G. Fournet 1955 *Small Angle Scattering of X-Rays*. Wiley, New York.
51. B. M. Yuri and G. D. Wignall, *J. Appl. Phys.*, 2007, **102**, 021101.
52. H. Hasegawa, S. Sakurai, M. Takenaka and T. Hashimoto, *Macromolecules*, 1991, **24**, 1813.
53. Noble prize in physics in 1994 (1994), URL http://nobelprize.org/nobel_prizes/physics/ laureates/1994/.
54. M. Akenaka, *Polymer*, 2013, **45**, 10.
55. P. A. Steward, J. Hearna and M. C. Wilkinson, *Adv. Colloid Interface Sci.*, 2000, **86**, 195.
56. R. Ullman, *Macromolecules*, 1986, **19**, 1748.
57. T. A. Vilgis, *Macromolecules*, 1992, **25**, 399.
58. T. Suzuki, *Macromolecules*, 2010, **43**, 1556.
59. S. Westermann, *Macromolecules*, 1999, **32**, 5793.
60. T. Kotani; S. S. Sternstein in *Polymer Networks*; Chompff, A. J., Ed.; Plenum: New York, 1971.
61. R. G. Kirste, W. A. Kruse and J. Schelten, *Makromol. Chem.*, 1973, **162**, 299.
62. D. G. Ballad, J. Schelten and G. D. Wignall, *Eur. Polym. J.*, 1973, **9**, 965.
63. J. P. Cotton, D. Decker, H. Benoit, B. Farnoux, J. Higgins, G. Jannink, R. Ober, C. Picot and J. Descloizeaux, *Macromolecules*, 1974, **7**, 863.
64. Jeffrey A. Hinkley, *Macromolecules*, July-August 1978, **11**(NO. 4).
65. Gabrys, B. J., Ed. *Applications of Neutron Scattering to Soft Condensed Matter*; Gordon and Breach: Paris, 2000.
66. R. Zorn, B. Frick and L. J. Fetters, *J. Chem. Phys.*, 2002, **116**, 845.

67. M. A. Adams, B. J. Gabrys, W. M. Zajac and D. G. Peiffer, *Macromolecules*, 2005, **38**, 160.
68. B. Frick and L. J. Fetters, *Macromolecules*, 1994, **27**, 974.
69. T. Karino, *Biomacromolecules*, 2007, **8**, 693.
70. P. A. Steward, *Adv. Colloid Interface Sci.*, 2000, **86**, 195.
71. T. Koga, T. Hashimoto, M. Takenaka, K. Aizawa, N. Amino, M. Nakamura, D. Yamaguchi and S. Koizumi, *Macromolecules*, 2008, **41**, 453.
72. G. Beaucage, *J. Appl. Cryst.*, 1995, **28**, 717.
73. K. Yamauchia, S. Akasakaa, H. Hasegawaa, S. Koizumib, C. Deeprasertkulc, P. Laokijcharoend, J. Chamchange and A. Kornduangkaeo, *Composites, Part A*, 2005, **36**, 423.
74. C. A. Rezende, F. C. Bragança, T. R. Doi, L.-T. Lee, F. Galembeck and F. Boué, *Polymer*, 2010, **51**, 3644.

CHAPTER 23

Microscopy of Natural Rubber Composites and Nanocomposites

LUCIA CONZATTI*[a] AND MAURIZIO GALIMBERTI[b,c]

[a] Istituto per lo Studio delle Macromolecole (ISMAC), Consiglio Nazionale delle Ricerche – UOS Genova, Via De Marini 6, 16149 Genova, Italy; [b] Politecnico di Milano, Dipartimento di Chimica, Materiali e Ingegneria Chimica 'G. Natta', Via Mancinelli 7, 20131 Milano, Italy; [c] Istituto per lo Studio delle Macromolecole (ISMAC), Consiglio Nazionale delle Ricerche, Via Bassini 15, 20133 Milano, Italy
*Email: conzatti@ge.ismac.cnr.it

23.1 Introduction

Optimized rubber composites for specific applications are very complex materials commonly composed of elastomers, fillers, chemical vulcanization aids and other chemical additives used to improve processing and ageing behaviour. The selection of the appropriate fillers and additives is strategic for achieving the target performances of the ensuing rubber composites. The state of distribution and dispersion of fillers and additives steers their effect in the composites and it is thus the subject of a massive research activity both in academic and industrial worlds,[1–3] with the aim of developing efficient processing technologies and advanced characterization techniques.

The most important rubber application is in tyre compounds, about 70% of the worldwide natural and synthetic rubber consumption. A conventional tyre for passenger cars contain more than ten different rubber compounds, developed as a function of the specific requirements of the various tyre parts and thus based on optimized combinations of rubbers and other ingredients.

RSC Polymer Chemistry Series No. 8
Natural Rubber Materials, Volume 2: Composites and Nanocomposites
Edited by Sabu Thomas, Hanna J. Maria, Jithin Joy, Chin Han Chan and Laly A. Pothen

Published by the Royal Society of Chemistry, www.rsc.org

A common feature of tyre compounds is the presence of natural rubber (NR), the most important rubber for highly demanding dynamic applications, such as the ones in tyre, basically as a consequence of its matchless elasticity.

For understanding and controlling the properties of elastomeric composites based on NR, it is of the outmost importance to assess:

(i) distribution and dispersion of fillers and additives;
(ii) structure of networks present in the rubber matrix, built in particular by fillers;
(iii) state of the interface between fillers and ingredients and the rubber matrix.

They are hot topics of the worldwide research and are the subject of the present chapter, which is in particular focused on fillers as the rubber composites ingredients.

In the scientific literature, nuclear magnetic resonance (NMR),[4–7] bound rubber measurements[8–11] and glass transition (T_g) determination through calorimetric analysis[12–16] are preferentially adopted for investigating the filler-rubber interaction, whereas microscopic analysis is in particular selected for assessing filler distribution and dispersion and for depicting the nature of the filler network.[17–23]

This chapter discusses the role of microscopic analysis for investigating all the above mentioned (i) – (iii) aspects, presenting a rationalized overview of available results. As it is of increasing evidence that only a multidisciplinary approach can lead to a more accurate picture of a NR-based composite, the information brought about by microscopic analysis is also discussed as complementary to findings arising from other analytical techniques.

23.2 Fillers for Rubber Composites

At the beginning of the last century, white tyres without fillers were prepared for the car of the German emperor Wilhelm and people were reluctant to add carbon black to tyre compounds, because of the black colour. Nowadays, rubber vulcanizates could not be used, particularly for applications in tyre compounds, without the addition of reinforcing fillers, which are mainly spherical particulate fillers with the diameter of primary particles ranging from about 10 to about 70 nm.[1,3] These low diameters ensure medium to high surface areas, thus a high interfacial area with the elastomeric matrix. These primary particles, even though are joined together by non-covalent bonds, still form strong aggregates that cannot be brought back to particles through thermo-mechanical mixing. These types of fillers are thus known as nanostructured and the most used in rubber composites are carbon black (CB) and silica. Aggregates form agglomerates and the dynamic equilibrium between aggregates and agglomerates deeply affects the elastomeric composite properties.

Spherical particles with higher diameter (up to about 90 nm) have a low surface area and thus do not have a reinforcing ability. They are essentially

used to infer specific properties such as colour, volume, conductivity, absorption of radiation or sound as well as to reduce costs.

Reinforcement of elastomers by particulate fillers is pursued in order to improve, by an order of magnitude, static and dynamic moduli as well as ultimate properties such as tensile strength and elongation at break. The simultaneous improvement of modulus and elongation is known as the 'paradox of elastomers'.

The reinforcement of elastomers by fillers has been studied in depth in numerous investigations[1,3,24–27] and, as shown in Figure 23.1, it is generally accepted that it arises from a combination of different contributions, such as the rubber network, hydrodynamic effects, and elastomer–filler and filler–filler interactions.

Moreover, it is accepted that the elastic modulus at high strain amplitudes is essentially due to the so-called 'filler structure', that means the ability of fillers to accommodate polymer chains into the macro-cavities of their aggregates. The filler structure is determined through *iso*-butylphthalate absorption measurements, which give an indication of the amount of polymer chains that could be adsorbed. The mobility of polymer chains is restricted as a consequence of their adsorption in filler macro-cavities as well as of their immobilization on the filler surface.

The modulus at minimum and low strain amplitudes is due to the so-called *filler network* and it is accepted that the filler surface area, as well as the surface activity, play a major role in establishing a filler network, determining the effective contact area between filler particles and between filler particles and the elastomer matrix. The stress assisted disruption of the filler network causes the reduction of the modulus as the strain amplitude increases, giving rise to the non-linearity of the dynamic-mechanical behaviour of the rubber composite. This phenomenon is known as the Payne effect and it is (to a certain extent) reversible. The disruption and re-formation of the filler network is

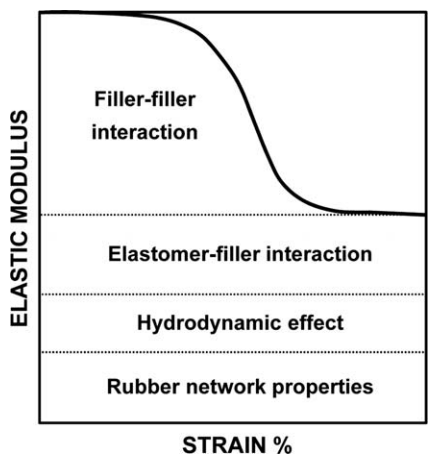

Figure 23.1 Contributions to the elastic modulus vs strain.

known as *filler networking* and it is clearly a source of dissipation of energy, that much contributes to the so-called rolling resistance of a tyre, when it occurs in a tyre tread compound of a rolling tyre. Much debate in the scientific community is focused on the molecular origin of the modulus reduction: is it essentially due to the dynamic equilibrium between filler aggregates (as in the original interpretation by Payne) or the detachment of glassy rubber shells from the filler particles surface plays also a role? As reported in the Introduction, microscopic analyses are important tools for this investigation, giving fundamental information on structure and extension of the filler network as well as on the amount of filler required to be established.

The theory of reinforcement of polymers and elastomers refers to the Guth–Gold–Smallwood equation[28–30] (Equation (23.1)) to correlate the composite initial modulus (E_c) with the filler volume fraction (ϕ):

$$E_c = E_m(0.67f\phi + 1.62f^2\phi^2) \tag{23.1}$$

where E_m is the initial modulus of the unfilled matrix and f is a shape factor of particle/aggregate of the filler. The quadratic term accounts for the mutual disturbance of the filler particles and the deviation from the Guth equation occurs when filler particles get to percolation. It is known that fillers with a high surface area require a low concentration to get to mutual disturbance and percolation and, thus, as commented above, are the ideal fillers for promoting a remarkable non-linearity of dynamic-mechanical properties (that means a remarkable Payne effect). Moreover, it is evident from Equation (23.1) the key role played by the aspect ratio of the filler, often indicated as shape factor f, that is the ratio between the longest and the shortest dimension of the filler particles/aggregates. The higher is f, the higher are the values obtained for the dynamic-mechanical moduli.

23.3 Nanofillers for Rubber Nanocomposites

The last decades have seen, both in the academic and industrial worlds, a steadily increasing research activity on rubber composites based on the so-called nanofillers.[2,31–40] Nanofillers are made by primary particles with at least one dimension of one or few nanometres that can be individually dispersed into a polymer matrix and, in this respect, are different from nanostructured fillers such as CB and silica. Their very large surface area potentially implies a large interfacial area between filler particles and between filler particles and polymer matrix, leading to: (i) high moduli at low strain; (ii) low filler content necessary to form a percolated filler network; and (iii) overall high reinforcement at low nanofiller concentration. The chance of nanofillers to be reduced to their primary particles presents to scientists the challenging need of assessing the nanocomposite structures, and investigating the state of nanofiller aggregation.

Most used nanofillers are inorganic clays, such as smectites (and among them montmorillonites),[2,31–33,40–48] carbon nanotubes (CNTs)[19,34–36,40,49–52] and graphites[37–39] made by few layers of graphene. Said nanofillers have, as a

common feature, a layered structure and present the great opportunity to integrate the findings obtained from microscopic analyses with results from other analytical techniques, namely X-ray diffraction (XRD) analysis. The complementary information that arises, for example, from electron microscopy and XRD analysis and its correlation with final properties of the material nanocomposites will be discussed in Section 23.5.2.

23.4 Microscopic Techniques for the Characterization of Filler Dispersion

Filler dispersion is defined at different levels: macro-dispersion, which characterizes the incorporation of fillers into the matrix, micro-dispersion, which describes the random distribution of aggregates, tactoids and primary particles within the polymer matrix, and nano-dispersion, which is fundamental for obtaining structural information on nanofillers.

As shown in Figure 23.2, depending on the information required, several types of equipment can be used: optical microscopy (OM),[19,21–23,43,52–56] scanning electron microscopy (SEM),[21,22,36,38,43,44,51,52,55,57–82] atomic force microscopy (AFM),[19–22,34–36,43,44,49–51,53,83–93] and transmission electron microscopy (TEM).[6,19,21–23,34–36,38,39,43,45–50,52,55–57,62,63,65,69,70,73,74,78–80,82–84,86,93–135]

Indeed, morphological characterization is usually performed at different length scales by using different microscopic techniques: at the macroscopic level to obtain information on the incorporation of the filler into the rubber and,

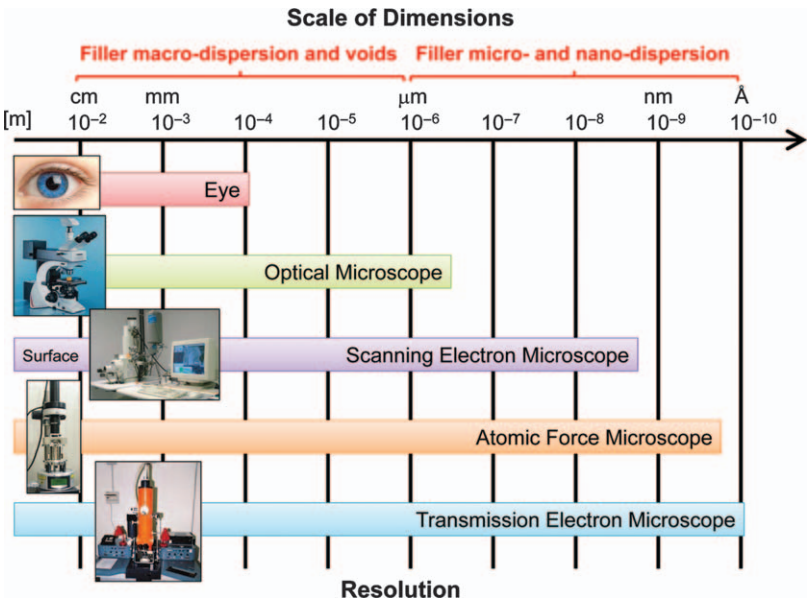

Figure 23.2 Resolution and scale length of different microscopies.

consequently, on the effectiveness of the mixing process; at the micro- and nanoscopic levels to achieve details on the distribution and size of filler aggregates/primary particles and then on the elastomer–filler interactions. In particular, OM is typically used to characterize the macro-dispersion of the fillers and to identify macro-defects.[19,43,52–56,66] SEM analysis is carried out on fracture surfaces of the composite materials to gain information on the micro-dispersion of the filler and mainly on the degree of bonding between matrix and reinforcement.[21,22,36,38,43,44,51,52,55,57–82] Anyway, most of the literature on the morphological characterization of rubber micro- and nanocomposites deals with the use of TEM[6,19,21–23,34–36,38,39,43,45–50,52,55–57,62,63,65,69,70,73,74,78–80,82–84,86,93–135] and AFM[19–22,34–36,43,44,49–51,53,83–93] that provide important and useful information on filler micro-dispersion in bulk and at the sample surface, as well as on topography.

The potential of all the microscopic techniques has been nowadays greatly implemented by the possibility of using automated image analysis (AIA), which allows to obtain structural details and to have quantitative information on the filler dispersion.

23.4.1 Optical Microscopy

Optical Microscopy (OM) has been and continues to be a useful tool for rapid analysis of filler macrodispersions in polymer matrices because of its relative simplicity and minimal sample preparation.[19,43,52–56,66] Traditionally, however, an optical microscope possesses two drawbacks: i) it can only be applicable to dark or strongly refracting materials, ii) its resolution power (calculated as approximately 200 nm) is limited due to the wavelength of the visible light and to the lens resolution. Therefore, OM is suitable to obtain information only on the sub-millimeter scale range, where, in the case of rubber composites, instead of observing filler aggregate dispersion one can obtain information about undispersed pellet fragments or macrodefects.

The OM analysis is carried out on thin cryosections of about 1 mm, as required for light transmittance. In correspondence of filler agglomerates or aggregates the light scatters, giving dark areas. With image analysis techniques, it is possible to calculate the surface of these areas and to evaluate a macrodispersion index,[19,43,52,55,56] as later described in the Section 24.5.2.2 for CNT-rubber nanocomposites. In this case, this parameter was successfully used to correlate the conductance measured during mixing with filler dispersion on the macroscopic scale.

However, for making a reliable and representative analysis, a large number of thin sections, obtained by cryomicrotomy from different zones of the composite, are required. Moreover, during the preparation of the thin cryosections, cutting artefacts can be produced in the case of highly loaded rubber and plastics. They appear as dark striations with the same opacity of the filler agglomerates and they must be eliminated by image analysis software.

In conclusion, despite this technique allowing the quantifying the filler macrodispersion, more sensitive microscopic techniques, such as SEM, AFM

and TEM, must be considered in order to achieve a comprehensive characterization of the filler dispersion at different nanoscales.

23.4.2 Scanning Electron Microscopy

Scanning electron microscopy (SEM) is generally used to observe the surface morphology of fractured composites, giving information mainly on the cause of crack initiation and the failure process. Sample preparation is minimal, requiring only the fragile fracture under liquid nitrogen of the specimens and their coating with a thin layer of conducting material (commonly carbon or gold).

SEM can visualize the filler dispersion in a comparatively large area of the specimen; however, due to its intrinsic lower resolution with respect to AFM and TEM, it is useful only for the determination of the filler dispersion at the micron length scale.[21,22,36,38,44,51,52,57–65,67–82] Several examples of micro- and nanocomposites morphologically characterized by SEM are reported in the literature.[21,22,36,38,44,51,52,57–65,67–82] In the particular case of nanocomposites, also TEM and AFM investigations were performed in order to obtain information on the filler dispersion at different length scales.[36,38,44,51,52,57,62,63,65,69,70,74,79,80]

Field emission SEM (FESEM), characterized by both improved spatial resolution (down to 1 nm) and minimized sample charging and damage, was recently developed. This technique was also applied to the morphological characterization of NR based composites containing CNTs[65] giving important information on the adhesion between filler and matrix.

23.4.3 Atomic Force Microscopy

Atomic force microscopy (AFM) has been shown to be particularly well suited to the characterization of filled elastomers and, more generally, of heterogeneous systems with components of different stiffness, providing information on surface topography, adhesion, mechanical and other properties on scale from a few hundred micrometres to nanometres.[19,20,34–36,43,49–51,53,86,87,91,92,136–138]

This technique has several advantages over the optical and scanning electron microscopes. Even if these latter can easily generate two-dimensional images of a sample surface, with a magnification as large as 1000× for an optical microscope, and ~100,000× for a SEM, they cannot measure the vertical dimension (*z*-direction) of the sample, that is the height (*e.g.* particles) or depth (*e.g.* holes, pits) of the surface features. AFM, which uses a sharp tip to probe the surface features by raster scanning, can image the surface topography with extremely high magnifications. Indeed, its resolution in the *Z*-direction is normally higher than that in the *x*–*y* plane.

Additionally, the coating of SEM specimens with metal or graphite, that is irreversible and may cause artefacts, is not required for AFM. Most of AFM modes can work perfectly in ambient air or even a liquid environment, whereas SEM (and also TEM) needs an expensive vacuum environment for proper operation. However, AFM has some disadvantages compared to SEM: i) AFM has a focal depth on the order of only microns, whereas that of SEM is deeper

on the order of only millimeters; ii) incorrect selection of a probe for the required resolution can also lead to image artefacts; and iii) being the scan speeds for AFM lower than for SEM, in a typical scan for an entire image it is necessary to spend several minutes.

With respect to TEM, AFM allows the analysis of filler dispersion at larger scales and does not require any particular preparation of the specimens if only their surface must be observed and the use of tapping mode minimizes damage of soft polymers surface during scanning.[20,34,87,91,92] Moreover, it has been recently used to study the dependence of filler structures from uniaxial deformation in SBR- and EPDM-based composites loaded with silica or CNT.[50,88] By evaluating the state of filler dispersion after removal of the strain and during second stretching, invaluable information on understanding the Mullins effect was also obtained.

Topography, error signal and phase imaging can be simultaneously recorded in order to get topographic and compositional mapping of the sample surface. Indeed, topography and error signal reveal surface roughness; while, phase imaging, which provides variation of surface stiffness, is particularly useful in elastomeric composites filled with inorganic fillers or CNTs in account of huge differences in moduli between the two phases.

However, to achieve information on the morphology of the bulk it is necessary to prepare sections, generally about 4 μm thick, by using cryomicrotomy, as for TEM specimen preparation. Moreover, the resolution of AFM is lower than that of TEM, as evidenced also in the literature.[34,87]

In the field of elastomer composites, this technique can provide also information on adhesion, as well as mechanical and other properties. In particular, the mechanical properties, such as the Young's modulus, can be calculated at a single point from AFM force–distance curves.[139–142] More recently, Wang *et al.*[91,92] obtained topography, elastic modulus and adhesive energy maps at the same point and at the same time in a single scan for NR–CNT composites. They employed the force–volume technique to obtain force–distance curves over a two-dimensional area, which were analysed using a procedure based on the combination of Johnson–Kendall–Robert (JKR)[143] contact mechanics and 'two-point method'.[144] The ensuing adhesive energy maps were thus used to identify and characterize heterogeneity of such composites. The interfacial regions formed around the CNTs together with CNTs divided elastomer matrix into small 'cells' in which NR is occluded. Therefore, the greatly enhanced mechanical properties of the composites were considered to be due to the three-dimensional structure formed by CNTs and the interfacial regions bound to them.

In the literature only few papers deal with the statistical analysis of filler dispersions in elastomers by using AFM/AIA technique.[20,53,87,90,145] The distribution of the aggregate areas of the filler in SBR-, EPDM- and silicone-based compounds loaded with different amounts of precipitated silica (up to 50 phr) was evaluated by using tapping mode phase imaging. The beneficial effect given by the addition of TESPT as a coupling agent was evidenced:[90] as compared to untreated silica, a significant amount of much smaller particles was detected.

Le *et al.*[53] quantitatively evaluated and successfully correlated in silicone rubbers macro- and microdispersion of CB with the electrical conductivity measured during mixing. OM and AFM both aided with AIA were used for the analysis of macro- and microdispersion, respectively. A comparison between the average particle size, determined on AFM and TEM images, is given by Clément *et al.* for silicone-loaded composites.[87] Even if a good agreement between the results obtained with the two techniques was found, TEM values are always slightly lower, due to the higher resolution of TEM, as compared to AFM.

Very recently, Morozov *et al.*[20,89] developed a new method for the quantitative analysis of the structure of filled rubbers by AFM. This method was tested for several EPDM-, SBR-, IR- and NR-based composites containing different amounts of CB or silica and involves the splitting of the surface relief of the material into separate clusters in order to determine the level at which the geometry of the clusters best reproduces the structure of the filler network. Calculations of filler distribution and structural parameters (area, size, perimeter, fractal characteristics, *etc.*) of clusters were thus performed. These morphological characteristics together with orientation and distance between neighbouring pairs of aggregates were also evaluated in materials subjected to tension.[89]

23.4.4 Transmission Electron Microscopy

Transmission electron microscopy (TEM) is widely recognized as an effective analytical method for studying nanostructures in general. In the particular case of elastomer-based composites it was extensively used to investigate the micro- and nano-dispersion of the filler, *i.e.* the random distribution of aggregates and primary particles in the matrix. Furthermore, if the loading is not too high, it also enables to recognize different fillers simultaneously present in the compound, as for example CB and silica or particulates and layered nanofillers. However, the great potential of this technique can be fully exploited only after a suitable sample preparation; indeed, high quality TEM specimens are required to be quite uniform and less than 100 nm thick, to be comparable with the mean free path of the electrons that travel through them (only a few tens of nanometers). To this purpose, the rubber specimens, cooled at least 40 °C below the glass transition, are microtomed with a cooled diamond knife. Moreover, to obtain meaningful results a large number of cryosections (several hundreds) 1 mm^2 of surface, obtained from different zones of each sample, must be investigated.

Since a conventional TEM produces a projected three-dimensional (3D) image on a two-dimensional (2D) plane, quantitative information on the filler dispersion can be attained by using AIA techniques.[6,95–97,99,102,115,125,127,134] In this way, it is possible to recognize, select, measure and compare size and shape of the complex structures dispersed in the matrix through the use of descriptors based on geometrical parameters, such as area, perimeter, diameter and morphometric parameters, such as shape ratio and roundness (Figure 23.3). However, TEM image analysis of filler microdispersions is more difficult to

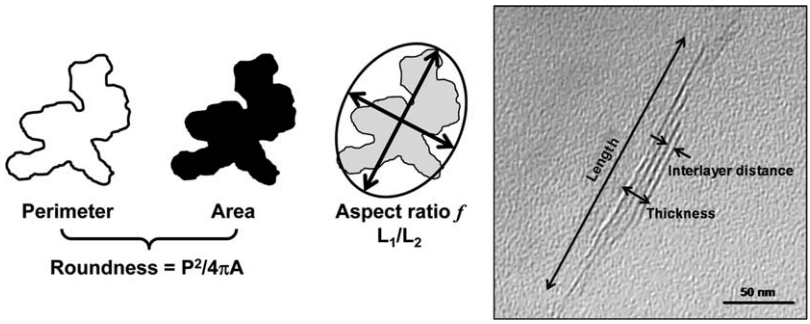

Figure 23.3 Morphometric descriptors for micro- and nanofillers.

interpret than optical analysis of agglomerates. This is particularly true at the high loadings typically used in elastomer compounds, *i.e.* CB or silica aggregates are not fully separated in the images of thin cryosections. As reported in Section 23.2, the *f* aspect ratio of a filler plays a fundamental role in the reinforcement of an elastomeric matrix. Microscopic analysis is thus of great importance for fitting experimental values of mechanical moduli with theoretical equations, allowing the determination of this parameter.[38,118,119,122,124,133]

Figure 23.3 also shows an innovative application of TEM analysis: measurement of the distance between opposite layers in a layered nanofiller.[105,146]

In recent years, TEM has been combined with electron tomography for 3D structural observation at the nanometre scale, fundamental for the study of highly loaded NR composites.[101,107–110,112–114,116,117,147] As TEM specimen holders typically allow for the rotation of a sample by a desired angle, multiple views of the same specimen can be obtained by rotating the sample angle along an axis perpendicular to the electron beam. By taking multiple images of a single TEM sample at various angles (typically with 1–2° increments) a set of images known as a 'tilt series' can be collected and used to construct a 3D representation of the sample. Image analysis techniques can be also applied.

Some examples of filler distribution quantitatively evaluated by 2D and 3D-TEM combined with AIA in rubber-based microcomposites will be reported in Section 23.5.1.

Different magnifications are typically used to characterize each sample: low magnifications (3000–12000×) give indications on the overall dispersion and they are useful to control the global homogeneity of the filler dispersion into the rubber matrix; medium magnifications (20000–50000×) enable to provide an accurate morphometric characterization of the system through the application of selected morphological descriptors used to identify, count and measure the aggregates; high magnifications (>50,000×) are helpful in the investigation of morphological details at the nanometric level.

23.5 Morphology of Natural Rubber Composites

Physical and mechanical properties of filled rubber composites are strongly influenced by chemical nature, microstructure and molecular weight of the

elastomers, as well as by some filler characteristics, such as particle size and surface activity, aggregate structure and morphology.

Due to their high spatial resolution and to the sufficient contrast between filler and matrix, microscopic techniques involving mainly electron microscopy have been extensively used to characterize structure and morphologic organization of fillers, such as CB, silica, layered silicates, CNT and graphite, both in their dry state and into the elastomer matrix.

However, depending on structural and chemical characteristics of the filler and on its ability to disperse into the matrix, different approaches have to be considered. Indeed, the filler dispersion must be investigated at different length scales and in some cases the combination with other techniques, such as image analysis, 3D reconstruction or XRD, can be helpful in correlating morphological features with final properties of the material.

In the following sections some of the most important examples are reported for micro- and nanofillers.

23.5.1 Microcomposites

The reinforcement of rubber composites by CB and/or silica is greatly affected by the rubber–filler interactions, the agglomeration of the filler particles within the rubber matrices, and the occlusion of the rubber into the internal voids of the dispersed aggregates. Furthermore, filler–elastomer interactions play a major role in the filler dispersion achievable during mixing process.

From a practical point of view, an accurate morphological characterization of the filler dispersion allows us to ascertain the homogeneity of the filler network, responsible for the material's performance, as well as to detect structural differences in the filler aggregates and to relate them to the final properties of the composite material.

Simple morphological characterization by TEM gives only qualitative information on the filler micro-dispersion and it becomes more difficult on increasing the amount of the filler, as shown in Figure 23.4.

The combination of TEM and AIA techniques makes it possible to obtain quantitative and representative information on the filler distribution in the elastomer matrix (homogeneity of the dispersion, size and shape distribution of the aggregates) and, consequently, on the filler–elastomer interactions.

This method was implemented in the last 10 years mainly for rubbers loaded with silica;[6,17,95–97,99,102,115,127,134] different elastomer matrices were explored even if SBR was the most considered.

In a series of papers[6,127,134] aimed at investigating the effect of the secondary network of silica on the reinforcement SBR and NBR, image analysis was performed on digital binary images converted from TEM micrographs determining the average size of filler aggregates. This parameter was measured in composites containing silicas with different surface activity and it was correlated with stress–strain and Payne effect curves. The following conclusions were drawn: the higher is the hydrophilic character of silica surface (number of silanols groups per unit surface area of silica), the larger is the size of

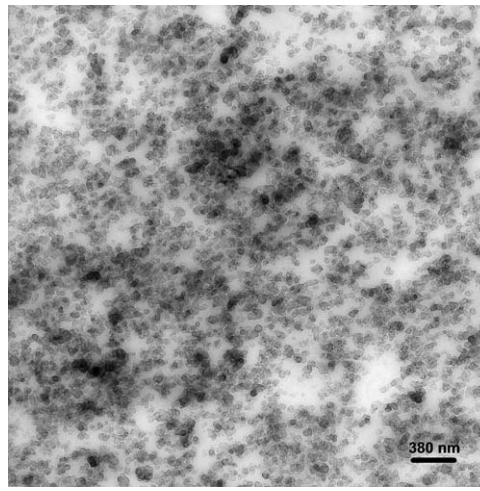

Figure 23.4 TEM image of NR loaded with 60 phr CB.

agglomerates; the larger are the aggregates the higher is the content of bound rubber entrapped.

Rubber microcomposites based on different matrices (BR, NR, SBR) and loaded with the same amount of unmodified silica were analysed by TEM/AIA following a procedure optimized in order to achieve, in a reasonably short time, quantitative information on the filler dispersion by considering several morphometric descriptors.[96,99,102]

This procedures is carried out on several (at least 10) digitalized TEM images taken at the same magnification taken in different zones of the sample. It involves the use of image analysis software (*e.g.* Image Pro® Plus, Media Cybernetics) and the following steps:[17,102]

- application of an appropriate calibration scale;
- application of an appropriate filtering procedure to identify exactly all the filler aggregates, with their irregular and complex perimeters, and to make sure that any single particle is selected;
- subtraction of the polymer matrix background, given by the lowest intensity grey, and identification of the grey tones corresponding to the filler;
- application of the most appropriate morphometric descriptors (*e.g.* area, perimeter, aspect ratio, roundness, *etc.*) to the filler particles automatically identified by the software;
- collection of the data in a spreadsheet where a statistical elaboration can be done.

A significant difference in terms of number, size and shape of the dispersed particles was found as a function of the matrix considered: in NR and BR the number of filler particles was smaller than that counted in SBR. In particular,

by using as a morphological descriptor the area to perimeter ratio, A/P, it was found that aggregates with similar surface area have quite different perimeters, *i.e.* different shape. The overall results indicated favoured interactions between silica and the SBR matrix.

This TEM/AIA procedure was thus extended from one of the authors to SBR composites containing increasing amounts of as received or silane-modified silica.[17,95,97] Considering two composites containing the same amount (35 phr) of silica, the selection and application of morphometric descriptors such as A/P and roundness ($P^2/4\pi A$) through the AIA procedure allowed to show that two morphologies apparently similar from a qualitative analysis are different on size and shape of the dispersed particles. In particular, in spite of having similar area, aggregates of modified silica are characterized by higher perimeter, that means higher contact surface between filler and elastomer. This morphological information supported tensile and dynamic-mechanical properties of the composites.

Because TEM micrographs are 2D projections of the observed sample, on increasing filler loading (Figure 23.4), a morphometric analysis based on the same procedure becomes more difficult and can give apparently contradictory results. The superimposition of the aggregates, which can easily occur due to the high amount of filler and can be favoured if the filler is well dispersed, together with the difficulty of identifying exactly the contact surface area between the filler and the matrix, might be responsible for what is stated above. A further contribution to the surface area covered by the filler might be given by the bound rubber, according to the results reported by Yatsuyanagi *et al.*[134]

As a consequence, to characterize composites containing high amounts of filler, different methods must be exploited, taking into account also the 3D distribution of the filler aggregates.

In recent years, since the progress on computerized simulation and modelling, new approaches based on 3D reconstruction of TEM images have been developed.[107–110,112–114,116,117,147]

A conventional TEM was combined with electron tomography (3D-TEM) to visualize and quantify the 3D distribution of CB and/or SiO_2 in NR and NR/BR microcomposites.[109,110,112,116] The vulcanized samples were first subjected to extraction by organic solvents to remove Zn compounds (*e.g.* zinc stearate and organic zinc salts), which derive from ZnO, one of the additive commonly used for sulfur curing, and can detrimental to the contrast between the inorganic phase and the rubber matrix. A series of 2D projections TEM images were thus acquired with a CCD camera by tilting a very thin cryomicrotomed sample from -70° to $+70^\circ$ by 2° steps. The pixel size was calibrated using colloidal gold sized ca. 10 nm, taken as a reference.[148] The 2D projections were aligned by using IMOD software, and the sequential tilted images were converted to image slices showing the mass density distribution at each angle. The AMIRA software was thus used to reconstruct 3D images from the obtained image slices. The 3D images showing nanoscale morphology of silica and CB aggregates in NR matrix were successfully visualized confirming the formation of a 3D filler network. Moreover, in each aggregate the primary filler particles

are physically in contact, and the aggregates are recognized as the primary existing species of filler. The number, the radius, the aspect ratio of silica aggregates and their distribution in a definite volume, as well as the volume of each particle and, consequently, the total volume of filler were calculated from 3D-TEM. The 3D structure of the filler network was thus visualized by drawing a line connecting the gravity centres of neighbouring aggregates,[149] and quantitatively characterized by measuring the number of crosslinked and branched filler chains. Interesting results were obtained concerning the correlation with physical properties, such as electron conductivity.

By using 3D-TEM combined with electron energy loss spectroscopy (EEELS), the 3D structure of a NR composite containing both CB and SiO_2 was investigated by Jinnai *et al.*[109,110] CB and silica are difficult to be distinguished by conventional TEM/AIA techniques because of the overlap of the two fillers in the section of the analysed sample; however, they appeared different by 3D-TEM. In the image slice of the 3D-TEM reconstruction, CB and silica particles appeared to be hollow and solid particles, respectively. With this approach the two fillers were found to form in the NR/BR matrix aggregates made of only one species, not single aggregates containing both CB and SiO_2.

However, the analysis of 3D-TEM images yields an enormous amount of data and until now the biggest problem is the availability of software to be used for the calculations. As a consequence, only very little areas (of surface less than 500 nm^2) can be until now analysed with this technique, giving information not representative of the entire composite material.

Another problem is that no method has been established yet for evaluating the exact resolution in 3D-TEM measurements.

23.5.2 Nanocomposites

As reported in Section 23.3, research on rubber nanocomposites has remarkably increased over the last decades, both in the academic and industrial worlds. Nanofillers bring about appreciable improvements of the following properties of a rubber matrix: mechanical, rheological, barrier, thermal, degradation, flame resistance.

In Section 23.2 was discussed the theory of reinforcement of polymer and elastomers which refers to the Guth-Gold-Smallwood equation (Equation (23.1)) to correlate the compound initial modulus (E_c) with the filler volume fraction (ϕ). Moreover, it was already commented on the key roles played by the surface area and by the aspect ratio (f). Basic feature of nanofillers, such as clays, CNTs and nanographites, is the nano-dimension of primary particles and thus their high surface area. This allows creating filler networks at low concentrations, much lower than those typical of nanostructured fillers, such as CB and silica, provided that they are evenly distributed and dispersed in the rubber matrix. In this case, low contents of nanofiller particles are required to mutually disturb each other and to get to percolation. Moreover, said nanofillers are characterized by an aspect ratio f that can be remarkably higher than 1. Barrier properties are improved when fillers (such as clays and nanographites) made by

platelets, are disposed orthogonally to gas diffusion. Thermal properties are related to the thermal conductivity of nanofillers, such as CNT and nanographites, when they are able to establish a continuous network; whereas degradation and flame resistance properties are improved when platy nanofillers reduce the diffusion of gaseous molecules.

On these bases, it is clear that the achievement of the improvements above reported is first based on the ultimate distribution and dispersion of nanofillers. However, also the control of nanofiller particles organization, in aggregates and agglomerates, plays a key role. To pursue advanced properties moving from the nanocomposite structure, the multiscale organization of nanofillers in the polymer matrix has to be assessed.

23.5.2.1 Clays as Nanofillers

The available literature on rubber–clay nanocomposites essentially refers to cationic clays and those of the smectite family have been the most investigated. Montmorillonite (Mt) is a natural mineral filler belonging to this family, made of stacked layers whose atoms are joined together by iono-covalent bonds (Figure 23.5).[41,150] The layers are bound to each other in the perpendicular direction through weak forces and alkaline/alkaline-earth cations are located in the interlayer space. A single clay layer has lateral dimensions from 100 to 1000 nm and a thickness of about 1 nm, and presents oxygen atoms on its faces and oxygen atoms and hydroxide groups on its edges.

As sketched in Figure 23.5(b), the aspect ratio f is given in this case by the ratio between the longest lateral side of the layer and the height of clay stacks. The highest f value is thus obtained in the case of a single layer. As it will be discussed below, a higher f value means a more pronounced improvement in the rubber matrix. Therefore, the exfoliation of a clay not only favours a better clay dispersion but also improves the modulus of the compound. However, the hydrophilic nature of these clays implies that a nanometric dispersion in a hydrophobic polymer is hard to achieve. The alkaline and alkaline-earth

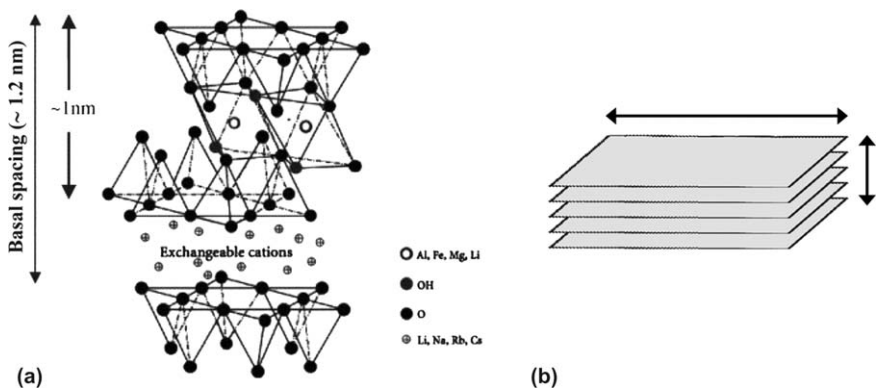

Figure 23.5 Structure of (a) montmorillonite clay and (b) schematic representation of a stack of some clay layers.

cations of Mt are therefore replaced by hydrophobic compensating cations, typically ammonium cations bearing long alkyl chains. This exchange reaction is usually carried out in a water/alcohol mixture and the so formed organoclay (OC) is characterized by a larger basal spacing with respect to Mt.[151] An alternative approach was also reported, performing the exchange reaction directly in the polymer medium, either elastomeric[105,106,152,153] or thermoplastic.[152]

The multiscale clay mineral organization in the polymer matrix has been widely studied in the scientific literature,[18,43,45–48,86,154–156] as it has been identified as the key feature determining the nanocomposite material properties. The analysis of the multiscale clay organization is typically focused on:

(i) ascertaining both distribution and dispersion of the silicate in the rubber matrix;
(ii) studying the lowest level of clay organization, from the distance between two opposite layers to the presence of molecules in the interlayer space, if any.

Figure 23.6 shows the types of composites formed from the interaction of clays and polymers.

If the clay, either pristine or organically modified, is not efficiently dispersed in the polymer matrix, micron-sized agglomerates made of stacks of layers are present (Figure 23.6(a)). The material properties typical of microcomposites.

If an efficient dispersion of clays is achieved and the size of the dispersed particles is in the 'nanoscale', clay nanocomposites (Figure 23.6(b) to (d)) are formed. In the polymer matrix individual layers and/or stacks of few layers are present. Depending on the specific clay organization, the literature distinguishes between:

Exfoliated nanocomposites (Figure 23.6(b)). Individual clay layers are separated in a continuous polymer phase, with the clay loading affecting their relative distance.[156] The terms exfoliation and delamination are synonymously adopted.

Intercalated nanocomposites (Figure 23.6(c)). This expression refers to the presence of polymer chains in the space between two opposite layers. A minor extent of intercalation of preferentially extended polymer chains was assumed

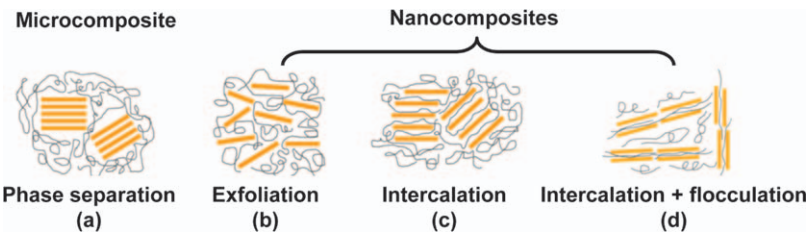

Figure 23.6 Structure of polymer–clay nanocomposites.

to occur[155,156] in order to justify both: (i) the somewhat limited expansion of the interlayer distance and (ii) the presence of a crystalline order.

Intercalated and flocculated nanocomposites (Figure 23.6(d)). In this case, polymer chains are intercalated between two opposite layers that are 'flocculated due to hydroxylated edge–edge interaction'.[156]

However, in practice, the organization of the clay layers in the matrix is more complicated: isolated layers, stacks of a variable number of layers, nano- and micron-sized aggregates coexist and their relative ratio affects the final material properties.

As reported in Table 23.1, TEM and XRD are the techniques typically used to describe the clay organization in a polymer/rubber matrix.[43,46,47,57,62,63,69,79,80,94,98,100,103,105,106,111,120,121,123,126,131,157]

In particular, TEM and SEM analyses give information on homogeneity of distribution and degree of dispersion within the polymer matrix, allowing to conclude that dispersion and distribution of clay particles in NR matrix essentially depend on: (i) the type of clay, either pristine or organically modified, (ii) the nature of the amphiphilic compensating cation (with or without a polar group) (iii) the blending technology.

Melt and solution blending of pristine clays with NR led to poor dispersions. In particular, melt blending of pristine Mt with NR led to a simple incorporation of agglomerated clay,[158] to undispersed aggregates[126] and to the formation of microcomposites,[159,160] with some big clay aggregates. It appears thus that the high molecular mass of NR and the strain induced crystallization mechanism (supposed to give rise to an enhancement of the mixing stress) are not enough to achieve an efficient clay dispersion. The same findings were reported in synthetic isoprene (IR) matrix,[106] although the clay aggregates were smaller than those present in the pristine clay. Prevailingly agglomerated clays were observed by SEM analysis.[161] A conventional microcomposite with typical clay aggregates was obtained from a toluene solution of a masterbatch based on NR and containing ZnO, sulfur, stearic acid and a sulfenamide.[111]

An excellent Mt dispersion, also at a level of 20 phr, was observed when emulsion blending was adopted,[162] with both individual and stacking silicate layers with a thickness of about 10–30 nm.

Organically modified clays achieved a good dispersion in the NR matrix. Mt modified with octadecylamine ammonium chloride was melt blended with NR,[158] a water suspension of a C_{18} based organoclay (the other substituents being three methyl groups) was slowly added to a NR latex.[163] OC was also

Table 23.1 Techniques typically used to analyse the multi-scale clay organization in NR-based nanocomposites.

Clay organization in rubber nanocomposites	*Characterization techniques*
Distribution and dispersion	SEM, TEM
Affinity with other fillers	TEM
Aspect ratio	TEM/AIA
Interlayer distance	XRD, TEM/AIA

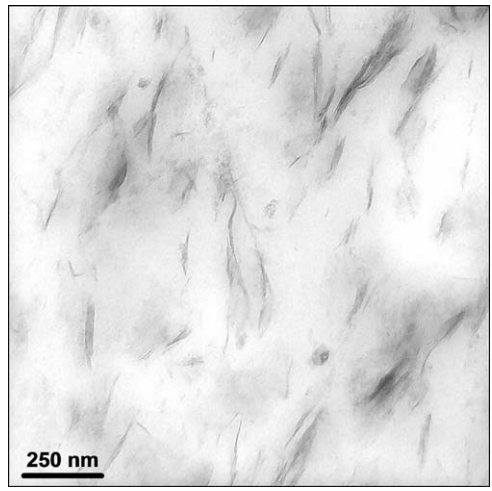

Figure 23.7 TEM image of an isoprene rubber nanocomposite containing organoclay.

formed *in situ* in the NR matrix from Mt and an ammonium cation with two methyls and two talloyls as substituents:[105] Figure 23.7 shows the good dispersion of the OC in the NR matrix.

Less exfoliation and more agglomerated particles were observed when the ammonium cation contained a polar group,[120] with properties resembling those of microcomposites.

The even dispersion of OC allowed percolation to be achieved at low OC concentration. This was demonstrated by the sudden increase in the initial modulus, occurring at OC concentrations between 5 and 8 phr. Natural[123] and synthetic[103] isoprene rubber were examined. TEM analysis supported these findings, identifying continuous clay networks in the rubber matrix.

The easy formation of filler networks allows thus the achievement of remarkable reinforcement of the rubber matrix at low clay content. To mention just an example, a comparable mechanical reinforcement of a NR matrix was obtained with 10 phr Mt modified with octadecylamine and 40 phr CB. The low amount of nanofiller allowed almost double elongation at break to be achieved, a lower compression set and similar abrasion loss.[164] Moreover, a much lower heat built up was obtained with respect to 50 phr CB.[165]

By applying AIA techniques analogous to those discussed in Section 23.5.1, the aspect ratio of the clay particles in a rubber matrix can be determined.[118,119,122,124,133] For example, the high aspect ratio of stacked and distorted fluorohectorite layers was observed in TEM micrographs and was correlated with the reinforcing effect brought about by this silicate.[131]

The investigation of the lowest level of the clay organization, that means the organization of layers in aggregates, is of great importance. As shown in Figure 23.6, most authors believe that rubber chains can intercalate in the interlayer space (Figure 23.6(c)). This event is seen prodromic to clay

exfoliation and can also be considered relevant for rubber reinforcement, thanks to the immobilization of rubber chains. The intercalation of polymer chains should clearly lead to an expansion in interlayer distance and XRD analysis is selected as the tool to determine the distance between consecutive layers in clay stacks. However, when reflections disappear from the XRD pattern, TEM analysis is the only tool to verify if exfoliated clay layers are in the rubber matrix. Other authors proposed an alternative mechanism for the formation of exfoliated clays in the rubber matrix: the so-called 'delamination mechanism'.[153] Layers are progressively peeled off from clay stacks, without the intercalation of polymer chains. These authors prepared, through the synthesis in the rubber matrix (*in situ* synthesis), organoclays with different interlayer distances and explained these different values with the intercalation of low molecular mass substances. Outstanding correspondence was found between the values detected through XRD and the ones measured from the analysis of TEM images.[105] Figure 23.3 shows that from a TEM image it is possible to determine the distance between layers regularly placed in a clay stack. Moreover, the analysis of TEM images allows to observe the platy nature of clay layers and also to determine the aspect ratio f. By performing the investigation on a large number of micrographs, the average value of f was determined and thus introduced in the equations that describe the dependence of modulus on the filler volume fraction, such as the Guth-Gold-Smallwood equation reported above (Equation (23.1)). TEM analysis allows thus to discriminate among models and equations used to describe the reinforcement of rubber matrices, through the determination of structural parameters of nanofillers.

23.5.2.2 Carbon Nanotubes as Nanofillers

Among nanofillers, carbon nanotubes (CNTs) have gained much attention because of their superior electrical, mechanical, and thermal properties.[166] They are nanotubes, made by wrapped graphene layers, with a diameter of few nanometres, a length from a few microns up to millimetres, and a graphite-like structure. They can be single walled (SWCNT) or multi walled (MWCNT). In this paragraph, results refer to MWCNT, unless otherwise indicated.

CNTs are not available as individual tubes (independently of the number of walls), but as tangled webs; indeed, they tend to form rope-like bundles due to their long aspect ratios ($\sim$1000) and the strong anisotropic interactions between them.[167] TEM and high-resolution TEM (HRTEM) are the most useful techniques for the investigation of CNT dispersion before incorporation into the polymer matrix.[34,35,65,73,76,84]

Reports available in the scientific literature clearly show the remarkable improvement of material properties, namely the Young (initial) modulus and the direct current (DC) electrical conductivity, when they are incorporated in an elastomeric matrix.[19,34–36,55,56,58,64,65,71,73,74,76,77,84,101,104,128,129,168–170]

However, the properties of the manufactured materials are still far from theoretical values, as a consequence of the still not completely satisfactory

Table 23.2 Microscopic techniques typically used to characterize CNTs in NR-based nanocomposites.

CNT in rubber nanocomposites	*Characterization techniques*
Macro-dispersion	Optical microscopy/AIA
Micro-dispersion	SEM, AFM, TEM
Nano-dispersion Structure of the filler network	TEM
CNT/NR adhesion	SEM
Adhesive energy distribution maps	AFM

dispersion of CNTs, that are still, at least in part, present in bundles and/or agglomerates, which act as materials defects. As a matter of fact, the dispersion of CNTs as individual particles is still the subject of major research efforts.[171–173] Microscopy plays thus a key role in assessing not only the state of dispersion but also the integrity of CNT in the rubber matrix.

As summarized in Table 23.2, different microscopic techniques are used to characterize the dispersion of CNTs at different length scales.

Optical microscopy has been used to analyse the CNT macrodispersion[19,52,55,56] and to quantify the presence of non-dispersed agglomerates (average diameter larger than 6 μm).[19,52] Indeed, by using a method described by Leigh-Dugmore *et al.*[174] for CB filled compounds and modified by Le *et al.*[175] and an image analysis program, the area of larger CNT aggregates present on several pictures was calculated. The macro-dispersion index D was thus assessed as the amount of the non-dispersed agglomerates (A/A_o) by using Equation (23.2):

$$D = f\frac{A/A_0}{\phi} \tag{23.2}$$

where ϕ is the volume fraction of the filler and f[176] is the aspect ratio of filler particles estimated from TEM images of pure CNTs.

As already discussed in Section 23.4.2, SEM analysis of fractured surfaces gives information both on the CNT micro-dispersion in a comparatively large area of the specimen and on the adhesion between CNTs and rubber matrix.[52,58,64,65,71,73,74,76,77,170] However, to obtain thorough characterization of the micro-dispersion of the CNTs, AFM and TEM have to be also used.[19,34–36,49,50,52,55,56,74,128,129]

Filler micro-dispersion, structure of the composite materials and filler networks are visualized through TEM;[19,34–36,52,55,56,74,104,128,129] while AFM was also recently used for investigating topography and adhesive energy between CNT and NR.[34,49,91,92] In particular, as previously discussed in Section 23.4.3, adhesive energy distribution maps were used to identify and characterize the interfacial regions around the CNTs dispersed in the rubber matrix.

From the investigations based on the commented microscopy techniques, it appears that the state of the dispersion and the integrity of CNTs in the rubber matrix depend on: (i) blending technology (ii) functionalization of CNT.

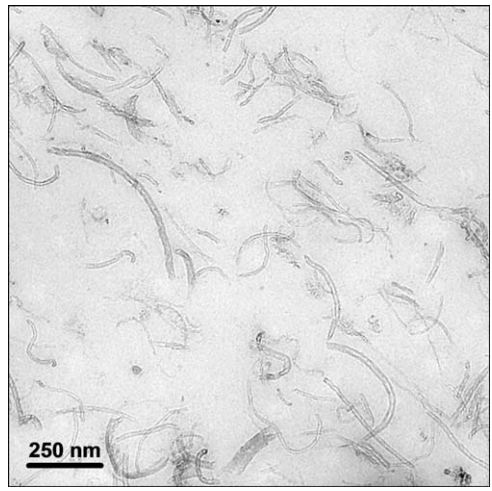

Figure 23.8 TEM image of an isoprene rubber nanocomposite containing CNTs.

The direct dispersion of CNTs in NR by melt mixing[19,34,49,52,55,56,71,77,91,92,104,170] process takes advantage of the high shear stress produced during mixing by rubbers, such as IR and NR, for achieving an easier CNT dispersion. It appears that a high shear is able to promote a better dispersion but also brings about, at the same time, a remarkable reduction in tube length, which means of the tube aspect ratio. Figure 23.8 shows the even CNT dispersion in synthetic isoprene rubber and also that tube length was remarkably decreased by mixing from the original micron size.[104]

Through physical-mechanical measurements it was determined that the CNT percolation occurred at low nanofiller concentration and TEM images supported this finding, revealing a continuous CNT network for filler concentrations above the percolation threshold.[104]

To overcome the problem of damaging tubes through melt mixing, CNT/NR nanocomposites were formed by incorporating CNT in a polymer solution and subsequently evaporating the solvent.[35,58,64,65,73,76,84,128,129] CNTs were dispersed homogeneously, as observed through SEM, field emission SEM (FESEM) and/or TEM, allowing to hypothesize an excellent interface between CNTs and NR.

TEM revealed that the surface functionalization of CNT with phenol[129] or 1-octadecanol[128] improved their dispersion in a NR matrix.

Furthermore, nanocomposites were prepared from NR latex and CNT with cavities filled by magnetic species.[36] Surfactants were used to achieve a stable aqueous CNT dispersion. TEM and SEM analyses showed the even CNT dispersion, in line with findings from other techniques such as IR and Raman spectroscopy, X-ray microtomography, which revealed a good adhesion between CNT and the polymer matrix.

A combined self-assembly and latex compounding technique was used for preparing NR-based composites containing positively charged CNTs.[74] TEM and SEM indicated that the CNTs were homogeneously distributed into the NR as single tubes and their interfacial adhesion with the matrix was good.

23.5.2.3 *Nanographite as a Nanofiller*

Nowadays, a steadily increasing interest is for graphene, a two-dimensional sheet made of sp2-hybridized carbon atoms in an extended honeycomb network.[177] At the origin of said interest are its excellent thermal, electrical and mechanical properties and its layered structure.[178] Remarkable efforts are thus made in order to prepare graphene or graphitic nanofillers made by few layers of graphene. These nanofillers are mainly named as graphite nanoplatelets (GNPs), but can be also called as graphite nanosheets and graphite nanoflakes. Considering the size of a single graphene layer and of graphene stacks, they can be considered as nanographite. In a recent review,[179] GNPs are defined as a type of graphitic nanofiller composed of stacked 2D graphene sheets. The control of GNP thickness, which means of the number of stacked layers, is attempted through a variety of techniques, namely: intercalation, oxidization, heat treatment, microwave irradiation, and ultrasonic treatment, *etc.*[180–183]

GNP deserve increasing interest as fillers for polymers[38] and in the literature papers relating to elastomers filled with it can be found.[38,39,59,67,68,70,72,75,81,83,94,135,179,184–188] Among them, only very few examples are reported on NR nanocomposites.[38,39,70,72,83,135,188] AFM and HRTEM are typically used for the determination of thickness and dimensions of GNP both before and after dispersion in the rubber matrix;[38,189,190] while SEM and TEM are used for the visualization of the GNP dispersion in the composite materials.[38,39,70,72,83,135,188] Figure 23.9 shows TEM images of a platy single layer obtained by exfoliating GNP (Figure 23.9(a)) and of a nanocomposite obtained by melt blending nanographite in isoprene rubber (Figure 23.9(b)).

Also in this case, the aspect ratio f of the GNP particles dispersed in NR was quantified with a TEM/AIA approach.[38] An excellent fit was found between experimental and theoretical (evaluated on the basis of Equation (23.1) by using the measured f) modulus values.

From preliminary results[191] it appears that nanographite is able to establish a network at a concentration remarkably lower with respect to carbon black, but also appreciably higher with respect to OC and CNTs. TEM analysis supports these findings, as already observed for clays and CNTs.

Information from other techniques, such as XRD and Raman spectroscopy, are required to perform the investigation at the lowest level of nanographite organization. In fact, the distance between two successive graphene layers is too small (<1 nm) to be determined by electron microscopy. In particular, XRD analysis is generally performed to assess the crystalline structure of GNP, both in the pristine material and in the polymer composites. The D_{hkl} correlation length, thus the dimension of crystallites, in particular in the directions orthogonal and parallel to structural layers, can be determined. From this

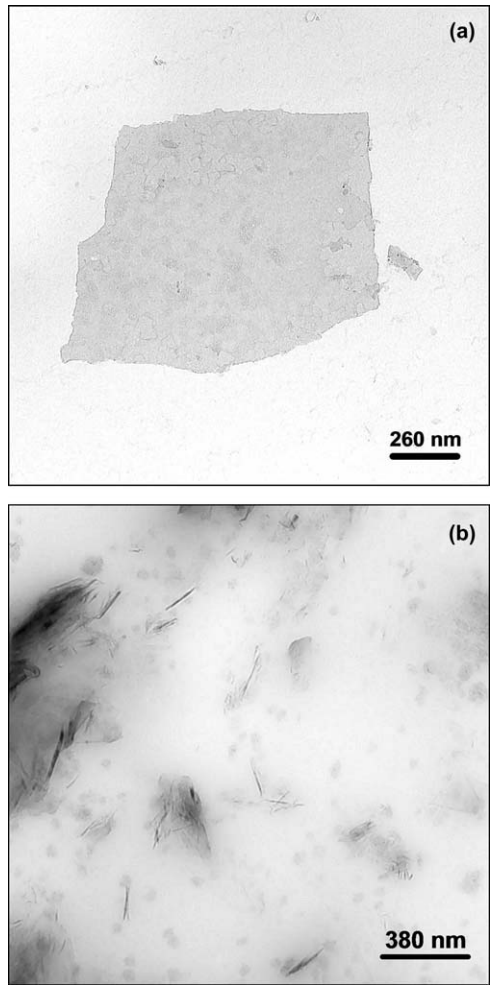

Figure 23.9 TEM images of (a) a graphene platy single layer and (b) an isoprene rubber nanocomposite containing nanographite.

determination, it is possible to calculate the ratio between the crystallite dimensions in directions orthogonal and parallel to structural layers, which is defined as shape anisotropy.[192]

23.5.2.4 Nanofillers in Combination with Carbon Black

A large-scale application of rubber nanocomposites, such as the one in the tyre industry, reasonably implies the use of hybrid filler systems, with a minor amount of nanofiller added to a major part of a traditional filler, such as silica or carbon black.

The most reasonable approach seems to add a carbonaceous nanofiller, such as CNT or nanographite, to CB. In fact, very few reports have recently

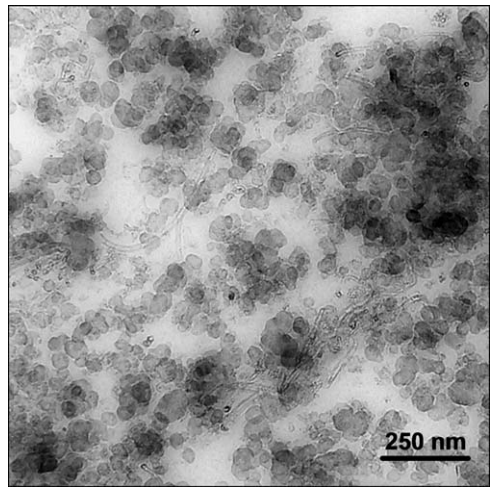

Figure 23.10 TEM image of an isoprene rubber nanocomposite containing CNTs and CB.

appeared in the literature on CNT–rubber composites containing also a further filler,[55,56,77,85,104] either CB[77,85,104] or silica.[55,56] In the particular case of samples filled with CB and increasing amounts of CNT,[104] the two fillers were found to develop synergistic effects on mechanical and dynamic-mechanical properties of the ensuing materials and the existence of a continuous hybrid filler network between CNT and CB was confirmed by TEM analysis, as shown in Figure 23.10. Microscopy thus confirmed the high affinity between the two carbon allotropes, as expected.

Preliminary results are available for hybrid filler systems based on nanographite and CB in isoprene rubber.[191] The high affinity between the two carbon allotropes, as also revealed by the TEM images in Figure 23.11 (nanographite adheres to CB particles) leads to the formation of a continuous filler network.

In the literature an increasing number of studies considering OC–CB isoprene rubber nanocomposites is becoming available.[18,98,103,106] CB was used at a level typical of commercial applications (higher than 50 phr). The most important finding from these studies, to some extent surprising, was the synergism developed by the two fillers. XRD and TEM analyses led to conclude that both stacked and isolated layers are present in the nanocomposites, with a high amount of exfoliated clay. Figure 23.12 shows a surprising finding: OC layers and aggregates prefer to stay close to CB particles rather than staying in the polymer matrix.

An unexpected affinity of OC for CB is thus revealed. Static and dynamic-mechanical measurements demonstrated that the OC was able to give rise to a hybrid filler network with CB and resulted in the continuous hybrid filler system being responsible for the remarkable enhancement in material dynamic-mechanical properties.

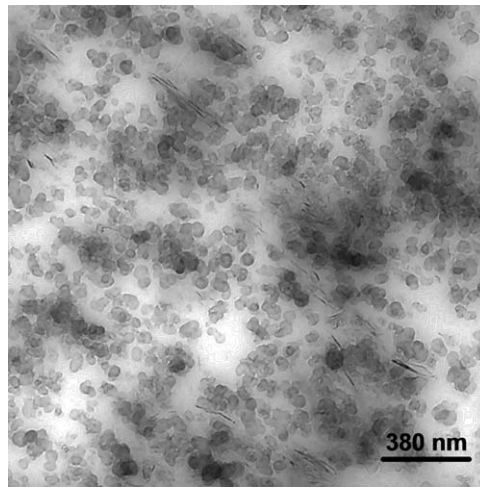

Figure 23.11 TEM image of an isoprene rubber nanocomposite containing nanographite and CB.

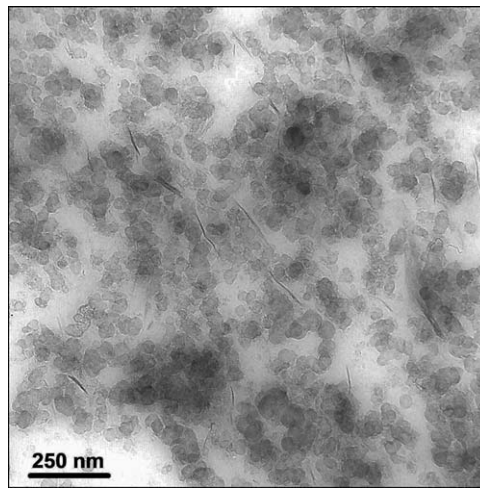

Figure 23.12 TEM image of an isoprene rubber nanocomposite containing organoclay and CB.

References

1. J. B. Donnet and E. Custodéro, in *The Science and Technology of Rubber*, 3rd ed., eds. J. E. Mark, B. Erman and F. R. Eirich, Academic Press, San Diego, Editon edn., 2005, pp. 367–400.
2. M. Galimberti, *Rubber Clay Nanocomposites – Science, Technology, Applications*, Wiley and Sons, Hoboken, NJ, 2011.

3. A. I. Medalia and G. Kraus, in *The Science and Technology of Rubber*, 2nd ed., eds. J. E. Mark, B. Erman and F. R. Eirich, Academic Press, San Diego, Editon edn., 1994, pp. 387–418.
4. S. Bracco, P. Valsesia, L. Ferretti, P. Sozzani, M. Mauri and A. Comotti, *Micropor. Mesopor. Mater.*, 2008, **107**, 102–107.
5. N. K. Dutta, N. R. Choudhury, B. Haidar, A. Vidal, J. B. Donnet, L. Delmotte and J. M. Chezeau, *Polymer*, 1994, **35**, 4293–4299.
6. N. Suzuki, F. Yatsuyanagi, M. Ito and H. Kaidou, *J. Appl. Polym. Sci.*, 2002, **86**, 1622–1629.
7. J. L. Valentin, I. Mora-Barrantes, J. Carretero-Gonzalez, M. A. Lopez-Manchado, P. Sotta, D. R. Long and K. Saalwachter, *Macromolecules*, 2010, **43**, 334–346.
8. A. Ansarifar, H. P. Lim and R. Nijhawan, *Int. J. Adhes. Adhes.*, 2004, **24**, 9–22.
9. S. S. Choi, I. S. Kim, S. G. Lee and C. W. Joo, *J. Polym. Sci., Part B: Polym. Phys.*, 2004, **42**, 577–584.
10. W. Kaewsakul, K. Sahakaro, W. K. Dierkes and J. W. M. Noordermeer, *Rubber Chem. Technol.*, 2012, **85**, 277–294.
11. S. Wolff, M. J. Wang and E. H. Tan, *Kautsch. Gummi Kunstst.*, 1994, **47**, 102–107.
12. N. D. Alberola, K. Benzarti, C. Bas and Y. Bomal, *Polym. Compos.*, 2001, **22**, 312–325.
13. W. Chonkaew, W. Minghvanish, U. Kungliean, N. Rochanawipart and W. Brostow, *J. Nanosci. Nanotechnol.*, 2011, **11**, 2018–2024.
14. G. Ramorino, F. Bignotti, S. Pandini and T. Riccò, *Compos. Sci. Technol.*, 2009, **69**, 1206–1211.
15. P. C. Thomas, S. P. Thomas, G. George, S. Thomas and J. Kuruvilla, *J. Polym. Res.*, 2011, **18**, 2367–2378.
16. J. X. Zhai, H. Wang, X. Y. Shi and S. G. Zhao, *J. Macromol. Sci., Part B: Phys.*, 2012, **51**, 496–509.
17. L. Conzatti, G. Costa, L. Falqui and A. Turturro, in *Rubber Technologist's Handbook*, Volume 2, eds. S. K. De, K. Naskar and J. White, Smithers Rapra Press, Shawbury, Shrewsbury, UK, Editon edn., 2009, vol. 2, pp. 1–27.
18. M. Galimberti, V. Cipolletti and S. Giudice, in *Rubber Clay Nanocomposites – Science, Technology and Applications*, ed. M. Galimberti, Wiley and Sons, Hoboken, NJ, Editon edn., 2011, pp. 181–240.
19. H. H. Le, G. Kasaliwal, S. Ilisch and H. J. Radusch, *Kautsch. Gummi Kunstst.*, 2009, **62**, 326–333.
20. I. A. Morozov, B. Lauke and G. Heinrich, *Kautsch. Gummi Kunstst.*, 2011, **64**, 24–27.
21. W. M. Hess, C. R. Herd and E. B. Sebok, *Kautsch. Gummi Kunstst.*, 1994, **47**, 328–341.
22. H. Miyagawa, in *Rubber nanocomposites. Preparation, properties, and applications*, eds. S. Thomas and R. Stephen, John Wiley & Sons (Asia), Singapore, Editon edn., 2010, pp. 255–290.

23. L. Nikiel, M. Gerspacher, H. Yang and C. P. O'Farrell, *Rubber Chem. Technol.*, 2001, **74**, 249–259.
24. J. Frohlich, W. Niedermeier and H. D. Luginsland, *Compos. Part. A-Appl. S.*, 2005, **36**, 449–460.
25. A. R. Payne, *Reinforcement of Elastomers*, Wiley-Interscience, New York, 1965.
26. A. R. Payne and R. E. Whittaker, *Rubber Chem. Technol.*, 1971, **44**, 440–459.
27. W. Niedermeier, J. Frohlich and H. D. Luginsland, *Kautsch. Gummi Kunstst.*, 2002, **55**, 356–366.
28. E. Guth, *J. Appl. Phys.*, 1945, **16**, 20–25.
29. E. Guth and O. Gold, *Phys. Rev.*, 1938, **53**, 322.
30. H. M. Smallwood, *J. Appl. Phys.*, 1944, **15**, 758–766.
31. R. Sengupta, S. Chakraborty, S. Bandyopadhyay, S. Dasgupta, R. Mukhopadhyay, K. Auddy and A. S. Deuri, *Polym. Eng. Sci.*, 2007, **47**, 1956–1974.
32. S. N. Bhattacharya, M. R. Kamal and R. K. Gupta, *Polymeric Nanocomposites: Theory and Practice*, Hanser Verlag, Munich, 2008.
33. M. Maiti, M. Bhattacharya and A. K. Bhowmick, *Rubber Chem. Technol.*, 2008, **81**, 384–469.
34. L. Bokobza, *Polymer*, 2007, **48**, 4907–4920.
35. S. Bhattacharya, C. Sinturel, O. Bahloul, M. L. Saboungi, S. Thomas and J. P. Salvetat, *Carbon*, 2008, **46**, 1037–1045.
36. C. F. Matos, F. Galembeck and A. J. G. Zarbin, *Carbon*, 2012, **50**, 4685–4695.
37. R. Sengupta, M. Bhattacharya, S. Bandyopadhyay and A. K. Bhowmick, *Prog. Polym. Sci.*, 2011, **36**, 638–670.
38. J. R. Potts, O. Shankar, L. Du and R. S. Ruoff, *Macromolecules*, 2012, **45**, 6045–6055.
39. Y. H. Zhan, M. Lavorgna, G. Buonocore and H. S. Xia, *J. Mater. Chem.*, 2012, **22**, 10464–10468.
40. D. Feldman, *J. Macromol. Sci., Part A: Pure Appl. Chem.*, 2012, **49**, 784–793.
41. F. Bergaya, B. K. G. Theng and G. Lagaly, *Handbook of Clay Science*, Elsevier Science, Amsterdam, 2006.
42. B. Chen, E. J.R.G., H. C. Greenwell, P. Boulet, P. V. Coveney, A. A. Bowden and A. Whiting, *Chem. Soc. Rev.*, 2008, **37**, 568–594.
43. Z. Ali, H. H. Le, S. Ilisch, K. Busse and H. J. Radusch, *J. Appl. Polym. Sci.*, 2009, **113**, 667–677.
44. A. Samadi and M. R. Kashani, *J. Appl. Polym. Sci.*, 2010, **116**, 2101–2109.
45. M. Bhattacharya and A. K. Bhowmick, *J. Mater. Sci.*, 2010, **45**, 6126–6138.
46. M. Bhattacharya, S. Biswas, S. Bandyopadhyay and A. K. Bhowmick, *Polym. Adv. Technol.*, 2012, **23**, 596–610.
47. S. Rooj, A. Das, K. W. Stockelhuber, N. Mukhopadhyay, A. R. Bhattacharyya, D. Jehnichen and G. Heinrich, *Appl. Clay Sci.*, 2012, **67–68**, 50–56.

48. S. Rooj, A. Das, K. W. Stockelhuber, D. Y. Wang, V. Galiatsatos and G. Heinrich, *Soft Matter*, 2013, **9**, 3798–3808.
49. L. Bokobza, *Vib. Spectrosc.*, 2009, **51**, 52–59.
50. L. Bokobza, B. Bresson, G. Garnaud and J. X. Zhang, *Comp. Interf.*, 2012, **19**, 285–295.
51. J. S. Choi and A. I. Isayev, *Rubber Chem. Technol.*, 2012, **85**, 14–37.
52. H. H. Le, X. T. Hoang, A. Das, U. Gohs, K. W. Stoeckelhuber, R. Boldt, G. Heinrich, R. Adhikari and H. J. Radusch, *Carbon*, 2012, **50**, 4543–4556.
53. H. H. Le, S. Ilisch, H. J. Radusch and H. Steinberger, *Plast. Rubber Compos.*, 2008, **37**, 367–375.
54. S. Otto, O. Randl, O. Goncalves and B. Cantaloube, *Kautsch. Gummi Kunstst.*, 2005, **58**, 390–393.
55. J. Fritzsche, H. Lorenz and M. Kluppel, *Macromol. Mater. Eng.*, 2009, **294**, 551–560.
56. H. Lorenz, J. Fritzsche, A. Das, K. W. Stockelhuber, R. Jurk, G. Heinrich and M. Kluppel, *Compos. Sci. Technol.*, 2009, **69**, 2135–2143.
57. M. Arroyo, M. A. Lopez-Manchado, J. L. Valentin and J. Carretero, *Compos. Sci. Technol.*, 2007, **67**, 1330–1339.
58. A. A. Azira, D. H. A. Hassim, A. B. Suriani and M. R. Mahmood, *Nano Hybrids*, 2012, **1**, 81–97.
59. X. Bai, C. Y. Wan, Y. Zhang and Y. H. Zhai, *Carbon*, 2011, **49**, 1608–1613.
60. J. Hrachova, I. Chodak and P. Komadel, *Chem. Pap.*, 2009, **63**, 55–61.
61. H. Ismail and P. K. Freakley, *Polym.-Plast. Technol. Eng.*, 1997, **36**, 873–889.
62. H. Ismail and R. Ramli, *J. Reinf. Plast. Compos.*, 2008, **27**, 1909–1924.
63. Q. X. Jia, Y. P. Wu, Y. Q. Wang, M. Lu and L. Q. Zhang, *Compos. Sci. Technol.*, 2008, **68**, 1050–1056.
64. H. X. Jiang, Q. Q. Ni and T. Natsuki, *Adv. Mater. Res.*, 2009, **79-82**, 417–420.
65. H. X. Jiang, Q. Q. Ni and T. Natsuki, *Polym. Compos.*, 2011, **32**, 236–242.
66. J. Kruzelac, S. Ilisch, I. Hudec and R. Dosoudil, *Smart Mater. Res.,* Hindawi Publishing Corporation, Editon edn., 2012, vol. 2012.
67. Y. Q. Li, Q. H. Wang, T. M. Wang and G. Q. Pan, *J. Mater. Sci.*, 2012, **47**, 730–738.
68. H. Q. Lian, S. X. Li, K. L. Liu, L. R. Xu, K. S. Wang and W. L. Guo, *Polym. Eng. Sci.*, 2011, **51**, 2254–2260.
69. Y. B. Liu, L. Li, Q. Wang and X. Zhang, *J. Polym. Res.*, 2011, **18**, 859–867.
70. A. Malas, C. K. Das, A. Das and G. Heinrich, *Mater. Design*, 2012, **39**, 410–417.
71. C. Nah, J. Y. Lim, B. H. Cho, C. K. Hong and A. N. Gent, *J. Appl. Polym. Sci.*, 2010, **118**, 1574–1581.
72. B. Ozbas, S. Toki, B. S. Hsiao, B. Chu, R. A. Register, I. A. Aksay, R. K. Prud'homme and D. H. Adamson, *J. Polym. Sci., Part B: Polym. Phys.*, 2012, **50**, 718–723.

73. Z. Peng, C. F. Feng, Y. Y. Luo, Y. Z. Li and L. X. Kong, *Carbon*, 2010, **48**, 4497–4503.
74. Z. Peng, C. F. Feng, Y. Y. Luo, Y. Z. Li, Z. F. Yi and L. X. Kong, *J. Appl. Polym. Sci.*, 2012, **125**, 3920–3928.
75. V. K. Singh, A. Shukla, M. K. Patra, L. Saini, R. K. Jani, S. R. Vadera and N. Kumar, *Carbon*, 2012, **50**, 2202–2208.
76. G. Sui, W. H. Zhong, X. P. Yang, Y. H. Yu and S. H. Zhao, *Polym. Adv. Technol.*, 2008, **19**, 1543–1549.
77. G. Sui, W. H. Zhong, X. P. Yang and S. H. Zhao, *Macromol. Mater. Eng.*, 2007, **292**, 1020–1026.
78. P. L. Teh, Z. A. M. Ishak, A. S. Hashim, J. Karger-Kocsis and U. S. Ishiaku, *J. Appl. Polym. Sci.*, 2004, **94**, 2438–2445.
79. P. L. Teh, Z. A. M. Ishak, A. S. Hashim, J. Karger-Kocsis and U. S. Ishiaku, *Eur. Polym. J.*, 2004, **40**, 2513–2521.
80. P. L. Teh, Z. A. M. Ishak, A. S. Hashim, J. Karger-Kocsis and U. S. Ishiaku, *J. Appl. Polym. Sci.*, 2006, **100**, 1083–1092.
81. L. L. Wang, L. Q. Zhang and M. Tian, *Mater. Design*, 2012, **39**, 450–457.
82. H. Y. Xu, Y. Y. Cao, X. L. He, Y. F. Wu, Y. M. Zhang and C. F. Wu, *J. Macromol. Sci., Phys.*, 2009, **48**, 1190–1200.
83. M. Bhattacharya, M. Maiti and A. K. Bhowmick, *Rubber Chem. Technol.*, 2008, **81**, 782–808.
84. L. Bokobza and M. Kolodziej, *Polym. Int.*, 2006, **55**, 1090–1098.
85. L. Bokobza, M. Rahmani, C. Belin, J. L. Bruneel and N. E. El Bounia, *J. Polym. Sci., Part B: Polym. Phys.*, 2008, **46**, 1939–1951.
86. A. Choudhury, A. K. Bhowmick, C. Ong and M. Soddemann, *J. Nanosci. Nanotechnol.*, 2010, **10**, 5056–5071.
87. F. Clement, A. Lapra, L. Bokobza, L. Monnerie and P. Menez, *Polymer*, 2001, **42**, 6259–6270.
88. A. Lapra, E. Clement, L. Bokobza and L. Monnerie, *Rubber Chem. Technol.*, 2003, **76**, 60–81.
89. I. A. Morozov, B. Lauke and G. Heinrich, *Rubber Chem. Technol.*, 2012, **85**, 244–263.
90. D. Trifonova-Van Haeringen, H. Schonherr, G. J. Vancso, L. van der Does, J. W. M. Noordermeer and P. J. P. Janssen, *Rubber Chem. Technol.*, 1999, **72**, 862–875.
91. D. Wang, S. Fujinami, K. Nakajima, S. Inukai, H. Ueki, A. Magario, T. Noguchi, M. Endo and T. Nishi, *Polymer*, 2010, **51**, 2455–2459.
92. D. Wang, S. Fujinami, K. Nakajima, K. Niihara, S. Inukai, H. Ueki, A. Magario, T. Noguchi, M. Endo and T. Nishi, *Carbon*, 2010, **48**, 3708–3714.
93. A. K. Bhowmick, M. Bhattacharya, S. Mitra, K. D. Kumar, P. K. Maji, A. Choudhury, J. J. George and G. C. Basak, in *Advanced Rubber Composites*, ed. G. Heinrich, Springer-Verlag, Berlin, Editon edn., 2011, vol. 239, pp. 1–83.
94. A. K. Bhowmick, M. Bhattacharya and S. Mitra, *J. Elastom. Plast.*, 2010, **42**, 517–537.

95. M. Castellano, L. Conzatti, A. Turturro, G. Costa and G. Busca, *J. Phys. Chem. B*, 2007, **111**, 4495–4502.
96. M. Castellano, L. Falqui, G. Costa, A. Turturro, B. Valenti and G. Castello, *J. Macromol. Sci. Phys.*, 2002, **B41**, 451–471.
97. L. Conzatti, G. Costa, M. Castellano, A. Turturro, F. M. Negroni and J. F. Gerard, *Macromol. Mater. Eng.*, 2008, **293**, 178–187.
98. L. Conzatti, P. Stagnaro, G. Colucci, R. Bongiovanni, A. Priola, A. Lostritto and M. Galimberti, *Appl. Clay Sci.*, 2012, **61**, 14–21.
99. G. Costa, G. Dondero, L. Falqui, M. Castellano, A. Turturro and B. Valenti, *Macromol. Symp.*, 2003, **193**, 195–207.
100. A. Das, K. W. Stockelhuber, R. Jurk, D. Jehnichen and G. Heinrich, *Appl. Clay Sci.*, 2011, **51**, 117–125.
101. F. Deng, M. Ito, T. Noguchi, L. F. Wang, H. Ueki, K. Niihara, Y. A. Kim, M. Endo and Q. S. Zheng, *ACS Nano*, 2011, **5**, 3858–3866.
102. L. Falqui, G. Costa, M. Castellano, A. Turturro and B. Valenti, *Rubber Chem. Technol.*, 2003, **76**, 899–911.
103. M. Galimberti, M. Coombs, V. Cipolletti, P. Riccio, T. Ricco, S. Pandini and L. Conzatti, *Appl. Clay Sci.*, 2012, **65–66**, 57–66.
104. M. Galimberti, M. Coombs, P. Riccio, T. Riccò, S. Passera, S. Pandini, L. Conzatti, A. Ravasio and I. Tritto, *Macromol. Mater. Eng.*, 2013, **298**, 241–251.
105. M. Galimberti, S. Senatore, L. Conzatti, G. Costa, G. Giuliano and G. Guerra, *Polym. Adv. Technol.*, 2009, **20**, 135–142.
106. M. Galimberti, S. Senatore, A. Lostritto, L. Giannini, L. Conzatti, G. Costa and G. Guerra, *E-Polymers*, 2009.
107. Y. Ikeda, *Kautsch. Gummi Kunstst.*, 2005, **58**, 455–460.
108. Y. Ikeda, A. Katoh, J. Shimanuki and S. Kohjiya, *Macromol. Rapid Commun.*, 2004, **25**, 1186–1190.
109. H. Jinnai, Y. Shinbori, T. Kitaoka, K. Akutagawa, N. Mashita and T. Nishi, *Macromolecules*, 2007, **40**, 6758–6764.
110. H. Jinnai, R. J. Spontak and T. Nishi, *Macromolecules*, 2010, **43**, 1675–1688.
111. S. Joly, G. Garnaud, R. Ollitrault, L. Bokobza and J. E. Mark, *Chem. Mater.*, 2002, **14**, 4202–4208.
112. A. Kato, Y. Ikeda, Y. Kasahara, J. Shimanuki, T. Suda, T. Hasegawa, H. Sawabe and S. Kohjiya, *J. Opt. Soc. Am. B. Opt. Phys.*, 2008, **25**, 1602–1615.
113. A. Kato, S. Kohjiya and Y. Ikeda, *Rubber Chem. Technol.*, 2007, **80**, 690–700.
114. A. Kato, J. Shimanuki, S. Kohjiya and Y. Ikeda, *Rubber Chem. Technol.*, 2006, **79**, 653–673.
115. H. Kishimoto, Y. Shinohara, Y. Amenya, K. Inoue, Y. Suzuki, A. Takeuchi, K. Uesugi and N. Yagi, *Rubber Chem. Technol.*, 2008, **81**, 541–551.
116. S. Kohjiya, A. Kato and Y. Ikeda, *Prog. Polym. Sci.*, 2008, **33**, 979–997.
117. S. Kohjiya, A. Katoh, J. Shimanuki, T. Hasegawa and Y. Ikeda, *Polymer*, 2005, **46**, 4440–4446.

118. D. J. Lowe, A. V. Chapman, S. Cook and J. J. C. Busfield, *J. Polym. Sci., Part B: Polym. Phys.*, 2011, **49**, 1621–1627.
119. D. J. Lowe, A. V. Chapman, S. Cook and J. J. C. Busfield, *Macromol. Mater. Eng.*, 2011, **296**, 693–702.
120. K. N. Madhusoodanan and S. Varghese, *J. Appl. Polym. Sci.*, 2006, **102**, 2537–2543.
121. A. P. Meera, P. S. Thomas and S. Thomas, *Polym. Compos.*, 2012, **33**, 524–531.
122. S. Praveen, P. K. Chattopadhyay, P. Albert, V. G. Dalvi, B. C. Chakraborty and S. Chattopadhyay, *Compos. Part. A-Appl. S.*, 2009, **40**, 309–316.
123. G. Ramorino, F. Bignotti, L. Conzatti and T. Ricco, *Polym. Eng. Sci.*, 2007, **47**, 1650–1657.
124. C. A. Rezende, F. C. Braganca, T. R. Doi, L. T. Lee, F. Galembeck and F. Boue, *Polymer*, 2010, **51**, 3644–3652.
125. N. Roy and A. K. Bhowmick, *J. Mater. Sci.*, 2012, **47**, 272–281.
126. Y. H. Sun, Y. F. Luo and D. M. Jia, *J. Appl. Polym. Sci.*, 2008, **107**, 2786–2792.
127. N. Suzuki, M. Ito and F. Yatsuyanagi, *Polymer*, 2005, **46**, 193–201.
128. P. S. Thomas, A. A. Abdullateef, M. A. Al-Harthi, M. A. Atieh, S. K. De, M. Rahaman, T. K. Chaki, D. Khastgir and S. Bandyopadhyay, *J. Mater. Sci.*, 2012, **47**, 3344–3349.
129. P. S. Thomas, A. A. Abdullateef, M. A. Al-Harthi, A. A. Basfar, S. Bandyopadhyay, M. A. Atieh and S. K. De, *J. Appl. Polym. Sci.*, 2012, **124**, 2370–2376.
130. S. Varghese and J. Karger-Kocsis, *Polymer*, 2003, **44**, 4921–4927.
131. S. Varghese and J. Karger-Kocsis, *J. Appl. Polym. Sci.*, 2004, **91**, 813–819.
132. S. Varghese, J. Karger-Kocsis and K. G. Gatos, *Polymer*, 2003, **44**, 3977–3983.
133. Y. P. Wu, Q. X. Jia, D. S. Yu and L. Q. Zhang, *Polym. Test.*, 2004, **23**, 903–909.
134. F. Yatsuyanagi, N. Suzuki, M. Ito and H. Kaidou, *Polymer*, 2001, **42**, 9523–9529.
135. Y. H. Zhan, J. K. Wu, H. S. Xia, N. Yan, G. X. Fei and G. P. Yuan, *Macromol. Mater. Eng.*, 2011, **296**, 590–602.
136. H. J. Butt, B. Cappella and M. Kappl, *Surf. Sci. Rep.*, 2005, **59**, 1–152.
137. B. D. Huey, in *Annu. Rev. Mater. Res.*, Editon edn., 2007, vol. 37, pp. 351–385.
138. J. Song, D. Tranchida and G. J. Vancso, *Macromolecules*, 2008, **41**, 6757–6762.
139. B. Cappella and G. Dietler, *Surf. Sci. Rep.*, 1999, **34**, 1–103.
140. B. Y. Du, O. K. C. Tsui, Q. L. Zhang and T. B. He, *Langmuir*, 2001, **17**, 3286–3291.
141. Y. J. Sun, B. Akhremitchev and G. C. Walker, *Langmuir*, 2004, **20**, 5837–5845.
142. P. Achalla, J. McCormick, T. Hodge, C. Moreland, P. Esnault, A. Karim and D. Raghavan, *J. Polym. Sci., Part B: Polym. Phys.*, 2006, **44**, 492–503.

143. T. Noguchi, S. Inukai, H. Uekii and A. Magario, in *SAE Technical Paper*, Editon edn., 2009.
144. Y. J. Li and H. Shimizu, *Macromolecules*, 2009, **42**, 2587–2593.
145. P. Mele, S. Marceau, D. Brown, Y. de Puydt and N. D. Alberola, *Polymer*, 2002, **43**, 5577–5586.
146. A. Di Gianni, G. Colucci, A. Priola, L. Conzatti, M. Alessi and P. Stagnaro, *Macromol. Mater. Eng.*, 2009, **294**, 705–710.
147. Y. Ikeda, A. Kato, J. Shimanuki, S. Kohjiya, M. Tosaka and S. Poompradub, *Rubber Chem. Technol.*, 2007, **80**, 251–264.
148. J. Frank, *Electron Tomography: Three-dimensional Imaging with Transmission Electron Microscope*, Plenum Press, New York, 1992.
149. S. Kohjiya, A. Katoh, T. Suda, J. Shimanuki and Y. Ikeda, *Polymer*, 2006, **47**, 3298–3301.
150. F. Bergaya, M. Jaber and J.-F. Lambert, in *Rubber Clay Nanocomposites – Science, Technology and Applications*, ed. M. Galimberti, Wiley and Sons, Hoboken, NJ, Editon edn., 2011, pp. 3–44.
151. F. Bergaya, M. Jaber and J.-F. Lambert, in *Rubber Clay Nanocomposites – Science, Technology and Applications*, ed. M. Galimberti, Wiley and Sons, Hoboken, NJ, Editon edn., 2011, pp. 45–86.
152. M. Galimberti, S. Giudice, V. Cipolletti and G. Guerra, *Polym. Adv. Technol.*, 2010, **21**, 679–684.
153. M. Galimberti, A. Lostritto, A. Spatola and G. Guerra, *Chem. Mater.*, 2007, **19**, 2495–2499.
154. E. P. Giannelis, R. Krishnamoorti and E. Manias, *Adv. Polym. Sci.*, 1999, **138**, 107–147.
155. M. Alexandre and P. Dubois, *Mat. Sci. Eng.*, 2000, **28**, 1–63.
156. S. S. Ray and M. Okamoto, *Prog. Polym. Sci.*, 2003, **28**, 1539–1641.
157. P. Y. Li, L. Wang, G. J. Song, L. L. Yin, F. Qi and L. D. Sun, *J. Appl. Polym. Sci.*, 2008, **109**, 3831–3838.
158. J. Sharif, W. Yunus, K. Dahlan and M. H. Ahmad, *Polym. Test.*, 2005, **24**, 211–217.
159. M. Hernandez, J. Carretero-Gonzalez, R. Verdejo, T. A. Ezquerra and M. A. Lopez-Manchado, *Macromolecules*, 2010, **43**, 643–651.
160. Y. P. Wu, H. H. Huang, W. Zhao, H. F. Zliang, Y. Q. Wang and L. Q. Zhang, *J. Appl. Polym. Sci.*, 2008, **107**, 3318–3324.
161. N. Rattanasom and S. Prasertsri, *Polym. Test.*, 2009, **28**, 270–276.
162. Y. P. Wu, Y. Q. Wang, H. F. Zhang, Y. Z. Wang, D. S. Yu, L. Q. Zhang and J. Yang, *Compos. Sci. Technol.*, 2005, **65**, 1195–1202.
163. L. L. Qu, G. S. Huang, Z. Y. Liu, P. Zhang, G. S. Weng and Y. J. Nie, *Acta Mater.*, 2009, **57**, 5053–5060.
164. M. Arroyo, M. A. Lopez-Manchado and B. Herrero, *Polymer*, 2003, **44**, 2447–2453.
165. B. Jurkowska, B. Jurkowski, M. Oczkowski, S. S. Pesetskii, V. Koval and Y. A. Olkhov, *J. Appl. Polym. Sci.*, 2007, **106**, 360–371.
166. J. P. Salvetat, S. Bhattacharyya and R. B. Pipes, *J. Nanosci. Nanotechnol.*, 2006, **6**, 1857–1882.

167. J. A. Fagan, B. J. Landi, I. Mandelbaum, J. R. Simpson, V. Bajpai, B. J. Bauer, K. Migler, A. R. H. Walker, R. Raffaelle and E. K. Hobbie, *J. Phys. Chem. B*, 2006, **110**, 23801–23805.
168. A. Das, K. W. Stockelhuber, R. Jurk, M. Saphiannikova, J. Fritzsche, H. Lorenz, M. Kluppel and G. Heinrich, *Polymer*, 2008, **49**, 5276–5283.
169. L. D. Perez, M. A. Zuluaga, T. Kyu, J. E. Mark and B. L. Lopez, *Polym. Eng. Sci.*, 2009, **49**, 866–874.
170. C. Nah, J. Y. Lim, R. Sengupta, B. H. Cho and A. N. Gent, *Polym. Int.*, 2011, **60**, 42–44.
171. Z. Spitalsky, D. Tasis, K. Papagelis and C. Galiotis, *Prog. Polym. Sci.*, 2010, **35**, 357–401.
172. N. Grossiord, J. Loos, O. Regev and C. E. Koning, *Chem. Mater.*, 2006, **18**, 1089–1099.
173. M. Moniruzzaman and K. I. Winey, *Macromolecules*, 2006, **39**, 5194–5205.
174. C. H. Leigh-Dugmore, *Rubber Chem. Technol.*, 1956, **29**, 1303–1308.
175. H. H. Le, S. Ilisch, I. Prodanova and H. J. Radusch, *Kautsch. Gummi Kunstst.*, 2004, **57**, 355.
176. A. I. Medalia, *J. Coll. Interf. Sci.*, 1970, **32**, 115–131.
177. K. S. Novoselov, A. K. Geim, S. V. Morozov, D. Jiang, Y. Zhang, S. V. Dubonos, I. V. Grigorieva and A. A. Firsov, *Science*, 2004, **306**, 666–669.
178. A. K. Geim and A. H. MacDonald, *Physics Today*, 2007, **60**, 35–41.
179. B. Li and W. H. Zhong, *J. Mater. Sci.*, 2011, **46**, 5595–5614.
180. H. L. Fan, L. L. Wang, K. K. Zhao, N. Li, Z. J. Shi, Z. G. Ge and Z. X. Jin, *Biomacromolecules*, 2010, **11**, 2345–2351.
181. A. V. Yakovlev, A. I. Finaenov, S. L. Zabud'kov and E. V. Yakovleva, *Russ. J. Appl. Chem.*, 2006, **79**, 1741–1751.
182. T. Ramanathan, S. Stankovich, D. A. Dikin, H. Liu, H. Shen, S. T. Nguyen and L. C. Brinson, *J. Polym. Sci., Part B: Polym. Phys.*, 2007, **45**, 2097–2112.
183. J. P. Li, H. F. Lin, W. F. Zhao and G. H. Chen, *J. Appl. Polym. Sci.*, 2008, **109**, 1377–1380.
184. M. Bhattacharya, M. Maiti and A. K. Bhowmick, *Polym. Eng. Sci.*, 2009, **49**, 81–98.
185. V. Sridhar, A. M. Shanmugharaj, J. K. Kim and D. K. Tripathy, *Polym. Compos.*, 2009, **30**, 691–701.
186. W. E. Mahmoud and A. A. Al-Ghamdi, *Polym. Int.*, 2012, **61**, 51–54.
187. W. E. Mahmoud, A. A. Al-Ghamdi and F. R. Al-Solamy, *Polym. Adv. Technol.*, 2012, **23**, 161–165.
188. B. Ozbas, C. D. O'Neill, R. A. Register, I. A. Aksay, R. K. Prud'homme and D. H. Adamson, *J. Polym. Sci., Part B: Polym. Phys.*, 2012, **50**, 910–916.
189. Y. Hernandez, V. Nicolosi, M. Lotya, F. M. Blighe, Z. Y. Sun, S. De, I. T. McGovern, B. Holland, M. Byrne, Y. K. Gun'ko, J. J. Boland, P. Niraj, G. Duesberg, S. Krishnamurthy, R. Goodhue, J. Hutchison,

V. Scardaci, A. C. Ferrari and J. N. Coleman, *Nat. Nanotechnol.*, 2008, **3**, 563–568.
190. H. Persson, Y. Yao, U. Klement and R. W. Rychwalski, *Expr. Polym. Lett.*, 2012, **6**, 142–147.
191. M. Galimberti, M. Coombs, V. Cipolletti, L. Giannini, T. Riccò, S. Pandini, L. Conzatti, M. Mauro and G. Guerra, in *ACS Rubber Division – 181st Spring Technical Meeting*, San Antonio, TX USA, Editon edn., 2012.
192. M. Mauro, V. Cipolletti, M. Galimberti, P. Longo and G. Guerra, *J. Phys. Chem. C*, 2012, **116**, 24809–24813.

CHAPTER 24

NMR Studies of Natural Rubber Composites from Macro- to Nanoscales – A Review

DEEPALEKSHMI PONNAMMA,[a] KISHOR KUMAR SADASIVUNI[b] AND SABU THOMAS*[a,c]

[a] School of Chemical Sciences, Mahatma Gandhi University, Kottayam, Kerala, India; [b] Center for Advanced Materials, Qatar University, Qatar; [c] Centre for Nanoscience and Nanotechnology, Mahatma Gandhi University, Kottayam, Kerala, India
*Email: sabupolymer@yahoo.com; kishor_kumars@yahoo.com

24.1 Introduction

Nuclear magnetic resonance (NMR) spectroscopy has great relevance in the area of investigation of molecular structures. Many studies using NMR spectroscopy and microscopy have been reported in elastomer based systems.[1–6] Due to the possibility of reuse of samples after the analysis (NMR is non-destructive) NMR attracts many material scientists to select this technique for characterization. In the case of polymers NMR is specifically useful in finding out the crosslink density. Since the crosslink density is related to the size of pores or cavities inside solid polymers, this method points towards the structural elucidation of polymers. From the parameters such as magnetic relaxation[7] and the dipolar correlation effect[8] obtained from the NMR spectrum, crosslink density can be calculated. In addition to the crosslink density, the behaviour of small particles inside the polymer matrices can also be

RSC Polymer Chemistry Series No. 8
Natural Rubber Materials, Volume 2: Composites and Nanocomposites
Edited by Sabu Thomas, Hanna J. Maria, Jithin Joy, Chin Han Chan and Laly A. Pothen

Published by the Royal Society of Chemistry, www.rsc.org

monitored by this technique. The pore sizes and their distribution in mesoporous silica gels using NMR have been published[9,10] by several research groups. NMR can reveal the conformation of polymer chains. Also free volume in amorphous polymers can be determined using NMR and Positron Annihilation Lifetime Spectroscopy (PALS).[10]

Among the various polymers, an industrially important elastomer, natural rubber (NR) has been the subject of extensive research. Curing agents such as sulfur, different accelerators, activators like zinc oxide and reinforcing fillers, such as carbon black, calcium carbonate, clay and silica, are added to enhance the mechanical and various other properties of NR.[11–13] Of the various filler particles, carbon black is the most popular in rubber compounds. Depending on the dimensions of the filler materials, micro- and nanocomposites of rubber are fabricated. The presence of the filler and its concentration affect the cure characteristics and crosslink density[14–16] of the composites. Again, the crosslink density of the composite determines the properties such as modulus, elongation at break, strength, hardness, resilience, and responses to solvents.[17] It can also be influenced by the process of thermal ageing.[17–22] Although NMR provides several useful parameters, a correlation between the crosslink density and the NMR parameters was demonstrated for the first time by Sakdapipanich *et al.*[23] They could derive a relationship, based on the intensity ratio between two small ^{13}C signals. Using the ^{129}Xe-NMR, they also showed a linear relationship between the chemical shift and degree of solvent swelling. The ^{1}H-NMR is also helpful in estimating the crosslink density and can also be applied to the sample in the liquid state.

By using the ^{1}H and ^{13}C solid-state NMR, the structure and dynamics of quite a lot of rubber composites were derived.[24] This will be discussed in detail in the subsequent sections. Solid-state NMR analysis of clay-reinforced samples reveals the influence of layered silicate platelets on the growth of the crystalline phase of the polymer. The crystalline and non-crystalline phases can be easily recognized by ^{13}C cross-polarization magic angle spinning (CPMAS) experiments. This chapter is aimed at providing a basic understanding about the usefulness of NMR spectroscopy in characterizing NR and its various composites. Various NMR methods used for characterization are also discussed following the basic theory behind the studies. The dispersion of the fillers inside the matrix can be revealed by knowing the local conformation and dynamics of the entrapped molecules. Even though different composite systems of NR are addressed, this study focuses mainly on the structural and dynamic information about the elastomer composites.

24.2 Basic Theory of NMR Spectroscopy and Instrumentation

NMR occurs when nuclei of certain atoms placed in a static magnetic field are exposed to a second, oscillating, magnetic field. NMR experiments provides wide range of knowledge varying from qualitative information such as

connectivities of atoms or groups of atoms and the magnetic equivalence of atoms in a compound to quantitative structural values like the J-coupling constant and cross-relaxation rates. The quantitative parameters are useful in elucidating the local conformation, distances, bond angle and local mobility of atoms within the molecules.[24,25]

The major components of an NMR spectrometer are illustrated in Figure 24.1.[24] This is essential to understand the details of the techniques and interpretation in the following discussion. The main parts of the spectrometer are connected by arrows drawn with heavy lines in the figure. The instrument is controlled by a computer, from where the data and spectrum are also obtained. All other parts perform specific functions and indirectly control the computer signals. The essential components of the NMR instrument include the highly stable magnet, sample probe, source of radio frequency radiation, phase-sensitive detector and data processing unit.

When the nucleus of an atom is considered, it possesses spin angular momentum depending on the number of protons and neutrons present in it. The nuclei experiences different energy levels when they are placed in an external magnetic field. Depending on the net spin of the protons and neutrons the nucleus can have 1/2, 1 or 0 spin value. A nucleus with spin 1/2 will have two possible orientations when placed in the external magnetic field, and its energy level splits. But in the absence of the external field, these orientations are of equal energy. Based on the stability, the lower energy level will be highly populated than the higher. The electromagnetic radiation of particular frequency is used to flip the alignment of nuclear spins from the low energy spin aligned state to the higher energy spin opposed state and vice versa. The energy required for this transition depends on the strength of the magnetic field applied.

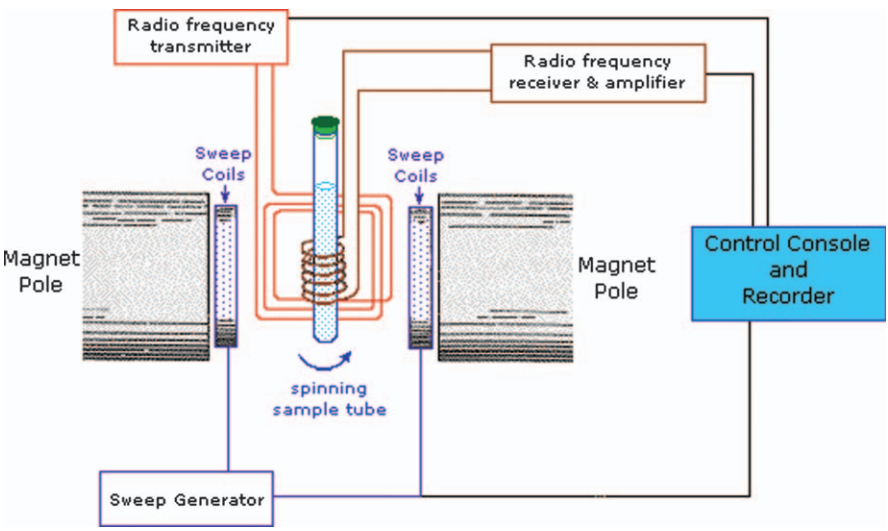

Figure 24.1 Block diagram of NMR spectrometer.[24] Copyright 2007.

In a mathematical way, it can be said that the spin angular momentum is associated with the intrinsic magnetic momentum of the nucleus and both are proportional to each other. The spin angular momentum:

$$L = m\hbar \tag{24.1}$$

where m is the spin quantum number and $\hbar$ is Planck's constant. m can have any of the values $m = -I,\ -I+1 \ldots I\ -\ 1,\ I$, that is in total $(2I+1)$ possible values.

The component of the magnetic moment (μ) along the field direction z is related to the gyro magnetic ratio (γ), which is a constant for all nuclei of a given isotope:

$$\mu z = \gamma L \tag{24.2}$$

$$\mu z = \gamma m\hbar \tag{24.3}$$

The spinning nucleus undergoes precessional motion in the presence of a magnetic field H_0. The frequency of this motion is known as the Larmor frequency and is given by:

$$\omega = 2\pi\nu = \gamma H_0 \tag{24.4}$$

Also the energy of a magnetic dipole in a magnetic field with a flux density H_0 is related to the magnetic moment by the following equation:

$$E = -\ \mu z H_0$$

$$E = -\ \gamma m\hbar H_0 \tag{24.5}$$

When the energy difference between two consecutive levels of the nucleus is taken as ΔE, it can be obtained as:

$$\Delta E = E_2 - E_1 = \gamma\hbar H_0 \tag{24.6}$$

When the frequency of the electromagnetic radiation (radiofrequency (rf)) pulse equals the precessional frequency of the nuclei (ω) in magnitude, at this resonance level, energy is absorbed and the nucleus excites from one level to another. This is the key part of the process and it is at this condition the spectrum is taken.

The splitting of energy levels in the external magnetic field is shown by Figure 24.2.

The difference in energy is related to the ratio of the number of nuclei populating the high-energy state $(N+)$ to the low energy state $(N-)$ according to Boltzmann statistics as:[26]

$$\frac{N+}{N-} = \exp(-\Delta E\ /\ K_B T) \tag{24.7}$$

where K_B is the Boltzmann constant and T is the absolute temperature.

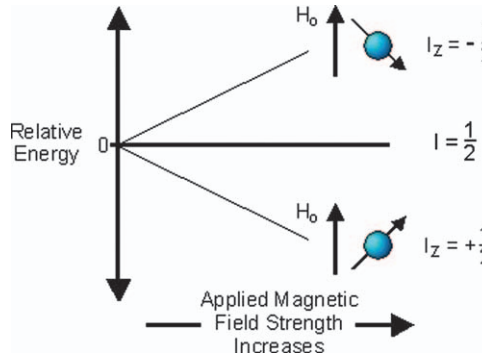

Figure 24.2 The energy difference between two adjacent energy levels as a function of the magnetic flux density.[25]
Copyright 2007.

NMR spectroscopy is a unique technique to study the physical, chemical and biological properties of matter. Depending on the type of processes, design of the instrument and nature of analysis, NMR spectroscopy is of different types. It is the subject of another vast study and cannot be included in the topic of a single chapter. However the principles of two commonly used methods and the solid-state NMR technique are explained here by emphasizing the importance of such studies in elastomer composites.

24.2.1 Spin–Spin Relaxation and Spin Echo

When a large number of nuclei are considered, the resultant magnetization M will be a sum of individual magnetic moments at resonance. When an isolated spin system is at equilibrium in a static magnetic field H_0 (along the z-axis), there will be no net magnetization in the xy-plane. At equilibrium, let M_0 represent the magnetization along the z-axis. In a spin echo process, the Hahn spin echo sequence (90 – τ – 180 – τ – echo) is used to obtain the spin echo. At zero time, a 90° rf pulse is set to produce a free induction decay (FID) and the vector M flips into the xy plane.[27] A magnetic field H_1 rotating about the z-axis is created by this pulse with its angle of rotation proportional to H_1.

$$\Theta = \gamma H_1 t \tag{24.8}$$

where t is the precession time. Also at resonance, the derivative of M with respect to precession time can be given as:

$$\frac{\partial M}{\partial t} = \gamma M \times H_1 \tag{24.9}$$

The component of the magnetization vector in the xy plane M_{xy} has significance as it is related to the transverse relaxation time. This is defined as a time constant in NMR, characterizing the rate at which M_{xy} decays in the transverse magnetic plane. In other words, it is the time taken by the transverse

signal to reach 37% of its initial value after flipping in to the magnetic transverse plane. This can be represented by the following equation:

$$M_{xy}(t) = M_0 e^{-t/T_2} \tag{24.10}$$

The decay of transverse magnetization is governed by two important factors, the molecular interactions (results in pure T_2 molecular effect), and the variations in H_0 (results in an inhomogeneous T_2 effect). When both these factors are combined, the time constant becomes T_2* and it can be related to both T_2 coming from molecular processes and from inhomogeneities by the following equation:

$$1/T_2^* = 1/T_2 + 1/T_{2in\,\mathrm{hom}\,o} \tag{24.11}$$

Figure 24.3 explains all the points discussed by demonstrating the timing of radio frequency and magnetic field gradient pulses and their effect on the NMR spin echo.[27] The net magnetization vector precesses around the z-axis at the Larmor frequency. During the first relaxation time delay, the magnetization evolves according to its chemical shift (and field inhomogeneity), and then a 180° pulse is applied. This 180° pulse applied along the x- or the y-axis inverts the magnetization. This is followed by another delay and during this time, the magnetization refocuses. The reconverged phases are known as spin echo.

24.2.2 Pulsed Gradient Spin Echo Diffusion

The process of diffusion is often described by Fick's laws, which relates the local macroscopic concentration of different molecule to an equilibrium value.[28]

In one dimension, the law is explained by:

$$\partial C/\partial t = -\,Dc\partial 2C/\partial x_2 \tag{24.12}$$

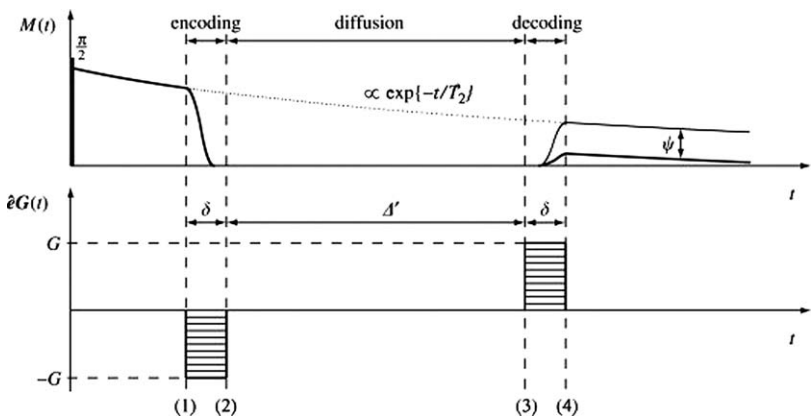

Figure 24.3 Timing of r_f and magnetic field gradient pulses and their effect on the NMR spin echo.[27]
Copyright 2007.

and in three dimensions

$$\partial C/\partial t = -Dc \tag{24.13}$$

where $\partial C = \mathrm{i}\partial/\partial \mathrm{x} + \mathrm{j}\partial/\partial \mathrm{y} + k\partial/\partial \mathrm{z}$, C is the concentration of the diffusing species (mol/m^2) and Dc is the mutual diffusion constant (m^2/s), and it is proportional to the velocity of the diffusing particles. The velocity of movement of particles undergoing diffusion depends on the temperature, viscosity of the fluid and the size of the particles. This is the mathematical explanation of Fick's first law.

In order to correlate the displacement of different individual molecules, according to Brownian movement, Fick's second law is employed.[28]

According to this law:

$$\partial \mathrm{P}(r,t)/\partial \mathrm{t} = Ds\,\mathrm{P}(r,t) \tag{24.14}$$

where P(r, t) is the probability of finding a particle with displacement r at a time t and Ds is the molecular self-diffusion constant. The spin echo experiments measure self-diffusion coefficients (Ds) rather than Dc and in the presence of a steady magnetic field gradient G_0, the effect of diffusion can be described by:[28,29]

$$A(2\tau, G_0) = A(2\tau, 0)\exp(-2/3\gamma^2 D_s G_0^2 \tau^3) \tag{24.15}$$

where A is the echo height as a function of time, and τ is the time between radio frequency pulses.

To amplify the effects of diffusion, a pair of magnetic field gradient pulses of magnitude G is applied in addition to the small value G_0 of steady gradient. According to Stejskal and Tanner, the amplitude of the attenuated spin echo is given by:[28,30]

$$A(2\tau, X = A(2\tau, 0)\exp(-\gamma^2 D_s X)$$

where

$$X = \delta^2 G^2(\Delta - \delta/3) - \delta G G_0(\cos\theta)[(t_1^2 + t_2^2) + \delta(t_1 + t_2) + 2(\delta^2/3) - 2\tau^2] \tag{24.16}$$

Here, Δ is the time separation between the gradient pulses, t_1 is the delay between the radio frequency pulse and the corresponding gradient pulse, δ is the width of the gradient pulse, and $t_2 = 2\tau - \Delta - t_1$.

24.3 Solid-State Study of Elastomer Nanocomposites

Elastomer nanocomposites can better be characterized with the help of NMR studies as illustrated in the introduction section. Solid-state NMR is the best choice as the sample is in the solid state, but the same information is obtained from the liquid state NMR as well, in fact this latter method is rather simple and has better sensitivity and resolution. Both these methods determine the crosslink density of composites from the differences in chemical shift values between the bulk solvent and trapped molecules. Prior to the NMR spectral

analysis, the composite samples are usually swollen in deuterated tetrachloroethane ($C_2D_2Cl_4$).

24.3.1 Structure and Dynamics

NMR can provide structural details of all composite samples. In composites, two types of interactions exist, namely filler–elastomer type and filler–filler type. Depending on the interfacial interactions between filler and elastomer, loosely bound and tightly bound layers of bound rubber can be formed over the filler particles. This formation of two layers of bound rubber content was analysed using NMR in the case of carbon black reinforced *cis*-polybutadiene.[31] NMR revealed the restricted motion of rubber chains as many segments of the rubber molecules in the tightly bound rubber layer are fixed to the surface of carbon black. This tightly bound layer of rubber has a higher density compared to the free rubber molecules resulting in gradual density change from the filler surface to the matrix. The thickness of this tightly bound rubber between carbon black and *cis*-polybutadiene is calculated by O'Brien *et al.*[32] in their studies and the value is found to be 0.4–1.3 nm.[33]

NMR is also helpful in understanding the mechanism of interaction within the fillers. This is really important when fabrication of composites is considered, because good interfacial interaction depends on the filler morphology. The ^{1}H-NMR characterization done for the silane-functionalized CNTs is illustrated in Figure 24.4.[34] Aminosilane-functionalized CNTs exhibit peaks at $d = 0.9$ (2 H; NH_2–CH_2–CH_2–CH_2–Si– group); $d = 1.2$ (3H; –O–CH_2–CH_3 group); $d = 1.6$ (2H; NH_2–CH_2–CH_2–CH_2– group); $d = 2.2$ (2H; NH_2–CH_2–CH_2–CH_2–) and a small peak $d = 2.0$ (2H; NH_2–CH_2– CH_2–CH_2–Si) indicating the presence of 3-aminopropyltriethoxysilane on the surface. The elemental analysis of functionalized CNTs indicates that the atomic percentage of nitrogen is 4.3% relative to carbon, confirming the introduction of aminosilane on the nanotube surface. The –OH groups formed on the nanotube surface interact with the ethoxy groups of silane and this leads to the chemical grafting of silane through Si–O–C linkages. Also there is a possibility of hydrogen

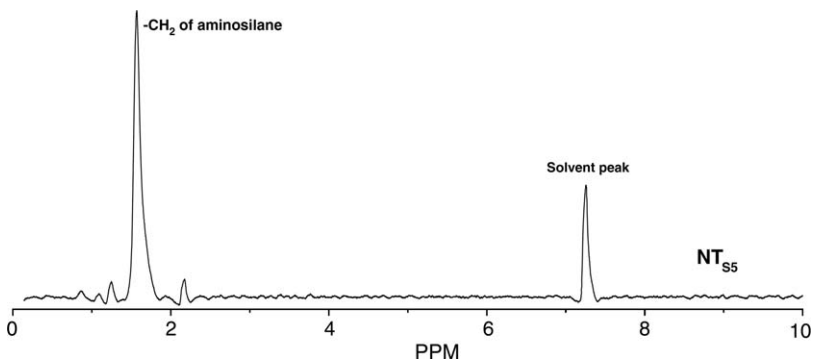

Figure 24.4 ^{1}H-NMR spectra of silane-functionalized CNTs.[34]
Copyright 2007. Reproduced with permission from Elsevier Ltd.

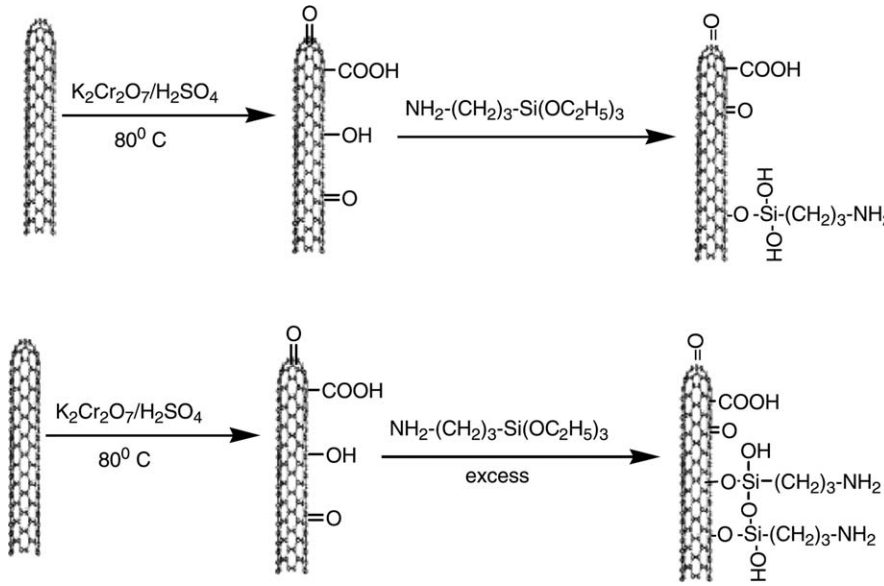

Figure 24.5 Probable mechanism of interaction between aminosilane and CNTs.[34] Copyright 2007. Reproduced with permission from Elsevier Ltd.

bonding interaction between the –CO groups on CNTs with hydrolysed silane on the surface of CNTs. The probable mechanism for all these kinds of interaction is included in Figure 24.5.[34]

NR is an industrially important material and many rubber products are available on the market. Due to the usage of vulcanized rubber products, its recycling is of significant concern and the increasing stockpiles of used rubber products, particularly tyres, present a serious threat to the environment. The three-dimensional highly vulcanized network is difficult to devulcanize because the process is non-reversible in nature, thus making the rubber recovery a difficult process. The chemical bonds within the crosslinked rubber can be broken by many methods, and among them, the relatively new high-power ultrasound technique is the most promising. This process does not use any solvent or chemicals. The NMR in solutions is capable of analysing chemical structures of soluble polymers and small molecules. However, solid-state NMR is necessary for the analysis of undissolvable vulcanized elastomers.[35] Experiments using high-power ultrasound for the devulcanization, and non-spectroscopic solid-state NMR techniques to study molecular dynamics and diffusion of the rubbers, have been performed on a wide variety of rubbers.

The NMR spectra of NR obtained from the two source plants (Hevea and Goldenrod) are illustrated in Figure 24.6. The structure is very clear from the various proton chemical shift values.[36]

The morphology of composite can be better explained using the solid-state NMR studies. For instance both the crystalline and amorphous components of polymer have distinct chemical shifts in the ^{13}C spectrum. The observed

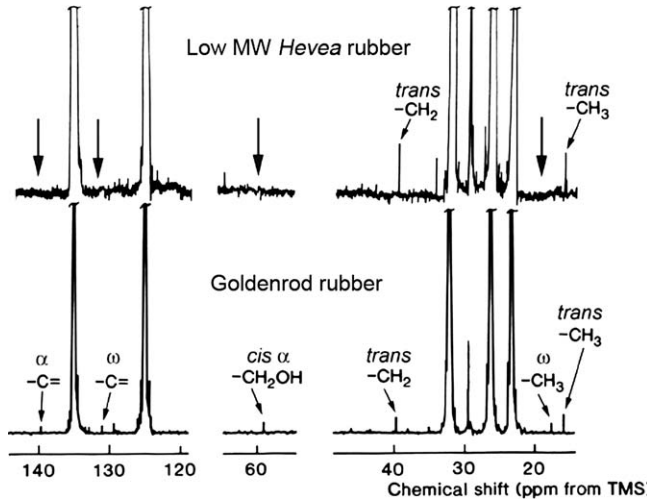

Figure 24.6 ^{13}C-NMR spectra of low-molecular weight fraction of *Hevea* rubber and rubber from Goldenrod.[36]

intensity can be easily converted to crystallinity. The ^{1}H-NMR wide line spectrum gives different degrees of molecular motion depending on the crystalline and amorphous domains. Usually the rigid, crystalline material gives a broad line whereas amorphous highly flexible chains narrow the line. Deconvolution of the signal is employed in order to calculate the relative amounts of each component. Crystallization induced due to strain is a common phenomenon observed in the case of NR-based materials. This property of NR is addressed by Lin *et al.* using high-resolution solid-state ^{13}C-NMR experiments.[37] They performed tests on both unstretched and *in situ* stretched NR samples and observed the formation of small crystals at room temperature from the ^{13}C cross-polarization and magic angle spectra (CP/MAS). The ^{13}C spin-lattice relaxation time and ^{1}H spin–spin relaxation time of *in situ* stretched samples again gave proof for the existence of crystallites. Also the ^{13}C dipolar decoupling spectra (DD/MAS) revealed the increase in crystalline signals with the draw ratio. The high-resolution NMR spectra concluded that the strain-induced crystallization starts when the draw ratio is about 2.0 and maximum crystallinity of NR is 19.3%. The presence of fillers lowered the crystallization as well.[37]

24.3.2 Filler Dispersion

The dispersion of filler within the polymer matrix is an important parameter to be addressed while manufacturing composite materials. NMR techniques are helpful in determining this filler effect. Since the protons are located in side groups attached to the main carbon chain of the polymer, the proton NMR spectroscopy characterize the elastomer composites very clearly. The transverse

magnetic relaxation studies can reveal interchain kinetics. In the case of vulcanized rubbers, the transverse relaxation (τ_2) gives molecular and segmental motions of the rubber chains, kinetics and dynamics near the sulfur crosslinkings.[35] The segments having restricted mobility produce one or more short τ_2 components, whereas highly mobile polymer chains (neat polymer) produce long τ_2 component.[35] In general, two-component or three-component exponential methods are practiced to determine the relaxation spectrum of dispersed systems. The relaxation spectrum will also show an additional intermediate τ_2 component when the molecular weight distribution of the pristine melt and of the extractable sol is particularly wide. This is due to the presence of unentangled sol molecules and dangling network chain ends and in this case the three-component exponential model gives better reproduction of the relaxation spectrum. A well-defined relaxation spectrum of devulcanized elastomer is characterized by a long τ_2, indicating the extractable and unentangled sol formed in it, and a short τ_2 indicating the presence of unextractable gel and entangled sol.[38] This was explained by a two-component exponential model whereas in a three-component exponential model, the relaxation decay of devulcanized rubber, is described by three components in the rubber which include a short τ_2 component due to the physically entangled and chemically crosslinked networks, an intermediate τ_2 component due to the unentangled light sol and the dangling network chain ends, and the long τ_2 component due to unreacted oligomers.[35]

Rubbers such as NR, butyl rubber (IIR), *etc*. are extensively used in tyres, after adding proper vulcanizing agents and fillers. More than 98% of the NR molecules used in the tyre industry are chemically *cis*-1,4-polyisoprene and these chains exhibit stress-induced crystallization to a great extent. This property influences the strength and fatigue properties of the isoprene rubber[26] and vulcanization further improves many properties like modulus, hardness, tensile strength, abrasion and tear resistance. In industry carbon fillers again impart better properties by manufacturing composites. As processing agents, oils promote good dispersion of carbon fillers as well, when added in small amounts. At high amounts, oils lower the uncured compound's viscosity and the vulcanizate's stiffness and hardness.[35] The molecular mobility and all the information regarding the fabrication of tyres is obtained using proton solid-state NMR spectroscopy. Before the analysis, the rubber is devulcanized by using high-power ultrasound techniques. NMR provided the transverse relaxation, and the diffusion of light sol and the data were analysed to study molecular mobility of cured and devulcanized samples. By the analysis, information about the destruction of network, network segmental mobility, and the mobility of the diffusing sol molecules are well explained.

The sample for NMR spectral study is usually heterogeneous in nature, *i.e*., solid rubber composite in liquid chloroform, and due to this reason it is difficult to shim. In some samples, automatic gradient shimming (top shim) is possible whereas in some others, shimming has to be done manually. This low level of shimming can lead to the broadening of the peak in the NMR spectrum. Chemical exchange of atoms is another reason for peak broadening.

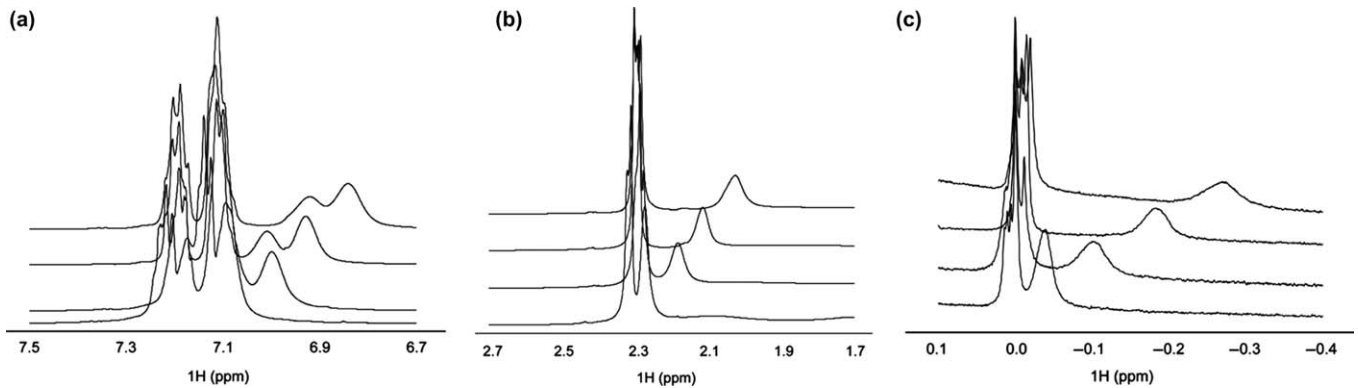

Figure 24.7 NMR spectra of the unaged rubber composite with different carbon black contents: (a) the splitting of the aromatic regions, (b) splitting of methyl regions, (c) signals for toluene methyl groups.[39]

Figure 24.7(a) and (b) illustrates the splitting of both the aromatic and methyl regions of a plot of four spectra of the unaged rubber composite samples with different carbon black contents.[39] The splitting of peaks into two groups corresponds to the toluene molecules present outside and inside the rubber strip while swelling the samples in toluene. Moreover the peaks arise from toluene shifts to upfield on increasing the carbon black concentration from 20 to 80 phr. When both aromatic and methyl signals are compared, the former exhibit severe overlap and so it is better to take the methyl resonance as the basis to analyse the carbon content. On the basis for NMR, tetramethyl silane (TMS) also shows the same behaviour as those of toluene in their methyl group signals, but a little complicated in shape than the toluene methyl groups (Figure 24.7(c)). It is also observed that the signal from the outside toluene also broadened and moved slightly upfield.[39]

This splitting of signals and broadening can be attributed to the inhomogeneous magnetic field around the sample. Also, the toluene molecules present outside the rubber composite sample interact with the sample surface. Due to this reason, the chemical shift change is usually measured as the difference between two methyl signals in the same sample and not between those of the sample and reference toluene liquid. The toluene reference showed its methyl signal at 2.34 ppm, while toluene present outside the samples showed in the range of 2.29–2.33 ppm. The actual chemical shift values do not show any relation with the filler concentration, indicating the difference in heterogeneity of both samples and magnetic field.

Apart from carbon black, silica also enhances the mechanical properties of rubbers. The exact reason for the improved mechanical strength of the filler reinforced composites is explained on the basis of molecular mechanisms, coming from the modification of the rubber chain properties in filled systems. Due to the large surface area of the fillers, most of the polymer chains can interact with the filler surface. As a result of the filler–elastomer interaction, the polymer chain mobility is restricted and the ^{1}H unresolved NMR spectral studies can reveal the local dynamics, in both unfilled and filled elastomers. The restricted chain mobility can be calculated using the NMR analysis provided λ, the shift factors required on the timescale, Ve,Vx and V_{f} respectively, the density of topological constraints due to entanglements, crosslinker molecules, and fillers are known. Since the residual NMR interactions from the different constraints are additional, the average length of the equivalent chain for any filled elastomers is

$$V = V\mathrm{x} + V\mathrm{e} + V_{\mathrm{f}} \tag{24.16}$$

The values for various constraints are represented by certain relations between λ and V.

For unfilled chemically crosslinked elastomer:

$$\lambda_{\mathrm{u}} = 1 + V\mathrm{x} / V\mathrm{e} \tag{24.17}$$

For filled non-chemically crosslinked elastomer (NC):

$$\lambda_{\mathrm{f}}^{\mathrm{NC}} = 1 + V_f / V\mathrm{e} \tag{24.18}$$

And for the filled chemically crosslinked elastomer (C):

$$\lambda_f^C = 1 + (V\mathrm{x} + V_f) / V\mathrm{e} \quad (24.19)$$

As already discussed, the ^{1}H-NMR allows measurement of the crosslink density and entanglements.[2,40] In composites, multifunctional crosslinking points exist consisting of crosslinker molecules and fillers particles.[41] The heterogeneous mobility of the two micro-domains can also be probed by ^{1}H-NMR. At the interface, the segment layers are immobilized, and the chains far from the particle surface remain highly mobile.[31,41,42] All these depend on the interfacial interaction and the grafting of the filler particle surface with suitable molecules which can control the mobility.[43,44] In order to understand the role of filler–elastomer interaction, model materials containing perfect spherical particles of silica (60 nm diameter) dispersed homogeneously in elastomer matrix following Joseph *et al.*[45] is addressed. Here in this system, the silica beads are coated with a coupling agent and bound with rubber chains either covalently or by van der Waals interactions. Thus the two classes of materials having highly different strengths of interactions could reveal the filler contribution to the total network structure, the chain mobility at the interface and thickness of the immobilized layer.

An important property of elastomer nanocomposites is ageing and is a very important cost and reliability factor in industry. Solid-state NMR microscopy provides analysis of thermal ageing of the elastomer composite since their partial liquid-like properties create a good environment for imaging compared with solids. The inhomogeneities in the network density and the filler content, ageing and diffusion fronts, stress pictures, *etc.* were also addressed. Ageing of elastomeric materials is very complex in nature, and it takes place mainly under the influence of heat, oxygen (ozone), other free radicals, radiation and/or mechanical stress.[46] Generally, the two competing processes – scission and linking of the polymeric chains – dominate the ageing process.[46] The network modifications take place without the use of crosslinker, but with the support of free radicals, arising easily in the presence of oxygen. Chain scissions also dominate the ageing process in synthetic polyisoprene or butyl rubber, whereas new crosslinks will arise in the case of styrene butadiene rubber.[46] Even though a lot of factors affect the ageing process, the presence of oxygen (ozone) besides the thermal damage and/or mechanical stress is the most important. This creates free radicals at the polymer backbones and leads to additional crosslinking. Oxygen diffusion also influences ageing velocity,[46] but at the same time, ageing can take place in the absence of oxygen also. During thermal ageing, the modulus and the crosslink density can go through a maximum and then decrease with additional curing due to the loss of network structure.[47] For vulcanized samples, desulfurization occurs during thermal ageing and as a result modified species such as cyclic sulfides, shorter sulfur crosslinks, *etc.* can be formed and this process is known as reversion. This process is the first step of an ageing process, and is called soft ageing. As a next step, the above-mentioned oxygen-consuming reactions can

occur and olefinic double bonds break, which is known as hard ageing.[48] The ^{1}H-NMR is applied to find out the role of the oxygen in ageing in different gaseous environments like air and nitrogen for carbon black filled NR composites.[49] The behaviour of elastomer chains near and far from the filler particles is an important factor determining the reinforcement. ^{2}H-NMR provides information about the orientations of chains far from the filler surface having a high mobility ($\sim$ 80 °C above T_g). The extension of the amorphous polymer chains of filled and unfilled rubber define a strain amplification factor, whose value depends on the property analysed and the technique used.[50]

For carbon black filled soft cured NR systems, under the ageing conditions of 100$\sim$ in air or nitrogen a soft ageing regime is observed. At short (0–20 h) times a decay of spin–spin relaxation time T_2 is seen. This is due to the desulfuration process. Also the inhomogeneously cured spheres becomes more homogeneous. After 20–70 h of ageing, T_2 becomes longer, indicating a higher molecular mobility, might be due to lower crosslink density. At still longer ageing times the olefinic double bonds get destroyed and new crosslinks can be formed. Here T_2 becomes shorter and the behaviour is more solid-like. It was Kuhn *et al*. who observed this decrease of relaxation time T_2 by NMR spectral studies.[48] They explained that at shorter ageing times chemical bonds with low activation energies such as sulfidic will be broken by thermal treatment and lead at least to crosslink decompositions. While at longer times (hard aging) the olefinic double bonds in the backbone will be broken and make the formation of new crosslinks possible.

The variable contact-time (VCT) experiments performed on SBR and SBR/TiO_2 nanocomposites synthesized by following a colloidal route is shown in Figure 24.8.[51] The spectrum of the non-degraded SBR/TiO_2 nanocomposite is identical to the pure SBR elastomer in the number, shape and relative intensities of the peaks, but is dislocated 5 ppm to higher chemical shift, indicating the presence of a strong interaction between the polymer chains and the TiO_2 nanoparticles. It is clear from the figure that two domains with different molecular mobilities exist in the samples – a large and flexible domain for the neat SBR and nanocomposites and a rigid domain for the SBR/TiO_2 photodegraded samples (Figure 24.8(c)). The intensity of NMR signals during the cross-polarization depends on the rate of cross-polarization from the ^{1}H nuclei to neighbouring ^{13}C nuclei, thus helping in the determination of proton spin-lattice relaxation time.[52] But in the case of atactic and amorphous flexible polymers (*e.g*. polybutadiene), the molecular motion reduces the interaction of the dipole moments and thus the cross-polarization is a slow process.[52] Figure 24.8(a) and (b) shows peaks located at long contact times arising from the rubbery materials. Figure 24.8(c) indicates the rigid domain of SBR/TiO_2 photodegraded nanocomposite. This is attributed to some crosslinking reactions occurring between the polymer chains during the degradation process, making the material more rigid and less soluble. These reactions occur particularly on the chains containing a,b-unsaturated carbonyl groups.[53,54]

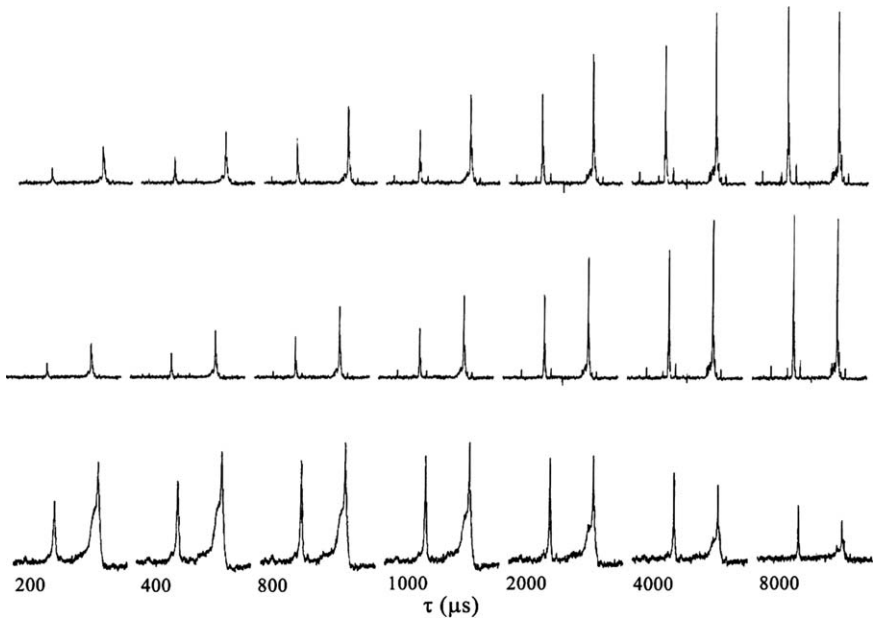

Figure 24.8 ^{13}C-NMR CP/MAS spectra with variable contact-time experiment (VCT): (a) SBR, (b) SBR/TiO_2 nanocomposite and (c) SBR/TiO_2 photodegraded nanocomposite.[51]
Copyright 2009. Reproduced with permission from Elsevier Ltd.

Table 24.1 Proton spin-lattice relaxation time in the rotating frame values for all resolved ^{13}C of SBR, SBR/TiO_2 nanocomposite, SBR/TiO_2 photodegraded nanocomposite.[51] Copyright 2009. Reproduced with permission from Elsevier Ltd.

d (ppm)	*SBR* $T_{1\rho H}$ *(ms)*	*SBR/TiO₂* $T_{1\rho H}$ *(ms)*	*SBR/TiO₂ Photodegraded* $T_{1\rho H}$ *(ms)*
38	13.5	–	–
36	10.3	–	2.2
31	25.7	–	–
29	43.2	393	–
133	–	–	7.3

The values of proton spin-lattice relaxation time in the rotating frame ($T_{1\rho}{}^{H}$) for the resolved carbons were calculated and listed in Table 24.1.[51] The non-uniformity in the values of $T_{1\rho}{}^{H}$ shows the heterogeneous nature of the system and the structural changes. $T_{1\rho}{}^{H}$ evaluates the changes in the microstructure and the molecular mobility in polymer blends. It also permits verification of the homogeneity in the polymer systems, as it is sensitive to the spatial proximity of chains. In general, for a compatible blend, only one value of $T_{1\rho}{}^{H}$ is present, and more than one value indicates the existence of two domains with distinct mobilities.[55]

In polymers, the strongly adsorbed polymer layer exhibits a different and higher glass transition temperature than bulk.[56–58] Similarly, in rubber

composites, Struik[59] observed a glassy shell around the filler particles. The thickness of such a glassy layer varies with temperature and anchoring strength and the layer volume increases with the anchoring strength. In the case of polymers as well as the composites, strong anchoring can slow down the dynamics of the polymer chains over a distance of a few nanometres. The thickness decrease with temperature is attributed to a glass transition gradient at the interface.

In short, solid-state NMR is a direct measurement and sample preparation is easy.[60] The solid-state spectra is of similar quality to that of the traditional liquid NMR. Also the techniques such as magic angle spinning (MAS) and cross-polarization (CP) can reduce line broadening and can increase the signal sensitivity. NMR also gives a mean value, with a high accuracy, of the local extension of the amorphous chains during the processes of crystallization and melting, during stretching and recovery.[61] Thus NMR is a significant tool in addressing the homogeneity and domain structures during the analysis of polymers, polymer blends, composites and polymer nanocomposites.[2,62–66] The CP rates in NMR are related to the crosslink density in elastomers.[67,68] The presence of dynamic, physical and chemical crosslinks in elastomers leads to a non-zero average of the homonuclear and heteronuclear dipolar couplings, and results in the NMR relaxation behaviour.[2]

24.4 Conclusions

Solid-state NMR is an emerging technique in the study of the structure and dynamics of elastomer nanocomposites. It helps in a clear identification of the variation in the elastomer structure, the filler and its mode of dispersion. These results not only complement FTIR data but also provide new insights into the dispersion and confinement. Moreover the application of NMR techniques is more general. The arrangement of polymer chains in the nanocomposites depends on the interfacial interaction between polymer chains and filler particles. This can be better investigated by NMR as it provides information about the behaviour of polymer chains as a function of the distance from the filler. In other words the mobility of polymer chains depends on their arrangement and conformation in the interlayer region. Other composite properties like ageing, degradation, curing behaviour, *etc*. can also be addressed using NMR technique. The nature of filler dispersion within the elastomer matrix is also understood by this method. Thus NMR helps the manufacture of rubber composites and contributes to technology and industry both directly and indirectly. However challenges do exist, from the fabrication of elastomer composites to the derivation of NMR spectrum and as a solution technology focus more on the development of very sophisticated devices.

Acknowledgements

The authors would like to acknowledge the University Grants Commission and the Department of Atomic Energy Consortium. Thanks are also due to the

Department of Science and Technology and the Nanomission scheme of DST, New Delhi.

References

1. D. E. Demco, S. Hafner, C. Fulber, R. Graf and H. W. Spiess, *J. Chem. Phys.*, 1996, **105**, 11285.
2. P. Sotta, C. Fulber, D. E. Demco, B. Blumich and H. W. Spiess, *Macromolecules*, 1996, **29**, 6222.
3. W. Kuhn, P. Barth, P. Denner and R. Muller, *Solid State Nucl. Magn. Reson.*, 1996, **6**, 295.
4. R. Graf, D. E. Demco, S. Hafner and H. W. Spiess, *Solid State Nucl. Magn. Reson.*, 1998, **12**, 139.
5. M. Schneider, D. E. Demco and B. Blumich, *J. Magn. Reson.*, 1999, **140**, 432.
6. M. Schneider, L. Gasper, D. E. Demco and B. Blumich, *J. Chem. Phys.*, 1999, **111**, 402.
7. V. M. Litvinov and A. A. Dias, *Macromolecules*, 2001, **34**, 4051.
8. M. Garbarczyk, F. Grinberg, N. Nestle and W. Kuhn, *J. Polym. Sci., Part B: Polym. Phys*, 2001, **39**, 2207.
9. W. O. Parker, A. Ferrando, D. Ferri and V. Canepari, *Macromolecules*, 2007, **40**, 5787.
10. T. Emmler, K. Heinrich, D. Fritsch, P. M. Budd, N. Chaukura, D. Ehlers, K. Ratzke and F. Faupel, *Macromolecules*, 2010, **43**, 6075.
11. K. I. Winey and R. A. Vaia, *MRS Bull.*, 2007, **32**, 314.
12. J. Oberdisse, *Soft Matter*, 2006, **2**, 29.
13. A. C. C. Esteves, A. B. Timmons and T. Trindade, *Quim. Nova*, 2004, **27**, 798.
14. E. F. Devlin, *Rubber Chem. Technol.*, 1986, **59**, 666.
15. S.-S. Choi, *J. Appl. Polym. Sci.*, 2004, **93**, 1001.
16. S.-S. Choi, K. J. Hwang and B. T. Kim, *J. Appl. Polym. Sci.*, 2005, **98**, 2282.
17. N. J. Morrison and M. Porter, *Rubber Chem. Technol.*, 1984, **57**, 63.
18. S.-S. Choi, *Bull. Korean. Chem. Soc*, 2000, **21**, 628.
19. S.-S. Choi, *J. Appl. Polym. Sci.*, 2000, **75**, 1378.
20. S.-S. Choi, D.H. Han, S.W. Ko and H.S. Lee, *Bull. Korean Chem. Soc.*, 2005, **26**, 1853.
21. S.-S. Choi and J. C. Kim, *J. Ind. Eng. Chem.*, 2007, **13**, 950.
22. S.-S. Choi, J. C. Kim, S. G. Lee and Y. L. Joo, *Macromol. Res.*, 2008, **16**, 561.
23. J. T. Sakdapipanich, T. Kowitteerawut, S. Tuampoemsab and S. Kawahara, *J. Appl. Polym. Sci.*, 2006, **100**, 1875.
24. http://www2.chemistry.msu.edu/faculty/reusch/VirtTxtJml/Spectrpy/nmr/nmr1.htm.
25. Driguana, http://www.chembio.uoguelph.ca/cgi-bin/cc.exe?dbase = cc&user = &item = 27O1FM&action = v_article.

26. F. M. Herman in *Encyclopedia of Chemical Technology*, ed. Polyisoprene, Wiley, New York, 1978, pp. 582–592.
27. F. Stallmach and P. Galvosas, *Annu. Rep. NMR Spectrosc.*, 2007, **61**, 51.
28. X. Sun, The devulcanization of unfilled and carbon black filled isoprene rubber vulcanizates by high power ultrasound, PhD dissertation, university of Akron, 2007.
29. E. L. Hahn, *Phys. Rev.*, 1950, **77**, 297.
30. R. Hamzah, M. Abu Bakar, M. Khairuddean, I. A. Mohammed and R. Adnan, and , *Molecules*, 2012, **17**, 10974.
31. S. Kaufman, W. P. Slichter and D. O. Davis, *J. Polym. Sci.*, 1971, **9**, 829.
32. J. O'Brien, E. Cashell, G. E. Wardell and V. J. McBierty, *Rubber Chem. Technol.*, 1977, **50**, 747.
33. K. Yamauchi, S. Akasaka, H. Hasegawa, S. Koizumi, C. Deeprasertkul, P. Laokijcharoen, J. Chamchang and A. Kornduangkaeo, *Composites, Part A*, 2005, **36**, 423.
34. A. M. Shanmugharaj, J. H. Bae, K. Y. Lee, W. H. Noh, S. H. Lee and S. H. Ryu, *Compos. Sci. Technol.*, 2007, **67**, 1813.
35. S. Kariyo and S. Stapf, *Macromolecules*, 2002, **35**, 9253.
36. J. T. Sakdapipanich and P. Rojruthai, Molecular Structure of Natural Rubber and Its Characteristics Based on Recent Evidence, *Biotechnology – Molecular Studies and Novel Applications for Improved Quality of Human Life*, ed. R. Sammour, InTech, 2012.
37. W. Lin, M. Bian, G. Yang and Q. Chen, *Polymer*, 2004, **45**, 4939.
38. A. Vieyres, R. Pérez-Aparicio, P. A. Albouy, O. Sanseau, K. Saalwächter, D. R. Long and P. Sotta, *Macromolecules*, 2013, **46**, 889.
39. Y. K. Chae, W. Y. Kang, J. Jang and S. Choi, *Polym. Test.*, 2010, **29**, 953.
40. G. Simon, K. Baumann and W. Gronsky, *Macromolecules*, 1992, **25**, 3624.
41. V. M. Litvinov and P. A. M. Steeman, *Macromolecules*, 1999, **32**, 8476.
42. H. Luchow, E. Breier and W. Gronsky, *Rubber Chem. Technol.*, 1997, **70**, 747.
43. Y. C. Ou, Z. Z. Yu, A. Vidal and J. B. Donnet, *J. Appl. Polym. Sci.*, 1996, **59**, 1321.
44. A. P. Legrand, N. Lecomte, A. Vidal and E. Papirer, *J. Appl. Polym. Sci.*, 1992, **46**, 2223.
45. R. Joseph, S. Zhang and W. T. Ford, *Macromolecules*, 1996, **29**, 1305.
46. W. Kleemann, Mischungen ∼r die Elastverarbeitung, VEB Deutscher Verlag ∼r Grundstoffindustrie Leipzig, 1982, p. 132.
47. L. Koenig, M. Andreis in *Solid State NMR of Polymers*, L. Mathias, Plenum Press, New York, 1991.
48. W. Kuhn, E. Koeller and I. Theis, *Economic Analysis*, 1976, 217–236.
49. M. Knirgen, U. Heuert, H. Schneider, P. Barth and W. Kuhn, *Polym. Bull.*, 1997, **38**, 101.
50. S. Trabelsi, P. A. Albouy and J. Rault, *Macromolecules*, 2003, **36**, 9093.
51. T. M. Arantes, K. V. Leão, M. I. B. Tavares, A. G. Ferreira, E. Longo and E. R. Camargo, *Polym. Test.*, 2009, **28**, 490.

52. M. R. G. Coelho, R. A. S. San Gil and M. I. B. Tavares, *Polym. Test.*, 1996, **15**, 485.
53. J. A. Bousquet and J. P. Fouassier, *Eur. Polym. J.*, 1987, **23**, 367.
54. C. Adam, J. Lacoste and J. Lemaire, *Polym. Degrad. Stab*, 1989, **26**, 269.
55. E. P. Silva and M. I. B. Tavares, *Polym. Bull.*, 1998, **41**, 307.
56. J. H. Van Zanten, W. E. Wallace and W. L. Wu, *Phys. Rev. E.*, 1996, **3**, 2053.
57. H. Fujiwara and S. Nishimura, *Polym. J*, 2012, **44**, 832.
58. J. L. Forrest, K. Dalnoki-Veress and J. R. Dutcher, *Phys. Rev. E*, 1997, **56**, 5705.
59. L. C. E. Struik, *Polymer*, 1987, **28**, 1521.
60. H. Luo, M. Klüppel and H. Schneider, *Macromolecules*, 2004, **37**, 8000.
61. J. Rault, J. Marchal, P. Judeinstein and P. A. Albouy, *Macromolecules*, 2006, **39**, 8356.
62. S. H. Zhu, M. K. Cheung and C. M. Chan, *Polymer*, 1998, **39**, 6099.
63. E. R. Andrew and E. Szczesniak, *Progr. Nucl. Magn. Reson. Spectros.*, 1995, **28**, 11.
64. M. I. B. Tavares and E. E. C. Monteiro, *Polym. Test.*, 1995, **14**, 273.
65. B. Garnaik and S. Sivaram, *Macromolecules*, 1996, **29**, 185.
66. R. F. Nogueira and M. I. B. Tavares, *Polym. Test.*, 2001, **20**, 379.
67. A. P. M. Kentgens, W. S. Veeman and J. Van Bree, *Macromolecules*, 1987, **20**, 1234.
68. J. W. ten Brinke, V. M. Litvinov, J. E. G. J. Wijnhoven and J. W. M. Noordermeer, *Macromolecules*, 2002, **35**, 10026.

CHAPTER 25

ESR Studies of Natural Rubber Composites and Nanocomposites

ARUNA KUMAR BARICK AND YOUNG-WOOK CHANG*

Polymer Nano Materials Laboratory, Department of Chemical Engineering, College of Engineering Sciences, Hanyang University, Ansan 426-791, Republic of Korea
*Email: ywchang@hanyang.ac.kr

25.1 Application of ESR in Polymer Systems

25.1.1 Introduction

Electron spin resonance (ESR) or electron paramagnetic resonance (EPR) spectroscopy is a sophisticated technique for studying materials with paramagnetic properties (unpaired electrons). Application of ESR in polymer chemistry has a long history.[1] Generally, characterization of polymers by ESR is impossible because polymers are the most stable macromolecules having all the electrons in paired state. In order to make the polymers be ESR active, stable free radicals such as a nitroxide free radical are added into the polymer matrix, which can act as a tracer molecule.[2,3] Figure 25.1 shows representative resonance structures of the nitroxide free radical with delocalized unpaired electrons.[4] The most popular stable nitroxide radicals (2,2,6,6-tetramethylpiperidin-1-yl)oxyl, or (2,2,6,6-tetramethylpiperidin-1-yl)oxidanyl (TEMPO) are red-orange sublimable solids, first discovered by Lebedev and Kazarnovskii.[5,6] Huber has depicted the molecular orbital (MO) of the nitroxide free radical in detail.[7] The nitroxide radical possesses a free electron

RSC Polymer Chemistry Series No. 8
Natural Rubber Materials, Volume 2: Composites and Nanocomposites
Edited by Sabu Thomas, Hanna J. Maria, Jithin Joy, Chin Han Chan and Laly A. Pothen

Published by the Royal Society of Chemistry, www.rsc.org

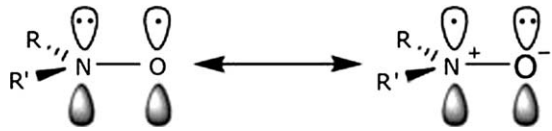

Figure 25.1 Representative resonance structures of the nitroxide free radical. (Reproduced from ref. 4 with permission from the Royal Society of Chemistry.)

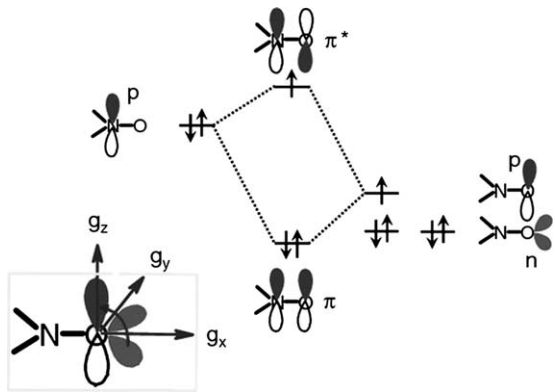

Figure 25.2 Schematic representations of the frontier orbitals of the nitroxide group. (Reproduced from ref. 7 with permission from Springer.)

that resides on the nitroxide group (>N–O•) and occupies the P_z orbital of the nitrogen atom. Figure 25.2 shows the outermost orbital of the nitroxide group.[7]

The TEMPO or its derivatives are widely used as a radical trap, a structural probe/label of ESR for investigation of organic systems, a selective oxidizing agent for organic synthesis, and an active mediator in controlled/living free radical polymerization.[8] Kocherginsky and Swartz, and Likhtenshtein *et al.* have published books regarding preparations, reactions, properties, and application of nitroxides.[9,10] Miwa *et al.* employed the microwave power saturation (MPS) method of site-specific spin labelling ESR to determine glass transition temperature (T_g) and β relaxation temperature (T_β) around chain ends of polystyrene (PS).[11] The segmental dynamics of polymers in polymer/clay nanocomposites were studied by spin labelling ESR experiment.[12] Grassie published a scientific report on the study of polymer degradation by ESR.[13] A small amount of nitroxide radicals (>1 wt%) can be implanted into a polymer matrix through spin probe (diffused or dispersed into a polymer matrix) or spin label (covalently bonded to a polymer) method for ESR studies on polymers. ESR analysis of the nitroxide radical as a spin probe or spin label can provide structural information on organic and biological systems because mobility of the nitroxide radical is strongly influenced by the dynamics and local structures of the matrix materials. That is to say, the stability of nitroxide radical is generally attributed to the delocalization of the free electron centre and steric

hindrance by neighbouring conjugative bulky or sterically inhibiting groups (generally methyl groups).[14] The miscibility between the nitroxide and a polymer matrix as well as the size, shape, polarity, substituent groups, and flexibility of nitroxide must be considered together for studying a particular polymeric system.[15,16] In spin label method, the nitroxide can be exactly placed within a polymer backbone through chemical reactions, while in the spin probe method, the nitroxide can be physically incorporated into a polymer matrix by simple solution mixing technique. Didović *et al*. have studied the effect of temperature at which a spin probe was incorporated into a polymer on the quality of ESR spectrum.[17] Pace and Snow have reported the effect of probe size of various nitroxide radicals and hydrogen bonding interactions of the radicals on the mobility of spin probe or spin label.[18] Veksli and Miller have studied the effect of solvents on the molecular motion of nitroxide free radicals in covalently labelled PS and poly(methy1 methacrylate) (PMMA).[19] Magnetic dipole–dipole interactions (dipolar couplings) between two electrons make it a most feasible technique for measurement within the most applicable range of 1.5–8 nm. The ESR works out a specified characterization tool for amorphous samples with a high selectivity and sensitivity, which has no long range orders.[20] ESR is a suitable instrumentation technique to identify the segmental molecular motions and microstructural parameters of different types of polymeric systems such as polymer blends and polymer composites or nanocomposites filled with different fillers. The ESR experiments for the polymeric systems may provide insights into a reinforcement mechanism in polymer composites by evaluation of interfacial interactions between filler and polymer matrix, heterogeneity in structure and mobility, and degree of phase separation on a nanoscale length in polymer blends. The spin label and spin probe methods produce a suitable signal-to-noise ratio without altering the inherent material properties of polymer matrix.

This chapter reviews the ESR studies of natural rubber (NR) and some selective other polymer composites and nanocomposites based on literature surveys.

25.1.2 Theoretical Background

Electronic spin state of unpaired electrons of nitroxide free radical is split into two degenerated energy states, denoted as $m_s = \pm\frac{1}{2}$, when it is placed under an externally applied magnetic field. Alignment of the electron spin, oriented along and opposite to the direction of the applied magnetic field result in lower ($m_s = -\frac{1}{2}$) and higher ($m_s = +\frac{1}{2}$) energy states, respectively. The spin Hamiltonian for nitroxide free radical (H_{NO}) resulted from the interactions of the unpaired electrons with the N^{14} nucleus ($I = 1$) magnetic moments and the external magnetic fields, which is measured by the electron and nucleus Zeeman interactions, and hyperfine coupling, respectively, as given in Equation (25.1):

$$H_{NO} = \beta_e g_e B_0 S - (\beta_N g_N/\hbar) B_0 I + SAI \tag{25.1}$$

where β_e ($e\hbar/2m_e$, where e is the elementary charge, $\hbar$ (h/2π) is reduced Planck's constant, and m_e is electron rest mass) is the Bohr magneton ($\approx 9.27400968 \times 10^{-24}$ Joules/Tesla), g_e (≈ 2.0023 for a free electron) is Landé g-factor for electron or spectroscopic splitting factor, B_0 is external magnetic field, S is spin angular momentum, β_N is nuclear magneton ($\approx 5.05 \times 10^{-27}$ J/T), g_N is the nuclear g-factor, A is the hyperfine coupling tensor, and I is the nuclear spin of N^{14}.

Electron Zeeman interaction (EZ) splits the energy state of a nitroxide free radical into two levels, and each level is further divided into three sublevels due to nuclear Zeeman interaction (NZ) and each Zeeman level has different energy states due to hyperfine interactions (HF). Figure 25.3 shows an energy level diagram in which the energy state of the electron (E) is plotted against applied magnetic field (H_0). In Figure 25.3, vertical arrows denote allowed ESR electronic transitions with corresponding first derivative spectral lines. The nitroxide free radical shows three allowed ESR transitions derived from the selection rules ($\Delta m_s = \pm 1$ and $\Delta m_I = 0$). The g-factor indicates a centre of the resonance that split into three lines due to hyperfine interactions with a

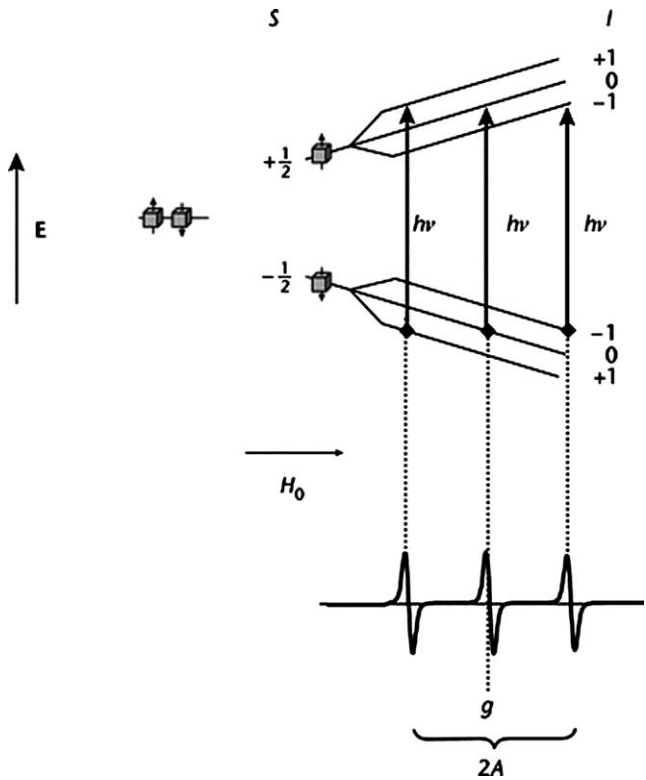

Figure 25.3 Energy level diagram of the Zeeman and hyperfine interactions of nitroxide with first derivative spectrum.
(Reproduced from ref. 21 with permission from John Wiley & Sons.)

separation of tensor component '*A*', which are degrees of interaction between unpaired electrons and perturbing nuclei.[21]

25.2 ESR Studies of Natural Rubber Composites and Nanocomposites

Very few papers on ESR studies of NR composites and nanocomposites are available in the literature.[22]

25.2.1 ESR Studies of NR

Marinović *et al*. have examined the effect of temperature on the ESR signals of TEMPOL (4-hydroxy-2,2,6,6-tetramethylpiperidin-1-yl)oxyl) spin probe embedded NR.[23] The temperature dependence of ESR spectra is due to change in rotational motion of the nitroxide radicals, characterized by the rotational correlation time (τ_R).[24] The representative ESR spectra of spin probed NR measured over a wide range of temperature are given in Figure 25.4(a). The separation of the outer maxima ($2A_{zz}$) is maximum for the spectrum of immobilized spin probe molecules at −120 °C and is slightly decreased with the increase in temperature. The shape of the spectral lines are separated when temperature approaches the glass transition temperature (T_g) (−20 °C) and above it, referred as $T_{5\,mT}$ (the temperature at which the separation between the $2A_{zz}$ attains 5 mT).

The quantitative relationship between the T_g of polymer and $T_{5\,mT}$ is shown in Equation (25.2):[25]

$$T_{5\,mT} = T_g/(1 - 0.03T_g/\Delta H_a) \tag{25.2}$$

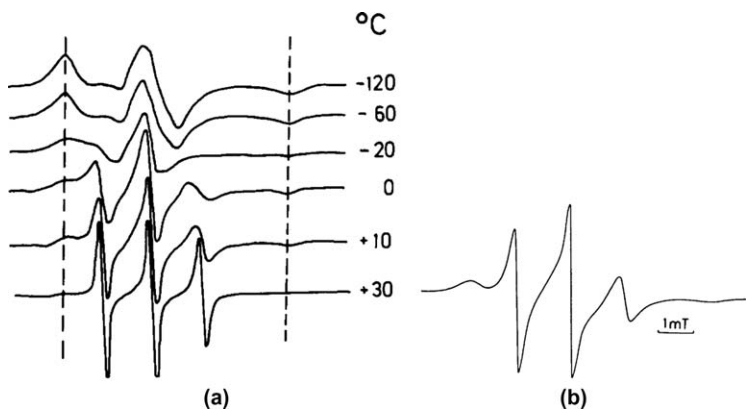

Figure 25.4 (a) Temperature dependence of the ESR spectra of spin probed NR and (b) simulated ESR spectrum for two non-interconverting nitroxide spin probe motions.
(Reproduced from ref. 23 with permission from Springer.)

where ΔH_a is the apparent activation energy for the T_g relaxation process.

Kusumoto *et al.* have proposed a mathematical equation by considering the volume of the spin probe and the segmental size of the polymer as given in Equation (25.3).[26]

$$T_{5\,mT} - T_g = 52[2.9f(\mathrm{In}1/f + 1) - 1] \tag{25.3}$$

where f is the ratio of the volume of the probe to that of the segment.

Hwang *et al.* have interpreted that the value of $T_{5\ \mathrm{mT}}$ increases with increasing pore size and molar mass that causes the increase in the intermolecular interactions between the spin probe and polymer molecular chains, which leads to the better coupling of rotational motions of spin probe with that of polymer segment.[27]

The spin probed NR exhibits a composite spectrum in the glass transition region. The composite ESR spectrum consists of superposition of the narrow and broad components as a consequence of the separation of spin probes dispersed in the crosslinked network of different local density or available free volume.[28] The narrow component originates from the slow motion of nitroxide spin probes located in the regions undergoing main chain segmental mobility, which is characteristic of an amorphous polymer above T_g. The broad component corresponds to the nitroxide spin probes populated in the regions with restricted segmental motions of large rotational mobility.[29] The origin of bimodal ESR spectra for nitroxide spin probe NR is due to the partition of the probes into two different environments related to local matrix density. The intensity of the narrow component is increasing at the expense of the broad component with rise in temperature. However, the outermost peak-to-peak separation of the remaining broad component does not change with change in temperature. The improvement of the narrow component with temperature is expected due to the increase in free volume. The simulated spectrum shown in Figure 25.4(b) is made up of two non-interconverting nitroxide motions having τ_R of 7×10^{-10} and 7.8×10^{-8} s, respectively, with a slow component of 30%, which is very similar to the ESR spectrum of NR recorded at 10 °C.

Kusumoto *et al.* have reported that a small sub-splitting appears at 16 °C for NR vulcanizates and its intensity increases with increase in both temperature and combined sulfur (S_c) content as shown in Figure 25.5, which is attributed to two kinds of spectra with broad and narrow line separation being superimposed.[26]

Figure 25.6 displays the ESR spectra of four different types of nitroxide spin probes (TEMPO (I), TEMPOL (II), EGONO (4-ethylene glycoloxy-TEMPO) (III) and BZONO (4-benzyloxy-TEMPO) (IV)) dispersed in NR matrix. The molecular weights and molecular volume are different for different types of spin probes. The spin probes (I, II and III) in the NR matrix show composite spectrum but the only difference between them is the intensity of the broad component, which increases with increasing molecular volume of the probes. Alternatively, the largest spin probe (IV) exhibits only one component in

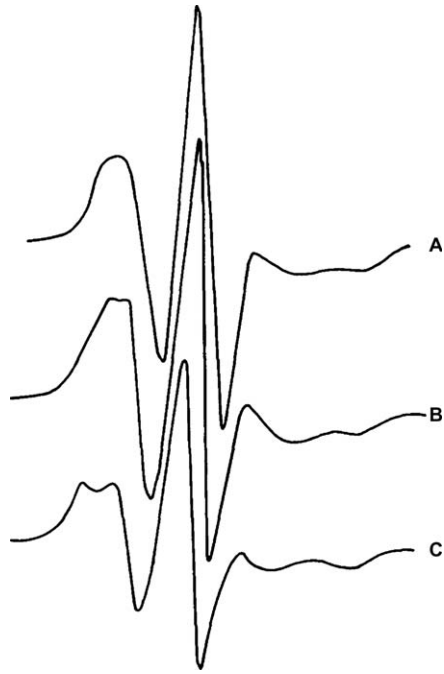

Figure 25.5 ESR spectra of NR vulcanizates of (A) 1.1% S_c at 16 °C, (B) 7.5% S_c at 25 °C, and (C) 15.1% S_c at 33 °C.
(Reproduced from ref. 26 with permission from Elsevier.)

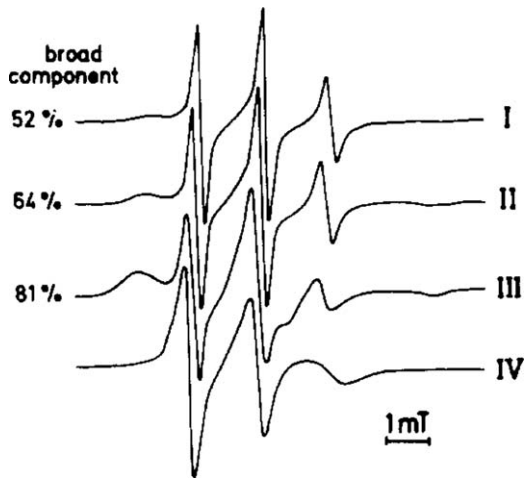

Figure 25.6 ESR spectra of NR doped with different types of spin probes (I, II, III and IV) measured at 20 °C.
(Reproduced from ref. 29 with permission from Elsevier.)

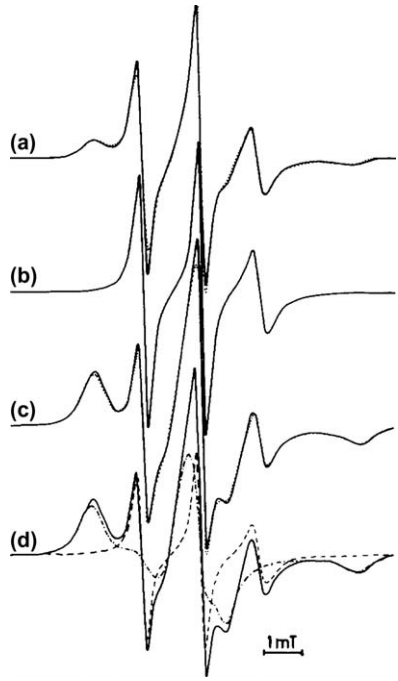

Figure 25.7 ESR spectra of (a) NR, (b) NR sol and (c, d) NR gel at 20 °C doped with spin probe (II). The dotted line corresponds with the simulated spectrum. Spectrum (d) displays the broad and narrow component as the best fit to an experimental spectrum.
(Reproduced from ref. 29 with permission from Elsevier.)

spectrum that resembles with the fast nitroxide motion, which conclude that it cannot penetrate into the high density domains with smaller free volume sizes.

The bimodal spectra generated for spin probe NR confirms the presence of the gel phase within NR matrix. The extracted sol and gel phases of NR were spin probed and ESR spectra are investigated to further ascertain the phenomena as shown in Figure 25.7. The sol phase exhibits a three line spectrum attributed to the fast spin probe motion, while the gel phase shows a composite spectrum. The bimodal spectrum for NR gel is assigned to the heterogeneous distribution of regions of immobilized molecular chains and improvement of segmental movements above $T_{5\ \mathrm{mT}}$.

Veksli *et al.* have investigated the effect of molecular weight, molecular weight distribution, and gel phase on the heterogeneity in the NR matrix by a spin probe ESR method.[30] The temperature dependence of ESR spectra of spin probe embedded low and high molecular weight NR are shown in Figure 25.8(a) and (b). The ESR spectra were evaluated both above the T_g and $T_{5\ \mathrm{mT}}$ of the NR matrix in order to obtain the population of spin probes contributing to the slow and fast motions. The intensity of the fast component increases with increasing the temperature at the expense of the slow component, which is expected due to the gradual increase in local free volume or segmental

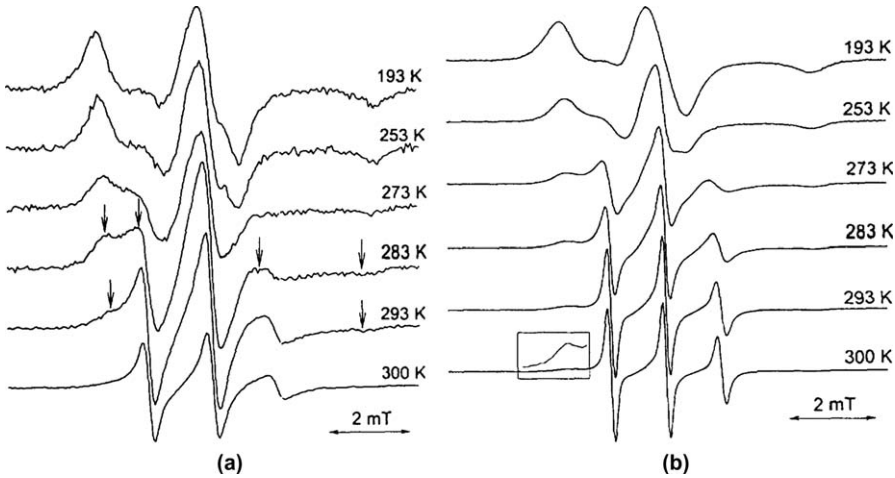

Figure 25.8 ESR spectra of (a) low and (b) high molecular weight spin probe added NR matrix at indicated temperatures.
(Reproduced from ref. 30 with permission from Elsevier.)

motion of molecular chains above T_g. The slow component of the ESR spectra of high molecular weight NR matrix is still present well above the T_g and the corresponding $2A_{zz}$ is unaltered in the studied temperature range, which is assigned to the spin probes associated with the regions of relatively rigid chains of the NR matrix.

The spin probed ESR spectra of extracted sol and gel phases of the high molecular weight NR matrix are displayed in Figure 25.9 in order to probe the ESR spectra of slow component above T_g, which reflects the restricted motion of entangled and physically crosslinked NR chains (gel phase). The ESR spectra of the gel phase are characteristic of restricted NR chains below T_g with a constant $2A_{zz}$ value, whereas the ESR spectra of the sol phase indicate a continuous increase in mobility of spin probes with increasing temperature. The existence of a broad component in the isolated sol phase of the NR matrix confirms the presence of a certain extent of heterogeneity in the movement of spin probe above T_g. However, the intensity of the broad component in the sol phase disappears at a much faster rate at higher temperatures by the expense of the narrow component as compared with the behaviour of the extracted gel phase.

Veksli *et al.* have investigated the NR crosslinked networks prepared by two-stage γ-irradiation of rubber latex with different spatial heterogeneity.[31] The irradiated latex emulsions (L-network) and dried latex (S-network) have different crosslink density. The ESR spectra of spin probe dispersed in both L- and S-rubber networks at different temperatures are shown in Figure 25.10(a) and (b). The shapes of the spectral line of the spin probed L- and S-rubber networks are different at and above -23 °C, referred to the $T_{5\ mT}$ and correlates with T_g of NR matrix. The improvement of narrow component with increase in temperature is higher for S-network in comparison

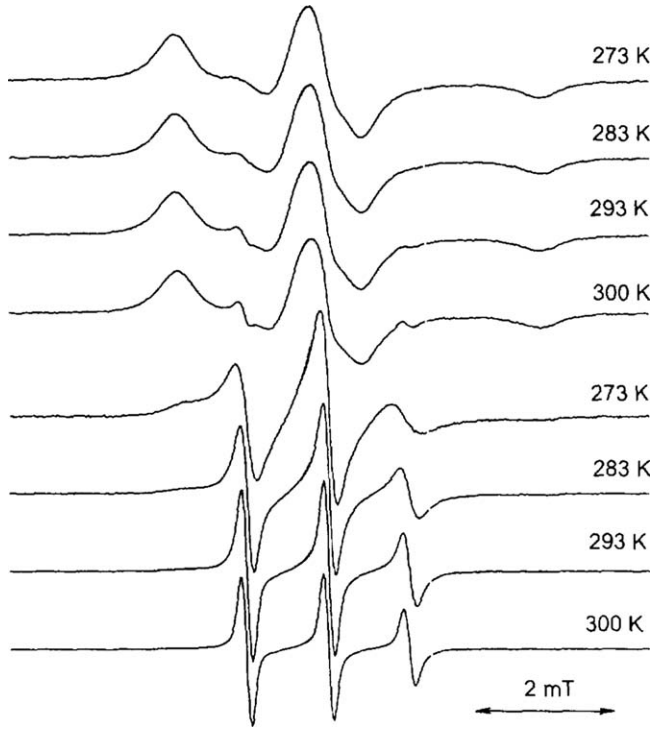

Figure 25.9 ESR spectra of the gel (upper four spectra) and sol (lower four spectra) fractions of high molecular weight spin probed NR matrix at indicated temperatures.
(Reproduced from ref. 30 with permission from Elsevier.)

with the L-network but the amount of broad component is more for L-network than that of S-network. The significant enhancement of the narrow components in case of S-network is attributed to the change in free volume with increasing temperature. Although, the predominant contributors for the broad components are crosslinked domains and network structures but on the other hand, molecular weight, molecular weight distribution, gel phase, and chain branching also contribute to the matrix heterogeneity.[32]

Dubrović *et al*. have studied the NR films crosslinked by γ-irradiation under both relaxed and uniaxial deformation state by ESR.[33] Figure 25.11 shows the ESR spectra of the spin probe diffused non-irradiated and irradiated NR matrix at relaxed state. The intensity of the broad component is more pronounced and the narrow component is strongly reduced in case of the 200 kGy irradiation dose applied crosslinked NR films in comparison with the non-crosslinked NR films at unstretched condition. The ratio of intensity for narrow (I_n) to broad (I_b) spectral lines reduces with application of irradiation, which is due to the decrease in sol components by irradiation induced crosslinking process. The amount of broad component is not pronounced at higher irradiation doses, which may be attributed to the heterogeneous distribution of

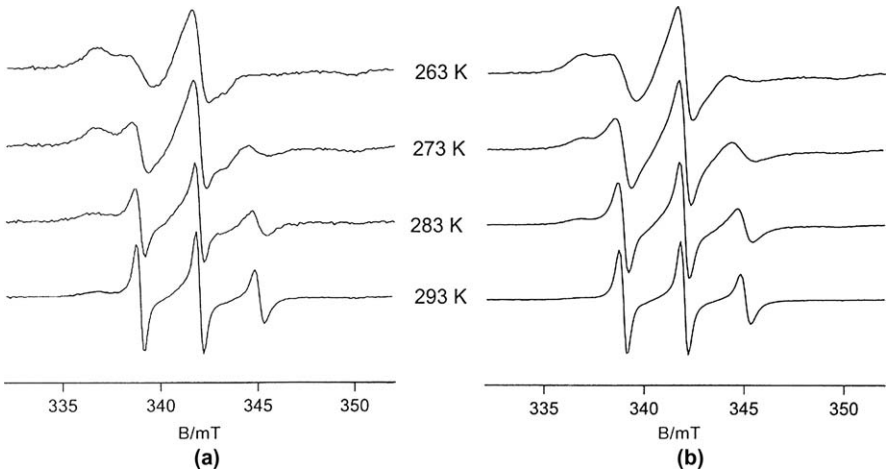

Figure 25.10 ESR spectra of (a) L- and (b) S-natural rubber networks at indicated temperatures.
(Reproduced from ref. 31 with permission from Elsevier.)

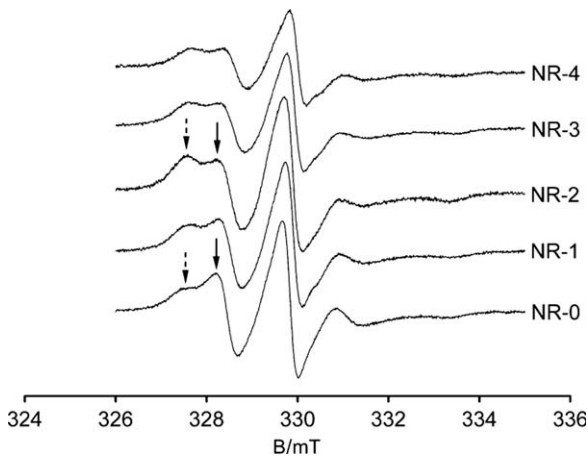

Figure 25.11 ESR spectra of the spin probe incorporated in non-irradiated (NR-0) and irradiated (NR-1, NR-2, NR-3, NR-4 with 100, 200, 300 and 400 kGy irradiation doses, respectively) NR measured at $T_{5\ mT}$. The dashed and full line arrows indicate the broad and narrow lines, respectively.
(Reproduced from ref. 33 with permission from Elsevier.)

the probe molecules in the NR matrix, rather than to the lower amount of high density restricted mobility regions. Actually, higher amount of local density regions are developed at higher irradiation doses, which hinder the spin probe molecules to easily penetrate into the highly dense part of the NR matrix.

ESR spectra of the spin probe in NR films irradiated with 200 kGy at various deformation ratios are shown in Figure 25.12. The shapes of the spectral lines

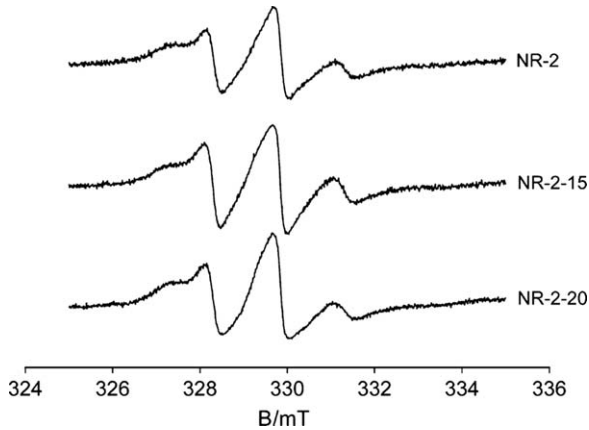

Figure 25.12 ESR spectra of spin probe in NR matrix irradiated with 200 kGy dose for NR-2 ($\lambda = 1.0$), NR-2-15 ($\lambda = 1.5$) and NR-2-15 ($\lambda = 2.0$) samples observed at 6 °C.
(Reproduced from ref. 33 with permission from Elsevier.)

are almost similar and no noticeable change is observed in the intensity of the narrow spectral lines. The values of I_n/I_b ratios for spin probe implanted NR matrix irradiated with 200 kGy dose at undeformed ($\lambda = 1.0$), and uniaxial deformed ($\lambda = 1.5$ and $\lambda = 2.0$) conditions measured at 6 °C are 1.72, 192, 1.71, respectively. It is concluded that the lower deformation ($\lambda = 1.5$) induces effective structural changes within the NR matrix that influence the mobility of the spin probes, contributing to the narrow spectral component. The narrow component is substantially reduced at higher deformation ($\lambda = 2.0$) due to the presence of lower amount of mobile phase in NR matrix. It is noteworthy to mention that the dynamics of spin probe are associated with molecular chain segmental mobility and its orientation.[15] The anisotropic spin probe motions along with slow motion participate for an additional increase in the broad component of ESR spectra. It can be deduced that the polymer chain segmental motion prevails at lower deformation, while the orientation behaviour predominates at higher deformation.

Čulin *et al.* have analysed the effect of thermal oxidative ageing on the network morphology of crosslinked unfilled NR vulcanizate of three model networks with different sulfur cure systems (efficient (NR-A), semi-efficient (NR-B) and conventional (NR-C) by applying spin probe ESR technique.[34] The ESR spectra of three different NR networks (NR-A, NR-B and NR-C) at 20 °C aged with different periods of times are shown in Figure 25.13(a) to (c). The ESR spectra of both aged and unaged rubber networks demonstrate different amounts of broad component. The spin probes in NR-A matrix (monosulfidic sulfur bonds) undergoes restricted motion because tumbling of free probes dispersed in NR matrix depends on available free volume while most of probe molecules exhibit slower motion, which is associated with smaller holes present in the NR matrix. Presence of monosulfidic sulfur bonds in NR-A matrix has small accessible free volume, leading to increase in number

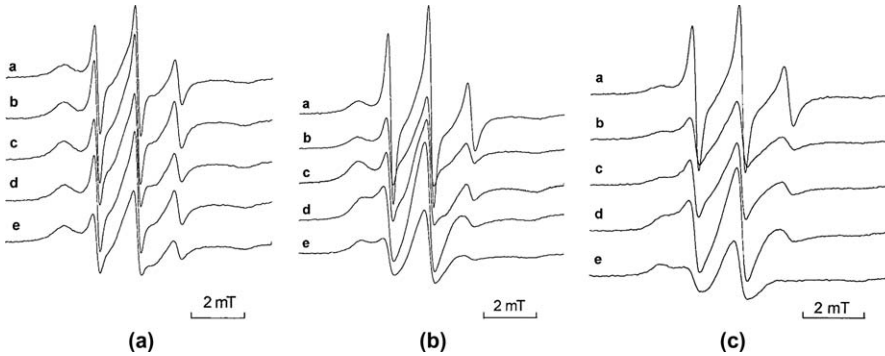

Figure 25.13 ESR spectra of (a) efficiently (NR-A), (b) semi-efficiently (NR-B) and (c) conventionally (NR-C) crosslinked NR vulcanizates at 20 °C aged for (a) 0 h, (b) 48 h, (c) 96 h, (d) 144 h and (e) 240 h.
(Reproduced from ref. 34 with permission from the Society of Chemical Industry.)

of spin probes with restricted motion. The unaged NR-B and NR-C networks (polysulfidic sulfur bonds) exhibit lower amount of broad component due to the larger accessible free volumes in the NR matrix. After 48 h ageing, the ESR spectrum of NR vulcanizate with monosulfidic bonds does not change but the broad component of NR vulcanizates with polysulfidic bonds increases considerably. However, the increase in slow component of NR-A vulcanizate is comparatively higher than that in NR-B and NR-C vulcanizates after 48 h ageing. The restricted spin probes increase with increasing the local density of NR matrix because of the transformation of the initial polysulfidic bonds into mono- and disulfidic bonds.[35] The polysulfidic bond decomposes and recombines at the time of ageing process due to the relatively low bond energy of the polymeric sulfur chains. The excess sulfurs were produced during the desulfurization process without addition of any further curing agents but it is a slow process.[36] The network density of NR-B and NR-C attains lowest value after 96 h ageing because of the formation of cyclic sulfide structures and unreactive pendant groups during thermal ageing,[37] which provide the free volume available for the accommodation of probe molecules. In addition to the modification of molecular backbone chain, main chain scission during the thermal ageing process alters the network structure and crosslink density. The NR-A networks are not changed by the ageing up to 48 h and then broad component increased between 48 and 96 h ageing, but it decreases with further ageing up to 240 h due to reduction in network density. The width and shape of the spectral line for broad component is marginally changed in NR-A but it considerably changed in NR-B and NR-C by the thermal ageing process, resulting in the change in spin probe motions in different network structure. The effects of thermal ageing are also observed in the narrow component, which is associated with the soluble phase. The width of spectral line for narrow component and corresponding τ_R significantly increase after 48 h ageing and it is more pronounced in NR-B and NR-C vulcanizates than in NR-A

vulcanizate, which is due to the change in the local structure of NR matrix with prolonged thermal ageing. The bimodal distribution of the spin probe motion is still present after 240 h ageing, while the shape of spectra lines for both broad and narrow components are broadened due to the wide distribution of τ_R.

25.2.2 ESR Studies of NR Composites

The Jachym research group has conducted ESR experiments in order to investigate the interactions between the NR matrix and carbon black in NR/carbon black composites.[38–41] ESR spectra of free radicals formed during compounding of NR with various carbon blacks were examined in detail. Figure 25.14(a) show ESR spectra of 10–70 phr carbon black-filled NR compounds. In Figure 25.14(a), quite spectral and narrow lines appeared for the composites while a broad spectral line appeared for carbon black alone. Figure 25.14(b) shows ESR spectra of 70 phr carbon black-filled NR compounds prepared at different milling times. It can be seen in the figures that the amplitude of the narrow line is independent of the milling time while it is directly proportional to carbon black content in the compounds. The figures showed that width of the spectral lines is independent of the milling time and

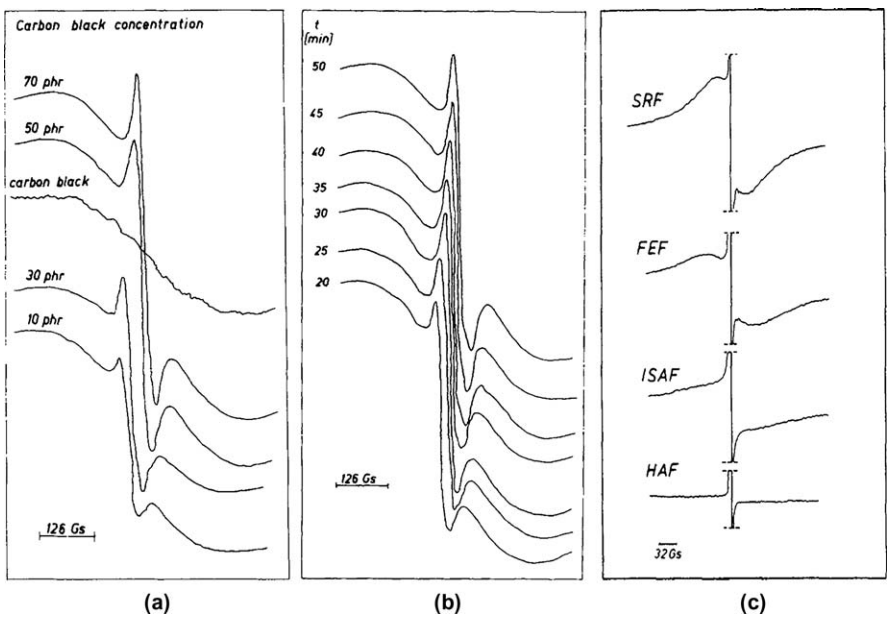

Figure 25.14 ESR spectra of NR/carbon black compounds: (a) with various phr of carbon black loading at 40 min milling time, (b) with various milling times at 70 phr carbon black content, and (c) with various types of carbon blacks at 70 phr carbon black content and 40 min milling time. (Reproduced from ref. 40 with permission from the American Chemical Society.)

amount of carbon black in the systems. It is to be noted in Figure 25.14(a) that position and intensity of the narrow line is changed with the increase in carbon black loading in the composites, which were thought to be related to the presence of interactions between NR and carbon black. Formation of 'bound rubber' resulting from interfacial attractions between NR matrix and carbon blacks has been considered as an important factor for an effective reinforcement in the NR/carbon black composites. Figure 25.14(c) shows ESR spectra of NR/carbon black compounds with various types of carbon blacks. ESR spectra of NR compounds filled with semi-reinforcing furnace (SRF) carbon blacks and fast extruding furnace (FEF) carbon blacks consist of both small broad and demarcated narrow spectral lines. The broad line is diminished for intermediate SAF (ISAF) carbon black-filled system and it is completely disappeared in high abrasion furnace (HAF) carbon black-filled system.

The same research group examined ESR spectra of the NR/carbon black compounds extracted with benzene. ESR spectra of gels and soluble parts of the solvent extracted NR/carbon black compounds are shown in Figure 25.15(a) and (b), respectively. ESR spectrum corresponding to (a) NR matrix, (b) carbon black and (c) interface region of NR matrix and carbon black are observed in the figures. The narrow signals (b and c) also were observed by Sullivan and Wise in ESR spectrum of styrene butadiene rubber (SBR)/ISAF mixtures at cryogenic temperatures.[42] Waldrop and Kraus reported that this narrow ESR component is attributed to the formation of stabilized rubber macro-radicals, resulting from the cleavage of SBR macromolecules that catalysed by the interaction with carbon black particles and this

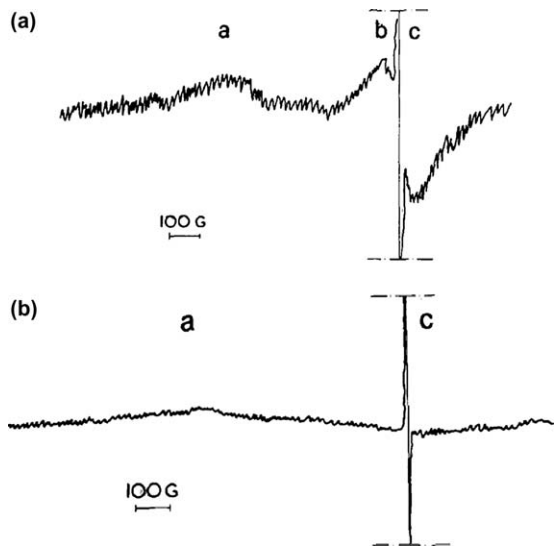

Figure 25.15 ESR spectrum of (a) natural rubber/SRF carbon black gel and (b) soluble parts of NR/carbon black mixtures.
(Reproduced from ref. 39 with permission from Elsevier.)

characteristic spectrum is called as 'rubber spectrum'.[43] Furthermore, Harbour and Walzak showed that the styrene acrylate copolymer/carbon black composites reveal a spectral line derived from the superposition of narrow and broad ESR signals.[44] This broad signal is a conduction ESR (CESR) signal due to the charge carriers within the bands of the carbon blacks.[45] The narrow signal originates from the carbon black, which can accept free electrons from the polymer.[46] However, Cashell and McBrierty reported that a similar signal was not shown at ambient temperature for carbon black-filled polybutadiene (BR).[47] Ellis and Baugher noted that this permanent asymmetric free radical ESR signal must be due to the presence of some paramagnetic impurities in the pure masticated SBR rubber,[48] which was confirmed by O'Brien *et al.*'s studies on the unfilled BR.[49,50] Mead *et al.* employed ESR measurement to study the oxidation of peroxide crosslinked BR and polyisoprene (IR) after uniaxial deformation at cryogenic temperatures.[51,52] Effects of oxygen, UV radiation, temperature and heat treatment on the oxidation of diene rubbers are extensively investigated via ESR spectra of the samples. Kawakubo and coworkers showed ESR spectra for carbon black and silica filled IR vulcanizates are similar in shape and having identical *g*-value (2.0001), as shown in Figure 25.16(a) and (b).[53] The spectrum of carbon black-filled IR is marginally broader as compared to that of the silica-filled IR at the same filler loading and the spectra showed almost equal intensity. Kawakubo *et al.* also reported that the signal intensity of the carbon black-filled NR increases upon stretching without changing the shape and the *g*-value, while the pure gum and the silica-filled rubbers show little change in the intensity.[53] Brosseau *et al.* reported that the size distribution of the carbon black aggregates affects the ESR spectral

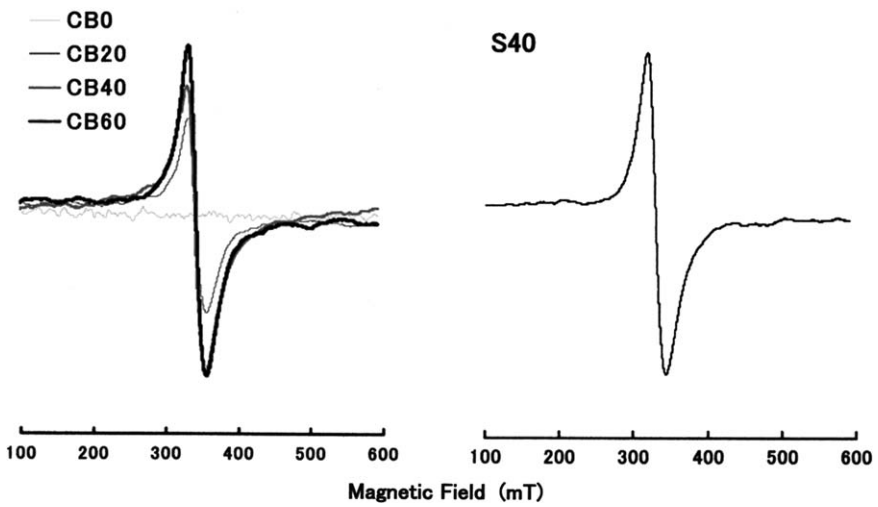

Figure 25.16 The ESR spectra of IR (CB0), 20 phr (CB20), 40 phr (CB40) and 60 phr (CB60) carbon black filled and 40 phr (S40) silica filled IR vulcanizates. (Reproduced from ref. 53 with permission from the American Chemical Society.)

feature, which result in either symmetrical or asymmetrical line shapes.[54] The spectral lines for the gel and soluble parts are varied with types of carbon blacks, content of carbon blacks, and time of milling. Spectrum for gel consists of three conventional first derivative peaks, whereas the spectrum for soluble parts displays only two lines. Broad and narrow lines are present for the gel and soluble parts, whereas small lines are not shown in spectrum for soluble parts. In the spectrum for the extract, a small intensity ESR spectral line, which was appeared in the spectrum of both soluble parts of NR/carbon black mixtures and carbon black alone was not observed, even though the extract contains carbon blacks. This can be an evidence for the presence of chemical interactions between carbon black radicals and NR macro-radicals in the NR/carbon black compound. For NR/carbon black compounds with low carbon black contents, all reactive centres present on the carbon black surface are completely occupied by NR microradicals and thereby no coherent space lattice is created in the system. ESR spectra of soluble parts of extract showed only one line, which is assigned to the plasticized NR matrix,[38] and the intensity of the spectral line is greatly affected by the types and content of carbon black as well as the milling time. But, the intensity of the narrowest spectral line of the gels is unaltered with filler content and milling time.

Figure 25.17 shows that intensity of the narrowest line of the soluble parts of the extract depends on the carbon black content as well as milling time. Concentration of free radicals in NR/carbon black gels was calculated from intensity of the narrowest spectral line and the value is about 4×10^{17} sp/g. The results indicate that the quantity of the reactive centres, which is responsible for the formation of the stable gels due to the NR and carbon black interactions, is constant.

The concentration of unpaired spins corresponding to the carbon black only is calculated from the ESR spectral intensity of the broad component line. The relationship between the number of unpaired spins and compounding time is the same for all the NR compounds filled with various carbon blacks. The

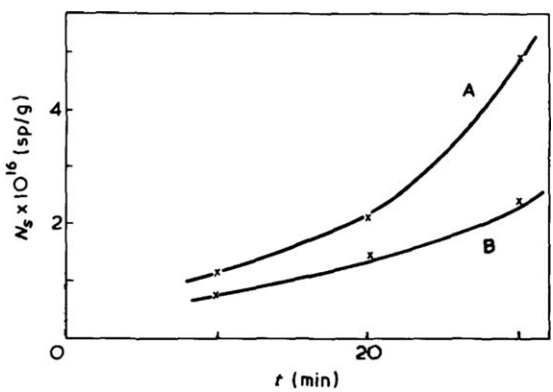

Figure 25.17 Variation of unpaired spin concentration (N_s) with milling time (t) for NR/SRF carbon black compounds extract.
(Reproduced from ref. 39 with permission from Elsevier.)

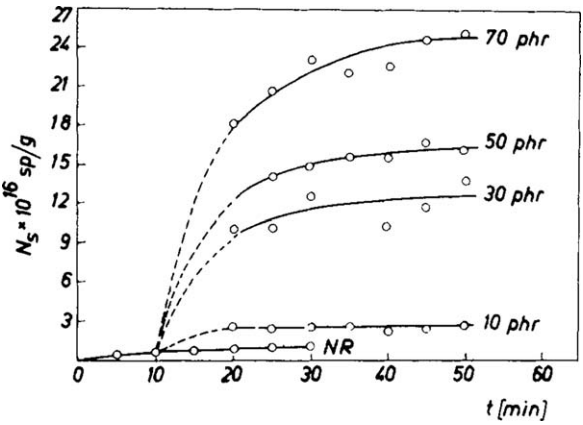

Figure 25.18 Dependence of unpaired spin concentration (N_s) on the milling time (t) for NR/carbon black compounds with various carbon black loading. (Reproduced from ref. 40 with permission from the American Chemical Society.)

number of carbon black radicals is not affected by the milling time but it is varied at initial stage of mastication process, which is due to the reduction in size of the carbon black particles as well as increased active surface area that facilitates the mutual interactions. Further, Figure 25.17 shows that the narrow spectral line component is affected by the milling time.

Figure 25.18 shows the variation of N_s as a function of milling time for NR/carbon black compounds with different carbon black loading. The plots are the same for all types of carbon black (SRF, FEF, ISAF, and HAF) filled NR systems. Initially, 10 min milling time is required for generation of adequate number of unpaired spin and then the concentration of unpaired spin is increased at a maximum rate. Subsequently, rate of increase in radical concentration decreased with increased mastication time and finally it reached a constant value where the applied shearing force does not cause any further cleavage of the NR chains. The saturation value for unpaired spin is achieved at higher milling time with increasing carbon black content. The concentration of free radicals for NR/carbon black compounds with different carbon black loading is substantially higher than that of plasticized unfilled NR.

Figure 25.19 shows the maximum unpaired spin concentration versus specific surface area of various carbon blacks. The increasing order of the free radical concentration of various types of carbon blacks is TM-15 $<$ HAF $<$ SRF $<$ FEF $<$ ISAF. The results are related to the concentration of free radicals on the surface of carbon blacks, *i.e.* concentration of free radicals for the carbon blacks become higher for the carbon blacks having higher specific surface area. This indicates that the interfacial interactions between NR matrix and carbon black are governed by the active surface area of the carbon blacks.

Figure 25.20(a) and (b) show the variation of unpaired spin concentration as a function of TM-15 and HAF carbon blacks content in NR compounds,

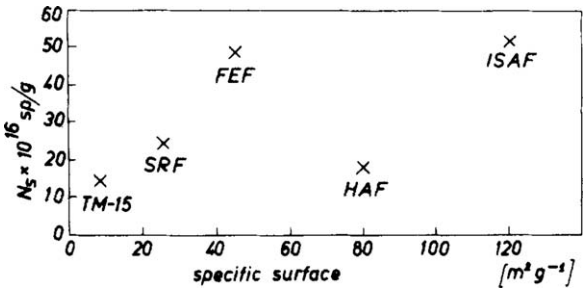

Figure 25.19 The maximum unpaired spin concentration versus specific surface area of various carbon blacks.
(Reproduced from ref. 40 with permission from the American Chemical Society.)

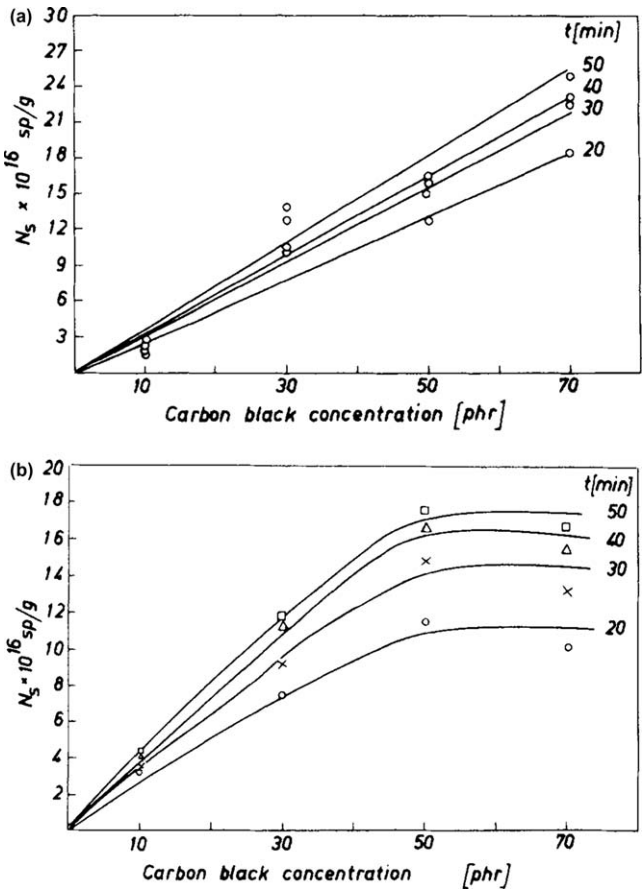

Figure 25.20 The variation of unpaired spin concentration as a function of (a) TM-15 and (b) HAF carbon black content in NR compounds.
(Reproduced from ref. 40 with permission from the American Chemical Society.)

respectively. For TM-15 carbon black-filled NR compounds, the relationship between unpaired spin concentration and carbon black content is linear over a whole range of the carbon black content investigated. For HAF carbon black-filled NR compounds, the linear relationship is retained up to 50 phr filler content and the unpaired spin concentration reached a saturation value with higher carbon black content. The highest level of NR–carbon black gel phase occurred at 50 phr active carbon black loaded NR compounds. Previously, it was reported that the maximum reinforcing effects is achieved at 50 phr carbon black loaded rubber compound.[55] The deviation of the relationship from linearity for higher carbon black loadings is most probably due to the increase in mutual interaction among them, which reduces the effective surface area required for NR–carbon black interactions. These relations are in good agreement with electron microscopy and gel permeation chromatography analysis.[56,57]

Siswanto *et al.* reported the ESR studies on NR/carbon black composites filled with four different types of carbon blacks.[58] The ESR spectra of unfilled NR matrix and HAF carbon black is shown in Figure 25.21. ESR signal of the unfilled NR matrix is not detected even at a high modulation or a high magnetic field. The ESR spectrum of HAF carbon black displays a broad spectral signal with *g*-value close to that for the free electron. Figure 25.22(a)–(c) show ESR spectra of 10, 25 and 45 phr HAF carbon black-filled NR compounds at 298 K and 77 K, respectively. Figure 25.23(a) to (c) show the ESR spectra of 45 phr Vulcan P, Vulcan XC-72 and Black Pearls 2000 carbon blacks filled NR compounds at 298 K and 77 K, respectively. The ESR spectra showed that shapes of spectral lines are varied with the types of carbon blacks. The *g*-values and line widths obtained from the spectra are summarized in Table 25.1. It is observed from Table 25.1 that magnitudes of the *g*-values for various carbon black-filled NR composites are slightly higher than those of the free electrons without any evidence of orbital momentum. The detected *g*-values

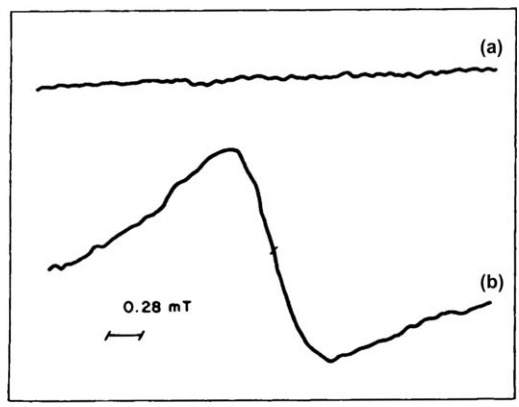

Figure 25.21 The ESR spectra of (a) unfilled NR matrix and (b) HAF carbon black. (Reproduced from ref. 58 with permission from the American Chemical Society.)

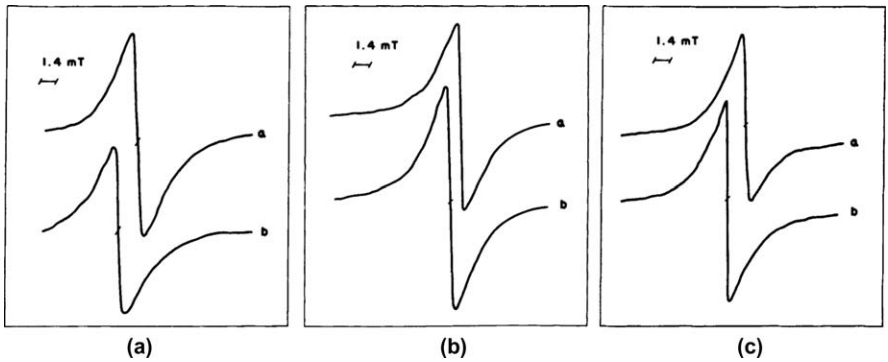

Figure 25.22 The ESR spectra of (a) 10 phr, (b) 25 phr and (c) 45 phr HAF carbon black filled NR compounds at (a) 25 °C and (b) −196 °C.
(Reproduced from ref. 58 with permission from the American Chemical Society.)

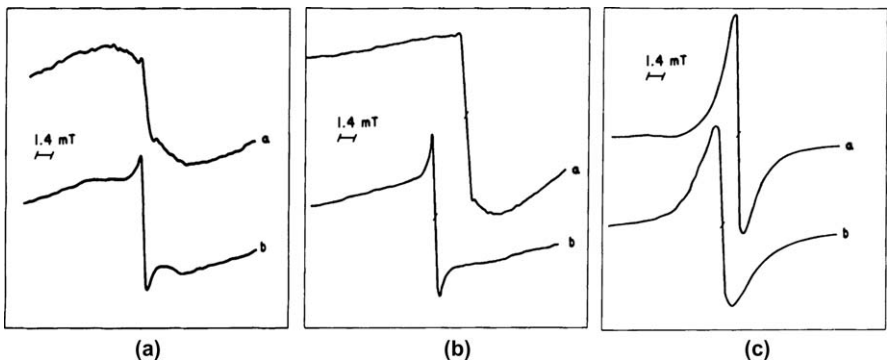

Figure 25.23 The ESR spectra of 45 phr (a) Vulcan P, (b) Vulcan XC-72 and (c) Black Pearls 2000 carbon black filled NR compounds at (a) 25 °C and (b) −196 °C.
(Reproduced from ref. 58 with permission from the American Chemical Society.)

Table 25.1 ESR spectral characteristics of different carbon black-filled NR composites. (Reproduced from ref. 58 with permission from the American Chemical Society.)

Carbon black type	*Concentration (phr)*	*g-value*	*Line width (gauss) (298 K)*	*77 K*
HAF	10	2.0027	10.0	8.0
HAF	25	2.0028	9.0	4.6
HAF	45	2.0028	6.3	3.6
Vulcan P	45	2.0029	11.5	4.4
Vulcan XC-72	45	2.0028	11.0	4.7
			47.0	50.0
Black Pearls 2000	45	2.0028	17.6	18.2

were unaltered with temperature. Line width of ESR spectra of NR/carbon black composites are much narrower than that of pure carbon black, which is caused by the paramagnetic centres that formed in the chemically modified NR matrix present at the interface region between the carbon black aggregates. The nature of the paramagnetic centres acting as traps depends on both types of carbon blacks and chemical nature of the composites. Basically, two types of ESR spectra are detected in HAF and Black Pearls 2000 carbon blacks filled NRs and in Vulcan P and Vulcan XP-72 carbon blacks filled NRs, which are further supported by the space charge limited current (SCLC) characteristics.[58]

ESR spectra of 10, 25 and 45 phr filled NR composites consist of a high intensity single spectra line as presented in Figure 25.22(a)–(c), respectively. Line widths of these spectral lines measured both at 298 K and 77 K noticeably decrease with the increase in HAF carbon black content without any shift in the *g*-values, which is a result of enhanced exchange narrowing due to the increase in electron spin concentration or non-orbital electrons. Amplitudes of the spectral lines substantially increase with an increase in carbon black content. It is also noticed that the line widths significantly narrowed at 77 K than that at 298 K because of the dimensional change, *i.e.* shrinkage of the NR matrix induced the increase in the spin concentration but other things remain unaltered.

ESR spectra for Vulcan P and Vulcan XC-72 carbon black loaded NR composites comprised of two distinct lines as shown in Figure 25.23(a) and (b), respectively. The spectra show better resolution at lower temperature and narrow line were saturated faster than the spectral line at higher temperature. These two spectral lines support that trap is distributed with energy that occurred well below the edge of conduction band (deep), which are consistent with the SCLC characteristics. The existence of electrons within a trap spread across a certain energy range results in the observed broadening of the ESR lines. Figure 25.23(c) shows spectra of Black Pearls 2000 carbon black-filled NR composites in which a single line was observed and the line width of the single lines is slightly broader at 77 K than at 298 K. The ESR and SCLC results are in good agreement with the model of electron hopping transport where traps play a prominent role. The distribution of traps depends on the types of carbon blacks present in the NR matrix.

Baccaro *et al.* have investigated the chemical interactions between N375 carbon black and NR matrix under electron beam irradiations.[59] In their ESR studies, effects of radiation dose on free radical concentration were evaluated by applying 191 kGy, 499.5 kGy and 1 MGy irradiation doses to the compounds at 2 kGy/h dose rate. The results are shown in Figure 25.24(a). The shapes of the ESR spectra remain unchanged with different radiation doses, whereas intensity of the derivative peaks change with the radiation doses. It is assumed that the radiation-induced free radical concentration may be proportional to the peak-to-peak intensity signal. The intensity of the spectra lines increases up to 499.5 kGy and then decreases at 1 MGy radiation dose. The

high concentrations of carbon black radicals favour recombination between themselves at higher radiation dose.

Effects of dose rate on free radical concentration are shown in Figure 25.24(b). It is observed that the peak intensity attained maximum value at around 500 kGy and then decreases. Because the free radicals are also formed in un-irradiated carbon blacks at the preparation process, the peak-to-peak ESR signal value recorded before the application of radiation (H_0)

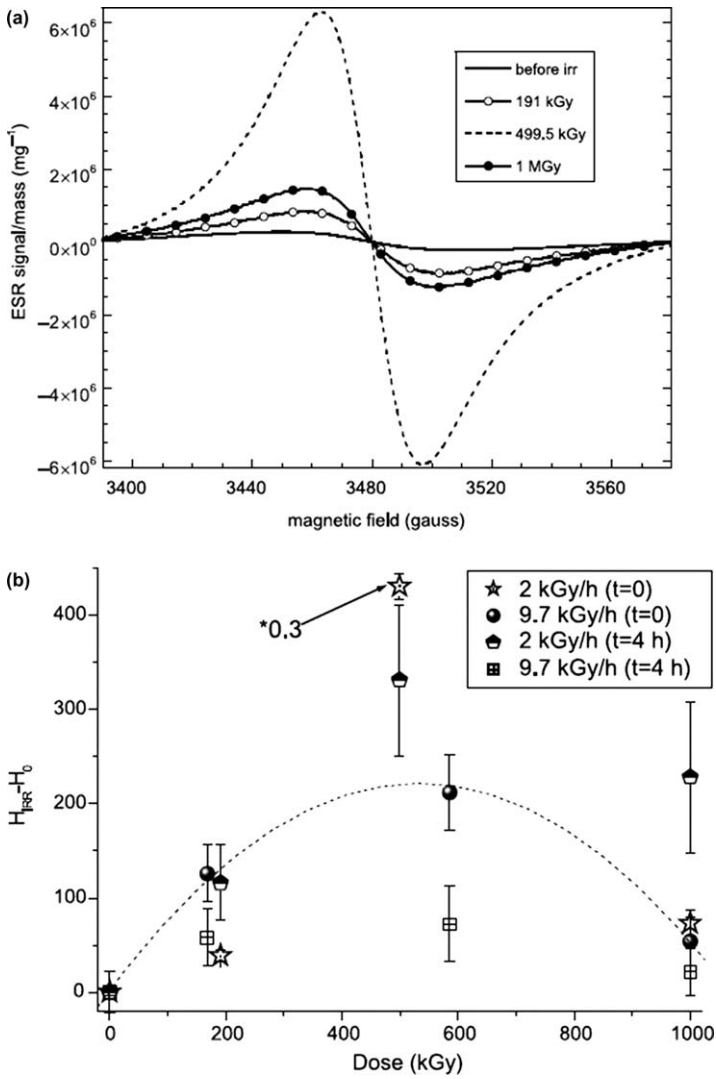

Figure 25.24 ESR spectra of carbon black (a) after different irradiation doses and (b) after different radiation dose rate.
(Reproduced from ref. 59 with permission from Elsevier.)

must be subtracted from each signal measured after the radiation (HIRR). The concentration of radiation-induced free radicals depends on the applied radiation dose rate but the peak intensity for 2 kGy/h dose rate is higher than that for 9.7 kGy/h dose rate.

Effects of dose rate on the concentration of free radicals were examined by performing the test at 163 kGy dose with a dose rate of 1 kGy/h, and the results are shown in Figure 25.25(a). Concentration of free radicals decreases with increasing dose rate, *i.e*. the lower dose rate produced higher concentration of radicals. Decay kinetics of the radiation-induced carbon black free radicals were measured by taking ESR of samples at an interval of 3–5 min after withdrawal of the radiation source. Figure 25.25(b) shows the measured decay

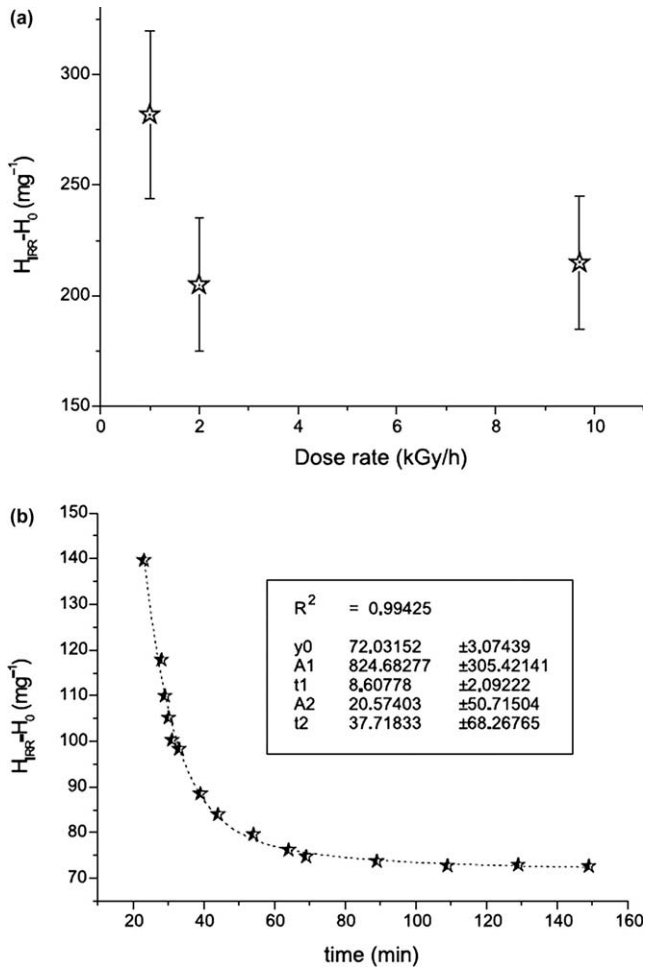

Figure 25.25 ESR signal of carbon black (a) dependence on the dose rate and (b) decay kinetic.
(Reproduced from ref. 59 with permission from Elsevier.)

kinetics of the radiation-induced carbon black free radicals by the superposition of two exponential components with two time constants of 8.6 and 37.7 min after 585.5 kGy irradiation doses. The ESR signal intensity did not change after 1 h of removal of radiation source and shows a characteristic plateau region. The results indicated that the chemical bonds between the NR and carbon black are formed by the combination of free radicals existed in NR and at the surface of carbon blacks, which are not destroyed in the decay process.

Scotti *et al*. have carried out the ESR measurements to study the extent of crosslinking of NR matrix in the NR/differently modified silica composites.[60] The ESR spectra for uncured NR/silica composites embedded with the TEMPOL spin probe by toluene swelling procedure was investigated after the removal of uncrosslinked NR chains by a solvent extraction. Typical representative ESR spectrum of NR/silica composites is shown in Figure 25.26(a). The spectra of both unmodified silica and modified silica filled NR composites show very strong broad anisotropic signals (I_{ani}) of nitroxide, which are due to low movement of spin probe in a highly crosslinked matrix. The much less intense narrow isotropic signals (I_{iso}) were overlapped by resonances due to fast motion of spin probe units. The separation between the outer components of the ESR signals ($2A_{zz}$) increases from $\approx$ 30 Gauss for I_{iso} to 72 Gauss for I_{ani}. The results revealed that mobility of the spin probe is comparatively very low in crosslinked NR/silica composites due to the high density of NR matrix as well as the presence of small number of free volume holes. The small amount of fast motion signals is attributed to the presence of residual free volumes in the crosslinked NR/silica composites. The intensity ratios (peak height of I_{ani} to I_{iso}) of signal were evaluated to estimate the contribution of the two overlapping species of NR/silica composites, as shown in Figure 25.26(b). The higher magnitude of I_{ani}/I_{iso} indicates the prevention of slow motion components which are related to the higher degree of crosslinking of the NR/silica composites and lower size of free volume holes.

Suzuki *et al*. studied the effect of applied initial strain on the radical concentration of unfilled and silica filled SBR vulcanizates.[61] Figure 25.27(a) shows the ESR spectra of unfilled SBR vulcanizates (UF) imposed with different strains, which were measured after one week of sample preparation at $-100\ ^{\circ}C$. UF samples show a broad ESR absorption curve in the unstretched state. The *g*-value and the line width at the maximum slope (ΔH_{msl}) for the absorption curve were 2.004 and 1.5 mT, respectively, which was assigned to the polyenyl free radicals ($-(C{=}C)_n-C$).[62,63] The intensity of ESR signals for UF samples increases with increasing strain without altering the *g*-value and ΔH_{msl}, which suggest that the allyl radicals formed during the stretching at room temperature were transformed into polyenyl radicals.

The first derivatives of ESR curves for unmodified silica filled SBR vulcanizates (UM-1) with different initial strains are shown in Figure 25.27(b). The results were qualitatively similar to those for unfilled SBR vulcanizates. The UM-1 sample shows a broad absorption curve with the *g*-value of 2.004 and ΔH_{msl} of 1.5 mT, which is independent of the initial strain. The intensity of

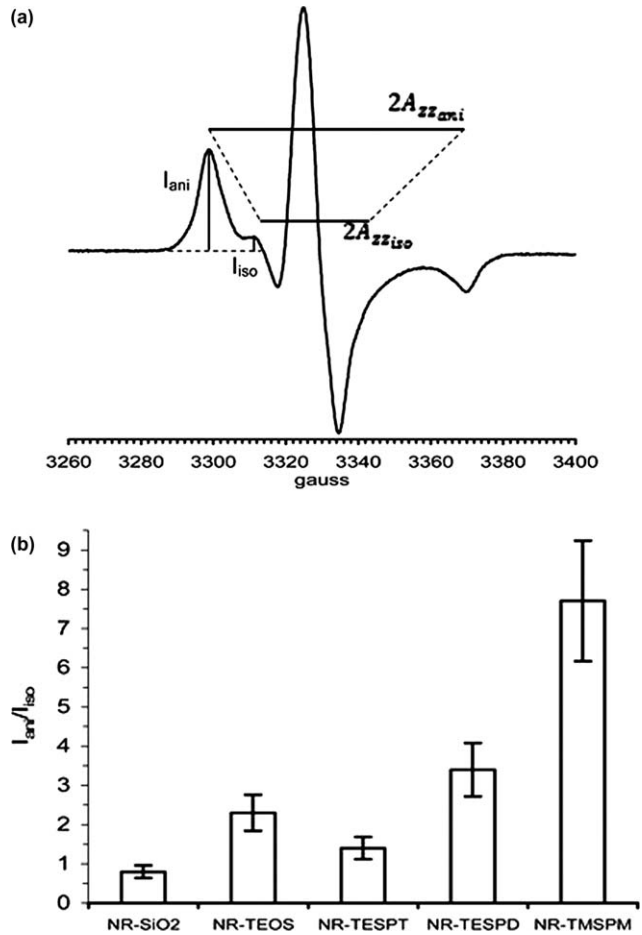

Figure 25.26 (a) Representative ESR spectrum of NR/silica composites and (b) I_{ani}/I_{iso} ratios of NR/silica composites.
(Reproduced from ref. 60 with permission from the Royal Society of Chemistry.)

ESR signals increases with increasing initial strain. The intensity of ESR signals of filled and unfilled SBR vulcanizates are different from each other due to the difference in the degree of chain scission caused by the considerably higher mixing torque for silica filled system than that for unfilled system.

Ito *et al*. examined the ESR spectra of surface modified silica filled SBR unvulcanizates to get information on the filler/rubber interactions.[64] The ESR spectra of vinyl trimethoxy silane (VS) modified silica filled SBR unvulcanizates (U-VS) and (bis(triethoxysilyl propyl)-tetrasulfide (TESPT) modified silica filled SBR unvulcanizates (U-TESPT) measured at −100 °C and at different initial strains are shown in Figure 25.28(a) and (b), respectively. It is found that the intensity of signals increases with increasing initial strain without changes in

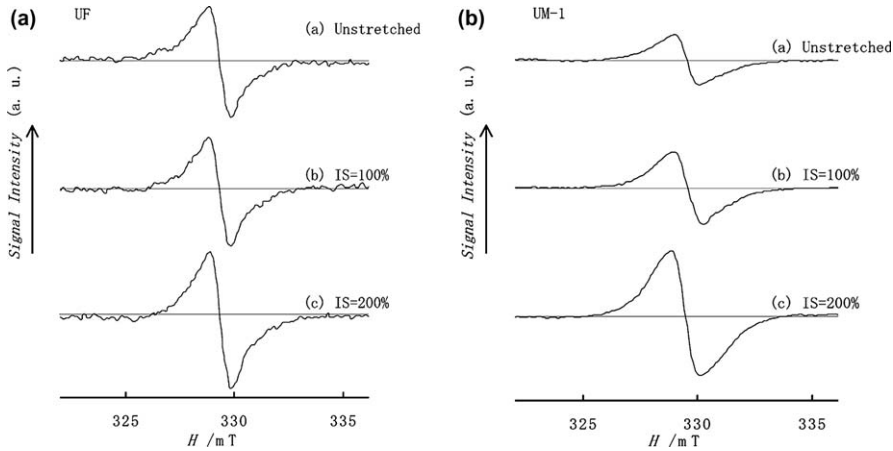

Figure 25.27 ESR spectra of (a) unfilled and (b) silica filled SBR vulcanizates at different strain.
(Reproduced from ref. 61 with permission from Elsevier.)

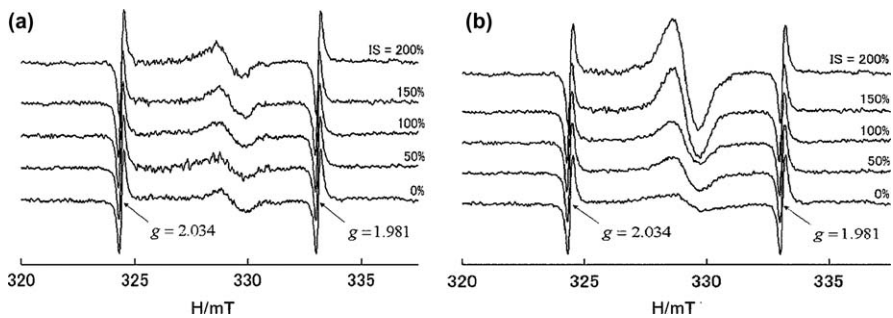

Figure 25.28 ESR spectra of (a) U-VS and (b) U-TESPT with different ISs at −100 °C.
(Reproduced from ref. 64 with permission from Wiley Periodicals.)

the *g*-value and ΔH_{msl}. The unstretched samples also show spectral line corresponding to small amount of rubber macro-radicals during mixing at high shear. The mixing torque increases by the incorporation of silica into SBR matrix, thereby the concentration of free radicals enhances in the filled rubber.

Figure 25.29(a) and (b) show the variation of radical concentration produced by the stretching (ΔC_R) with strain for unvulcanized and vulcanized silica filled SBR composites with different coupling agents, respectively. The magnitude of ΔC_R is comparatively higher for vulcanized samples than that of unvulcanized samples because of the effective interconnected crosslinked network structures in the vulcanizates. The crosslinked networks successfully suppress the chain slippage during tensile stretching and thereby the stress applied on the molecular chain is higher for vulcanizates than for unvulcanizates. The values of ΔC_R slightly increases up to 100% strain for methyl trimethoxy silane modified

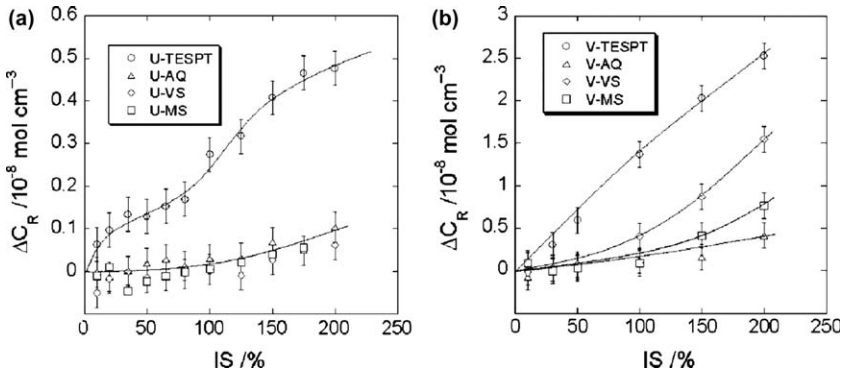

Figure 25.29 Dependence of ΔC_R on IS for (a) the unvulcanizates and (b) the vulcanizates.
(Reproduced from ref. 64 with permission from Wiley Periodicals.)

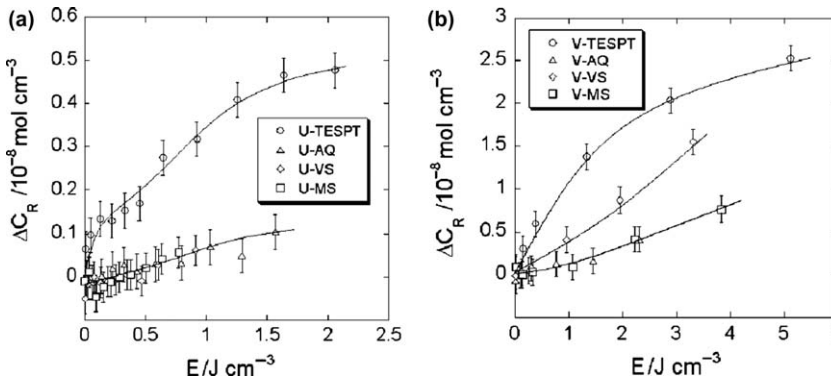

Figure 25.30 Relationship between the mechanical energy (E) and ΔC_R for (a) the unvulcanizates and (b) the vulcanizates.
(Reproduced from ref. 64 with permission from Wiley Periodicals.)

silica, and precipitated silica filled SBR vulcanizates without coupling agent and unvulcanizates, followed by a gradual increase with increasing IS. It is noted that the rates of increase in ΔC_R values with IS are significantly larger in case of U-TESPT and V-TESPT as compared to other samples. However, the values of ΔC_R for U-TESPT and V-TESPT (TESPT modified silica SBR vulcanizate) gradually increase with increasing IS.

Figure 25.30(a) and (b) show the variation of ΔC_R of unvulcanizates and vulcanizates with applied mechanical energy (E) at a given stretching. The values of E are calculated from the area of stress–strain curves at a certain strain. The values of ΔC_R for U-VS, U-MS and U-AQ are almost independent of E up to 0.5 J/cm^3 due to the breakdown of least amount of –C–C– linkages but then slightly increase with the increasing E values after a critical point. Mono-functional coupling agents with alkyl groups (VS and MS) act as

plasticizer for unvulcanized rubber matrix, which causes chain slippage under tensile deformation, which diminished the efficient chain extension and results in low ΔC_R values. Comparatively, in U-TESPT, the ΔC_R values improved noticeably with increasing E values even below 0.5 J/cm^3, which is more prominent in V-TESPT. It is also found that the magnitudes of ΔC_R of vulcanizates at a given E value is much large than those of the unvulcanizates, because the applied strain is effectively transferred into the rubber molecular chains without any chain slippage in the vulcanizates. The value of ΔC_R for the U-TESPT shows a stepwise increase with the increasing E values, while it shows a continuous increase for the V-TESPT.

Klepac extensively studied the effect of uniaxial deformation on the molecular chain segmental mobility of linear low density polyethylene (LLDPE) by ESR spin probe method.[65] The simulated ESR spectra of undeformed and deformed (parallel and perpendicular) LLDPE samples at 0 °C are shown as dotted line in Figure 25.31. The results obtained by simulations indicate that the amount of slow components and corresponding τ_R of LLDPE films deformed in both parallel and perpendicular directions are significantly larger than those of the undeformed LLDPE films. However, the amount of fast components decreased in the deformed sample. It was concluded from the results that uniaxial deformation reduces the molecular chain segmental mobility in the amorphous region and increased the amount of crystalline phase of the LLDPE films.

Funatsu *et al*. examined the change in free radical concentration of sulfur and peroxide cured *cis*-1,4-polyisoprene rubber (IR) vulcanizates during tensile deformation.[66] Figure 25.32 shows the first derivative ESR curves determined

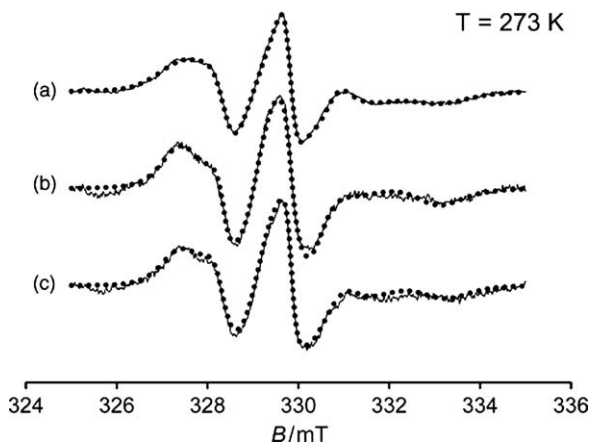

Figure 25.31 ESR spectra of (a) undeformed ($\lambda = 1.0$), (b) parallel deformed ($\lambda = 2.0$) and (c) perpendicularly deformed ($\lambda = 2.0$) LLDPE films at 0 °C (continuous and dotted lines represent experimental and simulated spectra, respectively).
(Reproduced from ref. 65 with permission from the Society of Chemical Industry.)

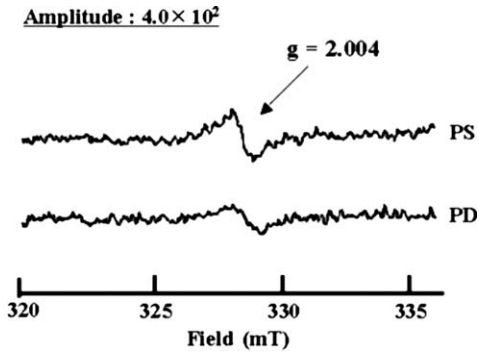

Figure 25.32 ESR spectra of vulcanized samples with 200% strain at −20 °C. (Reproduced from ref. 66 with permission from Wiley Periodicals.)

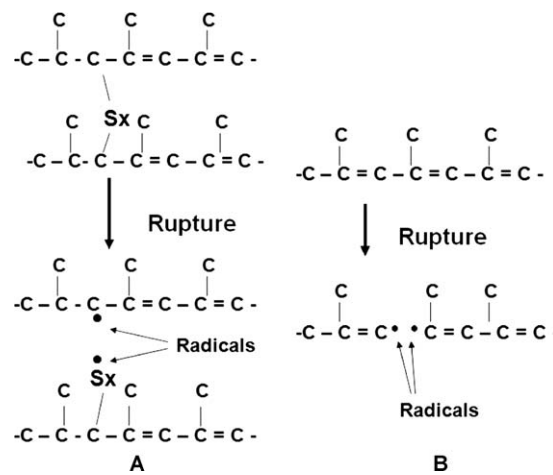

Figure 25.33 Schematic models of rupture process of sulfur vulcanization and carbon–carbon bond. (A) sulfur network and two radicals (sulfur and carbon radical) after rupture, and (B) molecular chain and carbon radicals after rupture.
(Reproduced from ref. 67 with permission from Elsevier.)

at −20 °C for both sulfur cured IR and peroxide cured IR when they are under 200% strain. Both rubber vulcanizates show broad signals with *g*-value of 2.004 and ΔH_{msl} of 1.55 mT, which are caused by the cleavage of –C–C– bond in peroxide cured IR and by cleavage of both –C–C– bond, –C–S_x–C– ($x = 1$ to 8) bond and –C–S–C– bond in sulfur cured IR.[62,63] The rupture of crosslinked network and polymer chains occur during the deformation and generate carbon (–C·) and sulfur (–S·) free radicals. A schematic model to represent the phenomena is shown in Figure 25.33.[67] It is observed that the intensity of the signals is substantially higher in sulfur cured IR than in peroxide cured IR. The radical concentration values calculated from spectra is higher for sulfur cured IR (3.8×10^9 mol/cm^3) than that of peroxide cured IR (0.9×10^9 mol/cm^3),

because the –C–S–S–C– and –C–S–C– bond break more easily than the –C–C– bond due to smaller binding energies of the latter bonds.[68]

25.2.3 ESR Studies of NR Nanocomposites

Valić applied TEMPOL spin probe ESR technique to nano-silica and nanoclay particles filled NR nanocomposites.[69] Figure 25.34 shows the ESR spectra of 10 phr nano-silica filled NR nanocomposites doped with spin probe obtained at the temperature range of −100 to 80 °C. The shape and width of the spectral lines significantly changed with test temperatures. The spectra obtained at temperature below glass transition temperature ($T_g \approx -57$ °C from differential scanning calorimetry (DSC) analysis) of NR are composed of three

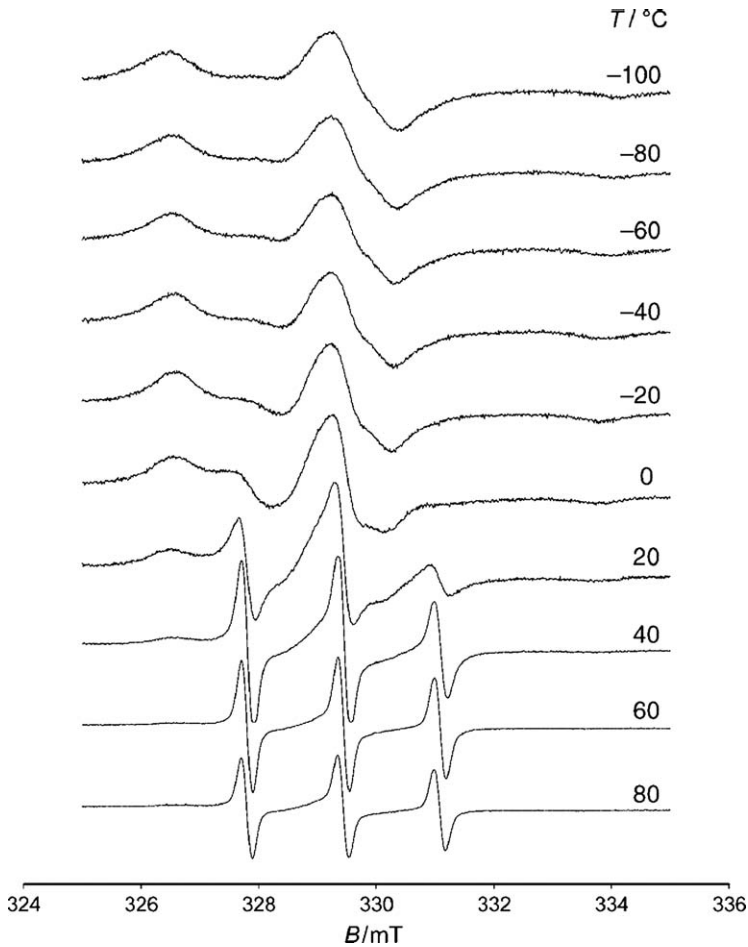

Figure 25.34 ESR spectra of spin probe for 10 phr nano-silica-based NR nanocomposites at different temperatures.
[Reproduced from ref. 69 with permission from John Wiley & Sons.)

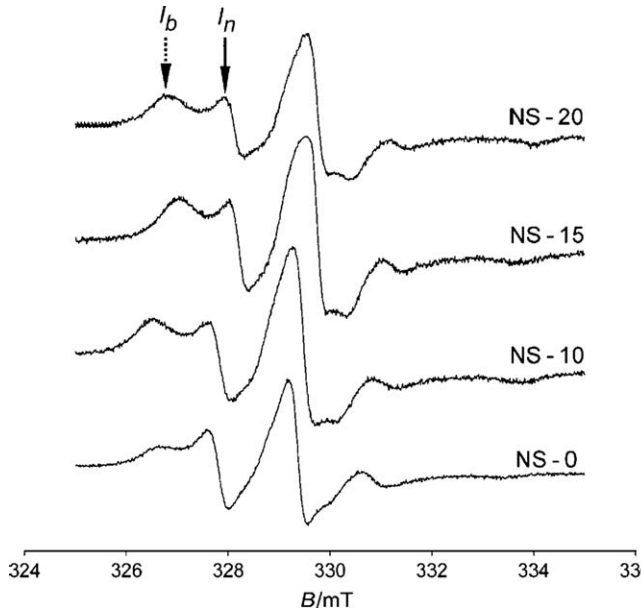

Figure 25.35 ESR spectra of spin probe for 0, 10, 15 and 20 phr nano-silica-filled NR nanocomposites at 10 °C.
(Reproduced from ref. 69 with permission from John Wiley & Sons.)

superimposed broad lines which were attributed to the characteristics of a solid matrix, whereas three distinct narrow lines are shown at a higher temperature region, which are due to rapid mobility of the spin probes.[15] The spectra obtained at both 0 °C and 20 °C constitute three broad and three narrow lines, which imply the existence of two dynamically different spin probe populations assigned to the slow and fast movements.

Figure 25.35 represents the ESR spectra of spin probe for NR nanocomposites containing 0, 10, 15, and 20 phr nano-silica. It is observed that the intensity of the broad (I_b) and narrow (I_n) spectral lines mostly depends on the concentration of nano-silica in the NR matrix. The magnitude of ratios of I_n/I_b continuously decreased from a unit of 1.72 to 0.92 with increase in nano-silica content from 0 to 20 phr. However, a substantial distinction is present among the unfilled NR vulcanizate and NR nanocomposites filled with various amounts of nano-silica. Height of a broad component in the ESR signal for the nanocomposites significantly increases with the increasing nano-silica content. Movement of spin probe is restricted by the interfacial interactions between nano-silica and NR matrix in the nanocomposites, and the interactions increase with increasing nano-silica content in the nanocomposites. The segmental mobility of the spin probe is also affected by the aggregation tendency of the nano-silica as at higher filler loading.

Effect of the coupling agent on the motion of spin probe was examined by incorporation of 4 phr coupling agent into 10 phr silica nanoparticle filled NR nanocomposites. The ESR spectra of spin probe for NR/nano-silica

nanocomposites with and without coupling agent are shown in Figure 25.36. The ESR spectral line of NR/nano-silica nanocomposites without coupling agent shows prominent narrow component. However, it is completely diminished by the addition of coupling agent. The values of I_n/I_b ratios for NR/nano-silica nanocomposites with and without coupling agent are 0.31 and 0.96, respectively.

Figure 25.37 shows the variation of the $2A_{zz}$ of ESR spectra as a function of temperature. The broad component of the ESR spectral lines for

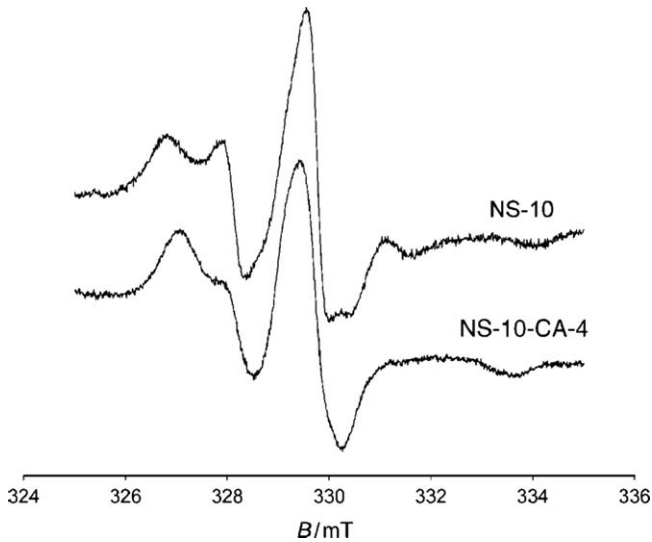

Figure 25.36 The ESR spectra of spin probe for 10 phr nano-silica-based NR nanocomposites at 10 °C without and with 4 phr coupling agent. (Reproduced from ref. 69 with permission from John Wiley & Sons.)

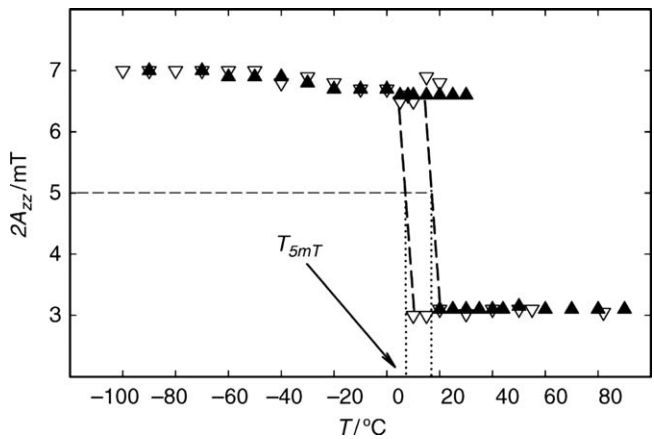

Figure 25.37 The temperature dependence of the $2A_{zz}$ of ESR spectra for the NR/nanosilica nanocomposites with (▲) and without (▽) coupling agent. (Reproduced from ref. 69 with permission from John Wiley & Sons.)

NR/nano-silica nanocomposites with coupling agent is present up to 30 °C, while it disappeared at 20 °C for the nanocomposites without coupling agent. Values of $T_{5\ mT}$ calculated from the plot are 16 and 7 °C for NR/nano-silica nanocomposites with and without coupling agent, respectively. The change in the shape of the ESR spectra and value of $T_{5\ mT}$ revealed that presence of coupling agent in NR/nano-silica nanocomposites effectively enhanced the interaction between nano-silica and NR matrix; as a consequence, the segmental motion is hindered by the presence of coupling agent.

ESR spectra of spin probe for NR/nanoclay nanocomposites (10 phr Cloisite 20A) measured in the temperature range of −100 to 80 °C are shown in Figure 25.38. The ESR spectra investigated above 20 °C show pronounced broad component for NR/nanoclay nanocomposites but it is completely disappeared for NR/nano-silica nanocomposites, which indicates that the spin

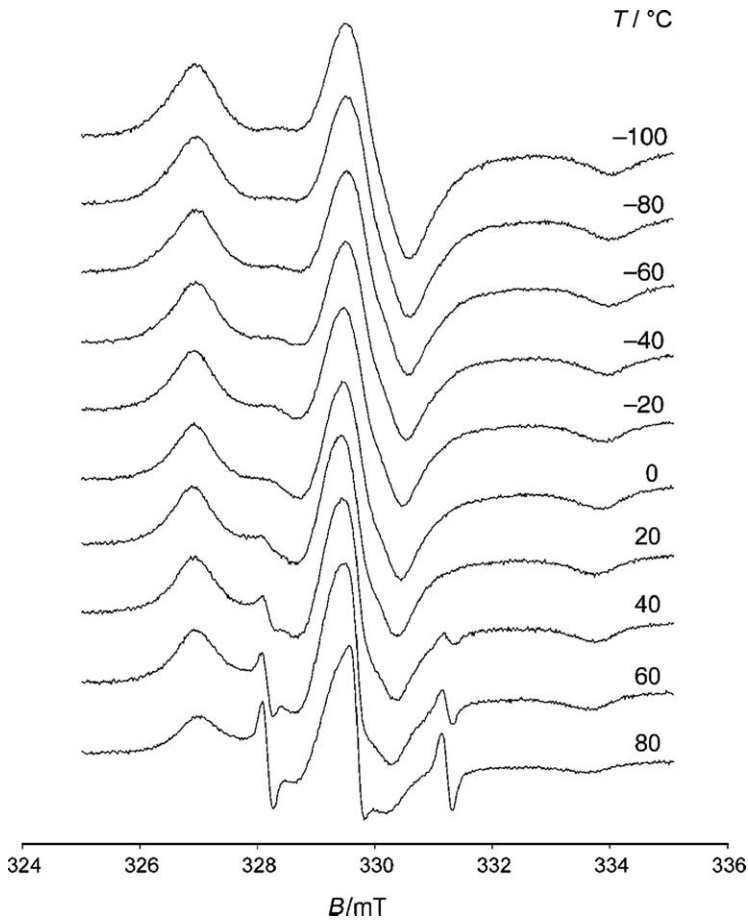

Figure 25.38 ESR spectra of spin probe for 10 phr nanoclay-based NR nanocomposites at different temperatures.
(Reproduced from ref. 69 with permission from John Wiley & Sons.)

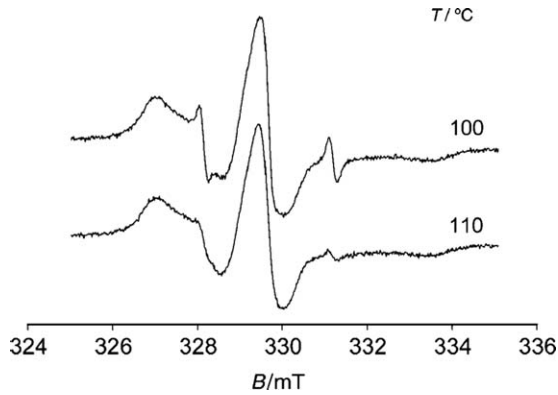

Figure 25.39 ESR spectra of spin probe for 10 phr nanoclay-based NR nanocomposites at 100 and 110 °C.
(Reproduced from ref. 69 with permission from John Wiley & Sons.)

probe motion is more highly restricted in the nanoclay filled rubber as compared to the nano-silica filled rubber. It is reported by Ammala *et al.* that interactions between nanoclay and polymer matrix reduce the free volume, as determined by positron annihilation lifetime spectroscopy (PALS) measurement.[70] which further support the restriction imposed by nanoclay as demonstrated by the segmental mobility of spin probes observed by ESR study.

ESR spectra of spin probe for NR/nanoclay nanocomposites at 100 and 110 °C are shown in Figure 25.39. ESR spectra of probe for NR/nanoclay nanocomposites measured at temperature above 80 °C show broad lines along with the usual narrow line, which were also reported in the NR/nano-silica nanocomposites. These observations confirm that the mobility of the spin probe is restricted in presence of nanoclay.

Zhang *et al.* have studied the effect of γ-radiation source on free radical concentration of neat OMMT (organophilic montmorillonite), pure SBS (styrene–butadiene–styrene), and SBS/OMMT nanocomposites.[71] Figure 25.40(a) shows the ESR spectra of DPPH (2,2-diphenyl-1-picrylhydrazyl), a reference sample, and OMMT before and after γ-radiation. A doublet ESR resonance is observed for OMMT before the irradiation, which is due to the presence of active paramagnetic species within the silicate layers. A large amount of free radicals are formed in the samples after exposing them to γ-radiation, which is attributed to the cleavage of clay modifying agent (octadecyl trimethyl ammonium bromide (OTAB)) by the γ-ray. Figure 25.40(b) and (c) show the ESR spectra of pure SBS and SBS/clay nanocomposites before and after expose to the γ-radiation, which revealed that large amount of radicals formed after the radiation. It can also be observed that the ESR spectra of pure SBS and SBS/OMMT nanocomposites are almost the same before and after irradiation. But, the intensity of the ESR peaks of SBS/OMMT nanocomposites is comparatively much more intense than that of pure SBS after expose to radiation, which is due to synergistic effect of the radicals originating from SBS and

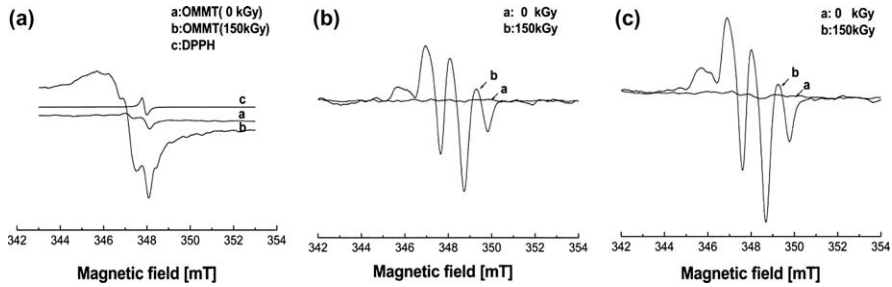

Figure 25.40 ESR spectra of (a) DPPH and OMMT, (b) pure SBS and (c) SBS/clay nanocomposites before and after irradiation.
(Reproduced from ref. 71 with permission from the Royal Society of Chemistry.)

OMMT. Further, the layers of OMMT can absorb a large amount of radiation and protect the SBS molecular chains, and can produce a large number of free radicals, which may cause recombination of free radicals of SBS chain or grafting of the SBS chains onto the surface of the layers of the OMMT via covalent bonding.

25.3 Summary and Future Scope

ESR is a sophisticated characterization technique to investigate and estimate the molecular dynamics and structural parameters in the polymer composites and nanocomposites in detail. Almost all polymers are diamagnetic in their normal state and become paramagnetic by the incorporation of foreign stable free radicals, *i.e.* ESR active species, using physical or chemical means. Generally, spin probe or spin label technique is employed to insert nitroxide free radical into a polymer matrix. The spin label method is relatively simple as compared to the spin probe method, and thereby is suitable for laboratory and industrial applications. The incorporation of spin probe into the inhomogeneous polymeric system needs sufficient cautions to achieve best performance. The shape, size, stereochemistry, polarity, and flexibility along with its bonding ability of the spin probe with polymer matrix should be thoroughly considered for its successful implementation. Novelty of the spin probe system is that it requires very minute quantity of nitroxide radical, which produces very good signal-to-noise ratio as well as no noticeable effect on the inherent materials properties of polymer matrix.

In this chapter, ESR studies on NR composites and nanocomposites are extensively reviewed based on available published literatures. A very few ESR studies on rubbers were conducted due its complexity and specific natures. Interactions between both carbon black and silica particles with NR matrix were well established by conducting the ESR study. Variations of the ESR spectra and the concentration of the unpaired spins of NR/carbon black composites with carbon black concentration, milling time, types of carbon

blacks, temperature, and specific surface area of the carbon blacks were thoroughly evaluated. Effects of irradiation dose, dose rate, and time after removing radiation source on the concentration of carbon black free radical were systematically analysed by ESR. The NR nanocomposites based on nano-silica and nanoclay were also characterized by ESR measurement. The effect of test temperature and coupling agent on the ESR spectra of spin probe for the nanocomposites were depicted successfully.

Acknowledgements

This review work is supported by the research fund of Hanyang University, ERICA Campus, Republic of Korea (HY-2012-P). The postdoctoral research fellowship provided by Hanyang University is gratefully acknowledged by one of the authors (A. K. Barick).

References

1. S. E. Bresler and E. N. Kazbekov, *Russ. Chem. Rev.*, 1967, **36**, 298.
2. H. Fischer, *Proc. Roy. Soc. Lond. Ser. A Math. Phys. Sci.*, 1968, **302**, 321.
3. D. J. T. Hill, J. H. O'Donnell and P. J. Pomery, in *Electron Spin Resonance*, ed. P. B. Ayscough, The Royal Society of Chemistry, London, UK, 1982, **vol. 7**, p. 1.
4. M. Lucarini and L. Pasquato, *Nanoscale*, 2010, **2**, 668.
5. O. A. Lebedev and S. N. Kazarnovskii, *Treatises Chem. Chem. Technol., Gorky*, 1959, **8**, 649.
6. O. L. Lebedev and S. N. Kazarnovskii, *Zhur. Obshch. Khim.*, 1960, **30**, 1631.
7. M. Huber, *Photosynth. Res.*, 2009, **102**, 305.
8. T. Fukuda, T. Terauchi, A. Goto, K. Ohno, Y. Tsujii, T. Miyamoto, S. Kobatake and B. Yamada, *Macromolecules*, 1996, **29**, 6393.
9. N. Kocherginsky and H. M. Swartz, *Nitroxide Spin Labels: Reactions in Biology and Chemistry*, Crc Press, Boca Raton, FL, 1995.
10. G. Likhtenshtein, J. Yamauchi, S. Nakatsuji, A. I. Smirnov and R. Tamura, *Nitroxides: Applications in Chemistry, Biomedicine, and Materials Science*, Wiley-VCH Verlag GmbH & Co. KGaA, Boschstraβe, Weinheim, Germany, 2008.
11. Y. Miwa, O. Urakawa, A. Doi, K. Yamamoto and S. Nobukawa, *J. Phys. Chem. B*, 2011, **116**, 1282.
12. Y. Miwa, S. Schlick and A. R. Drews, in *Characterization Techniques for Polymer Nanocomposites*, ed. V. Mittal, Wiley-VCH Verlag GmbH & Co. KGaA, Boschstraβe, Weinheim, Germany, 2012, p. 283.
13. N. Grassie, *Pure Appl. Chem.*, 1968, **16**, 389.
14. A. R. Forrester and R. H. Thomson, *Nature*, 1964, **203**, 74.
15. Z. Veksli, M. Andreis and B. Rakvin, *Prog. Polym. Sci.*, 2000, **25**, 949.
16. G. Jeschke, *Macromol. Rapid Commun.*, 2002, **23**, 227.
17. M. Didović, D. Klepac and S. Valić, *Macromol. Symp.*, 2008, **265**, 144.

18. M. D. Pace and A. W. Snow, *Macromolecules*, 1995, **28**, 5300.
19. Z. Veksli and W. G. Miller, *Macromolecules*, 1977, **10**, 686.
20. M. N. Junk, in *Assessing the Functional Structure of Molecular Transporters by EPR Spectroscopy*, Springer-Verlag, Heidelberg, Berlin, Germany, 2012, p. 7.
21. P. G. Fajer, in *Encyclopedia of Life Sciences*, John Wiley & Sons, Inc., Hoboken, NJ, USA, 2001, p. 1.
22. S. Valić, M. Andreis and D. Klepac, in *Handbook of Multiphase Polymer Systems*, eds. A. Boudenne, L. Ibos, Y. Candau and S. Thomas, John Wiley & Sons, Ltd., Chichester, West Sussex, UK, 2011, p. 551.
23. T. Marinović, Z. Veksli, M. Andreis and D. Fleš, *Polym. Bull.*, 1984, **12**, 457.
24. J. John, D. Klepac, M. Didović, C. J. Sandesh, Y. Liu, K. V. S. N. Raju, A. Pius, S. Valić and S. Thomas, *Polymer*, 2010, **51**, 2390.
25. P. L. Kumler and R. F. Boyer, *Macromolecules*, 1976, **9**, 903.
26. N. Kusumoto, S. Sano, N. Zaitsu and Y. Motozato, *Polymer*, 1976, **17**, 448.
27. J. S. Hwang, M. M. Saleem and C. P. Tsonis, *Polymer*, 1991, **32**, 231.
28. I. M. Brown and T. C. Sandreczki, *Macromolecules*, 1985, **18**, 2702.
29. T. Marinović, S. Valić, M. Andreis and Z. Veksli, *Polymer*, 1991, **32**, 2519.
30. Z. Veksli, M. Andreis and D. S. Campbell, *Polymer*, 1998, **39**, 2083.
31. Z. Veksli, M. Andreis, S. Valić, T. Marinović and F. Ranogajec, *Radiat. Phys. Chem.*, 1997, **51**, 207.
32. K. N. G. Fuller and W. S. Fulton, *Polymer*, 1990, **31**, 609.
33. I. Dubrović, D. Klepac, S. Valić and G. Žauhar, *Radiat. Phys. Chem.*, 2008, **77**, 811.
34. J. Čulin, D. Gembarovski, M. Andreis, Z. Veksli and T. Marinović, *Polym. Int.*, 2000, **49**, 845.
35. N. J. Morrison, *Rubber Chem. Technol.*, 1984, **57**, 86.
36. P. P. Chattaraj, A. K. Kalidaha, R. Mukhopadhyay and D. K. Tripathy, *Angew. Makromol. Chem.*, 1996, **235**, 81.
37. A. V. Chapman and M. Porter, in *Natural Rubber Science and Technology*, ed. A. D. Roberts, Oxford University Press, new York, USA, 1988, p. 511.
38. M. Jamroż, K. Kozłowski, M. Sieniakowski and B. Jachym, *J. Polym. Sci. Polym. Chem. Ed.*, 1977, **15**, 1359.
39. K. Kozłowski, M. Jamroż, T. Słupkowski and B. Jachym, *Polymer*, 1978, **19**, 709.
40. M. Jamroż, K. Kozłowski, M. Sieniakowski and B. Jachym, *Rubber Chem. Technol.*, 1978, **51**, 81.
41. K. Kozłiowski, *Acta Polym.*, 1979, **30**, 547.
42. A. B. Sullivan and R. W. Wise, in *Proceedings of the 5th International Rubber Conference*, MacLaren & Son, Ltd., London, UK, 1967, p. 235.
43. M. A. Waldrop and G. Kraus, *Rubber Chem. Technol.*, 1969, **42**, 1155.
44. J. R. Harbour and M. J. Walzak, *J. Colloid Interf. Sci.*, 1987, **119**, 150.

45. L. S. Singer, in *Proceedings of 5th Carbon Conference*, Pergamon Press, Oxford, UK, 1963, **vol. II**, p. 37.
46. J. R. Harbour, M. J. Walzak and R. P. Veregin, *J. Colloid Interf. Sci.*, 1990, **138**, 380.
47. E. M. Cashell and V. J. McBrierty, *J Mater Sci*, 1977, **12**, 2011.
48. B. Ellis and J. F. Baugher, *J. Polym. Sci. Polym. Phys. Ed.*, 1973, **11**, 1461.
49. J. O'Brien, E. Cashell, G. E. Wardell and V. J. McBrierty, *Macromolecules*, 1976, **9**, 653.
50. J. O'Brien, E. Cashell, G. E. Wardell and V. J. McBrierty, *Rubber Chem. Technol.*, 1977, **50**, 747.
51. W. T. Mead, R. S. Porter and P. E. Reed, *Macromolecules*, 1978, **11**, 56.
52. W. T. Mead, R. S. Porter and P. E. Reed, *Rubber Chem. Technol.*, 1980, **53**, 915.
53. M. Kawakubo, K. Tsunoda, H. Yajima, T. Ishii, H. Kaidou and A. Ahagon, *Rubber Chem. Technol.*, 2005, **78**, 644.
54. C. Brosseau, F. Boulic, P. Queffelec, C. Bourbigot, Y. Le Mest, J. Loaec and A. Beroual, *J. Appl. Phys.*, 1997, **81**, 882.
55. C. M. Blow, ed., *Rubber Technology and Manufacture*, Newnes-Butterworths, London, UK, 1971.
56. B. B. Boonstra, E. M. Dannenberg and F. A. Heckman, *Rubber Chem. Technol.*, 1974, **47**, 1082.
57. A. I. Medalia, *Rubber Chem. Technol.*, 1974, **47**, 411.
58. M. G. Siswanto, N. P. Bo, Parangtopo, H. Neubacher and L. C. Burton, *Rubber Chem. Technol.*, 1988, **61**, 269.
59. S. Baccaro, F. Cataldo, A. Cecilia, A. Cemmi, F. Padella and A. Santini, *Nucl. Instrum. Methods Phys. Res. Sect. B Beam Interact. Mater. Atoms*, 2003, **208**, 191.
60. R. Scotti, L. Wahba, M. Crippa, M. D'Arienzo, R. Donetti, N. Santo and F. Morazzoni, *Soft Matter*, 2012, **8**, 2131.
61. N. Suzuki, M. Ito and F. Yatsuyanagi, *Polymer*, 2005, **46**, 193.
62. P. Carstensen, *Makromol. Chem.*, 1970, **135**, 219.
63. P. Carstensen, *Makromol. Chem.*, 1971, **142**, 131.
64. M. Ito, H. Isago and N. Suzuki, *J. Appl. Polym. Sci.*, 2008, **108**, 1385.
65. D. Klepac, M. Ščetar, M. Kurek, P. E. Mallon, A. S. Luyt, K. Galić and S. Valić, *Polym. Int.*, 2012, **62**, 474.
66. J. Funatsu, R. Takagi and M. Ito, *J. Appl. Polym. Sci.*, 2009, **113**, 2791.
67. S. Toki, R. Takagi, M. Ito and B. S. Hsiao, *Polymer*, 2011, **52**, 2453.
68. F. W. H. Kruger and W. J. McGill, *J. Appl. Polym. Sci.*, 1992, **45**, 1545.
69. S. Valić, in *Rubber Nanocomposites: Preparation, Properties, and Applications*, eds. S. Thomas and R. Stephen, John Wiley & Sons, Ltd., Chichester, West Sussex, UK, 2010, p. 391.
70. A. Ammala, S. J. Pas, K. A. Lawrence, R. Stark, R. I. Webb and A. J. Hill, *J. Mater. Chem.*, 2008, **18**, 911.
71. W. Zhang, J. Zeng and L. Liu, *J. Mater. Chem.*, 2004, **14**, 209.

CHAPTER 26

Applications of Natural Rubber Composites and Nanocomposites

ALDO E. JOB,*[a] FLÁVIO C. CABRERA,[a] LEANDRA O. SALMAZO,[a] MIGUEL A. RODRIGUEZ-PEREZ,[b] ALBERTO LÓPEZ GIL,[b] ALEXANDRE F. DE SIQUEIRA[a] AND FELIPE S. BELLUCCI[a]

[a] Department of Physics, Chemistry and Biology, Faculty of Sciences and Technology – FCT, Univ Estadual Paulista – UNESP, Roberto Simonsen St., 305, Postal Code 19060-900, Presidente Prudente, SP, Brazil; [b] Cellular Materials Laboratory – CellMat, Condensed Matter Physics Department, University of Valladolid – UVA, 47011, Valladolid, Spain
*Email: job@fct.unesp.br

26.1 *Leishmania brasiliensis* Promastigotes and Natural Rubber Membranes

26.1.1 Introduction

The first material known as rubber was a polyisoprene produced from latex extracted from *Hevea brasiliensis* trees.[1] Currently latex world production is concentrated in three areas: Asia (93,3%), Africa (4,5%) and Latin America (2,2%).[2,3] In Latin America the production reaches 195,000 tons, subdivided between Brazil, Ecuador, Guatemala and Mexico, and 54% of this production refers to Brazilian supply, with approximately 105 thousand tons, representing 1.2% of world production.[4,5]

RSC Polymer Chemistry Series No. 8
Natural Rubber Materials, Volume 2: Composites and Nanocomposites
Edited by Sabu Thomas, Hanna J. Maria, Jithin Joy, Chin Han Chan and Laly A. Pothen

Published by the Royal Society of Chemistry, www.rsc.org

Natural rubber (NR) may be characterized as latex submitted to thermal treatment, presenting a glass transition temperature (T_g) below room temperature, composed of flexible and long chains, arbitrarily clustered. These mechanical properties are attributed to the rotation of C–C single bonds, which allow different chain conformations.[6–8]

Another sector that has attracted attention of scientific world today is the synthesis of metallic nanoparticles. Generally the aim is to improve knowledge about these materials as well as controlling the formation of nanoparticles with desired size and shape, which can influence the evolution of electronic, optical, catalytic and other properties resulting from nanocomposite system.

NR can be included in the list of materials with possibility of application on nanostructures synthesis by green chemistry. In literature is possible to find the synthesis of nanoparticles using latex extracted from other trees of Euphorbiaceae family, such as *Jatropha curcas*,[9] as well as the seed extract[10] used as liquid compound and inserted directly into an aqueous solution of $AgNO_3$.

Latex use for synthesis of silver nanoparticles was also found in the literature,[11] however using only one phase obtained after centrifuging the latex, inserting the silver salts in the dilute phase volume in water, subsequently produced films including the route of synthesis, irradiation with ultraviolet light of these films, which makes obtaining nanoparticles an arduous process. Epoxidized natural rubber (ENR) was also used for fabrication of platinum and gold nanoparticles after dissolved in toluene, and mixed in colloids with nanoparticles reduced using sodium borohydride, such that ENR works only as a nanostructure stabilizer.[12,13]

26.1.2 Latex Extraction

Latex shown in this application was obtained by bleeding process, in different trees from RRIM 600 clone, in Presidente Prudente region, São Paulo state, Brazil. The process is exerted on the stem to a height of approximately 1.2 m from the ground with a *jebong*, a cutting tool in 'U' form. The cut is made at an angle of 30° related to the horizontal, to about half the circumference of the trunk, removing about 1.5 mm of cortex for each incision. Finally, latex was stored in dark coloured glass containers, in order to prevent latex degradation by sunlight action.

26.1.2.1 Gold (III) Chloride

For accomplishment of this application metal salts of gold chloride in oxidation state +3 was used, named 'Gold (III) chloride 99.99%' and purchased from Sigma-Aldrich.

26.1.3 Preparation of Natural Rubber Membranes

NR membranes were obtained by a casting technique; 10 ml of latex was used, annealed at temperatures of 65, 80 and 120 °C and thermal

treatment time of 10 h. The thermal treatment time was defined according to the minimum time required for latex drying to membranes at 65 °C and maintained for membranes at 80 and 120 °C. Latex is stabilized with ammonia at a 2% proportion, and supported on Petri dishes of 9.5 cm inner diameter. The thermal treatment is made using a drying oven with forced air circulation, to form NR membranes with thickness of approximately 0.6 mm.

26.1.3.1 Synthesis of Gold Nanoparticles

Initially, NR membrane is placed in a beaker with distilled water, so their pores can expand. Thereafter, gold chloride ($AuCl_3$) salt is diluted in a concentration of 3.1×10^{-4} M, chosen according to colloid preparation methods by chemical reduction,[14] at a temperature of 80 °C. Membranes are then placed in the solution, where occurs reduction of gold (Au) and withdrawn at 6, 9, 15, 30, 60 and 120 minutes of reduction.

Spectrophotometry is determined by the relative characteristics of atoms or molecules to absorb or emit electromagnetic energy, referring to a region comprised in the spectrum. Measurements are basically determined by Beer–Lambert law, which establishes the relationship between transmittance, sample thickness and concentration of the species responsible for absorption. UV-Vis is given by incidence of polychromatic light, with wavelengths between 380 and 780 nm (which characterizes the '*vis*' description – *visible*, region of wavelengths that excite the human retina).[15] The spectrophotometry used operates in a range of 190–1100 mm.

Formation and growth of the AuNPs within the NR membranes, by reduction of Au^{3+}, was monitored following the plasmon absorption band. The reducing agents for formation of AuNP are likely to be the carboxylic functional groups present in the NR. Nanoparticle growth was carried out for reaction times of 6, 9, 15, 30 and 60 min, which produces an increase in the intensity of the distinctive plasmon absorption band of AuNPs centred at $\sim$560 nm, as shown in Figure 26.1.[16]

Analyses performed by scanning electron microscopy (SEM) were performed for NR membranes with gold nanoparticles, obtained at a 30 min time reduction (Figure 26.2). Apparently, there is a homogeneous distribution of nanoparticle occupying the entire surface of the membrane, but by amplifying the images, one can observe the formation of many nanoparticles in sites, and among them, nanoparticles dispersed on the surface of the polymeric matrix. In Figure 26.2(d) the small spherical nanoparticles can be seen agglomerated over reduction sites, forming an exorbitant amount of aggregates. The sizes of nanoparticles were measured and are very similar, with an average of approximately 48 nm. These results are in agreement with the analysis by UV-Vis spectroscopy, and show that the amount of nanoparticles decreased as a function of collection; more properly, based on the composition of the latex obtained.

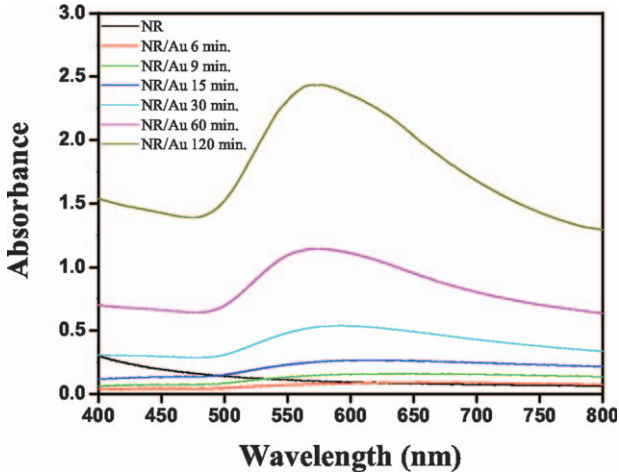

Figure 26.1 UV-Vis spectroscopy for different reduction times of gold nanoparticles compared to raw natural rubber membrane, obtained at 65 °C.

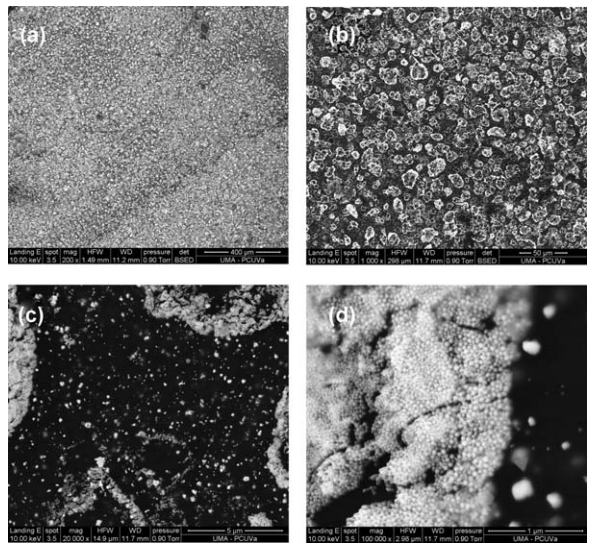

Figure 26.2 SEM analysis of NR/Au membrane obtained at 30 min of reduction. Magnification of (a) 200 times; (b) 1000 times; (c) 20,000 times; (d) 100,000 times.

26.1.4 Studying the Influence of NR/Au Composites on the Physiology of *Leishmania brasiliensis* Promastigotes

Polymeric materials have been the focus of biomedical research due both to their biocompatible and non-toxic properties, but also with an emphasis on the control of structures at molecular level, allowing *in vitro* study of drug

incorporation in biomolecular systems.[17–19] Polymers allow systematic drug incorporation and release or protein functionalization; composites can be used to induce angiogenesis observed by formation of blood vessels in ulcer treatment, or even applied to promote the activity of bone regeneration,[20–24] which opens up the possibility of future applications such as *in vivo* implants.

Recent studies regarding the use of gold nanoparticles in medicine have shown great potential, from diagnosis to treatment of diseases, through controlled release of systematized drugs.[25–27] On the other hand, when dealing with nanostructures, their properties are intimately modified, presenting different optical and electrical characteristics, so that recent studies have challenged the use of nanoparticles, whether cutaneous character or even intravenous injection with respect to the toxicity of these nanoparticles.[28–30] The development of these studies may define the dosage of these nanoparticles as metabolic inhibitors or as adjuvants for the immune system, thus elevating the development of nanomedicine.

In this section NR membranes with colloidal incorporation of gold nanoparticles are used, synthesized by an *in situ* method (NR/Au) at different reduction times, in order to evaluate the physiological behaviour of *Leishmania braziliensis* promastigotes cultured in axenic medium, in a colony of 7 weeks old, evaluating the increase in kinetics in relation to the permanence time of the membranes in the culture medium as a function of reduction time and temperature of preparations of NR membranes.

26.1.4.1 Leishmania brasiliensis Parasites

The parasites used in this study were isolated from four clinical cases of cutaneous leishmaniasis in the municipality of Santa Cruz do Rio Pardo, São Paulo, Brazil, in 1997, where these patients had only ulcerated skin lesions (strain SCP-1/WHO-M).

26.1.4.2 Cultivation System

Amastigotes were isolated from nodular lesions of experimental animals and cultured on BHI ('Brain Heart Infusion', BBL, São Paulo, Brazil) plus 10% FCS, 2% filtered urine, 1000 UI/mL of potassic penicillin G 100 and μL/mL of streptomycin sulfate. The cultures remained in a biological stove (26 °C) for 10 days. The cultivation of promastigotes was also given in BHI environment.

26.1.4.3 Population Growth Kinetics

With an inoculum of 5×10^5 promastigotes, the culture medium was included in growth tanks with a thermo-controlled oven (36.5 °C) along with samples of membrane adhering to the bottom and the population growth of promastigotes *in vitro* was followed, by estimating through a Neubauer chamber every 3 h for 1 week. The entire experiment was performed in triplicate and the results were statistically analysed in order to represent a significant sample.

For the accounting of promastigotes adhered to the membrane, the membrane extraction medium was performed by washing with a saline phosphate solution with pH 7.0 for the disconnection of protozoans, in a totally sterile and temperature-controlled environment. Subsequently, the membranes were reintroduced in order that the adsorption process is restarted, until the next third hour counting.

26.1.4.4 Evaluation of NR/Au membranes as Inhibitors of in vitro Growth of Leishmania brasiliensis Protozoans

Evaluation of growth kinetics of promastigotes in culture medium was performed separately for the membranes of pure and NR with different times of gold nanoparticles reducing, as evaluated in previous work.[31]

The inclusion of NR/Au membrane in culture generates a delayed onset of growth in culture until about 24 h, with a reduction in the development population proportional to the time reduction of the gold nanoparticles. It is noted also that the NR/Au 120 min. membrane presents the best results with regard to growth inhibition of promastigote population in culture medium. NR/Au 30 min. membrane has a sharper decline in curve kinetics attributable to death of promastigotes from 120 h. Upon analysis completion of growth medium, the membranes prepared for times of 30, 60 and 120 minutes showed similar results, with the number of promastigotes in solution smaller than inserted into the initial population.

Some of this decrease can be explained by the natural dynamics of promastigotes in the culture medium. It is expected that after 150 h population drop occurs because of nutritional deficit and saturation of the cellular environment with cellular excreta generated during this period of growth log phase and stationary,[32] but the presence of gold nanoparticles anticipates this drop in the number of the population, probably because these metal components do not provides nutrient absorption of environment through permeases and transplasmalema transport channels. The count of promastigotes adhered in membranes by optical microscopic technique, with the average yield of living microorganisms were evaluated in previous work.[31]

The percentage of adhered promastigotes widens with increasing reduction time up to 30 minutes. For this reduction time is assigned maximum functionality of the nanoparticles, presenting to longer reduction times the resorption of the components responsible for the reduction of nanoparticles, reacting with the nanoparticles incorporated in the surface of membranes.[33] This amount of adhered promastigotes decreases when observed to the NR/Au membranes for reduction times of 60 and 120 minutes.

The logarithmic phase is characterized by very intensive growth of the population due to the use rich environment in the nutritional point of view. At this stage, almost all of the parasites are in a procyclical state because the metacyclogenesis process starts only when there is a stabilization of the cellular catabolic

processes and the onset of specific gene expression inhibited until this instant. For this fact, all the test means, in the presence of any NR/Au membrane, the sample adhered promastigotes is low due to the small concentration of those glycoconjugates and their waste is expected to have an affinity for the whole researched. It is noticed also that, in the stationary phase, the concentration of live and adhered to the membrane promastigotes remains high with growth with increasing concentration of nanoparticles within 30 minutes of reduction.

The decline of adhesion can be explained by the process of cellular stress common during fall phasis, where there are few nutrients in the medium and the microorganism in question is in a process of internal reserves spent, thus degrading the surface glycoconjugates as artifice to synthesis survival for a longer period of time.[34]

According to the results the best allowed reduction time is 120 minutes, due to its greater population growth inhibition, and was then assessed the influence of the thermal treatment by the casting preparation method of membrane NR to temperatures of 60, 80 and 120 °C, and then used as substrates for the reduction of nanoparticles.

In an attempt to develop a smart skin bandage were covered the membranes of pure NR and with incorporation of gold nanoparticles using methylene blue molecules, due to the drug photosensitivity. This composites NR/Au-MB were inserted in the culture medium and evaluated the behaviour of *Leishmania braziliensis* promastigotes through the population growth kinetics and morphophysiological analysis. Results regarding population growth obtained for protozoans eluted to membranes prepared at 120 °C of thermal treatment are presented in Figure 26.3.

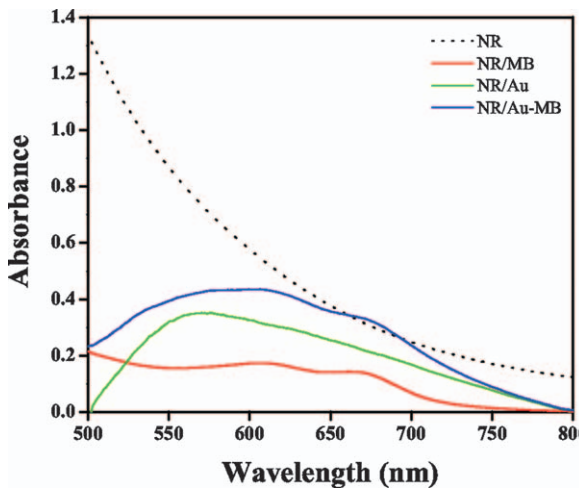

Figure 26.3 Molecular spectroscopy in the UV-Vis region of natural rubber membranes with gold nanoparticles for the 120 min time reduction and functionalization with molecules of methylene blue compared to pure natural rubber membrane.

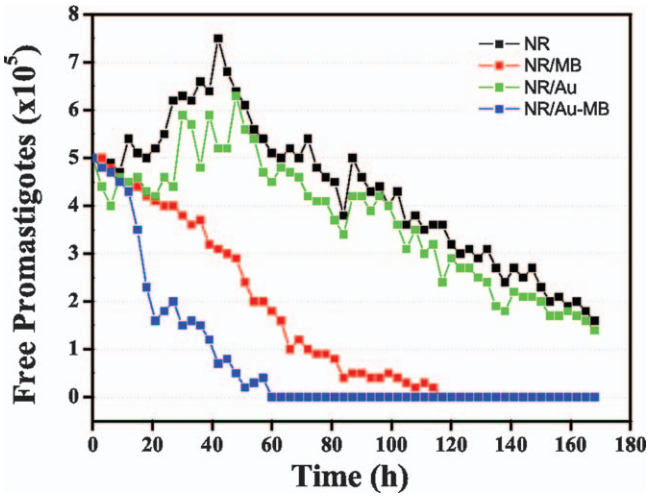

Figure 26.4 Evaluation of increase kinetics of promastigotes in solution in the presence of natural rubber membranes incorporating gold nanoparticles and methylene blue molecules, inserted separately into the culture medium, compared with the pure natural rubber membrane, and exposed to blue light.

The characteristic spectrum of the NR membrane shows no characteristic bands when evaluated in the UV-vis area. Absorption bands are observed around 560 nm, attributed to the plasmon resonance of the gold nanoparticles. The incorporation of the blue methylene molecules is observed through the absorption bands at 595 and 667 nm, assigned to π–π* electronic transitions. These membranes were then evaluated in culture medium of promastigotes of *Leishmania brasiliensis*, when irradiated with blue light, and the results are shown in Figure 26.4.

The incorporation of methylene blue (MB) molecules does not show toxic interaction with promastigotes, since the population growth usually develops when inserted membranes are NR/MB. Moreover, when irradiated culture media contain MB molecules, a deficit in the population growth is observed. For NR/MB membranes irradiated with blue light total elimination of promastigotes is observed in about 120 h, whereas when MB molecules are deposited on gold nanoparticles this time decreases to about 60 h. This fact is attributed to the amplification effect of surface commonly evaluated by micro-Raman spectroscopy, so that the metallic particles act as sites for amplification of energy absorbed by the anchored molecules. Thus the electrons assume an excited energy state, and during the release of the absorbed energy active radicals are generated, with interaction with the environment where are the MB molecules. In the first instance, electrons from the MB molecules, when returning to the ground state emit enough energy to excite the oxygen present in the medium converting to superoxides or peroxides radials. This transfer may occur also by interaction with hydrogen atoms present in other molecules to form radicals, *e.g.* hydroxyl, also with potential toxic to cells, or as in this case,

the promastigotes. If the emission energy is derived from a transition to a triplet state of the photosensitizer, one can obtain the formation of a singlet oxygen molecule and an oxidizing agent more toxic to cells.[35–39]

26.2 Thermoplastic Starch and Natural Rubber Blends

26.2.1 Introduction

The food packaging industry has traditionally used materials such as paper, glass and metal to produce trays, cups, *etc*. However, during the last 60 years plastic has been progressively introduced into the packaging market due to its excellent properties such as low density, low cost, good mechanical and physical properties, resistance to corrosion and ease of processing.[40] This huge increment in the production of plastics (Figure 26.5) has generated many environmental concerns. Despite the rise in recycling rates worldwide, the lifetime of landfills has been progressively shortened and marine and street litter pollution are starting to become one of the main concerns of local and regional governments. Last but not least, petroleum prices are continuously rising and so, therefore, is the price of plastic raw materials.

In order to try to solve these environmental concerns, biopolymers are starting to emerge as an alternative to traditional synthetic polymers in the food packaging market. Oil-based polymers take at least 400 years to be completely degraded. However, biopolymers are fully biodegradable under certain atmospheric conditions in a few months, which avoids excessive accumulation in landfills.

Starch is one of the most promising biopolymers for the production of food packaging trays for several reasons:[41] It is bio derived and fully biodegradable; its cost is very low (0.7 €/kg) and its production is abundant worldwide. Nevertheless, up to now the introduction of starch in the food packaging market has been restricted because it presents several drawbacks: native starch,

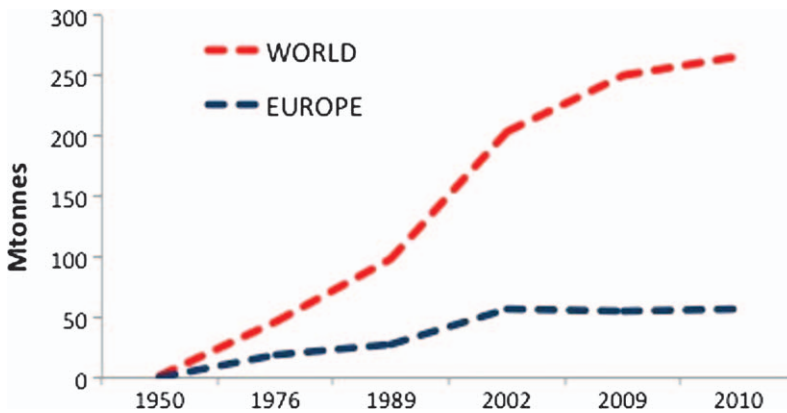

Figure 26.5 World and European production of plastics since 1950.

Figure 26.6 Pellets of thermoplastic starch (TPS).

after being thermoformed becomes brittle and breaks easily, it is hydrophilic and therefore moist products cannot be packed, and its density is higher (1400 kg/m^3) than common synthetic polymers employed in the food packaging market such as polystyrene (1070 kg/m^3).

With the aim of improving the flexibility and strength of starch after being thermoformed, several strategies have been followed. One of them is the plasticization of starch with water and polyols[42] (Figure 26.6). However, the moisture affinity of starch is not avoided with the use of polyols as plasticizers. In order to combine both strategies, improvement of mechanical properties and reduction in water uptake, blends of thermoplastic starch (TPS) with NR seem to be a promising approach.[43] Characteristics of NR such as its high elasticity and its hydrophobic nature make it a suitable choice to produce blends with TPS.

The challenge here is the achievement of good compatibility between both polymers because of their different chemical affinities: starch is hydrophilic and NR is hydrophobic. With the aim of improving the compatibility, some examples can be found in literature such as the chemical modification of starch by an esterification process[44] and the generation of a graft copolymer in the starch–NR blends by potassium persulfate.[45]

This research work has been focused on the production and vulcanization of TPS and NR blends. Vulcanization is a well-known method of crosslinking NR, which considerably improves its strength.[46] The aim of this work is the vulcanization of TPS and NR blends in order to, on the one hand, improving the compatibility between both polymers and, on the other hand, reducing the water affinity of TPS and increase its flexibility.

26.2.2 Production of Vulcanized TPS–NR Blends

Several production steps were followed in order to produce the vulcanized TPS–NR blends. Figure 26.7 shows a scheme of the production route.

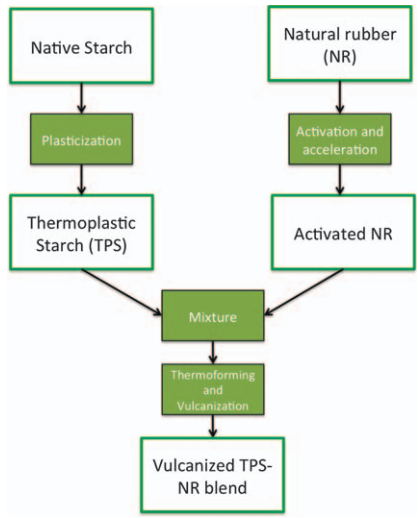

Figure 26.7 Production route of vulcanized TPS–NR blends.

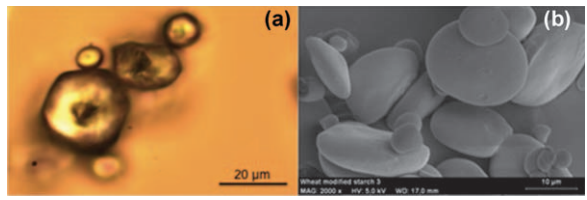

Figure 26.8 Native wheat starch: (a) microscopic image; (b) SEM image.

Figure 26.9 Equipment employed in the production of the blends: (a) twin-screw extruder; (b) hot-plates press.

First of all, native wheat starch (Figure 26.8) was plasticized through a twin-screw extruder (Figure 26.9). Native starch was manually premixed with glycerol and then introduced into the extruder. Temperature profile and screw speed were set to 90-110-130-150-110 °C and 100 rpm respectively. During the extrusion, the native granular structure of starch is completely disrupted by the plasticizer and it becomes a thermoplastic material. A drastic change in the thermal transitions of starch, such as T_g, takes place during the disruption of starch granules. The T_g drops by more than 200 °C in the case of native starch,

Table 26.1 Activation of NR system.

Name	*Chemical Formula*	*Phr*[a]
Zinc Oxide	ZnO	4
Stearic Acid	$CH_3(CH_2)_{16}COOH$	3
Sulphur	S_8	2
2-Mercaptobenzotiazol	$S_2NC_7H_7$	1

[a]Parts per hundred of natural rubber.

to temperatures below 100 °C in the case of TPS.[47] This drop in the T_g enhances the processability of starch in common industrial plastic equipment as well as improving its mechanical properties as far as plasticity is concerned. Once the starch is plasticized, it is removed from the extruder, air dried and pelletized.

Secondly, NR was activated. The activation system used to prepare the vulcanized TPS–NR blends is shown in Table 26.1.

NR, stearic acid and zinc oxide were mixed for 20 min at 40 °C in an internal mixer. This mixture was stored at room temperature and without exposure to light for 24 h. During this time, the following reaction took place between zinc oxide and stearic acid to obtain zinc stearate:

$$(C_{17}H_{35}COOH) + ZnO \Rightarrow (C_{17}H_{35}COO^-)_2 \cdot Zn^{2+} + H_2O$$

Once the reaction was developed, the vulcanized agents, sulfur and mercaptobenzothiazole were added using also an internal mixer for 10 minutes at 40 °C. Having finished the mixing of NR with the vulcanized agents, the activated NR was obtained and was ready to be mixed with TPS.[48]

Finally, both polymers, TPS and activated NR, were mixed in the same internal mixer previously employed for the activation of NR. The blend, after being completely mixed, was removed and introduced in square-shaped moulds. The mould with the blend inside was then placed in a hot-plates press (Figure 26.9) where the vulcanization and thermoforming process was carried out at the same time. Production parameters such as temperature and pressure were set up to 2.5 MPa and 150 °C for 8 min 30 s.[48]

26.2.3 Characterization of Vulcanized TPS–NR Blends

Vulcanized TPS–NR blends were mechanically and morphologically characterized in order to evaluate on the one hand the compatibility between both polymers and on the other hand the mechanical response as far as elasticity and strength is concerned.

Four formulations were produced. One of them without NR and the other three with different proportions of NR: 1%, 3% and 5%. TPS was plasticized previously with 30% of glycerol. These formulations are summarized in Table 26.2.

Little amounts of NR were chosen taking the required condition of biodegradability of these materials into account. NR is a bio derived product but is resistant to microbial degradation because of its hydrophobic character,

Table 26.2 Blends Produced.

Blend	*TPS*	*NR(%[a])*
SNR0	TPS (30% Glycerol)	0
SNR1	TPS (30% Glycerol)	1
SNR3	TPS (30% Glycerol)	3
SNR5	TPS (30% Glycerol)	5

[a]All percentages are by weight.

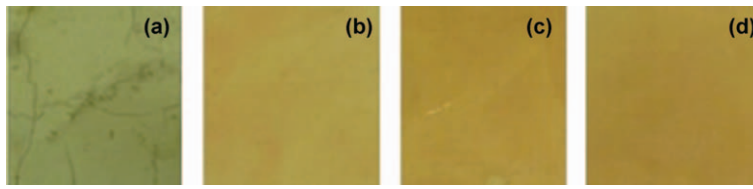

Figure 26.10 Surface images of vulcanized TPS–NR blends: (a) SNR0, (b) SNR1, (c) SNR3, (d) SNR5.

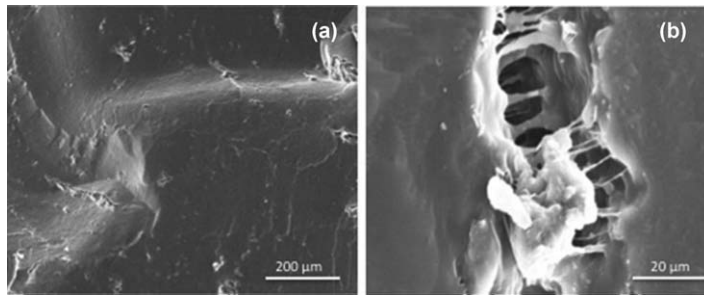

Figure 26.11 SEM images of vulcanized TPS–NR blends with 5% of NR (SNR5): (a) surface; (b) crack on the surface.

especially if it is crosslinked through vulcanization by sulfur.[49,50] For these reasons, small amounts of NR were blended with TPS.

Figure 26.10 shows surface images of the materials produced. The neat TPS formulation has several cracks and holes through the surface. Nevertheless, the TPS blended with NR shows neither cracks nor holes on the surface. NR was homogeneously distributed among the TPS matrix. A drastic change in colour was also observed.

Figure 26.11 shows SEM micrographs of the blend with 5% of NR (SNR5). As is shown in the image on the left the surface is very homogeneous. Only a small amount of particles are observed, which could be due to the presence of granules of starch not being completely disrupted after the plasticization process or to NR that was not well mixed after the blending process. On the other hand, the adhesion between TPS and NR was also qualitatively analysed using SEM images. The image on the right (Figure 26.11(b)) shows a small crack on the surface where it is possible to observe how the NR completely adheres to the TPS matrix.

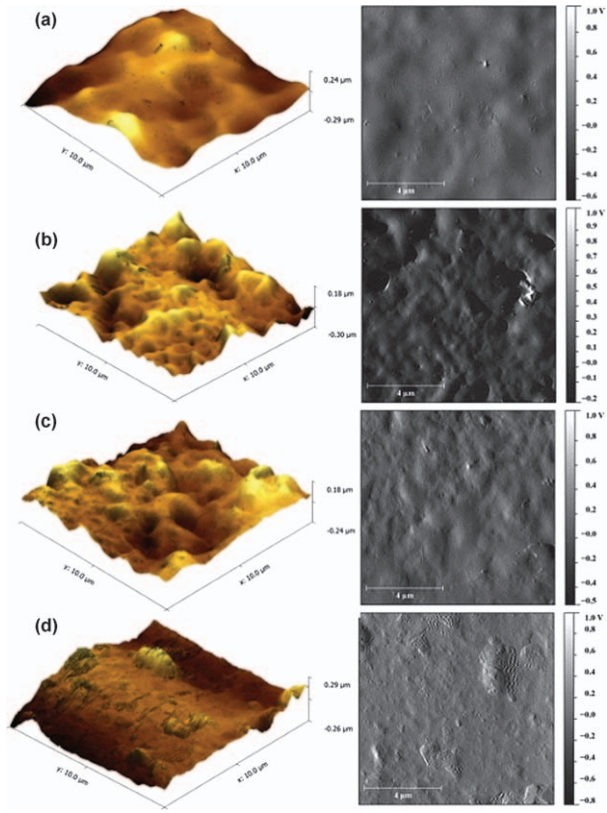

Figure 26.12 AFM images of vulcanized TPS–NR blends: (a) SNR0, (b) SNR1, (c) SNR3, (d) SNR5.

In order to gain a deeper insight into the morphology of these blends, AFM images were also obtained and are shown in Figure 26.12. Figure 26.12(a) (SNR) shows a smooth surface characteristic of the thermoplastic materials, as mentioned earlier. As the concentration of NR in the blends is increased (Figure 26.12(b), (c) and (d)) this smooth surface was substituted by irregular surfaces due to the presence of NR. These microscopic features of the blends could not be observed in the images in Figure 26.12 (much lower magnification) where blends showed a high homogeneity.

Tensile tests were carried out in order to evaluate the influence of the addition of NR to the TPS matrix and the vulcanization process. The test was carried out to 50 mm/min and the extensometer length was 25 mm. Average stress–strain curves of the blends produced are shown in Figure 26.13.

Figure 26.14 shows the results obtained from the tensile tests regarding elastic modulus (Figure 26.14(a)) and tensile strength (Figure 26.14(b)).

On the one hand, elastic modulus, although decreasing linearly when the amount of NR in the blends increases, was not influenced to a large extent by the addition of NR. Neat TPS elastic modulus was 107 MPa and with the addition of 5% of NR, elastic modulus dropped to 92 MPa. The crosslinking of

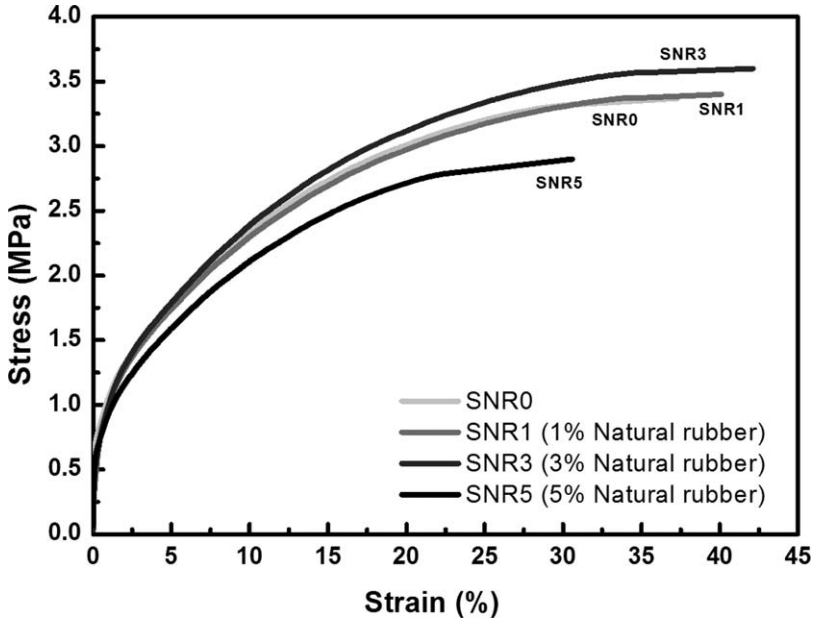

Figure 26.13 Average stress–strain curves of the blends produced.

starch by sulfur and the low amounts of NR employed in the production of the blends could explain the small decrease in mechanical properties regarding stiffness. On the other hand, tensile strength increased, although only slightly, up to 3.6 MPa in the case of 3% of NR. Tensile strength decreased only when blends of 5% of NR are considered.

Regarding the elongation at break (Figure 26.15), the same trend was observed with respect to tensile strength. Elongation at break was increased when NR concentrations of 1% and 3% are incorporated. The introduction of 5% of NR causes a decrease in the elongation at break.

To sum up with respect to mechanical properties, although elastic modulus decreased linearly with the concentration of NR in the blends, this decrease was lower than expected taking the low stiffness of NR into account. On the contrary, tensile strength and elongation at break were improved with concentrations of 1% and 3% of NR.

Regarding the water uptake of starch, several tests are currently being performed in order to evaluate the influence of blending TPS with NR. These tests comprise, firstly, the measurement of water uptake by the total immersion of the materials produced in water. The samples are weighed before and after the immersion in order to measure the water uptake. Secondly, the measurement of the equilibrium contact angle of a drop of water placed over the surface of the materials. Taking the hydrophobic nature of NR into consideration and the high compatibility reached between both polymers in this research, a decrease in water uptake is expected.

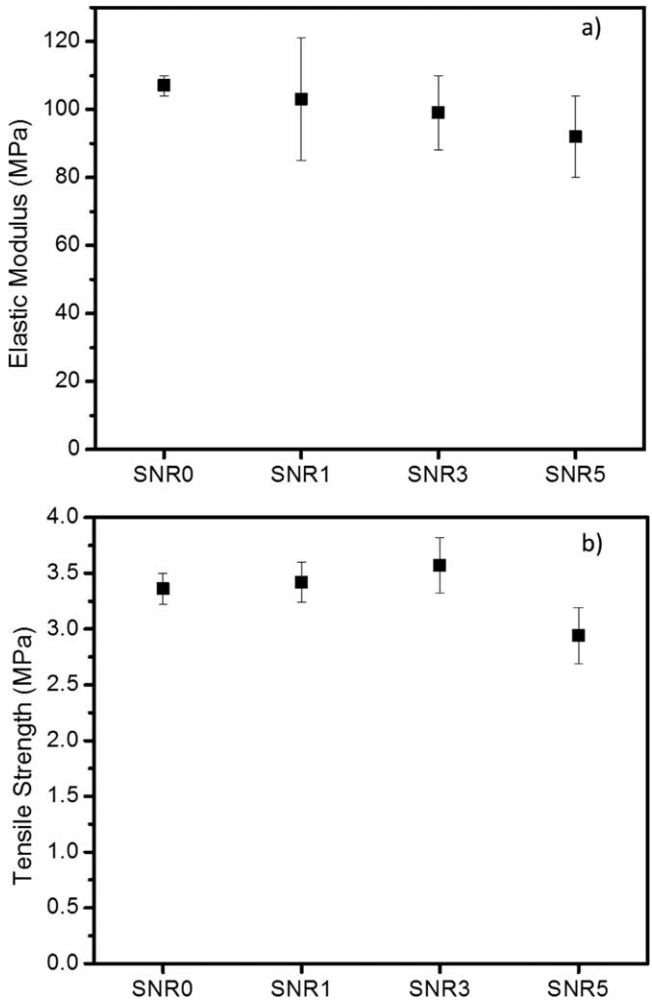

Figure 26.14 (a) Elastic modulus. (b) Tensile strength.

26.2.4 Conclusions

Several objectives were set up at the beginning of the research with regards to blending TPS with NR. The first one was the compatibility between both polymers. Not only a high homogeneity but also high adhesions between both polymers were observed from the pictures and SEM micrographs. Secondly, an improvement of the mechanical properties was also one of the main challenges. Elongation at break was improved with the addition of 3% NR and higher strengths were also achieved with concentrations of NR of 1% and 3%. Concentrations of NR higher than 3% resulted in a worsening of both, flexibility and strength. Nevertheless, It is fair to point out that further work must be performed in order to evaluate the suitability of these materials for the

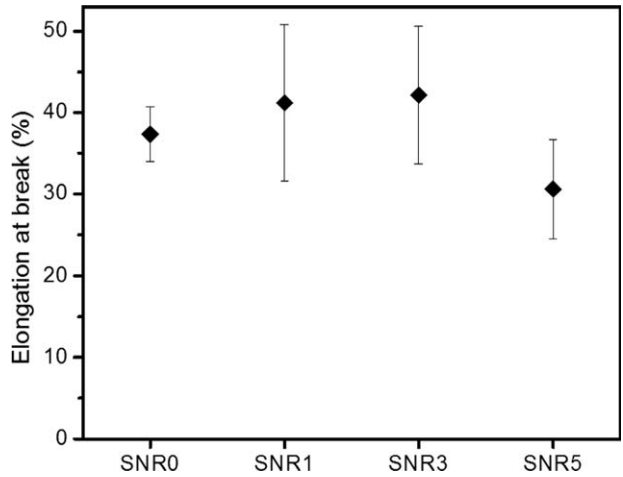

Figure 26.15 Elongation at break (%).

production of food package trays. Water absorption measurements and biodegradation tests of the blends produced will be carried out in order to fully characterize the materials produced.

26.3 Production and Characterization of Dry Natural Rubber Foams

26.3.1 Introduction

Foams are generally defined as a solid network composed of struts and/or faces enclosing a gaseous phase in cells. There are very common foams in nature such as sponge, wood, cork and coral but man has also been capable of producing foams such as honeycomb-like materials, polymeric foams and even metallic, glass and ceramic foams (Table 26.3). The polymeric foam industry dates back to the first half of the 20th century. Nevertheless, the wide range of properties of these materials (Figure 26.16) have been the driving force behind the continuous growth of polymer foam products and the development of foaming technologies during the second half of the 20th century.[51,52] Examples of polymer foams are shown in Figure 26.17.

There are three kinds of polymers used for making foams: thermoplastics, thermosets and elastomers. Elastomers are a special kind of polymers composed of linear chains with a few widely spaced crosslinks attaching each molecule to its neighbours. The main difference with respect to thermoplastics and thermosets is their T_g, which is well below room temperature (−60 °C).[53] Due to the presence of the spaced crosslinks, elastomers can undergo deformations of up to 500%. However, when unloaded, the material returns to its original shape.[54]

Table 26.3 Common foamed products.

Natural:	Pumice, Tree, Trunk, Wood, Cork, Marine Organisms
Synthetic:	
• Food:	Steamed Rice, Flour Dough, Popped Cereal...
• Plastic:	Seat cushion, Life jacket, Insulation Board...
• Automotive:	Armrest, Liner, Bumper...
• Sports:	Helmet Pad, Knee Protection, Surfing Board
• Medical:	Tape, Gasket Seal.

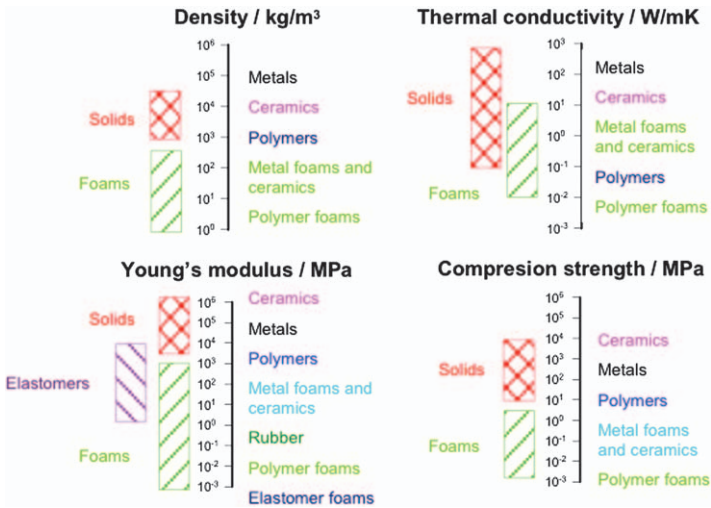

Figure 26.16 Properties of foams and solids.

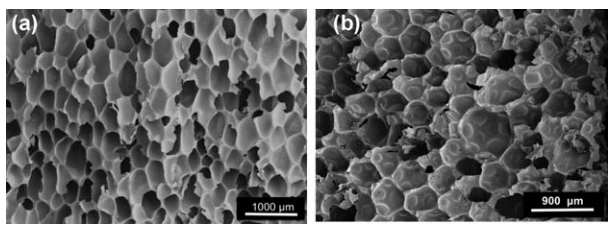

Figure 26.17 Examples of polymer foams: (a) polypropylene foam, (b) rigid polyurethane foam.

NR is a naturally existing elastomer composed mainly of *cis*-1,4-polyisoprene. It is collected from more than 400 different species of plants but the main source is *Hevea brasiliensis*. The collection is in the form of latex, a colloidal solution of NR, which contains about 70% of water and other materials in smaller quantities such as proteins, fatty acids, resins, *etc*. After removing the excess water by centrifugation two products based on NR can be obtained: concentrated latex and dry natural rubber. Concentrated latex has about 60%

Figure 26.18 Dry natural rubber.

of NR and dry natural rubber (Figure 26.18) is completely solid. NR has applications in several industrial sectors such as tyres, industrial and general rubber goods, bridge and earthquake bearings, expansion joints, *etc*.[55]

Currently, most of the foams found on the market based on NR are produced from the colloidal suspension commonly called latex. Two methods have been traditionally used to produce latex foams: Dunlop and Talalay.[56] Mattresses and pillows are common examples of products obtained through these processes. Nevertheless, foams produced by dry natural rubber are unlikely to be found in the market and it is a topic which has not been studied in depth yet. Only few studies concerning dry natural rubber foams are found in the literature.[57–59] Also, prices of dry natural rubber ($\approx$6 €/kg) are extremely high in comparison with synthetic rubber materials such as styrene butadiene rubber ($\approx$2.3 €/kg).

Several industrial sectors such as automotive, aeronautics, sports, footwear, packaging and toys are currently employing NR foams because of its low density, thermal insulation, acoustic absorption and high abrasion and impact strength.[60] When it comes to the footwear industry, it is noteworthy the employment of NR foams for the production of insoles. On the other hand, the construction industry employs NR foams in order to improve the thermal and acoustic absorption of roofs, walls, air conductions, pipes, floors, *etc*.[61]

Therefore, this research work aims to produce and characterize low-density cellular materials based on dry natural rubber in order, on the one hand, to reduce the density and consequently the price of this raw material, and on the other hand to provide further knowledge about the topic. A production process, which combines the crosslinking by sulfur, commonly called vulcanization, and the foaming of NR by decomposing a chemical blowing agent inside a closed mould, was developed. Finally a study of the correlation between density, cellular structure and mechanical and acoustic absorption properties of the foams produced has been carried out.

26.3.2 Production of Vulcanized Natural Rubber Foams

The formulation employed for the production of vulcanized NR foams are summarized in Table 26.4. Raw materials are classified depending on the process: vulcanization or foaming.

Table 26.4 Formulation.

Name	*Chemical Formula*	*Molar Mass*	*Phr*[a]
Vulcanization:			
Zinc Oxide	ZnO	129.39	4
Stearic Acid	$CH_3[CH_2]_{16}COOH$	284.47	3
Sulphur	S_8	167.24	2
2-Mercaptobenzotiazol	$S_2NC_7H_7$	284.47	1
Foaming:			
Azodicarbonamide	$C_2H_4O_2N_4$	116.00	5
Zinc Oxide	ZnO	129.39	0.25

[a]Parts per hundred of natural rubber.

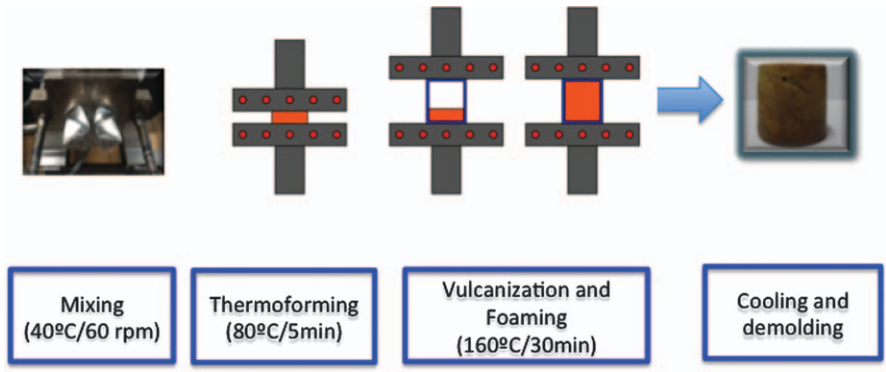

Figure 26.19 One-step process.

Two different production routes were developed in order to decrease the density of NR materials: the first involves only one step, in which vulcanization and foaming take place simultaneously without a previous pre-vulcanization of NR. This production route was called one-step process. The second one, on the contrary, was carried out in two steps: first, NR is pre-vulcanized and later vulcanized and foamed at the same time. This production route was called the two-step process. The one-step process is described schematically in Figure 26.19.

Firstly, dry natural rubber was mixed with stearic acid and zinc oxide in an internal mixer at a temperature of 60 °C and using a speed of 60 rpm. Then, the mixture was stored at room temperature without light exposure for 24 h. This storing time is required so as to complete the reaction of activation of NR. Once the reaction was performed, the materials employed for the vulcanization of NR, sulfur and mercaptobenzothiazole, and the chemical blowing agent employed for foaming, in this case azodicarbonamide, were added and mixed with the activated NR in the same rheometer using the same processing conditions. It is fair to point out that an additional amount of zinc oxide (0.25 phr) was also added in order to catalyse the chemical decomposition of azodicarbanamide.[62]

Secondly, the mixture produced is thermoformed in a hot-plates press at 80 °C for 5 min using a pressure of 1 ton with the aim of obtaining circular samples. The thermoformed sample of activated NR was then introduced into a circular mould. The mould was also placed in the hot-plates press where the vulcanization and foaming process were performed simultaneously. The reason for choosing a hot-plates press instead of a conventional oven was that the heat transfer is faster in a press than in an oven, which consequently allows a reduction in the production time. Nevertheless, no pressure was applied to the material. The plates of the press were only in contact with the upper and lower surfaces of the mould. Temperature and time were set up respectively to 160 °C and 30 min. During this time, NR was crosslinked and expanded due to the decomposition of azodicarbonamide in gases, mainly N_2 and CO, allowing NR to fill the mould completely. Finally, the mould was water cooled and the foam was removed from it.

The two-step process, as well as the one-step process, is described schematically in Figure 26.20.

As shown in Figure 26.20, the two-step process also involves a pre-vulcanization step. The reason for introducing a pre-vulcanization step was to study the influence of the crosslinking degree by sulfur in the cellular structure. Different cellular structures regarding cell sizes, open cell content, anisotropy, *etc*. that could be obtained by different degrees of crosslinking, should influence to a large extent mechanical and acoustic properties.

The production route is exactly the same as in the one-step process, with the exception of introducing the pre-vulcanization step immediately after the thermoforming of NR. In this step, temperature and time were set up respectively to 140 °C for 5 min.

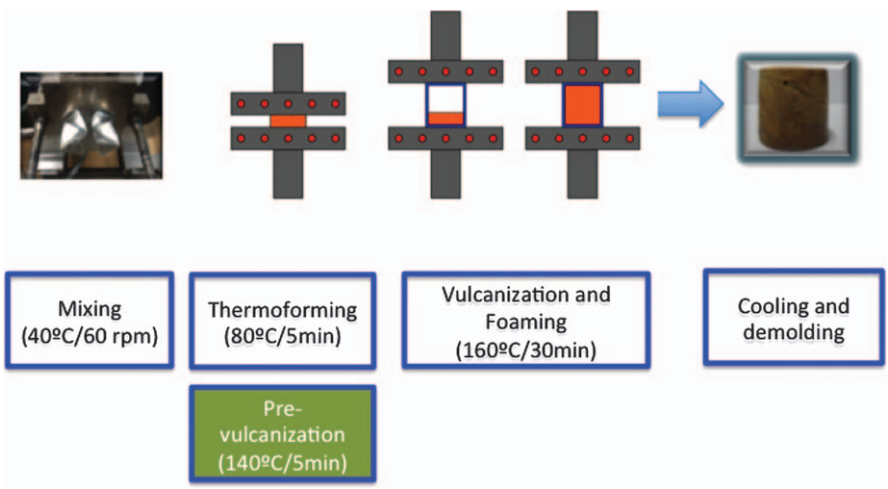

Figure 26.20 Two-step process.

26.3.3 Characterization of Vulcanized Natural Rubber Foams

The main objective of this characterization is to establish a relationship between the degree of crosslinking of the NR matrix and the foams density, cellular structure and mechanical and acoustic properties.

26.3.3.1 Density

No significant differences were observed for the foams produced by the one-step process and the two-step process. Figure 26.21 shows a comparison between NR density and the average density of the foams produced by both methods. This foaming process allowed reductions in density of up to 2.3 times with respect to solid NR.

26.3.3.2 Cellular Structure

Figure 26.22 shows images of vulcanized NR foams produced by the one-step and two-step processes in the expansion direction and in the transversal direction of expansion. Clear differences can be seen.

SEM images of both foams were obtained in order to better characterize not only cell size and cell distribution but also anisotropy. These SEM images are shown in Figure 26.23. In order to quantify the observed differences, image analysis was conducted.

Figure 26.24(a) shows how cell size is greatly influenced by the production method employed. Cell sizes are smaller when foams are produced by the two-step process. Moreover, cell size is also greater in the expansion direction than

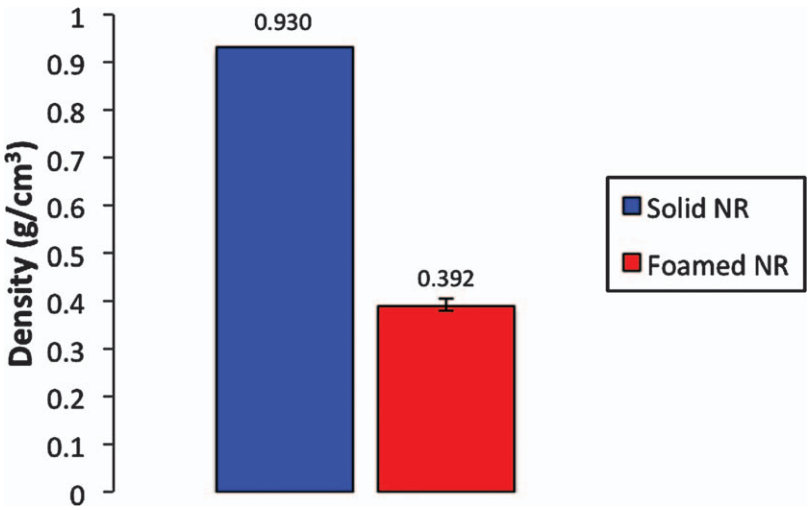

Figure 26.21 Density of the solid material and the foams produced.

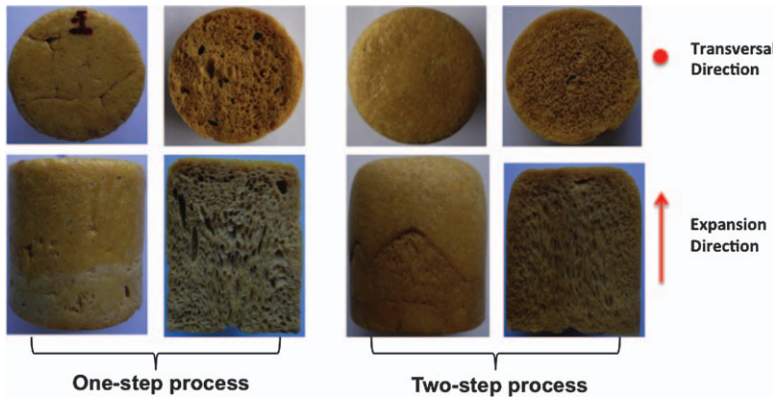

Figure 26.22 Images of the foams produced.

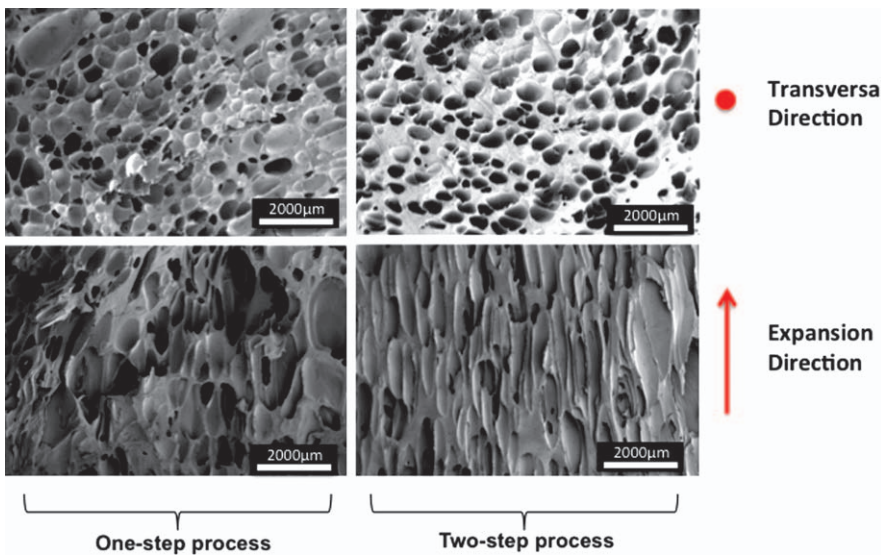

Figure 26.23 SEM images of the foams produced in two perpendicular directions.

in the transversal direction. Figure 26.24(b) shows how cell size distribution is also influenced to a large extent by the production method because a narrower, and therefore more homogeneous distribution of cell size is observed for the two-step method. Last but not least, cell anisotropy in the expansion direction of the foam produced by the two-step process is higher than that of the foam produced by the one-step process.

The two-step process is supposed to increase the degree of crosslinking of the NR matrix prior to foaming due to the pre-vulcanization step. The NR matrix, after being pre-vulcanized, increased its strength and viscosity and this results in the production of foams with higher homogeneities regarding cell

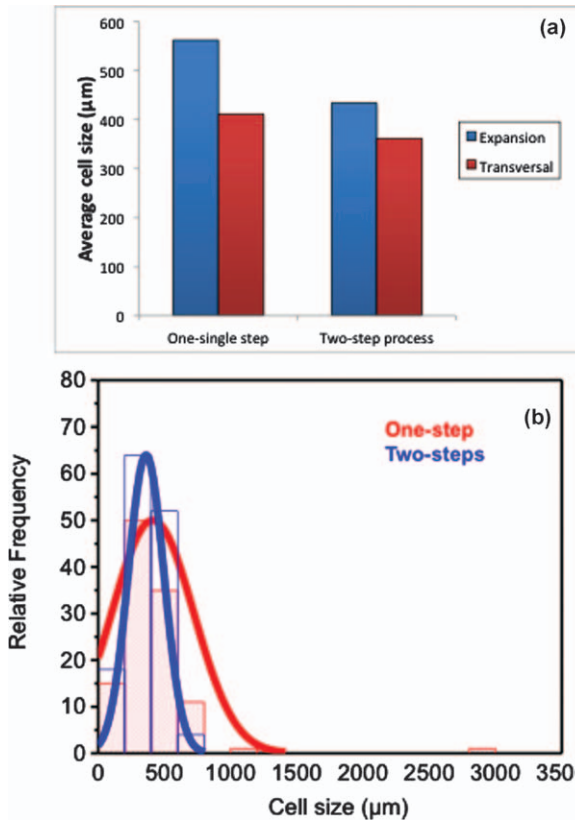

Figure 26.24 Morphological characterization: (a) cell sizes, (b) cell size distribution.

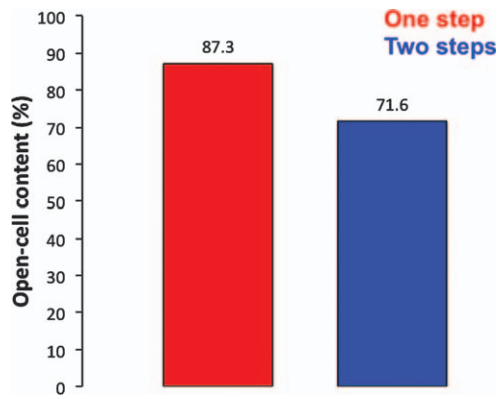

Figure 26.25 Open-cell content.

sizes and cell size distribution and a higher anisotropy in the foaming direction. Moreover, open cell content was decreased up to 15.6%, as shown in Figure 26.25.

26.3.3.3 Acoustic Absorption

NR has been traditionally employed as a sound absorber. The NR foams sound absorption capacity is generally higher in the regions of lower (1000–200 Hz) and higher (5500–6400 Hz) frequencies. The maximum absorption capacity is 83% in the range of high frequencies. Sound absorption capacity is influenced by the cellular structure, relative density and the crosslinking density.[57] Several mechanisms of sound absorption have been described in the literature.[63–65] When a sound wave reaches a surface such as metal or a rigid closed cell foam is mostly reflected. Only a small proportion of the wave energy is absorbed by the material. On the contrary, in the case of open cell foams, most of the sound wave penetrates the foam structure. Once the sound wave goes through the foam cells, sound pressure is considerably reduced due to the air friction against the cell walls. Higher times of the sound wave travelling through the foam, results in higher sounds absorptions. Figure 26.26 shows how the foams produced with the one-step process, with higher open cell contents, presented higher sound absorptions in all the frequency ranges under study. As the foams are mainly closed cell, the acoustic absorption is in general low.

26.3.3.4 Mechanical Properties

A five-cycle compression test was carried out under the standard ISO 3386-1:1986. Results are shown in Figure 26.27. Not only was a comparison between the foams produced by the different production methods obtained but also with a commercial latex foam. Commercial latex foam (density = 300 kg/m^3), even after the first compression test, clearly showed a high hysteresis and therefore, a loss in the capacity of absorbing energy. Nevertheless, vulcanized NR foam showed almost no hysteresis even after completing the five-cycle compression test.

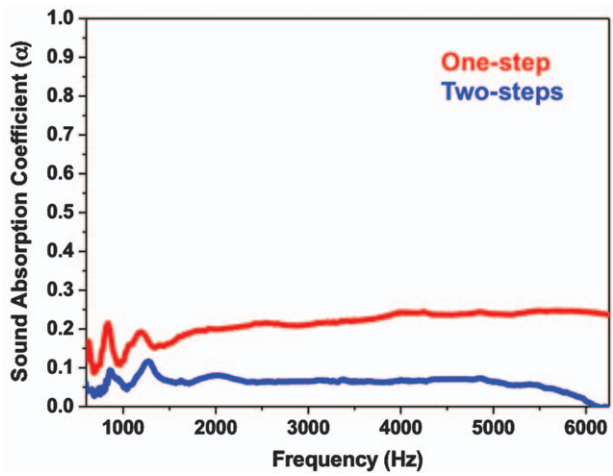

Figure 26.26 Sound absorption coefficient measurements.

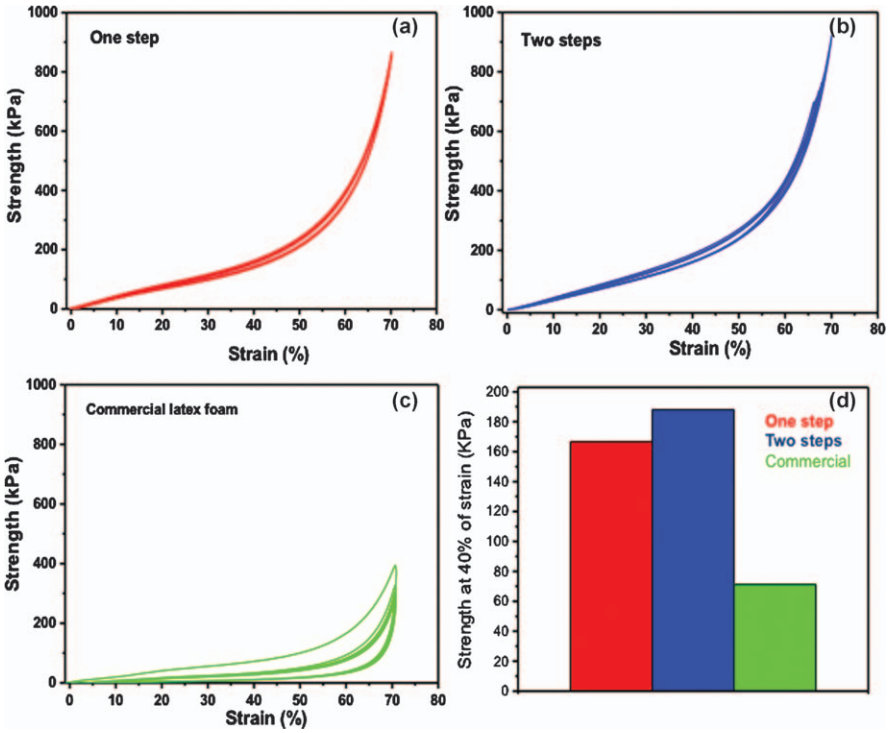

Figure 26.27 Five-cycle compression tests: (a) one-step process, (b) two-step process, (c) commercial latex foam, (d) strength at 40% of strain.

Foams produced by the two-step process have slightly better compressive stress than foams produced by the one-step method, as shown in Figure 26.27(d). This result can be explained by taking several factors into consideration. First of all, the two-step foams have a higher degree of cross-linking due to the pre-vulcanization step and therefore, the vulcanized NR matrix is stronger. Secondly, the open cell content of the two-step foams is slightly lower and cell anisotropy is higher than that of the foams produced by a single step. One of these effects, or a combination of them, resulted in better mechanical properties for the foams produced by the two-step process.

26.3.4 Conclusions

Significant reductions in NR density were achieved by means of foaming methodologies based on the decomposition of a chemical blowing agent inside a closed mould. By introducing a pre-vulcanization step (two-step process), different cellular structures regarding open cell content, anisotropy, cell size and cell size distribution were obtained. These variations in the cellular structure resulted in different mechanical behaviours and acoustic absorption. Foams produced by the two-step process allowed higher strengths to be obtained and foams produced by the one-step process presented higher open cell

contents and therefore higher acoustic absorption. Finally, a comparison with a commercial latex foam showed how the mechanical behaviour is clearly different with respect to dry natural rubber foams. Dry natural rubber foams presented almost no hysteresis, while the commercial latex foam presented a high hysteresis even after the first compression cycle.

Acknowledgements

The authors would like to acknowledge the Brazilian research agencies FAPESP, CAPES and CNPq for financial support, and also the research groups NanoBioNet, NanoBioMed, INEO, the graduate programme of Materials Science and Technology – POSMAT, Carlos Gomes Barboza-Filho for the biological tests and also Dr Ricardo F. Aroca and Ariel Guerrero for the AFM measurements.

References

1. W. Hofmann, *Rubber technology handbook*, ed. Hanser Publishers, Oxford University Press, 1989, 674.
2. International Rubber Study Group, *Rubber Industry Report*, 2009, **8**, 7.
3. The Association of Natural Rubber Producing Countries (ANRPC), *Monthly Bulletin of Rubber Statistics*, 2009, **1**, 1.
4. A. C. Dall'Antonia, M. A. Martins, R. M. Moreno, L. H. C. Mattoso, A. E. Job, F. C. Ferreira and P. S. Gonçalves, Avaliação de clones de borracha natural crua por ensaios padrão e analise dinâmico-mecânica, *Polímeros: Ciência e Tecnologia*, 2006, **16**(3), 239–245.
5. M. A. Martins, L. A. Forato, L. A. Colnago, A. E. Job, R. M. B. Moreno, L. H. C. Mattoso and P. S. Gonçalves, Avaliação da Borracha Natural de Clones da Série IAC por RMN 13C no Estado Sólido, Associação Brasileira de Polímeros, Anais 8° Congresso Brasileiro de Polímeros, 2005, Águas de Lindóia, 105.
6. E. B. Mano, L. C. Mendes, *Introdução a Polímeros*, ed. Edgard Blücher, 2, 1999.
7. W. J. S. Nauton, *Ciencia y tecnologia del caucho*, ed. Compania Editorial Continental, 1, 1967.
8. C. M. Blow, *Rubber technology and manufacture*, ed. Institution of the Rubber Industry, 2, 1975.
9. H. Bar, D. Kr. Bhui, G. P. Sahoo, P. Sarkar, S. Pyne and A. Misra, Green synthesis of silver nanoparticles using latex of Jatropha curcas, *Colloids and Surfaces A: Physicochem. Eng. Aspects*, 2009, **339**, 134–139.
10. H. Bar, D. Kr. Bhui, G. P. Sahoo, P. Sarkar, S. Pyne and A. Misra, Green synthesis of silver nanoparticles using seed extract of Jatropha curcas, *Colloids and Surfaces A: Physicochem. Eng. Aspects*, 2009, **348**, 212–216.
11. N. H. H. Abu Bakar, J. Ismail and M. Abu Bakar, *Materials Chemistry and Physics*, 2007, **104**, 276.

12. M. Abu Bakar, J. Ismail and C. H. Teoh, *Journal of Rubber Research*, 2008, **11**, 4, 196.
13. M. A. Bakar, J. Ismail, C. H. Teoh, W. L. Tan and N. H. H. A. Bakar, *Journal of Nanomaterials*, 2008, Article ID 130295, DOI: 10.1155/2008/130295.
14. K. C. Grabar, R. G. Freeman, M. B. Hommer and M. J. Natan, Preparation and Characterization Monolayers, *Anal. Chem.*, 1995, **67**, 735–743.
15. F. Cienfuegos, D. Vaitsman, *Análise Instrumental*, ed. Interciência Ltda., **1**, 2000.
16. R. F. Aroca, R. A. Alvarez-Puebla, N. Pieczonka, S. Sanchez-Cortez and J. V. Garcia-Ramos, *Adv. Colloid Interface Sci.*, 2005, **116**, 45–61.
17. C. M. Petty, *Langmuir-Blodgett Films – an Introduction*, ed. Cambridge University Press, 1, 1996.
18. A. Cavalli, G. Borissevitch, M. Tabak and O. N. Oliveira Jr, *Thin Solid Films*, 1996, **284-285**, 731–734.
19. G. Ladam, P. Schaaf, G. Decher, J. C. Voegel and F. J. G. Cuisinier, *Biomolecular Engineering*, 2002, **19**(2-6), 273–280.
20. R. D. Herculano, C. P. Silva, C. Ereno, S. A. C. Guimaraes, A. Kinoshita and C. F. O. Graeff, *Materials Research*, 2009, **12**(2), 253–256.
21. M. Ferreira, R. J. Mendonça, J. Coutinho-Netto and M. Mulato, *Brazilian Journal of Physics*, 2009, **39**, 3.
22. F. Mrué, *Neoformação tecidual induzida por biomembrana de látex natural com poli-lisina. Aplicabilidade na neoformação esofágica e da parede abdominal. Estudo experimantal em cães*. 2000, Ribeirão Preto, São Paulo, Brazil: Faculty of medicine of Ribeirão Preto, USP.
23. M. A. Frade, R. V. Valverde, R. V. de Assis, J. Coutinho-Netto and N. T. Foss, *International journal of dermatology*, 2001, **40**(3), 238–240.
24. D. L. S. Agostini, C. J. L. Constantino and A. E. Job, *Journal of Thermal Analysis and Calorimetry*, 2008, **91**, 703.
25. U. A. Gunasekera, Q. A. Pankhurst and M. Douek, *Targ. Oncol.*, 2009, **4**, 169.
26. S.-Y. Jeong, S.-J. Park, S. M. Yoon, J. Jung, H. NaWoo, S. L. Yi, S. Y. Song, H. J. Park, C. Kim, J. S. Lee, J. S. Lee and E. K. Choi, *Journal of Controlled Release*, 2009, **139**, 239–245, DOI: 10.1016/j.jconrel.2009.07.007.
27. W. H. Jong and P. J. A. Borm, *International Journal of Nanomedicine*, 2008, **3**(2), 133.
28. H. C. Fischer and W. C. W. Chan, *Pharmaceutical biotechnology*, 2007, **18**, 565.
29. N. R. Panyala, E. M. Peña-Méndez and J. Havel, *J. Appl. Biomed*, 2009, **7**, 75.
30. K. L. Aillon, Y. Xie, N. El-Gendy, C. J. Berkland and M. L. Forrest, *Advanced Drug Delivery Reviews*, 2009, **61**, 457–466, DOI: 10.1016/j.addr.2009.03.010.
31. C. G. Barboza-Filho, F. C. Cabrera, R. J. dos Santos, J. A. S. Saez and A. E. Job, *Journal Experimental Parasitology*, 2012, **130**, 152.

32. L. H. P. da Silva, M. Camurate, K. A. Costa, S. M. P. Oliveira, N. L. Cunha e Silva and E. M. B. Saraiva, *Int J Parasitol.*, 2002, **3**, 1371–1377.
33. N. Kimblin, N. Peters, A. Debrabant, N. Secundino, J. Egen, P. Lawyer, M. P. Fay, S. Kamhawi and D. J. Sacks, *PNAS*, 2008, **105**(29), 10125–10130.
34. M. F. Sernee, J. E. Ralton, Z. Dinev, G. N. Khairallah, R. A. O'Hair, S. J. Williams and M. J. McConville, Leishmania β-l,2-mannan is assembled on a mannose-cyclic phosphate primer, *PNAS*, 2006, **103**(25), 9458–9463.
35. L. S. Peloia, C. E. G. Biondo, E. Kimura, M. J. Politi, M. V. C. Lonardoni, S. M. A. Aristides, R. C. C. Dorea, N. Hioka and T. G. V. Silveira, Photodynamic therapy for American cutaneous leishmaniasis: The efficacy of methylene blue in hamsters experimentally infected with Leishmania amazonensis, *J. Exp. Para.*, 2011, **128**(4), 353, DOI: 10.1016/j.exppara.2011.04.009.
36. R. A. Prates, A. M. Yamada Jr., L. C. Suzuki, M. C. E. Hashimoto, S. Cai, S. Gouw-Soares, L. Gomes and M. S. Ribeio, Bactericidal effect of malachite green and red laser on Actinobacillus actinomycetemcomitans, *Journal of Photochemistry and Photobiology B: Biology*, 2007, **86**, 70–76.
37. M. Wainwright, *Journal of Antimicrobial Chemotherapy*, 1998, **42**, 13.
38. M. Miyabe, J. C. Junqueira, A. C. B. P. da Costa, A. O. C. Jorge, M. S. Ribeiro and I. S. Feist, Effect of photodynamic therapy on clinical isolates of Staphylococcus spp, *Braz. oral res.*, 2011, **25**(3), 230–234.
39. J. P. F. Longo and R. B. Azevedo, *J. Dent. Clin. Res.*, 2010, **6**(3), 249.
40. G. Davis and J. H. Song, *Industrial Crops and Products*, 2006, **23**, 147.
41. J. BeMiller, R. Whistler, *Starch. Chemistry and Technology*, ed. Elsevier, 2009.
42. R. Zullo and S. Iannace, *Carbohydrate Polymers*, 2009, **77**, 376.
43. A. J. F. Carvalho, A. E. Job and N. Alves, *Carbohydrate Polymers*, 2003, **53**, 95.
44. Z. Wang, Z. Peng, S. Li, H. Lin, K. Zang, X. She and X. Fu, *Composites Science and Technology*, 2009, **69**, 1797.
45. V. Tanrattanakul and W. Chumeka, *Journal of Applied Polymer Science*, 2009, DOI: 10.1002/app.
46. J. E. Mark, B. Erman, F. R. Eirich, *The Science and Technology of Rubber*, ed. Elsevier, 2005, ISBN 0-12-464786-3.
47. L. Janssen, L. Moscicki, *Thermoplastic Starch. A Green Material for Various Industries*, ed. Wiley-VCH, 2009, ISBN 978-3-527-32528-3.
48. F. S. Bellucci, L. O. Salmazo, E. R. Budemberg, M. R. da Silva, M. A. Rodríguez-Pérez, M. A. L. Nobre and A. E. Job, *Journal of Nanoscience and Nanotechnology*, 2012, **12**, 2691.
49. R. V. Roy, M. Das, R. Banerjee and A. K. Bhowmick, *Process Biochemistry*, 2006, **41**, 181.
50. R. V. Roy, M. Das, R. Banerjee and A. K. Bhowmick, *Bioresource Technology*, 2006, **97**, 2485.
51. L. J. Gibson, M. F. Ashby, *Cellular Solids. Structure and properties*, ed. Cambridge University Press, 1997, ISBN 0 521 49560 1.

52. S. Lee, C. B. Park, N. S. Ramesh, *Polymeric Foams: Science and Technology*, ed. Taylor and Francis Group, 2007, ISBN 0-8493-3075-0.
53. M. A. Mansilla, L. Silva, W. Salgueiro, A. J. Marzocca and A. Somoza, *Journal of applied polymer science*, 2012, **125**(2), 992.
54. A. P. Meera, R. Tlili, A. Boudenne, L. Ibos, V. Poornima, S. Thomas and Y. Candau, *Journal of Elastomers and Plastics*, 2012, **44**, 369.
55. M. Morton, V. N. Reinhold, *Rubber technology*, ed. New York, 1987.
56. D. Eaves, *Handbook of polymer foams*, ed. Rapra Technology Limited, 2004, ISBN 1-85957-388-6.
57. N. N. Najib, Z. M. Ariff, A. A. Bakar and C. S. Sipaut, *Materials and Design*, 2011, **32**, 505.
58. N. N. Najib, Z. M. Ariff, N. A. Manan, A. A. Bakar and C. S. Sipaut, *Journal of Physical Science*, 2009, **20**(1), 13.
59. Z. M. Ariff, Z. Zakaria, L. H. Tay and S. Y. Lee., *Journal of Applied Polymer Science*, 2008, **107**, 2531.
60. N. Sombatsompop, *Cell Polym*, 1998, **17**, 63.
61. G. Lin, X. J. Zhang, L. Liu, J. C. Zhang, Q. M. Chen and L. Q. Zhang, *European Polymer Journal*, 2004, **40**, 1733.
62. A. Zoller and A. Marcilla, *Journal of Applied Polymer Science*, 2011, **122**, 2981.
63. Z. Hong, L. Bo, H. Guangsu and H. Jia., *J Sound Vibrat*, 2007, **304**, 400.
64. X. Liu, M. Zhan and K. Wang, *High performance polymers*, 2012, **24**(7), 646.
65. Z. Hong, L. Bo and H. Guangsu, *Mater Lett*, 2006, **60**, 3451.

CHAPTER 27

Diffusion and Transport of Liquids, Vapours and Gases Through Natural Rubber Composites and Nanocomposites

THANAPORN AMNUAIKIT

Faculty of Pharmaceutical Sciences, Prince of Songkla University, Hat Yai, Songkhla, 90112, Thailand
Email: chomchan1@yahoo.com; chomchan.a@psu.ac.th

27.1 Fundamental Theories of Diffusion and Transport of Liquids, Vapours and Gases

The transport of liquids, vapours and gases through rubber is an important property that must be considered for utilizing the rubber material in various applications, such as in biomedical products, packaging, tyre industry and *etc*. The diffusion of such penetrants through the rubber materials has been shown as a critical factor in the existing shelf life of products made of these rubber materials. In packaging, materials that protect liquids, vapours and gases which pass through them is required. This is one of the criteria for polymer composite and nanocomposite system which have been developed as an increasing barrier in order to minimize the penetration of liquids, vapours and gases. Therefore, the basic knowledge of theories of diffusion and transport behaviours could be stated to determine the suitable property and understand their mechanism.

RSC Polymer Chemistry Series No. 8
Natural Rubber Materials, Volume 2: Composites and Nanocomposites
Edited by Sabu Thomas, Hanna J. Maria, Jithin Joy, Chin Han Chan and Laly A. Pothen

Published by the Royal Society of Chemistry, www.rsc.org

Liquid, vapours and gases can pass through materials by different processes, depending on the nature or physical property of the materials. In the case of porous materials, such as rock or wood, the gas or liquid flows through the holes within the materials. On the other hand, liquids, vapours and gases pass through non-porous materials such as rubber via permeation processes of absorption and diffusion, as shown in Figure 27.1.

The quantity of liquids, vapours and gases that can pass through the materials will be determined as the constant value at steady or equilibrium state. The diffusion of molecules of liquids, vapours and gases into materials depends on the physicochemical properties of both permeants and the permeable materials.[1–4] Free volume or holes that exist in the rubbery matrix is one of the critical factors influencing diffusion process of liquid, vapour and gas molecules to migrate from hole to hole. The transport of liquid, vapour and gas through non-porous polymer under applied driving force was described on variety models of solution–diffusion that contain a large number of diffusion parameters and equilibrium constant.[5] The suitable model depends on experimental data that fit the most of model's parameters which is highly system specific to the permeating species. However, the general parameters which are important to describe the permeation process through permeable material, the so-called solubility S and diffusivity D are displayed in Equation (27.1):[6]

$$P = D^{*}S \tag{27.1}$$

where P is the permeation coefficient, a direct measure of the permeation process; D is the diffusion coefficient of a gas or liquid molecule inside the

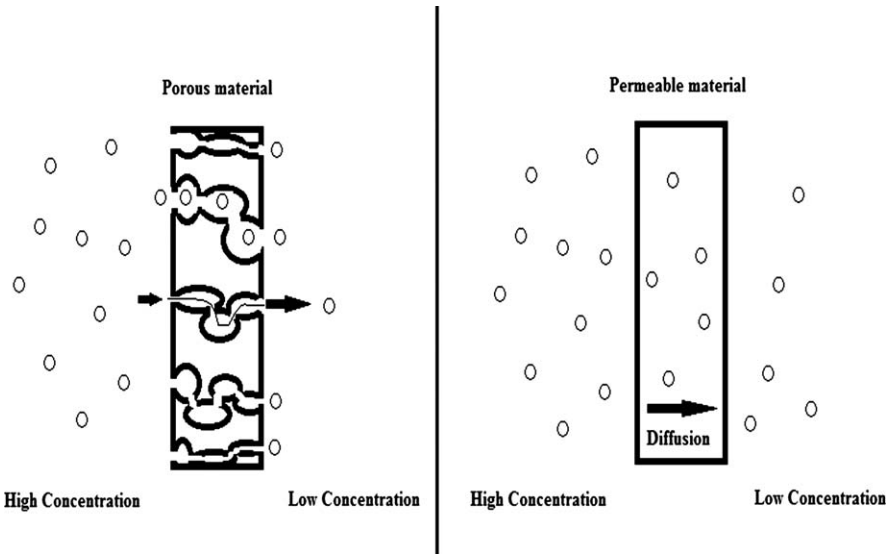

Figure 27.1 Diffusion and transport of substances through the materials: porous material (left) and permeable material (right).

polymer network; S is the soluble value of the total amount of gas or liquid trapped in the rubbery matrix.

Therefore, the diffusion process is a kinetic parameter depending on the free volume within the permeable material, segmental mobility of polymer chains, polymer structure, the size and shape of penetrant molecule and crystallinity.[4,7] The diffusion coefficient D is described by the following equation:[8]

$$D = \pi\left(\frac{h\theta}{4Q_\infty}\right)^2 \tag{27.2}$$

where h is rubber sample thickness, θ is the slope of the initial linear portion of the sorption curve Q_t *vs* $t^{[1/2]}$, Q_t and Q_∞ are the number of mole of liquid or gas sorbed by gram of rubber sample at time t and at equilibrium, respectively.

The thermodynamic solubility parameter S is estimated by the number of grams of liquid or gas sorbed per gram of rubber compound, which is given as:[8]

$$S = \frac{\text{weight of solvent uptake of equilibrium}}{\text{initial weight of rubber sample}} \tag{27.3}$$

Several diffusion models have been used to propose transport mechanism of liquid, vapour and gas molecules through the polymer. A model described by Fick's laws is frequently used and known as Case I or Fickian diffusion. The diffusion behaviour in the rubbery polymers, represented by permeation, migration and sorption processes, can be described by the equation of Fick's first law:[5]

$$J = -D\frac{\partial\phi}{\partial x} \tag{27.4}$$

where J is the flux density of the solute molecules through the rubbery matrix, D is the liquid, vapour or gas diffusion coefficient, $\partial\phi/\partial x$ is the concentration gradient applied across the rubbery matrix and ϕ is the concentration of the dissolved liquid, vapour or gas given as the amount of dissolved molecules per cubic centimetre of rubbery matrix.

In non-steady state diffusion, the concentration of dissolved molecules changes with respect to time in one direction within diffusion volume. This phenomenon is described by Fick's second law of diffusion:[5]

$$\frac{\partial\phi}{\partial t} = D\frac{\partial^2\phi}{\partial x^2} \tag{27.5}$$

Although Fickian diffusion has been used to describe the diffusion mechanism of liquid through the rubbery material because of its simplicity and mathematical tractability, most of the rubber–solvent systems do not fit such a simplified explanation.[9] Then, non-Fickian diffusion was developed. The case of non-Fickian diffusion was investigated using the following equation:[9,10]

$$Q = kt^n \quad \text{or} \quad \log Q_t / Q_\infty = \log k + n\log t \tag{27.6}$$

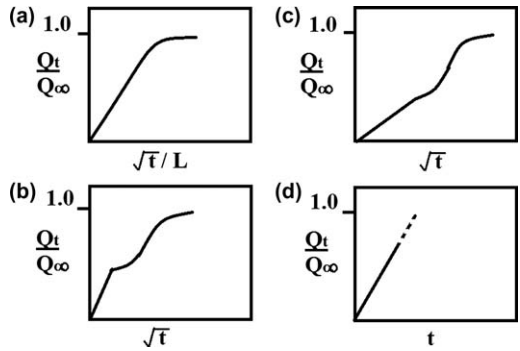

Figure 27.2 Different types of non-Fickian diffusion: (a) classical, (b) two steps, (c) sigmoidal, (d) Case II.
(This figure was modified from ref. 9.)

where Q represents mass uptake, which at equilibrium swelling or sorption Q_t becomes Q_∞, k is the value due to the structural features of the polymer and n is the value for determining the diffusion mechanism.

Whereas the value of n equals 0.5, the mechanism of diffusion described by Case I of Fickian model, when n values range between 0.5 and 1 that exhibits anomalous transport model and when n value equals 1, Case II of non-Fickian model is used to determine. Fickian model describing the rate of diffusion of penetrant molecule is much less than the relaxation rate of polymer chains while Case II of non-Fickian diffusion representing rate of diffusion is rapid than relaxation process. For the anomalous transport model, both solvent diffusion rate and polymer relaxation rate are comparable. Figure 27.2 shows various types of non-Fickian model; anomalous transport and Case II of non-Fickian are included in this group.[9]

For diffusion of liquid through rubbery polymer composites, Fickian and non-Fickian diffusion theories are frequently used to describe the mechanism of transport, but for gas or vapour, other models have been developed to fit experimental data of diffusion profiles. The models of gas transport include Maxwell's model,[11] free volume increase mechanism,[11] solubility increase mechanism,[11] nanogap hypothesis,[11] Nielsen model,[5,10,12] Bharadwaj model,[5,10,12] Cussler model[5,10,12] and Gusev and Lusti model,[5,12] *etc.*

Maxwell's model has been used to describe the behaviour of gas which permeates through a polymer added with roughly spherical impermeable inorganic nanoparticles. Addition of the molecules results in reduction of the gas permeability at the steady state. It is described by the following equation:[11]

$$P_c = P_p\left(\frac{1-\Phi_f}{1+0.5\Phi_f}\right) \tag{27.7}$$

where P_c and P_p stand for the permeability of the nanocomposite and the pure polymer matrix, respectively, and Φ_f represents the volume fraction of the nanofiller.

From Equation (27.7) of Maxwell's model, the numerator denotes the loss of rubbery matrix solubility due to the loss of polymer volume available for sorption. The denominator denotes a decrease in diffusivity due to increasing the penetrant diffusion pathway length. Both factors affect a decrease of permeability with increasing particle volume fraction.

Free volume increase mechanism was proposed by Cohen and Turnbull. The concept of this model deals with the effect of polymer free volume on penetrant diffusion coefficient. The model equation express for penetrant diffusion coefficient, D as following given:

$$D = A \exp\left(\frac{-\gamma V^*}{V_f}\right) \tag{27.8}$$

where A is a pre-exponential factor weakly dependent on temperature, γ an overlap factor introduced to avoid double-counting free volume elements, V^* the minimum free volume of polymer size that can accommodate a penetrant molecule, and V_f represents the average free volume in the polymer matrix accessible to penetrants for transport.

According to Equation (27.8), an increase in polymer free volume is expected to enhance penetrant diffusion. It could be described that the increased free volume results from the disruption of nanofillers in polymer-chain packing. Thus, gas diffusion through rubbery polymer is enhanced and subsequently increased gas permeability.

Solubility increase mechanism depends on the interaction between the penetrants and nanofillers. The functional groups of nanofillers such as hydroxyl when occur on the surface of the inorganic nanofiller phase in rubber composites may interact with polar gases such as SO_2. This condition can increase the penetrant solubility in the nanocomposite rubbers and, in turn, increase the gas permeability. The solubility increase mechanism model due to permeation coefficient parameter of gas, P is described using the Arrhenius equation:

$$P = P_0 \exp\left(\frac{-E_p}{RT}\right); \quad E_p = E_d + \Delta H_s \tag{27.9}$$

where P_0 is a pre-exponential factor, E_p the apparent activation energy equal to the activation energy of diffusion (E_d) plus the enthalpy of sorption (ΔH_s), R the ideal gas constant, and T is absolute temperature.

Nanogap hypothesis was developed for determining some experimental data that did not follow the free volume increase mechanism model. Because the increased gas permeability did not result from the disrupted polymer-chain packing of nanofiller. Cong *et al.*[11] proposed this hypothesis to their finding that the polymer chains could not tightly contact the silica nanoparticles due to the poor compatibility between the silica surface and the polymer, therefore forming a narrow gap surrounding the silica particles (Figure 27.3). The gas diffusion path was shortened and thus the apparent gas diffusivity and permeability were increased. In contrast, in the system containing nanoparticles

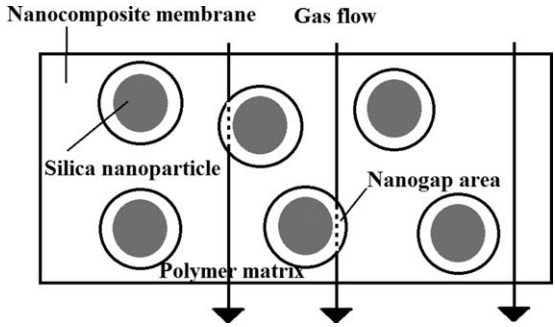

Figure 27.3 Nanogap formation in the silica nanocomposite membrane. (This figure was modified from ref. 11.)

with surface compatible with the polymer, the nanogaps could not form any more due to the tight contact between the polymer and the filler particles.

The Nielsen model has been a popular theory, originally used to explain polymer–clay nanocomposites. This model is used to describe the tortuosity effect of plate-like particulates of filled rubber polymer composite on the gas permeation.[10] An increase in barrier properties of gas permeation of rubber polymer nanocomposites is a result of the impermeable nature of filler particles which creates a long path of penetrant molecule by directing them around the particle.

This model system consists of uniform platelets homogeneously dispersed in the polymer matrix and oriented parallel to the polymer matrix surface. The model can be applied using the equation:

$$\frac{P}{P_0} = \frac{1-\phi_f}{1+(L/2W)\phi_f} \quad \text{or} \quad \frac{P}{P_0} = \frac{1-\phi_f}{1+(\alpha\phi_f/2)} \tag{27.10}$$

P is the permeability of the nanocomposite polymer, P_0 is the permeability of the polymer matrix and ϕ_f is the volume fraction of the clay. L and W are length and width of the clay sheets, respectively, and its ratio L/W defines the aspect ratio α of the fillers.

Bharadwaj model was modified from Nielsen model by incorporating an orientation parameter, S. The range of relative orientations of the clay sheets with respect to each other is represented by θ, the angle between the direction of preferred orientation and the normal sheet.

The Bharadwaj model expresses the equation accompanied by orientation parameter as shown in Equation (27.11):

$$\frac{P}{P_0} = \frac{1-\phi_f}{1+\alpha\phi_f(2S+1)/6}; \quad S = \frac{1}{2}(3\cos^2\theta - 1) \tag{27.11}$$

This model assumed that the orientation of platelet clay layers in nanocomposite polymer is random $S=0$, then the tortuosity decrease with orientation and diffusion is facilitated as opposed to parallel orientation, $S=1$

or Nielsen model. However, in the case of the latex nanocomposites prepared by solution casting, the majority of the clay layers orient in the same direction rather than randomly. Thus, the Bharadwaj model cannot be applied to the latex nanocomposite.[12]

The Cussler model focuses on the diffusion of small gas molecules through a polymer matrix which is partly filled of impermeable flakes which are oriented perpendicular to the direction of diffusion. Therefore, the diffusion process is mainly related to three factors: the tortuous wiggles to get around the flake, the tight slits between the flakes, and the resistance of going from the wiggle to the slit.[10] This model proposes that the diffusion depends on the volume fraction of the impermeable filler and the aspect ratio. Then, a permeability model of Cussler can be obtained by multiplying the diffusion by the appropriate solubility as following equation:

$$\frac{P}{P_0} = \frac{1 - \phi_f}{1 + (\alpha\phi_f / 2)^2} \tag{27.12}$$

The aspect ratio calculated using the Cussler model is much higher than that calculated using the Neilsen model. This model will agree with a very low clay loading and a better homogeneous dispersion in polymer matrix as a model fit. However, it is not suitable for the latex nanocomposite system.[10]

The Gusev and Lusti model[12,13] was developed by the concept of performing a series of finite-element analyses of random dispersion of non-overlapping impermeable round platelets for a number of values of α and ϕ_f. The result of this model in the form of permeation could be represented by the stretched exponential function.

$$\frac{P}{P_0} = \frac{1 - \phi_f}{\exp\{(\alpha\phi_f / 3.47)\}^{0.71}} \tag{27.13}$$

Recently, many models for predicting the diffusion and permeation pattern or mechanism still have been developed to fit the experimental data in various types of polymer composite as well as nanocomposite. Many researchers try to clearly know a characteristic of composite and nanocomposite polymer with different type, shape and amount of filler in the polymer matrix. This basic knowledge of diffusion mechanism of composite rubber material is useful for industrial field to develop the suitable material in several conditions of usage such as a long duration of tires in automobile industrial. However, most of other models have been developed by modification from Neilsen model as a basic equation.

27.2 Testing of Diffusion and Transport of Liquids, Vapours and Gases through Rubber

There are several testing protocols and equipment for diffusion and permeation study of liquids, vapours and gases through the rubber. In case of liquids and

vapours, the swelling or sorption test is an important measurement for determining transport parameters. Equation (27.1) reveals that permeation is the result of diffusivity and solubility of penetrant molecule in rubbery matrix. Solubility is obtained from a swelling measurement value of solvent uptake in polymer at equilibrium state.[10,14] Then, a diffusion coefficient can be calculated following Equation (27.2) using the slope of the initial linear portion of the sorption curve profile to determine this parameter.[14,15] For gas diffusion and transport through rubber, although the diffusion and transport parameters are the same as liquid and vapour, testing protocols and equipment are mostly different because of the specific characteristics of gases. The testing methods of liquids, vapours and gases could be divided into two parts. The first part is the method for standard procedure according to standard organization as the American Society for Testing and Materials (ASTM), British Standard (BS), the International Organization for Standardization (ISO) and the German Institute for Standardization (DIN). The second part composes of modified techniques and experimental protocols of testing studies. However, the modified techniques still base on the standard method.

27.2.1 Standard Methods or Procedures

Swelling or sorption test of liquids and vapours through the rubber is obtained by the standard method of ASTM D 814[16] and ISO 6179: 2010[17] as a general method for various types of rubber. Other standard methods to test liquid and water vapour transmission rate are displayed in Table 27.1. Gas permeation test is obtained by the standard method of ASTM D 1434-82[18] and ISO 2782[17] as a general method, especially for oxygen gas mostly using ASTM D 3985[19] as a protocol for measurement. Table 27.2 exhibits the standard methods of gas permeability test.

ASTM D 814[16] is a method for measuring water or volatile liquid vapour permeability. This method detects the quantity of vapour transmitted by changing in weight. The test apparatus consist of glass vapour transmission jars with approximate volume 236 cm^3, an opening of 60.3 $\pm$ 0.4 mm in inside diameter and a wall 3.2 mm in thickness at the opening. The opening should be equipped with a metal screw ring clamp holding a smooth edged, flat, sheet metal ring 55.6 $\pm$ 0.4 mm in inside diameter and approximately 68.3 in outside diameter. The screw clamp is tightened to form a leak proof seal without subjecting the specimen to torsional strain. Then a suitable rack for supporting the jars in an inverted position in such a way as to allow free circulation of air over the surface of the specimen and finally, it should be kept in a constant temperature cabinet at 23 $\pm$ 2 °C (73.4 $\pm$ 3.6 °F). In case of specimens, they should consist of circular disks of 68 mm in diameter, cut with a sharp edged die from a sheet of the material being tested and the thickness of the sheet which should not exceed 3.2 mm measured by a dial micrometer. Three specimens having the same thickness within a tolerance of $\pm$ 3% are tested. The procedure of this test is described as follows, set the jar in an upright position, place 200 cm^3 of the test liquid in it, after which fit the test specimen over the mount

Table 27.1 The standard methods for testing liquids and vapours through rubber or polymer materials.[20–22]

Title of standard method	*Detail of testing*
ASTM D814	Standard Test Method for Rubber Property – Vapour Transmission of Volatile Liquids
ASTM D570	Standard Test Method for Water Absorption of Plastics
ASTM E96	Standard Test Methods for Water Vapor Transmission of Materials
ASTM E398	Standard Test Method for Water Vapor Transmission Rate of Sheet Materials Using Dynamic Relative Humidity Measurement
ASTM F739	Standard Test Method for Permeation of Liquids and Gases through Protective Clothing Materials under Conditions of Continuous Contact
ASTM F1249	Standard Test Method for Water Vapor Transmission Rate Through Plastic Film and Sheeting Using a Modulated Infrared Sensor
ASTM F2298	Standard Test Methods for Water Vapor Diffusion Resistance and Air Flow Resistance of Clothing Materials Using the Dynamic Moisture Permeation Cell
ISO 2528[20]	Sheet materials – Determination of water vapour transmission rate – Gravimetric (dish) method
ISO 6179	Rubber, vulcanized or thermoplastic – Rubber sheets and rubber coated fabrics – Determination of transmission rate of volatile liquids (gravimetric technique)
BS 903: Part A46:1991 (withdrawn standard)	Physical testing of rubber, Method for determination of the transmission rate of volatile liquids
BS EN ISO 62	Plastics. Determination of water absorption
DIN 53122	Determination of the water vapour transmission rate of plastic film, rubber sheeting, paper, board and other sheet materials by gravimetry

of the jar, place the ring and wire screen in position, and screw down the screw ring clamp lightly. Hold the assembly in the constant temperature cabinet as described before with the test disk lightly in place until temperature equilibrium is obtained. Then screw down the ring tightly and allow the assembly to stand in an upright position for 2 h. Make a tare assembly using a duplicate jar and a test specimen with same size but without the addition of the test liquid. Place a suitable weighing material such as lead shot in the tare jar to bring its mass to approximately that of the assembled jar and contents. Condition the tare jar at the test temperature in a manner similar to that used for the test jar. Test and tare jar are weighing on a balance with capacity capable of weighing to 0.005 g. Adding weights as required for equilibrium. After weighing invert each test jar and place on the rack, supporting each in such a way that the entire inner surface of the specimen remains contact with the liquid throughout the test. Twenty-four hours after inverting the jar, again weigh it against the tare jar. Any excessive loss of mass indicates that leakage due to improper seal is

Table 27.2 The standard methods for testing gases through rubber or polymer materials.[17,21]

Title of standard method	*Detail of testing*
ASTM D1434	Standard Test Method for Determining Gas Permeability Characteristics of Plastic Film and Sheeting
ASTM D3985[19]	Standard Test Method for Oxygen Gas Transmission Rate Through Plastic Film and Sheeting Using a Coulometric Sensor
ASTM F2298	Standard Test Method for Permeation of Liquids and Gases through Protective Clothing Materials under Conditions of Continuous Contact
ISO 1399	Rubber, vulcanized – Determination of permeability to gases – Constant volume method
ISO 2782	Rubber, vulcanized or thermoplastic – Determination of Permeability to gases. Differential-pressure methods, Equal-pressure methods
ISO 7229	Rubber or plastics coated fabrics measurement of gas permeability
BS 903: Part A30:1996 (withdrawn standard)	Physical testing of rubber, Method for determination of permeability to gases
BS EN ISO 2556	Plastic. Determination of the gas transmission rate of films and thin sheets under atmospherics pressure. Manometric method
BS ISO 15105	Plastic. Film and sheeting. Determination of gas transmission rate. Differential-pressure methods, Equal-pressure methods
DIN 53380	Determination of permeability of rubber to gases
DIN 53536	Determination of permeability of rubber to gases

occurring. Remove old assemblies and replace them with new ones which have been properly prepared. Return the assemblies to the rack and reweigh against the tare after periods of 120 ± 2 h and 192 ± 2 h from the initial inversion. Consider the difference in mass between those obtained at 120 h (5 days) and 192 h (8 days) divide by three as the average mass of liquid lost per 24 h. The result expresses as the vapour transmission rate (VTR) of each test liquid with respect to the rubber employed and calculated via the equation that follows:

$$\text{VTR, mg}/(\text{s}\cdot\text{m}^2) = 4.77 \times \text{average mass in grams of liquid lost per 24 h} \tag{27.14}$$

Although the ASTM D 814 has been generally used as a method for rubber testing recently, the classical method of measuring water vapour has been still used the gravimetric or dish method. Such a method is detailed in ISO 2528[20] and similarly in ISO 6179[17] which can be applied to any sheet material with flat, thin and can be processed to form a vapour resistant barrier such as plastic films, fabrics coated with rubber or plastics. The procedure deals with the dishes containing a desiccant and closed by the material to be tested are placed in a controlled atmosphere. The dishes are weighed at suitable interval of time

and WVTR is determined from the increase in mass when this increase has become a proportional to the time interval. A WVTR value is expressed in grams per square meter per 24 h [g/(m^2 · d)]. With the difference from ISO 2528, ISO 6179 specifies two methods which are particularly useful for comparing the relative transmission rates of one volatile liquid through different materials, or of several volatile liquids through one material.

For gas permeation measurement,[21] there are three concepts of conditions test methods. First is a constant volume, second is a constant pressure and third is a carrier gas method.

The constant volume method[21] such as ASTM D 1434, ISO 1399 consists of metal cell having two cavities separated by the test piece. The high pressure cavity is filled with the test gas at the required pressure between 0.3 and 0.5 MPa with accuracy. The cavity should be at least 25 ml volume to minimize pressure loss during the course of the test. The low pressure cavity should be a small volume using rigid porous packing to support the test piece against the pressure of the test gas. A capillary U tube manometer is used for determination of pressure in the low pressure cavity side. The test piece is a disc, suitable dimensions being between 50 mm and 65 mm diameter and thickness between 0.25 mm and 3 mm. It is essential that there must be no leakage of gas occurring. After the cell and test piece have been assembled and the high pressure side filled with gas at the test pressure, the increase in pressure on the low pressure side is measured as a function of time. The conditioning period of time to reach steady state is suggested at least 16 h. Throughout of the test period, the test cell should be enclosed in a constant temperature bath to maintain the temperature within ± 1 °C (for temperatures up to 175 °C). In the steady state, a plot of pressure change against time should be linear. Any deviation from linearity in the direction of increasing slope with time indicates that the steady state has not been reached.

The constant pressure method,[21] the test cell used in this protocol is similar to that for constant volume method. The main difference is that the low pressure side is connected to a device for measuring the volume increase as gas diffuses to the low pressure side while the test system is maintained as constant pressure. In ISO 2782, a graduated capillary tube is used to measure the volume change and the tube may be arranged either vertically or horizontally. The operation of the apparatus is very similar to the constant volume procedure. In the horizontal arrangement of capillary, only a straight length is needed which contains a single drop of liquid which is pushed along as volume increases and then the movement of the liquid drop is monitored as a function of time. Recently, ISO 2782:2012 has been established part I for differential pressure method and part II for equal pressure method which the most convenient procedure is to use the constant volume method with an apparatus equipped with modern pressure transducers.

The carrier gas method[21] such as ASTM D 3985 is the commonly used for film oxygen permeability test. The test gas, oxygen flows on one side of the test piece and a second gas, nitrogen as carrier gas, flows on the other side and is quantitatively analysed to determine the quantity of test gas which has passed

through the test piece by the coulometric detector where it produces an electric current. The magnitude of which is proportional to the amount of oxygen flowing into the detector per unit time.

27.2.2 Modified Techniques and Experimental Studies

Many experimental studies sometime could not use the equipment or apparatus test as same as the standard protocol of testing due to financial policy or other reasons such as unsuitable existing protocols that fit to test the new interesting material models. Therefore, the modified techniques and apparatus are developed mostly based on standard protocol as a primary design. A measurement of liquid and vapour transmission rate of rubbery materials according the standard method of swelling or water sorption, many studies[4,8,10,23–28] following the gravimetric technique with different sizes of circular sample of diameter which range from 0.2 to 5 cm, with different shape such as rectangular[15] (2 × 2 cm) have been performed. A typical procedure describes that the cut samples are weighed on an electronic balance having an accuracy of 0.001 g and were put into bottle with cover an amount 15–20 ml of testing liquid or water. The bottles are placed in a thermostatically controlled hot air oven throughout the testing under different three temperatures range from low until high values such as 28, 50, 70 °C[29] and 35, 55, 65 °C[30] as for example. When the bottle of samples are equilibrated for different time interval, at the expiration of the specified time, the rubber sample is removed from the bottle, wiped free of adhering solvent and weighed using the electronic balance. The weighing is continued until equilibrium swelling or sorption is attained. Besides following the standard method, some techniques such as unidirectional injection experiments have been performed for permeation study by Francucci *et al.*[31] to study capillary flow effect theory. For determination of water vapour transmission rate according to ASTM F 1249, Osman *et al.*[32] measured polyamide foil coated film using Permatran-W 3/31 as an instrument of testing with condition of 23 °C, 1 atm and 100% RH. Exposure area for the WVTR measurements of this test was 50 cm^2 and thickness of the film sample was 300 μm. Water vapour transmission rate is done through plastic film and rubber sheeting using a modulated infrared sensor.

In case of gas permeation testing, there is an instrument that is produced according to ASTM D 1434-82, procedure V-Volumetric.[33] The instrument is CSI-135 Permeability Cell of Custom Scientific Instruments, Inc. The test temperature is controlled by water bath and helium is used for test gas. In addition to the same standard method, other experiments have been used an ATS FAAR gas permeability tester in nanometric method to measure permeability of O_2 and N_2 gases through EVA composites at various pressures.[34] An another one, the oxygen gas transmission rates of the rubbery samples is measured at 20 °C and 90% RH with GDP-C 150 (Germany) instrument.[35] Lyssy Manometric Gas Permeability Tester L100-2402 instrument is mostly used to measure air permeability of the natural rubber (NR) layered silicate membranes.[10,23,36] The test gas used is oxygen, nitrogen and carbon dioxide at a

flow rate of 500 ml/min with temperature of 25 ± 1 °C and 65 ± 0.5% RH. Oxygen transmission rate is usually measured according to ASTM D 3985 standard method; various instruments have been commercially produced such as an OX-TRAN Model 2/20[32] and oxygen permeability tester (model 8001) of Systech Instruments Ltd. Oxon, UK.[12] These instrument models are tested under the same condition of 1 atm pressure, relative humidity of 0%. Whereas, Model 8001 using three different temperatures which is different from OX-TRAN Model using one temperature at 23 °C.

The condition of gas permeation through rubbery materials in case of high pressure measurement recently becomes interesting because many industrial utilities in the real situation often encounter the high pressure stress application. Then various test models have been developed to explain and evaluate a true value of diffusion profiles. Since standard methods are still not valid enough for this condition, many studies try to investigate and create new models of testing. The novel techniques[21] such as measurement of gas absorption under high pressures is monitored using the change of resonant frequency of a rubber test piece/steel rod assembly. The other technique is a measurement of sorption and diffusion at high pressure by pressure decay techniques. Furthermore, Wang *et al.*[37] developed oxygen measurements at high pressures using vertical cavity surface-emitting lasers. However, the newest model comes all time nowadays due to the knowledge of advanced high technology in the present day.

27.3 Diffusion and Transport Profiles of Various Rubber Types

The pristine NR polymers are flexible depending on a property of glass transition temperature value. If any rubbers have low value of glass transition temperature, its network structure of rubber chain will tend to easily mobilize at room or ambient temperature. Therefore, the penetrant can diffuse through the network structure of rubber chain easily. In addition, the orientation and functional group of rubber chains are factors that also affect the diffusion and transport of liquid, vapour and gas molecules through rubber by penetrant–rubber chain interaction.[5] Changing of chain structure of rubber from flexible to rigid property is one of strategies for decreasing the diffusion of penetrant molecules by improved packing order and increased crystallinity of rubber materials. Composite systems have been provided to the pristine NR in order to improve barrier property and prevent the free flow of permeant through network structure of polymer. Rubber composite is a system which composes of rubber as a continuous phase and impermeable particulate or plate-like fillers as a disperse phase. In the case of nanocomposites, the nanosize fillers are incorporated in the system. It is known that the diffusion and transport profile of the pristine, composite and nanocomposite rubber are different due to a change of network structure of rubber by many factors which are described later. Figure 27.4 shows the effect of the fillers in NR on solvent uptake compared to the unfilled NR.

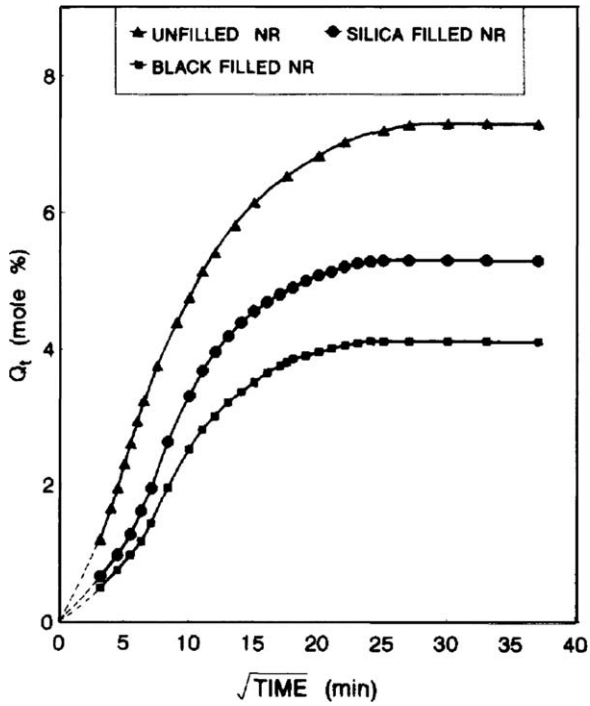

Figure 27.4 Mole percent benzene uptake for unfilled, black-filled and silica-filled natural rubber.
(Reproduced from ref. 27 with permission from Elsevier Science Ltd.)

27.3.1 Natural Rubber

NR or India rubber is a mixture of polyisoprene and small amounts of organic compounds as same as water. This material is classified as an elastomer which is obtained from latex, a milky colloid produced by some plants. Most NR latexes come from the rubber tree (*Hevea brasiliensis*). However, polyisoprene can also be produced synthetically as well. Although their properties normally are very stretchy, flexible and extremely waterproof, they permit a minute amount of liquid vapour and water molecules to pass through them. The structure of rubber has an important effect on diffusion and transport of liquid, vapour and gas. When rubber chain segment is not interfering by solvent molecule, the diffusion follows a Fickian mechanism.[9] A swelling of rubber chain segments that is induced by the presence of solvents make the diffusion pattern deviate from the Fickian model. It means that not only the structure of rubber that has an important effect on diffusion and transport but also the molecular structure of the permeating liquid or gas as well. Especially, due to the molecular size of liquid, the small molecules could permeate through rubber membrane rapidly than large molecules. In addition, the polarity of liquid plays and important

role in permeation such as in case of non-polar liquids, water could permeate more slowly than non-polar toluene in non-polar rubber membrane.[9] The others are reversed in the case of polar membranes. It could conclude that the permeability of rubber is determined by many structural and morphological properties of both polymer matrix and the species of permeant. The morphological properties of NR are controlled by the number and distribution of crosslinks between rubber chains as one of many factors. A crosslinking value of rubber depends on the technique of vulcanization which is a system that is used to improve the quality of rubber making it less soluble, more durable and harder.[26,38] This system is to chemically link the rubber chain together to form a three-dimensional network by accelerated sulfur formulations. Unnikrishnan and Thomas[26] studied the swelling behaviour in aliphatic hydrocarbons of NR crosslinked by the four vulcanization systems viz., conventional (CV), efficient (EV), dicumyl peroxide (DCP) and a mixture consisting of sulfur and peroxide (mixed). Theirs results showed that the order of solvent uptake increased following the systems of DCP < EV < mixed < CV because of different degrees and distribution of crosslinking along the rubber chains. In addition to their chemical nature of the crosslinks, they can also contribute to the liquid sorption behaviour of rubbers as well. The structure of the networks formed by different vulcanization systems and solvent uptake profiles of each system are depicted in

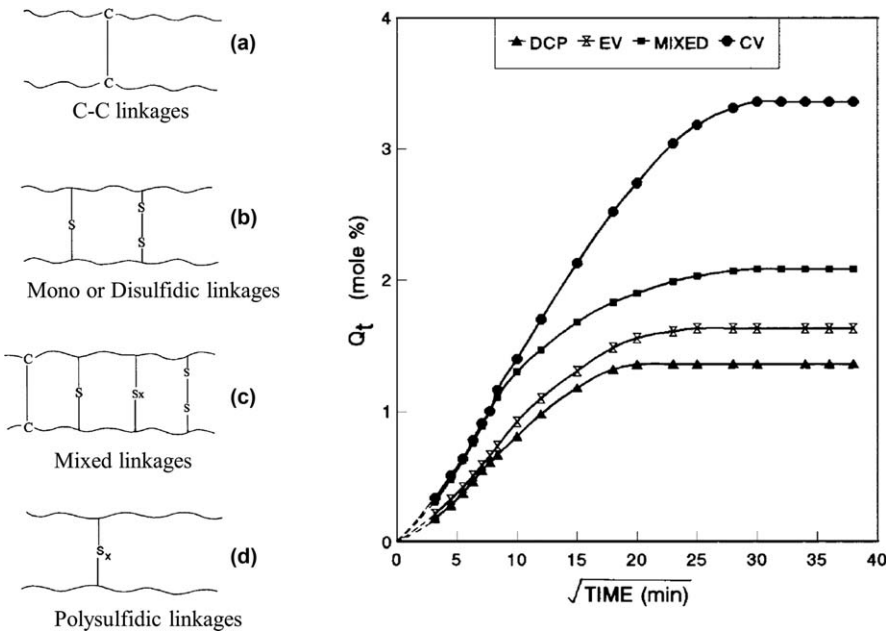

Figure 27.5 Structure of the networks formed by the four vulcanization techniques: (a) DCP, (b) EV, (c) mixed, (d) CV (left) and mole percent *n*-hexane uptake of natural rubber with different crosslinking systems (right). (Reprinted from ref. 26 with the permission of Copyright © 1997 John Wiley and Sons, Inc.)

Figure 27.5. As described earlier, the decrease in diffusion coefficient values is based on the increase in molecular weight of the solvent or permeant. However, the study by Unnikrishanan and Thomas[26] revealed that even though a solvent such as heptane has a molecular weight higher than hexane, the solvent uptake value of heptane is higher than hexane in the rubber, the opposite of what is expected. The conclusion of this finding is that not only molecular weight of penetrant affects permeability but also the rubber–solvent interaction as well. Then the permeation coefficient value is the sums of total effect of each factor are included. The mechanism of transport of most solvent through the NR in various vulcanization systems follows by anomalous diffusion describing that the diffusion and relaxation time are comparable. As same as liquids, gases pass through the NR dealing with diffusivity and solubility.[33] Diffusivity of gas greatly depends on the size of the gas molecule, the smaller the size of the gas molecule, the faster the diffusivity. Additional, thickness and area of rubber membrane effect diffusion of gas which thicken and smaller area of membrane result in less total gas diffusion. Solubility depends on the polarity of both the gas molecule and nature of rubber. If the gas molecule has a similar polarity to rubber chain functional group, it has a higher solubility in rubber membrane. Therefore, factors that affect both diffusivity and solubility could easily increase the permeability of gas through rubber.

27.3.2 Natural Rubber Composites

NR composites have been classified into two categories: non-layered and layered. Two categories are divided by types of filler which are incorporated to rubbery matrix. The first category composes of particulate fillers such as spherical silica, titanium dioxide and fibres or whisker such as natural cellulose fibre. The latter, layered composite composes of layered sheet of fillers such as clay, layered silicate (montmorillonite, hectorite, saponite, fluoromica, fluorohectorite, vermiculite and kaolinite).[39] The loading of fillers in conventional composites is high ratio 30–60 vol% as compared to the nanocomposite (1–5 wt%). This is one of factor different between conventional composite and nanocomposite that effect on permeation profiles. In the rubber composite, the diffusion and transport through filled rubber membranes depend on the nature of the fillers, dimension and shape of the fillers, the degree of adhesion and their compatibility with the rubber matrix. In addition, size, surface area, state of aggregation, and quantity of the fillers also make an effect on the diffusion and transport.[7,39,40] The inert and compatible fillers create free volume in matrix of rubber then give a tortuous path for the permeating molecules pass through membranes. On the other hand, the incompatible filling create a void or space at the interface, increasing free volume of the system which affect permeation of penetrant easily through membranes. Improving the performance of rubber products by adding inorganic filler has long been worked. Especially, rubbery polymers are often reinforced with particulate fillers such as carbon blacks, talcum and silica to provide the suitable requirement of mechanical, thermal, chemical and permeation properties. However, there are some disadvantages of

conventional fillers. The high loading of conventional fillers with micronized size affects distribution of fillers bringing down important properties such as mechanic, thermo dynamicity and including permeation, in addition the process to produce also difficultly. The orientation of microcomposite rubber represents as phase separation that affects the whole characteristic of polymer composites when adding layered silicate fillers at higher loadings as well.

In recent years, natural fillers have been used to incorporate in NR again. They are becoming popular because of their economic and ecological aspects. However, the use of natural composites has existed for very long time since Egyptian period.[41] The natural fibres such as sisal, oil palm, coir, jute, bamboo, are well known as reinforced materials of polymer in many fields with the advantages of high performance, environmental friendly biodegradable, renewable and cheap fulfilling the economic interest of industry. One of the major problems is their high moisture sensitivity because of hydrophilic properties of them so their affinity toward moisture, leading to low degree of an adhesion between fibre and matrix of rubber. Disadvantage can be remedied in the form of chemical modifications. Jacob *et al.*[42] studied the water sorption of natural fibre reinforced NR composites. Their results concluded that moisture uptake was found to be dependent on the properties of the biofibres. The mechanism of diffusion in the rubber gum was found to be Fickian in nature, while in the loaded composites, it was non-Fickian. In addition, chemical modification was seen to decrease the water uptake in the composites. Their findings are agreed with many studies.[8,24,41] Due to nature of natural fibre being lignocellulose with hydrophilic, incorporation of these materials into rubber composites thus generally increase the rates of water sorption ability. The mechanisms of moisture uptake of fibres are related to diffusion, capillarity and transport via micro cracks which diffusion mechanism plays an important role.[42] In the case of hybridized composites between two or more fibres show the water sorption characteristic depending on the intrinsic properties of both or more fibres.[24,42] There can be two states of water molecules existing in the fibre reinforced rubber composites: unbounded in the nanohole of the polymer and bonded with hydrogen bonds to the polymer. The waxy materials present on the fibre will additionally help to retain the water molecule on the fibre. Therefore, the increase in content of fibre fillers results in an increase in water uptake in rubber composites as shown in Figure 27.6. There are various types of chemical modification to improve water resistant of fibre surface such as mercerization, silane chemical coupling and alkali treatment with sodium hydroxide.[8,24,41,42] Alkali treatment is more effective with natural fibres than other methods.[24,42] It can lead to breaking down of fibres into smaller ones that provide a large surface area and give better mechanical interlocking between the fibre and the matrix, resulting in a decrease in water uptake value. The mechanism of solvent transport seems like a Fickian model when increase the concentration of sodium hydroxide for treated fibre. Figure 27.7 shows the effect of sodium hydroxide treatment compared to untreated fibre of rubber composite in SEM images.

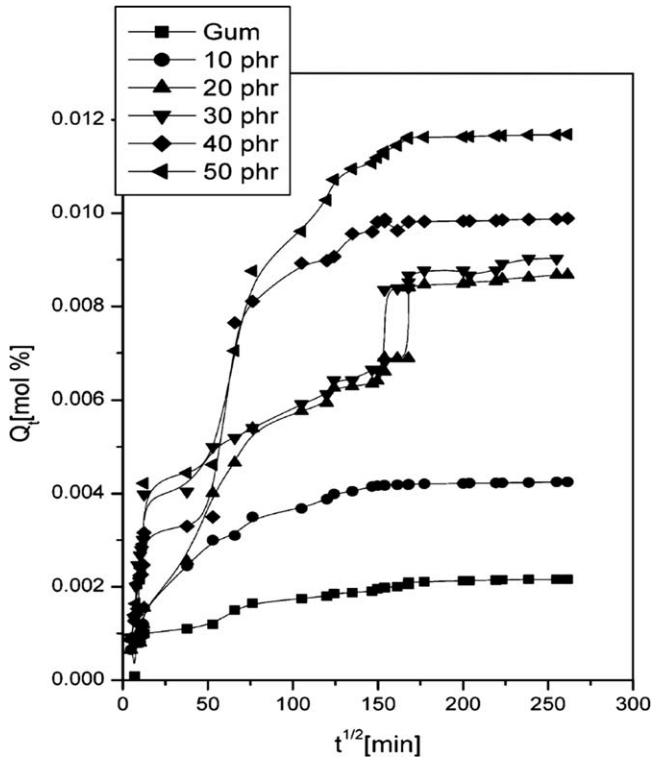

Figure 27.6 Variation in molar water uptake of various contents of fibre loading in rubber composites.
(Reprinted from ref. 42 with the permission of Copyright © 2005 American Chemical Society.)

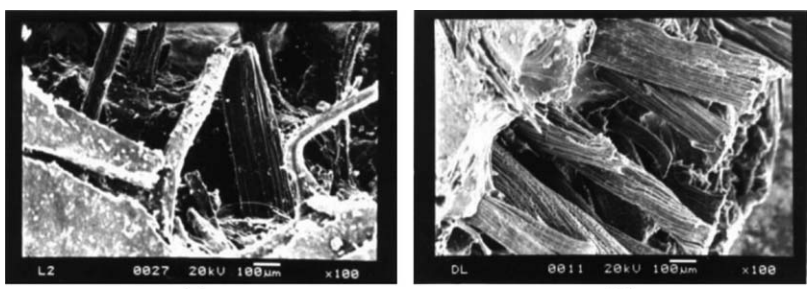

Figure 27.7 SEM tensile fracture surface of untreated (a) and 4% NaOH treated (b) sisal/oil palm reinforced natural rubber composites.
(Reprinted from ref. 42 with the permission of Copyright © 2005 American Chemical Society.)

27.3.3 Natural Rubber Nanocomposites

Solving problems of disadvantages of conventional composites, the nanosize (1 nm = 10^{-9} m) of fillers have been used to incorporate into the rubber materials called nanocomposites. They are reported to be the materials of 21st century in the view of possessing design uniqueness and property combinations that are not found in conventional composites.[39] Two main categories still have been classified as same as general rubber composites, but the difference between conventional and nanocomposites is the orientation of layered silicates of nanofillers. They can be arranged in two patterns, represented as intercalated and exfoliated nanocomposites (Figure 27.8). The pattern of filler arrangement and loading in the rubbery matrix is an important role of liquids, vapours and gases permeation.[7,39,40,43] Additionally, as dimensions reach the nanometre level, interactions at phase interfaces become largely improved, and this is important to enhance material properties.

The spherical inorganic particulate fillers such as fumed silica and carbon black are also considered impermeable by gas molecules. Therefore, the incorporation of inorganic fillers in the rubbery matrix can enhance the barrier properties by forcing the penetrant molecules to follow a more tortuous path, slowing down the progress of the permeation. Gas barrier in rubber composites were conventionally explained by the theory originally proposed by Nielsen to describe the tortuosity effect of plate-like particulate structure.[5] The impermeable nature of filler particles create a long path for the diffusing molecule by directing them around the particle, leading to an increase in barrier

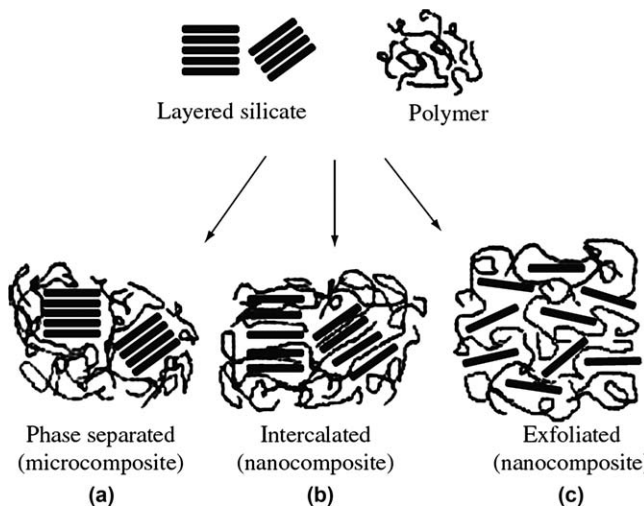

Figure 27.8 Different types of composites arising from the interaction of layered silicates, polymers: (a) phase-separated microcomposite; (b) intercalated nanocomposite and (c) exfoliated nanocomposite.
(Reprinted from ref. 40 with the permission of Copyright © 2000 Elsevier Science Ltd.)

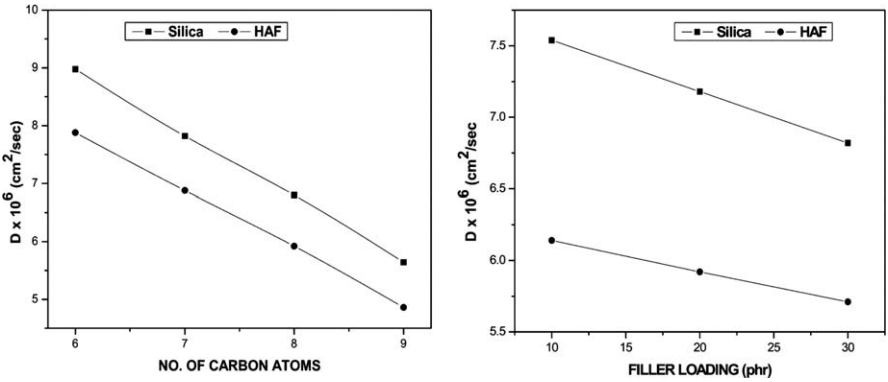

Figure 27.9 Effect of number of carbon atoms of permeant (left) and filler loading (right) on diffusivity of rubber nanocomposite.
(Reprinted from ref. 38 with the permission of Copyright © 2012 American Chemical Society.)

properties. In the case of solvent sorption through the non-layered particulate filler composite[38] has the same concept of gas permeation, the decrease of solvent uptake depend on the increase of tortuous pathway. Factors that affect diffusion coefficient such as size of permeate molecule, polymer matrix–filler interaction, the amount of filler loading are mentioned before, the same as conventional rubber composites. Figure 27.9 shows the effect of molecular weight of various carbon atom of permeant and fillers loading on diffusivity of rubber nanocomposites.[38] The larger molecule of penetrant increasing with number of carbon atoms provides the decrease of diffusivity. The filler loading at only small level about (1–5 wt%) could decrease diffusivity of rubber nanocomposites which inversely result in conventional composites. The study by Dufresne and coworkers[44] found that the absorption value of NR filled with waxy maize starch nanocrystals decreased when the starch content increased which was concluded that the reduction of swelling upon the addition of starch nanocrystals might also be due to the interaction between starch and NR.

The layered silicate type, especially individual clay layers are separated in a continuous polymer matrix by an average distance that depends on clay loading. Generally, the clay content of an exfoliated nanocomposite is much lower (4–5 wt%) than that of an intercalated (11–34 wt%).[5,40] The exfoliated nanocomposite is more completely and uniformly dispersed than intercalated which highly affect diffusivity of gas and solvent (Figure 27.8). This system displayed reduction in the permeability of small molecule gases, *e.g.* O_2, H_2O, He, CO_2 and ethyl acetate vapours.[4,11,14,23] The effect of different types and shapes of fillers (2 wt%) such as organoclay, either exfoliated montmorillonite, synthetic mica or intercalated clay tactoids (hectorite and saponite), on water permeability of both partially and totally exfoliated polyimide-based nanocomposites has been reported.[45] Results of this study are shown in Figure 27.10, where a drastic decrease in relative permeability can be observed with the increasing length of the clay.

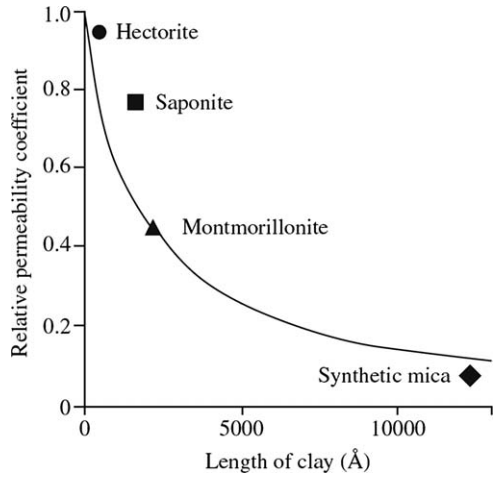

Figure 27.10 Clay length dependence on the relative permeability coefficient for poly(imide)/clay nanocomposites.
(Reprinted from ref. 45 with the permission of Copyright © 1997 John Wiley & Sons Inc.)

In the case of natural nanofibres, many recent studies have been done to develop and characterize the bio-based nanocomposites as a relatively new class of nanomaterial because of their biodegradability, biocompatibility and surprisingly, improved rubber properties.[24] The transport behaviour of three aromatic organic solvents, namely benzene, toluene, and p-xylene in NR nanocomposite membranes containing cellulose nanofibres and cellulose nanowhiskers was studied. The result showed that the uptake decreased with increased penetrant size; being the highest for benzene and the lowest for p-xylene. Both the nanocelluloses have restricted the molecular mobility at the interphase and thereby decreased the transport of solvents through the materials even at concentrations as low as 2.5 wt%.[24] Furthermore, the study of synergistic of montmorillonite and nanocellulose whisker on the improvement of gas barrier found that this synergism effect, the most efficient effect being observed for montmorillonite contents higher than 2.5 wt%.[46] The transport mechanism of liquid uptake of rubber nanocomposites reveals mostly non-Fickian behaviour as anomalous sorption.[4,5] In the other hand, the transport mechanism of gas permeation mostly follows by Neilsen model as tortuous path for a diffusing penetrant. However, the gas permeation might increase as a function of filler loading because the aggregation of fillers is formed with increase in concentration of fillers resulting in the weakening of polymer chains.[34]

27.4 Effect of Temperature on Diffusion and Transport Parameters

Temperature is effect on permeability with two aspects;[33] first, the free volume of many types of rubber depends on temperature. If the ambient temperature is

lower than the glass transition temperature of the polymer, permeability is significantly reduced. The second, the mobility of gas molecule depends on temperature as well. Lower temperature is resulting in slow gas mobility which is an effect on lower gas diffusivity and permeability. Thus, temperature also affects the solubility of gas molecules in rubber as shown in Equation (27.5):

$$S = S_{0^e} \frac{-\Delta H_s}{RT} \tag{27.15}$$

where S is solubility, ΔH_s is the enthalpy of solution, S_0 is a pre-exponential factor, R is the gas constant, *and* T is Kelvin temperature. ΔH_s can be negative or positive. If solution enthalpy is negative or discharging heat, gas solubility increases with decreasing temperature. If solution enthalpy is positive or absorbing heat, gas solubility decreases with decreasing temperature. The gas solubility is proportional to polymer permeability.

The thermodynamics of the system has also been studied by the calculation of enthalpy, entropy, and free energy. In addition, the thermodynamic parameter of the sorption process can be calculated from diffusion data. The activation energy of the sorption process can be calculated and described using the Arrhenius equation as shown before in Equation (27.9). Equation (27.9) can be simplified by taking logarithms of the diffusion coefficient (Equation (27.16)). Then a plot of log D against $1/T$ gives the value of the activation energy from the slope of the curve.[26,27,38]

$$\log D = \log D_0 - E_D / RT \tag{27.16}$$

where D is the diffusion coefficient, D_0 is a constant, and E_D is activation energy. R is the gas constant, T is Kelvin temperature.

There is an increase in the rate of diffusion and the maximum solvent uptake with an increase in temperature. Therefore, in the process of sorption or solvent uptake of rubbery polymer, when the absorption obtain the equilibrium, sorption constant parameter could be determined from the amount of liquid sorbed by a given mass of the polymer, the equilibrium sorption constant K_s for the samples at different temperature has been computed as:[26,38]

$$K_s = \frac{\text{No. of mole penetrant sorbed}}{\text{Unit mass of the polymer}} \tag{27.17}$$

From the values of K_s, enthalpy ΔH and entropy ΔS of sorption have been determined using the Van't Hoff relation:[26,38]

$$\log Ks = \frac{\Delta H}{2.303R} - \frac{\Delta S}{2.303RT} \tag{27.18}$$

From enthalpy ΔH, entropy ΔS and Kelvin temperature T, the free energy of sorption process ΔG has been obtained by adopting Gibbs's thermodynamics expression (Equation (27.19)).[38]

$$\Delta G = \Delta H - T\Delta S \tag{27.19}$$

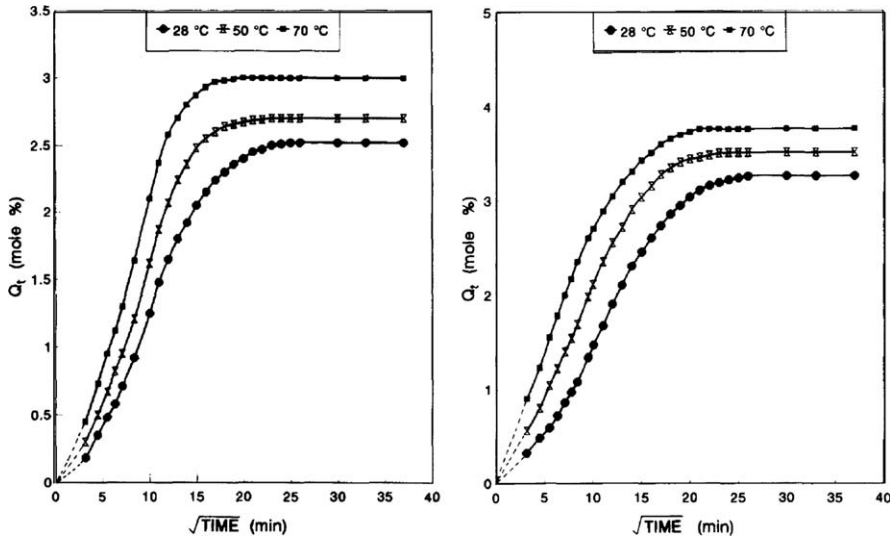

Figure 27.11 Effect of temperature on solvent uptake; mesitylene through filled natural rubber with carbon black (left) and silica (right).
(Reprinted from ref. 27 with the permission of Copyright © 1997 Elsevier Science Ltd.)

All of the equations from (27.16) to (27.19) dealing with effect of temperature are used to calculate for describing the liquids, vapours and gases when they pass through various rubber types such as the pristine NR or composite system. That means the temperature is one of most effect factors on diffusion and transport parameters. Many studies.[4,8,10,26,27,29,33,38,42] have been concluded that there is an increase in the rate of diffusion and the maximum solvent uptake with an increase in temperature. Figure 27.11 shows the effect of temperature on solvent uptake of filled NR with carbon black and silica, which is in agreement with many of the mentioned studies.

Segmental mobility of polymer and free volume within the matrix are increased at higher temperature which affect the diffusion rate of liquids, vapours and gases pass through the rubber membrane. The kinetic energy of the penetrant also increases with increasing temperature because of crystalline region disruption.[38] In the case of filled rubber composites have a decrease value of diffusion coefficient as a function of filler concentration. This effect on the activation energy needed for the diffusion of penetrant molecules is found to be higher than that of pristine rubber.[4] As mentioned before, the value of ΔH can be negative or positive, but in many studies[26,27,38] showed the negative value of ΔH. This result could indicate an increased exothermicity of the sorption process with increase in molecular size of solvent. The negative value of entropy, ΔS means the sorption molecules remain in liquid state throughout the process. And the negative value of ΔG also describe the tortuosity of the diffusion process[38] which more negative value results in more tortuosity in the rubbery matrix as well.

27.5 Application of Improved Barrier Property Rubbers

It was well known that NR, an elastomer has been widely used in tire production. One of application areas is leading to automotive field that consider the improved barrier property of rubber as a material for ecology, safety, durability and easy production.[39] Especially, the excellent air retention properties of butyl/halo butyl and chemically modified rubbers are widely used in the inner tube and inner line of automotive tires.[5] In addition, the materials for packaging which is resistant to moisture and oxidation are provided. The gas barrier, reinforcement and flame retardant properties of improved rubber have also been exploited such as heat-resistant polymer nanocomposites are used to make fire fighter protective clothing and lightweight materials suitable to work in high temperature and stress condition.[39] Additional, a barrier coating with scratch and tear resistance can prevent the diffusion of corrosive gases and liquids.[5] Polymer nanocomposites can replace conventional materials in food and drink container seals, medical container seals for blood collection tubes, stoppers for medical containers, stoppers for blood collection tubes, baby pacifiers and other products needing both flexibility and barrier properties.[5] Regarding the variety of applications of polymer nanocomposites, prominent impacts over the automotive industry can be highlighted, including their use in tires, fuel systems, gas separation membranes in fuel cells.

In the case of natural fibre reinforced polymer composites,[41] in 1996 this material was used for making aeroplane seats and fuel tanks. The last decade has been used widely because of biodegradability and high specific properties. Currently, nanobiofibre composites are also provided for material revolution in technical application which is taking place in the automobile and packaging industrial.

27.6 Conclusions

NR is a widely used material in a multiplicity of applications, particularly in the automotive industry and as packaging in the food and beverage industries. However, the permeation property of pristine NR is found to be a drawback while it is used in the packaging or automotive industries. Therefore a conventional composite with large size fillers is being used for a long period for such applications. The properties of even such composites have not reached the desired level. With the advent of nanotechnology, new nano rubber materiels suited for such applications are being produced. The use of nanocomposite might get the most significant improvement in various rubber properties such as decrease permeation of liquids, vapours and gases that pass through rubber. The existence of nanofiller in the rubbery matrix results in barrier property improved by creating a tortuous path for the diffusion penetrant molecules. The degree of dispersion, orientation of filler particle, volume fraction of filler, type of filler modifier and temperature

greatly influence the permeability of barrier materials. Therefore, to understand the mechanism of diffusion and transport through the membrane of different penetrants and types of rubber polymer, the various models are constructed to describe all of factors that affect characteristic of them. The mechanism of sorption and diffusion of permeant depends on the geometry and nature of the barrier material, the solubility of the penetrant, the concentration gradient of the penetrant in bulk and in the interfacial region including temperature effect. Various experimental studies are reported in the literature on the barrier properties of different types of barrier material to give an idea for a unique perspective of composites and nanocomposites rubber system.

References

1. I. Q. Garrido, J. M. B. Rienda and G. Frutos, Diffusion of erucamide (13-cis-docosenamide) in isotactic polypropylene, *Macromolecules*, 1996, **29**, 7164.
2. E. Foldes, Transport of small molecules in polyolefins. II. Diffusion and solubility of irganox 1076 in ethylene polymers, *J. Appl. Polym. Sci.*, 1993, **48**, 1905.
3. J. Klein and B. J. Briscoe, Diffusion of long molecules through solid polyethylene. II. Measurements and results, *Journal of Polymer Science Part B-Polymer Physics Edition*, 1977, **15**, 2065.
4. R. Stephen, S. Varghese, K. Joseph, Z. Oommen and S. Thomas, Diffusion and transport through nanocomposites of natural rubber (NR), carboxylated styrene butadiene rubber (XSBR) and their blends, *Journal of Membrane Science*, 2006, **282**, 162.
5. C. Nah, M. A. Kader, Barrier Properties of Rubber Nanocomposites. In: S. Thomas, R. Stephen (Eds.), *Rubber Nanocomposite: Preparation, Properties and Applications*, John Wiley and Sons (Asia) Pte Ltd., Singapore, 2010, 499.
6. C. A. Kumins, T. K. Kwei, Free volume and other theories. In: J. Crank and C. S. Park (Eds.), *Diffusion in Polymers*, Academic Press, N.Y., 1968, 165.
7. T. Naylor. Permeation properties, In: C. Booth and C. Price (Eds.), *Handbook of Comprehensive Polymer Science*, 1st ed., Pergamon Press: Oxford, U.K., 1982, Vol. 2, 643.
8. V. G. Geethamma and S. Thomas, Diffusion of Water and Artificial Seawater Through Coir Fiber Reinforced Natural Rubber Composites, *Polymer Composites*, 2005, 136.
9. D. De Kee, Q. Liu and J. Hinestroza, Review Viscoelastic (Non-Fickain) Diffusion, *The Canadian Journal of Chemical Engineering*, 2005, **83**, 913.
10. A. Jacob, P. Kurian and A. S. Aprem, Transport Properties of Natural Rubber Latex Layered Clay Nanocomposites, *Journal of Applied Polymer Science*, 2008, **108**, 2623.

11. H. Cong, M. Radosz, B. F. Towler and Y. Shen, Review Polymer-inorganic nanocomposite membranes for gas separation, *Separation and Purification Technology*, 2007, **55**, 281.
12. M. Bhattacharya, S. Biswas, S. Bandyopadhyay and A. K. Bhowmick, Influence of the nanofiller type and content on permeation characteristics of multifunctional NR nanocomposites and their modeling, *Polym. Adv. Technol.*, 2012, **23**, 596.
13. A. A. Gusev and H. R. Lusti, Rational design of nanocomposites for barrier applications, *Advanced Materials*, 2001, **13**, 1641.
14. V. Sridhar and D. K. Tripathy, Barrier Properties of Chlorobutyl Nanoclay Composites, *Journal of Applied Polymer Science*, 2006, **101**, 3630.
15. M. Balachandran and S. S. Bhagawan, Mechanical, Thermal, and Transport Properties of Nitrile Rubber–Nanocalcium Carbonate Composites, *Journal of Applied Polymer Science*, 2012, **126**, 1983.
16. ASTM D814, 1995; 2000. Standard Test Method for Rubber Property – Vapour Transmission of Volatile Liquids. https://law.resource.org/pub/us/cfr/irb/003/astm.d814.1995.pdf. Accessed on 20 October 2012.
17. ISO-Rubber Information Centre. www.rubber.org/standard/standard.php?stand = ISO. Accessed on 20 October 2012.
18. ASTM 2003. Standard Test Method for Determining Gas Permeability Characteristics of Plastic Film and Sheeting, D1434. West Conshohocken, PA: American Society for Testing and Materials.
19. ASTM 2005. Standard Test Method for Oxygen Gas Transmission Rate Through Plastic Film and Sheeting Using a Coulometric Sensor. D3985. West Conshohocken, PA: American Society for Testing and Materials.
20. ISO 2528, 1995. Sheet materials – Determination of water vapour transmission rate – Gravimetric (dish) method. http://www.permeabilita-imballaggi.it/pdf/ISO%202528-1995.pdf Aceesed on 20 October 2012.
21. B. Roger. Chapter 17 Permeability. In: B. Roger (Ed.) *Physical testing of rubber*, 4th ed.; Springer Press: New York, USA, 2006, p. 349.
22. Moisture vapour transmission rate From Wikipedia, the free encyclopedia. http://en.wikipedia.org/wiki/Moisture_vapor_transmission_rate. Accessed on 20 October 2012.
23. P. S. Thomas, P. A. Sreekumar, A. S. Aprem and S. Thomas, Poly(ethylene-co-vinyl acetate)/calcium phosphate nanocomposites: Mechanical, gas permeability, and molecular transport properties, *Journal of Applied Polymer Science*, 2011, **120**, 1974.
24. P. M. Visakh, S. Thomas, K. Oksman and A. P. Mathew, Cellulose Nanofibres and Cellulose Nanowhiskers Based Natural Rubber Composites: Diffusion, Sorption, and Permeation of Aromatic Organic Solvents, *Journal of Applied Polymer Science*, 2012, **124**, 1614.
25. E. Basavaraj, B. Ramaraj and A Siddaramaiah., Study on Mechanical, Thermal, and Wear Characteristics of Nylon 66/Molybdenum Disulfide Composites Reinforced With Glass Fibers, *Polymer Composites*, 2012, 1570.

26. G. Unnikrishnan and S. Thomas, Sorption and Diffusion of Aliphatic Hydrocarbons into Crosslinked Natural Rubber, *J. Polymer Sci. B: Polym Phys*, 1997, **35**, 725.
27. G. Unnikrishnan, S. Thomas and S. Varghese, Sorption and Diffusion of Aromatic Hydrocarbons through filled natural rubber, *Polymer*, 1996, **37**, 2687.
28. A. P. Mathews, S. Packirisamy, R. Stephen and S. Thomas. Transport of aromatic solvent through natural rubber/polystyrene, *J. Membrane Sci.*, 2002, **201**, 213.
29. G. Unnikrishnan and S. Thomas, Molecular Transport of Benzene and Methyl-Substituted Benzenes into Filled Natural Rubber Sheets, *Journal of Applied Polymer Science*, 1996, **60**, 963.
30. H. C. Obasi, O. Ogbobe and I. O. Igwe, Diffusion Characteristics of Toluene into Natural Rubber/Linear Low Density Polyethylene Blends, *Inter. J. Polymer Sci.*, 2009, 1.
31. G. Francucci, A. Vázquez, E. Ruiz and E. S. Rodríguez, Capillary Effects in Vacuum-Assisted Resin Transfer Molding With Natural Fibers, *Polymer Composites*, 2012, 1593.
32. M. A. Osman, V. Mittal, M. Morbidellis and U. W. Suter, Polyurethane adhesive nanocomposites as gas permeation barrier, *Macromolecules*, 2003, **36**, 9851.
33. H. Zhang and A. Cloud. The Permeability Characteristics of Silicone Rubber. The 2006 SAMPE Fall Technical Conference, Global Advances in Materials and Process Engineering, proceedings, Coatings and Sealants Section, November 6–9, 2006, Dallas.
34. S. A. Kumar, H. Yuelong, D. Yumei, Y. Le, M. G. Kumaran and S. Thomas, Gas Transport Through Nano Poly(ethylene-*co*-vinyl acetate) Composite Membranes, *Ind. Eng. Chem. Res.*, 2008, **47**, 4898.
35. Y. Mohammadpour and A. A. Katbab, Effects of the Ethylene–Propylene–Diene Monomer Microstructural Parameters and Interfacial Compatibilizer Upon the EPDM/Montmorillonite Nanocomposites Microstructure: Rheology/Permeability Correlation, *Journal of Applied Polymer Science*, 2007, **106**, 4209.
36. A. P. Meera, P. S. Thomas and S. Thomas, Effect of Organoclay on the Gas Barrier of Natural Rubber Nanocomposties, *Polymer Composites*, 2012, 524.
37. J. Wang, S. T. Sanders, J. B. Jeffries and R. K. Hanson, Oxygen measurements at high pressures with vertical cavity surface-emitting lasers, *Applied Physics B: Lasers and Optics*, 2001, 1.
38. P. V. A. Kumar, K. T. Varughese and S. Thomas, Effect of Rubber – Filler Interaction on Transport of Aromatic Liquids through High Density Polyethylene/Ethylene Propylene Diene Terpolymer Rubber Blends, *Industrial & Engineering Chemistry Research*, 2012, **51**, 6697.
39. P. H. C. Camargo, K. G. Satyanarayana and F. Wypych, Review: Nanocomposites: Synthesis, Structure, Properties and New Application Opportunities, *Materials Research*, 2009, **12**, 1.

40. M. Alexandre and P. Dubois, Polymer-layered silicate nanocomposites: preparation, properties and uses of a new class of materials, *Materials Science & Engineering*, 2000, **28**, 1.
41. S. Taj, M. A. Munawar and S. Khan, Review Natural Fiber-Reinforced Polymer Composites, *Proceedings of the Pakistan Academy of Sciences*, 2007, **44**, 129.
42. M. Jacob, K. T. Varughese and S. Thomas., Water Sorption Studies of Hybrid Biofiber Reinforced Natural Rubber Biocomposites, *Biomacromolecule*, 2005, **6**, 2969.
43. M. Maiti and A. K. Bhowmick, Effect of Polymer–Clay Interaction on Solvent Transport Behavior of Fluoroelastomer–Clay Nanocomposites and Prediction of Aspect Ratio of Nanoclay, *Journal of Applied Polymer Science*, 2007, **105**, 435.
44. H. Angellier, M. Boisseau, L. Lebrum and A. Dufresne, Processing and structural properties of waxy maize starch nanocrystals reinforced natural rubber, *Macromolecules*, 2005, **38**, 3783.
45. K. Yano, A. Usuki and A. Okada, Synthesis and properties of polyimide-clay, *Journal of Polymer Science and Polymer Chemistry*, 1997, **35**, 2289.
46. A. Bendahou, H. Kaddami, E. Espuche, F. Gouanvé and A. Dufresne, Synergism Effect of Montmorillonite and Cellulose Whiskers on the Mechanical and Barrier Properties of Natural Rubber Composites, *Macromolecular Materials and Engineering*, 2011, **296**, 760.

Subject Index